JOINT EUROPEAN TORUS JET

EUR 1113

JET JOINT UNDERTAKING

PROGRESS REPORT 1986

EUR 11113 EN
EUR-JET-PR4

JET JOINT UNDERTAKING

PROGRESS REPORT 1986

MARCH 1987

This document is intended for information only
and should not be used as a technical reference.

EUR 11113 EN (EUR-JET-PR4) March 1987.
Editorial work on this report was carried out by B.E. Keen
The preparation for publication was undertaken by
the Documentation Service Units, Culham Laboratory.

Printed in England

Contents

Foreword

This is the fourth JET Progress Report which covers the third full year of JET's operation. These Progress Reports were introduced in 1983 to provide a more detailed account of JET's scientific and technical progress than that contained in the JET Annual Reports.

The first two Reports (in 1983 and 1984) described the main activities and advances made on JET during the relevant periods, and concentrated on the scientific and technical involvement of the relevant JET Departments. As an experiment, it was decided in 1985 to change the format of the Progress Report, so that it provided an overview summary of the scientific and technical advances during the year, and was supplemented by appendices of detailed contributions (in preprint form) of the more important JET articles produced during that year.

The early Progress Reports provided good reference documents of developments and results during the early operation period, before JET advances were published in the conventional literature. Now, JET results receive world-wide dissemination at International Conferences and meetings and in various scientific journals, at an earlier stage. Therefore, there is now less need for such a detailed record of all JET events, as the machine now operates almost in a routine manner. This change in format was introduced to reflect that change in circumstances, and comments from recipients showed that they appreciated this new format. Consequently, this Report follows that revised scheme.

The document is still aimed not only at specialists and experts engaged in nuclear fusion and plasma physics, but also at a more general scientific community. To assist in meeting these general aims, the Report contains a brief summary of the background to the Project, describes the basic objectives of JET and the principal design aspects of the machine. In addition, the Project Team structure is included as it is within this structure that the activities and responsibilities for machine operation are carried out and the scientific programme is executed.

There is no doubt that 1986 provided another successful year for JET both from the technical and scientific viewpoints. The Project completed Phase IIA of its programme devoted to the first stage of additional heating studies to observe the effects on plasma temperatures and confinement properties of large powers of ion cyclotron resonance heating (ICRH) and of neutral beam heating, singly and in combination.

Most of 1986 was devoted to machine operations with a previously planned major shutdown starting at the end of November. More time was devoted to tokamak operations during 1986 than in any year since the experimental programme started in 1983. The total number of pulses achieved was 4,900, an increase of 56% on the previous year. In the operational period, the machine operated routinely and reliably at its maximum design level with toroidal fields up to 3.4T and plasma currents exceeding 5MA. In spite of the complexity of operation with the introduction of new systems, there was a clear shift to the use of higher plasma currents compared with operations in previous years.

An important aspect of the JET programme during the year was the introduction, commissioning and operation of the first neutral beam heating system. The expected level of operation was reached and up to 10MW of power was injected into the torus with an 80keV deuterium beam. The first stage of the radio-frequency heating system, which started in 1985, also reached its planned capability for this phase with 12MW of output power from the generators, and 8MW of net power launched into the torus. This level exceeded considerably that previously used on a tokamak.

An important advance during the year was the establishment on JET of stable discharges with a separatrix or X-point in the magnetic configuration, which formed a clear magnetic limiter for JET plasmas. This scheme has been maintained with a plasma current of 3MA in a single-null and a 2.5MA with a double-null configuration. A significant break-through was a transition to high plasma confinement (H-mode) for about 2s which was achieved in the single-null configuration using neutral beam heating levels above 5.5MW.

These major technical achievements have formed the basis for the most encouraging scientific results obtained during the year. During neutral beam heating experiments in normal discharges, temperatures up to 6.5keV have been attained with ion densities $n = 3 \times 10^{19} m^{-3}$. With radio-frequency heating, the peak ion temperature achieved was 5keV with a peak density $n = 3.5 \times 10^{19} m^{-3}$. In both cases, the energy confinement times degraded as the heating power was increased, irrespective of the heating method being used.

The fusion product $\langle n\ T\ \tau \rangle$ obtained in material limiter configurations was similar for all heating methods as gains made in density and temperature were offset by degradation in confinement time. Under these conditions, the value for the fusion parameter was $\langle n\ T\ \tau \rangle = 1 \times 10^{20} m^{-3}.s.keV$. Operations with the X-point magnetic limiter configuration using a single-null in the H-mode has yielded a record value for the fusion parameter of $2 \times 10^{20} m^{-3}.s.keV$ within a region directly relevant for achieving reactor conditions. If tritium has been introduced into the machine under these conditions,

it would correspond to a fusion power production above 1MW. These results announced at the '11th IAEA Conference on Plasma Physics and Controlled Nuclear Fusion' held in Japan during November, were widely acclaimed and firmly established JET as the world's leading nuclear fusion experiment.

The scientific results so far achieved on JET are most encouraging. In terms of plasma parameters - density, temperature and confinement - JET has already reached the stage where each of these parameters is within a factor of two or three of those needed for fusion reactor. Considerable effort has been devoted towards the design, procurement and commissioning of equipment for installation during the 1987 shutdown and at later stages. This task is of utmost importance as these preparations will determine the future performance of JET.

New additions proposed for JET aim to build up a high density and high temperature plasma in the central region, where α-particles could be observed, while maintaining a sufficiently high energy confinement time. This is planned by: tailoring the current profile by lower hybrid current drive and neutral beam injection to eliminate or reduce sawteeth oscillations to obtain improved temperatures; increasing the central density by high velocity pellet injection; reducing edge density by edge pumping; achieving high central temperatures by on-axis ICRF heating and high energy neutral beam heating. In addition, the confinement will be improved by increasing the plasma current to 7MA in limiter discharges and to 4MA in X-point magnetic limiter configurations. This represents a major modification to the poloidal field coil system to allow these plasma currents to be achieved. Since operations at these plasma currents constitute a considerable extension of the original design parameters, a study has been undertaken to reassess the machine and its power supplies.

The most encouraging results obtained to date are a tribute to the dedication and skill of all who work on the Project. They also reflect the continuous co-operation and assistance received from the Associated Laboratories and from the Commission of the European Communities. They support the confidence and guidance given to the management of the Project by the JET Council, JET Executive Committee and JET Scientific Council.

I have no doubt that with such devotion from all sides, the Project will face with confidence the many problems and challenges that are likely to be encountered in the future.

Introduction, Background and Report Summary

Introduction

The first two JET Progress Reports (EUR-JET-PR1 and EUR-JET-PR2) described activities and advances up to the end of 1983 and 1984, respectively, and concentrated mainly on the scientific and technical activities of the relevant Departments in JET. The Reports provided detailed records of JET's achievements and advances in all its aspects reported on a Division by Division basis. However, the staff effort involved in preparation and compilation of the detailed reports was considerable and the information was already outdated by the time of publication. As an experiment for the 1985 version (EUR-JET-PR3), it was decided that, in order to speed up the production process and to minimise the staff effort involved, a Progress Report would be produced which provided an overall summary of the scientific and technical advances achieved during the year, following by appendices of detailed contributions (in preprint form) of the most important JET technical articles produced during that year. In view of many favourable comments received, especially on the timely production of the 1985 edition, it was decided that the 1986 JET Progress Report would follow the same format as that in 1985.

For completeness, this section contains a brief summary of the background to the Project. It describes the basic objectives of JET and the principal design aspects of the machine. In addition, the Project Team structure is detailed, as it is within this structure that the activities and responsibilities for machine operation are carried out and the scientific programme is executed.

Background

Objectives of JET

The Joint European Torus (JET) is the largest single project of the nuclear fusion research programme of the European Atomic Energy Community (EURATOM). The project was designed with the essential objective of obtaining and studying plasma in conditions and with dimensions approaching those needed in a fusion reactor.

The studies are aimed at

(a) investigating plasma processes and scaling laws, as plasma dimensions and parameters approach those necessary for a fusion reactor;

(b) examining and controlling plasma-wall interactions and impurity influxes in near-reactor conditions;

(c) demonstrating effective heating techniques, capable of approaching reactor temperatures in JET, in the presence of the prevailing loss processes (particularly, RF and Neutral Beam Heating processes);

(d) studying alpha-particle production, confinement and subsequent plasma interaction and heating produced as a result of fusion between deuterium and tritium.

Two of the key technological issues in the subsequent development of a fusion reactor are being faced for the first time in JET. These are the use of tritium and the application of remote maintenance and repair techniques. The physics basis of the post-JET programme will be greatly strengthened if other fusion experiments currently in progress are successful. The way should then be clear to concentrate on the engineering and technical problems involved in progressing from an advanced experimental device like JET to a prototype power reactor.

Basic JET Design

To meet these overall aims, the basic JET apparatus was designed as a large tokamak device with overall dimensions of about 15m in diameter and 12m in height. A diagram of the apparatus is shown in Fig.1 and its principal parameters are given in Table I. At the heart of the machine, there is a toroidal vacuum vessel of major radius 2.96m having a D-shaped cross-section 2.5m wide by 4.2m high. During operation of the machine, a small quantity of gas (hydrogen, deuterium or tritium) is introduced into the vacuum chamber and is heated by passing a large current (up to 5MA at present but may be enhanced to 7MA subsequently) through the gas. This current is produced by transformer action using the massive eight-limbed magnetic circuit, which dominates the apparatus (see. Fig.1). A set of coils around the centre limb of the magnetic circuit forms the primary winding of the transformer with the plasma acting as the single turn secondary. Additional heating of the plasma is provided by propagating and dissipating high power radio frequency waves in the plasma and by injecting beams of energetic neutral atoms into the system.

The plasma is confined away from the walls of the vacuum vessel by a complex system of magnetic fields, in which the main component, the toroidal field, is provided by 32 D-shaped coils surrounding the vacuum vessel. This field, coupled with that produced by the current flowing through the plasma, forms the basic magnetic field for the tokamak confinement system, which provides a full design field at the centre of 3.45T. The poloidal coils, located around the outside of the vacuum vessel, shape and position the plasma in operation.

Initial experiments have been undertaken using hydrogen and deuterium plasmas, but in the later stages of operation, it is planned to operate with deuterium-tritium plasmas, so that fusion reactions can occur to produce significant α-particle heating in the plasma.

In order to reach conditions close to those relevant to a fusion reactor, a plasma density of $\sim 10^{20} m^{-3}$ at a temperature of 10keV would be needed. Even with a current of 5MA in JET, this would be inadequate to provide the temperature required using ohmic heating

TABLE I
Principal Parameters

Parameter	*Value*
Plasma minor radius (horizontally), a	1.25m
Plasma minor radius (vertically), b	2.10m
Plasma major radius, R_o	2.96m
Plasma aspect ratio, R_o/a	2.37
Plasma elongation ratio, e=b/a	1.68
Flat top pulse length	10s
Toroidal magnetic field (plasma centre)	3.45T
Plasma current, D shaped plasma	4.8MA
Volt-seconds available	34Vs
Toroidal field peak power	380MW
Poloidal field peak power	300MW
Additional heating power (into torus)	~50MW
Weight of vacuum vessel	108t
Weight of toroidal field coils	364t
Weight of iron core	2800t

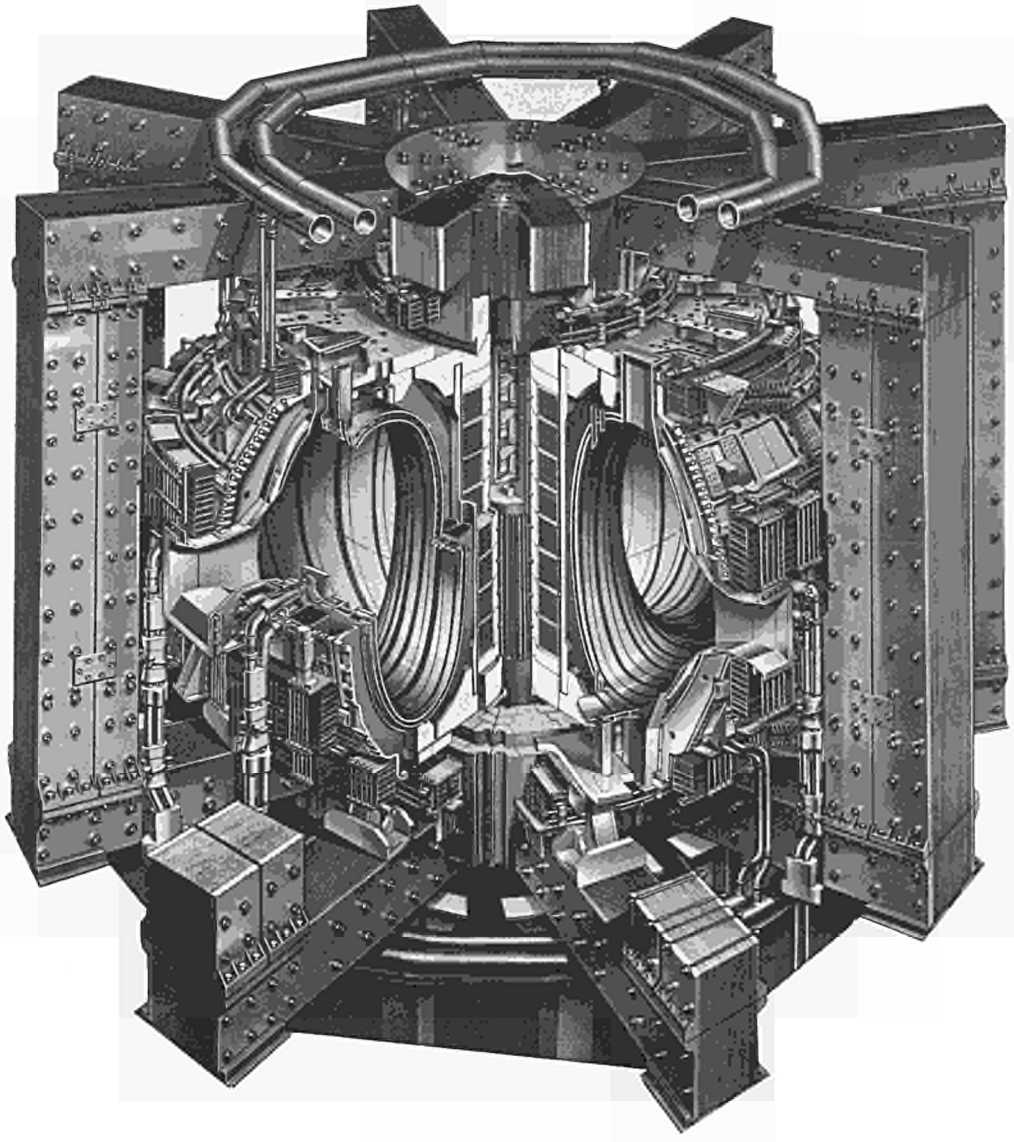

Fig. 1: Diagram of the JET Tokamak.

alone. Consequently, additional heating is required and two main systems are being added to JET as follows:

- Injection into the plasma of highly energetic neutral atoms (Neutral Injection Heating)
- Coupling of high power electromagnetic radiation to the plasma (Radio Frequency (RF) heating).

The total power into the torus will increase in discrete steps up to ~50MW.

Project Team Structure

A rationalisation of the Project Structure was undertaken at the beginning of 1986 and the structure adopted, for management purposes, was divided into four Departments (see Table II):

- Machine and Development Department
- Experimental Department
- Heating and Theory Department
- Administration Department

The main duties of the Administration Department have been described in previous JET Annual Reports. This Report concentrates on progress made in the scientific and technical Departments during 1986. To aid this description, the functions of these technical Departments are described below.

Machine and Development Department

The Machine and Development Department is responsible for the performance capacity of the machine as well as equipment for the active phase, together with directly related enhancements (excluding heating) and the integration of any new elements on to the machine. In addition, the Department is responsible for machine services. The Department contains three Divisions:

(a) Magnet and Power Supplies Division, which is responsible for the design, installation, operation, maintenance and modification of all power supply equipment needed by the Project. In addition, the Division is responsible for maintenance and operation of the coil systems, structural components and machine instrumentation;

(b) First Wall Division, which is responsible for the vital area of plasma wall interactions. Its main tasks include the provision and maintenance inside the vacuum vessel of conditions leading to high quality plasma discharges. The Division develops, designs, procures and installs first wall systems and components, such as limiters, wall protections and internal pumping devices. The area of responsibility encompasses the vacuum vessel as a whole together with its associated

TABLE II

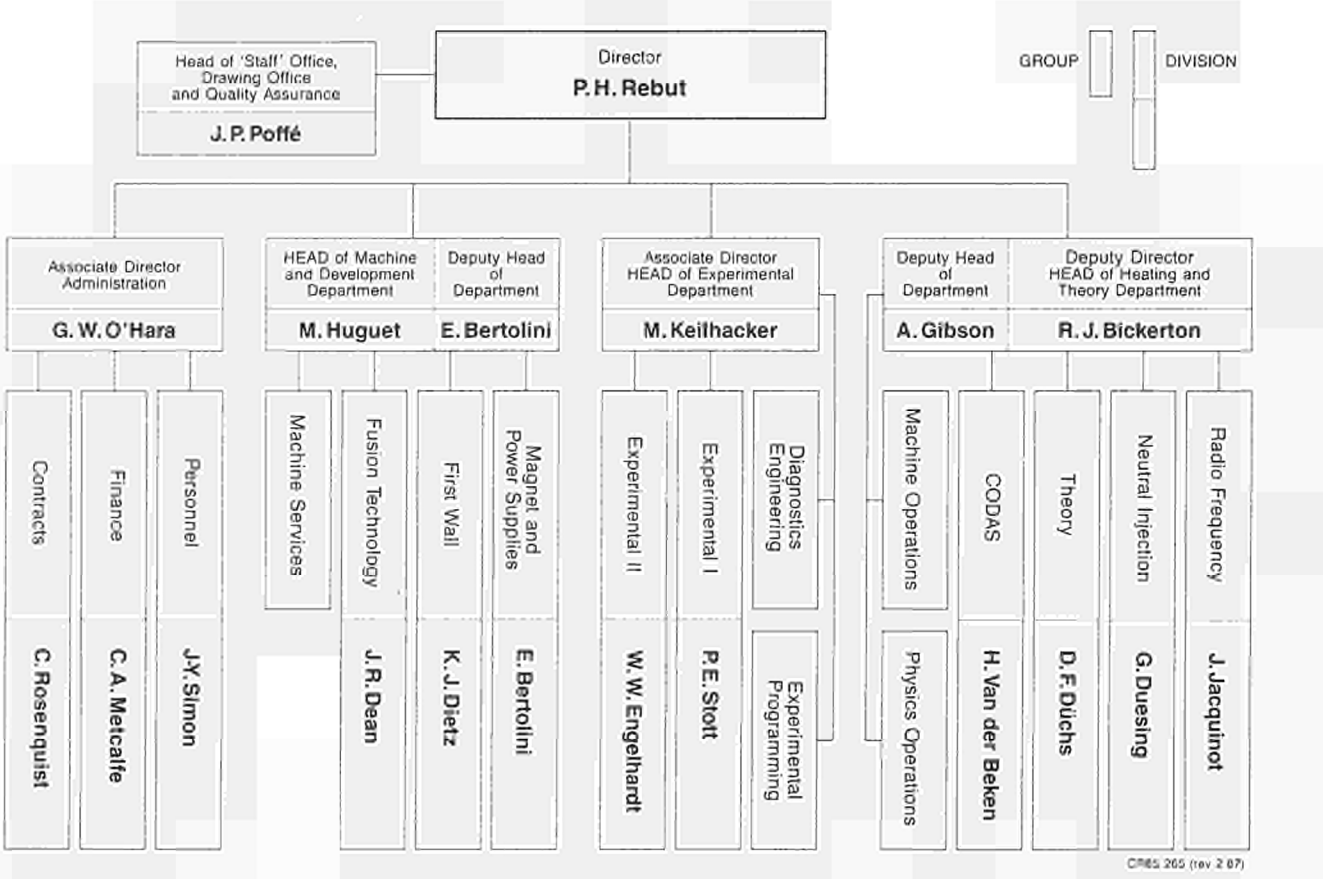

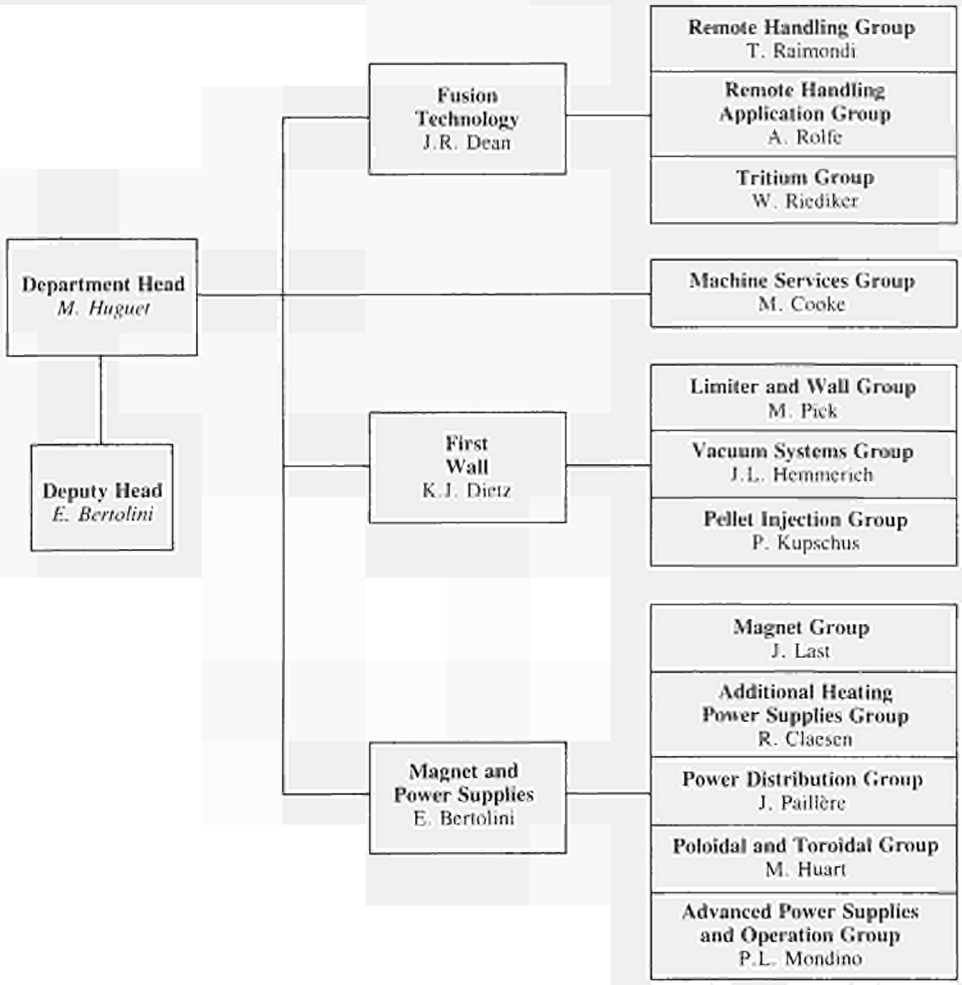

Fig. 2: Machine and Development Department, Group Structure (December 1986).

systems, such as pumping, bake-out, gas introduction and pellet fuelling;

(c) Fusion Technology Division, which is responsible for the design and development of remote handling methods and tools to cope with the requirements of the JET device, and for maintenance, inspection and repairs. Tasks also include the design and construction of facilities for handling of tritium.

The Structure of the Machine and Development Department to Group Leader level is shown in Fig.2 and the list of staff within the Department is shown in Fig.3.

Experimental Department

The main functions of the Department relate to the measurement and validation of plasma parameters. The main tasks are:

- to conceive and define a set of coherent measurements;
- to be responsible for the construction of necessary diagnostics;
- to be responsible for the operation of the diagnostics, the quality of measurements and the definition of the plasma parameters;
- to play a major role in the interpretation of data.

The Department contains two Groups (Diagnostics Engineering Group and Data Processing and Analysis Group) and two Divisions:

(a) Experimental Division 1 (ED1), which is responsible for specification, procurement and operation of approximately half the JET diagnostic systems. ED1 undertakes electrical measurements, electron temperature measurements, surface and limiter physics and neutron diagnostics;

(b) Experimental Division 2 (ED2), which is responsible for specification, procurement and operation of the other half of the JET diagnostic systems. ED2 undertakes all spectroscopic diagnostics, bolometry, interferometry, soft X-ray array and neutral particle analysis.

The structure of the Experimental Department to Group Leader level is shown in Fig.4 and the list of staff in the Department is shown in Fig.5.

Heating and Theory Department

Heating and Theory Department is responsible for heating the plasma, the theory of tokamak physics, the organisation of experimental data, and the day to day

MACHINE AND DEVELOPMENT DEPARTMENT

Head of Department: M. Huguet
Deputy Head of Department: E. Bertolini

D Carre	Mrs A Cranstone
M Cooke	L Nickesson

MAGNET AND POWER SUPPLIES DIVISION
Head: E Bertolini

Mrs C Allen	D Halliwell	A Santagiustina
P Bertoldi	M Huart	K Selin
T Bonicelli	A Keymore	S Shaw
I Borch	J R Last	A Skinstad
O Buc	V Marchese	S Turley
D Cacaut	G Marcon	J van Veen
J Carwardine	L Mears	N Walker
C Christodoulopoulos	A Moissonnier	Mrs L T Wall
R Claesen	P Mondino	C R Wilson
E Daly	G Murphy	G C Wilson
P Doidge	Mrs J Nolan	M E Young
B T Eriksson	P Noll	L Zannelli
H T Fielding	J Paillere	J Zwart
J Goff	C Raymond	

FUSION TECHNOLOGY DIVISION
Head: J R Dean

S J Booth	Mrs M E Jones	W Riediker
P G Brown	P D Jones	J Schreibmaier
R Cusack	A Konstantellos	L Sonnerup
Mrs M Daish	A Nowak	A Tesini
L Galbiati	P Presle	M Tschudin
A Galetsas	T Raimondi	M Wykes
E Gebler	J Removille	

FIRST WALL DIVISION
Head: K Dietz

W P Bailey	M Gadeberg	P McCarthy
B Bignaux	K Grabenstätter	J Orchard
A Boschi	L Grobusch	M Pick
H Buttgereit	J Hemmerich	R L Shaw
G Celentano	D Holland	K Sonnenberg
Mrs D Cranmer	Mrs I Hyde	R Thomas
W Daser	G Israel	E Usselmann
C Froger	H Jensen	M Walravens
E Deksnis	P Kupschus	T Winkel

Fig.3: Project Team Staff in Machine and Development Department (December 1986)

operation of the machine. The main functions of the Department are:

- following the theory of tokamak physics;
- heating the plasma and analysis of its effects;
- centralising the interpretation of experimental results and investigating their coherence;
- organising data acquisition and computers;
- preparing and co-ordinating operation of the machine across the different Departments.

The Department is composed of three groups (Machine Operations Group, Physics Operation Group and Data Management Group) and four Divisions:

(a) Control and Data Acquisition System Division (CODAS), which is responsible for the implementation, upgrading and operation of computer-based control and data acquisition systems for JET;

(b) Neutral Beam Heating Division, which is responsible for the construction, installation, commissioning and operation of the neutral injection system, including development towards full power operation of the device. The Division also participates in studies of the physics of neutral beam heating;

(c) Radio Frequency Heating Division, which is responsible for the design, construction, commissioning and operating the RF heating system during the different stages of its development to full power. The Division also participates in studies of the physics of RF heating;

(d) Theory Division, which is responsible for prediction by computer simulation of JET performance, interpretation of JET data and the application of analytic plasma theory to gain an understanding of JET physics.

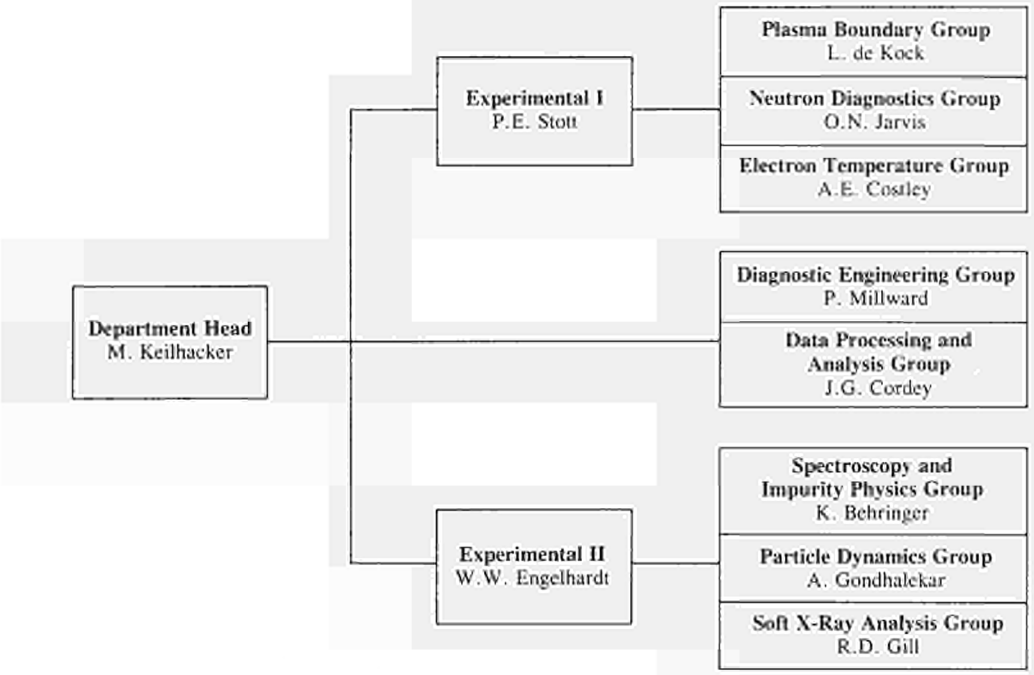

Fig. 4: Experimental Department, Group Structure (December 1986).

EXPERIMENTAL DEPARTMENT
Head of Department: M Keilhacker

M Barnes	Miss J Kedward	Miss K Slavin
C H Best	R C Lobel	Mrs P Stubberfield
C Caldwell-Nichols	P Millward	A R Talbot
J Christiansen	E Oord	A Tiscornia
J G Cordey	Miss A Reichenau	E Van der Goot
N Foden	J Reid	M L Watkins
J Gowman	P J Roberts	C H Wilson
C J Hancock	F Sieweke	D Wilson
J Hoekzema		

EXPERIMENTAL DIVISION I
Head: P Stott

Miss N Avery	S Gregoli	R Prentice
D Bartlett	P J Harbour	P Roach
B W Brown	M Hone	G Sadler
D Campbell	I Hurdle	A Stevens
J Coad	O Jarvis	Miss D Strange
A Costley	J Källne	D Summers
L de Kock	G Neill	P van Belle
J Fessey	C Nicholson	J Vince
C Gowers	P Nielsen	

EXPERIMENTAL DIVISION II
Head: W Engelhardt

K Behringer	A Gondalekar	J O'Rourke
J L Bonnerue	J Holm	A Ravestein
G Braithwaite	Mrs S Humphreys	J Ryan
A D Cheetham	E Källne	B K Scheidt
S Corti	L Lamb	Mrs C Simmons
Miss G Denne	G Magyar	M Stamp
A Edwards	J L Martin	B Viaccoz
Mrs A Flowers	P Morgan	M von Hellerman
R Gill		

Fig. 5: Project Team Staff in Experimental Department (December 1986)

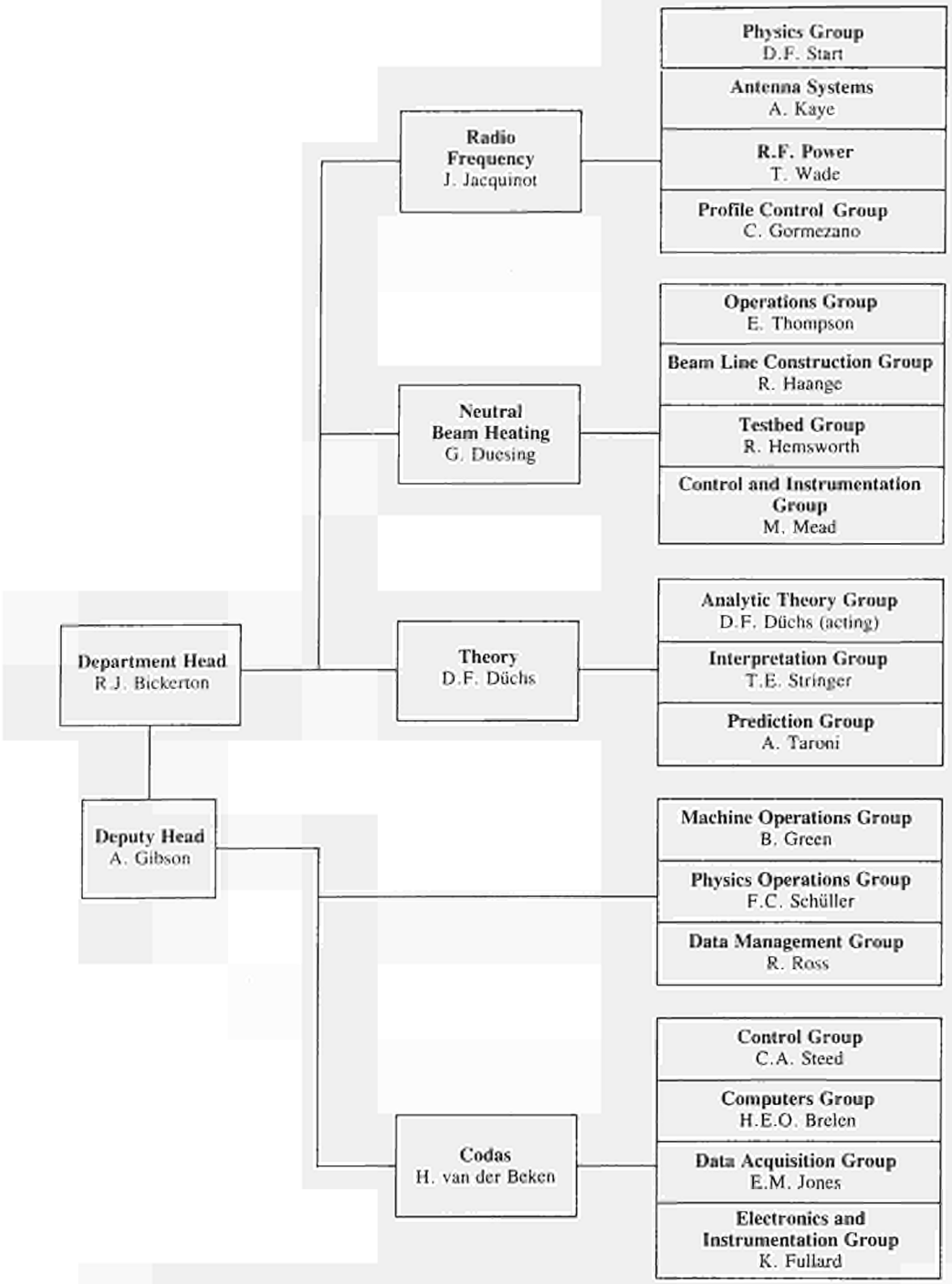

Fig. 6: Heating and Theory Department, Group Structure (December 1986).

The structure of the Heating and Theory Department to Group Leader level is shown in Fig.6, and the list of staff in the Department is shown in Fig.7.
In addition, all Divisions are involved in:

- execution of the experimental programme;
- interpretation of results in collaboration with other appropriate Divisions and Departments;
- making proposals for future experiments.

Report Summary

Section 1 of this Report provides a brief introduction and some background information relevant to the Report. Section 2 sets out an overview of progress on JET during 1986 and with a survey of scientific and technical achievements during 1986, sets these advances in their general context. This summary is specifically cross-referenced to reports and articles prepared and presented by JET staff during 1986. The more important of these articles which are of general interest, are reproduced as appendices to this Report.

In Section 3, certain developments are considered which might enable additional improvements/ modifications of the machine to further improve its overall performance. These improvements are considered to overcome certain limitations encountered generally on Tokamaks, particularly concerned with

HEATING AND THEORY DEPARTMENT

Head of Department: R J Bickerton
Deputy Head of Department: A. Gibson

K Adams
P Chuilon
A Conway
D Cook
S Cooper
T Dale
B Glossop
B Green
N Green
R Hausherr
C Hookham
M Hughes
P Lomas
M Malacarne
Mrs M Pacco
D Pratt
R Rigley
R T Ross
Mrs M E Rowe
P Rutter
F C Schüller
W Smith
Miss A Strange
A Tanga
P Thomas
R Thomson
M Walker

THEORY DIVISION

Head: D F Düchs

M Brusati
W Core
Mrs S Costar
Mrs M Ellis
A Galway
N A Gottardi
T Hellsten
Mrs S Hutchinson
B Keegan
E Lazzaro
Miss M Nave
H Sack
R Simonini
P Smeulders
E Springmann
T E Stringer
A Taroni
J Wesson

NEUTRAL BEAM HEATING DIVISION

Head: G Duesing

H Altmann
G Beaumont
A Browne
A Burt
C D Challis
D Cooper
J F Davies
G Deschamps
A Dines
D Ewers
H Falter
J Gallacher
Mrs S Gerring
A Goede
R Haange
R Hemsworth
F Hurd
J Jensen
A Jones
T T C Jones
D Kausch
E Küssel
F Long
J Lundqvist
D Martin
P Massmann
C Mayaux
M J Mead
W Obert
S Papastergiou
D Raisbeck
R Roberts
Mrs M Sinclair
D Stork
R Tivey
E Thompson
D Young
M Watson

RADIO FREQUENCY HEATING DIVISION

Head: J Jacquinot

R J Anderson
S C Booth
G Bosia
F Brandl
M Brandon
H Brinkschulte
Mrs L Brookes
M Bures
G Cottrell
J Dobbing
D T Edwards
A Franklin
M Gammelin
C Gormezano
E Hanley
R Horn
G Jessop
A Kaye
Miss J Maymond
P Murray
M Pain
J Plancoulaine
F Sand
M Schmid
A G Sibley
D Start
T Wade
C Walker

CONTROL AND DATA ACQUISITION SYSTEMS DIVISION

Head: H Van der Beken

Mrs A M Bellido
M Botman
H Brelen
W Brewerton
M L Browne
T Budd
P Card
J J Davis
Mrs L M Dines
S E Dorling
K Fullard
R F Herzog
E M Jones
N Kidd
J G Krom
Miss E Mathia
D Nassi
J P Nijman
I Piacentini
C G Pollard
G Rhoden
J Saffert
C A Steed
J E Van Montfoort
B A Wallender
I D Young

Fig. 7: Project Team Staff in Heating and Theory Department (December 1986)

density limits, with plasma MHD behaviour, with impurities and with plasma transport. Some attention has been devoted to methods of surmounting these limitations and these are detailed in this section.

The Appendices contain a list of work topics carried out under Task Agreements with various Association Laboratories, and selected articles prepared by JET authors are reproduced in detail, which provide some details of the activities and achievements made on JET during 1986. In addition, a full list is included of all Articles, Reports and Conference papers published in 1986.

Technical Achievements during 1986

Torus Systems

Many new elements had been added to the machine vacuum system during the late 1985 shutdown, ready for 1986 operation. Eight carbon limiters (instead of the previous four) were fitted symmetrically on the outboard periphery of the vacuum vessel wall, and additional graphite protection was installed to further reduce the contamination of the plasma by metal impurities. The inboard protection was extended by eight discrete poloidal rings covering the octant joints and the inner wall was covered with tiles to ±1m of the mid-plane. Graphite tiles were also fitted at the outboard wall in the vicinity of the Octant No.5 horizontal port, to protect the vessel wall against tangential neutral beams, originating from Octant No.8. As well, the second neutral injection box with its high vacuum rotary valve and a third RF antenna were connected to the main vacuum system, and a number of new diagnostics were also installed. However during 1986, nearly the whole year was dedicated to machine operation, and few new systems could be brought into service. It was necessary for the various machine systems to prove their reliability, especially those elements added to the machine during 1985.

Vacuum Systems

The pumping systems performed reliably during 1986, and in addition, all vacuum related systems operated without major problems. The year was mainly dominated by a gradual increase in power of neutral beam heating. During this programme, several incidents occurred which demonstrated both the strength of the vessel and the vacuum system, but also indicated the need for improvement in some areas, related to rotary valves and vacuum instrumentation.

Leak testing has been a problem since deuterium was first introduced into the vessel. Standard leak detectors as well as quadrupole mass analysers cannot easily separate deuterium (mass 4.028) from helium (mass 4.003). As a consequence, outgassing of deuterium, previously implanted in the wall during discharges, masked the helium normally used as a tracer gas. Employing other gasses such as neon or argon does not relieve the situation as normally these elements are masked by various deuterated chemical compounds. Since this situation was no longer tolerable, a different type of mass analyser - the omegatron - was adopted by JET and brought into operation. Leak detection can now be carried out in the presence of deuterium with helium as a tracer gas [1].

The tritium phase of JET requires careful screening of the compatibility of vacuum components with the envisaged tritium environment. One point of concern was the compatibility of the main turbopumps. An experiment was devised by JET and carried out at the KFA Jülich, F.R.G., to clarify this situation. A simulation experiment, with a tritium dose equivalent to 250 years of JET operation, was set up to investigate the changes in the viscosity of the pump oil. The viscosity of the lubricant is the determining parameter for the life of a turbopump, and since no changes were found, it can be concluded that the JET turbopumps are fully compatible with the expected tritium operation [2].

In-Vessel Components

The eight discrete limiters worked reliably and showed virtually no surface damage at the end of the operational period, indicating that the design criteria were properly chosen. Beam shine-through and port protection tiles were also in an excellent condition at the end of 1986 operation.

The inner wall graphite tiles were initially designed as protection against disruptions only, but subsequently were extensively used as a limiter. This operation mode was extremely useful for controlling the density at the end of a discharge and to achieve particle pump-out during discharges. This allowed JET to run low density, high temperature discharges as well as slide-away discharges. However, some wall damage occurred mainly during these modes, but the extent was not as severe as to endanger operation. Three areas of the inner wall especially, in which tiles protruded by 5-10mm, showed strong marks, and required special attention.

The U-joint graphite protection tiles, initially designed as wall protection against vertical instabilities, were used as dump plates during X-Point operation. Initial power limits of 10MW for 1s did not allow H-mode discharges. Under these conditions, surface temperatures of the protection tiles exceeded 3000°K locally. A design modification was made and new tiles installed during 1986. The power handling capability was 16MW for 2s without exceeding the design limit surface temperature of 2000K. Amongst other things, this increase in perform-

ance was a prerequisite to achieving H-mode operation in JET.

The procurement of additional graphite tiles to cover the bellows protection plates continued satisfactorily and most tiles together with their support plates were ready for assembly in the vessel at the end of the year. The manufacture of the belt limiter was also nearly complete and by the end of 1986, many limiter sectors were delivered and successfully leak tested at elevated temperatures in the JET oven. Assembly was planned to start in January 1987. For the belt limiter, both graphite and beryllium tiles were procured in 1986, but a decision was taken to use graphite first. Beryllium will be used later, probably early in 1988, and this decision will be confirmed before the end of 1987.

Electromagnetic Systems

For the containment of forces occurring during vertical instabilities, new supports linking the main vertical ports of the vessel to the magnetic limbs were designed in 1985 (see Fig.8). The procurement of these supports went ahead satisfactorily during 1986 and deliveries, already started in December, were expected to be complete in January 1987. These new supports involved the replacement of the existing flanges at main vertical ports with new rigid forged pieces.

During the whole of 1986, the toroidal field and poloidal field coils systems were operated routinely and reliably at their maximum design parameters. No major change of the coil system took place in 1986, except that

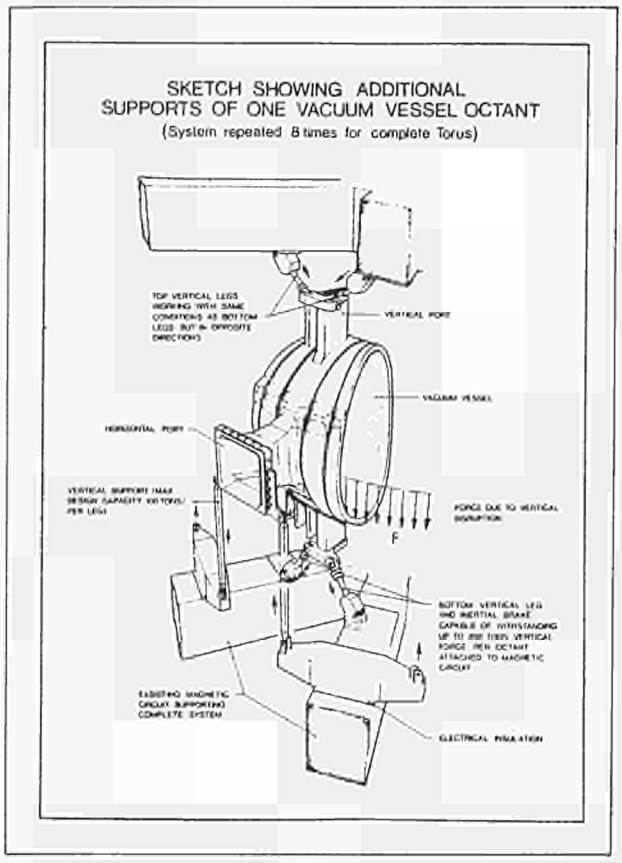

Fig.8: Final design of vacuum vessel supports

for X-point operation in the single null configuration, the poloidal shaping field circuit was used in an assymetric configuration with the upper coils only. This new mode of operation was completely successful but, if used routinely, would require a modification of the safety system (DMSS) which detects electrical faults. A new system was designed for implementation early in 1987.

Major modifications of the poloidal field coil system were decided in 1986 and planned for implementation during the 1987 shut-down. These are:

a) the central poloidal field coil stack will be increased from eight to ten sub-coils in order to reduce stray fields and improve discharge breakdown and plasma start-up conditions;
b) additional busbars connecting the six centre sub-coils will be manufactured and installed in order to allow separate control of the current flowing in these six centre sub-coils with respect to the current flowing in the four top and bottom sub-coils. This new circuit configuration will require a new power supply and will make use of the PVFA-5-6 which was being erected at the end of 1986.

The new poloidal field coil configuration is extremely versatile and opens up a wide range of operational scenarios. In particular, it allows:

a) compensation of stray fields by means of small differential currents flowing in the six centre sub-coils;
b) an increase of the total flux swing by driving the current in the six centre sub-coils above the design value of 40kA. This should allow plasma current flat-tops of 7s at 7MA;
c) an increase of the plasma current achieveable in the X-point mode of operation (up to 4MA).

Preparation and procurement for these far-ranging modifications were carried out during the second half of 1986, and work started on the machine in December. By the end of December, the central poloidal field coil stack was extracted from the machine and dismantled into elementary coils. At this stage, some slight damage was observed on the sub-coils. Keys which located and interlocked the sub-coils together were fractured due to a tendency for the sub-coils to rotate with respect to each other. This rotation was driven by the large twisting moment acting on the mechanical structure and the forces involved were considerable. Some design modifications were being prepared to prevent the re-occurrence of this effect.

The modifications of the poloidal field coil system were in line with the enhancement of JET performance up to a current of 7MA in the limiter mode of operation, and up to 4MA in the X-point mode of operation. Since this enhancement calls for a considerable extension of the original design parameters, a major design review (The 7MA and X-point Study) was launched in 1986. The aim of this study is to reassess the machine and its power supplies from the mechanical, thermal and electrical point of view and identify safe operation boundaries. A task force was established to carry out this work. By the

end of the year, a number of study contracts had been placed and work was proceeding along several lines. Major results are expected by July 1987.

References

[1] T Winkel, J L Hemmerich
Helium leak detection in JET in the presence of high deuterium partial pressures
J Vac. Sci. Tech. (1987) in publication

[2] R Lasser, K H Klatt, D Triefenbach, J L Hemmerich
Tritium compatibility measurements of turbomolecular pump oil in a miniaturised viscosimeter
J. Nucl. Mat. (1987) in publication

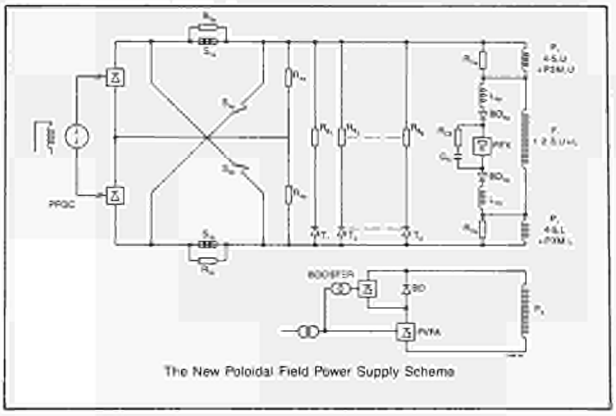

Fig.9: The new poloidal circuit.

Power Supplies and Plasma Control

Since the machine was in operation throughout most of 1986, the priority duty was to maintain and operate, in good operational condition, the JET power supplies for the tokamak systems, for the additional heating and for power distribution. Therefore, little intervention was allowed for modifications and improvements on the power supplies. However, certain problems arising during operation have been analysed and necessary modification work has been carefully prepared for implementation during the 1987 shutdown. In addition, as part of the JET development programme towards performance well beyond the original design parameters, some major design work has been undertaken, on both tokamak and additional heating power supplies, leading to a considerable number of contracts being placed with manufacturers for construction.

Development

This activity includes both systems related to the extension to full performance and systems related to the new JET development plan.

Tokamak Power Supplies and Plasma Control

The highlight in this area has been activities associated with development of the Poloidal System to allow operation up to 7MA plasma current with a material limiter and up to 4MA operation with a magnetic limiter (X-Point) configuration. Efforts have been devoted to design work, preparation of technical specifications, contracts, and installation and commissioning of components for the implementation of the new Poloidal Circuit (see Fig.9).

The present status is that: the Thyristor Power Supplies for PFX (the new PVFA 5,6 with the existing PVFA2) and the Additional Switching Network are on site and commissioning work has started; the contract for the Booster Amplifiers has been placed; one of the blocking diodes (BDXa) is on site, while for the other (BDXb) the procurement process has started; and the design of the resistors RXa, RXb and of the inductors LXa, LXb has been completed. All the required new busbars have been ordered.

Although all components may not be available by June 1987, it is expected to have all the essential components operational during 1987, so that both 7MA and 4MA operation in the respective machine configurations can be achieved. A study to enhance the poloidal power supply capability (PVFA 1, 2, 3, 4, 5, 6) up to 40kA for 10s has been initiated.

Another important achievement has been digitalisation of the Plasma Current Control and the study to change the Plasma Position Control from analog to digital operation has started. An assessment of Plasma Shaping has shown that it could be achieved in all present and future operating conditions by using only one Amplifier (PVFA 1), thus releasing PVFA2 for use eventually as part of PFX together with the newly acquired PVFA 5,6. Installation is in progress for PVFA 5,6 and the New Switching Network.

Additional Heating Power Supplies

During early 1986, the first set of eight Neutral Beam PINI Power Supplies started to supply the first PINI Box, to inject up to 10MW of neutral beam power into the plasma. The second set of eight PINI Power Supplies has been installed and fully commissioned on dummy loads. The Power Supplies for the PINI Test-Bed have been rearranged to supply the PINI's at 160kV and a comprehensive test programme has been undertaken: one injector has been tested up to 160kV and 45A for 5s.

All eight power supplies for the ICRH system have been installed and three of these have been used in continuous operation to supply the three RF antennae during the 1986 experimental period. The design for upgrading these power supplies to cater for the new 2MW RF generating tubes has been completed. A call for tender has been issued and offers received: orders will be placed in February 1987.

Power Distribution

A significant achievement has been the successful completion of further negotiations with UK Central Electricity Generating Board (CEGB) to revise the operational limits foreseen in the existing agreement.

This relates to voltage drops and power derivatives and is an essential feature required to operate JET at the future enhanced performance, without increasing the modest size of the active and reactive power compensation equipment already foreseen in development plans. Other major activities have been the rescheduling of the load feeders in the 33kV substation. This will allow simpler isolation procedures during operation and the installation of feeder metering equipment at 11kV and 3.3kV and the installation of a new 33kV/11kV, 30MVA transformer of improved design to supply the two flywheel generators.

Operation and Maintenance

So far, operation has been carried out with separate responsibilities for the tokamak and for the additional heating power supplies. As soon as the latter achieves the same reliability as the former, these responsibilities will be unified, with an expected reduction in total number of staff involved. The reliability achieved by the tokamak power supplies must be considered satisfactory, since, on average, as few as three faults a week have led to some loss in operating time.

Regular maintenance and prompt distribution throughout the project has been successfully carried out making use of a team of twelve electricians. The successful maintenance organisation set up for power distribution and for tokamak power supplies will be extended to the additional heating power supplies.

Studies

A number of studies of new power supplies and/or modifications of existing ones have been initiated. In particular, high frequency supplies (0-10kHz) to plasma disruption control coils to be fitted inside the vacuum vessel, a third set of power supplies for a new PINI Box and the possibility of enhancing the power output of the existing PINI power supplies, have all been investigated. As part of the 7MA enhancement study to assess the ultimate capability of JET, a comprehensive investigation of the capability of the overall JET power supplies to match the requirement of plasma performance beyond design value has also started. In addition, a new AC/DC power supply system has been designed to supply the twenty-four lower hybrid resonance heating (LHRH) klystrons with 500kW each.

A detailed analysis has also been undertaken of the effect on the CEGB grid of the planned JET operating scenarios, and a preliminary assessment of the active and reactive power compensation has been completed.

Neutral Beam Heating System

Beamline Construction

The first beamline system was successfully brought into full operation at the beginning of 1986, and the first experimental programme, in which hydrogen beams were injected into deuterium target plasmas, was carried out with few technical problems. The computer control and data acquisition system [1] proved to be particularly valuable in setting parameters and in ease of operation of this complex subsystem. The complete setting-up and operation of the eight-source beamline system plus associated subsystems can be carried out by one operator. Furthermore, it was confirmed that injector conditioning pulses were not required between tokamak pulses.

The injection system is capable of operation in two distinct modes:

(a) independent of tokamak operation in which the beams are intercepted by the beam-line calorimeter (ASYNCH mode);

(b) fully synchronised with the machine, in which the beams are injected into the plasma (SYNCH mode).

Following operation with hydrogen, the working gas was changed to deuterium to increase the injected power and to investigate D° injection into deuterium plasmas. The maximum power levels so far injected into the torus have been

- 5.5MW H° beams at 65kV extraction voltage;
- 10MW D° beams at 80kV extraction voltage.

Pulse lengths of up to 7s have been used. Over 700 pulses have been injected into the torus at power levels >1MW and pulse lengths >1s.

Beamline performance [2] has been extensively monitored during both operation modes using thermal and optical diagnostics and results were similar to those obtained during single beam operation in the Testbed (Fig.10), except for one significant deviation during SYNCH operation. Due to a higher than expected interaction between the injected beam and the stray machine magnetic field, a sideways deflection of the beams and a higher power interception on some of the beam-line components occurred. A single mechanical realignment of the beams was sufficient to compensate for the stray magnetic field over the range 1-3MA plasma current but additional realignment was necessary to compensate for higher plasma currents.

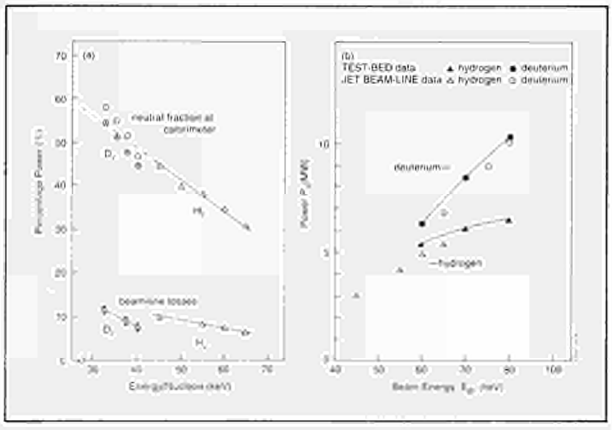

Fig.10: Measured performance of beamlines;
(a) measured power to beamline calorimeter and losses downstream of calorimeter as a percentage of extracted power;
(b) power to tokamak compared with predictions from single source operation on the JET Testbed.

The otherwise high overall mechanical and vacuum reliability of the injectors was marred by two incidents, which resulted in the melting of the water-cooled nickel liner in the beam entrance port. These incidents were due to excessive re-ionisation losses due to anomalously high gas pressure. These highlight one of the additional (but not fundamental) problems associated with long pulse operation.

For the JET beamline, ~4% of the 80keV D° beams are re-ionised by collisions with the background gas downstream of the deflection magnets, corresponding to ~400kW of beam swept out by the stray poloidal magnetic field. This leads to high localised power densities caused by magnetic focussing effects in the entrance duct. Instrumentation installed subsequent to the two incidents has determined that although the 2D design computations were broadly correct, both the position and magnitude of the peak re-ionised power is different from original predictions. More extensive 3D computations indicate better agreement with measurements due to the inclusion of vertical focussing of the re-ionised particles and a more accurate representation of the stray magnetic field.

In addition, measurements of the D_α light emission from thc background duct gas have indicated the importance of cleanliness of the duct walls. Unless the duct surfaces are well outgassed prior to beam operation, considerable gas is released from surfaces which intercept the re-ionised beams. An extensive programme of duct conditioning is necessary to avoid excessively high power densities in this region. Consequently, more robust copper cooling structures have been installed in the duct, relying on thermal capacity to absorb energy during the beam pulse and then cool during the inter-pulse period. Operational experience has shown that this system has a much higher safety margin and should prevent any re-occurrence of such incidents.

Heating Experiments

Injection experiments have been carried out over a wide range of target plasma conditions and have resulted in major extensions of the plasma parameters achieved in JET. The most obvious feature of first experiments was the plasma density increase obtained during injection. High density disruptions at the end of the 5s pulses were avoided by moving the plasma to the inner graphite covered vessel wall, co-incident with a staggered switch-off of the beams. This method of discharge termination, which relies upon the inner wall pumping effect to lower the plasma density prior to the current decay, has been used routinely for all neutral injection heated limiter discharges. Inner wall pumping has also been used to produce low density target plasmas. Experiments with H° injection produced ion temperatures of ~6.5kV for this type of discharge [3,4]. Subsequently, deuterium ion temperatures of ~12.5keV were achieved using D° injection into low density deuterium plasmas. In this case, wall pumping was further enhanced by pre-conditioning the wall using tokamak discharges in helium.

Other major features expected from neutral beam injection have been observed, including beam fuelling, beam driven current, plasma rotation and reduced energy confinement consistent with L-mode scaling. In addition, experiments with combined NB and RF heating were carried out at a total power level of ~15MW.

Modification and Testing of the Prototype 160KV Source

The JET PINI's were originally designed to allow modification from the initial 80kV, 60A operation with hydrogen to 160kV, 30A with deuterium. Modification of a prototype 80kV PINI for higher voltage operation and testing was carried out at the EURATOM-CEA Association Laboratory, Fontenay-aux-Roses (FAR), France [5]. Successful operation with a Periplasmatron type plasma source at 160kV with a perveance matched current of 38A was achieved. Further source modifications were necessary. As a temporary and reversible measure, it was advantageous to operate at a slightly lower beam energy but higher power. As a consequence, it was decided to optimise the upgraded sources at 140kV, 30A, rather than 160kV, 30A. In addition, the deuterium yield of the JET bucket plasma sourses is sufficiently higher than that obtained from the Periplasmatron source [3], that even at the reduced voltage of 140kV, the perveance matched current would be >30A.

The modified source was installed on the JET Testbed in January 1986. Few problems were encountered with either conditioning the source or with the operation of the power supplies, and operation at 160kV, 40A was achieved by the end of April 1986. The optimum perveance was exactly that required. However, the measured power loads on the grids were found to be above the predicted levels, but below acceptable limits. The power loadings on other parts of the system (neutraliser, box scraper, etc.) were also determined and found to be within acceptable limits. The principal characteristics of the extracted beam were determined by obtaining self consistent fits to calorimetrically measured profiles and these were within acceptable limits.

Testing the Second Central Column

The central column of the injection system is suspended from the lid of the Neutral Injector Box (NIB); it carries the main water flow into the NIB and supports the beam deflection magnets and their liners, the various ion dumps and the beamline calorimeter. It can be installed directly into the NIB that forms part of the Testbed. However, for these tests the lower Full-Energy Ion Dumps (FEID) were not installed in order to reduce water flow requirements. As only the upper four PINI positions could be used in the Testbed, this did not restrict the proposed experimental programme. During the test of the first Central Column, it had been found that the measured profile of the deflected full-energy ion beam differed significantly from the predicted profile. Consequently, it was decided to modify the magnet slightly by the addition of shims to the input and exit faces of the pole pieces.

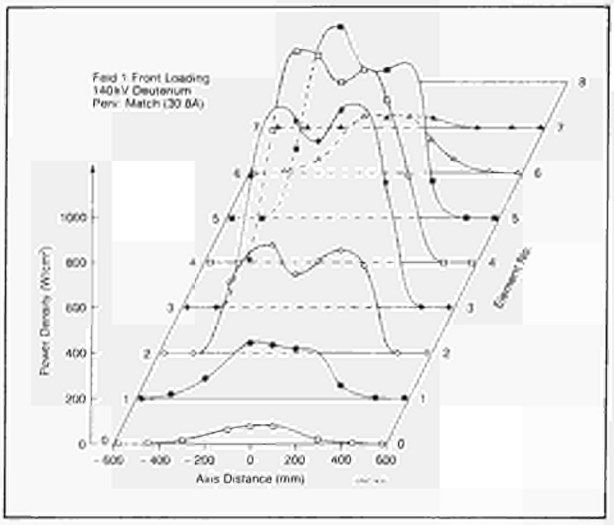

Fig.11: Power density on the Full Energy Ion Dump (FEID) from the Lower Beam.

The basic instrumentation installed on the Central Column does not enable a precise measurement of the deflected beam profile. Therefore, for this second Central Column test, extensive additional thermocouple instrumentation was installed on one of the dumps. Deflected profiles were measured for beams from both the upper and lower positions for one quadrant of the Central Column for a range of deuterium gas flows and perveance values for energies up to 140kV. Two PINI's simultaneously could not be operated as the schedule did not allow sufficient time for commissioning of the second set of auxiliary power supplies installed in the Testbed.

The power density profile on the surface of the dump due to a 140kV, D beam (30A extracted) from the lower PINI is shown in Fig.11 (the dump vapotrons are 'opened out' in order to clarify the presentation). Similar data was obtained for beams from the upper PINI. These data demonstrated that the power density everywhere on the dump was within the safe operating range for the vapotrons and that the beams were contained within the dumps. However, extrapolation of these data indicate that the dumps would be overloaded for 160kV, 30A beams. Several parameter scans were carried out to establish the safe operating regime; including variation in gas flow, (i.e. neutralisation); magnet current; extracted current at fixed extraction voltage (perveance scan); and beam alignment.

The results were consistent with the first tests, which showed beam broadening for highly deflected beam currents. Low gas flow gave low neutralisation, and hence a higher deflected beam current. High perveance (constant voltage) also gave a relatively high deflected beam current. Measurements were made of the neutralisation efficiency by comparing the power to the Testbed Beam Dump with and without the deflection magnet energised. The data [6] showed a neutralisation efficiency significantly below that expected.

Operational Experience with Main Mechanical Components

In deuterium, components downstream of the deflection magnets, (i.e. the calorimeter, the box scrapers, the fast shutter, the wall protection system in the rotary high vacuum valve (RHVV), and the duct scraper assembly) received about twice the power with hydrogen. Even under these severe conditions, beamline operation was generally satisfactory. However, focussed reionised particle beams occurring in the duct area led to power density levels greatly exceeding design values. This necessitated installation of additional copper protection plates in October 1986 (as mentioned previously). During the 1987 shutdown, the Octant No.8 duct scraper assembly will be replaced and the liner side walls will be protected by water-cooled copper plates allowing a much higher duty cycle. The increased beampower also led to overloading of the calorimeter for long pulses and restricted pulse lengths to the calorimeter to $\leq$1s. However, the reduced pulse length allowed acceptable beam source conditioning and an indication of beam alignment.

Several heat transfer components were originally made by galvanic copper deposition, which permits incorporation of water-cooling channels into thin copper structures. However, during manufacture, it proved difficult to consistently produce copper of UHV quality especially with concave surfaces (and corners) and to achieve equal deposition rates over large areas. After manufacture, these components were all subjected to stringent acceptance tests including thermal cycling in vacuum furnaces to temperatures well in excess of those expected during operation. Only after passing these tests were galvanoplastically formed components assembled into the beamlines. Nevertheless, some of these components developed leaks after assembly and during injector operation. These leaks occurred especially at concave geometries and transitions. Therefore, it was decided to replace these components (except neutralisers and grids) with simpler designs avoiding copper deposition.

The fast shutter has been operated routinely during 1986 and the conductance after initial running-in was well within specification. During the 1987 shutdown, the actuator penetration through the front wall of the NIB is being modified to include a double bellows arrangement, allowing interspace leak detection which is a prerequisite for the tritium phase and the flexible hose system for the water inlet and exit to the water-cooled shutter doors is being modified to allow a cycle life time in excess of 100,000 shutter closing and opening movements.

During operation, stray magnetic fields from the plasma and poloidal coil system affect the neutral injection system. To minimise these, part of the beamline is fitted with a magnetic shield of 5cm thick soft iron. The shielding design was based on a 3D computer computation which predicted stray fields of $<10^{-4}$T around the beam sources. However, the measured fields exceeded this value. Thus, the stray field deflects ionised beams on passing through the neutraliser. The remedy requires offset beam steering, depending on the stray field strength.

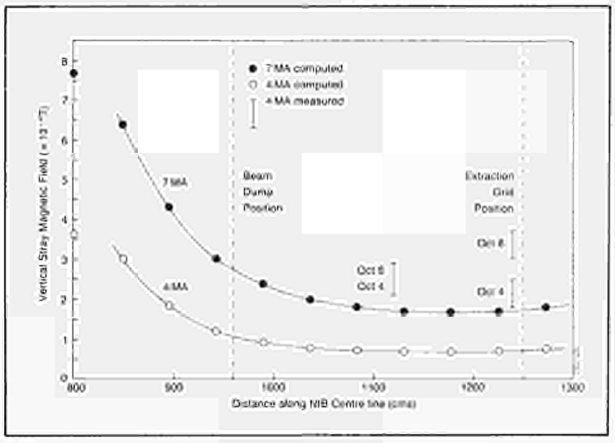

Fig.12: Computed and measured stray fields for I_p=4MA and computed value for I_p=7MA.

In practice, beam resteering is required for I_p>3MA. Extrapolation from I_p=5MA up to I_p=7MA, (required for later operation) shows that unacceptably high stray fields would leak through the magnetic shielding. Consequently, installation of an active magnetic shield is planned during the 1987 shutdown. The basic system consists of both horizontal and vertical axis coils fitted inside the existing shielding and passing around the outer perimeter of the system. Computations suggest that a 60 turn coil with a 130A current would be sufficient to cancel a stray field of $\sim 10^{-3}$T. Fig.12 shows the computed and measured stray fields for I_p=4MA and the computed value for I_p=7MA when the value is expected to reach 10^{-3}T. The system is designed to cancel stray fields up to 1.5×10^{-3}T near the beam sources and neutraliser positions.

Procurement and Testing of Components for the Second Injector

The central column assembly for Octant No.4 beamline system was completed in early 1986 and transferred for tests in the Testbed. In summer 1986, leaks developed in Inconel bellows of the calorimeter. A combination of high material hardness due to plastic forming of the convolutions and of induced vibrations led to rapid high cycle fatigue failure. Ways of damping and avoiding vibration together with improved forming methods are being investigated. Meanwhile, the Inconel 600 bellows will be replaced with stainless steel double-ply bellows during the 1987 shutdown.

During 1986, contracts were placed for the procurement of a third central column assembly, which will allow quick replacement, in case of problems with those at Octants No.8 and No.4. The only components not yet ordered are full-energy ion dumps, which await results of Testbed performance tests of a modified design with increased safety margin in power handling capability.

Cryosystem

The main achievements on the cryosystem were the successful operation of the Octant No.8 cryopump, commissioning of the Octant No.4 cryopump from the cryoplant, procurement of the cryopump system for the multi-pellet injection system and preparation of a substantial upgrade of the cryosupply system of LHe and LN_2 required for the pellet injection system in parallel with the Octant No.4 and No.8 cryopumps. The Octant No.8 cryopump system was continuously operational and provided the necessary NIB vacuum for the NI beam injection. The cryoplant, cryolines and cryopump have operated reliably, but the overall control and fail-safe approach needed modification following operational experience in early 1986. In most failure modes, the cryopumps are now supplied from a LHe dewar, allowing a considerable margin for plant restart after failure without unplanned regeneration of the cryopump.

Commissioning of the Octant No.4 cryopump system has started and showed that a second cryopump can be cooled and operated during continuous operation of the first one. Tests simulating operation of the future multi-pellet injection system have been successfully carried out. A complete cryopump system for the JET multi-pellet injector has been procured together with the necessary cryotransfer lines, including those for the pellet launcher.

References

[1] "Overview and Operation of the Control, Safety and Interlocks on the JET Neutral Beam Injector". D. Stork et al, 14th Symposium of Fusion Technology, Avignon, France, 1986 and JET-P(86)39;

[2] "Performance of the First JET Neutral Beam Injector". A.P.H. Goede et al, 14th Symposium on Fusion Technology, Avignon, France, 1986 and JET-P(86)39;

[3] "First Neutral Beam Heating Experiments on JET". G. Duesing P. Lomas, A. Stäbler, P. Thomas, E. Thompson, Royal Society, London, U.K., (1986) and JET-P(86)11;

[4] "First Results of Neutral Beam Heating on JET". The JET Team, paper presented by G. Duesing, 13th Eur. Conf. on Contr. Fusion and Plasma Heating, Schliersee, F.R.G., 1986 and JET-P(86)27;

[5] FAR 160kV Prototype Test
H. Fumelli, P. Bayetti, R. Becherer, F. Bottiglioni, M. Desmons, F. Jequier, J. Paméla, P. Rainboult and F.P.G. Valckx, Rev. Sci. Inst. *57*, No.7, (1986) pp1266-1273;

[6] Neutralisation Efficiency - First Quadrant Test.
A. Stäbler and R.S. Hemsworth,
JET Divisional Note, JET-DN-C(85)14.

Radio Frequency Heating System

Three main lines of work have dominated the activities of the RF Division during 1986 [1];

a) on-line plasma operation [2] with three antennae

TABLE III
Conditions and Parameters During Plasma Operation

Power launched in plasma with 3 antennae	8MW
Power launched with the monopole antenna	4.2MW
Maximum energy launched (3 antennae)	40MJ
Maximum pulse length	10s
Typical conditions	6MW for 2s
Frequency range explored	25 to 47MHz
Automatic matching during the pulse by frequency modulation	

and up to four generators each capable of 3MW output;

b) continuation and testing of the equipment necessary for the second stage of the ICRF programme. This second stage starts in 1987 with the installation of eight new water-cooled antennae;

c) conception and initial preparations for a Lower Hybrid Current Drive system (see a separate section in this Report).

On-Line Plasma Operation

Three antennae were available during twelve months of continuous plasma operation (November 1985 to November 1986). For most of this period, each antenna was connected to a generator unit delivering 3MW at its output. As expected, about two-thirds of the output power was delivered to the plasma, the remaining power being lost in the antenna conductors, in the transmission lines or in reflected power due to imperfect matching between the antenna and source.

In the last two months of operation, two generator units were coupled to a single antenna in order to test its power limit. This experiment demonstrated that a net power of 4.2MW could be launched by a single antenna. In this experiment, the total power from all three antennae reached 8MW for 2s. Table III summarises the maximum parameters achieved, which far exceed the original design parameters based on 1.5MW for 1s per antenna.

In normal operation with the plasma lying on the outboard limiters or on the inner wall, the systems reached full power after one or two plasma pulses which were used to determine the matching parameters. During X-point operation with the large antenna-plasma distance necessary for the occurrence of the H-mode, the antenna loading resistance became small and launching the full power would have required a large antenna voltage (typically ~40kV). Arcing in the antenna or vacuum transmission lines occurring between 20-25kV prevented the attainment of full power. After a number of design improvements, the new water-cooled antennae (A_1) did not show similar arcing behaviour.

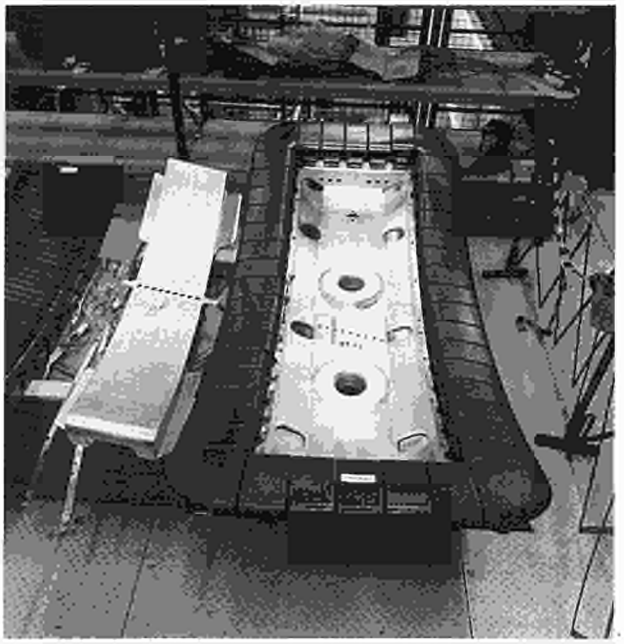

Fig.13 The main components of the A_0 antenna (monopole) after removal from the torus.

Fig.13 shows the main antenna components after removal from the torus. The antenna is remarkably free of damage or deterioration, with the exception of a small zone on the screen sides near the equatorial plane. These marks come from steady arcs which appear during high current discharges. They exist during ohmic discharges but are enhanced by additional heating.

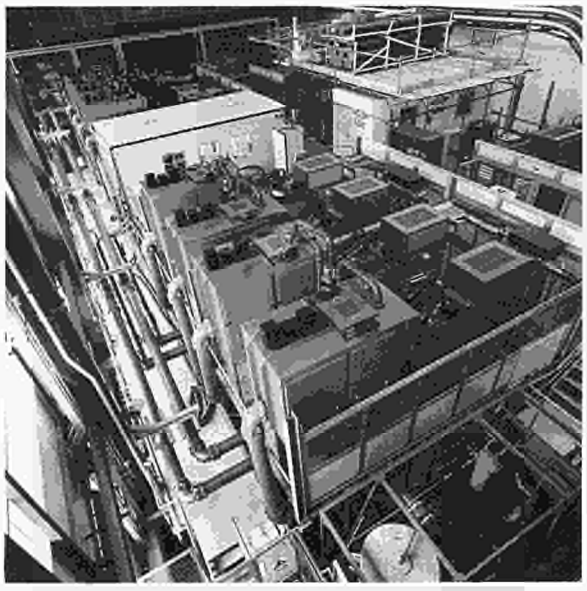

Fig.14 The ICRF power source installed in the North Wing of the Torus Hall. Two 3MW units are seen in the foreground. Six units were installed by the end of 1986.

Enhancement of the ICRF Power Plant and Transmission Lines

The ICRF power plant (Fig.14) has been enhanced using line trimming devices which allowed operation in a wider range of conditions. The installation of a phase shifter (trombone construction) on each output transmission line allowed all the transmission lines to be precisely set to the same length, which was a necessary condition to operate the antennae as a matched phased array. Two antennae have been operated in this phased mode and the possibility of matching this configuration has been demonstrated. Furthermore, the phase shifter allows a balance of matching between the two halves of the antenna.

A variable capacitive tuning stub has been installed in one of the three antennae. The element is placed just after the vacuum window and can match the antenna by itself in two frequency bands around 30 and 35MHz. This mode minimises losses and voltage requirements on the main transmission lines. This element can also be used in combination with the motorised tuning stub located at the generator end. This second mode of operation combined with the frequency feedback loop has been used to match a highly variable load during a pulse. The system worked successfully with loads varying from 4Ω to 1Ω in X-point discharges. Fig.15 shows the main components of the capacitive stubs [3].

When completed, 1.5km of coaxial lines (24cm external diameter) will link the generators in the North Wing to the antennae in the vacuum vessel. Nearly half of the supply is now installed. The lines have to withstand a peak RF voltage of 50kV, a value which proved to be difficult to achieve. It required the development of ceramic insulators of a particular conical shape. Tin plating, used in some Stage 1 components, developed whiskers which considerably reduced the power handling performance. These faulty elements have been eliminated during 1986 and the installed equipment has reached the full design value [4].

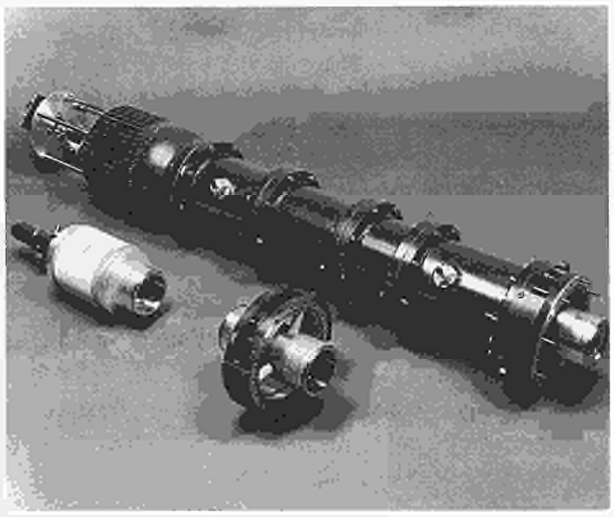

Fig.15 The main elements of a capacitive tuning stub placed closed to the antenna which has allowed dynamic matching on varying loads.

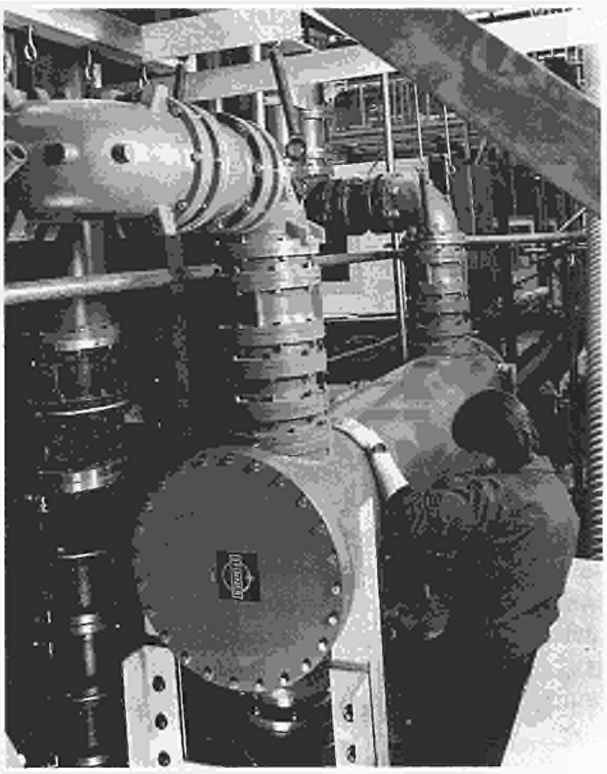

Fig.16 One of the two RF power combiners used in the experiments demonstrating the 4MW capability of a single ICRF antenna.

Before being fully committed to upgrading the ICRF system to 4MW per unit, an experiment has been performed combining two ICRF generators into a single antenna. Purpose designed combining units (Fig.16) have been procured and installed in 1986. The experiment required precise phase control of the four output circuits of the generators. During plasma heating experiments 4.2MW was effectively launched by a single antenna and this value appears to constitute a power limit as hot spots started to appear on the antenna structure.

Seven (3MW) generators have been delivered to JET. One has been installed in the testbed area and feeds the prototype water-cooled antenna. The others are installed in the North Wing of the Torus Hall and have been either in operation or undergoing commissioning. The eighth unit is being tested, at the contractor's site, in its upgraded 4MW version [5]. In the initial tests, the required peak power has been obtained and the tests will continue on the JET site where the installed DC power supplies will allow long pulse operation. It is planned to upgrade all the generators by stages during 1987.

Construction of the Second Generation Antennae

The three prototype antennae (A_0) installed during the 1986 experiments were designed to test, at moderate pulse length, various internal antenna configurations. Fig.13 shows one of these antennae constructed in the monopole configuration. A compromise must be found between the coupling efficiency and the radiated wave spectrum for minimum impurity production. Experimental results have shown that the most interesting

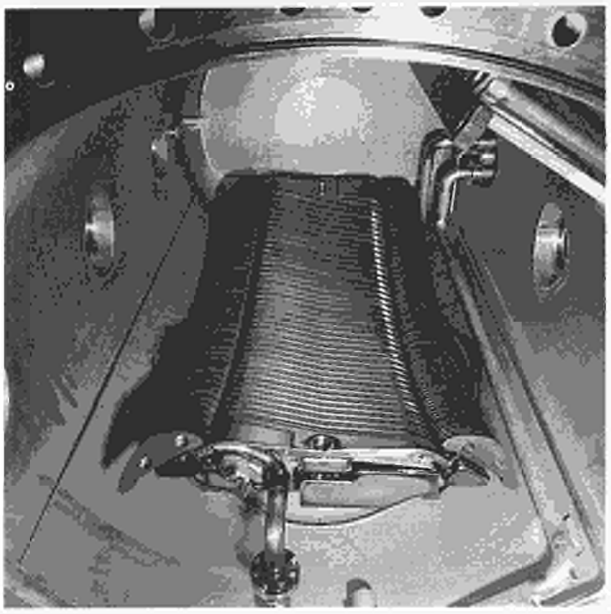

Fig.17 A complete water-cooled A_1 antenna installed in the Testbed. Graphite tiles cooled by nickel fins can be seen on each side. The nickel bars acting as an electrostatic screen are drilled to allow internal water flow.

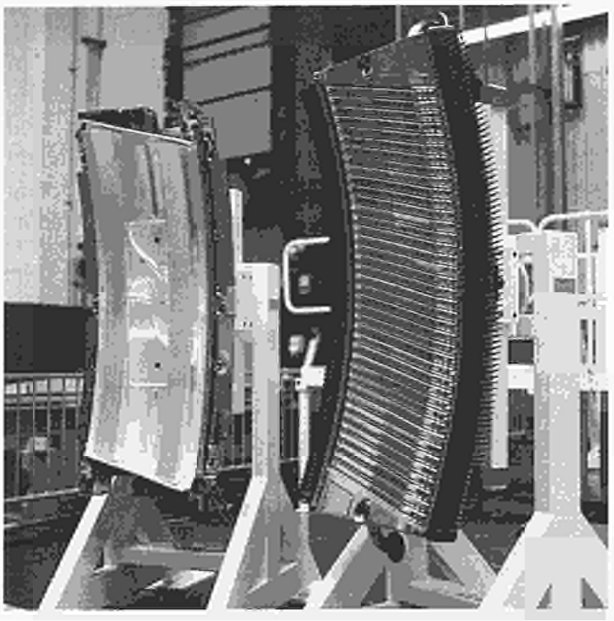

Fig.18 Components of the A_1 antenna. The A_1 antenna housing is seen on the left. The screen assembly without graphite tiles is on the right and this fits on top of the housing.

configurations are the monopole (all RF currents in phase) for its high power coupling capability or a toroidal dipole for its low perturbation of the plasma edge.

A new configuration has been designed to allow both of these modes to be achieved with the same antenna. After successful operation on the Testbed this new configuration has been chosen for the new antennae.

The eight second generation antennae (A_1) are being installed between the two toroidal limiters and are actively cooled by water flowing inside each screen element [4]. The graphite (or later beryllium) protection tiles are located between nickel fins in order to increase the radiation transfer to the water cooled manifold. Fig.17 illustrates the new arrangement photographed inside the testbed vessel. The main antenna components can be seen on Fig.18.

The vacuum transmission lines are cooled by a closed circuit airflow. The turbomolecular vacuum pumping system of the prototype antennae has been replaced by renewable getter pumps [5] (zirconium, iron) which combined simplicity and reliability. The coaxial vacuum feedthroughs are now all using an assembly of two brazed conical ceramic windows with high voltage capability.

The Testbed Facility

The JET ICRF Testbed was first constructed and installed at EURATOM-CEA Association Laboratory, Fontenay-aux-Roses, France and operated for JET on the prototype antenna by CEA. It then was moved to JET to test the second generation antennae. It has been extensively used in 1986 to validate antenna or transmission line components and to perform endurance tests of a complete antenna assembly at full reactive power. Pulses of 50kV and 20s duration were routinely achieved after the correction of a number of weaknesses in the design of the insulators and central conductors.

References

[1] For an overview of the JET RF systems see "The JET Annual Report 1986";
For a detailed description see "Radio Frequency Heating System", A. Kaye, J. Jacquinot, P. Lallia, T. Wade, Fusion Technology **11**, No.1, p203 (1987);

[2] "RF Heating on JET" by the JET Team (presented by J. Jacquinot), 11th International Conference on Plasma Physics and Controlled Nuclear Fusion Research, Kyoto, Japan, 1987, Paper IAEA-CN-47/F-1-1;

[3] "Overview of the JET ICRF Power Plant Operation and Development", R.J. Anderson, J. Plancoulaine and M. Schmid. Proceedings of the 14th Symposium on Fusion Technology, SOFT, Avignon (1986);

[4] "Design and Manufacture of the Water Cooled Electrostatic Screens for JET ICRF Antennae", C.I. Walker, A.S. Kaye, H. Brinkschulte, R.A. How, J. Plancoulaine, D. Sigournay, G. Bevilacquay, F. Anselni, Proceedings of the 14th Symposium on Fusion Technology, SOFT, Avignon (1986);

[5] Non evaporable getter pumping for JET ICRF antennae, C.I. Walker, A.S. Kaye, R.A. How, F. Mazza, Proceedings of the 14th Symposium on Fusion Technology, SOFT, Avignon (1986).

Remote Handling

Further progress has been made in specifying, acquiring and commissioning major items of remote handling equipment. This equipment comprises special tools to suit the features and to provide access to JET components; end-effectors to lift and attach large components; large, high-precision transporters to carry the equipment to all parts of the JET machine; and control systems for all this equipment.

During 1986, further efforts were devoted to analysis of tasks inside and outside the vessel to provide the basis for specifications of equipment and to supply material for data bases which will be used to direct operations.

The introduction of tritium into the machine, which will require that all work on the JET machine is performed by remote control from outside the Torus Hall, is now proposed for mid-1991. Until this time, increasing background radiation, the generation of slightly activated dust and the use of beryllium will necessitate special equipment and methods for gaining access and carrying out hands-on work safely inside the torus.

Transporters

An additional joint, which extends the reach of the articulated boom to the whole vacuum vessel from a single post was procured and commissioned. The local capacity of the boom is 350kg in this new configuration. The boom extension was completed and a family of grabbers was designed, procured and tested for handling the belt limiter segments, the antenna housing and screen.

A micro-processor based control system was specified and procured. It provides the functions:

- "teach and repeat", to achieve an automatic repetition of the difficult manoeuvre of inserting the boom into the post of the vessel and positioning it in the working area;
- resolved motion to permit the operator to move the end effector with a joystick in an absolute or relative co-ordinate frame;
- single joint, velocity controlled or positioned controlled operation.

The articulated boom is being used for the installation of the belt limiters and antennas in the 1987 shutdown (see Fig.19).

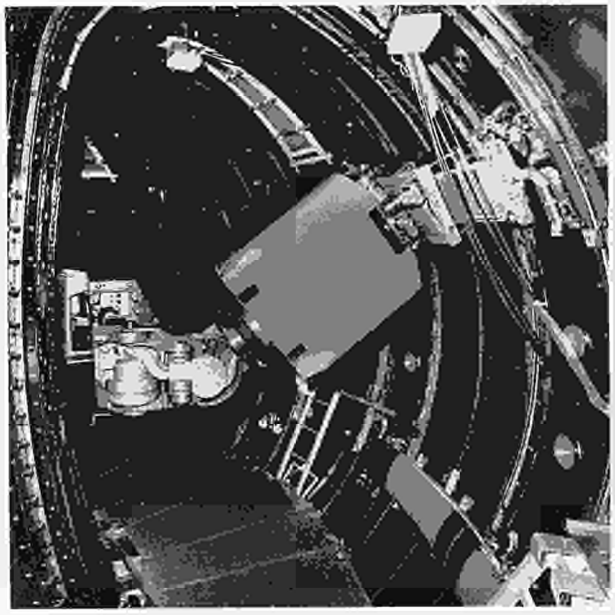

Fig.19: Articulated boom being used for installation of belt limiters.

The conceptual study of a crane mounted telescopic arm able to carry the manipulator all around the machine has been carried out. This will be mounted on the existing 150 tonne crane and provided with TV cameras supported by articulated arms. Finite element calculations have been undertaken on critical parts of this very large structure. Specifications for an international call for tender are being prepared and will be issued at the end of March 1987.

A low level transporter was specified and procured for the handling of turbo-pump, valves and diagnostic equipment which cannot be reached with the crane. This transporter, without remote control, was commissioned and due for delivery to JET in February 1987 and will be used to install seven pumps during the machine shutdown in March and April. Its remote control unit will be specified and ordered before the end of the year. The vehicle used is a modified conventional electric fork-lift truck, which should result in a fairly high level of reliability. However, the end-effectors are specially designed and manufactured one-off items. The load carrying capacity of the truck is 2 tonnes, which should allow pick-up of 200kg components with an horizontal extension of approximately 4m where access is difficult. The vertical lift of the mast is 2m.

Servomanipulators

The contract for manufacture of the two sets of Mascot 4 servomanipulators is close to completion. This has needed the resolution of a number of technical issues regarding the mechanisms and more particularly the new advanced microprocessor based serial link controller. Special gaiters with rotary seals have been developed for the servomanipulator, including, the arm and the tongs. A remotely operated connector has been designed and procured for either manipulator or grabber. It provides both automatic mechanical attachment and electrical and pipe connection. The wiring and piping for all services through the manipulator shoulders up to a remotely operated connector is being installed. These services include electric and gas lines for arc welding and high pressure water for cutters.

Tools

The self-propelled welder and cutter trolleys for the standard U joints have been completed in their reduced size version. They are able to negotiate corners with a minimum radius of 60mm and all the rectangular parts will be radiused accordingly (see Fig.20). A flexible microprocessor based controller for the various cutting

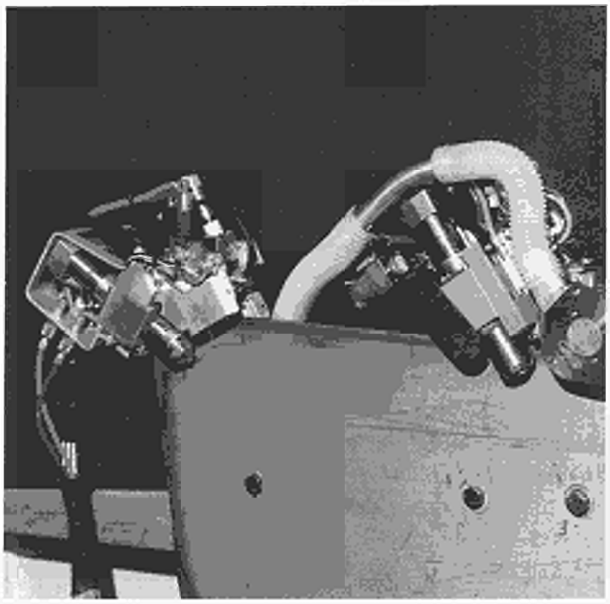

Fig.20: Welding and cutting trolleys on a simulated vertical port loop joint.

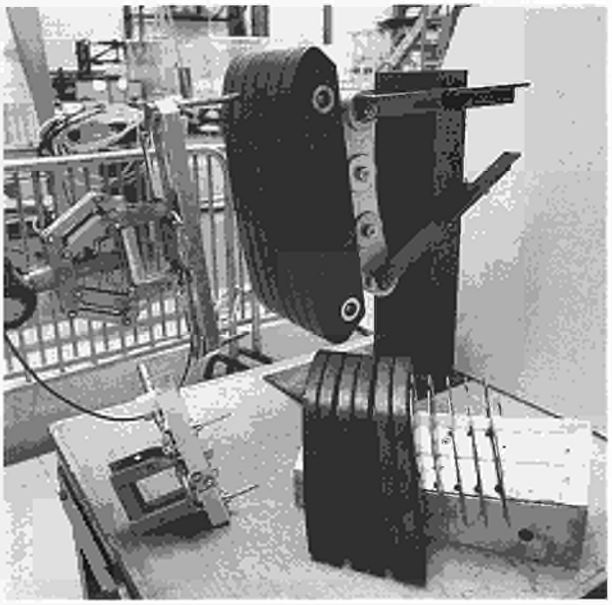

Fig.21: Tool used for installing belt limiter tiles.

tools, providing control for the cutting parameters and sequences has been developed and will be commissioned in early 1987.

Television

The in-vessel inspection vacuum system has been re-designed to include more reliable valves and separate getter pumps. This will improve reliability and allow for individual leak detection of the four viewing units. The system will be installed in the 1987 shutdown.

An upgraded version to inspect the vessel under vacuum at 300°C has been developed. This uses a special thin cylindrical water jacket, retaining the already existing viewing probe and glass cylinders. Tests have shown that these can withstand the temperature gradients and regain transparency impaired by radiation through exposure to the operating temperature. Light pipes are being developed to give continuous illumination of the vessel to ease operation, which was difficult with flash-lights only.

Light, waterproof and high resolution cameras on articulated arms have been manufactured for the work with the manipulator and the boom grabbers.

Remote Handling Controls

A prototype remote handling work-station has been specified and built but not yet used extensively. The full remote handling CCTV system requirements have been specified and the system ordered. This will facilitate display of up to 40 video pictures from any of 70 camera inputs including those on the transporters and the Torus Hall walls.

A Servo Manipulator Master Station, the concept of which was derived in an Article 14 study undertaken by EURATOM-CEA Association, Saclay, France, has been designed and procured. This will be fully evaluated in 1987.

Special Tools

A fully remote handling compatible welding power pack for all remote handling tools has been specified, tendered and ordered. Three hands-on units have been procured for use in the 1987 shutdown and these will be modified for remote handling compatibility later in 1987.

A single remote handling connector for connection of all tools to their service lines has been specified, designed and about 50 manufactured. This facilitates connection of weld current, high and low pressure hydraulics, pneumatics and electrical signals through a single type of connector.

In addition, the design and manufacture of 20 different types of tool was completed for use in the 1987 shutdown to install vacuum vessel windows of all sizes, belt limiter segments, A_1 RF antennae shields and housings, NBH shine-through protection tiles and the belt limiter and antennae tiles (see Fig.21).

Active Handling

The manufacture was completed and delivery taken of the torus access cabin (see Fig.22) which was described in the 1985 Progress Report. This will be in daily use in the 1987 shutdown, to provide clean entry, services and communications. It will continue to be used, particularly when beryllium in introduced into the vessel. A beryllium laboratory to test monitoring samples is being installed and a strategy has been derived for maintenance of machine components during the period that beryllium is installed and prior to the active phase.

Tritium Handling

During 1986, development and testing continued on components for the plant needed to handle the exhaust gases from the JET machine and its auxiliary systems, notably the neutral beam injectors. The exhaust streams consist mostly of hydrogen isotopes in various mixtures,

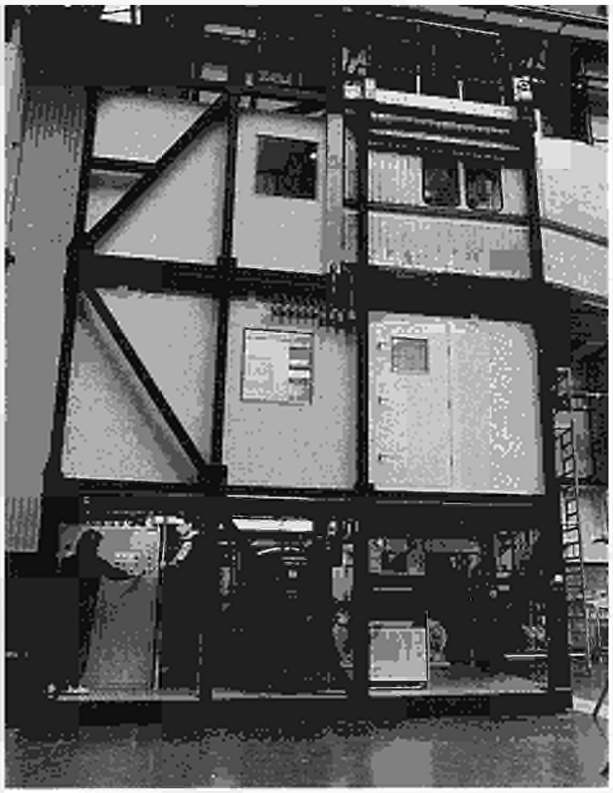

Fig.22: Torus Access Cabin.

but also contain impurities, water, methane and carbon-oxides. A cryogenic transfer pump, accumulator, cold trap and gas chromatagraphy column were successfully demonstrated.

The level of methane in the exhausts, due to the use of graphite as wall-lining material, is found to be much greater than expected earlier, so that methane cracking to strip the tritium from the waste could be essential. Also, hydrogen isotopes deposited in the wall materials could need to be removed by extensive glow discharge cleaning employing oxygen, and the water so produced would need to be cracked to strip it of tritium.

Results obtained during 1986 point to eventual pellet injection and neutral beam injection not only with deuterium but also with tritium beams and pellets. For these reasons, a tritium purification and separation plant is now envisaged to cater for a much greater range of isotope mixtures, impurities, throughput and product purity than envisaged earlier. As a result, studies were made of a cryodistillation plant for separating the isotopes, which is capable of giving a much greater throughput than the previously proposed gas chromatography separation plant. It will be used in conjunction with a small gas chromatography unit, better suited to small quantities, unpredicted isotope mixtures, and intermittent operation during commissioning of JET with tritium and operation with scenarios needing limited throughputs.

Decisions were taken to proceed with the tritium plant in this way, and implementation started in 1986. The basic design of the cryodistillation plant is established and it will be put to tender in Spring 1987.

Control and Data Acquisition System (Codas)

The Control and Data Acquisition System (CODAS) Division is responsible for the design, procurement, implementation, upgrade and operation of the computer-based control and data acquisition system of JET. This system, based on a network of NORSK DATA minicomputers, allows centralised control and monitoring. The various components of JET have been logically grouped in subsystems like Vacuum, Toroidal Field, Poloidal Field, etc. Each subsystem is controlled and monitored by one computer and the various computer actions are co-ordinated by supervisory software running on the machine console computer. This supervisory function includes the countdown sequences for each plasma discharge.

The allocation and configuration of all CODAS computers is given in Table IV, and Table V provides other quantitative data. Recent publications related to CODAS are given in the reference list [1,2].

The main achievements during 1986 are summarised, as follows:

- Development and commissioning of the digital feedback to control the plasma current;
- Development and commissioning of the plasma density validation which monitors and correlates various diagnostic channels;
- Modification and improvement of the plasma fault protection system (PFPS) to provide better machine protection and accommodate density diagnostic disturbances related to pellet injection;
- Development and commissioning of hardware and software to allow usage of Westward terminals on the IBM Computer through a Gandalf terminal multiplexer and the IBM 7171 interface unit;
- Design, manufacture, installation and commissioning of 15 CODAS interface cubicles;
- Design and installation of the first Remote Handling workstation and part of its software;
- Design, development and commissioning of the sequencer unit required by the pellet launcher built by Oak Ridge National Laboratory (ORNL), USA, and due to be installed at JET in early 1987;
- Improvement of data collection and archiving throughput to accommodate the larger amount of data collected at each pulse (about 9 MByte per pulse);
- Introduction of larger mass storage devices based on Winchester technology;
- Completion of the suite of on-line test programs for all standard CODAS CAMAC modules;

Table IV
CODAS Computer Configuration at the end of 1986

Subsystem	*Usage*	*Model*	*Memory (MByte)*	*Disks (MByte)*
AH*	NI Additional Heating	ND100	2.0	1×75 1×450
AS	Assembly Database	Compact	0.75	1×45
CA*	Message Switcher A	ND100	0.5	1×75
CB	Message Switcher B	ND100	0.5	1×75
CP	Cable Database	ND530	5.0	1×75 1×288
DA*	On-line diagnostic	ND520	3.0	2×75
DB*	On-line diagnostic	ND520	3.0	1×75 1×288
DC*	On-line diagnostic	ND520	3.0	2×75
DD*	On-line diagnostic	ND520	3.0	2×75
DE*	Off-line diagnostic	ND520	3.0	2×75
DF*	On-line diagnostic	ND520	3.0	2×75
DG	Diagnostic Commissioning	ND520	5.0	2×75
EC*	Experiment Console	ND570	5.0	1×75 1×288
EL	Electronic	ND100	1.0	1×75
GS*	General Services	ND100	1.5	1×75
HL*	Harwell Link	ND100	1.5	1×75
MC*	Machine Console	ND100	1.5	1×75
PF*	Poloidal Field	ND100	2.0	1×75
PL	Pellet Launcher	ND100	2.0	1×75
RB*	Radio Frequency Test Bed	ND100	1.25	2×75
RF*	Radio Frequency	ND530	3.0	2×75
RH	Remote Handling	ND100	1.5	1×75
SA*	Storage & Analysis	ND560	3.0	1×75 1×288 1×450
SB	Standby-System/Backup	ND100	1.5	2×75 1×288
SD	Built-in, Pool, Computer db	Compact	0.75	2×45
SS*	Safety & Access	ND100	1.5	1×75
TB*	NI Test Bed	ND100	1.5	1×75 1×450
TF*	Toroidal Field	ND100	1.5	1×75
TR	Tritium	ND100	1.5	1×75 1×288
TS	Test	ND100	1.5	1×75
VC*	Vacuum	ND100	2.0	1×75
YB	Integration	ND530	3.0	2×75
YC	CODAS Commissioning/NIB-C	ND100	1.5	1×75 1×450
YD	Sc Dpt Development	ND570	5.0	1×75 1×288
YE	CODAS Development	ND520	5.0	1×75 1×288

*indicates on-line computers.

- Installation on the Main Frame Computer of terminal handling and PLOT-10 software;
- Installation of hardware and software to allow access to all CISS logical states by CODAS, so that full CISS MIMICs could be displayed on the consoles.

A breakdown of electronics modules is given in Table VI comparing the end of 1985 and the end of 1986 figures.

References

[1] M L Browne, CODAS - A Large Scale Multi-Computer Control System for the JET Project, IFAC Conf. on Distributed Control (1986);

[2] K Fullard, SE Dorling, JE van Montfoort, Computer to Process Interface in JET's Control and Diagnostic System, 14th Symposium on Fusion Technology, SOFT, Avignon, France, (1986);

TABLE V
Quantitative Information on CODAS Installation at end of 1986

CODAS Interface Cubicle	128
CAMAC Crates	198
CAMAC Modules	2,982
Eurocard Modules (Signal Conditioning)	6,254
Computer Terminal	238
CAMAC Serial Loop (Fibre Optic)	21
On-line Computers	20
Off line and Commissioning Computers	15
Size of JPF	9MB
Number of diagnostics on-line with CODAS	26
Number of diagnostics under commissioning with CODAS	8

TABLE VI
Review of CODAS Electronics Stock Holding (Installed, Pre-procurement and spares)

	End 85	*End 86*
1. CAMAC system modules	705	760
2. CAMAC digital I/O modules	662	738
3. Timing system (CAMAC & Eurocard)	910	1,073
4. CAMAC analogue I/O modules	803	1,073
5. CAMAC display modules	265	377
6. CAMAC Auxiliary controllers	110	110
7. CAMAC powered crates	187	227
8. U-port adaptor	140	155
9. CISS modules	753	753
10. CCTV	414	470
11. Cubicle frames	223	280
12. Console devices (not CAMAC)	344	387
13. Power supply modules	1,350	1,570
14. Intercom, Public Address		
15. Pool	818	889
16. Analogue I/O in Eurocard	1,816	2,006
17. Digital I/O in Eurocard	3,923	4,584
18. Eurocard sub-racks	744	751
	14,564	17,490
Increase	2,923	20%

Diagnostic Systems

The status of JET's diagnostic systems at the end of 1986 is summarised in Table VII and their general layout in the machine is show in Fig.23. The staged introduction of the diagnostic systems onto JET has proceeded from the start of JET operation in June 1983 and is now nearing completion. The present status is that of 39 systems in total, 24 are in routine operation, 10 are being installed/ commissioned and 5 have still to be constructed. Operational experience has been good and many of the systems are now operating automatically with minimal manual supervision. The resulting measurements are of a high quality in terms of accuracy and reliability, and provide essential information on plasma behaviour in JET.

Magnetic Measurements

The magnetic diagnostics have been described in previous JET Annual and Progress Reports and have continued to work routinely and reliably during the year. The diamagnetic loop measuring the plasma energy content has been a most useful tool during additional heating studies and information on MHD oscillations has been extended to include monitors of modes of distinct toroidal mode number n up to n=3, as well as of locked (ie. non-oscillating) n=1 modes.

Extensive use has been made of the facility to interconnect a large number of pick-up coils in different poloidal and toroidal locations into different data recording channels with selectable time windows. Very accurate correlation studies have been made for many different fluctuating plasma quantities, using soft X-ray detectors, ECE, probes and reflectometers.

Plasma Boundary Probes

Measurements of the plasma temperature, density and heat flux in the region outside the limiters have been routinely made with Langmuir probes in the carbon protection tiles of the RF antennas. Similar probes have been used on a system that is introduced from the top of the machine by a vertical probe drive. This system has been mainly used in discharges with a single null at the top of the machine. The collected data are important to develop models for the plasma boundary layer and to assess impurity production mechanisms.

Plasma-Wall Interactions

The systems designed to expose samples in order to measure the hydrogen, deuterium and impurity fluxes in the boundary are now operational. One system that introduces the time resolving collection probe from the top has successfully monitored standard ohmically heated discharges.

The other system that is based on a train powered by linear motors and running in a vacuum tube, can transfer probes from the Diagnostic Hall to the torus on a shot-by-shot basis. Langmuir probes and time resolving collector probes have been successfully exposed. A surface analysis system is directly coupled to this system and surface collector probes can be analysed immediately after exposure to the plasma without leaving an ultra high vacuum environment. This system has been installed and is in the last stage of commissioning.

The programme of exposing long term wall samples in the vessel was continued. These samples which are accessible only at shutdowns show the actual state of the vessel wall as a function of poloidal and toroidal locations. Also representative samples of the limiters, the protective tiles of the RF antennae and inner wall have been taken routinely. All data obtained from post-mortem surface analyses provide valuable information on the release mechanisms of the impurities from surfaces in contact with the plasma.

TABLE VII
Status of JET Diagnostic Systems

System Identifier	Diagnostic	Purpose	Association	Status Dec. 1986	Date of Operation in JET
KB1	Bolometer Array	Time and space resolved total radiated power	IPP Garching	Operational	Mid 1983 partly Early 1984 fully
KC1	Magnetic Diagnostics	Plasma current, loop volts, plasma position, shape of flux surfaces	JET	(1) Operational (2) Enhancement	Mid 1983 Late 1985
KE1	Single Point Thomson Scattering	T_e and n_e at one point several times	Riso	Operational	Mid 1984
KE3	Lidar Thomson Scattering	T_e and n_e profiles	JET and Stuttgart University	Commissioning	Mid 1987
KG1	Multichannel Far Infrared Interferometer	$\int n_e ds$ on 7 vertical chords and 3 horizontal chords	CEA Fontenay-aux-Roses	Operational	Mid 1984 partly Early 1985 fully
KG2	Single Channel 2mm Interferometer	$\int n_e(r) ds$ on 1 vertical chord in low density plasmas ($<10^{20}$ m^{-3})	JET and FOM Rijnhuizen JET	Operational	Mid 1983
KG3	Microwave Reflectometer	n_e profiles and fluctuations	JET	(1) Prototype system operating (2) Multichannel system in construction	Mid 1984 End 1987
KG4	Polarimeter	$\int n_e B_\phi ds$ on 6 vertical channels	CEA Fontenay-aux-Roses	Under construction	Mid 1987
KH1	Hard X-ray Monitors	Runaway electrons and disruptions	JET	Operational	Mid 1983
KH2	X-ray Pulse Height Spectrometer	Plasma purity monitor and T_e on axis	JET	Operational	Early 1986
KJ1	Soft X-ray Diode Arrays	MHD instabilities and location of rational surfaces	IPP Garching	Operational	End 1985
KJ2	Toroidal Soft X-ray Detectors	MHD instabilities	JET	Under construction	Mid 1987
KK1	Electron Cyclotron Emission Spatial Scan	$T_e(r,t)$ with scan time of a few milliseconds	NPL, Culham Lab and JET	Operational	Late 1985
KK2	Electron Cyclotron Emission Fast System	$T_e(r,t)$ on microsecond time scale	FOM, Rijnjuizen	Operational	Early 1985
KL1	Limiter surface temperature	Monitor of hot spots on limiter and RF antennae	JET and KFA	Operational	Mid 1984
KL2/3		Temperature of wall and limiter surface	JET	KL2 Operational KL3 Under development	1986 Mid 1987
KM1	2.4 MeV Neutron Spectrometer	Neutron spectra in D-D discharges, ion temperatures and energy distributions	UKAEA Harwell	Commissioning	Mid 1987
KM3	2.4 MeV Time-of-Flight Neutron Spectrometer		NEBESD, Studsvik	Commissioning	Mid 1987
KM4	2.4 MeV Spherical Ionisation Chamber		KFA Julich	Commissioning	Mid 1987
KM2	14 MeV Neutron Spectrometer	Neutron spectra in D-T discharges, ion temperatures and energy distributions	UKAEA Harwell	Under construction	1990
KM5	14 MeV Neutron Spectrometer		NEBESD, Gothenberg	Under construction	1990
KM7	Time resolved 14 MeV Neutron Yield Monitor	Triton burn up studies	JET-Harwell	Operational	Mid 1986
KN1	Time Resolved Neutron Yield Monitor	Time resolved neutron flux	UKAEA Harwell	Operational	Mid 1983
KN2	Neutron Activation System	Absolute fluxes of neutrons	UKAEA Harwell	Operational	Mid 1986 partly Mid 1987 fully
KN3	Neutron Yield Profile Measuring System	Space and time resolved profile of neutron flux	UKAEA Harwell	Commissioning	Mid 1987
KN4	Delayed Neutron Counters	Absolute fluxes of neutrons	Mol	Commissioning	Mid 1987
KP2	Fusion Product Detectors	Charged particle produced by fusion reactions	JET	Prototype operational Upgrade	1985 Mid 1987
KR1	Neutral Particle Analyser Array	Profiles of ion temperature	ENEA Frascati	Operational	Mid 1984 partly End 1985 fully
KS1	Active Phase Spectroscopy	Impurity behaviour in active conditions	IPP Garching	Commissioning	Mid 1987
KS2	Spatial Scan X-ray Crystal Spectroscopy	Space and time resolved impurity density profiles	IPP Garching	Commissioning	Mid 1987
KS3	H-alpha and Visible Light Monitors	Ionisation rate, Z_{eff}, impurity fluxes	JET	Operational Poloidal Scan, Operational	Early 1983 Mid 1986
KS4	Active Beam Diagnostics (using heating beam)	Fully ionized light impurity concentration, $T_i(r)$, rotation velocities	JET	Provisional system Under construction	Early 1986 Mid 1987
KT1	VUV Spectroscopy Spatial Scan	Time and space resolved impurity densities	CEA Fontenay-aux Roses	Operational	Mid 1985 partly Mid 1987 fully
KT2	VUV Broadband Spectroscopy	Impurity survey	UKAEA Culham Lab.	Operational	Early 1984
KT3	Visible Spectroscopy	Impurity fluxes from wall and limiters	JET	Operational	Mid 1983
KT4	Extreme Ultraviolet Spectrometer	Impurity survey, rotation velocities, $T_i(r)$	UKAEA Culham Lab	Operational	Mid 1986
KX1	High Resolution X-ray Crystal Spectroscopy	Ion temperature by line broadening	ENEA Frascati	Operational	Early 1986
KY1	Surface Analysis Station	Plasma wall and limiter interactions including release of hydrogen isotope recycling	IPP Garching	Commissioning	Mid 1987
KY2	Surface Probe Fast Transfer System		UKAEA Culham Lab.	Operational	Mid 1986
KY3	Plasma Boundary Probe	Vertical probe drives for electrical and surface collecting probes	JET, UKAEA Culham Lab, IPP Garching	Operational	Mid 1984-86
KZ1	Diagnostic Pellet Launcher	Particle transport, fueling	IPP Garching	Operational	Mid 1986
KZ3	Laser Blow-off	Injection of trace elements	JET	Being designed	End 1987

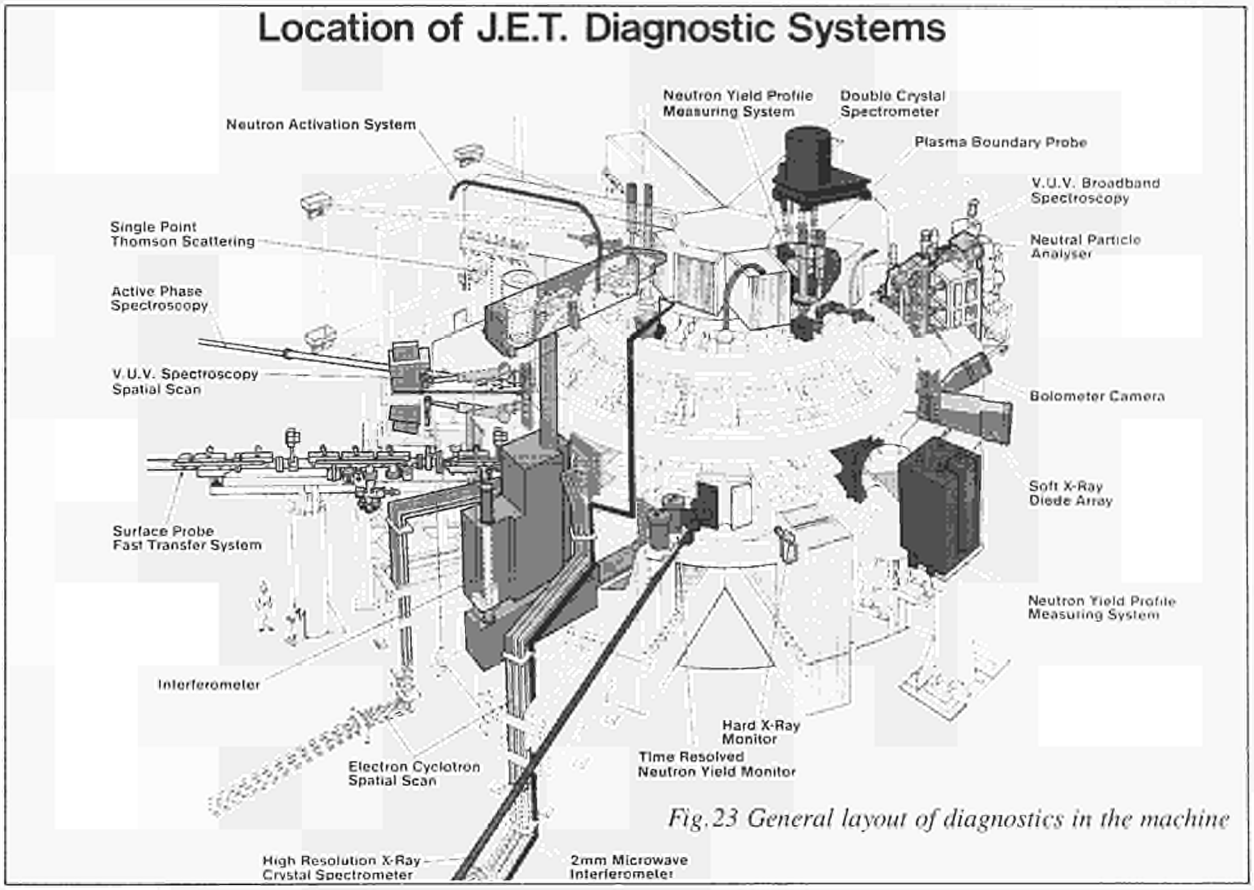

Fig.23 General layout of diagnostics in the machine

Limiter Diagnostics

The interaction of the plasma with the limiters and wall surfaces has been routinely monitored and recorded by means of a video system based on infra-red cameras. As well as routine monitoring of the limiters and RF antennae, observations of the target plates near the single null during X-point operation have been of great importance for maintaining safety limits on the machine. This camera system is excellent in detecting hot spots and excessive temperatures but lacks the dynamic range for accurate temperature measurements. A new system working at a wavelength of 3-5μm has become operational. This is based on a cooled infra-red diode array of 32 x 32 pixels and has successfully monitored the spatial temperature distribution of one of the JET limiters.

Electron Cyclotron Emission Measurements

Radiation measurements of electron cyclotron emission (ECE) have been made routinely during the year using the Michelson and Fabry Perot interferometers and the grating polychromator described in previous reports. From the measurements, the electron temperature is determined with good temporal and spatial resolutions and with an absolute accuracy of about 10%.

Several significant developments have been achieved in 1986. Automation of the instrumentation has been completed and during normal tokamak operating periods only occasional manual monitoring of the system is now necessary. The measured temperatures have been compared systematically with those measured by Thomson scattering and, with only a few exceptions, the measurements agreed within the estimated experimental uncertainties. This has given a high degree of confidence in the electron temperature measurements. Measurements made with Michelson interferometers along four different viewing chords have been combined to derive the lines of constant temperature (ie. isothermals) in the poloidal cross-section. Extensive use has been made of a special code developed by EURATOM-CNR Association, Milan, Italy in the interpretation of this data. A code for interpreting non-thermal ECE spectra has been developed by EURATOM-FOM Association, The Netherlands. A novel technique for improving the relative calibration of the Michelson interferometers has been developed and the shape of the electron temperature profile is now determined to an accuracy of $\pm 5\%$.

The measurement system has also been extended. A high resolution Michelson interferometer has been commissioned and preliminary plasma measurements carried out. This device will provide measurements of the temperature over the entire plasma cross-section instead of covering half, as is the case with the present Michelson interferometers. In addition, a heterodyne system has been constructed and commissioned. This system provides the time dependence of the temperature at eight different locations with a spatial resolution ~ 1.5 cm, and a time resolution $\sim 10\,\mu$s and a signal to noise of typically 100/1. At B = 3.4T, the system probes the edge region of the plasma ($3.8 < R < 4.0$ m).

Electron temperatures determined from ECE measurements have been used extensively in many physics studies on JET. In particular, they have played a central role in studies of energy confinement, disruptions, sawteeth and heat pulse propagation.

Thomson Scattering

The Single Point Thomson scattering system, which measures the electron temperature at a single position in the plasma several times during a pulse, has operated reliably and routinely throughout the year. A source of systematic error due to chromatic aberration has been identified and rectified, and the measured temperatures now agree well with those measured by ECE. The system has been made fully automatic and only occasional monitoring of the system is necessary during tokamak operation.

All the major components of the LIDAR Thomson Scattering system, which will measure the spatial profile of the electron temperature by a time of flight technique, have been constructed. A provisional installation was achieved late in 1986 and some promising first plasma measurements obtained. The system will be completed and brought into full operation in 1987.

Microwave Transmission Interferometry and Reflectometry

The microwave transmission interferometer has continued in routine use for measurements of the line-of-sight electron density and for plasma control purposes. The system has a high reliability and no further developments are planned.

The provisional microwave reflectometer which uses one of the ECE waveguides, has been used extensively in studies of several different phenomena, such as plasma fuelling and particle transport. In addition, this reflectometer has tested successfully the novel operating mode of the new 12 channel reflectometer. The design of the 12 channel system has been completed and contracts placed for all the major components. This system will be installed during the 1987 shutdown.

Neutron Flux Measurements

Routine measurements of the time-resolved neutron yield are made using ^{235}U fission chambers fixed to the magnet limbs. The absolute detection efficiency of these chambers for one particular machine configuration has been established using a neutron source inside the JET vacuum chamber during a previous shutdown. Unfortunately, the detector response is sensitive to changes to other equipment close to the detectors and to changes to JET itself, especially at the horizontal diagnostic ports.

These dependencies can be avoided by determining the total neutron yield from activation measurements with samples for irradiation being placed just outside the vacuum vessel but within the coils and support shell. In such a position, the measurement will be independent of changes to the external equipment or to the ports. A pneumatic transfer system has been installed to facilitate the removal of activated samples to a remote counting station for analysis. Four lower irradiation positions have been installed (beneath the median plane of JET), leaving four upper positions to be installed during the present shutdown. A preliminary examination of the first measurements with this system, using indium foils, provide neutron yields somewhat lower than those estimated from the fission chambers.

The deduction of the total neutron yield from either the fission chamber or the activation measurements depends on a knowledge of the geometry of the neutron emitting region of the plasma. Information on the shape of this neutron source can now be obtained using the neutron yield profile measuring system which was installed on JET late in 1986. The performance of this diagnostic is only now being evaluated. For ohmic discharges, the electron temperature profiles can be used to obtain a broadly acceptable prediction of neutron emission profile but the profile for neutral beam heating with D° injection is much flatter. The diagnostic also shows that the local neutron emission exhibits the familiar sawtooth inversion effect.

Neutron Spectroscopy

Continued work with a ^{3}He ionization chamber in the Roof Laboratory has provided ion temperature measurements which agree well with results from neutral particle analysis (NPA) and from the nickel impurity X-ray spectrometer. The operating position originally planned for the ^{3}He spectrometer was within a shielded enclosure positioned in the Torus Hall as close as possible to the diagnostic port to obtain high neutron fluxes. This shield has now been installed (see Fig.24) and results from this

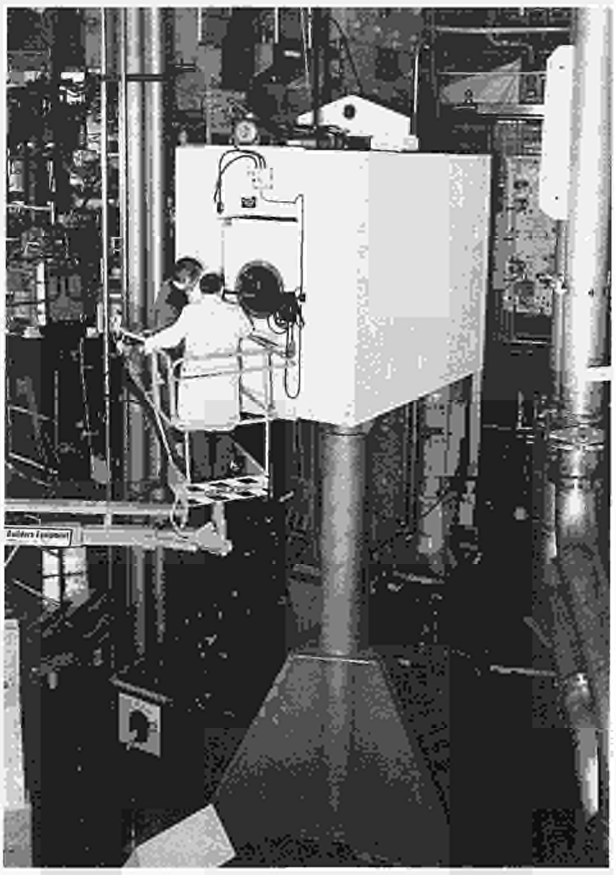

Fig.24: The photograph shows the substantial radiation shield opposite Octant No: 4 which has been provided for the neutron spectrometer (^{3}He ionisation chamber).

diagnostic have been obtained. In future, ^{3}He spectrometers in both positions (Roof Laboratory and Torus Hall) will be operated.

The major challenge for neutron spectrometry will be to measure and interpret the energy spectra of neutrons emitted from deuterium beam-heated discharges. Adjustable collimators will be fitted on the torus to control the neutron fluxes falling on the ^{3}He spectrometers. The time-of-flight neutron spectrometer, also in the Roof Laboratory, operates with the full flux available from present JET plasmas and has provided measurements which are being analysed.

Two contracts have recently been placed, with UKAEA Harwell, U.K., and Chalmers University, Gothenburg, Sweden, for 14MeV neutron spectrometers for operation during the tritium phase of JET operations.

Charged Fusion Products

A prototype detector mounted inside the vacuum vessel has been used to study the emission of 14.6MeV protons from the $^3He + d \rightarrow p + \alpha$ reaction. Based on experience gained, an upgraded version has been constructed which should be operational by mid-1987.

Fusion Gamma-Ray Studies

With the 14.6MeV proton measurements, it is difficult to obtain the total proton yield, since most of the protons are confined by the high plasma currents. The 16.5MeV gamma-rays emitted from the $^3He + d \rightarrow {}^5Li + \gamma$ reaction are not so constrained. Measurements of the gamma-ray emission strength lead to a calibration of the proton experiment. Strong gamma-ray emission has been observed from D plasma with RF heating of ^{3}He minority ions, for which conditions the d-d neutron emission is weak. The results (see Fig.25) indicate the presence of ions heated by the RF waves to energies of -200keV or higher.

Triton Burn-up Studies

The study of the confinement and slowing down of the 1MeV tritons emitted from the $d + d \rightarrow t + p$ reaction is useful as an analogue to the 3.5MeV alpha-particle emitted by the d-t reaction and thus has a bearing on the alpha-heating of deuterium-tritium plasmas. The tritons are easily studied through the emission of 14MeV neutrons by the $t + d \rightarrow n + {}^4He$ reactions which take place as they slow down in the plasma.

The pneumatic transport system has been applied to the measurement of the ratio of the 14MeV to 2.5MeV neutron fluxes through the activation of copper and indium samples, respectively. A preliminary analysis of the measurement indicates that the burn-up fraction of tritons varies with operating conditions over the range 0.3 to 0.8%, the higher values being obtained for X-point configuration plasmas. A simple classical calculation for the burn-up, including prompt losses of the tritons, predicts a typical burn-up of 1.2%.

The triton burn-up has also been studied with a silicon detector placed just outside the vacuum vessel. This technique exploits the high (n,α) and (n,p) reaction thresholds in silicon to disciminate the 14MeV neutrons from the dominant 2.5MeV neutron flux; the detector is therefore a poor energy resolution spectrometer which gives the time-resolved yield of the 14MeV neutrons. The time dependence of the 14MeV neutron emission relative to that of the 2.5MeV neutrons is shown in Fig.26, which exhibits clearly the time delays associated with 1MeV tritons slowing down in the plasma following a brief period of deuterium beam heating. Detailed calculations aimed at reproducing the observed time

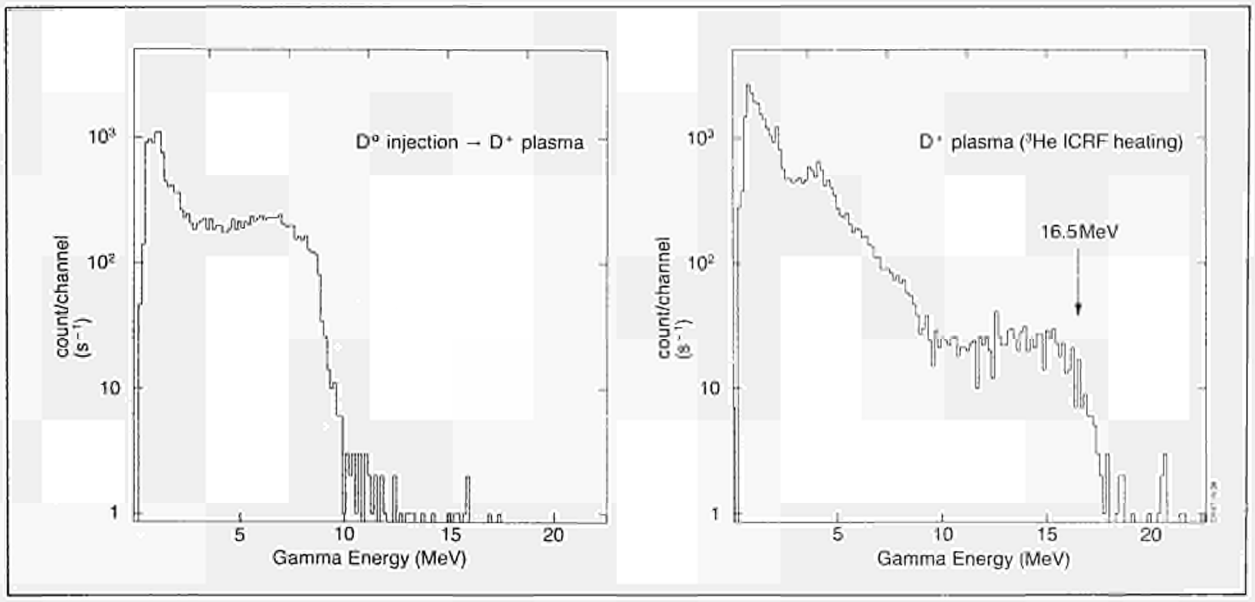

Fig.25: Gamma-ray energy spectra observed with a large NaI(Tl) crystal scintillator viewing the plasma from the Roof Laboratory. The left-hand spectrum was obtained under conditions of high neutron production from deuterium neutral beam injection into a deuterium plasma and shows only gamma rays from neutron capture in structural materials. The right-hand spectrum was obtained for ^{3}He minority ICRF heating of deuterium plasma, with low neutron production: the 16.5MeV gamma-rays from the $^3He + d \rightarrow {}^5Li + \gamma$ reactions are clearly visible.

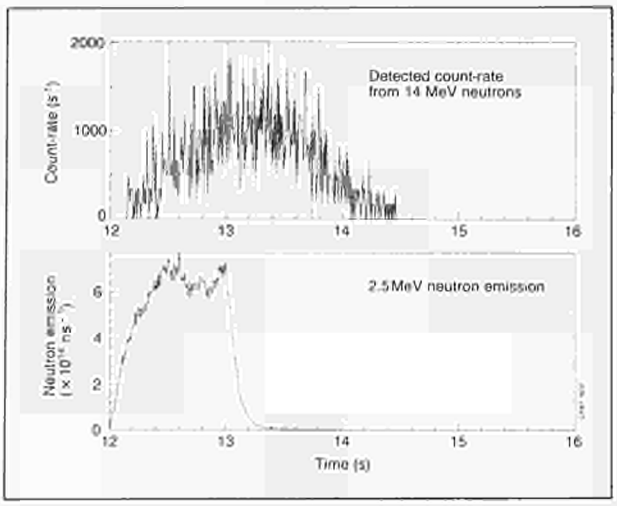

Fig.26: Illustrating the burn-up tritons from the d+d→t+p branch of the d-d reaction. The lower curve shows the 2.5MeV neutron flux (d+d→^{3}He+n) whilst the upper curve shows the 14MeV neutron flux from the t+d→^{4}He+n reaction. The good confinement of the 1MeV tritons is clearly displayed.

structure from the measured machine parameters are in progress.

H_α and Visible Radiation Monitors

The intensity of H_α/D_α emission is measured absolutely at several points in the torus, at the limiters, RF antennae, the inner wall and at the top and bottom wall. This enables the ionisation rate to be calculated and, by establishing the particle balance in the plasma, the global particle confinement time and the recycling coefficient can be deduced. In addition, measurements of the absolute bremsstrahlung emission provide information on the effective ion charge (Z_{eff}) of the plasma.

The light collected through windows in the torus is relayed by optical fibres to the Diagnostic Hall, where it is analysed by filters or spectrometers and detected by photomultipliers. Recently, the capabilities of the system have been enhanced by the addition of a 13-channel array, aligned in a common poloidal cross-section of the plasma. The array has been used to determine the radial profile of Z_{eff} and its temporal evolution. In particular, the abrupt drop in Z_{eff} (r) over its whole profile has been observed following the injection of a deuterium pellet into the plasma. Data from the H_α/D_α emission have been used to determine the poloidal variations in recycling at the plasma edge, which are considerable during the formation of discharges limited by a magnetic separatrix.

Visible Spectroscopy

Some of the optical fibres of the H_α monitor are equipped with visible spectrometers, provided under a Task Agreement with EURATOM-UKAEA Association, Culham Laboratory, UK or are fitted with interference filters for observing impurity emission. In addition, a spectrometer closely coupled to the torus is installed for limiter observation. In this way, the influx of impurities can be measured from various different sources such as walls, limiters and antennae.

Charge Exchange Recombination Spectroscopy

The active beam diagnostic system based on charge exchange recombination spectroscopy (CXRS) uses the neutral beams as probe beams. During the first year of neutral beam heating, ion temperatures deduced from Doppler broadened charge exchange recombination spectra of fully ionized light impurity atoms and local particle densities calculated from absolutely calibrated CXRS photo fluxes were measured in a wide range of plasma parameters. Two viewing lines providing localised data from the plasma centre (R=3.1m) and another active volume at R=2.3m were commissioned. Six different recombination lines of the main light impurities and the bulk of a JET plasma such as deuterium, hydrogen, helium, carbon and oxygen were analysed. A dual spectrometer arrangement, employing the same viewing line twice, has enabled simultaneous measurement of two different CXR spectra. The deduced low-Z ion temperatures of helium, carbon and oxygen were found to agree within 15%.

Absolute calibration of the detection system has enabled determination of local densities of carbon, oxygen and helium between 1 and 10% of the electron density. Simultaneous measurement of carbon and oxygen concentrations has given values of Z_{eff} in approximate agreement with independent measurements. The effective CXR excitation rates which were used for the quantitative analysis of the observed photon fluxes were corrected for cascading and l-mixing effects and modelled to the actual plasma parameters such as electron temperature and bulk ion density. The total error of the resultant impurity densities are estimated to be approximately 50%. Further detailed modelling including experimental data gained on JET and on other tokamaks is under progress.

During the 1987 shut-down, a multi-chord viewing system will be installed providing a dual-Z radial profile of ion temperature, toroidal velocity and low-Z impurity density.

Vacuum Ultraviolet Spectrometry

The combined 1-250 nm range of the JET VUV and XUV spectrometers allows a study of light emission from most impurities as these emit mainly in this band due to the high temperature of JET. A multi-channel broadband instrument, covering the wavelength range 10-170 nm, is used for time-resolved line identification. It has been absolutely calibrated and thus allows quantitative monitoring of impurities. The instrument has been routinely operated since May 1984.

This system is complemented by a XUV instrument in the range 1-33 nm, with two multichannel detectors. Due to its higher spectral resolution, it can solve line identification problems and allows estimates of ion temperatures and plasma rotational velocities from Doppler-broadening measurements. The system became

operational in June 1986. The two systems share the same port.

The spatial distribution of impurities can be measured by an instrument resolving in the 10-250 nm range, which views the plasma through an additional rotating mirror. It scans the plasma for 80 ms, repeatedly. Two lateral channels, viewing the top and bottom half of the plasma, have been installed. Each channel can monitor two lines simultaneously (and a visible line for branching ratio calibration). The third channel, viewing the plasma vertically through a bottom port, will be installed during the 1987 shutdown.

Wide Band X-Ray Spectroscopy

In order to determine concentrations and radial distributions of highly stripped light impurities (such as 0) and metal impurities (such as Ni and Cr), two double crystal monochromators have been built during the year under contract with IPP EURATOM-Association, Garching, F.R.G.. Both the monochromators will be able to record X-ray emission from the plasma in the wavelength range 1 to 24Å . This range covers emission from H- and He-like Ni, Ne-, Na- and Mg-like Ni, H- and He-like O. These ionisation stages are of importance for mapping the impurity content of the plasma, the equilibrium conditions and particle transport processes.

The spatial scan monochromator has been delivered and preliminary tests were made on JET at the end of the 1986 operation phase. The instrument is close coupled to a top vertical torus port in order to get a sufficiently wide horizontal aperture for the spatial scan (see Fig.27). The two crystals have the capability to scan wavelength and plasma radii during a single plasma discharge and the instrument has a resolution $E/\Delta E \sim 500$ which is sufficient for intensity measurement of the resonance lines. The monochromator was removed from the machine after preliminary tests to allow further calibrations with an absolutely calibrated X-ray laboratory source and will be reinstalled in 1987 with a new vacuum interface compatible with the new torus support structure.

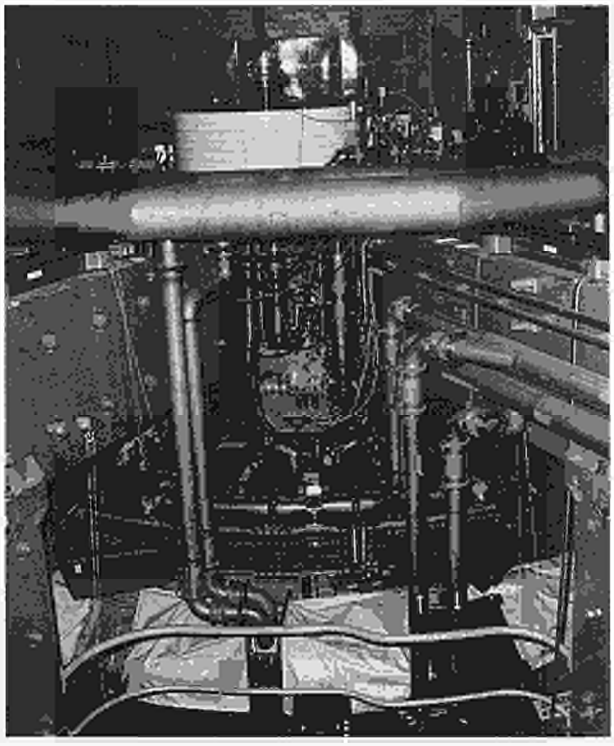

Fig.27: The spatial scan X-ray Spectrometer showing close coupling to a top vertical torus port.

The second double crystal monochromator was delivered in late-1986 and installed in a newly built concrete shielding outside the biological wall of the Torus Hall. The monochromator is planned for active phase operation on JET, as one of the main impurity survey diagnostics. The monochromator has a horizontal line-of-sight to the plasma through one of the main horizontal ports adjacent to the scanning vacuum ultraviolet monochromators. The precision scans of the two crystals were tested both optically and with X-rays and the instrument will be capable of both survey measurements with a resolution of 500 and line broadening measurements with a resolution of 6000. During 1987, the high vacuum beam line connecting the torus with the monochromator will be installed, and both double crystal monochromators are expected to operate.

High Resolution X-Ray Spectroscopy

A high resolution curved crystal spectrometer (radius of curvature 24m) was installed and operated in 1986. The instrument measures characteristic X-ray spectra in the wavelength region of 2Å which covers H- and He-like ionisation stages of metal impurities such as Cr and Ni. During 1986, H- and He-like Ni spectra were recorded with a resolution of 20 which is sufficient to measure accurately the widths of Doppler broadened line profiles over a wide temperature range. Nickel ion temperatures have been measured routinely during the various operational scenarios of JET, with temperatures in the range of 1.5-14keV. The time resolution achievable is dependent on the signal to noise level at the detector and varies from 20ms to several seconds, the latter being limited by the low nickel concentrations in the plasma during certain operation schemes. In addition to measuring the central impurity ion temperature, the X-ray spectra provide information on plasma rotation from line-shifts. Toroidal velocities of $5x10^4$-$3x10^5 ms^{-1}$ have been recorded during neutral beam injection. During 1987, new crystals will be installed to increase the possible time resolution in order to respond better to fast varying phenomena in plasma behaviour.

Soft X-Ray Pulse Height Analysis

A three detector pulse height analysis (PHA) system has been installed on JET to measure continuum and line radiation in the X-ray region.

This diagnostic makes measurements of the plasma electron temperature, impurity concentrations and deviations of the distribution function from a Maxwellian and has operated throughout 1986. Comparisons made with other diagnostics have shown good overall agreement.

In addition, the X-ray spectra have been modelled using a radiation code to form a consistent picture of the X-ray emission from the plasma centre. In 1987, the diagnostic is being reconfigured to allow operation into JET's active phase. The detectors will be moved behind the Torus Hall biological walls, which will act as an efficient neutron shield. This new configuration will be operating after mid-1987.

Soft X-Ray Diode Array

The Diode Array system, built by EURATOM-IPP Association, Garching, F.R.G,. consists of two X-ray imaging cameras, which view the plasma from orthogonal directions. The diagnostic is used to investigate MHD plasma properties and to measure the radiation profiles with coarse energy resolution using different absorption filters. The system was fully operational during 1986 and has obtained several important new results.

The sawtooth instability has now been very closely studied and it has been shown that all sawteeth crashes proceed as a rapid displacement of the hot central plasma followed by an equally rapid collapse of this hot zone. The measurements have also greatly clarified the role of sawtooth precursor and successor oscillations. These results have had important consequences for the theory of the sawteeth instability.

During pellet injection, the diode array has provided detailed measurements of the pellet ablation and the penetration of the pellet into the plasma. Immediately following the pellet injection, a striking new phenomenon has been discovered called the "snake", due to its characteristic appearance in the X-ray cameras (see Fig.28). The snake is a small long lived region of high plasma density and is thought to be caused by a small magnetic island. It is important, as it gives information on the internal q-profile of the plasma.

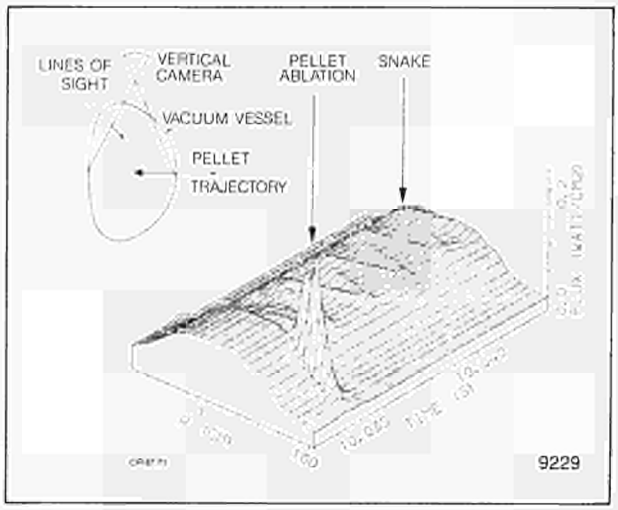

Fig.28: Soft X-Ray flux profile as a function of time following pellet injection, indicating the phenomenon of the 'snake'.

Detailed studies of disruptions in JET have shown many similarities with observations in other machines, but a new phase had also been identified during which a rapid plasma collapse occurs. This does not seem readily explicable in terms of existing theoretical ideas.

The diagnostic has also provided detailed measurements on ELMS and profile broadening observed during X-point (or separatrix) magnetic configurations.

The radiation shield design for the horizontal camera has been completed. This shield will extend the usefulness of the diagnostic into the D-D phase. A satisfactory alternative detector system, less sensitive to neutron induced effects, has not yet been identified although work continues in this area.

Bolometry

This diagnostic measures the total radiation power of the plasma in the energy range 5eV-9keV, resolved in time and space. Two horizontal arrays of bolometers (10 each) and an orthogonal array of 14 provide data, with ~20ms time resolution.

The relative radiation power loss, P_{rad}/P_{input}, depends sensitively upon the plasma density and upon the influx of impurities. In discharges where a magnetic separatrix with one or two stagnation points is formed inside the vacuum vessel, reduced particle influx results in power loss as low as about 20%. Increase of the density leads to an increase of the power loss. In discharges with improved confinement properties (H-mode) the significant increase in density results in power losses up to about 60%. In all cases, the radial emissivity profile is hollow. Pellet injection causes a jump in the plasma density and thus an enhanced power loss which, typically, is moderate if the pellet is deposited deeply inside the plasma region, but up to 100% if the pellet is ablating further out.

Interferometry

Electron density is one of the fundamental plasma parameters, which must be measured reliably every discharge. On JET, this task is fulfilled by a far-infrared (195 μm) multi-channel interferometer. It serves not only to obtain the profile of electron density as a function of time, but also as a safety interlock signal for neutral beam injection and a feed-back signal for gas puffing. The system has 7 vertical and 3 lateral channels. The vertical part has been operated routinely since September 1984. The lateral channels require compensation for mechanical vibrations as they use retro-reflectors in the vacuum vessel. The short wavelength laser beam originally envisaged for this purpose was difficult to maintain alignment, so it is being replaced by a 119 μm laser during the 1987 shutdown.

During 1986, measurements of the density profiles were used to study particle transport and wall pumping in inner-wall, X-point and limiter configurations. Increased particle confinement and a broadening of the density profile are signatures of the transition from L-mode to H-mode (in the single null X-point configuration), which was one of the most important observations during 1986.

Finally, the evolution of the density profile in pellet injection experiments has permitted more reliable measurements of the particle transport coefficients in the centre of the plasma.

Polarimetry

The magnetic field of the plasma interacts with the linearly polarized laser beam of the interferometer to cause rotation of the plane of polarization (Faraday effect). Hence, information on the poloidal field and, after some manipulation, on the plasma current distribution can be obtained. During the 1987 shutdown, the vertical channels of the far-infrared interferometer will be equipped with the additional optics and detection necessary for such measurement as part of a contract with EURATOM-CEA Association, Cadarache, France.

Neutral Particle Analysis

An array of five passive neutral particle analysers has been in operation since the end of 1985. The system, constructed for JET by EURATOM-ENEA Association, Frascati, Italy, has been extensively used during 1986 operation in all plasma scenarios to infer information on neutral particle behaviour and ion temperatures.

In collaboration with the Frascati NPA Group, particular emphasis has been given to the development of data analysis codes which have allowed:

- the evaluation, together with data from other diagnostics, of information on the ion temperature profile;
- the study of the minority tail during ICRH heating to infer the RF power deposition profile;
- the study of the slowing down of the neutral particles injected during NB operation.

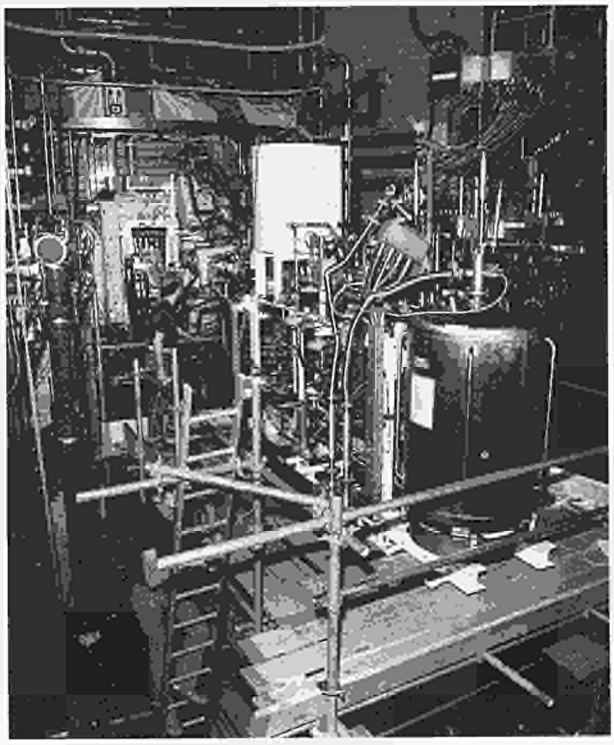

Fig.29: Single-shot pellet injector.

Single Shot Pellet Injector

A single shot pellet injector was installed in May, and following commissioning was ready for operation at the end of June (see Fig.29). The rapid installation and short commissioning period for such complex apparatus were made possible by careful planning and preparation of the hard- and soft-ware interfaces and by the dedicated efforts of those involved.

The injector was operational for three months and a total of 170 pellets were fired into JET plasmas with high reliability. The cylindrical pellets with diameters of 3.6 mm or 4.6 mm with velocities between 0.8 and 1.2 km s^{-1} were injected into various target plasma configurations (limiter, inner-wall and X-point) using different combinations of the available heating methods (OH, ICRF and NBI). The results of these investigations are described elsewhere in this report.

The single shot pellet injector will be reinstalled with the new multi-pellet injector for the next operational period. The two systems will be operated independently but will use a common cryo-pump box to exhaust the propellant gas and a common protection system to inhibit pellet injection when the machine conditions are not suitable. It is planned to use the facility of the single shot injector to supply pellets of deuterium, hydrogen or known mixtures of both and also to dope any of these with trace amounts of neon, to further the studies of particle/impurity transport, confinement, recycling and fuelling in JET plasmas.

Summary of JET Technical Achievements

During 1986, the toroidal magnetic field (B_T) operated routinely at its maximum design value of 3.4T. The plasma current ($\pm<3\%$), horizontal plasma position ($\pm<10$mm), plasma elongation $\epsilon(\pm5\%)$ and shape were all controlled by feedback circuits acting on poloidal field coils. Following considerable work on these systems, stable control has been obtained with elongations in the range 1.2 -1.7. However the plasma vertical position is naturally unstable due to both the quadrupole poloidal field necessary for the elongated plasma and destabilising effect of the iron magnetic circuit. Loss of vertical position feed-back control at higher elongations can lead to large vertical forces on the vessel. Some additional vessel supports have been introduced, but the plasma current, I_p, was still restricted within the operating regime given by $I_p^2(\epsilon\text{-}1.2)<5.0(MA)^2$. So far, the full inductive flux (34Vs) has not been used as the maximum premagnetisation current creates stray fields, which inhibit reliable plasma breakdown.

The vacuum vessel has usually been operated with wall temperatures at 250-300°C and with a base pressure of

10^{-7}mbar H and 10^{-9}mbar residual impurities. To reduce the level of metallic impurities and oxygen, the torus walls have been carbonised by glow discharge cleaning in a mixture of hydrogen or deuterium and hydrogenic methane (CH_4). Difficulties in controlling the density during Tokamak discharges following carbonisation limited the number of carbonisations performed in 1986. The vessel is also conditioned by glow discharge cleaning in hydrogen and/or deuterium.

Eight carbon plasma limiters were located symmetrically on the outer equatorial plane of the vessel. Since disruptions mostly terminated on the inner walls, these have been covered by carbon tiles to a height of ±1m around the mid-plane. Similar tiles also protected the frames of the RF antennae, eight octant joints, and the outer wall from neutral beam shine-through. Additional tiles were installed to protect the top and bottom of the vessel during X-Point (Separatrix) operation. The total surface area covered is 45m^2, corresponding to ~20% of the vacuum vessel area. The inner wall tiles used as limiters and those for X-Point protection provided powerful pumping (with speeds up to 100mbar.l.s^{-1}). This allowed operation at low density near the plasma edge and was used to reduce the density after neutral injection to avoid disruptions. Recently, helium discharges prior to normal operation have improved the inner wall tiles pumping capacity.

RF Heating System

Three RF antennae were installed at the outer equatorial wall. Power was transferred to the plasma at a radiation frequency (25-55MHz) equal to the cyclotron resonance of a minority ion species (H or He^3). Each antenna was fed by a tandem amplifier delivering up to 3MW in matched conditions. The three units have been regularly operated up to 7.2MW for 2s pulses. Experiments with 8s pulse duration were also performed delivering ~40MJ to the plasma. Recently, a fourth RF generator has been installed so that two generators fed one antenna, and over 4MW was coupled to the plasma in this configuration.

Neutral Beam System

A long pulse (~10s) neutral beam (NB) injector with eight beam sources operated on JET from early 1986. H° beams were injected into D plasmas with particle energies (in the full energy fraction) of up to 65keV. The neutral power fractions were 69%, 23% and 8% in the full, half and one-third energy components, respectively, giving a total beam power of ~5.5MW injected into the torus. D° beams have also been injected into D plasmas, with particle energies up to 75keV (injected power fractions of 76%, 17% and 7%) giving a total power up 10MW. Up to 40MJ was delivered to the plasma during a pulse.

Scientific Achievements during 1986

General Plasma Characteristics and Global Confinement

Experiments have been performed with ICRF and NBI to determine the response of the plasma to additional heating. Up to 7MW of ICRF and 9MW of neutral beam injection (NBI) have been applied to a wide range of plasmas (B_T= 1.7-3.4T, I_p= 1-5MA and <n> = 1-5x$10^{19}m^{-3}$) with fixed plasma dimensions (R ~ 3.0m, a = 1.2m and b/a = 1.45). The plasma behaviour is similar to that observed in other smaller tokamaks [1]. Discharges with a magnetic separatrix (X-point) inside the chamber can make a transition to a régime of improved confinement, called the H-mode [2]. The X-point plasmas obtained in JET are described in another section of this report. This section deals with plasmas bounded by the outboard limiters or inner-wall protection tiles, which have not made the H-mode transition and are in the L-mode.

The central electron and ion temperatures, for two different conditions, are shown as a function of density in Figs.30 and 31. The first shows the result of deuterium

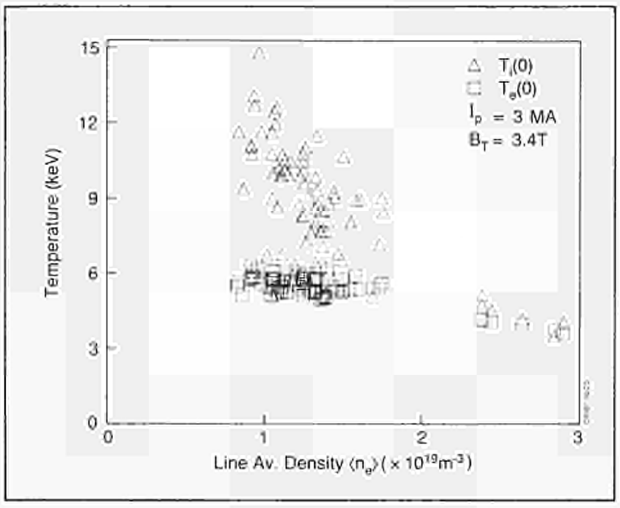

Fig.30: The central ion and electron temperatures versus line average electron density for I_p=3MA, B_T=3.4T deuterium plasmas with deuterium neutral beam injection giving a total power between 5 and 7MW.

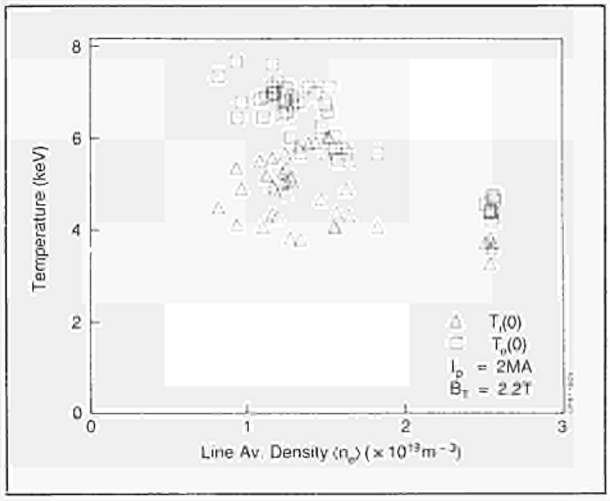

Fig.31: The central ion and electron temperatures versus line average electron density for I_p=2MA, B_T=2.2T, He^3 plasmas with hydrogen minority ion cyclotron heating giving a total power between 5 and 7MW.

NBI on deuterium plasmas at I_p=3MA and B_T=3.4T. At medium to high densities, the thermal ions and electrons are quite strongly coupled and the temperatures of both fall with increasing density. At low densities, where the thermal ions receive most of the NBI power and can decouple from the electrons, the electron temperature saturates and ion temperatures of up to 14.5±1keV have been obtained. The various plasma ions can have different temperatures during heating, and these have been obtained by the Doppler broadening of an X-ray emission line of Ni^{26+}. The deuterium ion temperature is estimated to be ~ 1.5keV less at the highest nickel temperature shown.

In contrast, Fig.31 shows some hydrogen minority ICRF data at I_p=2MA and B_T=2.2T where the power transfer is calculated to be due primarily to the electrons. In this condition at low densities, the ion temperature saturates and electron temperatures of 7.5keV have been obtained. From these heating results, it can be concluded that the power transfer from ICRF and NBI is at least qualitatively as expected. As described in the section of RF heating, the quantitative agreement between the calculated ICRF heating rates and those observed experimentally is also good.

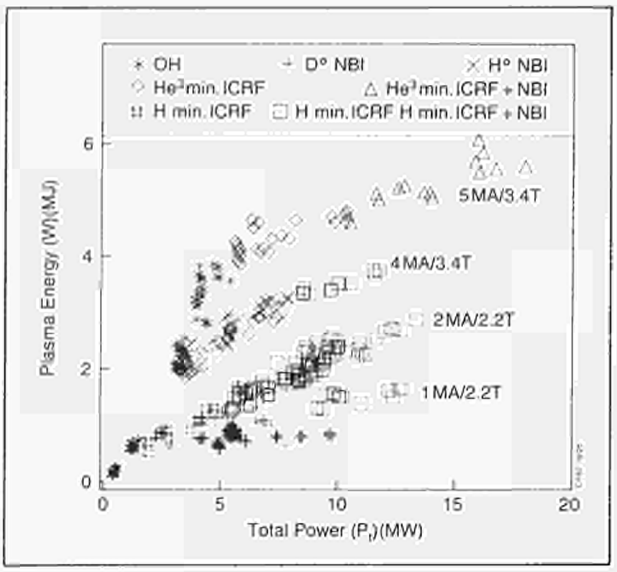

Fig.32: The total plasma energy content against total input power for various plasma currents and toroidal fields.

The global properties of the plasma thermal insulation are best described by plotting the plasma energy content (W) against total heating power P_t. This is shown for a number of plasma currents and toroidal fields in Fig.32. The main features of this data are:

(i) Ohmic heating alone is the most effective.

(ii) When additional heating is applied the energy confinement is degraded and the rate at which the energy content increases with power (or the incremental confinement time, $\tau_{inc} = \Delta W/\Delta P$) is less than that with Ohmic heating alone;

(iii) For much of the data, τ_{inc} is independent of power so that $W = W(0) + \tau_{inc} P_t$. However for some scans, τ_{inc} falls with increasing power, so the heating is less effective, particularly in those plasmas using the main outboard limiters;

(iv) The energy content is proportional to plasma current and independent of toroidal field;

(v) The best results from each heating scheme are similar and imply that there are no fundamental differences in effects on the plasma.

The main deviations from this summary, such as variations in τ_{inc} with power or reductions in heating effectiveness, are associated with changes in the power deposition or radiation profiles.

To demonstrate that the power deposition profile can affect the heating effectiveness, a scan of hydrogen ion cyclotron resonance position was performed at $I_p = 2MA$ and $B_T = 2.2T$, with ICRF heated hydrogen minority in ^{3}He plasmas. Helium plasmas were used as these have a low impurity content and, unlike most deuterium plasmas, do not radiate more or, worse still, disrupt as the power source is moved away from the centre of the chamber. The half-width in minor radius of the power deposition around the resonance position is approximately 0.2-0.3m. A plot of τ_{inc} against the minor radius of the resonance is shown in Fig.33. τ_{inc} has its maximum value when the resonance intersects the magnetic axis and falls to zero when it reaches the edge of the plasma. The solid curve is the prediction of a simple power balance model in which the thermal conductivity increases quadratically with minor radius. These results show that unfavourable heating profiles, such as those obtained when NBI is used at high plasma density, will reduce the heating effectiveness. If radiation is regarded as a negative heating source, Fig.33 demonstrates that peripheral radiation can have little or no effect but a shift of the profile towards the plasma interior will reduce τ_{inc}. Such changes in the radiation profiles do occur as shown in Fig.34. The difference between inner-wall and limiter plasmas, mentioned above, and the poor

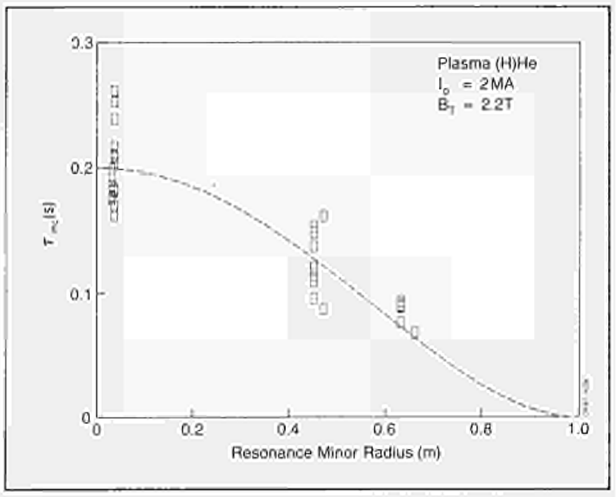

Fig.33: The incremental energy confinement time versus the minor radius of the ion cyclotron resonance for a number of I_p=2MA, B_T=2.2T, He^3 and H-minority ion cyclotron heated plasmas.

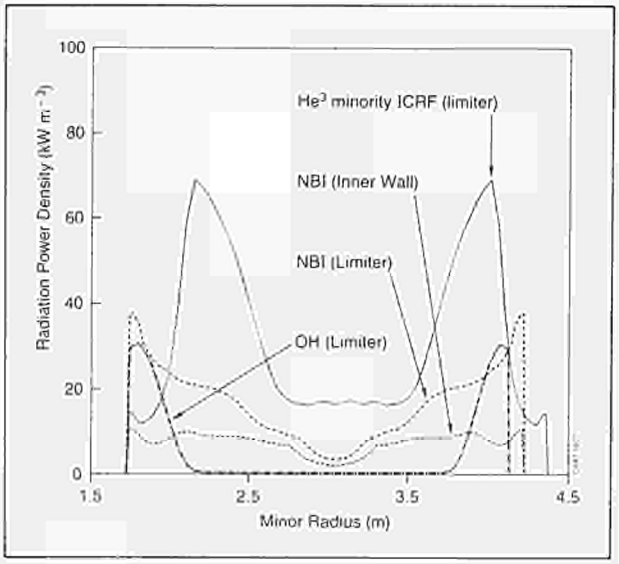

Fig.34: The total radiation power density versus minor radius for various different heating conditions. The radiation power density in the central region is poorly determined for these profiles.

performance of some ^{3}He minority ICRF plasmas, whose UV spectra show unusually high metal contamination, are examples where the radiation profile has an important effect.

It is clearly of interest to know whether the confinement deterioration is an effect of additional heating or whether it already manifests itself in ohmically heated plasmas. The latter possibility is suggested because the high density ohmic heating points usually lie on the same line as those with additional heating in the energy content against total power plots (see Fig.32). The strongest evidence in support of this has been obtained from the propogation of the heat pulse which follows the sawtooth collapse. The measurements of the electron heat pulse have been made using an absolutely calibrated grating polychromater sensitive to the plasma electron cyclotron emission. The transient response of the electron temperature can be analysed to yield a value for the electron thermal conductivity. The measured conductivity is plotted against input power for I_p=3MA and B_T=3.4T data in Fig.35. The thermal conductivity does not vary significantly from Ohmic heating to full power additional heating plasmas. Therefore, the confinement degradation has already occurred with Ohmic heating alone. Furthermore, the mean value of the thermal conductivity, χ_{hp}, so determined, is consistent with the value of the incremental confinement time (ie $\chi_{hp} = \chi_{inc} \sim ab/4\tau_{inc}$).

Two alternative pictures for the power balance are suggested by these results. The first has the confinement degradation associated with the passage through a threshold in a quantity such as temperature or pressure gradient. The alternative picture is that the outward diffusive power flow is nearly balanced by a constant inward convective flow or heat pinch. As additional heating or the sawtooth heat pulse are supposed only to excite the diffusive part of the power flow, confinement

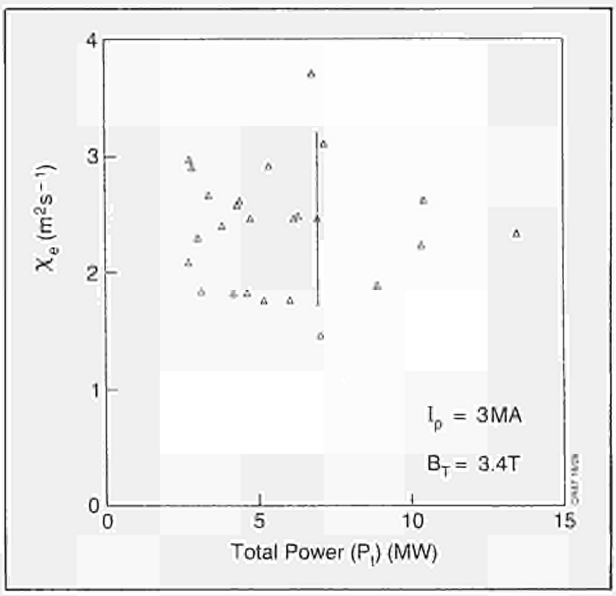

Fig.35: The thermal conductivity, χ_e, determined using sawtooth heat pulse propogation measurements against the total input power in I_p=3MA, B_T=3.4T plasmas.

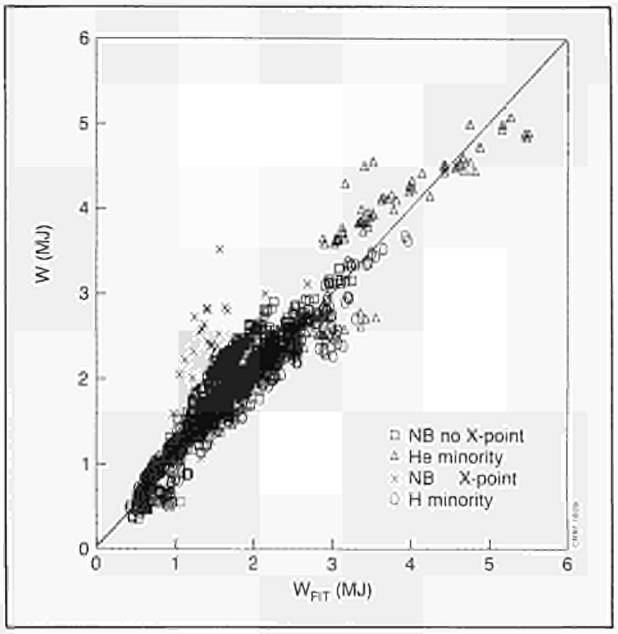

Fig.36: The plasma energy content against the unconstrained off-set linear fit for different plasma conditions (as marked on the figure).

degradation is observed. Whatever the correct picture, the above discussion underlines the importance of study of the dynamic behaviour of the plasma in an effort to understand the transport processes.

The global confinement data has been fitted with a number of different scaling forms. When the scaling law is unconstrained by theoretical models, the intention is to pick out the main parametric dependences of the data. This approach has been applied to the data for the total energy content using the linear dependence on total power described above. A good fit to the NBI data is found using standard regression techniques: it is $W(0)(MJ) = 0.225 n^{0.6}(10^{19}m^{-3}) I_p^{0.5}(MA) B_T^{0.4}(T)$, where $\tau_{inc}(s) = 0.047 I_p(MA)$. A comparison with the complete dataset is shown in Fig.36. The scatter around the fit is thought to be due to the variations in deposition and radiation profiles described above. It should be noted that the behaviour of the intercept, W(0), is essentially that of the Ohmic heating data. Since a strong density rise usually occurs with additional heating whose magnitude depends on plasma current, the total power, plasma current and density dependences of any scaling law must be checked for correlations between them. This has been done for plasma current dependence in τ_{inc} by testing that all the density dependence in the energy content is in W(0). In other words, the change in energy content with additional heating is independent of density.

An alternative approach to scaling the global confinement data is to use only those parameters which are invariants under the scale transformations of theoretical models. This method has the advantage that it offers guidance as to which model describes the data even when the model cannot be solved. The most restrictive model which gives a good fit to the data from plasmas dominated by additional heating is resistive MHD. In the

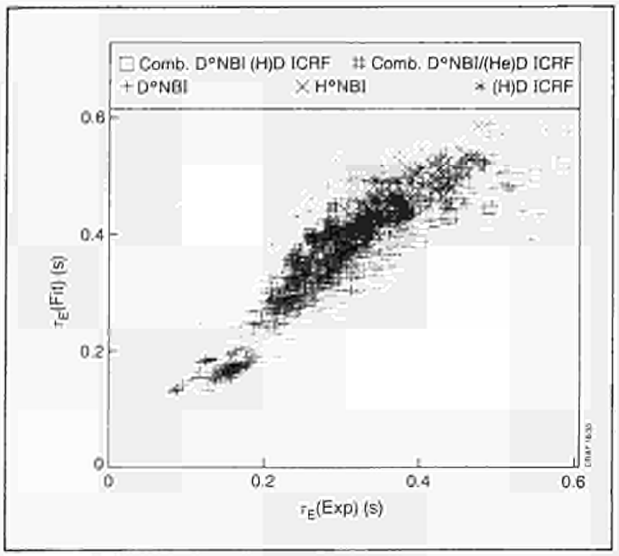

Fig.37: The fitted energy confinement time for the resistive MHD model against the values obtained in JET plasmas with different heating conditions ($P_t > P_\Omega$).

resistive MHD model, the total energy confinement time, $\tau_E = W/P_t$, can be described by $\tau_E = \tau_{Ap} f(S, P_t/P_\Omega)$, where τ_{Ap} is the poloidal Alfvén time, S is the magnetic Reynold's number and P_Ω is the Ohmic heating power. The magnetic Reynold's number is defined by $S = \tau_R/\tau_{Ap}$ where τ_R is the resistive skin time of the plasma. The JET data, $P_t/P_\Omega > 2$, are best fitted by $\tau_E = 0.91\ \tau_{Ap}\ (P_t/P_\Omega)^{-0.5} S^{0.75}$, as shown in Fig.37. At first sight, this scaling law appears to be inconsistent with the linear scaling of the energy content. However the implicit dependence of P_Ω and S on total power make the two indistinguishable. The simplicity of this form for the energy confinement and the lack of significant normalising constants encourage the belief that resistive MHD processes are implicated in the confinement degradation. When data from machines other than JET are included in the fit, a dependence on the aspect ratio (ϵ = a/R) must be included. The result is $\tau_E = 0.53\ \tau_{Ap}\ (\epsilon P_t/P_\Omega)^{-0.46} S^{0.74}$, which is compared with the data in Fig.38. It can be seen that the data are fitted well over a range of nearly three orders of magnitude. It can easily be shown that the fit is equivalent to $\tau_E \sim (\tau_{Ap}\ \tau_R)^{1/2}\ (\epsilon\beta_t)^{-1}$, where β_t is the poloidal beta, which has a satisfying simplicity. The reason this form is not used in fits is that both τ_E and β_t depend on the same measurement so that errors are amplified. Nevertheless, this form compares reasonably well with the data as shown in Fig.39.

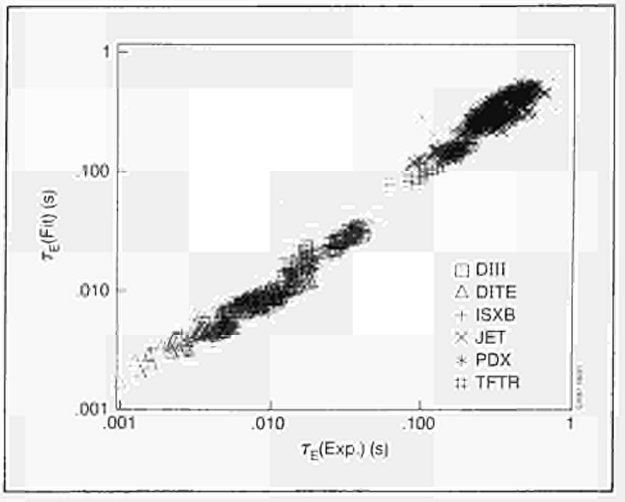

Fig.38: The fitted energy confinement time for the resistive MHD model against the experimental values for various tokamak devices ($P_t > 4P_\Omega$).

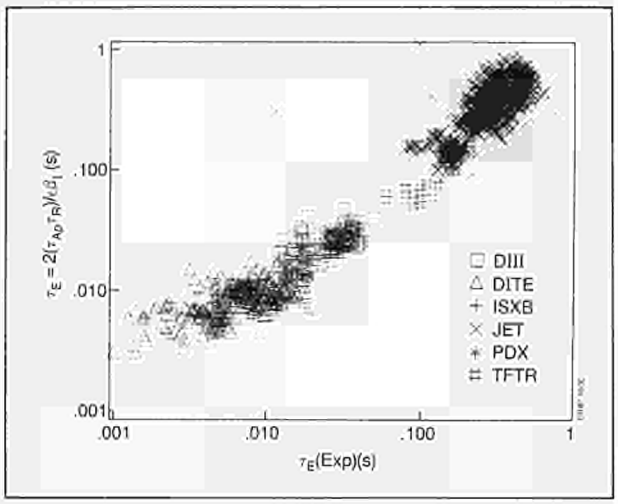

Fig.39: The transformation of the resistive MHD fit ($\tau_E = 2(\tau_{Ap}\ \tau_R)/\epsilon\beta_t$)) against the experimental energy confinement time for different tokamak devices.

Heat Transport

A Heat Transport Topic Group has been set up whose role is to study the response of the JET plasma to externally applied power, leading to a dynamical equilibrium pattern of sources and sinks which maintain the plasma stored energy. A main aim of JET is to optimize the efficiency of the plasma energy build-up in order to reach thermonuclear conditions at the highest input power levels planned in the JET programme. Therefore, it is important to identify the physical mechanisms by which the plasma loses energy and particles; the scaling of their effectiveness with the main plasma parameters in the different regimes in which JET is presently operating; and, ultimately, the theoretical models which describe the observed behaviour.

Within the Heat Transport Topic Group, these problems are being tackled through the detailed local analysis of experimental data provided by the JET diagnostic systems. A necessary prerequisite for this analysis to take place is assembling consistent and fully validated information from different diagnostics. This information is then fed into sophisticated computer codes which ultimately compute the local fluxes of energy (conduction) and particles (convection) which are compatible with the dynamics of the plasma discharge.

In general, it is found that, in all regimes of JET operation analyzed so far (ohmic, NBI, RF, X-point, and pellet injection), electrons and ions lose energy at comparable rates and their energy confinement times are typically longer than their equipartition time. As a consequence, electron-ion coupling accounts for a substantial fraction of the total power input to the plasma and must be taken into account when assessing the physics which describes electron and ion behaviour.

In particular, attention has been focussed on the phenomenology of electron confinement in trying to assess the validity of theoretical models when describing electron losses. So far, it has been found that none of the models presently available (electron viscosity, drift induced, MHD instabilities) satisfactorily describes the electron behaviour in all types of JET discharges. A further possibility remains, in that a systematic correlation is found between broad-band magnetic fluctuations and plasma confinement, indicating that the former can play a leading role in affecting transport. It has been established that the electron heat conductivity increases approximately linearly with the total input power, with no apparent scaling with plasma current or toroidal magnetic field. However, the analysis in this area is in a preliminary state and continuous refinement is in progress.

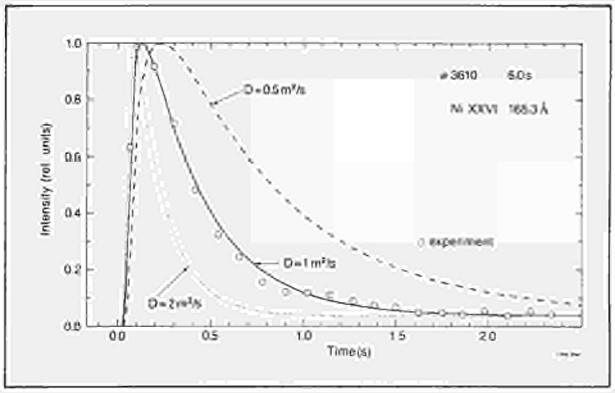

Fig. 40: Ni XXVI intensity after accidental nickel injection ($n_e=2x10^{19}$ m^{-3}, $I_p=2.8$ MA). Simulations using different D values are shown ($V_D=-2Dr/a^2$). Recycling at the limiters leads to a finite level after the event.

Impurities and Radiation Losses

In 1986, the JET VUV spectroscopy was complemented by a grazing incidence spectrometer (KT4) allowing measurements of the C VI and O VIII resonance lines. Preliminary results from this diagnostic essentially confirmed previous impurity data based on the VUV survey spectrometer (KT2). Resonance lines of He- and H-like nickel were observed by the high resolution crystal spectrometer (KX1) and were mainly used for measuring ion temperatures and rotation velocities. For impurity studies, charge-exchange recombination spectroscopy (CXRS) in the visible spectrum (KS4) proved to be a most useful diagnostic, enabling measurement of light impurity concentrations at the plasma centre. An overview of present spectroscopic diagnostics on JET [1] and results dealing particularly with plasma-surface interactions [2] have been previously reported. A more recent summary on impurity behaviour has been published [3]. Some general impurity results are discussed in the following paragraphs.

Impurity Transport and Impurity Confinement

Emission shells of light impurities and low metal ionisation stages in JET, measured by the spatial scan spectrometer (KT1), are clearly transport dominated requiring a diffusion coefficient D $\approx$ 1 m^2s^{-1} to explain their position and width [4]. Information about transport was also obtained from accidental injections of iron and nickel. At an electron density $n_e=2x10^{19}m^{-3}$, simulations using D=1 m^2s^{-1} agree well with the observed rise and decay of nickel line intensities as shown in Fig.40 for Ni XXVI. There are indications that the diffusion coefficient decreases with electron density and increases during additional heating. Investigations of hydrogen particle transport [5] show similar transport coefficients to those found for the impurities.

A diffusion coefficient D=1 m^2s^{-1} and a drift velocity $V_D=-2Dr/a^2$ are used in standard interpretation of VUV and X-ray spectra and for calculating radiated power losses of individual impurity species by means of an impurity transport code [6]. The resulting moderately peaked total ion density profiles are confirmed within a factor of two by analysis of a number of metal ionisation stages at different radial positions (eg Ni XVII-Ni XXVII). Sawtooth oscillations, observed on lines of higher ionisation stages, can only be partly explained by pertinent variation of electron temperature profiles. It must be assumed that impurities are expelled from within the q=1 surface during the sawtooth crash.

Impurity particle confinement times, derived from measured influxes and concentrations, agree roughly with calculations on the basis of a simple diffusion model [2] and D=1 m^2s^{-1}, if an energy of a few eV is assumed for the neutral particles produced at the limiters. A good correlation of impurity influxes and densities has been observed throughout JET operation, both as a function of plasma parameters and of vessel conditions.

Occasionally, when a steep increase in the Cr influx was observed due to chromium evaporation, the metal concentration in the bulk plasma did not change [2]. These slow particles are ionised in the immediate vicinity of the limiter surfaces and have a high redeposition probability before entering the plasma. This observation demonstrates that the usual impurity influxes of C, O and metals must have a significant kinetic energy to give rise to the measured impurity concentrations.

Impurity Production

The impurity behaviour of JET limiter discharges was dominated by the limiter fluxes (wall contribution ≈ 20% during OH). Metal concentrations were only significant (>0.1% n_e) if the carbon limiters were metal-coated after accidental melting and evaporation of wall material (Inconel droplets and $>2x10^{21}m^{-2}$ uniform coverage [8]). Recently, this has been prevented by covering large areas of the torus by carbon protection plates. A particular metal problem during ICRH will be discussed later. During discharges limited by the inner-wall protection tiles, these took over the role of the limiters leading essentially to the same plasma behaviour.

The release of metals from the limiters can be explained by a combination of sputtering by deuterium and by light impurities taking into account the respective surface coverage of the carbon tiles (ϕ_M/ϕ_D = 0-0.02). The metal fluxes decrease with n_e and increase with I_p; they are inversely correlated with the light impurity behaviour. These trends, previously observed on many other tokamaks, are due to the temperature dependence of the metal sputtering yields. In JET, oxygen gettering by chromium has been observed to be a further reason for this anti-correlation.

The carbon concentration in JET has remained consistently at a level of a low percentage of the electron density (few % n_e) throughout operation periods. The carbon production rate behaves similarly to that of the metal release, but the dependencies are less pronounced [2]. This observation and the fact that the produced C particles must have significant kinetic energy suggest physical sputtering as the prevailing production mechanism. Furthermore, during temperature excursions of the limiter surface from 300°C to over 1000°C, no change in carbon production rate was observed. This means that chemical sputtering, expected to manifest itself by an increased yield at about 600°C, is not an important process. There is some evidence for carbon sputtering by oxygen, but only at unusually high oxygen levels [2]. The carbon yields measured ($\phi_C/\phi_D \approx$ 0.05-0.1) can be explained by a combination of deuterium, oxygen and self-sputtering at high electron temperature values at the edge of the plasma (T (a) >100 eV).

The oxygen fluxes and concentrations in JET varied primarily with vessel conditions. The vessel walls constitute the most important oxygen source and, once in the plasma, oxygen recycles at the limiters. This is apparent from the tendency of oxygen limiter fluxes to increase throughout a discharge, even if other parameters are stationary. If the recycling occurs in the form of CO molecules, the O atoms must gain energy in Franck-Condon or charge-exchange processes. Since no dependence of the oxygen yield on plasma parameters is observed, the energy threshold for the respective production mechanism must be very low. During ^{3}He discharges, carbon fluxes remained unchanged ($\phi_C/\phi_{He} \approx 0.13$) while oxygen was substantially reduced. Therefore, chemical processes or charge-exchange neutrals must be responsible for the O production.

During ICRF heating on JET, screen material (Cr, Ni) has been observed to enter the plasma from the ICRH antennae [2,9]. The measured chromium flux from a Cr coated antenna (10^{16} cm^{-2} s^{-1}MW^{-1}) decreased by a factor 5 during five months' operation and was reduced temporarily (some 10 discharges) by two orders of magnitude by means of heavy carbonisation (15% CH_4, 12 hrs). In the course of ICRH operation, screen material was deposited on the limiters and eroded again by the plasma resulting in higher basic metal levels during an ICRH campaign. The metal coverage of the limiter carbon tiles was removed by a few OH or NBI discharges in accord with model predictions [10]. The release mechanism of the screen material is not yet understood.

ICRH and NB co-injection

Both hydrogen and impurity influxes increased during additional heating, leading to a substantial increase in n_e, unless the plasma was at the inner wall, which appears to have an efficient pumping capability. Although the wall fluxes gained in importance, the plasmas were still dominated by the limiters. The n_e-profile flattened during ICRH, and was unchanged or peaked during neutral beam injection (NBI). The hydrogen and impurity particle confinement times decreased in both cases.

Due to the higher electron densities during NBI, oxygen was the most important impurity. The increase in the O/C ratio is well demonstrated by the charge exchange recombination spectrometry (CXRS) results [11], the trends of which are in excellent agreement with the usual VUV spectroscopic results, while they tend to give somewhat higher carbon concentrations. Z_{eff} decreased during NBI, but not to a lower level than that of OH discharges at the respective higher densities. For constant n_e, the radiated power fraction P_{rad}/P_{tot} fell with increasing NBI power. However, due to the pertinent n_e-evolution, radiation losses remained around 45% P_{tot}, on average. These radiation losses were caused by light impurities, in particular, by oxygen (1-2% n_e).

The metal release from the antennae screens during ICRH led to significant metal densities in the plasma (≈ 0.1% n_e, contribution to P_{rad} ≈ 20% P_{tot}) except immediately after heavy carbonisation. Z_{eff} remained essentially at the OH value before RF (ie there was no benefit of the higher electron densities). For individual campaigns, the radiated power fraction increased somewhat with RF power input (P_{RF}) and was generally in the range 40-70% P_{tot}. Hydrogen minority heating led to higher metal densities in the plasma than with ^{3}He minority heating but the difference in P_{rad} is within the scatter of the data points.

During combined NBI and ICRH, the consequences of the two heating schemes essentially added. The metal densities in the plasma corresponded to the respective RF power. Basic metal levels and limiter coverage built up as during ICRH alone. Z_{eff} and P_{rad}/P_{tot} values for OH plasmas and additional heating are summarised in Fig.41 for 1986 JET limiter discharges. At higher electron densities, Z_{eff} was about 2.5 for NBI, ICRH and combined heating, essentially caused by oxygen and carbon.

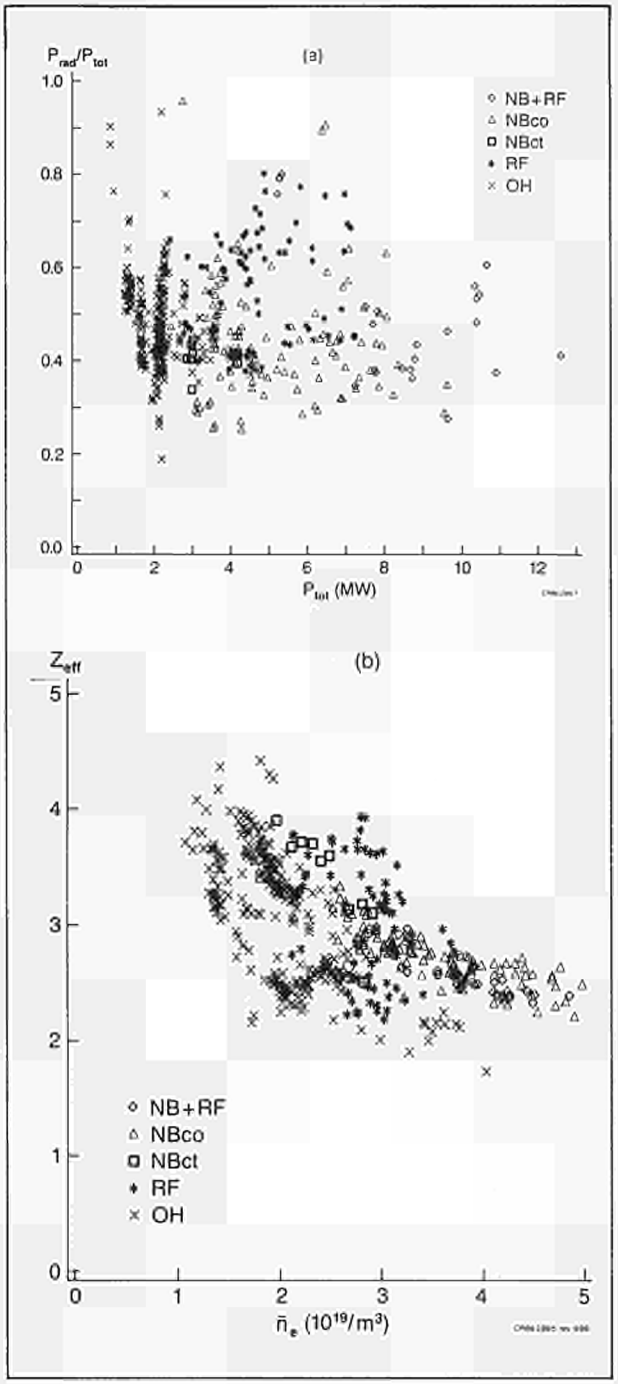

Fig. 41: JET 1986 limiter discharges. (a) P_{rad}/P_{tot} as a function of P_{tot}; and (b) Z_{eff} versus n_e; for OH, ICRH (RF), co- and counter-NBI and combined heating (NB+RF).

Magnetic Separatrix

The magnetic separatrix configuration has been successfully generated in JET (X-point plasmas [12]). In this case, the top and bottom vessel protection tiles act as X-point neutraliser plates. Even when these plates consisted of Inconel (June 1985), no significant metal concentrations were detected in X-point plasmas. With carbon plates, the carbon level was reduced compared to the respective limiter discharges during the OH phase. During NBI, carbon concentrations increased in contrast to the behaviour of limiter discharges, as demonstrated again by CXRS [11]. The behaviour of carbon and metals indicates a low plasma temperature in front of the neutraliser plates during OH discharges and therefore a low sputtering yield. After argon puffing into X-point plasmas, no retention of Ar in the X-point regions was observed, as the same amount was found in the bulk of X-point and corresponding limiter discharges, in contrast to that found in Doublet III [13].

The oxygen concentration was no different from that in limiter plasmas ($\approx$ 1.5% n_e). Since metal concentrations were generally low, X-point operation resulted only in a minor reduction of Z_{eff} ($Z_{eff} \approx 3$ at $n_e = 1.5 \times 10^{19}$ m^{-3} and $I_p = 2$ MA). The radiation losses of the bulk plasma were also somewhat lower, but there was an additional contribution of the X-point regions of $\approx$ 50% P_{bulk}. The total radiation losses amounted to $\approx$ 50% P_Ω at low densities ($n_e = 1 \times 10^{19}$ m^{-3}) and approached 100% at higher densities. NBI into X-point plasmas led to a low level of wall material in the plasma, probably due to charge exchange particles hitting the walls. The oxygen concentration did not change significantly during NBI.

NB Counter Injection

Counter injection both into limiter and X-point plasmas has been studied for a limited period in JET. The impurity behaviour of these discharges was virtually indistinguishable from the corresponding co-injection cases (see Fig.41). Some peaking of soft X-ray emission profiles was observed and the line intensities of higher metal ionisation stages appeared to increase more than the lower ones. However, the standard analysis taking into account the respective electron density n_e - and temperature T_e - distributions resulted in the usual impurity ion density profiles, within experimental errors. For the present NBI power levels (< 7 MW) and plasma parameters, no accumulation of impurities has been observed.

References

[1] K Behringer, Rev. Sci. Instrum. **57** (1986) 2000

[2] K Behringer, 7th Int. Conf. on Plasma-Surface Interactions (Princeton, U.S.A., 1986) J. Nucl. Mater. **145** & **146** (1987)

[3] K Behringer et al., Proc. of the 11th Int. Conf. on Plasma Physics and Controlled Nuclear Fusion Research, Kyoto, Japan, 1986

[4] K H Behringer et al., Proc. of the Workshop on Basic and Advanced Fusion Plasma Diagn. Techn., Varenna, Italy (1986)

[5] A Cheetham et al, Proc. of the 13th European Conf. on Contr. Fusion and Plasma Heating, Schliersee, FRG (1986) 240

[6] K Behringer et al., Nucl. Fusion **26** (1986) 751

[7] E R Müller et al., Nucl.Fusion **22** (1982) 1651

[8] R Behrisch et al., 7th Int. Conf. on Plasma-Surface Interactions (Princeton, U.S.A., 1986) J. Nucl. Mater. **145** & **146** (1987)

[9] JET Joint Undertaking Progress Report, 1985, (EUR-10616EN, EUR-JET-PR3)
[10] G M McCracken et al., 7th Int. Conf. on Plasma-Surface Interactions (Princeton, U.S.A., 1986) J. Nucl. Mater. **145 & 146** (1987)
[11] M G von Hellermann et al, Proc. of the Workshop on Basic and Advanced Fusion Plasma Diagn. Techn., Varenna, Italy (1986)
[12] A Tanga et al, Proc. of the 11th Int. Conf. on Plasma Physics and Controlled Nuclear Fusion Research, Kyoto, Japan, 1986
[13] M Ali Mahdavi et al., Phys. Rev. Lett. **47** (1981) 1602

Plasma Boundary Phenomena

The physics of the scrape off layer (SOL) plasma outside the last closed flux surface defined by material or magnetic limiters (X-point) is relevant to the release and transport of impurities; to recycling, retention, and transport of hydrogen isotopes; and to the energy confinement properties of the core plasma.

Studies of this edge plasma and surrounding structures have progressed along several lines. A survey of the SOL parameters has been undertaken, using Langmuir probes, to produce detailed temperature and density scalings for OH, RF, and NB plasmas and a more limited data set during the single-null X-point discharges showing the transition from L to H mode. The impurity coverage on the limiters and its spatial distribution have been analysed in terms of erosion and deposition in the SOL, of which parameters are known. An erosion rate of up to 10^{22} atoms $m^{-2}.s^{-1}$ is found [1], showing that the steady state distributions on areas close to the plasma edge are rapidly established since the measured impurity coverage is around 10^{21} atom m^{-2}. The calculated erosion gives an impurity influx which is in broad agreement with spectroscopic measurements. Progress has been made in understanding the overall gas inventory, wall pumping and other phenomena affecting the evolution of the total plasma particle content during the pulse. It has been shown that plasma edge parameters, plasma transport rates and material properties all affect wall pumping.

The plasma in the SOL interacts with the limiters. By folding the power flux with the mushroom shape of the limiter, two discrete interaction zones appear. The separation between the zones depends on the e-folding length of the power flux λ_p. Using charge coupled device (CCD) or diode array TV cameras with narrow-bandwidth filters, these zones can be automatically recorded and directly monitored with good temporal and spatial resolution throughout plasma pulses. After analysis, the surface temperature, the spatial distribution of H_α and impurity lines can be obtained [2]. Real-time display of this information allows an impression of events occurring near the plasma edge.

More detailed measurements of limiter surface temperature have been made using a cooled 32x32 pixel IR array, which is sensitive at longer wavelengths than CCD cameras. This enables the evaluation of the power loading on the limiters throughout the pulse [3]. However, since the power flow to the other limiters, the RF antennae and inner wall has not been measured, it has been possible to construct an overall power balance based on these measurements.

The CCD camera was also used to observe carbon tiles installed near the separatrix of single-null X-point plasmas to assess excessive power loading. Initially, power loading at the inner and outer intersections of the flux surfaces appeared to be approximately equal but, after pulses with intense NB heating, tiles around the inner intersection point were displaced so that they received a much higher heat load. This was confirmed by post-mortem examination. The maximum power loading inferred was 1.5kW cm^{-2} for the highest NB power and 850W cm^{-2} during the H-mode.

To investigate the relation between the plasma conditions in the edge and the global plasma properties, a survey of SOL parameters using Langmuir probes has been completed over a wide range of plasma currents, I_p, average densities $\langle n_e \rangle$ and additional heating powers. For steady state conditions (i.e. at the end of the plasma current flat-top and total input power constant), it was found (see Fig.42(a)) that the edge density scaled as $\langle n_e \rangle^2$ and the edge temperature as $\langle n_e \rangle^{-2}$ (see Fig.42(b)). In the scaling of the edge temperature, the dependence on I_p reflects the variation of the power conducted to the SOL, while the scaling of the edge density depends mainly on the ionisation of the neutral hydrogen and therefore did not show a strong relation to I_p. For constant I_p and q, it was found experimentally that the density e-folding length λ_{n_e} was inependent of $\langle n_e \rangle$, which suggested that the perpendicular diffusion coefficient, $D_\perp$, varied according to $T_e^{1/2}$.

The power deposited on the limiters calculated from SOL parameters $P_d = \gamma(T_e) I_{sat} T_e$, showed a linear variation with $P_\Omega - P_{rad}$ but, however, P_d was smaller in magnitude by a factor $\times 2$. This is attributed to the uncertainty in the extrapolation to the last closed flux surface. From consistent measurements at three different poloidal and toroidal locations, it is concluded that in JET with eight discrete limiters and three RF antennae at the outer midplane, the SOL appears to be reasonably uniform.

During ICRH heating, all parameters in the SOL increased. This increase was almost independent of radius but rose with ICRH power. Radial profiles showed exponential decays with an e-folding length which increased with the ICRH power. The observed increase in the density e-folding length could be due to an increase in the perpendicular diffusion $D_\perp$ and/or increased ionisation in the SOL [4]. The rise time of particle flux increase in the boundary was 0.25-3ms at ICRH switch-on. This short timescale was also observed for C-III and H_α radiation. In contrast, the central density rose only slowly, suggesting a fuelling from the edge. The edge temperature rise could be a result of direct heating of the edge by ICRH power [4,5].

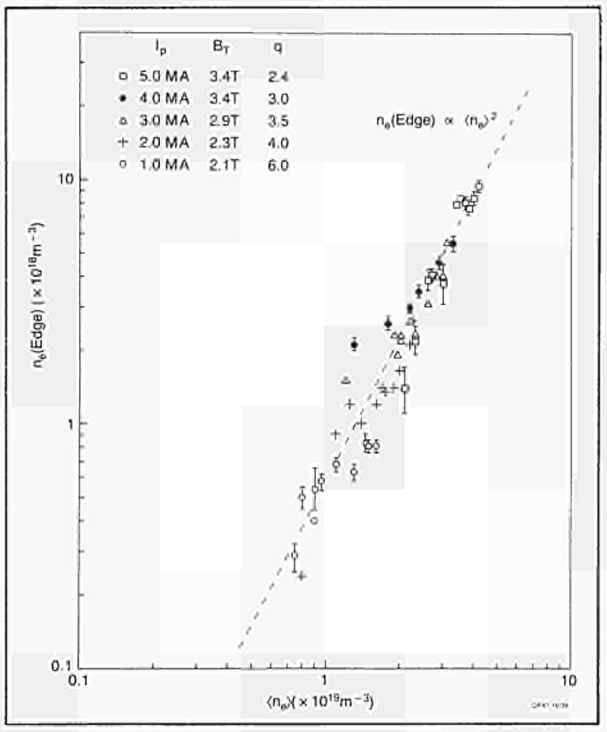

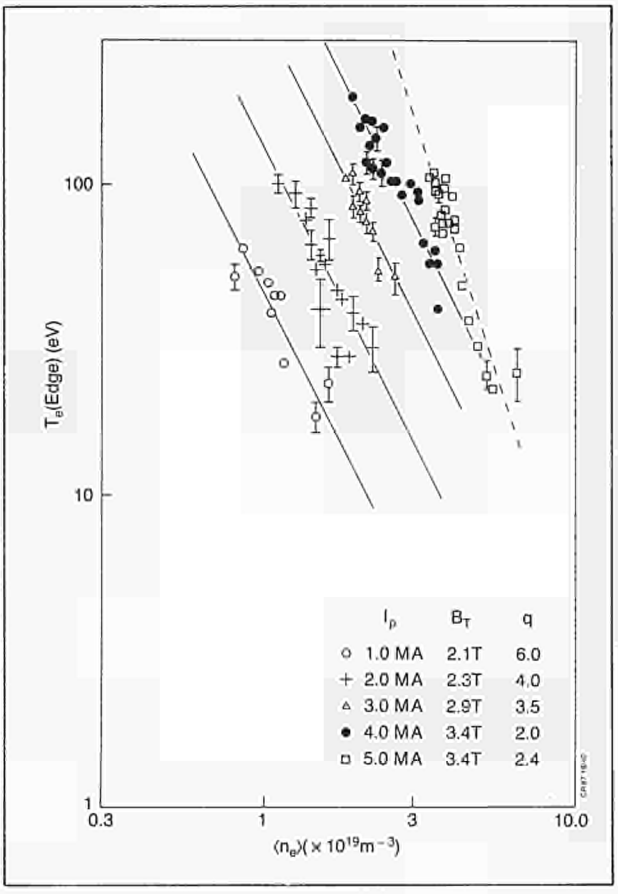

Fig.42: The scaling of (a) edge density and (b) edge temperature as a function of average density $<n_e>$ for different plasma currents (I_p).

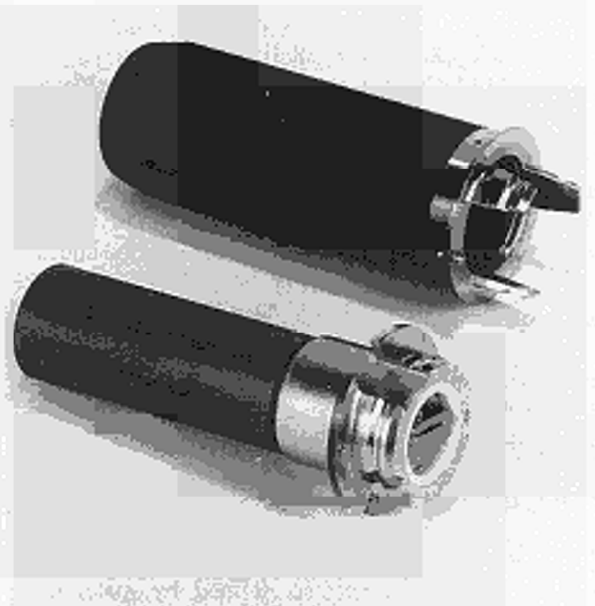

Fig.43: Standard time resolving collector probe after exposure. Shield and collector separated.

During NB heating, it is found that no flattening of the SOL profiles was observed in contrast to ICRH heating. All SOL parameters rose approximately linearly with NB power. No general scaling with $<n_e>$ could be found, since in limiter NB heated discharges, no steady state was obtained.

During the year, time resolved collector probes have been exposed for the first time in the boundary plasma region using the Fast Transfer System (FTS) which inserts probes horizontally and the Plasma Boundary Probe System (PBPS), which inserts probes vertically. In each case, the probes are cylinders of 31.5mm diameter which can rotate during a plasma pulse within a shield of 50mm OD with two longitudinal slits one facing the ion drift direction and one the electron drift direction. The first probes exposed had carbon shields and collectors, but due to the interest in carbon impurity measurements in the plasma boundary, some silicon collector/inconel shield probes have been exposed. Fig.43 shows a carbon probe that was exposed to four discharges. The image of the slit at the bottom represents the start up phase on the ion-drift side, the upper one represents the ramp down phase from the electron drift side. The probe was only rotated during the current flat-top.

Preliminary observations from analysis of collectors and shields are:

(a) the carbon flux in the boundary is about two orders of magnitude greater than metal impurities flux for ohmic discharges and about one order of magnitude greater than the oxygen detected;

(b) during the flat-top and close to the plasma (<50mm), the carbon flux collected is about 10% of the ion flux;

(c) the majority of carbon deposited deep in the boundary (>100mm), exceeds the ion fluence predicted from extrapolated Langmuir probe measurements and implies a different mechanism

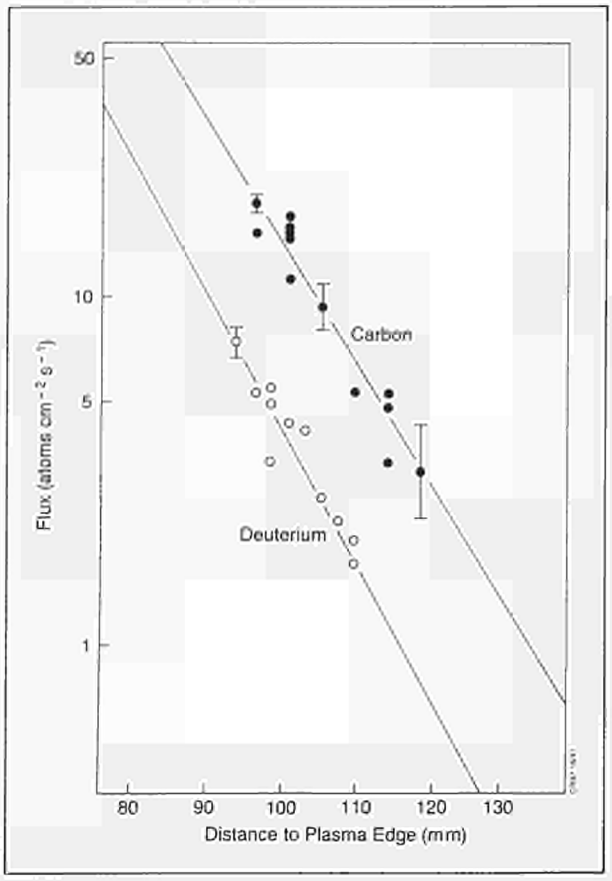

Fig.44: Deuterium and carbon concentration on a silicon collector exposed using the Fast Transfer System to a single 5MA discharge (Pulse No:10903), as a function of distance to the plasma.

may be operating in this region particularly during rampdown;

(d) the amount of deuterium observed is a constant fraction of the amount of carbon observed for ohmic discharges suggesting co-deposition of D and C [6]. (However, this may not be true for RF-heated discharges). Fig.44 shows the amounts of D and C observed on a silicon collector exposed to a I_p=5MA discharge;

(e) during ramp down (including pushing the plasma to the inner wall to control density), flat distributions were observed for all the detected species, indicating relatively high fluxes deep into the boundary region.

A further set of long-term samples was exposed in the vessel during 1986 and together with samples of 1986 limiters and inner wall tiles will be examined during early 1987. Additional analyses of samples from 1985 have confirmed that the average surface (up to ~1μm) concentration of deuterium over the vessel graphite components or vessel wall is about 5×10^{17} atoms cm^{-2}: this gives a total near surface content of about 10^{24} atoms of deuterium after the operations phase, and the hydrogen content is of a similar order. Much of this gas can be regarded as available for recycling and is of importance for plasma density control. Together with the large amounts of hydrogenic material present deeper (though at lower concentrations) in the walls and tiles, it is also of importance for the tritium inventory when tritium operations commence. About 10% of all the gas fed into the vessel would be necessary to account for the deuterium found trapped in the near surface region in these post-mortem analyses.

Gas fuelled plasmas moved to the carbon tiles on the inner wall are frequently characterised by an initially rapid decay of the electron density, with a 1s characteristic time. Pellet-fuelled inner-wall (PFIW) discharges have shown two distinct modes of density behaviour when no gas puffing is added. These are illustrated in Fig.45. Of the fourteen PFIW plasmas, ten behaved as in Fig.45(b), where the volume-averaged electron density $\langle n_e \rangle$ decreased back to its pre-pellet value in a "scallop-like" fashion and the other four discharges showed a much slower and smoother density decay which did not result in $\langle n_e \rangle$ returning to its pre-pellet value (see Fig.45(a)) [7].

The decrease of $\langle n_e \rangle$, whether slow or rapid, requires two sequential processes: the transport of plasma ions to material surfaces; and then the adsorbtion or absorption of these plasma ions by the materials. The scallop-wise density decay is always accompanied by synchronous minor disruptions at the q=2 surface. These cause increases in n_e and T_e at the edge giving rise to higher wall fluxes with increased penetration of the hydrogen into the carbon. During the temperature spikes, the H_α emission from the inner wall tiles decrease by a factor ×4. Modelling of the density behaviour shows that changes in plasma edge parameters, plasma transport rate and material properties are required to simulate the observations.

With neither pellet fuelling nor gas feed during the steady-state portion of a discharge, the plasma density is

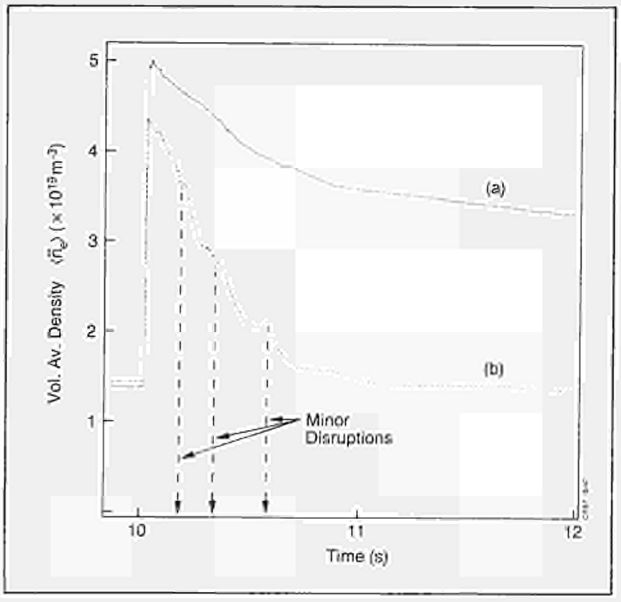

Fig.45: Two discharges with pellet fuelling, showing volume averaged electron density as function of time; a) slow decay and residual density remaining; b) scallop-like decay and no density remaining.

relatively constant if the plasma position, current, and configuration are held fixed. This indicates a global recycling near unity. For the same gas prefill, the steady-state density is lower in X-point and inner-wall discharges than in the outer limiter discharges. Movement of the plasma, during a single discharge, back and forth between the inner wall and outer limiters results in the total inventory of particles in the plasma oscillating between a high level (outer-limiter operation) and a low level (inner-wall operation). This behaviour shows no saturation, and is repeatable for tens of consecutive discharges, equivalent to hydrogen fluences in excess of $10^{18}cm^{-2}$ and $10^{17}cm^{-2}$ on the outer limiters and inner wall, respectively. The density decay during the transfer of the plasma to the inner wall corresponds to a maximum pumping speed of the inner wall of $3x10^{21}$ atoms.s^{-1}. An example of such a discharge is shown in Fig.46. In parallel, investigations have started to relate the total gas inventory and especially the gas released after the pulse to the observed pumping. Peak pressures of $6x10^{-5}$mbar are observed about 20s after the pulse giving maximum release of $3x10^{19}$atoms.s^{-1}. These investigations are continuing.

The standard bath-tub [8] or local mixing [9] models of hydrogen trapping in graphite are not adequate to explain hydrogen retention for more than a single discharge with typical parameters of $\tau_p \sim 0.3$s and $N_T \sim 3x10^{21}$ electrons.

Two models are being studied, which can independently cause the observed retention of hydrogen for tens of sequential inner wall discharges. The first model assumes that, due to the finite dwell-time of a hydrogen atom which has been implanted into a material surface and then diffuses out, pumping is exhibited by increasing the dynamically retained H-inventory by increasing the dwell-time. The capacity of removing particles from the plasma depends then on the diffusion coefficient of hydrogen in the respective wall areas with which the plasma ions and neutrals mainly interact. Assuming the same material properties for inner wall and limiters, the important parameter is the respective surface temperature during plasma shots being larger on the limiter than on the inner wall, and subsequently a smaller diffusion coefficient at the inner wall and a large pumping there.

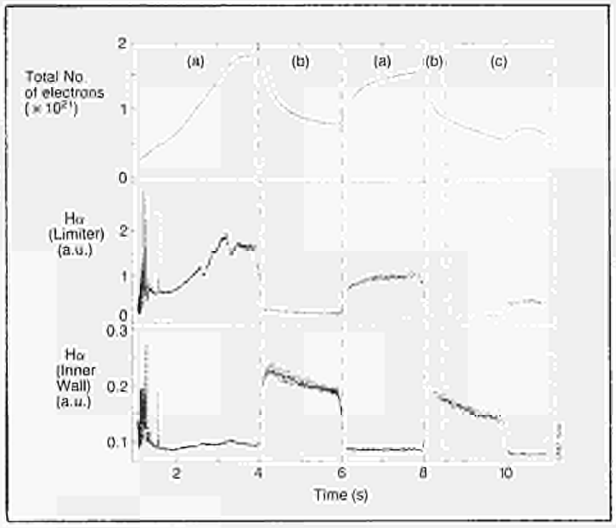

Fig.46: Example of an OH discharge which was started on the limiter (a) and moved twice between the limiters and inner wall (b). Total volume averaged density $<n_e>$ and H_α wall/limiter emissions are shown.

The second model assumes that the level of plasma density depends on two things: a source, which is assumed to be outgassing from the wall due to implantation of gas during the plasma breakdown phase, and sinks, at the limiter or the inner wall, which however have different pumping strengths. These remove particles by erosion of carbon and subsequent codeposition of C and H forming saturated H-C layers. The most important difference between this model and the proceeding one is that removed particles are not recoverable. Any later increase of density can only be due to the outgassing from the wall or limiters.

So far there is experimental evidence for both of these models suggesting the idea that both processes may take place, depending on the prevailing conditions of wall and plasma.

References

[1] G. McCracken and J. Ehrenberg, 7th International Conference on Plasma Surface Interactions in Controlled Fusion Devices, Princeton, 1986 and Journal of Nucl. Mat. **145-147** (1987)

[2] C. Lowry, Workshop on High Temperature Plasma Diagnostics, Varenna, Italy, 1986;

[3] D. Summers, Workshop on High Temperature Plasma Diagnostics, Varenna, Italy, 1986;

[4] S.K. Erents and J.A. Tagle, 7th International Conference on Plasma Surface Interactions in Controlled Fusion Devices Princeton, 1986, 100;

[5] H.W. Brinkschulte, 13th European Conference on Controlled Fusion and Plasma Heating, Schliersee, 1986;

[6] R. Behrisch and J. Ehrenberg, 7th International Conference on Plasma Surface Interactions in Controlled Fusion Devices, Princeton, 1986, 213;

[7] A. Gondhalekar, 11th International Conference on Plasma Physics and Controlled Nuclear Fusion Research, Kyoto, Japan (1986) and JET Report JET-P(86)44;

[8] G.M. McCracken et al, Nuclear Fusion, **18** (1978) 35;

[9] B.L. Doyle et al, J. Nucl. Mat., **93** and **94** (1980) 551.

MHD Activity and Stabilisation

Introduction

The study of sawtooth behaviour has been separated from the general mhd topic and the remaining work has mainly concentrated on understanding and controlling disruptions.

There has been a clarification of the boundaries of operation imposed by disruptions both for the operational aspects and the theoretical model. Basically, there are three types of disruption on JET.

a) the high density disruption at $q_\psi > 3$ when the density is so high that a radiation contraction of the plasma column takes place;
b) the low-q disruption, when q_ψ falls to 2.0 ± 0.1;
c) the rise-phase disruption when dI/dt is too large.

In the basic model describing the density limit disruptions, the radiation increases with density until ~ 100% of the power input is radiated. The plasma then contracts and ultimately becomes disruptively mhd unstable. From this model, it was expected that the density limit would be increased with additional heating. This increase is found to occur for neutral beam heating but not for RF heating. The explanation of the RF results seems to be that impurities and neutral gas are introduced when RF is applied.

The mhd instability phase of the disruption has been studied both theoretically and experimentally. Numerical simulations of the radiation contraction show that, beyond a certain point, the m=1 internal mode and the m=2 tearing mode drive each other more unstable leading to a disruption. Experimentally, the growth of the external magnetic fluctuation level seems consistent with the tearing mode model but internal measurements of soft X-ray emission and electron temperature have not provided clear evidence of the associated magnetic island.

Since disruptions at large plasma currents might cause damage to the machine, a study is being made of their stabilisation using magnetic feedback. A system is being designed in which the magnetic fluctuation of the instability is detected and the appropriate time dependent correcting field is applied.

Other areas of work include the study of the low mode number mhd activity and of the lower amplitude broadband fluctuations at higher frequency.

Disruptions

High Density Disruptions

The total radiation level rises to 100% of the total input power. The ohmic contribution to the total power also increases but not enough to stay above the radiated power.

The thickness of the radiation mantle grows until just before the energy quench when it reaches the $q_\psi = 2$ surface. The radiation mantle is often poloidally asymmetric forming a so-called marfe.

The electron temperature in the outer region falls and the T_e-profile shrinks, the T_e-gradient inside the radiative layer staying more or less the same. Apparently, the current density profile follows, since l_i increases. This explains the increase in ohmic input power during the precursor phase. When the radiative layer has come close to the q=2 surface, an m=2, n=1 instability arises, at first rotating toroidally and later locking in space. At this time, the temperature gradient is steep inside the q=2 surface and flat outside.

These results make it plausible that a radiation induced column contraction underlies the high density disruption. Thus, if one can predict the radiation loss one can predict the high density limit.

A theoretical model has been developed on this basis and the critical density is found to be [1,2]

$$\bar{n}_{crit} = 3.5 \times 10^{16} \left[\frac{P_\Omega + P_{AH}}{Z_{eff} - m^{-3}} \frac{q_{cyl}}{R_{ab}(q_{cyl} - 2a/b)} \right]^{1/2}$$

where P_Ω and P_{AH} are the ohmic and additional heating powers, R is the major radius, a and b are the horizontal and vertical half-widths of the plasma and $q_{cyl} = 2\pi abB_T / \mu_0 IR$. As Z_{eff} approaches unity, other edge cooling mechanisms become dominant. This relation holds for practically all high density disruptions in JET for ohmic and additionally heated discharges.

Exceptions are found for disruptions after pellet injection, in the current decay phase which showed a higher limit, and in the current rise phase which showed a lower limit than predicted from the above formula. Although the radiation was 100% of the input power in these cases, the explanation has been found in the change of n(edge)/$\bar{n}$ which is remarkably insensitive to external parameters during the flat-top but decreases for pellet-injection and during the current decay and increases during the current rise.

The mhd mechanism of the energy quench phase is not yet completely clear. The rotating predominantly m=2, n=1 mode measured by magnetic diagnostics shows up in temperature variations at the q=2 magnetic surface and soft X-ray emission variations which have a more "kink" type than "tearing" mode character. According to a model for tearing mode islands based on thermal isolation [3,4], one would have expected a cool spot in the island. However, at present, the spatial resolution is not quite sufficient to settle this question. In the actual quench, the kinetic plasma energy is redistributed over the cross-section in about 1 ms whilst the subsequent loss of energy to the limiter/wall takes place in a surprisingly fast 200μs.

Disruption at the $q_\psi = 2$ Boundary

The planned 7MA operation of JET at $q_\psi = 2.2$-2.4 requires modifications to the poloidal field system to be implemented in the 1987 shutdown. Information on the stability of such a low q discharge is needed and has been obtained from a half value analogue plasma at 3.5MA/1.7T with the same shape: a=1.2m; R=2.97m; b/a=1.35. This resulted in discharges with $q_\psi = 2.2$ and $q_{cyl} = 1.5$. Excursions to disruption boundaries were made in the second half of the pulse by: (i) increasing the density and (ii) lowering q_ψ by reduction in cross-section towards the limiter or to the inner wall or by reducing elongation, by lowering the toroidal field or by increasing the current.

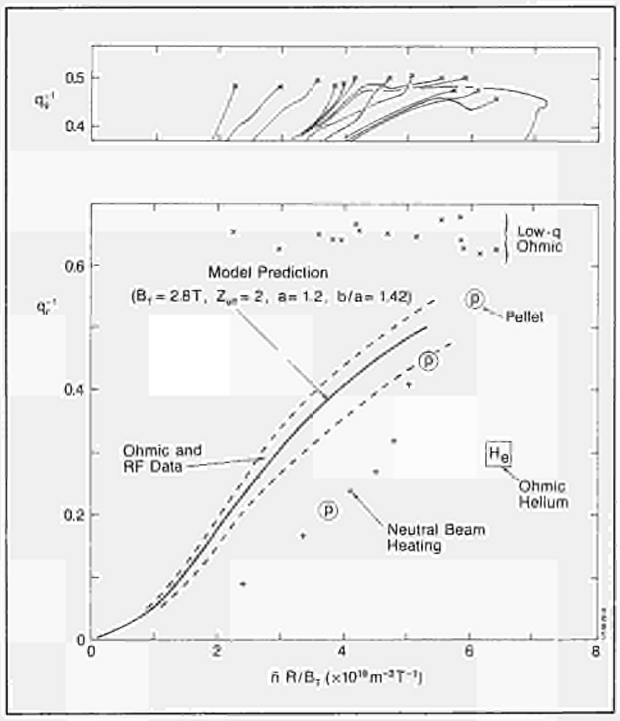

Fig.47: Hugill diagram summarising the limits of stable operation in JET. The preliminary results of single pellet injection into ohmic discharges which did not disrupt are also shown. The low q limit is more consistently plotted in terms of q_ψ as shown in the upper figure.

The results are shown by the excursions in the Hugill-diagram of Fig.47. The following observations are made:

a) every excursion to $q_\psi = 2.0 \pm 0.1$ led to a disruption except one pulse with b/a>1.5. A sawtooth collapse is likely to initiate the disruption, the radiative collapse and column contraction being absent;
b) very high densities were reached at $q_\psi = 2.2$ leading to a record Murakami parameter of $\bar{n}R/B = 7.2 \times 10^{19} m^{-2} T^{-1}$. However, even at these high densities a radiative column contraction was not observed with P_{rad}/P_Ω typically only 70%;
c) the discharges with q_ψ just above 2.0 were most reproducible. The sawtooth inversion radius was 55% of the minor radius. The energy confinement time of 450ms agreed well with the general scaling law of JET [1];
d) a mode lock occurred shortly (10ms) before the energy quench at a variable position in contrast with high density disruption where mode-locks are often observed more than 1s before the quench. The mhd phenomena during the quench were similar.

The similarity of the mhd phenomena during the quench between q=2 and high density disruptions suggests that both types of disruption may be due to surface kink instabilities. The high density disruption should then be seen as a current carrying column with q=2 at its current boundary surrounded by a passive, almost currentless cold radiative layer acting as a gaseous limiter.

Disruptions during the Current Rise

Depending on current rise rate, constant or expanding aperture and density programming, hard disruptions sometimes occur during the rise-phase. The rate of incidence is highest in the band of q_ψ values between three and four but is unrelated to the density limit. The probability of this type of disruption increases with $\delta I/\delta t$ and for a growing aperture such that q_ψ (t) stays more or less constant. Also, these type of disruptions are preceeded by a spatially locked mode but the radiation loss is modest. A speculative explanation is that skin effects keep the current-profile flat except at the very edge, whilst the magnetic topology does not change since q_ψ is kept constant.

MHD Activity

Direct information about MHD instabilities has been greatly improved this year due to the addition of hardware monitors of discrete oscillating mode activity for n=1, 2 and 3 modes, locked n=1 activity providing both the amplitude and phase of the locked mode, and the very recent commissioning of the latest ECE system which provides very fine spatial resolution in the radial direction. The discrete n monitors allow immediate toroidal mode identification of any low n MHD activity present in the discharge. They have been particularly valuable in identifying the large n=2 activity often observed after monster sawteeth. Before density limit disruptions, an oscillating mode grows and locks at a finite amplitude, making it invisible on an ordinary coil signal. The locked mode monitors then take over from the oscillating monitors showing that the mode, though locked in space, continues to grow until the disruption occurs. Finally, very recent data from the high spatial resolution ECE system has provided detailed information on the size and character of the oscillating modes observed before the mode locks. Such information may enable us to determine the precise nature of the disruptive instability.

Fluctuation Studies

Low amplitude broadband fluctuations have been observed in visible light and magnetic measurements performed at the plasma edge [5].

The visible light emitted by the plasma edge has been recorded by soft X-ray diode arrays with a sampling rate of 200kHz. Fluctuations have a total normalised amplitude, $\tilde{n}_e/\langle n_e \rangle$, of up to 10^{-2}. Their amplitude decreases with frequency from 0 to 100kHz. Correlation analysis indicates that the fluctuations generally have a toroidal velocity of about $5 \times 10^3 ms^{-1}$ in the electron diamagnetic drift direction, independent of frequency, and have high m numbers ($10 < m < 100$).

The magnetic signal is detected by poloidal field pick-up coils located inside the torus wall. It is either recorded with a sampling rate of 40kHz and analysed by cross-correlation techniques or directly monitored by eight hardware band-pass filters (from 5 to 56kHz). The total normalised amplitude of the incoherent fluctuations measured at the plasma edge is typically $\tilde{B}_\theta/\langle B_\theta \rangle$

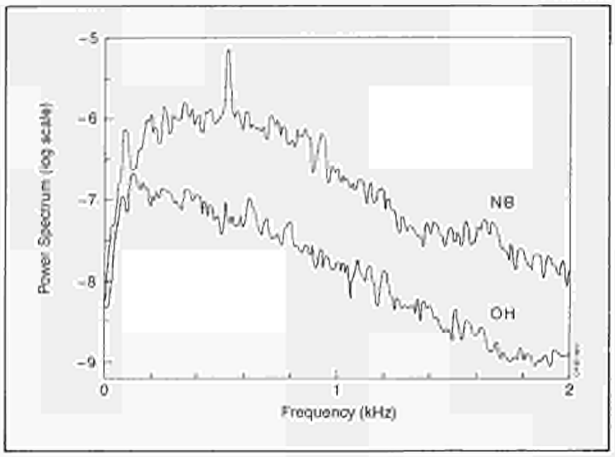

Fig.48: Frequency spectrum of $\tilde{B}_\theta$ for two similar pulses during ohmic (OH) and neutral beam (NBI) heating.

$\sim 10^{-4}$-10^{-5}. Their frequency spectrum covers the range studied here and monotically decreases with frequency: $B_\theta \propto f^{-1.5 \pm 0.5}$ above 2kHz. The incoherent fluctuations are strongly correlated along the magnetic field lines. In the frequency band 2-5kHz, their poloidal and toroidal numbers are $0<m<8$ and $0<n<4$ respectively and they are often observed to propagate in the electron diamagnetic drift direction with a velocity of 4-6x10^3ms^{-1}, independent of additional power and frequency. In the range 15-20kHz, there is no propagation and the dominant modes are $2<m<q_\psi$ and $0<n<2$, the largest mode have m equal to the integer below q_ψ at the edge. In limiter discharges, these fluctuations are not observed to be directly correlated with visible light data.

The magnetic fluctuation level above 2kHz increases with additional heating. This is shown in Fig.48, which compares the results obtained for two similar discharges, on being heated by 4MW of NB power.

Data analysis indicates that the inverse of the confinement time τ_E^{-1} linearly increases with the square of $\tilde{B}_{\theta N}$ ($=\tilde{B}_\theta.B_T/B_\theta$) for the frequency range 10-56kHz. The case of fluctuations around 40kHz is shown in Fig.49. A more detailed study of the relationship between $\tilde{B}_{\theta N}$ and the confinement is now in progress.

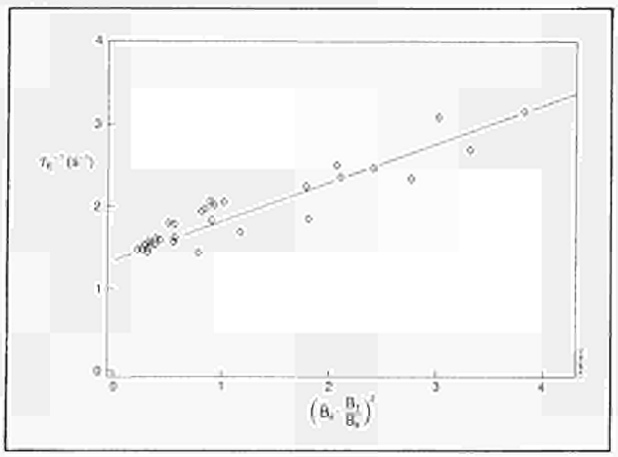

Fig.49: τ_E^{-1} versus $(\tilde{B}_{\theta N})^2$.

Although the pick-up coils are mainly sensitive to the plasma edge, the above observations suggest that a part of the detected random fluctuations might be induced by magnetic perturbations located more deeply inside the plasma.

Stabilisation of Disruptions

In JET, as in all other tokamaks, the minimum safety factor q (and thus the maximum discharge current) and the maximum plasma density for stable operation are limited by disruptions. Whilst these limits will permit stable operation of JET up to currents of 7MA, considerable care is needed to programme the plasma density decay at the end of the discharge, particularly after additional heating is turned off, in order to avoid disruptions occurring at high plasma currents. If these occur too frequently there may be a risk of damage to the JET machine.

Proposals are being studied to try to stabilise disruptions using magnetic feedback. The present design study would consist of four pairs of large coils mounted inside the vacuum vessel. Each coil pair would consist of a coil at the top and bottom of the vessel, extending poloidally down to the belt limiters, and toroidally covering two octants. The coils will be connected via vacuum feedthroughs to powerful amplifying power supplies which form part of a feedback loop. The disruptions are preceeded by slowly growing magnetic perturbations (frequency $\sim$ 1kHz) which are generated by the growth of mhd instability. These perturbations are detected by diagnostic pick-up coils and these signals after suitable real-time processing will be used as error signals for the feedback loop. Thus the feedback coils will induce a correcting magnetic field which will suppress the growth of the instability. The detailed design of this system is proceeding with installation planned for the 1988 shutdown.

References

[1] F.C. Schüller et al, 12th Euro. Conf. Fusion and Plasma Physics, Budapest, Hungary (1985);

[2] K. Behringer et al, Paper A-IV-1, 11th Int. Conf. on Plasma Physics and Controlled Nuclear Fusion Research, Kyoto, Japan (1986).

[3] P.H. Rebut and M. Hugon, Plasma Physics and Controlled Nuclear Fusion Research (Proc. 10th Int. Conf., London, U.K., 1984) Vol.2, IAEA, Vienna (1985) 197.

[4] J. Wesson et al, Controlled Fusion and Plasma Physics (Proc. 12th Eur. Conf., Budapest, Hungary, 1985) Vol.I 147.

[5] M. Malacarne an P.A. Duperrex, JET Report JET-P(86)31, JET Contributed papers at the International Workshop on Small Scale Turbulence and Anomalous Transport in Magnetised Plasmas (Cargèse, Italy, July 1986).

Sawteeth Oscillations

Sawtooth oscillations have for many years been recognized as one of the fundamental instabilities of tokamak plasmas. However, experimental measurements have shown, that several aspects of the sawteeth observed in JET are substantially at variance with predictions of the conventional theory. Experimental and theoretical studies are underway to elucidate the true nature of the instability. Furthermore, when powerful auxiliary heating is applied in JET, sawteeth dominate the behaviour of the central plasma, limiting temperature and density. This has drawn attention to the deleterious effects of this instability in reactor plasmas, and, as a consequence, considerable efforts have been devoted to understanding recent observations, which indicate that sawteeth may be spontaneously stabilised for long periods up to 1.6s (3 to 5 energy confinement times).

Analysis of soft X-ray emission and electron cyclotron emission (ECE) during a sawtooth collapse has shown that the dynamics of the collapse are significantly different from those predicted by models based on tearing modes which give rise to magnetic islands. Tomographic reconstruction of contours of local X-ray emissivity show that the collapse begins as a displacement of the plasma core caused by the formation of a cold plasma 'bubble'. As shown in Fig.50, the hot core then deforms into a crescent shape, and it is the rotation of this structure which is commonly observed as successor oscillations. Studies with a toroidally and poloidally spaced ECE array have confirmed that the collapse has an m=n=1 structure.

Discrepancies between experimental results and existing models have led to a reexamination of the theory of the m=1 mode. Using the assumption that $|1-q| \sim 10^{-2}$ in the central region of the plasma, a new theory of the sawtooth instability has been developed, which is based on a quasi-interchange mode. Results of a non-linear numerical calculation of the evolution of this mode are shown in Fig.51. The striking similarities between the predicted behaviour of the instability and that observed experimentally (Fig.50) are clear. In addition, quantitative analysis of plasma flows associated

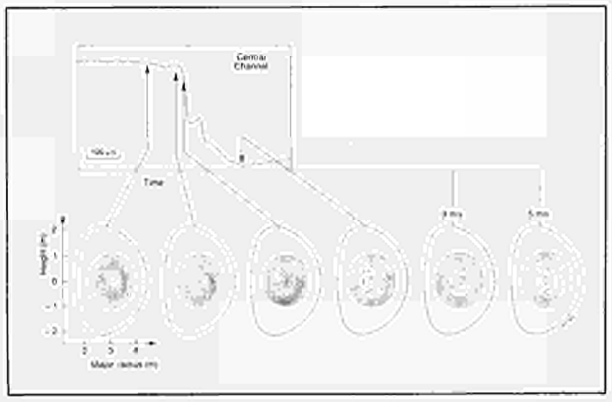

Fig.50: Contours of local soft X-ray emissivity during a sawtooth collapse.

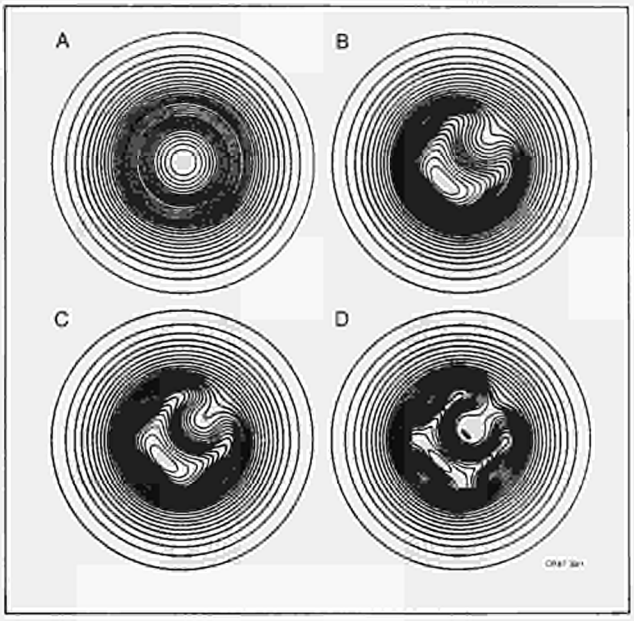

Fig.51: Results of a non-linear calculation of the evolution of a quasi-interchange mode in cylindrical geometry with $q_0=1.005$. Several stages (A to D) in the evolution of plasma flux surfaces during a sawtooth collapse are shown.

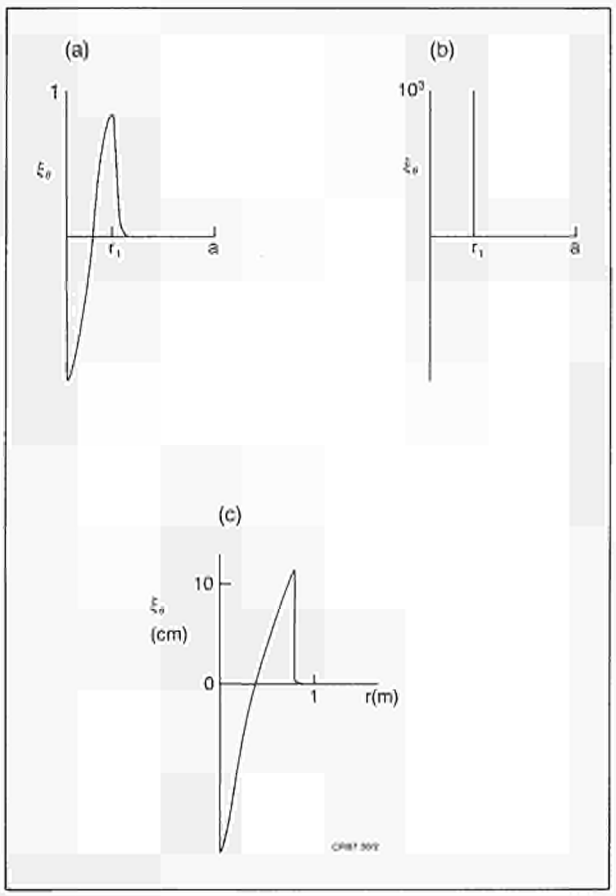

Fig.52: Comparison of the azimuthal displacement eigenfunctions $\xi(\theta)$ for several cases: (a) quasi-interchange mode; (b) tearing mode; (c) experimentally observed instability.

with this instability has yielded excellent agreement between theoretical and experimental results. Fig.52 shows the azimuthal displacement eigenfunctions for three cases:

- quasi-interchange mode;
- tearing mode;
- the experimental instability (derived from soft X-ray measurements).

A wide variety of mhd activity is observed during sawteeth in JET. In particular, 'partial' sawteeth are common: these have certain features of the full sawtooth collapse but with little or no effect on central temperature. Previously, it has been thought that this phenomenon was due to a magnetic reconnection occurring away from the plasma axis. However, detailed measurements have revealed significant similarities between the full and partial sawtooth instabilities. Fig.53 shows the behaviour of the electron temperature in the central region of the plasma during (a) a full sawtooth and (b) a partial sawtooth. In both cases, the crucial feature is the rapid displacement of the central core during a time period ~100μs. In the full collapse, the displacement is substantial (~25cm), and ultimately leads to a flattening of the central profile. However, during the partial collapse, the displacement of the central core is smaller (~5cm), and the core rapidly returns to its original position. There is little residual effect on the central temperature, but a flattening of the temperature profile occurs around the sawtooth inversion radius. A second type of partial sawtooth has also been identified which occurs on a slower timescale (~10ms) and which gives rise to a small inversion and a redistribution of the location of the accompanying m=1 activity.

Studies of the scaling of the sawtooth period with plasma parameters have continued. It has been confirmed that, during the ohmic phase, the sawtooth period scales linearly with plasma density, and that, the sawtooth inversion radius is found to be inversely proportional to the edge safety factor. No satisfactory systematic scaling law for the sawtooth period has been obtained for additional heating conditions. This probably reflects the complexity of the experimental situation, since such

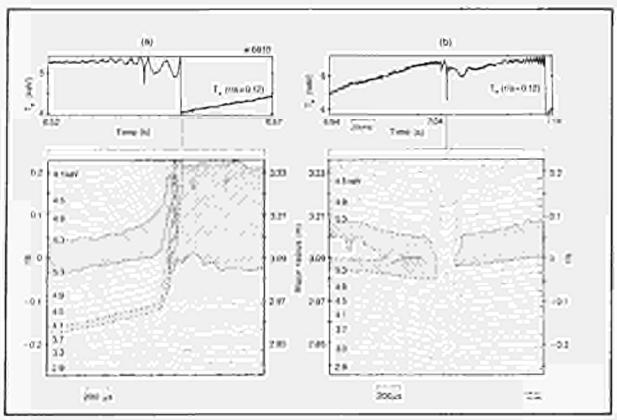

Fig.53: Temperature contours in the central region of the plasma during (a) a full sawtooth collapse; (b) a partial sawtooth collapse.

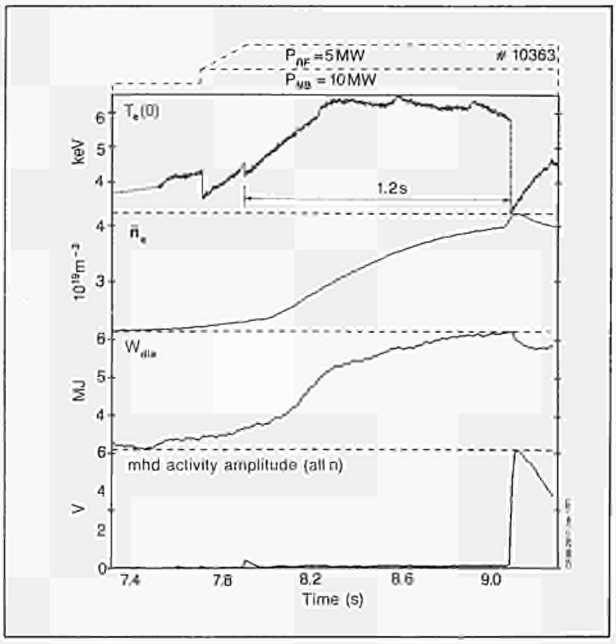

Fig.54: Evolution of central temperature $T_e(0)$, line average electron density, total plasma energy from diamagnetic measurements W_{dia} and the amplitude of total MHD activity during a 5MA discharge with a 'monster' sawtooth lasting 1.2s.

factors as the heating profile, direction of neutral beam injection and changes in impurity levels become important.

During additional heating experiments, some sawteeth have very long duration (up to 1.6s). These were first observed in relatively low current discharges (I_p=2MA) with combined additional heating (NBI and ICRH). However, similar phenomena ('monster' sawteeth) have now been observed at high current (I_p=5MA), as shown in Fig.54, and in discharges with ICRF heating alone. There is also preliminary evidence that they occur in discharges with NBI heating alone. These sawteeth are characterised by unusually low levels of coherent m=1 activity, suggesting that they are not simply sawteeth with particularly long periods, but that the m=1 mode has been stabilised. The possible stabilisation mechanisms are under investigation, but at present the strongest possibility is that additional heating leads to a favourable modification of the current profile. A major advantage of this regime is that the quiescent sawtooth-free period lasts 3-5 energy confinement times, permitting analysis of the benefits of full sawtooth stabilisation on transport and confinement. While there may be a small (~20%) improvement in the global energy confinement time during these stable periods, present studies suggest that the principal benefits will be the increased fusion power production (due to the peaking of temperature and density profiles), and the reduction in the losses of high energy particles which usually occur at sawtooth collapses.

Experiments with injected pellets have revealed a remarkable new phenomenon which may yield important diagnostic information on the q-profile within the

plasma. A very localised density and temperature perturbation with m=n=1 topology has been observed following the injection of a pellet. This perturbation exists for a very long time (>2s) and appears to be associated with the q=1 surface. Similar structures are seen with m=3, n=2 symmetry at the q=3/2 surface. Fig.28 shows the behaviour of the soft X-ray emission profile during pellet injection. The spike of emission associated with the ablation of the pellet identifies the time of injection, and the snake-like modulation of the soft X-ray emission which remains is clear. As the location of this modulation shifts considerably in minor radius ($\Delta/r \sim 40\%$) during a sawtooth period, it may be inferred that the q=1 surface undergoes a similar shift. However, the long duration of the perturbation does require further investigation. Since the particle confinement time is much shorter (~ 0.3s) than the lifetime of the snake, the most likely explanation is that the plasma perturbation induced by pellet injection gives access to a new non-axisymmetric equilibrium involving a magnetic island.

Separatrix Experiments

The main objectives of measurements with a magnetic separatrix (or X-Point) configuration are (i) to compare the global confinement characteristics of separatrix and limiter discharges and (ii) to study the conditions for the creation of a high density, highly radiative, cool plasma region near the X-point capable of screening and isolating the bulk plasma. In these configurations, the plasma is detached from both the limiter and the inner wall and recycling occurs in an open divertor region near the X-point. Experiments have been carried out with plasma currents up to 2.5MA in a double null (DN) and up to 3.0MA in the single null (SN) configurations. A maximum additional power of 9MW has been injected (D° into D^+) into the confined plasmas. Compared to similar limiter discharges, the thermal energy content of single null (SN) X-point discharges is roughly a factor x2 higher. Plasmas with even modest separation between X-point and target plates show typical signatures of H-mode discharges. Multi-channel infrared interferometer measurements provide evidence of the formation of a high density diverted plasma with average density $\sim 10^{20}m^{-3}$, an order of magnitude higher than the main plasma. Measurements with a bolometer camera array show that, in high density discharges with additional power, up to 40% of the input power is radiated within a $\sim 0.2x0.2m^2$ toroidal region around the torus.

Formation of a Magnetic Separatrix

A magnetic separatrix can be formed within the vacuum vessel of JET using the multipolar field normally used to control the elongation and triangularity of the plasma

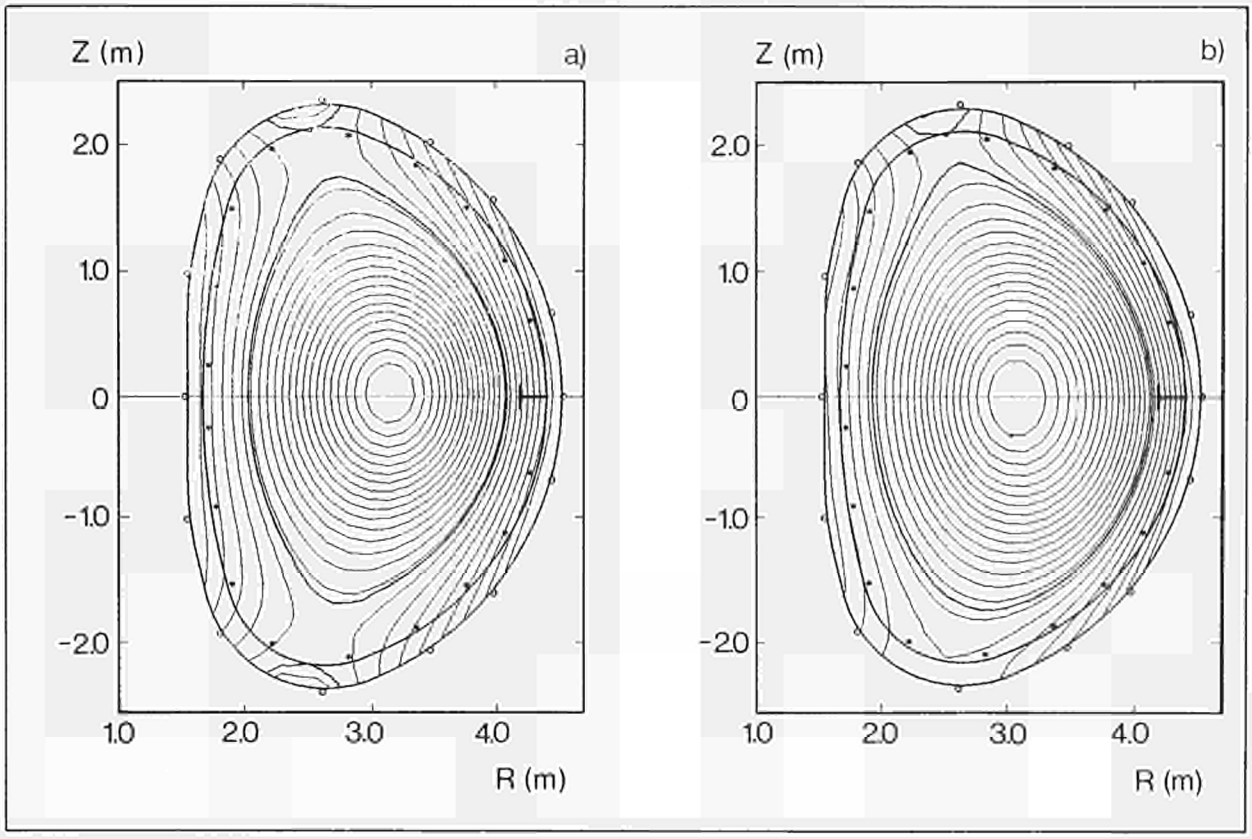

Fig.55(a): Flux plot of a double null configuration. Plasma current = 2MA, toroidal field = 2.8T, average electron density = $3x10^{19}m^{-3}$, poloidal beta = 0.44, plasma elongation = 1.8.
(b): Flux plot of a single null configuration. Plasma current = 2MA, toroidal field = 2.2T, average electron density = $3x10^{19}m^{-3}$, poloidal beta = 0.6, plasma elongation = 1.65 (Pulse No:10237, t=13.5s).

cross-section. In the DN configuration, the present poloidal field equipment allows operation at plasma currents up to 2.5MA. The resulting plasma has an elongation of 1.8; the vertical position is unstable with an open loop growth rate of $150s^{-1}$.

The separation between the X-point and the graphite target plates is a linear function of the current in the shaping coils. For the DN configuration in Fig.55a, the separation is ~0.10m. In the SN configuration (Fig.55b), plasma currents up to 3.0MA have been produced with an elongation of 1.65; the growth rate of the vertical instability is substantially smaller than for the DN configuration.

The maximum separation between X-point and the target plates obtained so far at 2MA has been ~0.13m with the SN configuration and may be increased by displacing the magnetic axis below the midplane. The radial position of the null point is held constant during the discharge, to within a few cms. The distance between the separatrix and the antennae for ICRH is finely controlled by the radial position feedback system and this can allow good coupling of ICRH to the plasma. In both DN and SN configurations, Langmuir probe measurements give the e-folding length for the decay of the density and temperature at 0.06m and 0.10m, respectively.

Location of the separatrix has been corroborated to within a few cms by observations with a bolometer camera array and TV cameras and by the separation between the erosion marks on the graphite target tiles. The magnetic configuration is only slightly sensitive to changes in the internal parameters, such as the poloidal beta and internal inductance.

The formation of a magnetic separatrix within the vacuum vessel produces a significant change in the discharge characteristics. For separations between the plasma and the limiter larger than 0.07m, deuterium recycling (monitored by D_α signals) shifts from the limiters to small regions near the X-points. Both the D_α monitors and TV observations in the near infra-red show the formation of bright regions (~0.2m across) coinciding with the X-points. In high density DN discharges, only one bright region is observed. The application of a radial magnetic field shifts the toroidal plasma column vertically and the bright region moves correspondingly, indicating that the formation of only a single bright region is not connected with slight up-down asymmetries in the poloidal field. Simultaneous with the shift in recycling characteristics, stronger gas-fuelling is needed to sustain the average plasma density; Z_{eff} is reduced; and the bolometer camera array shows a decrease in bulk plasma radiation and a large increase in the radiation from the X-point region.

Improved Confinement with Additional Heating

Double Null (DN) X-point discharges show an energy confinement time some 20-30% higher than similar limiter or inner wall discharges. However, no clear H-mode transition was identified at the power levels available. Recent experiments have therefore concentrated on the SN configuration. First results show a

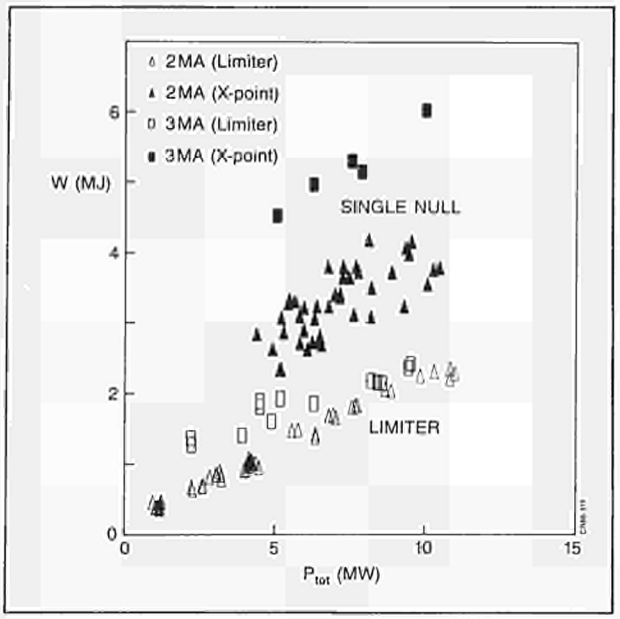

Fig.56: Total plasma thermal energy content as measured by diamagnetic loop versus total input power for single null and limiter configurations.

substantial improvement of energy confinement in SN X-point discharges compared to similar limiter or inner wall discharges. The experiments have been carried out with neutral beam injection heating with up to 9MW power. Ion cyclotron heating has been applied in some of the shots with a power of up to 4MW (but keeping the total input power, $P_t = P_\Omega + P_{NBI} + P_{RF} < 10MW$).

In Fig.56, the variation of the total plasma thermal energy content with total input power P_t for two series of SN X-point discharges at plasma currents of 2MA and 3MA is compared with the corresponding data sets for limiter discharges. While the separation of the X-point and the target plates is ~0.13m at $I_p = 2MA$, this is reduced to ~0.05m at $I_p = 3MA$ and is then rather close to the wall. For either plasma current, the energy content of the X-point discharges is up to a factor x2 larger than that of the corresponding limiter discharge with the same additional power. In general, the trend with increasing heating power is also similar in all cases.

The electron temperatures (and also the central ion temperatures) for such an X-point H-mode plasma are substantially higher than for a limiter plasma with the same parameters of plasma density, plasma current, toroidal field and P_t (see Fig.57). It should be noted that the electron temperature profile is broader, with the edge temperature at R=4.0m being ~2.5 times higher.

As already mentioned, the SN discharges at $I_p = 2MA$ exhibit clear indications of a transition into an H-mode. As show in Fig.58, the edge D_α signal (f) drops and the line integrated electron density (d) increases more rapidly. These events occur shortly after the crash of a sawtooth when the edge temperature (e) increases abruptly. The power flow to the target plates (b) is substantially reduced. This phase is subject to an abrupt termination when the average density reaches some limiting values (as evidenced more clearly in other JET

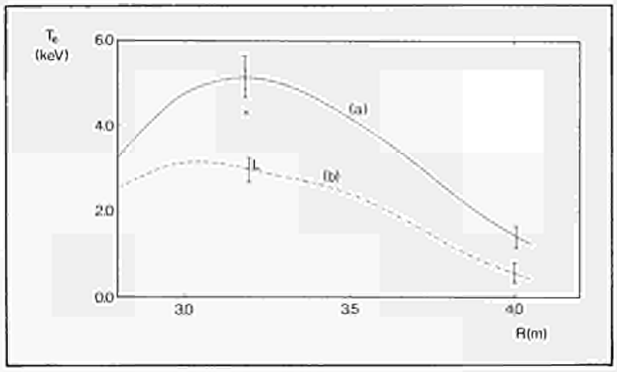

Fig.57: Electron temperature profiles a) X-point (Pulse No:10237 t=13.5s) and b) Limiter discharge (Pulse No:7709). Central ion temperatures for SN (X) and Limiter (L) discharge are also marked.

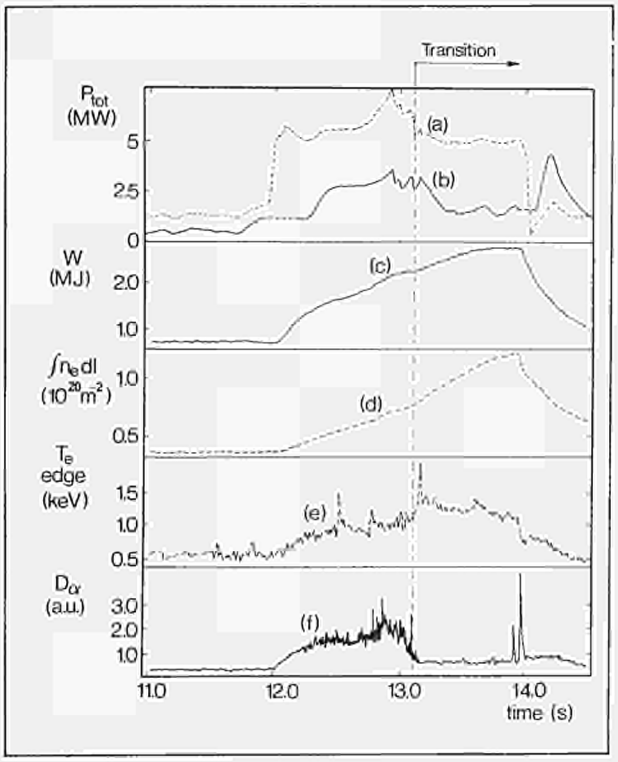

Fig.58: a) Total input power, P_{tot} for Pulse No:10237;
b) Power conducted to the target plates from bolometric analysis, P_t-P_{rad}-dW/dt;
c) Total energy content from the diamagnetic loop, W;
d) Line electron density, $\int n_e dl$;
e) Plasma edge temperature, T_e^{edge};
f) D_α signal from the plasma boundary.

Pulses where his event is not obscured by the end of additional heating). The average density, temperature and thermal energy content (c) fall in about 40ms, accompanied by a spike in the X-point radiation. During the H-phase the plasma density profile broadens with steep gradients developing at the edge.

Impurity radiation from the plasma edge (O VI, C IV) falls by about a factor x2 at the transition to the H-regime. At this time, the ICRH power ceases to be coupled to the plasma (probably due to the changed edge conditions) and the nickel influx from the antenna screen falls to zero. Nevertheless the total nickel content, as observed from the Ni XXV and Ni XXVI line intensities, remains constant indicating substantially improved confinement of metals in the interior of the plasma. However, as indicated by the soft X-ray radiation profiles, this does not lead to accumulation of impurities.

Conclusions

Separatrix operation appears to induce substantial changes in the plasma behaviour compared to limiter operation. This is possibly a result of the high shear at the boundary of the plasma. Even with a modest separation of the X-point from the target plates, a high recycling regime has been observed in this region at high plasma densities. With additional heating, the stored energy increases substantially above that for corresponding limiter discharges. A further increase in stored energy is observed for both 2MA and 3MA discharges leading to global energy confinement times in excess of 0.6s, which is about a factor x2 higher than for the corresponding limiter discharges. These discharges also exhibit other signatures (e.g., reduced edge recycling) normally associated with H-modes.

Radio Frequency Heating

The level of RF heating power on JET has been steadily improved throughout 1986, and a maximum of 8MW power coupled to the plasma for 2s has been achieved using three antennae. Two antennae were in dipole configurations with a 3MW peak power ICRF generator connected to each. These operated successfully with a constant relative phasing in preparation for current drive experiments and to test the effect of k// spectrum shaping on edge effects, coupling and power absorption. The third antenna was a monopole configuration connected to two generators by means of a purpose designed combining unit. This system launched up to 4.2MW RF power into the plasma and established that the power handling capability of the antenna would be sufficient for the full performance system of 8 antennae fed by 32MW total generator output.

The majority of experiments have been carried out with H and ^{3}He minority heating in deuterium plasmas and H minority in ^{3}He plasmas. A wide variety of conditions have been studied, such as outer limiter, inner wall, single-null X-point discharges, combined operation with neutral beams and pellet injection. The minority fundamental cyclotron resonance was usually placed at the plasma centre ('on-axis' heating) although some 'off-axis' heating studies have been made. The most significant results [1,2] are summarised below.

The central role played by minority ions in the wave absorption process has been firmly established. One piece of impressive evidence is indicated in Fig.59 which shows results of experiments which included both ^{3}He and H minority ions in a D^+ plasma. As the RF was

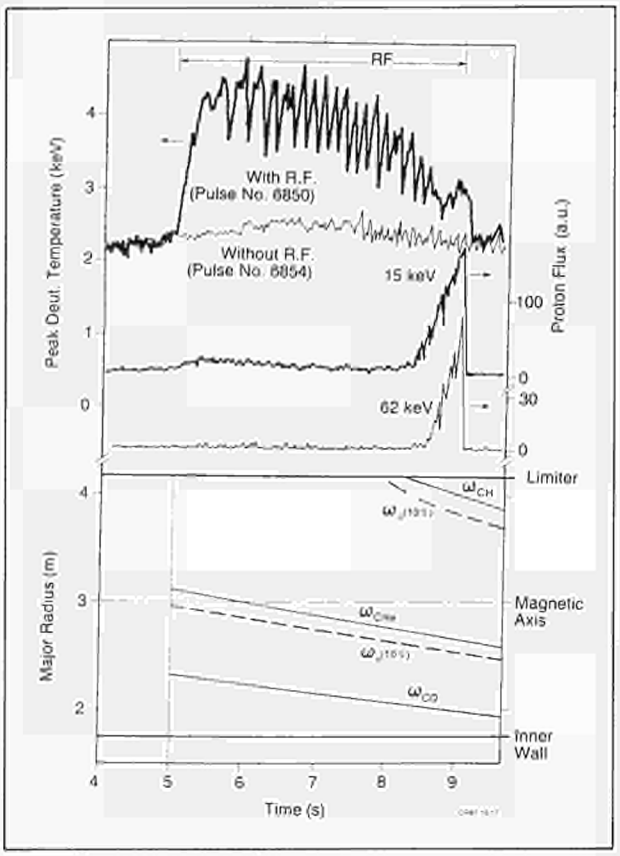

Fig.59(a) Time evolution of the central deuteron temperature with and without 3.4MW ICRF, and of the proton flux at 15keV and 62keV during a toroidal field ramp down. The plasma current was maintained constant at 2MA.
(b) Radial position of the proton and ^{3}He cyclotron layers during the above pulse. The approximate position of the corresponding hybrid layers is indicated by the dotted lines.

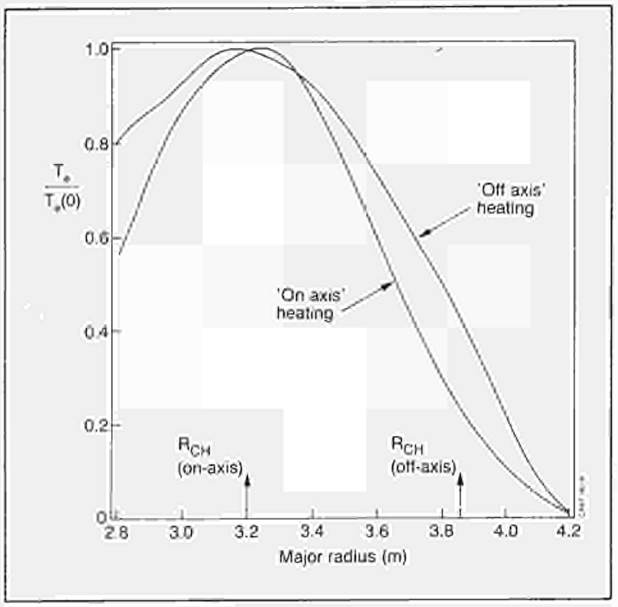

Fig.60 Normalised electron temperature profiles during on-axis and off-axis ICRF heating. The respective cyclotron resonance positions are indicated.

switched on, the ^{3}He resonance was on-axis and the central deuterium temperature $T_D(0)$ showed strong sawteeth, characteristic of central heating. At this time, the H minority resonance was outside the plasma. During the RF pulse the toroidal field was ramped down which moved the ^{3}He minority resonance position away from the axis and $T_D(0)$ decreased. Eventually, the toroidal field became sufficiently low to allow the H minority resonance into the plasma. When this occurred, 100keV protons were detected with a time delay which increased with increasing energy, in accordance with theory. Theory also predicted a transition from bulk ion heating to electron heating as the energy of the minority species was raised by increasing the RF power. The transition was expected to occur at a lower power for (H)D than for (^{3}He)D and this difference was seen as the RF power was raised above 4MW.

The effect on heating efficiency of varying the cyclotron resonance layer has been studied for the (H)D scenario. The maximum increase in central electron temperature, global stored energy, and D-D reaction rate were all achieved with the ion-ion hybrid resonance inside the sawtooth inversion radius. The volume average electron temperature was insensitive to resonance position but off-axis heating produced a broader T_e profile than did on-axis heating, contrary to the concept of 'profile consistency' but confirmed by recent (H)^{3}He off-axis heating experiments (see Fig.60).

Power deposition profiles have been deduced by amplitude modulating the ICRF and observing the corresponding time behaviour of the electron temperature, T_E, to obtain the rate of change of electron energy content. The local change in T_e was measured with a 12 channel ECE polychromator with the signal-to-noise ratio enhanced by box-car techniques. The power density transferred to the electrons is shown in Figs.61(a) and 61(b) for central and off-axis heating, respectively. In each case, the maximum lies close to the minority cyclotron resonance and the width is ~60cm for on-axis heating and ~20cm for off-axis heating. Fig.61 also compares the results with ray tracing calculations. There is excellent agreement in the off-axis case but the central heating is somewhat broader than predicted, possibly due to redistribution by sawtooth activity.

Combined deuterium neutral beam injection and hydrogen minority ICRF experiments in D^+ plasmas have indicated that RF power can be coupled to the beam ions at the harmonic resonance. The distribution function of the beam ions is shown in Fig.62. The distribution shape above the beam energy (62keV) was increased from 5keV to 16keV on applying 6.9MW of 32MHz RF with the H minority resonance on axis. Fokker-Planck calculations indicated that a substantial fraction of the RF power was coupled to the beam ions and predict that the effect should enhance both neutral beam current drive and fusion reactivity.

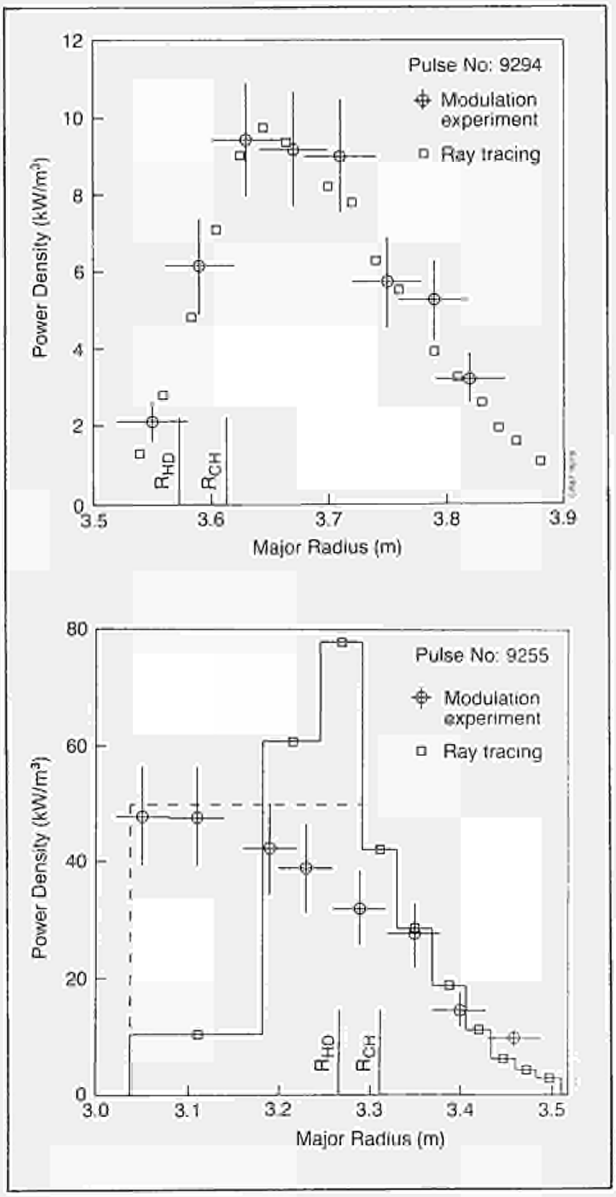

Fig.61 Comparison of experimental and theoretical power deposition profiles for a) on-axis heating and b) off-axis heating using the H(D) scenario.

High power central RF heating, both alone and in conjunction with neutral beam heating, has produced plasmas that have central electron temperatures as high as 7.2keV and are free from internal disruptions for times ~1s. The longest such period (~1.6s) was obtained with H minority heating in a ^{3}He plasma ($n_e = 3 \times 10^{19} m^{-3}$) using 7MW RF power at 32MHz, $B_T = 2.1T$ and 2MA. The central electron temperature time evolution is shown in Fig.63, indicating saturation at about 6keV. However, the plasma had not attained steady state as the density continued to rise throughout the RF pulse. Other characteristics of this new regime included reduced MHD activity and an enhancement of global energy confinement (~20%) compared to discharges with normal sawteeth-free behaviour. Studies of this regime should help to quantify the benefits of sawtooth stabilisation for producing significant α-particle heating.

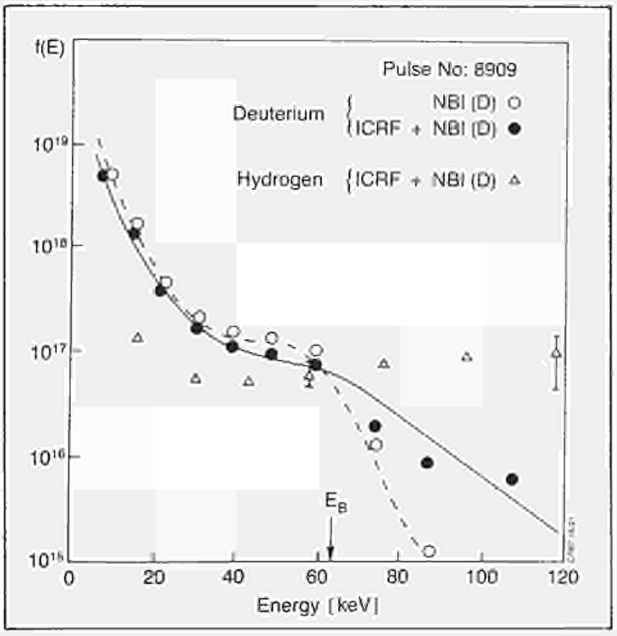

Fig.62 Distribution function for the D^+ beam ions deduced from neutral particle analysis. The open circles refer to no RF and the full circles to 6.9MW RF power. The triangles show the H minority species distribution.

Towards the end of the 1986 experimental period, some RF heating studies were carried out in single null X-point discharges using the (H)^{3}He scheme. The sawtooth-free regime was accessed and preliminary analysis indicated that the increase in stored energy and global confinement time were somewhat better (~10%) than in corresponding limiter discharges. However, H-mode plasmas have not been achieved with RF only, possibly because the power into the plasma is limited by a large antenna-plasma separation. This situation will be improved as more ICRF power becomes available in the next period of operation.

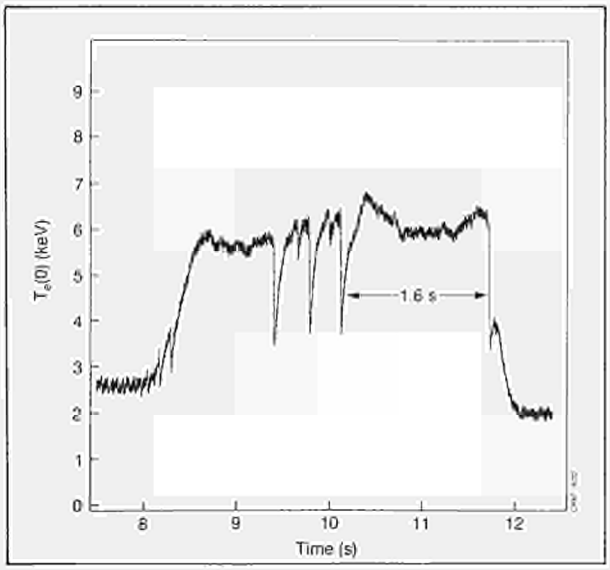

Fig.63 Time evolution of central electron temperature during central (H)^{3}He minority ICRF heating showing the formation of prolonged sawtooth-free periods.

References

[1] P.P. Lallia et al, Plasma Physics and Controlled Fusion, **28**(1986)1211.

[2] J. Jacquinot et al, Proceedings of 11th IAEA International Conference on Plasma Physics and Controlled Nuclear Fusion Research, Kyoto, Japan, 1986.

Neutral Beam Heating

During the first experimental campaign started in January 1986, hydrogen (H°) beams were injected into deuterium (D) plasmas at energies up to 65keV and powers up to 5.5MW. In later campaigns, the injection system was switched to deuterium (D°) beams at energies up to 80keV and powers up to 10MW. The beams were used alone and in combination with ICRF heating, with a maximum total combined power up to 17MW. All possible JET plasma configurations were used as target plasmas including outboard limited plasmas; inner wall limited plasmas; and separatrix plasmas in double- and single-null configurations.

The characteristics of the experiments with H° injection into D plasmas have been reported previously [1]. The gross effects of energy confinement in additionally heated plasmas was not substantially altered in most discharges obtained in later campaigns. As described in the 1985 JET Progress Report, confinement properties of JET ohmic discharges depended on plasma density, current and toroidal field. With high power neutral beam heating (NBH), confinement times were at the low end of the range obtained with ohmic heating alone for the same values of I_p and B_T (i.e. comparable to those found in low density ohmic discharges but a factor ~x3 lower than those in high density ohmic discharges). This is illustrated in Fig.64(a), which includes data from plasmas limited by the outboard carbon limiter or inner-wall tiles and for double-null separatrix plasmas. Counter-injection beam data is also shown, which is largely the same as co-injection. Similar behaviour is observed in combined NB-ICRF heated discharges, which exhibit the same power law fit for the stored energy (W) as a function of power as that found in NBH only discharges, i.e.

$W_{NBH} = 0.27\ P_{TOT}^{0.37} I_p^{0.67} \langle n_e \rangle^{0.41} B_T^{0.24}$(MJ)

Fig.64(b) shows that this is a reasonable description for discharges with combined-heating. All discharges covered by this data exhibited typical 'L-mode' behaviour.

In plasmas with a single null separatrix configuration, a transition to a regime occurred in which the confinement time improved by ~x2, becoming comparable to typical ohmic-phase values. This behaviour has only been observed for injected beam power P_{NBH}>4.5MW, and is similar to H-mode behaviour. The confinement studies with NBH are described more fully in the section on General Plasma Characteristics and Global Confinement, and the H-mode behaviour is covered in the section on Separatrix Experiments.

The global behaviour of ion and electron temperatures has been studied in NBH plasmas. From all data (shown in Fig.65), the central ion temperature ($T_i(0)$) scales more strongly than $P_{bi}/\langle n_e \rangle$, where P_{bi} is the NBH power transferred to the ions (as calculated from beam deposition codes). However, when subdivided by plasma current, there is a tendency for $T_i(0)$ to increase with I_p at fixed values of $P_{bi}/\langle n_e \rangle$. The most effective ion heating has occurred in 3MA plasmas. At low densities, even with modest (5MW) beam powers, high ion temperatures were attained. The peak ion temperature

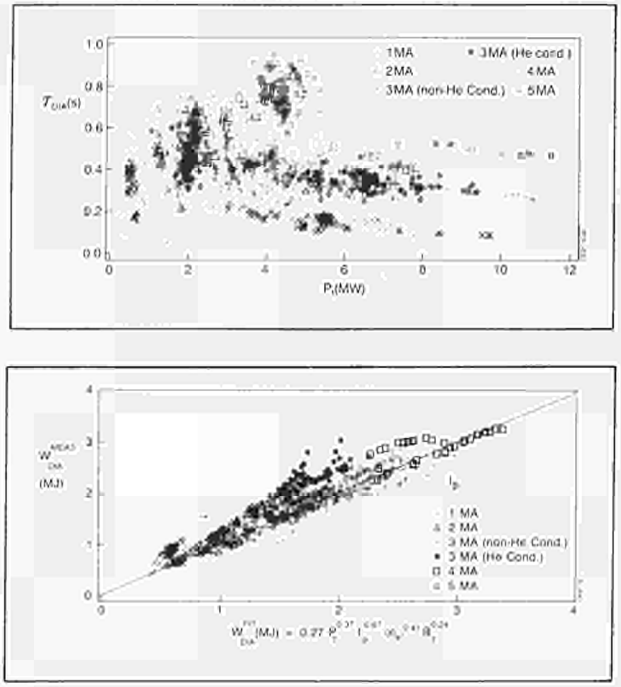

Fig.64(a) Energy confinement time (τ_E) as a function of total power into the plasma (P_{TOT}) for various plasma currents and discharge configurations for NBH plasmas. (b) Best power law fit to the stored energy in the discharge (W^{DIA}) as measured by the diamagnetic loop in NBH discharges. (Note that the 'He-conditioned' discharges are not included in the fit).

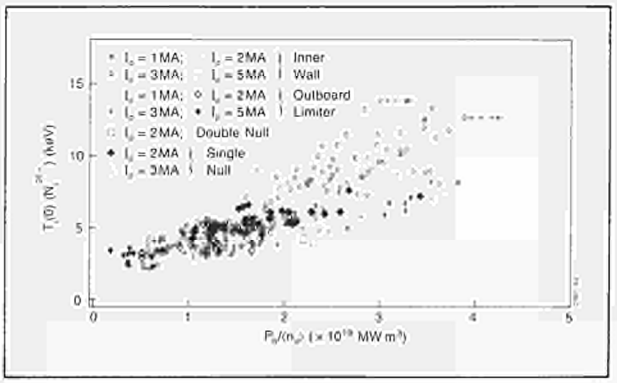

Fig.65 Central ion (Ni^{26+}) temperatures in NBH discharges as a function of code-derived power to the ions from the beams.

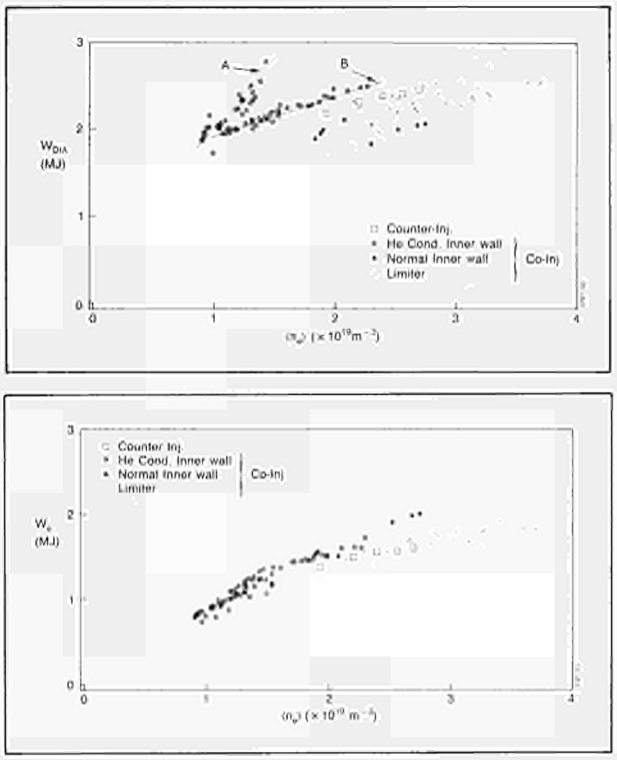

Fig.66(a) Diamagnetically-derived stored energy (W^{DIA}) in I_p=3MA, P_{NBH}=5.5(±0.5)MW plasmas as a function of volume averaged electron density.
(b) Electron stored energy (W^e) as a function of volume averaged electron density $\langle n_e \rangle$ for the discharges shown in (a).

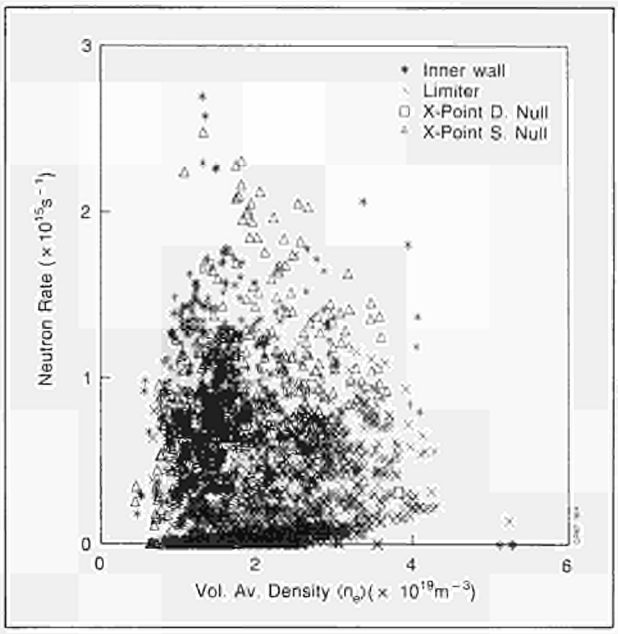

Fig.67 Neutron yield for JET NBH plasmas.

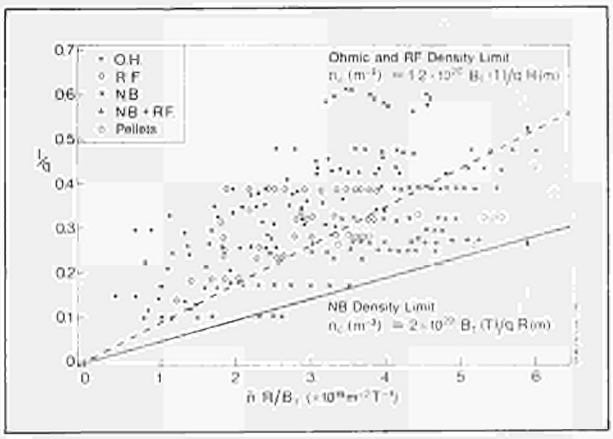

Fig.68 Hugill-Murakami diagram for JET plasmas showing extension of operating range achieved with neutral beams.

(from Doppler broadened Ni^{26+} ions) reached 14.5 ± 1.0keV, corresponding to a peak deuterium temperature of 12.5 ± 1.0keV. High $T_i(0)$ values were obtained using the inner wall carbon tiles as limiters, after special conditioning procedures with helium plasmas, producing low recycling at the wall. In these discharges, electron temperatures were higher at $T_e(0) \sim 5.5$-6.0keV. The low density He-conditioned plasmas also showed strong rotation with central toroidal velocities greater than $2x10^5 ms^{-1}$ (determined by X-ray crystal Doppler-shift spectroscopy on N_i^{26+} ions). It was also noted that a higher efficiency of electron heating takes place in NBH single-null X-point discharges with high (5keV) peak electron temperatures, occurring at very modest values of $P_{hi}/\langle n_e \rangle$.

The helium conditioned inner wall discharges showed somewhat higher stored energy, determined by diamagnetic loop (W^{DIA}), compared with the parameterised fits to the stored energy in other materially-limited discharges (see Fig.64(b)). If W^{DIA} is plotted against $\langle n_e \rangle$ for discharges with a restricted range of beam power at a fixed plasma current, the helium conditioned inner wall discharges display higher values (see Fig.66(a)). On closer inspection, these discharges appear to have W^{DIA} values in two distinct branches (A and B in Fig.66(a)). The discharges in branch A are characterised by lower recycling and all have density histories which show constant or very slowly increasing values once the initial response to the beam power has occurred. In branch B, the beam fuelling of the discharges is normal, with a strong linearly increasing density and hence more recycling. The type A discharges usually resulted from the first deuterium discharge on a newly-conditioned wall. The exact role of reduced recycling in these discharges is unclear and is under investigation. The low density helium conditioned shots resulted in the highest neutron yields obtained in JET discharges, with peak values of $2.8x10^{15} s^{-1}$ being attained. The comparative neutron yields for NBH discharges are shown in Fig.67.

A major extension to the density operating range was achieved with NBH discharges. The Hugill diagram for JET is shown in Fig.68, where the operating domain is limited by disruptive instabilities. For ohmically and RF heated discharges, the density limit was $n_e(OH/RF)(m^{-3}) = 1.2x10^{20} B_T(T)/qR(m)$, depending on plasma purity. In NBH plasmas, the limit was substantially increased to $n_e(NB)(m^{-3}) = 2.0x10^{20} B_T(T)/qR(m)$.

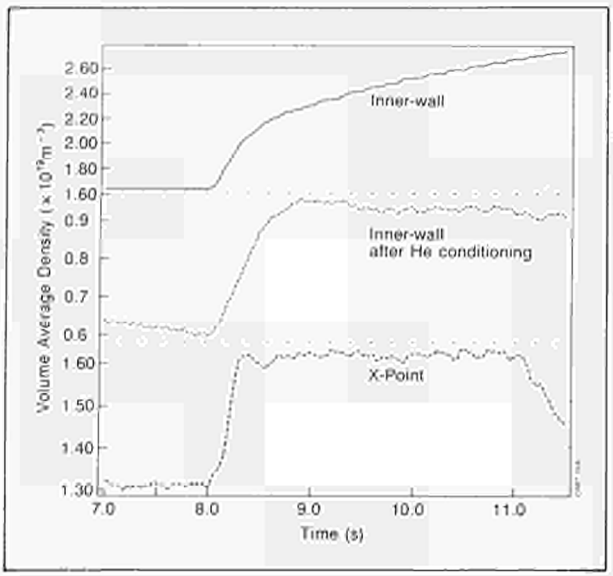

Fig.69 Time behaviour of plasma density after beam injection.

When the beams are switched off at high density, the plasma disrupts, indicating that the power input plays an important role in the disruption mechanism. This is further emphasised by the observation that NBH discharges have density limits which scale like the ohmic discharges as $\langle n \rangle_{crit} = 3.5 \times 10^{16}(P_t q_c/Z_{eff}-1)Rab(q_c-2a/b))^{1/2} m^{-3}$, where P_t is the total input power [2]. This density limit is predicted by a model in which the density limit disruption occurs when the radiated power outside the q=2 surface is equal to the power input. The increased density limit for NBH is consistent with the large increase in P_t on injection and also by the slight decrease which occurs in Z_{eff}.

A feature of the density behaviour in JET with beam heating is the near constancy of the density profiles despite an increase in the electron source rate with NBH of about two orders of magnitude [3]. Density profiles tend to broaden slightly with increasing P_{NBH} and density. The response in density behaviour is shown for three different plasma configurations in Fig.69. The behaviour of the edge recycling has been studied for these discharges and there is evidence that the sudden transient in $\langle n_e \rangle$ is due to an influx of particles from the limiter/wall surfaces. After this transient, for outboard limiter and H-mode single null discharges, the density continues to rise linearly corresponding to an asymptotic beam fuelling efficiency, ϵ, whilst for inner wall and ordinary separatrix plasmas some measure of density control is achieved. This behaviour is not yet fully understood but analysis on the outboard limited NBH discharges [4] shows that the plasma particle confinement time, τ_p, showed a generalised q dependence, which increased with increasing I_p and decreased with increasing B_T. τ_p also decreased with increasing NBH power.

In beam-driven current experiments, substantial non-inductive currents up to 0.6MA were driven in up to 3MA low-density plasmas. The currents were deduced from the plasma loop voltages, as shown in Fig.70(a). The effects were larger than those due to a change in

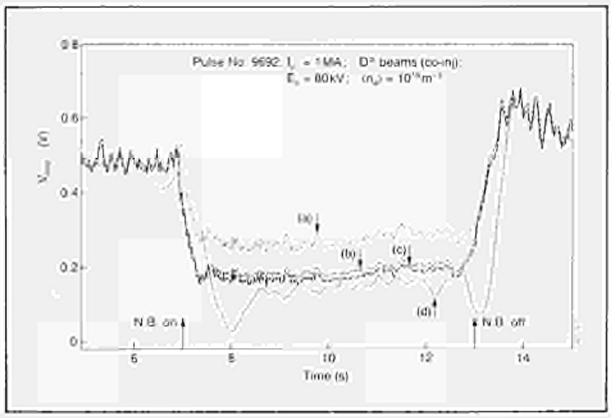

Fig.70 Measured plasma loop voltage V_{loop} during beam injection into a low current (1MA) discharge, compared with theoretical predictions for certain effects.
(a) predictions from conductivity change only;
(b) conductivity change plus beam driven current;
(c) conductivity change plus beam driven current plus bootstrap current;
(d) measured value.

plasma resistivity from the beam plasma heating. A comparison of several discharges showed good agreement with the observations if the predicted beam driven current including trapped-particle effects was taken into account. The difference between observations, and predictions is still sufficient to allow for the existence of the neo-classical 'bootstrap' current [5], predicted to be ~50kA in the Ohmic phase and ~100kA during NBH. The JET injection geometry (with beams nearer to perpendicular than parallel to the plasma current) has the effect that fast-ion trapping is an important effect in the outer regions of the plasma and thus the predicted beam driven current decreases rapidly with increasing density and resultant poorer beam penetration, as shown in Fig.71. The predicted beam driven current profile (Fig.72)) is relatively insensitive to plasma parameters and is centrally peaked, and probably more peaked than the ohmic profile.

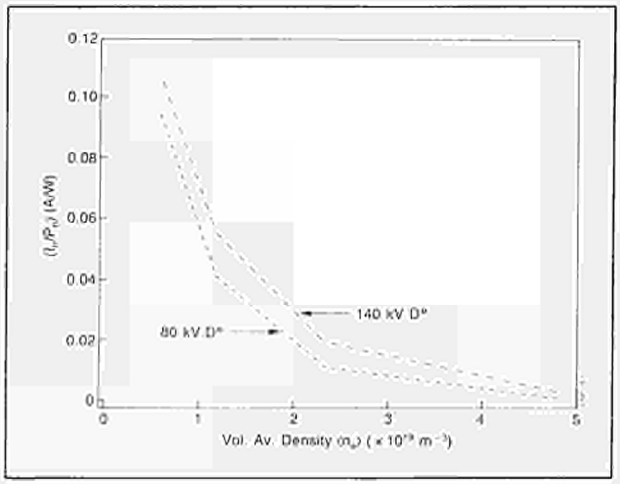

Fig.71 Predicted beam driven current per unit input beam power for 80keV and 140keV D° beams as a function of plasma density.

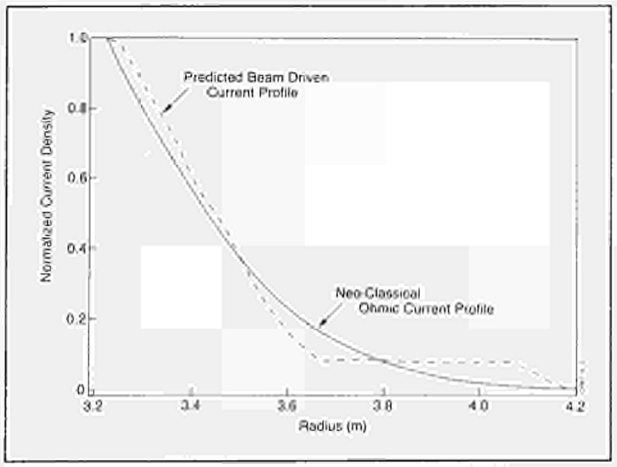

Fig. 72 Current profile for predicted beam driven current for 80keV D° beams at $<n_e>=1.2x10^{19}m^{-3}$ compared with the neo-classical ohmic current profile.

In NBH discharges, strong plasma rotation at toroidal velocities in excess of $2x10^5 ms^{-1}$ was seen. The toroidal rotation velocities show a saturating dependence on the power per particle input from the beams ($P_b/<n_e>$). The values have little dependence on plasma current alone. Only preliminary evidence exists on the radial profiles of the toroidal velocity but this indicates that the profiles are very much flatter than obtained in smaller tokamaks. Transport of momentum in the plasma is highly correlated with significant MHD activity ($\delta B_\theta/B_\theta > 10^{-4}$) as evidenced by the rapid reduction in rotation velocity at the collapse of a sawtooth (Fig.73). When a high level of MHD activity exists, the velocity profile of the fluid appears to be flat. This is evidenced by the frequency of MHD (m=1; n=1) from the centre of the discharge (r/a ~ 0.3) which appears to be the same as the (m=3,4; n=1) activity from the edge of the discharge, indicating a uniform $v_\phi(r)$ profile (see Fig.74(a)). For cases of 'significant' MHD activity, the rotational angular velocity, determined from the edge MHD frequency

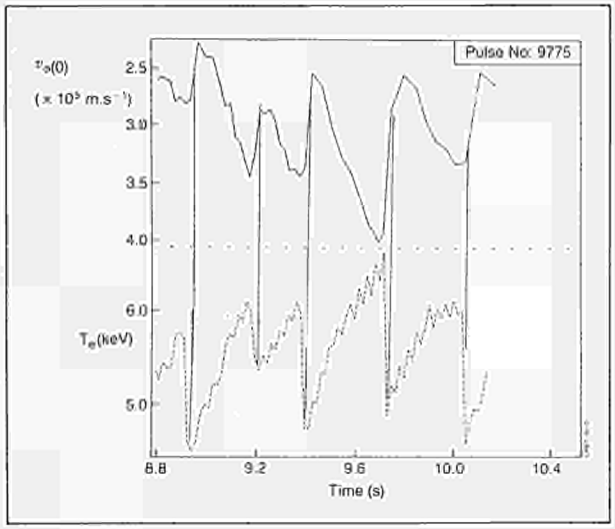

Fig. 73 Correlation of rapid collapse of central rotation velocity (as measured by X-ray crystal spectrometer) and sawtooth collapse in electron temperature.

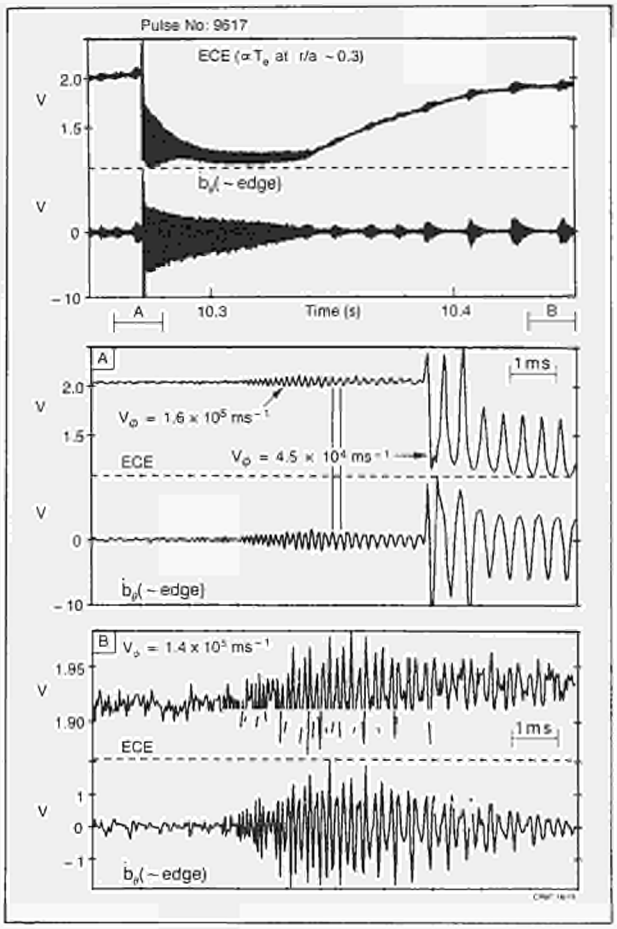

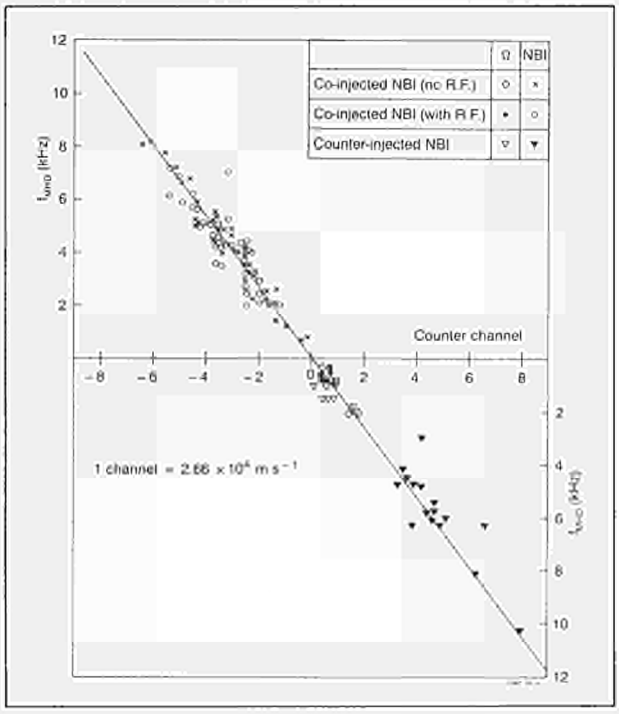

Fig. 74 Correlation in the rotation speeds inferred from central (ECE) and edge (Magnetic coils) MHD activity. (b) Frequency of MHD (m=3,4; n=1) activity for NBH discharges against central rotational velocity from the Ni^{26+} Doppler shift.

($\omega_\phi^{MHD}(R=R_o+a)$), correlates well with the central toroidal rotation velocity determined by the Doppler shift of Ni^{26+} ions ($v_\phi^{Ni}(R=R_o)$ viz:

$$2\pi f^{MHD} = \omega_\phi^{MHD}(R_o+a) \simeq R_o \cdot v_\phi^{Ni}(R_o)$$

as shown in Fig.74(b) which again indicates a relatively flat rotational velocity profile.

References

[1] 'First Results of Neutral Beam Heating on JET', The JET Team (presented by G. Duesing), 13th Eur. Conf. on Controlled Fusion and Plasma Heating (Schliersee, FRG, 1986). Plasma Physics and Controlled Fusion, **28**, 1429 (1986).

[2] D.J. Campbell et al, Proc. 11th International Conference on Plasma Physics and Controlled Nuclear Fusion Research, IAEA, Kyoto, 1986.

[3] A. Cheetham et al, 13th European Conf. on Controlled Fusion and Plasma Heating (Schliersee, FRG, 1986). Europhysics Conference Abstracts, Vol.10c Part 1 p240 (1986).

[4] 'Density Behaviour in JET Neutral Beam Heated Discharges', T.T.C. Jones, O. Kaneko, J.W. Cuthbertson, A. Gondhalekar, P.J. Lomas, P.D. Morgan, J. O'Rourke, A Staebler, D. Stork and E. Thompson, 28th APS Annual Meeting of the Division of Plasma Physics (Baltimore, 1986).

[5] R.J. Bickerton, J.W. Connor and J.B. Taylor, Nature (Physical Science) **229**, 110 (1971).

Particle Transport and Fuelling

Control of electron and ion (fuel) density and their spatial distributions are essential for optimisation of plasma performance and fusion reactivity in JET. Attention has focussed on three aspects of this question: (i) behaviour of particle fluxes at the plasma edge during Ohmic, RF and NB heating, and the contribution of the edge neutral sources to the plasma density; (ii) analysis of electron density profile and related transport in the bulk of the plasma; and (iii) fuelling of the plasma using single-shot pellet injection.

Behaviour of Edge Fluxes during Ohmic, ICRF and NBI Heating

The study is based on simultaneous measurements of absolute H_α and D_α emissivity at the graphite limiters, ICRF antennae, inner and outer walls, and the top and bottom walls of the vacuum chamber, yielding neutral fluxes ϕ. A seven chord interferometer provides the electron density distribution and the total electron content N_e. Information about H and D effluxes is derived from measurements with an array of neutral particle analysers. Optical spectroscopic measurements are employed to deduce the electron source due to, and dilution of the fuel ions by, impurity influx at the plasma edge.

In OH discharges, after a steady state in plasma density has been established during the current flat-top, the influx of H or D atoms from limiters and walls varies as n_e^2 [1]. However, the exact values of the influxes are dependent on surface conditions in the vacuum vessel. Following a few days pause in JET operations, a hysteresis behaviour is observed in the $\phi_{H,D} \propto n_e^2$ dependence during a sequence of discharges. The increase in electron content upon application of heating power is indistinguishable whether OH, ICRF, NBI or combinations of these are applied. The increase, ΔN_e, scales approximately linearly with applied heating power [2].

The injection of a D pellet into an OH discharge produces a sudden increase of density, by factors $\leqslant 2$, with corresponding increases in the H and D influxes. However, the fluxes are considerably lower than for a gas-fuelled discharge of the same density. Consequently the global particle confinement time is higher than in the non-pellet case. Also, the particle recycling behaves markedly differently. Whereas for gas-fuelled discharges $(1-R) \leq 0$, with pellet fuelling $(1-R) \geqslant 0$, which corresponds to a net removal of particles (i.e. pellet-induced pumping). A similar reduction in impurity influxes and in Z_{eff} is also observed. Eventually, on a time scale $\approx 4s$, τ_p, $(1-R)$ and Z_{eff} revert to values characteristic of gas fuelling [3].

An important limitation of ICRF heating in JET is the uncontrolled density increase during application of RF power. Influx of all neutral species from the limiters, walls and other structures increases roughly in proportion to the applied power, and Z_{eff} and the ratio P_{rad}/P_{in} remain nearly constant. Consequently, the density limit during ICRF heating is at most 10% higher than the corresponding value with OH only. The time evolution of the total electron inventory N_e can be associated with two time scales for the evolution of edge neutral fluxes. The neutral flux from the walls, and a fraction of the limiter flux ($\sim 20\%$) is released immediately ($\tau \lesssim 10ms$) upon application of ICRF power. Additional neutral flux from the limiters is released on a slower timescale approximately equal to the confinement time ($\approx 0.25s$). The total limiter flux is usually 5-10 times larger than the total wall flux. These observations may be understood in terms of some of the applied ICRF power coupling to the edge plasma and immediately reaching the wall and limiters, while a large fraction is coupled to the bulk plasma and reaches the outside on a slower timescale. Analysis of these observations for different ICRF coupling configurations, and various wall conditioning strategies is in progress.

High power neutral beam (NB) injection heating has been applied to JET plasmas in various configurations (outer limiter, inner wall, magnetic separatrix in single and double-null operation), and also differing wall conditioning histories (with and without carbonisation or He discharge conditioning). Depending on conditions, the plasma density responds to the application of NB heating in markedly different ways. Nevertheless, there is generally an initial increase in the total plasma electron content N_e, at a rate several times greater than the beam fuelling rate ϕ_{NB}, followed either by a phase in which

asymptotically $dN_e/dt \approx \phi_{NB}$, or by a steady-state phase with constant N_e for constant ϕ_{NB}. The latter behaviour implies that some areas of the exposed material surfaces effectively pump the escaping plasma particles throughout the duration of the NB pulse ($\approx$5s). This steady-state behaviour has been observed with many different operating conditions. The various kinds of observed density evolution, together with the corresponding recycling behaviour have been modelled. Using the parameters of particle confinement time in the plasma, surface residence time and surface reflection coefficient for the particles, the model describes dN_e/dt, assuming that the process is due to the disturbance of dynamic equilibrium of particles exchanged between the plasma and the surfaces surrounding the plasma [4]. The model can be generalised to describe the total plasma electron inventory N_e on application of ICRF, and pellet fuelling.

Electron Density Transport in the Bulk Plasma

A striking feature of density build-up in JET is that, in the steady state, the spatial electron density profile shape is nearly constant. The profiles can be represented as $n_e(r) = n_e(0)\{1-r^2/a^2\}^m$ where a is the minor radius of the plasma column, and $0.4 \leqslant m \leqslant 0.8$. This approximate profile constancy prevails throughout a large range of plasma parameters and variation in particle sources. The behaviour is observed when the particle source at the plasma edge ($0.8 \leqslant r/a \leqslant 1.0$) is suddenly increased by a factor 3-5 by application of ICRF power and when the particle source at the plasma centre ($0 \leqslant r/a \leqslant 0.2$) is increased by a factor $x10^{12}$ by application of NB power [2].

The rate of rise of central electron density, $dn_e(0)/dt$, during the discharge may be compared to the electron source, $n_e n_o \langle\sigma v\rangle_I$, due to ionisation of the calculated neutral density associated with the edge neutral source. Impurity contributions at most double the electron source. It is deduced that $dn_e(0)/dt$ cannot be supported by these sources alone. The rate of increase of central electron density suggests an inward convection of edge density at $V_p(r=1) \leqslant 0.2 ms^{-1}$. An analysis of refuelling of the centre of the discharge between density sawteeth affords a method of evaluating the magnitude of the pinch velocity in the region $q \leqslant 1$. The measured density sawtooth parameters have been used in the evaluation for a number of discharge conditions. The measured pinch velocity is compared to the corresponding neo-classical pinch velocity. For refuelling the centre of the plasma column between sawteeth, a pinch with the neoclassical pinch velocity is found to be sufficient. Globally, however, the required convection is much larger than, and its radial dependence different from, the neo-classical pinch [5].

For global analysis, the measured electron flux $\Gamma_e(r)$ is interpreted in terms of a model of electron transport consisting of diffusive and convective driving terms $\Gamma_e(r) = -D(r)\Delta n_e(r) + n_e(r)V_p(r)$. Analysis of electron density profile evolution from one steady state to another, induced by a sudden increase in the electron sources due to application either of ICRF or NBI heating power has yielded a volume-averaged particle diffusion coefficient $D \approx 0.6 m^2 s^{-1}$. Moreover, it is found that D(r) increases towards the plasma boundary. The corresponding inward pinch velocity $V_p(r)$ increases as r^α with $\alpha \sim 2$-3, and has a magnitude of approximately $0.2 ms^{-1}$ at half radius. Analysis has been carried out for a large number of discharges covering a wide parameter range $2.3 \leqslant B_T(T) \leqslant 3.4$, $2 \leqslant I_p(MA) \leqslant 4$, $1.5 \leqslant n_e(10^{19} m^{-3}) \leqslant 3$, $0.7 \leqslant P_{RF}(MW) \leqslant 2.2$, and $P_{NB}(MW) \leqslant 5.4$. D and V_p show a large scatter but no systematic dependence on the plasma parameters or heating mode [2,5].

A more sensitive determination of the transport coefficients in the plasma core, $0.25 \leqslant r/a \leqslant 0.7$, can be made in pellet fuelled plasmas by analysing evolution of an initially hollow profile ($dn_e/dr<0$) to a peaked profile ($dn_e/dr>0$ everywhere). Such analysis yield values of D and V which are consistent with our previous evaluations of these coefficients. More importantly, the ratio $V_p(r/a \sim 0.5)/D$, which previously did not show much variation, increases by a factor >2 immediately after pellet injection, giving more peaked electron density profiles. The peaking of the density profile becomes more pronounced with deeper pellet fuelling [3].

Pellet Fuelling of Jet Plasmas during Ohmic, ICRF and NB Heating

Pellet fuelling experiments have been performed on JET using a single-shot injector giving 4.6mm ($4.5x10^{21}$ D atoms) and 3.6mm ($2x10^{21}$ D atoms) diameter pellets with velocity $0.8 \leqslant V(kms^{-1}) \leqslant 1.2$. Most of the pellet mass was deposited at radial positions $0.25 \leqslant r/a \leqslant 0.5$. Using such pellets, regimes of higher plasma density and improved purity have become accessible. The previous high density limit obtained with ohmic heating and deuterium gas feed has been exceeded by a factor ~ 2, and $Z_{eff} < 1.5$ with $n_D/n_e \sim 1$ on axis have been obtained.

The electron density profile evolution with pellet fuelling has been examined for several different target plasma conditions and pellet deposition profiles. In JET, significant peaking of the density profile is not obtained unless there is pellet deposition in the $q \leqslant 1$ region. The magnetic configuration also plays a role. The most peaked profiles, giving $n_e(0)/n_e = 2$ with $n_e(0) = 1.2x10^{20} m^{-3}$, have been observed in a magnetic separatrix configuration formed during single-null X-point operation [3].

Detailed ablation modelling has been performed for pellet injection into OH, OH+ICRF and OH+NBI heated plasmas. A single modified neutral gas shielding model based on bulk plasma parameters successfully describes the pellet ablation data. At present levels of auxiliary heating power, no additional ablation processes associated with the application of ICRF or NBI power have been identified [3].

Novel diagnostic applications of pellet injection have been discovered. X-ray imaging methods and magnetic fluctuation measurements have revealed unique MHD phenomena caused by pellet injection. The most striking is a 'snake' oscillation, characterised by a dense cooler plasma region at the q=1 radius with m=1/n=1 helical

symmetry. The small spatial extent and long life-time of the structure imply formation of a magnetic island at q=1 location due to local cooling and associated current perturbation alone a helical flux tube. Thus, the 'snake' is a valuable monitor of the dynamic behaviour of the q=1 surface during sawtooth activity. Firstly, the radial position of the q=1 surface is deduced. Secondly, the radius of the q=1 surface is observed to grow by up to 35% during a sawtooth ramp. If the q-profile is assumed parabolic for radii less than the q=1 surface radius, then it is deduced that $q(0) \approx 0.97$ before the sawtooth crash. Thirdly, the observation that the q=1 surface exists throughout a sawtooth cycle [3] is valuable in excluding some models in the discussion of sawtooth activity.

References

[1] P.D. Morgan et al, 12th European Conference on Controlled Fusion and Plasma Physics, Budapest 1985, Europhysics Conference Abstracts, Vol.9F, Part II, p.535;

[2] A. Cheetham et al, 13th European Conference on Controlled Fusion and Plasma Physics, Schliersee 1986, Europhysics Conference Abstracts, Vol.10c, Part I, p.240;

[3] A. Gondhalekar et al, 11th IAEA Conference on Plasma Physics and Controlled Nuclear Fusion Research, Kyoto, Japan, 1986. Paper IAEA-CN-47/I-I-6;

[4] T.T.C. Jones et al, Bull. Am. Phys. Soc. **31** (1986) 1590;

[5] A. Gondhalekar et al, Bull. Am. Phys. Soc. **30** (1985) 1525.

Theory

Theoretical work at JET concentrates on the prediction of JET performance by computer simulation, the interpretation of JET data, and the application of analytic plasma theory to gain an understanding of plasma behaviour in JET.

Interpretation plays a key role in the assessment of plasma performance, and hence in optimisation studies and programme planning. Prediction work continuously checks the measured behaviour against the different computational models, and provides a basis for long term programme planning. A major role of analytic theory is to compare the observed behaviour against that expected from existing analysis, and to modify the latter when there is divergence. However, effort within JET on analytic theory has been limited, in the expectation that Visiting Scientists and staff from within the Associations would provide support by extended visits and by work under Article 14 Contracts. Valuable assistance has been provided during 1986.

The central task has been to provide a quantitative model of tokamak plasmas, with particular attention to JET. This plasma model should ultimately reproduce all important measured plasma effects (i.e. it should be a concise description of the JET experimental plasma) and allow prediction of future tokamak plasmas in JET and other devices. Although empirical prescriptions for some plasma effects can satisfy the first objective, it is obvious that analytically derived (i.e. theoretically understood) plasma physics mechanisms are preferable and finally necessary for predictions. This requires continuous review of plasma theory literature, assessment and adaptation to JET conditions of proposed theories. In addition, it is not possible to dispense with theory development, either in-house or through contracts.

The other key issue concerns the validation of the model (i.e comparison with experimental data). This task requires the identification and computation of sensitive parameters from theory. The derivation of the corresponding data banks from directly measured quantities often requires very complex mathematical and computational procedures.

Activities during 1986 can be subdivided under the following headings:

- Data Banks and Data Management Software:
- Code Development for Code Library;
- Data Interpretation;
- Modelling of JET Plasmas;
- Predictive Computations;
- Analytic Plasma Theory.

Highlights of activities in these areas are summarised below.

As a general contribution to data evaluation, a report was prepared for the Consultative Committee on the Fusion Programme (CCFP) on the status, quality and utilisation of tokamak data banks in Europe, which summarised the results of a corresponding workshop. Its main conclusions were that:

(a) data should be made available not only by JET but also by other tokamaks;

(b) a common data base management system would be desirable;

(c) data validation and reduction should be an explicit part of tokamak operation planning;

(d) "data reports" with *complete* and intelligible data sets for important discharges should be published regularly.

In contrast to other tokamaks, JET has succeeded in providing a (rather gross) systematically complete collection of *all* plasma discharges in the Survey Data Bank. The included data are derived from raw data to a level such that they can be understood by plasma physicists. At JET, the bank has been made easily accessible through computer terminals, and exploitable by means of a commercial data base management system (NOMAD2). This collection is released periodically in printed volumes to all Association Laboratories.

For the purpose of comparison with theoretical predictions, data banks with well checked plasma data (including dependence on geometrical and velocity space coordinates and on time) are being prepared for a few *selected discharges*.

The line of emphasising the investigation of local fluxes in anomalous transport - in contrast to the more

common automatic scaling study of global confinement time - has found general acceptance. The comparison of available theoretical predictions of anomalous transport with measurements on JET revealed that the mechanisms responsible are still not fully understood. However, it is possible to describe JET plasma behaviour quite well, especially when empirical flux formulae exploit the observed electron temperature "profile consistency".

The JET method of utilising full and consistent plasma models ("transport codes") for consistency checks and evaluation of the measured quantities produced another interesting result. Within the errors, in many JET discharges, the ion thermal flux can be remarkably different, in magnitude and parameter dependence, from neoclassical values, (i.e. the conductivity χ_i cannot be described by an ansatz $\alpha\chi_i$ (neo) with a constant α in the range 1-5).

General theoretical activities are described in further detail in Appendix I, which summarises the Work of Theory Division at JET.

Summary of JET Scientific Progress and Perspective

During the major shutdown in late 1985, new systems were added to the machine, such as the first neutral beam injection box, new carbon protection tiles in the vessel, a third ICRF antenna and a single deuterium pellet launcher. During 1986, experiments were pursued to determine the effects of these new additions, and were reported at various International Conferences (see Appendix V).

The main parameters of JET are summarised in Table VIII, which compares the progress achieved during 1986 with situation at the end of 1985. The most significant improvements were:

a) the extension of 5MA discharges to flat-top durations of 4.5s;
b) the demonstration of stable discharges at $q_\psi \approx 2.1$ with $B_T = 1.7T$ and $I_p = 3.5MA$, in simulation of future operations at 7MA;
c) the total input power to the plasma reached 18MW;
d) the plasma energy content reached close to 6MJ in both limiter and separatrix plasma cases;
e) the plasma temperature increased up to 12.5keV for the peak deuterium temperature in low density discharges with NBI and up to 8keV for the peak electron temperature in He discharges with ICRF;
f) a record value of the fusion parameter $\langle n_i(0)\, T_i(0)\tau_E\rangle = 2\times10^{20}m^{-3}.keV.s$ obtained during separatrix limited plasmas with enhanced confinement (H-mode).

Pellet Injection

Single deuterium pellets of 3.6 or 4.6mm diameter have been injected at speeds of 1-1.2km/s into JET plasmas in various conditions of magnetic configuration (limiter or separatrix discharges) and heating (ohmic only, ICRF or NBI). Pellet injection permitted an increase in the density limit in JET and reduced the effective charge Z_{eff} of the plasma. Z_{eff} values close to 1 were observed. In combined operations with NBI, peak electron densities exceeding $10^{20}m^{-3}$ were obtained lasting 0.5s after pellet

TABLE VIII
Summary of Main Jet Parameters
(NOT NECESSARILY IN THE SAME PLASMA PULSE)

		LATE-1985	*LATE-1986*
Toroidal Field	$B_T(T)$	$\leq$ 3.4	3.4
Plasma Current	$I_p(MA)$	$\leq$ 5.0	5.0
Duration of Max. I_p	$t_p(S)$	$\leq$ 0.5	4.5
Plasma Major Radius	$R_o(m)$	$\leq$ 3.0	3.0
Horiz. Minor Radius	a(m)	$\leq$ 1.2	1.2
Vert. Minor Radius	b(m)	$\leq$ 2.0	2.0
Elongation	b/a	$<$ 1.65	1.80
Safety Factor at Plasma Boundary	q_{cyl} q_ψ	$\geq$ 1.8 $\geq$ 2.6	1.5 2.1
Vol. Average Electron Density	$\bar{n}(10^{19}m^{-3})$	$\leq$ 4.0	5.0
Central Electron Temp.	$T_e(keV)$	$\leq$ 5.0	8.0
Central Ion Temp.	$T_i(keV)$	$\leq$ 4.0	12.5
Global Energy Conf. Time	$\tau_E(s)$	$\leq$ 0.8	0.9
Fusion Performance Param.	$\langle n_i(0)T_i(0)\tau_E\rangle$ $(10^{19}m^{-3}.keV.s)$	$\leq$ 5.0	20.0
Input ICRF Power	$P_{RF}(MW)$	$\leq$ 5.0	7.0
Input NBI Power	$P_{NB}(MW)$	$\leq$ —	9.0
Total Input Power	$P_{TOT}(MW)$	$\leq$ 8.0	18.0
Stoed Plasma Energy	$W_p(MJ)$	$\leq$ 3.0	6.1

injection, with a corresponding peak electron temperature down to 1keV. On-axis ICRF heating of high density plasma was not seriously attempted but the observed compatibility of pellet injection and ICRF heating provides encouragement for experiments with multiple pellet injection in 1987. Pellet ablation is well described by a model taking into account shielding effects provided by neutral gas and plasma surrounding the pellet. Additional heating does not introduce any abnormality in the process.

Following pellet injection in JET, a zone of lower electron temperature (by 20%) and higher density (by up to 100%) has been observed at the radius of sawtooth inversion by the Soft X-ray camera and the ECE temperature measuring system. This non-axisymmetric zone (nick-named the "snake") which extends 0.15m radially and 0.25m poloidally can be associated with an m=1, n=1 perturbation (m and n being the poloidal and toroidal wave numbers respectively). It can be identified with a magnetic island located at the radius, where the safety factor q is equal to unity. The perturbation can be observed for as long as 1s after pellet injection, implying that the insulation with the surrounding plasma is good and that it survives the sawtooth crash.

Ultra Long Sawteeth Oscillations

Sawtooth oscillations occur in almost all JET discharges. With central deposition of additional power, especially ICRF, sawteeth may develop large amplitudes (up to doubling the central electron temperature) and long periods (up to 0.6s). It has been observed that ultra-long sawteeth (nick-named "monsters") can occur, with durations up to 1.6s. During this time period, the central electron temperature can reach values above 7keV; usually, the ion temperature rises too and thermonuclear reactivity is improved. A strong reduction of MHD activity with low m, n numbers is observed and there is no apparent impurity accumulation. These ultra-long sawteeth were initially observed in combined heating situations in H minority plasmas at I_p=2MA. Subsequently, these phenomena have been observed in various conditions: NBI only, ICRF only (in He plasma) even after injection of a deuterium pellet, limiter or separatrix discharges and at values of plasma current up to 5MA. The only necessary condition seems to be a threshold in the input power per particle of $\sim 5\times10^{-19}$ MWm^3 in deuterium plasmas but down to 3×10^{-19} MWm^3 in He plasmas, where charge exchange losses and outgassing are strongly reduced. The mechanism maintaining high central electron temperatures and preventing the usual crash characteristic of sawtooth oscillations is still conjectured. The most plausible explanation is a slight change in current profile, possibly caused by the bootstrap current, raising the central value of the safety factor q(0) above unity.

Magnetic Separatrix Operations

Stable discharges with a magnetic separatrix (or X-point) inside the vessel have been maintained in JET for several seconds, at plasma currents up to I_p=3MA with a single null and up to I_p=2.5MA with a double null. The single null discharges have an elongation of 1.65 compared with 1.80 for the double null situation and, therefore, are more stable against vertical displacements. While interaction of the discharges with the limiters were curtailed, localised power deposition on the top and bottom target plates has so far limited the total input power to 8MW.

When compared to discharges leaning on the limiters or on the inner wall, the magnetic separatrix discharges without additional heating showed the existence of a dense plasma near the X-point with an average density of $1\text{-}2\times10^{20}$m^{-3} (which is an order of magnitude higher than the average plasma) and an improved confinement time.

With neutral beam injection power larger than 5.5MW, a transition to enhanced plasma confinement (H-mode) has been obtained in single null operation, at B_T=2.2T. The usual features of the H-mode were observed; such as decreased D_α light emission at the plasma boundary; reduced broadband magnetic fluctuations near the X-point; a rise in plasma density and in energy content; and a sudden increase of the electron temperature near the separatrix producing a pedestal to the temperature profile. The H-mode can be sustained for durations approaching 2s. The continuous density rise increases the radiated power from the bulk plasma and is probably the cause for termination of the H-mode even though there is no indication of peaking of the impurity profile. While the energy content reaches a quasi-steady state for a time approaching 1s, the electron temperature may reach a maximum before the end of the H-mode. In those conditions, a plasma energy content of 6MJ has been achieved with 8MW of NBI in addition to an ohmic power of 2MW at a plasma current of 3MA. The global confinement time more than doubled the value obtained in limiter or inner wall discharges. Increasing the magnetic field raised the power threshold required to obtain an H-mode, which so far has prevented the occurrence of a transition above 2.8T. H-modes have not yet been achieved in "double null" operations.

ICRF heating has been applied during X-point discharges, alone or in combination with NBI. In optimum conditions for an H-mode with NBI, the separatrix to antenna distance was ~10cm and the coupling resistance of the ICRF antenna was halved compared with "limiter" discharges. The plasma was moved radially to decrease this distance but no H-modes were observed in D plasma with ICRF alone up to the operational limit of the input power. Furthermore, at moderate power (>1MW), ICRF usually provoked the termination of an H-mode, previously triggered by NBI. This difference between heating methods may be linked to the usual increase in charge exchange and in radiation losses at the plasma boundary during ICRF pulse. Indeed, when these losses were reduced, in a ^{3}He plasma with proton minority, some of the features of an H-mode were observed with ICRF alone, (i.e. reduction of broadband MHD fluctuation level, decrease in light emission at the plasma periphery while the density was rising; attainment of $T_e(0)$ and $T_i(0)$ close to 8 and 6keV respectively for an

ICRF power of 6.5MW at a volume averaged density of $1.5x10^{19}m^{-3}$).

Global Plasma Behaviour

Impurities and Effective Charge of the Plasma

In most cases, impurity radiation losses were mostly caused by carbon and oxygen and originated mainly from the plasma edge. In limiter discharges, the metal concentrations were only significant (i.e. $>0.1\%n_e$), if the carbon limiters were metal-coated following accidental melting and evaporation of wall material. The release of metals from the limiters can be explained by a combination of sputtering by deuterium and by light impurities. The metal fluxes decreased as the plasma density increased and the plasma current increased. These fluxes were inversely correlated with the light impurity behaviour. At high plasma density, radiation losses were mainly caused by oxygen.

The effective plasma charge Z_{eff} ranged usually between 2 and 3 for line averaged electron density n_e greater than $3x10^{19}m^{-3}$. Z_{eff} was reduced and approached unity for a time duration exceeding 0.5s after the injection of a deuterium pellet.

Density Limits

In ohmic phases, the density limit was $n_e(OH)(m^{-3}) = 1.2x10^{20}\ B_T(T)/qR(m)$, and depended on plasma purity. In RF heated discharges, it was only slightly increased, possibly because the effect of the extra power was cancelled by an increase in impurities. In neutral beam heated plasmas, the limit was substantially increased to $n_e(NB)(m^{-3})=2.0x10^{20}B_T(T)/qR(m)$. Switching off neutral beams at high density caused the plasma to disrupt, which indicated that the power input played an important role in the disruption mechanism. Preliminary experiments with a single-shot pellet injector have also exceeded the OH density limit.

Plasma Temperature

Electron and ion temperatures were observed to react differently on application of additional power. At a power input per particle $P/\bar{n} > 4x10^{-19}MW.m^3$, the on-axis ion temperature greatly exceeded the electron temperature and reached ~12.5keV in JET. The ion temperature profile was broadened in cases of off-axis ICRF heating.

The peak electron temperature could be raised significantly above the value reached in the ohmic phase as exemplified by the ultra-long sawteeth, where $\Delta T_e(0)$ has exceeded 4keV. By contrast, the electron temperature at the sawtooth inversion radius ($q\sim1$ surface) showed only a weak dependence with the power input per particle ($P/\bar{n}$) for a given plasma current and toroidal field; T_e increased from 2.5keV to 4keV when $P/\bar{n}$ varied from 2 to $8x10^{-19}MW.m^3$. The normalised temperature profile outside the inversion radius can be well described by a Gaussian type expression, $T_e(R)=T_e(R=4m)\exp\alpha_T[1-(R/4)^2]$, where R is the radial position relative to the vertical axis. It is found that $\alpha_T=1.8\pm0.1$ for the majority of the JET plasmas. Only very highly additionally heated and high q discharges are fitted by a different value of α_T. In that respect, the electron temperature profile although stiff, is not rigidly "consistent".

Energy Confinement

The definition of the total energy confinement time used at JET is $\tau_E=W_k/[P_t-dW_k/dt]$, where W_k is the kinetic energy and P_t is the total input power to the plasma without subtracting radiation losses. Reported values of τ_E are quasi-stationary.

TABLE IX
(MAXIMUM VALUES OF $<n_i(0)\tau_E T_i(0)>$

Experimental Programme	*Peak Density* $n_i(O)$ $(x10^{19}m^{-3})$	*Energy Confinement* τ_E (s)	*Ion Temperature* $T_i(O)$ (keV)	*Fusion Product* $<n_i(O)\tau_E T_i(O)>$ $(x10^{19}m^{-3}.s.keV)$	Q_{DT} *Equivalent* Q_{DT}	*Plasma Current* I_p (MA)
Ohmic (4.6MW)	4.2	0.8	3.0	10	0.010	5
ICRF (7MW)	3.7	0.3	5.4	6	0.012	3
NBI (6MW)						
High "	4.4	0.4	4.0	7	0.10*	3
Low "	1.5	0.4	10.0	6	0.20*	3
Combined NBI + RF (14MW)	5.0	0.5	3.5	7	0.10*	3
X-point (NB-10MW)	5.0	0.65	6.0	20.0	0.15*	3

*Beam-Plasma reactions are dominant

Independently of the type of additional heating, whether RF, NB or combined, the confinement time degrades with increasing input power, as seen in a number of other experiments. The rate of increase in W_k with $P_t(=\Delta W_k/\Delta P_t)$ appears to reach a limit of 0.1-0.3MJ/MW (=s) at high powers. This suggests a lower limit to the global confinement time, τ_E, of 0.1-0.3s in JET. The confinement time depends weakly on plasma density but scales favourably with plasma current.

While the global confinement time results could be fitted by a Goldston type law, the measured radial propagation of heat pulses prior to sawtooth crashes strongly supports a linear offset relation between W_k and P_t, in the form:

$$W_k(P_t) = W(0) + \tau_{inc}P_t$$

The best fit to the data has been found by use of standard regression techniques in the cases of limiter or inner wall discharges, and gives $W(0)=0.225n^{0.6}I_p^{0.5}B_T^{0.4}$ and τ_{inc} $=0.047I_p$ (in units of MJ, $m^{-3}x10^{-19}$, MA, T, and s).

In the H-mode, the energy confinement time was observed to be more than twice that obtained in limiter discharges. Degradation was also observed as the input power was increased and a similar offset linear scaling of W_k with P_t seems likely. It is too early to say how the corresponding incremental confinement time compares with that obtained in limiter discharges, but in both cases, higher plasma current looks beneficial.

Thermonuclear Reactivity

The best performance of thermonuclear reactivity under various conditions are summarised in Table IX. The record value of the fusion product $\langle n_i(0)T_i(0)\tau_E\rangle \approx$ $2x10^{20}m^{-3}.keV.s$ has been achieved with 10MW of neutral injection heating during an H-mode. For limiter or inner wall discharges, the values of the fusion parameter are similar for ohmic heating only, RF, NBI and combined heating cases, degradation in confinement time with additional heating off-setting gains in the other parameters. Neutron yields up to $4x10^{15}n.s^{-1}$ have been obtained in the hot-ion mode with neutral injection, but mainly from beam plasma D-D reactions. The best ratio of fusion power to input power obtained was Q_{DD} $=3.5x10^{-4}$ which is equivalent to $Q_{DT}\sim 0.2$ and would have corresponded to a fusion power production of $\sim$2MW.

Developments and Future Plans

In 1978, the original aims of JET were set out in the JET Design Proposal, EUR-JET-R5, which described the objectives as follows:

"The essential objective of JET is to obtain and study a plasma in conditions and dimensions approaching those needed in a thermo-nuclear reactor. These studies will be aimed at defining the parameters, the size and the working conditions of a Tokamak reactor. The realisation of this objective involves four main areas of work:

(1) the *scaling of plasma behaviour* as parameters approach the reactor range;
(2) the *plasma-wall interaction* in these conditions;
(3) the study of *plasma heating*; and
(4) the study of *alpha-particle production, confinement* and consequent plasma *heating*.

The problems of plasma-wall interaction and of heating the plasma must in any case be solved in order to approach the conditions of interest.

An important part of the experimental programme will be to use JET to extend to a reactor-like plasma, results obtained and innovations made in smaller apparatus as a part of the general Tokamak programme. These would include: various additional heating methods, first wall materials, the control of the plasma profiles, and plasma formation."

Nine years' later, the objectives of JET are unchanged and the same four areas of work remain the focus of the Project's activities. The study of energy confinement and its degradation with additional heating is covered by areas 1 and 3. The study of different low-Z (i.e. low atomic number) materials, edge effects, exhaust and fuelling is covered by area 2. The study of α-particles, area 4, must clearly wait until area 2 and 3 have been successful addressed, as α-particles will need to be produced in sufficient quantities for their effect on the plasma to be observed.

The JET aims clearly state that JET is an experimental device and that, to achieve its objectives, the latest developments in Tokamak physics must be allowed to influence its programme. The proposed programme now includes some new additions and enhancements to overcome confinement degradation and to push the parameters of the JET plasma closer to those needed in a thermonuclear reactor. This is in complete agreement with the original objectives laid down for JET.

While present achievements show that the first three objectives of JET are being actively addressed and substantial progress is being made, the strategy for JET can now be summarised as a strategy "to optimise the fusion product $<n_i(0)\tau_E T_i(0)>$". For the energy confinement time, τ_E, this involves maintaining, with full additional heating, the values that have been already reached with ohmic heating alone, which means avoiding confinement degradation. For the density and ion temperature, it means increasing their central values $n_i(0)$ and $T_i(0)$ to such an extent that D-T operation would produce α-particles in sufficient quantity to be able to analyse their effects on the plasma.

New additions proposed for JET aim through the following mechanisms to build up a high density and high temperature plasma in the centre of the discharge, where α-particles could be observed, while maintaining an acceptably high global energy confinement time:

(a) to decouple the temperature profile from the current density profile through the use of *lower hybrid current drive and neutral beam injection* to ensure that, at higher central temperatures, the current density in the centre does not reach the critical value that causes sawteeth oscillations;
(b) to reduce the edge density by *edge pumping*, since it is observed that the temperature at the $q=1$ surface is higher when the edge density is lower. Other advantages of lowering the density in the outer region are the inhibition of disruptions and a higher efficiency for the lower hybrid current drive system;
(c) to increase the density of deuterium and tritium ions in the central region to $1\text{-}2\times10^{20}m^{-3}$ by *high velocity pellet injection*;
(d) to achieve high central temperatures (12-15keV) by the combination of 'on-axis' ion cyclotron resonance frequency (ICRF) heating, neutral beam injection at 160keV and *current profile control*, which is aimed at maintaining the conditions of giant sawteeth for longer periods.

Such a scheme will be attempted in two configurations: (a) with a *magnetic separatrix* (X-point operation) at 4MA; and (b) with low-Z material limiters at the higher currents up to 7MA, which represents a further enhancement of the JET machine.

The following sections describe various developments which are underway on JET to implement these additions and enhancements.

Future Separatrix Experiments

Upgrading of plasma current and power capabilities for X-point operations are scheduled during the period 1987-1989, as summarised in Table X. Modifications of the poloidal circuit will increase the shaping magnetic fields, thus allowing the production of X-point configurations up to plasma currents of 4MA both in the single null and in the double null configurations. Predicted magnetic flux plots are shown in Figs.75 and 76 for the double null and for the single null cases. New cladding with water cooled tiles inside the vacuum vessel region near to the X-points will permit operations with large plasma heating powers (up to 40MW), for maximum pulse lengths of 10s.

The achievement of the H-mode in JET in the X-point configuration opens the way to studies of plasma transport in this regime, in conditions which should be relevant to reactor plasma. At the same time, it can be expected that, with the upgrading capabilities, the plasma parameters (such as global confinement time, plasma density, ion temperatures and hence thermonuclear reactivity) in the H-mode could be comparable if not better than those achievable at I_p=7MA in the limiter configuration. In fact, despite the limited data set of H-mode discharges, it was observed that, in H-mode, global confinement was linearly dependent on plasma current. Moreover, although in the H-mode a certain amount of confinement degradation with additional power was present, the values of global confinement time were at least a factor x2 larger than in limiter discharges. The increased power capability should produce a plasma temperature increase, thus increasing the Q values.

A conservative extrapolation can be based on the assumption that the confinement time in the H-mode is double than in limiter discharges and scales linearly with plasma current. This leads to the conclusion that the values of thermonuclear Q achievable with the H-mode at a plasma current of 4MA could be similar or better than those with limiter discharges at 7MA. Comparative studies of these two configurations will help the choice of parameters of future machines. At the same time, while the fact that an H-mode has been achieved in JET indicates that the magnetic separatrix configuration is a key element in the improvement in global confinement times, the studies of particle fluxes, edge radiation and impurity influxes and transport need to be pursued because these results can provide basic knowledge needed for long pulse burning plasmas, if the next step device is constructed with a divertor configuration.

TABLE X

	1986	*1987-1988*	*1989*
Plasma Current Single Null	3.0MA	4.0MA	4.0MA
Plasma Current Double Null	2.5MA	3.8MA	3.8MA
Power Capability	10MW	20MW	40MW
Pulse Duration	2s	4s	10s

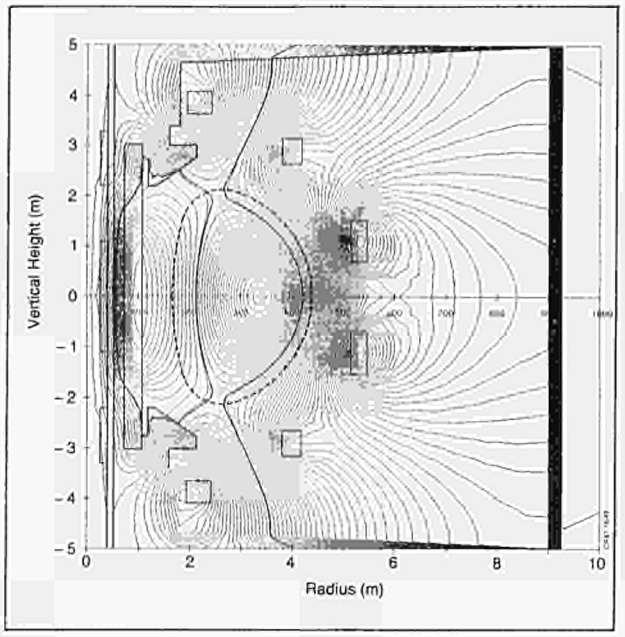

Fig.75: Predicted magnetic flux plot for double null configuration at I_p=4MA.

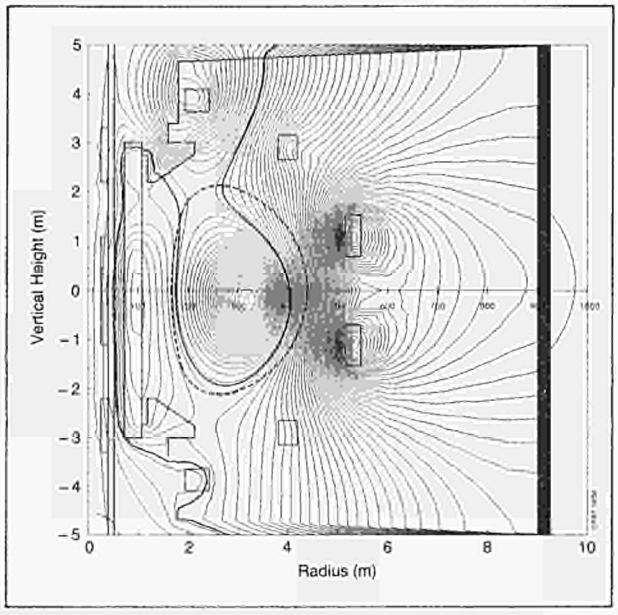

Fig.76: Predicted magnetic flux plot for single null configuration at I_p=4MA.

Current Drive and Profile Control

The main goals for controlling the current profile on JET are:

(a) to reduce the peaking tendency of current density profile, thereby eliminating the sawtooth instability which limits the electron temperature inside the q=1 surface;

(b) to decouple (at least, partially) the current density and electron temperature (set by ohmic heating) and, thus, provide a means of reducing the constraints of profile consistency which might be responsible for confinement degradation during additional heating.

In addition, a suprathermal electron population, which can be generated by lower hybrid injection into a thermal plasma, may have a beneficial effect on MHD stability.

The JET proposal makes use of Article 14 contract work on lower hybrid systems (IPP, Garching, F.R.G. and CEA, Grenoble, France) and electron cyclotron resonance (FOM, The Netherlands and UKAEA, Culham, U.K.), as well as conclusions from a Workshop on Profile Control organised by and held at JET in May 1986.

There is a large database of information available on lower hybrid current drive (LHCD) and, by contrast, there are presently technical limitations on electron cyclotron resonance (ECR) systems and a lower current drive efficiency with electron cyclotron resonance heating (ECRH). Consequently, a lower hybrid wave system is preferred as the main additional tool for active current profile control. The physics of the proposed JET LHCD system has been extrapolated from data obtained from many experiments, especially those from sawteeth stabilisation experiments which have been performed over a wide range of plasma parameters and in neutral beam and ICRH heated plasmas. A high frequency (HF) driven current of between 25% and 50% of the total current is estimated to be required in JET for sawteeth stabilisation.

The proposed LHCD system is designed to launch 10MW wave power into the torus, producing 1-2MA of HF driven current in JET with an average density of $5 \times 10^{19} m^{-3}$. The current drive efficiency used in this estimate is approximately four times higher than experimental efficiencies obtained in PETULA and ASDEX experiments, and is justified by an improved wave spectrum, better directivity, and by much higher electron temperatures obtained in the JET experiment. Such an improvement with increased temperature may be the cause of the high LHCD efficiency recently obtained in neutral beam heated plasmas in the Japanese JT-60 experiments.

The choice of frequency is a compromise representing both technical and scientific considerations. Losses in the transmission line and grille are greater at higher frequencies but the achievable power density at the grille mouth is also higher. The density limit for current drive is higher at higher frequencies. Moreover, the resonant energy of ion interaction with the LH wave, which is undesirable for this application, increases with frequency. Therefore, to avoid coupling to energetic ions created by the other heating methods, a higher frequency is preferable. A frequency of 3.7GHz has been chosen, based on the above considerations and the availability of klystrons with large output power per unit (0.5MW), in the required time schedule.

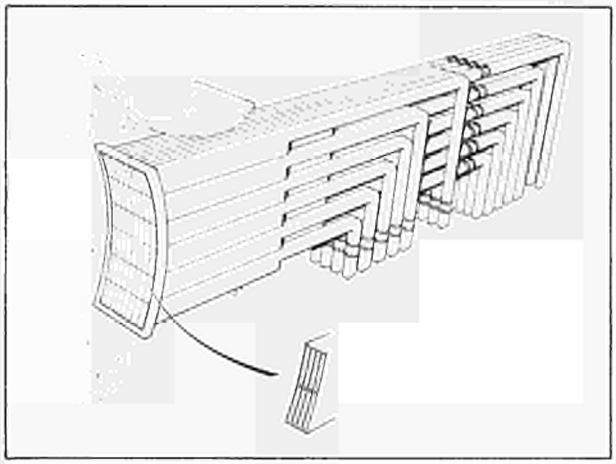

Fig. 77 Single grille structure for launching lower hybrid waves into the JET plasma.

The grille technology to be applied in JET is based on the multijunction grille which has already been tested in LHCD experiments in PETULA. The multijunction grille has been demonstrated to exhibit a good match to the klystron over a wide range of plasma conditions, and thus provides flexibility in the acceptable position of the grille relative to the plasma surface. The power will be injected through a single grille structure that occupies an entire port (Fig.77), from which some diagnostics must be removed. The proposed power density of $4 kW/cm^2$ appears attainable with routine grille conditioning techniques (baking at high temperature and appropriate surface coatings). By means of control feedback techniques on the HF power, phasing between klystrons and controlling the grille position relative to the plasma, the central value of the parallel wave spectrum will be varied in the range 1.2-2.4 and the overall HF reflection coefficient kept at a low value ($\leq$3-5%) over a large range of plasma densities and plasma configurations.

The system is scheduled for installation in JET during the major shutdown at the beginning of 1990. The project is presently in the design phase of the various subsystems, as follows:

- the generator (24 klystrons)
- the transmission line (40m long)
- the launcher (384 waveguides into 48 units)
- the control command logic and data acquisition.

An intermediate step is planned in which a prototype system of 4 klystrons with the corresponding launcher will operate on a testbed and may be placed in JET by the end of 1988. To obtain this, an initial set of 5 klystrons

TABLE XI
Summary of Current Profile Control Systems for JET

	NBI	*ICRH*	*NBI + ICRH*	*ECRH*	*LHCD*
Current Drive Data	Observed (Jet, TFTR)	Predicted	Predicted	Not yet observed	Abundant Database
Requirements for Jet	2 Beam Units E=80-160keV	8 Phased Antennae	2 NBI Units + 8 Antennae	15 Gyrotrons at f=60-80GHz (Top Launch or Inner Wall Reflector)	24 Klystrons at f=3.7GHz
Power Coupled to Current Carrying Particles (MW)	21	5	12	3	7
Power at the Generator (MW)	52	32		4	12
Power from the Mains	65	53		10	28
Current Drive (MA) ($n_e=2\times10^{19}m^{-3}$)	0.5			0.5	3 to 4.5
Current Drive (MA) ($n_e=5\times10^{19}m^{-3}$		0.4	1-2	0.3	1 to 1.5
Availability of the Full System	To be operated in 1987	To be operated in 1987	To be operated in 1987		Being Considered 1990

was ordered at the end of 1986 and should be delivered by the end of 1987.

At relatively low plasma densities, the total required current of 2-4MA should be driven by the LH current drive system alone. At higher densities, additional methods of non-inductive current drive provided by the other auxiliary heating systems on JET (see Table XI), must be utilised to generate sufficient current for profile control.

Estimates for neutral beam current drive effects have been based on simulations of results recently obtained in JET with NBI at 80keV beam energy. Reasonably good agreement between the experimental results and the numerical modelling have been seen when the effect of fast ion trapping, which results in a rapid fall of the current drive efficiency with density, is taken into account. Simulations show that the beam driven current is peaked at the plasma centre and that the beam driven current profiles are relatively insensitive to plasma and injection parameters. This localisation of the beam driven current at the plasma centre can be exploited by employing the neutral beam in a counter injection mode so that the current is flattened in the plasma centre while additional current is generated off-axis by lower hybrid waves.

Ion cyclotron resonance frequency (ICRF) current drive can be obtained by properly phasing the eight antennae which will be installed during the 1987 shut-down. Although the estimated efficiency of ICRF current drive is relatively poor when used alone, the good localisation properties of ICRF wave power deposition can be used to locally shape the plasma current density, particularly in conjunction with other more efficient current drive methods which are sensitive to temperature. Beneficial synergistic effects resulting from simultaneous use of NBI and ICRF, or LH and ICRF, can be foreseen so that the current profile can be effectively shaped for the required range of plasma parameters.

Multi-Pellet Injection for Fuelling and Refuelling

The multi-pellet injection system and its development activities are aimed at achieving pellet speeds higher than $1.5kms^{-1}$ but the initial multi-pellet injector will employ state-of-the-art techniques, in collaboration with the U.S. Department of Energy. The basic ideas for fuelling and refuelling were outlined in the 1985 Progress Report and do not need revision, following successful operation of the single-shot diagnostic pellet injector on JET. These experiments confirmed previous findings on other experiments.

Although the Agreement on Pellet Injection Collaboration with the US Department of Energy (within the framework of the EURATOM - USDoE Bilateral Agreement on Fusion Research) is not yet formally signed, work by both parties is progressing well, as planned.

During the next three years the Agreement calls for a collaborative team effort of on average ~4 man years per year from each side to jointly perform a programme, with the main aim of plasma performance improvement by pellet injection. A pellet injector will be formed by joining an Oak Ridge National Laboratory (ORNL) launcher to a JET interface. The launcher is similar to the RPI type initially employed on TFTR at Princeton University, USA. The interface is composed mainly of a differential pumping system consisting of a pellet injector box (PIB) of the same type as a neutral injection box (NIB) with its large cyropump. During 1986, a number of interface meetings took place in which JET and ORNL discussed, expanded and amended the basic conception and the according agreements were laid down in a JET/ORNL interface document.

The ORNL launcher is termed a temporary installation as it does not fulfil the requirements of tritium and remote handling compatibility. It comprises three guns, with repetitive firing capability during a tokamak pulse, combined in one general vacuum housing. The system is specified for delivery of deuterium or hydrogen pellets in sizes according to the barrel diameter at maximum speeds of around $1.5 kms^{-1}$. The initial choice of barrel diameters were 6, 4 and 2.7mm with the minimum number of pellets per tokamak pulse 6, 8 and 10, respectively, at a repetition rate of $5s^{-1}$ for the smallest pellets, and less for others. The launcher will be accompanied by its complete control and pellet data acquisition system on the basis of a programmable controller and a high-level control computer interfacing with CAMAC equipment for particular tasks. Both the launcher hardware and the control equipment are in an advanced state of assembly and pre-checking and commissioning starts in early 1987. Apart from providing the CAMAC data acquisition module, JET has also contributed directly by designing and building the firing sequencer governing the internal timing of each gun-line. This device was delivered to ORNL and integrated into their controls; its conception permits its use for a later JET injector in which the number of timing steps and gun lines can be increased, as necessary. The launcher, fully commissioned at ORNL by using a test stand vacuum and target arrangement, should arrive at JET in early 1987.

Besides the PIB with its cryopump system, the JET interface comprises conventional turbomolecular vacuum pump, and forevacuum system, the local LHe system and pellet diagnostic systems. The PIB and its rear launcher platform integrated into the PIB support structure have been delivered, and so has the cryopump system which is already assembled awaiting first LHe cool-down and final leak test. Other components are in various states of procurement and preparation for commissioning and all preparations should converge to join the launcher and the interface at the end of the 1987 shut-down, ready for injector operation when machine operations restart.

Apart from the launcher, most other equipment should be compatible with the active phase and a considerable effort was made to design, manufacture and prepare accordingly. A modification of the single-pellet injector periscope for the imaging of pellet generated D_α-light is underway and upgrading of the multi-pellet recording is being investigated.

In principle, the ORNL launcher for use during the next two operational periods should fulfil all parameter requirements, except that of increased pellet speeds. It will not be possible to investigate whether larger plasma penetration depths can be achieved and lead to advantages of plasma performance. To apply the high-speed feature with a prototype high-speed gun in 1989 and, if successful to incorporate it into the design of the final tritium and remote handling compatible injector, development effort is proceeding. This should clarify the basic physics and the technology elements of obtaining high pellet speeds with a pneumatic gun using high-temperature driver gas.

This development is underway in collaboration with several laboratories and, currently, JET is constructing a pellet injector testbed in support of development and for maintenance of launchers. At present, the task-sharing is as follows: CENG, CEA, Grenoble, France (Article 14 contract) treats all problems in connection with formation, the material properties of ice pellets and the technical means of formation and fast repetitive loading of the gun; Risø National Laboratory, Denmark (Article 14 contract) will develop acceleration methods using an electric arc heater type gun; EMI, Ernst-Mach-Institut der Fraunhofer-Gesellschaft, Freiburg, F.R.G., will employ acceleration methods by means of a two-stage gun, in its ultimate form using considerable adiabatic compression heating.

AT CENG, 6mm diameter, 6mm long pellets have been formed by in-situ cryo-condensation of deuterium directly into the barrel. The understanding of the cryo-condensation process and the pellet shape resulting from it was improved by testing a variety of freezing cell designs and by varying the formation parameters. The development is directed towards optimising conditions for higher reliability of the formation process. Even with an advanced fast valve design (300 bar) yielding $1850 ms^{-1}$ with a 0.5m barrel, pellets cannot be accelerated to values higher than $5 \times 10^6 ms^{-2}$. Preparations are underway to transfer to CENG a piston device along the lines of the EMI work and to complete tests with higher acceleration in early 1987.

Work at Risø has concentrated on three items:

(a) attempts are being made to overcome limitations of supplying driver gas by cryo-condensation into the arc chamber before igniting the arc by using pre-injection of frozen hydrogen pellets into the arc chamber. So far, the method has been successful and attention is now being turned to sufficiently large pellets required for a high-speed gun;

(b) the design of an arc chamber suitable for pressures up to 1000 bar with minimum dead volume, initiated by JET, is now being pursued at Risø. The arc chamber design is now compatible

for gas feeds from either pellets, fast valve (CENG) or piston device (EMI) and matches the CENG cryostat for the deuterium pellets, which is now under construction. Test stand preparations have been carried out;

(c) a ramp generator power supply and matching transformer for the arc equipment has been successfully commissioned into a ohmic load.

In the work at EMI, F.R.G., work has been carried out with a piston driven pneumatic amplifier, which in its simplified form uses a bursting disc as a fast valve delivering the pressure pulse to the pellet. Deuterium pellets have been simulated by 6mm diameter, 6mm long polystyrol foam pellets (close to the specific density of deuterium) and these have been accelerated in a 1m long barrel to 2.8km.s^{-1}, which is about a factor 1.6 larger than the highest pellet velocity achieved with conventional pneumatic guns. It appears, however, that the pressure wave entering the pellet is too slow to follow the pellet. Now a new device has been brought into operation which allows not only a pressure amplification but also a substantial temperature increase of the propellent gas by adiabatic compression. Using a 1m long compression cylinder, a much higher velocity of 4.3kms^{-1} has been achieved which is closer to the theoretically expected value of about 5kms^{-1}. It follows from Fig.78, that the driving pressure at the pellet can be kept up even further down the barrel.

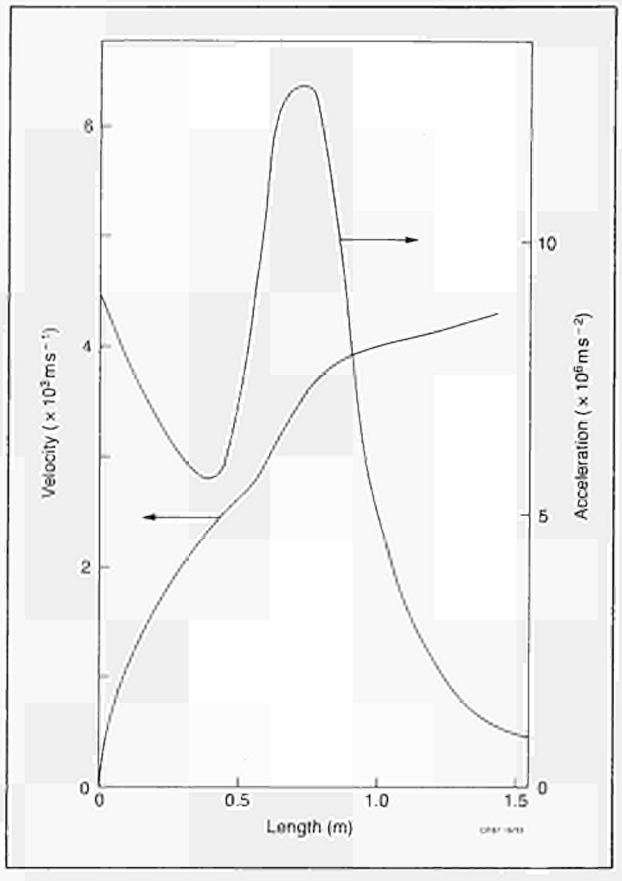

Fig. 78: Velocity and acceleration of pellet achieved as a function of compression cylinder length.

Although high velocities have only been achieved for plastic pellets, the fact that the acceleration did not substantially exceed 10^7m.s^{-2} provides hope that similar velocities can be expected for deuterium ice pellets. The present device seems to be suitable to investigate further deuterium ice properties and if technically matured, could probably be developed into a higher speed gun.

JET has placed a contract with CENG for the delivery of two cryostats and controls of the type which have successfully demonstrated the in-situ pellet forming, one of each to go to the arc gun and two-stage gun development effort so that the different elements are joined up already in an early phase of the development.

From these results, JET tends to favour the two-stage gun approach in the short term, with the arc gun being considered as a longer term solution with potential for even higher gas temperatures. Accordingly, the pellet injection testbed will continue the work on the adiabatic compression heating scheme from the middle of 1987 onwards and a first version of such a gun is under design. A platform for the pellet injection testbed has been erected, services are being installed and supporting steelwork and vacuum tanks for two gun lines have been prepared; other ancillary components are in preparation.

Density Control

Introduction

The overall JET aim is to improve the fusion parameter $\langle n_i(0)T_i(0)\tau_E\rangle$ and hence increase the α-particle production rate to allow α-particle heating and confinement to be studied in JET. This will necessitate an increase in the central density in JET well above the limits observed so far in ohmic discharges. However, this increased central density should not be accompanied by an increased edge density as this would cause loss of plasma stability. Consequently, a particle exhaust system is proposed, capable of controlling the edge density during discharges with additional heating and pellet injection. In addition, it will permit controlled pulse termination by reducing the average density to corresponding ohmic levels at the end of high power and high density discharges.

At this stage, the required particle removal rates can only be roughly estimated. Recent experiments have shown that the global particle confinement time increases when pellets are injected. An extrapolation from these data suggests particle confinement times of $\sim$2s. The particle outflux would then reduce to half of the influx. For 5mm diameter pellets fired into the plasma at a rate of 1s^{-1}, the average increase in particle content is 6 x 10^{21}s^{-1}. To maintain a low boundary density, 3 x 10^{21} particles per second would have to be pumped. It should be noted that for such particle influxes about 10MW heating needs to be coupled to the particles to heat them to 10keV. This shows that an influx of 6x10^{21}s^{-1} is probably a practicable upper limit.

Maintaining constant density during additional heating or density reduction after heating are easily achieved by

these particle removal rates. JET is following two concepts to provide these: using wall pumping and pump limiters.

Wall Pumping

A strong wall pumping effect is observed in JET when the plasma is moved towards the inboard graphite protection tiles. This allows particle removal rates of up to $4x10^{21}$ s^{-1}. This strong pumping lasts typically for only about 1s, and then, it decreases to much lower values, but is still sufficient for controlled pulse termination. The density for discharges with additional heating can be reduced to values below the Murakami limit for ohmic discharges. The wall pumping does not show saturation from discharge to discharge.

To understand the basic mechanisms of this effect, a group at Sandia, Livermore, USA has taken on the task of performing hydrogen recycling measurements on graphite. A Penning discharge with graphite cathodes has shown that a strong pumping effect can be generated by carbon sputtering and subsequent co-deposition of hydrogen and carbon, or by redeposition of chemically sputtered hydrocarbons. Studies are continuing and will be extended to beryllium.

With a tritium plasma source, the group has also studied the transient pumping effect for carbon - diffusion and solution of hydrogen limited by recombination at the surface. The results indicate that this is not a sufficiently effective mechanism to account solely for the wall-pumping observed at JET. Possibly, transient pumping and co-deposition both play a role in wall pumping. To date, it cannot be concluded unambiguously which of the two mechanisms is the dominant one in JET. If it turns out to be co-deposition, the use of pumping panels (or even large graphite areas in JET) must be assessed with respect to the consequences for tritium handling and retention.

Pump Limiter

If similar pumping speeds could be achieved to those obtained during strong wall pumping, the pump limiter would have the advantage of constant pumping throughout the whole JET pulse. Therefore, the second concept of particle exhaust is to employ pump limiters.

The first step will be to install a prototype pump limiter in 1988 to determine the pumping efficiency possible with the JET boundary conditions by positioning the pump limiter somewhat behind the leading edge of the belt limiter. As a simplification, the prototype will only be inertia cooled during the plasma discharge. An approximate estimate, using a simple plasma model, showed that a measurable effect of the prototype on the plasma density could be expected and so the conceptual design has been started. To optimise the design, detailed numerical calculations have been started to determine the plasma edge parameters for JET boundary conditions and to determine the neutral particle transport inside the pump limiter.

Conceptual Design

The prototype pump limiter incorporates two pumping modules. One scrapes the plasma between the belts and one scrapes the plasma above and below the belt limiter. Both modules can be activated independently from outside by moving the central blade and by internal flaps. Using the internal flaps, the electron and ion side of the pump limiter also can be activated independently. For final removal of the particles scraped off the plasma, a cryopump positioned in the pumping chamber will be used.

The prototype pump limiter will consist of an Inconel box as the basic structure and the scrape-off blade and neutralizer plates will be constructed of carbon fibre reinforced graphite or pyrolitic graphite. An integral design for the scrape-off blade and neutralizer plate has been selected.

To avoid overheating of the scrape-off blades, the pump limiter can be kept in the pumping position for only 1-2s if carbon reinforced graphite is used for the blades. The whole pump limiter box is moved to bring the pump limiter into the pumping position and to retract it. If pyrolitic graphite is used as a blade material, it appears that the heat load can be sustained on the blade for a 10s plasma pulse. In this case, only a slow driving mechanism would be required and more importantly the pump limiter could be used for density control. The latter concept is now being followed closely.

Plasma Transport Calculations

JET has started plasma transport calculations for a circular plasma cross-section and a single belt limiter. The formation and dissociation of H molecules has been included in these calculations since they effect the transport strongly. The calculations have been performed for a total power input of 40MW, and no radiation from impurities has been taken into account. The model requires the input of the plasma density about 0.1m in front of the limiter as input for the calculation.

Typical edge parameters for a density of $2x10^{19}m^{-3}$ at this radius are:

n(edge) = $1.2x10^{19}m^{-3}$

T(edge) = 100eV

Γ(edge) = $2.5x10^{23}m^{-2}$ s^{-1}

P(edge: perpendicular to field lines) = $10^{8}Wm^{-2}$

The calculations will be extended to D-shaped plasma and to the two belt limiter case.

Using plasma edge parameters derived from plasma transport calculations for a circular plasma and a single belt limiter, Monte Carlo calculations have been used to optimise the geometry, particularly that of the pump limiter mouth and neutralizer plate.

For a geometry indicated in Fig.79, typically 40% of the incoming particles will be trapped in the pump limiter, 50% will be lost by reionisation after neutralisation at the reflector plate and 10% will be lost as neutral particles through the mouth. Taking into account that part of the reionized particles will be neutralized again, more than 50% of the incoming particles can be expected to be trapped in the pump limiter. Assuming a particle removal

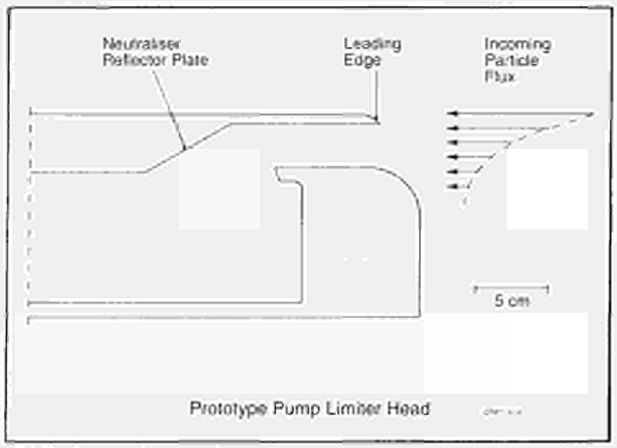

Fig. 79: Prototype pump limiter head.

efficiency of 80% for the cryopump, a total pumping efficiency of = 40% seems to be possible. In absolute terms, about $2x10^{21}$ particles s^{-1} can be pumped (for 1-2s using carbon fibre reinforced blades and up to 10s using pyrolitic graphite blades). This particle removal rate corresponds to time constants for a density decrease of about 5s.

Conclusions

It is proposed to develop both a pump limiter and pumping panels for density control. Detailed calculations show that it should be possible to provide particle exhaust rates with the pump limiter which are comparable with those obtained by wall pumping. In addition, the pump limiter does not show a saturation effect during a discharge. On the other hand, pumping panels are much simpler, but the processes leading to wall pumping in graphite are not yet fully understood and more effort will be required.

Appendix I

Work of Theory Division in 1986

(Division Head: Dr. D.F. Düchs)

In the 1985/86 reorganisation of the JET Project, Theory Division became part of the Heating and Theory Department. The Division remained responsible for the prediction of JET performance by computer simulation, the interpretation of JET data, and the application of analytic plasma theory to gain an understanding of plasma behaviour in JET. However, it was able to shed some of the non-theoretical activities such as the responsibility for peripheral computer hardware and extensive data validation. These necessary tasks absorbed effort from the more essential plasma theoretical and modelling activities which were the main thrust of the Division's activities.

Theory Division interacts with experiment much more strongly than in most plasma physics Theory Divisions. Interpretation plays a key role in the assessment of plasma performance, and hence in optimisation studies and programme planning. Prediction work continuously checks the measured behaviour against the different computational models, and provides a basis for long term programme planning. A major role of analytic theory is to compare the observed behaviour against that expected from existing analysis, and to modify the latter where they diverge. The effort allocated within JET to analytic theory was limited, in the expectation that Association staff and Visiting Scientists would provide support, by extended visits and by work under Article 14 Contracts. Valuable assistance has been provided in this and the other areas, over the past year.

The central task of the Division is to provide a quantitative model of tokamak plasmas, with particular attention to JET behaviour. The ultimate objective is to include in this model all the important effects observed in JET and other tokamaks. Although it is preferable to understand each effect theoretically, in some cases it may be necessary to rely on an empirical description.

The other key issue concerns the validation of a model (i.e. the comparison with experimental data). This task requires the identification and computation of sensitive parameters from the theory side; the derivation of the corresponding data banks from directly measured quantities often requires very complex mathematical and computational procedures.

In view of these working areas, the Division continued to be composed of three groups: Analytic Theory Group (under T.E. Stringer until June 1986, later under D.F. Düchs, as acting Group Leader), Interpretation Group (early 1986 under D.F. Düchs as acting Group Leader, since June 1986 under T.E. Stringer), and Prediction Group (under A. Taroni). There is much natural overlap between their roles requiring extensive collaboration between the Groups, as well as strong interaction with experimental groups.

During 1986, the Division hosted the following visitors:

As Associated Staff members: Dr. W. Feneberg (IPP Garching, F.R.G.), Dr. H. Hamnén (Chalmers University, Gothenberg, Sweden), Dr. P. Mantica (CNR Milano, Italy), Dr. F. Romanelli (ENEA, Frascati, Italy), Prof. H. Schlüter (Ruhr-Universität Bochum, KFA Jülich, F.R.G.), and Dr. R. Sillen (FOM Jutphaas, The Netherlands).

As Visiting Scientists: Prof. J. Callen (University of Wisconsin, USA), Dr. Z. Jankowicz (Institute of Atomic Energy, Otwock-Swierk, Poland), Prof. H. Schamel (Ruhr-Universität Bochum, F.R.G.).

Under other arrangements (fellowships, contracts etc.): Dr. M. Kovanen, Dr. L. Lauro-Taroni, Mrs. M. Lorentz-Gottardi, Dr. A. van Maanen-Abels, Mr. A. Pichlmaier, Dr. F. Tibone, Mr. D. Ward.

Additional important support to theoretical work was provided through Article 14 contracts with the Associations and other contracts.

Article 14 contracts with Associations:

Numerical simulation of sawtooth behaviour in tokamaks	CEA, Cadarache, France.
Development of an ICRF global wave code	CEA, Cadarache, France.

Equilibrium transport code for a multispecies free boundary plasma	ENEA, Bologna, Italy.
Analytic models for predicting the velocity distributions in JET with the ICRF heating Sweden.	SERC, Gothenburg, Sweden.
A toroidal global wave numerical model of ICRF heating on JET	CRPP, Lausanne, Switzerland.
Code for simulation of non-thermal aspects of the ECE spectra	FOM, Jutphaas, Netherlands.
Extension of studies on polarisation and on non-thermal ECE from JET plasmas	CNR, Milano, Italy.
A critique of present theories of anomalous transport with relevance to JET	UKAEA, Culham, U.K.
By other contracts: The influence of plasma flows on plasma/magnetic field equilibrium configurations	CYFRONET, Institute of Atomic Energy, Otwock-Swierk, Poland.

The Division's 1986 activities can be presented under the following headings:

- Data Banks and Data Management Software
- Code Development for Code Library
- Data Interpretation
- Modelling of JET Plasmas
- Predictive Computations
- Analytic Plasma Theory

The Division's progress is described in the following sections.

Data Banks and Data Management Software

JET Survey Data Bank
(P. Smeulders, A. Galway, B. Hodge, M.G. Pacco)
Survey Data from all JET plasma discharges are stored in this bank. At present, it contains data sets for 5900 shots and ~140,000 time traces for a total of 330MB: on average ~55K bytes per pulse. The data for the Survey Bank are obtained either from the existing processed pulse files (PPF's) or from the raw data: the JET pulse files (JPF's). The original time traces can now be reduced using routines (specially written by P. Smeulders, D.F. Düchs and A. Pichlmaier) and then stored in the data base. In this way space is saved but all the important features of the original signals are kept. Existing programs at present run independently of JET discharges. A new program has recently been completed and, when installed in the JET data processing chain, will provide a one page shot overview with 18 selected time traces. This will allow a rapid comparison with earlier JET discharges to be made in the control room.

Survey Data Bank Software
(M.G. Pacco, B. Hodge, A. Pichlmaier)
The Survey Data Bank was implemented in a prototype version in 1985 and has now been brought to a production version. Its files have been reconstructed in order to save disc space and to increase efficiency. During the operation period, the Survey Data Bank is updated daily from PPF's and JPF's.

The Survey Data Bank consists mainly of three tables.

(a) S-PULSE, contains scalar parameters characterising a pulse, including gases, maxima of plasma current, density, RF and NB powers, times of switching on/off the NB and the RF heating, time of pellet injection, etc.;
(b) S-TIME-GRP, contains scalar parameters calculated at some specified time points for each pulse. Part of these parameters are loaded from the Transport Data Bank (J.G. Cordey, P. Lomas, K. Thomsen). Several validation checks have been introduced for these data;
(c) the largest table contains a set of time traces extracted from PPF's and JPF's.

A user interface has been developed, so that this Data Bank can be accessed without any knowledge of the NOMAD2 system. It allows searches on the data, print of selection lists or of function values, plot of the functions, statistical plots, etc.

Journal Data Bank Software
(B. Hodge, M.G. Pacco)
The Journal Data Bank contains the journal data existing on the NORD computer system until June 1986. Subsequent data will be loaded shortly. From the next operation period, journal data will be sent directly from the local NORD to the IBM computer system. Data stored includes: session aims, duty personnel, PF/TF/RF machine settings, vacuum parameters, daily pulse summary, pre- and post-pulse comments. A user interface allows an easy search through the data base. The Journal data base can be accessed directly from the Survey Data Bank.

Predictive Code Database
(B. Hodge, F. Tibone)
A database system has been made available in NOMAD to provide the possibility of storing the most significant results obtained from predictive transport codes. The system can also be used to store results from other codes. It allows code users to retrieve quickly recent and old results and it includes a flexible graphics utility for comparisons of results from the same or different codes and comparisons of computed and experimental results.

Database for Local Transport
(M. Brusati, S. Corti, A. Galway, N. Gottardi, P. Smeulders)
Specialised databases have been set up containing, for example, ion temperature profiles from neutral particle analysis, or spatial distribution over the cross-section of the radiation measured by bolometers. Such data bases are particularly necessary for the local transport analysis. Results from the local transport analysis code (JICS) are also stored. In this process, a standardised data handling and storage system is being developed.

Radiation Profiles
(N. Gottardi, P. Smeulders, A. Galway)
A data bank for the low energy radiation from the plasma, derived from the bolometer signals (KB1), has been established in the NOMAD environment. It is regularly filled with the surface averaged profiles obtained from the two-dimensional spatial distribution of the radiation (Fig.A1).

Simple Reduction of Data
(D.F. Düchs, A. Pichlmaier)
For most purposes, it is not expedient to use all data points of a measured signal. A very general and flexible procedure has been devised and programmed to reduce the number of data points without losing essential physics information. The program has been tested and applied to measured JET signals; reduction factors (number of retained points/original number) of about ten were easily achievable.

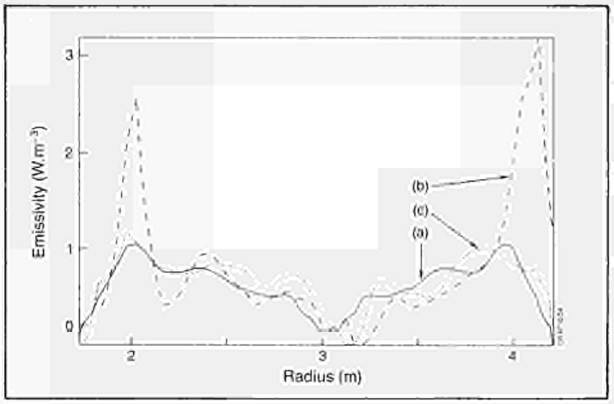

Fig.A1: Plasma radiation give by bolometer cameras:
(a) volume averaged emissivity: equatorial plane;
(b) original tomographic projection - equatorial cross-section;
(c) original tomographic projection - vertical mid-plane cross-section projection onto equatorial plane.

Code Development for Code Library

Equilibrium-Transport Codes and Related Packages
(W. Core, C. Sack, E. Springmann, A. Taroni, F. Tibone, G. Cenacchi*, F. Romanelli*) - (*ENEA Bologna, Italy) (*ENEA Frascati, Italy).
The 1½-D code JETTO has been updated both with respect to the equilibrium and the transport package. The equilibrium package ESCO can now be used for all possible cases of free boundary equilibria of interest in JET: limiter, inner wall and X-point configurations and compression experiments. The code is remarkably flexible, allowing arbitrary profiles of pressure and safety factor to be prescribed.

Several transport coefficients (both for electron and ion energy) derived from different theories have been included in the transport part of the code with the purpose of checking against JET experimental results. A transport coefficient, χ_e, based on a generalised definition of profile consistency has also been derived and included in the code. JETTO has also been linked to data bases where JET experimental results are stored. This is achieved by means of a generalised package allowing use in the code of any subset of measured quantities (either time traces or profiles as a function of time). In this way, the task of testing models and the consistency of measured quantities is remarkably simplified.

Plasma Boundary Code
(Z. Jankowicz, R. Simonini, A. Taroni, W. Feneberg*) - (*IPP Garching, F.R.G.)
The 2-D boundary code EDGE2D developed at JET has been coupled to the output of MHD codes (IDENTC or ESCO) providing the magnetic flux surface configuration of JET plasmas. The computational mesh of EDGE2D is thus derived for realistic magnetic configurations and for both limiter and X-point cases (see Fig.A2). The code has also been extended to take into account simple models for radiation loss and work is in progress to include the radial electric field and two temperature equations.

Orbit-Following Code for Particles Produced by Fusion Reactions (W. Core, H. Hamnén, M. Kovanen)
The charged particle orbit following code - CPOF - has been developed and provides the possibility of tracing the charged particle orbits with three different methods:

- solving the full equation of motion for charged particles (P. van Belle and G. Sadler)
- using guiding centre approximation
- using the constants of motion method for guiding centre.

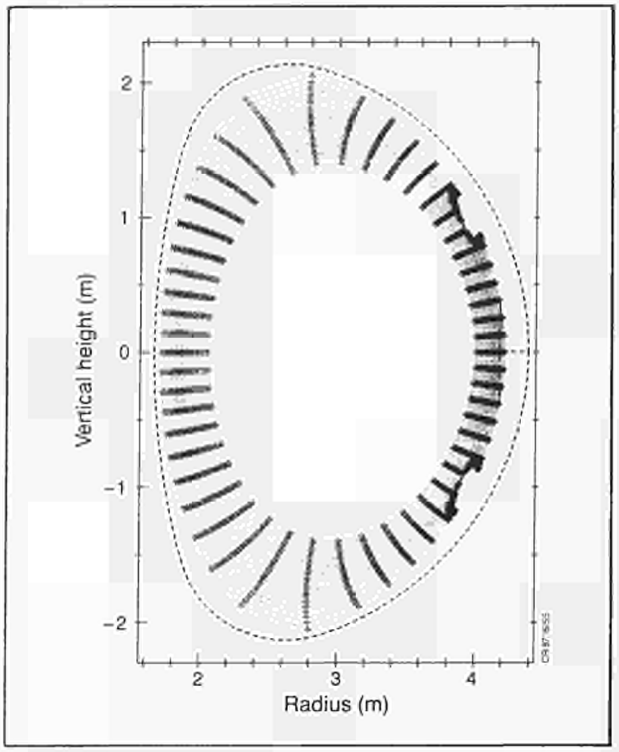

Fig.A2: Magnetic flux surface configuration using EDGE2D (limiter case).

The code can be used for both circular and non-circular plasma cross-sections.

The poloidal magnetic field is presently based on an analytical model derived from the Lao-Hirshman representation of the poloidal flux function. The toroidal magnetic field is calculated from $B_T = R_0 B_0 / R$, where B_0 is the toroidal field strength in the centre of the vessel. For the slowing-down calculations, the Coulomb scattering on the background ions and electrons is included by calculating the new values for the particle energy and the magnetic momentum after each time step. The code is being linked to experimental databases in the same way as transport code JETTO, and will be suitable for studying a wide range of problems related to the production of particles by thermonuclear reactions.

Mapping of Magnetic Field Lines

(C. Sack)

A new code, developed at Bochum University, FRG, has been implemented at JET to compute perturbed magnetic field lines. The code is based on a transformation of the field line equations to a general Hamiltonian formulation that is suitable for comparisons with existing theoretical results referring to the ergodisation of magnetic field lines.

Identification of Plasma Equilibrium from Experimental Data

(E. Lazzaro, P. Mantica)

The identification of the current profile from experimental data is still an open problem. It has been demonstrated that finding the current profile whose computed poloidal magnetic field best fits that measured internally, does not reliably determine the real profile. This is because the external field is insensitive to the profile in the central region. However, the addition of independent information, such as the value of the diamagnetic flux, the location of the q rational surfaces provided by the ECE heterodyne system, and possibly the Faraday rotation measurements, could help to restrict the possible current profiles. A new code embodying these features is being designed and will be produced in cooperation with J. Blum, INRIA, France.

Design of Double and Single Null Magnetic Separatrix Experiments

(E. Lazzaro, B. Keegan, P. Rutter)

Extensive improvements have been made to the magnetic equilibrium code INVERSX to allow accurate design of special plasma configurations, extending the plasma current range to 7MA. The iron model has been revised, including detailed permeability curves for eight materials, and the results have been benchmarked against experimental measurements of stray fields. The design of separatrix configurations for the 1986 experimental campaign was extended to single null configurations with currents up to 3MA. The response of the configuration to variation of the shaping currents was analysed and made available in a data bank. The experiment (carried out with A. Tanga and the JET Operations Group) proved to be highly successful. Transition to the H-mode was observed in over 30 discharges with single null configurations at plasma currents of 2 and 3MA. Confinement times of over 0.7s were obtained, with additional power levels about 5 times the ohmic power.

An attempt to extend this promising regime to 4MA plasma current will be made next year. To produce a

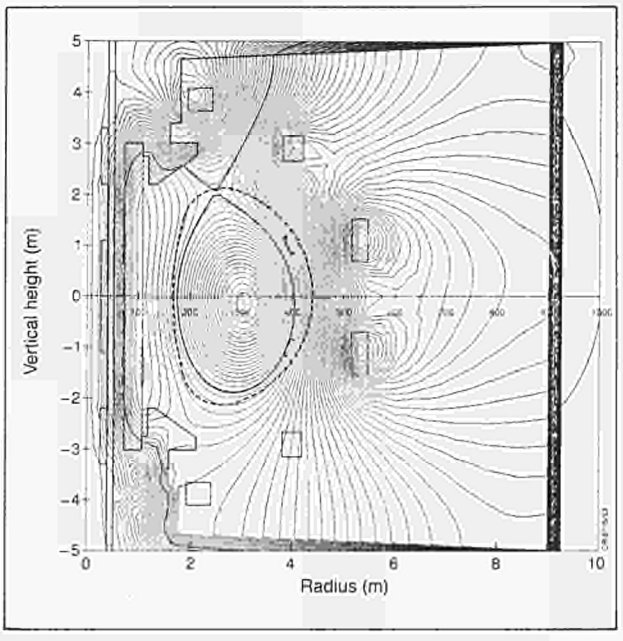

Fig.A3: Computed magnetic flux configuration for a single null separatrix at I_p=4MA.

double or single X-point configuration at this current, the shaping action must be supplemented by a controlled leakage field from the primary OH coil. This requires the addition of an extra pan-cake and non-uniform distribution of the inductance matrix, and the local forces and fields for these extended configurations have been provided. Fig.A3 shows a computed X-point configuration at 4MA.

Derivation of Electron Density Profiles
(N. Gottardi, E. Springmann)
A public user-friendly program (NEPROF) has been produced to allow general access to the line integrated data from the multichannel interferometer (KG1) stored in the JET Pulse File (JPF), and to produce electron density profiles. The same program allows specified people to store profiles of general interest in a newly established data bank in the NOMAD environment. The program uses the generalised Abel inversion (projection) method for deriving electron density profiles in very difficult critical situations, e.g. X-point, inner wall, and pellet injection pulses. An example of its versatility is illustrated in Fig.A4, which shows the time evolution of the density during the pellet injection phase of Pulse No.:9377.

Radiation Profiles
(N. Gottardi, P. Smeulders, A. Galway)
A 2-D distribution of radiation losses has been obtained using a new and very fast code, based on a tomographic method already successfully used for the analysis of the soft X-radiation from ASDEX. A user-friendly program to allow general access to the data bank has also been developed.

The code allows the line integrated measurements to be inverted when the radiation is strongly asymmetric in the poloidal direction, which is the case in almost all JET discharges. This method fails to deliver the profile only in certain cases (e.g. X-point configurations), where the number of useful measuring channels is reduced. The old (slow) projection method has also been implemented to deal with these special situations.

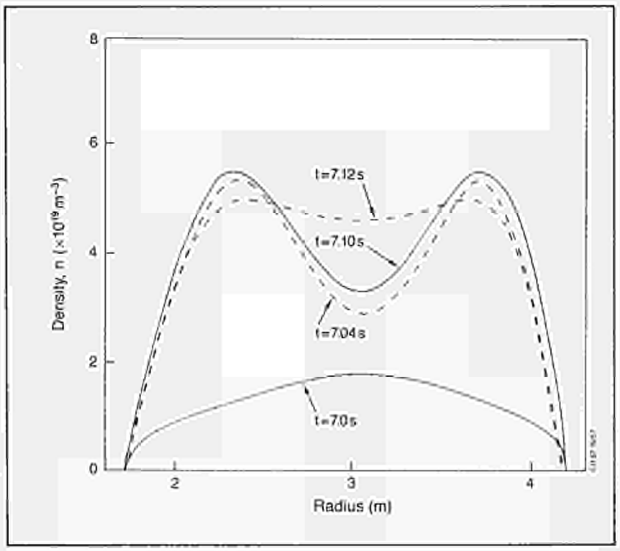

Fig.A4: Electron density profile following pellet injection at t=7.0s.

Data Interpretation

Installation of the ECE code NOTEC
(R.M.J. Sillen*) - (*FOM Institute for Plasma Physics, Nieuwegein, The Netherlands)
The ECE code NOTEC, developed at the FOM Institute for Plasma Physics was installed on the Harwell Computer System. Programs using the PLOT10 package to show the results of NOTEC, were developed and tested. NOTEC was applied to the ECE spectra measured during the slide-away discharges and the results were most promising. NOTEC can simulate ECE spectra from plasmas that include suprathermal populations.

Neutral Beam Current Drive
(H. Hamnén, C. Challis, J.G. Cordey)
An analysis of neutral beam heated plasmas has been undertaken to assess the magnitude and profiles of non-inductive currents driven by the beams. In typical JET discharges, the currents driven are about 0.5MA.

Second Harmonic ICRH Heating of Fast Injected Ions
(W.Core, H. Hamnén, G. Cottrell)
An analysis of ICRH/NB heated JET plasmas has been undertaken to assess coupling of the ICRH to fast injected ions via second harmonic heating. In typical present day conditions, the fraction of the RF-power absorbed by the injected ions could reach 10%.

Bootstrap Current Drive
(H. Hamnén)
An assessment has been made of the magnitude of the expected bootstrap current in JET. In present day operating conditions, it would be typically ~ 100kA. If the present confinement degradation persists, it might be difficult to reach a bootstrap dominated JET plasma even with the future power capacity.

Local Transport Analysis
(M. Brusati, D.F. Düchs, A. Galway, T.E. Stringer, N. Gottardi, E. Lazzaro)
The JICS interpretation code evaluates the individual components in the local energy balance, and so derives the heat flux due to conduction and convection. The number of pulses for which the complete analysis is possible has been limited so far by the availability of a complete set of diagnostic data. Figs.A5 and A6 show, for typical ohmic and RF heated pulses, how the volume integrated electron energy sources (ohmic, RF) and sinks (radiation, electron-ion transfer) vary with radius, together with the derived electron thermal energy flux, F_e.

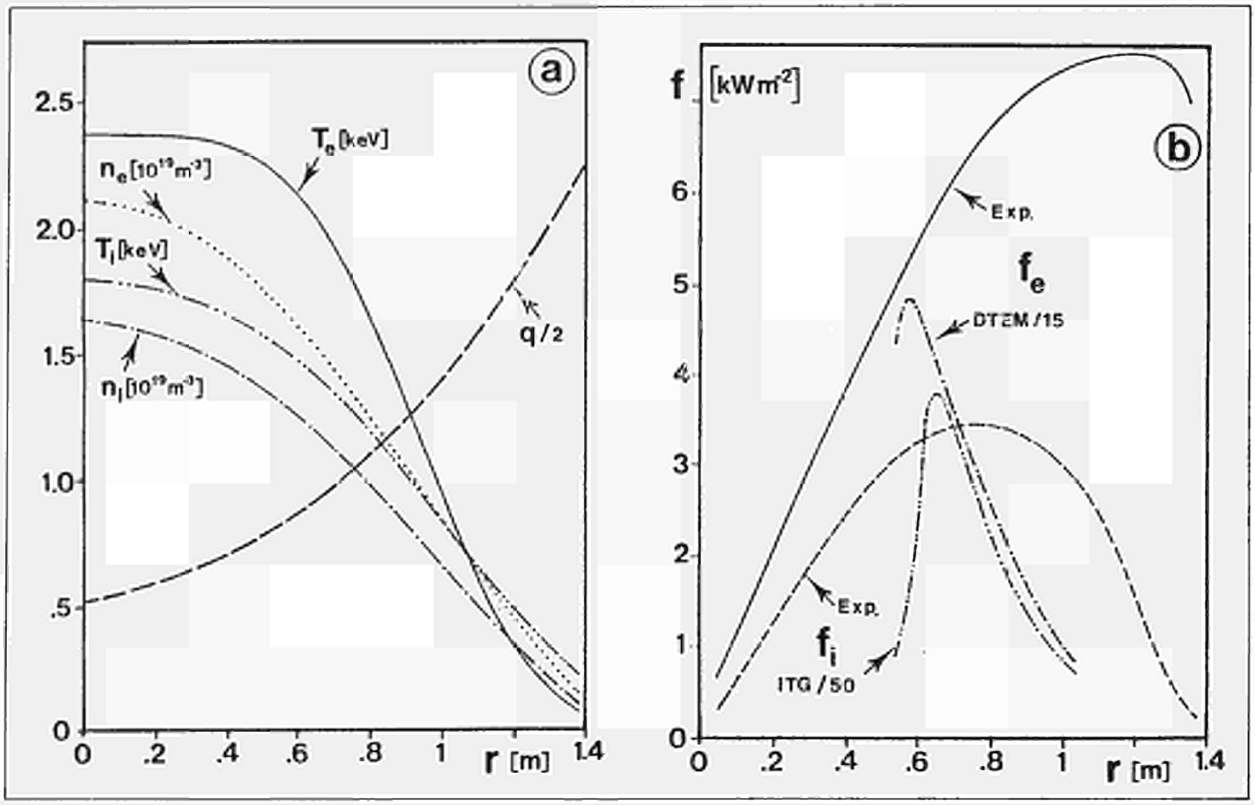

Fig. A5: Measured surface averaged thermal fluxes f for electrons and ions (b) for the ohmically heated JET plasma with plasma parameter profiles as in (a). Scaled down theoretical prediction (by factor of 15) from dissipative trapped electron mode (DTEM) for electrons and ion temperature gradient instability (ITG) for ions are added in (b).

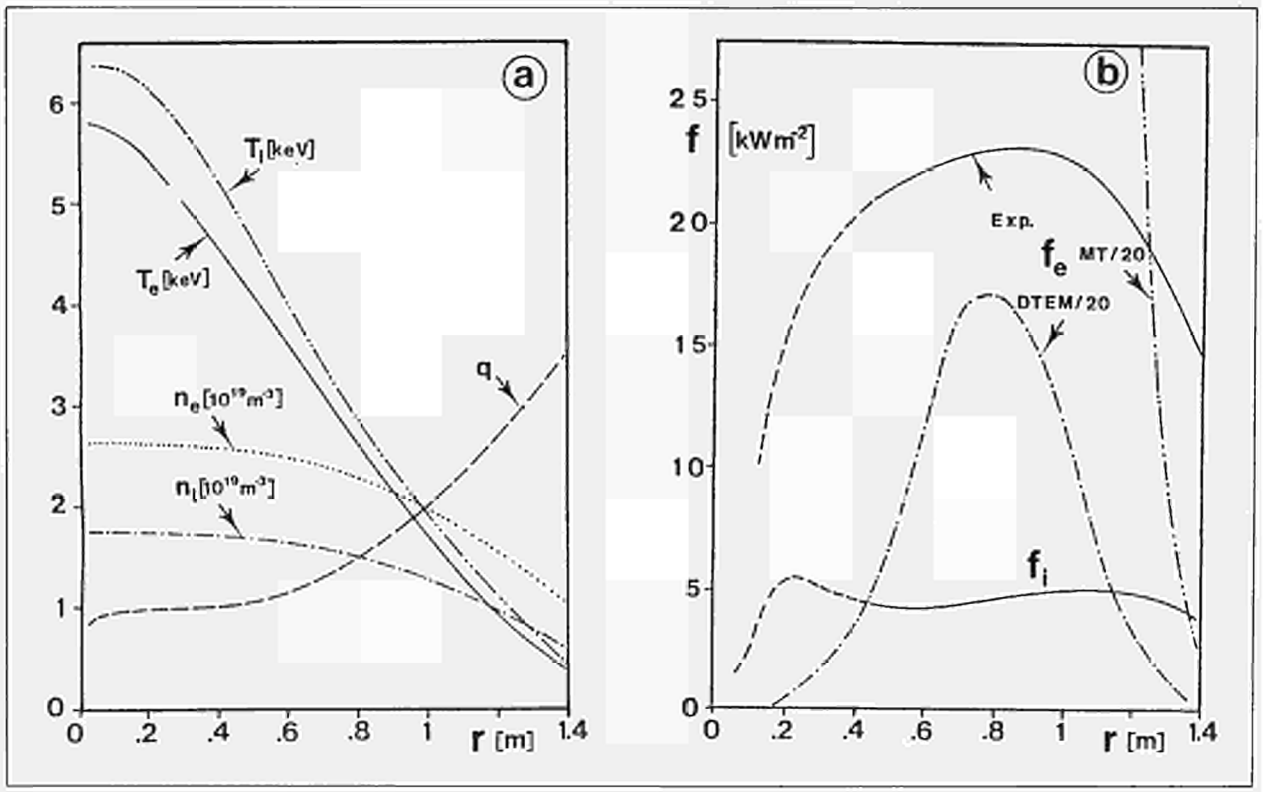

Fig. A6: Surface averaged thermal fluxes f for electrons and ions (b) for an RF heated JET plasma characterised by plasma parameter profiles shown in (a). The uncertainty of f is enhanced within the sawtooth region (dashed (b)). The electron heat fluxes predicted for the DTEM and microtearing modes MT (scaled down) are shown in (b).

The electron and ion energy fluxes have been compared with theoretical prediction for various plasma instabilities. The magnitudes of the fluxes are less than the maximum predicted for the dissipative trapped electron mode and the ion temperature gradient mode, though still within the uncertainty in the estimate of the saturation level. The radial variation in the conductivity, however, cannot be explained by either of these modes.

Modelling of Temperature Profiles and Transport Scaling in Auxiliary Heated Tokamaks
(J.D. Callen*, J.P. Christiansen, J.G. Cordey, P.R. Thomas, K. Thomsen) - (* University of Wisconsin, Madison, U.S.A.)
The temperature profiles produced by various heating profiles are calculated using two rudimentary local heat transport models (constant heat pinch or excess ΔT, and nonlinear χ) that are consistent with local measurements of heat transport. The model predictions are shown to agree with JET data for a variety of heating profiles ranging from peaked on-axis, through approximately flat (NBI at high density), to localised off-axis (ICRH). The modest temperature profile responses predicted ($\leq 20\%$ for physically relevant heating profile changes) clarify why temperature profiles in many tokamaks are often characterised as exhibiting a high degree of "profile consistency". Global transport scaling laws are also derived from the two models and compared with JET data. The constant heat pinch or excess ΔT model, which provides the best description of present local and global JET heat transport data, leads naturally to the offset-linear scaling law for the stored energy, and to a definition of the heating efficiency as a function of the heating profile.

Modelling of JET Plasmas

Modelling of Ion Cyclotron Heating
(T. Hellsten)
Ion cyclotron heating has been modelled for various heating scenarios, using the codes LION and ISMENE to determine the wave propagation and absorption, and BAFIC and other semianalytical prescriptions to calculate the energy transfer to the background plasma species.

For minority heating of hydrogen, finite gyroradius effects have been found to become important in determining the evolution of the velocity distribution. The timescale for energy transfer to the electrons is strongly reduced compared to the Spitzer time. This explains the relatively short energy transfer time currently being observed during modulation experiments.

Analyses of Wave Propagation by Global Wave Codes
(K. Appert*, T. Hellsten, J. Vaclavik*, L. Villard*) - (*CRPP Lausanne, Switzerland)
Wave propagation in tokamak plasmas is computed using the global wave codes LION and ISMENE. The coupling spectra of the magnetosonic wave during ICRH has been analyzed. For the heating scenarios and parameters currently used, it is found that the coupling spectra are characterised by a compound resonance peak. The wave spectrum launched is narrower than when reflection is not included. This compound resonance also modifies the coupling resistance. This has been compared with the oscillations of the measured coupling resistance during ramp down of the toroidal magnetic field, and good agreement has been found. This supports the present model for magnetosonic wave propagation in JET. A study of mode conversion in toroidal plasmas showed that the amount of mode conversion depends only weakly on the details of the absorption mechanism, and that the mode conversion surfaces are aligned with the magnetic surfaces.

Analysis of the Velocity Distribution During ICRH
(D. Anderson$^+$, W. Core, L-G. Eriksson$^+$, H. Hamnén, T. Hellsten, M. Lisak$^+$) - ($^+$Chalmers University, Göteborg, Sweden)
A simplified model has been developed to calculate the velocity distribution during ion cyclotron heating, including finite gyroradius effects and heating due to the electric field component rotating in the opposite direction to the ions. This model can treat fundamental cyclotron heating as well as second harmonic heating of an injected species and ions produced by fusion reactions. Although the model assumes an isotropic distribution, quantities like energy transfer to electrons and ions, fusion yield and modification of the cyclotron absorption show good agreement with the results of 2-D calculations using a more exact Fokker-Planck code (BAFIC).

Changes in Magnetic Topology and Associated Heat Flow
(M. Brusati, A. Galway)
A theoretical model of plasma transport is being developed which is based on partial ergodisation of magnetic field lines associated with small magnetic islands. The perturbed field topology is sustained by fluctuations in plasma current driven by local heat flow, and leads naturally to a rigidity of the electron temperature profile in the confinement zone. This model describes the coexistence of ergodic and non-ergodic field lines as a dynamic equilibrium between two phases in the plasma-magnetic field system, triggered by the electron temperature reaching a critical gradient.

Local Energy Transport Study
(A. Taroni, F. Tibone, D.F. Düchs, T.E. Stringer, M. Brusati, N. Gottardi, T. Hellsten, F. Romanelli*) - (*ENEA Frascati, Italy)
An extensive study of the energy transport properties of JET plasmas has been performed. It has been shown that available "theoretical" transport coefficients cannot be used to simulate the large variety of plasma regimes

found in JET (Ohmic, ICRH and NB heating in various conditions, including H-modes). Adjustment coefficients larger than those claimed in the literature seem to be required. Work is in progress to provide theoretical justification (i.e. a more accurate derivation of χ_e and χ_i) for the cases of the so-called dissipative trapped electron and ion temperature gradient modes.

This study has pointed out that the local transport coefficient, χ_e, must either be abandoned on the basis of "profile consistency" arguments, or modified to introduce a dependence on local gradients. The situation is more complex in the case of χ_i, as reliable T_i profiles are not available, but there is "circumstantial evidence" that χ_i is neither neoclassical nor proportional to neoclassical. The same study has also pointed out that in JET:

- the confinement properties of the central region ($q < 1$), during the time between sawtooth collapses, are similar to those outside this zone;
- the boundary region could play an important role in determining the overall energy confinement properties of JET.

Predictive Computations

Effect of Sawteeth on α-Particle Power
(J.A. Wesson)
In pulses with substantial additional heating, the central temperature in JET can fall to half its peak value during a sawtooth collapse. Given the associated fall in density and the strong dependence of the thermonuclear reaction rate on temperature and density, the loss of α-particle power under thermonuclear conditions could be substantial. Calculations were therefore carried out to assess the improvement in α-particle power which would result from the stabilisation of sawteeth.

The two basic parameters are the volume affected by sawteeth and the confinement properties of the central core. In the limit where the confinement is the same as the general confinement, a substantial enhancement in α-particle power is possible provided the core region is sufficiently large. The α-power improvement factor depends on the amplitude of the sawteeth being stabilised, but in JET an improvement factor of up to 5 could be obtained.

Predictive Computations of Plasma Boundary Properties with Belt Limiters
(R. Simonini, A. Taroni)
The 2-D plasma boundary code EDGE2D and the 2-D Monte-Carlo neutral particle code NIMBUS, have been extensively used to provide information on the design of pumped limiters in JET. In particular, density and temperature profiles and particle and energy fluxes at the limiters and wall have been evaluated, pointing out the importance of an accurate simulation of all aspects of the problem, from molecular and atomic physics to geometry. This work is still in progress and has motivated a further development of the EDGE2D code and its interface with NIMBUS to take into account a detailed description of the geometry of the limiters and of the flux surfaces close to the limiters.

ICRH Current Drive
(H. Hamnén)
Non-inductive current drive by ICRH heating of a minority species has been studied in terms of efficiency and compared to ICRH heating of a species injected by the beams. The first scheme has been found to suffer from serious drawbacks and only when tuned to the beams does the efficiency of ICRH current drive reach acceptable levels.

Analytic Plasma Theory

Stability of the m=1 Mode
(J.A. Wesson, F. Nave)
Following the realisation that the behaviour of the ideal $m=1$ mode in toroidal geometry is sensitive to the q-profile, an analytic stability calculation was carried out. For simple algebraic profiles, the $m=1$ mode is stable up to a critical central $\beta_p \sim 0.3$. If such a q-profile having a central value of q given by $q_o = 1-\Delta q^*$, is flattened within the $q=1$ surface, so that the value of q_o increases to $1-\Delta q$, then the critical value of β_p is lowered to

$$\beta_p = \left[\frac{13}{144}\,\frac{3\Delta q}{\Delta q + 2\Delta q^*}\right]^{1/2}, \quad q_o < 1$$

Thus for small Δq, the critical β_p is much reduced. If $\Delta q<0$, corresponding to an off-axis minimum in q at $q=1$, the ideal $m=1$ mode is unstable for any β_p. These results have important implications for understanding sawtooth behaviour.

Non-Linear Tearing Modes
(J.A. Wesson, F. Nave)
A theory of the non-linear behaviour of tearing modes in the presence of a conducting wall has been developed. At high phase velocities, the wall behaves as a good conductor and has a stabilising effect on the tearing mode. However, as the amplitude of the mode grows, there is a momentum transfer to the plasma arising from the imaginary part of the well known Δ' function. This results in a reduction of the phase velocity and a consequent reduction in the stabilising effect of the wall. This behaviour proceeds with increasing rapidity and ultimately the mode locks to the wall. A computer code based on the analytic model has been written and this is being used to solve for the time dependent development of the magnetic island and the phase velocity.

MHD Simulations of Sawteeth
(P. Kirby*, J.A. Wesson) - (*Culham Laboratory, U.K.)
The understanding of sawtooth oscillations requires non-linear calculations to explore the feasibility of the various models proposed, and to clarify certain crucial elements

of the physical processes involved. Several such simulations have been carried out. Perhaps the most interesting are those which study cases with low shear in the central core. Although the calculations are cylindrical, they demonstrate clearly the bubble formation seen in the tomographic reconstructions of the soft X-ray emission in JET. For somewhat higher shear, partial bubble formation is found, the plasma rearrangement being localised to the region around the $q=1$ surface. This may correspond to the observed partial sawtooth collapse. A comparison of a flat q simulation with experimentally observed soft X-ray contours is shown in Fig.A7 to illustrate the general similarity in the behaviour.

Fig.A7 shows the development of contours of equal soft X-ray emission during the sawtooth collapse. A numerical simulation of the quasi-interchange instability is compared with the tomographic reconstruction of a sawtooth collapse on JET. The shaded region indicates the hotter part of the plasma to clarify the distinction between the observed behaviour and that of the classical model involving island formation in the colder plasma.

Analysis of Feedback Stabilisation of Tearing Modes
(E. Lazzaro, M.F.F. Nave, J.A. Wesson)
The operation of JET at high currents implies working at low values of the safety factor at the edge, and hence increased danger of disruptions. To prevent and control disruptions, detailed technical studies for stabilising coils are being undertaken in JET. The physics description of the stabilisation of tearing modes presents a number of open questions which are being addressed in a cylindrical model. Stabilisation of a single helicity mode is considered by modifying the boundary conditions using a single helicity external current. The instability is characterised by both the growth in island width and rotation. The current and power needed to control this is being estimated, taking into account the finite resistivity of the wall.

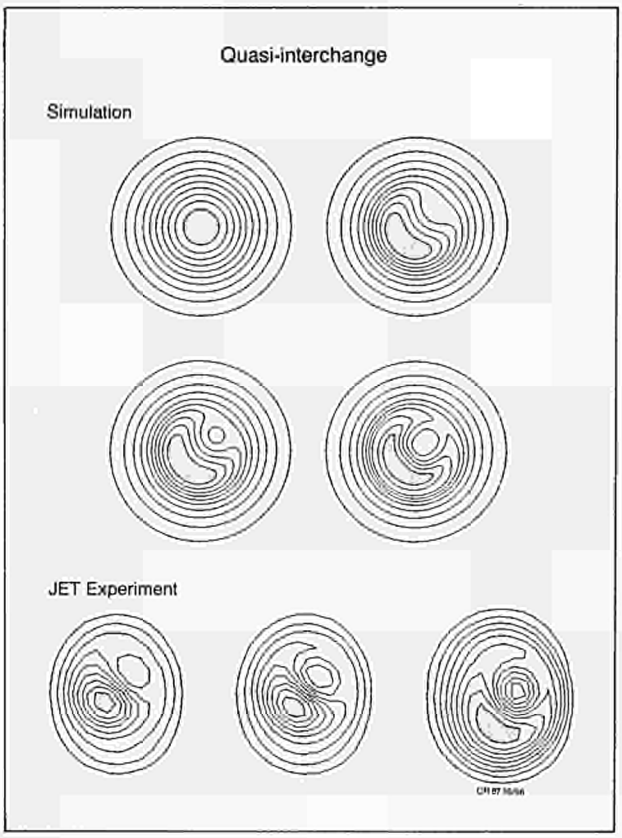

Fig.A7: Development of contours of equal soft X-ray emission during a sawtooth collapse:
(a) simulation of the quasi-interchange mode:
(b) as seen experimentally in JET.

Anomalous Transport Theory
(T.E. Stringer)
There is an apparent discrepancy between the thermal diffusivities derived from confinement and from the sawtooth heat pulse propagation in JET and TFTR. One possible cause is that the energy transport law contains an inward convection term, in addition to the usual outward diffusion. The effect of such an inward convection of the energy confinement would be much greater than on the heat pulse propagation. The observation that additional heating significantly reduces the confinement, but has little effect on the heat pulse, would then imply that additional heating significantly reduces the inward convection, but not the diffusion.

The analytic derivation of the energy flux due to various instabilities has been re-examined, in a search for an inward convection mechanism. The heat and particle flows due to drift wave instabilities are found to have the required form. Whereas the diffusive component depends on bulk parameters, the convective component depends on the gradient of the electron velocity distribution function. The change in this due to additional heating is not negligible, but does not appear to be large enough to account for the degradation in energy confinement.

Analytic Investigation of Temperature Isotropization
(H.K. Schamel, D.F. Düchs, T.E. Stringer)
The energy relaxation of an anisotropic bi-Maxwellian distribution function caused by like-particle Coulomb collisions is investigated in detail taking full account of the non-linearity in the Fokker-Planck description. Combining KOGAN's expressions for $\dot{T}_\parallel$ and $\dot{T}_\perp$, a single equation is derived describing the time evolution of $\epsilon = T_\perp/T_\parallel$. The complete time history is presented for ϵ for both regimes $T_\perp < T_\parallel$ and $T_\perp > T_\parallel$. For $T_\perp \ll T_\parallel$, a logarithmic singularity is found in the rate of relaxation exhibiting the non-linear character of the isotropization process.

Enhancement of Collisional Drag by Anisotropy
(H. Schamel, H. Hamnén)
The collisional drag particles experience due to like-particle Coulomb collisions is investigated for anisotropic waterbag distributions. A general increase is found in comparison with the drag for isotropic distributions.

described by enhancement factors. For $T_{\parallel} >> T_{\perp}$, as in e.g. runaway situations, it becomes logarithmically singular in agreement with a similar behaviour of the rate of energy relaxation.

Scaling Methodology
(D.F. Düchs, L. Lauro-Taroni)
The limits and expediency of the usual power product ansatz has been clarified. For a given number of experiments (data sets), the maximum number of independent variables can now be determined by a simple procedure. In addition, it has been investigated how given experimental error bars can be exploited to identify possible inner relations between the (assumed) independent variables. A corresponding computer programme has been applied to statistically analyse various JET plasma parameters such as electron and ion temperatures, voltages and confinement times.

Non-Linear Double-Tearing Mode
(M. Lorentz-Gottardi)
The non-linear evolution of the double-tearing instability has been investigated with special respect to anomalous current penetration in tokamak discharges. Allowing for current rise and diffusive transport in a non-linear MHD code (RSF), it was shown that in the presence of a hollow current density the double-tearing instability considerably enhances current penetration when low mode numbers (m=2,3,4) are involved. Interaction of diffusive transport with the instability then levels the q(r)-profile starting from its minimum value q_{min} right across the plasma centre. The flattening process scales with the resistive time, τ_R, and is by a factor 0.01-0.1 faster than τ_R, depending on the shape of the current density and resistivity profiles. For high mode numbers ($m \leq 6$), the double-tearing mode does not contribute to current penetration. The model predicts, for a hollow current density profile, a sequence of magnetic perturbations with falling mode number m, where each mode occurs only once, when $q_{min} < m$. The perturbations grow stronger as m decreases and lead to flattening of the current density for low m. Preliminary comparison with experiment shows good agreement.

Appendix II

Data Processing and Analysis

(Group Leader: J.G. Cordey)
The Data Processing and Analysis Group was set up in February 1986 to co-ordinate the acquisition, processing and analysis of JET data. The group is strongly task-driven with staff working in several different areas. Most of the diagnostics and their accompanying software have now been installed and a significant part of the Group's effort has now been directed to improving data processing by the introduction of more sophisticated codes and in improving the manipulation and display of the data. This has also included a study of the use of personnel computers for presentation graphics and data manipulation. A brief description of the Group's data interpretation activities is also presented.

Diagnostic Software Development
The group is responsible for developing software for diagnostics and for handling their computer interface to the CODAS computers. During 1986, the following diagnostics have been successfully interfaced to CODAS.

Limiter Temperature Monitors (KL2)
(K. Slavin and C. Best)
A complex data acquisition system to digitise the outputs of an infra-red Mesa array viewing the limiters has been developed and commissioned. On-line display software was written to give a colour contour map of the temperatures in the control room. An analysis program has also been developed to yield the power loading during a JET pulse.

Pellet Injector Diagnostic (KZ1)
(C. Best)
The software to provide full remote control from a CODAS console has been commissioned. A set of MIMICS touch panels and a real time program have been successfully used during operation of this diagnostic.

Neutron Diagnostics (KN3 and KM3)
(K. Slavin and D. Wilson)
The data acquisition systems for the Neutron Yield Profile (KN3) and Time of Flight Spectrometer (KM3) have been implemented and are now operational. The KM3 system required the development of a real-time program to control a wedge scintillator position during a JET pulse. This is necessary to handle the wide variation in neutron fluxes.

The Fast Transfer System (KY2)
(K. Slavin and D. Wilson)
The data acquisition system has been implemented and first data produced for this diagnostic. A flexible software system to handle and analyse data from a variety of probes is under development.

Calibration (KT2)
(F. Sieweke)
A calibration dataset has been set up for the KT2 Spectrometer. It contains several tabulated calibration curves which are used by the data calibration procedures to convert pixel numbers into wavelengths, to compensate for the high voltage, or to convert the raw ADC values into real light intensities. Another dataset identifies the various spectral lines with their position on the pixel array.

Transport Data (KT2)
(F. Sieweke)
The transport data base contains information for selected pulses at selected time points. A program has been written to interpolate time histories at the time points of the transport data base. The result can be visually verified at a terminal before it is stored together with the transport data. The combined KT2 and transport data base is then filed as SAS datasets.

Soft X-ray Camera (KJ1), X-Ray Crystal Spectrometer (KX1), Active Beam Diagnostic (KS4)
(E. Oord)
During 1986, the Soft X-ray Camera (KJ1) data retrieval and display software were completed. This permits data with different sampling rates (or time windows) to be superimposed on one graph and the speedy detection of detector saturation. The High Resolution X-ray Crystal Spectrometer (KX1) was also successfully brought on-line. An interactive bandfit procedure was developed mainly for incorporation in the Active Beam Diagnostic (KS4) data analysis software. However, it is available as a stand-alone package and can be used when the automatic fit procedure fails.

X-Ray Pulse Height Analysis Software (KH2)
(E. van der Goot)
Analysis software for the X-Ray Pulse Height Analysis System has been developed on the NORD computer and ported to the IBM mainframe using NICE. The IBM version has been extended to enable the production of PPF's in interactive and in batch mode. The software now produces automatically a PPF containing the electron temperature, the concentration of metal impurities, the X-ray anomaly factor and Z_{eff}.

Lidar Thomson Scattering (KE3)
(T. Gadd)
The Lidar diagnostic uses fast oscilloscopes to digitise the detected back scattered laser light from the plasma. These oscilliscopes have been interfaced to the NORD computer system to allow remote control and data acquisition. Programs have been written for commissioning the diagnostic and were used for first operations on JET. Display and analysis software was developed to process these first results. The software is installed on both the IBM and NORD computers. Current developments are in the design of software for the full operation under CODAS.

FORTRAN Source Code Conversion
(E. van der Goot)
A utility program, NICE, has been developed to allow easy transfer for programs that have been written on the NORD computers to the IBM mainframe environment. The program, written in Pascal, converts most of the non-standard FORTRAN extensions. It also reformats the source code, so that the generated source is easy to read and to maintain. It offers several additional features to make the transfer as easy as possible.

Other Software Support
(C. Best, E. Oord and D. Wilson)
The group has also supported various upgrades to existing diagnostics. Upgrades to the magnetics diagnostic (KC1) has involved considerable effort, and a new method for accurately recording events such as disruptions has been developed.

Automatic diagnostic status checks have been implemented into JET operations. During the JET countdown, the failure of an essential diagnostic will inhibit a pulse. The status of all diagnostics is monitored and displayed on a central MIMIC. This system required the development of several real time programs. Of particular note is the magnetics (KC1) check program. This program performs on automatic validation of the data after a pulse can detect ADC failures, drifting integrators, etc..

Considerable effort has been devoted to unifying the NORD and IBM analysis software. A series of methods to ease transfer of software from the NORD to the IBM have been developed. This has involved installing a graphics package IGL, the terminal handling system and GETDAT on the IBM system. Several application programs have been transferred to the IBM mainframe computer. Procedures have also been developed for writing new analysis software which will enable them to run easily on either computer system. This provides diagnosticians with a standard software image irrespective of which computer system they use. As an example, the BROWSE display program developed on the NORD, now provides the same interactive graphics to any JPF or PPF signal on the IBM system.

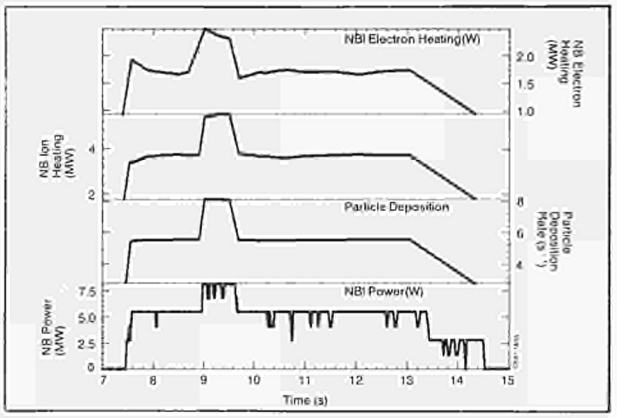

Fig.A8: Fast ion heating and deposition parameters as a function of time during Pulse No: 9775.

Data Processing Software Enhancements

Integrated Analysis
(J.P. Christiansen)
Improvements have been made to the integrated analysis of JET data applied to most JET plasma pulses. Data from a series of similar JET pulses with positive - negative field and current in four combinations established a plasma current coupling to the diamagnetic loop signal and the data also improved the calibration required to compensate for toroidal field coil expansion. The ion temperature data from the crystal X-ray spectrometer has been included to produce one further kinetic estimate of plasma energy. To facilitate data reprocessing due to hardware and software errors and faults, extensive computerised logging procedures of the latter have been produced.

The Neutral Beam Injection Code PENCIL
(D.G. Muir and P. Stubberfield)
In order to understand the interaction of neutral beams with JET plasma, the prediction code PENCIL [1] has been modified into an on-line data analysis code and integrated into the JET processing chain. The deposition of fast ions, particle heating, current drive and other effects associated with neutral beam heated plasmas are now determined inter-shot. Fig.A8 shows the fast ion deposition and heating for Pulse No:9775.

PENCIL has undergone considerable development during 1986. It has been linked to another program [2] which solves a simplified Fokker-Planck equation in order to model the evolution of the thermalising fast ion distribution. In addition, this Fokker-Planck solver has been updated to include the effects of toroidal geometry and the trapping of fast ions, which are important in the simulation of the beam driven current. Finally, the

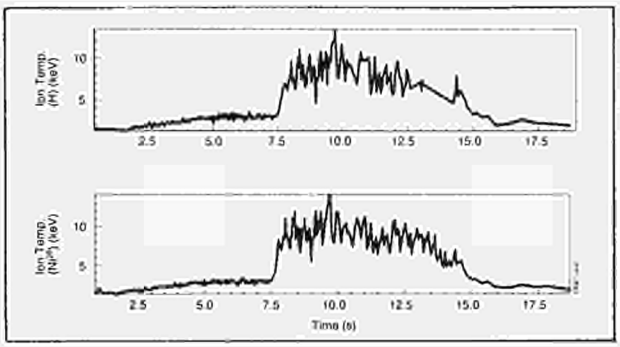

Fig.A9: X-Ray Crystal Spectrometer (KX1) data of H and Ni^{26} impurity ion temperatures as a function of time during Pulse No:9775.

geometrical modelling of the magnetic flux surfaces in JET have been revised.

In addition to neutral beam data analysis, PENCIL has been used as a production code with the results of predictions written to the PPF data base and the SAS package used to analyse results. This combination has proved a very powerful tool in exploratory studies of upgrades of the neutral injection system.

The pellet injection code, PELLET has been reconstructed so that electron density and temperature data from the PPF database can be accessed. This work is in preparation for the integration of pellets into the intershot processing chain during 1987.

In association with M. Shaw, a data analysis code has been written which determines a hydrogenic ion temperature from the observed KX1 spectroscopic measurement of the Ni^{26+} impurity temperature (see Fig.A9). The calibration is based on a simple energy balance model [3] taking account of the stronger impurity heating during NBI. This program is currently undergoing final testing before it is integrated into the intershot processing chain in 1987.

Ion Temperature from X-ray Crystal Spectrometer (KX1)
(M. Shaw)

Improvements have been made to the KX1 analysis program. The fit of the experimental data has been modified and more peak position and peak intensity points have been produced by the addition of a second fit lower statistics.

A new program has been developed to calculate the hydrogenic ion temperature from the KX1 nickel ion temperature data. The fractional abundance of Nickel and the power transfer from ions to electrons are also calculated. Fig.A9 shows both the KX1 impurity temperature and the hydrogenic ion temperature for Pulse No:9775.

Transport Database
(J.G. Cordey, P. Lomas, A. Parker and K. Thomsen)

The collection of data for the transport database has been re-organised. This contains for each shot a selected number of time slices. The results from pure ohmic and separatrix experiments are first inserted in an "Ohmic" transport database. The neutral beam injection results are stored in a NBI database and results from ICRH heating experiments are stored in an ICRH database. The three different databases contain a common set of variables which are relevant to the particular heating technique. The data is first checked in these three databases and the common set is then transferred to the transport database.

In this way, comparisons of all results can easily be made using the transport database, while more detailed selections can be made in the three sub databases. All four databases are available too all JET users.

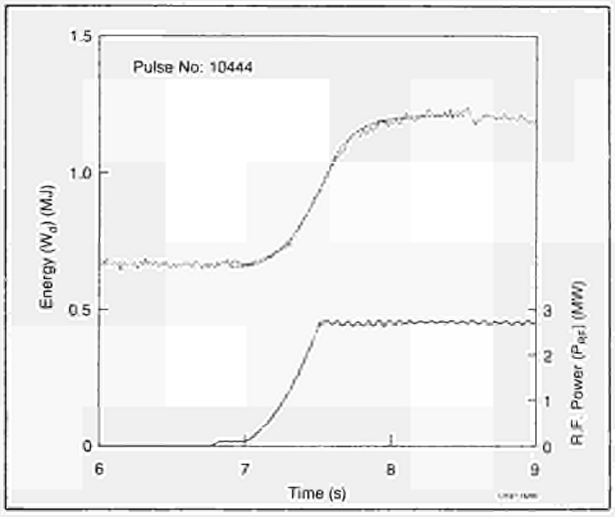

Fig.A10: The energy (W_d) as a function of time when ICRF power (P_{RF}) in switched on and the fitted curve (dashed curve, $\tau_{inc}=0.24s$, $d_w=0.554$) for Pulse No:10444.

Calculation of ICRH Power Input
(K. Thomsen)

A chain of programs has been set up, which makes it possible to fit the plasma energy time evolution given that the auxiliary power is turned on as a step function or increased quadratically (see Fig.A10). The results are automatically saved in a database. This technique gives independent estimates of both the absorbed power and the incremental confinement time.

Personal Computers
(E. van der Goot and A.R. Talbot)

Personal Computers have been co-ordinated within the project. Models from two manufacturers are being supported, the IBM PC XT and Olivetti M24 for general applications. The IBM AT and Olivetti M28 systems are used for applications which require greater processing power or need an IBM AT or compatible system to run. Configurations always include a hard disk of at least 20Mb capacity and a hardware floating point processor. Other standard items include a fully passive current loop interface for use on the Gandalf network and a backup tape interface. Additional features such as colour monitor and enhanced graphic cards are obtained only if required for the specific application. Olivetti M28 systems are always purchased with an additional 360kb floppy disk drive in order to maintain compatibility with the M24 systems.

A major use of personal computers has been for the production of presentation graphics, using the GEM range of software products, in particular, GEM Draw. Usually, the final output is printed directly onto a transparency using a laser printer. Colour output can be produced using an ink jet printer. A new GEM application has been written at JET which enables the graphical output from programs, using PLOT10 on the mainframe computer, to be included in GEM Draw pictures.

Data Interpretation

(J.P. Christiansen, J.G. Cordey and K. Thomsen)

Analysis of local transport, confinement and temperature profile consistency has been made. A study of data from neutral beam power scan experiments has shown [4,5] that simple local transport models can be used to interpret measured electron temperature profiles and their changes during auxiliary heating. Comparisons between the heat flow calibrated from ohmic - neutral beam power deposition profiles and the density and local temperature gradient yield estimates of the heat diffusivity. The latter is found to depend mostly on the plasma current. The local heat transport models also reproduce the experimentally observed scaling laws for global confinement in JET.

References

[1] P.M. Stubberfield, M.L. Watkins, "Multiple PENCIL Beam", JET Divisional Note DPA/87/06

[2] M. Cox, "FOKMEG: A Package to Determine the Fast-Ion Distribution Function for the JET Interpretation Code Suite", Report KR5-33-04.

[3] D.G. Muir, M. Shaw, "Determination of Hydrogenic Ion Temperature from the Nickel Temperature" JET Divisional Note DPA/86/9/1.

[4] J.G. Cordey et al, 11th Int. Conf. on Plasma Phys. and Contr. Nuclear Fusion Research (Kyoto, Japan, 13-20 November 1986) paper A-II-3.

[5] J.D. Callen, J.P. Christiansen, J.G. Cordey and K. Thomsen, JET Report JET-P(87)10.

Appendix III

JET Task Agreements 1986

Title	*Associations (JET Responsible Officer)*	*Duration of Agreement*	*Present Status*
RF HEATING DIVISION			
ICRF CURRENT DRIVE EFFECTS – ● Asymmetric heating of minority species ions, ● Absorption of fast magnetosonic waves by TTMP of suprathermal electrons, ● ICRF enhancement of beam driven currents	EUR-UKAEA CULHAM LABORATORY (CUL/TA6) (J Jacquinot)	November 1984–May 1987	● work continuing
RF ANTENNA DEVELOPMENT, TESTING, COMMISSIONING AND OPERATION	EUR-CEA FAR (FAR/TA2) (J Jacquinot)	Sept 1984–July 1987	● testbed operational ● A_1 antennae tests underway
ICRH HEATING – ● The operation of ECRH antennae, ● The evaluation of the heating performance and the comparison to theoretical expectations, ● The theory of RF current drive.	EUR-CEA (FAR/TA3/GREN/TA1). (J Jacquinot)	Sept 1984–April 1987 analysis of results obtained with ICRF.	● Since January 1985, FAR staff have been participating actively in
ICRH HEATING – ● Coupling calculations of ICRH antennae. ● Calculations of the power deposition profile by the method of ray tracing.	EUR-ERM/KMS (ERM/TA2) (J Jacquinot)	1 Feb 1985–30 Sept 1986	● Work completed
EXPERIMENTAL DIVISION 1			
PHYSICS OF SHAPED CROSS-SECTIONS	CULHAM, UK (CUL/TA4) (P E Stott)	March 1983–May 1987	● Work continuing.
EDGE PLASMAS & PLASMA SURFACE INTERACTIONS	CULHAM, UK (CUL/TA2) (P E Stott)	June 1983–June 1989	● Work proceeding
PLASMA WALL INTERACTIONS	GARCHING, FRG (IPP/TA2) (P E Stott)	January 1984–December 1986	● Work proceeding
MHD ACTIVITY, DISRUPTION AND RF WAVEFIELDS, EDGE PLASMAS UNDER INTENSE RF FIELDS.	LAUSANNE, SWITZERLAND (CRPP/TA1) (P E Stott)	March 1984–March 1986	● Work proceeding
NEUTRON PRODUCTION, RELATED PHYSICS AND ASSOCIATED DIAGNOSTICS	SWEDEN (SERC/TA1) (P E Stott)	January 1984–December 1986	● Work proceeding

Title	*Associations (JET Responsible Officer)*	*Duration of Agreement*	*Present Status*
PLASMA SURFACE INTERACTIONS	SWEDEN (SERC/TA2) (P E Stott)	July 1984–June 1987	● Work proceeding
NEUTRON PRODUCTION RELATED PHYSICS	HARWELL, UK (HAR/TA1) (P.E. Stott)	August 1985–April 1987	● Work proceeding
NEUTRON PRODUCTION RELATED PHYSICS AND ASSOCIATED DIAGNOSTICS	FRASCATI, ITALY ENEA/TA3	January 1986–January 1989	● Work proceeding
ECE MEASUREMENTS	FOM, NETHERLANDS (FOM/TA1)	March 1985–March 1988	● Work proceeding
EXPERIMENTAL DIVISION 2			
BULK IMPURITY PHYSICS AND IMPURITY RELATED DIAGNOSTICS	EUR-IPP FRG (W W Engelhardt)	Started February 1983	● Work proceeding
IMPURITY ANALYSIS	EUR-UKAEA CULHAM LABORATORY (CUL/TA1) (W W Engelhardt)	Started February 1983	● Work proceeding
SPECTROSCOPIC MEASUREMENTS:	EUR-CEA	Started July 1984	● Work proceeding
INTERPRETATION AND IMPURITY	FAR (W W Engelhardt)		
PHYSICS OF ION AND ELECTRON ENERGY TRANSPORT AND RELATED DIAGNOSTICS	EUR-ENEA CREF (W W Engelhardt)	Started October 1983	● Work proceeding
PHYSICS OF NEUTRAL BEAM HEATING	EUR-UKAEA	July 1983–July 1986	● Work terminated
OPTIMISATION	CULHAM LABORATORY (CUL/TA3) (W W Engelhardt)		
THEORY DIVISION			
TESTING THEORETICAL TRANSPORT MODELS AGAINST JET DATA	EUR-UKAEA CULHAM LABORATORY (CUL/TA5) (T.E. Stringer)	Started December 1986	● Work proceeding

Appendix IV

Articles, Reports and Conference Papers Published 1986

1. Distortion of ion velocity distributions in the presence of ICRH: a semi-analytical analysis.
   Anderson D., Core W., Eriksson L-G., Hamnén H., Hellsten T., Lisak M.
   Controlled Fusion and Plasma Heating 13th Euro. Conf., held in Schliersee, 14-18 April 1986.
   Geneva, European Physical Society. 1986.
   Vol.2, pp.97-100.
2. Distortion of ion velocity distributions in the presence of ICRH. A semi-analytical analysis.
   Anderson D., Eriksson L.G., Hellsten T., Core W., Hamnén H., Lisak M.
   Joint European Torus JET. 1986.
   Report (JET-R(86)09. 25p.
3. Overview of the JET ICRF power plant operation and development.
   Anderson R.J., Bosia G., Plancoulaine J., Sand F., Schmid M., Wade T.J.
   Fusion Technology 14th Symp. held in Avignon, 8-12 September 1986. Avignon, SOFT. 1986.
   Paper No. B O.02.
4. Textbook finite element methods applied to linear wave propagation problems involving conversion and absorption.
   Appert K., Hellsten T., Vaclavik J., Villard L.
   Computer Physics Communications.
   Vol.40 No.1 May 1986 (Procs. 3rd Euro. Workshop on Problems in the Numerical Modelling of Plasmas (NUMOP 85), 10-12 September 1985, Varenna, Italy).
   pp.73-93.
5. Energy transport in JET with ohmic and auxiliary heating.
   Bartlett D.V., Bhatnagar V., Bickerton R.J., Brusati M., Bures M., Campbell D.J., Christiansen J.P., Cordey J.G., Corti S., Costley A.E., Cottrell G.A., Duesing G., Edwards A., Fessey J., Gibson A., Gill R.D., Gottardi N., Gondhalekar A., Gowers C.W., Hendricks F., Jacquinot J., Jarvis O.N., Källne E., Källne J., Kissel S., de Kock L., Lallia P., Lazzaro E., Lomas P.J., Morgan P.D., Nielsen P., Prentice R., Ross R.T., O'Rourke J., Sadler G., Schüller F.C., Stamp M.F., Stott P.E., Summers D.R., Tanga A., Taroni A., Thomas P.R., Thompson E., Tibone F., Tubbing B.J., Watkins M.L., and others.
   Controlled Fusion and Plasma Heating 13th Euro. Conf., held in Schliersee, 14-18 April 1986.
   Geneva, European Physical Society. 1986.
   Vol.1, pp.29-32.
6. Investigation of electron temperature profile behaviour in JET.
   Bartlett D.V., Bindslev H., Brusati M., Campbell D.J., Cordey J.G., Costley A.E., Kissel S.E., Stott P.E., and others.
   Controlled Fusion and Plasma Heating 13th Euro. Conf., held in Schliersee, 14-18 April 1986.
   Geneva, European Physical Society. 1986.
   Vol.1, pp.236-239.
   (Also Report JET-P(86)15).
7. Ultra-long sawteeth during combined additional heating JET.
   Bartlett D.V., Campbell D.J., Costley A.E., Cottrell G.A., Duperrex P.A., Edwards A.W., Gowers C.W., Gill R.D., Granetz R.S., Jacquinot J., Kissel S.E., Lallia P.P., Lopes Cardozo N., Nave F.M.M., Stork D., Stott P.E., Thomas P.R., Thompson E., Tonetti G., Tubbing B.J.D., Weller A., Wesson J.A., Snipes J.A.
   American Physical Society. Bulletin.
   Vol.31 No.9 October 1986.
   (Abstracts of 28th Annual Meeting Division of Plasma Physics, Baltimore, 3-7 November 1986).
   Paper 8P 30, P.1591.
8. Impurity and radiation studies during the JET ohmic heating phase.
   Behringer K.H., Denne B., Decker G., Engelhardt W., Gill R., Gottardi N., Källne E., Krause H., Magyar G., Mansfield M., Mast F., Morgan P., Stamp M.F., Summers H.P. Carolan P.G., Forrest M.J., Hawkes N.C., Peacock N.J.
   Nuclear Fusion.
   Vol.26 No.6 June 1986.
   pp.751-768.
9. Metal sources and general impurity behaviour in JET plasmas during ICRH.
   Behringer K.J., Denne B., Kaye A., Morgan P.D.,

Stamp M.F., Summers H.P., Tallents G., Forest M.J., Hawkes N.C., Peacock N.J. Controlled Fusion and Plasma heating 13th Euro. Conf., held in Schliersee, 14-18 April 1986.
Geneva, European Physical Society. 1986.
Vol.1, pp.176-179.

10. Radiation behaviour during additional heating of JET plasmas.
Behringer K.H., Edwards A., Gill R.D., Granetz R., Gottardi N., Jaeckel H., Magyar G., and others.
Controlled Fusion and Plasma Heating 13th Euro. Conf., held in Schliersee, 14-18 April 1986.
Geneva, European Physical Society. 1986.
Vol.1, pp.180-183.

11. Spectroscopic diagnostics on JET (invited).
Behringer K.H.
Review of Scientific Instruments.
Vol.57 No.8 pt.II August 1986 (Procs. 6th Topical Conf. on High Temperature Plasma Diagnostics, Hilton Head Island, South Carolina, 9-13 March 1986).
pp.2000-2005.
(Also Report JET-P(86)10).

12. Development of the JET poloidal electromagnetic system.
Bertolini E., Last J.R., Mondino P.L., Noll P.
Fusion Technology 14th Symp. held in Avignon, 8-12 September 1986. Avignon, SOFT. 1986.
Paper No. I I.02.

13. Operation and development plans of JET.
Bertolini E.
Fusion Engineering 11th Symposium, held in Austin, 18-22 November 1985.
New York, IEEE. 1986.
Vol.1, pp.8-18.
(Also Report JET-P(85)26).

14. The JET magnet power supplies and plasma control systems.
Bertolini E., Mondino P.L., Noll P.
Fusion Technology, Vol.11 No.1 January 1987 (Special issue on design, construction, and first operational experience on the Joint European Torus (JET)) pp.71-119.

15. Fusion Reactor Design IV (Report on the 4th IAEA Technical Committee Meeting and Workshop, Yalta, 26 May - 6 June 1986).
Bertolini E., and others.
Nuclear Fusion.
Vol.26 No.10 October 1986.
pp.1377-1428.

16. Comparison between H and He^3 minority ICRF heating experiments in JET.
Bhatnagar V.P., Corti S., Ellis J.J., Jacquinot J.
Controlled Fusion and Plasma Heating 13th Euro. Conf., held in Schliersee, 14-18 April 1986.
Geneva, European Physical Society. 1986.
Vol.2, pp.165-168.
(Also Report JET-P(86)15).

17. Theory of excitation of asymmetric k-parallel spectrum by phasing the JET ICRF antennae.
Bhatnagar V.P., Evrard M.P., Jacquinot J.
Controlled Fusion and Plasma Heating 13th Euro. Conf., held in Schliersee, 14-18 April 1986.
Geneva, European Physical Society. 1986.
Vol.2, pp.77-80.
(Also Report JET-P(86)15 and Report JET-R(86)05).

18. Comparison between Experiment and Theory.
Bickerton R.J., Taroni A., Watkins M.L., Wesson J.
Royal Society Discussion Meeting on the JET Project and the Prospect for Controlled Nuclear Fusion, London, 1986.
(Also JET-P(86)28).

19. Early results from large tokamaks in Europe, Japan and the United States.
Bickerton R.J.
American Physical Society. Bulletin.
Vol.31 No.4 April 1986 (Program of the 1986 Spring Meeting, Washington, 28 April - 1 May 1986).
Abstract DA3, p.792.

20. Latest results from JET.
Bickerton R.J., Bartlett D.V., Behringer K.H., Bertolini E., Best C., Bonicelli T., Brusati M., Campbell D.J., Christiansen J., Chuilon P., Coad J.P., Cordey J.G., Corti S., Costley A.E., Denne B., Diëtz K.J., Düchs D.G., Edwards A., Engelhardt W.W., Eriksson B.T., Gibson A., Gill R.D., Gondhalekar A., Gottardi N., Gowers C., Green B.J., Hemmerich J., Huart M., Huguet M., Jacquinot J., Jarvis O.N., Jones E.M., Källne E., Källne J.C., Kissel S., de Kock L., Lallia P., Last J., Lazzaro E., Lomas P., Magyar G., Malarcarne M., Mansfield M., Marchese V., Mondino P.L., Morgan P.D., Murphy G., Nave M.F.F., Nielsen P., Noll P., O'Rourke J., Prentice R., Rebut P.H., Ross R., Sadler G., Santaquistina A., Schüller F.C., Stamp M.F., Steed C.A., Stott P.E., Stringer T.E., Summers D., Summers H.P., Tanga A., Taroni A., Thomas P.R., van Belle P., van der Beken H., Watkins M.L., Wesson J.A., Carolan P.G., Erents S.K., Forrest M.J., Goodall D., Hawkes N.C., McCracken G., Morris A.W., Peacock N.J., Robinson D.C., Turner M., and others.
Plasma Physics and Controlled Fusion.
Vol.28 No.1 pt.A January 1986 (Controlled Fusion and Plasma Physics, 12th Euro. Physical Society Plasma Physics Division Conf., 2-6 September 1985, Budapest, Hungary. Invited papers).
pp.55-69.
(Also Report JET-P(85)15).

21. Latest results from JET.
Bickerton R.J.
American Physical Society. Bulletin.
Vol.31 No.9 October 1986.
(Abstracts of 28th Annual Meeting Division of

Plasma Physics, Baltimore, 3-7 November 1986). Paper 1I3, pp.1383-1384.
22. Tokamak experiments.
Bickerton R.J., Keen B.E.
Joint European Torus JET. 1985.
38p.
Report JET-P(85)24.
Presented at the Course and Workshop on Basic Physical Processes of Toroidal Fusion Plasmas, Varenna, 26 August - 3 September 1985.
23. Contact maintenance on JET into the active phase.
Booth S.J.
ENC 86 Transactions Conf. on Nuclear Energy of Today and Tomorrow, held in Geneva, 1-6 June 1986. Incorporates ENC4, 4th Int. ENS/ANS Conf. and Foratom IX: 9th Foratom Congress.
Berne, European Nuclear Society. 1986.
Vol.3, pp.51-56.
24. Experimental determination of the ICRF power deposition profile and comparison with ray tracing calculations.
Bosia G., Jacquinot J., Lallia P.P, Malacarne M. and others.
Controlled Fusion and Plasma Heating 13th Euro. Conf., held in Schliersee, 14-18 April 1986.
Geneva, European Physical Society. 1986.
Vol.2, pp.193-196.
25. JET ICRF system automatic matching procedure.
Bosia G.
Joint European Torus JET. 1986.
Report JET-R(86)06. 10p.
26. Behaviour of plasma boundary during ICRF in JET.
Brinkschulte H., Tagle J.A., Bures M., Harbour P.J., Huld T., Kaye A.S., Lowry C., Erents S.K., McCracken G.M.
Controlled Fusion and Plasma Heating 13th Euro. Conf., held in Schliersee, 14-18 April 1986.
Geneva, European Physical Society. 1986.
Vol.1, pp.403-406.
(Also Report JET-P(86)15).
27. CODAS: A large scale multicomputer control system for the JET project.
Browne M.L.
JET Report JET-P(86)37.
28. JET pulse termination network.
Browne M., Green B., How J., Lomas P., Noll P., Schueller F., Steed C., van der Beken H.
Fusion Technology 14th Symp. held in Avignon, 8-12 September 1986. Avignon, SOFT. 1986.
Paper No. GP 06.
29. Analysis of current and temperature profile formation in JET.
Campbell D.M., Christiansen J.P., Lazzaro E., Morris A.W., Nave M.F.F., Schueller F.C., Thomas P.R.
Controlled Fusion and Plasma Heating 13th Euro. Conf., held in Schliersee, 14-18 April 1986.
Geneva, European Physical Society. 1986.
Vol.1, pp.268-271.
(Also Report JET-P(86)15).
30. Current and temperature profile evolution in JET.
Campbell D.J., Christiansen J.P., Cordey J.G., Lazzaro E., Nave M.F.F.
Report JET-P(86)46
Submitted to Nuclear Fusion.
31. Sawtooth activity in ohmically heated JET plasmas.
Campbell D.J., Gill R.D., Gowers C.W., Wesson J.A., Bartlett D.V., Best C.H., Coda S., Costley A.E., Edwards A., Kissel S.E., Niestadt R.M., Piekaar H.W., Prentice R., Ross R.T., Tubbing B.J.D.
Nuclear Fusion.
Vol.26 No.8 August 1986.
pp.1085-1092.
(Also Report JET-P(86)05).
32. The JET belt limiter.
Celentano G., Deksnis E., Shaw R., Sonnenberg K., Walravens M.
Fusion Technology 14th Symp. held in Avignon, 8-12 September 1986. Avignon, SOFT. 1986.
Paper No. BP 24.
33. Electron density transport in JET.
Cheetham A., Christiansen J.P., Corti S., Gondhalekar A., Hendriks F., Morgan P.D., O'Rourke J., Watkins M,. Hugill J.
Controlled Fusion and Plasma Heating 13th Euro. Conf., held in Schliersee, 14-18 April 986.
Geneva, European Physical Society. 1986.
Vol.1, pp.240-243.
34. Integrated analysis of data from JET.
Christiansen J.P.
Joint European Torus JET. 1985. 52p.
Report JET-R(86)04.
35. Temperature density and current profile changes caused by auxiliary heating in JET.
Christiansen J.P., Cordey J.G., Lazzaro E.
American Physical Society. Bulletin.
Vol.31 No.9 October 1986.
(Abstracts of 28th Annual Meeting Division of Plasma Physics, Baltimore, 3-7 November 1986).
Paper 5E 10, p.1503.
36. Additional heating power supplies: Design concept and first operation.
Claesen R., Baur U., Carwardine J., Celentano G., Christodoulopoulos C., Dobbing A., Mondino L.
Fusion Engineering 11th Symposium, held in Austin, 18-22 November 1985.
New York, IEEE. 1986.
Vol.1, pp.93-98.
(Also Report JET-P(85)26).
37. Neutral beam injection and radio-frequency power supplies.
Claesen R., Mondino P.L.
Fusion Technology, Vol.11 No.1 January 1987 (Special issue on design, Constructon, and first operational experience on the Joint European Torus (JET)), pp.141-162.

38. The JET neutral injection 160kV power transmission lines, the associated snubbers and the SF6 tower for the termination of the transmission lines, housing of the snubbers and voltage breaks.
Claesen R., Baur U., Bertolini E., Celentano G., Mondino P.L., Rebut P.H.
Fusion Technology 14th Symp. held in Avignon, 8-12 September 1986. Avignon, SOFT. 1986.
Paper No. CP55.

39. Determination of poloidal beta in JET.
Cordey J.G., Christiansen J.P., Tonetti G.
JET Contributions to 13th Euro. Conf. on Controlled Fusion and Plasma Heating, Schliersee, 14-18 April 1986.
Joint European Torus JET, 1986.
pp.25-28.
Report JET-P(86)15.

40. Prospects for alpha particle heating in JET in the hot ion regime.
Cordey J.G., Keilhacker M., Watkins M.L.
Symposium on the Role of Alpha-Particle in Magnetically Confined Fusion Plasma, Sweden, 1986.
(Also JET-P(86)38).

41. Unification of ohmic and additionally heated energy confinement scaling laws.
Cordey J.G.,
Joint European Torus JET. 1985. 6p.
Report JET-P(85)28.

42. The effect of neutral beam injection on wave propagation in the ion cyclotron range of frequencies.
Core W.G.F.
Controlled Fusion and Plasma Heating 13th Euro. Conf., held in Schliersee, 14-18 April 1986.
Geneva, European Physical Society. 1986.
Vol.2, pp.73-76.
(Also Report JET-P(86)15).

43. A solution of the ICRF Fokker-Planck equation.
Core W.G.F.
Joint European Torus JET. 1985. 24p.
Report JET-P(85)30.
Submitted to Physics of Fluids.

44. T_i profile studies during ICRF heating in JET.
Corti S., Brusati M., Bures M., Gondhalekar A., Hendriks F., Sand F., Taroni A., Tibone F., Zanza V. and others.
Controlled Fusion and Plasma Heating 13th Euro. Conf., held in Schliersee, 14-18 April 1986.
Geneva, European Physical Society. 1986.
Vol.1, pp.109-112.
(Also Report JET-P(86)15).

45. Beam acceleration with ICRF heating on JET.
Cottrell G.A., Evrard M.P., Bures M., Cordey J., Core W., Corti S., Hamnén H., Hellsten T., Jacquinot J., Sand F., Watkins M., Zanza V.
American Physical Society. Bulletin.
Vol.31 No.9 October 1986.
(Abstracts of 28th Annual Meeting Division of Plasma Physics, Baltimore, 3-7 November 1986).
Paper 8P 29, p.1590-1591.

46. Identification of ion cyclotron emission from charged fusion products.
Cottrell G.A., Lallia P.P., Sadler G., van Belle P.
Controlled Fusion and Plasma Heating 13th Euro. Conf., held in Schliersee, 14-18 April 1986.
Geneva, European Physical Society. 1986.
Vol.2, pp.37-40.
(Also Report JET-P(86)15).

47. Ion cyclotron emission from charged fusion products.
Cottrell G.A., Lallia P.P., Sadler G., van Belle P.
Joint European Torus JET. 1986.
Report JET-P(86)33. 8p.
Submitted to Plasma Physics and Controlled Fusion.

48. Measurements of ion cyclotron emission from ohmic and ICRF discharges in JET.
Cottrell G.A.
Joint European Torus JET. 1985. 6p.
Report JET-P(85)13.

49. Papers presented at 7th Int. Conf. on Plasma Surface Interactions in Fusion Devices, Princeton, 5-9 May 1986.
de Kock L., and others
Joint European Torus JET. 1986.
Report JET-P(86)35. 256p.

50. JET remote maintenance during active operation.
Dean J.R., Raimondi T.
Fusion Technology, Vol.1 No.1 January 1987 (Special issue on design, construction, and first operational experience on the Joint European Torus (JET)) pp.253-281.

51. Preparation for DT phase operation in JET.
Dean J.
Fusion Technology 14th Symp. held in Avignon, 8-12 September 1986. Avignon, SOFT. 1986.
Paper No. GI.02.

52. Metal sources and general impurity behaviour in JET plasmas during ICRH.
Denne B., Behringer K., Kaye A., Morgan P.D., Stamp M.F., Summers H.P., Tallents G., Forrest M.J., Hawkes N.C., Peacock N.J.
JET Contributions to 13th Euro. Conf. on Controlled Fusion and Plasma Heating, Schliersee, 14-18 April 1986.
Joint European Torus JET, 1986.
pp.101-104.
Report JET-P(86)15.

53. Wall protection in JET.
Diëtz K.J., Sonnenberg K. Deksnis E., Shaw R.
Tokamak Start-up: Problems and scenarios related to the transient phases of a thermonuclear fusion reactor. Procs. 7th Course of the International School of Fusion Reactor Technology, held in Erice, 14-20 July 1985.

54. Quantitative modelling of JET plasmas by computational methods.
Düchs D.F.
Royal Society Discussion Meeting on the JET Project and the Prospect for Controlled Nuclear

Fusion, London, 1986.
(Also JET-P(86)30).

55. First results of neutral beam heating on JET.
Duesing G.
Joint European Torus JET. 1986. 7p.
Report JET-P(86)20.
Presented at the 13th Euro. Conf. on Controlled Fusion and Plasma Heating, Schliersee, 14-18 April 1986.

56. First neutral beam heating experiments on JET.
Duesing G., Lomas P., Stäbler A., Thomas P., Thompson E.
Joint European Torus JET. 1986. 22p.
Report JET-P(86)11.
Paper for the Royal Society Discussion Meeting on the JET Project and the Prospects for Controlled Nuclear Fusion, London, March 1986.

57. Neutral beam injection system.
Duesing G., Altmann H., Falter H., Goede A., Haange R., Hemsworth R.S., Kupschus P., Stork D., Thompson E.
Fusion Technology, Vol.11 No.1 January 1987 (Special issue on design, construction, and first operational experience on the Joint European Torus (JET)) pp.163-202.

58. Neutral beam heating for JET, construction and test of a quasi-stationary plasma heating system at the 10MW level.
Duesing G.
JET Joint Undertaking. 1985. pp.757-760.
Report CUL 5484.
Jahrestagung Kerntechnik, Munchen, 21-23 May 1985.

59. The vacuum systems of the nuclear fusion facility JET.
Joint European Torus JET. 1986. 22p.
Report JET-P(86)08.
Invited paper presented at Vacuum 86, Glasgow, 25-27 March 1986.

60. JET soft x-ray diode array diagnostic.
Edwards A.W., Gill R.D., Oord E., Tsuji S., Fahrbach H-U., Granetz R., Schramm G., Weller A. Zasche D.
Review of Scientific Instruments.
Vol.57 No.8 pt.II August 1986 (Procs. 6th Topical Conf. on High Temperature Plasma Diagnostics, Hilton Head Island, South Carolina, 9-13 March 1986).
pp.2142-2144.
(Also Report JET-P(86)16).

61. Rapid collapse of a plasma sawtooth oscillation in the JET tokamak.
Edwards A.W., Campbell D.J., Engelhardt W.W., Fahrbach H-U., Gill R.D., Granetz R.S., Tsuji S., Tubbing B.J.D., Weller A., Wesson J., Zasche D.
Physical Review Letters.
Vol.57 No.2 14 July 1986 pp.210-213.
(Also Report JET-P(86)12).

62. Erosion and redeposition of metals and carbon on the JET limiters.
Ehrenberg J., Behrisch R., Stott P.E., Coad J.P., de Kock L., McCracken G.M.
Controlled Fusion and Plasma Heating 13th Euro. Conf., held in Schliersee, 14-18 April 1986.
Geneva, European Physical Society. 1986.
Vol.1, pp.391-394.
(Also Report JET-P(86)15).

63. The state of limiters and walls in plasma machines.
Ehrenberg J.
JET Joint Undertaking. 1985. pp.725-728.
Report CUL 5476.
Jahrestagung Kerntechnik, Munchen, 21-23 May 1985.

64. Wall effects and impurities on JET
Engelhardt W.W.
Royal Society Discussion Meeting on the JET Project and the Prospect for Controlled Nuclear Fusion, London, 1986.
(Also JET-P(86)27).

65. Probe measurements of the density and temperature profiles in the JET plasma boundary.
Erents S.K., McCracken G.M., Tagle J.A., de Kock L., Stangeby P.C.
Nuclear Fusion.
Vol.26 No.12, December 1986.
pp.1591-1603.

66. Probe measurements of the density and temperature profiles in the JET plasma boundary.
Erents S.K., McCracken G.M., Tagle J.A., de Kock L., Stangeby P.C.
Joint European Torus JET. 1986. 25p.
Report JET-P(86)07.

67. Comparison of theoretical and experimental ICRF antenna-plasma coupling resistance in JET.
Evrard M.P., Bhatnagar V.P., Bures M., Sand F.
Controlled Fusion and Plasma Heating 13th Euro. Conf., held in Schliersee, 14-18 April 1896.
Geneva, European Physical Society. 1986.
Vol.2, pp.133-136.
(Also Report JET-P(86)15).

68. Operational test of the JET neutral injection system in the JET test bed.
Falter H., Hemsworth R., Deschamps G.H., Goede A., Jones T., Massmann P., Mead M.J., Stäbler A.
Fusion Engineering 11th Symp., held in Austin, U.S.A., 18-22 November 1985.
New York, IEEE. 1986.
Vol.2, pp.786-790.
(Also Report JET-P(85)26).

69. Operational test of the second JET neutral injection with deuterium beams at extraction voltages of less than 160kV.
Falter H., Deschamps G.H., Hemsworth R.S., Massmann P.
Fusion Technology 14th Symp. held in Avignon, 8-12 September 1986. Abstracts.
Avignon, SOFT. 1986.
Paper No. DP 52.

70. Neoclassical impurity transport and observations of poloidal asymmetries in JET.
Fenebcrg W., Mast F.K., Gottardi N., Martin P.
Report JET-R(86)07.
71. Computer-to-process interface in JET control and diagnostic systems.
Fullard K., Dorling S.E., van Montfoort J.E.
Fusion Technology 14th Symp. held in Avignon, 8-12 September 1986. Avignon, SOFT. 1986.
Paper No. GP 15.
72. Experimental ICRF power deposition profile and power balance during heating of JET plasmas.
Local transport behaviour during ICRH.
Gambier D.G., Evrard M.P., Thomsen K., Tubbing B., Zanza V.
American Physical Society. Bulletin.
Vol.31 No.9 October 1986.
(Abstracts of 28th Annual Meeting Division of Plasma Physics, Baltimore, 3-7 November 1986).
Paper 5E 12 p.1504.
73. Experimental determination of the ICRF power deposition profile and comparison with ray tracing calculations.
Giannella R., and others
JET Contributions to 13th Euro. Conf. on Controlled Fusion and Plasma Heating, Schliersee, 14-18 April 1986.
Joint European Torus JET, 1986. pp.41-44.
Report JET-P(86)15.
74. High resolution X-ray spectroscopy of highly ionised impurities at JET.
Giannella R., Bombarda F., Källne E., Panaccione L., Tallents G.
American Physical Society. Bulletin.
Vol.31 No.9 October 1986.
(Abstracts of 28th Annual Meeting Division of Plasma Physics, Baltimore, 3-7 November 1986).
Paper 8P 28, p.1590.
75. Sawtooth activity during additional heating in JET.
Gill R.D., Bartlett D.V., Campbell D.J., Corti S., Costley A.E., Edwards A.W., Engelhardt W.W., Gowers C.W., Granetz R., Kissel S.E., Magyar G., O'Rourke J., Oord E., Prentice R., Wesson J.A., and others.
Controlled Fusion and Plasma heating 13th Euro. Conf., held in Schliersee, 14-18 April 1986.
Geneva, European Physical Society. 1986.
Vol.1 pp.21-24.
(Also Report JET-P(86)15).
76. Tomographic analysis of soft X-ray data from JET.
Gill R.D., Edwards A., Fahrbach H.U., Granetz R.S., Tsuji S., Weller A., Zasche D.
American Physical Society. Bulletin.
Vol.31 No.9 October 1986.
(Abstracts of 28th Annual Meeting Division of Plasma Physics, Baltimore, 3-7 November 1986).
Paper 8P 31, p.1591.
77. Performance of the first JET neutral beam injector.
Goede A.P.H., Challis C., Jones T.T.C., Stäbler A., Stork D., Thompson E.
Fusion Technology 14th Symp. held in Avignon, 8-12 September 1986. Avignon, SOFT. 1986.
Paper No. DP 47.
78. Electron density transport in JET.
Gondhalekar A., and others.
JET Contributions to 13th Euro. Conf. on Controlled Fusion and Plasma Heating, Schliersee, 14-18 April 1986.
Joint European Torus JET, 1986. pp.49-52.
Report JET-P(86)15.
79. The tritium safety programme at JET.
Gordon C.W.
IAEA Technical Committee Meeting on Fusion Reactor Safety, Culham, 1986.
(Also JET-P(86)41).
80. JET - what relation does it have to a future fusion power reactor?
Green B.J.
Joint European Torus JET. 1986. 16p.
Report JET-P(86)04.
UKAEA Prototype and Research Reactors Managers Conf., 18-20 March 1986, Warrington.
81. JET neutral injection beamline system, manufacture and assembly.
Haange R., Altmann H., Papastergiou S., Tivey R., Watson M.J.
Fusion Engineering 11th Symp. held in Austin, 18-22 November 1985.
New York, IEEE. 1986.
Vol.2, pp.1259-1264.
(Also Report JET-P(85)26).
82. Ion current drive using ICRF and combined ICRF/NBI.
Hamnén H.
Controlled Fusion and Plasma Heating 13th Euro. Conf., held in Schliersee, 14-18 April 1986.
Geneva, European Physical Society. 1986.
Vol.2, pp.425-428.
(Also Report JET-P(86)15).
83. Coupling spectra for ion cyclotron heating in large tokamaks in presence of eigenmodes.
Hellsten T., Appert K.
Controlled Fusion and Plasma Heating 13th Euro. Conf., held in Schliersee, 14-18 April 1986.
Geneva, European Physical Society. 1986.
Vol.2, pp.129-132.
(Also Report JET-P(86)15).
84. Neutralisation measurements for the JET injector.
Hemsworth R.S., Stäbler A., Falter H.D., Massmann P., Deschamps G.H., Goede A.P.H.
Controlled Fusion and Plasma Heating 13th Euro. Conf., held in Schliersee, 14-18 April 1986.
Geneva, European Physical Society. 1986.
Vol.2, pp.297-300.
85. The effects of finite-beta and shaping on tearing modes in JET.
Hender T.C., Robinson D.C., Hastie R.J.
Controlled Fusion and Plasma Heating 13th Euro. Conf., held in Schliersee, 14-18 April 1986.
Geneva, European Physical Society. 1986.

Vol.1, pp.65-58.
86. Ion temperature, rotation velocity and low Z impurity density measurements on JET using charge exchange recombination spectroscopy.
Horton L.D., von Hellermann M.G.V., Summers H.P., Peacock N.J.
American Physical Society. Bulletin.
Vol.31 No.9 October 1986.
(Abstracts of 28th Annual Meeting Division of Plasma Physics, Baltimore, 3-7 November 1986).
Paper 8P 26, p.1590.
87. Operation of the JET magnet power supplies. Reliability and improvements.
Huart M., Moissonnier A., Eriksson T., Raymond C.
Fusion Technology 14th Symp. held in Avignon, 8-12 September 1986. Avignon, SOFT. 1986.
Paper No. CP46.
88. Direct measurement of the electron diffusion coefficient on JET using a microwave reflectometer.
Hubbard A.E., Ward D., Stringer T.E.
Controlled Fusion and plasma Heating 13th Euro. Conf., held in Schliersee, 14-18 April 1986.
Geneva, European Physical Society. 1986.
Vol.1, pp.232-235.
(Also Report JET-P(86)15).
89. A simple fixed frequency reflectometer for plasma density profile measurements on JET.
Hubbard A.E., Costley A.E., Gowers C.W.
Joint European Torus JET. 1985. 18p.
Report JET-P(85)32.
90. Alpha particle diagnostics.
Hughes T.
Report JET-R(86)10.
91. Design, manufacture and assembly of the JET machine.
Huguet M.
Joint European Torus JET. 1986. 31p.
Report JET-P(86)14.
Paper given at the Royal Society Discussion Meeting on the JET Project and the Prospect for Controlled Nuclear Fusion, London, 12-13 March 1986.
92. Limiters and first wall on JET.
Huguet M., Booth J., Celentano G., Deksnis E., Diëtz K., Rebut P.H., Shaw R., Sonnenberg K.
Fusion Engineering 11th Symp. held in Austin, 18-22 November 1985.
New York, IEEE. 1986.
Vol.2, pp.1238-1248.
(Also Report JET-P(85)26).
93. Main features implemented in the JET facility for D-T operation.
Huguet M., Bertolini E.
ANS Transactions.
Vol.52 1986 (Annual meeting, Reno, Nevada, 15-19 June 1986) pp.28.
94. Main features implemented in the JET facility for deuterium-tritium operation.
Huguet M., Bertolini E.
7th Topical Meeting on the Technology of Fusion Energy, Reno, Nevada, U.S.A., June 1986.
(Also JET-P(86)23).
95. Technical aspects of the new JET development plan.
Huguet M.
Fusion Technology 14th Symp. held in Avignon, 8-12 September 1986. Avignon, SOFT. 1986.
Paper No. I I.01.
96. The JET machine: Design, construction and operation of the major systems.
Huguet M., Diëtz K., Hemmerich J.L., Last J.R.
Fusion Technology. Vol.11 No.1 January 1987 (Special issue on design, construction, and first operational experience on the Joint European Torus (JET)) pp.43-70.
97. Comparison between two global wave propagation codes for studying ICRF waves.
Itoh K., Itoh S.I., Hellsten T., Fukuyama A.
Joint European Torus JET. 1986. 11p.
Report JET-R(86)01.
98. Analyses of ICRF waves on JET plasmas.
Itoh S.I., Itoh K., Fukuyama A.
Joint European Torus JET. 1985. 17p.
Report JET-R(86)02.
99. Radiation behaviour during additional heating of JET plasmas.
Jäckel H., and others.
JET Contributions to 13th Euro. Conf. on Controlled Fusion and Plasma Heating, Schliersee, 14-18 April 1986.
Joint European Torus JET, 1986. pp.57-60.
Report JET-P(86)15.
100. Additional heating experiments on JET using ion cyclotron waves.
Jacquinot J., Bhatnagar V., Brinkschulte H., Bures M., Corti S., Cottrell G.A., Evrard M., Gambier D., Kaye A., Lallia P.P., Sand F., Schüller C., Tanga A., Thomsen K., Wade T.
Joint European Torus JET. 1986. 17p.
Report JET-P(86)18.
Talk at The Royal Society Discussion Meeting on "The JET Project and the Prospect for Controlled Nuclear Fusion"
(London, 12-13 March 1986).
101. Current profile control in JET.
Jacquinot J.
Fusion Technology 14th Symp. held in Avignon, 8-12 September 1986.
Avignon, SOFT. 1986.
Paper No. I I.04.
102. Heating and current drive scenarios with ICRF.
Jacquinot J.
Tokamak Start-up: Problems and scenarios related to the transient phases of a thermonuclear fusion reactor. Procs. 7th Course of the International School of Fusion Reactor Technology, held in Erice, 14-20 July 1985.
New York, Plenum. 1986. pp.259-268.
(Also Report JET-P(85)12).

103. ICRF studies on JET.
Jacquinot J., Anderson R.J., Arbez J., Bartlett D.V., Behringer K.H., Bertolini E., Bonicelli T., Bosia G.F., Brinkschulte H.W., Browne M.L., Brusati M., Bures M., Campbell D.J., Christiansen J.P., Christodoulopoulos C.O.A., Chuilon P., Claesen R., Coad J.P., Cordey J.G., Corti S., Costley A.E., Cottrell G., Denne B., Diëtz K., Eriksson B.T., Fullard K., Gill R.D., Gottardi N., Green B., Hellsten T., Hemmerich J.L., Huguet M., Jarvis O.N., Jones E., Kaye A.S., de Kock J., de Kock L., Lallia P.P., Last J., Lazzaro E., Lomas P.J., Magyar G., Mansfield M., Marchese V., Mondino P., Morgan P., O'Rourke J., Plancoulaine J., Rebut P.H.,Rhoden G., Sadler G., Sand F., Santaquistina A., Schmid M.S., Schüller F.C., Sibley A., Stamp M.F., Steed C., Stott P.E., Summers D., Tanga A., Thomas P.R., Valisa M., van der Beken H., Watkins M., Wade T.J., Walker C.I., Erents S.K., Hawkes N.C., McCracken G.M., and others.
Plasma Physics and Controlled Fusion.
Vol.28 No.1 pt.A January 1986 (Controlled Fusion adn Plasma Physics, 12th Euro. Physical Society Plasma Physics Division Conf., 2-6 September 1985, Budapest, Hungary. Invited paper). pp.1-15.

104. Overview of RF heating studies in tokamaks after the Aachen Conference.
Jacquinot J.
European Tokamak Programme, 2nd Workshop, held in Saulx les Chartreux, 30 November - 2 December 1983.
CEA, 1983. pp.66-75.

105. Summary talk on RF heating workshop.
Jacquinot J.
European Tokamak Programme, 2nd Workshop, held in Saulx les Chartreux, 30 November - 2 December 1983.
CEA, 1983. pp.118-128.

106. Neutron spectrometry at JET (invited).
Jarvis O.N., Gorini G., Hone M., Källne J., Sadler G., Merlo V., van Belle P.
Review of Scientific Instruments.
Vol.57 No.8 pt.II August 1986 (Procs. 6th Topical Conf. on High Temperature Plasma Diagnostics, Hilton Head Island, South Carolina, 9-13 March 1986).
pp.1717-1722.
(Also Report JET-P(86)09).

107. Nuclear data involved in present day fusion reactors.
Jarvis O.N.
Joint European Torus JET. 1985. 29p.
Report JET-P(85)22.
Presented at the KTG/ENS Int. State of the Art. Seminar on Nuclear Data, Cross-Section Libraries and their Application in Nuclear Technology, Bonn, 1-2 October 1985.

108. Status of the JET control and data acquisition system CODAS.
Jones E.M.
Nuclear Instruments and Methods in Physics Research. Section A: Accelerators, Spectrometers, Detectors and Associated Equipment.
Vol.A247 No.1 1 June 1986.
pp.58-67.

109. Design and Operation of the JET articulated boom.
Jones P.D.F., Maisonnier D., Raimondi T.
Fusion Engineering 11th Symposium, held in Austin, 18-22 November 1985.
New York, IEEE. 1986.
Vol.1, pp.144-147.
(Also Report JET-P(85)26).

110. Density behaviour in JET neutral beam heated discharges.
Jones T.T.C., Cuthbertson J., Gondhalekar A., Lomas P.J., Morgan P.D., O'Rourke J., Stäbler A., Stork D., Thompson E.
American Physical Society. Bulletin.
Vol.31 No.9 October 1986.
(Abstracts of 28th Annual Meeting Division of Plasma Physics, Baltimore, 3-7 November 1986).
Paper 8P 25, p.1590.

111. Measurements of the burn-up of fast ^{3}He and ^{3}H ions in deuterium plasmas.
Källne J., Gorini G., Jarvis O.N., Martin G., Merlo V., Sadler G., van Belle P.
Symposium on the Role of Alpha Particles in Magnetically Confined Plasmas, Sweden, 1986.
(Also Report JET-P(86)34).

112. Engineering design and preliminary performance of the JET ICRF system.
Kaye A., Anderson R., Arbez J., Bosia G., Beaumont B., Bures M., Jacquinot J., Lallia P., Plancoulaine J., Sand F., Schmid M., Wade T., Walker C.
Fusion Engineering 11th Symp. held in Austin, 18-22 November 1985.
New York, IEEE. 1986.
Vol.2, pp.1204-1209.
(Also JET-P(85)26).

113. Radio-frequency heating system.
Kaye A., Jacquinot J., Lallia P., Wade T.
Fusion Technology, Vol.11 No.1 January 1987 (Special issue on design, construction and first operational experience on the Joint European Torus (JET)), pp.203-234.

114. Dr. Hans-Otto Wüster, 1927-1985: An appreciation and dedication.
Keen B.E.
Fusion Technology, Vol.11 No.1 January 1987 (Special issue on design, construction and first operational experience on the Joint European Torus (JET)) pp.9-10.

115. Preface: Special issue on the Joint European Torus.
Keen B.E.
Fusion Technology, Vol.11 No.1 January 1987 (Special issue on design, construction and first operational experience on the Joint European

Torus (JET)) pp.11-12.

116. Financial planning and control at JET.
Kind P.
Int. Structural Comparison of Research Centres 4th Symposium on Research Centres and their Financial Environment, held in Petten, 7-9 October 1985.
Hague, ECN. 1985.
pp.233-244.

117. Nature of JET as a project.
Kind P.
Int. Structural Comparison of Research Centres 4th Symposium on Research Centres and their Financial Environment, held in Petten, 7-9 October 1985.
Hague, ECN. 19856.
pp.233-231.

118. Plasma heating in JET.
Lallia P.P., and others.
Plasma Physics and Controlled Fusion.
Vol.28 No.9A September 1986 (Controlled Fusion and Plasma Heating: 13th Euro. Physical Society Plasma Physics Division Conf., 14-18 April 1986, Schliersee, FRG. Invited papers).
pp.1211-1223
(Also Report JET-P(86)21).

119. Status and prospects of RF waves in tokamaks.
Lallia P.P.
Joint European Torus JET. 1985. 13p.
Report JET-P(85)29.

120. The JET magnets: operational experience and plans for upgrade.
Last J.R., Cacaut D., Zwart J.W.
Fusion Technology 14th Symp. held in Avignon, 8-12 September 1986. Avignon, SOFT. 1986.
Paper No. HP 07.

121. Magnetic separatrix operation in JET.
Lazzaro E., Bartlett D., Bickerton R., Christiansen J., de Kock L., GIbson A., Gottardi N., Keilhacker M., Nowak S., Tagle J., Tanga T., Erents S.
American Physical Society. Bulletin.
Vol.31 No.9 October 1986.
(Abstracts of 28th Annual meeting Division of Plasma Physics, Baltimore, 3-7 November 1986).
Paper 5E 11, p.1503-1504.

122. Reference data for plasma shaping and magnetic separatrix formation in the JET poloidal field system.
Lazzaro E., Keegan B.
Report JET-R(86)08.

123. Neutron detection techniques for plasma diagnostics at the Joint European Torus (JET).
Lees E.W., Argyle J.P., Dixon P., Huxtable G.B., Swinhoe M.T., Talbot A.R., Jarvis O.N., Sadler G., Källne J., van Belle P.
Radiation Effects, Vol.95 No.1-4 1986 pp.253-270.

124. Global heating and confinement with neutral beams in JET limiter plasmas.
Lomas P.J., Bombarda F., Brusati M., Challis C., Christiansen J.P., Cordey J.G., Corti S., Duesing G., Giannella R., Hendriks F., Horton L., von Hellermann M., Jones T.T.C., Källne K., Stäbler A., Stork D., Thomas P.R., Thomsen K., Thompson E., Watkins M.L.
American Physical Society. Bulletin.
Vol.31 No.9 October 1986.
(Abstracts of 28th Annual Meeting Division of Plasma Physics, Baltimore, 3-7 November 1986).
Paper 8P 24, p.1590.

125. Modelling and control of large robots for tele-operation systems.
Maisonnier D.
Joint European Torus JET. 1986. 23p.
Report JET-P(86)02.

126. JET contributed papers at the Int. Workshop on Small Scale Turbulence and Anomalous Transport in Magnetised Plasma (Cargese, July 1986). 1. Observations of turbulence in the JET tokamak. 2. Magnetic fluctuations and confinement in JET.
Malacarne M., Duperrex P.A.
Joint European Torus JET. 1986. 8p.
Report JET-P(86)31.

127. JET contributions to 14th symposium on fusion technology (SOFT): Part 1 - invited papers.
Many Authors.
Report JET-P(86)39.

128. JET contributions to 14th symposium on fusion technology (SOFT): Part 2 - contributed papers.
Many Authors
Report JET-P(86)40.

129. JET papers presented to Workshop on High Temperature Plasma Diagnostics, Varenna, 1986.
Many Authors.
Report JET-P(86)45.

130. The JET nuclear fusion project.
Maple J.H.C.
Electronics and Power
Vol.32 No.10 October 1986 pp.731-734.

131. The JET project - a major step to harness energy from fusion.
Maple J.H.C.
Endeavour Vol.10 No.4 1986 pp.177-183.

132. 15MeV proton emission from JET plasmas exhibiting sawtooth behaviour: results and interpretation.
Martin G., Jarvis O.N., Källne J., Merlo V., Sadler G., van Belle P.
Report JET-P(86)26.

133. Carbon protection tiles for JET.
Massmann P., Deksnis E., Falter H.D., Hemsworth R.S., Shaw R., Stäbler A.
Fusion Technology 14th Symp. held in Avignon, 8-12 September 1986. Avignon, SOFT. 1986.
Paper No. BP 19.

134. The interpretation of plasma edge conditions in tokamaks.
McCracken G.M., Stangeby P.C.
Joint European Torus JET. 1985. 15p.

Report JET-P(85)27.

135. Aspects of interfacing JET diagnostic systems.
Millward P., Caldwell-Nichols C.J., Ainsworth A., Barnes M., Foden N., Gowman J., Hancock C.J., Lobel R., Oliver B., Reid J., Roberts P.J., Tiscornia A., Wilks J.A., Wilson C.
Fusion Engineering 11th Symposium, held in Austin, 18-22 November 1985.
New York, IEEE. 1986.
Vol.1, pp.568-570.
(Also JET-P(85)26).

136. Engineering aspects of JET diagnostic systems.
Millward P., Ainsworth A., Caldwell-Nichols C.J., Lobel R., Hancock C.J.
Fusion Technology, Vol.11 No.1 January 1987 (Special issue on design, construction and first operational experience on the Joint European Torus (JET)) pp.235-252.

137. Design, commissioning and early operation of the power supply and protection system for the extraction grid of the JET neutral injectors at 160kV.
Mondino P., Claesen R., Dobbing J.A., Baigger P.
Fusion Technology 14th Symp. held in Avignon, 7-12 September 1986. Avignon, SOFT. 1986.
Paper No. CP 54.

138. The development of the JET poloidal field power supplies for maximising the flux swing capabilities.
Mondino P.L., Bonicelli T., Huart M., Santagiustina A.
Fusion Technology 14th Symp. held in Avignon, 8-12 September 1986. Avignon, SOFT. 1986.
Paper No. CP43.

139. JET technical and scientific performance and future plans.
Mondino P.L.
ANS Transactions.
Vol.52 1986 (Annual meeting, Reno, Nevada, 15-19 June 1986) pp.282-283.

140. The JET technical and scientific performance and future plans.
Mondino P.L., Bertolini E.
Joint European Torus JET. 1986. 11p.
Report JET-P(86)32.
Paper presented at the 7th Topical Meeting on the Technology of Fusion Energy, Reno, 15-19 June 1986.

141. Fast wave electron current drive.
Moreau D., Jacquinot J., Lallia P.P.
Controlled Fusion and Plasma Heating 13th Euro. Conf., held in Schliersee, 14-18 April 1986.
Geneva, European Physical Society. 1986.
Vol.2, pp.421-424.
(Also JET-P(86)15).

142. Stabilisation of vertical position and control of plasma shape in JET.
Noll P., Aigle R., Browne M.L., Corbyn D., Eriksson T., Froger C., Huguet M., Rebut P.H., Santagiustina A., Sonnerup L., Watkins J.R., Wesson J. Niedermeyer H.
Fusion Engineering 11th Symposium, held in Austin, 18-22 November 1985.
New York, IEEE. 1986.
Vol.1 pp.33-40.
(Also JET-P(85)26).

143. Operation and performance of the large scale JET cryopump system.
Obert W., Haange R., Jones A., Kuessel E., Mayaux C., Roberts R.
Fusion Technology 14th Symp. held in Avignon, 8-12 September 1986. Avignon, SOFT. 1986.
Paper No. BP 09.

144. Current density profile control on JET using ECRH current drive.
O'Brien M.R., Cox M., Hender T.C., Robinson D.C., Start D.F.H.
Controlled Fusion and Plasma Heating 13th Euro. Conf., held in Schliersee, 14-18 April 1986.
Geneva, European Physical Society. 1986.
Vol.2, pp.270-273.

145. Phenomenological relations for tokamak transport.
O'Rourke J.
Joint European Torus JET. 1986. 16p.
Report JET-P(86)13.

146. The JET in-vessel inspection system.
Raimondi T., Presle P., Galbiati L.
Fusion Technology 14th Symp. held in Avignon, 8-12 September 1986. Abstracts.
Avignon, SOFT. 1986.
paper No. HP 41.

147. The impact of the first JET results on the development of fusion.
Rebut P.H.
Fusion Technology 14th Symp. held in Avignon, 8-12 September 1986. Avignon, SOFT. 1986.
Paper No. AI.04.

148. JET contributions to 11th International Conference on Plasma Physics and Controlled Nuclear Fusion Research, Japan, 1986.
Rebut P.H., et al.
(Also JET-P(86)44).

149. JET: Evolution, status and prospects.
Rebut P.H., Lallia P.
Joint European Torus JET. 1986. 21p.
Report JET-P(86)17.
Talk given at the Royal Society Discussion Meeting on the JET Project and the Prospect for Controlled Nuclear Fusion, London, 12-13 March 1986.

150. The JET experiment: Evolution, present status and prospects.
Rebut P.H., Keen B.E.
Fusion Technology, Vol.11 No.1 January 1987 (Special issue on design, construction and first operational experience on the Joint European Torus (JET)) pp.13-42.

151. The Joint European Torus. Installation, first results and prospects.

Rebut P.H., Bickerton R.J., Keen B.E.
Joint European Torus JET. 1985. 18p.
Report JET-P(85)07.
Nuclear Fusion, Vol.25, No.9, (1985) pp.1011-1022.

152. Magnetic topology, disruptions and electron heat transport.
Rebut P.H., Brusati M.
Plasma Physics and Controlled Fusion
Vol.28 No.1 pt.A January 1986 (Controlled Fusion and Plasma Physics, 12th Euro. Physical Society Plasma Physics Division Conf., 2-6 September 1985, Budapest, Hungary. Invited papers.)
pp.113-124.

153. Electron temperature measurements from line ratios of He- and H-like argon in the Alcator C tokamak.
Rice J.E., Marmar E.S., Källne E., Källne J.
Review of Scientific Instruments.
Vol.57 No.8 pt.II August 1986 (Procs. 6th Topical Conf. on High Temperature Plasma Diagnostics Hilton Head Island, South Carolina, 9-13 March 1986).
pp.2154-2155.

154. Observation of charge-transfer population of high N levels in AR(sup +16) from neutral hydrogen in the ground and excited states in a tokamak plasma.
Rice J.E., Marmar E.S., Terry J.L., Källne E., Källne J.
Massachusetts Institute of Technology. Plasma Fusion Centre. October 1985. 15p.
Report PFC/JA-85-34.
Submitted to Physical Review Letters.

155. The JET cryogenic supply system.
Roberts R.L., Jones A., Kupschus P., Kussel E., Mayaux C., Mead M.J., Obert W., Steed C.A., Wallender B.A., Spath F.
Advances in Cryogenic Engineering.
Vol.31 1986 (Pocs. 1985 Cryogenic Engineering Conf. held 12-16 August 1985, in Cambridge, Mass.) pp.595-606.
(Also Report JET-P(85)14).

156. Remote maintenance of the JET tokamak.
Rolfe A.C.
Joint European Torus JET. 1986. 15p.
Report JET-P(86)03.
Published in the Procs. of UK Prototype and Research Managers Conf., Culcheth, 18-20 March 1986.

157. Fusion product measurements on JET.
Sadler G., van Belle P., Hone M., Jarvis O.N., Källne J., Martin G., Merlo V.
Controlled Fusion and Plasma Heating 13th Euro. Conf., held in Schliersee, 14-18 April 1986.
Geneva, European Physical Society. 1986.
Vol.1, pp.105-108.
(Also Report JET-P(86)15).

158. Effect of off axis ICRF power deposition in JET.
Sand F., Bures M., Corti S., Jacquinot J., Lallia P.P., Tanga A. and others.
Controlled Fusion and Plasma Heating 13th Euro. Conf., held in Schliersee, 14-18 April 1986.
Geneva, European Physical Society. 1986.
Vol.2, pp.197-200.
(Also Report JET-P(86)15).

159. The high voltage grid interface in the present and future JET operational requirements.
Selin K.I., Ciscato D., Claesen R., Marchese V., Mondino P.L., Ashmole P., Jervis B.
Fusion Technology 14th Symp. held in Avignon, 8-12 September 1986. Abstracts.
Avignon, SOFT. 1986.
Paper No. CP 44.

160. 3-D Monte Carlo computations of the neutral temperature and density distribution in JET discharges.
Simonini R., Taroni A.
Controlled Fusion and Plasma Heating 13th Euro. Conf., held in Schliersee, 14-18 April 1986.
Geneva, European Physical Society. 1986.
Vol.1, pp.164-167.
(Also Report JET-P(86)15).

161. A comparison between theory and experiment for multiple helicity modes during auxiliary heating on JET.
Snipes J.A., Haynes P.S., Hender T.C., Robinson D.C., Morris A.W., Tonetti G.
Controlled Fusion and Plasma Heating 13th Euro. Conf., held in Schliersee, 14-18 April 1986.
Geneva, European Physical Society. 1986.
Vol.1, pp.152-155.

162. First wall concepts and density control in JET.
Sonnenberg K., Diëtz K.J., Kupschus P.
Fusion Technology 14th Symp. held in Avignon, 8-12 September 1986. Avignon, SOFT. 1986.
Paper No. I I.03.

163. Mechanical design assessments of structural components and auxiliaries of the Joint European Torus.
Sonnerup L.
Nuclear Engineering and Design. Fusion Vol.3 No.3 1986. pp.233-247.

164. Mechanical design assessments of structural components and auxiliaries of the Joint European Torus.
Sonnerup L.
Structural Mechanics in Reactor Technology 8th Int. Conf., held in Brussels, 19-23 August 1985. Vol.N. Mechanical and thermal problems of fusion reactors.
Amsterdam, North Holland. 1985. pp.1-6.
(Also Report JET-P(85)19).

165. The recombination and level populations of ions. III - The role of charge exchange from neutral hydrogen.
Spence J., Summers H.P.
Joint European Torus JET. 1986. 55p.
Report JET-P(86)01.

166. Neutralisation measurements for the JET neutral

injector.
Stäbler A., and others.
JET Contributions to 13th Euro. Conf. on Controlled Fusion and Plasma Heating, Schliersee, 14-18 April 1986.
Joint European Torus JET, 1986.
pp.97-100.
Report JET-P(86)15.

167. Commissioning and operation of the control, safety and interlock on the JET neutral beam injector.
Stork D., Jones T.T.C., Cooper D., Davies J.F., Ewers D., Nijman J.P., Stäbler A., Starley K.
Fusion Technology 14th Symp. held in Avignon, 8-12 September 1986. Abstracts.
Avignon, SOFT. 1986.
Paper No. GP 13.

168. Plasma rotation during JET neutral beam heated discharges.
Stork D., Bombarda F., Campbell D., Giannella R., Horton L., Källne E., Lopes-Cardozo N., Tallents S., Tonetti G., von Hellermann M.
American Physical Society. Bulletin.
Vol.31 No.9 October 1986.
(Abstracts of 28th Annual Meeting Division of Plasma Physics, Baltimore, 3-7 November 1986).
Paper 5E 9, p.1503.

169. Plasma measurements for JET.
Stott P.E.
Royal Society Discussion Meeting on the JET Project and the Prospect for Controlled Nuclear Fusion, London, 1986.
(Also JET-P(86)48).

170. Summary of recent results in JET: Conf. Report on the 4th Euro. Tokamak Programme Workshop, Copenhagen, 4-6 December 1985.
Stott P.E.
Plasma Physics and Controlled Fusion.
Vol.28 No.8 August 1986.
pp.1193-1199.

171. Anomalous transport in toroidal confinement.
Stringer T.E.
Joint European Torus JET. 1985. 26p.
Report JET-P(85)17.
Lecture given at the Int. School of Plasma Physics, Varenna, 26 August - 3 September 1984.

172. Computational models for wave-particle interactions.
Succi S., Appert K., Core W., Hamnén H., Hellsten T., Vaclavik J.
Computer Physics Communcations.
Vol.40 No.1 May 1986 (Procs. 3rd Euro. Workshop on Problems in the Numerical Modelling of Plasmas (NUMOP 85), 10-12 September 1985, Varenna, Italy).
pp.137-151.

173. Interpretation of emission from ions out of ionisation balance.
Summers H.P., Behringer K.H., Boileau A., Forrest M.J., Horton L., Peacock N.J., Stamp M.F., von Hellerman M.
Report JET-P(86)42.

174. Radiative gaunt factors.
Summers H.P.
Joint European Torus JET. 1986. 29p.
Report JET-P(86)06.

175. Recombination and population structure
Summers H.P., Behringer K.H., Denne B.
Report JET-P(86)43.

176. Recombination of neon-like and adjacent ions in plasmas.
Summers H.P., Behringer K., Wood L.
Joint European Torus JET. 1986.
Report JET-P(86)36. 16p.

177. Errors in measuring electron temperatures using a single langmuir probe in a magnetic field.
Tagle J.A., Stangeby P.C., Erents S.K.
Report JET-P(86)22.

178. Effects of major radius compression in JET.
Tanga A., Gottardi N., Hubbard A. Lazzaro E., Noll P., Springmann E., Taroni A.
Controlled Fusion and Plasma Heating 13th Euro. Conf., held in Schliersee, 14-18 April 1986.
Geneva, European Physical Society. 1986.
Vol.1, pp.264-267.
(Also Report JET-P(86)15).

179. Start-up of the ohmic phase in JET.
Tanga A., Thomas P.R., Cordey J.G., Christiansen J.P., Ejima S., Kellman A., Lazzaro E., Lomas P.J., Morgan P., Nave M.F., Noll P., Schüller F.C.
Tokamak Start-up: Problems and scenarios related to the transient phases of a thermonuclear fusion reactor. Procs. 7th Course of the International School of Fusion Reactor Technology, held in Erice, 14-20 July 1985.
New York, Plenum. 1986. pp.159-180.
(Also Report JET-P(85)23).

180. A numerical study of the dependence of an MHD equilibrium configuration on variations of p and q profiles.
Taroni A., Springmann E.
Joint European Torus JET. 1986. 26p.
Report JET-R(86)03.

181. Profile consistency and electron energy transport models.
Taroni A., Tibone F.
Controlled Fusion and Plasma Heating 13th Euro. Conf., held in Schliersee, 14-18 April 1986.
Geneva, European Physical Society. 1986.
Vol.1, pp.160-163.

182. Confinement and heating of plasmas in the JET tokamak.
The JET Team (presented by R.J. Bickerton)
Institute of Physics Annual Meeting, Oxford, 1986.
Report JET-P(86)47.
Submitted to Plasma Physics and Controlled Fusion.

183. Impurity behaviour in JET
The JET-Team (presented by W.W. Engelhardt).

13th EPS Conference on Controlled Fusion and Plasma Heating, Schliersee (F.R.G.).
(Also JET-P(86)25)
Submitted to Plasma Physics and Controlled Fusion.

184. Energy confinement in tokamaks.
Thomas P.R.
Controlled Fusion and Plasma Heating 13th Euro. Conf., held in Schliersee, 14-18 April 1986.
Vol.1, pp.37-40.
(Also Report JET-P(86)15).

185. An overview of neutral beam injection experiments on JET.
Thompson E., Behringer K., Campbell D.J., Challis C., Christiansen J., Cordey J.G., Corti S., Costley A., Duesing G., Goede A.P.H., von Hellermann M., Jaeckel H., Jarvis O.N., Jones T.T.C., Källne E., Lomas P., Morgan P., Sadler G., Stabler A., Stork D., Thomas P., Watkins M.L.
American Physical Society. Bulletin.
Vol.31 No.9 October 1986.
(Abstracts of 28th Annual Meeting Division of Plasma Physics, Baltimore, 3-7 November 1986).
Paper 5E 8, p.1503.

186. Energy transport in JET with ohmic and auxiliary heating.
Thomsen K., and others.
JET Contributions to 13th Euro. Conf. on Controlled Fusion and Plasma heating, Schliersee, 14-18 April 1986.
Joint European Torus JET, 1986. pp.1-4.
Report JET-P(86)15.

187. Profile consistency and electron energy transport models.
Tibone F., Taroni A.
JET Contributions to 13th Euro. Conf. on Controlled Fusion and Plasma Heating, Schliersee, 14-18 April 1986.
Joint European Torus JET, 1986. pp.17-20.
Report JET-P(86)15.

188. Determination of poloidal beta in JET.
Tonetti G.G., Christiansen J.P., Cordey J.G.
Controlled Fusion and Plasma Heating 13fth Euro. Conf., held in Schliersee, 14-18 April 1986.
Geneva, European Physical Society. 1986.
Vol.1, pp.113-116.

189. Measurement of the energy content of the JET tokamak plasma with a diamagnetic loop.
Tonetti G.G., Christiansen J.P., de Kock L.
Review of Scientific Instruments.
Vol.57 No.8 pt.II August 1986 (Procs. 6th Topical Conf. on High Temperature Plasma Diagnostics, Hilton Head Island, South Carolina, 9-13 March 1986).
pp.2087-2089.

190. Technical planning and control.
Trevalion P.
Int. Structural Comparison of Research Centres 4th symposium on Research Centres and their Financial Environment, held in Petten, 7-9 October 1985.
Hague, ECN. 1985. pp.245-254.

191. CODAS: The JET control and data acquisition system.
van der Beken H., Best C.H., Fullard K., Herzog R.F., Jones E.M., Steed C.A.
Fusion Technology, Vol.11 No.1 January 1987 (Special issue on design, construction and first operational experience on the Joint European Torus (JET)) pp.120-137.

192. First spectroscopic charge exchange measurements during neutral injection on JET.
von Hellermann M., Engelhardt W.W., Horton L., Carolan P.G., Forrest M.J., Peacock N.J.
Controlled Fusion and Plasma Heating 13th Euro. Conf., held in Schliersee, 14-18 April 1986.
Geneva, European Physical Society. 1986.
Vol.1, p.120-123.
(Also Report JET-P(86)15).

193. The technology of the upgraded JET ICRF heating system.
Wade T.J., Kaye A.S., Jacquinot J.
ANS Transactions.
Vol.52 1986 (Annual meeting, Reno, Nevada, 15-19 June 1986) pp.283-284.
(Also Report JET-P(86)24).

194. Design and manufacture of water cooled electrostatic screens for JET.
Walker C., Kaye A.S., Brinkschulte H., Hora R.A., Sigournay D., Bevilacqua G., Anselmi F.
Fusion Technology 14th Symp. held in Avignon, 8-12 September 1986. Avignon, SOFT. 1986.
Paper No. CP 21.

195. Non evaporable getter pumping for JET ICRF antennae.
Walker C.I., Kaye A.S., Horn R.A., Mazza F.
Fusion Technology 14th Symp. held in Avignon, 8-12 September 1986. Avignon, SOFT. 1986.
Paper No. CP 22.

196. The vacuum vessel of JET.
Walravens M.J.
Proc. Instn. Mech. Engrs., Vol.200, No.A1, 1986, pp.9-30.

197. Predictive studies of neutral beam and pellet injection on JET.
Watkins M.L., Houlberg W.A., Kupschus P., Stubberfield P.M., Taroni A.
Controlled Fusion and Plasma Heating 13th Euro. Conf., held in Schliersee, 14-18 April 1986.
Geneva, European Physical Society. 1986.
Vol.1, p.156-159.
(Also Report JET-P(86)15).

198. A fast shutter system for the JET neutral injectors.
Watson J., Haange R., Tivey R., Stork D.
Fusion Technology 14th Symp. held in Avignon, 8-12 September 1986. Avignon, SOFT. 1986.
Paper No. DP 48.

199. Soft X-radiation losses during additional heating in JET.

Weller A., Behringer K., Edwards A., Engelhardt W.W., Fahrbach H.U., Gill R.D., Granetz R., Pasini D., Zasche D.
American Physical Society. Bulletin.
Vol.31 No.9 October 1986.
(Abstracts of 28th Annual Meeting Division of Plasma Physics, Baltimore, 3-7 November 1986).
Paper 8P 27, p.1590.

200. Sawtooth oscillations.
Wesson J.A.
Plasma Physics and Controlled Fusion.
Vol.28 No.1 pt.A January 1986 (Controlled Fusion and Plasma Physics, 12th Euro. Physical Society Plasma Physics Division Conf., 2-6 September 1985, Budapest, Hungary. Invited paper).
pp.243-248.
(Also Report JET-P(85)25).

201. Helium leak detection in JET in the presence of high deuterium partial pressure.
Winkel T., Hemmerich J.L.
Joint European Torus JET. 1986. 13p.
Report JET-P(86)29.
Paper presented at the Joint 10th Int. Vacuum Congress, 6th Int. Conf. on Solid Surfaces and 33rd National Symposium of the American Vacuum Society, Baltimore, 27-31 October 1986.

202. Remote handling tools for JET.
Wykes M., Galbiati L., Mills S., Presle P., Raimondi T., Schreibmaier J., Tesini A.
Fusion Technology 14th Symp. held in Avignon, 8-12 September 1986. Avignon, SOFT. 1986.
Paper No. HP 42.

203. JET Annual Report 1985
Euratom, Joint European Torus JET.
Abingdon, JET 1986, 99p.
EUR 10615 EUR-JET-AR8 (Edited by P.J. Kind, J.H.C. Maple, G.W. O'Hara and I.E. Pollard.

204. JET Progress Report 1985.
Euratom. Joint European Torus JET.
Abingdon, JET. 1986. 350p.
EUR 10616 EUR-JET-PR3 (Edited by B.E. Keen)

205. First results of neutral beam heating on JET.
JET Team.
Plasma Physics and Controlled Fusion.
Vol.28 No.9A September 1986 (Controlled Fusion and Plasma Heating: 13th Euro. Physical Society Plasma Physics Division Conf., 14-18 April 1986, Schliersee, FRG. Invited paper).
pp.1429-1434.

206. Impurity behaviour in JET.
JET Team.
Plasma Physics and Controlled Fusion.
Vol.28 No.9A September 1986 (Controlled Fusion and Plasma Heating: 13th Euro. Physical Society Plasma Physics Division Conf., 14-18 April 1986, Schliersee, FRG. Invited papers).
pp.1401-1412.

207. The status of JET.
JET Team.
European Tokamak Programme, 2nd Workshop, held in Saulx les Chartreux, 30 November - 2 December 1983.
CEA, 1983. pp.188-205.

Appendix V

Reprints of JET papers

(a) JET-P(86)21 Plasma Heating in JET (Invited paper at 13th European Conference on Controlled Fusion and Plasma Heating (Schliersee, F.R.G., April 1986));

(b) JET-P(86)25 Impurity Behaviour in JET (Invited paper at 13th European Conference on Controlled Fusion and Plasma Heating (Schliersee, F.R.G., April 1986));

(c) JET-P(86)20 First Results of Neutral Beam Heating on JET (Paper at 13th European Conference on Controlled Fusion and Plasma Heating (Schliersee, F.R.G., April 1986));

(d) JET-P(86)15 Contributed JET papers to 13th European Conference on Controlled Fusion and Plasma Heating (Schliersee, F.R.G., April 1986));

(e) JET-P(86)39 Invited papers presented at 14th Symposium on Fusion Technology (SOFT) (Avignon, France, September 1986);

(f) JET-P(86)40 Contributed papers presented at 14th Symposium on Fusion Technology (SOFT) (Avignon, France, September 1986);

(g) JET-P(86)32 The JET Technical and Scientific Performance and Future Plans (Invited paper to 7th Topical Meeting on Technology of Fusion Energy (Reno, U.S.A., June 1986));

(h) JET-P(86)23 Main Features Implemented in the JET Facility for D-T Operation (Paper at 7th Topical Meeting in Technology of Fusion Energy (Reno, U.S.A., June 1986));

(i) JET-P(86)44 JET papers presented at 11th International Conference on Plasma Physics and Controlled Fusion Research (Kyoto, Japan, November 1986).

Invited Paper at 13th European Conference on Controlled Fusion and Plasma Heating, Schliersee, FRG, April 1986

Plasma Heating in JET

P.P.Lallia

ABSTRACT

Heating the JET plasma well above temperatures reached in the ohmic phase is the aims of the two additional heating systems planned for JET: Ion Cyclotron Resonance Heating (ICRF) and Neutral Beam Injection (NBI). Operations with the latter started in February 1986, initially with Hydrogen injection, up to a power level of 7MW. ICRF power has been delivered to the plasma by three antennae and has reached power levels of 6MW for 2s. In most experiments, the frequency of the waves is adjusted to position the minority ion resonance layer close to the centre of the discharge, resulting in a centrally peaked power deposition profile. Results have also shown that the increase of the volume averaged electron temperature was much less dependent on the radial position of the ion resonance layer than were the central temperatures of both ions and electrons which can both approach 5keV. In cases of "on axis" heating, large increases in the sawtooth activity is observed with sawtooth periods exceeding 0.3s. Initial results with NBI have shown a decrease of the global energy confinement time with additional power similar to the one observed with ICRF heating. The scaling of the "incremental" confinement time (defined as the ratio of the plasma energy increase to the input power increase, $\Delta W/\Delta P$), is not yet available but figures between 0.15 and 0.3s have been observed. At present, the product $\hat{n}_i.\hat{T}_i.\tau_E$ is not significantly increased above the ohmic level ($\sim 6 \times 10^{19} m^{-3} keVs$). On the other hand, the neutron yield has exceeded $2.10^{15}/s$ in initial combined NBI/ICRF (D injection, H minority) with 14MW total input power as compared to $10^{14}.s^{-1}$ in the best ohmic conditions.

KEYWORDS

Thermonuclear Fusion Research; Plasma; Tokamaks; Joint European Torus; Additional plasma heating.

I. INTRODUCTION

Since mid-1985, (Jacquinot et al, 1985; Bickerton et al, 1985), the capabilities of heating the JET plasma have increased with the availability of a third ICRF antenna and RF generator, and, especially, the first Neutral Beam Injection box (Duesing et al, 1986). Studies of ohmically heated plasmas have been pursued and have resulted in maintaining a plasma current of 5MA for a 3 seconds flat-top, as illustrated in Fig. 1. The energy content was 3MJ for an ohmic input power of 5MW. While the density was kept at $n_e \simeq 4 \times 10^{19} m^{-3}$ well below the density limit, the Deuterium-Deuterium thermonuclear reaction yield reached $10^{14} s^{-1}$, corresponding to a peak ion temperature of 2.5keV.

Two types of discharges will be described in the following: (i) the so-called "limiter discharges" where the last closed magnetic surface on JET is tangential to eight graphite limiters located at a major radius of 4.17m and (ii) the so-called "inner wall" discharges, where the plasma leans on the graphite tiles protecting the central part of the vacuum vessel at a radius of 1.80m. The antennae protection tiles were recessed 8mm behind the carbon limiters and the metallic screens were 15mm further away.

All the results presented here have been obtained with a wall covered mostly by the carbon deposited early in 1985 (Engelhardt et al, 1986), with only a light carbonisation having been

performed in November 1985. The wall temperature was close to 300°C. The plasma cross-section was close to elliptical with an elongation ratio of 1.4 and the total plasma volume around 120m³. The ICRF antennae were used with a wavenumber spectrum centred on $k_{//} = 0$.

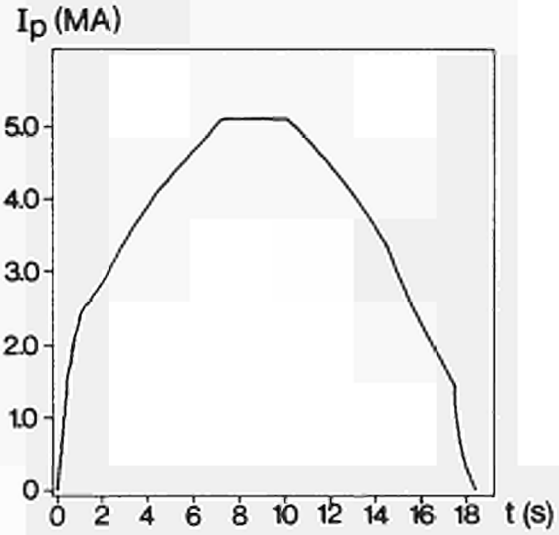

Fig.1 Time evolution of the plasma current showing the flat-top current at 5 MA. The other major parameters of this discharge were: B_T = 3.4 T; n_e = 4 x $10^{19}m^{-3}$; T_{eo} = 3 keV; $\langle T_e \rangle$ = 1.8 keV; T_{io} = 2.5 keV; Plasma Energy content: 3 MJ; Input ohmic power: 5 MW.

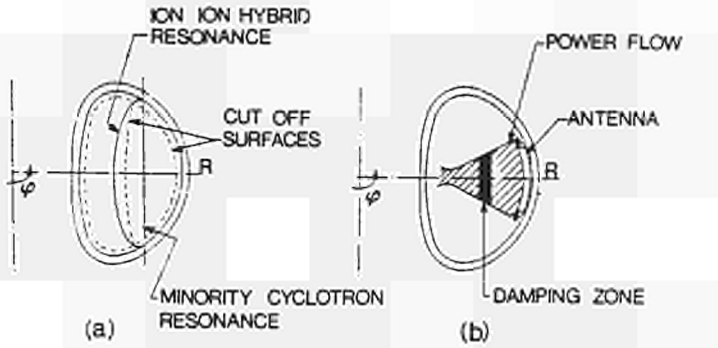

Fig.2 Cross-section of JET illustrating the various surfaces of CRF significance in ICRF heating.

II. ION CYCLOTRON RESONANCE HEATING

The basic scheme of ICRF minority heating in Tokamaks is to couple a compressional electromagnetic wave to the plasma. This type of wave can propagate freely into the plasma as long as the density exceeds a cutoff value (which depends on the Alfven speed and on the excited wave number), which is typically a few $10^{18}m^{-3}$. The presence of a minority ion species introduces locally near the so-called "hybrid resonance layer", a strong modification of the polarization of the compressional wave which increases the electric field component rotating in the same direction as the minority ions. In JET, the distance from the hybrid layer to the minority ion cyclotron resonance is about 5 to 15cm. For clarity, this distance has been exaggerated in Fig. 2, which shows the various surfaces of significance in ICRF heating. Those of the ions which experience both the current polarization and frequency (i.e. those for which the Doppler-shift exceeds the distance of the cyclotron layer - hybrid resonance layer) are strongly accelerated by the wave. The redistribution of power (by Coulomb collisions) to the electrons or the ions of the main plasma depends on the energy of the minority ions, which depends on the RF power per particle absorbed locally. Most of the RF power should be absorbed inside a volume, of which the characteristic radial extent is the perpendicular wavelength into the plasma (typically 20 to 30cm,) which is a small fraction of the minor radius of the JET plasma.

The two minority ion species used in JET are either Hydrogen or Helium-3 at a concentration relative to the Deuterium population varying between 5 and 10%. The proton concentration was monitored by a mass selective neutral particle analyser (Corti et al, 1986), while the actual concentration of He in JET was deduced from the density increase at the time of the ^{3}He gas puff and assuming a complete recycling at the plasma boundary.

Coupling of the RF antennae to the plasma showed fair agreement between results and the theoretical model, assuming strong absorption in the plasma (Evrard et al, 1986). In the absence of strong absorption, (i.e. in absence of resonating minority ions), eigenmodes should exist and have been observed, as shown in Fig. 3. Time evolution of the forward and reflected voltage along the RF transmission line are shown for three JET pulses. Without ^{3}He injection (Fig. 3a), the reflected trace shows fluctuations which disappear about 0.4s after the ^{3}He

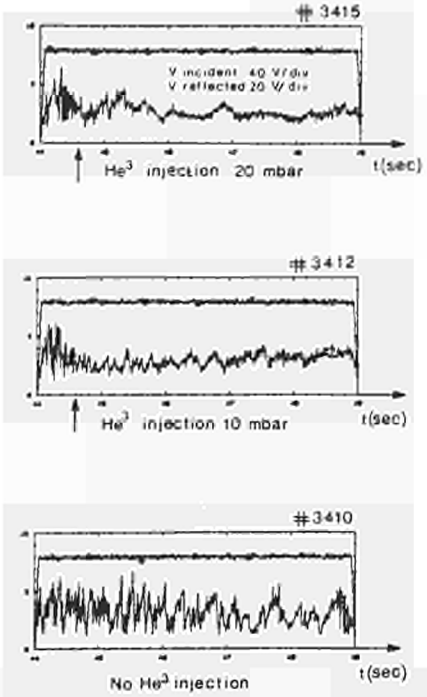

Fig.3 Time evolution of the incident and reflected voltage along the ICRF ion transmission line in case of on-axis ^{3}He resonance.
a) No ^{3}He injection.
b) The ^{3}He gas valve was opened at t = 44.3 s. The arrow indicates the estimated time when Helium reached the plasma axis.
c) As b) with higher He content.

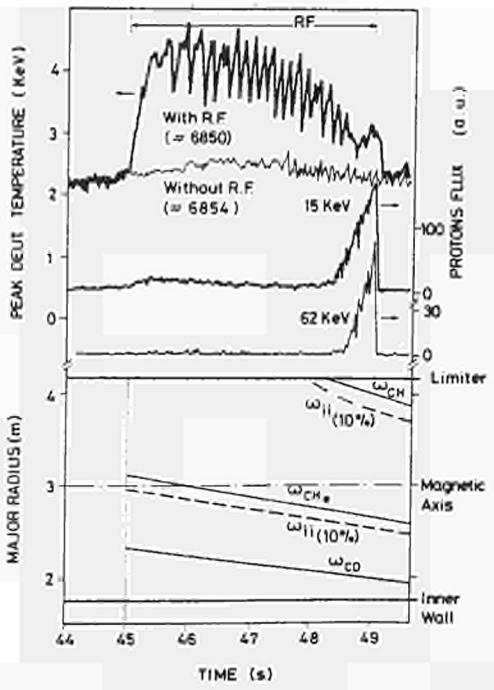

Fig.4 a) Time evolution of the central deuteron temperature with and without 3.4 MW ICRF, and of the proton flux at 15 and 62 keV during a toroidal field ramp down. The plasma current was kept constant at 2 MA.
b) Radial position of the proton and ^{3}He cyclotron layers during the above pulse. The approximate position of the corresponding hybrid layers is indicated by the dotted lines.

valve was opened at 44.3s, the arrow indicates the estimated time for the minority ions to reach the JET axis where the cyclotron layer existed.

Further evidence of the minority role in wave absorption is shown in Fig. 4. During this experiment, the toroidal magnetic field was ramped down so that the proton cyclotron layer entered the plasma at t = 48.3s, while the ^{3}He cyclotron layer was moving from the plasma axis towards the inner wall. A square RF pulse of 3.4MW was applied from t = 45 to t = 49s. The upper part of Fig. 4 shows an increase of 2keV in the peak Deuterium temperature deduced from the neutron flux, with the large sawteeth characteristic of "on axis" heating. The flux of 15keV protons seen by the neutral particle analyser increases at t = 45s, reflecting the ion temperature rise. At t = 47s, the central ion temperature decreases slightly, probably a consequence of both the density increase and the growing size of the volume inside the sawtooth inversion radius. However, the major change occurs when the proton cyclotron resonance enters the plasma: protons with energy up to 100keV are detected with a time delay increasing with energy and simultaneously the Deuterium temperature on axis drops further, indicating that a part of the RF power is now absorbed near the plasma boundary.

Ramping down the magnetic field during a JET pulse allowed a scan of the radial position of the cyclotron layer and permitted an observation of its effects on the heating efficiency of the plasma. This was performed using Hydrogen minority in a Deuterium plasma at a concentration of about 7% during a 2MA discharge. The wave frequency was 32MHz and the RF power ranged from 3.3 to 3.8MW. Figs. 5a, b, c and d show, respectively, the neutron flux, the central ion temperature deduced from this (Jarvis et al, 1985), and the central and volume averaged electron temperatures deduced from the absolutely calibrated ECE system (Costley et al, 1985), as a function of the radial position of the proton cyclotron layer. The axis of

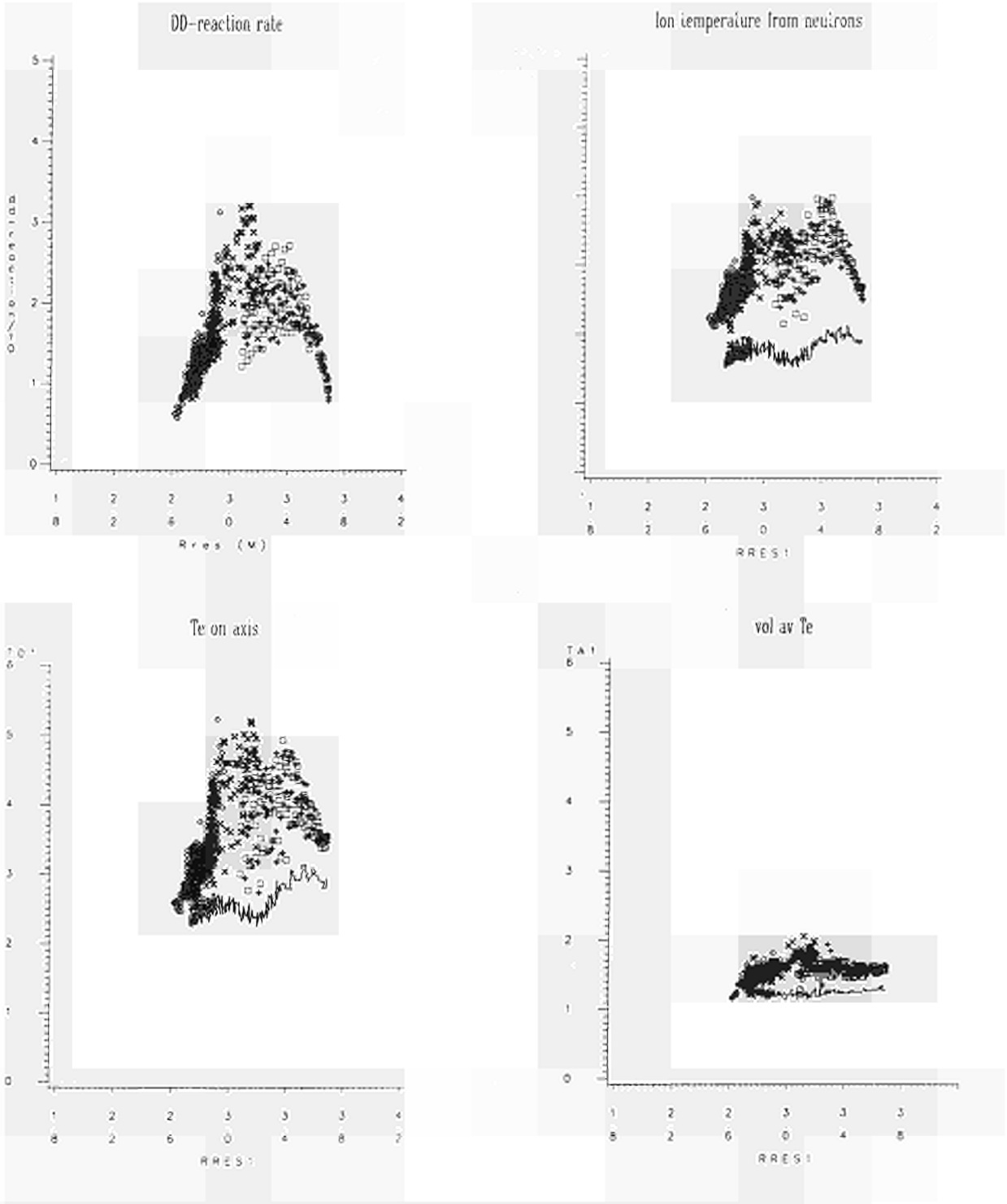

Fig.5 Variations with the position of the proton cyclotron layer of:
a) the D-D reaction rate; neutron flux;
b) the central ion temperature from neutron flux;
c) the central electron temperature from ECE;
d) the volume averaged electron temperature.

The data are taken during a ramp down of the toroidal field and the continuous line corresponds to a pulse without ICRF. The plasma boundaries are at R ≈ 4.2 and R ≈ 2.8 m. The sawtooth inversion radius is at R ≈ 3.4 and 2.8 m. The plasma axis is at R ≈ 3.1 m.

the discharge was close to 3.1m. The inner and outer boundaries of the plasma were at 1.80m and 4.17m, respectively.

The q profile changed somewhat during the scan but on average the sawtooth inversion radii were at 2.8m and 3.4m. The position of the ion-ion hybrid layer, where the maximum absorption was expected, was at a radius of -0.1m smaller than the cyclotron layer. The squares and crosses represent the data during RF, non-averaged over the sawteeth, while the solid lines indicate the values during an ohmic reference pulse. Curves 5a, b and c show clearly a maximum increase of the central temperatures when the hybrid layer is inside the inversion radius of sawteeth. The dispersion of the RF data reflects the large amplitude of the sawteeth. On the other hand, Fig. 5c shows a much smaller increase of the volume-averaged temprature which seems less dependent on the position of the cyclotron layer.

A global estimate of the ICRF power transferred to the plasma was estimated by fitting the time evolution of the total plasma energy content W(t), deduced either from magnetic or diamagnetic measurements (Cordey et al, 1986) or from temperature and density measurements, to a relationship of the form (Ejima et al, 1985):

$$W(t) = W_0 + \tau^*(fP_{RF} + \Delta P_\Omega)\left[1 - \exp(-t/\tau^*)\right]$$

Here P_{RF} is the total RF power radiated by the antenna (i.e. the power RF delivered by the generator less the power ohmically dissipated in the transmission line and in the antenna), ΔP_Ω is the change in ohmic power during the RF pulse. The fit allows a determination of the quantities f and τ^*, (i.e. the fraction of RF power "observed" in the plasma and the replacement time of the additional energy, respectively). The results show that τ^* ranges from 0.1 to 0.3s and f from 60 to 80% (Thomsen et al, 1986). While part of the missing power can be explained by the sudden influx of energy detected in the scrape off layer (by Langmuir probes) in the first millisecond after switching on the RF power, the mechanism responsible for peripheral absorption or for the very fast transport to the plasma boundary of some 30% of the RF power, is not yet identified (Brinkschulte et al, 1986).

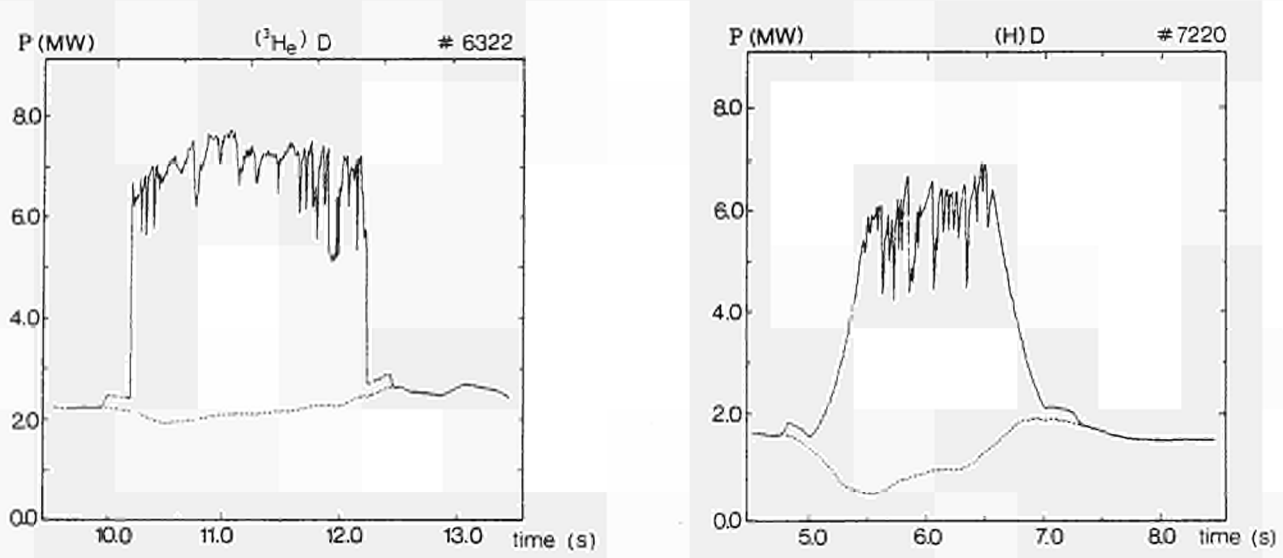

Fig.6 Time evolution of the ohmic and total input power in two ICRF heated pulses:
a) ^{3}He minority in Deuterium
b) H minority in Deuterium in Table I.

Previously reported experiments up to an RF power of 4MW had shown no significant dependence of the plasma heating results with the nature of the minority ions. At higher power, some difference in repartition of power between electrons and ions was identified. Figs. 6a and b show the time evolution of the total and of the ohmic input power during two "on axis" RF pulses; one with ^{3}He, the other with Hydrogen. The basic parameters of the discharge are given in Table 1. While the magnetic field and the plasma current were different, the peak

plasma density reached during the RF pulse was similar and close to $3 \times 10^{19} m^{-3}$. The larger ohmic power decrease was observed with Hydrogen and is supported by Fig. 7 which shows, for the same two pulses, the time evolution of central ion temperature T_{io} and of the peak, T_{eo}, and volume averaged electron temperatures $\langle T_e \rangle$. Higher $\langle T_e \rangle$ increase and higher sawteeth on T_{eo} are observed with Hydrogen with peak values of 6keV. On the other hand, higher sawteeth on T_i are observed with Helium and electron and ion temperatures are now close to each other, at peak values close to 5keV.

An estimate of the central deposition of ICRF power can be deduced either from the initial rise of the sawteeth or from the temperature modulation resulting from ICRF power modulation (Bhatnagar et al, 1986). Both methods are effective only inside the sawteeth inversion radius. Fig. 8 shows the central electron temperature evolution during an RF pulse of 5.5MW using Helium-3 as minority species (Gill et al, 1986) measured with the high time resolution ECE grating polychromator. The parameters of the discharge are similar to those indicated in Table 1.

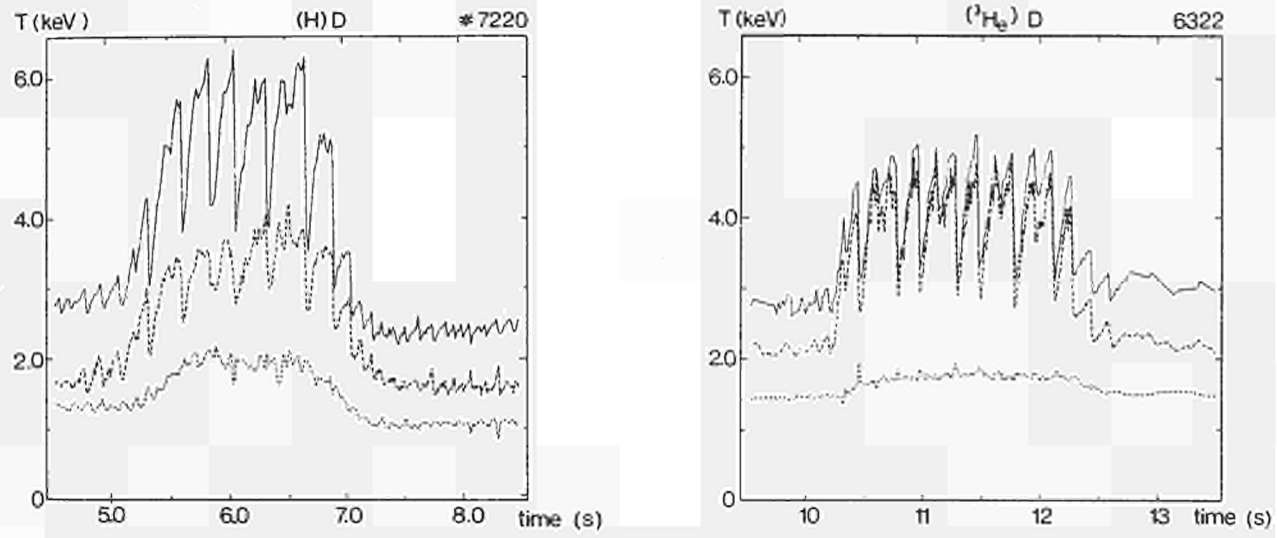

Fig.7 Time evolution of the central and volume averaged electron temperature and central ion temperature for the pulses shown in Fig.6.
a) $(^3He)D$
b) (H)D

TABLE I

Pulse No:	6322	7220
Gas mixture	$(^3He)D$	(H)D
Minority concentration (%)	6	5
Toroidal field (T)	3.0	2.3
Plasma current (MA)	3.5	2.0
q cylindrical	3.0	3.5
Electron density on axis ($10^{19} m^{-3}$)	3.5	3.2

Fig 9 shows the corresponding input power density on axis just after each sawtooth crash for both electrons and deuterons. The deduced values before and after the RF pulse are in agreement with the estimate of the ohmic input power density deduced from magnetic measurements (Taroni et al, 1986). The jump in power input to the deuterons, when the RF is switched on, appears to be larger than the corresponding one to electrons, while the distribution of power between electrons and ions is greater to the electrons in the ratio 1.4:1, when a steady state is reached. The peaking factor of RF power deposition (defined as the ratio of RF power

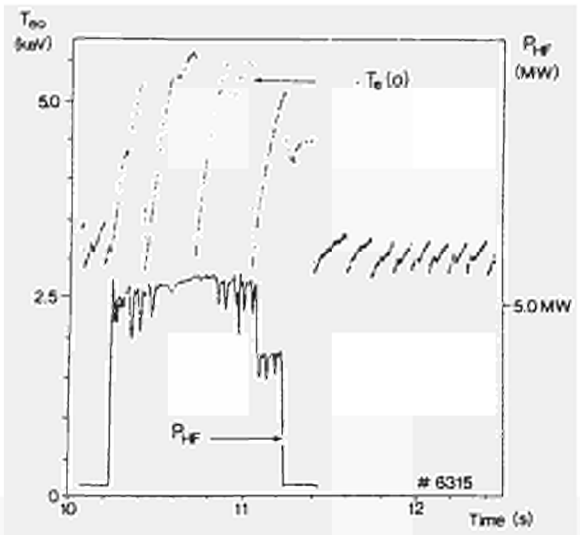

Fig.8 Time evolution of the central electron temperature as measured with the high time resolution ECE Grating polychromator for "on axis" heating with ^3He minority.

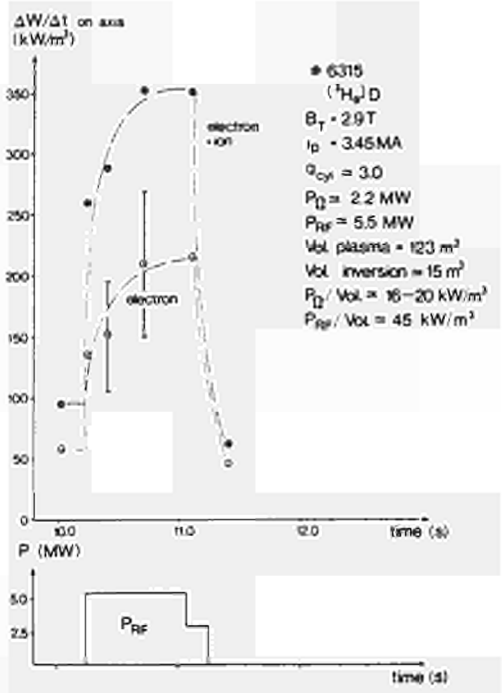

Fig.9 Time evolution of the central input power density deduced from the initial rise of the sawteeth shown in Fig.8 and from Neutron Flux detection.

density on axis to the volume averaged one), ranges from 5 to 8. These values compare favourably with the ohmic case of 3 to 4.

The assumption that the radial profiles of power deposition to the electrons and to the ions are similar leads to the conclusion that around 3MW of the 5.5MW coupled to the plasma are absorbed inside the sawtooth inversion radius. A similar analysis has been performed for the pulse of Fig. 6 with Hydrogen as minority ion. The results are summarised in Table II, together with the calculated values using "ray tracing" techniques and taking into account the redistribution of the minority energy to ions and electrons (Bhatnagar et al, 1986). The comparison between experiments with ^3He and H minorities shows that power deposition is more centrally peaked with ^3He, and that the ratio P_e/P_D of power to the electrons to that

Table II

	^{3}He MINORITY IN D PLASMA	H MINORITY IN D PLASMA
FROM EXPERIMENT	$P_{COUPLED}$ = 5.5 MW	$P_{COUPLED}$ = 5.5 MW
	$P_{ABSORBED}$ = 4.0 MW	$P_{ABSORBED}$ = 4.0 MW
	$\frac{P(\text{INSIDE } R_{INV})}{P_{ABSORBED}}$ = 0.75	$\frac{P(\text{INSIDE } R_{INV})}{P_{ABSORBED}}$ = 0.55
	$\frac{P_{ELECTRONS}}{P_{DEUTERIUM}}$ = 1.4	$\frac{P_{ELECTRONS}}{P_{DEUTERIUM}}$ = 3.8
FROM THEORY	$\frac{P(\text{INSIDE } R_{INV})}{P_{ABSORBED}}$ = 0.78	$\frac{P(\text{INSIDE } R_{INV})}{P_{ABSORBED}}$ = 0.85
	$\frac{P_{ELECTRONS}}{P_{DEUTERIUM}}$ = 1.2	$\frac{P_{ELECTRONS}}{P_{DEUTERIUM}}$ = 4.9

the deuterons is much larger with H minority. The comparison of experimental results with ray tracing models shows that the experimental deposition profile is broader than the theoretical one, especially with H minority but the dependence of P_e/P_D with the minority species is fairly well predicted. Direct RF absorption by the electrons cannot yet be quantified by lack of information on the minority behaviour, especially ^{3}He.

The previous statements are furthermore confirmed by Figs. 10a, b where the central temperature increment of both the electrons (from ECE) and of the ions (from the neutron yield) are plotted versus $P_{RF}/\langle n_e \rangle$ where P_{RF} is the RF power coupled to the plasma and $\langle n_e \rangle$ the volume averaged electron density. The squares refer to (H)D experiments and the crosses to (^{3}He)D. In spite of the dispersion of the data, averaged over 0.2s, a difference between the two schemes seems to emerge when $P_{RF}/\langle n_e \rangle$ is larger than $1.5MW/10^{19}m^{-3}$: the use of Hydrogen minority case produces larger ΔT_{eo} and smaller ΔT_{io} than the use of Helium-3.

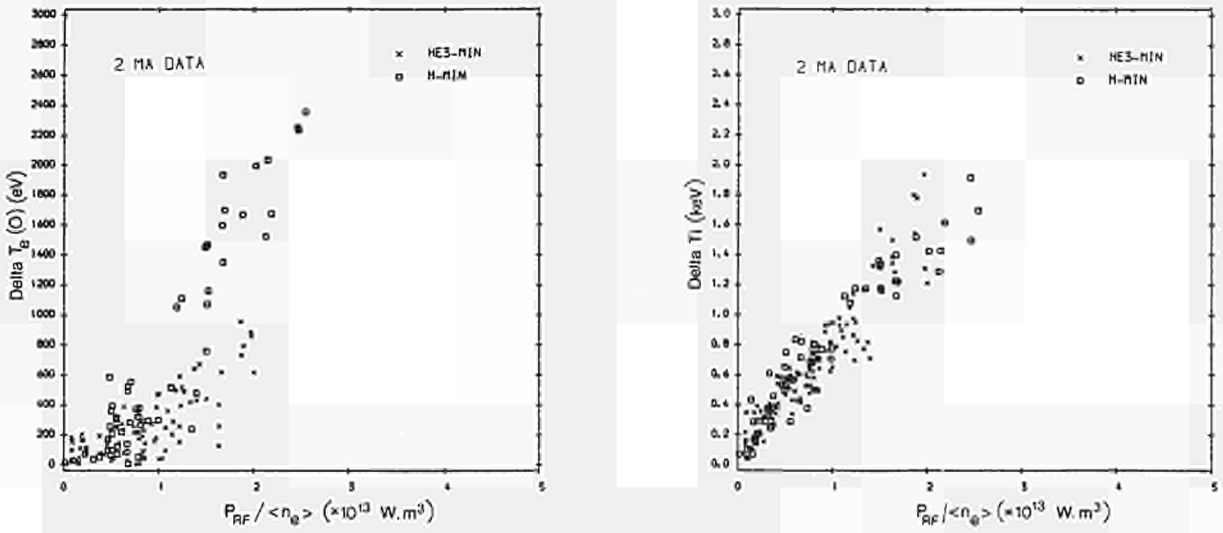

Fig.10 a) Central electron temperature increase
b) Central ion temperature increase versus $P_{RF}/\langle n_e \rangle$ during "on axis" heating at I_p = 2 MA, for ^{3}He(X) and H(□) minority experiments.

III. COMPARISON BETWEEN RADIO FREQUENCY AND NEUTRAL INJECTION HEATING

Degradation of energy confinement with ICRF in JET has already been reported and is well-illustrated by Fig. 11 showing the time trajectory in the plane of energy content versus power losses. During the ohmic phase, the energy increases up to 0.8MJ through the density increase while the power loss is constant and close to 1.8MW. When the RF pulse is switched on, the energy increases by around 1MJ while the losses are now of the order of 6MW. It is interesting to note the similar paths during the ramp up and ramp down of the RF power, which is reminiscent of the steady state pattern shown on Fig 12, where the energy content W of the plasma in steady state is plotted versus the total input power P_t, for two values of current (2 and 4MA), for either neutral injection or ICRF.

The additional power counted in this plot is either the total radiated by the ICRF antenna or the total beam power reaching the plasma, (i.e. shine-through losses are not subtracted). Hydrogen beams with a maximum energy ranging from 60 to 65keV have been used and around 80% of the power is provided by the main energy component. The ^{3}He ICRF resonance was on the plasma axis and the major parameters of the experiment are listed in Table 3. As shown, the general pattern of results is independent of the type of additional power, but slightly better for Neutral Injection, and suggest a dependence between the energy content and the input power of $W = W_o + \tau_{inc} P_t$, where τ_{inc} does not depend significantly on the plasma current at the present power level. It should be noted that the density is not constant over the scan and that part of the difference between NBI and ICRF may be due to higher density and lower radiation losses with NBI. The "incremental" confinement time, τ_{inc}, would identify with an assymptotic value of the global confinement time if the linear trend persisted at higher power levels. In summary, higher confinement times are obtained by increasing the plasma current I_p, but τ_{inc} has shown a limited dependence on both I_p and the type of heating (Thomsen et al, 1986).

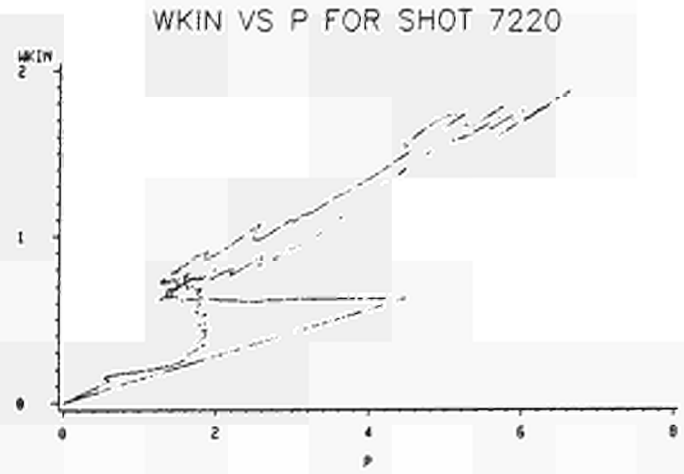

Fig.11 Time trajectory into the plasma W-P (Plasma energy content in MJ versus $P_\Omega + P_{RF}$ - W in MW) of a 2 MA discharge H minority in case of "on axis" heating.

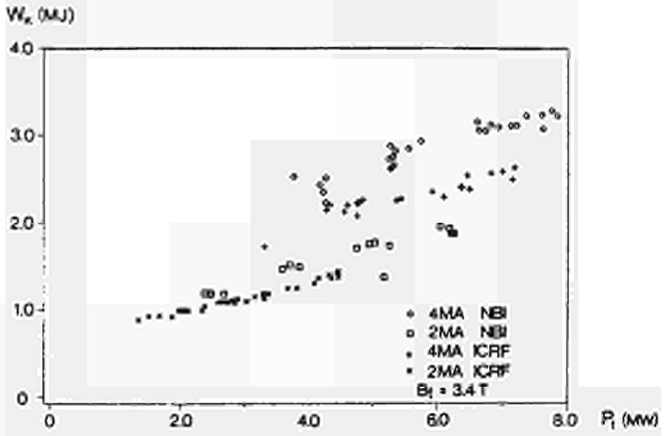

Fig.12 Plasma Energy content versus input power in steady state during Neutral Injection ($H^0 \rightarrow D$) and ICRF ($(^3He)D$, "on axis"). The parameter is the plasma current (B_T = 3.4 T).

TABLE III

	ICRF	NBI
Magnetic Field (T)	3.4	
Minor radius (m)	1.2	
Elongation	1.45	
Line averaged density ($10^{19}m^{-3}$)	1.5 to 3.2	1.5 to 5
$P_{Rad}/(P_\Omega + P_{ad})$	0.4 to 0.8	0.3 to 0.7
Z_{eff}	3 to 4.5	2.5 to 3.5
Ad Heating	$(^3He)D$; on axis	$H^0 \rightarrow D$; 60-65keV

On the other hand, the density limit can be doubled with NBI when compared to ohmic and ICRF results as illustrated by Fig. 13. The black squares represent NBI data in the operating diagram $1/q_{cyl}$ versus $\bar{n}R/B$ while the shadow area covers the ohmic and RF data: the increase in density limit with ICRF does not exceed 15% of the ohmic value. The explanation is likely to be found in one or both of the features of beam heating: most of the new charged particles are created near the plasma axis and the radiated power does not exceed 40% of the input power (Rebut, Hugon, 1984; Schüller et al, 1985; Wesson et al, 1985).

The product $\hat{n}_i.\hat{T}_i.\tau_E$, where n_i and T_i are the central ion density and temperature and the global energy confinement is plotted in Fig. 14 versus the total input power. The data correspond to the experiments shown in Table 3 and Fig. 12. The ion temperature is deduced from the neutral particle analyser measurements. As can be shown, there is no significant increase of $\hat{n}_i.\hat{T}_i.\tau_E$ above the ohmic level in either the ICRF case, Fig. 14a, or in the NBI case, Fig. 14b. On the other hand, and since the identification of $n_i.T_i.\tau_E$ with the ratio of the α particle power to the input power is valid only when the fusion cross-section is proportional to T_i^2, namely above 7keV, the neutron rate is strongly increased with the auxiliary power (Sadler et al, 1986). Fig. 15 shows the dependence of the ratio of thermonuclear power from the DD reaction to the input power P_{DD}/P_t versus the input power for ICRF heating. Initial combined operations of Deuterium neutral beam and ICRF heating on Hydrogen minority have resulted in increasing further P_{DD} by an order of magnitude for a total input power of 13MW, most of the neutrons being produced by beam plasma reactions.

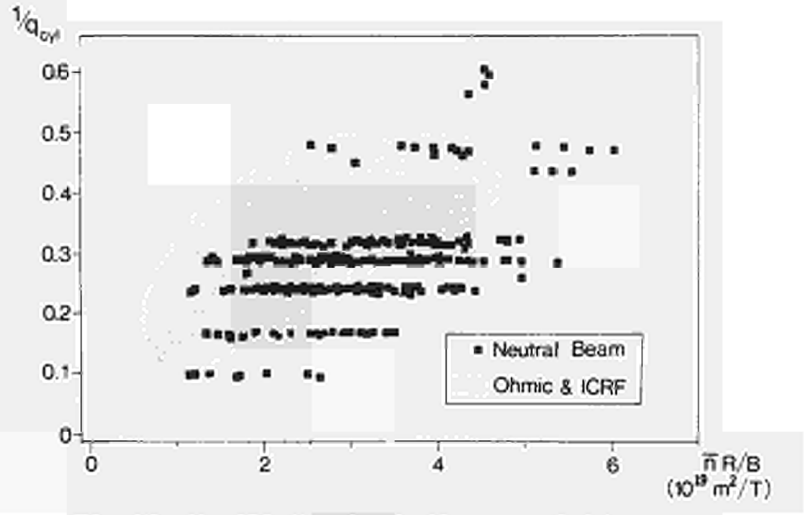

Fig.13 Hugill-Murakami diagram of $1/q_{cyl}$ versus nR/B_T for ohmic and RF heated plasma (shadowed area) and Neutral Injection heated plasma (squares).

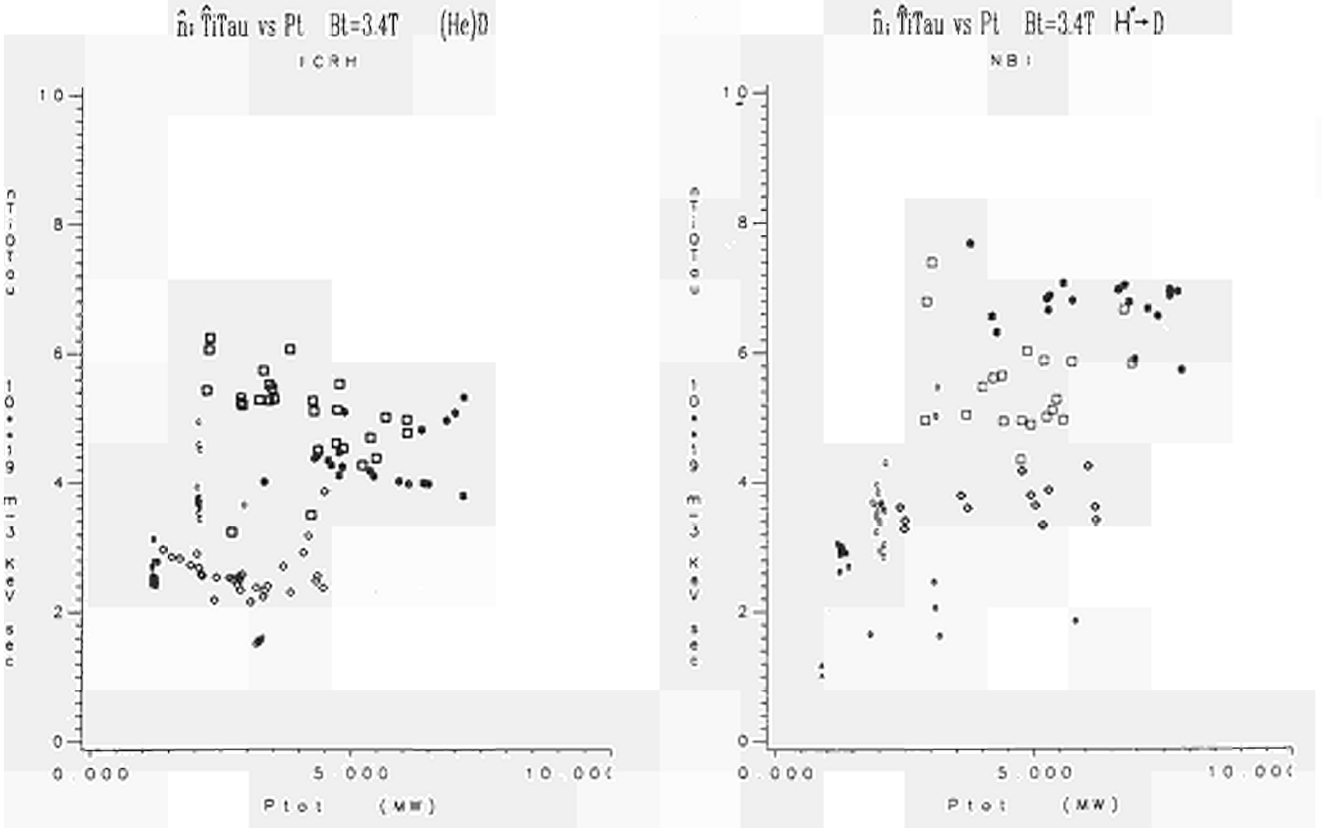

Fig.14 The Fusion Product $\langle \hat{n}_i . \hat{T}_i . \tau_E \rangle$ versus total input power for the data of Fig.12.

a) ICRF (^{3}He)D - on axis
b) NBI H° → D

Symbols

Ip (MA)	1	2	3	4
Ohmic	A	B	C	D
ICRF or NBI	○	◇	□	*

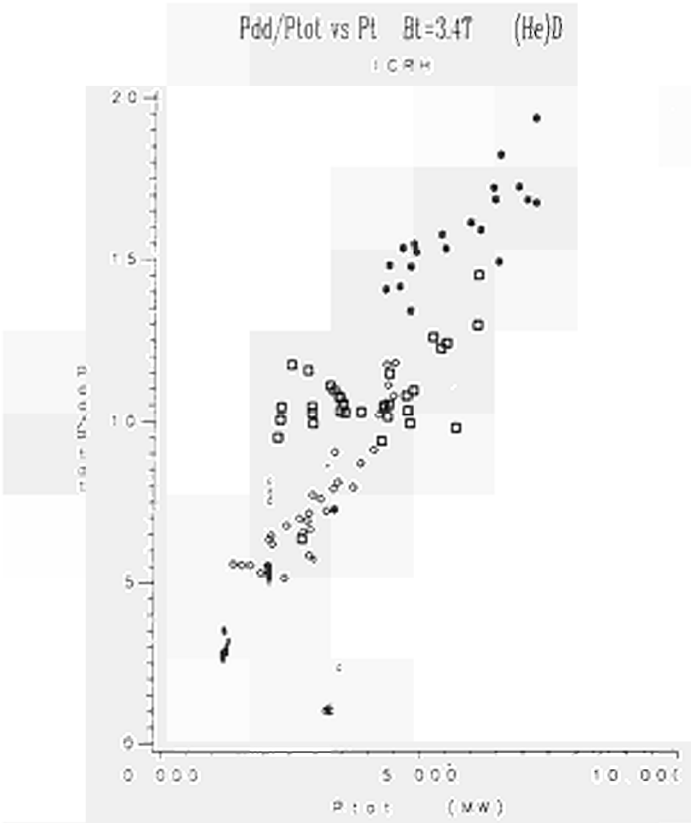

Fig.15 Ratio D-D thermonuclear power/Input power (x 10^{-6}) versus Input power during ICRF heating experiments ($(^3He)D$, "on axis", B_T = 3.4 T. The symbols are as in Fig.14.

IV. SUMMARY OF CONLUSIONS

1) A 5MA discharge has been achieved with a flat top duration exceeding 3s.

2) Neutral Injection heating operations have started, initially with Hydrogen beams and then with Deuterium beams. 7.7MW peak power and 35MJ of energy have been delivered to the plasma.

3) Ion Cyclotron heating operations have been pursued with three antennae. 6MW peak power and 21MJ of energy have been coupled to the plasma.

4) ICRF studies have shown:

   (i) About 70% of the RF power radiated by the antennae is required to acount for the observed initial rate of plasma energy increase.

   (ii) In conditions of "on axis" heating, 40% in (H)D and 55% in (^3He)D of the RF power radiated by the antennae is absorbed inside the volume defined by the sawtooth inversion radius.

   (iii) As expected, the maximum central temperature increases are observed during "on axis" heating experiments. However, the volume averaged electron temperature increase is much smaller and seems less dependent on the position of the cyclotron layer.

5) Preliminary comparative studies between NBI and ICRF have shown:

   (i) In both cases, the global energy confinement time τ_E is observed to decrease with increasing input power. While τ_E is larger at higher current, the rate of

increase of the plasma energy with the additional power seems neither significantly dependent on I_p nor on the heating method.

(ii) While the density limit is increased by only 10% with ICRF, it can be doubled with beam injection when compared to the ohmic limit and nRq/B reaches 20 x $10^{19}m^{-2}/T$.

(iii) In the best conditions so far achieved, the product $\hat{n}_i.\hat{T}_i.\tau_E$ with either NBI or ICRF is not significantly larger than the values with ohmic heating only, i.e. close to 6 x $10^{19}m^{-3}$.keV.s.

(iv) The neutron yield is strongly increased with additional heating and has exceeded $10^{15}s^{-1}$ with 80keV Deuterium beam injection into a Deuterium plasma.

6) Combined NB-ICRF operations have just started and with total power input of 13MW have shown a continuation of the trends presented above. Neutron yield exceeding 2 x $10^{15}s^{-1}$ have been measured.

7) Future experiments in JET will concentrate on achieving an "H mode" with additional heated plasmas in a magnetic separatrix configuration.

V. ACKNOWLEDGMENTS

The authors wish to acknowledge the hard work of technical staff of JET who modified and operated the machine and the heating systems for these experiments.

VI. REFERENCES

Bickerton, RJ and co-workers	Plasma Physics and Contr Fusion, 28, 55.
Bhatnagar, VP and co-workers	13th European Conference on Controlled Fusion and Plasma Heating, Schliersee, FRG, April 1986.
Brinkschulte, H and co-worker	13th European Conference on Controlled Fusion and Plasma Heating, Schliersee, FRG, April 1986.
Cordey, JG and co-workers	13th European Conference on Controlled Fusion and Plasma Heating, Schliersee, FRG, April 1986.
Corti, S and co-workers	13th European Conference on Controlled Fusion and Plasma Heating, Schliersee, FRG, April 1986.
Costley, AE and co-workers	Proc 12th European Conference on Controlled Fusion and Plasma Physics (Budapest 1985) Vol 9F p227.
Duesing, G and co-workers	13th European Conference on Controlled Fusion and Plasma Heating, Schliersee, FRG, April 1986.
Ejima, S and co-workers	27th Meeting of APS (San Diego 1985).
Engelhardt, W and co-workers	13th European Conference on Controlled Fusion and Plasma Heating, Schliersee, FRG, April 1986.
Evrard, M and co-workers	13th European Conference on Controlled Fusion and Plasma Heating, Schliersee, FRG, April 1986.
Gill, RD and co-workers	13th European Conference on Controlled Fusion and Plasma Heating, Schliersee, FRG, April 1986.
Jacquinot, J and co-workers	Plasma Physics and Contr Fusion, 28, 1.
Jarvis, ON and co-workers	Proc 12th European Conference on Controlled Fusion and Plasma Physics (Budapest 1985) Vol 9F p223.
Rebut, PH & Hugon, M	Proc 10th IAEA Conference on Plasma Physics and Controlled Fusion (London 1984) CN-44/AII.1.
Sadler, G and co-workers	13th European Conference on Controlled Fusion and Plasma Heating, Schliersee, FRG, April 1986.
Sand, F and co-workers	13th European Conference on Controlled Fusion and Plasma Heating, Schliersee, FRG, April 1986.
Schüller, FC and co-workers	Proc 12th European Conference on Controlled Fusion and Plasma Physics (Budapest 1985) Vol 9F p539.
Taroni, A and co-workers	13th European Conference on Controlled Fusion and Plasma Heating, Schliersee, FRG, April 1986.
Wesson, J and co-workers	Proc 12th European Conference on Controlled Fusion and Plasma Physics (Budapest 1985) Vol 9F p147.

APPENDIX I

THE JET TEAM

JET Joint Undertaking, Abingdon, Oxon. OX14 3EA, U.K.

A. Ainsworth, H. Altmann, R.J. Anderson, J. Arbez, D. Bartlett, W. Bailey, B. Beaumont[1], K. Behringer, E. Bertolini, P. Bertoldi, C.H. Best, V. Bhatnagar[4], R.J. Bickerton, G. Boissin, F. Bombarda[10], T. Bonicelli, S. Booth, A. Boschi, G. Bosia, M. Botman, G. Bracco[10], H. Brelen, H. Brinkschulte, M.L. Browne, M. Brusati, T. Budd, M. Bures, P. Butcher, H. Buttgereit, D. Cacaut, C. Caldwell-Nichols, D. Campbell, R. Carolan[11], J. Carwardine, G. Celentano, C.D. Challis, A. Cheetham, J. Christiansen, C. Christodoulopoulos, P. Chuilon, R. Claesen, J.P. Coad, M. Cooke, J.G. Cordey, W. Core, S. Corti, A.E. Costley, G. Cottrell, M. Cox[11], J. Dean, E. Deksnis, G.B. Denne, G. Deschamps, K.J. Dietz, J. Dobbing, S.E. Dorling, D.F. Düchs, G. Duesing, P. Duperrex[6], H. Duquenoy, L. de Kock, A. Edwards, J. Ehrenberg[2], W. Engelhardt, S. Erents[11], F. Erhorn, B. Eriksson, M. Evrard[4], H. Falter, N. Foden, M. Forrest[11], C. Froger, K. Fullard, M. Gadeberg[5], A. Galetsas, A. Gallacher, D. Gambier[1], R. Giannella[10], A. Gibson, R.D. Gill, A. Goede, A. Gondhalekar, D. Goodall[11], N.A. Gottardi, C. Gowers, R. Granetz, B. Green, S. Gregoli, F.S. Griph, R. Haange, J.H. Hamnén[3], C.J. Hancock, P. Harbour, N. Hawkes[11], P. Haynes[11], T. Hellsten, J.L. Hemmerich, R. Hemsworth, F. Hendriks, R.F. Herzog, L. Horton, J. How, M. Huart, A. Hubbard, J. Hugill[11], M. Hugon, M. Huguet, B. Ingram, H. Jäckel[2], J. Jacquinot, O.N. Jarvis, E.M. Jones, T.T.C. Jones, P. Jones, E. Källne, J. Källne, A. Kaye, B.E. Keen, M. Keilhacker, G. Kinahan, S. Kissel[2], A. Konstantellos, U. Küphnapfel[2], P. Kupschus, P. Lallia, J.R. Last, L. Lauro-Taroni, K.D. Lawson[11], E. Lazzaro, R.C. Lobel, P. Lomas, N. Lopes-Cardozo[7], M. Lorenz-Gottardi, C. Lowry, G. Magyar, D. Maisonnier, M. Malacarne, V. Marchese, P. Massmann, G. McCracken[11], P. McCullen, M.J. Mead, P. Meriguet, V. Merlo, S. Mills, P. Millward, A. Moissonnier, P.L. Mondino, D. Moreau[1], P. Morgan, R. Müller[2], G. Murphy, M.F. Nave, L. Nickesson, P. Nielsen, P. Noll, S. Nowak, W. Obert, B. Oliver, M. Olsson, J. O'Rourke, M.G. Pacco, J. Paillere, L. Pannacione, S. Papastergiou, J. Partridge[11], D. Pasini, N. Peacock[11], M. Pescatore, J. Plancoulaine, J-P. Poffé, R. Prentice, T. Raimondi, C. Raymond, P.H. Rebut, J. Removille, W. Riediker, R. Roberts, D. Robinson[11], A. Rolfe, R.T. Ross, G. Sadler, J. Saffert, N. Salmon, F. Sand, A. Santagiustina, R. Saunders, H. Schamel[12], M. Schmid, F.C. Schüller, K. Selin, R. Shaw, D. Sigournay, R. Simonini, P. Smeulders, J. Snipes[11], L. Sonnerup, K. Sonnenberg, A. Stäbler[2], M. Stamp, C.A. Steed, D. Stork, P.E. Stott, T.E. Stringer, D. Summers, H. Summers[13], J. Tagle[9], G. Tallents[14], A. Tanga, A. Taroni, A. Terrington, A. Tesini, P.R. Thomas E. Thompson, K. Thomsen[5], F. Tibone, R. Tivey, T. Todd[11], G. Tonetti[6], P. Trevalion, M. Tschudin, S. Tsuji[15], B. Tubbing[7], P. Twynam, E. Usselmann, H. van der Beken, M. von Hellermann, J.E. van Montfoort, J. von Seggern[8], T. Wade, C. Walker, B.A. Wallander, M. Walravens, K. Walter, M.L. Watkins, M. Watson, D. Webberley, A. Weller[2], J. Wesson, J. Wilks, T. Winkel, C. Woodward, M. Wykes, D. Young, L. Zannelli, J. Zwart

PERMANENT ADDRESS

[1] Commissiariat A L'Energie Atomique, F-92260 Fontenay-Aux-Roses, France.
[2] Max Planck Instituut Für Plasmaphysik, D-8046 Garching bei Munchen, F.R.G.
[3] Swedish Energy Research Commission, S-10072 Stockholm, Sweden.
[4] EUR-EB Association, LPP-ERM/KMS, B-1040 Brussels, Belgium.
[5] Risó National Laboratory, DK-4000 Roskilde, Denmark.
[6] CRPP/EPFL, 21 Avenue des Bains, CH-1007 Lausanne, Switzerland.
[7] FOM Instituut voor Plasmafysica, 3430 Be Nieuwegein, The Netherlands.
[8] Kernforschungsanlage Jülich GmbH, D-5170 Jülich, F.R.G.
[9] Junta de Energia Nuclear, Avda. Complutense, Madrid 3, Spain.
[10] ENEA-CENTRO Di Frascati, I-00044 Frascati, Roma, Italy.
[11] Culham Laboratory, Abingdon, Oxfordshire, U.K.
[12] Ruhr-Universitaat Bochum, D-4630 Bochum, F.R.G.
[13] University of Strathclyde, 107 Rottenrow, Glasgow, G4 ONG.
[14] The Australian National University, Research School of Physical Sciences, Canberra ACT 2600, Australia.
[15] Japan Atomic Energy Research Institute, Naka-machi, Naka-gun, Ibaraki-ken, Japan.

Invited Paper at 13th European Conference on
Controlled Fusion and Plasma Heating, Schliersee, FRG, April 1986

Impurity Behaviour in JET

W. W. Engelhardt

I INTRODUCTION

It is one of the main objectives of JET to control impurities at conditions approaching the reactor regime. Investigation of the impurity behaviour is therefore a major task in the JET programme. There are two main reasons why impurity concentrations must be kept sufficiently low close to ignition conditions:

1) Impurities dilute the reacting hydrogen plasma reducing thereby the available fusion power. If the electron density is limited, the fusion power density is reduced by a factor $(1-\alpha Z)^2$, where α is the relative concentration of an impurity with charge number Z. If a β-limit cannot be exceeded, the reduction is $(1-\alpha Z)^2/(1-\alpha(Z-1)/2)^2$. An impurity level of 5% carbon would decrease the fusion power by a factor of 2 or 1.6, respectively.

2) Highly charged impurity ions increase the radiation losses by emission of bremsstrahlung, recombination and line radiation. If the radiation losses are enhanced over hydrogen bremsstrahlung by a factor of 35, ignition is impossible. Heavy impurities of the order of 1% would already make up for this factor.

Impurities can be released from limiters and wall by the impinging ion flux. They leave the surface in the neutral state, penetrate into the plasma and become ionized within an ionisation length λ_I. If the impurity ions obey a diffusion law, a gradient of ions builds up and in steady state the charged and the neutral flux must be the same:

$$D \frac{\partial n_I}{\partial r} = \Gamma_I$$

where D is the diffusion coefficient and Γ_I is the influx of neutral particles. The gradient may be replaced by an increment Δn_I divided by the ionization length /1/. Adding the boundary value to the increment the impurity concentration in the plasma is approximately /2,3/

$$n_I = \frac{\Gamma_I(\lambda_I + \lambda_{SOL})}{D}$$

λ_{SOL} is the thickness of the scrape-off layer in the limiter shadow where ions flowing parallel to the magnetic field are intercepted by the limiter. This consideration can also

* For definition, see Appendix I of P P Lallia (1986) Proceedings of the 13th E.P.S Conference on Controlled Fusion and Plasma Heating (Schliersee, F.R.G, April 1986).

be applied to hydrogen and if the same transport law applies, the relative concentration does not depend on the diffusion coefficient:

$$\frac{n_I}{n_H} = \gamma \frac{\lambda_I + \lambda_{SOL}}{\lambda_H + \lambda_{SOL}}$$

γ is the ratio of impurity to hydrogen flux and λ_H the ionization length of hydrogen. The above formula is obtained under the assumption that the impurities are mainly released at the limiter and the ionisation length is short compared to the plasma radius so that a plane geometry can be applied. In this case it follows immediately that no difference in impurity concentrations is expected for big and small tokamaks, provided the conditions at the plasma edge are about the same. The release rate γ depends on the surface conditions, on the energy of the impinging particles and on the release processes involved. In the simplest case it is just a sputtering coefficient. In many cases $\lambda_I < \lambda_{SOL}$ and $\lambda_H > \lambda_{SOL}$ so that the concentrations are smaller than the release rate coefficient γ .

On JET γ is measured by comparing line intensities emitted by low ionization stages of various impurities with hydrogen lines at different locations like limiters, wall, antennae /4/. An atomic model is required to relate the line emission rate to the ionization rate /5/. The ratio of these rates is dependent on the electron temperature, which must be measured in the region where the lines are emitted /6/.

Langmuir probes are used to give this information in the scrape-off layer /7/. They measure also the electron density, which enters into the ionization length and the thickness of the scrape-off layer λ_{SOL}. The surface conditions both at the wall and at the limiters are monitored by samples of various materials, which are analysed along with the limiter tiles after major openings of the vessel /8/.

When impurities diffuse from the edge into the interior of the plasma, they are distributed according to the prevailing transport law. This leads in most cases to a moderately peaked density profile, but accumulation processes in the plasma centre can occur. The distribution among different ionisation stages is governed by the 'corona equilibrium' in large tokamaks, significant deviations, however, occur in the outer zones. The usual spectroscopic methods ranging from the visible to the soft X-rays are applied on JET to measure the concentrations of impurity ions and their spatial distribution. Global quantities like total radiation losses and the effective ion charge Z_{eff} are determined by bolometer arrays and by monitoring the visible bremsstrahlung at 523.5 nm respectively.

In order to obtain a consistent picture, these measurements must be accompanied by numerical impurity transport simulations /9,5/. It is assumed that a simple transport law applies for all fluxes:

$$\Gamma = -D\frac{\partial n}{\partial r} - v_o \frac{r}{a} n$$

v_o is chosen to be 2D/a. The code allows to predict measured line intensities, Z_{eff}, total radiation, if the profiles of electron density and temperature are known. Comparisons are made both with line integrated and with local measurements obtained from Abel inversion.

In the following an overview of the main results obtained on JET is presented. Sect. II deals with the measures to control the impurity contamination and the resulting wall and limiter conditions. The impurity situation during ohmic discharges is reviewed in Sect. III and the main effects resulting from auxiliary heating are given in Sect. IV.

II WALL AND LIMITER CONDITIONS

JET has an inconel vessel which is armoured with carbon tiles at the inboard wall. Eight carbon limiters of .4x.8 m^2 each protruding in the midplane from the outboard wall take the conducted power losses. Three antennae with either chromium of nickel screens and protected by carbon tile picture frames are located a few centimeters outside the limiter radius.

The vessel is baked to 300°C also during tokamak operation. During many hours of glow discharges volatile surface contaminations are removed. In some instances the glow discharges were seeded with methane in order to cover all metallic surfaces seen by the plasma with a layer of 10-100 nm of carbon /10/. In addition it is hoped that carbon oxide formation helps to reduce the oxygen contamination.

Analysis of limiter tiles after longer periods of operation showed that the surface is covered with metals, mainly nickel and chromium. The central area of the limiter where the plasma-wall interaction is strongest according to infrared photographs has typically a surface concentration of 10^{21} m^{-2}. Towards the limiter edge the concentration is increasing by at least an order of magnitude. This observation suggests that the limiters have been covered by metals, probably during violent plasma-wall interactions (disruptions) /8/. Subsequently, the plasma has eroded the metals in the centre and deposited the material at the edge. In cases where the initial coverage was thin (see Sect.IV), a cleaning effect after some discharges was indeed observed. If, however, the contamination is very strong and the metals are sitting on the limiter in the form of droplets, a metal free surface cannot be reached. In this case carbonisation helps to cover the metals for a while until the carbon layer is eroded again. Depending on the thickness of the layer the carbon erosion takes place within 20-200 discharges.

III OHMIC DISCHARGES

In the following the main results on impurity measurements will be discussed for ohmic discharges. The important aspects of impurity behaviour will be established as a reference point to be compared with in cases where auxiliary heating is applied.

1) Boundary Layer:

By introducing an array of Langmuir probes through a vertical port up to a distance of 3 cm from the last closed magnetic surface the profile of electron density and temperature in the

limiter shadow is measured. For a typical ohmic discharge with B_T = 3 T, I_p = 3 MA and $\bar{n}_e$ = $2 \cdot 10^{19}$ m^{-3} the e-folding length of the density is about 4 cm and that of the temperature profile is about 6 cm. Extrapolation to the limiter edge yields T_e ~ 50-100 eV and n_e ~ $2\text{-}3 \cdot 10^{18}$ m^{-3}. Due to the compression of the flux surfaces towards the midplane the e-folding lengths at the limiter are about a factor of 3 shorter. This is confirmed by measurements with Langmuir probes located in the graphite protection of the RF-antennae /11/ and also by unfolding the power loading on the limiter as measured in the near infrared. There is a tendency that the e-folding length of the electron density and the edge temperature decrease with increasing plasma density.

The spatial decay of the scrape-off plasma parameters is in accordance with similar observations on many other tokamaks. It is commonly explained by the balance between fast parallel and slow anomalous cross-field transport. Due to the widening of the flux surfaces the scrape-off thickness in JET varies and it is difficult to derive a diffusion coefficient as the correct averaging is not known. Taking a thermal speed $V_T = 10^5$ m/s for the parallel transport, a connection length of L = 50 m and an anomalous diffusion coefficient of D = 1 m^2/s (see below), an e-folding length of $\lambda_{SOL} = \sqrt{DL/V_T}$ = 2.2 cm is calculated. This appears to be a fair average between the thicknesses measured at the top and at the midplane of the torus. Under these conditions the ionization lengths of impurities are practically always shorter than the scrape-off thickness.

2) Impurity Fluxes:

Flux measurements by visible spectroscopy have been made at various locations, in particular at the limiters /5/. It is found that both the hydrogen flux and the flux of light impurities (C, O) increase with plasma density, the increase of oxygen flux being stronger (Fig.1) /6/. The ratio $\gamma = \bar{\Gamma}_I / \bar{\Gamma}_H$ stays therefore approximately constant, but at low density carbon is dominant and at high density oxygen is taking over. For carbon we find typically γ_C ~ ·1 at medium density, a value which is nearly independent of the vessel conditions. For oxygen there is a much broader range γ_O ~ ·01 ÷ ·05 depending, not surprisingly, on the vessel status. After an opening the oxygen flux decreases in the course of operation, provided there are no leaks.

The metal fluxes are substantial when the limiters are covered with metals as reported in Section II. They are, however, strongly decreasing with plasma density (Fig.1) and they vary appreciably depending on the metal deposits (γ_M ~ 0 ÷ ·02) /4/.

The fluxes as measured at the limiter can account for the observed concentrations in the plasma, the wall fluxes do not contribute significantly. An exception is oxygen, where both the limiter and the wall fluxes cannot make up for the oxygen concentration observed in the bulk plasma. We must assume that some unidentified sources from portions of the wall, which are not in the field of view, contribute to the total flux. This is supported by the fact that often a steady increase of the limiter flux is observed during a discharge, suggesting a recycling of the wall contribution at the limiter.

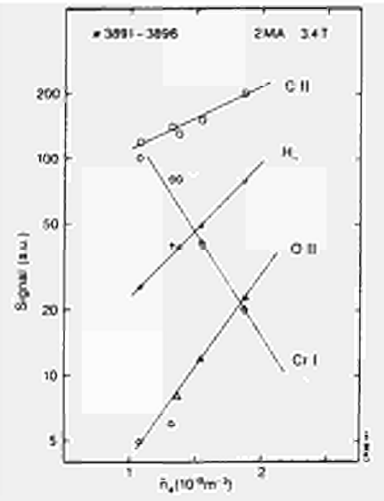

Fig.1 Dependence of line emission from various low ionization stages on electron density. The line emission is representative for the influx of the particle species /5/.

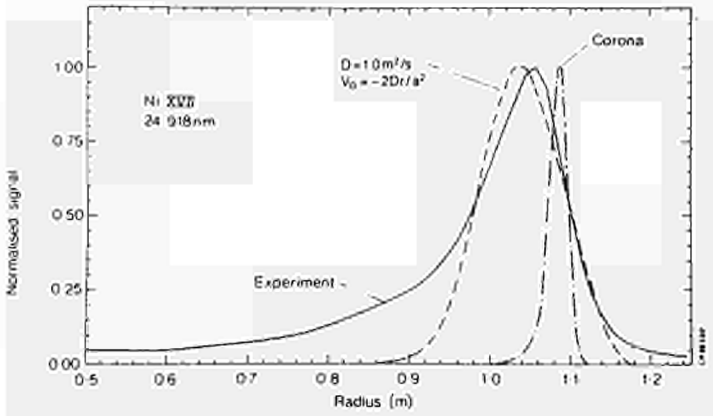

Fig.2 Emission profile of Ni XVII as a function of major radius. Solid line: measurement, broken lines: transport simulation and "corona" prediction.

The results of the flux measurements can be used to draw conclusions on the release mechanisms. For metals we consider sputtering (including impurity and self-sputtering) as the most likely process. This is concluded from the measured release rate, the surface coverage and the relevant sputtering coefficients at the measured plasma edge temperature. The decrease with increasing plasma density is explained by the accompanying reduced edge temperature which leads to a strong reduction of the sputtering yield /6/. In cases where the limiter surface reached very high temperatures (~ 1500°C) at the end of a discharge, the metal influx was enhanced by up to a factor of 30 due to evaporation. The metal concentration in the bulk plasma, however, did not increase at all /6/. This is explained by the very short ionization length expected for particles with practically room temperature. They are immediately diffusing back to the limiter surface in accordance with our picture of the penetration process as discussed in the Introduction. On the other hand,

this observation rules out evaporation as a normal release process. The particles must have a few electron volts to penetrate appreciably into the plasma. This energy can only be provided by sputtering processes.

The release of carbon is less clear. The measured release rate of 10% is typical for chemical sputtering, but the expected dependence on the surface temperature of the limiter is not observed. Furthermore, chemical processes would lead to very low particle energies and a similar penetration behaviour, as observed in the case of metal evaporation, would be expected. On the other hand, physical sputtering processes can explain the measured release rates within the error bars, if sputtering by oxygen and self-sputtering are taken into account. They are in basic agreement with the observed dependence on the edge temperature. From these considerations we tend to believe that chemical sputtering is not a major release mechanism /6/. More detailed studies, however, will be necessary to clarify this point.

The release of oxygen is even more obscure, as already indicated. The lacking knowledge of all sources makes it difficult to arrive at a conclusion. Oxygen appears to originate mainly from the vessel walls and to recycle at the limiters /6/.

3) Transport Properties:

Profiles of line emission from nickel have been obtained by scanning the plasma cross-section with rotating mirrors. Fig.2 shows an example, together with a transport simulation and the 'corona' prediction. The observed profile is clearly transport dominated with a diffusion coefficient of $D \sim 1\ m^2/s$. In some instances a small amount of nickel fell into the plasma, leading to a rise of line emission with a subsequent decay. Such events have also been simulated with the transport code using the same diffusion coefficient. The very good agreement of the calculated time evolution of the line emission with the measured one confirms independently the magnitude of the anomalous diffusion coefficient. This measurement is in fact more precise than the comparison of profiles: The emission shell width depends on $\sqrt{D}$, whereas the characteristic decay time depends on D^{-1}.

For the interpretation of line intensities in terms of concentrations it is necessary to know the radial position, the width and the relative maximum of the relevant ionisation stage density. These data are obtained from the code simulations using the measured diffusion coefficient. In the calculations an inward velocity of $v_o = -2Dr/a^2$ was assumed which leads to a moderate peaking of the total impurity density profile and a nearly constant relative impurity concentration. Since we find the same concentrations using line emission from ionisation shells at different radii, strong accumulation of impurities must be excluded /12/. This result is, however, not very precise. Within the experimental error the inward velocity could also be zero, the derived diffusion coefficient would then be $\cdot 7\ m^2/s$.

4) Impurity Concentrations:

The measured impurity concentrations follow roughly the behaviour of the fluxes to which

they are proportional. Light impurities are therefore fairly constant with respect to density changes, whereas metals vary quite strongly. The following trends can be observed: carbon is almost independent of the vessel status, but has a tendency to increase with plasma current and to decrease at higher electron density. Oxygen depends on the vessel status (major openings, leaks) and increases somewhat with electron density. Low density discharges contain therefore more carbon than oxygen and the trend is reversed for high density discharges. Metals depend very much on the limiter conditions. They are abundant when the limiter has been contaminated with metals and they nearly disappear when the limiter tiles are clean or covered by carbonisation with a fresh carbon layer. In addition they decrease strongly with increasing electron density, but increase somewhat with plasma current. Typical concentrations are 2-4% carbon, 1-2% oxygen and 0.001-0.3% metals giving Z_{eff} values ranging between 2 and 5 and a dilution fraction n_H/n_e between ·6 and ·8. The best values are obtained at the highest achievable electron density /12/.

These results are in broad agreement with the Z_{eff} measurements based on the emission of visible bremsstrahlung. Z_{eff} decreases with increasing electron density because of the reduction of metals and carbon. At high density, however, a minimum value of $Z_{eff} \sim 2$ is reached independent of density. It is mainly oxygen which prevents a further reduction of Z_{eff}.

It may be appropriate in this context to comment on the effect of carbonisation /13,10/. It has already been mentioned in Section II that excessive metal contamination of the limiters is irreversible, but can be covered by carbonisation. In addition, we have observed a gradual decrease of oxygen, which does not manifest itself immediately after a fresh carbonisation, but seems to be a long term effect. It is worth mentioning that carbonisation does not cause an enhanced carbon concentration. The main disadvantage of the method is that it does not lead to stationary conditions. After carbonisation it is difficult for the first discharges to control the hydrogen density as a large amount of hydrogen has been co-deposited with the carbon and is slowly released. The metals, which indeed disappear immediately, come gradually back when the carbon layer is eroded. Only very thick layers provide a metal free plasma for the order of 100 discharges. On the other hand, metals are no problem at high electron density as they strongly decrease with density anyway. The situation may be different when metals are excessively released during ion cyclotron heating. In this case carbonisation may be useful to prevent strong radiation losses.

5) Radiation Losses:

The total radiation losses in JET vary between 30% and 80% of the ohmic input power. The higher values occur at high density and reach sometimes even 100% or more when the density limit is approached. The metal contributions to this radiation is never more than 20%. The profiles are generally hollow, the central input exceeding the radiative losses by a factor of 5-10. Only at very low densities with relatively high metal concentrations central radiation losses become significant. Over two thirds of the minor radius the power losses are usually transport dominated.

TABLE I

Main impurity concentrations determined from spectroscopic measurements. Z_{eff}^{calc} is calculated on the basis of these measurements, Z_{eff}^{meas} is obtained from absolute bremsstrahlung measurements. P_{rad}^{meas} is determined by bolometry, P_{rad}^{calc} is predicted by the impurity transport simulation code using the measured concentrations.

	discharge # 7145 neutral injection I_p=4 MA, B_t=3.4 T		discharge # 5486 radio frequency heating I_p=4 MA, B_t=3.4 T	
	before heating	during heating	before heating	during heating
Auxiliary power	-	5.2 MW	-	3.9 MW
Ohmic power	3.2 MW	2.5 MW	3.7 MW	3.5 MW
$n_e(0)$	$3.2 \cdot 10^{19}$ m^{-3}	$6.0 \cdot 10^{19}$ m^{-3}	$3.0 \cdot 10^{19}$ m^{-3}	$4.1 \cdot 10^{19}$ m^{-3}
Impurity concentrations(%)				
C	2.5	1.0	3.1	3.9
O	2.0	1.9	0.7	0.9
Ni	0.006	0.001	0.08	0.09
Z_{eff}^{calc}	3.1	2.5	3.1	3.6
Z_{eff}^{meas}	3.3	2.7	3.4	3.0
P_{rad}^{calc}	1.0 MW	3.9 MW	1.5 MW	4.1 MW
P_{rad}^{meas}	1.2 MW	3.5 MW	1.7 MW	4.1 MW

IV DISCHARGES WITH AUXILIARY HEATING

When the plasma is heated by either radio frequency or neutral beam injection, the limiter fluxes of all particles increase proportional to the applied power (Fig.3). As a result both the hydrogen and the impurity densities increase, but Z_{eff} remains approximately constant. The total radiation is enhanced, but its ratio to the input power is generally not exceeding the ohmic value /13/. These global results are summarized in Fig.4. A detailed analysis of the impurity concentrations obtained from line intensity measurements has been performed for individual discharges. The results are in reasonable agreement both with the measured Z_{eff} values and with the radiation losses within the expected uncertainties. Two examples selected for comparable discharge parameters are given in Table I.

Although there is quite a scatter of data in Fig.3, a tendency is observed that Z_{eff} and the relative radiation losses are somewhat lower during neutral injection. The reason for this behaviour is mainly additional fuelling by the hydrogen beams. The electron density increases more strongly than in RF-discharges so that the relative importance of impurities becomes less.

In addition to these general features radio-frequency discharges show a peculiar behaviour of the metal impurities /14/. When the power is switched on, a strong influx of the screen

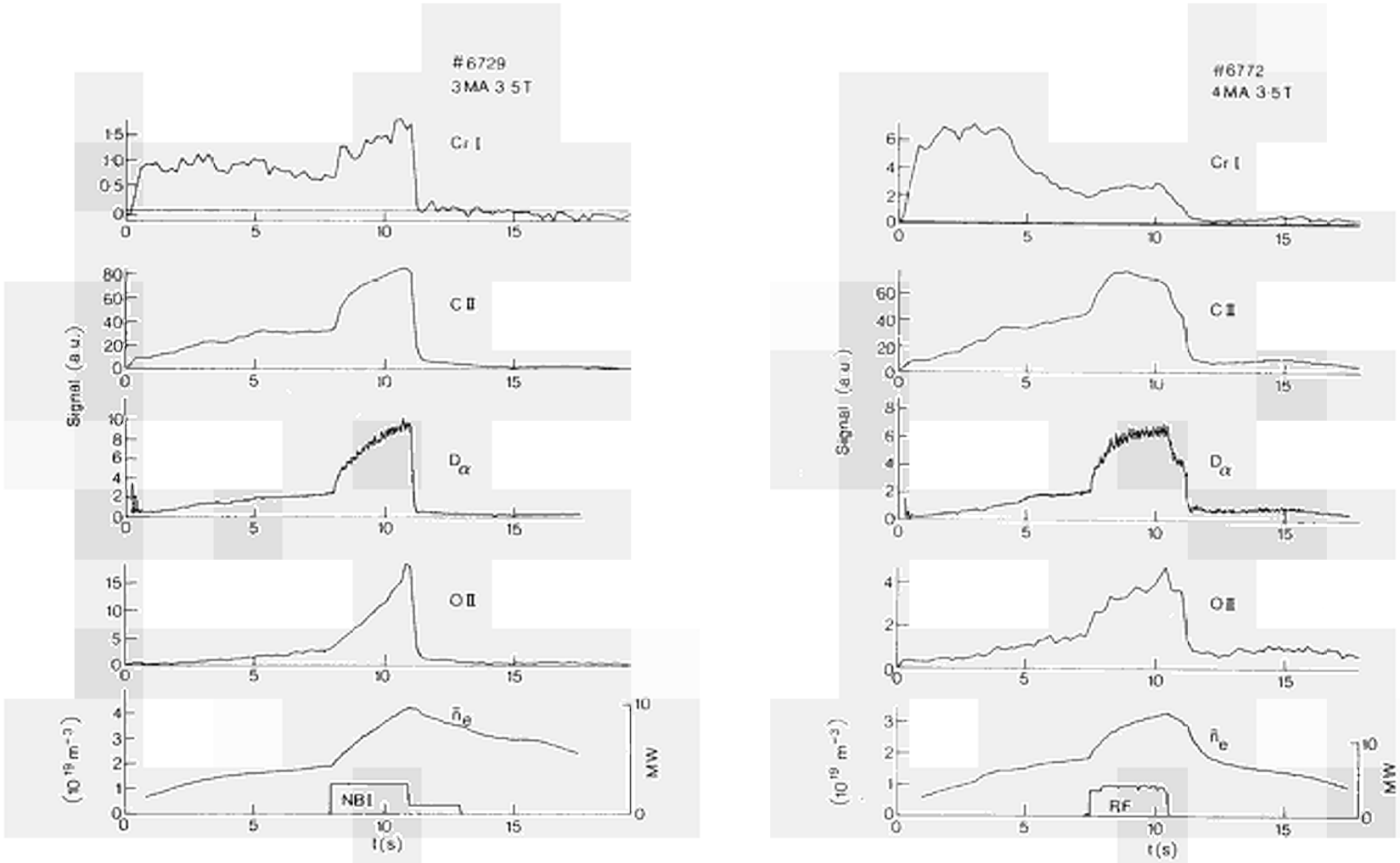

Fig. 3 Increase of emission lines from various low ionization stages when auxiliary heating is switched in.
a(neutral Injection b) Radiofrequency

P\86\25

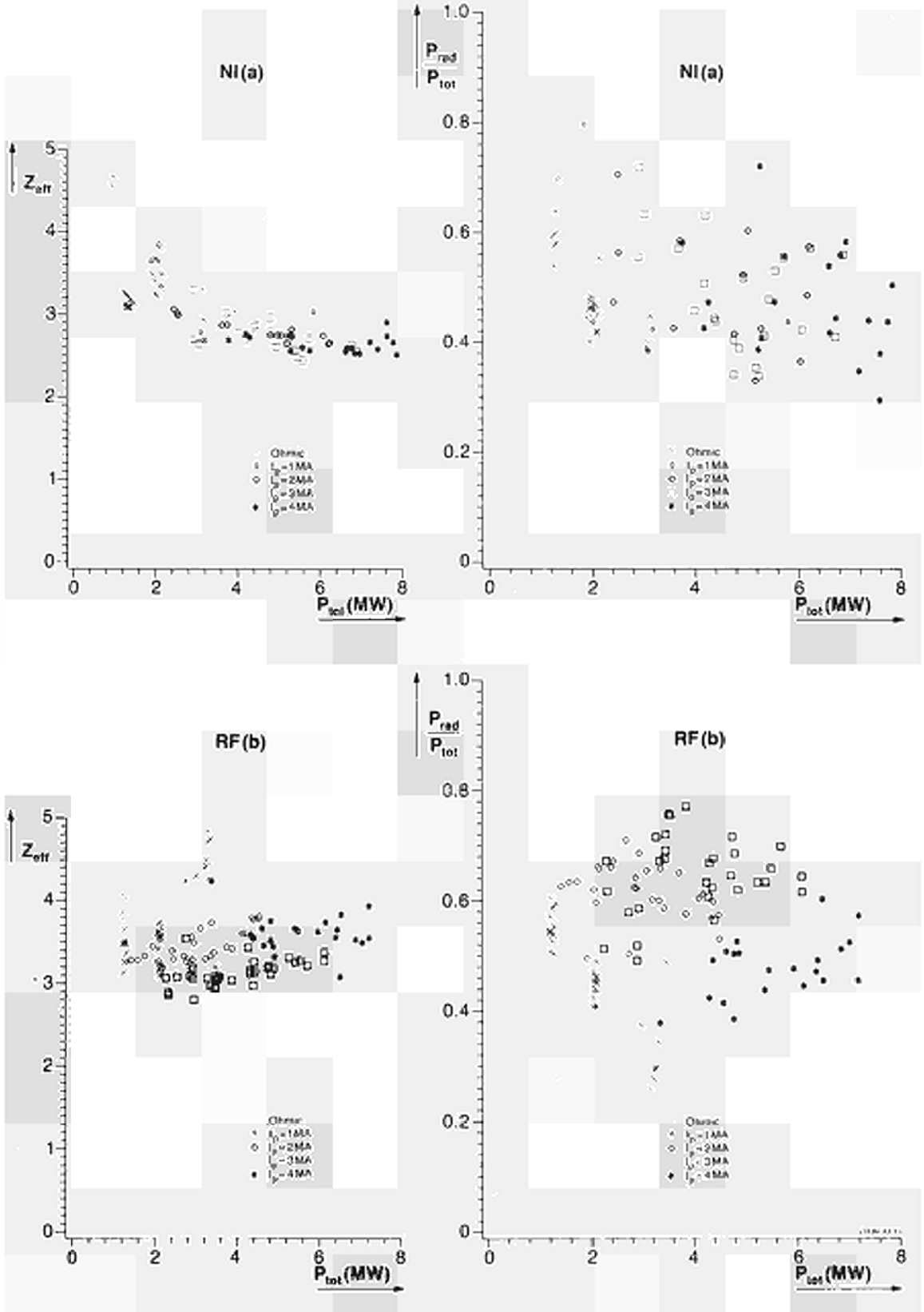

Fig. 4 Variation of Z_{eff} and relative power with total heating power.
a) neutral inection b) radiofrequency heating.

P86125

material is observed at the antennae and the corresponding metal impurity increases in the plasma depending on whether a chromium or a nickel coated antenna is activated. Furthermore the metal flux at the limiter builds up to a saturated level within a few discharges. Subsequent ohmic discharges erode the limiters again and the metal impurities are being reduced. The mechanism of this metal release at the antenna screens is not clear. It seems, however, that a broadening of the boundary layer, which is simultaneously observed by probe measurements, leads to a stronger plasma-screen interaction. It should be noted, however, that also in RF-discharges the relative contribution of the metal radiation to the total radiation is not more than 20% /14/. The radiation profiles remain hollow and the bulk plasma is still transport dominated. In this respect JET seems to be different from other tokamaks, which frequently suffer from excessive metal contamination when ion cyclotron heating is applied. The reason is probably the relative size of the plasma in comparison to the antennae which leads to a focussing of the waves and a centrally peaked power deposition.

V CONCLUSIONS

The impurity concentrations in JET are not significantly different from smaller ungettered tokamaks with carbon limiters. Strong metal contaminations can be avoided when the limiters are kept free of metals by preventing violent plasma wall interactions during disruptions. Minor, more homogeneous metal coatings are eroded by the plasma.

The anomalous diffusion coefficient (D-1 m^2/s) is similar as in small tokamaks, a somewhat surprising result in view of the enormous differences in plasma current or gradients of temperature and density. Catastrophic impurity accumulation does not occur.

The boundary layer can be described with the usual simple model balancing parallel and anomalous perpendicular transport.

The relative radiation losses are in a similar range as in smaller tokamaks, the bulk plasma is transport dominated.

During auxiliary heating the particle influxes from the limiters increase substantially, but Z_{eff} and the relative radiation losses compared to the input power remain approximately constant.

Ion cyclotron heating broadens the boundary layer and leads to a metal release from the antennae screens. The metals build up on the limiters, but they are eroded again by ohmic discharges. The metal concentrations in the plasma remain nevertheless low and cause not more than 20% of the radiation losses.

Neutral beam injection fuels the plasma with additional hydrogen. The discharges are therefore somewhat cleaner and have a very low metal concentration.

With the present impurity concentrations in JET no severe problems with respect to radiation losses are expected when approaching thermo-nuclear conditions. The present dilution would reduce the α-power by a factor of about 2. Higher electron densities which must be achieved in future could reduce impurities further.

ACKNOWLEDGEMENTS

Special acknowledgement is made to the JET Spectroscopy and Impurity Physics Group led by K Behringer, who contributed most of the interpretation in this paper. Important contributions from the Plasma Boundary Group, led by L de Kock, are also greatly appreciated. It is a pleasure to thank particularly H Brinkschulte, B Denne, J Ehrenberg, S K Erents, M Forrest, P Morgan, R Müller, H Jäckel, M Stamp, D Summers, H Summers, J A Tagle and K Thomsen for providing the actual data used in this work.

REFERENCES

/1/ W Engelhardt, W Feneberg, J. Nucl. Mater. 76 & 77 (1978) 518

/2/ W Engelhardt, G Becker, K Behringer et al., J. Nucl. Mater. 111 & 112 (1982) 337

/3/ K Lackner, D E Post, Proc. of the NATO Summer School, Val Morin, Canada, 1984

/4/ M F Stamp, K H Behringer, M J Forrest et al., Proceedings of the 12th European Conference on Contr. Fusion and Plasma Physics, p.539, Budapest 1985

/5/ K H Behringer, 6th Topical Conference on High Temperature Plasma Diagnostics (APS), Hilton Head Island, S.C. USA 1986

/6/ K H Behringer, 7th Int. Conf. on Plasma-Surface Interactions in Contr. Fusion Devices, Princeton, USA 1986

/7/ S K Erents, J A Tagle, G M McCracken, et al., submitted to Nuclear Fusion

/8/ R Behrisch, J Ehrenberg, H Bergsåker et al., 7th Int. Conf. on Plasma-Surface Interactions in Contr. Fusion Devices, Princeton, USA 1986

/9/ K Lackner, K Behringer, W Engelhardt, W Wunderlich, Z Naturforsch 37a (1982) 931

/10/ J P Coad, K H Behringer, K J Dietz et al., 7th Int. Conf. on Plasma-Surface Interactions in Contr. Fusion Devices, Princeton, USA 1986

/11/ H Brinkschulte, J A Tagle, S K Erents et al., this conference

/12/ K Behringer, P G Carolan, B Denne et al., Nucl. Fusion 26 (1986) in print

/13/ B Denne, K H Behringer, W Engelhardt et al., Proceedings of the 12th European Conference on Controlled Fusion and Plasma Phys. I, p.379, Budapest 1985

/14/ B Denne, K H Behringer, M Forrest, this conference

Paper at 13th European Conference on
Controlled Fusion and Plasma Heating, Schliersee, FRG, April 1986

First Results of Neutral Beam Heating on JET

G. Duesing

Operating Parameters

A long pulse (~ 10 s) neutral beam injector [1] with eight beam sources and one integrated beam-line system [2] has been taken into operation on JET. The sources are arranged in two vertical groups, and the injection geometry is shown in Fig.1.

H^0 beams were injected into D^+ plasmas with particle energies (in the full energy fraction) of ≤ 65 keV. The neutral power fractions at this energy are 69%, 23% and 8% in the full, half and third energy components respectively, giving a total beam power of ≤ 5.5 MW injected into the torus. Most recently, D^0 beam heating experiments were started with D^+ plasmas. The beam particle energy was 75 keV, the injected power fractions 76% : 17% : 7% and the total power and energy into the torus 7.7 MW and 35 MJ, respectively. The data presented in this paper are mainly from the 65 keV H^0 beam experiments.

At 5.5 MW the particle source rate into the plasma (~ 120 m³ volume) was 7×10^{20} s^{-1}. Under all operating conditions, the density profiles of the fast-ion deposition [3] were peaked on axis, though only weakly so at the highest plasma densities.

Experiments were performed over a wide range of plasma parameters, i.e. plasma current I_p = 1 - 4MA, toroidal fields B_t = 1.7 - 3.4 T and safety factors q_{cyl} = 1.7 - 10.5. Beam power scans were performed by firing various numbers of beams. When possible, the density time evolution n(t) was maintained during power scans by adding gas fuelling to compensate the reduced beam fuelling at lower powers.

High Density Plasmas

With beam injection, stable plasma operation at high density was achieved. Fig 2 shows a typical example of a 4 MA plasma with 5.5 MW beam power (pulse # 7145). The drop in ohmic power P_{OH} at the beam onset reflects the drop in loop voltage due to a combination of beam driven current, electron heating and reduced effective ionic charge Z_{eff}. The plasma was first in contact with the outer wall limiters, and was moved towards the inner wall at the end of the

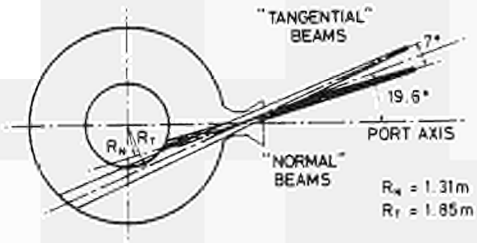

Fig.1 Plan view of the injection geometry.

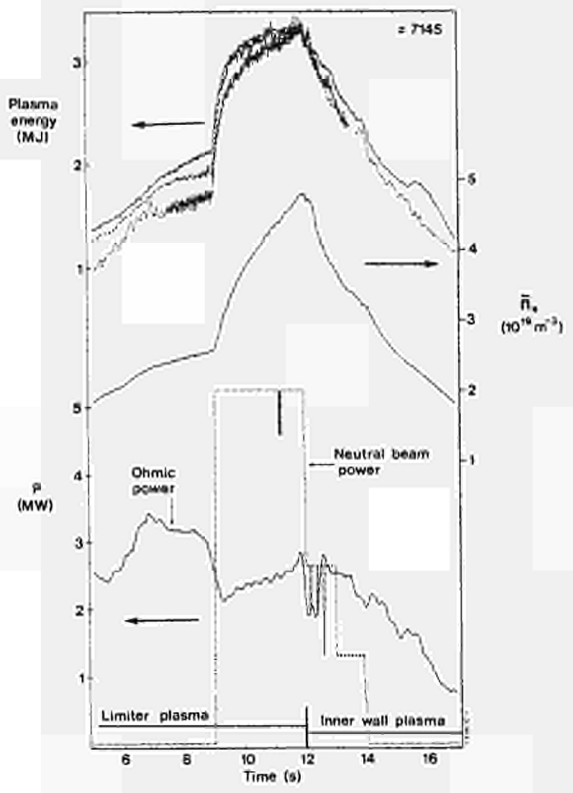

Fig.2 Input power, line averaged density $\bar{n}_e$, and plasma stored energy (from 3 different measurements) in a 4 MA limiter plasma, which is terminated on the inner wall. Plasma current flat-top from 7 to 12 s.

main beam pulse. This discharge termination scenario was routinely used, as the inner wall apparently is able to pump the high density build-up by the beams. In addition, density limit disruptions during the density decay are avoided by staggering the beam switch-off. The initial rise rate $\langle \dot{n}_e \rangle$ of the volume averaged density is larger than the beam fuelling rate. The almost constant $\langle \dot{n}_e \rangle$ close to the density maximum is I_p and B_t dependant. It amounts to 1/3 and 2/3 of the beam fuelling rate at 1 and 4 MA, respectively, for 3.4 T. With lower B_t, $\langle \dot{n}_e \rangle$ is reduced.

In limiter discharges, the density profile was found to remain constant from the ohmic part of the discharge all through the beam pulse. The density profile was, however, changed in a different experiment, when plasmas were shifted to the inner wall early in the beam pulse and subsequently had no or little density increase. In a power scan with such plasmas the reduced beam fuelling rate at lower beam power was replaced by external gas introduction in order to maintain the density evolution unchanged from pulse to pulse. The result was a 40% higher ratio of n_e^o / $\langle n_e \rangle$ for the beam-fuelling-only over the gas-fuelling-only case (n_e^o central density).

In pulse # 7145, the ion temperature close to the plasma axis increased from 3.1 keV to 4.1 keV at the beam onset with a subsequent slight reduction to 3.9 keV during the density rise. The electron temperature on axis was raised from the ohmic value of 3.8 keV to 5.0 keV (median value through ≤ 1 keV sawteeth), but then dropped smoothly during the density increase to 3.3 keV at the end of the beam pulse. (The absolute values of the ion temperatures given here need further corrections by $\lesssim$ 20%.)

Impurities

In general beam heated pulses showed an impurity situation very much like in high density ohmic discharges.

In pulse # 7145, Z_{eff} was reduced from 3.2 to 2.7 due to the beam injection. A reduction in Z_{eff} is also found in an evaluation of all NBH plasmas as a function of the beam power, which is proportional to the beam fuelling rate. This reduction amounted to 20% at the highest power level.

The most prominent impurity concentrations in # 7145 (with graphite outer wall limiters, graphite inner wall tiles, and the wall carbonised several months before the experiments) were changed by the beam injection as follows [4]: C was reduced from 2.9 to 1.0% and O from 2.0 to 1.9%, Cl was unchanged at 0.07%, and the most important metallic impurity Ni was reduced from 0.006 to 0.0008%.

reduced from 0.006 to 0.0008%.

The radiated power [5] both in limiter and inner wall discharges very closely follows the density time evolution (except when approaching a disruption).

In the limiter discharge # 7145, P_{rad}/P_{tot} dropped from 40 to 24% on beam onset, and subsequently increased to 42% during the density rise. The radiation profiles stayed unchanged, in particular no relative increase of the core radiation was observed.

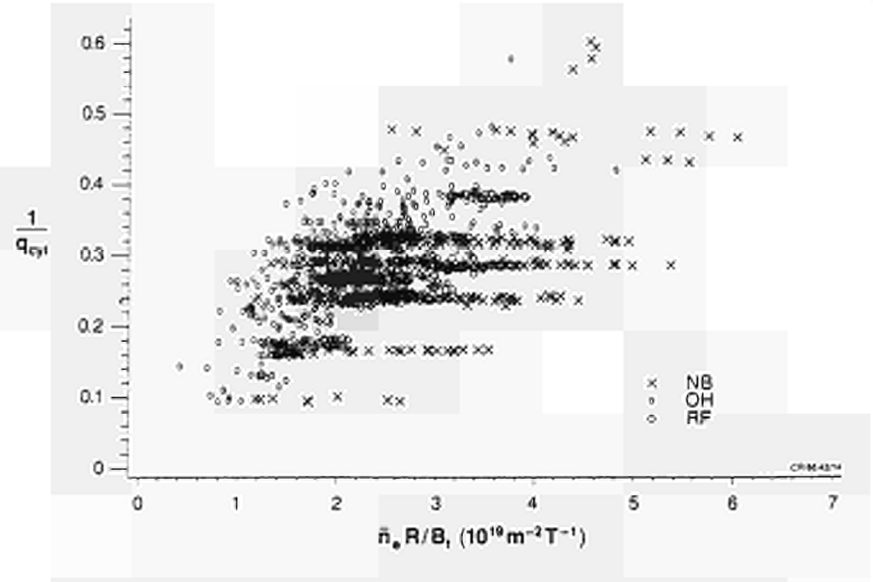

Fig.3 Hugill diagram for all JET discharges with a substantial plasma current flat-top.

Operating Regime

The Hugill diagram in Fig.3 contains NBH discharges over a wide range of I_p (1 to 4 MA) and B_t (1.7 to 3.4 T). The extension of the accessible operating regime by beam injection is substantial. The densities are increased by approximately 70% over ohmic and RF heated cases. A value of $\bar{n}_e R q_{cyl}/B_t$ of 20 has been exceeded compared to values of 11 quoted for JET so far [6].

n_e^{max} (Fig.4) increases with P_{tot} but indicates the beginning of a saturation. A $\sqrt{I_p}$ dependence of n_e^{max}

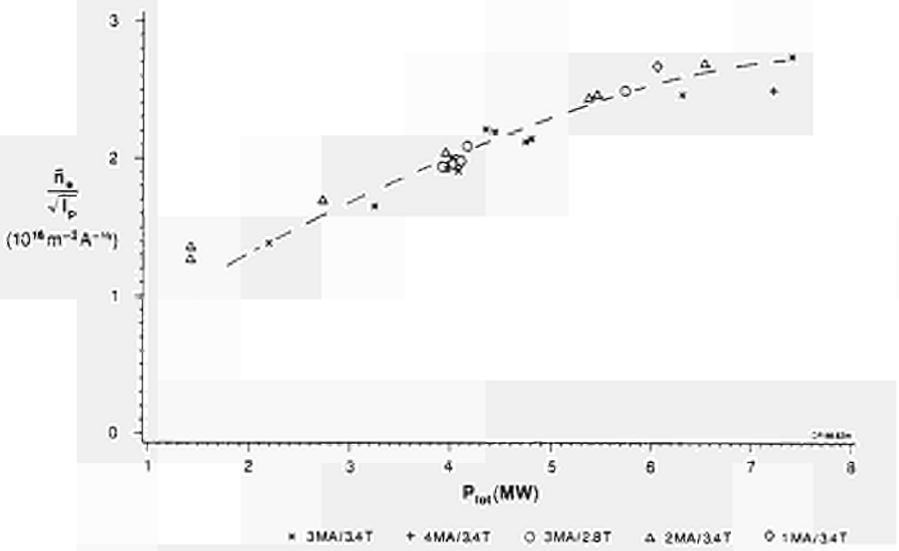

Fig.4 Maximum densities vs input power for disruptive neutral beam heated limiter discharges, normalised to $I_p^{1/2}$.

describes the measurements well (all pulses with $q_{cyl} \geq 3$) as reported before [7] from NBH experiments in Asdex, and different from the apparent linear I_p dependance in ohmic plasmas.

High Ion Temperatures

The inner wall pumping was found effective in controlling the plasma density rise during beam fuelling. In order to keep the initial densities low, plasmas were limited by the inner wall during the I_p ramp. Fig.5 shows pulse # 7155 where by this technique a line averaged density $\bar{n}_e = 2.3 \times 10^{19}$ m^{-3} was obtained and maintained during the 5.5 MW beam

pulse. The maximum P_{rad} during the pulse was 25% of P_{tot}, which is a typical value for inner wall NBH plasmas.

The central electron temperature T_e^o increased to ~ 4.8 keV for the median value during 1 keV sawteeth (Fig.6). The ion temperature T_i increased from 2.2 keV to ~ 6.5 keV (Fig.7) as measured from three diagnostics with an uncertainty of ± 1 keV. In NBH discharges of this type, T_i was substantially increased beyond T_e, unlike ICRH results on JET. During the main beam pulse in # 7155, the beam particle deposition profile [3] was strongly peaked on axis with a central particle source rate of 3.5 x 10^{19} $m^{-3}s^{-1}$, the central ion heating power was 1.8 x 10^{-5} W/m^3 and the central electron heating power 0.8 x 10^{-5} W/m^3.

A central velocity of plasma toroidal rotation of 1.6 x 10^5 m/s was measured by the X-ray crystal spectrometer during this pulse.

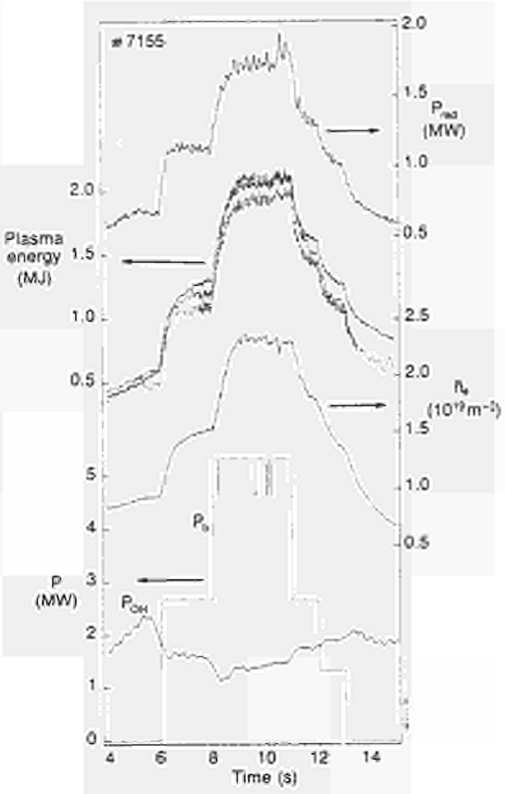

Fig.5 Beam power, ohmic power, line averaged density, stored energy and total radiated power in a 3 MA plasma (flat-top from 5 to 15 s) limited by the inner wall from 3 s.

Energy Confinement

Neutral beam power scans were performed with limiter plasmas at 3.4 T and various values of I_p between 1 and 4 MA. Fig. 8 shows the plasma stored energy W during the latter part of the beam pulses for these scans. The stored energy during the ohmic phase of the discharges, when the densities were much lower, is also shown.

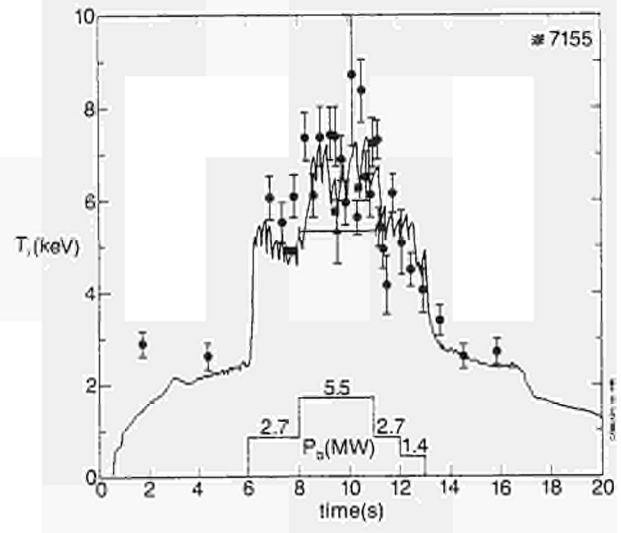

Fig.7 Ion temperatures for the plasma in Fig.5. ● X-ray crystal spectrometer (1.59 A Ni^{26+} resonance), ▲ neutron spectrometer, — neutral particle analyser (linear fit), ■ neutral particle analyser (complete fit).

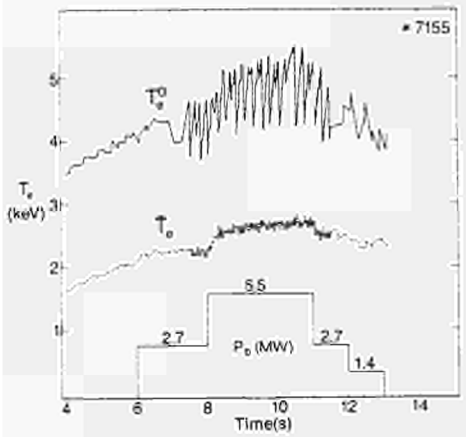

Fig.6 Central and average electron temperature for the same plasma as in Fig.5.

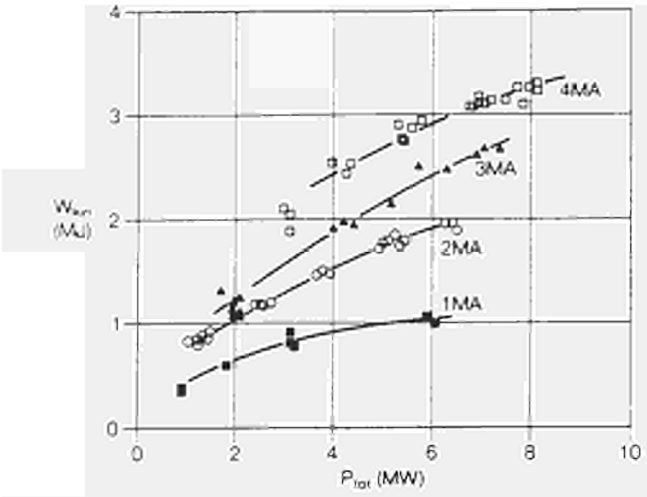

Fig.8 Stored energy from kinetic measurements vs total input power, for beam power scans in limiter plasmas at various I_p and at 3.4 T.

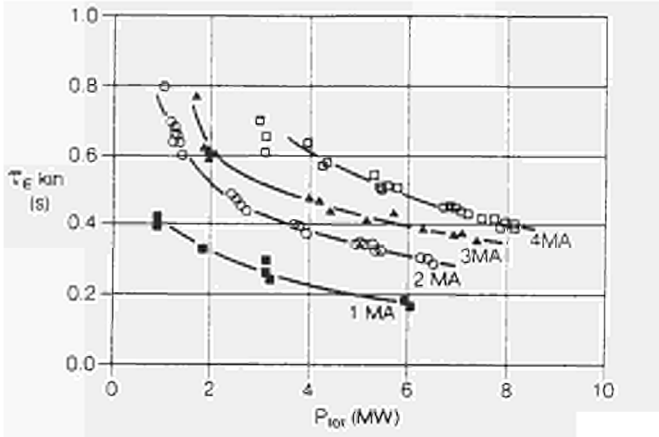

Fig.9 Global energy confinement time $\tau_{E\ kin} = W_{kin}/P_{tot}$ for the scans in Fig.8.

Lines have been drawn into the diagram only to guide the eye. Within the uncertainty of ± 15% for the W values, the slope of these lines is the same for the 2, 3 and 4 MA scans. The 1 MA scan appears to show a different slope and the onset of a saturation. A quantitative evaluation of this data in terms of linear fits and incremental confinement times is given in reference [8].

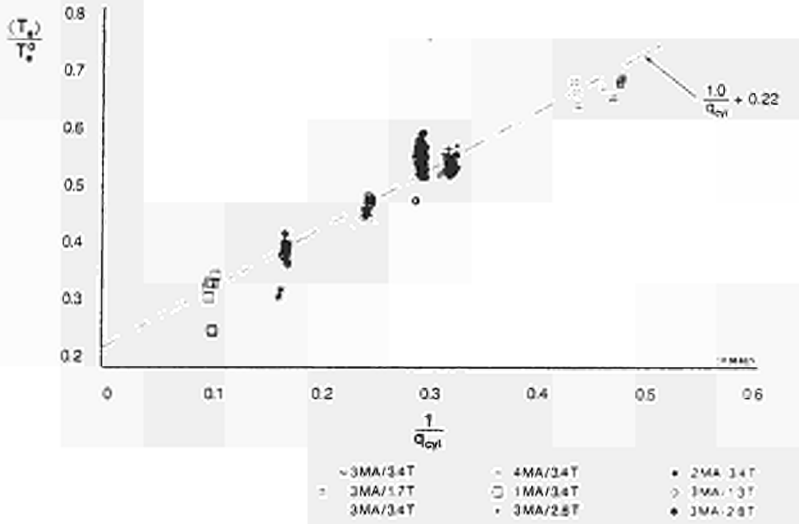

Fig.10 Width of T_e profiles for a wide range of beam heated plasmas. Each cluster of data is from a power scan with 0 to 5.5 MW beam power.

The global energy confinement time τ_E for the same data (Fig.9) qualitatively shows the expected [9] degradation. At the highest input power P_{tot} = 8 MW and I_p = 4 MA, the observed value is τ_E = 0.4 s. The available beam power is still too low ($P_b \sim 2\ P_{OH}$ at high I_p) for an unambiguous statement on a τ_E saturation with increasing power. Equally, the I_p scaling of τ_E in beam dominated plasmas cannot yet be quantitatively determined. At present power levels an I_p dependence is observed that is weaker than linear.

A weak density dependence has also been observed. The data is well described by various fits, e.g. a $\sqrt{n}$ dependence of τ_E or a τ_E definition [10] in the form of $\tau^{-2} = \tau_{OH}^{-2}(n) + \tau_{add}^{-2}$ with a linear density dependence of τ_{OH}.

Power scans at various B_t values between 1.7 and 3.4 T have been performed for 3 MA plasmas. For an assumed $W = W(0) + \tau_{incr}\ P_{tot}$ dependence, the values of τ_{incr} were 0.2 to 0.3 s, determined from different W measurements, and were independent of B_t. W(0) was

independent of B_t at higher B_t values . At lower values of B_t and hence of q, the W(0) values were somewhat lower.

The observed consistency of the T_e profile is presented in Fig. 10. The profile width is well described by a 1/q dependence. Each cluster of data represents power scans over a wide density variation in limiter and, to a lesser extent, inner wall discharges. The scatter of the data is mainly due to the sawtooth variation of T_e°.

Summary

Long-pulse neutral beam heating experiments with 65 keV hydrogen beams into deuterium plasmas have been performed over a wide range of plasma parameters (q_{cyl} = 1.7 - 10.5) and beam power (≤5.5 MW).

Impurities did not present a problem. Z_{eff} slightly decreased with increasing beam power and also during a beam pulse. Plasma radiation closely followed the beam-induced density build-up and stayed at low values, particularly in the case of inner wall plasmas.

At medium density the ion temperature was increased from ~ 2.2 to ~ 6.5 keV and in excess of the electron temperature.

The energy confinement degradation was close to L-mode scaling-law predictions. The confinement time at the highest input power and current was τ_E = 0.4 s, τ_E being a weakly increasing function of plasma current, density and toroidal field.

The operating regime for beam heated plasmas was much greater than for ohmic or RF heated plasmas. The maximum density increased with input power and with $I_p^{½}$. A Murakami parameter of 6 x 10^{19} m^{-2} T^{-1} was obtained.

Acknowledgements

The injector has been built and assembled by the beamline construction group (Group Leader R Haange), major parts tested by the test bed group (R S Hemsworth, H Falter), the final system commissioned by the neutral beam operation group (E Thompson) and the additional heating power supply group (R Claesen). The dedication and professional competence of the staff in these groups is highly appreciated. An important part of the injector, namely the beam sources, were jointly developed by JET, the CEA Fontenay-aux-Roses laboratory and the UKAEA Culham laboratory. P Lomas, A Stäbler, P Thomas and E Thompson made invaluable contributions to the planning and evaluation of the experiments.

References

[1] G. Duesing, Proc. 13th Symposium on Fusion Technology, Varese (1984), 59.
[2] R. Haange et al, Proc. 11th Symp. on Fusion Engineering, Austin (1985).
[3] M. Watkins et al, 13th Eur. Conf. on Contr. Fusion & Plasma Heating, Schliersee (1986).
[4] W. Engelhardt et al, in ref [3].
[5] H. Jäckel et al, in ref [3].
[6] R. Bickerton et al, Plasma Physics and Controlled Fusion 28 1A, 155 (1986).
[7] H. Niedermeyer et al, Proc. 12th Eur. Conf. on Controlled Fusion & Plasma Physics, Budapest (1985), 9F, part 1, 159.
[8] K. Thomsen et al, in ref [3].
[9] S. M. Kaye, R. Goldston, Nucl. Fus. 25 65 (1985).
[10] R. Goldston, Plasma Physics and Controlled Fusion 26 1A, 87 (1984).

APPENDIX I

THE JET TEAM

JET Joint Undertaking, Abingdon, Oxon. OX14 3EA, U.K.

A. Ainsworth, H. Altmann, R.J. Anderson, J. Arbez, D. Bartlett, W. Bailey, B. Beaumont[1], K. Behringer, E. Bertolini, P. Bertoldi, C.H. Best, V. Bhatnagar[4], R.J. Bickerton, G. Boissin, F. Bombarda[10], T. Bonicelli, S. Booth, A. Boschi, G. Bosia, M. Botman, G. Bracco[10], H. Brelen, H. Brinkschulte, M.L. Browne, M. Brusati, T. Budd, M. Bures, P. Butcher, H. Buttgereit, D. Cacaut, C. Caldwell-Nichols, D. Campbell, R. Carolan[11], J. Carwardine, G. Celentano, C.D. Challis, A. Cheetham, J. Christiansen, C. Christodoulopoulos, P. Chuilon, R. Claesen, J.P. Coad, M. Cooke, J.G. Cordey, W. Core, S. Corti, A.E. Costley, G. Cottrell, M. Cox[11], J. Dean, E. Deksnis, G.B. Denne, G. Deschamps, K.J. Dietz, J. Dobbing, S.E. Dorling, D.F. Düchs, G. Duesing, P. Duperrex[6], H. Duquenoy, L. de Kock, A. Edwards, J. Ehrenberg[2], W. Engelhardt, S. Erents[11], F. Erhorn, B. Eriksson, M. Evrard[4], H. Falter, N. Foden, M. Forrest[11], C. Froger, K. Fullard, M. Gadeberg[5], A. Galetsas, A. Gallacher, D. Gambier[1], R. Giannella[10], A. Gibson, R.D. Gill, A. Goede, A. Gondhalekar, D. Goodall[11], N.A. Gottardi, C. Gowers, R. Granetz, B. Green, S. Gregoli, F.S. Griph, R. Haange, J.H. Hamnén[3], C.J. Hancock, P. Harbour, N. Hawkes[11], P. Haynes[11], T. Hellsten, J.L. Hemmerich, R. Hemsworth, F. Hendriks, R.F. Herzog, L. Horton, J. How, M. Huart, A. Hubbard, J. Hugill[11], M. Hugon, M. Huguet, B. Ingram, H. Jäckel[2], J. Jacquinot, O.N. Jarvis, E.M. Jones, T.T.C. Jones, P. Jones, E. Källne, J. Källne, A. Kaye, B.E. Keen, M. Keilhacker, G. Kinahan, S. Kissel[2], A. Konstantellos, U. Küphnapfel[2], P. Kupschus, P. Lallia, J.R. Last, L. Lauro-Taroni, K.D. Lawson[11], E. Lazzaro, R.C. Lobel, P. Lomas, N. Lopes-Cardozo[7], M. Lorenz-Gottardi, C. Lowry, G. Magyar, D. Maisonnier, M. Malacarne, V. Marchese, P. Massmann, G. McCracken[11], P. McCullen, M.J. Mead, P. Meriguet, V. Merlo, S. Mills, P. Millward, A. Moissonnier, P.L. Mondino, D. Moreau[1], P. Morgan, R. Müller[2], G. Murphy, M.F. Nave, L. Nickesson, P. Nielsen, P. Noll, S. Nowak, W. Obert, B. Oliver, M. Olsson, J. O'Rourke, M.G. Pacco, J. Paillere, L. Pannacione, S. Papastergiou, J. Partridge[11], D. Pasini, N. Peacock[11], M. Pescatore, J. Plancoulaine, J-P. Poffé, R. Prentice, T. Raimondi, C. Raymond, P.H. Rebut, J. Removille, W. Riediker, R. Roberts, D. Robinson[11], A. Rolfe, R.T. Ross, G. Sadler, J. Saffert, N. Salmon, F. Sand, A. Santagiustina, R. Saunders, H. Schamel[12], M. Schmid, F.C. Schüller, K. Selin, R. Shaw, D. Sigournay, R. Simonini, P. Smeulders, J. Snipes[11], L. Sonnerup, K. Sonnenberg, A. Stäbler[2], M. Stamp, C.A. Steed, D. Stork, P.E. Stott, T.E. Stringer, D. Summers, H. Summers[13], J. Tagle[9], G. Tallents[14], A. Tanga, A. Taroni, A. Terrington, A. Tesini, P.R. Thomas, E. Thompson, K. Thomsen[5], F. Tibone, R. Tivey, T. Todd[11], G. Tonetti[6], P. Trevalion, M. Tschudin, S. Tsuji[15], B. Tubbing[7], P. Twynam, E. Usselmann, H. van der Beken, M. von Hellermann, J.E. van Montfoort, J. von Seggern[8], T. Wade, C. Walker, B.A. Wallander, M. Walravens, K. Walter, M.L. Watkins, M. Watson, D. Webberley, A. Weller[2], J. Wesson, J. Wilks, T. Winkel, C. Woodward, M. Wykes, D. Young, L. Zannelli, J. Zwart

PERMANENT ADDRESS

1 Commissariat A L'Energie Atomique, F-92260 Fontenay-Aux-Roses, France.
2 Max Planck Instituut Für Plasmaphysik, D-8046 Garching bei Munchen, F.R.G.
3 Swedish Energy Research Commission, S-10072 Stockholm, Sweden.
4 EUR-EB Association, LPP-ERM/KMS, B-1040 Brussels, Belgium.
5 Risó National Laboratory, DK-4000 Roskilde, Denmark.
6 CRPP/EPFL, 21 Avenue des Bains, CH-1007 Lausanne, Switzerland.
7 FOM Instituut voor Plasmafysica, 3430 Be Nieuwegein, The Netherlands.
8 Kernforschungsanlage Jülich GmbH, D-5170 Jülich, F.R.G.
9 Junta de Energia Nuclear, Avda. Complutense, Madrid 3, Spain.
10 ENEA-CENTRO Di Frascati, I-00044 Frascati, Roma, Italy.
11 Culham Laboratory, Abingdon, Oxfordshire, U.K.
12 Ruhr-Universitaat Bochum, D-4630 Bochum, F.R.G.
13 University of Strathclyde, 107 Rottenrow, Glasgow, G4 ONG.
14 The Australian National University, Research School of Physical Sciences, Canberra ACT 2600, Australia.
15 Japan Atomic Energy Research Institute, Naka-machi, Naka-gun, Ibaraki-ken, Japan.

JET Contributions to 13th European Conference on Controlled Fusion and Plasma Heating

Schliersee, F.R.G.

14—18 April 1986

JET CONTRIBUTED PAPERS TO THE 13TH EUROPEAN CONFERENCE ON CONTROLLED FUSION AND PLASMA HEATING (SCHLIERSEE, FRG, APRIL 14-18 1986)

* Poster Presentations.

ENERGY TRANSPORT IN JET WITH OHMIC AND AUXILIARY HEATING

K Thomsen+, D V Bartlett, V Bhatnagar, R J Bickerton, M Brusati, M Bures, D J Campbell, J P Christiansen, J G Cordey, S Corti, A E Costley, G A Cottrell, G Duesing, A Edwards, S Ejima*, J Fessey, M Gadeberg+, A Gibson, R D Gill, N Gottardi, A Gondhalekar, C W Gowers, F Hendricks, J Jacquinot, O N Jarvis, E Kallne, J Kallne, S Kissel, L de Kock, P Lallia, E Lazzaro, P J Lomas, P D Morgan, P Nielsen, R Prentice, R T Ross, J O'Rourke, G Sadler, F C Schüller, A Stäbler#, M F Stamp, P E Stott, D R Summers, A Tanga, A Taroni, P R Thomas, E Thompson, F Tibone, G Tonetti**, B J Tubbing, M L Watkins

JET Joint Undertaking, Abingdon, Oxfordshire, OX14 3EA
On attachment from *GA Technologies, USA; +Riso National Laboratory Denmark; #IPP, Garching, FRG; **CRPP, Lausanne, Switzerland

JET has now been operated with ohmic, ion cyclotron resonance and neutral beam injection heating. A wide range of plasma conditions have been studied with ohmic and ion cyclotron resonance heating while neutral beam injection heating has just recently been applied.

1. OHMIC HEATING

During 1984 and 1985 an extensive series of experiments with ohmic heating have been carried out in both Hydrogen and Deuterium discharges [1].

The ranges of variation in the main plasma parameters covered are: Toroidal magnetic field $1.7 < B_T < 3.4$ T; plasma current $1 < I_p < 4$ MA; line average density $0.5 \times 10^{19} < n < 3.6 \times 10^{19}$ m^{-3}; elongation $1 < K$ (= b/a) < 1.7; minor radius $0.8 < a < 1.23$ m; major radius $2.5 < R < 3.4$ m; cylindrical safety factor $1.7 < q < 12$; effective charge $2 < Z_{eff} < 8$; peak electron temperature $1.5 < T_e < 5$ keV; peak ion temperature $1 < T_i < 3$ keV.

The plasma geometry has been varied from fully elliptical to small circular plasmas limited on the inside wall or on the limiter. The discharges had long flat tops in current, density and temperature, 4 - 12 secs, which was sufficient in all but the 3.5 and 4 MA discharges for the magnetic field diffusion to have been completed before the end of the flat top. Values up to 0.8 s have been achieved for the energy confinement time defined by $\tau_E = W/(P_{tot} - \dot{W})$, where $W = 3/2 \int (n_e T_e + n_i T_i)\, dv$.

The scaling of τ_E with density for a few characteristic conditions is shown in Fig. 1. The general pattern is that at low densities the confinement time increases roughly linearly with density and then saturates at higher densities ($n \geq 3 \times 10^{19}$ m^{-3}). The precise reason for the saturation is not clear, both the impurity radiation and transport losses increase as the limiting τ_E is reached. Due to the large errors in separating the ion and electron losses at high densities, it is not possible to determine which is the dominant loss channel.

The scaling of τ_E with the plasma parameters has been investigated, Fig. 1 shows that the neo-Alcator scaling, $\tau_E \propto nqR^2a$, is a reasonable fit. A marginally better fit can be obtained by a regression analysis in the form $\tau_E \propto B_T^{\alpha} q^{\beta}$ etc. The result from such an analysis is (A is the atomic mass and $\varepsilon = a/R$ the inverse aspect ratio)

$$\tau_E = 0.013\ n^{0.38}\ q^{0.33}\ B_T^{0.57}\ K^{0.21}\ R^{3.2}\ \varepsilon^{1.7}\ A^{0.56} \qquad (1)$$

The range of variation of R and ε in the JET data set is very small so the uncertainty on their indices are rather large. The JET data set has been combined with the DIII data set to get a better estimate of the scaling with dimensions. The scaling law obtained from a regression analysis on this combined data set can in terms of q (cylindrical) be written as:

$$\tau_{Ee} \alpha\ n^{0.6}\ q^{0.5}\ B_T^{0.1}\ K^{0.3}\ R^{3.4}\ \varepsilon^{0.9} \qquad (2)$$

From analysis of the local transport properties with interpretative and predictive codes three distinct regions have been clearly identified; an inner region dominated by sawtooth activity, an intermediate region dominated by electron and ion thermal transport and an edge region dominated by impurity radiation and other atomic processes. The main loss channel at low and moderate densities in the second region is found to be via the electrons. The ion thermal conductivity is between 1 and 8 times neoclassical with the higher values of this anomaly factor occuring at lower densities. The electron thermal conductivity can be approximated by $\chi_e \sim 2.5.10^{19}/n$ at low densities, while for the highest JET densities it does not decrease with n. No clear dependence of χ_e on toroidal magnetic field or plasma current has been observed so far.

2. ION CYCLOTRON RESONANCE HEATING

Ion cyclotron resonance heating has been used in JET since the beginning of 1985. The heating system and characteristics of the different antennas are described elsewhere [2]. Various minority heating experiments have been performed in deuterium discharges with either H or ^{3}He as the minority gas.

It has been possible to couple up to 6 MW of RF power, P_{RF}, to the plasma. The increase of the total plasma energy during ICRH is partly due to a density increase. However, both the ion and electron temperatures have also been increased significantly.

In the first experiments the power scaling of W and τ_E was unclear [3]. Recent results seem to support a linear scaling of W with power in the form

$$W = W(o) + \tau_{inc}\ P_{tot} \qquad (3)$$

Fig. 2 shows W versus P_{tot} for different plasma currents obtained in D (^{3}He) limiter discharges with B_T = 3.4 T, K = 1.45 and a = 1.2 m using a frequency of 33 MHz for central power deposition. The results of fitting eq. (3) to the RF-points only are shown by dotted lines. The incremental confinement time τ_{inc}, obtained this way, ranges from 128 ms - 192 ms with no obvious current dependence.

At present no strong dependencies of τ_{inc} with respect to P_{RF}, B_T, I_p and n_e have been observed, however, comparing with results from other tokamaks there must clearly be a strong dependence on the plasma size [4]. The degradation of the total τ_E during ICRH is clearly seen in Fig. 3.

From Eq. (3) we may express the confinement of both ohmic and additional

heated plasmas in the form

$$\tau_E = \tau_E^{OH} \frac{P_\Omega(0)}{P_{tot}} + \tau_{inc} \left(1 - \frac{P_\Omega(0)}{P_{tot}}\right) \qquad (4)$$

where τ_E^{OH} and $P_\Omega(0)$ are the ohmic heating confinement time and power, respectively, in the absence of auxiliary heating. The present τ_{inc} is typically one third of τ_E^{OH}, which means we need to couple more than 10 times the ohmic power in order to confirm the saturation of τ_E.

By performing an exponential fit of the form $W(t) = W_o + \Delta W\ (1-\exp(-t/\tau))$ to the time evolution of W from the time of a change in RF-power level, we can estimate the fraction $f = (\Delta W - \tau \Delta P_\Omega)/\tau \Delta P_{RF}$ of RF-power which contributes to the increase in stored energy. This fraction f was typically ~ 70% in the experiments shown in Figs. 2, 3.

3. NEUTRAL BEAM INJECTION HEATING

Neutral beam injection heating (45 - 65 keV H into D plasma) has now been successfully applied to JET discharges [5]. Identical target plasmas have been used for NBI and ICRH making it possible to compare the two methods. Fig. 4 shows W versus P_{tot} for NBI heating, i.e. the equivalent of Fig. 2. Again a linear dependence of W with P_{tot} (eq. (3)) fits the data. In addition τ_{inc} shows an apparent current dependence which is present in all the estimates of the total plasma energy as is shown in Fig. 5.

In conclusion all NBI and ICRH experiments so far have produced values of τ_{inc} in the range 100 - 300 ms. Future heating experiments with more input power are needed to determine the dependence of τ_{inc} with power.

REFERENCES

[1] Cordey, J. G. et al., EPS Conference, Budapest (1985).

[2] Jacquinot, J. et al., Plasma Physics and Controlled Fusion 28, 1 (1986)

[3] Ejima, S. et al., APS Conference, San Diego, Paper 6p53 (1985)

[4] Jacquinot, J. et al., Royal Society Meeting, London (1986)

[5] Duesing, G. et al., Royal Society Meeting, London (1986)

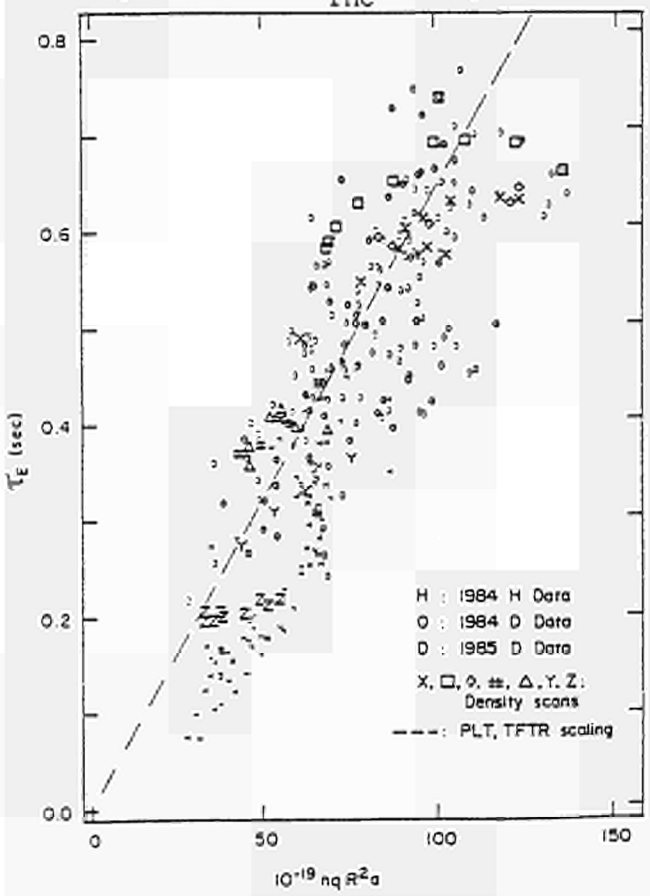

Figure 1 : Energy confinement time versus the neo-Alcator scaling. Ohmic data only.

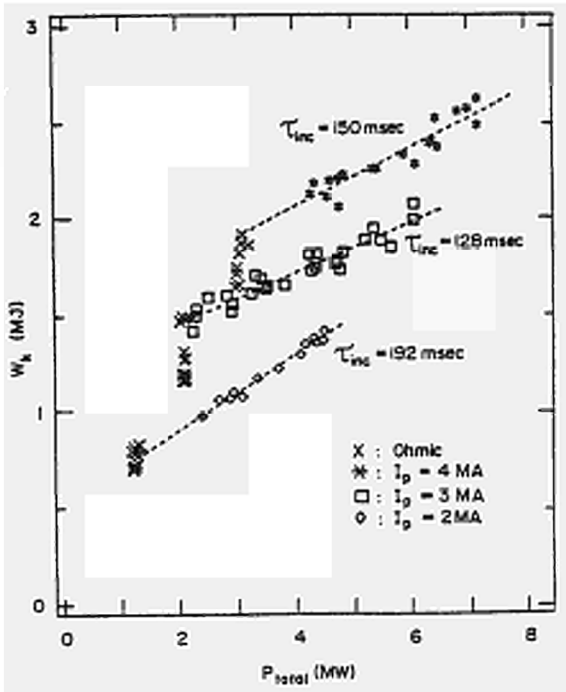

Figure 2 : Total kinetic plasma energy versus total input power from ICRH heating experiment.

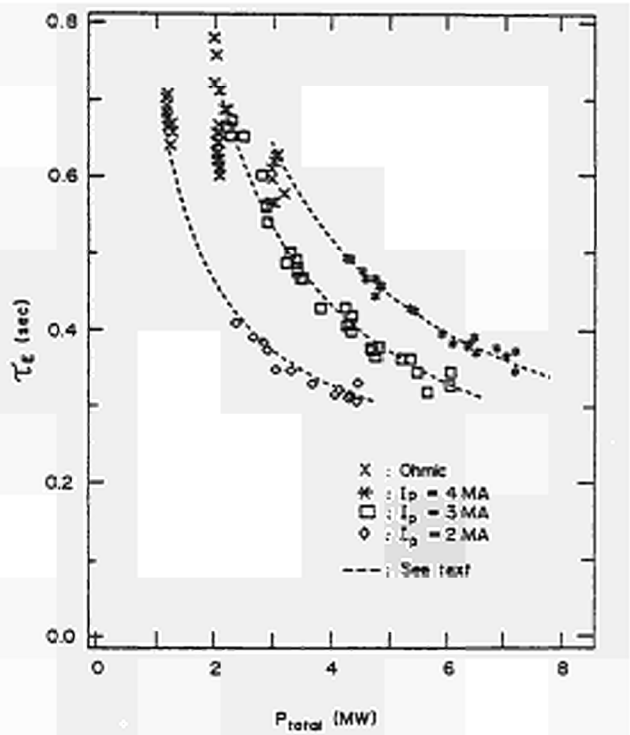

Figure 3 : Energy confinement time versus total input power from ICRH heating experiment. The dotted lines correspond to the fit lines in Fig. 2.

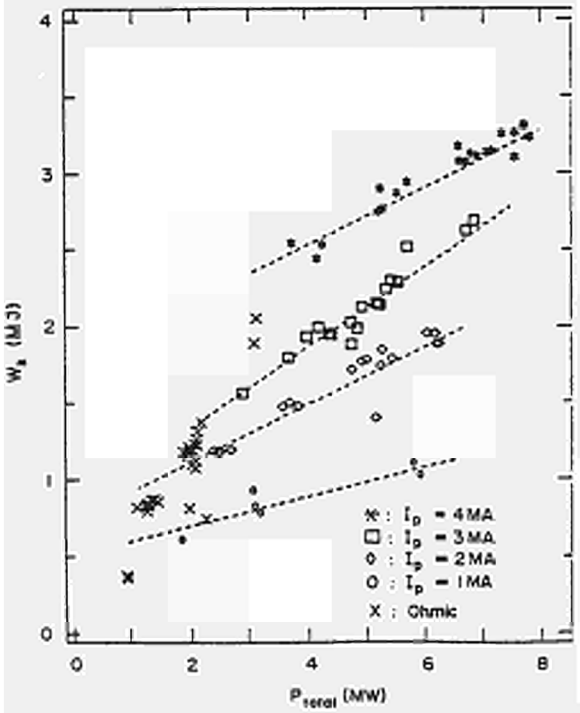

Figure 4 : Total kinetic plasma energy versus total input power from NBI heating experiment. The results of fitting the data to Eq. (3) are shown by dotted lines.

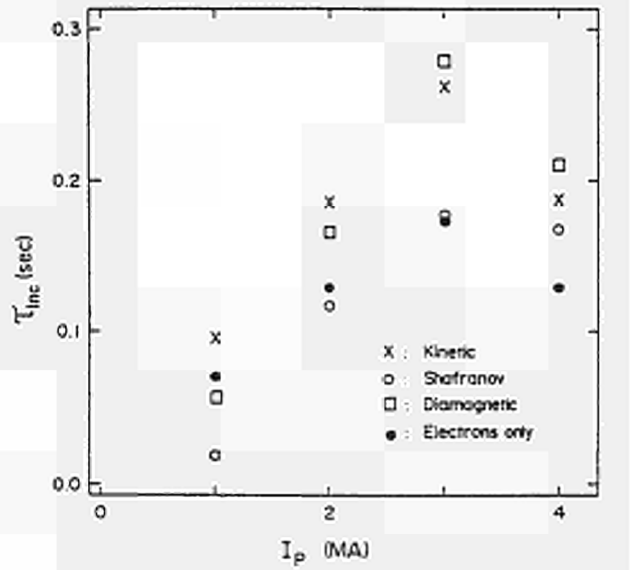

Figure 5 : The incremental confinement time, determined from the different estimates of plasma energy, shown versus plasma current, for the NBI heating experiment.

ENERGY CONFINEMENT IN TOKAMAKS

P R Thomas
JET Joint Undertaking, Abingdon, OX14 3EA, UK

1. INTRODUCTION

The presentation of the results of Ohmic and additional heating experiments on tokamaks has relied to a substantial degree on the parametric scaling of the total energy confinement time. Since the correct theory for transport in high temperature plasmas has not yet been identified, the range of validity of the resulting scaling laws is completely unknown. Also, it is not clear that the total energy confinement time is the appropriate quantity to represent the data and its use in scaling laws might even obscure the underlying physics. Tokamaks exhibit several confinement regimes with different scaling behaviour. It is proposed in this paper that tokamak plasmas can be viewed as have several phases separated by sharp transitions.

The use of the phraseology of phase transitions in thermodynamic systems is meant to suggest a framework for the representation of tokamak data. The applicability of the modern theory of phase transitions to driven systems which might not even posses a thermodynamic limit is the subject of an extensive literature [1]. In addition to discontinuous behaviour of observable quantities or their derivatives in an independent parameter, an important qualification for the theory to be useful is that the system possess a large scale order parameter. In some models of plasma turbulence [2], long wavelength pump modes appear to act as order parameters and the resulting transport exhibit the characteristics of second order phase transitions. However, the question as to whether or not tokamak plasmas undergo phase transitions will be left open here.

2. THE CONFINEMENT PHASES

There are two distinct, observable phases in tokamks. The growth of the energy density in the central region between sawtooth crashes indicates that a third (neoclassical?) phase exists within the q=1 surface. As given by Goldston [3], the low density Ohmic heating phase can be described by the neo-Alcator scaling

$$\tau_{E,OH} = 0.01\ n_e(10^{19}m^{-3})\ R^{2.04}(m)\ a^{1.04}(m)\ q^{0.5} \qquad (1)$$

whilst the high density ohmic and auxiliary heating phases are represented by

$$\tau_{E,aux} = \text{Const.}\ I_p(A)\ P_{tot}^{-0.5}(W)\ R^{1.75}(m)\ b^{0.5}(m)\ a^{-0.87}(m) \qquad (2)$$

The constant is in the range $3.7\text{-}7.4\times10^{-5}$ depending on the regime being represented. The variation in the constant is indicative of the neglect of a significant parameter from the description of a common transport mechanism.

In the neo-Alcator scaling, equation 1, is consistent with the Connor, Taylor constraints [4] for collisional high or low beta and collisionless

high beta models. This freedom of choice is perhaps the reason why so many explanations for neo-Alcator scaling have appeared!

The auxiliary heating scaling, equation 2, is consistent with collisional high beta and resistive MHD. The scaling of the resistive MHD model can be cast into the form

$$\beta_I = f\ (P_{tot}/P_{OH},\ S,\ q,\ a/R) \qquad (3)$$

where S is the magnetic Reynolds number and the other symbols have their usual meanings. It is assumed here that the plasma current is driven entirely by the transformer and that electron trapping is unimportant so that the Ohmic heating power is a consistent measure of the plasma resistivity. A simplified form of equation 3

$$\beta_I = 0.11((P_{tot}/P_{OH})\ (R/a)\ (b/a))^{0.5} \qquad (4)$$

is a quite good representation of the data [5] from several NBI dominated limiter experiments as shown in Figure 1. It is similar when transformed to a confinement time scaling to equation 2 and to the form expected of resistive ballooning mode turbulence [6].

3. THE NEO-ALCATOR TO AUXILIARY HEATING TRANSITION

The existence of a sharp transition between the neo-Alcator and auxiliary heating phases is indicated by several pieces of experimental data. The energy content of some 4MA, 3.4T ICRF heated JET plasmas is plotted against total power in Figure 2. The linearity and non-zero intercept imply the presence of an underlying confinement phase which supports most of the energy content. The propogation time of the sawtooth heat pulse was independent of input power for these discharges [7]. Furthermore, the thermal conductivity inferred from the beta pulse propogation is consistent with the characteristic time given by the slope in Figure 2. Therefore the thermal insulation has been broken down by the Ohmic heating and the application of auxiliary heating causes little or no further change. The transition becomes apparent when the energy content for Ohmic heating discharges with the same current and field are plotted against line average electron density. As can be seen in Figure 3, the transition is rather sharp and the energy content, becomes independent of density at high densities. The same behaviour has been observed in most machines.

Following the above comments, it is of interest to determine whether the transition to the high density Ohmic phase has any of the characteristics that might be expected of resistive MHD. The JET Ohmic heating data cluster around the transition and this results in the reported weak density dependence of the energy confinement time [8]. Consequently, the JET data are well represented by the form of equation 3 as shown in Figure 4. The aspect ratio dependence is striking and must reflect the importance of toroidal coupling of modes or the edge plasma. It is tempting to ascribe the behaviour shown in Figure 4 to a threshold beta for MHD instability.

4. THE NATURE OF THE TRANSITION

Simple addition of the neo-Alcator and auxiliary heating loss rates is not consistent with the data. In order to match the sharpness of the transition, Goldston combined the loss rates by

$$\tau_E = \left((1/\tau_{E,OH})^{\alpha} + (1/\tau_{E,aux})^{\alpha} \right)^{1/\alpha} \qquad (5)$$

with $\alpha=2$. This suggests that each loss channel gains complete control of its own phase. The best match of the JET data to equations 1 and 2 can be obtained by taking $\alpha \to \infty$, or the maximum loss rate! Therefore it is unlikely that the confinement transition is due to the passage through a local critical point. Instead the data point to a global mechanism for switching from one loss process to the other [9].

Additional heating data from several machines [10] indicate that the current density profile or the shape of the electron temperature profile are held rigid by some, as yet, unexplained process. If this picture is correct, the temperature scale would be determined by the region with the works loss rate in relation to the local power flow. A sharp confinement transition could then result form the switch of control between a region dominated by drift wave turbulence, for example, and another dominated by resistive MHD. Any model leading to the neo-Alcator scaling, in which the losses increase with electron temperature, would yield a confinement transition at a critical density which increases with heating power. Unfortunately the published data is rather sparse in this region. However there is some weak evidence in the JET data to suggest that the critical density increases slightly with power.

5. CONCLUSIONS

Complex, non-linear systems generally exhibit phenomena which can be described, at least phenomenologically, as phase transition. Tokamak plasmas are no exception and the transition from the neo-Alcator to auxiliary heating phases is a good example of such behaviour. The loss rate in the auxiliary heating phase and the critical beta in the Ohmic heating data are consistent with resistive MHD processes. However, the transition so sharp that local transport must be regulated by some global mechanism. This mechanics must reflect the dominance in tokamak plasmas of an unobserved phase transition associated with the shape of the electron temperature or current density profiles. A concerted experimental attack on the transition between the confinement phases would surely yield some insights into transport processes.

6. REFERENCES

1. See for example, H Haken, Rev. Mod. Phys., 47(1975)p67
2. R E Walz, Phys. Rev. Lett., 55 (1985)p1098
3. R J Goldston, Plas. Phys. and Cont. Fus., 26(1984)p87
4. J W Connor and J B Taylor, Nuc. Fus., 17(1977)p1047
5. The author gratefully acknowledges the use of data collected by S M Kaye and P J Lomas.
6. J W Connor, Plas. Phys and Cont. Fus., 26(1984)p1419
7. B Tubbing et al., Proc 12th EPS Conf. on Cont. Fus. and Plas. Phys., (Budapest 1985) Part 1, p215.
8. J G Cordey et.al, Proc 12th EPS Conf. on Cont. Fus. and Plas. Phys., (Budapest 1985) Part 1, p26.
9. B B Kadomstev, Comm. Plas. Phys and Cont. Fus., 9(1985)p227, has discussed a local switching of trasport processes.
10. J W Connor, Plas. and Cont. Fus., 26(1984)p1419.

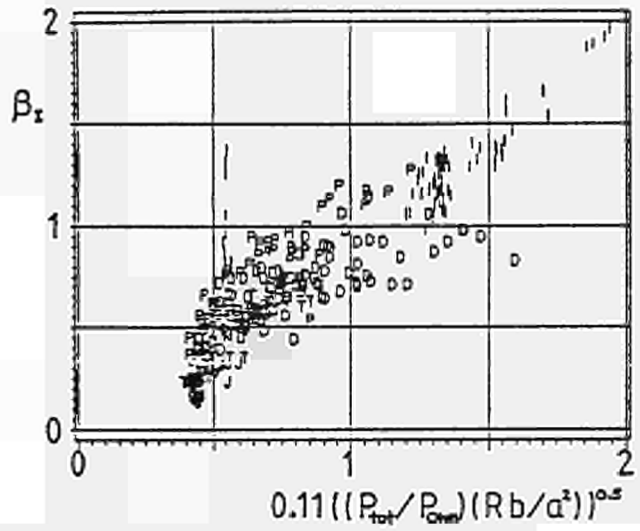

Figure 1: Equation 4 compared with data from DITE(C), DIII(D), ISXB(I), JET(J), PDX(P), TFR(F), and TFTR(T).

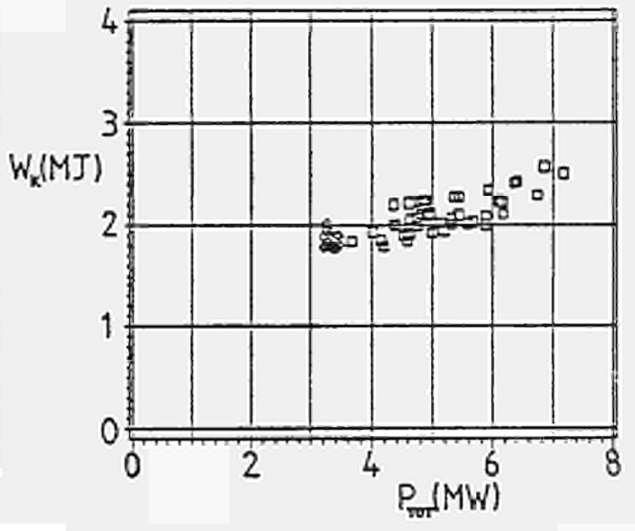

Figure 2: Total Plasma Energy vs total power for ◇ Ohmic and □ ICRF heated 4MA, 3.4T, $3.10^{19}m^{-3}$, a=1.2m JET discharges.

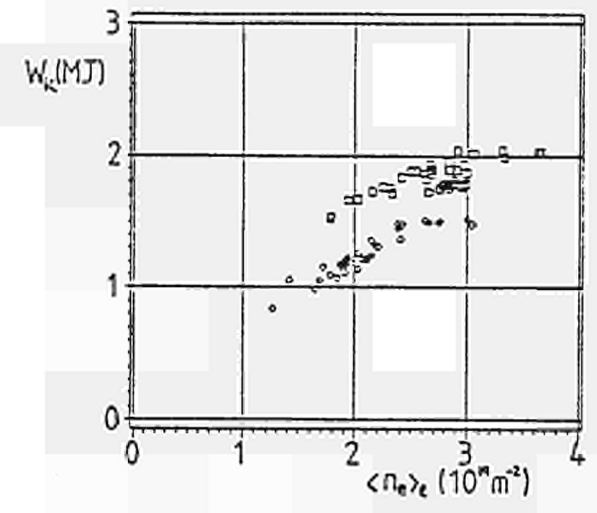

Figure 3: Total Plasma Energy vs. line average density for ◇ 3MA, 3.4T and □ 4MA, 3.4T JET discharges with a=1.2m and b/a = 1.4 - 1.55

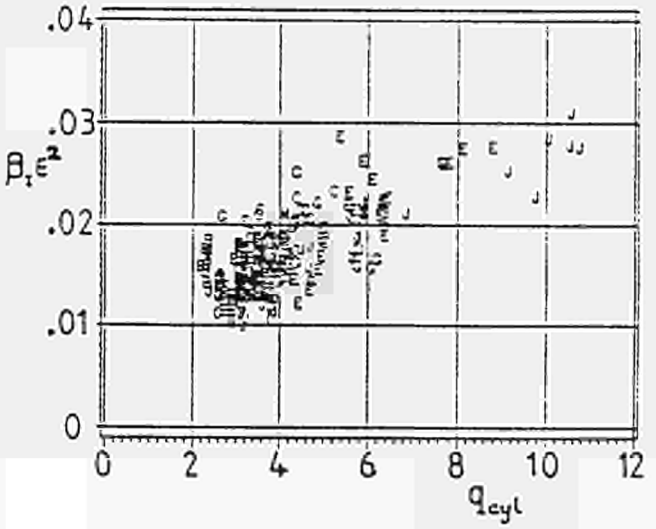

Figure 4: $\beta_I\varepsilon^2$ vs. Qcyl for JET OH discharges with toroidal field values A< 1.6T< B< 1.8T< C< 2.2T< D< 2.4T< E< 2.6T< F< 2.8T< G< 3.0T< H< 3.2T< I< 3.4T< J< 3.6T

SAWTOOTH ACTIVITY DURING ADDITIONAL HEATING IN JET

R D Gill, D V Bartlett, G Bracco[+], D J Campbell, S Corti, A E Costley, A W Edwards, W Engelhardt, H-U Fahrbach[°], D J Gambier[*], C W Gowers, R Granetz, A Hubbard[X], S E Kissel, N Lopes-Cardozoy, G Magyar, J O'Rourke, E Oord, R Prentice, S Tsuji[Z], B J D Tubbing[y], A Weller[°], J A Wesson, V Zanza[+] and D Zasche[°]

JET Joint Undertaking, Abingdon, Oxon, OX14 3EA, UK. [+] EURATOM-ENEA Association, Frascati. [°] EURATOM-IPP Association, Garching. [*] EURATOM- CEA Association, Fontenay-aux-Roses. [X] Imperial College of Science and Technology, London. [y] EURATOM-FOM Association. [Z]JAERI, Japan

ABSTRACT Sawtooth oscillations have been studied with a wide variety of diagnostics in JET in additionally heated discharges. Multichordal measurements, combined with tomographical reconstructions, have allowed a detailed experimental study of the sawtooth collapse with high time resolution. It is shown that the initial part of the collapse has m=1 topology.

1. INTRODUCTION Sawtooth activity has been studied in JET during both ohmically and additionally heated discharges using a large number of diagnostics, including two X-ray diode array cameras, a 12 channel ECE grating polychromator, four channel Fabry-Perot and Michelson ECE systems, a microwave transmission interferometer, a microwave reflectometer, bolometry and a multi-chord far infrared interferometer. Sawteeth have also been observed by the neutron diagnostics and on the particle fluxes and ion temperatures determined by a set of four neutral particle analysers.

2. SAWTEETH DURING ADDITIONAL HEATING During both neutral injection and radio-frequency heating the sawtooth oscillation increases in amplitude and its period becomes longer (Figure 1). The observation of partial sawteeth is common and the sawteeth are accompanied by a wide range of mhd activity in the plasma central region, generally with m=1.
In particular, we often observe: (i) strong successor oscillations following the sawtooth collapse; (ii) strong mhd activity accompanying the partial sawteeth; (iii) a large saturated m=1 mode which is sometimes seen before the sawtooth collapse during RF heating and (iv) a large amplitude m=1 mode seen during beam heating. The main sawtooth collapse generally occurs without mhd precursors. During ohmic heating typical mhd frequencies of ~ 1 kHz are seen and with ICRH this decreases, sometimes to 250 Hz. With 4.5 MW of tangential beam heating the frequency increases to ~ 5 kHz, corresponding to plasma rotation with $v = 10^5$ ms^{-1}. The radial location and poloidal mode number of the mhd activity in the central region has been studied with both the soft X-ray cameras and the ECE systems. For a particular discharge, the maximum amplitude of the mode occurs at approximately the same minor radius slightly inside the sawtooth inversion radius, regardless of its phase within the sawtooth

cycle. These modes are thought to occur on rational q surfaces and their relation to the q=1 surface is under investigation.

3. THE SAWTOOTH COLLAPSE A detailed study has been made on JET of the rapid (~ 100 μsec) part of the sawtooth collapse with the X-ray and the ECE systems. The two X-ray cameras view the plasma from vertical and horizontal ports at the same toroidal location with 38 and 62 detectors respectively. The detectors are shielded with 140 μgm of Be to enhance their sensitivity to radiation from the central region of the plasma from which the emission is due mainly to He-like Nickel for RF heated discharges and recombination for beam heated discharges.

Further information on the sawtooth collapse comes from the ECE diagnostics. In particular the electron temperature at a fixed radius is measured with very high time (10 μsec) and temperature resolution (30 eV) using a Fabry-Perot instrument and the sawtooth development in both time and radius along a fixed chord is measured with a 12 channel polychromator system with similar resolution.

A typical sawtooth collapse, with successor oscillations, taken during an RF heated discharge, is shown in Figure 2. The letters A-F indicate the times used for Figure 4. A contour plot showing the X-ray signal intensities from the vertical camera as a function of detector number and time, taken at 200 kHz sampling frequency (Figure 3a), shows that the collapse occurs in ≈ 100 μs and in this case with a rapid outward movement of the hot central plasma core. A similar plot for a different sawtooth collapse taken with the ECE polychromator with a digitization frequency of 20 kHz (Figure 3b) shows that the plasma temperature behaves in a similar way to that of the X-ray emission but in this case with an inward movement. These measurements indicate that the initial part of the sawtooth collapse is due to bulk motion of the hot centre of the plasma off axis to r/a ≈ 0.3.

The detailed nature of the collapse and its successors have been studied by tomographic analysis [1] of the data from both X-ray cameras. By fitting the experimental data with radial Zernicke polynamials $\ell=8$ and angular harmonics m=2 (but excluding sin 2θ), the line integrated data observed by each X-ray detector is reduced to a two dimensional function of X-ray emissivity as a function of plasma major radius and height. The tomographic reconstructions were carried out at 5 μs intervals throughout the sawtooth collapse. Some of these reconstructions are shown in Figure 4 in the form of contour plots and illustrate the main features of the collapse. On each plot the relative times are shown and the maximum radiated power, P_m. Initially the hot central core moves rapidly away from the centre with a maximum velocity of 2×10^3 ms^{-1} until it reaches r/a ~ 0.3 where the outward motion stops. The hot region then collapses on a time scale of 100 μs while at the same time the emissivity in the remainder of the central region increases. This implies a mixing of hot and cold plasma regions or rapid conduction of heat during this phase of the collapse. The final emissivity profile is not completely poloidally symmetric and it is the subsequent rotation of this distribution which is responsible for the observations of successor oscillations as can be

seen from Figure 4. In other sawtooth collapses, without successor oscillations, the final state is completely poloidally symmetric.

The tomographic analysis clearly determines the m=1 character of the initial phase of the collapse and the strong n=1 mode seen by the magnetic coils at the plasma edge [2] to accompany the sawtooth collapse then determine the sawtooth collapse as an m=n=1 mode. The initial fast plasma motion occurs at different poloidal angles as expected for m = 1.

Our observations do not generally seem in good agreement with existing theoretical models and in particular are in disagreement with models which require growing or static magnetic islands before the sawtooth collapse

However, a very recent theoretical model[3], in which the plasma motion occurs on a rapid time-scale due to an ideal m=1 mode would account for many of the features of our observations, particularly the observed initial plasma motion.

REFERENCES 1. R S Granetz and J F Camacho, Nuclear Fusion 25, 727 (1985). 2. P A Dupperex, R Keller, M Malacarne and A Pochelon, 12th European Conference on Controlled Fusion and Plasma Physics 1, 126 (1985). 3. J A Wesson, Plasma Physics and Controlled Fusion, 28, 243 (1986)

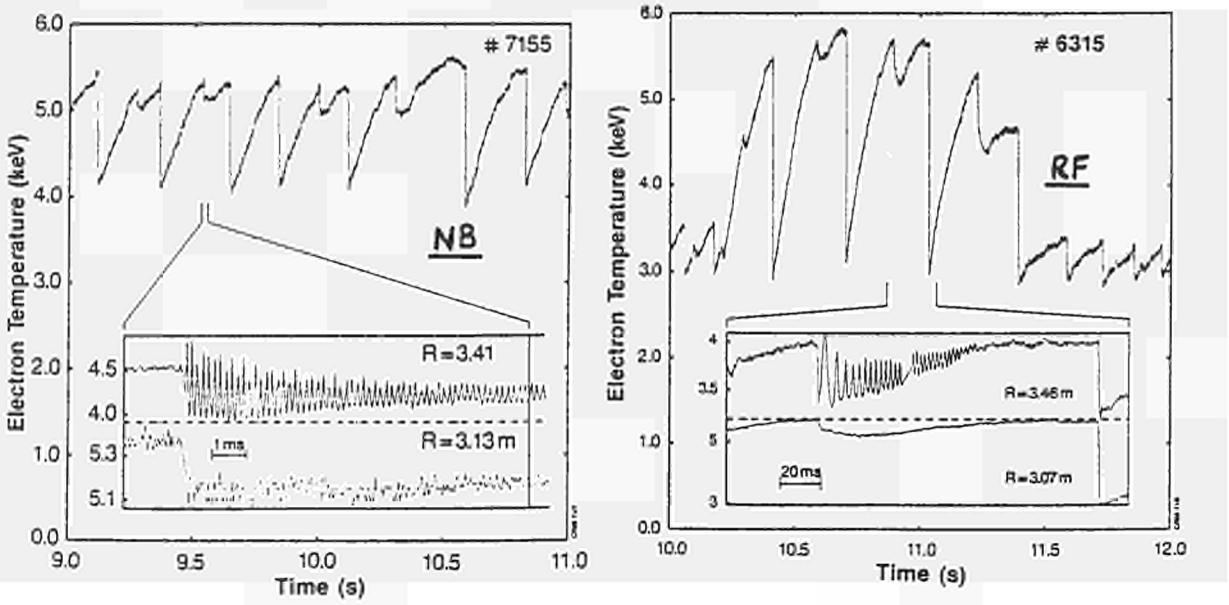

Figure 1 Sawteeth during additional heating. Note the much higher frequency mhd activity during the neutral beam heating.

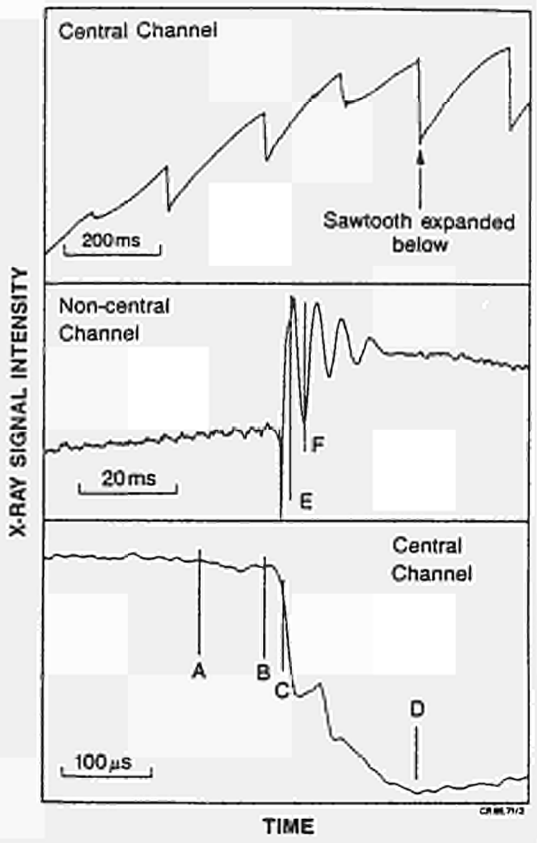

Fig. 2. X-ray signal on different timescales.

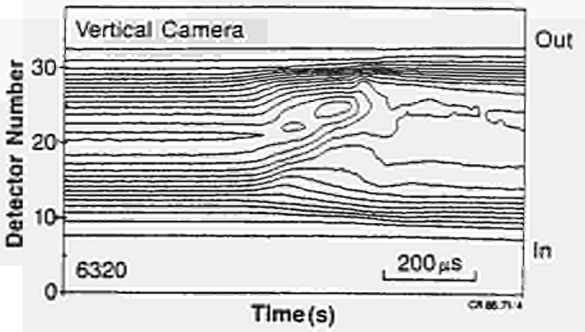

Fig. 3.(a). X-ray contour plot of line integrated intensity during sawtooth collapse

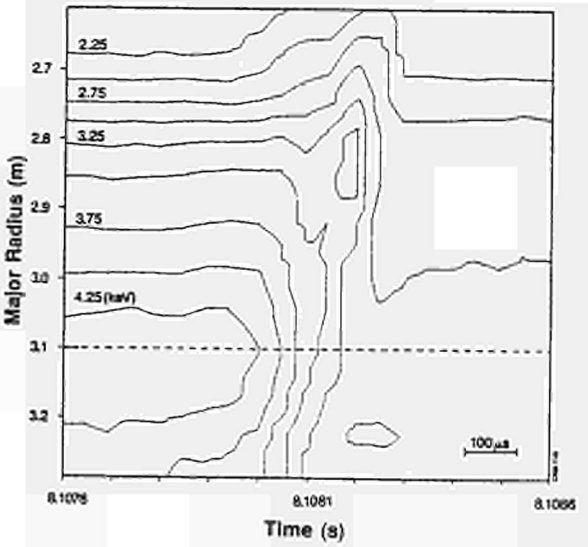

Fig. 3.(b). ECE electron temperature contour plot.

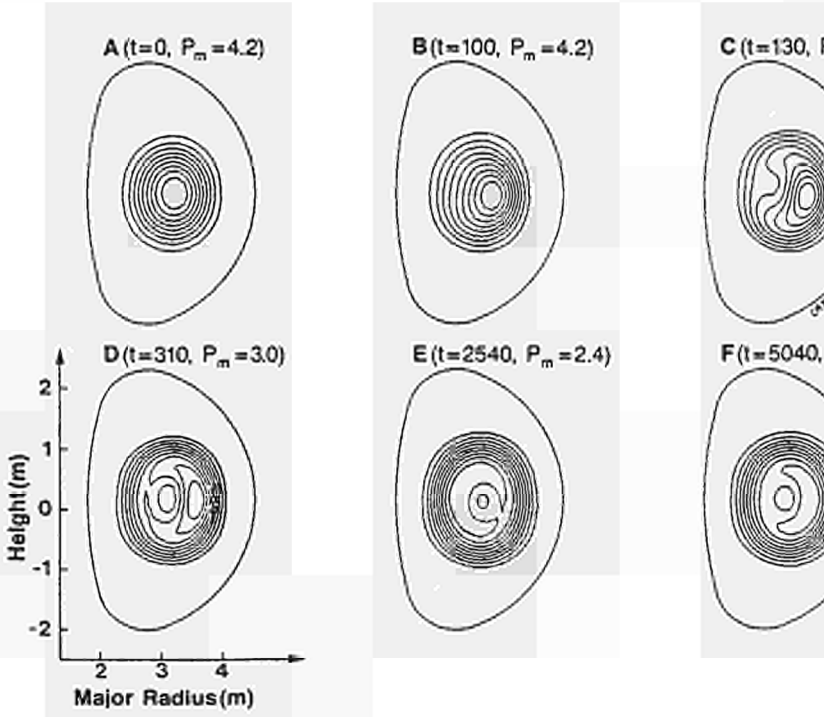

Fig. 4. Contour plots of X-ray intensity versus plasma height and major radius.

IDENTIFICATION OF ION CYCLOTRON EMISSION FROM CHARGED FUSION PRODUCTS

G.A. Cottrell, P.P. Lallia, G. Sadler, P. van Belle

JET Joint Undertaking, Abingdon, Oxon, OX14 3EA

Abstract We have made measurements of the Ion Cyclotron Emission (ICE) Spectrum from JET D^+ ohmic plasmas using an ICRF antenna in reception mode. The spectra (10-100 MHz) show a number of bright emission peaks with (a) frequencies proportional to the magnetic field and (b) intensities correlated with the total DD neutron yield (Y_{DD}) of the discharge. We have compared the observed intensities of the spectra with the thermal black body emission and find the peaks to be of superthermal origin. We examine the hypothesis that the peaks are generated by the confined charged fusion products from the DD reaction which emit ICE at harmonics of the cyclotron frequency and have used a particle orbit tracing code to generate model spectra to assist interpretation of the data.

1. Introduction

The possibility of observing optically thick ($\tau >> 1$) ICE in large and dense thermonuclear tokamak plasmas has stimulated experiments on TFR (CLARK 1984) and JET (COTTRELL 1985) to attempt to measure emission from the thermal ions. However, in large and hot D^+ plasmas, the superthermal population of fusion products radiate significantly in the ion cyclotron frequency range. For deuterium, the following primary reactions take place with equal probability:

$$ {}^2_1D + {}^2_1D \begin{cases} \xrightarrow{50\%} {}^3_2He\ (0.8MeV) + {}^1_0n\ (2.5MeV) \\ \xrightarrow{50\%} {}^3_1T\ \ (1.0MeV) + {}^1_1P\ (3.0MeV) \end{cases} \qquad (1) $$

In addition, secondary reactions can take place between the fast products of (1) and the thermal deuterium:

$$ {}^3_2He + {}^2_1D \rightarrow {}^1_1P\ (14.6MeV) + {}^4_2He\ (3.7MeV) \qquad (2) $$

$$ {}^3_1T + {}^2_1D \rightarrow {}^4_2He\ (3.6MeV) + {}^1_0n\ (14.7MeV) \qquad (3) $$

In experiments reported here we have attempted to identify the mechanism for producing the ICE as emission from charged fusion products. We have done this by deliberately replacing the D^+ plasma ions by H^+ ions in the plasma thereby changing its fusion reactivity and observing changes to the ICE intensity.

2. Experimental

In a sequence of discharges with almost constant overall conditions (I_p = 2.0MA, B_T = 2.6T, $\bar{n}_e = 1.5 \times 10^{19} m^{-3}$), the deuterium ionic fraction was varied by changing the torus filling gas from D_2 to H_2.

Complete replacement of D^+ with H^+ could not be achieved owing to the desorption of residual deuterium from the vessel walls. However, within the range of concentration studied the total DD reaction rate, Y_{DD} (derived from 2.5 MeV neutron flux measurements (JARVIS et. al 1984)) varied by a factor of ~ 6. ICE measurements were made with the system described earlier (COTTRELL 1985); frequency and amplitude calibration of the detection system being made by mixing two standard frequency calibrators (20 and 50 MHz) with the incoming signal. Figure 1 shows two

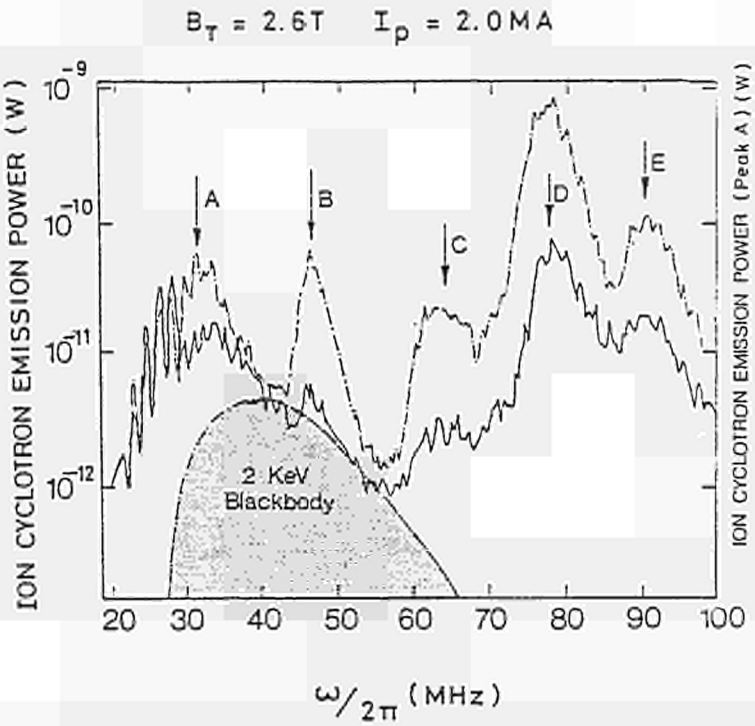

Figure 1: Ion Cyclotron Emission (ICE) spectra from two JET D^+ ohmic discharges with different DD fusion reactivities. Upper (dashed) curve obtained from a discharge with a total fusion neutron yield ~ 6 time the value corresponding to the lower (solid) curve. Other plasma parameters were almost constant. Also shown is the expected thermal black body spectrum ($\omega = 2\omega_{cD}$) from the majority ions.

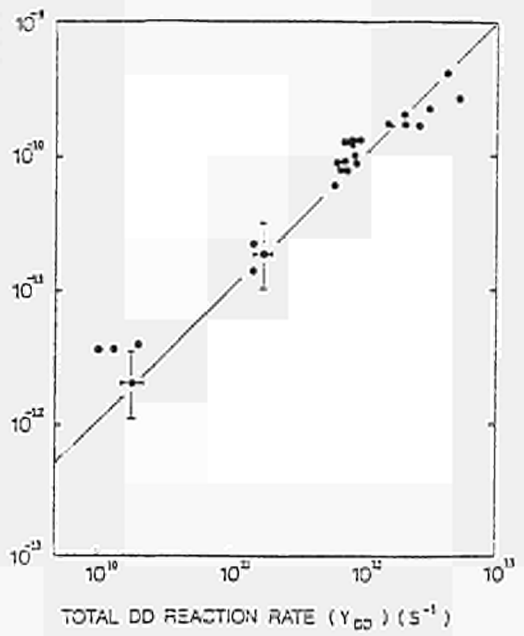

Figure 2: Variation of measured intensity of ICE peak A (see Fig 1) with the total DD reaction rate (Y_{DD}) determined from 2.5 MeV fusion neutron measurements.

superposed spectra from two discharges, each having different values of Y_{DD}. Prominent peaks can clearly be seen in both spectra; qualitatively these spectra are similar to ones published earlier (COTTRELL 1985) in which the frequencies of the peaks were found to be proportional to the applied magnetic field of the discharge indicating a cyclotronic origin. However, in the present experiments we have found the amplitude of the ICE to increase with total DD fusion yield Y_{DD} (Figure 2). The linear correlation of ICE power (of the 31MHz (peak A) in Fig 1) with Y_{DD} is consistent with emission from a primary DD fusion product (Eq.1).

It is of interest to compare the measured ICE level with the expected thermal black body level from the bulk ions (temperature T_i). In the (H)D minority regime we would expect the plasma to be close to optically thick.

The blackbody power which can be coupled to the antenna is then given by: $P_{BB} = kT_i \left[1 - \rho_c^2\right] \Delta f\, \Delta\Omega\, \Delta A$ where ρ_c is the voltage reflexion coefficient at the antenna-plasma interface and Δf, $\Delta\Omega$, ΔA are the receiver bandwidth, antenna solid angle and antenna area respectively. The antenna-plasma coupling resistance has been estimated for frequencies in the range (25-47) MHz by separate transmission and reflexion experiments. Assuming a parabolic form for the radial variation of $T_i(R)$, P_{BB} can be related to emission frequency in a manner analogous to that used in tokamak ECE measurements. The expected thermal spectrum is shown plotted in Fig 1 and suggests that the measured broad underlying component could be thermal radiation. However the bright, narrow emission peaks A, B and C etc are of non-thermal origin.

3. Model

We have attempted to model the basic features of the non-thermal spectrum on the basis that it represents cyclotron emission from the charged fusion products. Even though the birth distribution of the fusion products is strongly localised to the central region of the tokamak discharge, the high energies of these particles leads to significant orbital excursions. For this reason, we have used a code to model the distribution of ICE from the charged products. The code traces the full individual particle orbits (MARTIN 1985). We have modelled the D-shaped JET magnetic topology and have included the Shafranov shift, and divergence-free magnetic fields. At each point along the orbit the contribution to the harmonic cyclotron emission power is calculated. For cyclotron emission perpendicular to the magnetic field, the power radiated in the n^{th} harmonic of the cyclotron frequency, ω_{ci}, of a particle of charge + Ze and perpendicular velocity $v_\perp$ is

$$P_n = \frac{(Ze)^2\, \omega_{ci}^2 N}{8\pi^2\, \varepsilon_o c} \left[\frac{n\, v_\perp\, N}{c}\right]^2 J_n'^2 \left[\frac{n\, v_\perp\, N}{c}\right] \qquad (4)$$

where $N(\sim \omega_{pi}/\omega_{ci})$ is the refractive index of the medium, and J_n' is the derivative of the n^{th} order Bessel function (eg BEKEFI 1966). This expression shows the strong weighting for the emission to particles with high perpendicular velocities. The number of fast fusion products in the plasma is $N^* \sim Y_{DD}\, \tau_S$, where τ_S is the classical slowing down time. In our experiments $\tau_S \sim 0.3$s giving $N^* \lesssim 3 \times 10^{13}$, constituting a fraction $\sim 2 \times 10^{-8}$ of the plasma ions. The optical depth at $2\omega_{ci}$ is $\tau = \frac{\pi}{2} \beta_i R_o \frac{\omega_{pi}}{c}$ where β_i is the ratio of the pressure of the fusion products to the magnetic field pressure. We find $\tau \sim 10^{-5}$ and have therefore neglected the self-absorption of the ICE. In our model, test particles were lauched sequentially, scanning with increments in both velocity and real space in the discharge. By integration over the isotropic birth distribution function thus generated, ICE spectra were synthesized, using Eq. 4. We do not calculate the slowing down spectrum in this model.

For the plasma conditions relevant to the discharges in Fig. 1 we show in Fig.3 the calculated ICE source emission functions for the 3 primary products as well as the α-particle. The amplitude of the α-particle emission has been weighted by 0.02, corresponding to the expected burn-up (of T^-) fraction in the present conditions. The spectra show a number of harmonic emission peaks having the property $\omega \propto B_\phi$ (as seen experimentally), and a significant peak at $\sim$ 28 MHz (close to peak A)

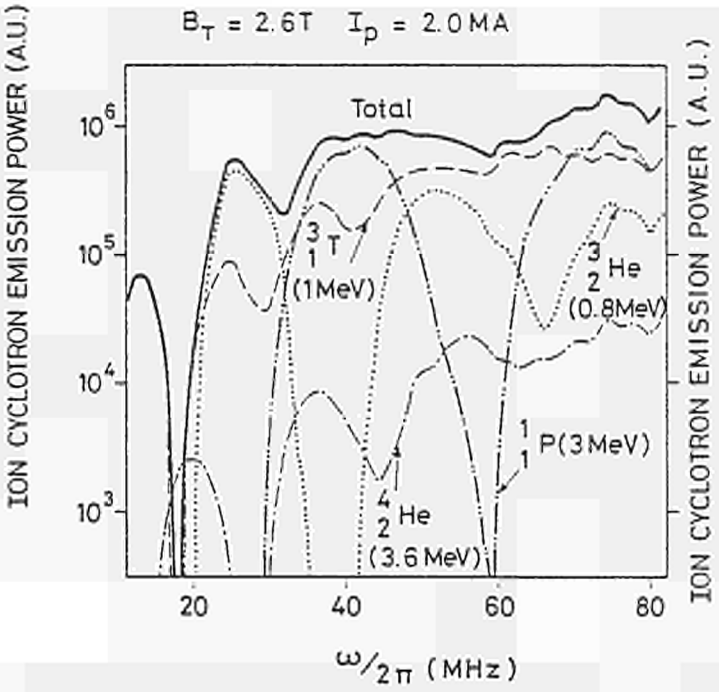

Figure 3: Calculated source emission spectrum from fusion products for conditions of Fig.1. No correction has been made for (i) slowing down of the fusion products, (ii) absorption.

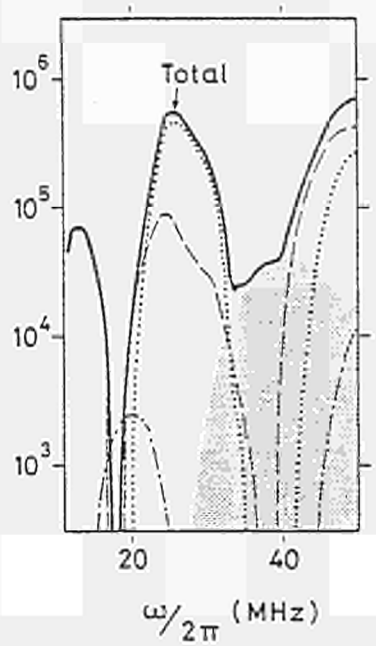

Figure 4: Same as Fig.3 except that absorption at $\omega = 2\omega_{cD}$ has been taken into account coupled with re-emission by the indicated blackbody spectrum (shaded).

coming predominantly from $^3_2$He fundamental radiation. Above 35 MHz the spectra become harmonically overlapped giving a quasi-continuum. Fig. 4 shows the effect of including a bulk plasma absorption model at $\omega = 2\omega_{cD}$. Here it is assumed that the fusion particle radiation from ω_{cH}, 2 ω_{c^4He} and 3 ω_{c^3T} is absorbed by the optically thick plasma and replaced by blackbody radiation at the bulk ion temperature (2 KeV). This model shows reasonable qualitative agreement with the experimental spectrum in the range 25-50 MHz. Above this frequency, uncertainties in the antenna response make detailed comparison more difficult. However we may expect to see bands of absorption at higher harmonic frequencies of the bulk plasma ions; these bands can be thought of as being analogous to the Fraunhofer absorption lines seen in solar spectra.

Acknowledgements:
It is a pleasure to thank Drs J Jacquinot, T Hellsten, C Lashmore-Davies and W Core for useful discussions and M Brandon for help in performing the experiments.

References

CLARK, W H M 1984 Proc. 4th Int Symposium on Heating in Toroidal Plasmas. Rome Vol 1, 385-391. (EUR 9341 EN)

COTTRELL, G A 1985 Proc Workshop on Application of RF Waves to tokamak Plasmas. Varenna Vol II, 710-716. (EUR 10333 EN)

JARVIS O N, GORINI G, HONE M, KALLNE J, MERLO V, SADLER G, VAN BELLE P 1985. Paper 185 in Proc of 12th European Conference on Controlled Fusion and Plasma Physicos, Budapest, Hungary.

BEKEFI, G 1966 Radiation Process in Plasmas. Wiley, Page 180

MARTIN, G 1985 Doctoral Thesis, Universite de Paris-Sud. Orsay N°694 France.

PROFILE CONSISTENCY AND ELECTRON ENERGY TRANSPORT MODELS

A. Taroni and F. Tibone

JET Joint Undertaking, Abingdon, Oxon. OX14 3EA, UK

INTRODUCTION

Results from several tokamaks have been recently interpreted invoking the concept of "Profile Consistency" (PC) first introduced by B. Coppi [1].

There does not seem to be a unique definition of PC (see for example [2-6]). Here we adopt the following definition: in tokamaks, with and without auxiliary heating, the plasma relaxes to a state with a "canonical" temperature profile

$$T_e(r) = T_{e2}\, f(r,\alpha), \tag{1}$$

T_{e2} being the temperature at a radius r_2 close to the plasma boundary and outside which atomic processes and transport not related to PC dominate [5,7]. α represents a "shape" parameter that can depend on global parameters such as q_a (safety factor at the boundary), I_p (total plasma current), B_t (toroidal field), poloidal or toroidal β. The family

$$f(r,\alpha) = \exp\left[\alpha\left(1 - \frac{r^2}{r_2^2}\right)\right] \tag{2}$$

was originally proposed [2] as "canonical" shape, and we shall mainly refer to it. However, we assume eq(1) to be valid in general only outside the region dominated by sawtooth activity ($r > r_1 \approx r(q=1)$). Thus other expressions for f may turn out to be more appropriate. Theory and/or experimental results are supposed to provide the information necessary to determine $f(r,\alpha)$ [8].

2. DERIVATION OF χ_{ePC}

Our approach will be an empirical one. We assume PC with some $f(r,\alpha)$ and derive a series of consequences for models used in transport codes, modifying and somewhat clarifying previous work in this direction [3].

Following [2,3,9] we derive χ_e from the steady-state electron thermal energy equation:

$$\chi_e(r) = -\frac{\int_{r_1}^{r}(P_\Omega + P_{aux} + S_e)r\,dr + \Phi_1}{r\, n_e(r)\, \partial T_e/\partial r} \tag{3}$$

where P_Ω is the ohmic input term, P_{aux} is the auxiliary heating term for electrons and S_e includes all other local sources and sinks in the equation. Φ_1 is proportional to the electron heat flux at $r=r_1$ and convection is neglected.

Eq.(1) can be used to eliminate $\partial T_e/\partial r$ from eq.(3) [3,9]. Furthermore, for any $f(r,\alpha)$ it is possible to eliminate T_{e2} by introducing $T_e(r)$, thereby obtaining a transport coefficient constrained by PC and expressed in terms of r, local quantities, α and integral quantities.

Clearly χ_e derived in this way (χ_{ePC}) cannot be expected to be valid far from the relaxed state. We assume it to be valid after the current distribution has relaxed (e.g. flat top of I_p in JET).

If the profile shape (2) is assumed, one obtains

$$\chi_{ePC} = \frac{1}{2\alpha} \frac{r_2^2}{r^2} \frac{\int_{r_1}^{r} (P_\Omega + P_{aux} + S_e) r dr + \phi_1}{n_e(r)\, T_e(r)} \qquad (4)$$

Notice that P_{aux} is treated on the same footing as P_Ω in this expression. If one considers a clean ohmic plasma with $T_e \sim T_i$, and $r_1 = 0$, then

$$\chi_{ePC} = \frac{1}{2\alpha} \frac{r_2^2}{r^2} \frac{E\, I(r)}{n_e(r)\, T_e(r)} = \frac{r_2^2\, V\, B_T}{2\alpha\, \mu_o\, R^2 n_e(r)\, T_e(r)\, q(r)} \qquad (5)$$

where E is the (radially constant) electric field, I(r) the current inside r, V the resistive loop voltage, R the plasma major radius and μ_o the vacuum magnetic permeability. Eq.(5) gives essentially the Coppi-Mazzucato-Gruber coefficient [10], which approximates the χ_e derived in [2].

The main difference between χ_{ePC} (5) and the coefficients proposed in [2,3] is due to the further assumption of a scaling, including a weak n(r) dependence, for some global quantity (e.g. V) made in [2,3]. It seems to us that if PC holds, any global scaling (including V, the energy replacement time and its degradation with auxiliary heating) must follow (given the density, a resistivity model, the impurity content and an ion transport model) from:

- choice of $f(r,\alpha)$ and possibly a scaling of α (i.e. numerical coefficient in χ_e) in terms of global quantities (PC contribution);
- plasma boundary model (or in its absence a scaling for r_2 and T_2);
- effects of sawtooth activity.

The problem of connecting the PC region of the plasma with the sawtooth dominated region needs further investigation. Sawtooth activity can be reconciled with steady state only considering time averages over a sawtooth period. For example one can assume $\phi_1 = \int_0^{r_1} (P_\Omega + P_{aux} + S_e) r dr$. This prescription is consistent with the simplest model of sawtooth activity: an enhanced χ_e for $r < r_1$. It can be used also with "reconnection" models and other choices of χ_e for $r < r_1$. However other expressions of $\phi_1 = \phi_1(t)$, possibly more consistent with a "pulsating" model of sawteeth, are to be looked for. Notice the connection between the choice of $\phi_1(t)$ and the problem of the velocity of propagation of the heat pulses induced by a sawtooth collapse.

We observe that other empirical transport coefficients are closely related to PC. For example the assumption $f(r,\alpha) = 1 + (\alpha/T_2)(r_2 - r/r_2)$ leads, under the same approximations used to derive eq.(5), to $\chi_e = \frac{r_2 V B_T r}{\alpha \mu_o R^2 n(r) q(r)}$. This coefficient is close to the Nec-Alcator one.

3. NUMERICAL RESULTS

The coefficient χ_{ePC} given by eq.(4) has been extensively and successfully tested for JET ohmic discharges. Encouraging preliminary results have been obtained also for a number of RF heated discharges.

Figure 1a shows the temperature profiles computed with χ_{ePC} in our transport code, for ohmic discharges at different densities. They have been obtained with $r_2 = a$ (the plasma radius) and prescribing T_{e2} according to the observed experimental trend (Fig.1b); $\alpha = 2.85$ has been used.

The influence of the plasma boundary transport model is illustrated in Fig. 2. We assumed $\chi_{eb} \propto \chi_{eBohm}$ when $r > r_2$ (= .8a). In this case T_{e2} changes by changing χ_{eb} and the entire temperature profile follows.

Figure 3 shows results obtained with χ_{ePC} and RF heating. Again T_{e2} was prescribed according to the experimental trend and $\alpha = 2.85$.

The acceptable agreement between computed and experimental temperature evolution implies that χ_{ePC} can indeed be used outside steady state.

4. CONCLUSIONS

Simple considerations allow to derive a transport coefficient χ_{ePC} that we regard as being "genuinely PC". In comparison, coefficients derived in [2,3,9] are to be considered as "quasi-PC". A particular choice of χ_{ePC} has been successfully tested in the simulation of JET discharges.

Our analysis shows that the success of $\chi_{eCMG} \approx \chi_{ePC}$ in simulating ohmic discharges in completely different devices can be explained by:

- the underlying "canonical profile" is close to reality and no strong change of α is needed in different cases;
- a "hidden" scaling is introduced in computations using χ_{eCMG} when the boundary value of T_e is changed. This aspect has alwaysbeen dispregarded in the past.

Choices other than (2), possibly less optimistic, are however possible for the "canonical profile", leading to other expressions for χ_{ePC}.

In the absence of a quantitative theory and of more detailed experimental observations on PC, our analysis and results are to be considered only as indications that transport models can be modified to introduce the constraint of PC. This must and can be done taking into account appropriate models for the central and the boundary plasma region.

REFERENCES

[1] B. Coppi, comments Pl. Phys. and Cont. Fus. 5, 261 (1980)
[2] B. Coppi and E. Mazzucato, Phys. Letters 71A, 337 (1980)
[3] B. Coppi, Fizika Plazmy 11, 83 (1985)
[4] P.H. Rebut and M. Brusati, Pl. Phys. and Cont. Fus. 28, 113 (1986)
[5] H. Furth, Proc. Varenna Workshop on Fusion Plasmas, 1985
[6] B.B. Kadomtsev, Pl. Phys. and Cont. Fus. 28, 125 (1986)
[7] R.J. Bickerton et al., Royal Society Meeting on the JET Project, 1986
[8] D. Bartlett et al., this conference
[9] F. de Luca et al., 27th An. Meeting of Division of Plasma Physics of APS, San Diego, USA, 4-8 November 1985
[10] O. Gruber, Nuc. Fus. 22, 1349 (1982)

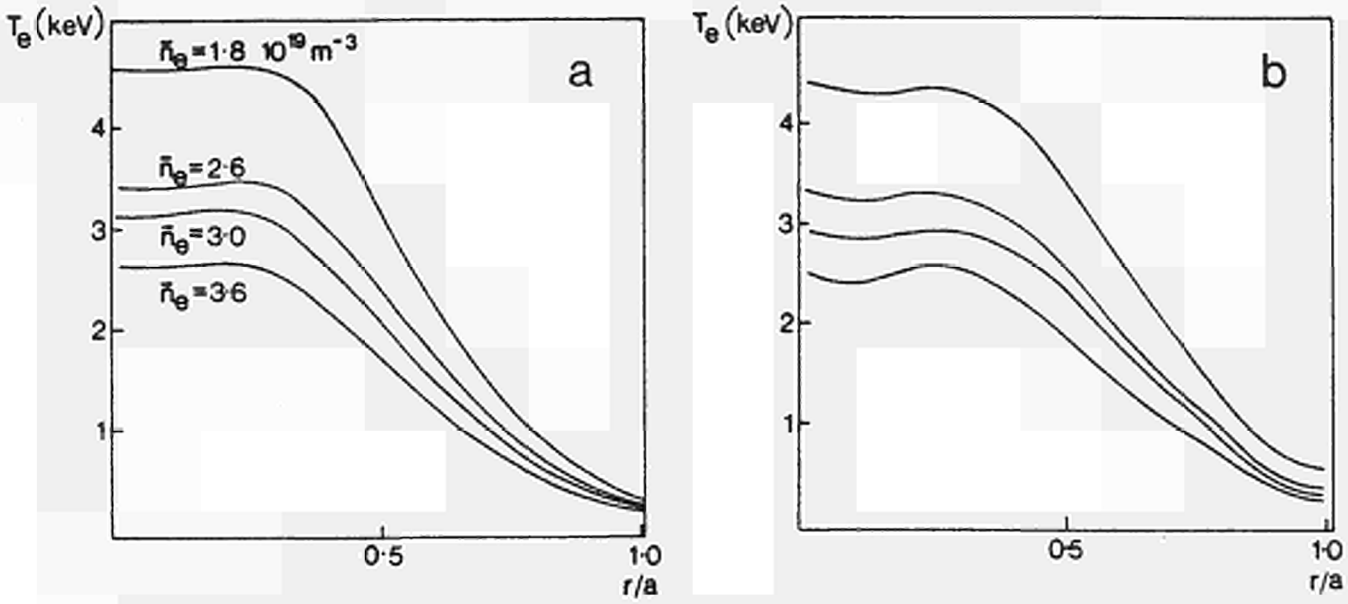

Fig.1 - Steady-state (sawtooth averaged) electron temperature profiles for a density scan at B_t= 3.4 T , I_p= 4.0 MA in JET : a) computed using $\chi_e(0<r<a) = \chi_{ePC}$; b) experimental data (ECE).

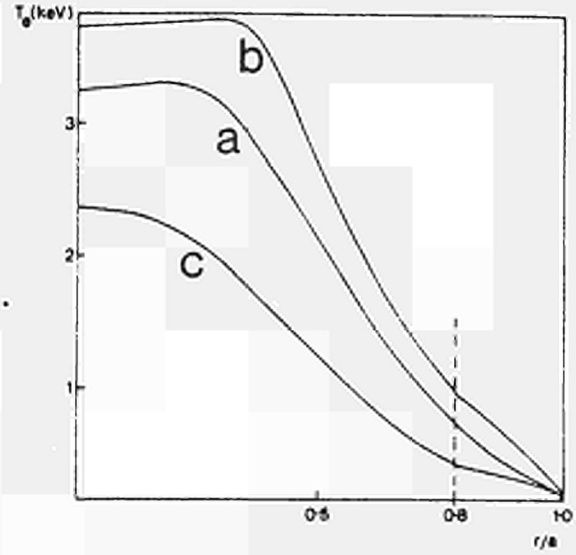

Fig.2 - Profile sensitivity to changes in the boundary model: three numerical experiments were performed using χ_{ePC} given by eq.(4), α=2.85 and
a) r = a
b) r = 0.8a and $\chi_e(r>r_2)$=0.1 χ_{eBohm}
c) r = 0.8a and $\chi_e(r>r_2)$= 2 χ_{eBohm} .

Fig.3 - Experimental data from ECE and numerical results (thicker lines) for an RF-heated JET discharge with $P^{tot}_{aux}/P_\Omega \sim 3$:
a) time evolution of peak and volume-averaged electron temperature ;
b) T_e-profiles before and during RF (three ECE profiles during the same RF-heated sawtooth are shown) .
In the simulation $\chi_e(r<r_1) \propto \chi_{eBohm}$ and T_{ea} is increased by 50% during RF.

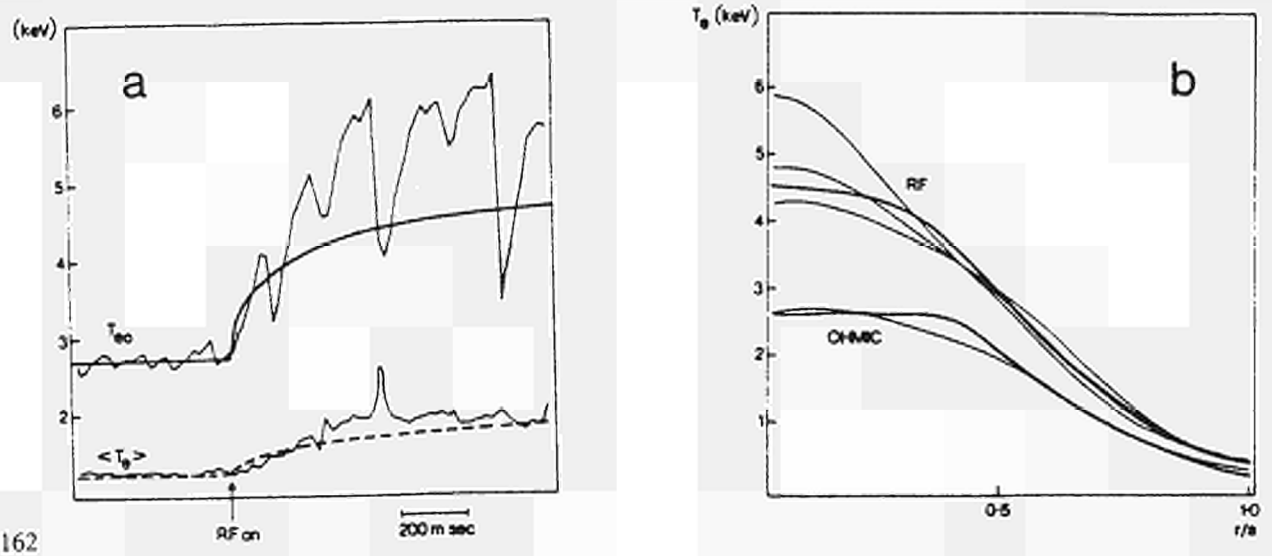

3-D MONTE-CARLO COMPUTATIONS OF THE NEUTRAL TEMPERATURE AND DENSITY DISTRIBUTION IN JET DISCHARGES

R. Simonini, A. Taroni

JET Joint Undertaking, Abingdon, Oxon., OX14 3EA, UK

INTRODUCTION - Detailed knowledge of the density and temperature of background neutrals in the JET bulk plasma is necessary for the interpretation of measurements such as charge-exchange emission spectra for NPA analysis. On the other hand, transport codes need averages of those quantities for evaluating source and sink terms.

The purpose of this work is to calculate as accurately as possible the distribution of the neutrals by means of 3-D Monte-Carlo codes, including the effects of toroidicity, non-circularity of the plasma cross-section and poloidal and toroidal asymmetries due to the limiters.

The results are used to assess the validity of simpler and faster models based on assumptions such as circular cylindrical plasma symmetry. Such codes are routinely used both for predictive and interpretative computations at JET.

Typical ohmic JET discharges at low and high plasma densities have been considered. For the calculations, the 3-D Monte-Carlo code NIMBUS [1] and an upgraded (3-D) version of the 1-D Monte-Carlo code AURORA [2] code have been used. For comparison with simpler models, the 1-D code FRANTIC [3] (upgraded so as to include a model of wall interactions) and the model for neutrals used in the ICARUS code [4] were selected.

GEOMETRY - The plasma and the chamber 3-D structure are considered in the following "complementary" way in codes AURORA and NIMBUS. NIMBUS does not allow for an exact treatment of toroidicity, but is otherwise very flexible in its geometry: it can model a general straight cylinder, with a largely arbitrary configuration in the poloidal plane; different materials can be assigned at various heights, with possibly periodic boundary conditions. Particle motion is fully 3-D. AURORA on the other hand can only model poloidal cross-sections defined by two matching semi-ellipses to allow for some degree of triangularity, but with full toroidicity. Taking into account these features, a configuration of eight 3-D limiters have been considered in NIMBUS, neglecting essentially only the toroidal curvature. In AURORA these limiters are replaced by a 2-D belt lying on the wall, thus the main approximation is the absence of any limiter shadow both in the toroidal and radial coordinate.

For the 1-D calculations, the toroidal elliptical shells are replaced by area-preserving cylindrical circular shells. The limiters are taken into account only for ion recycling, while their area is neglected for neutral reflection which is considered to take place on walls only.

PHYSICAL MODEL - The physical model in all codes assumes that the plasma characteristics remain fixed in the calculation. Electron temperature and density profiles are read from JET Processed Pulse File (PPF). The ion density profile is obtained by scaling the electron density by a depletion factor (typically, $n_i/n_e = 0.6\text{-}0.8$). The ion temperature is made up by

taking the axial and average temperatures and then setting up a profile that follows that of the electrons.

Test particles are neutral atoms or molecules (these for NIMBUS only). Target particles are electrons or deuterium ions. Impurities are only taken into account by assuming different densities for electrons and ions. No interaction neutral/impurity is considered.

Wall and limiters are assumed to be fully saturated, and the total ion flux to the first wall is considered to be one tenth of the total flux, the rest going to the limiters.

The neutrals are created either by recombination or by interaction of the scrape-off layer plasma with the carbon limiters and the chamber wall. Interactions with the chamber wall and the limiters are simulated by instantaneous backscattering or re-emission. NIMBUS allows for re-emission in both atomic and molecular state. The processes considered for neutral ion interactions are charge-exchange, ionisation by electron impact, recombination. In NIMBUS, also molecular dissociation and ionisation.

RESULTS AND DISCUSSION - We report here results from two typical ohmic shots, one at low density, $n_e = 8.4 \times 10^{12} cm^{-3}$, and one at high density, $n_e = 3.2 \times 10^{13} cm^{-3}$. Since NIMBUS and AURORA feature complementary approximations to a "full" 3-D geometry, a cross-check of their results has been performed to assess the relevance of these approximations. As for toroidicity for JET, AURORA has been run with different aspect ratios. It turns out that toroidicity plays a negligible role, all the discrepancies being well within the statistical errors. As for the importance of the 3-D structure of the scrape-off layer, comparisons of results from AURORA with results with NIMBUS averaged over the toroidal direction show that the presence of a 3-D scrape-off leads to an increase on the boundary neutral density of about 25%. Here NIMBUS was run with the option of re-emission in atomic state. One may add at this point that re-emission in molecular state leads to a decrease in neutral density of about 30%.

Poloidally averaged neutral density profiles computed by NIMBUS, namely $n_H(r,\phi)=1/(2\pi)\int n_H(r,\phi,\theta)d\theta$, are plotted in Figs. 1,2 along the toroidal direction as functions of the distance from the limiter centre. A molecule is counted as two atoms. At limiter level, the neutral density drops by almost two orders of magnitude over a distance of 1.5m.

The toroidally averaged neutral density profiles obtained by AURORA at various radii are shown in Figs. 3,4 for different minor radii at the mid-plane, as functions of the poloidal angle. A marked poloidal asymmetry is present. In this case, an asymmetry is present even in the neutral temperature. In the high-density case, the asymmetry is more localised in front of the limiter, and practically negligible as far as neutral temperature is concerned.

Poloidal and toroidal averages of neutral densities from 3-D AURORA are compared with 1-D (i.e. cylinders with circular cross-section) results in Figs. 5,6, including AURORA in the 1-D mode. For the Monte Carlo simulations, the statistical errors for the computed radial profiles are of the order of few percent at the boundary, and 15% at the centre of the discharge. We see that the shape of the plasma has some bearing in the case of low density. Here the circular 1-D AURORA overestimates the neutral density at the boundary and underestimates it at the centre by about 50%, due probably to the larger distance between source and centre in this boundary-recycling dominated case. For the same shot, the FRANTIC code

overestimates the central neutral density when compared to 1-D AURORA. ICARUS, instead, estimates the density well, but the central neutral temperature is somewhat overestimated. At high density, the agreement of the models is generally better, except for the density from ICARUS, which is overestimated by about 70%.

SOME SENSITIVITY RESULTS AGAINST BACKGROUND ASSUMPTIONS - The details of the plasma profiles in the scrape-off do not influence noticeably the toroidally and poloidally averaged neutral profiles in the bulk plasma (about 10% for relative variations of the scrape-off e-folding length from 0.5 to 2). In addition, variation of the ratio deuterium/electrons (keeping the electron concentration constant) from 0.8 to 0.5 amounts to negligible variations in the low-density case. For this case the neutral density is also rather insensitive to quite large (30%) changes in the temperature profiles by constant factors. At high density the sensitivity to both changes is larger: 15% at the centre for the variation of the depletion factor, 40% for the variation of the plasma temperature (recombination effects).

Finally, the neutral profiles are not very sensitive to the wall composition, the differences between cases with pure nickel or pure carbon wall being just above the statistical errors.

CONCLUSIONS - Toroidicity and the 3-D structure of the limiters do not appear to have a strong effect on poloidally and toroidally averaged neutral profiles in the bulk plasma, at least for the typical ohmic JET discharges examined.

The simple 1-D models reproduce sufficiently well the radial neutral profiles. This justifies the use of such models in transport codes where only averaged values of neutral profiles are required for source and sink terms. In such codes other inaccuracies are more relevant than those related to uncertainties in neutral profiles of the order estimated above.

However, strong poloidal and toroidal asymmetries in neutral profiles are indeed present. They could play a role that remains to be assessed for problems where only the local neutral density or an average over particular lines of sight is to be considered, e.g. the determination of the ion temperatures from NPA measurements.

REFERENCES -

[1] E. Cupini, A. de Matteis, R. Simonini, "NIMBUS - Monte-Carlo simulation of neutral particle transport in fusion devices", NET Report EUR XII - 324/9.

[2] M.H. Hughes, D.E. Post, "A Monte-Carlo algorithm for calculating neutral gas transport in plasmas", Princeton University Report, PPPL-1335 (1977).

[3] See for instance S. Tamor, "ANTIC: a code for calculation of neutral transport in cylindrical plasmas", JCP 40,104 (1981).

[4] M.L. Watkins et al., Plasma Physics and Controlled Nuclear Fusion Research, 1980 (Proc. 8th Int. Conf., Brussels, 1980) 1, IAEA, Vienna. (1981) 639.

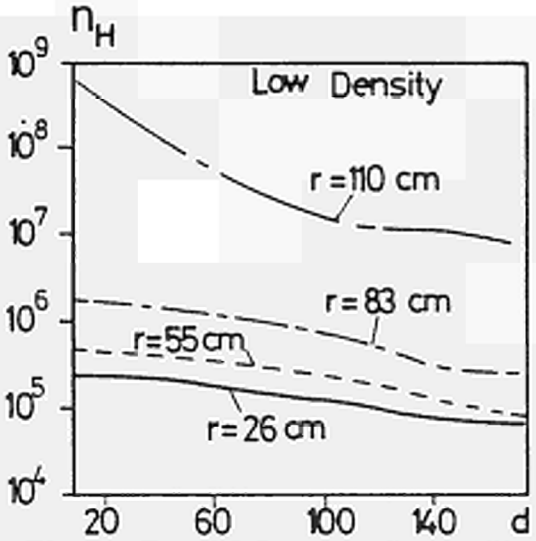

Fig.1 Toroidal neutral density as function of distance from limiter

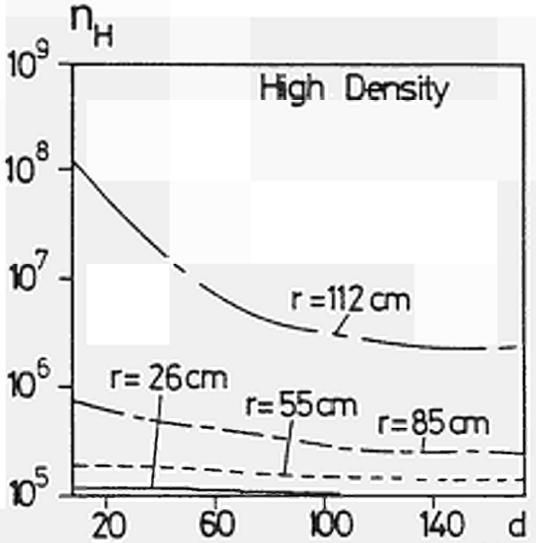

Fig.2 Toroidal neutral density as function of distance from limiter

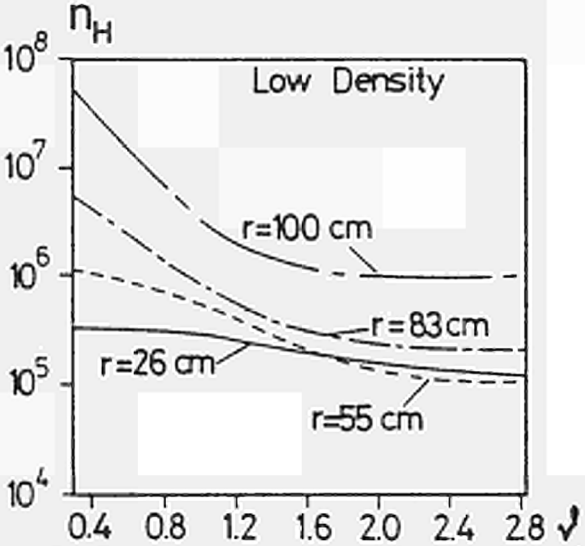

Fig.3 Poloidal neutral density at various radii.

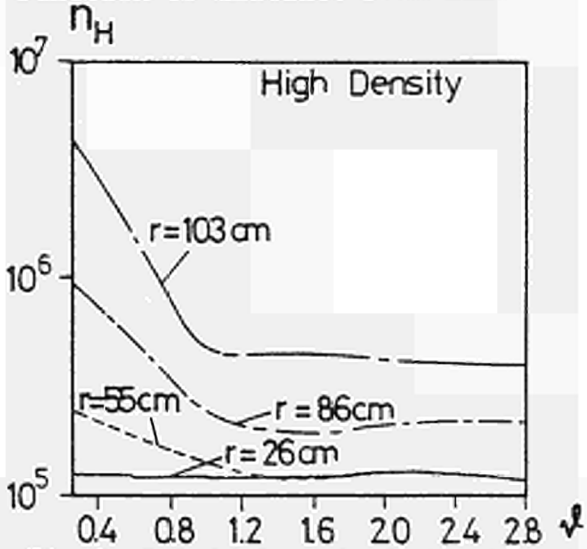

Fig.4 Poloidal neutral density at various radii.

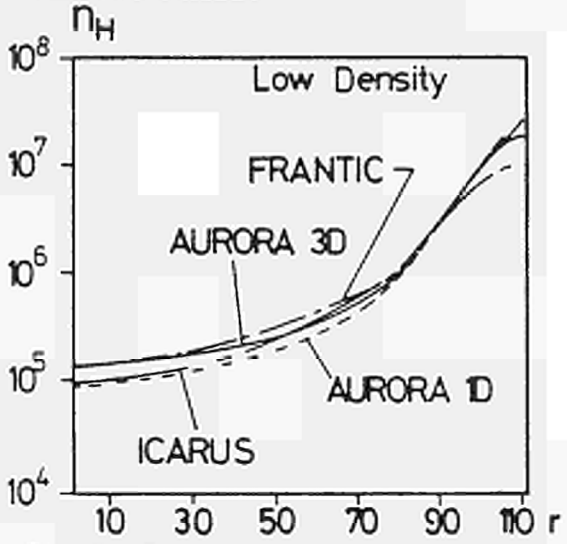

Fig.5 Comparison between models.

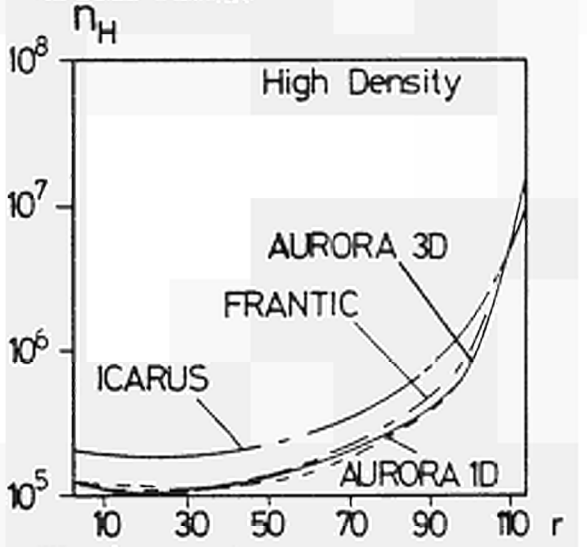

Fig.6 Comparison between models.

DETERMINATION OF POLOIDAL BETA IN JET

G Tonetti*, J P Christiansen, J G Cordey
JET Joint Undertaking, Abingdon, Oxon, OX14 3EA
*Euratom - CRPP Association, Switzerland

Abstract

Magnetic, diamagnetic, density and temperature measurements are used to calculate poloidal beta (β) by three independent methods. Comparison studies are made for a variety of plasma discharges in JET and error estimates are given. The results from the three methods are in good agreement for pulses with currents above 2MA.

1. Definitions and Relations

The poloidal beta (β), the internal inductance (ℓ_i) and the diamagnetic parameter (μ) are defined by the following integrals [1] over the plasma volume

$$\{\beta,\ \ell_i,\ \mu\} = \frac{4}{\mu_o I^2 R_o} \int \left\{p,\ B^2/2\mu_o,\ (B\phi_o^2 - B\phi^2)/2\mu_o\right\} dv \ . \qquad (1)$$

p, B, B_ϕ denote pressure, poloidal field and toroidal field; R_o is arbitary but in practice chosen to be the torus centre. If the plasma pressure is anisotropic and plasma flow is included values $\beta_\perp$, $\beta_{||}$, β_{ROT} are found from (1) by replacing the pressure p respectively with the perpendicular and parallel components of the pressure tensor and with the flow energy [2]. Neglecting the flow energy, two relations are derived [1,2] from (1).

$$\Lambda = \tfrac{1}{2}\beta_\perp + \tfrac{1}{2}\beta_{||} + \tfrac{1}{2}\ell_i = \tfrac{1}{2}S_1 + (1 - \tfrac{1}{2}\delta)S_2 \ , \qquad (2)$$

$$\beta_\perp - \mu = S_1 + \delta S_2 . \qquad (3)$$

The Shafranov integrals S_1, S_2 are evaluated on the plasma boundary via

$$\{S_1,\ S_2\} = \frac{4}{\mu_o I^2 R_o} \int B^2/2\mu_o \left\{r\ \bar{r}\cdot\bar{n},\ R_o\ \bar{R}\cdot\bar{n}\right\} R\ dl \ , \qquad (4)$$

the $\bar{}$ denoting unit vectors in the poloidal r, toroidal R and Z directions and $\bar{n}$ is normal to the boundary; δ in (2-3) is defined in [1]. In this paper we describe 3 calculations of β giving values referred to as follows:

$$\beta_{MHD} = \tfrac{1}{2}\beta_\perp + \tfrac{1}{2}\beta_{||} \ ; \quad \beta_{KIN} = \beta_\perp \ ; \quad \beta_{DIA} = \beta_\perp . \qquad (5)$$

These values are determined from (2), (1) and (3) respectively.

2. The MHD Beta

β_{MHD} is obtained from (2). Λ is given by the integrals (4) obtained from the plasma boundary calculations [3]. For an elongated plasma ℓ_i can be evaluated separately. An empirical formula for ℓ_i in terms of the elongation E, minor

radius a, major radius R_o and the current moment Y_2 has been given in [4].

$$\ell_i = \frac{2E}{1+E^2}\left(C_1 + C_2 \frac{Y_2}{(E^2-1)a^2} + C_3 \frac{8a^2\Lambda}{R_o^2(E^2-1)} \frac{5+E^2}{4}\right) + C_4 \qquad (6)$$

The constants C_1 - C_4 are adjustable parameters. From a study of more than 1000 JET pulses the following values were determined

$$C_1 = 2.15 \quad C_2 = 5.8 \quad C_3 = 1 \quad C_4 = -0.36 \; . \qquad (7)$$

The values (7) have been obtained for JET pulses with $E>1.25$ and $0.9<\ell_i<2$.

3. The Kinetic Beta

The integral $\int pdv$ of (1) is written as

$$\int pdv = e\int_0^1 (n_e(x)\, T_e(x) + n_i(x)\, T_i(x))\, \Omega(x)dx \; , \qquad (8)$$

were $\Omega(x)$ is the volume between adjacent plasma surfaces described by the parameter $0 \leq x \leq 1$. The approximate geometry of the plasma surfaces is derived from the boundary geometry using the Lao-Hirshman parametric description [6]. The plasma profile quantities required to evaluate (8) are obtained or approximated as follows: $T_e(x)$ directly from electron cyclotron emission; $n_e(x)$ from a parametric fit to data from 7 FIR interferometer channels; the ion temperature is assumed to be either

$$T_i(x) = T_{io}^{\text{neutrons}} \frac{T_e(x)}{T_e(0)} \quad \text{or} \quad T_i(x) = T_{io}^{\text{NPA}}(1-x^2) \; , \qquad (9)$$

where the central values T_{io} are calculated from the neutron emission and from the neutral particle analyser (NPA) data respectively; the ion density is $n_i(x) = f_{HD}\, n_e(x)$ with the fraction of hydrogenic species being fixed (usually $f_{HD} \sim 0.5$).

4. The Diamagnetic Beta

This is calculated directly from (3) using S_1, S_2 and δ as previously described. The diamagnetic parameter μ is

$$\mu = \frac{8\pi B_{\phi o}}{\mu_o I^2} \Delta\Phi \; . \qquad (10)$$

In (10) the flux change $\Delta\Phi$ is derived from the measurement $\Delta\Phi_M$ of a diamagnetic loop. The derivation includes compensation techniques implemented by hardware and software. The latter is

$$\Delta\Phi = \Delta\Phi_M - \Delta\Phi_{CX} - \Delta\Phi_{PF} - \Delta\Phi_I \; . \qquad (11)$$

In (11) the subscripts refer to flux change due to: toroidal field coil expansion (thermal and mechanical), coupling from the poloidal coil currents and from the plasma current. The hardware of the diamagnetic loop compensates for toroidal field and eddy currents in the vessel. Further details are given in [5].

5. Comparison of β values

In an isotropic plasma the 3 β estimates should be in close agreement. For a non-isotropic plasma (eg. with strong beam heating) the relations (5) would apply. On JET the values β_{KIN} corresponds to $\beta_\perp$ since the ECE and the NPA diagnostics measure $T_\perp$. For the JET pulses obtained so far non-isotropic effects are small and should not affect the comparison. Figure 1 shows the time evolution of β for 2 JET pulses with ICRH and neutral beam heating. All three methods are in good agreement on the increase of β. A large selection of β values for pulses with different current, field and plasma shape are shown in Figures 2 and 3; each symbol represents a value from one JET pulse chosen at the end of current flat top. Figure 2 shows a good agreement between β_{MHD} and β_{KIN} for the whole range of pulses. Figure 3 also shows a good agreement between β_{DIA} and β_{KIN} for currents above 2MA. For pulses with lower currents further studies of the coupling term $\Delta\Phi_I$ in (11) is needed.

The errors on β_{MHD} arise from the separation formulae (6-7) and are typically ± 0.05.

The errors on β_{KIN} are due to 1) approximate surface geometry ($\Omega(x)$ of(9)) in the axial region, 2) the density profile fit, 3) assumed profiles for n_i, T_i, 4) errors on raw data. The horizontal error bar in Figure 2, 3 assumes relative errors on T_e of 10% and on the density of 5%.

The error on β_{DIA} is proportional to B_ϕ/I^2 times the error on $\Delta\phi$. From measured residual fluxes the error $\Delta\beta_{DIA} = \pm 0.02$ is found for I = 4MA, B_ϕ = 3.4T. A systematic error related to $\Delta\phi_I$ is apparent at low plasma current (Fig 3).

6. Conclusion

For a variety of JET pulses with I>2MA the results from the 3 independent methods of determining β are found to be in good agreement. For I<2MA the compensation of the diamagnetic flux needs to be improved.

References

[1] V D Shafranov, Plasma Physics 13 (1971)757
[2] L L Lao, H St John, R D Stambaugh, W Pfeiffer, GA report A117611 (1984)
[3] J P Christiansen, Integrated analysis of JET data. Submitted to J Comp Physics. JET Report JET-R(86)04.
[4] J G Cordey, E Lazzaro, P Stubberfield, P Thomas, M L Watkins, Workshop on Transport Analysis codes PPL (March 1984)
[5] G Tonetti, J P Christiansen, L de Kock, 6th APS topical conf. on High Temperature plasma diagnostics, Hilton Head Island, South Carolina (March 1986)

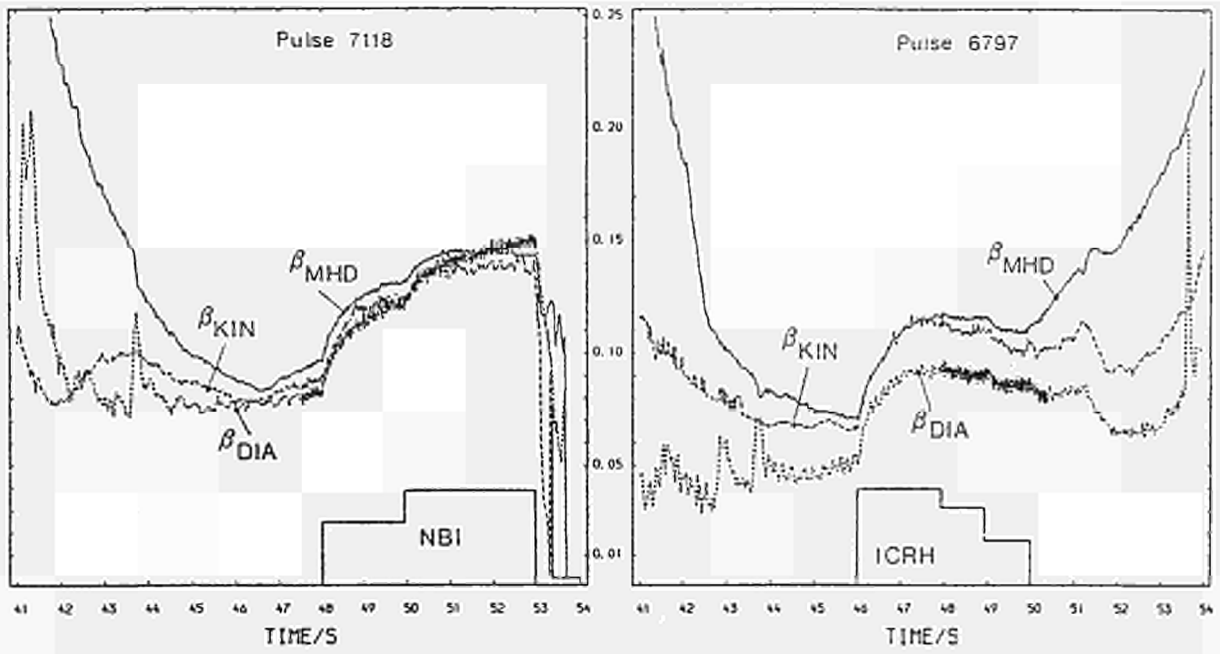

Fig. 1. Time evolution of poloidal beta for a neutral beam heated and an ICRH heated JET pulse. The increase in β is in good agreement for the 3 independent methods.

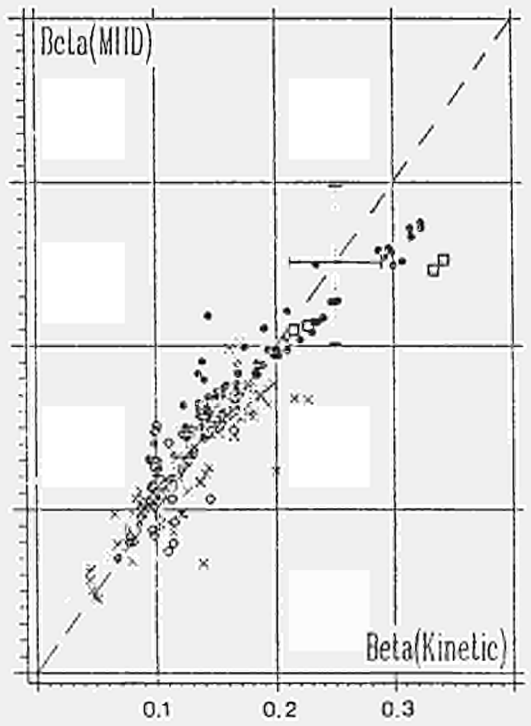

Fig. 2. Values of β_{MHD} vs β_{KIN} for the 1986 (Jan - March) JET pulses. The symbols denote different discharge parameters.

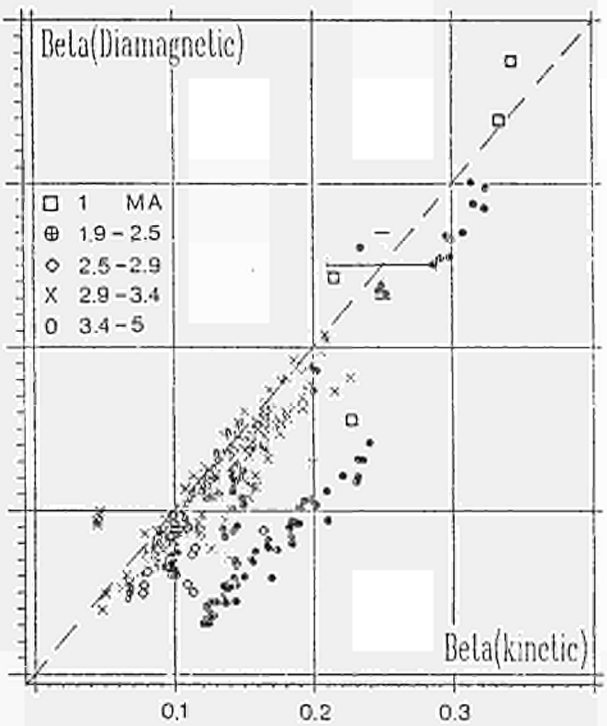

Fig. 3. Values of β_{DIA} vs β_{KIN} the points lying below the line correspond to pulses with currents under 2 MA.

THE EFFECT OF NEUTRAL BEAM INJECTION ON WAVE PROPAGATION IN THE ION CYCLOTRON RANGE OF FREQUENCIES

W.G.F. Core

JET Joint Undertaking, Abingdon, Oxon., OX14 3EA, UK

1. Introduction - The possibility of using neutral injection combined with the fast magnetosonic wave as additional heating of tokamak plasmas is currently of considerable interest and has received some attention in the literature [1]. As is well known, the injection of fast neutral particles leads to the formation of hot energetic ion tails on the bulk plasma ion species. These velocity space distortions modify the dielectric properties of the plasma, and in particular, for heating at the second harmonic frequency, can significantly enhance the absorption of wave energy [2].

In this paper, the effect of NBI on the propagation of waves in the IC range of frequencies is examined. The fast ion component is modelled by superimposing on the bulk plasma ions displaced Maxwellians of the form,

$$f(v_{\parallel},v_{\perp}) = N \exp\left\{-(v_{\parallel}-v_{\parallel_0})^2/\alpha - (v_{\perp}-v_{\perp_0})^2/\beta\right\}. \qquad (1)$$

Using this form of representation for the ion distribution functions the components of the dielectric are obtained in a form which is amenable to efficient computation. The resulting dispersion equation is then solved numerically for fast wave propagation into the beam/ICRF-plasma systems.

(i) Hydrogen beam injection during fundamental ($\omega=\omega_{cH}$) heating of a minority H/D plasma;

(ii) The seeding of a D-plasma with fast deuterons during bulk ICRF heating at ($\omega=2\omega_{cD}$).

2. The Dispersion Equation - Starting from the Maxwell field equations for electromagnetic wave propagation in a hot multi-component magnetoactive plasma the dispersion equation is readily obtained and can be written as

$$\left|k^2\delta_{ij}-k_ik_j-\frac{\omega^2}{c^2}\varepsilon_{ij}\right| = 0, \qquad (2)$$

where the components of the dielectric tensor in the cylindrical coordinate system $\underline{v}=(v_{\parallel},v_{\perp})$ in velocity space takes the form [3]

$$\varepsilon_{ij} = \delta_{ij} - \sum_S \left(\frac{\omega_{ps}}{\omega}\right)^2 \left\{\delta_{ij} + \sum_{n=-\infty}^{n=\infty} \int d\underline{v} \left(\frac{n\omega_s}{v_{\perp}}\frac{\partial f}{\partial v_{\perp}} + k_{\parallel}\frac{\partial f}{\partial v_{\parallel}}\right) \frac{\pi^s_{ij}}{k_{\parallel}v_{\parallel}+n\omega_{cs}-\omega}\right\}, \qquad (3)$$

where $\omega_{ps}^2 = \frac{4\pi Z_s^2 n_s}{m_s}$, $\omega_{cs} = \frac{Z_s B}{m_s c}$, $k_{\parallel}=\underline{k}\cdot\underline{B}$, $\pi_{11}^s = \lambda_n^2 J_n^2$, $\pi_{12}^s=-\pi_{21}^s = iv_{\perp}\lambda_n J_n J_n'$,

$\pi_{13}^s = \pi_{31}^s = v_{\parallel}\lambda_n J_n^2$, $\pi_{22} = v_{\perp}^2 J_n'^2$, $\pi_{23}^s=-\pi_{32}^s = -iv_{\parallel}v_{\perp}J_n J_n'$, $\pi_{33}^s = v_{\parallel}J_n^2$, $\lambda_n = \frac{n\omega_{cs}}{k_{\perp}}$,

$J_n = J_n(v_{\perp}/\lambda_n)$, $J_n' = dJ_n(x)/dx$, and the summation is over all the plasma species (s).

In the local frame of the toroidal magnetic field, where $k_x=k_{\perp}$, $k_y=0$, $k_z=k_{\parallel}$, Eq.(2) takes the form,

$$A_0 k_{\perp}^4 - 2A_1 k_{\perp}^3 + 4A_2 k_{\perp}^2 - 2A_3 k_{\perp} + A_4 = 0, \qquad (4)$$

where $A_0=\varepsilon_{\parallel}$, $A_1=\varepsilon_{13}k_{\parallel}$, $4A_2=k_{\parallel}^2(\varepsilon_{\parallel}+\varepsilon_{33}) - \varepsilon_{\parallel}(\varepsilon_{22}+\varepsilon_{33}) + \varepsilon_{13}^2-\varepsilon_{12}^2$,

$A_3 = k_{\parallel}^3\varepsilon_{13} + k_{\parallel}(\varepsilon_{12}\varepsilon_{23}-\varepsilon_{13}\varepsilon_{22})$,

$A_4 = k_{\parallel}^4\varepsilon_{33} - k_{\parallel}^2(\varepsilon_{11}\varepsilon_{33}+\varepsilon_{22}\varepsilon_{33}-\varepsilon_{23}^2-\varepsilon_{13}^2)$

$- \varepsilon_{11}\varepsilon_{22}\varepsilon_{33}-\varepsilon_{11}\varepsilon_{23}^2+\varepsilon_{33}\varepsilon_{12}^2-\varepsilon_{22}\varepsilon_{13}^2+2\varepsilon_{12}\varepsilon_{23}\varepsilon_{31}$.

3. Calculation of Permitivity Tensor Components ε_{ij} - Introducing plasma species distributions of the form, Eq.(1) into Eq.(3) the components of the tensor ε_{ij} after some reduction take the form:

$$\varepsilon_{11} = 1 - \sum_{i,e}\left(\frac{\omega_{pj}}{\omega}\right)^2 \{1 - 4\pi^{3/2}\sum_{n=-\infty}^{n=\infty}\{(\frac{n\omega_{cj}}{\alpha k_{\parallel}} Z - \frac{1}{2\sqrt{\beta}} Z')I_{n,n}^1 - \frac{n\omega_{cj}v_{\perp o}}{\alpha k_{\parallel}} Z\, I_{n,n}^o\}\},$$

with similar expressions for the remaining ε_{ij}, and where in the above expressions, $Z(x)$ is the plasma dispersion function, $Z' = dZ/dx$, $x = (\omega-n\omega_{cs}-k_{\parallel}v_{\parallel o})/k_{\parallel}\sqrt{\beta}$, and

$$I_{p,q}^m = \int_o^{\infty} dv_{\perp} v_{\perp}^m J_p\left(\frac{k_{\perp}v_{\perp}}{\omega_{cs}}\right) J_q\left(\frac{k_{\perp}v_{\perp}}{\omega_{cs}}\right) \exp\left\{-\frac{(v_{\perp}-v_{\perp o})^2}{\alpha}\right\},$$

$$= \frac{\left(\frac{k_{\perp}}{2\omega_{cs}}\right)^{p+q}}{\left\{\frac{2}{\beta} + \frac{k_{\perp}^2}{2\omega_{cs}^2}\left(\frac{1}{p+1}+\frac{1}{q+1}\right)\right\}^{\frac{p+q+m+1}{2}}} \exp\left\{-\frac{v_{\perp o}^2}{2\beta}\,\frac{2+\frac{k_{\perp}^2\beta}{2\omega_{cs}^2}\left(\frac{1}{p+1}+\frac{1}{q+1}\right)}{1+\frac{k_{\perp}^2\beta}{2\omega_{cs}^2}\left(\frac{1}{p+1}+\frac{1}{q+1}\right)}\right\}$$

$$\cdot \frac{\Gamma(p+q+m+1)}{\Gamma(p+1)\Gamma(q+1)} D_{-(p+q+m+1)}(\mu),$$

where $\mu = \frac{2v_{\perp o}}{\beta}\left\{\frac{2}{\beta} + \frac{k_\perp^2}{2\omega_{cs}^2}\left(\frac{1}{p+1} + \frac{1}{q+1}\right)\right\}^{-\frac{1}{2}}$, and $D_{-a}(\mu)$ is the Parabolic cylindrical function [4].

4. Computational Considerations - To determine the fast wave propagation from the plasma edge to the centre of the discharge Eq.(4) is solved recursively with the full plasma and hot ion dielectric tensor according to the prescription

$$A_o(k_{\perp r-1})k_{\perp r}^4 \ldots A_4(k_{\perp r-1}) = 0.$$

The bulk plasma species profiles take the form

$$T_e(r)=T_i(r)=T(0)\{1-C_1(r/a)^p\}^q,\quad n_e(r)=n_i(r)=n(0)\{1-C_2(r/a)^p\}^q,$$

and in order to model the beam, and in particular, the effects of slowing down, energy diffusion, and pitch angle scattering, we take 3-terms of the form given by Eq.(1), with N_i, α_i, β_i, $v_{\parallel oi}$, $v_{\perp oi}$, i=1,2,3, where for component energy E_i, energy spread ΔE_i, and beam angle θ, $\alpha_i = 2\Delta E_i/m\cos^2\theta$, $v_{\parallel oi}^2 = 2E_i/m\sin^2\theta$, with similar expressions for β_i, and $v_{\perp oi}^2$.

5. Numerical Results - For the aforementioned beam plasma systems we take the standard JET parameters, plasma species temperature $T_e(0)=T_i(0)=2.5$keV, electron density $n_e(0)=3\times10^{13}cm^{-3}$, p=2, q=1, $C_1=0.9$, $C_2=1.0$, beam injection angle at the toroidal axis 45°, minor radius a=125cm, and major radius R_o=296cm. For the beam deposition profile p=2, q=4.

Hydrogen beam injection during fundamental ($\omega=\omega_{cH}$) heating of a minority H/D plasma.

For this configuration, we take E_i=80,60,30keV; ΔE_i=1,5,15keV, N_i=1, magnetic field at the toroidal axis B(0)=2.0T, wave frequency f=33.3MHz, and $k_\parallel = 4\times10^{-2}cm^{-1}$.

In Fig.1 the fast magnetosonic wave propagation characteristics from the edge of the plasma to the centre of the discharge in a minority H/D plasma seeded with energetic protons is shown. For a 15% concentration of plasma minority hydrogen and no beam ions no significant single pass absorption occurs. The effect of increasing the fast ion concentration and maintaining the total minority concentration at 15% leads to enhanced selective wave damping by the injected ions. For 15% concentration of fast ions strong single pass absorption is indicated.

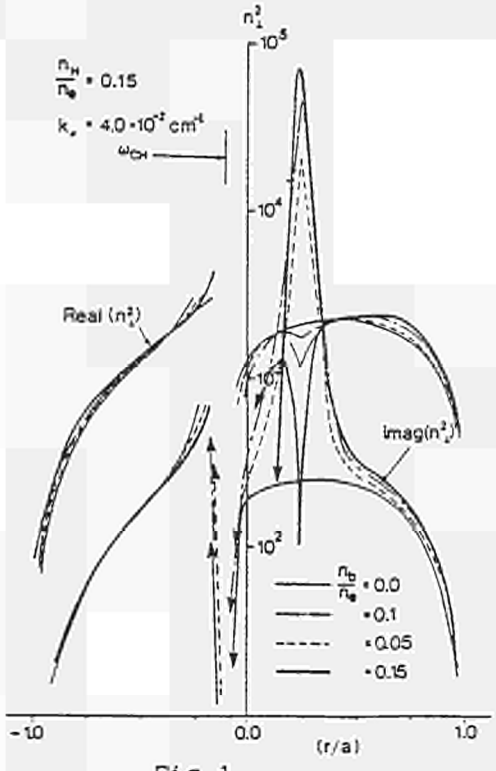

Fig.1

Fast Deuteron injection during ICRF heating of a bulk D-plasma at ($\omega=2\omega_{cD}$).

For this configuration, we take E_i=160,120,60keV, ΔE_i=2,10,30keV, N_i=1, magnetic field at the toroidal axis B(0)=2.03T, wave frequency f=29.8MHz, and $k_{\parallel}=4\times10^{-2}cm^{-1}$.

In Fig.2 the effect of introducing energetic deuterons into a D-plasma on the fast wave propagation characteristics during bulk second harmonic heating is shown. For no concentration of fast ions the absorption occurs on or near the resonant surface $\omega=2\omega_{cD}$. The presence of the fast ion components leads to additional damping at the Doppler shifted resonance surface at R, where $\omega=2\omega_{cD}(R)+k_{\parallel}v_{\parallel}$. The build-up of the fast ion concentration gives rise to strong increasing single pass absorption. However, here finite Larmor radius effects play a crucial role in the damping process.

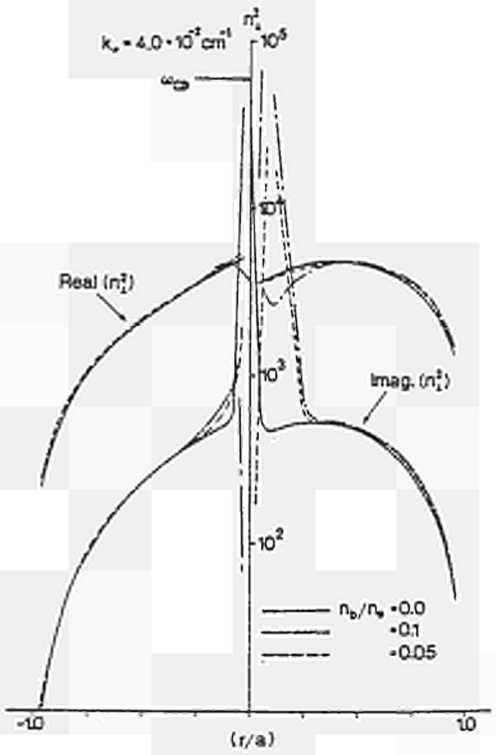

Fig.2

6. Summary - For the model configurations considered here, the preliminary results indicate that the seeding of ICRF heated tokamak plasma systems with fast resonant ions leads to

(i) Strong selective absorption of wave energy by the injected fast ions;

(ii) Damping of the fast wave during fundamental heating of minority ion admixtures is significant even at relatively large concentrations of fast ions.

(iii) For a given injection energy, and for fundamental ICRF operations, near tangential beam injection $\theta\approx0$, provides optimum damping. While for heating at the second harmonic frequency, where finite Larmor radius effects are important, injection in the region of $\theta=\pi/2$ is to be preferred.

Finally, for JET operations with a deuterium bulk, and either hydrogen or deuterium injection, strong damping by the fast particles is predicted.

References

[1] S-I. Itoh, A. Fukuyama and K. Itoh, Nucl. Fusion 24 (1984) 224.
[2] T. Hellsten, K. Appert, W. Core, H. Hamnén and S. Succi, 12th Eur. Conf. on C.F.P.P. (1985) 124.
[3] A. Sitenko, Electromagnetic Fluctuations in Plasmas, A.P. (1967).
[4] M. Abramowitz and I. Stegun, Handbook of Mathematical Functions.

PREDICTIVE STUDIES OF NEUTRAL BEAM AND PELLET INJECTION ON JET

M L Watkins, W A Houlberg*, P Kupschus, P M Stubberfield, A Taroni.

JET Joint Undertaking, Abingdon, Oxon, OX14 3EA, UK.
*Oak Ridge National Laboratory, Oak Ridge, Tennessee, 37831 USA.

1. INTRODUCTION

A 1½-D transport code is used to examine the importance of energy confinement degradation, beam deposition profile, central plasma fuelling and edge pumping in JET plasmas with neutral beam and pellet injection.

2. MAIN FEATURES OF THE TRANSPORT MODEL

The transport models used to simulate JET ohmic plasmas (including target plasmas for neutral beam injection and pellet injection) are basically those used previously [1-3] and include: anomalous electron thermal diffusivity of the ALCATOR-INTOR or Coppi-Mazzucato-Gruber form ($\chi_{eAI} = 5.10^{19} n_e^{-1}$ or $\chi_{eCMG} = 3.10^{15} a B_T n_e^{-0.8} (RqT_e)^{-1} A_p^{-0.5}$); ion thermal diffusivity of the Chang and Hinton form [4]; anomalous diffusive and convective particle fluxes; oxygen/carbon and nickel impurities; neoclassical resistivity; classical energy transfer between electrons and ions; and the K a d o m t s e v reconnection model for sawteeth.

Following [2,3], a full calibration of the ECE temperature measurement removed the need for excessively high anomaly factors ($\alpha_i \geq 10$) on the ion thermal diffusivity, thereby allowing a "conventional" transport model with $\chi_i \leq 5\chi_{iCH} \leq \chi_e$ to be acceptable. The present calculations use $\alpha_i = 4$.

3. NEUTRAL BEAM INJECTION

Neutral beam heating of JET plasmas is simulated using a multiple pencil beam model for additional power and particle sources and by increasing the transport coefficients over their ohmic values.

The birth profile of fast ions is obtained from the attenuation of many filamentary neutral currents by electron impact ionisation, proton ionisation and charge exchange, including capture by impurities. The energy partition to the background ions and electrons is obtained by solving a Fokker Planck equation for the slowing down of fast ions. The power mix assumed for hydrogen and deuterium injection at different energies is given in the Table.

Table

Full Energy/Species (E_o)	Power		
	Fractions at E_o: $E_o/2$: $E_o/3$ (%)	At full energy (MW)	Total (MW)
65kV/H	69:23:8	3.7	5.4
80kV/H	63:29:8	4.2	6.6
80kV/D	76:17:7	7.8	10.3

Confinement degradation during NBI is simulated by increasing outside the q = 1 region the electron thermal diffusivity for ohmic plasmas [2,3] by either a fixed factor, $\alpha_e \leq 2$, or a power-dependent factor, $\alpha_{ep} = {}_o\int^V P_{total,e} dV / {}_o\int^V P_{OH} dV$.

Simulations of the ohmic deuterium discharges of [2,3] but with hydrogen or deuterium neutral injection at 80kV indicate that maximum central temperatures are reached after only 0.8-1.3s of additional heating and subsequently decrease as the centre is shielded from the neutral beams with increasing density from beam fuelling. The highest temperature is achieved at the lowest starting density and with deuterium injection. These effects have been observed in the first experiments with NBI on JET. In particular, simulation of the medium density discharge (JET Pulse #7145) fuelled to high densities by neutral injection at 65kV shows the subsequent fall in the electron temperature from its peak after approximately 0.5s of heating (Figure 1). The calculated beam deposition profiles at the beginning and end of injection are shown in Figure 2. High ion temperatures have been achieved in low density plasmas by pumping the edge particle flux by moving the plasma off the outer limiters, towards the inner wall. The low density discharge (JET Pulse #7155) heated to high ion temperatures by neutral injection at 65kV is also well simulated (Figure 3). Even higher ion temperatures are predicted with the above models with deuterium injection at 80kV, provided beam fuelling is compensated by edge pumping (Figure 4).

4. PELLET INJECTION

The penetration of frozen hydrogenic pellets is calculated using a model that has been tested against TFTR, ISX-B and ALCATOR-C data [5]. The pellet surface is protected by a neutral gas shield of thickness given by the hydrodynamic solution of the gas expansion assuming spherical symmetry [6] and a "tube" of cold ionised plasma, which extends along the magnetic field. The heat flux to the pellet surface is calculated from convective flows of electrons along the magnetic field through both the tube of cold plasma and the dense neutral gas shield and fast neutral beam ions normal to the magnetic field only through the neutral gas shield, which they can enter since their gyro-orbits are larger than the effective pellet ionisation radius.

Calculations using the stand-alone code for pellet injection indicate that pellets up to 6mm diameter and speeds up to at least $10 kms^{-1}$ are necessary to penetrate to the centre of JET discharges with central densities and temperatures up to $10^{20} m^{-3}$ and 10keV respectively. Solid curves in Figure 5 show the penetration for electron ablation only and a fixed ratio between the thickness of the ionised plasma tube and the cold neutral gas shield. It should be added that when the thickness of the ionised plasma tube is kept fixed at 0.35cm (as derived from TFTR bench mark tests) smaller gains in the penetration depth are found with increasing pellet speed. For these cases, the penetration of low speed pellets, in particular, is strongly reduced by ablation by fast ions from 10MW of deuterium injection at 160kV (dashed curves).

Full transport code calculations indicate that lower edge recycling fluxes are achieved with peaked density profiles maintained by continuous pellet injection and pumping. However, radiated power losses equal to the ohmic input power can result after relaxation of the density profile, and although this situation can be avoided by additional heating, when all this power has been used to reach conditions close to ignition, reheat of the plasma is not possible with this model in which pellet injection does not lead to improved confinement.

5. CONCLUSIONS

The expectations of neutral beam injection theory and confinement degradation are borne out by NBI on JET, with respect to both high density plasmas, in which the electron and ion temperatures are similar and the energy confinement is severely reduced and high temperature plasmas, in which the ion temperature exceeds the electron temperature and energy confinement is little affected when pumping the edge particle flux allows low densities to be maintained.

The predictions of pellet injection on JET indicate that a push towards $10 kms^{-1}$ appears to be warranted for JET, with somewhat improved penetration in the absence of fast ion effects and as a means of recovering penetration to the central plasma in the presence of fast ions. The potential disadvantages, including substantial radiation losses and the failure to recover ignition-like conditions after pellet injection (unless confinement improves) should be considered together with the potential benefits, including lower edge fluxes, peaked densities and high edge temperatures obtained with continuous pellet injection and pumping.

ACKNOWLEDGEMENTS

We are indebted to members of the JET Experimental Department for the experimental data we have presented or quoted.

REFERENCES

[1] Behringer, K.H. et al, in Plasma Physics and Controlled Nuclear Fusion Research (Proc. 10th Int. Conf., London, 1984) 1, IAEA, Vienna (1985)291.

[2] Taroni, A. et al, Proc. 12th Eur. Conf. on Cont. Fusion and Plasma Physics, Budapest, 1985, 9F(I), EPS (1985)22.

[3] Taroni, A. et al, Varenna Workshop August/September 1985 (1985).

[4] Chang, C. S. and Hinton, F. L., AMPC Report 14-011 (To be published in Physics of Fluids) (1985).

[5] Houlberg, W.A. et al, Bull. Am. Phys. Soc. 30 (1985)1630.

[6] Milora, S.L. and Foster, C.A., IEE Trans. Plasma Sci. PS-5 (1978)12.

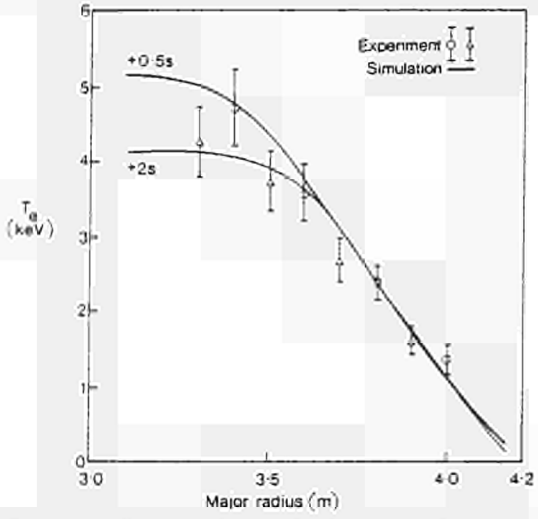

Fig 1: Comparison between theory and ECE measurements of the electron temperature profile for JET pulse #7145 after (a) 0.5s of NBI, model $2\chi_{eCMG}$ and α_{ep} and (b) 2s of NBI, model $0.4\chi_{eAI}$ and α_e=1.5.

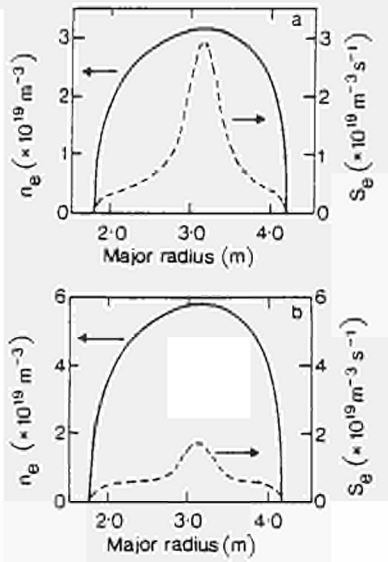

Fig 2: Density profiles and particle source rates at (a) the beginning and (b) the end of neutral injection.

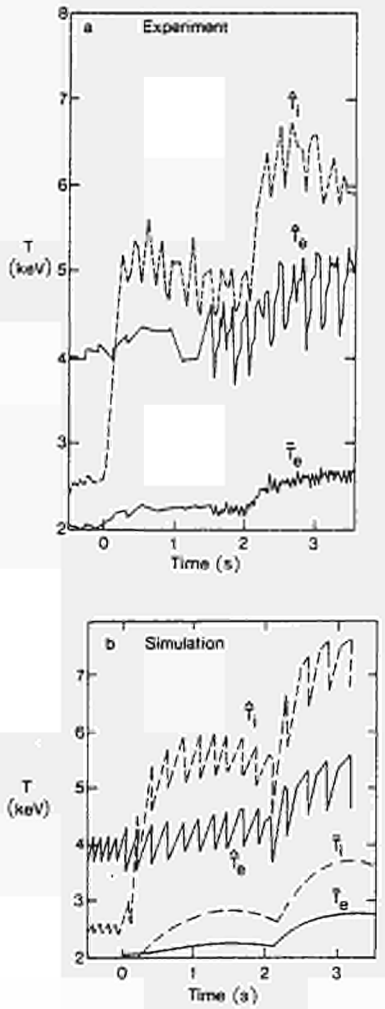

Fig.3: Comparison between experiment and theory for the temporal variation of the peak and mean electron and ion temperatures for JET pulse #7155 (a) ECE and NPA measurements, and (b) simulation with $4\chi_{eCMG}$ and α_{ep}. 2.7MW is applied at 0s and a further 2.7MW at 2s.

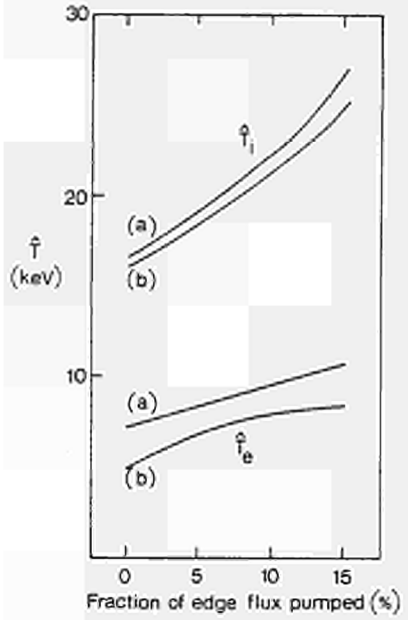

Fig.4: Predicted peak ion and electron temperatures with deuterium injection at 80kV and various levels of edge pumping for (a) $0.4\chi_{eAI}$ and α_e=1.5 and (b) $4\chi_{eCMG}$ and α_{ep}.

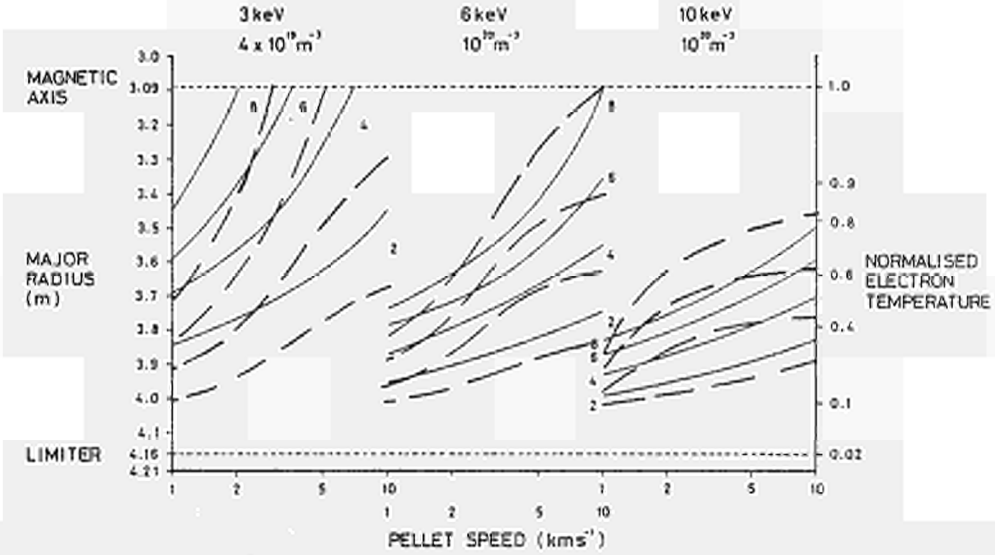

Fig.5: The position of maximum source density immediately after pellet injection when the thickness of the tube of cold plasma is fixed (a) relative to the thickness of the cold gas shield (—) and (b) at 0.35cm (- - -).

COUPLING SPECTRA FOR ION CYCLOTRON HEATING IN LARGE TOKAMAKS IN PRESENCE OF EIGENMODES

T. Hellsten and K. Appert*

JET Joint Undertaking, Abingdon, Oxon. OX14 3EA, UK
*CRPP Ecole Polytechnique, Federale de Lausanne, Switzerland

1. Introduction - The wave spectrum radiated from an antenna during ICRH is of importance for the radiation resistance, current drive efficiency, power deposition and partition to the various species. The wave coupling problem is usually treated by assuming single pass absorption. In general, this is not the case when coupling to the magneto-acoustic wave from the low field side in a tokamak. Instead, the coupling problem is characterised by the presence of eigenmodes. Global codes have recently been developed which can treat the wave coupling problem in presence of reflection [1-3]. In this note we discuss the structure of the wave spectra for some JET scenarios.

2. Characteristics of the Coupling Spectrum - A crude description of the coupling spectrum can be obtained from the dispersion relation for the magneto-acoustic wave in a plane geometry

$$(\varepsilon_\perp - k_z^2)(\varepsilon_\perp - k_x^2 - k_y^2 - k_z^2) - \varepsilon_{xy}^2 = 0. \qquad (1)$$

Here $\varepsilon_\perp$ and ε_{xy} are the diagonal and off-diagonal elements of the perpendicular components of the dielectric tensor. The magnetic field is assumed to be parallel to the z-axis. Let us identify x,y and z with the radial, poloidal and toroidal directions, respectively, in a tokamak of minor radius a and major radius R. Consequently, one has to imagine the components of $\vec{k}$, the wave vector, to be quantized with typical values $n_x\pi/a$, n_y/a and n_z/R where n_x,n_y and n_z designate the quantum numbers. In a calculation k_y and k_z can be chosen whereas k_x or rather n_x, the number of radial nodes of the eigenmode, is obtained as a result when a resonance condition of the form (1) is met. Assume for a moment that k_z could be treated as a continuous variable: a typical coupling spectrum (antenna load versus k_z) then has a structure as schematically shown in Fig.1. Essential for Fig.1 is that $|k_y|, |k_z| << |\varepsilon_\perp|, |\varepsilon_{xy}|$ and $n_x >> 1$. The spacing between modes with different n_x is greater than between modes with the same n_x but different n_y and n_z.

The amplitude and the width of a single resonance peak in Fig.1 are inversely proportional and proportional to the absorption, respectively. The amplitude further depends on the distribution of the current in the antenna, the distance between the antenna and the cut-off, wave frequency, k_y and $k_z$as in the case when single pass absorption is assumed. In general, the coupling with higher k_y and k_z is less effective. As the absorption increases, the resonances corresponding to different eigenmodes start to overlap and compound resonances are the result.

The probability for the antenna to couple to a resonance with a given $k_y$depends on the width of the resonance and the interval between the discrete k_z modes. A critical value of the absorption coefficient a*, can then be defined for which the width equals the separation of k_z modes. The

absorption coefficient is here defined as the fraction of the wave not reflected back to the antenna. Calculations with the ISMENE code [3] give for JET parameters $a^* \approx 0.25$. For $a<a^*$ the coupling resistance is determined by a single or a few single modes and hence may vary rapidly due to small changes in the plasma equilibrium, i.e. density, magnetic field etc. For $a>a^*$ the antenna couples to a large number of modes and the total resistance varies less when the equilibrium conditions evolve. We further note that since the amplitude and the width of the resonances vary in opposite ways with respect to the absorption, the mean value is independent of the absorption. However, as it falls below a^*, fluctuations will increase around this mean value.

The radiation spectra for antennae like the JET monopole and dipole antennae, which essentially couple to low k_z are characterised by a compound resonance peak in the interval $[0,k_z^*]$ where k_z^* is defined by

$$\pi = \int [k_x(0,0) - k_x(0,k_z^*)]dx. \qquad (2)$$

Typical values of k_z^* in JET are $0.05cm^{-1}$. Eq.(2) applied to Fig.1 implies that the antenna mainly couples to the first group of modes, i.e. $n_x=20$.

Since the wave number k_x is roughly proportional to $\sqrt{n}/B$ the wave spectrum will be sensitive to small variation of the density or the magnetic field strength. If the density increases or the magnetic field decreases the resonances will be displaced towards higher k_z. However, there will in general be one compound resonance peak in the interval $[0,k_z^*]$ which dominates the coupling thus leading to a fluctuation of the radiation spectrum and coupling resistance as the equilibrium parameters evolve. In Fig.2 we show how the radiation spectrum for fundamental heating of hydrogen in deuterium varies for small variation of the density as computed with the ISMENE code. The change due to a finite k_y is also shown. To obtain the spectrum for a finite sized antenna or antennae the spectra shown here have to be weighted with the Fourier components of the antenna current. In Fig.3 we show how the spectrum changes as the toroidal field varies. These calculations can be compared with the measured oscillations of the antenna resistance when the toroidal field was ramped down from 2.6-1.4 tesla in 10s (see Fig.4). The code calculations predict that the compound resonance peak will be localized at the same k_z for a change of B with 0.08T. This corresponds to an oscillation time of 0.67s compared to 0.45s of the experiment.

Predictions of the structure of the coupling spectra can then be based on studying the absorption coefficient. In Fig.5 we show how the absorption coefficient varies with respect to k_z for the case shown in Fig. 2 and for some other heating scenarios in JET:

$\omega=2\omega_{CH}$, $n_H(0)=3\times10^{13}cm^3$, $T_H(0)=2.5keV$, $B_o=1.1T$ and $f=33.3MHz$;

$\omega=2\omega_{C\,^3He}$ in D, $n_{^3He}/n_D=0.15$, $T_D(0)=2.5keV$, $T_{^3He}(0)=5keV$, $B_o=1.7T$ and $f=33.3MHz$;

$\omega=\omega_{C\,^3He}$ in H, $n_{^3He}/n_H=0.02$, $n_D(0)=3\times10^{13}cm^{-3}$, $T_{^3He}(0)=T_H(0)=2.5keV$, $B_o=3.4T$ and $f=33.3MHz$;

$\omega=\omega_{C\,^3He}$ in D, $n_{^3He}/n_D=0.04$, $n_D(0)=3\times10^{13}cm^{-3}$, $T(0)=2.5keV$, $B_o=3.4T$ and $f=33.3$ MHz.

Heating scenarios with "weak" absorption like fundamental heating of ^3He in D will be subjected to sharp resonances as can be seen in Fig.6. Since the resonances for different k_y appears at different k_z the antenna will still see a relatively broad compound resonance.

3. Discussion - Ion cyclotron heating by magneto-acoustic waves being launched from the low field side is characterised by coupling via eigenmodes. When the absorption coefficient, which determines the width and amplitude of the resonances, exceeds a critical value (typical 0.25 for JET) the antenna will couple to a large number of eigenmodes. The average value of the coupling resistance does not depend on the absorption. Antennae which couple to small k_z, will have a narrower radiation spectrum than if single pass absorption is assumed and the spectrum will be characeterised by a compound resonance in the interval $[0,k_z^*]$ whose position is very sensitive to small variations in the equilibrium. This will have consequences on current drive where a prescribed wave spectrum is important for the efficiency. Further, it may affect the partition of power absorbed by electrons and ions.

Acknowledgement - The authors wish to thank Dr M Bures for valuable discussions.

References

[1] S.I. Itoh, et al. Plasma Physics and Controlled Nuclear Fusion Research, IAEA, Vienna, 1985, Vol.1, pp.
[2] S.C. Chiu and T.K. Mau. Nucl. Fus.23 (1983) 1613.
[3] K. Appert, T. Hellsten, J. Vaclavik and L. Villard. 3rd European Workshop on Problems in the Numerical Modelling of Plasmas, NUMOP 85, Varenna, Italy, 1985.

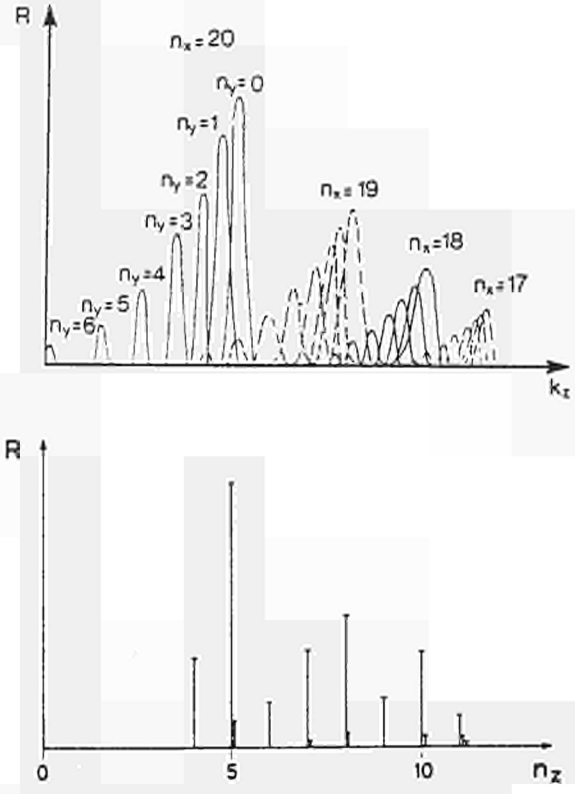

Fig. 1 Schematic picture of the coupling spectrum. Above for a continuous spectrum and below the corresponding one for a discret spectrum.

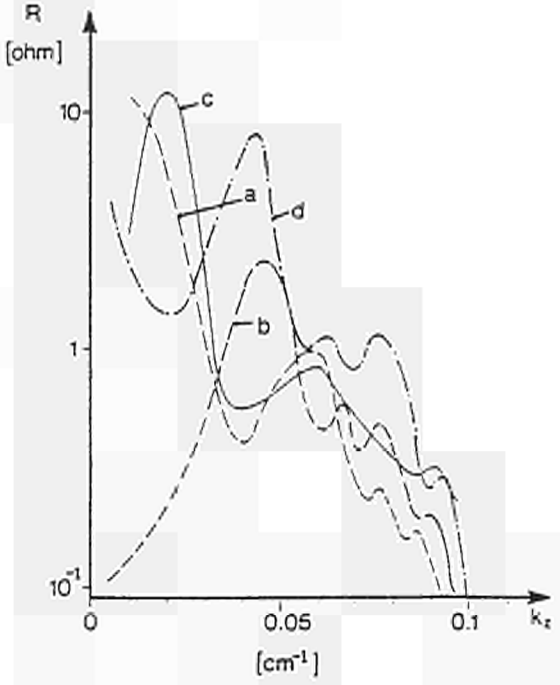

Fig. 2 Computed coupling resistance of the individual Fourier components for $\omega=\omega_{CH}$, $n_H/n_D=0.04$, $B_0=2.3T$, $T(0)=2.15keV$, $k_y=10^{-4}cm^{-1}$ in a-c.
a) $n_D(0)=3.1\times10^{13}cm^{-3}$
b) $n_D(0)=2.8\times10^{13}cm^{-3}$
c) $n_D(0)=2.5\times10^{13}cm^{-3}$
d) as b) except $k_y=0.04cm^{-1}$

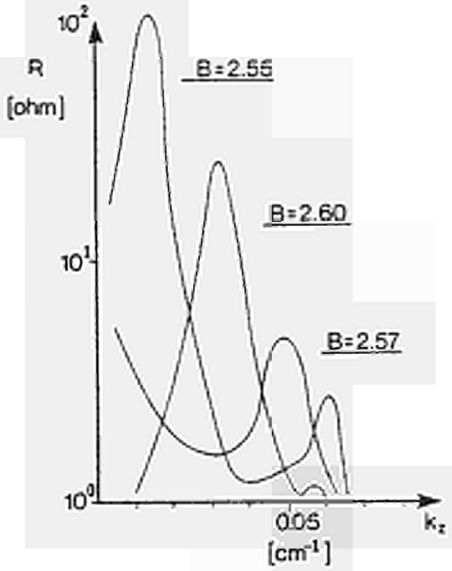

Fig. 3 Computed coupling spectrum for $\omega=\omega_{CH}$ for various magnetic fields.

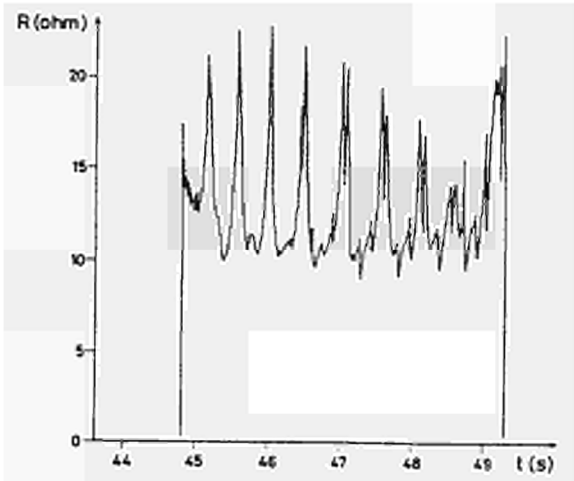

Fig. 4 Measured coupling resistance on a JET antenna during ramp down of the toroidal field. The resistance has been transformed by the short reactive stub close to the antenna.

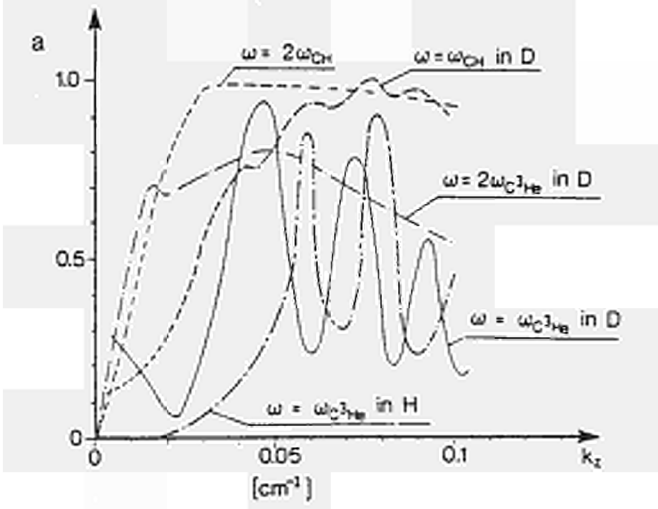

Fig. 5 Absorption coefficient vs. k_z

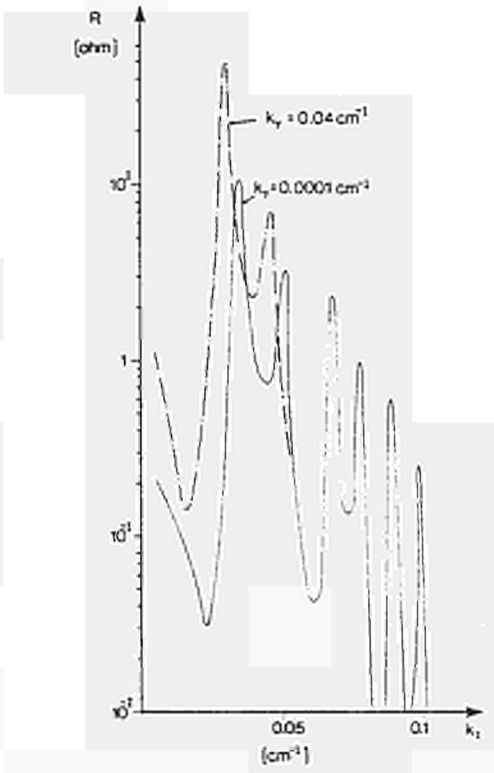

Fig. 6 Computed coupling spectrum for $\omega=\omega_{C^3He}$ in D.

EXPERIMENTAL DETERMINATION OF THE ICRF POWER DEPOSITION PROFILE AND COMPARISON WITH RAY TRACING CALCULATIONS

V.P. Bhatnagar*, E. Barbato⊕, G. Bosia, M.P. Evrard*, D. Gambier**, R. Giannella***, J. Jacquinot, P.P. Lallia, M. Malacarne, K. Thomsen#, B. Tubbing+, V. Zanza⊕

JET Joint Undertaking, Abingdon, Oxon, OX14 3EA, UK
*From LPP-ERM/KMS; EUR-EB Association, 1040 Brussels, Belgium
**From EUR-CEA Association, Fontenay-aux-Roses, France
***From EUR-ENEA Association, Frascati/Roma, Italy
#From Risó National Laboratory, Roskilde, Denmark
+From EUR-FOM Association, "Rijnhuizen", The Netherlands
⊕EUR-ENEA Association, Frascati/Roma, Italy

I INTRODUCTION

A detailed knowledge of the ion-cyclotron resonance heating (ICRH) power-deposition profile is a prerequisite in carrying out a meaningful power balance in the plasma. It is also an essential input to the tokamak transport codes which predict the evolution of plasma heating.

Three ICRH antennae located on the low-field side have been energised in JET which couple power to the fast magnetosonic waves in a deuterium plasma with H^+ or He^3 minority species. In this paper, ICRH power deposition profiles in JET determined both theoretically (ray-tracing) and experimentally (several methods; see below) are compared.

(i) Ray Tracing : A sophisticated ray-tracing code [1], which includes the effects of poloidal field, has been used to generate the ICRH power-deposition profiles in the D-shaped JET plasmas. The initial conditions of ray tracing are obtained by the full-wave solution of a realistic antenna plasma coupling model. The ray-tracing analysis shows that the ICRH power-deposition profiles are narrow and that the energy is deposited somewhat locally due to the large plasma parameters and large damping per pass.

(ii) Change of Slopes of Sawteeth : The RF power deposition in electrons can be estimated from [2,3]

$$P^e_{RF} = \left.\frac{\partial W_e}{\partial t}\right|_{+\varepsilon} - \left.\frac{\partial W_e}{\partial t}\right|_{-\varepsilon} \qquad (1)$$

where $\pm\varepsilon$ represent an infinitesimal time difference just after and before the application of a square wave RF pulse. Such a procedure assumes that the other source and sink terms (such as P_Ω, $-P_{ei}$, $-P_{rad}$ etc) remain unchanged at such short time intervals. Experimentally, the RF is square wave modulated and the difference of the slopes of a sawtooth in the electron-cyclotron emission (ECE) diagnostic of the 12-channel grating polychrometer [4] allows the determination of electron power deposition profile.

(iii) Modulation Experiments : When the antenna radiated power is amplitude modulated, the bulk temperatures in the plasma where RF power is deposited oscillate at the modulation frequency. The amplitude and phase of the oscillating signal of a temperature diagnostic at different radial positions lead to the knowledge of the power deposition profile of the additional heating [5,6]. The presence of large sawteeth in JET renders the signal analysis by correlation technique difficult especially when $\nu_m \approx \nu_{st}$, where ν_m is the RF modulation frequency and ν_{st} is the average sawtooth frequency. For $\nu_m > \nu_{st}$ or ν_m close to a harmonic of ν_{st}, the

ratio of signal to this extraneous disturbance is poor. However, when $\nu_m < \nu_{st}$, this technique gives useful results.

(a) Correlation function technique Consider the equation, $c(\tau) = \int \bar{f}(t)\, g(t+\tau)\, dt$. If $\bar{f}(\omega)$ and $\bar{g}(\omega)$ are the Fourier transforms of f and g respectively then $\bar{c} = \bar{f}^* \cdot \bar{g}$ is the Fourier transform of c. We use the discrete Fourier Transform for the data sampled at a given number of points during the time interval of interest. The analysis program computes the auto-correlation spectra and the index m of the maximum modulus of the correlation function transform. It also displays the frequency ν_m as well as the values $2|\bar{f}_m|$ and $2|\bar{g}_m|$ that are the amplitudes of the two signals oscillating at that frequency and their relative phase θ_m.

(b) BOXCAR Technique : The "Boxcar" method is used to analyse non-Gaussian random signals. In this method, each period of RF modulation is treated as an independent event and the signal behaviour on many successive events is averaged. As the sawteeth and the RF modulation are not synchronous and as the sawtooth amplitude is greater than the RF-modulated amplitude by an order of magnitude, it is necessary to eliminate the effect of the sawteeth. First, the sawteeth crashes are suppressed, and we build a long period, high amplitude single sawtooth. Then, the linear trend is removed and the remaining signal is analyzed.

II. Plasma Response to RF Modulation

If sawteeth do not change the power balance, the modulated quantities in the power balance equation can be written as

$$\begin{aligned} i\omega \tfrac{3}{2} n_e \bar{T}_e &= \bar{P}_{HF}^{(e)} + \bar{P}_e - \frac{1}{\tau_e} \tfrac{3}{2} n_e \bar{T}_e \\ i\omega \tfrac{3}{2} n_D \bar{T}_D &= \bar{P}_D - \frac{1}{\tau_D} \tfrac{3}{2} n_D \bar{T}_D \end{aligned} \qquad (2)$$

where we have neglected $\bar{P}_\Omega$, $\bar{P}_{rad}$ and $\bar{P}_{cx}$ (localized at the edge), $\bar{P}_{HF}^{D}$ (mainly minority heating), $\bar{P}_{ei}$ ($\tau_{ei} \approx 150$ ms $>> \tau_e, \tau_i$) and $\bar{n}_j/n_j << \bar{T}_j/T_j, j=e,i$. $\bar{P}_{tot} = \bar{P}_{HF}^{(e)} + \bar{P}_e$ is the total (modulated) power going to the electrons through the minority and by direct mode conversion. Using the modulus/ phase representation of the complex modulated quantities, we write

$$\bar{T}_e = T_{oe}\, e^{-i\theta_e} \; ; \; \bar{P}_{tot} = P_{oe}\, e^{-\Psi_e} \qquad (3)$$

Where θ_e and ψ_e are the relative phases $\omega.\tau.$ to the RF power signal at the generator. This leads to the following expressions for amplitude and phase relating the measured quantities T_{oe} and θ_e to the power density in the electrons

$$P_{oe} = \tfrac{3}{2} n_e T_{oe} \frac{\omega}{\sin \phi_e} \quad \text{and} \quad \phi_e - \theta_e = -\Psi_e \qquad (4)$$

where we have defined a phase angle ϕ_e such that $\tan \phi_e = \omega\tau_e$ (5)

The local electron energy confinement time is estimated from the local plasma transport considerations to be as

$$\tau_e = \langle R \rangle^2 / \left(j^2_{o,1} \cdot D_e \right) \qquad (6)$$

where $j_{0,1}$ is the first zero of Bessel function $J_o(r)$, D_e is the electron diffusion coefficient (at the centre of the plasma) and $\langle R \rangle$ is an average radius of the zone of interest. For the ions, we obtain similarly

$$P_{oD} = \tfrac{3}{2} n_D T_{oD} \omega / \sin\phi_D \quad \text{with } \tan \phi_D = \omega\tau_D \text{ and } \tau_D = \frac{\langle R \rangle^2}{j^2_{0,1} D_D} \qquad (7)$$

III. Results

We present results of analysis of modulation experiments in which the antenna radiated power was square wave modulated at 5 Hz. The electron cyclotron emission (ECE) from the plasma was used as the T_e diagnostic by detecting the signal by Michelson interferometer [7] and a 12 channel polychrometer [4]. The correlation technique has been applied to the two diagnostics and the signal amplitude and phase for the two is plotted in Fig. 1 as a function of the major radius. The signal for the same shot was also analysed by using the boxcar technique outlined above and the peak amplitude of the temperature signal is plotted against the major radius at different time interval in a 3-D plot shown in Fig. 2.

Using the formulation presented in Section 2, the estimated e-power deposition profile points deduced from the correlation technique are shown in Fig. 3 for the two processing of the ECE signals. The power density points were obtained by estimating the value of the ϕ_e (from eq. 5) in which $\langle R \rangle$ and D_e were taken to be 0.25 m and 1 m^2/s respectively) which is found to be nearly the same as θ_e measured at the centre with its value $\theta_e \simeq 0.36$ rad. The points derived from the change of slope of sawteeth at a switch ON/OFF phase of the modulation are also shown. For the same shot in which the power coupled by the antenna was 1.25 MW with He^3-minority, prediction of the p-d-profile from ray-tracing are also shown where the predominantly absorbed power by the minority species is redistributed to electrons and background ions based on the Stix model [8]. In this case, at the low He^3-minority power density, a significant fraction of the power is transferred to the ions. The correlation technique performed on the neutron diagnostic signal gave the central ion-power density which has relatively large error bars. The value of central ion diffusion coefficient is estimated to be 3 m^2/s. Experimentally derived e-power deposition profiles by several methods are found to be in good agreement among each other as well as with ray tracing.

IV. Summary and Conclusions

ICRH power-deposition profiles determined by (a) Ray tracing, (b) Change of slopes of a sawtooth of an ECE signal and (c) Modulation experiments analysed by correlation technique and Boxcar technique, have been compared for a JET deuterium plasma in the minority heating scheme. The results of power densities obtained by different methods are found to be in good agreements. The RF power-deposition profile are found to be well localized and are relatively narrow with respect to the size of the plasma. When the modulation frequency is increased from 5 to 25 Hz, the plasma temperature response goes down and the signal to noise ratio is worse. The presence of the strong sawteeth complicates the data analysis. The power-deposition profile presented have been obtained from the data when the modulation frequency was 5 Hz. These results suffer from the effect of energy diffusion which broadens the deposition profile. The effect of sawteething, equipartition etc have been ignored.

References

[1] V.P. Bhatnagar et al, Nuclear Fusion, 24 (1984) 955
[2] Equipe TFR, Report EUR-CEA-FC-1046 (1980), Fontenay-aux-Rose, France
[3] D.J. Gambier et al, 12th Conf. Plasma Phys., Budapest, (1985) ppr. 394
[4] B.D.J. Tubbing, ibid, paper 142
[5] E. Barbato, R. Giannella, Physics Letters, 110A, No. 6 (1985) 309
[6] G.L. Johns et al, Nuclear Fusion, 26 (1986) 226
[7] A.E. Costley et al, 12th Conf. Plasma Phys., Budapest, (1985) ppr. 186
[8] T.H. Stix, Nucl. Fusion, 15 (1975) 737

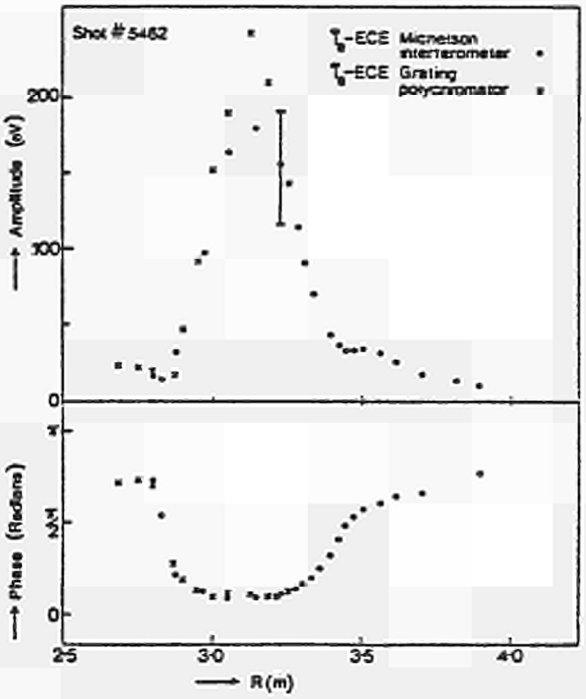

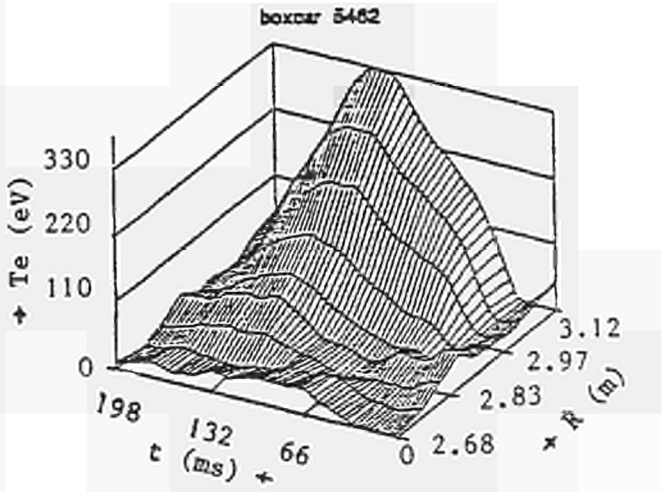

Fig. 2 The modulated electron temperature obtained from the boxcar technique is shown as a function of time for different positions along the major radius in a 3-D plot.

Fig. 1 Amplitude and phase θ_e of the Fourier transform at the modulation frequency for signals from two different ECE electron temperature diagnostics versus the major radius.

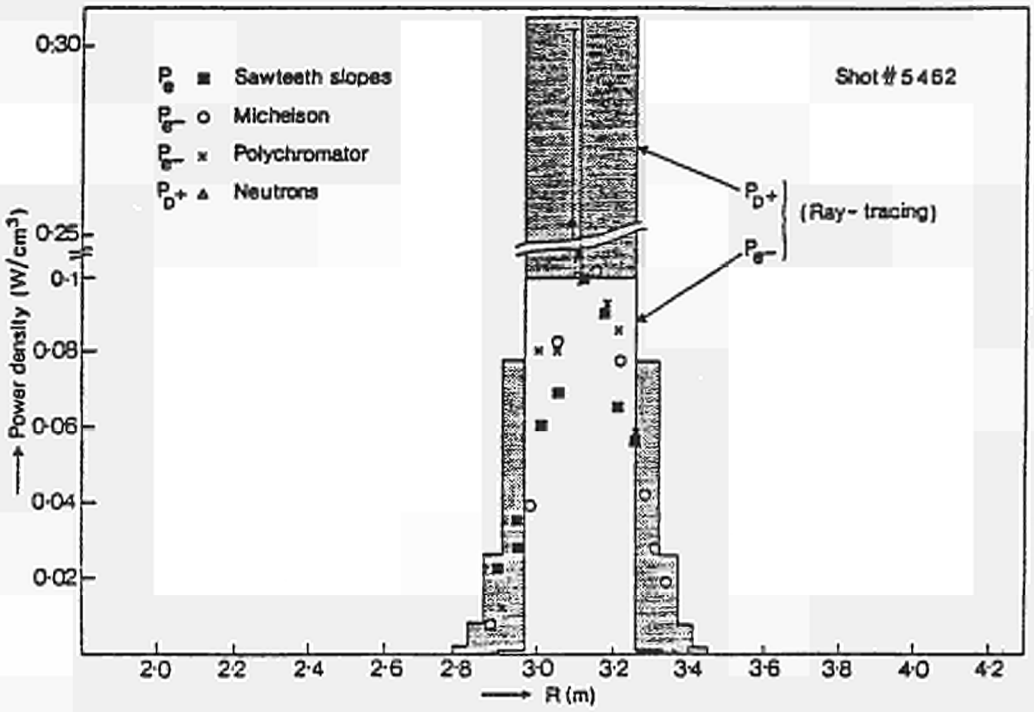

Fig. 3 Profiles of the RF power delivered to electrons as measured from sawteeth slopes (■) and from the correllation technique (o and x). An estimated value for the RF central power density to the ions deduced from the neutron signals is also shown (△). The slab deposition profiles shown are computed by the ray-tracing code.
NH_e^3/N_D = 0.18, B_o = 3.08 T, I_p = 2.7 MA, f = 29.9 MHz, T_{eo} = 3.2 keV, T_{io} = 2.2 keV, N_{eo} = 2.15 x 10^{13} cm^{-3}, P_{RF} = 1.25, P_e = 0.21, P_D = 0.79 MW, 0.25 MW is assumed not to be absorbed in the centre of the plasma.

ANALYSIS OF CURRENT AND TEMPERATURE PROFILE FORMATION IN JET

D.J. Campbell, J.P. Christiansen, E. Lazzaro, A.W. Morris[+], M.F.F. Nave, F.C. Schueller and P.R. Thomas

JET Joint Undertaking, Abingdon,Oxon, OX14 3EA, UK
[+]Balliol College, Oxford University

INTRODUCTION - The study of of current formation in a tokamak is important both at the practical operation level and at the fundamental level of identifying basic transport mechanisms and regimes. Here an analysis of observations on the formation of tokamak temperature and current profiles in JET is presented. The time evolution of these profiles has been studied for a large number of plasma discharges using the equilibrium identification codes IDENTC and FAST, and the ECE measurements of electron temperature profiles.

It is found that plasma resistivity is neoclassical during the current flat-top, from which we deduce that ECE temperature profile measurements are consistent with current profiles deduced independently from magnetic signals by the equilibrium codes. The effective resistivity is substantially higher than neoclassical during the initial stage of the current rise and, as a result, the current penetration occurs on a timescale which is much shorter than the neoclassical skin time. The penetration enhancement depends on the current and density ramp rates. Furthermore, during this early stage of the discharge substantial MHD activity is observed. The association between this activity and the process of current penetration has been investigated by analysing the path followed by typical discharges in the parameter plane (q_o, q_a), where q_a is the safety factor.

CURRENT PENETRATION BY RESISTIVE DIFFUSION

MAGNETIC ANALYSIS - The toroidal component of Ohm's law can be written

$$\eta_{eff} = E_\phi / J_\phi, \qquad (1)$$

where η_{eff} includes the resistive effects of any instabilities which may occur. For steady toroidal fields, this may be written

$$\eta_{eff} = \mu_o \frac{\partial \psi}{\partial t} \Big/ \left[R \frac{\partial}{\partial R} \frac{1}{R} \frac{\partial}{\partial R} + \frac{\partial^2}{\partial Z^2} \right] \psi. \qquad (2)$$

Equation (2) is solved for a time sequence of inverse Grad-Shafranov equilibria fulfilling Dirichlet boundary conditions plus an optimal fit of Neumann conditions [1] with current density profiles taken in the functional class:

$$J_\phi(R,\psi) = I_o \left[\alpha \, R/R_o \left(1-\psi+b(1-\psi)^2\right) + (1-\alpha) R_o/R \left(1-\psi+a(1-\psi)^2\right) \right], \qquad (3)$$

where a, b, α are the parameters to be determined. Once the calculation is validated by checks of compatibility with other diagnostics, the accuracy of the evaluation of q_o is of the order of 20% if the error in the data is 3%.

PLASMA RESISTIVITY - Profiles of plasma resistivity are derived from local parameters obtained by diagnostic measurements. The principal data are $T_e(r)$ from ECE [2], $n_e(r)$ from microwave or far-infrared interferometry, and Z_{eff} from visible Bremsstrahlung measurements. 'Spitzer' resistivity is calculated from

$$\eta_s = 1.034 \times 10^{-4} \, Z_{eff} \, \alpha(Z_{eff}) \, \ell n \, \Lambda / T_e^{3/2}, \qquad (4)$$

where T_e is in eV, and the neoclassical resistivity from

$$\eta^* = \beta \eta_s, \qquad (5)$$

where

$$\beta = \left(1-f_T/(1+\xi\nu_*)\right)^{-1} \left(1-C_R f_T/(1+\xi\nu_*)\right)^{-1}. \qquad (6)$$

Explicit forms of the coefficients $\alpha(Z_{eff})$, ξ, C_R, the electron trapping factor f_T, and the collisionality ν_* are given in [3]. The principal sources of error in these calculations arise from the measurement of $T_e(r)$ (±10%), and Z_{eff} (the profile is assumed to be flat).

RESULTS - The evolution of the principal parameters of a pulse selected for analysis is shown in figure 1. Figure 2 shows a comparison of radial profiles of η_{eff} (crosses), η_s (full line) and η^* (dashed line) at several times during the rise phase and flat top of this discharge. Once the plasma current has reached its equilibrium value, the profiles of resistivity derived from magnetic analysis and from temperature measurements are in very good agreement [4]. However, during the first 2s there are significant differences between the two, and particularly during the first 0.7s, where η_{eff} is significantly higher than η^*. Thus, the current penetration occurs more rapidly than can be explained by neoclassical resistivity, which leads to this enhancement in the calculated value of η_{eff} over η^*. This might be explained by magnetic relaxation, as discussed in the next section.

ROLE OF MHD INSTABILITIES IN CURRENT PENETRATION

TYPE OF INSTABILITIES PREDICTED FOR THE CURRENT RISE - to investigate the relationship between the observed MHD activity and the processes affecting current penetration, we have analysed the evolution of typical discharges in the parameter plane (q_o, q_a) [5]. By drawing the boundaries of various MHD instability regions, obtained from the model of [6], in this plane, it is possible to interpret the processes accompanying current penetration. Figure 3 shows a scatter plot of a sample of JET pulses in this plane. Several time points are included for each pulse. It is remarkable how few points lie centrally in the 'stable' region.

For clarity we discuss the trajectory of a particular pulse (2214) which, as shown in figure 4, passed through all regions of the plane. Identification of the times of interest which are labelled in the figure can be obtained from the plasma current trace in figure 1. Detailed magnetic equilibrium calculations show that the current profile initially exhibits a significant skin effect, and that it becomes gradually more peaked as the trajectory reaches the equilibrium state. It is also found that the trajectory reaches $q_o \sim 1$ at approximately the same time as sawteeth appear, and that it remains in this condition during a substantial period of the current decay. Thus, there is qualitative agreement between the form of the J (and q) profiles at various times and the region in which the trajectory lies.

This relationship between the J profiles and the regions of the (q_o, q_a) plane is further illustrated the two other cases shown in figure 4. These trajectories show very distinct patterns of evolution. Pulse 2442 starts in the $q_a < q_o$ sector and then remains entirely in the 'kink' sector before disrupting during the flat top. Its current density profile starts hollow and peaks 3s after breakdown, the trajectory then being in the 'kink' region. This is in contrast to pulse 2214 which has a similar slow rise, but enters the 'kink' region earlier and also becomes fully peaked earlier (after 2s), terminating within the 'tearing-internal' band. The third example (shot 2044) is rather unusual, but interesting, because it always has a peaked current profile and, as expected, it crosses only the 'tearing' region.

CURRENT REDISTRIBUTION BY MAGNETIC RELAXATION - The trajectories described here show a significant correlation with the spectra of MHD activity observed. Figure 5 shows the magnetic activity signal for pulse 2442 plotted as a function of the safety factor, q_a. Investigation over many pulses during the current rise shows that trajectories lying in the 'double-tearing'/'kink' regions exhibit MHD actvity spectra of this form,

i.e. with distinct peaks close to rational values of q_a, that is $q_a = m/n$ with n = 1 or, sometimes, n = 2. Evidence for the redistribution of J for pulses such as 2442 is shown in the plot of ℓi versus q_a (fig.6). This is further supported by observation of negative spikes in dI/dt. Trajectories which have crossed into the 'tearing' region have MHD spectra which are generally less structured with peaks of the signal often uncorrelated to integral values of q_a. The same is true for the evolution of ℓi.

CONCLUSIONS - The evolution of current and temperature profiles in JET may be understood in terms of the trajectory of the discharge in the (q_o, q_a) plane. It is found that the plasma evolves through regions in this plane which are predicted to be MHD unstable. While substantial MHD activity is observed, which is correlated with rapid current penetration, the occurrence of MHD instabilities generally has no deleterious effect on the flat-top performance. As the MHD activity decays, current penetration approaches the neoclassical value, and becomes neoclassical as the current plateau value is reached. Generally the plasma current flat-top is reached with $q_o \sim 1$, and this state is maintained into the decay phase.

REFERENCES

[1] J. Blum, B Thooris and J. Le Foll, JET Contract 9008.
[2] A.E. Costley et al. in Controlled Fusion and Plasma Physics (Proc. 12th Europ Conf., Budapest, 1985), 9F-I, 227 (1985).
[3] S.P. Hirschman and D.J. Sigmar, Nucl. Fus. 9, 1077 (1981)
[4] J.P. Christiansen, et al., in Controlled Fusion and Plasma Physics (Proc. 12th Europ Conf. Budapest, 1985) 9F-I 327 (1985)
[5] E. Lazzaro and M.F. Nave, JET-DN-T(85)24.
[6] J.A. Wesson, Nucl. Fus. 18 87 (1978)

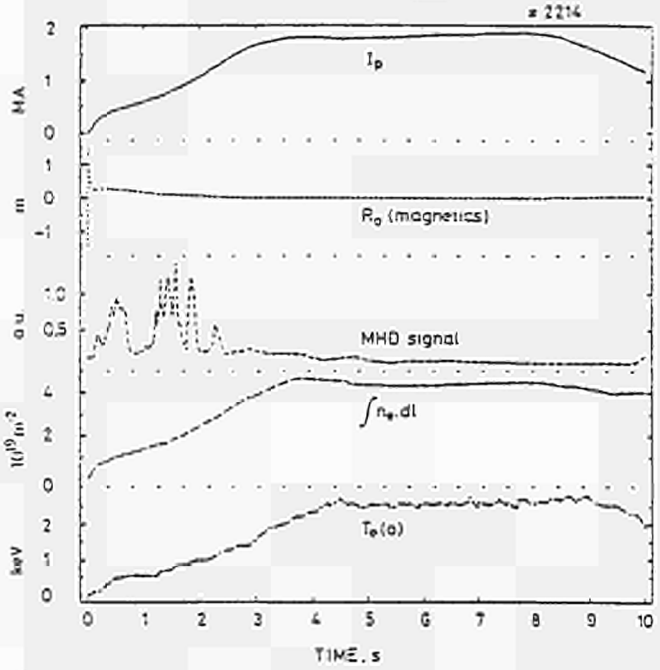

Figure 1 Evolution of several principal parameters during a JET pulse: plasma current, I ; magnetic axis, R_o; MHD activity signal; line integral of density, $\int n_e dl$; central electron temperature, $T_e(o)$.

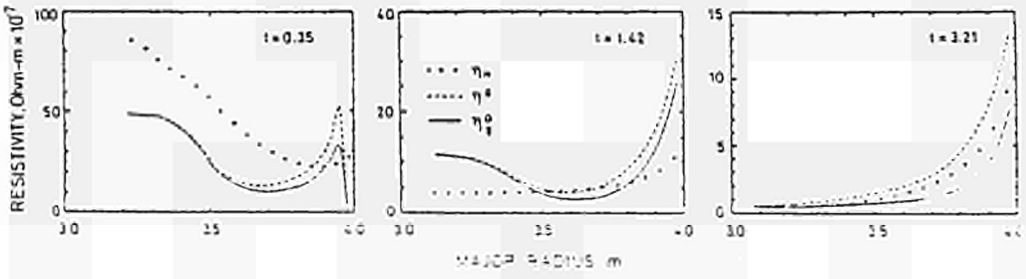

Figure 2 Comparison of radial profiles of η_{eff} (effective resistivity), η^* (neoclassical resistivity) and η_s (Spitzer resistivity) at three times.

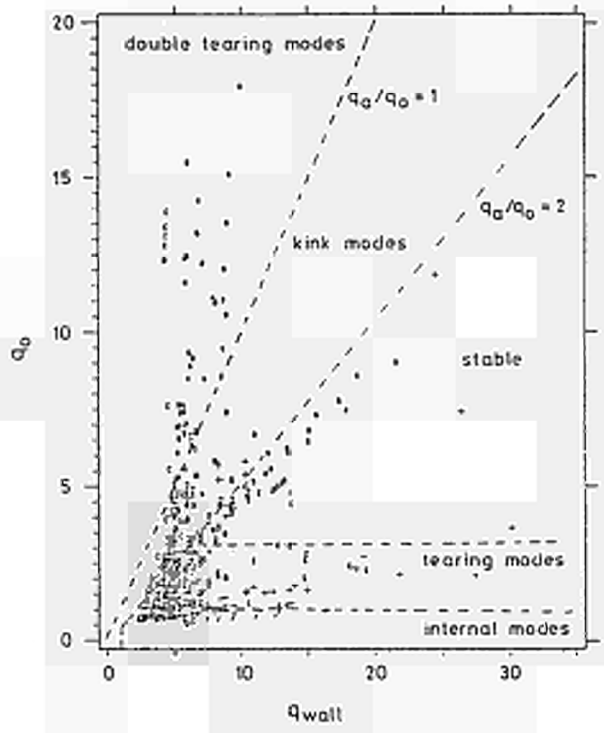

Figure 3 Scatter plot of JET pulses in the plane (q_o, q_a). The stability boundaries for various forms of MHD activity (derived from [6]) are superposed.

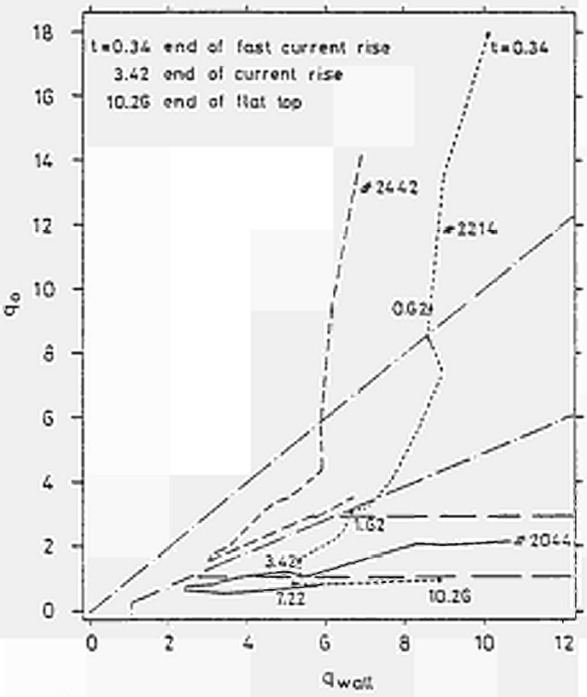

Figure 4 Trajectories of 3 JET pulses during their evolution and decay.

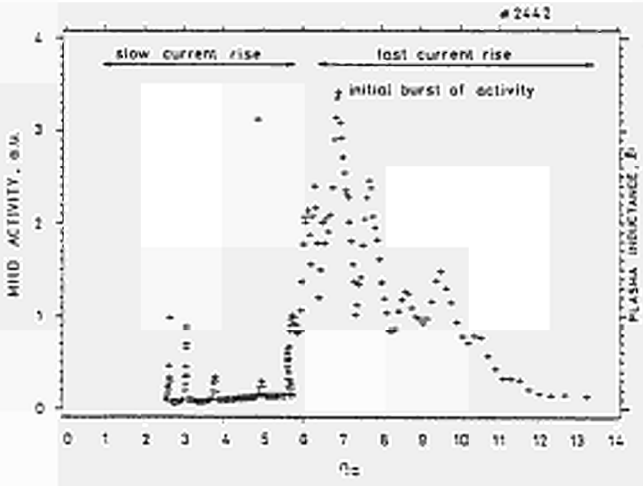

Figure 5 MHD activity signal for pulse 2442, plotted as a function of q_a.

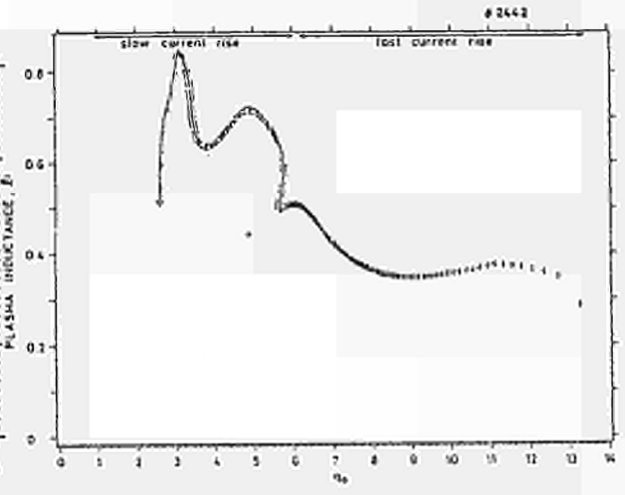

Figure 6 Internal inductance ℓi versus q_a for #2442.

ELECTRON DENSITY TRANSPORT IN JET

A Cheetham, J P Christiansen, S Corti, A Gondhalekar, F Hendriks
J Hugill*, P D Morgan, J O'Rourke and M Watkins

JET Joint Undertaking, Abingdon, Oxon OX14 3EA, UK
* Culham Laboratory, Abingdon, Oxon OX14 3DB, UK

This study is based upon absolute measurements of H_α or D_α emission at various locations, of electron density using a 7-channel FIR interferometer and of neutral particle effluxes using a NPA. Plasma fuelling with auxiliary heating is investigated and transport coefficients determined for a range of plasma parameters.

FUELLING AND PLASMA EDGE BEHAVIOUR

During an OH discharge, the density evolution closely follows that of the plasma current, [1]. The application of auxiliary heating pulses of duration a few seconds produces an increase in the electron inventory, ΔN_e, which scales approximately linearly with the additional power, Fig.1,while dN_e/dt falls throughout the heating pulse. During NBI, asymptotically the ratio of increase in electron inventory to the number of electrons injected by the beam, $\Delta N_e/N_{NBI}$, does not vary appreciably with N_{NBI}, Fig. 2, and is $\sim$ 0.8. In contrast, starting from the same initial conditions, admitting $N_g \sim 2.8 \times 10^{21}$ atoms into the torus by gas puffing produces a relative increase $\Delta N_e/N_g$ of $\sim$ 0.4.

During both ICRF and NBI, the global particle confinement time τ_{pg} drops during the heating pulse, consistent with the plasma being more impermeable to the recycled neutrals, due to its higher edge density. For a series of shots in which only the density is varied, and where the vessel has been conditioned by a number of discharges, τ_{pg} at current flat top varies inversely with $\bar{n}_e$ at densities $\gtrsim 1.5 \times 10^{19}\ m^{-3}$, (1). At lower densities the reverse dependence has been seen. However, for the same settings of the discharge parameters, the values of τ_{pg} obtained for a large collection of OH shots over a period of many months show a significant spread at a given $\bar{n}_e$, varing by a factor of 2 or more. Apart from uncertainties concerning the spatial uniformity of the H_α/D_α emission, the spread in τ_{pg} can be understood in terms of a shot-to-shot variation in the neutral influx from the limiters Φ_H^L, at fixed $\bar{n}_e$, depending on the recent history of the machine, Fig. 3.

ELECTRON DENSITY TRANSPORT IN JET

Density Profile Constancy is a striking feature of electron density build-up in JET. Figs. 4(a) and 5(a) show the line integrated density along seven vertical chords through the plasma. Fig. 4(a) is for a plasma with ICRF. Fig. 5(a) is for a similar plasma with NBI. Observe that, in both cases, after the plasma current and aperture become stationary, the ratios among the seven line integrated electron density signals remain nearly constant (within less than 5%) as the discharge evolves in time, indicating that the density profile shape remains nearly constant - see Figs. 4(b) and 5(b). This indicates that the magnitude of the electron density transport coefficients adjust themselves as the plasma heating source, electron source and electron density change, so as to maintain a nearly constant density profile.

In order to determine the electron density transport coefficients, the density transients as shown in Fig. 4(a) and Fig. 5(a) have been analyzed. The continuity equation governs the density evolution:

$$\frac{\partial n_e}{\partial t}(r,t) = S_e(r,t) - \nabla \cdot \Gamma_e(r,t).$$

The spatial form of the radial electron source function $S_e(r)$ is calculated using the neutral density profile arising from edge neutrals only, recombination neutrals do not contribute to the electron source. $S_e(r)$ is then normalized at the edge using the absolute H_α measurement. Ionization of impurities is also a source of electrons. We have simplified this by multiplying by a factor (usually 1.6) the electron source due to ionization of neutrals. Fig. 4(c) shows such a computation. This gives us a measurement of the radial electron flux.
In NBI discharges the electron source consists of, in addition to ionization of edge neutrals, ionization of beam neutrals. Fig. 5(c) shows the electron source function at the start of NBI. This source is strongly time dependent; as the plasma density increases, the beam-generated source flattens.

The measured electron flux $\Gamma_e(r)$ is interpreted in terms of a model of electron transport consisting of diffusive and convective driving terms, [2]:

$$\Gamma_e(r) = - D(r) \frac{\partial n_e(r)}{\partial r} + n_e(r)\, V_p(r).$$

$D(r)$ and $V_p(r)$ are assumed not to change during auxiliary heating. The magnitude of the diffusion coefficient D determined above is in agreement with that determined by analysis of density sawtooth propagation [3].

The analysis described has been performed for a large number of RF heated and a few NBI discharges, covering a large parameter range in B_ϕ, I_ϕ, P_{aux} and $\bar{n}_e$, Fig. 6.

CONCLUSIONS

1. ICRF and NBI heating produce increases in the plasma electron inventory, which are comparable under similar conditions, despite the differences in fuelling. The increase scales approximately linearly with applied power.
2. Hysteresis behaviour in the variation with $\bar{n}_e$ of the H or D influxes from the limiters leads to a spread in particle confinement time. Vacuum vessel conditions influence recycling and particle confinement.
3. The results of the electron density transport analysis, whilst yeilding credible results do not provide a detailed insight into the transport mechanisms. The transport coefficients do not depend in any systematic way on the externally controllable parameters. It seems plausible that transiently, the transport coefficients assume a magnitude so as to prevent the density profile deviating far from a preferred shape. Work is in progress to explore if the measured electron flux $\Gamma_e(r,t)$ is related to other driving terms such as the plasma pressure and its gradient.

REFERENCES

[1] P D Morgan et al, Proc 12th European Conf. on Controlled Fusion and Plasma Phys. Budapest 1985, Vol II, p.535

[2] B Coppi and N Sharky, Nuclear Fusion 21, 1981.

[3] A Hubbard et al., this conference.

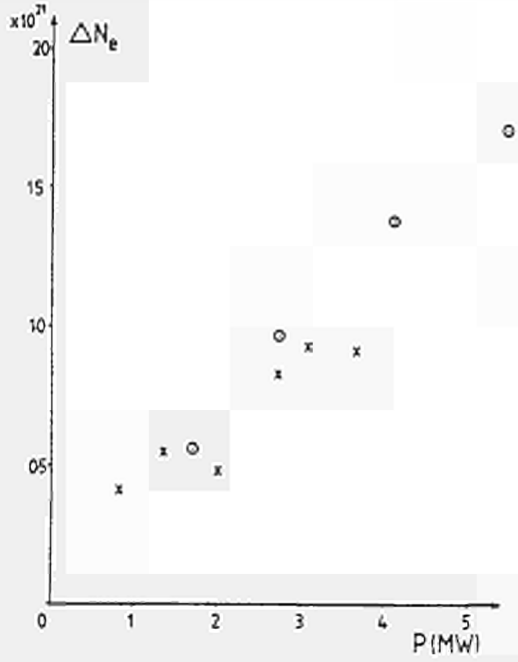

Fig. 1. Variation of increase in plasma electron inventory, ΔN_e, with auxiliary power, P, for discharges with ICRF (X) and NBI (O). I_p = 2 MA, B_ϕ = 3.4 T, D, plasma. *He minority or 65 keV H beam, length of auxiliary power pulse = 2 s.

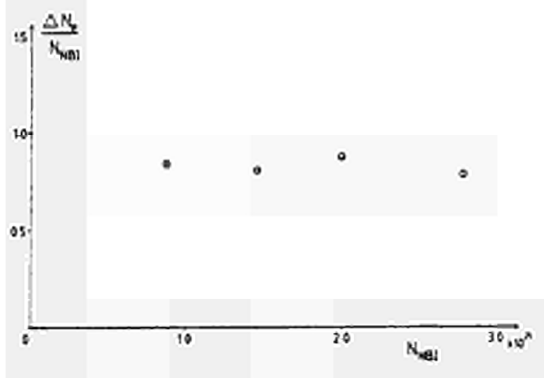

Fig. 2. Variation of ratio of increase in plasma electron inventory during NBI to total number of injected beam atoms, $\Delta N_e/N_{NBI}$, with number of injected atoms, N_{NBI}. I_p = 2 MA, B_ϕ = 3.4 T, D, plasma, 65 keV H beam, length of NBI pulse = 3.5 s.

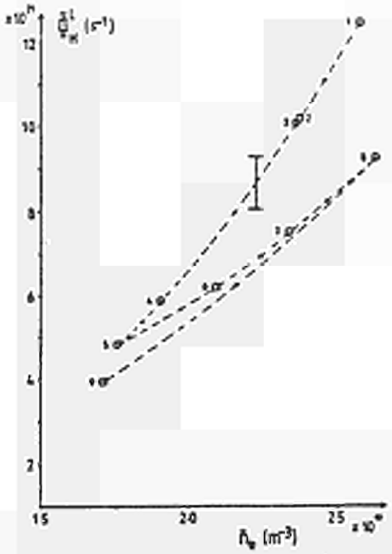

Fig. 3. Variation of total D influx time history, τ_E^{-1}, with average plasma density, $\bar{n}_e$, for a sequence of consecutive discharges. I_p = 3 MA, B_ϕ = 2.6 T, D, plasma. τ_E^{-1} exhibits hysteresis behaviour. The machine had not been operated previously for 3 days.

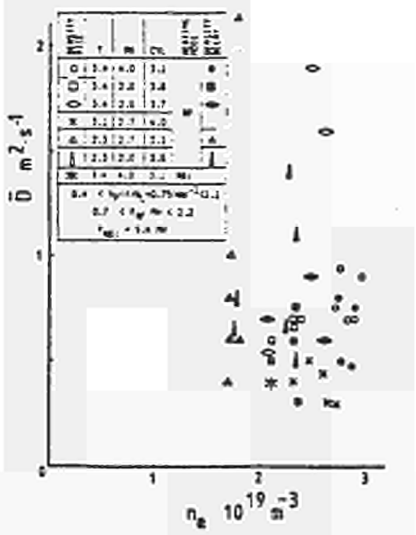

Fig. 4. The volume averaged diffusion coefficient $\bar{D}$, versus average electron density $\bar{n}_e$, for various plasma conditions.

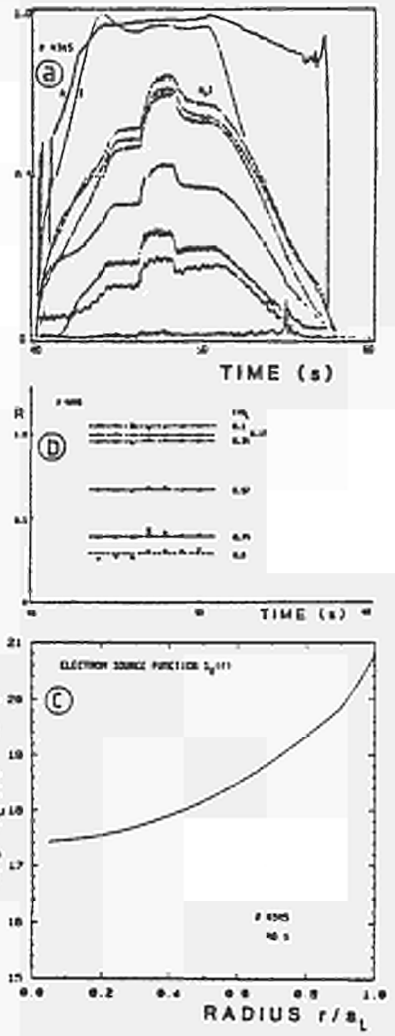

Fig. 4 . Plasma discharge in deuterium. B_T = 2.3 T, a/a = 1.4. 2 MW ICRF applied at 46.1 sec. for 2 sec. in hydrogen minority heating mode.
(a) Temporal evolution of plasma current, I, (2.1 MA full scale), plasma aperture, a, (5.86 m full scale), and seven vertical line-integrated measurements, n_eL, (8.53 x 10^{19}m^{-2} full scale).
(b) Ratios of the seven line-integrated density measurements to a central value, versus time. The constancy of these ratios indicates the constancy of the electron density profile during ICRF.
(c) Electron source versus normalized radius.

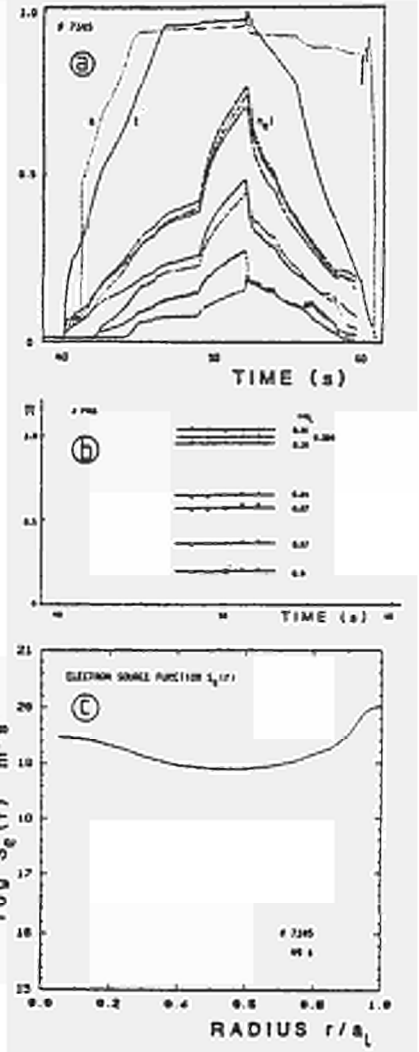

Fig. 5 . Plasma discharge in deuterium. B_T = 3.5 T, a/a = 1.46. 5.4 MW of 64 MHz hydrogen ICRF at 49 sec. for 1 sec.
(a) Temporal evolution of plasma current, I, (4.1 MA full scale), plasma aperture, a, (7 m full scale), and seven vertical line integrated measurements, n_eL, (19.5 x 10^{19}m^{-2} full scale).
(b) Ratios of the seven line-integrated density measurements to a central value, versus time.
(c) Electron source (including beam contribution) versus normalized radius.

ION CURRENT DRIVE USING ICRF AND COMBINED ICRF/NBI

H. Hamnén*
JET Joint Undertaking, Abingdon, Oxon., OX14 3EA, UK.
*On attachment from Chalmers University of Technology, Göteborg, Sweden.

Introduction

Among the various proposals to drive non-inductive currents in tokamaks are suggestions to use radio frequency current drive in the ion cyclotron range of frequencies. In the so-called minority regime, this could be done by heating a thermal minority ion species [1], or by heating a neutral beam injected minority species [2].

In the original proposal by Fisch [1], of current drive using minority ions, only a qualitative estimate of the current drive efficiency was done. In the subsequent papers [3,4], analytical studies based on the Fokker-Planck equation were carried out, for thermal and injected minority ions respectively.

In this paper, we will report on a numerical study of the current drive efficiency for these two schemes. Only the current carried by the minority ions will be included, leaving aside possible currents in the electron species. Electron currents could be created either by direct interaction with the wave through Landau- and transit-time damping, or as a "return current", resulting from momentum transfer from the minority ions.

For the calculations presented here, the effects of toroidicity on the particle motion along the field lines will be neglected. The Fokker-Planck equation for the minority ions then reads:

$$\frac{\partial f}{\partial t} = C(f) + Q(f) + S \qquad (1)$$

Here C(f) is the collision operator which has been derived assuming Maxwellian distributions of equal temperature for the background species, and using a linearised operator for the self-collisions [5]. Further Q(f) is the RF- operator, using the quasi-linear approximation [5], and S is a narrow Gaussian source function representing neutral beam injection. Also included in S is a low-temperature Maxwellian sink, with loss rate equalling the injection rate.

For the wave-particle interaction we will use the equation:

$$Q(f) = \frac{1}{v_\perp} \frac{\partial}{\partial v_\perp} \left(v_\perp D_o F(v_\parallel) \frac{\partial f}{\partial v_\perp} \right) \qquad (2)$$

Here D_o is a constant, dependent on the electrical field strength. For $F(v_\parallel)$ we will use the simple model:

$$F(v_\parallel) = \exp - \left(\frac{v_\parallel - v_o}{w} \right)^2 \qquad (3)$$

Numerical Results and Discussion

The scaling given by Fisch [1], for the minority ion current drive is

$$\frac{j}{P} \sim \frac{T}{n_e} \qquad (4)$$

where j is the current density and P is the power density.

The results presented here have been calculated using the 2-D finite-element code BAFIC, [6]. We have used one single set of plasma parameters. For the ion species we have chosen hydrogen minority ions and deuterium background ions, with $Z_{eff} = 1$, $T_e = T_i = 8keV$ and $n_e = 5 \times 10^{19}\ m^{-3}$. Throughout, the minority ion species concentration has been set at 5%. For the NBI cases, the injected power density has been set at $0.1MW/m^3$ and the injection point corresponds to a pitch angle of 15°.

Shown in Fig. 1 is the efficiency of the pure ICRF scheme for three different interaction velocities v_o vs absorbed power density, using a velocity space interaction width $w = 0.5v_{th}$. For interaction velocities $v_o \geq 3v_{th}$ it is difficult to achieve good numerical convergence. In spite of low power absorption (< $5kW/m^3$), very long high-energy tails are produced. Since the current drive is critically dependent upon the variation of the collision frequency, the best efficiency is found if the particles stay in a region of velocity space where this variation is strong. Being pushed too far out in the tail, electron collisions start to dominate and the collision frequency becomes almost constant. Thus, it seems to be difficult to achieve the optimum efficiencies predicted by Fisch [1], which occur for $v_o \sim 5v_{th}$, with the high power levels expected in forthcoming experiments.

By tuning the wave to a neutral beam injected species, one may hope to overcome this draw-back, simply because there are now more particles in the optimum interaction zone, implying less power per particle. That indeed this scheme has a much more favourable scaling with power is illustrated in Fig.2, which has been calculated setting the velocity space interaction velocity v_o (Eq.(3)), equal to the NBI injection velocity.

Both schemes are compared in Fig. 3, again using a very low RF power absorption (~ $1kW/m^3$). Also shown is Fisch's qualitative estimate [1]. Surprisingly good agreement is found. However, as noted above, raising the RF-absorption for the pure ICRF scheme, the peak efficiency drops drastically.

The efficiency for combined ICRF/NBI is shown in Fig. 4, for different values of the velocity space interaction width w (Eq.(3)), again setting the velocity space interaction velocity v_o equal to the NBI injection velocity. It is interesting to note that also with homogenous RF-interaction in velocity space ($w = \infty$ in Fig. 4), there will be considerable currents resulting from this scheme.

Conclusions

The current drive efficiency

$$\eta = \frac{1}{2\pi R} \cdot \frac{j}{P} \quad (A/W)$$

has been evaluated for pure ICRF minority heating and for combined ICRF/NBI (where for the latter scheme j/P denotes the incremental efficiency associated with the RF-interaction). For low RF-power, the efficiencies for both schemes agree well with Fisch's qualitative estimate [1]. The pure ICRF scheme, however, has a very strong power dependence, the efficiencies dropping dramatically for realistic power densities. This power dependence is much less pronounced for the combined scheme.

Using typical JET discharge parameters, it is found that currents of the order of 2-4MA could be driven with the planned ICRF- and NBI-capacity.

Acknowledgements

It is a pleasure to acknowledge a number of helpful discussions with Drs. T. Hellsten and W. Core.

References

[1] Fisch, N.J., Nucl. Fus. 21 (1981) 15.
[2] Okano, K., Inoue, N., Uchida, T., Nucl. Fus. 23 (1983) 235.
[3] Chiu, S.C., Chan, V.S., Hsu, J.Y., Guest, G.E., Prater, R., Rawls, J.M., Nucl. Fus. 23 (1983) 499.
[4] Cox, M., Start, D.F.H., Nucl. Fus. 24 (1984) 399.
[5] Stix, T.H., Nucl. Fus. 15 (1975) 737.
[6] Succi, S., Appert, K., Core, W., Hamnén, H., Hellsten, T., Vaclavik, J. (to be published in Comp. Phys. Comm.)

Figure Captions

Fig.1 Current drive efficiency vs. absorbed RF-power density for the pure ICRF case: a) $v_o=v_{th}$, b) $v_o=2v_{th}$ and c) $v_o=3v_{th}$. The velocity space interaction width $w=0.5v_{th}$.

Fig.2 Current drive efficiency vs. absorbed RF power density for the combined ICRF/NBI case: a) $v_o=5v_{th}$, b) $v_o=2v_{th}$ and c) $v_o=3v_{th}$. The NBI injection energy is 80keV and $w=0.5v_{th}$.

Fig.3 Current drive efficiency vs. velocity space interaction velocity for the two cases. The dashed curve shows Fisch's estimate, [1]. The absorbed RF power density was kept very low (< 5kW/m³).

Fig.4 Current drive efficiency for NBI only and the incremental efficiency for the combined case (for three different choices of interaction width), vs. NBI injection velocity ($v_o=v_{inj}$).

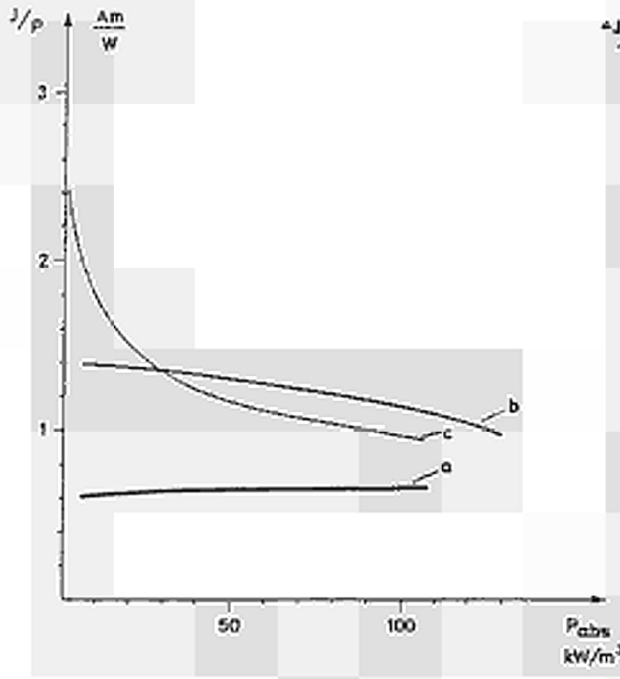

Fig.1

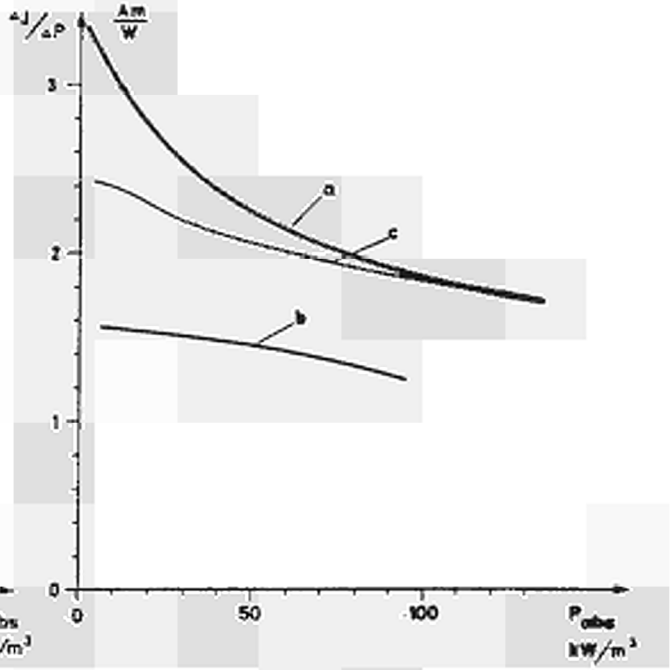

Fig.2

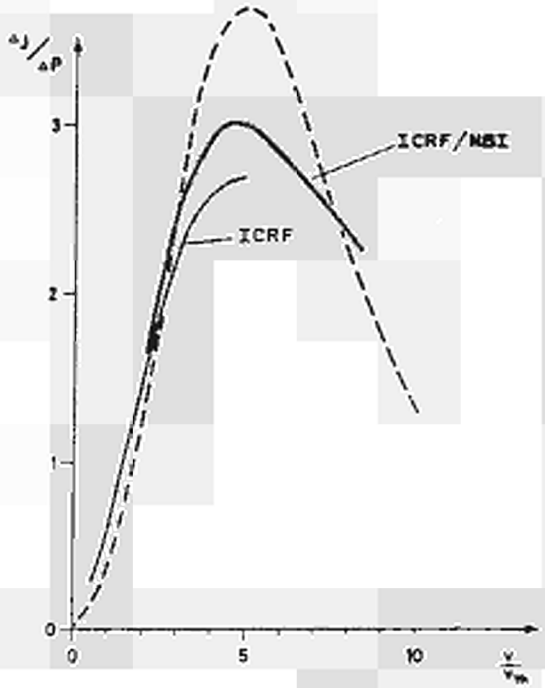

Fig.3

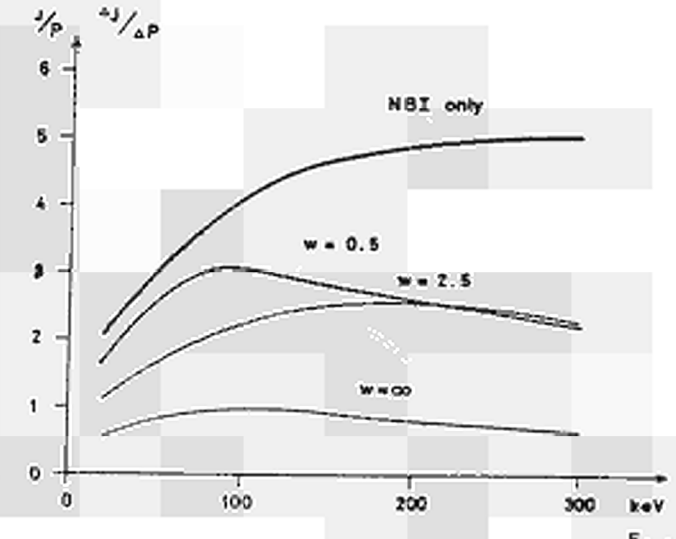

Fig.4

RADIATION BEHAVIOUR DURING ADDITIONAL HEATING OF JET PLASMAS

K Behringer, A Edwards, H-U Fahrbach[+], R D Gill, R Granetz, N Gottardi, H Jaeckel[+], G Magyar, E R Mueller[+], A Weller[+] and D Zasche[+]

JET Joint Undertaking, Abingdon, Oxon OX14 3EA, UK
[+]EURATOM-IPP Association, Garching

Abstract

Additional heating in JET with ICRH or NBI leads to an increase of the total radiated power. This is partly due to the density increase caused by the applied heating method. The relative power loss P_{rad}/P_{tot} reaches higher values with RF heating. The density increase can be partly controlled when the plasma is attached to the inner wall.

Radiation sources at the plasma edge lead to asymmetric radiation flux profiles. For this case the local emissivities can be derived from the bolometer measurement by a tomographic reconstruction method. Reliable values for the central radiation can be evaluated from the soft X-ray diagnostic when measuring with a 4.4 μm Be filter.

The radiative power loss of the JET plasma can be measured by bolometers in the energy range 5 eV $\leq E_{ph} \leq$ 9 KeV and with surface barrier diodes (soft X-ray diagnostic) in the range 300 eV $\leq E_{ph} \leq$ 10 KeV. The lower threshold energy of the diodes can be shifted to higher values by using Be-filters of different thickness. For both diagnostics two camera systems are available, viewing the plasma from the bottom ("vertical cameras") and the side ("horizontal cameras") on the same ports. In the immediate vicinity two RF antennae are installed which generate local radiation sources due to their interaction with the plasma. These sources contribute to the bolometer signal as well as to the soft X-ray signal (provided the latter is operated without filter). This may lead to an overestimation (up to about 10%) of the total radiated power derived from the vertical bolometer camera.

At present additional heating on JET with RF or NB provides similar maximum power levels ($P_{AH} \leq 5.5$ MW). The evolution of the electron density and hence of the radiated power during additional heating depends sensitively on whether the plasma is attached to the outer limiters or to the inner wall carbon protection plates. A strong increase of the electron density (particularly with NB-heating) and of the radiation loss is observed when the plasma is attached to the outer limiters. In inner wall operation, the density increase can be reduced or the density can even be kept constant. High radiation peaks may occur at the plasma edges. Fig.1 shows the radiation flux distribution for two NB-heated (Fig. 1a, 1b) and two RF-heated discharges (Fig. 1c, 1d) for limiter operation (top) and inner wall operation (bottom). The sudden appearance of a pronounced radiation peak at the inner plasma edge during the limiter bound discharge of Fig.1 is due to a shift of the plasma to the inner wall.

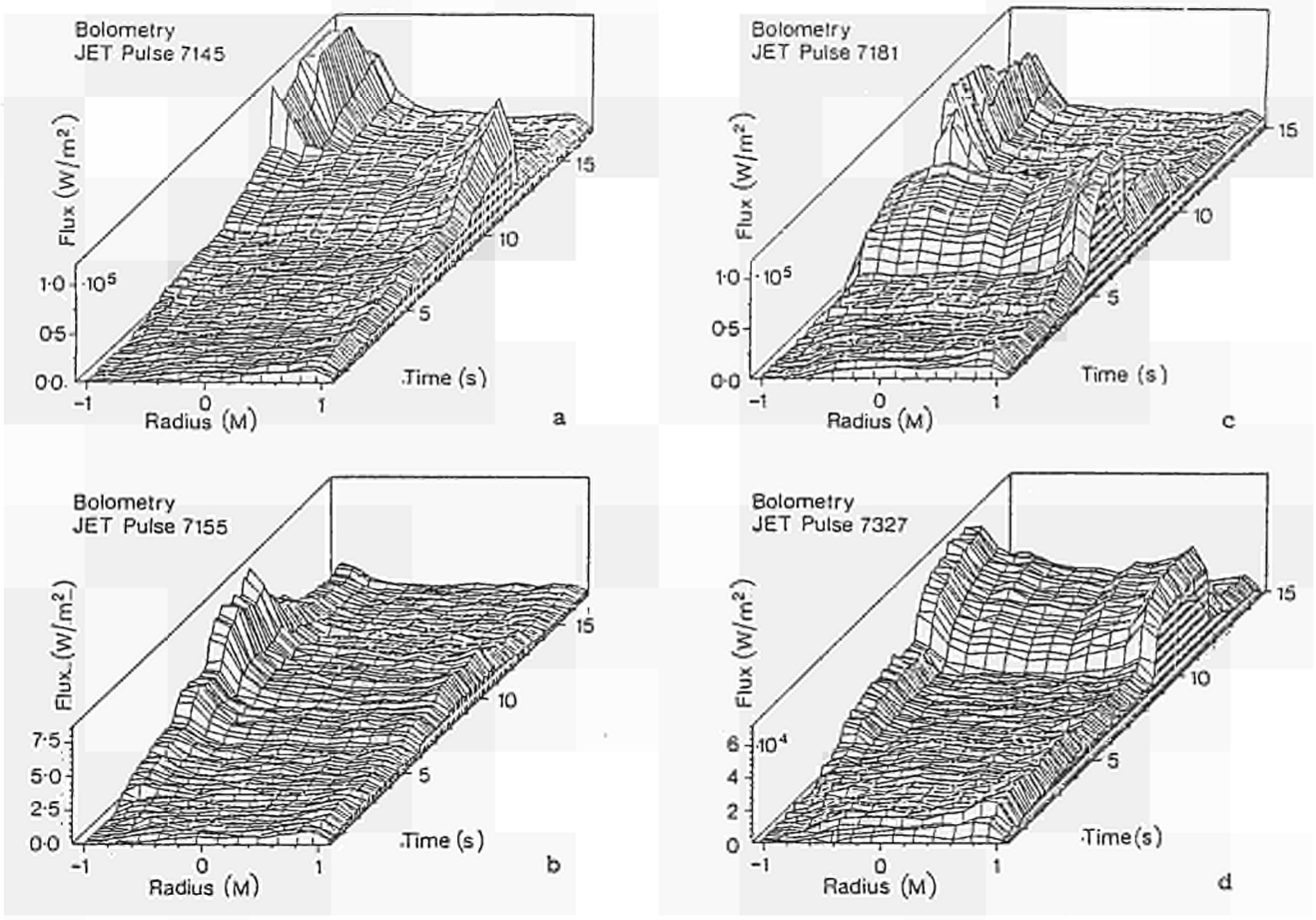

Fig. 1 Brightness distribution measured by the vertical bolometer camera for NB- (left) and RF-heated (right) discharges.

The relative power loss reaches 70% in the case of RF-heating (high <ne>). It can be kept quite low for NB-heating, when the density increase is controlled by shifting the plasma to the inner wall (Fig.2). Even in the high density NB-heated discharges the relative power loss is only about half of that in the corresponding RF-heated discharge.

The local emissivities can be evaluated by Abel inversion only for radially symmetric flux profiles. Using a tomographic reconstruction method /1/ one can derive local emissivities also when m = 1 and m = 2 deviations from the poloidal symmetry occur. Fig. 3 shows the emissivity distribution obtained from a tomographic reconstruction and from an Abel inversion (dashed curve) of the flux profile of the vertical bolometer camera. In the latter case the channels which are affected by the outer local radiation source have been omitted.

The emissivity in the centre cannot be derived accurately when asymmetries or hollow flux profiles occur. In that case the central emissivities can be obtained from soft X-ray measurements. Using a 4.4 µm Be filter ($E_{ph} \geq 750$ eV) leads to an attenuation of the radiation predominantly from the plasma edge and hence to radially almost symmetric emissivity profiles (Fig.4). In this case the m = 0 component gives reliable values for the central radiation. For the hollow radial profile shown in Fig.4 the contribution to the soft X-ray signal can arise from resonance lines of H-

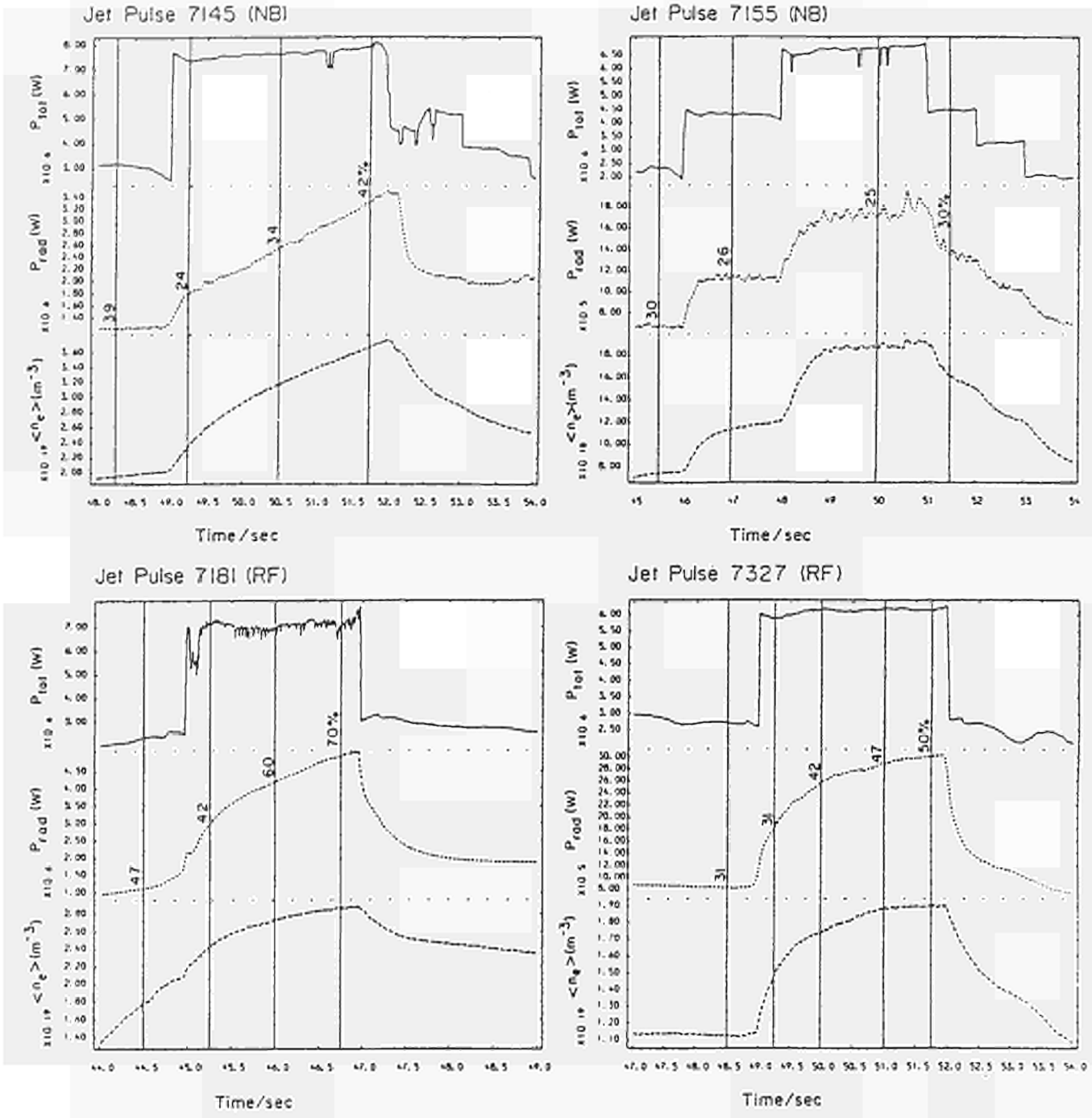

Fig. 2: Time history of the total radiated power (middle curves) and the volume averaged density <ne> (lower curve) for the input power given in the upper curves. The numbers at the middle curves give the relative power loss P_{rad}/P_{tot}.

and He- like oxygen and/or from metallic impurities in Ne- to Li-like states. Carbon line radiation is almost completely supressed by the 4.4 µm Be filter. For the discharge of Fig.4 a concentration of ~ 0.09% metallic impurties estimated from the soft X-ray measurements are in agreement with spectroscopic results /2/. For oxygen line radiation transport calculations usually show the radiation shell closer to the plasma edge than one would derive from the soft X-ray emission profile.

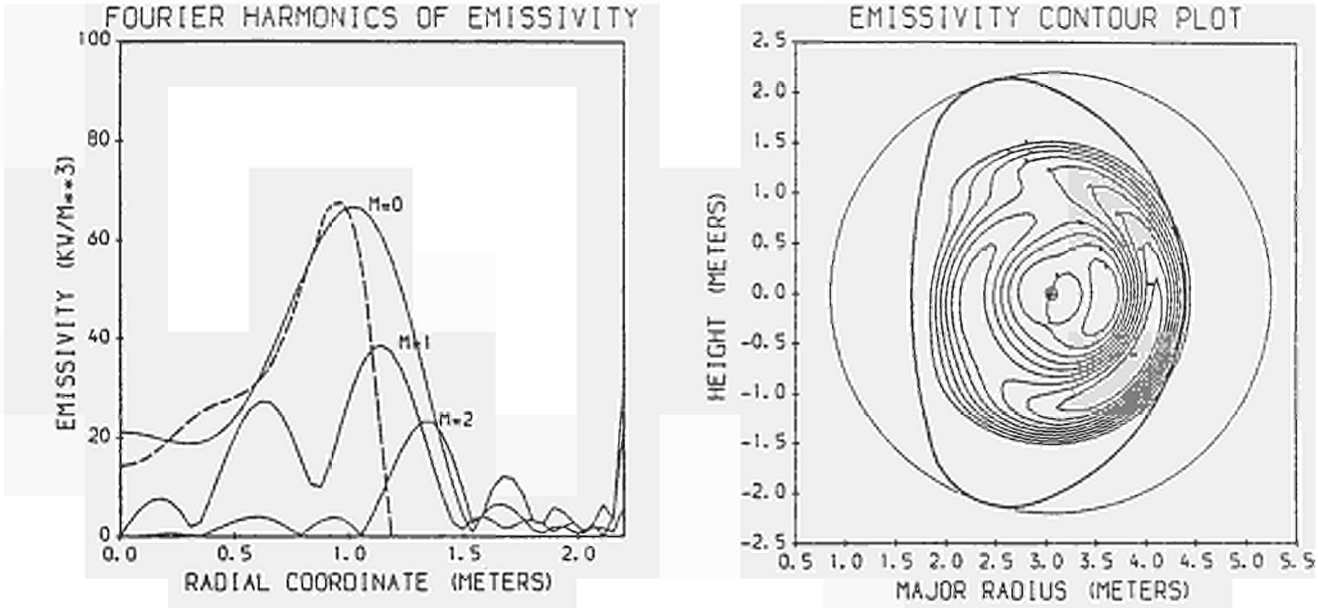

Fig. 3: Emissivity distribution of an RF-heated discharge derived by a tomographic method and by Abel inversion (dashed curve).

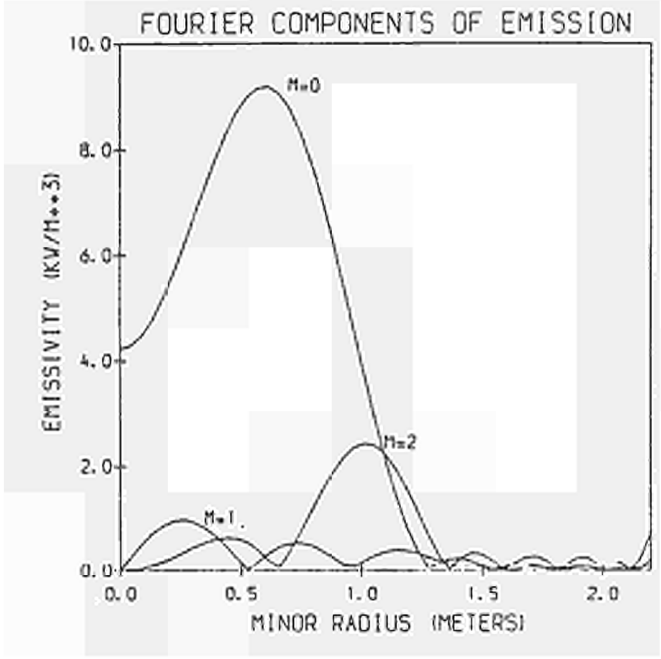

Fig. 4: Fourier components of the emissivity obtained from a soft X-ray measurement using a 4.4 µm Be filter.

References

/1/ R.S. Granetz and J.F. Camacho, Nucl. Fus. 25, 727 (1985)
and
J.F. Camacho and R.S. Granetz, Rev. Sci. Instr., 52, 417 (1986)

/2/ B. Denne, et al., this conference.

T_i PROFILE STUDIES DURING ICRF HEATING IN JET

S Corti, E Barbato*, G Bracco*, M Brusati, M Bures, A Gondhalekar*, F Hendriks, F Sand, A Taroni, F Tibone, V Zanza*

* JET Joint Undertaking, Abingdon, OX14 3EA, UK
* ENEA Euratom Association, Frascati, Italy

ABSTRACT

After a brief description of the analysis code used, some measurements performed with an array of four passive Neutral Particle Analysers are presented. The main result of this study is the evaluation of T_i profiles both during ohmic phase and ICRH phase of a JET plasma. A comparison of the experimental T_i profiles with those obtained from Transport analysis codes and a power balance computation performed using the JICS code are discussed.

This paper describes features related to the analysis of neutral particles and the ion temperature in JET as measured with an array of four passive Neutral Particle Analysers. Ten energies for two species (Hydrogen and Deuterium) are detected simultaneously in each analyser, so that the two energy spectra can be obtained at any time of a discharge and at different spatial locations. The neutral particles emitted by the plasma are ionised in a gas stripping cell and energy and mass analysed in a B//E geometry. The analysers have been absolutely calibrated both for H and D.

An analysis code /1/ taking into account all the relevant processes is available. This code, using the measured neutral particle fluxes, the measured T_e and n_e profiles, taking the edge neutral density as a free parameter allows to compute the neutral density and the T_i profiles. A value for n_i/n_e (ranging between 0.5 and 1) is assumed, constant in radius, throughout the calculation.

To start with a T_i profile is assumed as a parabola best fitting the four points obtained performing a linear fit on the spectra given by the different operational analysers. An iterative process is then adopted taking the χ^2 of the fitting to the experimental spectra as the key parameter.

In order to check the consistency of the calculated profiles with the experimental data, the value of the derivative of the spectra (i.e. the value of the temperature) corresponding to the radial location of each energy measured experimentally is superimposed to the final profile. In doing that, the assumption is made that T_i be constant on a given magnetic surface, so that all energies, measured along different lines of sight, can be plotted on the same radial scale.

In Fig. 1 the profile obtained during the OHMIC phase of a discharge is shown. The horizontal error bars correspond to the halfwidth of the relevant source functions.

During Ion Cyclotron Resonance Heating the ion temperature profile is modified according to the location of the resonant layer and of the power deposition. By varying the value of the toroidal field it is possible to have the position of the resonant layer changed during the same discharge. Figs. 2 and 3 show respectively the profiles obtained in case of central and off-axis heating.
The experimental T_i profiles obtained in this way have been compared for the ohmic phase of a discharge with those resulting from transport code simulations. The standard transport model for JET has been used: i.e. neoclassical resistivity, $\chi_e = 2\chi_{eCMG}$ and $\chi_i = 5\chi_{iCH}$, χ_{iCH} being the neoclassical ion thermal conductivity given in /27. The results are shown in Fig. 4. Good agreement is found between computed and measured profiles. The ion contribution to the energy replacement time in this case is half the electron contribution. This is mainly due to the deuterium depletion caused by impurities.

The same ion transport model is used to simulate the ICRH phase of the discharge. In this case a more detailed analysis is needed, especially at high RF power, where sometimes the consistency between the various T_i measurements failed. Results of the computation show that the NPA profiles can be consistent with the global power balance. However, when $P_{RF} \geq 2 - 3$ P_Ω, they would imply that a substantial portion (~80%) of the auxiliary power is absorbed by the main ions. The radial dependence of the ion neoclassical conductivity allows to obtain, in these cases, T_i profiles rather broad in the intermediate plasma region ($\nabla T_i < \nabla T_e$) while the height of the central peaking is inversely proportional to the width of the RF power deposition profile. If this picture was confirmed, it would have rather drastic implications on the global plasma parameters (e.g. τ_e would be much higher, during RF, than estimated so far.)

The analysis of the power balance has been performed, both for the Ohmic and the RF cases, using the JET analysis code JICS /3/. Experimental profiles for electrons and ions have been used to infer power terms and local conductivities.
The power balance follows the general Tokamak pattern, with most of the input power being lost by conduction mainly through the electron channel. This picture is maintained (fig. 5) during additional heating: ie conduction losses scale with the total input power for both ions and electrons.

References.

(1) - G BRACCO, S CORTI, V ZANZA et al: JET Report JET-IR(84)04.

(2) - C S CHANGE, F L HINTON: AMPC Report 14-011, June 1985
(to be published in Physics of Fluids)

(3) - M BRUSATI et al. : Workshop on Diagnostics for Fusion
Research Conditions, Varenna, Sept. 1982, p.235

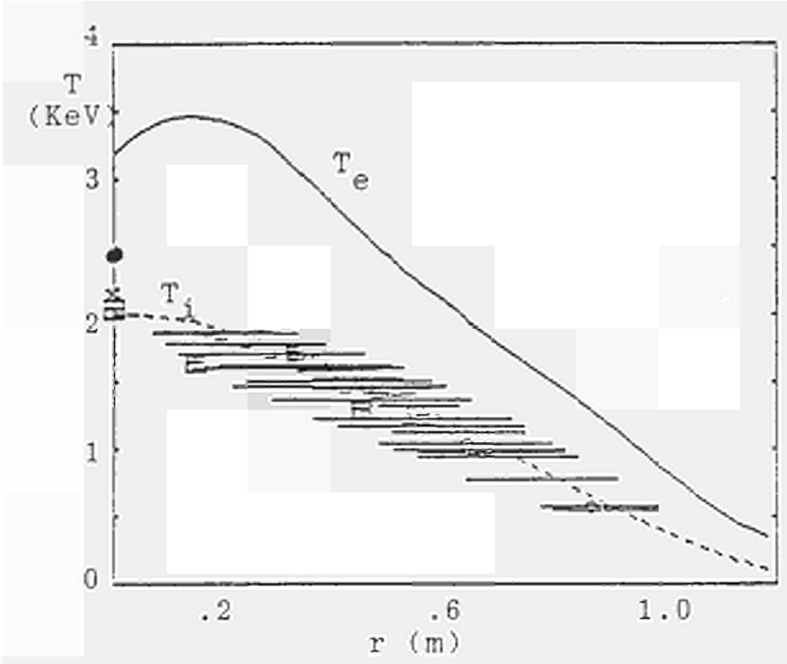

FIGURE 1 - T_i profile obtained during ohmic phase (shot 6850) (dashed line). The T_e profile from ECE measurements and the T_i values from x-ray spectroscopy on Ni (•) and from Neutron Yield (×) are also shown. The ⊞ represent linear fitting points.

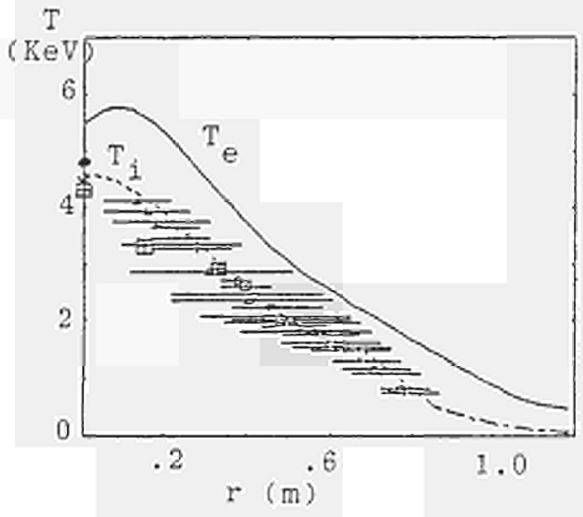

FIGURE 2 - As Fig. 1 but in case of ICRF central heating (shot 6850).

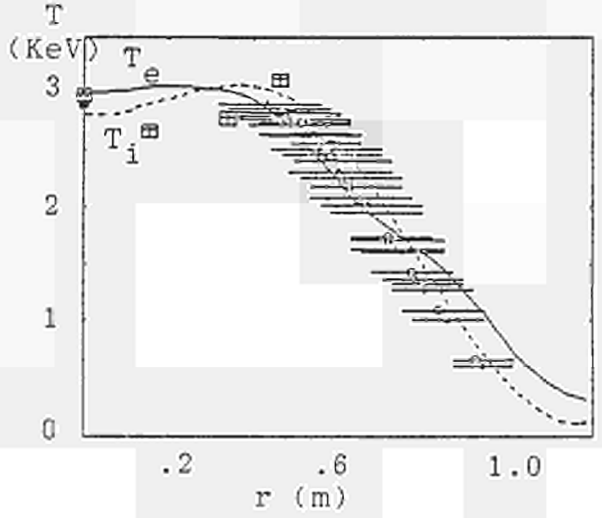

FIGURE 3 - As Fig. 1 but in case of ICRF off-axis heating (shot 6850) .

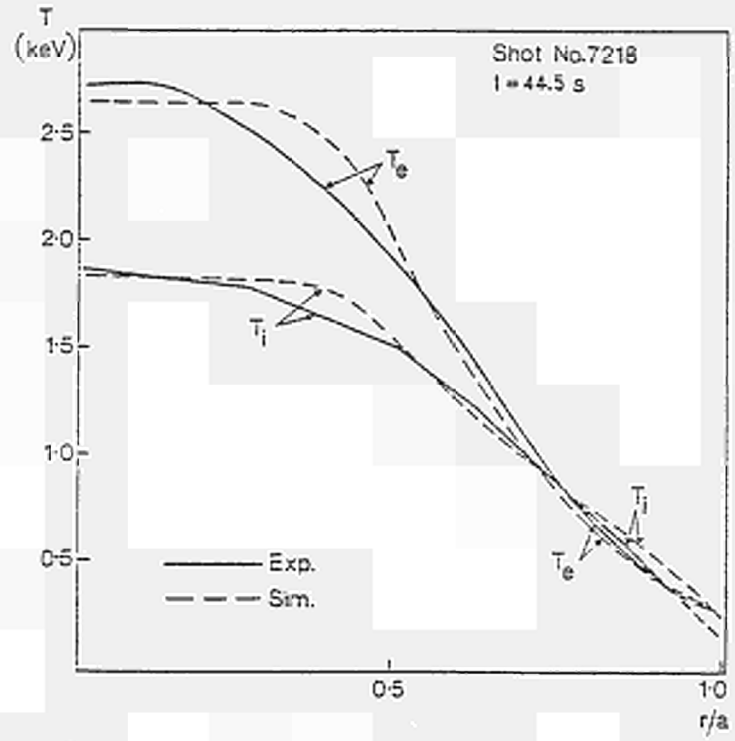

FIGURE 4

Comparison of experimental T profiles with those obtained by using Jet Transport Code in an ohmic case.

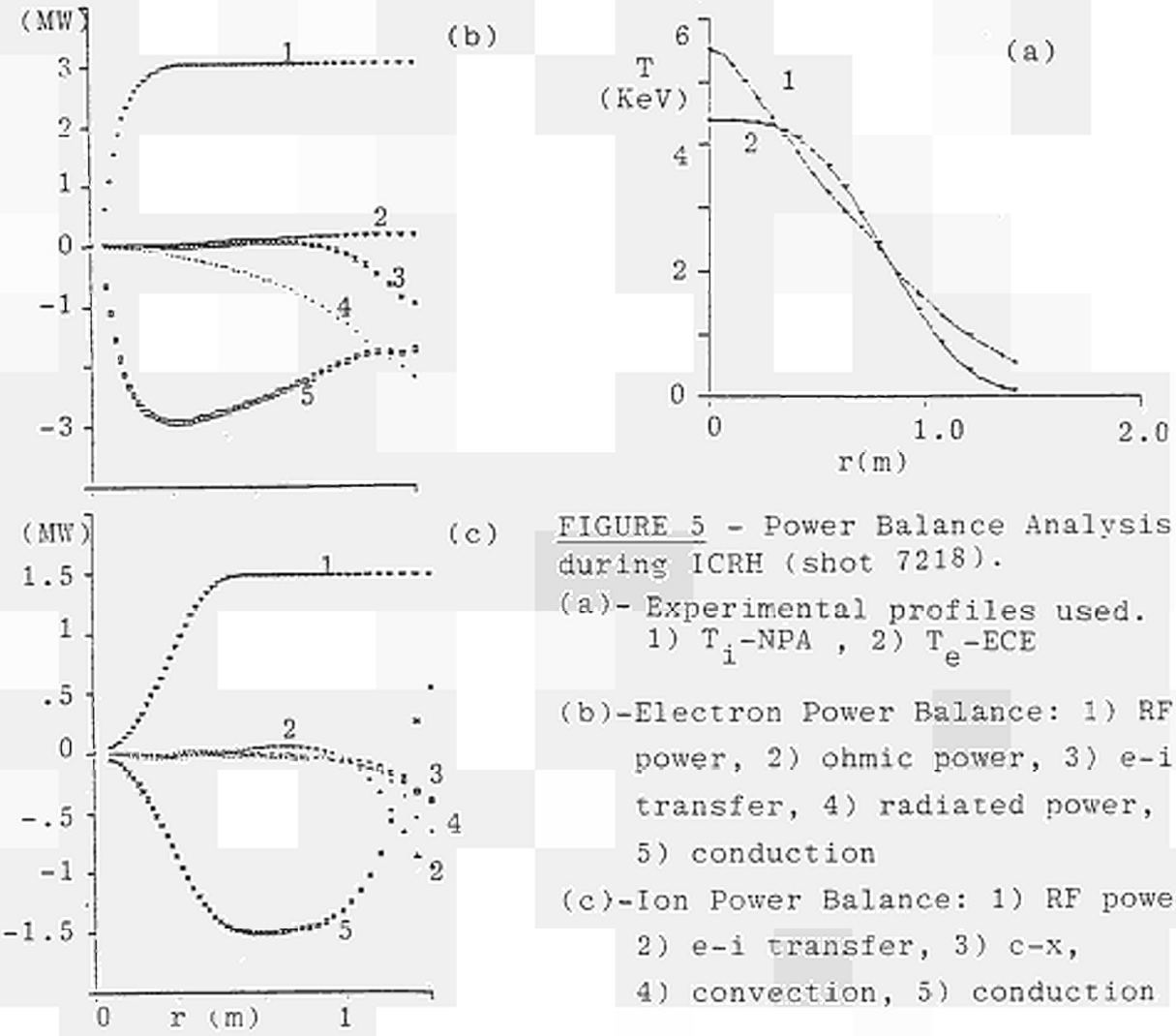

FIGURE 5 - Power Balance Analysis during ICRH (shot 7218).

(a)- Experimental profiles used. 1) T_i-NPA , 2) T_e-ECE

(b)-Electron Power Balance: 1) RF power, 2) ohmic power, 3) e-i transfer, 4) radiated power, 5) conduction

(c)-Ion Power Balance: 1) RF power, 2) e-i transfer, 3) c-x, 4) convection, 5) conduction

FAST WAVE ELECTRON CURRENT DRIVE

D. Moreau*, J. Jacquinot, P.P. Lallia

JET Joint Undertaking.
Abingdon, Oxon, OX14 3EA, UK

* From EUR-CEA Grenoble, France

Abstract

As a basis for investigating the possibility of controlling current profiles in JET we present a short analysis of transit time magnetic pumping of electrons by fast magnetosonic waves above the ion cyclotron frequency.

1. Introduction

The "profile consistency" observed to limit the performances of additionally heated tokamak discharges stressed the interest of decoupling their temperature and current density profiles.

The fast magnetosonic wave has been considered as an attractive candidate for non-inductive current drive /1-2/. Unlike the slow wave in the lower hybrid frequency range, it has indeed the potentiality of being efficient at high density and high temperature. Interaction with the bulk of the electron distribution in the centre of the discharge, although not the most efficient, would provide the required absorption of the RF power. In particular the fast wave could be very well suited for driving a reverse current in the central hot and dense plasma of large tokamaks, with the hope of suppressing "sawteeth relaxations" /3/.

A mode conversion current drive scheme near a two-ion hybrid resonance (Bernstein wave current drive) has been proposed /4/. As an alternative, we shall concentrate in this paper on direct electron current drive from the high frequency Alfvén wave itself. We shall draw some preliminary conclusions with respect to wave absorption by the electrons, bearing in mind that other loss channels such as absorption from ions at harmonics of Ω_{ci} or from high energy fusion products will have to be avoided or overcome.

2. Electrodynamics of the fast wave above the ion cyclotron frequency

We consider frequencies such that $\Omega^2_{ci} < \omega^2 < \Omega_{ci}\,\Omega_{ce}$ and densities higher than the lower hybrid resonance density ($\omega^2_{pi} \gg \omega^2$). The wave has both electrostatic and electromagnetic components, ie. $\vec{E} = -\frac{1}{c}\frac{\partial \vec{A}}{\partial t} - \nabla\phi$, its electric field is mostly perpendicular to the equilibrium magnetic field $\vec{B}_o$ and its magnetic field $\vec{B}$ parallel to $\vec{B}_o$. Parallel currents exist due to a small parallel electric field but also to the bulk $\mu\nabla B$ force exerted on the electron fluid. This force is the only thermal effect taken into account. Solving Maxwell's equations within these assumptions, one obtains the following results:

- at densities such that $\omega_{pi} >> \omega$ only the fast branch propagates and there is no problem of accessibility up to a few harmonics of Ω_{ci};
- near cutoff the wave has all the characteristics of the right handed circularly polarized whistler mode and then transforms itself into the high frequency Alfvén wave (HFAW), $n = n_A = \omega_{pi}/\Omega_{ci}$, at almost perpendicular propagation.
- if $\vec{B}_o$ is along $\vec{O}z$, $\vec{k}$ in the Oxz plane and if α is the angle between $\vec{k}$ and $\vec{O}x$ we find the following polarization for the HFAW:
$A_y = -jn_A \phi \cos\alpha \, \Omega_{ci}/\omega$, $A_x << A_y$, $E_y = j k_o A_y$, $B_z = j k_o n_A A_y \cos\alpha$ and $E_x = -j k_o n_A \phi \cos\alpha$;
- the energy density carried by the wave is mostly in magnetic and ion kinetic energy and can be expressed as
$W = W_m + W_i \approx 2W_m = B_z^2/\mu_o \approx 0.5 \, n_e T_e \beta_e \left| e\phi/T_e \right|^2$ where β_e is the usual ratio of electron pressure to magnetic pressure.

3. Interaction of the fast wave with electrons : TTMP vs. LANDAU DAMPING

Both parallel (-eE// force) and perpendicular ($-\mu\nabla//B$ force) electric fields act upon the parallel velocity of the guiding centre of the electrons. However, unlike ions in TTMP heating, electrons see opposite forces and the interaction vanishes at some critical perpendicular energy W_{crit}. Because the parallel electric field adjusts itself so as to give a zero net force on the bulk electron fluid (in the limit of zero electron inertia and $\omega_{pi} >> \omega$) we expect this critical energy to be near the thermal energy of the bulk electrons. TTMP diffusion will therefore be most efficient on electron tails having perpendicular energies a few times above thermal.

Our detailed calculations show that the total force applied on the guiding centre is

$$F// = j k_o e \phi n// \frac{\omega^2}{\Omega_{ce} \Omega_{ci}} \left[1 - \frac{W_\perp - \langle W_\perp \rangle}{mc^2} \frac{\omega^2_{pi}}{\omega^2} \cos^2\alpha \right]$$

so that the critical energy defined above is indeed

$$W_{\perp crit} = \langle W_\perp \rangle + mc^2 \, \omega^2/\omega^2_{pi}$$

where $\langle W_\perp \rangle$ is the average perpendicular energy of the electron fluid ($\langle W_\perp \rangle \approx T_e$). It is to be noted that at high density and low frequency (50 MHz) $W_{\perp crit}$ is indeed near T_e whereas at higher frequencies (800 MHz) it is much larger so that Landau damping is the dominant absorption process (cf. Fig. 1).

From the expression of the total force given above, it is straightforward to obtain the quasilinear diffusion coefficient and the corresponding damping rate. We assume a Gaussian distribution in k// space for the wave energy density and, after some algebra, we find that we can approximate the diffusion coefficient by the following expression:

$$D_{ql} = 0.5 \langle \Delta v//^2 \rangle / \Delta t \approx \frac{\sqrt{\pi}}{2m^2 k_o} \left| \frac{F//}{v//} \right|^2 \frac{}{\Delta n//} \exp \left[- \frac{n// - n//_o}{\Delta n//} \right]^2$$

where $n//_o$ is the peak parallel wavenumber and $\Delta n//$ the half width of the spectrum. The thermal velocity v_{te} is defined by $T_e = \frac{1}{2} m v^2_{te}$ and $\left| e\phi/T_e \right|^2$ is related to the average wave energy density $\bar{W}$ by the expression given at the end of the precedent section.

In high temperature plasmas and at moderate resonant velocities the

Maxwellian distribution will not be much distorted and we find the following damping rate for the wave energy:

$$2\gamma = dW/Wdt = (\sqrt{\pi}/4)\ \omega\ \beta_e\ x_e\ \exp(-x_e^2)\ \left[1 + \left(\frac{\omega^2}{\omega_{pi}^2} \cdot \frac{mc^2}{T_e}\right)^2\right]$$

where $x_e = \omega/k//v_{te}$.

4. Absorption of the fast wave and steady state current drive

The results sketched above have been inserted into a Fokker-Planck code developed at Culham /5/. For a given energy density, ie. a given maximum diffusion coefficient, we obtain the steady state current density and absorbed power density and we compute the corresponding absorption length $L_{abs} = v_A/2\gamma = v_A W.(dW/dt)^{-1}$, where v_A is the Alfvén velocity. Future calculations will include trapping and relativistic effects which may reduce the current drive efficiency.

An example of electron distribution that we obtained is displayed on Fig. 2 and it is clearly seen that substantial distortions from Maxwellian distributions take place at high perpendicular energy.

Fig. 3 shows the absorption lengths resulting from high power (~ 0.1 MW/m^3) quasilinear interaction, as a function of β_e and T_e. It is clear that high β_e values ($\geq$ 5%) and bulk interaction will be required if the wave is to be absorbed in a few passes. In this respect, the advantage that the centre of the plasma is accessible to waves with relativistic phase velocities along the magnetic field may turn out to be of little practical interest.

Nevertheless, as shown on Fig. 4, current drive based on bulk electron interaction seems feasible in JET with efficiencies ($\eta = j/2\pi R P_{abs}$) of the order of 0.1 A/W. This is of the same order of magnitude as lower hybrid current drive efficiencies; however, we must emphasize that fast wave current drive should occur basically at the centre of the hot and dense JET discharges whereas lower hybrid current drive should be more peripheral at high temperatures. Both schemes (LHCD and FWCD) seem therefore rather complementary as far as profile control is concerned and could provide the additional "knobs" that one seeks for improving tokamak performances.

Finally, a suggestion for enhancement of the T.T.M.P. absorption could be to start from a pre-formed non-Maxwellian distribution having high perpendicular energy ($\gamma \alpha W_\perp^2$). Slide-away discharges or synergic effects from combined lower hybrid and fast wave current drive could for instance be beneficial.

Acknowledgments

We are deeply indepted to M. O'Brien, M. Cox and D.F.H. Start for use of their "BANDIT" Fokker-Planck code and for fruitful discussions.

References

/1/ F.W. Perkins, in ORNL/FEDC-83/1, Oak Ridge, 1983
/2/ D. Moreau and C.M. Singh, in "IAEA Technical Committee Meeting on Non-Inductive Current Drive in Tokamaks", Culham, 1983
/3/ H. Hamnén and J.A. Wesson, private communication
/4/ J. Jacquinot, Erice Course on Tokamak Startup, Erice, 1985
/5/ M. O'Brien, M. Cox and D.F.H. Start, paper submitted to Nuclear Fusion, 1986

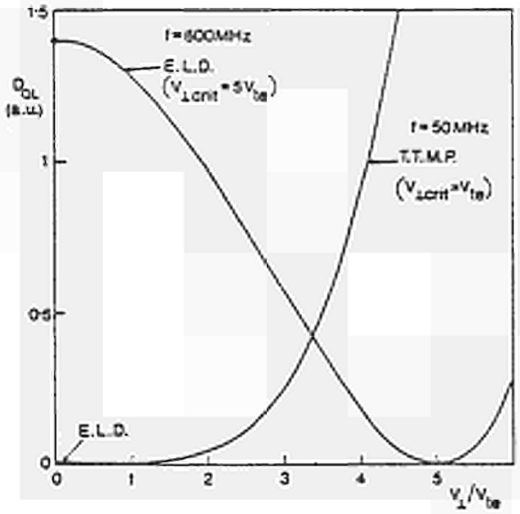

Fig. 1 Quasilinear diffusion coefficient versus perpendicular velocity at high (Landau damping) and low frequency (T.T.M.P.)

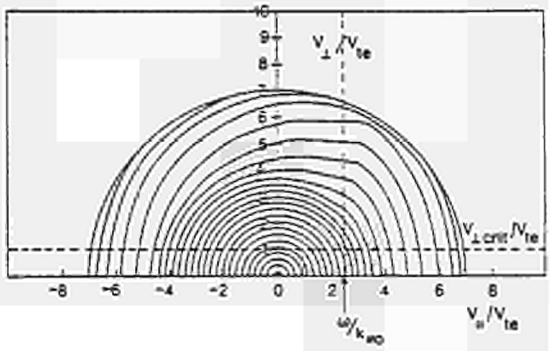

Fig. 2 Electron distribution contours for B_o = 2.2 T., f = 50 MHz, T_e = 5 keV, n_e = 1.8 x 10^{20} m^{-3} (β_e = 7.5%) in a H_2 plasma. The wave spectrum is Gaussian with $n//_o$ = 2.9 and $\Delta n//$ = 0.5

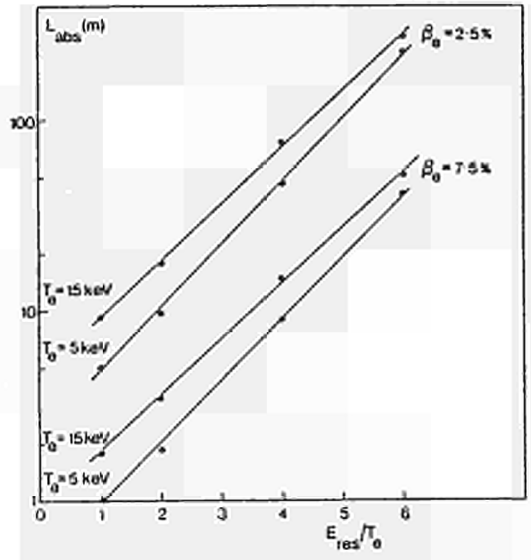

Fig. 3 Absorption length versus ratio of peak resonant energy to electron temperature (E_{res}/T_e) for β_e = 2.5% and 7.5%, and for T_e = 5 keV and 15 keV. Other parameters are B_o = 2.2 T., f = 50 MHz, $\Delta n//$ = 0.5 and H_2 plasma

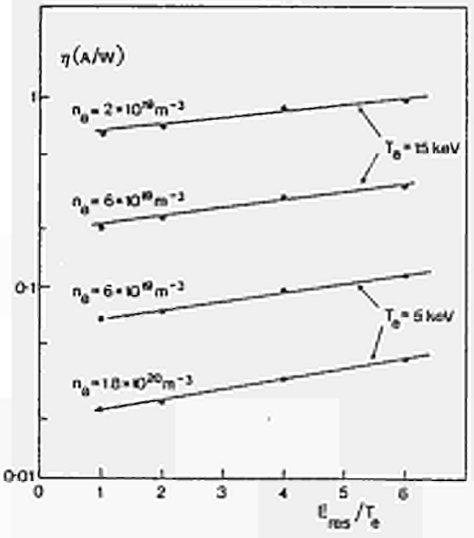

Fig. 4 Current drive efficiency versus E_{res}/T_e. Same cases as for Fig. 3 i.e. β_e = 2.5% and 7.5% and T_e = 5 keV and 15 keV

EFFECTS OF MAJOR RADIUS COMPRESSION IN JET

A Tanga, N Gottardi, A Hubbard, E Lazzaro, P Noll,
E Springmann, A Taroni.

JET Joint Undertaking, Abingdon, Oxon, OX14 3EA

Introduction

Major radius compression in tokamaks is a tool for achieving high plasma pressure [1,2,3,4]. Its attractiveness depends also on the fact that the compression can be made "adiabatic" and then the plasma quantities are expected to change according to simple laws ([1]).

In JET the application of a fast increase of vertical field has produced a displacement of the plasma column in major radius with the toroidal field constant in time. Typically the time necessary to detach the plasma from the limiter, until it reaches the final state in the contact with the inner wall, was 0.15 → 0.2s while the global energy confinement time was 0.5 → 0.7s. Parameters of the discharges analysed are presented in table I. Since the vertical field is not completely decoupled from the plasma, the increase of the vertical field causes an increase of poloidal flux. When the plasma is compressed the increase of plasma current is due for one third to the effect of the compression and for the rest to the increase of poloidal flux. The situation is illustrated in the figures 1,2,3. Fig 1 shows the flux contour as obtained by the equilibrium code INDENT B ([5]) before the radial compression. Fig 2 shows an analogous plot for the plasma, 0.19s later after the compression. The plasma is in contact with the inner wall and the cross section is hardly changed. The expected result in an ideal adiabatic case starting from the configuration of Fig 1 is shown for comparision in Fig 3. Here the equilibrium configuration was calculated using the code ESCO ([6]). The fluxes on the vacuum vessel are the same as in Fig 2 but the q profile and the toroidal and poloidal fluxes inside the plasma have been conserved and the adiabatic constraints ([7]) have been verified. It is evident that a pure adiabatic compression would have produced a smaller plasma. Moreover the increase in plasma current would have been only ~ 110kA against the ~ 360kA observed experimentally. The variation of flux as given in the table is in agreement with the changes in plasma current and variation of inductances.

Changes in plasma parameters

In terms of other plasma parameters a noticeable increase of the peak and of the volume average electron temperature has been measured by electron cyclotron emission and it is shown in Fig 4. It should be noticed that the increase of the peak and average electron temperatures is more slow than the compression which takes place between t = 8 and t = 8.2 seconds.

Some enhancement of the sawteeth activity is also present. The time evolution of the ion temperature, as deduced from neutron emission is shown in Fig 5. In Fig 6 the radial profile of the electron density is shown as obtained by Abel inversion of the interferometer data. There is a noticeable peaking of the electron density profile subsequent the radial compression. It should be also mentioned that n_e scales approximately as C^2, C being the initial major radius divided by the final one, as it is expected from the adiabatic scaling. The total radiated powers as obtained by the integration of the multichord bolometer camera, during the compression shows only a small variation (in this case a reduction), compared to the global input power. This fact would suggest that the resistive losses are not substantially enhanced by the radial compression.

Conclusions:

According to the adiabatic laws the temperature should scale with the compression ratio to the 4/3. Thus one would have expected a 10% increase in Te and Ti while the experimental values are respectively an increase by 20% and 30% shown in Table 1. This is probably due to the appreciable ohmic contribution as it is shown by the analysis of the magnetic data. It is obviously difficult to quantify in detail the balance of the power fluxes in a transient, however the increase of both the ion and electron central temperature is much faster than the resistive skin time and may this suggest the presence of an anomalous penetration of the plasma current which may contribute to the increase of the plasma temperature. The electron density scales in agreement with the adiabatic scalings. It should be stressed that, despite the elative changes in plasma parameters being small, there seems to be an enhancement in the thermal content of the discharge which seems to originate both from the flux variation and from the radial compression.

References

1) H P Furth and S Yoshikawa Phys of Fluids 13 2593 (1970)

2) V E Golant Plasma Physics and controlled Fusion 26 N° 1A, 77 (1984).

3) G Tait et al. in Plasma Physics and Controlled Nuclear Fusion Research London, Sep 12-19, 1984 (IAEA, Vienna, 1985) vol I, pp 141-154.

4) A Airoldi-Crescentini, G Grosso, G Lampis, L Lanzavecchia and E Lazzaro. Proc of the 2nd Joint Genoble-Varenna. Int. Symp. 1980 Vol II p 1059.

5) M Brusati et al. Comp. Phys. Rep 7-8, 345 (1984).

6) A Cenacchi, E Springmann, A Taroni to be published.

7) F L Hinton and R D Hazeltine Rev. of Mod. Phys. Vol. 48 N. 2 pp 305, 306. (1976)

TABLE I

	Ip	t	B_T	ϕ_T	ψ	q_b	Li
Before Compression	2.03	8.02	2.92	1.6	6.95	5.4	1.15
After Compression	2.39	8.19	2.92	1.8	7.34	5.6	1.09

Compression ratio C = 1.07

Adiabatic scalings(1)

$$T \to C^{4/3} = 1.09;\quad n \to C^2 = 1.15;\quad Ip \to C = 1.07$$

Experimental values

$$\frac{T_{e_2}}{T_{e_1}} = 1.20;\quad \frac{T_{i_2}}{T_{i_1}} = 1.30\quad \frac{n_{e_2}}{n_{e_1}} = 1.16$$

B_T = Toroidal field in tesla

t = time in seconds

ϕ_T = toroidal flux

ψ = poloidal flux

$T_{i1(2)}$ = ion temperature before (after) the compression

Ip = plasma curretn (MA)

q_b = safety factor at plasma boundary

β_p = poloidal beta

li = internal inductance

$T_{e(2)}$ = electron temperature before (after) the compression

$n_{en(2)}$ = electron density before (after) the compression

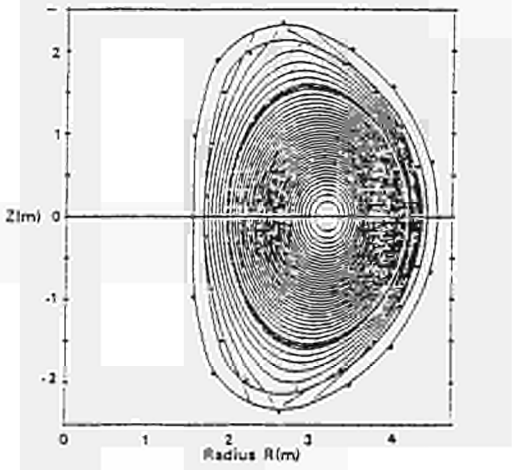

Fig 1

Poloidal flux contour of the plasma before the compression.

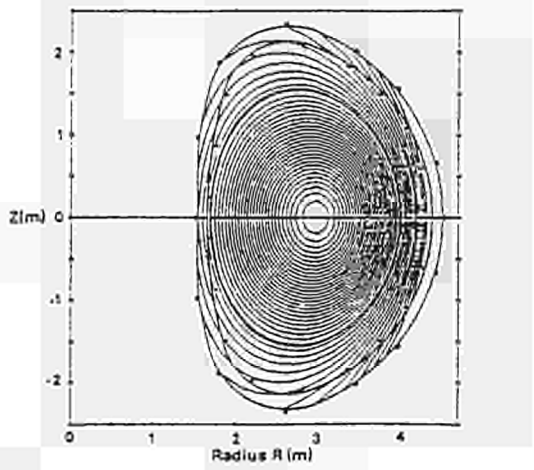

Fig 2

Poloidal flux contour of the plasma after the compression.

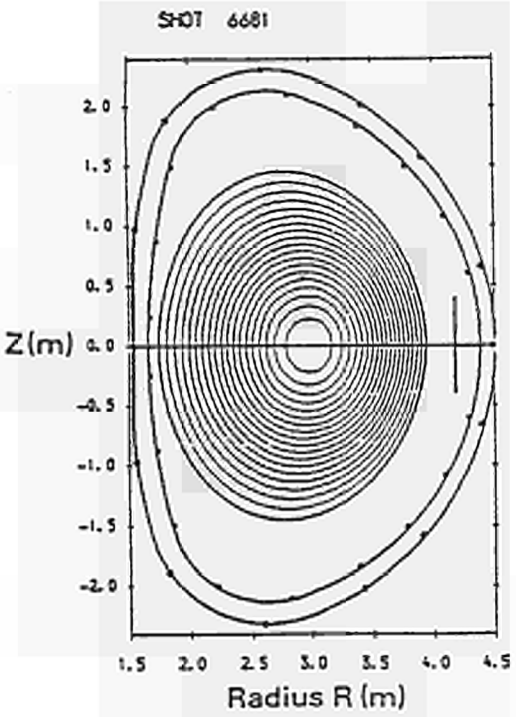

Fig 3

Poloidal flux contour of the plasma as it should have been if the compression were purely adiabatic.

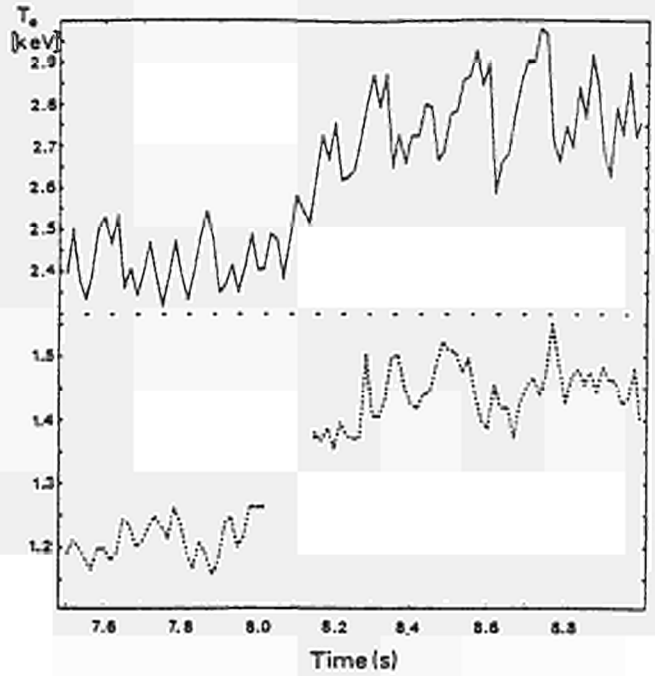

Fig 4

Time evolution of the peak electron temperature (top) and average electron temperature (bottom).

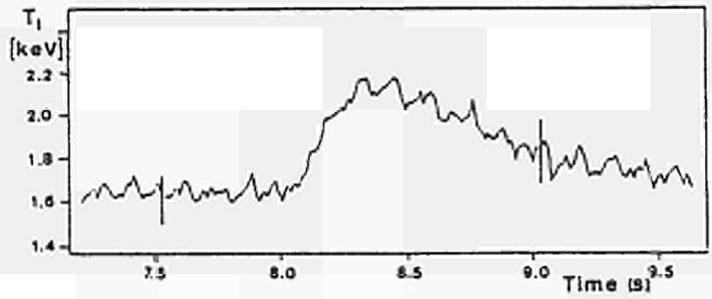

Fig 5

Time evolution of the peak ion temperature.

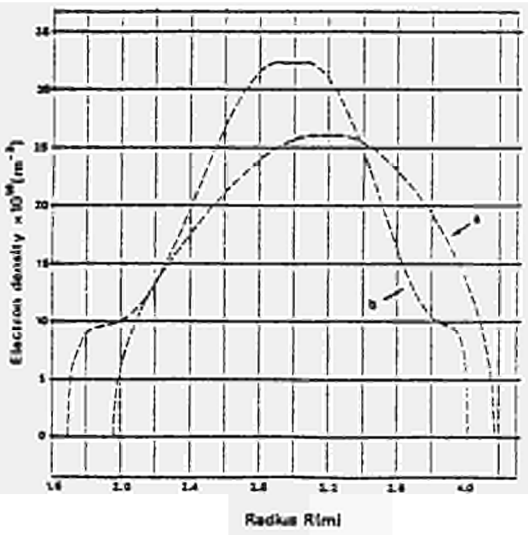

Fig 6

Electron density profile before compression (curve a) and after compression (curve b).

BEHAVIOUR OF THE PLASMA BOUNDARY DURING ICRH IN JET

H Brinkschulte, J A Tagle, M Bures, *S K Erents, P J Harbour, **T Huld, A S Kaye, ***C Lowry, *G M McCracken

JET Joint Undertaking, Abingdon, Oxon OX14 3EA, UK
* EUR-UKAEA Association, Culham Laboratory, Abingdon, Oxon OX14 3DB, UK
** Dept of Electro-Physics, Technical University of Denmark, Copenhagen
***Dept of Plasma Physics, Imperial College, London, UK

1. Introduction

A knowledge of the properties of the plasma boundary layer and their changes during the application of RF power is of general interest. Measurements of electron temperature and density are needed to understand the behaviour of impurities in the edge region. Radial profiles of electron density determine, in addition to other parameters, the coupling resistance of the ICRH antennae. The energy flux is needed for designing the limiters which are shaped to homogenize the radially dependent heat load. A very important parameter for the proper design of a limiter is the e-folding length for the energy flux. The total flux is also needed to understand the confinement of particles and energy during ICRH heating and from the density profile the diffusion coefficient $D_\perp$ in the boundary may be estimated.

2. Experimental

The JET scrape-off layer has been studied with 2 sets of single Langmuir probes mounted at two different poloidal and toroidal positions.

(i) A movable array of 4 probes (LPT in Fig. 1) introduced through a vertical port scans the boundary plasma near the top of the machine from the wall up to a minimum distance of 60 mm from the first closed flux surface defined by the limiters.

(ii) An additional set of two probes located in a side protection tile of an ICRH antenna (LP1 and LP2 in Fig. 1). These two probes monitor the plasma at distances of 15 mm and 27 mm, respectively, from the limiter separatrix (magnetic ripple taken into account).

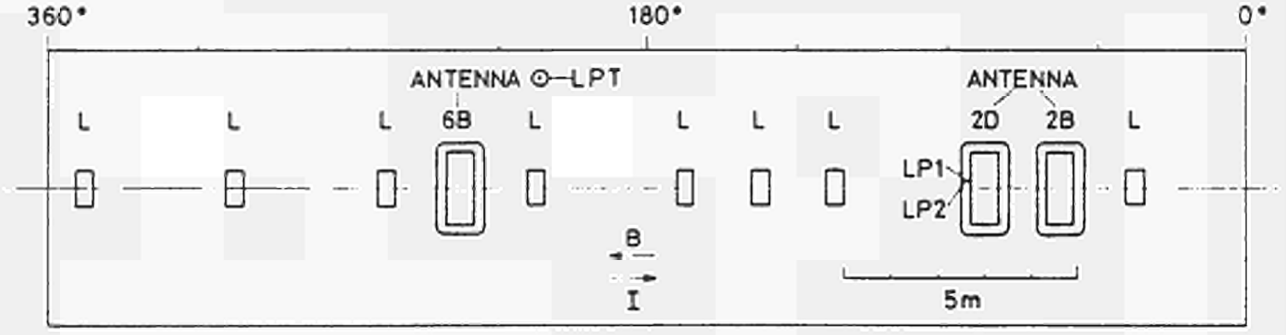

Fig. 1 Unfolded view of torus wall as seen from inside with 8 carbon limiters (L), 3 ICRH antennae (2B, 2D, 6B) and Langmuir probes (LP1, LP2, LPT).

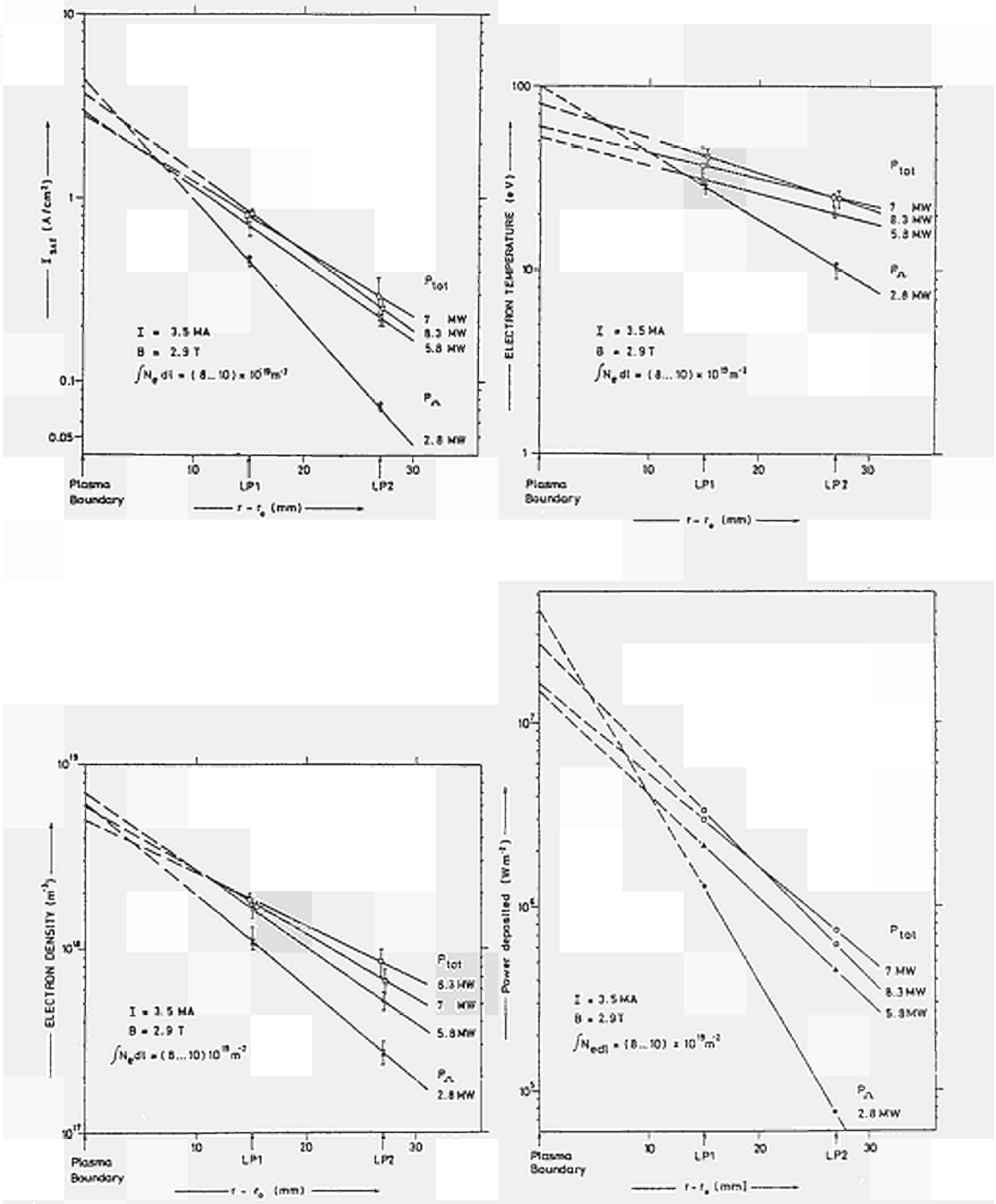

Fig. 2 Ion saturation current, electron density, electron temperature and power density versus distance from plasma boundary. Deuterium plasma with ^{3}He minority heating. JET pulses 6279...83.

Langmuir I-V characteristics ($-100\ V \leq V_p < +10\ V$) were taken at typically 0.5 second intervals during the plasma pulse, with a resolution of 50 ms for a single characteristic [1].

3. Results

Most of the results reported here have been obtained using the 2 antenna probes. The I-V scans have been arranged to determine the boundary properties before, during and after each 2 to 5 s long RF Heating pulse.

Fig. 2 shows the ion saturation current I_{sat}, the electron density n_e, the electron temperature T_e, the edge density n_e and the deposited power P_d versus radius for a typical discharge $\{I_p = 3.5$ MA, $B_T = 2.9$ T, $\int n_e dl = (8..10) \times 10^{19}\ m^{-2}\}$ in which up to 6 MW ICRH power was added to the 3 MW ohmic plasma. The density as calculated from I_{sat} and T_e is obtained by assuming $T_e = T_i$ and the deposited power flux density is derived from $\gamma I_{sat} T_e$ with $\gamma = 10$.

As a general observation all the parameters increase at both probes as RF power is applied, with an exponential decay of the parameters toward the torus wall[3]. The particle flux rises rapidly, with a time constant between 0.25 and 3 ms. The rise time in the RF power is ≈ 0.25 ms. Rise times in H_α and CIII light have also been measured, and these are faster than the sampling rate, (< 5 ms). We find that the e-folding length for I_{sat} increases from $\lambda_{Isat} = 6.6$ mm (for $P_{tot} = P_\Omega = 2.8$ MW) to 10.2 mm at $P_{tot} = 8.3$ MW (Fig. 2).

The density behaves similarly: λ_{n_e} increases from 9 mm for the ohmic target plasma to 13.2 mm at $P_{tot} = 8.3$ MW. The temperature rises from an average of 30 eV in the ohmic discharge to 45 eV with RF heating, as recorded by probe LP1. The T_e radial profile also flattens. The heat flux at the first probe rises from 1.3×10^6 W m^{-2} for $P_\Omega = 2.8$ MW to 3.3×10^6 W m^{-2} at 8.3 MW total power.

These profiles for I_{sat}, n_e, T_e and P_d are consistent with those measured with the top Langmuir probe array at similar discharge conditions if one takes into account that the field lines are compressed by a factor of 3 (mid-plane compared to top) [1-3].

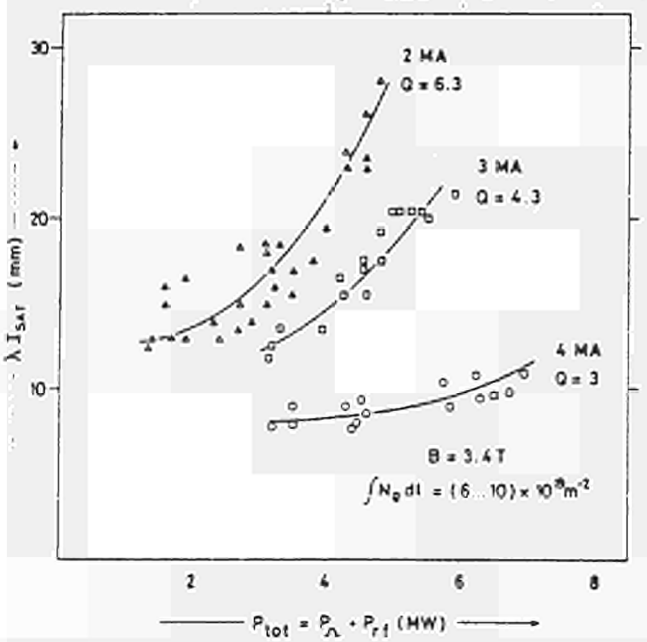

Fig. 3 e-folding length for ion saturation current versus total power for 3 different target plasmas (D with 5% ^{3}He).

The observed increase of all the e-folding lengths is more pronounced for a 2 MA discharge than at higher plasma currents (as demonstrated for λ_{Isat} in Fig. 3). The curves appear to steepen as more RF power is added to the discharge.

4. Discussion and Conclusions

It was found that electron density, temperature and hence deposited power all increased during ICRH. The relative increase is higher towards the wall - leading to a broader

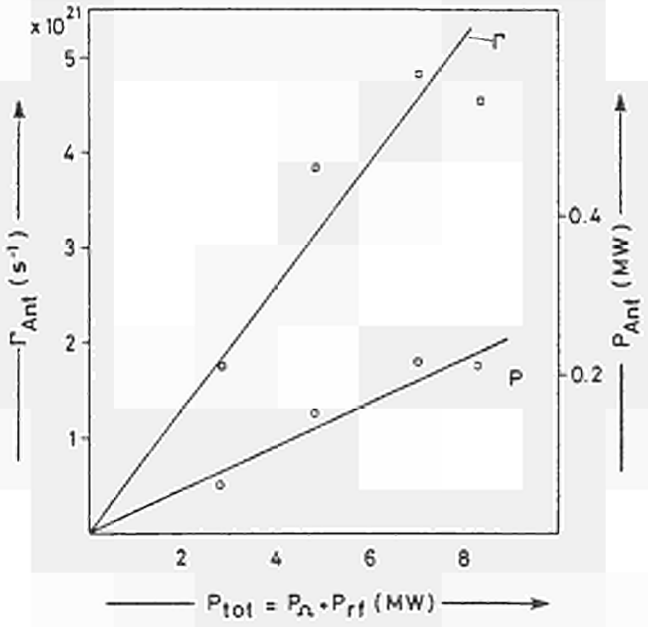

Fig. 4 Fluxes to the antenna limiters (at $r_s - r_o$ = 13 mm) versus P_{tot}.

boundary plasma during ICRH. (The absolute increases at the radii of LP1 and LP2 are similar.)

All parameters decay exponentially towards the torus wall. This is deduced from measurements taken between 15 mm and 60 mm from the separatrix. However one has to be cautious when extrapolating the measured data towards the plasma edge (dashed lines in Fig. 2).

The belt limiters for JET and the side protection tiles for the second generation ICRH antennae have been designed assuming a power flux e-folding length $\lambda_p \approx 10$ mm. The measured values are in that range. However, the increase in λ_p with power, taken in conjunction with the increases in I_{sat} and P_d, imply that the total particle flow and the total power flux to the limiters increase strongly with RF power. The calculated fluxes to the antenna limiters which are at $r - r_o$ = 13 mm are shown in Fig. 4. About 3% of P_{tot} is incident on the antenna limiters and up to 20% on the 8 carbon limiters. The increase of λ_p and P_d in the boundary with heating power is a matter of some concern.

The short timescale over which the boundary parameters increase (0.25-3 ms) is also observed for the CIII and H_α radiation. (The line averaged plasma density also increases during ICRH, but more slowly.) This implies that the plasma boundary is directly heated by the RF, the responsible mechanisms remain to be investigated.

The observed increase in e-folding lengths suggests an increase of perpendicular transport (and/or increased heating and/or ionisation in the S.O.L. [3]).

The rise in electron density with the associated flattening of the density profile should result in little change in antennae coupling resistance - which indeed has been observed.

References

1. S K Erents, J A Tagle, G M McCracken, P C Stangeby and L de Kock (Submitted to Nuclear Fusion).
2. P C Stangeby, S K Erents, J A Tagle, G M McCracken and L de Kock, 12th European Conference on Controlled Fusion and Plasma Physics (Budapest, Hungary, 2-6 September 1985), Vol. 9F,II,p 579
3. S K Erents, J A Tagle, P C Stangeby, G M McCracken, T Huld and L de Kock, to be presented at VIIth Int. Conf. on Plasma-Surface Interactions in Controlled Fusion Devices (Princeton, May 1986).

EFFECT OF OFF AXIS ICRF POWER DEPOSITION IN JET

F. Sand, **B. Beaumont, *V.P. Bhatnagar, M. Bures, S. Corti
J. Jacquinot, P.P. Lallia, A. Tanga

JET Joint Undertaking, Abingdon, Oxon, OX14 3EA, UK
** From EUR-CEA, Fontenay-aux-Roses, France
* From LPP-ERM/KMS; EUR-EB Association, 1040 Brussels, Belgium

1. Introduction

First tests were made in JET to assess off axis power effects on:
- confinement (including possible heating optimization q = 2 stabilization)
- sawteeth behaviour
- profile control.

The large dimension of the plasma cross section (2.50 m x 4 m) compared to the antennae dimensions and to the perpendicular wavelength of the wave together with a significant focalisation provide good localisation of the power deposition. The parameter range provided single pass absorption and little reflection.

2. Description of the Method

The JET RF system can cover a broad band in frequency (25-55 MHz) but in discrete steps requiring time consuming adjustments. It was therefore decided to alterna tively fix the frequency at a given value (~33 MHz) and to slip the resonant layer through the plasma cross section by a continuous change of the main toroidal magnetic field. The ramp duration is 10s and the magnetic value decreases either from 3.4 T to 2.1T (Case A, He^3 minority, 3 MA) or from 2.6 to 1.4T (Case B, H minority, 2 MA). The 4s RF pulse is superimposed at various times (45-49 or 48-52 or 51-55) to cover the full plasma cross section (Fig. 1).

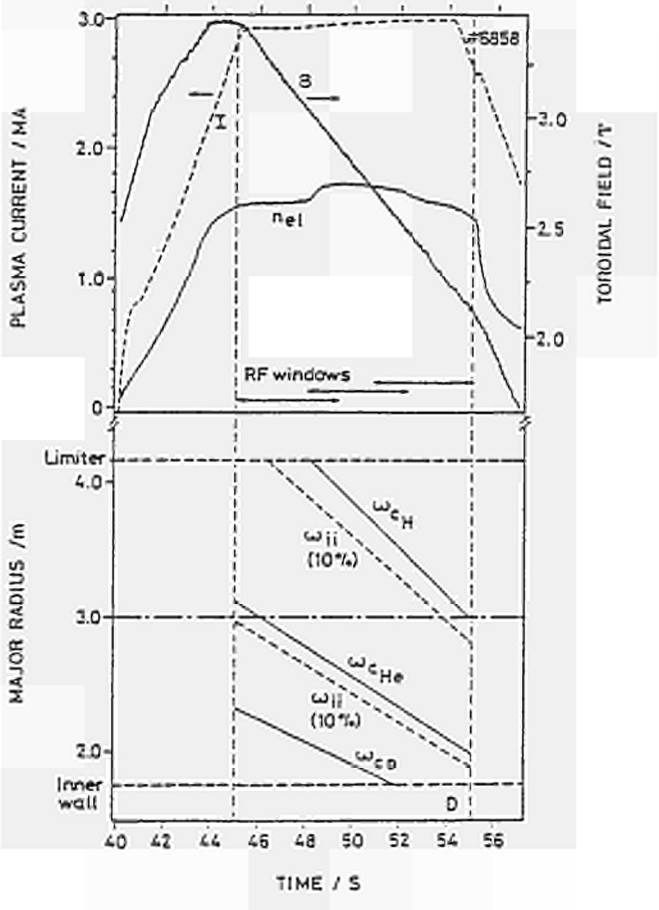

Fig. 1 Evolution during the ramping of the field of resonant layer position for case A-(3.4—2.1T)

3. Localisation expected

The elements playing a role in the broadening of the power deposition are mainly

(a) the natural thickness of the absorption zone.

(b) the difference in frequency at which each antenna is tuned (32.4 to 33.5 MHz) which scatter the resonant layers over 10 cm approximately.

(c) the vertical spread which, despite the focalisation, distribute the power on several successive magnetic surfaces.

The final distribution extends therefore over a domain whose thickness along R is typically between 30 and 50 cm and the expected effects are smoothed accordingly.

4. Experimental results

4.1 We have already reported /1/ that the dimensions of the sawteeth are dramatically increased when we heat the plasma inside the q = 1 cross section. This effect disappears when the resonant layer is moved outside q = 1.

4.2 Fig. 2 gives the $\Delta T/\Delta P$ plotted versus the position of the resonance layer.

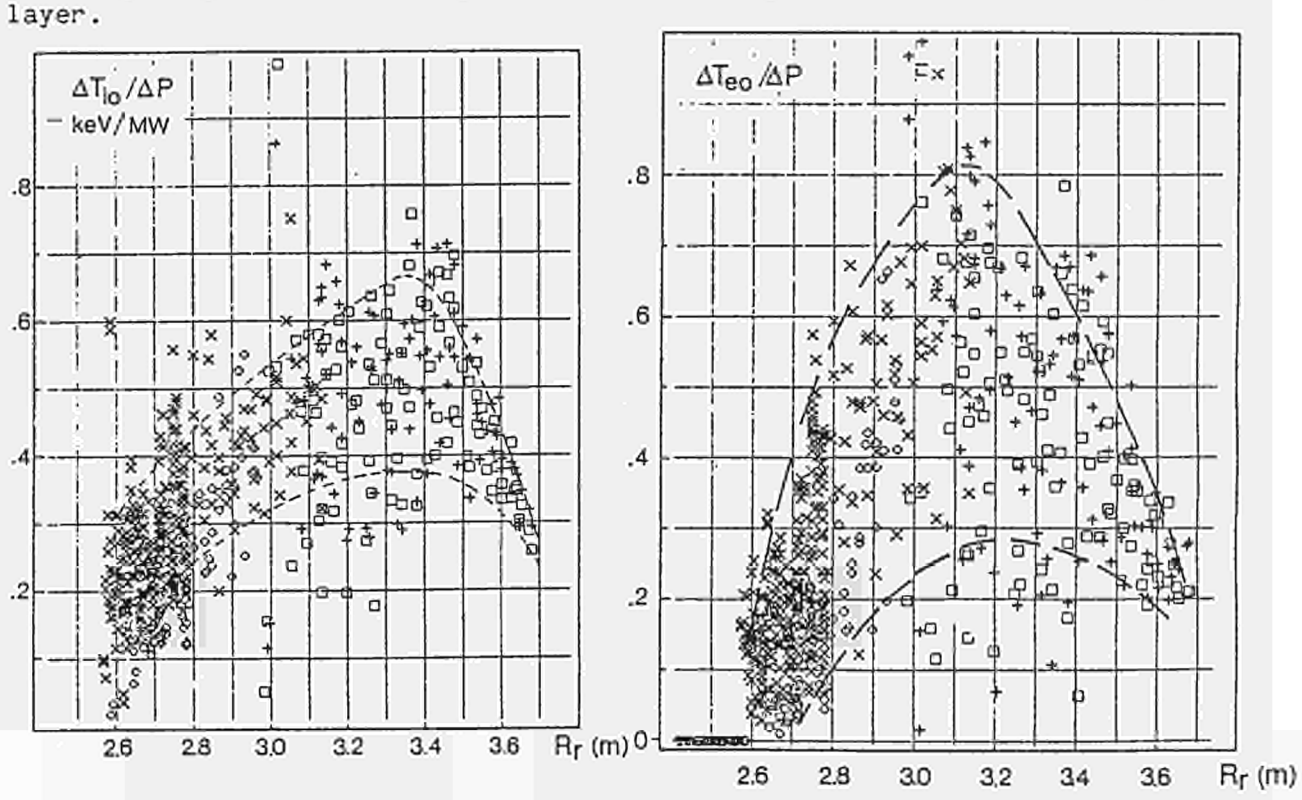

Fig. 2 : Ion and Electron temperature variation versus the position of the resonance layer

When plotting the total energy content of the plasma versus total power $P_{TOT} = P_{ohmic} + P_{RF}$ we find a linear dependence which could be described by : $W_{TOT} = \tau_{Eo} P_{\Omega o} + \tau_a (P_{TOT} - P_\Omega)$. We have reported (Fig. 3) for different conditions the τ_a-value versus the position of the resonance

layer. The resulting distribution exhibits a broad maximum in the central region (~ q < 1) and decreases outwards significantly. When moving from condition A (3.4 → 2.1 T, He^3 minority and I_p = 3 MA) to condition B (2.6 → 1.4 T, H minority and I_p = 2 MA), it is a striking result to find all the values merging in the same general curve.

Fig. 3 τ_a versus position of the resonnant layer

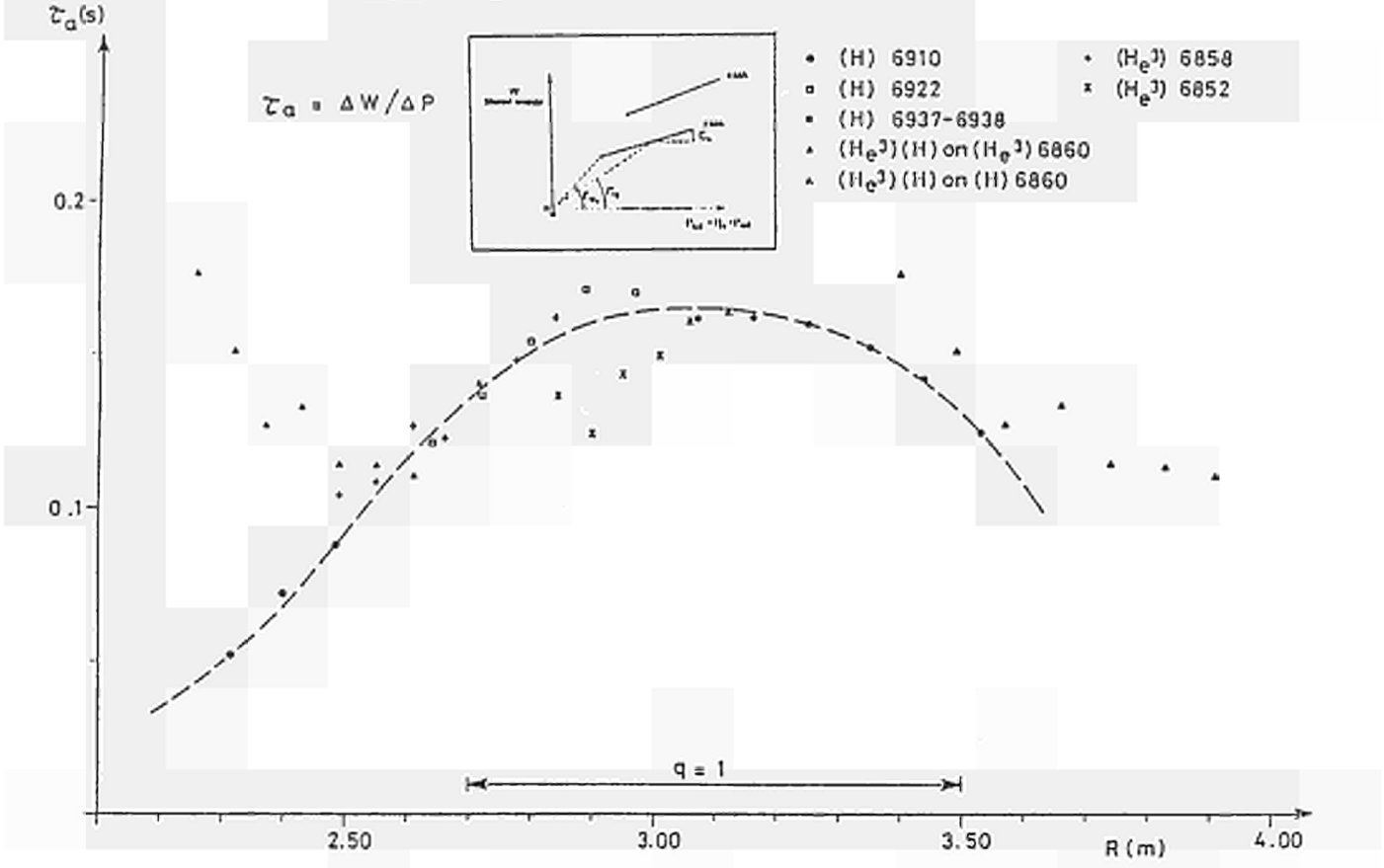

Several factors complicate the interpretation namely:

(a) The minimum mean hydrogen content in JET is around 5% of the Deuterium majority. Accordingly when the He^3 heating takes place at radius smaller than 2.8 m a second minority heating zone (H minority) enters the plasma from the LFS. Consequenly, when the magnetic field decreases an increasing heating efficiency on (H) competes with the decreasing heating efficiency on He^3.
(b) An adverse consequence of the RF heating is a moderate release of impurities increasing the radiated power which is thus more pronounced at the end of the RF pulse. Together with the density increase, this results in a decrease on τ_a at the later times and complicates the interpretation.

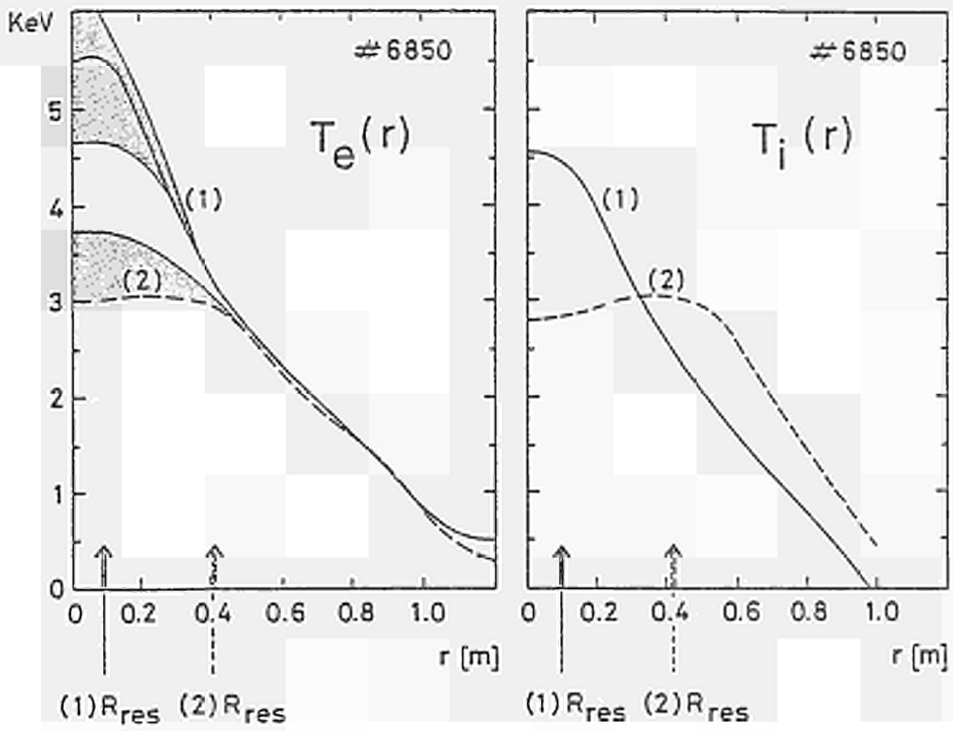

Fig. 4 Electron and ion temperature profiles with on axis (1) and off axis (2) RF heating

4.3 Significant effect on off axis heating on T_i -profile have been identified (Fig. 4). On the other hand, no change in T_e-profile outside q = 1 could be attributed to off axis heating despite the obvious mean increase observed in this case. This is in agreement with the so-called "profile consistency" observed on JET.

4.4 No evidence of any beneficial effects can yet be reported when heating around q = 2 surface. One could even discern an increased sensitivity to disruption possibly connected to impurity release when heating on the HFS q = 2 surface. This should however be reconsidered carefully with steady state condition before definite conclusions could be drawn.

Conclusion

So far, off axis heating did not achieve any major favourable results. The best heating efficiency has been obtained when the resonance zone is located close to the magnetic axis.

Reference:

/1/ ICRF Studies on JET - J. Jacquinot et al. 12th Eur. Conf. on Controlled Fusion and Plasma Physics, Budapest Sept. 1985

THEORY OF EXCITATION OF ASYMMETRIC $k_{//}$-SPECTRUM BY PHASING THE JET ICRF ANTENNAE

V.P. Bhatnagar*, M.P. Evrard*, J. Jacquinot

JET Joint Undertaking, Abingdon, Oxon, OX14 3EA, UK
*From LPP-ERM/KMS; EUR-EB Association, 1040 Brussels, Belgium

1. Introduction

A potentially important application of a radio-frequency heating scheme is the generation of RF driven currents to assist in the plasma equilibrium of a tokamak [1]. In large tokamaks such as JET, the ion-cyclotron resonance heating (ICRH) power-deposition profile is narrow and the power can be deposited locally [2,3]. This feature opens up the possibility of modification and control of current profile in tokamaks by driving current with waves in the ion-cyclotron range of frequencies (ICRF) with a view to stabilizing internal instabilities of a tokamak plasma. ICRF current-drive efficiencies are expected to be low [4] and therefore, no significant experiment of current drive by ICRF in a tokamak has yet been attempted, though, several advantages of ICRF over other RF schemes are evident such as good wave penetration property at high densities. Moreover, in this scheme, one could adjust several parameters like plasma composition, concentration and k//-spectrum for optimised experimental conditions [5].

To drive current in JET by waves in the ICRF either through cyclotron damping on a minority species or by absorption of the mode converted wave power by the plasma electrons via Landau damping, excitation of an asymmetric k//-spectrum is required. For the 1987 heating and current drive experiments in JET, four pairs of ICRF antenna systems will be regularly positioned around the torus. Such a system of antenna structures around the torus can be appropriately phased to produce the desired assymmetric k//-spectrum.

In this paper, we carry out a theoretical study, of the excitation of travelling ICRF waves in JET, based on a 3-D planar antenna-plasma coupling model. The antennae are progressively phased to excite a desired integral number of parallel wavelengths around the torus (n_o = 1, 2, 3 ... etc) where n_o = 3 or 4 is appropriate for mode conversion current drive and a somewhat higher number for the minority current drive.

Several sets of antenna combinations including that of a single pair alone have been analyzed and the results have been examined by looking at the directivity $D(n_o)$ defined as the asymmetry in k//-spectrum of the radiated power normalized to the total power radiated.

2. Theoretical Model

The analysis of excitation of fast magnetosonic waves by an ICRH antenna in a tokamak plasma is generally treated by a full-wave solution in the context of a semi-infinite, planar cold plasma model under single-pass absorption conditions [6,7]. The details of the model and the underlying assumptions have been published previously [6,7]. Applying the

induced emf method, analysis of the boundary value problem associated with this model is well known and is not repeated here, the details of which can be found in Ref. 6 and 7. The complex power radiated by the antenna and delivered to the medium can be written as $P = P_{TE} + P_{TM}$ where P_{TE} and P_{TM} are given in terms of a Fourier Series [6]. An array of antennae in the toroidal direction can be included by providing the appropriate spectrum of currents flowing in the phased antenna array. Travelling waves in a given direction can be excited by progressively phasing the antenna array. In order to gauge the asymmetry of the excited k//-spectrum of $R_e(P_{TE})$, we define a directivity D for a given toroidal mode number n_o as [8],

$$D\left(\frac{n_0}{r}\right) = \frac{\sum_{-m}^{m} Re\,\psi\left(\frac{n_0}{R}, \frac{m}{r}\right) - \sum_{-m}^{m} Re\,\psi\left(-\frac{n_0}{R}, \frac{m}{r}\right)}{\sum_{-n}^{n}\sum_{-m}^{m} Re\,\psi\left(\frac{n}{R}, \frac{m}{r}\right)} \qquad (1)$$

Where $2\pi r$ and $2\pi R$ are the poloidal and toroidal periodicities respectively, ψ is the TE radiated power spectrum and m and n represent the poloidal and toroidal mode numbers respectively. The above definition of directivity facilitates the examination of asymmetry for all toroidal mode numbers for a given case of progressive phasing. Note that this definition is related to the asymmetry of the spectrum and does not provide any direct information of the final current drive efficiency.

3. Results of Radiated Power Spectrum and Directivity

Several sets of antenna combinations including that of a single pair alone (as presently installed in JET) have been analyzed. The antennae are progressively phased to excite a desired integral number of parellel wavelengths around the torus (n_o = 1,2,3 ... etc). The results of the 3-D model described in Section 2, incorporate the effects of the finite-length of the antenna including the effect of the feeder currents and current propagation Constant β [7]. In this model, the radiation resistance per unit length (R_3) can be defined (see Ref. 7) by normalizing the quantity $2 \cdot R_e[\Psi]$ by the integral of the square of the current flowing, $I_c = \int I_o \cos^2 \beta_y \, dy$. These results can then be compared with R_2 obtained from a 2-D model in which the antenna (in the y-direction) is assumed to be infinetely long and the feeders are assumed to be located at infinity. However, in the comparison that is presented here, the product of 2-D $\left[R_e(\Psi(\frac{n}{R}))\right]$ and I_c is compared with 3-D $\sum_{-m}^{m} R_e\left(\Psi\left(\frac{n}{R}, \frac{m}{r}\right)\right)$. In this way, the effect of finite antenna length and β is incorporated in a rough way in the 2-D results, though the effects of the feeders are absent in this model. The radiated power spectrum for a pair of antenna described above is shown in Fig. 1(a) as a function of n for the 2-D and 3-D models. The principal difference exists for small $k// \leq k_o$ ($k_o \equiv$ vacuum propagation constant) related to the effects of feeder currents. (Fig. 1(b) shows the current spectra for the progressively phased antenna elements and the asymmetry is evident. The directivity defined in Section 2 is also plotted for each n nunmber and is shown in Fig 1(c). These curves are antisymmetric and therefore plotted only for positive n numbers.

Figure 2 shows similar plots when 4 pairs of antennae positioned symmetrically around the torus are energized with a progressive phase [8].

The imposed n_o number together with other mode numbers are found in the plasma and the directivity for $n_o = 3$ is about 29% with 3-D model and 22.5% with the 2-D model. The further narrowing and discretization of the excited spectrum is evident as the number of energized antennae is increased.

The results of directivity as a function of the imposed toroidal number by progressively phasing 8 antennae in several groupings obtained from the 2-D and 3-D models are shown in Fig. 3 and 4 respectively. In the 2-D results, the directivety is generally about 22.5%. The directivity values are lower for $n_o = 2$ and 6 in the case of 4G2H and for $n_o = 1$ and 7 in the case of 2G4H (2 groups of 4 housings each) as the phase difference between the corresponding antennae elements of different groups turns out to be an odd multiple of π (due to the fixed regular positioning of these groups of antennae). For $n_o = 0$ and 8, the phase difference is an even multiple of π, and the directivity values drop to zero. Similar behaviour is observed in the results of the 3-D model except that the value for small n numbers are higher (as compared to 2-D) since the 3-D model has higher values of radiated power near $k// \approx k_o$ due to the radial feeder current effects.

4. Summary and Conclusions

Eight travelling wave antennae are successful in imposing a desired toroidal mode number whereas a single pair of antenna system does not impose the desired n_o in the plasma. The asymmetry of the excited spectrum gauged by the directivity defined in Eq. 1 is found to be about 20%. Due to a finite number of antennae energized, it is found that the excited spectrum contributes significantly to other modes too. In current drive calculations and estimation of efficiency, this spectrum should be appropriately taken into account. These other modes may still be beneficial as they may heat the plasma instead. Moreover, the modes adjacent to the imposed one will also produce suprathermal electrons beneficial to current drive. In JET, for $n_o = 4$ at 33 MHz, the energy of the resonant electrons will be about 70 keV [2].

Acknowledgments: The computer codes used in the above calculations were initially developed in collaboration with Drs R. Koch and A.M. Messiaen. It is a pleasure to thank Mr J.J. Ellis for developing the plotting routines.

References

[1] Fisch, N.J., 2nd Joint Grenoble-Varenna Int" Symposium on "Heating in Toroidal Plasmas", Vol. II (1980) 1157
[2] Jacquinot, J., Paper presented at the ERICE Course on Toakamk Startup, Erice, Sicily, Italy 1985
[3] Jacquinot, J., et al, Invited paper, 12th European Conference on Controlled Fusion and Plasma Physics Budapest, hungary (1985)
[4] Cordey, J.G., Plasma Physics and Controlled Fusion, 26 (1984) 123
[5] Chiu, S.C., et al, Nuclear Fusion, 23 (1983) 499
[6] Bhatnagar, V.P., et al, Nuclear Fusion 22 (1982) 279
[7] Messiaen, A.M., et al, 3rd Joint Varenna Grenoble Int. Symp., Grenoble (1982) Vol. 1, 243
[8] Bhatnagar, V.P., et al, JET Report, Under preparation.

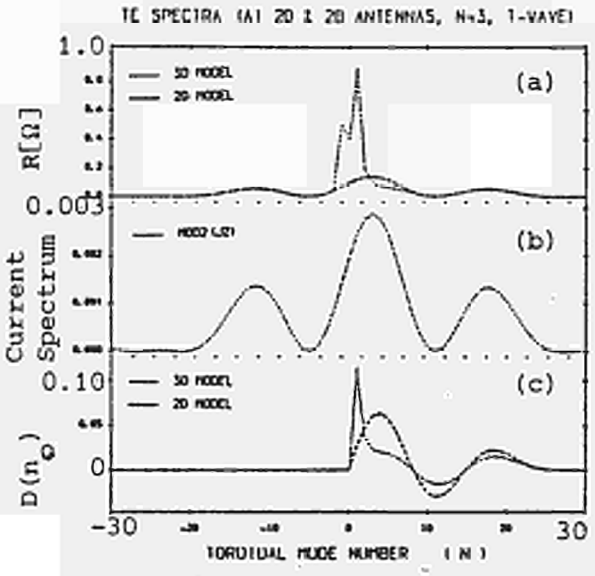

Fig. 1 R, Current Spectrum and D vs n for a pair of antennae

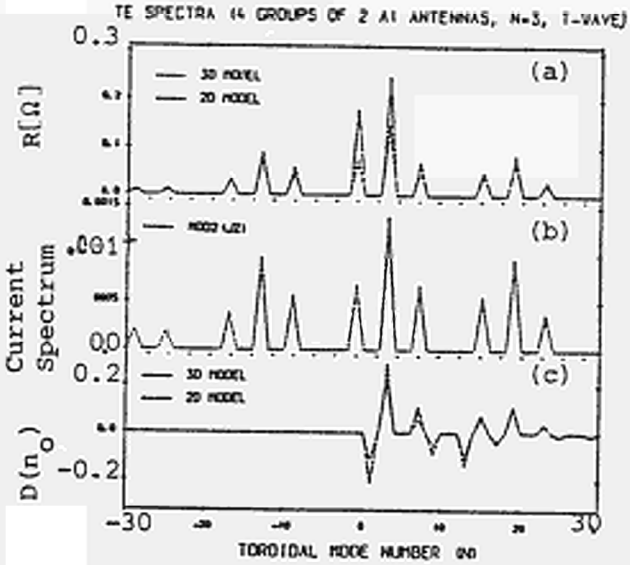

Fig. 2 R, Current Spectrum and D vs n for 8 antennae (4 groups of 2)

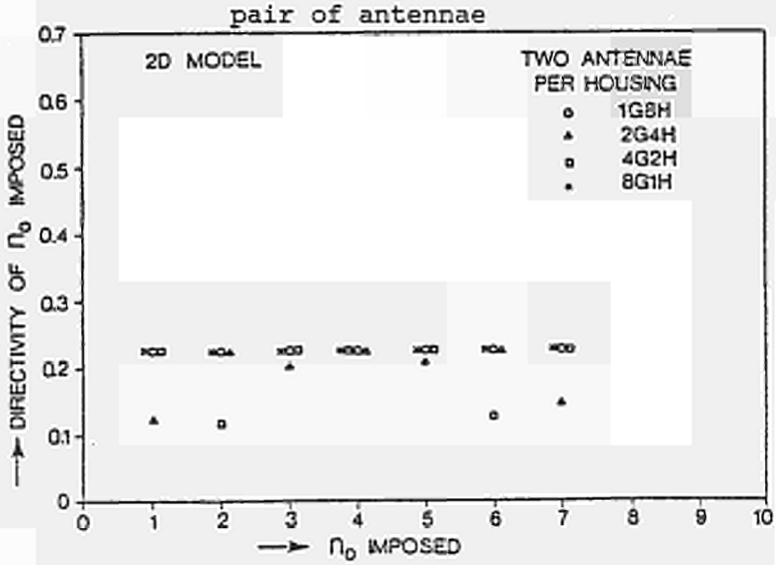

Fig. 3 Directivity vs n obtained from 2-D model for four different groupings of 8 JET antennae [8].

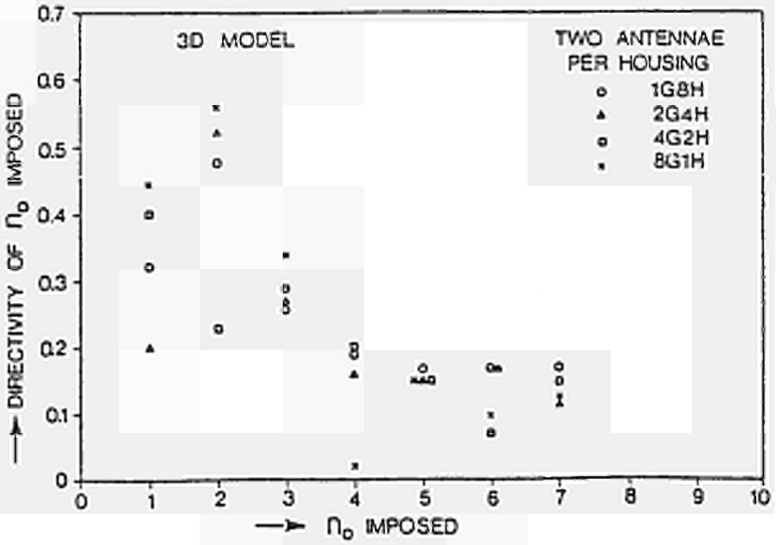

Fig. 4 Directivity vs n obtained from 3-D model for different grouping of 8 JET antennae [8].

COMPARISON OF THEORETICAL AND EXPERIMENTAL ICRF ANTENNA-PLASMA COUPLING RESISTANCE IN JET

M.P. Evrard*, V.P. Bhatnagar*, M. Bureš, F. Sand

*From LPP-ERM/KMS; EUR-EB Association, 1040 Brussels, Belgium

JET Joint Undertaking, Abingdon, Oxon, OX14 3EA, UK

1. Introduction

We present here a comparison of the predictions of different models for antennae coupling resistance with experimental measurements. We discuss the advantages and limitations of each model, and examine the importance of coaxial modes in JET. The influence of the current variation on the coupling resistance is studied and it is shown that a good agreement with experimental values can be found with a simple realistic current profile.

The effects of plasma edge parameters on the coupling resistance have also been investigated.

2. Coupling resistance measurements

The coupling resistance is deduced from voltage measurements made near the generators, 80 m away from the antennae. In the absence of additional fixed stubs, we can link the radiated power to the measurements by

$$\text{Re } P = \frac{1}{2} R_c I_{max}^2 = \frac{1}{2} R_{ant} \left| I_{ant} \right|^2 \qquad (1)$$

where I_{max} is the maximum current on the line and I_{ant} is the current at the antenna input. Losses in the line and in the screen have been estimated to contribute to the coupling resistance R_c by about 0.6 Ω at around 33 MHz. In the presence of fixed stubs near the antenna, relation (1) no longer holds. We need phase measurements to reconstruct the voltage pattern along the line, and to deduce the (complex) radiation impedance of the antenna which is at present not available.

3. Theoretical models for antenna impedance

Theoretical models for ICRH antenna impedance have been developed to a highly sophisticated level. Two models [1,2] are presently in use at JET, both allowing for realistic plasmas and using single pass absorption hypothesis in a slab geometry : the induced emf method and the variational method. In the variational method, we derive an equation for the current distribution which is solved, yielding eventually the coupling resistance. The induced emf method is faster and assumes a realistic current distribution and calculates the coupling resistance directly. The variational code takes into account the frame limiter in which the antenna is recessed but only the monopole configuration has been treated. The code based on the induced emf method does not consider the frame limiter but permits to choose between many different current distributions, including the four JET antenna configurations. Both models use the following expression for the radiated power:

$$P = \frac{1}{2} Z_{ant} \left|I_{ant}\right|^2 = \frac{1}{2} \int \frac{dk_{//}}{2\pi} \frac{dk_y}{2\pi} \psi(k_{//},k_y) \left|J(k_{//},k_y)\right|^2 \quad (2)$$

where $\psi(k_{//},k_y)$ depends on the boundary conditions and $J(k_{//}, k_y)$ depends on the Fourier transformed components of the current distribution. The code based on induced emf method also takes into account the periodicity of the torus by replacing the integrals in (2) by sums over multiple of $1/R$ and $1/a$ where R and a are the major and minor radius respectively. Due to the complex shape of the actual antenna conductors, the reactive part of the power which is very sensitive to the exact current distribution, specially on the lower conductors, is poorly described in the induced emf method where the antenna currents distribution is an input parameter. To be able to go from the real part of the antenna impedance to the coupling resistance with the help of eqn (1), we require the ratio $I_{max}(ant)/I_{max}(line)$. This has been experimentally measured to be about 1.2 in vacuum and is assumed to be unchanged in the presence of the plasma.

4. Effects of (possible) coaxial modes

Coaxial modes are described by $k_{//}^2 + k_y^2 \leq k_o^2$ and they propagate between the plasma surface and the machine wall. These modes could have adverse effects on the plasma edge conditions, leading to the release of impurities into the plasma. In JET, the geometrical dimensions and the ICRF frequency range permit only a minor contribution within the circle described by $k_{//}^2 + k_y^2 = k_o^2$ and the importance of coaxial modes depends on the sharpness of the integrand around this circle. For the JET monopole antenna configuration the coaxial modes contribution is largest, but the power spectrum as calculated without taking into account the frame limiter is not very peaked around $k_{//}^2 + k_y^2 = k_o^2$ (see Fig. 1) and the proportion of the contribution of coaxial modes to the total power is still less than 10%. The presence of the frame limiter should change the situation, and in the torus these modes could be shielded. The presence or absence of coaxial modes in JET has not been assesed experimentally, yet.

5. Influence of the current distribution along the antenna

We describe the current distribution as $I(y) = I_o \cos\gamma y$, where γ is the current propagation constant. To assess the effect of γ, we have studied the evolution of the coupling resistance of all four antenna configurations for a typical plasma ((He_3)-D, $B_o = 3.4T$, $f = 33$ MHz) where the antennae are nearly resonant. The expected γ for $\frac{\lambda}{4}$-resonant antennae of the size of those in JET is around $\gamma \approx 1.35\ m^{-1}$. Although the monopole and the quadrupole seem rather insensitive to changes of γ between $\gamma = 0$ (uniform distribution), and $\gamma = 2\ m^{-1}$, for both dipoles a choice of γ between 0 and $0.9\ m^{-1}$ would fit the experimental results better (Fig. 2). Choosing $\gamma = 0.9\ m^{-1}$ f.i. leads to Fig. 3 where a fairly good agreement with experimental data is found for the monopole, quadrupole and to a lesser extent for the dipoles. This behaviour reflects the fact that the dipole configurations, in which the current in the poloidal sections flow in mutually opposite directions, are difficult to be described by a single value of γ as we attempted in the induced emf method.

The variation of coupling resistance with frequency has been obtained by the variational method. As mentioned above, the induced emf method suffers from the need of redefining a new γ for each frequency, the variational methods is better suited. The resonance of $A\emptyset_1$ antenna in the monopole configuration is found to be at $f_{res} = 35$ MHz whereas experimentally, it is around 33 MHz.

6. Plasma edge effects on the coupling resistance

We have investigated the effects of the change of the density profile in the edge region of the plasma on the coupling resistance for the different antenna configurations. Variations of the plasma density at the limiter n(a), of the e-folding length in the S.O.L. and of the peaking factor of the bulk plasma density have been considered. The main dependance of the coupling resistance is on the plasma density at the limiter, for all the different antenna configurations. The $A\emptyset_1$ monopole and dipole, together with the $A\emptyset_2$ quadrupole show a marked dependance on the plasma edge density gradient through the peaking factor, the coupling resistance increasing with the steepest profile. But the dependance on the S.O.L. e-folding length is weak. The $A\emptyset_2$ dipole coupling resistance, in addition to show a somewhat lesser sensitivity to the plasma density at limiter than the others, does not seem to depend on the peaking factor. The sensitivity to the S.O.L. e-folding length is comparable to that of the other configurations.

Conclusions

Theoretical determinations of the coupling resistance for all four antenna configurations used in JET have been obtained and compared to experimental measurements. The coaxial modes have been found to be of little importaqnce in JET, and for the monopole antenna contribute less than 10%. Dependance of the coupling resistance on the current distribution has been studied. Though in practice γ may be slightly different for each antenna configuration, theoretically a value of $\gamma = 0.9\ m^{-1}$ gives a good agreement with experiment for all four antenna configurations. The behaviour of R_c with frequency for the monopole antenna has been verified.

The effects of edge conditions on coupling resistance have been investigated for all antenna configurations. R_c depends mainly on the plasma density at the limiter, increasing by about 20% when the edge density doubles.

References

[1] Bhatnagar, V.P., Koch, R., Messiaen, A.M., Weynants, R.E., Nuclear Fusion, 22 (1982) 279, and also Messiaen, A.M., Koch, R., Bhatnagar, V.P., Evrard, M.P., Luwel, M., Vandenplas, P.E., Weynants, R.R., Proc. 3rd Joint Varenna Grenoble Int. Sump. on "Heating in Toroidal Plasmas", Grenoble (1982) Vol 1. 243

[2] Theilhaber, K., Jacquinot, J., Nuclear Fusion, 24 (1984) No 5, p. 541, and Theilhaber, K., Nuclear Fusion, 24 (1984) 1383

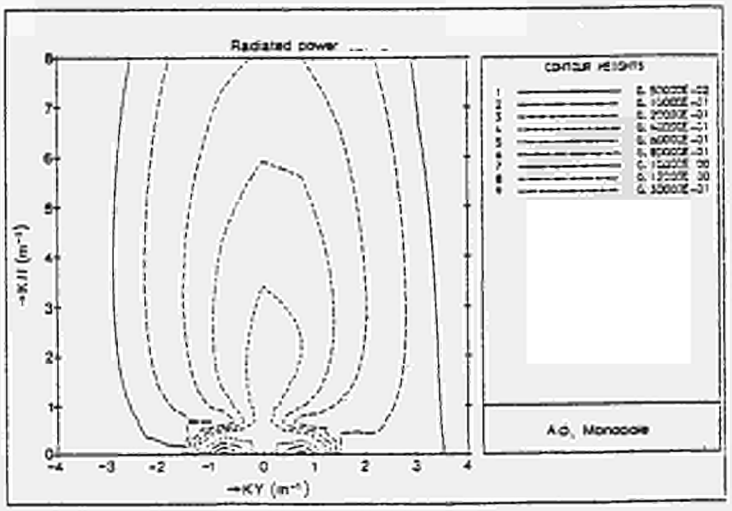

Fig. 1 The spectral density of the real part of the radiated power for a typical plasma (3.4T, He_3 minority, f = 33 MHz)

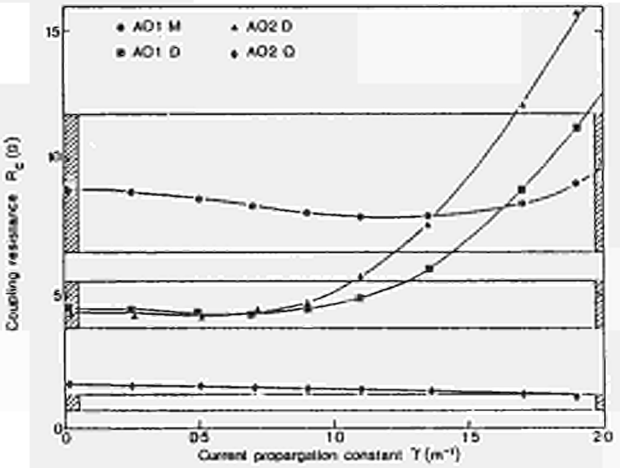

Fig. 2 Coupling resistance vs the propagation constant. The range of experimental values is indicated by shaded regions. The antenna limiter distance is 5.5 cm.

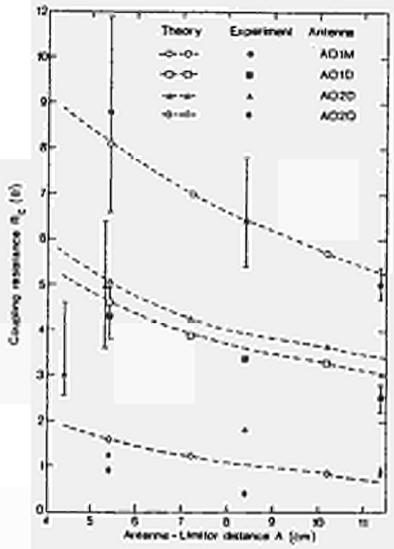

Fig. 3 Coupling resistance vs antenna to limiter distance.

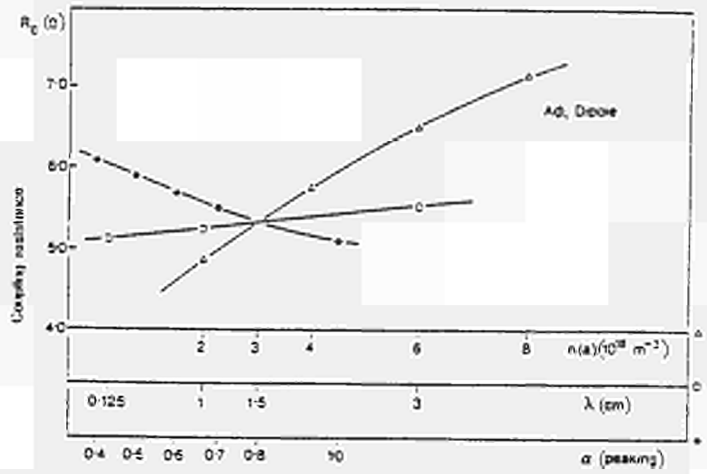

Fig. 4 Effect on coupling resistance of variations of the density at the limiter n(a), S.O.L. e-folding length γ and peaking factor α.

COMPARISON BETWEEN H AND He^3 MINORITY ICRF HEATING EXPERIMENTS IN JET

V.P. Bhatnagar*, S. Corti, J.J. Ellis, J. Jacquinot, P.P. Lallia, F. Sand

JET Joint Undertaking, Abingdon, Oxon, OX14 3EA, UK
* From LPP-ERM/KMS; EUR-EB Association, 1040 Brussels, Belgium

Introduction

In the ion-cyclotron resonance heating (ICRH) experiments in JET, the RF energy is coupled to the plasma via the cold-plasma fast magnetasonic waves which are generated by exciting ICRH antennae located on the low-field side of the takamak. In the minority species heating scheme, the minority ion (e.g. H^+ or ^3He in deuterium plasma) concentration $\eta = Nj/ND$ ($j = H^+$ or ^3He) is required to be below a certain critical concentration η_c [1] for a given k//, minority temperature and plasma density. For $\eta > \eta_c$, significant mode conversion to ion-Bernstein wave takes place. In the minority scheme, the RF power is primarily dumped into minority ions. The energy distribution of the minority ions is characterised by a tail and the distribution function is generally estimated based on the quasi-linear theory developed by Stix [2]. RF accelerated minority ions, which are sufficiently well confined in JET, act as an intermediate energy reservoir and transfer their energy to the background electrons and ions via the drag between minority ions and other plasma species.

In this paper, we analyse and compare the ICRH results obtained in JET with H^+ or ^3He minority in deuterium plasmas. Based on the experimental evidence, the aim is to present the merits and demerits of the heating with the two minority ion species and to establish which minority ion is better suited for plasma heating in JET.

ICRH experiments in JET have been carried out under a wide range of plasma conditions with torodial field (B_T) varying from 2 to 3.4 Tesla and plasma current (I_p) from 2 to 4 MA. But, most of the data for H-minority was taken with an I_p of 2 MA and therefore, for comparison we have selected He^3 data also at I_p = 2 MA. In the case of H-minority the frequency of operation was $\simeq$ 33 MHz and B_T was about 2.3 Tesla whereas in He^3-minority case, f = 25 → 31 MHz and B_T = 2.6 → 3.4 Tesla. A comparison of the efficiency of ion and electron heating, plasma stored energy, asymptotic energy confinement times, change in the radiated power and impurity production are presented.

Results

Figure 1 shows a comparison of bulk-ion (deuterium) heating with H^+ and ^3He minority species. For lower power levels such that $P_{RF}/\langle n_e \rangle \leq 1.5 \times 10^{-13}$ W·m^3, the increase in ion-temperature is practically the same in the two cases. However, for the values of $1.5 \leq P_{RF}/\langle n_e \rangle \times 1.0^{13} \leq 2.5$ W·m^3, the bulk ion heating in the H-minority case seems to degrade

somewhat in comparison to the He^3 case. Figure 2 shows the corresponding comparison of the central electron temperature. For $1.5 \leq P_{RF}/\langle n_e \rangle \times 10^{13} \leq 2.5$ W·m^3, the loss of efficient ion-heating in the case of H-minority is well compensated by the improved electron heating. Note that the T_e and T_i data points were plotted by averaging over the sawteeth.

The above data of plasma heating in JET can be represented by:

$$(\Delta T_{eo} + \Delta T_{io}) \approx \alpha \, P_{RF}/\langle n_e \rangle$$

where $\alpha \approx 1.5$ to 2×10^{13} (keV.W^{-1}m^{-3})

Figure 3 shows plasma stored energy when ICRH power is increased up to 5.5 MW. The slope of a line passing through H^+ data and that through ^{3}He data represent the asymptotic confinement times with values of τ = 0.15 s for H^+ and τ = 0.12 s for ^{3}He.

A comparison of the radiated power normalized by the line-averaged density square ($\langle n_e^2 \rangle$) shows that it is higher at a given power level of 4 MW by a factor of 1.7 in the case of H^+ minority than in the case of He^3-minority (see Fig. 4). Also the increase in metallic (Ni) impurity concentration was higher in the case of H^+-minority by a factor of about 2.5 compared to that with the ^{3}He case [3].

Summary and Conclusions

1. Bulk-ion heating is roughly the same for H^+ and ^{3}He-minority with $\Delta T_D \approx 1$ keV at a normalized RF power $R_{RF}/\langle n_e \rangle \approx 1 \times 10^{-13}$ W m^3. At higher power levels, ^{3}He seems to be a little better than H^+ minority from the point of view of ion heating. However, the poor ion-heating at higher power levels in H^+ case is well compensated by a better electron heating. These observations are consistent with the Stix theory [2] in which the strong tail formed in the case of H-minority, relaxes on electrons whereas He^3-minority tail relaxes on bulk-ions at the RF power densities achieved presently in JET. For example for JET parameters, at a minority power density of 0.4 W/cm^3, the fraction of power going to electrons is 0.85 and 0.2 in the case of H^+ and H^3 minority respectively. However, when RF heating power will be increased to tens of megawatts resulting in much higher minority power densities, both hydrogen and helium-3 minority are expected to transfer their energy primarily to electrons.

2. The asymptotic energy confinement times with ICRF in JET is marginally better in the case of H^+ than in the case of ^{3}He minority.

3. Both the (Bolometric) radiated power and the metallic impurities are worse in the case of H^+ than in the case for ^{3}He-minority.

References

[1] Equipe TFR, Report EUR-CEA-FC-1046, Fontenay-aux-Roses, France.
[2] T.H. Stix, Nuclear Fusion, 15 (1975) 737.
[3] B. Denne et al, these proceedings.

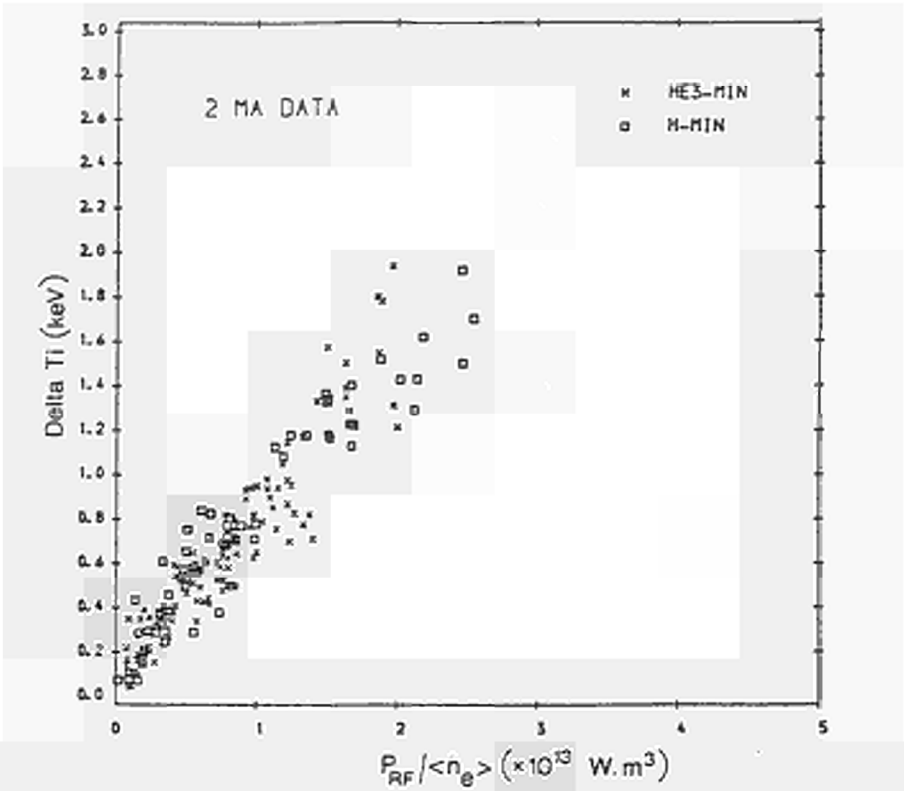

Fig. 1 Increase of bulk-ion (D+) temperature (measured by the neutron diagnostic) is plotted as a function of $P_{RF}/<n_e>$ both for H^+ and He^3 minority where P_{RF} is the ICRF power coupled from the antenna and $<n_e>$ is the line average density.

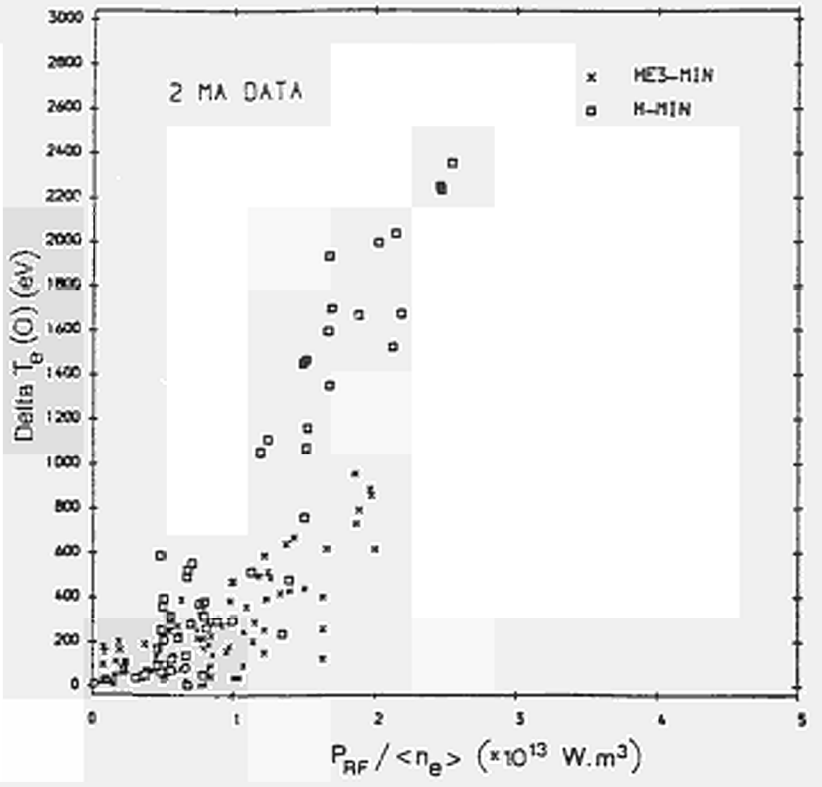

Fig. 2 A similar plot for central electron temperature (ECE) as in Fig. 1.

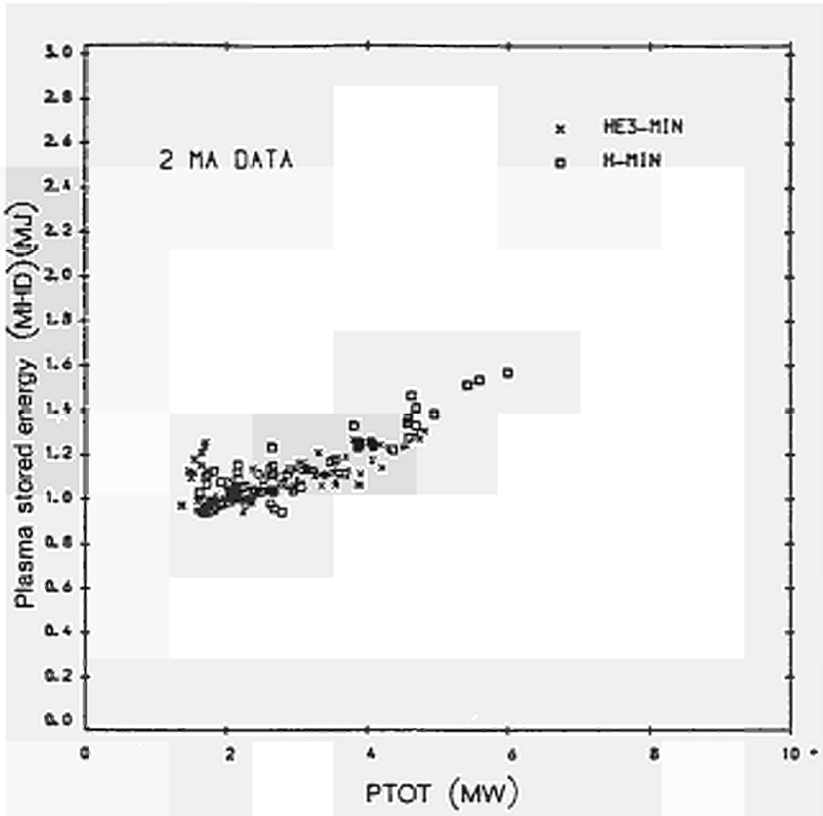

Fig. 3 Plasma stored energy (MHD) plotted as a function of total input power (P_{RF} + P_{OH}) for H^+ and He^3-minority cases.

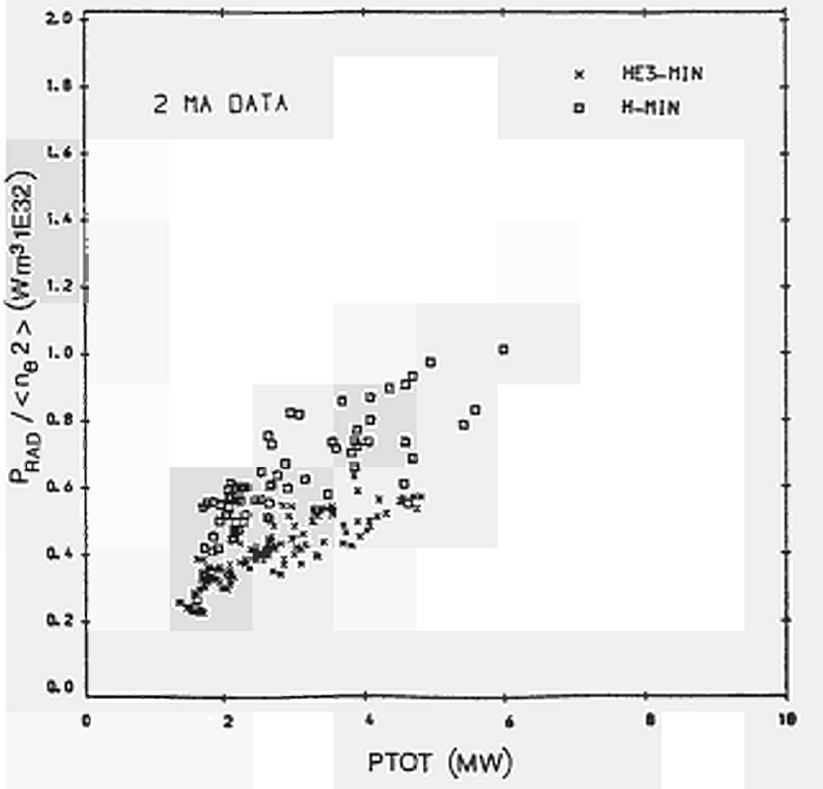

Fig. 4 Radiated power (Bolometer) normalized by $\langle n_e^2 \rangle$ is plotted as a function of total input power (P_{RF} + P_{OH}) for H^+ and He^3-minority.

FUSION PRODUCT MEASUREMENTS ON JET

G Sadler, P Van Belle, M Hone, O N Jarvis, J Källne,
G Martin+ and V Merlo

JET Joint Undertaking, Abingdon, Oxon, OX14 3EA, UK
+Association EURATOM-CEA-DRFC/TS. CEN Cadarache. France 13108

Neutrons from the D-D reaction and protons from the ^{3}He-D reaction have been used for diagnostic purposes during the past year of operation.

CODE CALCULATIONS OF FUSION PRODUCT SPECTRA (FSPEC)

It is well known that a measurement of the Doppler broadening of the 2.45 MeV neutrons from D-D reactions in a deuterium plasma affords a determination of the plasma ion temperature T_i. Several authors (refs 1-3) have shown that the Maxwellian ion energy distribution of a plasma in thermodynamic equilibrium leads to a neutron energy spectrum which is approximately Gaussian with a FWHM proportional to $\sqrt{T_i}$. These analyses include a number of approximations, e.g. the D-D reaction cross-section is usually assumed to be isotropic in the centre of mass (CM) system. The successful measurements of neutron spectra reported earlier (refs 4,5) have emphasised the need for a precise and reliable evaluation of the relationship between the neutron spectrum shape and ion temperature. A numerical simulation has been performed as follows.The birth energy spectrum of fusion products M_3 from the reaction $M_1 + M_2 \rightarrow M_3 + M_4 + Q$ taking place in a plasma is given by:

$$\frac{dN}{d\Omega_3 dE_3} = \int f_1(\vec{V}_1)\, f_2(\vec{V}_2)\, \frac{d\sigma}{d\Omega_3 dE_3 d\Omega_4 dE_4}\, \left|\vec{V}_1 - \vec{V}_2\right|\, dV_1^3\, dV_2^3\, dV_4^3$$

$$\text{where } \frac{d\sigma}{d\Omega_3 dE_3 d\Omega_4 dE_4} = \frac{d\sigma}{d\Omega_3 dE_3}\, \delta(E_3 - E_3^*)$$

$$\text{with } E_3^* = \tfrac{1}{2} m_3 V^2 + \frac{m_4}{m_3 + m_4}(Q+K) + \cos\Theta\; V \sqrt{\frac{2 m_3 m_4}{m_3 + m_4}(Q+K)}$$

Q = Energy release in reaction, V = CM velocity, K = Kinetic energy of reactants in CM, Θ = angle between relative velocity and velocity of fusion product in CM.

The above integral can be solved by Monte Carlo sampling on a computer. A code accepting numeric distribution functions of the form $f(\vec{V}) = f(V,\psi)$ has been developed, where ψ is the pitch angle of the reacting particle with respect to the total magnetic field. CPU usage is 7.5μs per sample on a Cray 1 (200μs on an IBM 3087). Neutron spectra from the anisotropic D-D reaction in a thermal plasma were calculated resulting in an almost perfect Gaussian shaped spectrum with a temperature dependent shift Δ and broadening $W = FWHM/\sqrt{T_i}$. A convenient representation for these

quantities, based on a series of calculations (each using $3 \cdot 10^7$ samples) is found to be:

$$W\ [\text{keV}^{1/2}] = 82.74 + 0.103\ T_i - 8.2\ 10^{-4}\ T_i^2 \pm 0.04 \text{ and}$$
$$\Delta\ [\text{keV}] = 2.94 + 3.41\ T_i - 0.034\ T_i^2 \pm 0.4 \qquad \text{for } 1 \leq T_i\ [\text{keV}] \leq 20.$$

APPLICATION TO NEUTRON MEASUREMENTS

Neutron spectra are obtained "routinely" during high yield discharges ($Y_n \geq 10^{14}$n/discharge) with a ^{3}He ionization chamber viewing the plasma vertically from the roof laboratory. The width of the spectrum is extracted by fitting the experimental data points (Fig. 1) with a gaussian convoluted with the detector response function using the maximum likelihood technique for Poisson distributions /4/. Computer simulations show that the correction which needs to be applied to the line of sight data to yield the central ion temperature is small (~9%) and depends only weakly (±1%) on profile shapes provided that the density profile is broader than the temperature profile.

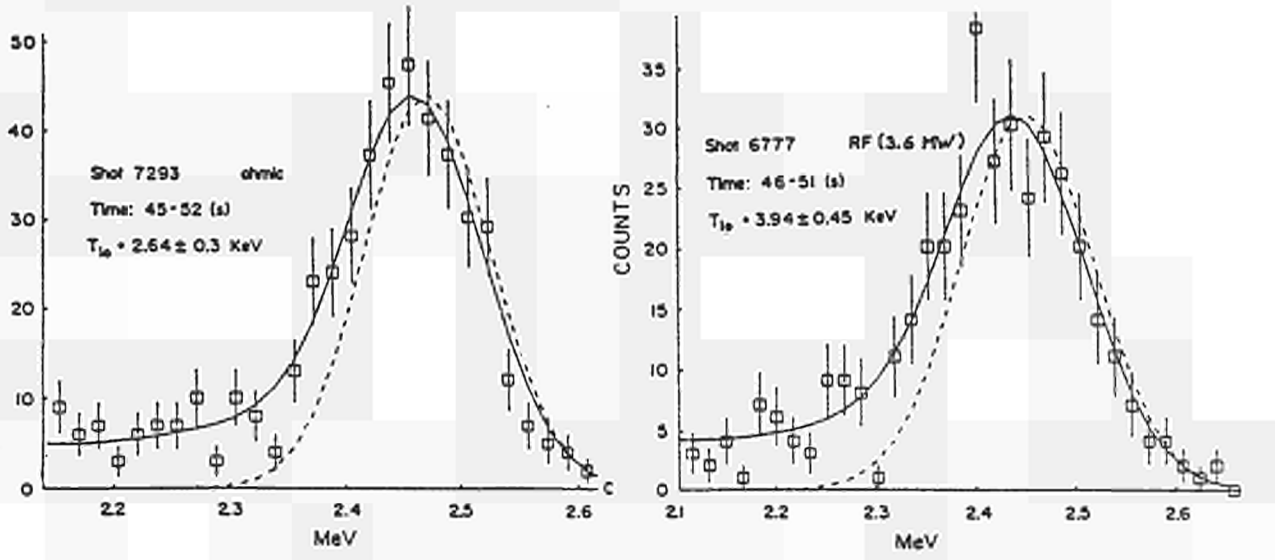

Fig. 1: Examples of measured pulse-height spectra and deduced central ion temperatures. The broken lines show the deduced neutron energy spectra.

The volume integrated neutron yield is measured with 3 pairs of absolutely calibrated fission chambers yielding a measurement of $\frac{1}{2}n_d^2 \langle\sigma v\rangle$ which can be used to deduce the deuteron density if $\langle\sigma v\rangle$ is calculated using the temperature measured with the spectrometer. This combination of measurements has shown that the ratio of $\hat{n}_d/\hat{n}_e$ for high yield discharges is noticeably low (between 0.8 and 0.3, reducing with $\hat{T}_e$). These results are obtained assuming the ion temperature profile is the same as the electron temperature profile.

One source of concern with the above analysis is that internal 'sawtooth' disruptions might lead to a preferential loss of fast ions from the central region of the plasma. A sensitivity analysis using FSPEC shows that the possible loss of all particles with E>27keV yields an over-estimate of 10% in $\hat{n}_d$ for a T_i = 3keV case; a more gradual treatment, eg. exp-(ln2xE/12), or preferential loss of particles with high $V_\perp$ would lead to a systematic error of less than 5%.

14.7 MeV PROTON MEASUREMENTS

Protons from the D + ^{3}He → ^{4}He (3.6MeV) + p (14.7MeV) reaction have been observed with the experimental arrangement shown below. The ^{3}He ions originated either as reaction products (D + D → n (2.45MeV) + ^{3}He (0.82MeV) reaction) or from the bulk plasma (by ^{3}He gas puffing).

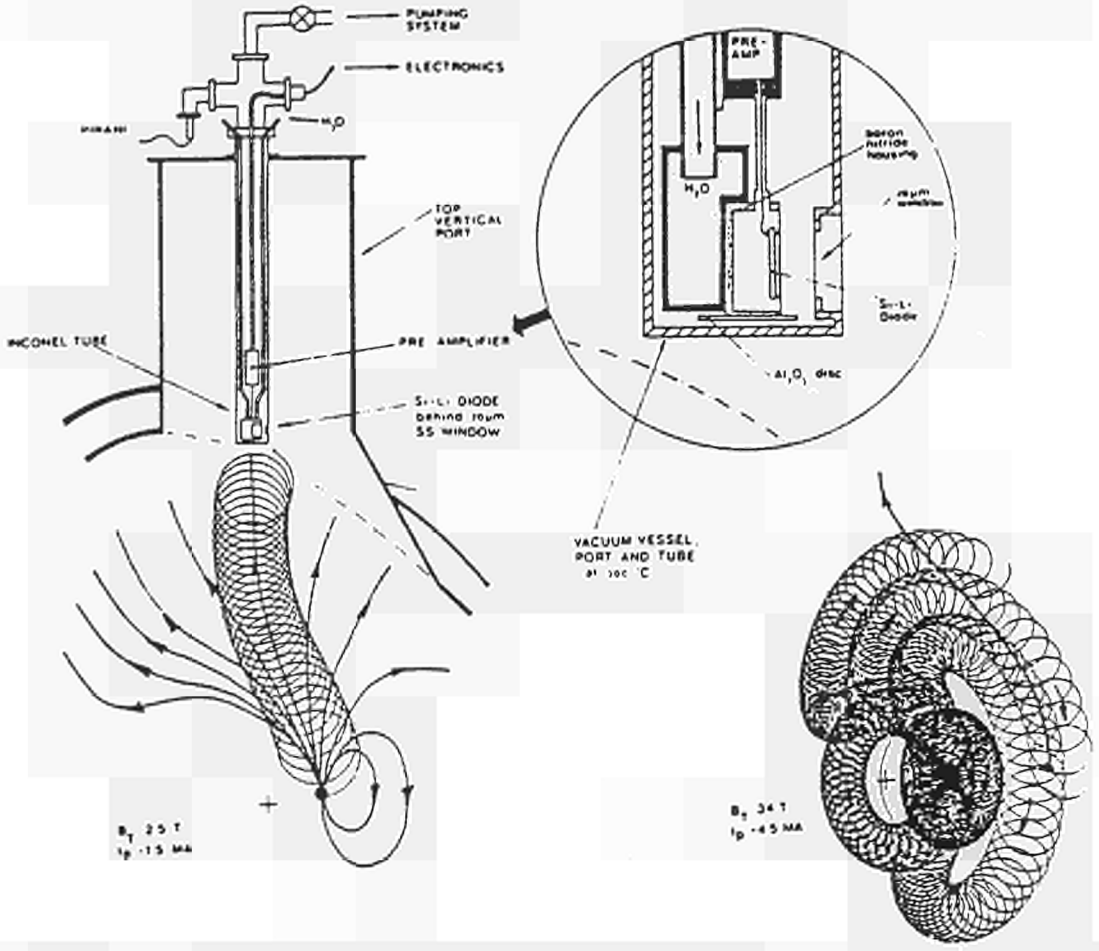

Fig 2: Detector arrangement with orbit examples at low and high current.

By collimation only protons with $V = V_\perp$ are accepted by the detector. The detector line-of-sight is determined with the help of an orbit code and depends strongly on the plasma current, the hot central core being visible only for currents below around 2.8MA (Fig. 2). The performance of the system was checked at plasma currents around 1.5MA (mainly during the current decay phase of discharges) yielding a Doppler broadening of the 14.7 MeV proton peak which was in agreement with other T_i measurements.

During H minority ICRF heating at low fields ($B_T \leq 2.6T$) and plasma currents ($I_p \leq 2.8MA$), protons originating from the central region of the plasma were observed. Enhanced sawtoothing could be clearly seen on the ECE signal (T_e) and the neutron yield. The proton yield, as derived from a single channel analyser showed the same trend but with less pronounced sawteeth. The 2.5MeV spread (FWHM) of the energy spectra around its nominal values was consistent with a 0.8MeV ^{3}He population slowing down in the plasma.

A systematic study of all discharges where data are available shows that the apparent ^{3}He burn-up fraction (= observed proton yield/ neutron yield) scales with T_e^7 while the expected burn-up fraction is proportional to $(n_d/n_e)T_e^{3/2}$, suggesting that the ^{3}He slowing down is influenced by the RF.

During ^{3}He ICRF minority heating the central part of the plasma is not visible but bursts of protons coinciding in time with the sawtooth collapse can be observed (Fig. 3). Spectra (Fig. 4) exhibit a downwards shift of ~1.5MeV which can be converted into a 75ms slowing down time for 15MeV protons (about half the sawtooth period) indicating that these protons were contained before being thrown out by the internal disruption. On the other hand the finite width (10-20 ms) of the proton bursts, being comparable to the decay time of the neutron sawteeth, rather suggests the burning up of expelled super thermal ^{3}He ions.

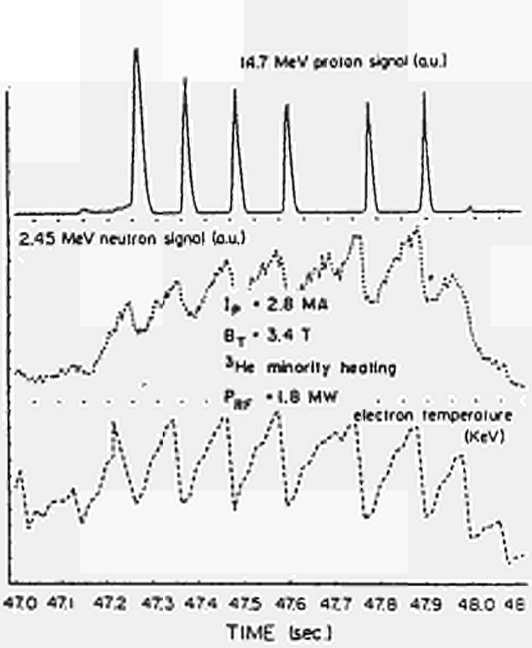

Fig. 3: Time dependence of 14.7MeV protons, neutrons and electron temperature during (^{3}He) ICRF.

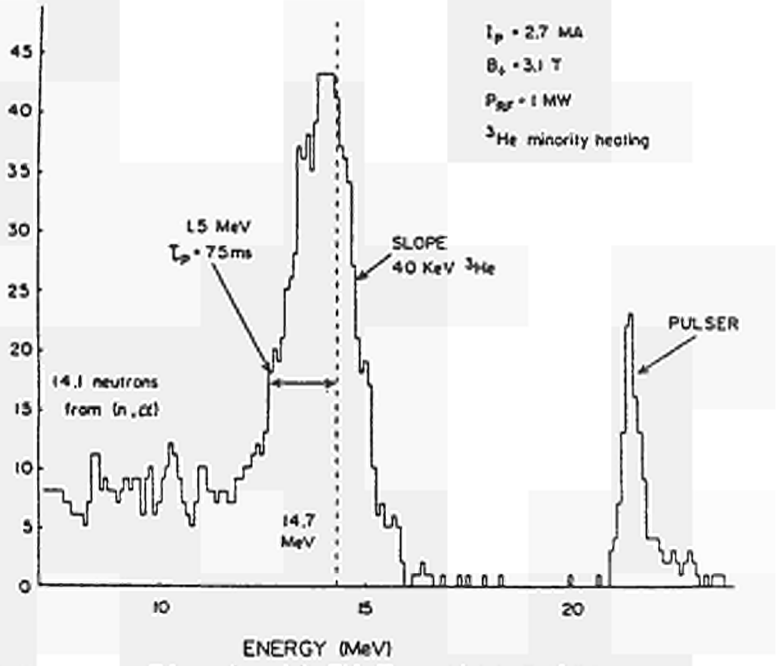

Fig. 4: 14.7MeV proton pulse-height spectrum during low power (^{3}He) ICRF heating.

SUMMARY AND CONCLUSIONS

* A highly efficient and exact code was used to calculate D-D neutron spectra from thermal plasmas.
* For high yields, $\hat{n}_d/\hat{n}_e$ ratios between 0.8 and 0.3 are measured.
* Intense bursts of 14.7MeV protons are observed at the collapse time of giant sawtooth disruptions during ^{3}He minority ICRF heating.
* The ^{3}He burn up fraction observed during ICRF(H) heating shows a very steep dependence on $\hat{T}_e$ indicating a possible interaction of the RF with the slowing down ions.

/1/ G Lehner and F Pohl Zeitschrift f Physik 207, 83, 1967
/2/ H Brysk, Plasma Physics, Vol 15, p 611, 1973
/3/ J Scheffel, Nuclear Inst. and Meth, Vol 224, No 3, p 519, 1985
/4/ V Merlo et al, Varenna, Course and Workshop, 26 Aug-3 Sept 1985
/5/ O N Jarvis et al, 12th EPS Conference, Budapest, Sept 1985

NEUTRALISATION MEASUREMENTS FOR THE JET INJECTOR

R S Hemsworth, *A Stäbler, H D Falter, P Massmann, G H Deschamps, and A P H Goede

JET Joint Undertaking, Abingdon, Oxon, UK. *Attached from I.P.P. Garching

Introduction

Neutralisation of the extracted beam is, of course, an essential part of any neutral injection system. During testing of the first JET injector in the Neutral Injection Test Bed, extensive measurements have been made of the neutralisation efficiency with both H_2 and D_2 as the working gas, for extraction voltages of up to 80kV. Careful measurements of the neutralisation target present in the absence of the beam enable an accurate comparison to be made between predicted and measured neutralisation efficiencies. The variation in the power in the fractional energy ions is independently determined and shown to support the conclusions from the neutralisation measurements.

Gas Target Measurements

The JET beam source (PINI) is equipped with a close coupled neutraliser consisting of two equally long stages with an overall length of 1.8m. The cross section is racetrack shape of typical dimensions 0.43m x 0.18m. The gas is fed into both the plasma source (Qs) and the neutraliser (Qn), in the latter case via the gap between the two stages. The line density with the nominal neutraliser gas flow (Qn = 18 Torr.l.sec^{-1}) has been measured by tracking a nude high pressure ionisation gauge along the centreline of the neutraliser (see Fig.1). The gauge was calibrated for H_2, in situ, against a Baratron capacitance manometer. For the case where Qs=0, there is no gas flow in the first stage neutraliser, so that the pressure is constant in this region. This pressure has been measured as a function of Qn; it is not linear as the system operates in the transition flow regime. The pressure profile due to Qs has not been measured, but it is assumed to be identical to that due to Qn along the second stage neutraliser and to extrapolate linearly back to the extraction grids. The pressure at the junction between the two neutraliser stages (Qs only, Qn=0) is consistent with this assumption. The gas pressure profile from combined flows of Qs and Qn is taken as a simple addition of the individual profiles.

It is worth noting that Qs is normally approximately equal to the equivalent flow due to the extracted current, so that the net flow from the source to the neutraliser is usually very small, hence the gas target due to Qs is also small.

Neutralisation Measurements

The experimental set-up consisted of the PINI and neutraliser connected to the Neutral Injector Box containing the deflection magnet, the beamline calorimeter, the various ion dumps and the Test Bed Box Scrapers. The NIB was connected to the Target Tank containing a simulation of the torus duct and the Test Bed Beam Dump. This set-up is shown schematically in Fig.2.

Most of the measurements of neutralisation consisted of simply comparing the power to either the TBBD or the Target Tank plus the

TBBS from similar, usually sequential, shots with and without the deflection magnet energised. The power to the TBBD and the Target Tank plus TBBS were determined by water flow calorimetry, the flow and water temperature rise being independently determined for the two sets of components. The neutralisation efficiency is calculated as:

$$\eta = \frac{\{E_{tbbd} / E_o\}\ \text{on}}{\{E_{tbbd} / E_o\}\ \text{off}} \qquad \text{and/or} \qquad \eta = \frac{\{E_{tt} / E_o\}\ \text{on}}{\{E_{tt} / E_o\}\ \text{off}}$$

where $\{E_{tbbd} / E_o\}$on is the energy to the TBBD with the deflection magnet energised, normalised to the extracted energy, E_o etc. (In practice the extracted energy was usually the same for both shots.) The agreement between the measurements was generally very good. Since the determination of ε involves the ratio of energies, and as the water flow was held constant, this frequently reduced to simply the ratio of the integrals under the water temperature rise versus time curve, such as shown in Fig.3. Overall the accuracy of this measurement is high $<\pm 5\%$.

The method described above could not generally be used when the beam was intercepted by the beamline calorimeter, since this is designed to accept only ≤ 1.4MW per beam. With the magnet energised and the beamline calorimeter intercepting the neutral beam, the total power leaving the neutraliser is deposited on the calorimeter and the components connected to the Central Support Column, i.e. the various ion dumps and the magnet liners. Thus the neutralisation efficiency is calculated as:

$$\eta = \frac{Ecal}{Ecal + Ecsc}$$

where Ecal is the energy deposited on the calorimeter etc. Again water flow calorimetry was used to determine the deposited energy, except this time absolute measurements of water flow and temperature were necessary. The error in these measurements is estimated to be $\sim\pm 10\%$.

Predicted Neutralisation Efficiencies

In order to predict the neutralisation efficiency from known charge transfer cross sections, the extracted species mix must be known. Extensive species measurements for the JET PINIs have been made with H_2 as the working gas([1]). Measurements of the extracted species with D_2 as the working gas have recently been made, both at Culham and during the course of this work ([2]), these two measurements being in good agreement.

Account must, of course, be taken of reionisation losses in the magnet region. It is estimated that ~ 5% of the neutral beam is reionised with a gas flow of 18 Torr.1.sec^{-1}.

Comparison of Measured and Predicted Neutralisation

The measured and predicted neutral power fraction versus the target gas density for extraction voltages of 60kV and 80kV with H_2 as the working gas and for 80kV with D_2 as the working gas are shown in Figs 4 to 6. Spot points are also shown at 60kV and 70kV with D_2 as the working gas. It is obvious that there is very poor agreement between measurement and prediction. Reasonable agreement can only be achieved by multiplying the n.l scale by a factor <1.

As the species extracted from the JET PINI is well known, as are the relevant cross sections, the neutralisation measurement is in fact a measure of the gas target, n.l, in the presence of the beam, i.e.

for the JET system the gas target in the presence of the beam is of the order of half that in the absence of the beam.

Supporting evidence for the conclusion that the gas target is reduced in the presence of the beam can be obtained from the independent measurement of the power in the deflected, dumped, fractional energy ions. Because of the complexity of the system, accurate absolute measurements of this power were not possible and the experimental data shown in Fig.7 have been 'normalised' for the purpose of comparison. It is clear that the variation in the power in the deflected fractional ions strongly supports the conclusion that the gas target in the presence of the beam is indeed 'thin': The power to the fractional energy ion dumps actually increases with the gas flow, whereas a decrease is expected. As substantial re-neutralisation of these ions occurs as they traverse the magnet the accuracy of determining the reduction in the gas target is poor and no significance is attached to the discrepancy between the reduction factor determined from these data c.f. that from the neutralisation measurement.

A likely explanation for the reduction in the gas target is significant heating of the gas, as recently suggested by Paméla ([3]). This is supported by another experimental observation: The Baratron capacitance manometer attached to the neutraliser at the gap between the first and second stages shows an increase in the pressure when the beam is turned on (see Fig.10). This is precisely the opposite of expectations. The beam transports particles from the source, effectively reducing the net flow into the neutraliser, so that a reduction in the neutraliser pressure is expected, typically of the order of 0.5m Torr. An increase in the measured pressure is expected if the neutraliser gas is heated because the system is set up for constant gas flow and it operates in the transition flow regime. (As the Baratron is at room temperature, at the end of a piece of relatively narrow bore tube, no pressure change would result from a temperature increase of the gas in the neutraliser if the system operated entirely in the molecular flow regime due to thermal transpiration effects between the gauge and the neutraliser.) In order to explain a reduction in the gas target by a factor of two, the gas temperature would need to be increased to approximately 1400°C.

Conclusion

The obvious consequence of the low neutralisation efficiency is that the neutral power to JET will be lower than predicted. This can be ameliorated to some extent by increasing the gas flow. The measured gas flow to create the design gas target in the absence of the beam is 18 Torr.l.sec^{-1}. This can be increased to 25 Torr.l.sec^{-1} without exceeding limits such as the power lost due to reionisation or the power loading to the extraction grids. Nevertheless the gas target in the presence of the beam will be substantially below the design figure of 10^{16}cms^{-2}. The reason for the low neutralisation is likely to be heating of the neutraliser gas by the beam. It is probable that the size of the neutraliser c.f. the mean free path of the molecules is significant in determining the equilibrium temperature of the gas and thus should be taken into account in the design of the future systems.

References

1. T.S.Green et al, Proc. 10th Int. Conf. on Plasma Physics & Contr. Fus. Res., London, 1984.
2. A.R.Martin, Culham Neutral Beam Development Grp., unpublished data.
3. J.Paméla, EUR-CEA-FC-1279, 1985.

Fig.1 MEASURED PRESSURE PROFILE ALONG BEAM PATH

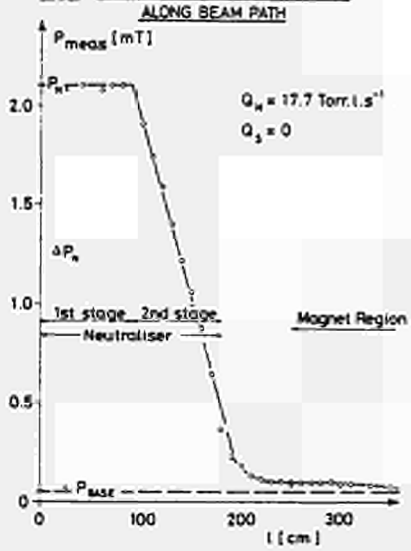

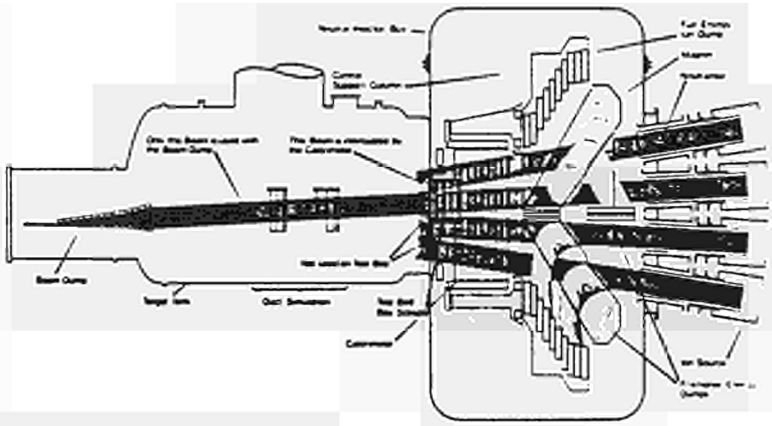

Fig.3 TEST BED TARGET TANK WATER TEMPERATURE WAVEFORM

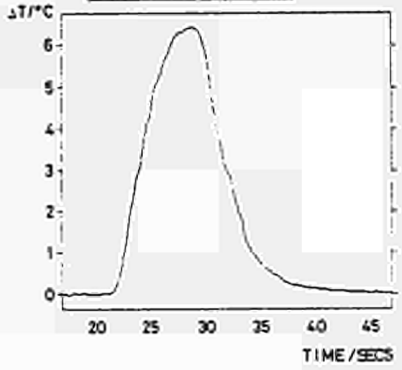

Fig.4 NEUTRALISATION DATA : 60kV/H_2

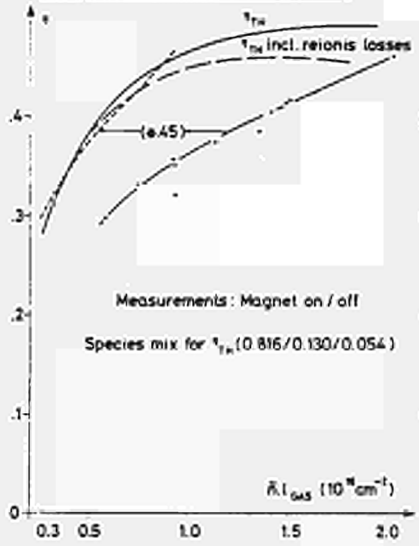

Fig.5 NEUTRALISATION DATA : 80kV/H_2

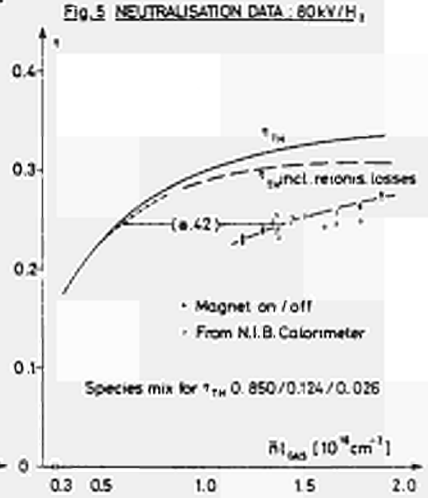

Fig.6 NEUTRALISATION DATA : D^0 BEAMS

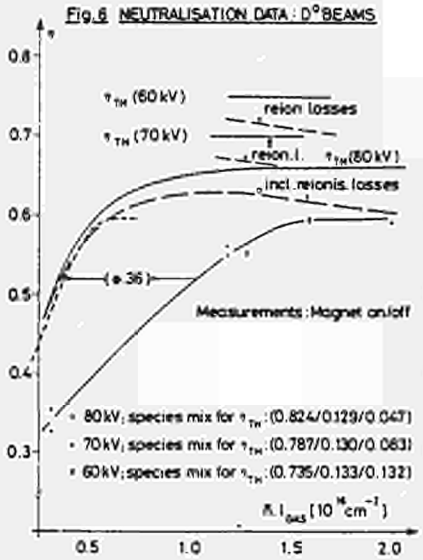

Fig.7 POWER IN DUMPED FRACTIONAL ENERGY IONS FOR 60kV (H_2) OPERATION

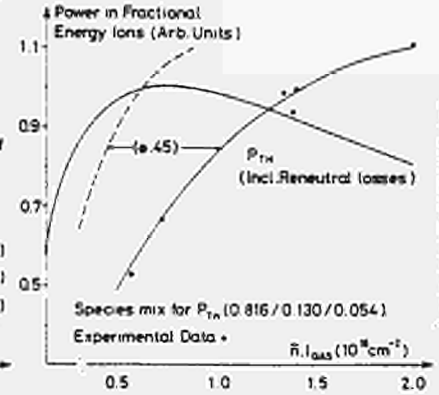

Fig.8

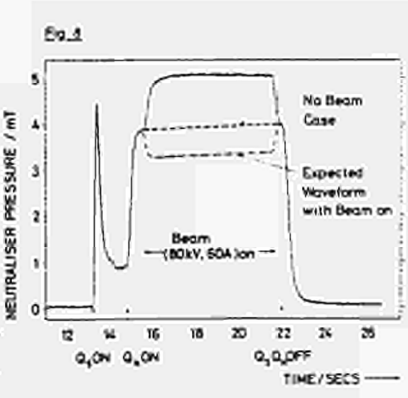

METAL SOURCES AND GENERAL IMPURITY BEHAVIOUR IN JET PLASMAS DURING ICRH

K Behringer, B Denne, M Forrest*, N C Hawkes*, A Kaye,
P D Morgan, N Peacock*, M F Stamp, H P Summers and G Tallents

JET Joint Undertaking, Abingdon, Oxon, UK
* EURATOM-UKAEA Association, Culham Laboratory, Abingdon, Oxon, UK

INTRODUCTION

The behaviour of impurities during ICRF heating after heavy carbonisation has been reported on before /1/. Further investigations have been carried out with modified antennae, clean limiter carbon tiles and an uncarbonised vessel.
Presently three ICRF antennae are installed in JET. Their Faraday screens are made of nickel; one of the screens (2D antenna) is chromium plated. The antennae are protected by surrounding carbon tiles. The vessel consists of Inconel 600 (72% nickel, 16% chromium, 8% iron). The discharges are operated either on eight poloidal carbon limiters or on the inner wall carbon protection tiles.

ORIGIN AND MIGRATION OF METALS DURING ICRH

During ICRF heating, an increase of Cr line brightness from the bulk plasma is observed when the 2D antenna is active; an increase of Ni intensity accompanies operation of the other antennae (2B or 6B). Thus it is evident that the antennae screens are the original sources of these metals. Observation of the 2D screen by visible spectroscopy proves the existence of chromium influx during RF manifesting itself in intense Cr I line radiation. In the course of operation with ICRH , screen material is deposited onto limiters and antennae protection tiles and subsequently eroded by the plasma. This is demonstrated by the behaviour of Cr I and Ni I lines in the respective visible spectra. As a consequence, the metal fluxes and concentrations in subsequent pulses increase in the ohmic part of the discharge before RF and higher concentrations result during RF for a given power. For constant RF energy, an equilibrium is established after a few pulses (Fig. 1 for the case of Cr). Lower RF energy or purely ohmic discharges lead to cleaning of the respective surfaces (Fig. 1). A beneficial result of the metal contamination is a reduction of oxygen influxes and oxygen concentrations in the plasma (gettering).

Cr INFLUXES AND RELEASE MECHANISM

Absolute Cr influx densities have been derived from Cr I intensities. They are roughly proportional to RF power and decrease during some months of operation. Indications are that H minority heating leads to somewhat higher Cr fluxes.
Combining an analysis of Cr densities in the plasma and total influx (using the antenna area) results in a Cr replacement time τ_D of $\approx$ 20 ms. This value agrees with simulations of the plasma edge conditions, if the Cr atom energy is some eV (ie sputtering, not evaporation). No significant shift (<0.1 Å) of Cr I lines in the visible spectrum could be

detected, which means that the energy of the atoms is < 50 eV. Visible He II line profiles yield an edge ion temperature of ≈ 80 eV which is not affected by the RF pulse. Concluding from these observations, the release mechanism of Cr is probably neutral atom or ion sputtering, but the details are not clear.

PARAMETER DEPENDENCE OF METAL DENSITIES

An estimate of the increase in Ni and Cr density during RF is provided by taking the incremental increase in Ni XXV and Cr XXII line intensities, corrected for the change in electron density, $\bar{n}_e$, by dividing the line intensity by $\bar{n}_e$. The behaviour of nickel as a function of RF power coupled to the plasma for a variety of conditions is shown in Fig. 2. Open symbols denote H-minority heating whereas filled symbols indicate ^{3}He-minority heating. In the ^{3}He-case it is seen that, for a given electron density, higher plasma current leads to a somewhat larger increase in nickel density (3/4 MA, 3 x $10^{19}m^{-3}$). Lower $\bar{n}_e$ leads to a higher nickel density, even at a lower plasma current (2 MA, 2 x $10^{19}m^{-3}$). This behaviour is also evident in the H-minority data (2 MA, 1.5/2 x $10^{19}m^{-3}$). H-minority heating leads to higher metal densities than ^{3}He heating, but the comparison in Fig. 2 overemphasises this fact because of lower $\bar{n}_e$ in some H cases. For several pulses the nickel concentration following from a detailed analysis is also shown in Fig. 2.

A study of the Cr density behaviour shows a steeper dependence on RF power than nickel does which is possibly due to the previous carbonisations of the nickel screens.

A heavy carbonisation (48 hrs, 17% CH_4) in 1985 led to a reduction of the OH metal concentrations of about a factor 100 and a very small increase during RF. Recovery to the usual behaviour was observed after about 200 plasma pulses, indicating an erosion of carbon layers on both antennae and limiters. The results measured towards the end of this campaign (reported in /1/) fit into the present data set (pulse 5486 in Fig. 2) obtained many months after the carbonisation.

IMPURITY CONCENTRATIONS AND RADIATED POWER

In spite of a substantial increase of metal line radiation during RF, the metal contribution to Z_{eff} and P_{rad} is relatively small (Table 1 and Fig. 3). Impurity concentrations and contributions to radiated power are derived from VUV line intensities using an impurity transport code /2/. About 20% of the radiated power during RF is due to metals. The local radiation in the plasma centre amounts to ≈ 10 mW/cm^3, as supported by bolometer and soft X-ray results/3/.

SUMMARY

The Faraday screens of the RF antennae have been identified as the original sources of metal impurities during ICRH in JET. Migration of metal impurites from the antennae screens to the limiters and protection tiles has been observed, leading to a build-up of metal concentrations in ohmic plasmas and aggravating the increase during RF. It has been observed that the limiters and protection tiles are cleaned by operation without RF within a few pulses.

Carbonisation leads to a temporary reduction of metals before and during RF heating.

In all cases, radiated power and Z_{eff} of the plasma are dominated by contributions from light impurities (C,O), and metals only contribute ≈ 20% to P_{rad}.

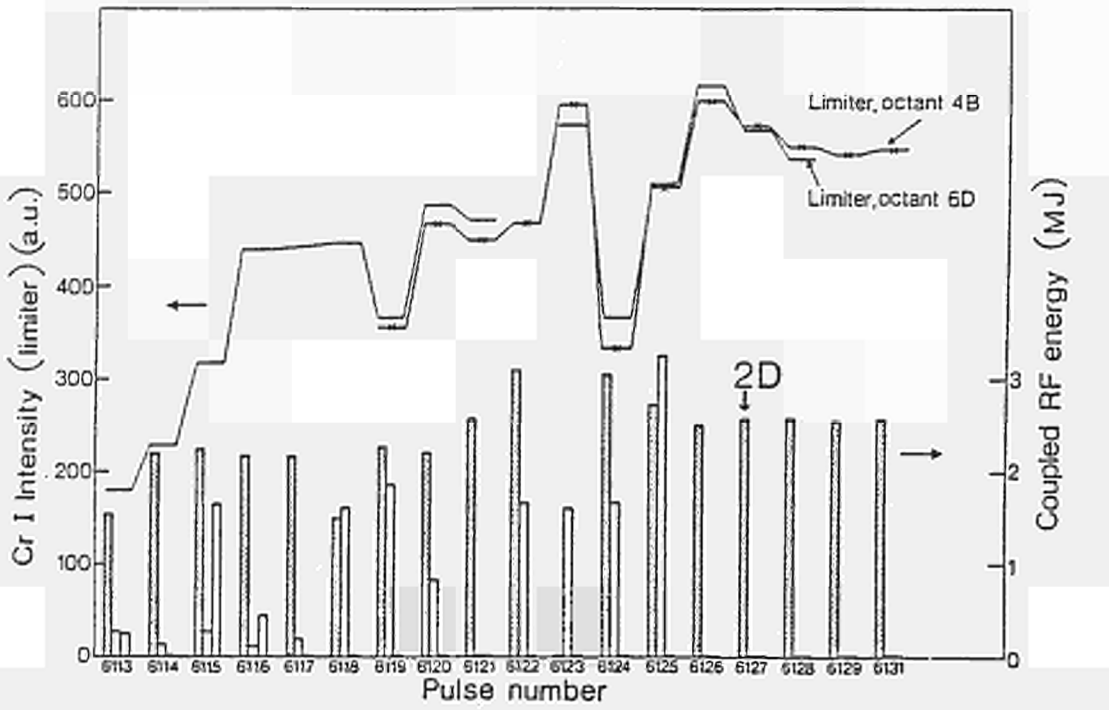

Fig.1 Cr I line intensity (two limiter views) before RF demonstrating the contamination and cleaning of the limiters as a function of preceding 2D antenna operation.

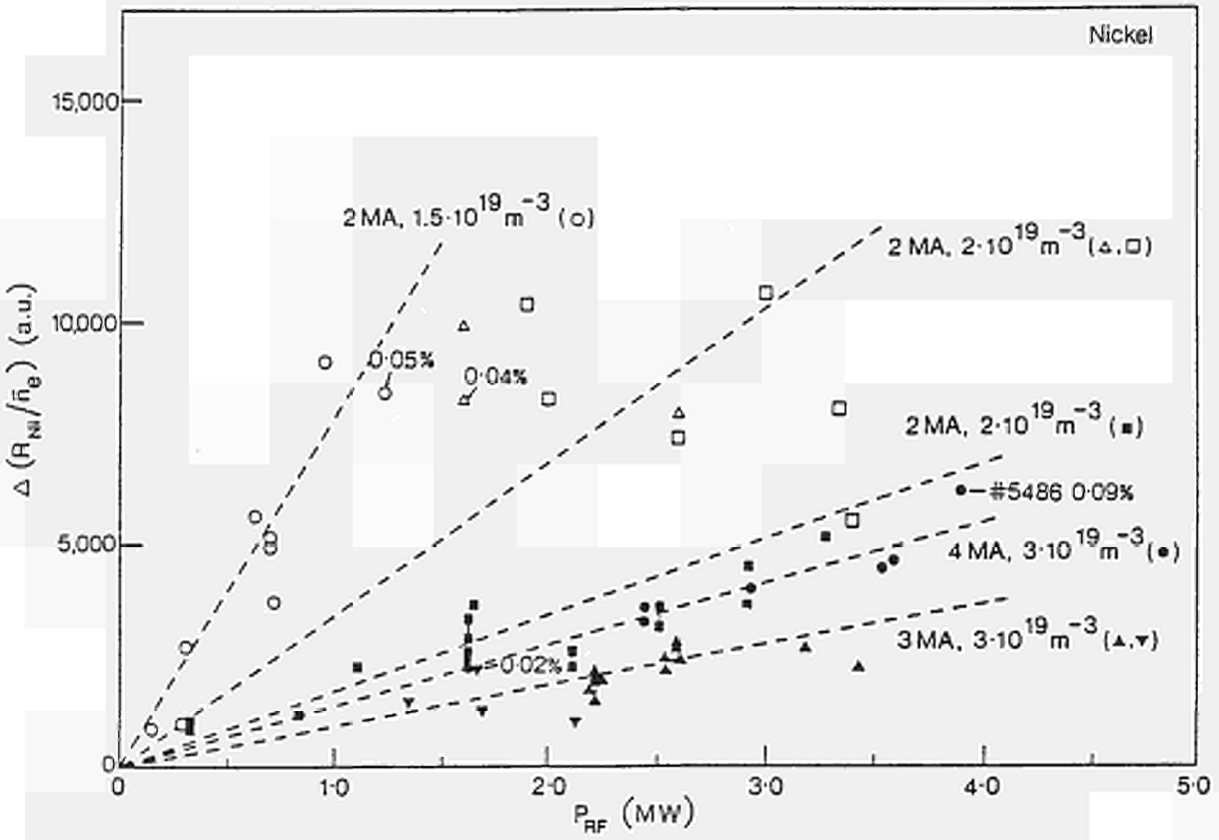

Fig.2 Increase of Ni XXV 117.9-Å line intensity divided by $\bar{n}_e$ during ICRH as a function of RF-power from the 2B and 6B antennae. The dashed lines are drawn to guide the eye only.

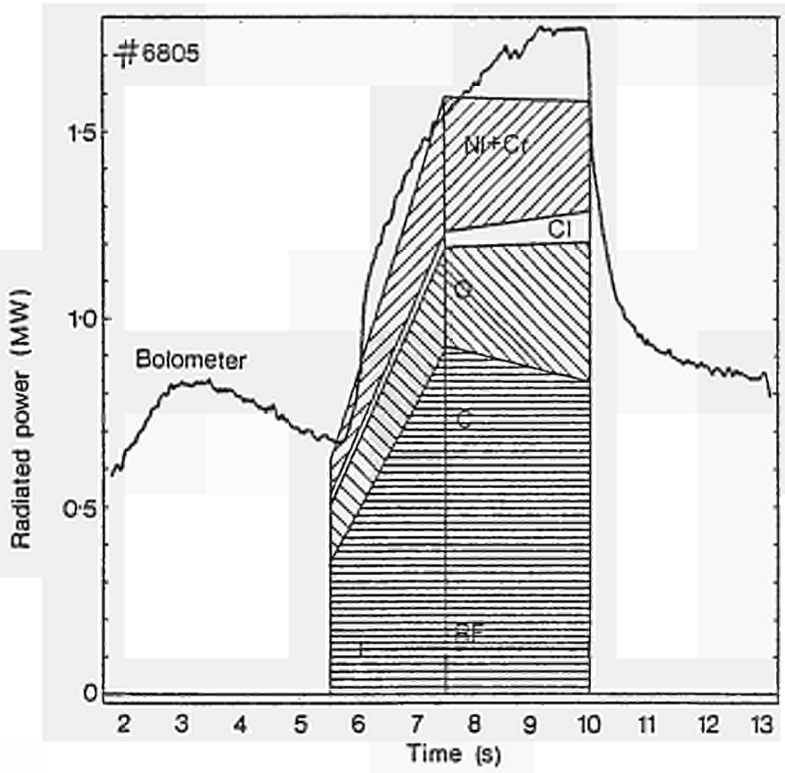

Fig.3
Calculated contributions from carbon, oxygen, chlorine and metals (nickel + chromium) to the total radiated power.
The calculation has been made for one time point before RF and two time points during RF. The result is compared with the total radiated power as measured by bolometry.

#6805
(^{3}He)D, 3.4 T, 2.0 MA, P_{RF} = 1.66 MW

	Before RF (t=5.5 s)	During RF (t=10.0 s)
C:	4.0% of n_e	4.7
O:	1.0	1.3
Cℓ:	0.04	0.06
Ni:	0.03	0.04
Cr:	0.02	0.02
Z_{eff}^{calc}:	3.2	3.6
Z_{eff}^{brems}:	4.0	3.5
$n_e(0)$:	1.93×10^{19} m^{-3}	2.79×10^{19} m^{-3}

Table 1 Analysis of the impurity content of JET pulse 6805 before and during RF heating. Z_{eff} is calculated from the impurity mixture for comparison with Z_{eff} from visible bremsstrahlung.

REFERENCES

/1/ B Denne et al., M F Stamp et al., Proc. of the 12th European Conf. on Contr.Fusion and Plasma Phys.I, p.379 and II, p.539, Budapest (1985)

/2/ K H Behringer et al., JET Preprint JET-P(85)08 (1985)

/3/ H Jäckel et al., this conference

EROSION AND REDEPOSITION OF METALS AND CARBON ON THE JET LIMITERS

J Ehrenberg*, G M McCracken+, R Behrisch*, P E Stott, J P Coad and L de Kock

JET Joint Undertaking, Abingdon, OX14 3EA, U.K.
* Max-Planck-Institut für Plasmaphysik, 8046 Garching bei München, FRG.
+ Culham Laboratory, Abingdon, OX14 3DB, U.K.

1. Introduction

It has been observed in JET and other tokamaks that the limiters become contaminated by material from the walls (1) (2) and in JET they are the main source of impurities in the plasma, although for current plasma discharges in JET the metals do not contribute significantly to the energy balance in the plasma centre. The analysis of the metal concentration on the limiter of JET gives indication on the erosion and redeposition processes for all impurities. These analyses have been carried out after the various periods of operation in 1983, 1984 and 1985 and have been described in detail elsewhere (3). The general features common to each period of operation are that the concentrations of metals have minima (~ 3×10^{20} atoms m^{-2}) near the centre and maxima (some 10^{21} atoms m^{-2}) near the edges. However the detailed distributions differ significantly for the three operating periods. In the present paper we discuss the possible mechanisms of contamination and some of the possible explanations for the observed spatial distributions.

2. Limiter Contamination and Cleaning Processes

The possible processes by which metals from the wall may be transferred to the limiter are: (a) Glow discharge cleaning (GDC). (b) Pulse discharge cleaning (PDC). (c) Disruptions or runaway electron interactions with the wall, leading to wall evaporation. (d) Arcing at the wall. (e) Charge exchange neutral sputtering of the wall. The contamination of the limiters by metals is clearly the integral effect of some or all of these processes. We have experimental evidence that all of these processes have occurred during the period of interest on JET.

Processes (a),(b) and (c) are expected to give a fairly uniform deposition flux onto the surface of the limiter. Process (c) may also result in discrete metal splashes and droplets on the limiter. Processes (d) and (e) would result in a deposition flux on the limiter peaked at the outside edge where material entering the scrape-off layer from the wall will be first ionized and swept along field lines onto the limiter.

However, the spatial distributions are modified by subsequent exposure of the limiter to tokamak discharges. Because of the limiter geometry in JET atoms sputtered from the limiter surface have a high probability of being ionized and entering the plasma. When these impurity ions subsequently diffuse out of the plasma they will be redeposited primarily on the limiter.

Direct experimental observations of impurity erosion from the limiter have been made spectroscopically. Early in the 1985 operating period one of the limiters was accidently contaminated by iron when a stainless steel probe was destroyed by a disruption. During the subsequent series of discharges the iron influx from this limiter was initially very high, but progressively fell to a negligable value after about 1 week. Similar results have been seen more recently when nickel and chromium deposited in discharges with r.f. heating have been removed in subsequent discharges without r.f.

3) Modelling of Erosion and Deposition Processes

In this section we examine in more detail the distribution of Ni on the limiter tiles from the 1983, 1984 and 1985 experimental period. Ni is chosen because it is the major wall (inconel 600) constituent. We first discuss empirical fits to the measured distributions and then propose a simple model which may explain some of the observed erosion and deposition phenomena.

Fig. 1 shows the Ni concentration per unit area of the limiter for the three limiter tiles of interest plotted as a function of the radial distance into the scrape-off layer X = r-a and divided by cos α to take into account the geometry of the limiter surface relative to the toroidal magnetic field lines. Where α is the angle between the surface normal and the toroidal magnetic field. We assume that the impurity distribution on the limiter is due to erosion and deposition and that this is composed of three terms:
(i) a uniform layer of metals C_o which represents the accumulated deposition due to glow and pulse discharge cleaning and to disruptions;
(ii) an erosion fluence $C_e \exp(-x/\lambda_e) \cos\alpha$ which represents the removal of metals from the limiter during tokamak discharges (iii) a redeposition fluence $C_d \exp(-x/\lambda_d) \cos\alpha$ which represents the redeposition of metals from the plasma. Thus the resulting concentration on the limiter surface is

$$C(x) = C_o - C_e \exp(-x/\lambda_e) \cos\alpha + C_d \exp(-x/\lambda_d) \cos\alpha. \qquad [1]$$

For simplication we will assume that $\lambda_e = \lambda_d$ and thus the difference $C_e - C_d$ represents the net erosion.
The date for the 1983 limiter is best fitted (figure 2) by $C_o = 2\ 10^{22}$ atoms m^{-2} and $C_e - C_d = 2.08\ 10^{22}$ atoms m^{-2}, ie. there is an initial uniform deposition consistent with the extensive glow clearing during this period of JET operations and a net erosion during subsequent tokamak discharges. It contrast the 1984 limiters is best fitted with a very small uniform deposit, Co ≈ 0, and with net redeposition in tokamak discharges, $C_d - C_e = 1.07\ 10^{22}$ atoms m^{-2}. The difference between the 1983 and 1984 cases is not fully understood. There may have been a lower ratio of glow cleaning per tokamak discharge in 1984, particularly towards the end of the operating period resulting in the initial contamination being completely redeposited. It may also be significant that during this period of operation the limiter surface temperature was raised to around 1500°C compared to ≤ 700°C during earlier operation. A detailed surface analysis (4) suggests that diffusion of Ni into the bulk of the limiter to a depth of several μm took place due to the higher surface temperature. This would allow Ni to accumulate in the limiter at a depth where it would be protected against erosion but subsequently measured by the PIXE analysis technique which measures to a depth of several μm. Using the alternative technique of Rutherford backscattering with which a surface layer of about 10nm can be analysed, the concentrations on the actual surface have been found to have a distribution similar to that found on the 1983 limiter.

The 1985 data (figure 1) has a distribution similar to that for 1983 near to the centre, but increases sharply at x ~ 20nm and is much higher on the outer part of the limiter. The step coincides with the radius of the leading edge of the carbon shield surrounding the RF antenna which had been installed at the start of 1985. It seems resonable that the carbon shields which also act as limiters affect the scrape off layer and reduce the net erosion on the outer part of the limiter.

To examine these processes further we have developed a more detailed model of erosion and redposition in the scrape-off layer of a tokamak discharge.

The model is presented in more detail elsewhere (5) and we only give here a brief summary. We assume that the Ni distribution on the limiter is eroded by sputtering due to deuterons, light impurities (carbon) and self sputtering during plasma discharges. We also assume that the eroded flux of Ni enters the confined plasma and is then redeposited on the limiter by diffusion perpendicular to the magnetic flux surfaces. We assume further that the sputtering coefficients are energy dependent and therefore decrease with increasing radial distance from the leading edge of the limiter. By using measured data for the relative particle fluxes, the relative coverage of the limiter surface with metal (described by the factor f in figure 3) the scrape-off layer decay lengths and the plasma temperature at the limiter we get the erosion and deposition rates as indicated in fig. 3.

One result is that the limiter is split into an erosion and deposition zone the formation of which depends on the plasma boundary parameters. In our example this deposition zones is at $x \geq 15$mm for kT=100eV.

Another result is that erosion rates on the limiter surface are about 10^{20}atoms/m^2.s at $x \approx 10$mm. Thus an initial thin film surface coverage of 10^{21}atoms/m^2 would be eroded off in 10s. This is consistent with spectroscopic observation of the rate of which a limiter appears to clean up following contamination.

Erosion of droplets, however, which have been detected with diameter of up to 100 μm on the limiter will take much longer to erode. They may represent a more persistent source of Ni.

In view of this model we suggest that the surface concentration on the limiter does not reach steady state, as long as processes are present which contaminate the limiter in its erosion zone. This may occur in processes as mentioned under (a) - (c) in section (2).

4) Conclusions

A more detailed analysis of the metal distribution found on the JET limiters from three different operational periods indicates that the final distribution is largely affected by erosion and deposition processes caused by the plasma. Contamination of the limiter surface is probably due to tokamak operational processes as GDC and PDC as well as transfer of metal from the walls to the limiter in disruptive discharges. For a complete description the results suggest that the limiter surface conditions (temperature) and the positioning of the limiter in the torus relative to other structures (r.f. antenna) have to be taken into account. A theoretical model describing the 1983 limiter erosion and deposition processes gives results which are qualitatively in agreement with experimental observations during discharges.

References

(1) G M McCracken et al. J.Nucl.Mat. 111 & 112 (1982) 159.
(2) R Behrisch et al., J.Nucl.Mat. 128 & 129 (1984) 470.
(3) J Ehrenberg et al., 12th Europ.Conf.Fus.Plasma Phys. Budapest 2-6 September 1985.
(4) J Ehrenberg and P Borgesen, Proceed.7th Int.Conf. Ion Beam Analysis Berlin 7-12 July 1985.
(5) G M McCracken et al Proceed. 7th Int. Conf. Plasma Surface Interactions, Princeton N.J. USA 5-9 May 1986.

Fig. 1 Ni concentration distributions on JET carbon limiters from three experimental periods.

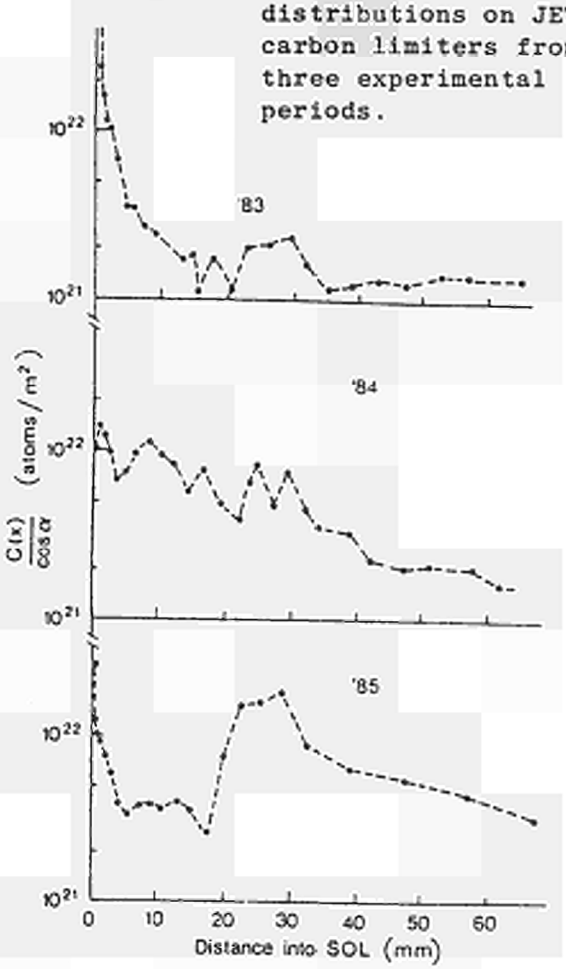

Fig. 2 Empirical fits to the Ni concentration distributions on JET limiters from two experimental periods

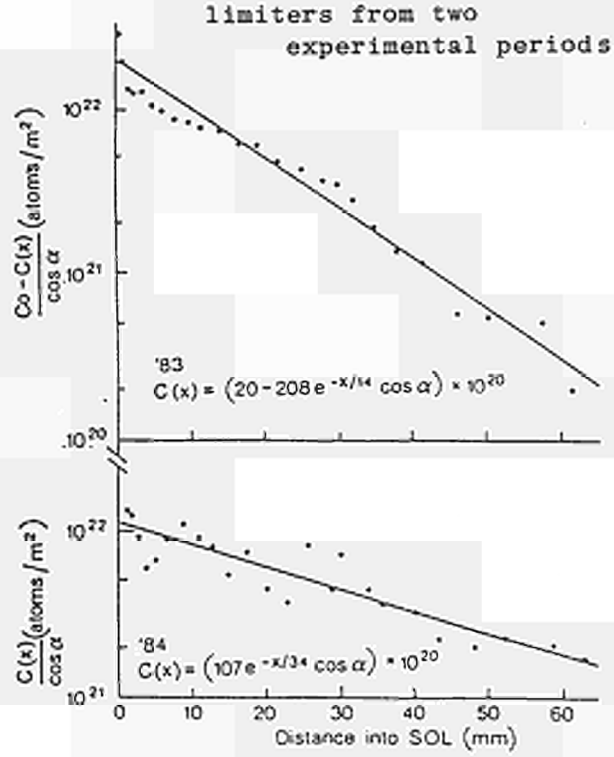

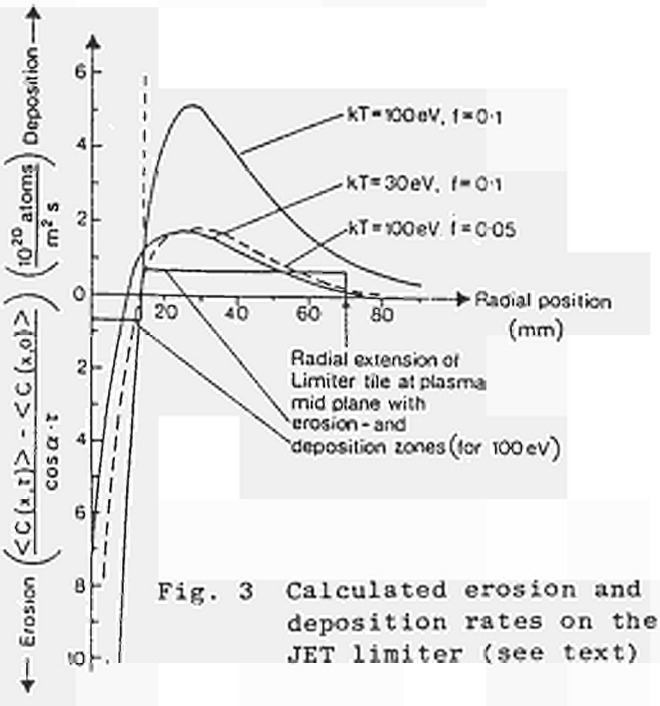

Fig. 3 Calculated erosion and deposition rates on the JET limiter (see text)

INVESTIGATION OF ELECTRON TEMPERATURE PROFILE BEHAVIOUR IN JET

D V Bartlett, H Bindslev, M Brusati, D J Campbell, J G Cordey, A E Costley, S E Kissel, N Lopes-Cardozo*, B van Milligen*, P E Stott

JET Joint Undertaking, Abingdon Oxon OX14 3EA, UK
* FOM Institute for Plasmaphysics, Rijnhuizen, Netherlands

1. INTRODUCTION

The characteristics of the electron temperature profile in JET have been examined for a wide variety of plasma conditions. Both ohmically heated plasmas ($2.1 < B_T < 3.5$ Tesla, $1 < n_e < 4 \times 10^{19}$ m^{-3}, $1 < T_{eo} < 5$ keV, $1 < I_p < 5$ MA) and those with strong additional heating (RF and Neutral Beam powers up to about 5 MW) have been studied.

The temperature data have been obtained from electron cyclotron emission measurements. The spatial and temporal resolution of the diagnostic systems employed permit a detailed study of the profile behaviour to be made.

In this paper, both global information (volume averaged quantities) and local information (eg. temperature gradients) are examined to see if they show any scaling with other plasma parameters, and whether this can be related to any of the theories of profile consistency [1,2,3].

2. THE ELECTRON TEMPERATURE DIAGNOSTICS

All the temperature data presented here have been obtained from measurements of the second harmonic (extraordinary mode) of the electron cyclotron emission (ECE). The observation direction is along a major radius on, or close to, the plasma mid-plane. These measurements provide reliable temperature information for all plasma conditions of interest here across a major radius range from just inside the plasma centre to almost the plasma edge (ie. R = 2.8 to ~ 4.0m). The measuring instruments and techniques used in the JET ECE diagnostic system have been described in detail elsewhere [4]. Two instruments are used in the present study:

1) All the temperature profiles are produced by an absolutely calibrated Michelson interferometer which measures the whole ECE spectrum about 300 times during each JET discharge. The spatial resolution of the profile both parallel and perpendicular to the line of sight is about 0.15 m, and the time taken for each measurement is 15 ms. An important characteristic of this instrument for the current investigations is that the temperatures deduced are absolutely calibrated to within ±10%, and the relative systematic error within any profile is about ±5%. Despite this accuracy, the uncertainties in the spectral response of this instrument are a limiting factor in the present analysis.
2) A 12-channel grating polychromator gives the time dependence of the temperature at fixed positions in the plasma. Its spatial resolution, about 0.06 m along the line of sight, and its response time, about 5 μs, are well suited to the present task.

3. GLOBAL TEMPERATURE BEHAVIOUR

Figure 1 shows the ratio of the peak temperature to the volume average as a function of q_{edge} for a large number of discharges with ohmic, ICRH and neutral beam heating. These data were taken at the end of the current flat top when the plasma was in a steady state and sawteeth were present. Although the peak electron temperature depends on a number of plasma parameters, the shape of the profile appears to be strongly linked to the safety factor at the edge of the plasma, q_{edge}. Also shown in figure 1 is the time development for a typical 4 MA (q_{edge} = 3) pulse. It is only when the plasma has reached a steady state with the current fully penetrated (about 3 seconds into the flat top) that the correlation of T_{eo}/T_{av} with q_{edge} is observed. The inductance shows similar correlation with T_{eo}/T_{av}.

The scatter in the T_{eo}/T_{av} plot is not due to sawteeth since the data is averaged over a time longer than the sawtooth period. It is probably related to the net input power profile (input power minus radiated power), the temperature profile being much narrower when the total radiated power is 90% of the input power. Plasmas of this type are shown by the crosses on figure 1. There is also an apparent tendency for the profile to be narrower during ICRH where the heating profile is very peaked (*), and broader during neutral beam heating which has a less peaked deposition profile (Δ).

The radius at which q = 1 (which we equate approximately to the sawtooth inversion radius measured by the 12 channel grating polychromator) is also closely correlated with q_{edge} as shown in figure 2. This, of course, is not surprising since the current density profile is determined by the temperature profile once the electric fields have fully penetrated the discharge. The confinement inside q = 1 is largely determined by sawtooth activity and the region of prime interest for confinement lies between q = 1 and q_{edge}. The parameter T_{eo}/T_{av} may be a fairly coarse measure of the profile shape in this confinement region and in particular scatter in the experimental data could mask significant differences in profile shape. We have therefore looked in more detail at the actual shape of the profiles.

4. LOCAL TEMPERATURE BEHAVIOUR

Figure 3a compares three temperature profiles measured in the steady state of ohmic plasmas with difference values of q_{edge}. Due to the different ohmic power inputs and densities the peak temperatures for these three discharges vary considerably. The gradients ($\nabla T_e = dT_e/dR$) of these three profiles are shown in figure 3b: again there are large differences. In part c) of the figure, the ratio $\nabla T_e/T_e$ is plotted. These curves show a trend with q_{edge}: across a wide region outside q = 1, the slope decreases with increasing q_{edge}. To examine this behaviour, it is convenient to fit a straight line to these curves (outside q = 1), which implies a Gaussian fit to the profiles. Figure 4 shows the slope of the fitted line as a function of q_{edge} for a number of ohmic discharges. Although the quality of the fit becomes poor at high q_{edge} (when the profile becomes more triangular) there is a correlation with q_{edge}.

With additional heating the picture becomes more complicated. The localised deposition of ICRH power inside the q = 1 surface produces greatly enhanced sawteeth, but little change in the electron temperature outside q = 1. Figure 5 shows an example of a plasma with 5 MW of ICRH (plus 2 MW of ohmic heating) and q_{edge} = 4. Even in this case, where the additional heating gives a slight increase in both the temperature and its gradient outside q = 1, the $\nabla T_e/T_e$ ratio remains constant.

With neutral injection, the temperature can increase across the whole profile. When the injected power is comparable to the ohmic input power, the $\nabla T_e/T_e$ shows a change of shape, as shown in figure 6. Since a number of plasma parameters are being changed simultaneously (eg. density), it is not clear which is responsible for this effect.

5. CONCLUSIONS

The analyses made so far on the JET data permit some tentative conclusions to be made. A range of temperatures and temperature gradients are obtained for different plasma conditions. The profile shape, represented by T_{eo}/T_{av} or the slope of $\nabla T_e/T_e$, also shows considerable variation but appears to be correlated with q_{edge}. A Gaussian fit to the profile shape outside q = 1 works well only at low and moderate values of q_{edge}. The changes in profile shape with additional heating are small, and more detailed analysis is required to determine their cause. Further work on these points is in progress.

6. REFERENCES

[1] B Coppi, Comments on P1. Phys. and Cont. Fus. 5, 261 (1980)
[2] P H Rebut and M Brusati, P1. Phys. and Cont. Fus. 28, 113 (1986)
[3] B B Kadomtsev, P1. Phys. and Cont. Fus. 28 125 (1986)
[4] A E Costley et al, 27th Meeting of APS, San Diego, USA (1985)

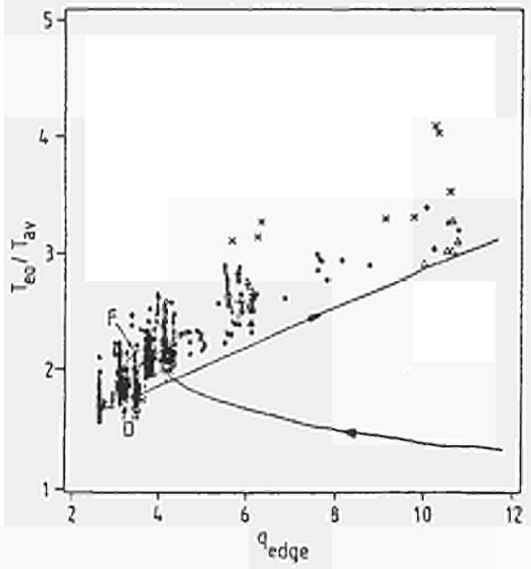

Figure (1): The ratio of peak to volume average electron temperature as function of q_{edge} for a large number of JET pulses. The symbols are:

- o Ohmic plasmas
- * With ICRH
- Δ With NB
- x High radiated power

The curve shows the time evolution for a typical q_{edge} = 3 plasma. The plasma current reaches its flat top at the point marked F, and begins to decay at D.

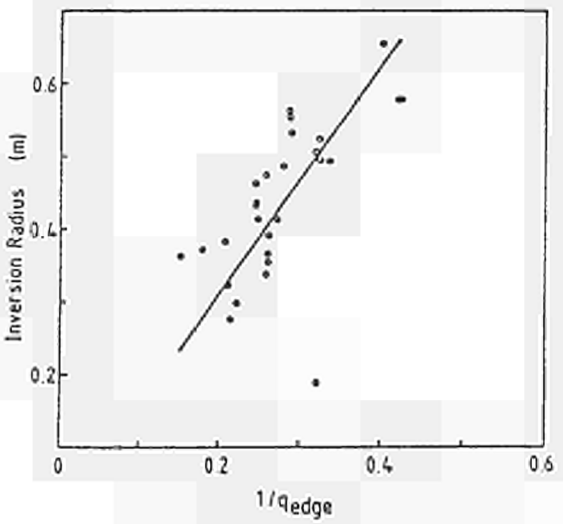

Figure (2): The sawtooth inversion radius as a function of q_{edge} for a number ofJET ohmic plasmas. The inversion radius is obtained by examination of the data from the twelve channel ECE polychromator.

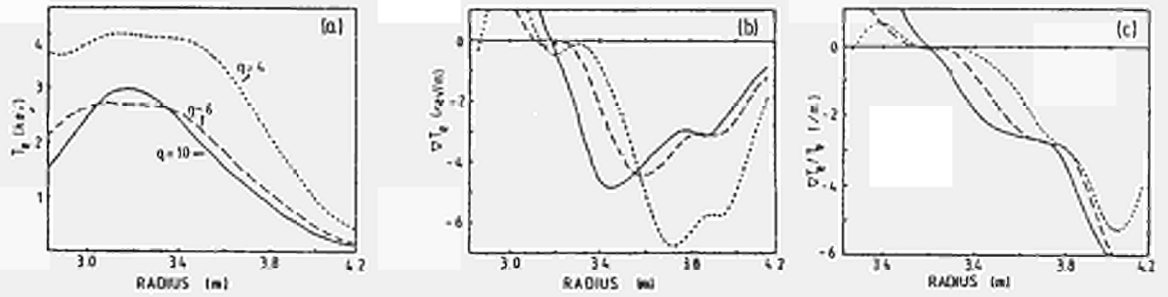

Figure (3): Variation of the profile shape with q_{edge}. The electron temperature (a), its gradient (b), and the ratio of the two (c) are plotted for 3 values of q_{edge}: solid line: q = 10, long dashes: q = 6, short dashes: q = 4

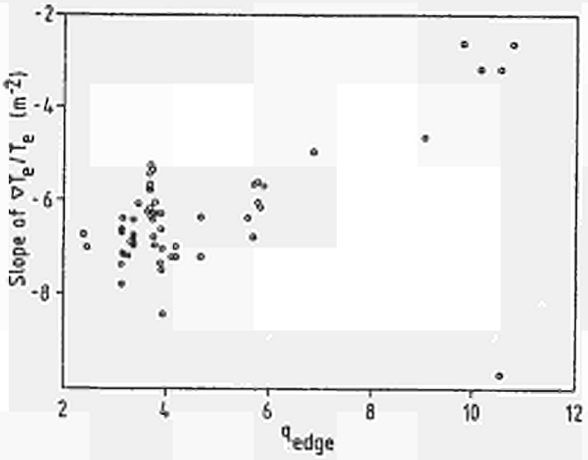

Figure (4):
The slope of the $\nabla T_e/T_e$ curve as a function of the cylindrical q at the edge of the plasma (q_{edge}) for a number of ohmic pulses.

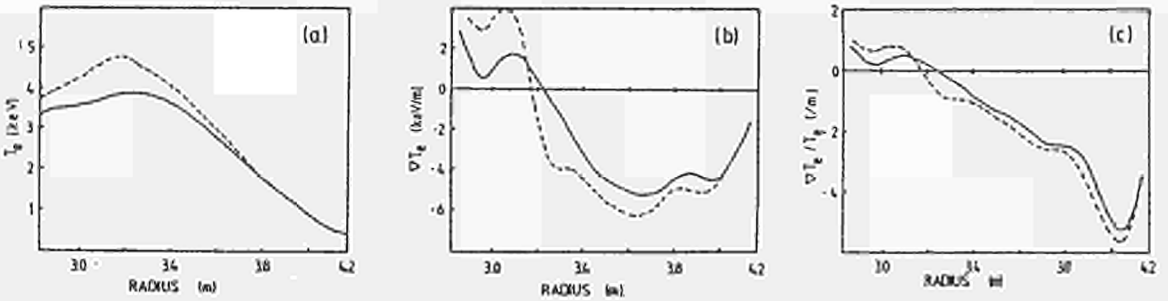

Figure (5): Variation of the profile shape with ICRH heating. The solid curve is the ohmic phase and the dashed curve 1 second after the start of 5 MW of ICRH. Although T_e and ∇T_e change, the $\nabla T_e/T_e$ curve shows only a slight outward shift.

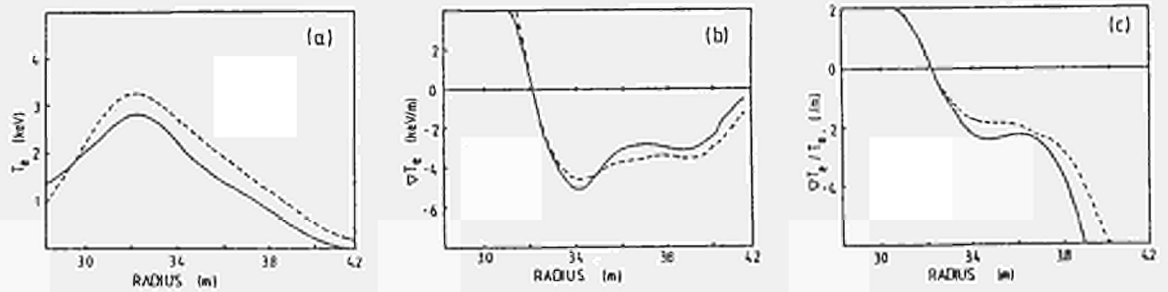

Figure (6): Variation of the profile shape with neutral beam heating. The solid curve is the ohmic phase and the dashed curve 1 second after the start of 5 MW of heating (several times the ohmic power). In this case the $\nabla T_e/T_e$ curve shows a distinct change of shape.

DIRECT MEASUREMENT OF THE ELECTRON DIFFUSION COEFFICIENT ON JET USING A MICROWAVE RELECTOMETER

A Hubbard* D Ward* and T E Stringer

JET Joint Undertaking, Abingdon, OX14 3EA, UK
*On attachment from Imperial College, London, UK

ABSTRACT

A fixed frequency reflectometer on JET is used to make localized measurements of density changes. During sawtooth oscillations, the effects of the central density collapse are clearly seen outside the mixing radius. The timing of these density pulses is compared with model predictions to derive the particle diffusion coefficient, D_p. Values of D_p = 0.5 - 0.8 m^2/s are derived, in good agreement with those obtained by other means.

EXPERIMENT

Measurements of electron density changes are made using a microwave reflectometer which launches waves at a fixed frequency F_o in the ordinary mode ($\underline{E}//\underline{B}$) /1/. Total reflection occurs where F_o equals the local plasma frequency. This corresponds to a critical density $n_c = F_o^2/80.6$ (MKS units). A simple interferometer detects movements in this layer throughout the plasma pulse. Gunn oscillators with frequencies of 20, 34.5, 49 and 60GHz have been used on different pulses to probe density layers at 5.10^{18}, 1.5×10^{19}, 3×10^{19} and 4.5×10^{19} m^{-3} respectively. In recent JET experiments the central density n_o was typically $3 - 5 \times 10^{19}$ m^{-3}, so that a 35GHz beam reflects well outside the sawtooth mixing radius.

The reflectometer uses a single antenna to launch and receive waves along the horizontal mid-plane (Figure 1). A long, oversized (WG10) transmission line directs radiation to a tunable crystal detector, which measures the interference signal. Signal/noise ratios of up to 200 are obtained. Using a low-pass filter to reduce the effect of MHD fluctuations with f > 500Hz, the delayed effect of the sawtooth collapse is clearly observed.

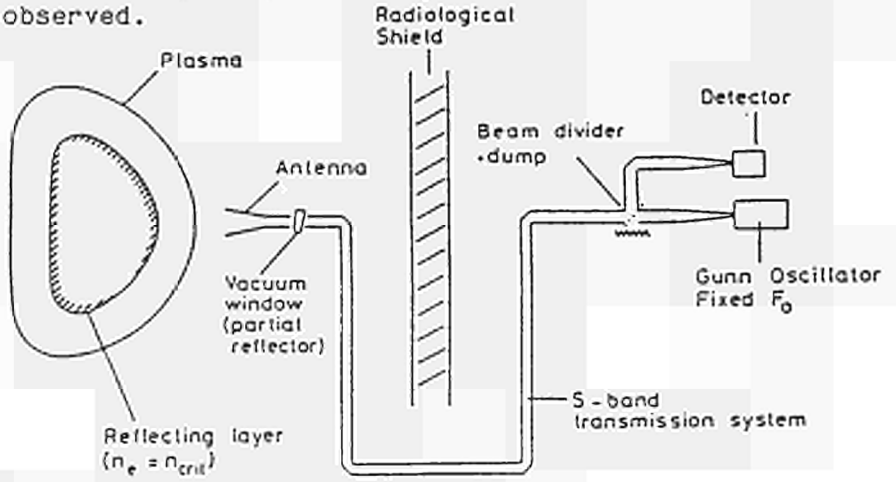

Fig. 1 Schematic of JET Reflectometer.

MODEL OF DENSITY PULSE PROPAGATION

A 1-dimensional numerical model is used to simulate the density profile of a sawtoothing plasma. First, an equilibrium is allowed to evolve assuming full recycling with a realistic neutral penetration depth, a uniform diffusion coefficient D_p and an anomalous pinch term $V_p = D_p\, r/a^2$. This gives a profile in good agreement with JET measurements. The sawtooth activity is now included by a periodic instantaneous flattening of the density profile in the central region out to the mixing radius R_m. This central perturbation then evolves on a diffusive time scale. The effect on the density at different radii is shown in Figure 2. For the region of interest, we find the time of arrival of the maximum density change (T_p) scales linearly with the distance from R_m.

In previous similar work on the propagation of the sawtooth temperature perturbation /2,3,4/, the time for the pulse to reach the edge, $T_p(a)$, was short compared to the sawtooth period τ_{st}, and consequently each pulse behaved independently. For density perturbations, however, the two times are comparable (both ~100ms on JET). This leads to a sensitive dependence of T_p on τ_{st}, which is summarized in Figure 3. Similar curves have been plotted for the time at which the pulse is first seen (T_i in Figure 2), which has a different scaling with radius.

The influence of the assumed pinch velocity on our results has been tested by using two different values: $V_p = 2D_p r/a^2$ and $V_p = 0.2D_p r/a^2$. The predicted delay times for these cases vary by less than five percent while the equilibrium density profiles are of course very different. This shows that the derived D_p is not sensitive to variations in the pinch term.

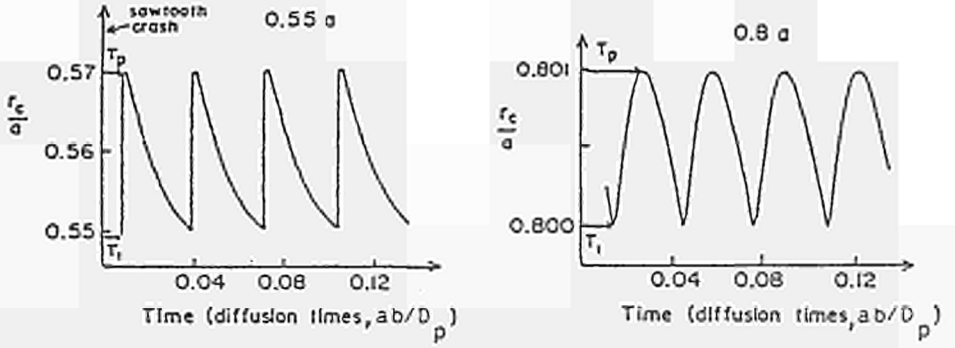

Fig. 2 Predicted movements of density layers at different radial positions across a sawtoothing plasma. (r_c = R_c - R_o).

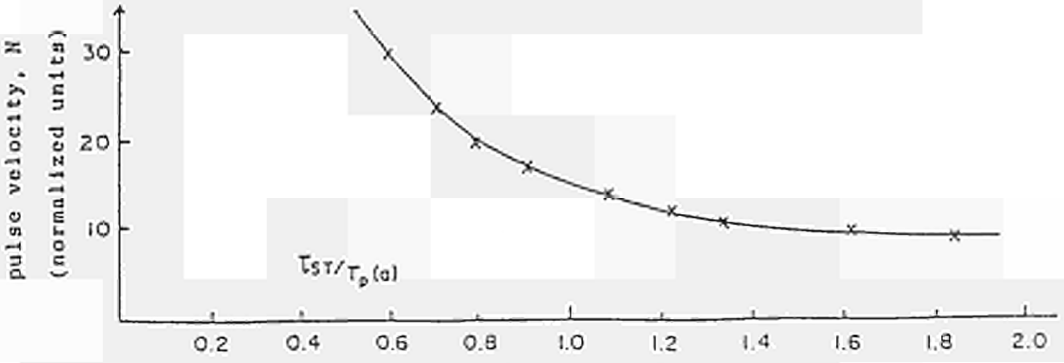

Fig. 3 Dependence of $N = (R - R_m)/T_p$ on sawtooth period.

DATA ANALYSIS AND RESULTS

To derive the diffusion coefficient we use density pulse times measured by the reflectometer during a series of similar sawteeth. Information from other diagnostics is also required. Data used for the ohmically heated JET discharge 7010 (I_p = 3MA, B_T = 2.9T) are summarized below.

Parameter	Value	Diagnostic
a	1.07m	Magnetics
b/a	1.45	
R_c(1.5 x $10^{19}m^3$)	4.04m	Multichannel FIR interferometer
R_m	3.75m	ECE grating polychromater, Soft X-rays
T_i	8ms	
T_p	51ms	Reflectometer and 2mm transmission
τ_{st}	93ms	Interferometer

T_p is compared to the model prediction as discussed above. For this case D_p = 0.81m^2/s. Using this value, we also fit the first arrival time T_i to within 1ms. Figure 4 shows the good agreement between the measured and predicted pulse shape. This gives confidence in the model as well as the values of R_m and R_c. For pulse 6276, which has higher density due to RF heating, we find D_p = .62 during heating and .48 afterwards. So far we have analysed insufficient data to determine whether there are systematic changes with RF heating or plasma parameters. Varying R_m, R_c and the delay times within experimental tolerances, we estimate an uncertainty of ± 30%. This could be improved significantly by using 2 or more frequencies simultaneously, reducing the sensitivity to R_m. Such an experiment is planned in the near future.

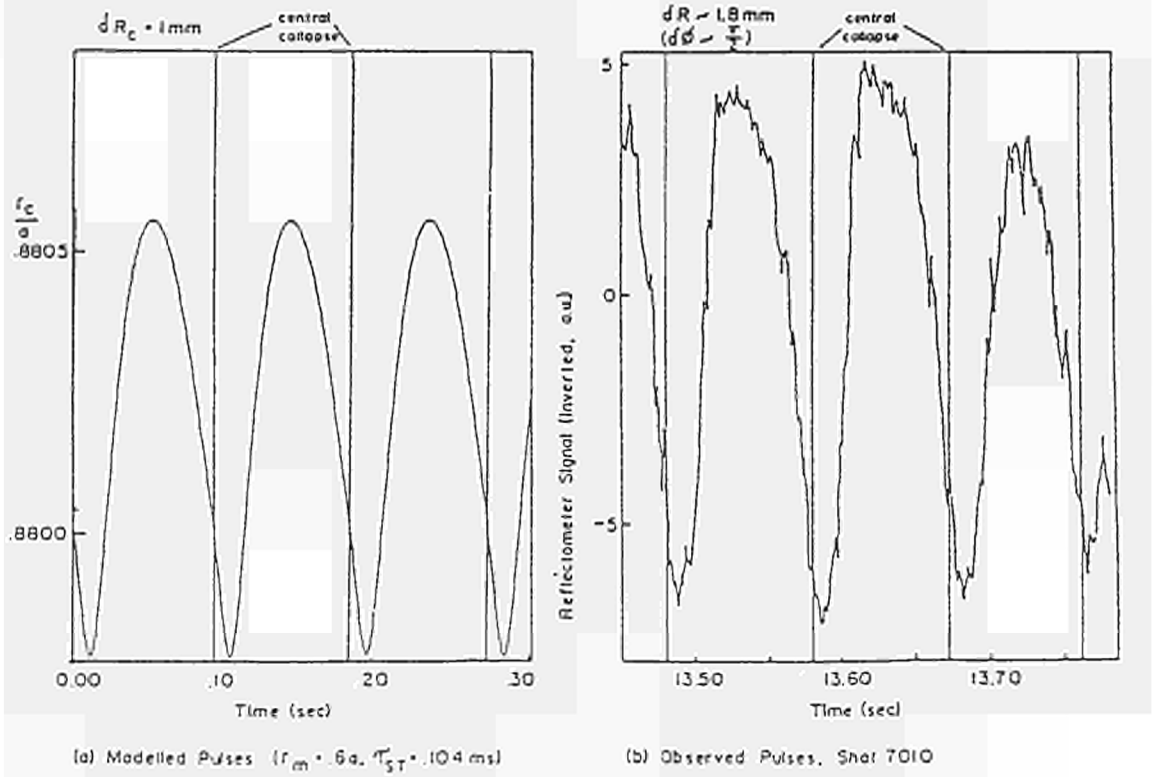

Fig. 4 Comparison of observed and predicted movements of R_c (Pulse 7010, D = 0.81 m^2/s).

CONCLUSIONS

- A simple fixed frequency reflectometer is able to make localised measurements of density perturbations in the outer regions of the discharge due to the sawtooth collapse. The shape and amplitude of the observed pulses agree with predictions of a numerical model. This gives a new and more direct technique of measuring particle diffusion.

- Detailed analysis of an ohmically heated JET discharge (pulse 7010) gives a value of $D_p = (0.81 \pm 0.25) m^2 s^{-1}$. On other discharges D_p falls in the range 0.5 to $0.8 m^2 s^{-1}$. No scaling with plasma parameters has yet been attempted.

- The cumulative effect of the sawtooth density perturbations is found to be important. With only one measurement point, the value of D_p is sensitive to experimental errors, in particular to error in the radius of the critical density, R_c. Thus we have at present an estimated uncertainty of $\pm$ 30% on D_p. This error would be reduced by having a larger number of data points (more reflectometer frequencies). A multichannel reflectometer is planned on JET.

- The results obtained are in good agreement with the mean values for D_p derived from density profile changes during RF heating /5,6/.

REFERENCES

/1/ A E Hubbard, A E Costley and C W Gowers, JET-PC(85)32 (Submitted for publication)

/2/ G L Jahns et al, Nuclear Fusion 18, 609 (1978)

/3/ J D Bell et al, Nuclear Fusion 24, 997 (1984)

/4/ H W Piekaar et al, 27th Annual Meeting of the Division of Plasma Physics of the APS (San Diego, 1985); JET-P(85)31/9.

/5/ A Gondhalekar et al, 27th Annual Meeting of the Division of Plasma Physics of the APS (San Diego, 1985); JET-P(85)31/3.

/6/ A Gondhalekar et al, this conference.

FIGURE CAPTIONS

Fig. 1 Schematic of JET Reflectometer.

Fig. 2 Predicted movements of density layers at different radial positions across a sawtoothing plasma. ($r_c = R_c - R_o$).

Fig. 3 Dependence of $N = (R - R_m)/T_p$ on sawtooth period.

Fig. 4 Comparison of observed and predicted movements of R_c (Pulse 7010, $D = 0.81\ m^2/s$).

FIRST SPECTROSCOPIC CHARGE EXCHANGE MEASUREMENTS DURING NEUTRAL INJECTION ON JET

M G V von Hellermann, W W Engelhardt, L D Horton
P G Carolan*, M J Forrest*, N J Peacock*

JET Joint Undertaking, Abingdon, Oxon, OX14 3EA, UK
* EURATOM-UKAEA Association, Culham Laboratory, Culham, Oxon OX14 3DB,UK

INTRODUCTION During the first phase of neutral beam heating on JET advantage has been taken of using the heating beams to develop an active beam diagnostic system based on charge - exchange - recombination - spectroscopy (CXRS). The diagnostic is based on the charge exchange interaction of fast injected neutrals as H^0 and D^0 with thermal fully stripped atoms such as H^+, D^+, He^{2+}, C^{6+} and O^{8+}. The first two represent the bulk of a a JET plasma and the other the dominant light impurities. The charge exchange reaction is:

$$H^0_{beam} + Z^z \rightarrow H^+_{beam} + Z^{z-1,*}(n,\ell)$$

H^0 or D^0 are the injected high energy neutrals, Z^z the thermal (fully) ionized impurity of charge z and $Z^{z-1,*}(n,\ell)$ the impurity atom excited in quantum state (n,ℓ).

The resulting recombination radiation can be analysed by suitable instrumentation. The most intense recombination lines are emitted from $\Delta n=1$ transitions and lie in the VUV or soft X-ray regions of the spectrum. At high beam energies ($E_{beam} > 25$keV/a.m.u.) there is appreciable recombination into high quantum states which emit in the visible region. The visible CXR lines have a particular appeal as diagnostic indicators in an active thermonuclear experiment such as JET since the collected light can be transferred via radiation hardened fibre guides into a remote diagnostic hall. CXRS enables diagnostic access to nuclei which are distributed widely throughout the bulk of the plasma, but which otherwise are not directly detectable in JET. In contrast to conventional line emission spectroscopy the geometric intersection of a line of sight and the neutral beam path determines a well defined active volume and hence gives a local measurement. The observed excited CXR flux is given by:

$$\frac{d\Phi(\lambda,L)}{d\lambda} = \frac{1}{4\pi} f(\lambda) \int_{-L/2}^{L/2} ds \cdot \left\{ n_Z(s) \sum_E n_H(s,E) \, (\sigma v)^{n,\ell}_{cx}(E) \right\}$$

Where : $n_H(s,E)$ is the neutral particle density at fractional energy E and location s, $n_Z(s)$ the local (impurity) density, $\sigma v^{n,\ell}_{cx}(E)$ the effective charge exchange excitation rate at beam energy E and quantum numbers n and ℓ, taking into account cascading and ℓ - mixing processess (cf. FONCK. [1]). Finally L the length of emitting intersection volume along line of sight s and $f(\lambda)$ is the spectral profile

$$f(\lambda) = \frac{1}{\sqrt{\pi}\lambda_D} e^{-((\lambda-\lambda_0)/\lambda_D)^2}$$

The Doppler width and Doppler shift allow a determination of the temperature and the bulk plasma velocity. The local fractional neutral beam particle density $n_{H^0}(R,E,t)$ can be derived by the recently developed PENCIL CODE (cf. WATKINS et al [2]). In addition to that code it is feasible to obtain the same information by measuring the electron impact excited and Doppler shifted Balmer-alpha spectra emitted by the fast injected neutrals (cf. PEACOCK et al [3]) The atomic physics data of the

involved excitation rates rely mostly on theoretical (cf. SUMMERS et al [4]) and partly on experimental data like those recently obtained from a CRX-experiment on ASDEX in pure helium discharges (PEACOCK et al [3]).

EXPERIMENTAL

The layout of the viewing chords and that of the heating neutral beams is described by Fig.1. At present two viewing chords are employed. A vertical line of sight in Octant 8 intersecting the neutral beams in the plasma centre (R=3.1m) and a second viewing line, which passes from a horizontal port in the adjacent Octant 1 to an intersection volume with the neutral beams at approximately half the minor radius (R=2.3 m). This viewing line enables measurement of toroidal plasma rotation. A multichord optical head, (8 fibres) which will allow a complete radial scan, will be installed during the next shut down of JET. The instrumental equip- ment is an optical head (F/1.6) followed by a 150m, PCS 1000, fibre link with an attenuation of 20 db/km at 500nm. The spectrometer is a 1m Czerny-Turner with a 2160g/mm grating. The 1024 element intensified detector array has a quantum efficiency of 8 photons/count at 500nm. The total sensitivity of the system was absolutely calibrated yielding a photon flux/count rate of 10^7 cm^{-2} sr^{-1} at the same wavelength.

RESULTS

The CXRS results obtained during the first NBI campaign have clearly demonstrated the potential for measurement of local ion temperature, toroidal plasma rotation and impurity concentration. The ion temperature derived from the Doppler broadened CX-line profiles of oxygen, carbon and helium agree reasonably with values determined by independent ion temperature diagnostics on JET. There seems to be a slight increase of derived ion temperature with increasing Z. This needs however, further systematic investigation. As an illustration of the CX characteristic features the time dependence of the oxygen 10 → 9 (6068A) spectrum before and during NBI is shown in Fig.2. Analysis of fitted line profiles and background level gives the ion temperature, line intensity and continuum intensity (Fig.3). A preliminary analysis of the calibrated photon fluxes making use of electron source rate data determined by the PENCIL code [2], excitation rates taking into account complete ℓ-mixing for the 10 → 9 transition [1], results in relative oxygen concentrations in the order of 2 % of the electron density. The concentration of oxygen relative to n_e appears to decrease during a NB pulse whereas the absolute level tends to increase slightly. This very preliminary analysis is based on the assumption that only the full energy component contributes to the CXR signal and that halo effects and excitation by meta stables from thermal atoms can be ignored.

Comparison of JET pulses with comparable NB and plasma parameters, the spectrometer being tuned to the spectra of O^{8+} and C^{6+} respectively, indicates a value n_C/n_O of 3 to 5 decreasing with increasing electron density during injection to ≈2. These values are in rough agreement with results obtained by the usual transport analysis (cf. BEHRINGER [5]). Further analyses are in progress which involve detailed modelling of the atomic physics and local neutral particle densities [2,4]. The tangential viewing line was used to measure temperature and toroidal plasma rotation at approximately half the minor radius (R = 2.3m). Typical values are in the order of a few times 10^6 cm/sec and the ratio of ion temperature Ti(R = 2.3m)/Ti (R = 3.0m)≈0.6 .

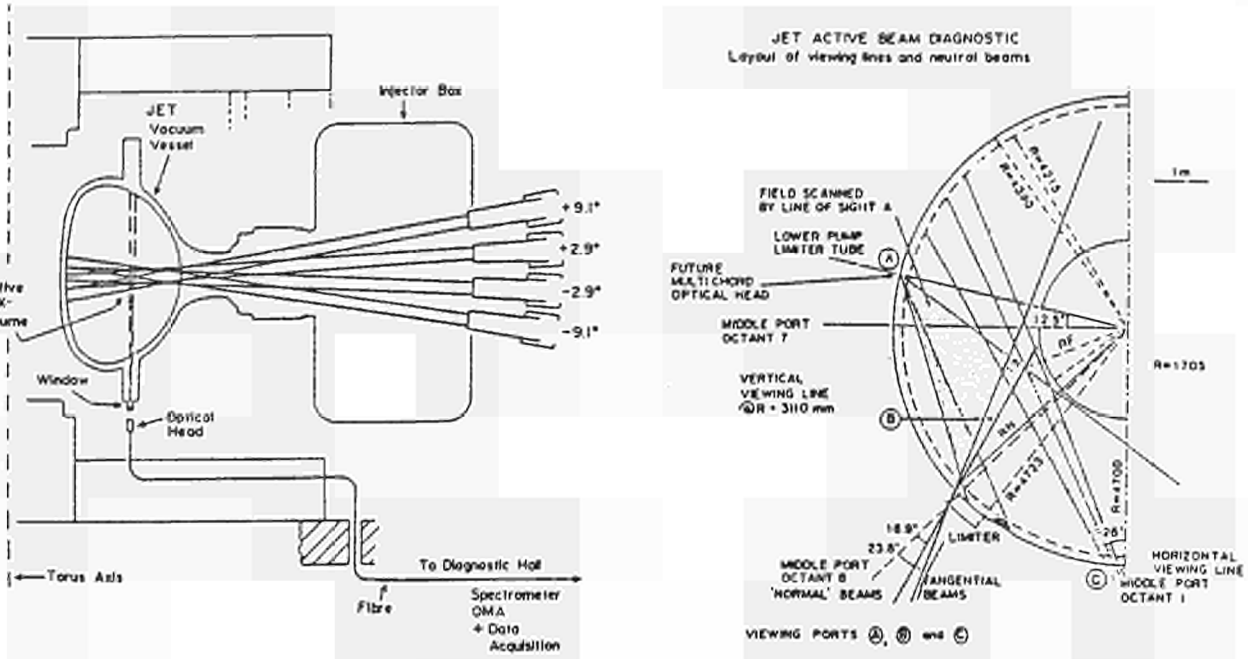

Fig. 1. Experimental layout showing viewing lines and neutral beams.

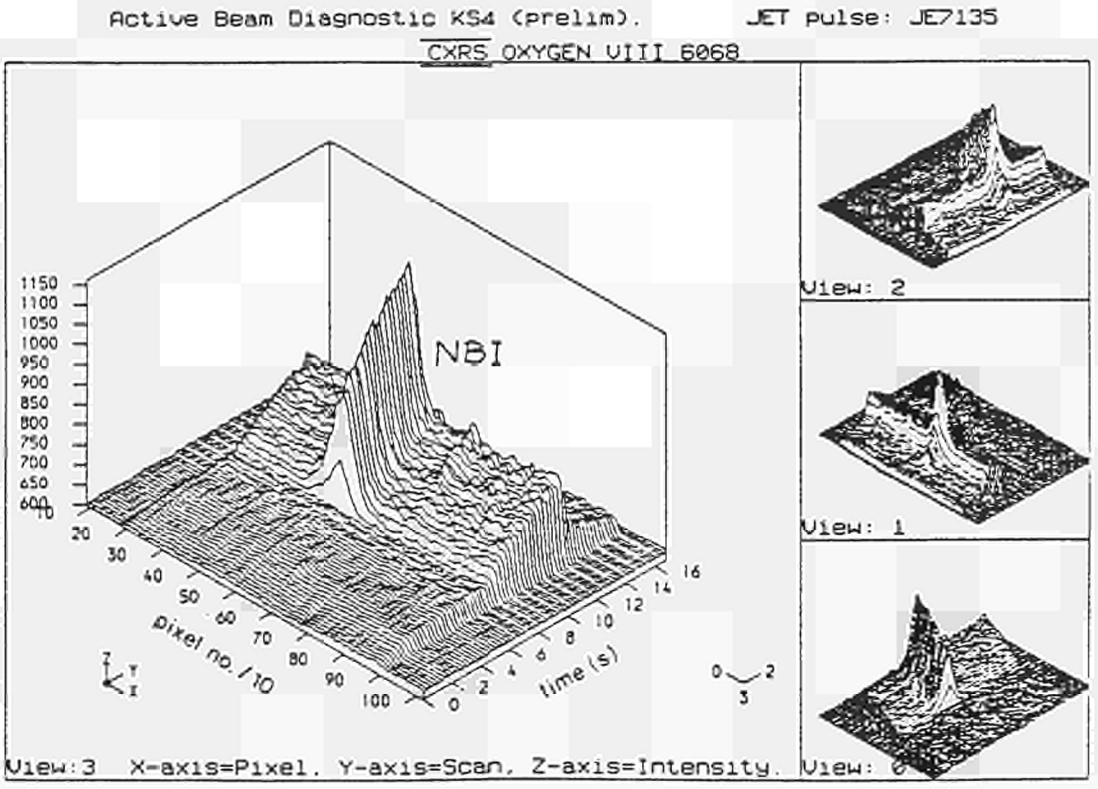

Fig 2. Time history of the O^{7+} (10 → 9) spectrum during NBI.

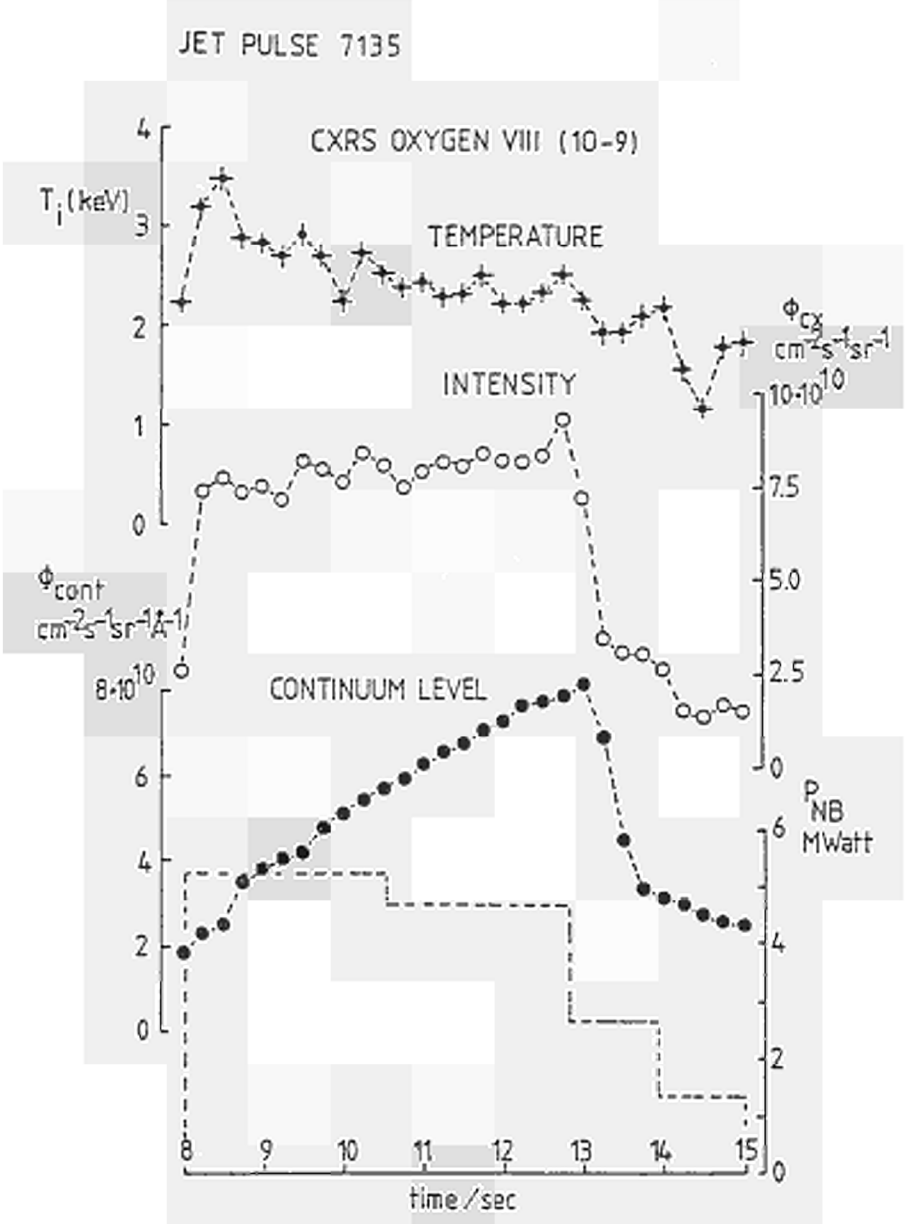

Fig 3. Calculated fit parameters a)CXR(O^{8+})-temperature b)CX-intensity, c)continuum intensity.

REFERENCES

[1]. FONCK el al, Phys. Rev. A29, 3288 (1983)
[2]. WATKINS et al, this conference
[3]. PEACOCK et al, to be published
[4]. H.P. SUMMERS, JET Report 1986, P (86) 01
[5]. BEHRINGER et al, this conference

JET Invited Papers at Fourteenth Symposium on Fusion Technology (SOFT), Avignon, France, September 1986

CONTENTS PAGE NO.:

THE IMPACT OF FIRST JET RESULTS ON THE DEVELOPMENT OF FUSION

The JET Team*

(Presented by P.H. Rebut)

JET Joint Undertaking, Nr. Abingdon, Oxon, OX14 3EA, U.K.

ABSTRACT

In the mid 1970's, when the objectives and parameters of JET were defined, certain problems were identified, for which solutions were needed, before a fusion reactor could be envisaged. These were associated with plasma-wall interactions, the need for additional plasma heating, and the eventual activation of the experimental device.

After three years of operation, JET has proved to be the world's best performing device in thermonuclear fusion research, but has also shown that plasma behaviour is even more complex than anticipated. The latest JET results show the many advances made over its operational period. In particular, the especially good confinement and high temperatures achieved with ohmic heating alone have exceeded expectations. However, certain limitations in plasma parameters have been encountered including density limits due to disruption phenomena; peak ion and temperature limitations due to sawtooth oscillations; impurity power losses; and confinement degradation and restricted temperatures with additional heating (in contrast with those reached with ohmic heating alone). The impact of this plasma behaviour on the JET programme and the necessary developments to approach closer to reactor conditions are described. In conclusion, the implications for a future reactor are considered.

1. INTRODUCTION

The Joint European Torus (JET) is the largest single project of the coordinated fusion research programme of the European Atomic Energy Community (EURATOM). Its main objective is to obtain and study plasma in conditions and with dimensions approaching those needed for a fusion reactor (ie $n = 2\times10^{20}m^{-3}$; $T > 10keV$, and $\tau = 1\text{-}2s$), and is the first device to be designed to study α-particle production, confinement and subsequent plasma heating in D-T plasmas.

The main parameters of JET, the details of its construction, its essential features and results from the initial ohmic heating phase have been described previously [1,2]. This paper concentrates on experiments and advances during the last 18 months (the first additional heating phase) using ion-cyclotron resonance frequency (ICRF) and neutral beam (NB) heating.

2. TECHNICAL ACHIEVEMENTS

2.1 Machine Status

Machine conditions were progressively improved during the early phase and all machine systems have now met the stringent design specifications. The toroidal magnetic field (B_T) now operates routinely at its maximum design value of 3.45T. The plasma current ($\pm < 3\%$), horizontal plasma position ($\pm < 10mm$), plasma elongation $\epsilon(\pm 5\%)$ and shape are all controlled by feedback circuits acting on poloidal field coils. Following considerable work on these systems, stable control has been obtained with elongations in the range 1.2-1.7. However, the plasma vertical position is naturally unstable due to both the quadrupole poloidal field necessary for the elongated plasma and the de-stabilising effect of the iron magnetic circuit. Loss of vertical position feedback control at higher elongations can lead to large vertical forces on the vessel. Consequently, until the vessel has been further strengthened, the plasma current, I_p, has been restricted within the operating range given by $I^2(\epsilon\text{-}1.2) < 5.0(MA)^2$. Final strengthening of the vessel will be implemented at the 1986 shutdown and should allow operation to the highest plasma current, at the full elongation of $\epsilon = 1.7$.

The plasma current has been increased to 5.1 MA (for a period of 3 s within a 20 s pulse), exceeding the design value of 4.8 MA. However, the elongation was limited to 1.4 in order not to risk machine damage from a vertical instability. In addition, plasma currents have been achieved routinely at 4 MA with flat-tops of 6 s duration. At present, the full inductive current drive (34 Vs) cannot be used as the nominal premagnetisation current creates stray fields, which inhibit reliable plasma breakdown. Changes are planned to increase the inductive drive capacity to enable longer duration current flat-tops and to permit the possibility of cautiously raising the plasma current towards a value of 7 MA.

The vacuum vessel is usually operated with wall temperatures at 250-300°C and with a base pressure of 10^{-7}mbar H and 10^{-9}mbar residual impurities. The vessel is conditioned by glow discharge cleaning (GDC) in hydrogen and/or deuterium. Gas introduction is made from four injection modules, each permitting fast puffing for pre-filling, and controlled addition of gas during the pulse. JET usually operates with carbonised walls since this type of conditioning reduces considerably the level of metallic impurities and oxygen, leading to reduced Z values. Carbonisation of the torus interior is achieved by glow discharge cleaning in a mixture of hydrogen or deuterium and hyrogenic methane (CH_4).

In most recent experiments, eight carbon plasma limiters have been located symmetrically on the outer equitorial plane inside the vessel. Since the relatively frequent radial disruptions mostly terminated on the inner walls, these have been covered by carbon tiles to a height of $\pm$ 1 m around the mid-plane. This tiling can also be

*See Appendix 1

used as a limiter defining the magnetic surface adjacent to the vessel inner walls: this configuration has been used for minor radius and major radius scaling experiments. These protections cover $\sim 45\,m^2$, in total, corresponding to $\sim 20\%$ of the vacuum vessel surface, and protects areas of the inner wall, the frames of three RF antennae, eight octant joints, the outer wall around Octant No.5 (neutral beam shine-through protection), and the eight limiters.

In early 1987, it is planned to cover the 32 bellows assemblies and protect one further horizontal port ready for introduction of the second neutral injector box. In addition, the existing limiters will be replaced with two toroidal 'belt' limiters (surface area $\sim 15m^2$), and the existing RF antennae will be replaced with eight water-cooled versions. These components will be covered first in graphite for early 1987 operation. The total graphite surface area seen by the plasma will be $\sim 128\,m^2$, amounting to ~ 5.6 tonnes in the vessel. In late 1987, these protections will be replaced by beryllium plates to observe the effects with this material covering.

2.2 RF Heating System

Since early 1985, three RF antennae have been installed. Power is transferred to the plasma by selecting a radiation frequency (25-55MHz) equal to the cyclotron resonance of a minority ion species (H or He^3). The power deposition in the plasma is local (half-width ~ 30cm) and can be varied across the plasma by changing either the toroidal field or the frequency. Each antenna is fed by a tandem amplifier delivering up to 3MW in matched conditions. The three units have been regularly operated up to 7.2MW for 2s pulses. Experiments with 8s pulse duration have also been performed delivering ~ 40MJ to the plasma.

When completed, the JET RF system will have eight generator-antenna units delivering 32MW for 20s pulses at the generator output. Each amplifier unit will be upgraded to 4MW, using a more powerful tetrode in the final amplification stage. New antennae have been designed for insertion inside the toroidal belt limiter. Active cooling of the side protections and of the screen elements will permit operation at full additional heating power (~ 40MW). The new antennae are presently being tested and should be installed during the 1987 shutdown. Ugrading to 4MW units should be completed in 1988.

2.3 Neutral Beam Heating System

A long pulse (~ 10s) neutral beam injector with eight beam sources and one integrated beam line system has been operated on JET, since early 1986. H beams have been injected into D plasmas with particle energies (in the full energy fraction) of >65keV. The neutral power fractions at this energy were 69%, 23% and 8% in the full, half and third energy components, respectively, giving a total beam power of >5.5MW injected into the torus. D beam heating experiments were also performed into D plasmas, with a particle energy of 75keV, injected power fractions of 76%, 17% and 7% and total power and energy into the torus of 9MW and 35MJ, respectively. The pulse lengths employed were 3-7s.

Under all operating conditions, the fast ion deposition profiles were peaked on axis. With 5.5MW H-beams, the particle source rate into the plasma was $7x10^{20}s^{-1}$. Stable plasma operation at high densities was achieved. Impurity production was not a problem and radiation from the centre was low, in all cases. Metal impurity concentrations dropped substantially during beam pulses, and the effective charge, Z_{eff}, decreased by $\sim 20\%$.

3. SCIENTIFIC RESULTS

3.1 Gross Parameters

After reaching full performance specifications in the Ohmic Heating configuration, the additional heating programme has been continually optimized, during the last eighteen months. Optimization of ohmic heating discharges was carried out below 4MA with limited elongation, to avoid the vertical instability and to reduce the number of radial disruptions. During the current plateau, peak ion and electron temperatures of 3keV and 4keV were achieved with a peak density $\sim 4.2x10^{19}m^{-3}$ and an energy confinement time of 0.8s.

In early 1985, RF heating was first applied to the plasma. Subsequently, three antenna have been installed and ~ 7MW of power coupled to the plasma, at which, the peak electron and ion temperatures have reached 5.5keV, with peak ion densities of $\sim 3.5x10^{19}m^{-3}$. However, the confinement time has dropped to $\tau = 0.3$s, during RF heating, at the higher power inputs.

In early 1986, the first neutral beam injector was operated on the machine and up to 5.5MW of neutral hydrogen (H°) beams and in excess of 9MW of neutral deuterium (D°) beams have been injected, producing ion temperatures up to 6.5keV at densities of $3x10^{19}m^{-3}$. At lower peak densities ($\sim 1.5x10^{19}m^{-3}$), ion temperatures >10keV have been observed. However, again there was a degradation in confinement time with additional heating. Recently, combined RF and neutral beam powers up to 14.5MW has been coupled to the plasma. Ion and electron, temperatures of ~ 7.5keV at densities of $3x10^{19}m^{-3}$ were obtained. Neutron yields up to $2.5x10^{15}s^{-1}$ were obtained with D injection, mainly from beam – plasma D – D reactions. The best ratio of fusion power to input power obtained was $Q_{DD} = 3.5 \times 10^{-4}$, which is equivalent to $Q_{DT} \sim 0.2$ and would have corresponded to a fusion power in excess of 1-2MW.

The best figure of merit (fusion product) $<\hat{n}_{DT_E}\hat{T}_i> = 10x10^{19}m^{-3}s.keV$ has been achieved in ohmic heating cases at 5MA (compared with the value $5 \times 10^{21}m^{-3}s.keV$ required in a reactor). The value is similar for ohmic heating only, RF, NB and combined heating cases at comparable plasma currents, due to the degradation in τ_E with additional heating offsetting gains

in other parameters.

3.2 Limitations on Plasma Parameters

Successful discharges without either gross instabilities or excessive development of a non-thermal distribution of electrons are limited to certai n ranges of plasma density and plasma current. In turn, this limits the temperatures (T_e and T_i) reached and the energy confinement time, τ_e, attained. There are certain physical processes (predicted theoretically and observed experimentally), which limit the maximum parameters achieved in Tokamaks, as follows:

(i) Current and Density Limits: Tokamak disruptions are observed in which plasma confinement is suddenly destroyed, followed by a complete loss of plasma current. These pose a major threat, as they limit the range of current and density operation, and their occurrence leads to large mechanical stresses and intense heat loads on the plasma vessel.
The operating diagram for JET plotted as normalized current ($=2\pi RI_p/AB_T = 1/q$, where A is the cross-sectional plasma area) versus normalized density ($=\bar{n}R/B_T$) is shown in fig.1. The operating region on JET is bounded on the high sides of both ($\bar{n}R/B_T$) and (1/q) by disruptive instabilities and, in ohmically heated plasmas, the density limit is $n_e(\mathrm{m}^{-3}) = 1.2\times10^{20}\, B_T(T)/qR(m)$. This limit depends on plasma purity and on power input. In neutral beam heated plasmas, this limit is substantially increased, as shown in fig.1, to $n_0(\mathrm{m}^{-3}) = 2\times10^{20} B_T(T)/qR(m)$. In addition, preliminary experiments with a diagnostic pellet injector have also increased the density limit. It is planned to further increase the density limit in JET by decreasing impurity levels, by high power additional heating and by the use of a high speed pellet injection.

At a given plasma density, if the current is ramped down, reducing 1/q, or when the additional heating is turned off at constant current, a disruption is inevitable, unless the density can be reduced by special pumping panels as the power is reduced, so that the discharge parameters remain on the right side of the limiting line in fig.1. At present the powerful pumping of the inner wall carbon tiles greatly assists this operation.

(ii) Sawtooth Instabilities: Sawtooth oscillations are seen in the centre of JET, from soft X-rays, neutron emission, electron and ion temperatures, and electron density particularly with RF additional heating (as shown in fig.2). These internal disruptions limit the peak ion and electron temperatures, and restrict the highest global energy confinement times. The electron temperature shows sawteeth in all regimes, with enhanced values of amplitude and period in additional heating situations. The deposition of additional power has the effect mainly of increasing the T_e amplitude of the sawteeth inside the inversion radius (q = 1) leaving the profile outside this radius largely unaffected. Fig.3 shows the electron temperature at the q = 1 surface is almost independent of the total power input per particle. However, inside the q = 1 surface, the peak temperature T_e can be raised significantly by the use of additional heating.

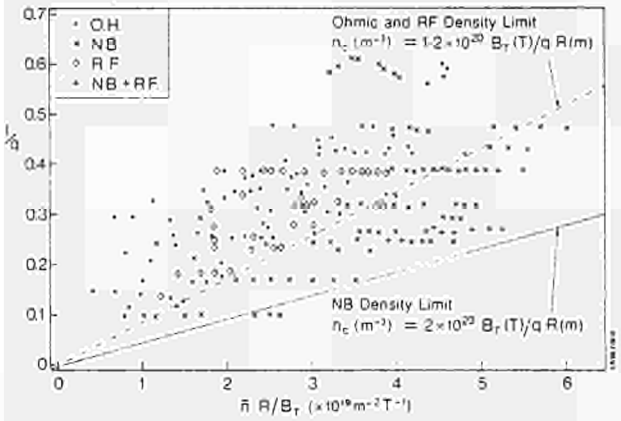

Fig.1: Normalized current [$=(2\pi RI_p/AB)=1/q$] versus normalized density [$=nR/B$];

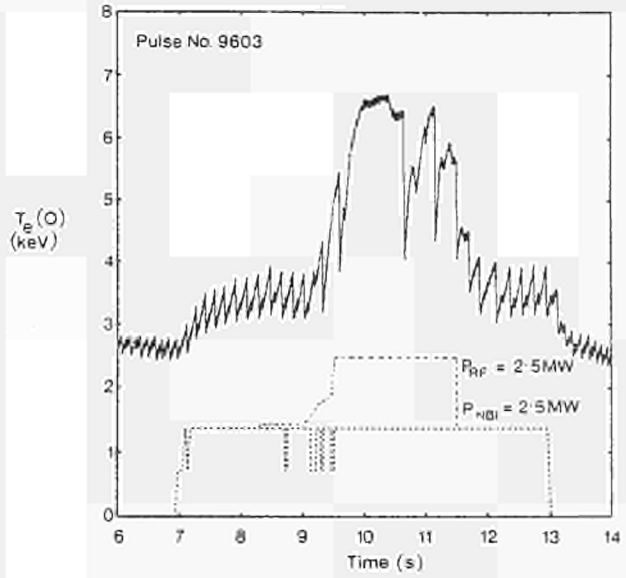

Fig.2: Sawtooth oscillations of the central electron temperature, showing the effects of NB and RF additional heating;

A theoretical model has been developed to explain these plasma phenomena [3]. In this model, three types of magnetic field topology can coexist across the plasma: (i) a central region with nested toroidal magnetic surfaces (q < 1, q[= 0); (ii) a transition region of magnetic islands centred on rational q values, and (iii) an outer region where the field lines show chaotic (ergodic) behaviour. In tokamaks, q increases from a value close to 1 at the centre to ~ 3-5 at the boundary. In the outer region (higher q values) the magnetic islands begin to overlay radially. Here energetic electrons can connect high and

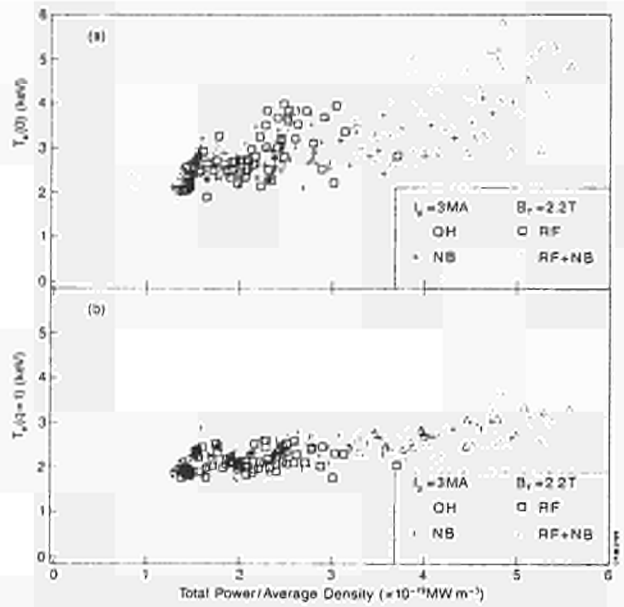

Fig.3: The electron temperature at (a) the centre and (b) the inversion radius (q = 1) as a function of the power input per particle, for ohmic, RF, NB and combined heating cases (I_p = 3MA; B_T = 2.2T);

low temperature regions by flowing along the magnetic field lines. The resulting electron heat transport is substantially larger than classical collisional radial diffusion and decreases the radial electron temperature gradient which can be achieved for a given input power, and consequently reduces the efficiency of any heating process.

This theory leads to a 'critical electron temperature gradient' directly linked to the degree of the magnetic field line chaos. Any additional power enlarges the volume of the chaotic zone, which limits the increase of the electron temperature gradient. A saturation phenomenon exists, when the resonance condition between the pitch of a perturbation and the pitch of the field line is destroyed by the chaocity itself. Then, the temperature gradient can increase again at the expense of a highly degraded thermal insulation. This phenomenon is predicted to be dominant when the radial q gradient (q′) is significant.

When q′ is small, only large islands are predicted to exist around rational q values and chaotic regions do not appear. This should occur inside the q ~ 1 surface (the inversion radius). The almost linear increase of the electron temperature in the central region during the growth of a sawtooth indicates a mean adiabatic heating and a much better confinement of energy than in the outer regions. The sudden and fast relaxation is probably caused by the rigid body-like motion of the central part of the discharge through the region developing around the q = 1 surface, as described by Wesson [4].

Among possible remedies being considered is current profile control using a contribution of Lower Hybrid Resonance and NB heating to maintain a flat current profile configuration (q ~ 1, q′ = 0) in the central region, which is stable to the relevant MHD instabilities, or which will prolong the sawtooth period significantly.

(iii) Impurities: Impurities present problems, as they cause; a reduction in effective plasma ions available for productive fusion interactions; power losses by radiation; and a reduction of the density limit at which major disruptions occur. Experiments with increased carbon tile protection plates on the inboard walls of the vessel, combined with carbonisation of the vessel, have shown decreased metal impurities and lower Z_{eff} values. This showed improved plasma performance with only low-Z material facing the plasma (including the limiters and most of the vessel walls). Only two materials are practicable with high temperature plasmas: carbon and beryllium.

Recently, eight graphite limiters have been used in JET. However, to cope with the additional wall loading which increased additional heating power, two toroidal belt limiters (to be covered by graphite and later with beryllium tiles) will be installed in early 1987 to replace the existing limiters.

(iv) Confinement Degradation: With additional heating, the confinement time, τ_E the so, degrades with increased power, as shown in fig.4, and has been confirmed in a number of experiments, including JET. It is seen that this degradation is independent of type of heating, whether RF, NB or combined. This degradation is also demonstrated in fig.5, which shows the evolution of the plasma energy content W_k versus the total power P_t into the plasma for both, RF and NB heating cases ($W_k/P_t = \tau_E$). The rate of the increase in W_k with P_t ($= \Delta W_k/\Delta P_t$) seems to reach a limit at high powers of 0.2 – 0.3 MJ/MW (= s), suggesting a limiting global confinement time, τ_E, of 0.2-0.3 s at these currents, independent of type of additional heating, which is consistent with fig.4.

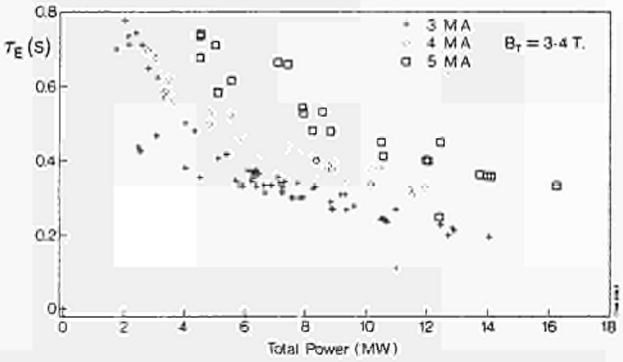

Fig.4: The energy confinement time as a function of additional heating power (at I_p = 3 MA, 4 MA and 5 MA, and B_T = 3.4 T);

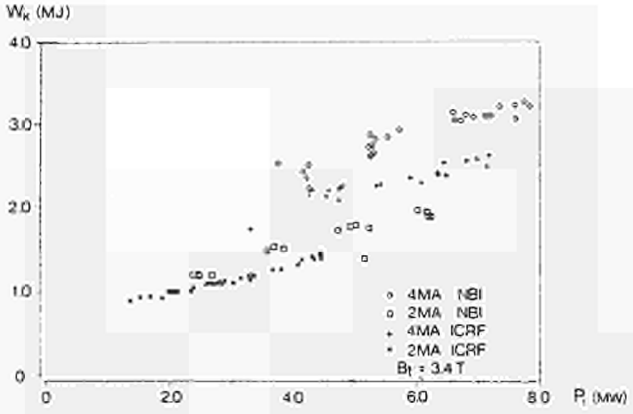

Fig.5: Plasma energy content W_k versus the total input power P_i, with NBI or ICRF heating (I_p=2 and 4MA; B_T=3.4T);

Since the plasma energy W_k is a function of n_i, T_e and T_i, the degradation in confinement time ($\tau_E = W_k/P_i$) can be seen as an inability of the energy W_k, to rise linearly with power input, P_i. This in turn is consistent with the observation that the electron temperature, T_e, outside the inversion radius (q = 1 surface) does not increase with power input and the central temperature (T (0)) increase is less than linear (see fig.3).

However, a better confinement regime with additionally heated plasmas has been observed (the so-called H-mode) in some Tokamaks with magnetic limiters or divertors, which manifests itself with a pedestal in electron temperature, T_e, to raise the whole temperature profile. In the H-mode, τ_E can be typically 2-3 times better. JET experiments have demonstrated a magnetic separatrix mode of operation and have studied technical questions related to stability and vessel heat loadings. The configuration was maintained stable for several seconds and interaction with the limiters curtailed. Improved confinement was seen although true H-mode operation was not achieved. It is believed JET can operate for several seconds at 4MA currents without major modifications.

Confinement with additional heating has been studied on JET with RF heating up to 7MW, neutral beam injection up to 9MW, and combined heating for a total additional heating power up to 14MW ($P_{add}/P_{oh} \sim 8$), corresponding to an increase in power per particle of $\times 4$ with respect to the ohmic heating cases. Confinement time degradation has been observed which is independent of the heating scheme. In fig.4, the plasma confinement time is shown as a function of the total input power. A weak dependence of the confinement degradation is found on the plasma density (or Z_{eff}), while the decay rate appears to scale favourably with plasma current. Work is underway to improve the inductive drive capacity to increase the plasma current towards 7MA, which should also provide decreased degradation (or improved plasma confinement).

4. THE JET STRATEGY

The proposed strategy for JET can be summarised as 'Optimization of the fusion product $<\hat{n}_i\hat{T}_i\tau_E>$. τ_E should be kept near to present values and $\hat{n}$ and $\hat{T}_i$ increased so that D-T operation would provide α-particle production large enough to analyse its effects on the plasma. In illustration of what should be an optimisation of $<\hat{n}_i\tau_E\hat{T}_i>$, fig.6 shows the radial dependence of n, T_e and q measured in JET during a discharge at 3.4MA/1.7T, simulating a future 7MA/3.4T pulse at low q.

JET with its additional equipment aims to build up a high density and high temperature plasma in the discharge centre, where α-particle power could be observed. Fig.7 shows the profile types which could be achieved using the proposed systems on JET. Time windows where NBI and LHCD are switched off will be implemented to allow high speed pellets to penetrate the q ~ 1 volume. Such a plasma would have an energy content of 20MJ and would produce 10MW of α-power. If $\tau \sim 0.3 - 0.4$s,

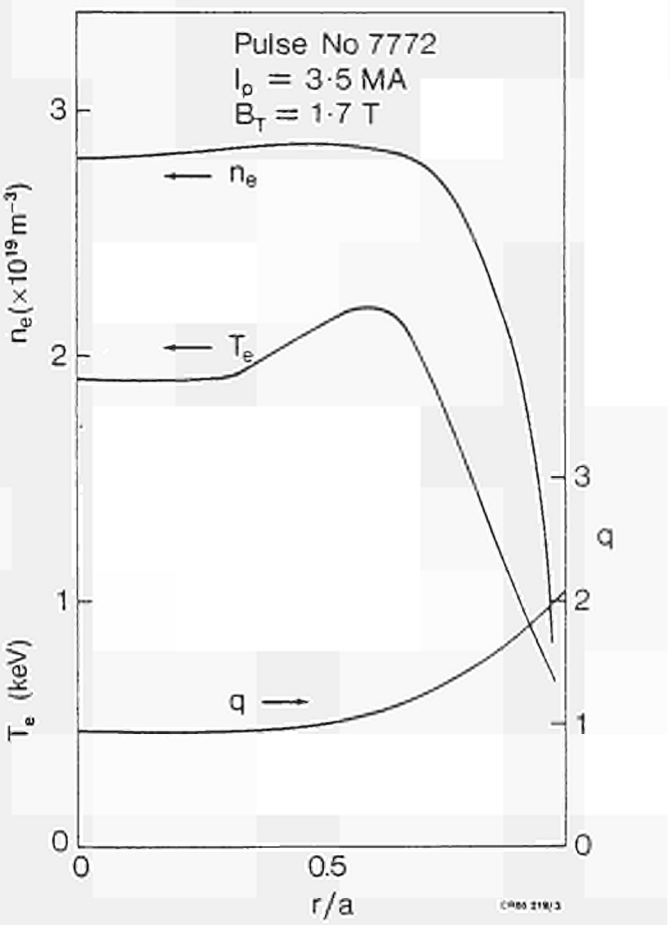

Fig.6: Density (n), electron temperature (T_e) and safety factor (q) profiles in a low q pulse (I_p=3.5MA; B_T=1.7T);

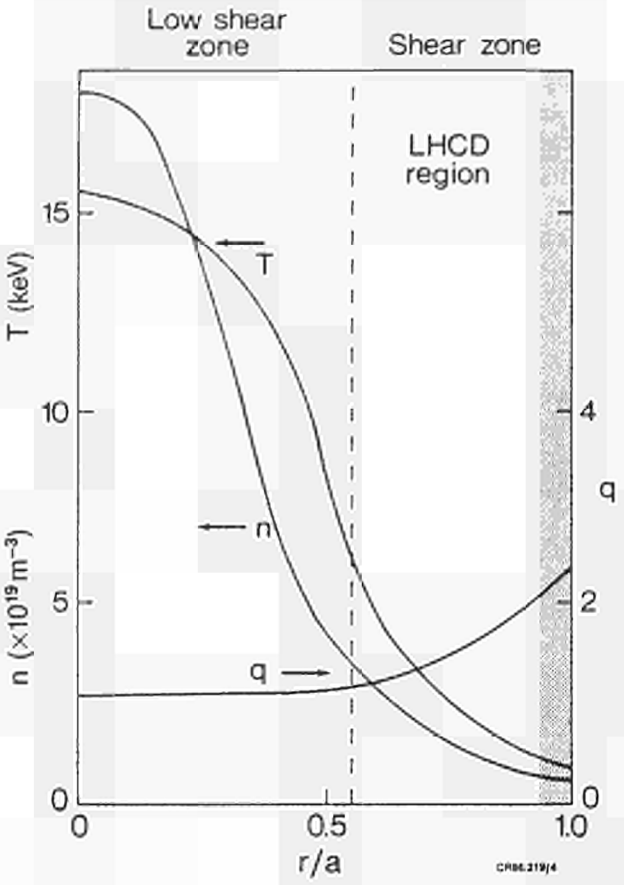

Fig.7: Density (n), temperature (T) and safety factor (q) profiles aimed for within the latest JET strategy. The shaded area represents the zone q=2;

Q_{DT} should reach 1 ~ 2. The role of proposed JET additions to achieve such a discharge is as follows

(i) Sawteeth oscillations should be absent or have periods of several confinement times as a consequence of a flat q profile ($q \approx 1$, $q' = 0$) over a large plasma section by working with a low q boundary and by driving part of the current (~ 1 – 2MA) in the outer plasma (the shear region) by Lower Hybrid Current Drive (LHCD) and with counter NBI near the centre to flatten the profile;

(ii) Radiation cooling between the q = 2 surface and the plasma boundary would be minimised to allow operation below the major disruption limit. Low Z material (C or Be) would be used to take advantage of its low ionization potential;

(iii) Since the temperature at q = 1 is higher when the density is lower, this would be kept low using edge pumping. The aim is to achieve temperatures ~ 7keV and densities ~ $2\text{-}5 \times 10^{19} m^{-3}$ at the transition with the central region. Further advantages of low densities in the outer region are the prevention of disruptions and higher efficiency for LHCD;

(iv) The D-T density on axis is increased up to $1 - 2 \times 10^{20} m^{-3}$ by high velocity pellet injection;

(v) High central temperature (~ 12 – 15keV) would be achieved by the combination of 'on axis' ICRF heating, NBI at 160keV and current profile control.

This scheme will be attempted in two configurations: (a) with a magnetic separatrix at 4MA and (b) with material limiters at current values up to 7MA (a value where the α – particles can be confined inside the central volume (q ~ 1)).

However, in this strategy, it is assumed that: (i) higher central temperatures can be achieved at low q; (ii) the scheme is based mainly on experimental observation without a full understanding of sawteeth mechanisms; and (iii) there is no β limitation in the central region of the plasma.

5. JET DEVELOPMENTS AND THE JET PROGRAMME

In order to meet the JET strategy, enhancements of the electromagnetic system are underway with two main goals: (i) to increase the flux swing capability of the ohmic heating system, beyond the 34V.s design value to provide 7MA plasma current with a ~ 10s flat-top time; (ii) to produce single and double null magnetic limiter discharges up to ~ 4MA plasma current. Both should permit improved confinement in JET.

To improve the central density well above present values, multipellet injection will be incorporated, using a staged approach. A single pellet injector able to launch pellets of 2.6 to 4.6mm diameter at speeds of 1.2-1.5km/s has been installed. During the 1986/87 shutdown, a multipellet injector will be installed capable of 2.6, 4 and 6mm diameter (same length) pellets at speeds of 1.5km/s with repetition rates of 10, 8 or $6 s^{-1}$ (for respective diameters). A development programme is underway to increase pellet speeds towards 10km/s. A single shot pellet injector with speeds 2-5km/s is planned for installation during 1988, whereas a multipellet injector with speeds 5-10km/s should be fitted during the 1989 shutdown.

An increased central density should be obtained without increasing the edge density. Therefore, a particle exhaust system is required to control the edge density during pulses with additional heating and pellet injection. Moreover, controlled pulse termination should be achieved by reducing the density to ohmic levels at the end of additional heating. A development programme has started, both of a pump limiter system and of pumping panels. Two steps are planned for the pump limiter. Firstly, a prototype will be installed in the 1988 shutdown: with a limiter blade movable radially by ~ 20-30mm at a power loading ~ $10 MW/m^2$ for 1-2s. At a density of $10^{20} m^{-3}$, the decay time should be ~ 4s. Secondly, the actively cooled pump limiter should withstand ~ $30 MW/m^2$ for 10s, with installation during the 1989 shutdown.

Pumping panels are being investigated as a consequence of the large pumping effect of the carbon walls observed on JET. Present estimates suggest $50 m^2$ radiation cooled pumping panels would be required. Installation is foreseen during the 1988 shutdown.

Control of current density profile should remove the strong correlation between the current density and the electron temperature caused by Ohmic heating ($J \propto T^{3/2}$). A flat current profile should avoid sawteeth and produce higher central electron temperatures. ICRH as a technique for current drive will be tested in JET after the 1986/87 shutdown using phase locked operation of the planned eight A_1 RF antennae. 10MW LHCD power at 3.7GHz should drive 1-2MA current in the outer plasma region. Broadening of the current profile in JET would be achieved by using, the two already available NB injectors (~0.5MA capability) in counter injection to reduce the current density in the central region.

The proposed JET programme of operations and shutdowns for introduction of new equipment and modifications is shown in fig.8. The addition of the new developments appear in Phases III and IV as follows.

5.1 Phase IIA (mid 1988 – Early 1990)

For this phase, the following will be installed: (i) prototype single shot high speed pellet injector; (ii) conversion of one NB injector to 160keV; (iii) prototype uncooled pump limiter or pumping panels; (iv) water–cooled dump plates for X–point operation; (v) sawteeth control system; (vi) disruption control system (internal saddle coils controlled by feedback).

The main aims will be to consolidate machine opeation with full additional heating power and to explore X–point operation for improving confinement.

5.2 Phase IIIB (Early 1990 - Late 1991)

For this phase, the following will be operational: (i) multiple pellet injector system (~5-10km/s injection); (ii) final LHCD profile control system; (iii)cooled pump limiters; (iv) both NB injectors at 160keV; (v) all remote handling systems required for the active phase. (The commissioning of the tritium plant will also start during this phase).

The main aim will be to reach maximum performance with deuterium plasmas before proceeding to the final phase, requiring introduction of tritium.

5.3 Phase IV (Late 1991 - End 1992)

The aim is to study α-particle production and heating. A level of α-particle power must be reached sufficient to analyse its effects on the plasma, and to answer the question whether α-particle heating degrades energy confinement similar to the other additional heating methods. Although, a positive answer is expected, it has direct consequences on the size of the next experimental device (Next Step).

The starting date for D-T operations is linked to the performance reached in Phase III: the performance in deuterium should have been optimised and the first three objectives of JET must have been achieved; and there should be a high degree of confidence in obtaining a measurable α-particle heating power relative to the other inputs (ie, $Q_{DT} > 0.5$);

6. IMPLICATIONS FOR A REACTOR

Tokamak research is progressing speedily, especially in the new generation of larger Tokamaks where the size and the associated longer characteristic times allow a better identification of the mechanisms prevailing in the plasma. Without doubt, the results obtained on JET and the understanding of the plasma behaviour are likely to play

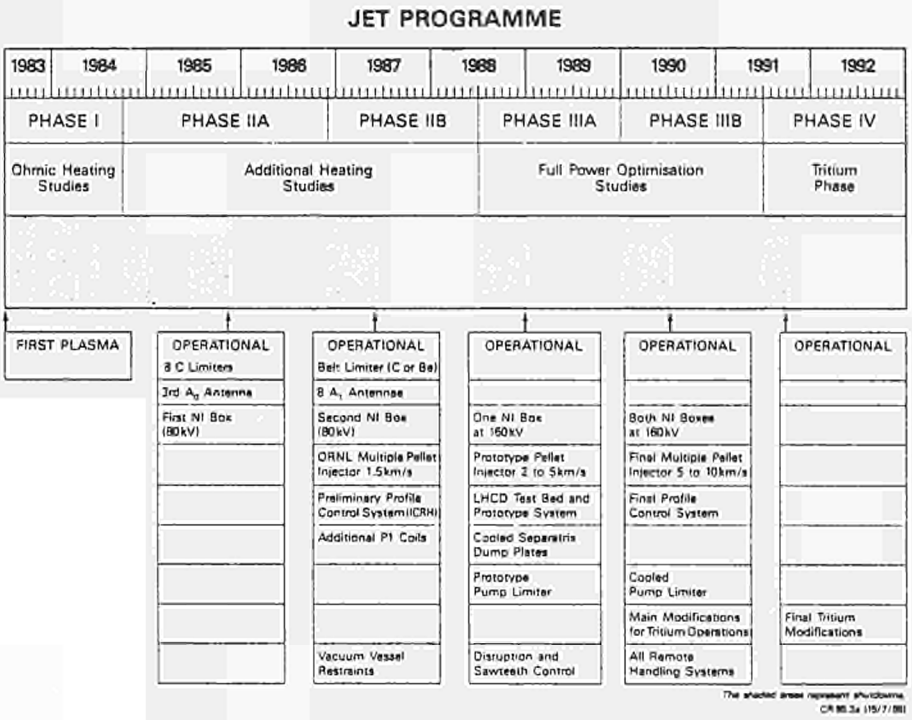

Fig.8 Proposed JET Programme.

an increasing role in the definition of a future reactor.

The magnetic field of the larger tokamaks is already operated in the range of 2-5T, which is appropriate to a reactor. Whilst not yet simultaneously achieved, the values of maximum density and temperature presently observed are not far from those required, and the confinement time obtained with ohmic heating alone is already significant. The extrapolation required now mainly concerns the size of the future device. Fig.3 shows that additional heating hardly increases the temperature in the large confinement volume outside the $q=1$ surface ($q>1$), and only achieves some heating in the smaller volume inside this surface. This suggests that a reactor must rely upon either a tight control of current profile and large power additional heating to provide sufficient stabilization of sawteeth oscillations, intense heating inside the $q=1$ surface and improved energy confinement (as proposed for JET), or it must depend upon a size increase to obtain the required ignition temperature.

Large increases of the electron temperature have been observed with increased plasma size, in agreement with the qualitative prediction based on magnetic topology, which suggests that it is possible to conceive a D-T burner Tokamak without external additional heating. The resulting simplification of the overall system could well compensate for the larger size. Scaling suggests that a major radius of $\sim$x2.5 that of JET, a plasma volume of $\sim 2000 m^3$ and a magnetic field slightly higher than JET, a 15keV plasma and a confinement time of 15-25s could be reached without ohmic heating at a density only 0.3-0.5 that in JET but still satisfying the ignition criterion. Then, the thermonuclear power output of the D-T burner should be increased by injecting fuel pellets: the thermal insulation should degrade as the additional heating provided by the α-particles increases, keeping the temperature approximately constant and the burn control would be performed entirely through density control. This stresses the importance of mastering the disruptive density limit.

7. CONCLUSIONS

(i) Both ICRF and neutral beam (NB) additional heating methods are effective in JET at injecting and localizing power deposition in the plasma ($>70\%$ power accounted for in the plasma).

(ii) Both methods demonstrate increased plasma energy, W, with increasing power input, P, but the rate of increase of energy with power input (dW/dP) ($\sim$0.1-0.3s) is much smaller than the confinement time, τ_E (confinement time degradation with additional heating).

(iii) It is only in the central region (inside the inversion radius), between sawtooth collapses that the heating is effective in increasing the electron temperature of the plasma (cf giant and monster sawteeth).

(iv) Outside the region, electron heating is poor. The electrons seem to be the main energy loss channel, which appears related to confinement properties and not to the heating process. (In particular, this could be related to the shear properties of the tokamak and the presence of chaotic (ergodic) lines of force).

(v) α-particle heating is expected to behave in a similar fashion to other heating methods.

(vi) Therefore, a reactor must either (i) work at moderate currents with sophisticated control of the central region; or (ii) work at high currents without the need for control of the central region.

(vii) In the latter case, a temperature of $\sim$7keV at the inversion radius is needed (at which thermonuclear reactions can start in the centre). This could be achieved without additional heating and leads to a reactor of large size and current (dimensions $\sim 2.5\times$JET, $V\sim 2\times10^{19} m^{-3}$, $\tau_E\sim$15-20s, and T $\sim$ 15 keV at the start. Additional heating would be from thermonuclear α-particles and would allow the density to be increased into the $10^{20} m^{-3}$ range, at the cost of a degraded τ_E. Further work is needed to clarify final requirements.

REFERENCES

[1] HUGUET, M. et al, 13th Symposium on Fusion Technology (SOFT), Varese, Italy, 24-28th September 1984. Proceedings Vol.I, pp 91-103

[2] BICKERTON, R.J. et al, Plasma Physics and Controlled Fusion, 28, 55 (1986)

[3] REBUT, P.H., and BRUSATI, M., Plasma Physics and Controlled Fusion, 28, 113, (1986)

[4] WESSON, J.A., Plasma Physics and Controlled Fusion, 28, 243, (1986)

APPENDIX I

The JET Team

A. Ainsworth, H. Altmann, R.J. Anderson, J. Arbez, D. Bartlett, W. Bailey, B. Beaumont[1], K. Behringer, E. Bertolini, P. Bertoldi, C.H. Best, V. Bhatnagar[4], R.J. Bickerton, G. Boissin, F. Bombarda[10], T. Bonicelli, S. Booth, A. Boschi, G. Bosia, M. Botman, G. Bracco[10], H. Brelen, H. Brinkschulte, M.L. Browne, M. Brusati, T. Budd, M. Bures, P. Butcher, H. Buttgereit, D. Cacaut, C. Caldwell-Nichols, D. Campbell, R. Carolan[11], J. Carwardine, G. Celentano, C.D. Challis, A. Cheetham, J. Christiansen, C. Christodoulopoulos, P. Chuilon, R. Claesen, J.P. Coad, M. Cooke, J.G. Cordey, W. Core, S. Corti, A.E. Costley, G. Cottrell, M. Cox[11], J. Dean, E. Deksnis, G.B. Denne, G. Deschamps, K.J. Dietz, J. Dobbing, S.E. Dorling, D.F. Düchs, G. Duesing, P. Duperrex[6], H. Duquenoy, L. de Kock, A. Edwards, J. Ehrenberg[2], W. Engelhardt, S. Erents[11], F. Erhorn, B. Eriksson, M. Evrard[4], H. Falter, N. Foden, M. Forrest[11], C. Froger, K. Fullard, M. Gadeberg[5], A. Galetsas, A. Gallacher, D. Gambier[1], R. Giannella[10], A. Gibson, R.D. Gill, A. Goede, A. Gondhalekar, D. Goodall[11], N.A. Gottardi, C. Gowers, R. Granetz, B. Green, S. Gregoli, F.S. Griph, R. Haange, J.H. Hamnén[3], C.J. Hancock, P. Harbour, N. Hawkes[11], P. Haynes[11], T. Hellsten, J.L. Hemmerich, R. Hemsworth, F. Hendriks, R.F. Herzog,

L. Horton, J. How, M. Huart, A. Hubbard, J. Hugill[11], M. Hugon, M. Huguet, B. Ingram, H. Jäckel[2], J. Jacquinot, O.N. Jarvis, E.M. Jones, T.T.C. Jones, P. Jones, E. Källne, J. Källne, A. Kaye, B.E. Keen, M. Keilhacker, G. Kinahan, S. Kissel[2], A. Konstantellos, U. Küphnapfel[2], P. Kupschus, P. Lallia, J.R. Last, L. Lauro-Taroni, K.D. Lawson[11], E. Lazzaro, R.C. Lobel, P. Lomas, N. Lopes-Cardozo[7], M. Lorenz-Gottardi, C. Lowry, G. Magyar, D. Maisonnier, M. Malacarne, V. Marchese, P. Massmann, G. McCracken[11], P. McCullen, M.J. Mead, P. Meriguet, V. Merlo, S. Mills, P. Millward, A. Moissonnier, P.L. Mondino, D. Moreau[1], P. Morgan, R. Müller[2], G. Murphy, M.F. Nave, L. Nickesson, P. Nielsen, P. Noll, S. Nowak, W. Obert, B. Oliver, M. Olsson, J. O'Rourke, M.G. Pacco, J. Paillere, L. Pannacione, S. Papastergiou, J. Partridge[11], D. Pasini, N. Peacock[11], M. Pescatore, J. Plancoulaine, J-P. Poffé, R. Prentice, T. Raimondi, C. Raymond, P.H. Rebut, J. Removille, W. Riediker, R. Roberts, D. Robinson[11], A. Rolfe, R.T. Ross, G. Sadler, J. Saffert, N. Salmon, F. Sand, A. Santagiustina, R. Saunders, H. Schamel[12], M. Schmid, F.C. Schüller, K. Selin, R. Shaw, D. Sigournay, R. Simonini, P. Smeulders, J. Snipes[11], L. Sonnerup, K. Sonnenberg, A. Stäbler[2], M. Stamp, C.A. Steed, D. Stork, P.E. Stott, T.E. Stringer, D. Summers, H. Summers[13], J. Tagle[9], G. Tallents[14], A. Tanga, A. Taroni, A. Terrington, A. Tesini, P.R. Thomas E. Thompson, K. Thomsen[5], F. Tibone, R. Tivey, T. Todd[11], G. Tonetti[6], P. Trevalion, M. Tschudin, S. Tsuji[15], B. Tubbing[7], P. Twynam, E. Usselmann, H. van der Beken, M. von Hellermann, J.E. van Montfoort, J. von Seggern[8], T. Wade, C. Walker, B.A. Wallander, M. Walravens, K. Walter, M.L. Watkins, M. Watson, D. Webberley, A. Weller[2], J. Wesson, J. Wilks, T. Winkel, C. Woodward, M. Wykes, D. Young, L. Zannelli, J. Zwart

Permanent Address

[1] Commissiariat A L'Energie Atomique, F-92260 Fontenay-Aux-Roses, France.

[2] Max Planck Instituut Für Plasmaphysik, D-8046 Garching bei Munchen, F.R.G.

[3] Swedish Energy Research Commission, S-10072 Stockholm, Sweden.

[4] EUR-EB Association, LPP-ERM/KMS, B-1040 Brussels, Belgium.

[5] Risö National Laboratory, DK-4000 Roskilde, Denmark.

[6] CRPP/EPFL, 21 Avenue des Bains, CH-1007 Lausanne, Switzerland.

[7] FOM Instituut voor Plasmafysica, 3430 Be Nieuwegein, The Netherlands.

[8] Kernforschungsanlage Jülich GmbH, D-5170 Jülich, F.R.G.

[9] Junta de Energia Nuclear, Avda. Complutense, Madrid 3, Spain.

[10] ENEA-CENTRO Di Frascati, I-00044 Frascati, Roma, Italy.

[11] Culham Laboratory, Abingdon, Oxfordshire, U.K.

[12] Ruhr-Universitaat Bochum, D-4630 Bochum, F.R.G.

[13] University of Strathclyde, 107 Rottenrow, Glasgow, G4 0NG, UK.

[14] The Australian National University, Research School of Physical Sciences, Canberra ACT 2600, Australia.

[15] Japan Atomic Energy Research Institute, Naka-machi, Naka-gun, Ibaraki-ken, Japan.

TECHNICAL ASPECTS OF THE NEW JET DEVELOPMENT PLAN

M. HUGUET
JET Joint Undertaking, Abingdon, Oxon, OX14 3EA, U.K.

ABSTRACT

Recent results from JET and other large tokamaks point to the need for JET to introduce new modes of operation and additional equipment to enhance performance, and as a result gain the full benefit of deuterium-tritium (D-T) operation. The principal new additions to the JET development plan concern: operation up to plasma currents of 7MA, magnetic limiter operation, disruption control, density control and current profile control.

The new additions to the JET programme entail only minor changes to the basic design of the machine itself. The ohmic heating coil stack will be reconstructed with 10 sub-coils instead of 8 sub-coils. This modification is important for magnetic limiter operation and is also desirable to achieve long flat-tops at plasma currents of 7 MA. For the magnetic limiter mode of operation, dump plates are foreseen inside the vessel in the vicinity of the X-points. The vacuum vessel supports will be reinforced to cope with the transient loads resulting from vertical instabilities.

Disruption control requires new saddle coils inside the vacuum vessel. Density control includes the use of pump limiters, the study of transient wall pumping, and deep fuelling by means of pellet injectors. Current profile control will probably involve a combination of lower hybrid frequency and neutral beam current drive techniques.

At the same time, the machine and all systems will be prepared for D-T operation. The varicus steps of the new JET programme are planned for implementation during major shutdowns scheduled until 1991. D-T operation is now planned to start by the end of 1991.

1. INTRODUCTION

After 3 years of operation, the JET experimental results are most encouraging. The best, but not simultaneous, plasma parameters achieved are $\hat{T}_i$ (peak ion temperature) = 10 keV $\hat{n}_i$ (peak ion density) = 6×10^{19} m^{-3}, τ_E (global energy confinement time) = 0.8s, while the best simultaneous combination gives a fusion product $\hat{T}_i \times \hat{n}_i \times \tau_E = 10 \times 10^{19}$ $keV.m^{-3}.s$.. D.D neutron production rates up to $5 \times 10^{15} s^{-1}$ have been measured. These results are not yet those required for D-T operation. A meaningful D-T phase on JET with significant alpha particle heating would require a fusion production of about 5 to 10×10^{20} $keV.m^{-3}.s$. In order to bridge the gap, a new development programme has been proposed. This programme includes the extension of the current capability in the limiter mode of operation

from 5 to 7 MA, a magnetic limiter (also called X-point) mode of operation with plasma currents up to 4 MA, disruption control, density control and plasma current profile control. The physics motivation of this programme is explained by Rebut [1].

This new development programme represents a considerable extension of the original plan and is justified and made credible by the fact that from the technical point of view, the JET operation has been entirely successful. The plasma current has reached 5.1 MA for 3 s., exceeding the design value of 4.8 MA. Additional heating systems have performed most satisfactorily and up to 14 MW of additional heating (NB + RF) power has been injected.

This paper summarizes the technical aspects of the new JET development plan, with an emphasis on the modifications and additions to the tokamak itself.

2. STUDY OF THE NEW EXTENDED OPERATING CONDITIONS

The new JET development plan includes modes of operation which call for a considerable extension of the original JET design parameters. In particular, it is proposed to operate up to 7 MA in the limiter mode, as compared to the design value of 4.8 MA. This will severely increase the thermo-mechanical stress on the coils, the structural components, the vacuum vessel and first wall. The magnetic limiter, or X point mode of operation was not considered in the original JET programme. This will introduce a new range of operation scenarios together with their associated thermo-mechanical problems.

Clearly, such a major step into new operating territory calls for a detailed and refined reassessment of the machine itself, of some power supplies and of the integrated behaviour of systems, from the electrical, mechanical and thermal point of view. This investigation called the "7 MA and X-point study", has been initiated and Table I shows some of the major items to be included. The outcome of the study will be known during the first half of 1987 and will provide a more accurate definition of the actual and safe boundaries of the new operating space. The figures quoted in this paper, as regards the expected level of performance, are supported by preliminary work and at this stage appear to be realistic targets. However, some changes may occur as a result of on-going work.

TABLE I

Major items of the 7 MA and X point study

Plasma and Pulse Parameters
Field Configuration and Magnetic Forces
Safe Limits
Machine Instrumentation
Mechanical Analysis
Thermal Effects on First Wall
Global Assessment on Machine Behaviour
Power Supplies Electrical, Mechanical, Thermal and Control Scenarious Analysis

3. CHANGES TO THE JET MAGNETS IN VIEW OF 7 MA AND X-POINT OPERATIONS

3.1 The toroidal field magnet

The performance of the toroidal field (TF) magnet will be reviewed with the aim of

increasing both the flat-top duration and field strength. The flat-top duration can be easily increased by chilling the cooling water. A 6 MW chiller plant connected on the site water side of the heat exchanger will cool the water down to 7°C before a pulse and will allow an extension of the flat-top duration from 12.5 to 19 s at full field. The pulse repetition rate will be of one pulse every 20 minutes. The chillers will be operational by the end of 1987.

It is planned to carry out a refined thermo-mechanical analysis of the TF coils with a view to assess their potential for operation at fields above the design value of 3.45 T. Tests may have to be carried out to characterize better the fatigue strength of copper brazed joints and epoxy-glass insulation. The results of such calculations and tests must however be examined cautiously since the behaviour of the actual coils could be impaired by undetected internal defects. For this reason, operation up to 4 T, if possible, will not be attempted before the final phase of the JET operation.

3.2 The primary winding of the poloidal field system

It has not been possible so far to use the full design value (34 V.s.) of the flux swing available from the primary winding. This is because plasma breakdown conditions are impaired by stray magnetic fields which develop when the centre pieces of the magnetic circuit saturate. Computed field mapping has shown that these stray fields can be dramatically reduced by increasing the length of the primary winding coil stack. For this reason, the primary winding will be removed from the machine during the planned 1987 shutdown, and will be rebuilt with 10 sub-coils instead of 8, by making use of existing spare sub-coils. The mechanical work involved is extensive since the upper limbs of the magnetic circuit must be dismantled, together with the services and diagnostics attached to them. The TF magnet is unaffected by this operation, the coils have only to be slightly retracted to permit the removal and reinsertion of the primary winding. Since the primary winding takes up the centripetal forces acting in the TF coils, it is also the structural reference for the whole machine and must be rebuilt to tight tolerances regarding cylindricity and verticality, and co-axiality with the mechanical structure.

3.3 The ohmic heating system

In its present configuration, the 8 sub-coils of the primary winding are all electrically connected in series as shown in fig. 1. It is planned to modulate the current flowing in the six centre sub-coils, with respect to the current flowing in the four top and bottom sub-coils. This requires an additional power supply and busbars as shown in fig. 1. This scheme is extremely versatile and opens up a wide range of new operational space. The following is a summary of the scenarious made possible with this new scheme. Details are given by Bertolini [2].

a) Stray field compensation: Stray field compensation may be further improved by a slight reduction of the current flowing in the 6 centre sub-coils. An optimization of breakdown conditions may save useful flux during the initiation of the discharge.

b) Increase of the flux swing: The current flowing in the 6 centre sub-coils could be raised beyond the design value of 40 kA, taking advantage of restraining external pressure of the TF coils. At 60 kA, the outward pressure due to the

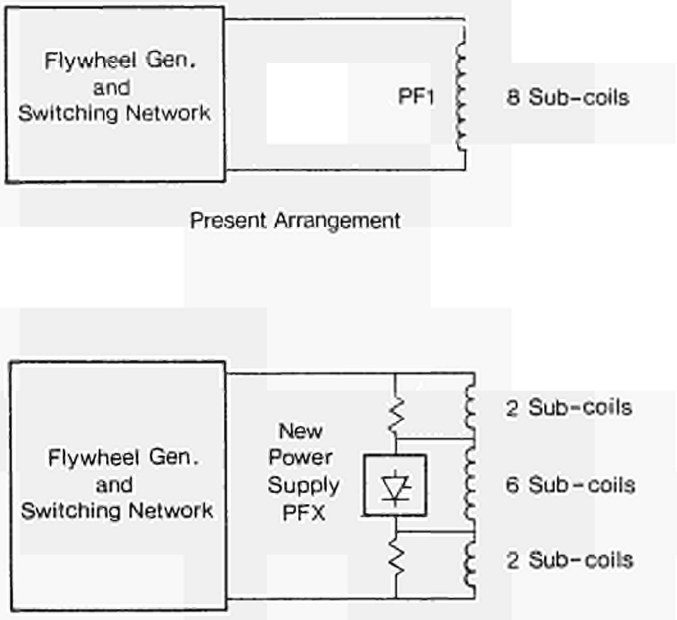

Fig. 1. Present and planned configuration of the ohmic heating circuit

coils own field would balance the inward pressure. A current of 60 kA, if possible, would give a total flux swing of 40 Wb, thus allowing a 10 s flat top at 7 MA in the limiter mode of operation.

A study is underway to evaluate the thermo-mechanical behaviour of the winding and its interaction with the mechanical structure and TF coils, under these new operating conditions.

c) X-point operation: A non uniform distribution of the current in the primary winding (for instance 40 kA in the 6 centre sub-coils and zero current in the upper and lower sub-coils) causes a large stray radial flux in the top and bottom areas of the plasma and promotes the formation of X-points inside the vacuum vessel. Calculations show that a double null configuration can be obtained up to 4 MA with X-points between 10 and 25 cm inside the vessel. This is a considerable improvement with respect to the present configuration which allows only a plasma current of 2.5 MA and a X point to wall distance of about 5 cm. Single null configurations can also be obtained by unbalancing the current in the top and bottom coils of the shaping circuit. In this case plasma currents up 4.5 MA and X-point to wall distances of 20 cm seem achievable.

4. MECHANICAL PROBLEMS

4.1 Twisting moments

The new modes of operation result in higher values and new distributions of the azimuthal forces acting on the TF coils. These forces are resisted by the mechanical structure. The behaviour of the structure will be checked by means of a comprehensive finite element model including the TF coils located inside the structure. It is expected that the structure is globally strong and stiff enough for the new modes of operation, but certain highly loaded areas have to be checked carefully.

The most critical areas, where the high level of stress is likely to set a limit to the machine performance, are the upper and lower portions of the D-shaped TF coils which are supported by the so-called collar teeth. There is no scope for any improvement of the design because of the lack of space in this area and the inaccessibility of the collar teeth. The critical stress is a shear stress in the TF coils insulation, which results from a combination of pure shear, torsion and bending.

A maximum allowable load of 45 tonnes on each tooth, gives a shear stress of 16 MPa and corresponds to the following operational limits.

a) In the limiter mode at 7 MA, the elongation b/a must be less than 1.5.

b) In the X-point mode, the current must not exceed 4 - 4.5 MA.

Full scale fatigue tests, using the prototype TF coil are planned to assess better this critical point.

4.2 Vertical supports for the vacuum vessel

The original flexible supports of the vacuum vessel were not designed to cope with the unexpectedly large vertical forces resulting from vertical instabilities [3]. By the end of 1984, the vessel was fitted with simple mechanical reinforcements able to resist vertical forces up to 350 tonnes. Under these conditions, the operational space is restricted in plasma current I_p and elongation $(\frac{b}{a})$ according to the following relationship:

$$I_p^2(\frac{b}{a} - 1.2) < 5\ MA^2$$

New vessel supports have now been designed and will be installed during the 1987 shut-down (fig. 2). These supports are designed to resist vertical forces up to 1600 tonnes. This specification exceeds the expected level since such a force would develop in the event of a vertical instability at a current of 7 MA and an elongation of 1.7 (limit value is 1.5). The new supports involve some modifications of the vessel itself, in particular the flanges at the vertical ports are used as anchoring points and have to be replaced by rigid forged pieces. Diagnostics attached to these ports must be modified to be made compatible with the new design.

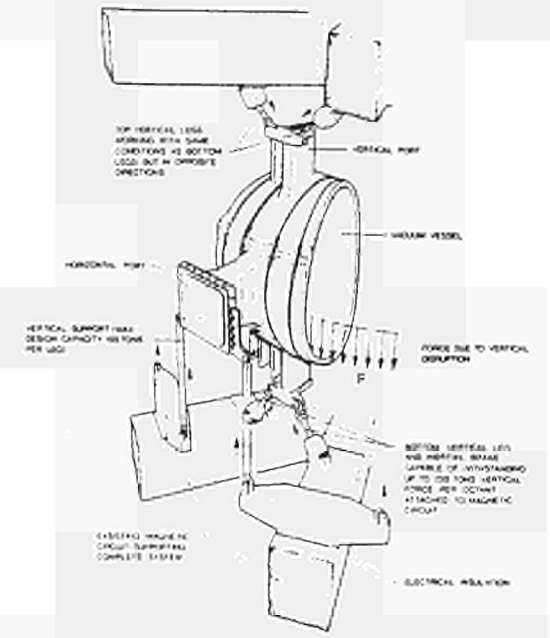

Fig. 2. Additional supports of the vacuum vessel (only one octant shown on the picture)

During vertical instabilities, the poloidal field coils are also subjected to vertical forces. Preliminary calculations show that these forces are within tolerable limits except in the case of the large outer coils P-4. The supports of these coils will be strengthened during the 1987 shut-down.

5. NEW FIRST WALL COMPONENTS

5.1 Present status of wall protection and limiters

The areas covered by graphite tiles include the inboard wall over a height of 2 m, 8 belts in the poloidal direction at the octant joints, and a zone at the outboard wall (Octant 5) acting as a protection against neutral beam shine-through. The total area covered is 40 m^2 or 20% of the inner surface of the vessel.

JET presently uses 8 discrete graphite limiters (area 3m^2) placed at the outboard

wall in the equatorial plane. The 3 RF antennae are also protected by graphite (area $6m^2$) and absorb some of the power conducted to the wall. Due to the fact that part of the power is radiated, it has been possible to cope with up to 16 MW of total power with the present limiter arrangement.

5.2 Planned development in 1987

Early in 1987, the bellows protection plates presently made of inconel will be replaced by graphite tiles. This will add 32 graphite belts to the existing 8. Neutral beam shine-through protection will also be added at Octant 1, in readiness for the start of operation of the second neutral beam system. The total area covered with graphite will be 100 m^2 or 50% of the inner surface.

The 8 discrete limiters will be replaced by the belt limiter which consists of 2 belts in the toroidal direction with a total area facing the plasma of approximately $15m^2$ [4]. This limiter will be able to absorb 40 MW during a 10 s pulse and is therefore adequate for operation at 7 MA and full additional heating power, including the expected alpha particle heating during the D-T phase. The existing RF antennae will be replaced by 8 new antennae with their associated side protections.

The JET aim is to use a low-Z and unique material for the wall protection and limiter. The two candidate materials are graphite and beryllium and JET will be ready to install either of these materials by the end of 1986. The expected advantages and drawbacks of these materials have already been discussed [5].

If graphite is used, the belt limiter will utilize solid graphite tiles. The vessel walls and antennae screens which are not covered with graphite tiles will be carbonized so as to offer a 100% graphite-carbon wall to the plasma.

If beryllium is used, the belt limiter will utilize solid beryllium tiles. The rest of the first wall, including metal parts and graphite tiles, will be coated with a thin layer of beryllium by means of four internal beryllium evaporators [6].

5.3 Dump plates for X point operation

The vessel requires additional protection, or dump plates, to absorb the power conducted and radiated to the wall in the vicinity of the X-points. In 1987 and early 1988, this function will be performed by the existing and planned (see above) graphite protection. This will impose some restrictions on power and pulse duration since the energy which can be safely absorbed in these tiles during a pulse is about 80MJ. In addition, the pulse repetition rate will be limited by the radiative cool-down time (1 hour) of the tiles.

In 1988, the top and bottom parts of the vessel will be completely covered with tiles (graphite or beryllium) mounted on a water cooled support structure. These dump plates will be able to receive a power of 40 MW for 10 s in the double null configuration, and will sustain a pulse repetition rate of one pulse every 10 minutes (fig. 3). A full description is given by Sonnenberg [6].

6. CONTROL OF DISRUPTIONS

The motivation for attempting to control disruptions on JET is to increase the overall performance by extending the limits for stable operation to lower values of the safety

factor q and higher plasma densities. Moreover, even if significant extension of the operating range is not achieved, the possibility of disruption free termination of discharges would be most desirable. It would allow operation of the machine without restriction at maximum current, high densities, and maximum heating power. Since switching off the heating power could be performed safely and quickly, this would also extend the useful flat-top duration.

Disruptions are characterized by unambiguous precursor magnetic activity some hundreds of milliseconds before the disruption, and thus feedback control seems to be feasible in principle. Since the magnetic activity appears essentially to be an m = 2, n = 1 mode, the scheme for stabilizing this is to provide a magnetic perturbation modulated by feedback control to counter the m = 2 mode perturbation.

The magnetic perturbation would be provided by a set of internal saddle coils. The optimum locations for these coils are the top (4 coils) and bottom (4 coils) parts of the vessel (fig. 3). These coils would carry a current of 5-10 kA and with 3 turns would create a magnetic perturbation of the order of 5-10 x 10^{-4} T. The radiation cooled conductor would consist of copper and inconel bars welded together for low resistivity and strength, and would be insulated and supported by alumina pads. Care must be taken in the design to provide strong supports able to sustain the large electromagnetic forces and vibrations due to the AC supply, and at the same time allow differential expansion between the coils and the vessel walls. A problem in the design, is that image eddy currents flowing in the vessel walls reduce dramatically the efficiency of the coils, and therefore a distance of approximately 15 cm is required between the coils and walls. The plasma aperture for limiter ($\frac{b}{a}$ = 1.6) or X-point configurations is however not significantly affected by the coils.

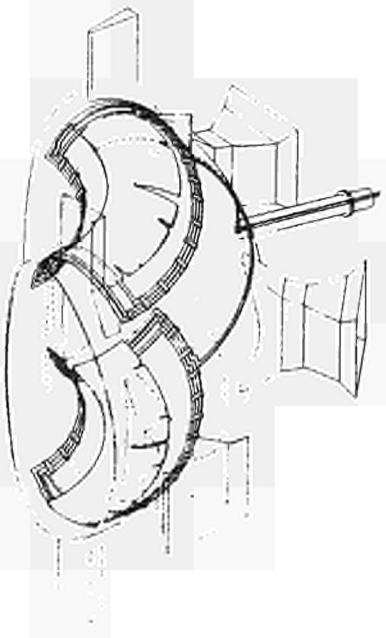

Fig. 3. Internal saddle coils for disruption control (only 2 octants are shown on the picture). Dump plates for X-point operation are also shown.

Graphite tiles will of course be required to protect the coils. The profile of the existing and planned wall protection tiles will have to be modified so that it blends smoothly with the coil protection. This work is planned in 1988 when the coils are installed.

Provisional estimates of the power requirements for these coils are 6 MW. The error signal for the feedback loop would be derived from the existing magnetic diagnostics.

7. DENSITY CONTROL

Density control aims at increasing the central density by deep pellet (and neutral beams) fuelling, and keeping the edge density low by pumping. The detailed plans are given in [6].

7.1 Pellet injection

A single shot injector able to launch pellets of 2.6, 3.6, 4.6 mm diameter at speeds of 1.5 km/s has been operational on JET since June 1986. By the middle of 1987, a multi pellet injector supplied by the Oak Ridge National Laboratory, U.S.A. will be able to fire 2.6, 4 and 6 mm diameter pellets at a repetition rate of respectively 5, 3, 2 Hz and speeds in the range of 1.5 km/s.

A development programme has been undertaken to increase the pellet speeds towards 5 and even 10 km/s to achieve deeper penetration inside the JET plasmas. In principle, these high velocities can be achieved by pneumatic guns if hot propellant gas is used. Heating of the propellant gas by adiabatic compression and electric arc is being investigated. A prototype single shot, high speed (5 km/s) injector should be available by mid-1988.

7.2 Pumping

Particle exhaust on JET has been achieved so far by a very effective wall pumping effect (up to 3×10^{21} particles.s^{-1}), although not understood. Simulation experiments have been undertaken in an attempt to understand the phenomenon and assess its potential for the future JET operation. In particular, saturation effects at high wall fluxes have to be evaluated. These experiments are being conducted for both graphite and beryllium.

JET is also planning to develop pump limiters in case wall pumping should prove insufficient. A prototype radiation cooled pump limiter, using carbon fibre reinforced graphite for the high heat flux components, could be installed in the machine by the end of 1988. Actively cooled pump limiters will take longer to develop and their possible use in JET cannot be envisaged before 1990.

8. CURRENT PROFILE CONTROL

The aim of current control is to achieve a flatter current profile. Such a current profile could keep the safety factor q above 1 everywhere in the plasma, thus avoiding sawteeth and achieving higher electron temperatures. Current profile control can also reduce the correlation between the current density and electron temperature ($J \propto T_e^{3/2}$) and this may lead to improved confinement.

The JET proposal is to use lower hybrid current drive. A 10 MW system at 3.7 GHz would be able to drive 1-2 MA in the outer regions of the plasma. The broadening of the current profile may be further enhanced by counter neutral beam current drive in the central region of the plasma. Details are given by Jacquinot [7].

9. MODIFICATIONS IN VIEW OF THE D-T PHASE

In addition to the development work in the areas of tritium and remote handling [8], some modifications will be necessary to make the machine and associated systems ready for tritium operation. However, these modifications are expected to be few, because, since the conceptual phase of JET, the requirements of the D-T phase have been the guiding factor in the definition process and detailed design of the machine and all associated facilities [9]. Nevertheless, it is planned to undertake in the near future, a major critical review of all systems, modes of operation and failure modes to check their compatibility with the use

of tritium. Necessary changes will be implemented during the 1988, 1990, and 1991 shut-downs. A few examples of modifications which have already been identified are listed below:

- Tritium permeation through the vessel walls may be driven by pressure or by particles fluxes. In order to eliminate the contribution from particle fluxes, it has been decided that the wall areas not covered with graphite would be clad with inconel plates.
- The small turbo-molecular pumps, used in large numbers for diagnostics vacuum systems will be replaced by static, fully sealed, regenerable getter pumps.
- The gas baking loop circulates a hot gas in the interspace between the two walls of the vacuum vessel. Helium will be used rather than nitrogen as a heat transport gas since helium is not activated by neutrons and can be decontaminated from tritium. The helium blower will be fully encapsulated to contain tritium emissions originating from the shaft seal.

10. TIME PLAN

Table II shows the new development programme which is 2½ years longer than the original JET plan. It must be pointed out that this plan should be considered as provisional since the necessary steps to seek approval from the JET supervisory bodies have been started recently. Four major shut-downs are planned before the start of the D-T phase, to implement the additions to the programme and make systems ready for tritium.

TABLE II

The new JET development plan

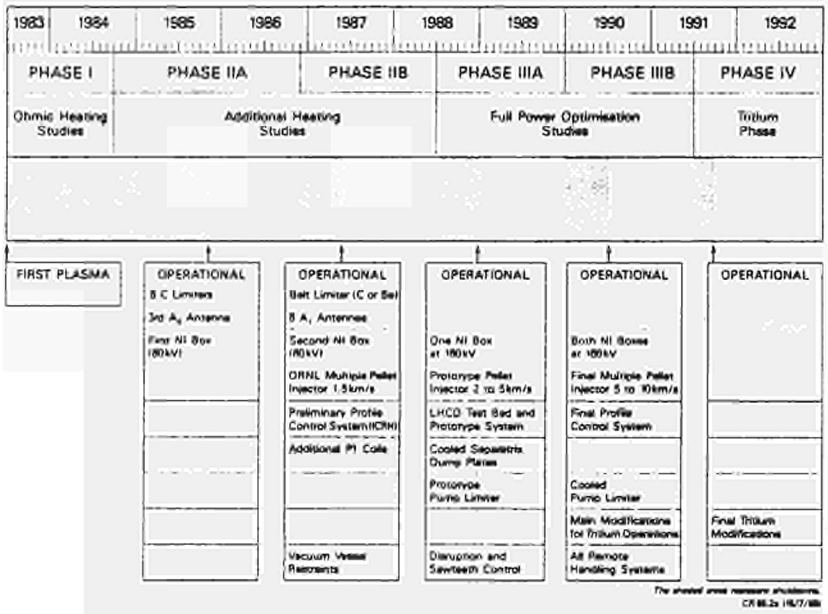

11. CONCLUSIONS

The major objective of the JET experiment is to use deuterium-tritium (D-T) fuel to study the confinement and heating effect of alpha particles produced by fusion reactions. The new JET development plan aims at an enhancement of the plasma physics performance so that a meaningful D-T phase with significant alpha particle heating can be achieved.

Although ambitious, the new development plan is technically justified by the results

obtained so far. The sound technical performance of the machine and the good overall reliability of the various sub-systems provide great confidence that the operational parameters can be stretched above the rated design values. New modes of operation can also be easily incorporated because of the inherent flexibility and versatility of the JET design which allows new equipment to be added without affecting the basic structure of the machine and the organization of sub-systems.

Therefore, the new development plan appears modest, in view of the existing investment, but a most valuable extension of the original programme, with the aim of making full use of the potential performance of the machine. It must be stressed that the JET objective of a sustained D-T operation phase of at least one year, is unique on the world scene of tokamak research, and will provide an essential and irreplaceable data base for NET.

ACKNOWLEDGEMENTS

This paper reports the work of the whole JET Team under the leadership of Dr. P.H. Rebut. The author wishes to thank K.J. Dietz and B. Keen for carefully reading the manuscript.

12. REFERENCES

[1] REBUT, P.H., The impact of the first JET results on the development of fusion. 14th Symposium on Fusion Technology, Avignon, 8-12 September 1986.

[2] BERTOLINI, E., The development of the JET electromagnetic system. 14th Symposium on Fusion Technology, Avignon, 8-12 September 1986.

[3] NOLL, P., et al, Stabilization of vertical position and control of plasma shape, 11th Symposium on Fusion Engineering, Austin (USA) 1985.

[4] CELENTANO, G., et al, The JET belt limiter, 14th Symposium on Fusion Technology, Avignon, 8-12 September 1986.

[5] REBUT, P.H., et al, Low Z material for limiter and wall surfaces in JET, JET report JET-R(85)03.

[6] SONNENBERG, K., DIETZ, K.J., KUPSCHUS, P., Wall concepts and density control for JET, 14th Symposium on Fusion Technology, Avignon, 8-12 September 1986.

[7] JACQUINOT, J., Plan for current profile control in JET, 14th Symposium on Fusion Technology, Avignon, 8-12 September 1986.

[8] DEAN, J., Preparation for D-T phase operation in JET, 14th Symposium on Fusion Technology, Avignon, 8-12 September 1986.

[9] HUGUET, M., BERTOLINI, E., Main features implemented in the JET facility for deuterium-tritium operation, American Nuclear Society meeting on Fusion Technology, Reno, Nevada (USA) June 1986.

THE DEVELOPMENT OF THE JET ELECTROMAGNETIC SYSTEM

Paper No. 11.02

E. Bertolini, J. R. Last, P. L. Mondino, P. Noll, A. Santagiustina

JET Joint Undertaking, Abingdon, Oxfordshire OX14 3EA, UK

ABSTRACT

A series of enhancements of the JET apparatus is in the process of being implemented to increase the fusion parameter $n_{iD}T_i\tau_E$ to values required for meaningful D – T operation.

Modifications to the electromagnetic system (magnets, power supplies and plasma control) are major features of the new JET development plans, for operation with magnetic limiter up to 4MA and with material limiter up to 7MA. Operation at these levels, well above design values, requires compensation of stray fields at breakdown, control of plasma current derivative during the early phase of the discharge, larger currents in the primary windings of the transformer (coil 1) and arrangements for establishing magnetic limiter configurations. To this end coil 1 will be made a 10 subcoil stack (now 8), a fast rise voltage shaping circuit and a DC power supply will be added to the present JET poloidal system, and the radial field control will be modified to cater for the magnetic limiter configuration with both one and two X-points.

If the electromagnetic, thermal and mechanical assessment of the machine and power supplies, now underway, shows that the indicated extensions of the JET engineering operating space are possible, flat top currents of duration 10s and magnitude 4 and 7MA will be achieved in magnetic and material limiter configurations, respectively.

1. INTRODUCTION

The experimental results obtained in JET during the first three years of operation have allowed the range of fusion relevant tokamak parameters to be greatly extended [1]. However a number of physics questions, such as plasma fuelling and exhaust, pulse termination, limitations on density and beta and degradation of the energy confinement time are still outstanding. As a consequence, the currently used key fusion parameters, central ion density, central ion temperature and global energy confinement time, cannot be raised to the required levels simultaneously, for meaningful studies of alpha particle confinement and heating in D – T [2, 3].

A comprehensive package of JET enhancements has been proposed, to overcome these difficulties and increase the performance of JET by extending the machine operating space: new equipment is being designed and some is under construction already and will be installed during the next major shutdown in early 1987 [4].

Although each one of these enhancements may positively effect more than one plasma parameter, the global energy confinement time is expected to be increased most effectively in two ways: operation of plasma current up to 7MA for several seconds with material limiter and up to 4MA with magnetic limiter with one or two nulls of the poloidal field inside the vessel. Both these scenarios are outside the original JET 'extended' performance (4.8MA with material limiter and magnetic limiter configuration not foreseen) and therefore their implementation represents a major undertaking. The achievement of this new operating space essentially relies on major modifications to the tokamak electromagnetic system, which will provide for the magnetic limiter configuration and for a substantial increase of the usable transformer magnetic flux swing.

At this stage the new plasma current values given above, have only to be considered as a reasonable target, suggested by preliminary work already undertaken [4, 5], since the operating scenarios eventually allowed will be the outcome of another major undertaking, the electromagnetic, thermal and mechanical assessment of the tokamak and of the power supplies ('7MA' study).

2. PRESENT CONFIGURATION

In the present configuration of the tokamak system [6,7], the primary winding of the transformer consists of 8 coil 1 subcoils (568 turns) and of 4-8 coil 3 turns (P3M) all connented in series, supplied with a DC current, which can be varied between + 40kA and – 40kA during a pulse. The operation of JET has shown that this configuration suffers from some important limitations.

The currently used level of premagnetization current is 25kA, because a larger current produces excessive stray fields at breakdown in a large part of the vacuum vessel volume: this leads to a considerable loss of driving magnetic flux ($\sim$ 5.5 Wb). The computed stray field mapping for 40kA of premagnetization current is represented in fig 1. It has been shown that satisfactory plasma formation is possible only when the ratio between the stray field B_S and the toroidal field B_T is $B_S/B_T < 10^{-3}$ [8]. In the present machine configuration this condition, at full premagnetization current (40kA), is satisfied only in a limited volume of the vessel (fig 2, diagram (a)).

The build-up of the plasma current should avoid too large a current derivative, which may lead to hollow current profiles, MHD instabilities and possible disruptions in the early part of the current flat top. On the other hand a high gas breakdown voltage would be desirable ($E_T B_T/B_S > 10^3$ V/m, E_T electric field induced in the plasma ring), for good ionization and to reduce the length of the plasma high resistivity phase (cold coulomb collision phase) [8, 9]. However the present poloidal circuit [6], a simplified schematic of which is shown in

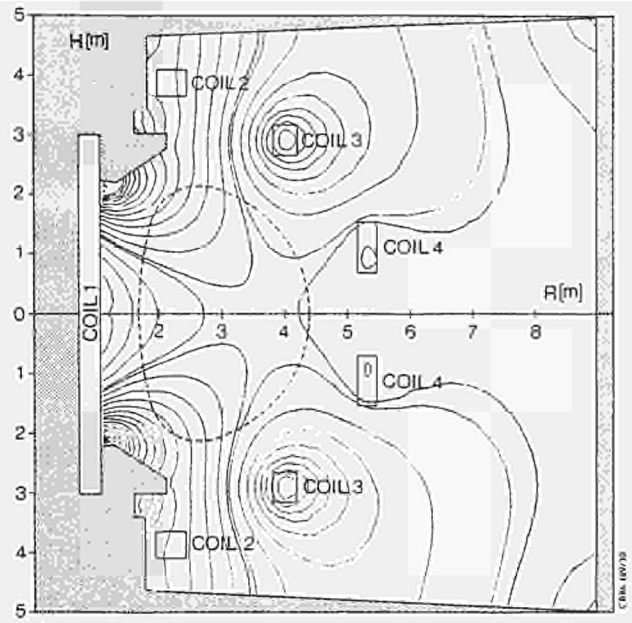

Fig. 1 Stray field patterns with present configuration of the poloidal system (8 coil 1 subcoils) at 40kA of premagnetization current.

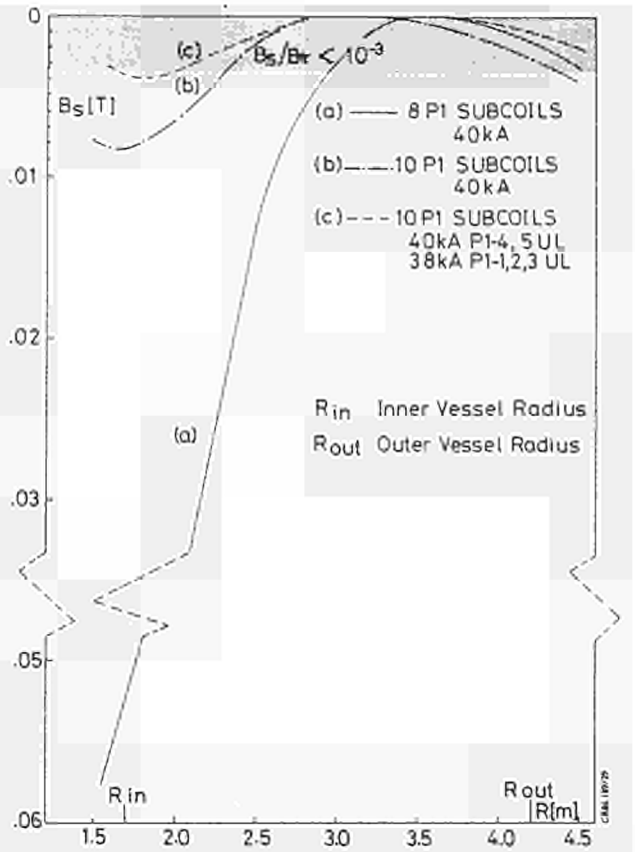

Fig. 2 Vertical component of the stray field across the vacuum vessel, for 8 coil 1 subcoils (a), for 10 coil 1 subcoils without (b) and with (c) active modulation of premagnetization current.

fig 3, allows the breakdown voltage to decay only according to the ohmic heating circuit time constant (300 ms in present configuration), thus leading to too high a voltage after breakdown and too high a current derivative, during the plasma current fast rise phase. There is an additional reason to limit the breakdown voltage: the present voltage capability (+ 2.8kV, − 2kV open circuit) of the vertical field amplifiers (PVFA), which control the radial position of the plasma by supplying

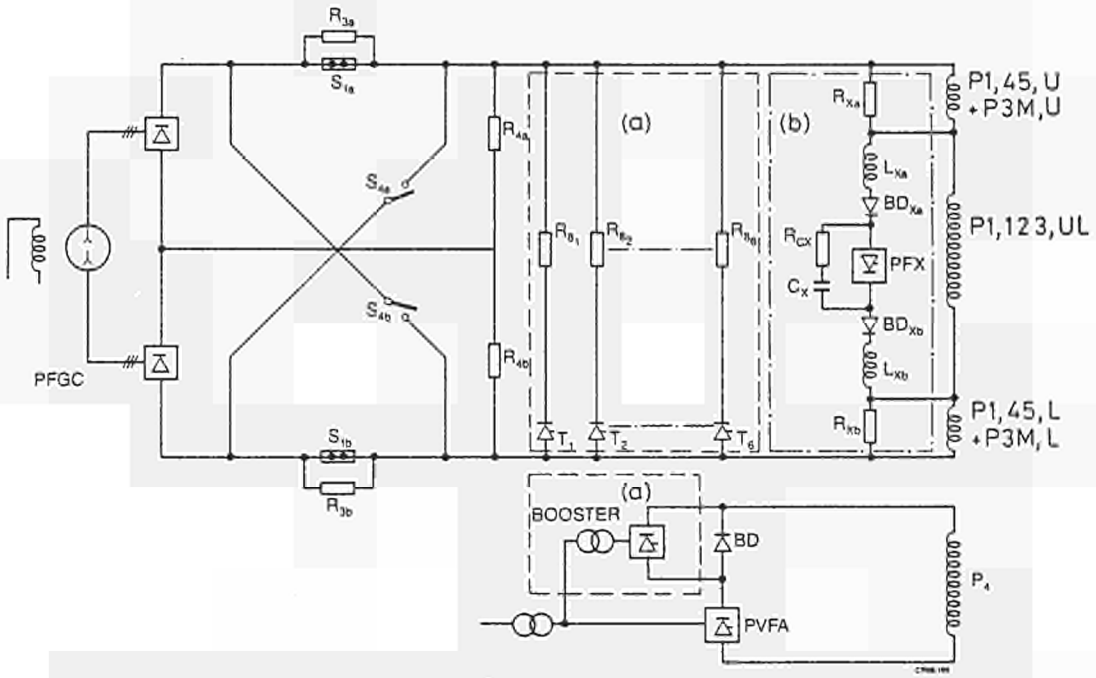

Fig. 3 Simplified schematic of the poloidal circuit, showing present and new configurations with additions for the control of the plasma current derivative (a), for stray field compensation, for increasing flux swing and for establishing a magnetic limiter configuration (b).

coil 4 (see fig 7). In fact the necessary single turn voltage to maintain radial equilibrium during the early phase of the discharge is

$$\frac{VP4}{NP4} = k\frac{VP1}{NP1} - h\,V_{RP}$$

(with k = 2.2, h = 1, geometric factors, VP1, VP4, NP1, NP4, voltages and turns of coils 1 (P1) and 4(P4) respectively, V_{RP} resistive voltage drop in the plasma ring). In order to limit the early plasma radial displacement to less then 30cm, NP4 is now reduced to 78 turn (out of a total available of 122), and VP1 to 12kV (25kA of premagnetization current).Therefore the loop voltage has to be limited at breakdown (−25 V): this leads to a long cold coulomb collision phase, a delayed start of the plasma current and to a poor use of the initial 1 to 2Wb of magnetic flux variation (fig 4) [9].

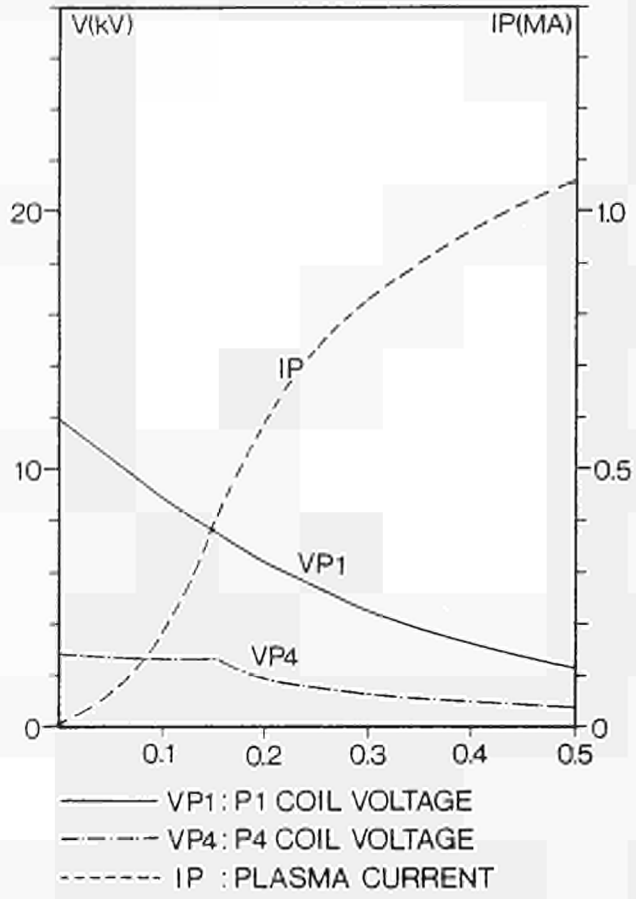

Fig.4 Coil 1 and coil 4 voltages during fast rise of the plasma current with the present poloidal system configuration. (6.8 Wb of flux swing used).

The total magnetic flux currently used for most JET discharges is 28.5 Wb and it is not sufficient for long plasma current flat tops at 4.8MA (design value). A four second flat top at 5MA (fig 5) has been achieved by a sophisticated start up scenario, which has allowed a premagnetization current of 30kA to be used. If a 10s flat top is required for a current of 7MA, improvements limited to the early phase of the discharge are not sufficient and a substantial increase in the flux swing has to

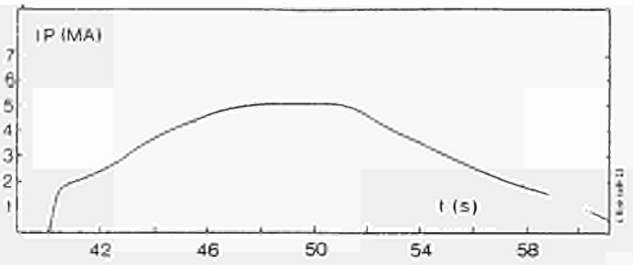

Fig.5 A material limiter 5MA plasma pulse (pulse 8865) with a 4s flat top achievable with the present poloidal system configuration.

be provided to take care of the late phase of the plasma rise and of the current flat top.

Magnetic limiter configurations with two X-points are currently established in JET up to plasma current of 2 to 2.5MA (fig 6): they are obtained by 'passive' means, i.e. taking advantage of the saturation of the upper and lower regions of the central column of the magnetic circuit (see fig 7) which starts at coil 1 current above 25kA, during flat top: the leakage flux has a radial component that creates X points in the poloidal field inside the vacuum vessel at currents up to 2 to 2.5 MA [10].

3. ENHANCEMENTS AND IMPROVEMENTS

The flexibility of the JET design and construction has made it relatively easy to make modifications and improvements to the electromagnetic system which address all the above issues.

3.1 Stray field compensation

The coil 1 stack (P1) has been designed to allow 10 subcoils to be installed, while only 8 subcoils and 2 'dummies' are used in the present assembly, the remaining

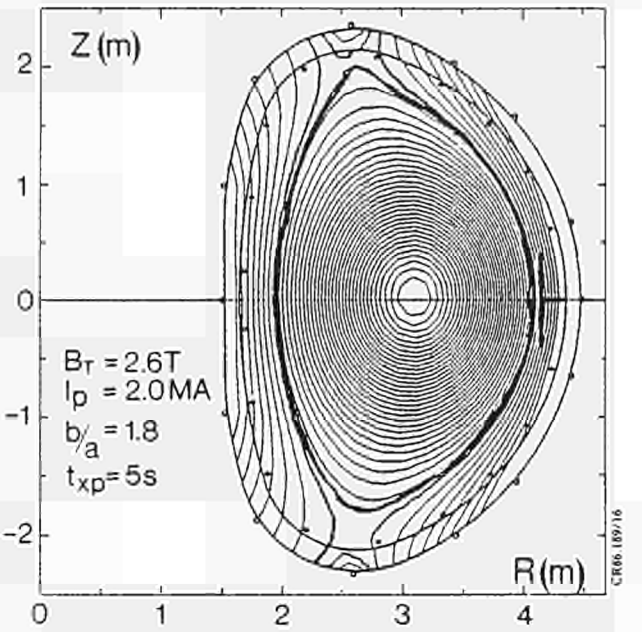

Fig.6 A magnetic limiter 2MA plasma pulse (pulse 5564), obtained with the present poloidal system configuration.

2 subcoils having been kept as spares. A 10 subcoil stack (fig 7) would bring only a marginal increase (~ 0.6 Wb) in the flux capability of the transformer, due to poor coupling with the plasma of the added end subcoils and increased reluctance of the magnetic circuit; but it considerably reduces the stray field at breakdown. In other words the vacuum vessel region, where the ratio of the vertical component of the stray field to the toroidal field satisfies the relation $B_S/B_T \gtrsim 10^{-3}$ (i.e. $B_T = 3.45$T, $B_S \gtrsim 0.0035$T) at 40kA of premagnetization current, would be greatly increased (fig 2, diagram (b)).

With the present P1 stack the computed stray field at the inboard side of the vacuum vessel of 0.052T is close to the measured value; this may suggest that calculated value of 0.008T with a P1 stack of 10 subcoils may also be close to the real value (the computations are for 40kA of premagnetization current).

The necessary work on the machine to implement the new configuration is scheduled for the November '86 – April '87 shutdown. This work is not simple at all: it is necessary to remove cooling water and vacuum rings, jumper cables, in vessel inspection system (IVIS) and many diagnostics at the top of the machine. Concerning the machine itself, the following components have to be removed: central iron pillars, upper limbs, upper coils 2 (P2), upper centre piece, upper dummy coil, upper ring, P1 stack and lower dummy coil. The P1 coil has then to be reassembled with 10 subcoils and the dismantling sequence reversed (fig 7) [4, 5].

The stray field can be further reduced if the P1 coil connections are modified from 2 busbars to 4, so as to allow the central 6 coils (P1 – 1, P1 – 2, P1 – 3, upper U and lower L) to be supplied with a somewhat lower current than the four end coils (2 upper and 2 lower, i.e. P1 – 4, P1 – 5 UL) as shown in fig.8(a). With a current difference of 2kA (5%), stray field satisfies the condition $B_S/B_T < 10^{-3}$ in practically the full volume of the vessel (fig 2, diagram (c)), with a loss of flux of only 0.6Wb.

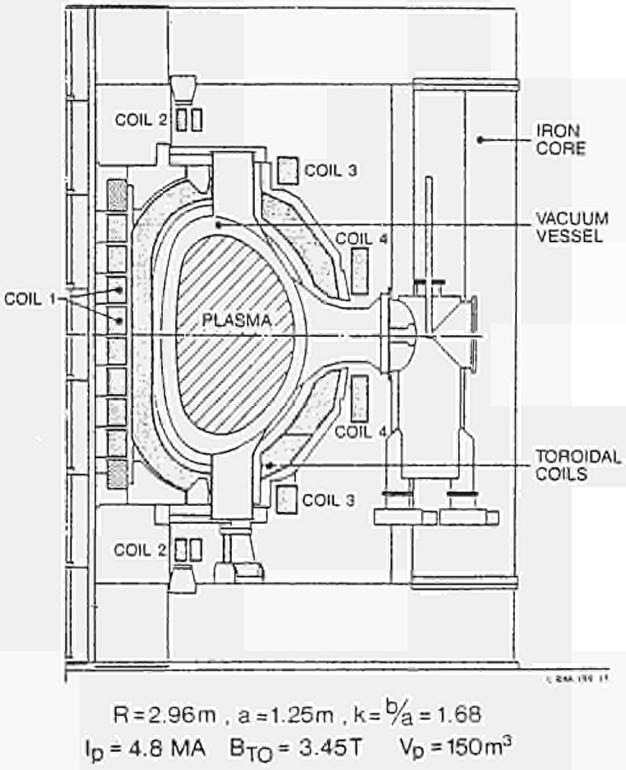

Fig.7 Cross sectional view of the JET tokamak, showing the future configuration with 10 coil 1 subcoils.

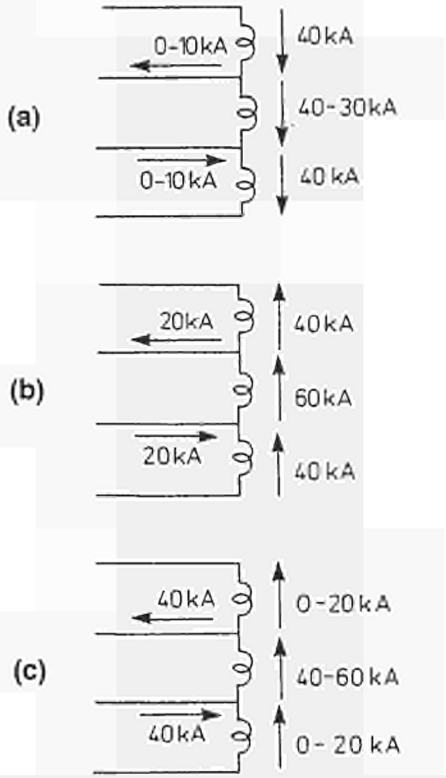

Fig.8 The four busbar connections to the magnetizing winding (P1 + P3M) for active compensation of stray field (a), for increasing flux swing (b) and for magnetic limiter configuration (c).

The 4 busbar P1 connections will also be implemented during the next shutdown, while the circuit for 'active' stray field compensation (which supplies these new busbars) is being designed in detail: its current capability will allow a reduction of the P1 – 1,2,3 UL current up to a value to be chosen between 5 and 10kA as compared with the current in P1 – 4,5 – UL (and P3M – UL), to make allowance for further stray field compensation and for any discrepancy between computed and experimental stray field values.

3.2 Plasma Current Derivative

Low stray field (< 0.0035T) and a relatively high loop voltage (> 30V) at breakdown have to be followed by a suitable control of the plasma current derivative during the early phase of the discharge in order to obtain a good plasma formation and to avoid MHD instabilities [8].

The high breakdown voltage and the limitation in the

plasma current derivative can be obtained by a suitable shaping of the P1 coil and correspondingly of the P4 coil voltages (fig 9). These voltage patterns can be produced by reducing the value of the resistance in parallel to P1: this is achieved by modifying the poloidal circuit as shown in fig 3. By inserting the resistors (R8) in the circuit, by means of the thyristors (T) and producing the appropriate triggering sequence, the desired P1 voltage (and therefore loop voltage) shaping can be achieved. The booster amplifier, designed for high voltage (~ 9.2kV), low current (~ 6kA) and short operating time (< 0.5s) allows P4 to be supplied with the voltage (up to ~ 12.0kV including existing PVFA) required to maintain plasma radial equilibrium from the early plasma current formation. The value of each new R_8 resistor is 0.9Ω and, to avoid expensive and complex thyristor switch off, the resistors are kept in the circuit during the complete pulse, with a maximum energy dissipation of 135MJ each. This is possible, again, thanks to the JET built in flexibility, in this instance the installed reserve of stored energy in the poloidal flywheel generator [11, 12].

The advantage of the new configuration (10 P1 subcoils, active stray field compensation and fast rise voltage shaping) in the early phase of current build – up, can be appreciated by comparing fig 4 with fig 9: with 6.8 Wb of flux swing it will be possible to obtain a larger plasma current (~ 1.4 MA as compared with ~ 1.05 MA).

3.3 Total Magnetic Flux

With the provisions described in 3.1 and 3.2, the total flux available, from the magnetizing coils (P1 and P3M) may be brought from the present 28.5 Wb to the original design value of 34 Wb. However higher values are required for reasonably long flat top times at 7MA of plasma current.

There is a particular feature in the design of the machine, which may allow increasing the ampere turns of P1 coil, by increasing the current in the centre 6 coils (P1 – 1,2,3 – UL) above the design value of 40kA. In fact the six central subcoils are maintained under compression by the inward forces of the toroidal coils (fig 7): preliminary evaluations indicate that a current of 60kA (50% larger than the design value) may be passed through P1 – 1,2,3 – UL while 40kA is still maintained through P1 – 4,5 – UL (and through P3M – UL), making use of the 4 busbar system that now supplies coil P1 (fig 8(b)) [5].

A total flux swing of 40.6 Wb may thus be achieved, i.e. an increase of 20% above the design value of 34 Wb and 40% above the present value of 28.5 Wb (fig 10). Assuming a plasma loop voltage of 0.5V during flat top,

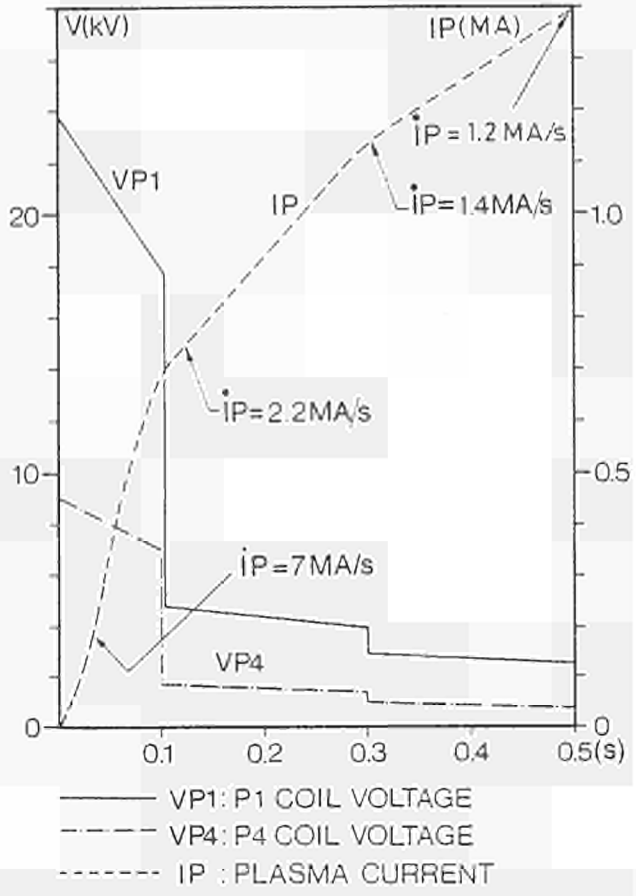

Fig. 9 Coil 1 and coil 4 voltages during fast rise of the plasma current with the new poloidal system configuration. (6.8 Wb of flux swing used).

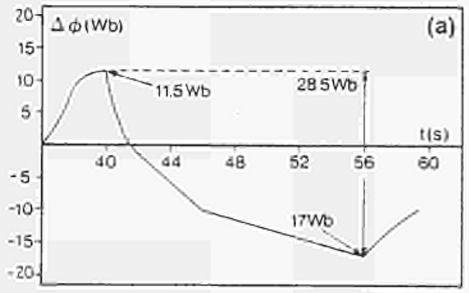

(a) 8 P1 subcoils
Premagnetisation 25kA
End of flat top –40kA

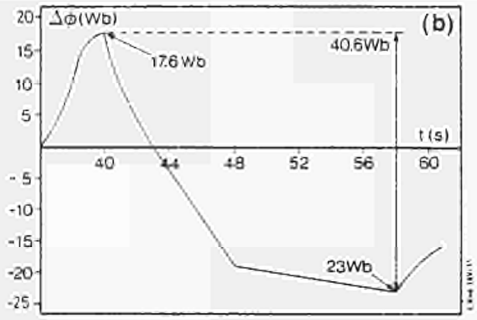

(b) 10 P1 subcoils

Premagnetisation	P1–4,5	40kA
	P1–1,2,3	38kA
End of flat top	P1–4,5	–40kA
	P1–1,2,3	–60kA

Fig. 10 Comparison between the currently available flux swing (28.5 Wb) and the one available with the new poloidal system (40.6 Wb).

a current of 7MA can be sustained for 10s with this new value of the flux swing, (fig 11).

3.4 Magnetic Limiter Configuration

In order to use the 'X – point' configuration for enhanced JET performance, the configuration has to be set up for currents well in excess of the values achieved so far (2 – 2.5 MA). The P1 four busbar system (fig 8(c)) allows P1 – 1,2,3 – UL to be supplied with a current of 40kA (or above), while P1 – 4,5 – UL (and P3M – UL) are supplied with a lower current (down to zero but not reversed), during flat top: in this way the leakage flux is higher than that achievable by 'passive' means (see section 2). The computed poloidal field shows that a configuration with 2 X points at 4MA is achievable with a distribution of current 0 – 40 – 0kA in P1 (fig 12). The leakage flux could be further increased, thus allowing larger X point plasma currents, by reversing the current in P1 – 4,5 – UL. However this will not be permitted as the consequence would be that the P1 stack would not all be in axial compression any more and a force tending to lift the upper limbs of the iron circuit would develop. Moreover, the shaping field crossing the toroidal coils near the 'X – points' would cause excessive shear stress in these coils.

4. NEW POLOIDAL SYSTEM

The new poloidal system is the result of combined and significant modifications in the machine assembly and in the poloidal power supplies.

The primary winding of the tokamak transformer

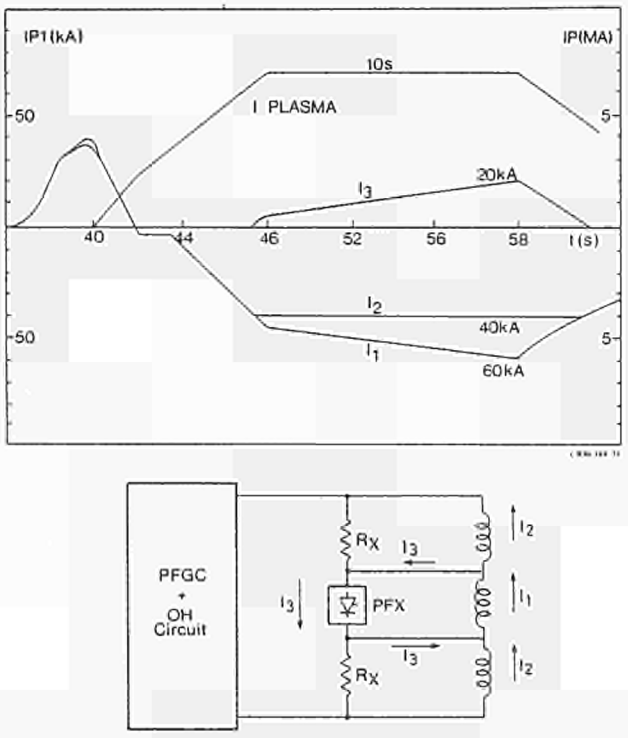

Fig. 11 Computed plasma current of 7MA with 10s flat top, achievable with 40.6Wb of flux swing.

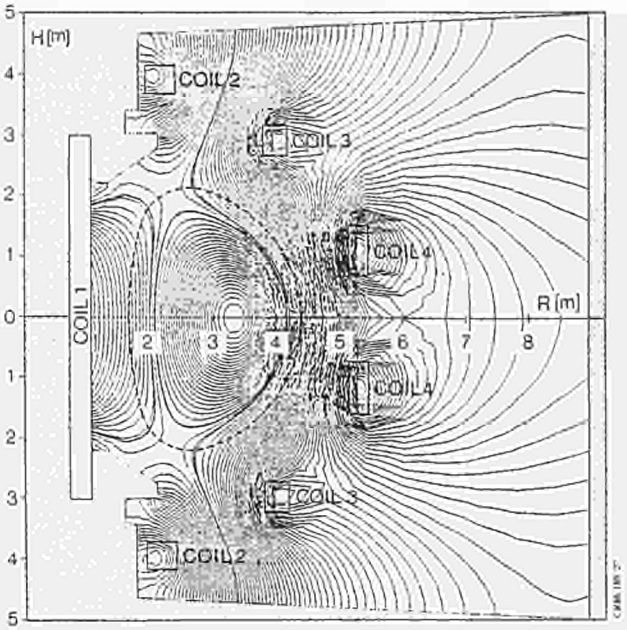

Fig. 12 Computed magnetic limiter configuration, obtained with the new poloidal system (2 X – points, 4MA for 10s, coil currents of 0kA in P1 – 4,5 + P3M and of 40kA in P1 – 1,2,3).

(coil 1) is now made by 10 subcoils (fig 7), 71 turns each, connected in series (R = 40 mΩ, L = 250 mH), supplied through the 4 busbar system (fig 8); the 6 inner subcoils can be supplied with currents up to 60 kA, while the outer 4 can be supplied with currents up to 40 kA.

The poloidal power supply systems have been modified with a number of additions as shown in fig 3: the circuit now includes the new features for active control of the stray field and of the plasma current derivative during rise, for increasing the flux swing capability and for establishing the X – point configuration at plasma current well above the previous limits.

The operational sequence of the new poloidal system will then be as follows (fig 13) [6]:

- The transformer windings (710 turns of P1 + 4 + 8 of P3M) will be premagnetized at 40kA by the poloidal flywheel generator converter leading to vertical components of the stray field according to diagram (b) of fig 2. If experiments indicate that this is too high, the thyristor power supply unit PFX will pass through P1 – 1,2,3 – UL (426 turns) a current of few kA in the opposite direction so that the current in the magnetizing windings will be 40kA in P3M + P1 – 4,5 and less than 40kA in P1 – 1,2,3, leading to a vertical component of the stray field as in diagram (c) of fig 2, or even less by adjusting the current difference.
- The S1a, S1b circuit breakers of the ohmic heating circuit will be opened in the usual way [6], thus producing the required high loop voltage for breakdown (~ 24kV primary, 34V secondary, fig 9). The few kA current, that was previously circulating in PFX (i.e. the 'difference' between P1 – 4,5 and P1 – 1,2,3 currents) will now be circulated in the resistors Rxa, Rxb designed

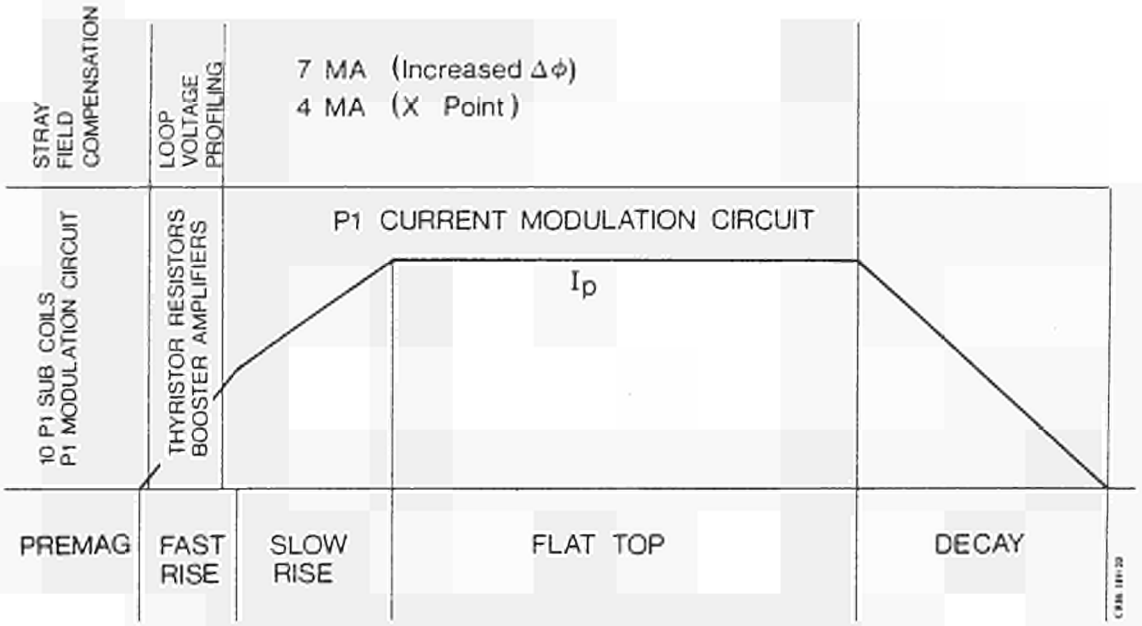

Fig. 13 Sequence of operation of the new poloidal system, showing functions of the new features at various stages of plasma current development.

to drain the required current. The combined effect of the filter Rcx – Cx, the inductances Lxa, Lxb, and the blocking diodes BDxa, BDxb, protects the low voltage (~ 3 kV) thyristor power supply PFX.

- The plasma current starts growing and the phase ('fast rise') where its derivative has to be controlled, starts. This is obtained by appropriately shaping the P1 voltage (i.e. the plasma loop voltage), by triggering (following the example of fig 9) the thyristor resistor banks connected in parallel to the magnetizing windings, in two steps, T1,2,3, and 4, 100ms, and T5 and 6, 300ms, after breakdown respectively, thus leading to the following plasma current derivatives: ~ 7MA/s after breakdown, 2.2MA/s after 100ms, 1.4MA/s after 300ms and finally 1.2MA/s toward the end of fast rise phase.

The plasma is kept in equilibrium throughout, by suitable matching of the P4 voltage using the high voltage booster amplifier connected in series with PVFA: at the end of this phase, with the current in P4 of few kA (< 6kA) the booster thyristors go to inversion, and the current supplied by PVFA goes through the bypass diode stack BD.

This circuit allows a great flexibility in optimizing the plasma current build up, permitting the balance between high plasma current derivative and plasma free of MHD instabilities to be found experimentally.

- The plasma current now continues to grow at moderate derivative, (slow rise phase, ~ 0.5 ÷ 1MA/s): when the voltage across the magnetizing winding is equal to the generator voltage, the reversing make switches S4a, S4b are closed and the generator can magnetize the coils in the opposite direction. When the plasma current reaches the desired value, this is maintained ('flat top') by controlling of the generator voltage [6].
- At this time (several seconds after breakdown, figs 3, 13), the circuit offers two choices:

  (a) increase the 'reverse' flux up to 23Wb (total flux swing 40.6Wb, see fig 10), by passing through the six central subcoils, up to 20kA more than in the outer subcoils, by using the PFX supply in mode (b) of fig 8; this operating scenario will allow a current of 7MA to be maintained for 10s (assuming 0.5V of loop voltage during flat top, see fig 11);

  (b) maintain a difference in current up to 40 kA between the 6 central and the 4 outer P1 subcoils (and P3M): in this way a radial leakage flux is produced which, according to a computed scenario (see fig 12) should allow a magnetic limiter configuration to be established at 4MA for several seconds.

5. RELATED PROJECTS

While the hard core of the JET electromagnetic system development has been summarised in section 4, there are other projects to be also implemented if the new electromagnetic system is to work correctly: they are only briefly mentioned here.

The *plasma vertical stabilization control* [6], has to be revised and to be made both more effective and more reliable, because the extreme plasma performance now envisaged for JET may increase the risk of vertical instabilities and the risk of damaging disruptions (as the JET elongated plasma is intrinsically vertically unstable), if appropriate measures to improve the related control system are not taken. While the stabilization of vertical plasma position is satisfactory up to an elongation factor k = 1.9 with material limiter configuration, the magnetic limiter configuration requires

operation close to the stabilization limit of the feedback system. A number of improvements are being considered at present.

Interference suppression may be obtained by simultaneous measurement at two opposite octants of the vacuum vessel.

The vertical stabilization system uses a change over switch from current feedback (used during premagnetization to maintain the radial field winding current to zero) to flux feedback to be started as soon as the plasma current begins to build up. For experiments with single X-point this system would become saturated and the stabilization would fail. It has been proven by plasma tests that where current and flux feedback are allowed to act simultaneously the stabilization is more effective: on fast time scale the flux feedback would prevail, as necessary for stabilization, and at slow time scale current feedback reduces the average current to zero.

Reliability will be substantially increased by implementing a complete dual plasma vertical position control system, each one with its own magnetic signals, control logic and power supply; the two power supplies are obtained by independent control of the existing four units of the radial field amplifiers (PRFA) in two modules of two units each (Fig. 14).

At present the ohmic heating circuit (OHC), the vertical field amplifiers (PVFA) and the shaping amplifiers (PSFA) have one busbar in common [6]. Full *galvanic separation* will now be implemented for the four poloidal circuits [5,9], since this will lead to lower voltages on the vertical and shaping field coils, less coupling between circuits, symmetrical coil voltages and easier debugging and testing.

The full *toroidal field* can be maintained, at present, for only 12,5s when, with the present cooling system, the maximum allowed coil copper temperature (~ 80°C) is reached. Both long pulses at moderate toroidal field (typically $I_p = 2MA$, $B_T = 2T$ for 60s) and high performance scenarios ($B_T = 3.45T$) require an increase in the I^2t capability of the toroidal coils. Chillers will therefore be installed in the cooling circuit, to allow an increase of the 3.45T toroidal magnetic field flat top length from 12,5 to 19 seconds [4, 5].

With the full additional heating system becoming available and with the planned new enhancements, the demand of *active and reactive power* on the CEGB 400 kV grid will increase as will the active power steps. Since in the CEGB supply contract, there must be limits on both reactive power swing and active power steps, a suitable scheme for a combined active and reactive power compensation scheme has been designed [13] and will be implemented to the extent required by the JET – CEGB negotiations, presently underway.

But the key issue on which the whole JET new development programme depends, is the answer to the following question: can the machine be operated well above the engineering design parameters? A qualified quantitative answer will come from the so-called *'7 MA' study*, now underway. This project involves many skills, since a comprehensive assessment of the machine capability as built has to be made, possibly leading to suggest further improvements and to a hopefully accurate definition of the JET new operating space [4, 5].

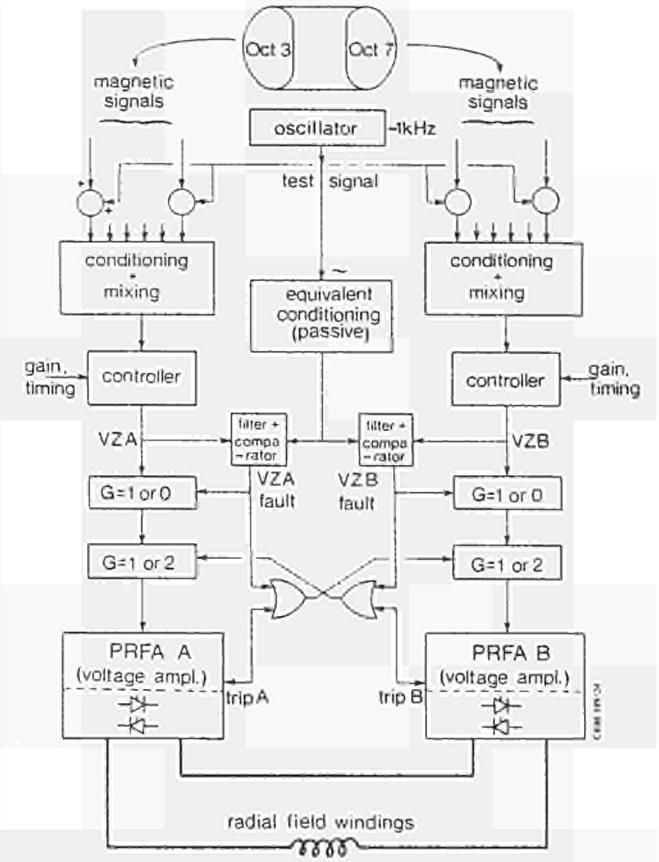

Fig.14 Schematic of the new dual control system for vertical stabilisation to achieve high reliability.

There are, in addition, a number of less complex, but still *important modifications* to be undertaken. Significant examples are the increase in the current capability up to 40 kA of the PVFA, PSFA thyristor bridges and above 3 kA of the PRFA thyristor bridges and the modification from analog to digital of the plasma position and current control (PPCC).

6. CONCLUSIONS

The implementation of the enhancements described for the JET electromagnetic system requires rearrangement of existing equipment and production of new hardware. This will involve a considerable investment in manpower and financial resources.

However the planning must be consistent with the JET development programme and therefore the development of the JET electromagnetic system has to conform to the procurement schedule of Table I.

In conclusion the modifications and additions to be implemented in the electromagnetic system will allow a considerable extension of the JET engineering operating space, well beyond the one originally foreseen, and it is hoped that this will allow extension of the physics

TABLE I

PLANNING FOR THE IMPLEMENTATION OF THE NEW JET ELECTROMAGNETIC SYSTEM AND RELATED PROJECTS.

1987
- 10 P1 subcoils
- separation of poloidal loads
- thyristor switched resistors
- thyristor power supply for P1 current modulation
- magnets additional cooling
- improvement in PPCC
- '7MA' study

1988
- booster amplifiers
- passive components for P1 current modulation
- increased current capability of PVFA, PSFA, PRFA power supplies
- further improvements

1989
- active power step compensation
- reactive power swing compensation

operating space as well, so that the main aim of JET, to show alpha particle confinement and heating, can be met.

In essence this means to be able to compare fusion relevant performance, with full additional heating and with the other facilities considered [4, 14, 15], of 7MA material limiter plasmas and 4MA magnetic limiter plasmas.

The actual values of the technically permitted currents and pulse lengths will be defined by the '7MA study', now underway, the ultimate aim of which is to clearly define the JET new performance operating space.

7. ACKNOWLEDGEMENTS

The authors wish to acknowledge the contribution of their colleagues in JET for the work described in this paper, E. Lazzaro, A. Tanga and F.C. Schüller for the physics background, T. Bonicelli, M. Huguet, K.I. Selin and L. Sonnerup for some of the engineering aspects. A special appreciation is due to P.H. Rebut for his cooperation in the choice of the basic concepts for the new magnetic configuration of coils and of power supplies.

REFERENCES

[1] P L Mondino, E Bertolini, 'The JET Technical and Scientific Performance and Future Plans' Proceedings of the 7th Topical Meeting on the Technology of Fusion Energy, Reno (USA), 16 – 19 June 1986.

[2] R J Bickerton, et al, 'Latest Results from JET', Proceedings of the 12th European Conference on Controlled Fusion and Plasma Physics, Budapest (Hu) 2 – 6 Sept 1985, published in the Europhysics Journal Vol 28, No 1A, pp. 55 – 69, January 86.

[3] P H Rebut, 'The Impact of First JET Results on the Development of Fusion', presented at the 14th Symposium of Fusion Technology, Avignon (F), 8 – 12 Sept 1986.

[4] M Huguet, 'JET Status and New Development Plans', presented at the 14th Symposium of Fusion Technology, Avignon (F), 8 – 12 Sept 1986.

[5] J Last, D Cacaut, J W Zwart 'The JET Magnets: Operational Experience and Plans for Upgrade', presented at the 14th Symposium of Fusion Technology, Avignon (F), 8 – 12 Sept 1986.

[6] E Bertolini, P L Mondino, P Noll, 'Magnet Power Supplies and Plasma Control in JET', to be published in Fusion Technology Journal, January 1987.

[7] M Huguet, K Dietz, J L Hemmerich, J Last, 'The JET Machine: Design, Construction and Operation of Major Systems', to be published in Fusion Technology Journal, January 1987.

[8] F C Schüller, et al, 'Plasma Evolution and Skin Effects in JET', Proceedings of 12th European Conference on Controlled Fusion and Plasma Physics, Budapest (Hu), 2 – 6 Sept 1985, pp 287 – 290.

[9] P L Mondino, T Bonicelli, M Huart, A Santagiustina, 'The Development of the JET Poloidal Field Power Supplies to Reach the Nominal Flux Swing Capability', presente at the 14th Symposium of Fusion Technology, Avignon (F), 8 – 12 Sept 1986.

[10] A. Tanga, et al, 'The Formation of a Magnetic Separatrix in JET', Proceedings of 12th European Conference on controlled Fusion and Plasma Physics, Budapest (Hu), 2 – 6 Sept 1985, pp 70 – 73.

[11] M Huart, 'Design, Fabrication and Erection of the Flywheel Generator Converters, for the JET Tokamak', Proceedings of the 9th Symposium on Engineering Problems of Fusion Research, Chicago (USA), Oct 1981, Vol I, pp 382 – 385.

[12] M Huart, A Moissonnier, T Eriksson, C Raymond, 'Operation of the Magnet Power Supplies: Reliability and Improvements', presented at the 14th Symposium of Fusion Technology, Avignon (F), 8 – 12 Sept 1986.

[13] K I Selin, D Ciscato, V Marchese, P Ashmole, B Jervis, 'The High Voltage 400 kV Grid Interface in the Present and Future JET Operational Requirements', presented at the 14th Symposium of Fusion Technology, Avignon (F), 8 – 12 Sept 1986.

[14] K Sonnenberg, K J Dietz, P Kupschus, 'Wall Concepts and Density Control for JET', presented at the 14th Symposium of Fusion Technology, Avignon (F), 8 – 12 Sept 1986.

[15] J Jacquinot, 'Current Profile Control in JET', presented at the 14th Symposium of Fusion Technology, Avignon (F), 8 – 12 Sept 1986.

WALL CONCEPTS AND DENSITY CONTROL FOR JET

K. SONNENBERG, K.J. DIETZ, P. KUPSCHUS
JET Joint Undertaking
Abingdon, Oxon, OX14 3EA, UK

SUMMARY

Only low-Z materials will be used for first wall components of JET. This is particularly important with regard to radiation losses in the outer region of the plasma which can lead to instabilities limiting the plasma density. To avoid implications from redistribution of wall material by erosion and redeposition, the first wall is intended to consist of one material only. Two alternative concepts are being developed. The first employs graphite tiles for limiter and wall protection, with the rest of the wall being carbonised, the second uses beryllium limiters and a thin beryllium layer on the graphite protection and the rest of the wall.

Density control will be achieved by Pellet Injection to increase the central density and by pumping at the plasma edge to control the recycling.

For the pumping two possibilities are studied. It has been frequently shown that the JET wall acts as an efficient pump. The effect is not understood and if it turns out to be insufficient for full performance conditions in JET pump limiter modules will be installed in the shadow of the main limiter. As a first step an inertia cooled prototype limiter will be built to find the optimal design parameters for the JET boundary conditions. The final pump limiter will be actively cooled to allow a continuous operation during a JET discharge.

For pellet injection JET will start with a single pellet injector followed by a multiple pellet injector with 3 barrels for different pellet sizes repetitive at a rate of 5 pellets per second both injectors with pellet velocities up to 1.5 km/s. In parallel JET has started a program for developing a high speed injector.

1. FIRST WALL CONCEPT

1.1 Introduction

The basic ideas of the JET wall concept have been discussed several times in the past [1, 2, 3]. In this paper only a brief summary shall be given concentrating on the technical aspects of the present status and of future enhancements of the first wall. At JET the main objectives are to use low-Z materials for wall components and to build the wall out of a uniform material. In several tokamaks improved performance has been observed

when a low-Z wall was employed: e.g. TEXTOR achieved its highest density values with the metal limiter and walls carbonized [4]; JET experienced problems in achieving high densities when the graphite limiters were heavily contaminated by metals from the inboard wall protection tiles. The situation improved when the metal protection tiles were exchanged by graphite tiles and a further improvement was achieved when wall, limiter and the metal screen of the RF antenna were carbonized. Recent experiments studying pellet injection in ASDEX [26] showed that even in divertor machines a low-Z wall can be essential.

Theoretically it is predicted [2,7] that disruptions due to high density limits would be strongly suppressed if radiation losses in the outer plasma zone can be reduced by employing a low-Z wall. Only low-Z impurities can be tolerated in higher concentrations without generating a thermal collapse of the plasma due to radiation losses. It should be noted, however that the experience in JET [5] shows that even impurities with low-Z such as carbon and oxygen still influence the density limits of the plasma. For this reason JET is prepared to use Beryllium as a low-Z wall material as an alternative to graphite.

In practically all tokamaks it has been observed that due to a series of erosion mechanisms wall material is redistributed over the first wall, resulting in limiters being contaminated [6] by wall material and vice versa. For this reason JET decided to employ a uniform material for all wall components. One can distinguish between erosion mechanisms which may damage the bulk of a wall component, e.g. melting or fracture by runaway electrons, disruptions or neutral beam shine-through and those which only lead to surface erosion due to sputtering. Since the wall components which are further back from the plasma such as the vacuum wall are only attacked by the sputtering processes it is sufficient to coat them only with a thin layer of a low-Z material whereas all other components (limiter, protection limiter for antennae, and wall protection tiles) will be built from solid low-Z material.

1.2 Present status of the first wall

Limiter: Presently JET is equipped with 8 graphite limiters (area ≈ 3 m^2) (see Fig. 1). The limiters are inertia cooled during the pulse and cooled down by radiation only between pulses within ≈ 30 min. The limiters are designed to take a maximum total power of ≈ 7.5 MW for 10s. Due to the fact that 30-40% of the power is radiated and that the antennae are equipped with graphite protection limiter (total area ≈ 6 m^2) which are also very close to the plasma and share the load, the maximum heating power can be ≈ 16 MW. Under these conditions the limiters reach surface temperatures of more than 2000°C.

Inboard and outboard wall protection: In the beginning of JET the inboard wall was protected by inconel tiles which suffered, however, from heavy damage by run away electrons during disruptions. Because of the larger transparency of carbon for high energy electrons the inconel tiles were exchanged with graphite tiles, which have survived about 1.5 years of JET operation without any major damage [8].

Part of the inboard protection tiles also act as a wall protection against NB shine-through. Under normal conditions the estimated power density from the NB shine-through is less than 500 W/cm^2 which the tiles can sustain for about 10s. An unattenuated beam however would generate about 2 kW/cm^2. As shown by tests and calculation such power

density builds up thermal stresses within 1 s sufficient to fracture the tiles. Tests performed on carbon, carbon fibre composite material (CCFC) showed that this material can sustain heat loads > 3 kW/cm² for more than 10 s [9]. For this reason JET will substitute the graphite tiles in the area of the NB shine-through with CCFC tiles.

The third function of the inboard wall protection is that it is used particularly during the pulse termination as a bumper limiter for the plasma, because it has been observed that pushing the plasma against the inner wall generates a strong wall pumping effect, which will be discussed later in this paper.

Since the NB shine-through also affects parts of the outboard wall some areas around the horizontal port on Octant 5 have been covered with graphite tiles (≈ 3 m²).

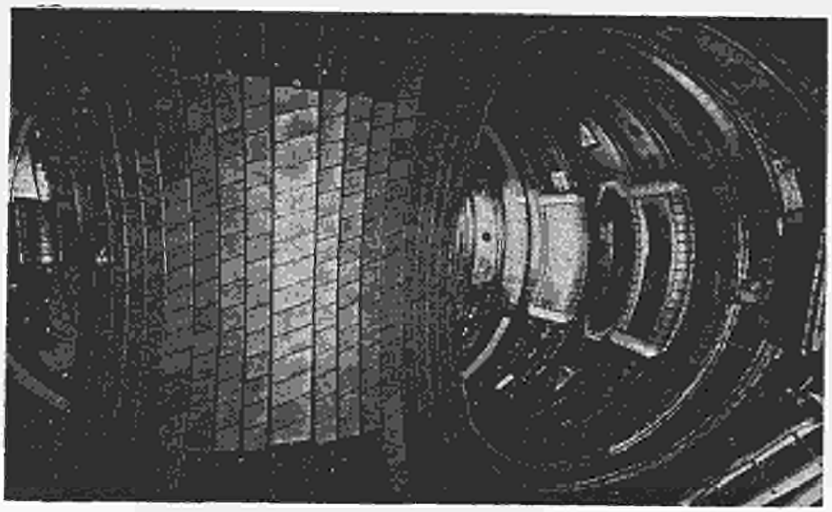

Fig. 1: Present status of the first wall

Separatrix dump plates: Apart from the normal limiter mode JET can also be operated in a separatrix (or X-point) mode [10]. For this operation the vacuum vessel requires additional protection on top and bottom of the vessel. Presently only 8 graphite protection rings (one at each octant joint) are available for this purpose. This allows X-point operation with a very limited power level since the total surface is less than 0.5 m² and the tiles are only cooled by radiation. Because the final wall protection will not be available before 1988 (see future enhancements), as a first measure, JET will increase the surface of the 8 protection rings by a factor two and will shape the tiles so that the heat load is distributed more homogeneously. This will allow X-point operation with a power level shown in Fig. 5 (See curve A).

Carbonisation in JET: At the present state ≈ 45 m² of the First Wall are already covered with graphite. The remaining wall consists of inconel and although much further away from the plasma still acts through the above mentioned erosion mechanism as a metal source. More important, however, are the Nickel screens (one screen is coated with chromium) of the RF antennae which are much closer to the plasma and it also seems that an increased erosion of the Ni and Cr screens occurs due to an increased particle flux during RF heating [11]. To prevent metal erosion from the wall and the antenna screen and to cover up existing metal contamination on the limiter JET uses carbonisation of wall and limiter [12]. Although this creates some difficulties in conditioning the machine (density control) and the carbon layer has to be renewed after about 2 days of operation, it does

improve the performance of JET (lower radiation and Z_{eff}, and somewhat higher density limits).

It should be noted, that even with this uniform low-Z wall the density limit is still determined by radiation in the outer plasma zone, approaching 100% of the power input at the density limit. Radiation from central plasma is negligible. The edge radiation is mainly caused by carbon and oxygen impurities. The high concentration of carbon and oxygen if unchanged, would also create a problem for the dilution of the fuel ($n_D \approx 70\% \, n_e$) reducing the α-particle production.

1.3 Future Enhancements

(i) Alternatively to the first wall consisting of graphite components with the rest of the wall carbonised JET is preparing the possibility to exchange the graphite with Beryllium and to coat the rest of the wall with a thin layer of Beryllium (see Table I). In contrast to carbon no line radiation is expected for Beryllium inside the limiter radius and in addition the oxygen level will be reduced substantially due to gettering by the Beryllium. This has been confirmed in the two tokamak experiments [13,14] performed until now with Beryllium limiters. Improvements can be also expected with regard to the dilution of the plasma if the Beryllium concentration is not much higher than the carbon concentration presently observed in JET (2.5%). Beryllium concentrations observed in the ISX-B experiment were only higher when large areas of the Beryllium limiter were melted during tests with heat loads exceeding the design limit. When initially heat loads within the design limit were used a Beryllium concentration of only ≈ 1% was observed.

Due to lower edge radiation for Be a higher edge temperature must be expected which will help to increase somewhat the central temperature. Higher edge temperatures are also typical for H-mode conditions.

One of the main arguments against Be was that it would have insufficient thermal resistance. Though graphite and particularly carbon fibre reinforced graphite is certainly superior in this respect, thermal fatigue test [15] under JET relevant conditions and the limiter experiment in ISX-B [13] proved that Be due to its high ductility at higher temperatures has excellent thermo-mechanical properties. The major drawback of Be is its toxicity imposing strict safety precautions, which are, however, well known from the Beryllium industry.

(ii) Belt limiter: For full performance of JET a new limiter will be required. It will consist of two toroidal belts with a total surface of ≈ 15 m^2 capable of taking about 40 MW for a 10s plasma pulse (equivalent to the total power including the expected α-particle heating). The principle of the limiter cooling is shown in figure 2 (for details see [16]). During a discharge the limiter surface is cooled by heat conduction into the limiter tiles and the heat is extracted mainly between pulses by

TABLE I

	BERYLLIUM WALL	GRAPHITE WALL
Limiter and Antenna protection	Beryllium tiles	Graphite tiles
Separatrix dump plates	Beryllium tiles	Graphite tiles
Wall protection	Graphite (some carbon fibre reinforced) tile coated with Beryllium	Graphite (some carbon fibre reinforced) tiles
Inconel wall	Beryllium coated	Carbonised
Antenna screens	Beryllium coated (later solid Be)	Carbonised

radiation from the large side surfaces of the tiles to water cooled nickel fins. The surface of both the limiter tile and the fin are coated to provide a high emmissivity for an improved radiation. This cooling method allows a very simple design; i.e. a simple mechanical attachment of the tiles to the fins. This is important for an easy exchange of the limiter material, when changing from a graphite to a Beryllium first wall (see Table I).

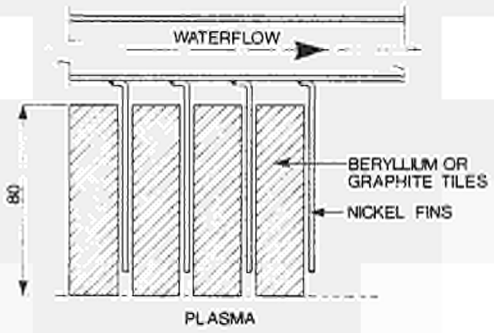

Fig. 2: Cooling of the belt limiter

(iii) Beryllium evaporator: For a "Beryllium" first wall (see Table I) only the tiles of the limiter, the antennae and the separatrix wall protection will be changed to Beryllium. The rest will only be covered with a thin Be layer (≈ 10 µm). For this purpose four evaporators (Fig. 3) are being prepared. The coating shall prevent the erosion and redistribution of high-Z impurities from the vacuum wall and the nickel screen of the antennae. Since the Beryllium coating will form an oxide layer on its surface rather quickly the evaporator will be employed periodically to deposit a fresh layer (a few Å's) of Beryllium onto the wall to eliminate the oxygen by gettering. The four evaporators are normally in a retracted position in the equatorial plane and can be moved into the torus by about 300 mm for evaporation. During evaporation the Beryllium head are radiation heated from the inside by electrically heated graphite coils.

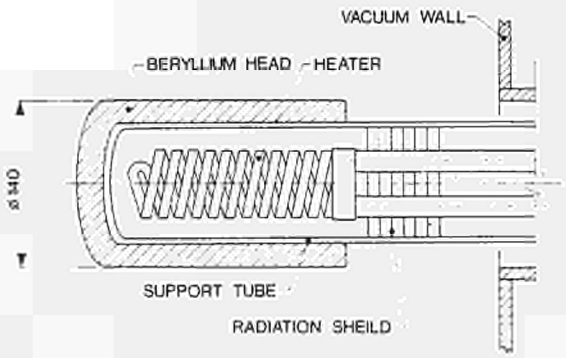

Fig. 3: Beryllium evaporator head

(iv) Separatrix dump plates: To allow X-point operation with higher power than possible with the current wall protection JET will increase the surface of the protection successively. The number of graphite protection rings will be increased to 40 (in 1987) allowing power loads as shown in curve B in figure 5. The final protection (1988) will cover the top and bottom section of the wall completely and will be mounted on a water cooled support structure (see curve C in Fig.5). Similar to the belt limiter the protection tiles will be kept cool during the discharge by thermal inertia. The heat will be extracted between pulses, however, by heat transfer through pressure contacts to the water cooled base structure as indicated in figure 4. As for the limiter, the design will allow an easy change from graphite to Beryllium tiles (see Table I).

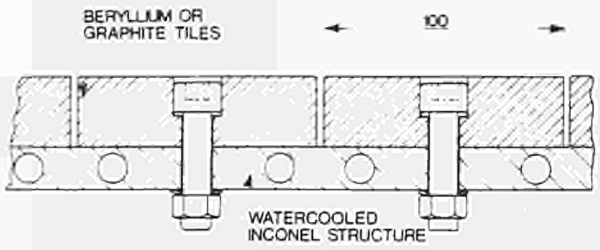

Fig. 4 Schematic diagram of Separatrix dump plates.

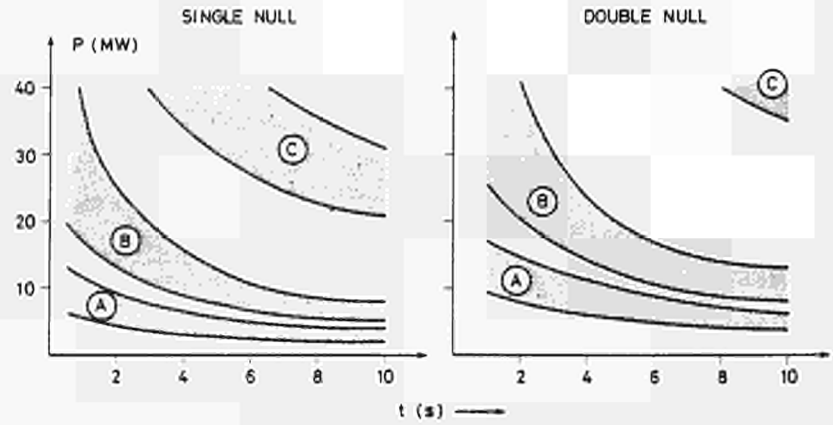

Fig. 5 Total power as a function of the pulse length to reach a surface temperature of the dump plates of 900°C for Be and 2200° for graphite.
Curve A: status in September 1986
Curve B: 40 graphite rings
Curve C: complete coverage with protection tiles.

The hatched areas are limited by curves representing different powers dissipated by radiation (upper limit 50%, lower limit 0% radiation).

2. PARTICLE CONTROL

The particle control in JET will be achieved through:

1. particle exhaust by adequate pumping and
2. particle fuelling by pellet and neutral beam injection. Only pellet injection shall be discussed here.

2.1 Particle exhaust

Introduction: An adequate pumping is necessary to avoid disruptions after switch off of the auxiliary heating by reducing the density below the safe limit for ohmic discharges. There is also hope that by pumping one can tailor the density profile during NB and pellet injection and improve thereby the plasma performance. Although it has been shown that the particle confinement time can be improved by pellet injection due to the still longer pulse

time of JET a substantial pumping will be required during pellet injection to keep the edge density sufficiently low while the central density is high. JET follows two concepts for pumping.

(i) Wall pumping

The first concept is used already routinely. When the plasma is moved towards the inboard graphite protection tiles a strong wall pumping effect is observed. The particle removal rate due to this effect is sufficient to reduce the plasma density obtained with the present level of auxiliary heating to values below the ohmic limit so that the discharge indeed can be terminated without a disruption. A typical example is shown in Figure 6. From this and other discharges particle removal rates of up to 3.10^{21} particles per second can be estimated corresponding to pumping rates of about 50 mbar l/s. The pumping rate sometimes decreases to values of ≈ 10 mbar l/s after a few seconds during pump down. No deterioration or satuturation of the pumping rate has been observed, however from shot to shot.

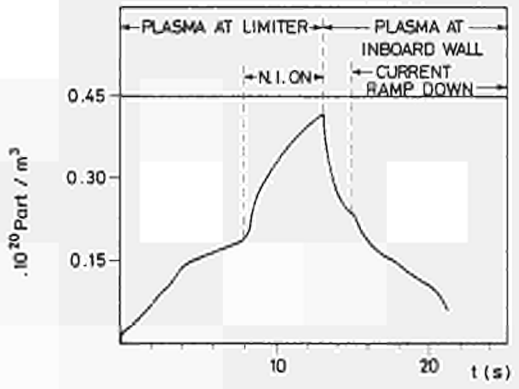

Fig. 6: Wall pumping effect in JET

Qualitatively the effect behaves somewhat like the transient pumping effect many times observed for hydrogen on metal surfaces [e.g. 17], however it has not been seen yet for graphite. It is unlikely that the metal wall above and below the inboard graphite protection tiles causes the effect, since the wall pumping is also observed for carbonised walls. Hydrogen trapping in a surface layer of the graphite has been found by several groups [e.g. 18], but the effect quickly saturates in contrast to the observation in JET. One group using a tritium plasma source to simulate the hydrogen flux did, however, find deeper penetration of the hydrogen at medium temperatures (above 300°C) probably due to a diffusion along the open porosity of the graphite [19]. Further measurements particularly with graphite used at JET and a plasma sequence simulating the JET plasma are required to find out whether this observation can explain the wall pumping in JET. The measurements will be extended also to address the question whether a similar wall pumping can be expected when JET is operated with a Beryllium wall. For this purpose hydrogen recycling measurements will be performed in the Nat. Lab. Sandia, Livermore, for graphite, for Beryllium coated graphite and for solid Beryllium. The simulation experiments in Sandia will also study another mechanism based on the sputtering of carbon from the graphite tiles and on a subsequent codeposition of carbon and hydrogen. Also the redeposition of hydro-carbon fragments resulting from chemical sputtering appear important. It should be noted that the existence of a temperature dependent chemical sputtering has recently been demonstrated for JET relevant fluxes as well as the existence of a redeposition regime for hydro-carbons [33].

ii. Pump Limiter

The second concept for particle exhaust in JET will employ pump limiter which proved in other tokamaks of being capable to remove 5 - 10% [20] of the total particle outflux from the plasma core. JET has started a programme to develop pump limiters as a back-up solution if the observed wall pumping turns out to be insufficient. The pump limiter modules will be positioned somewhat behind the main belt limiter thereby protected against runaway electron damage. Since the plasma edge parameters under these conditions are not yet known JET will follow a two step strategy. A prototype of simple design and only inertia-cooled (operational only for 1-2s per discharge) shall be used to measure the pumping efficiency possible under the JET boundary conditions (i.e. belt limiter being the main limiter). In a second step an actively cooled pump limiter shall be installed which can be operated continuously during a JET pulse.

The prototype pump limiter will be built out of carbon fibre reinforced graphite because this material - as tests at JET [9] have shown - has the highest thermal resistance. With a leading edge only cooled by inertia we expect that heat loads of about 2 kW/cm^2 can be sustained but only for 1 or 2 secs. This means that the limiter must be designed with a movable blade to retract the leading edge after less than 2 seconds by a few e-folding lengths. For removing the particles from the pump limiter JET will concentrate on developing conventional pumping through two main horizontal ports using, e.g. cryopumps in the JET pumping chambers. If this turns out to be insufficient pumping panels (Zr-Al getter or Titanium sublimation getter) inside the pump limiter as used in other pump limiter experiments [20] will be studied. We have estimated the pumping efficiency as a function of the scrape-off length using a simple 1-dimensional edge model. The result is shown in figure 7.

We have started more detailed calculations using a 2-dimensional plasma transport model to provide better plasma edge parameter as input data for a 3-dimensional Monte Carlo Code[20] calculating the neutral gas transport inside the pump limiter module.

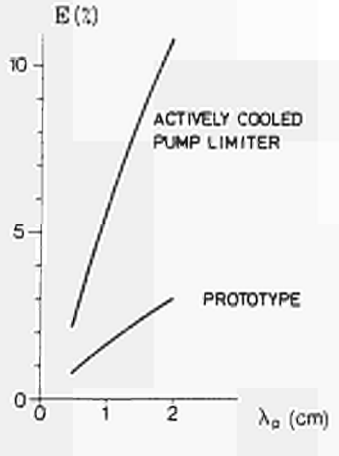

Fig. 7 Pumping efficiency, E as a function of the scrape off length λ_p. The following assumptions have been made:

* density, flux and temperature decay exponentially with the same e-folding length for density and temperature
* a high electron temperature at the plasma edge T_{el} = 300 eV (low radiation in case of Beryllium)
* total particle efflux from the plasma core of $7.5.10^{22}$ part/s
* length of the leading edge (2 m for prototype and 8 m for actively cooled limiter)
* thickness of leading edge (1 cm for prototype and 1.5 cm for actively cooled limiter)
* 50% of all particles entering the limiter throat will be pumped.

The calculations will be performed for two different designs of the prototype limiter. In one case the pump limiter will be positioned between the two belt limiters close to a pumping chamber providing a short pumping duct but having the disadvantage of a small-scrape off length due to a short connection length between the two belts of the limiter. Alternatively the pump limiter can be positioned above or below the belts of the limiter where a much larger scrape off length can be expected but it would require a rather long pumping duct to the pumping chamber. Also parts of the belt limiter would have to be removed to provide space for this duct.

For the actively cooled pump limiter a leading edge is envisaged which can sustain a stationary heat load of 3 kW/cm^2 and will be plated by either Graphite or Beryllium to be compatible with the low-Z concept of JET. The pumping efficiency which can be expected for an actively cooled pump limiter is shown in Figure 7.

Since the prototype pump limiter will not be installed before 1987 and in order to have as soon as possible sound input data for the design of the actively cooled limiter JET is planning to install simple plasma scrape-off probes to measure the plasma edge parameter after installing the belt limiter. It has been shown [22] that simply by measuring the pressure built up in a tube behind a scrape off blade the particle flux in the scrape off layer can be estimated (see Fig. 8).

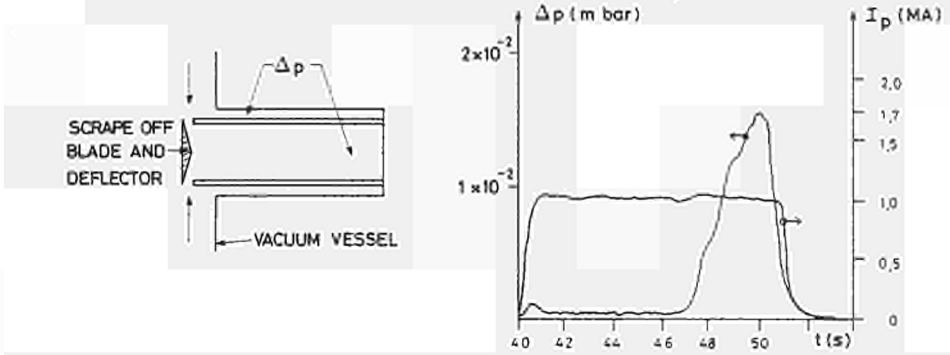

Fig. 8: Schematic diagram of the plasma scrape-off probe and a typical pressure signal (A total flux into the throat of the probe of about 10^{21} part/s can be estimated).

2.2 Particle fuelling

Introduction: It has been shown by several groups [23, 24, 25, 26] that pellet fuelling far beyond the recycling zone can result for ohmic discharges

- in an increase (recently as much as a factor five [25]) of the central plasma density with the edge density essentially being unchanged
- in a remarkable improvement of the plasma confinement data. The effect on plasmas heated by a large amount of neutral beam power is less clear.

The hope of diluting impurities in the plasma core by pellet injection as earlier claimed by PDX and ALCATOR did not receive supporting evidence from recent experiments; however differences are notable, e.g., between ASDEX and ALCATOR on the one hand, finding density limits due to high-Z radiation (Fe and Mo, resp.) in the plasma centre and TFTR on the other hand where only low-Z radiation and Bremsstrahlung are dominant. It is not yet clear whether these differences are connected with the fact that the pellets in TFTR penetrated deeper into the plasma. There are, however, indications from TFTR that the plasma performance improves with the penetration depth of the pellet.

There is theoretical and experimental evidence [27;28] that the pellet penetration depth is strongly affected by the electron temperature, where as the influence of high energy ion from NB injection on the penetration is less clear [26]. Estimating the pellet penetration for JET relevant conditions with the neutral shielding model [27] it appears that pellet injection beyond q=1 would require much higher pellet velocities ($\geq$ 5000 m/s) than available with present injectors (1500 m/s). JET is therefore following a two-way strategy ie to study from 1986 onwards the plasma behaviour with technical available low speed (= 1500 m/s) pellet injection and to develop high speed injectors in parallel.

(i) Low speed injectors

For initial studies JET presently uses a single pellet injector. The unit allows to fire one pellet (choices are 2.6; 3.6; or 4.6 mm diameter) per discharge with a maximum injection speed of about 1500 m/s. From the middle of 1987 a multipellet injector will be available. As shown in Fig. 9 it consists of a triple barrel launcher supplied by Oak Ridge National Laboratory, and a JET vacuum interface composed of a differential pumping system employing a cryopump and a vacuum vessel as used for the neutral beam injectors of JET and connecting it to the Torus via three flow restrainer tubes and shut-off valve.

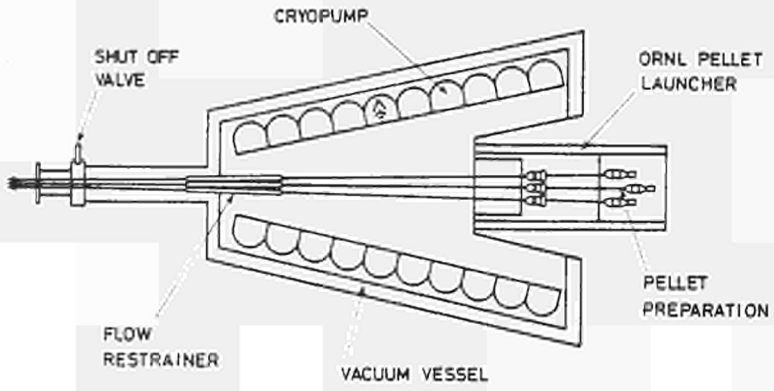

Fig. 9: Schematic diagram of multipellet injectors

The ORNL-injector can fire 2.6, 4 and 6 mm diameter pellets, with a maximum repetition rate of 5 per second. The repetition rate required depends strongly on the particle confinement time achieved with pellet injection but taking into account the limited capability for particle removal* and for heating the particles** it is certain that the repetition rate of the ORNL injector is sufficient. The ORNL injector uses pneumatic guns with up to 120 bar pressure of the propellant gas resulting in maximum pellet speeds of about 1500 m/s. The pellet is punched out of a solid deuterium ribbon prepared by an extrusion technique.

The cryopump provides a pumping speed of about 10^7 l/s which allows to fire pellets at the rate mentioned above using up to 3 barl of propellant gas for each pellet. Under these conditions propellant gas would enter the torus through the three restrainer tubes at a rate of less than 0.01 mbar l/s. The capacity of the cryopump (= 4000 barl) is sufficient for one day of operation before regeneration.

---

* compare particle removal rate of $3\text{-}8.10^{21}$ part/s with 3.10^{21} particles in a 4 mm diameter pellet.

** 7 MJ required to heat 3.10^{21} particles to 5 keV.

(ii) For the development of high speed injector JET will concentrate on pneumatic guns, other concepts such as a rail gun development for hydrogen pellets appear unlikely to be completed within the time frame of JET. The presently used pneumatic guns do not allow high pellet velocities because only low temperature propellant gas is employed. It has been shown theoretically [29] that much higher velocities could be achieved with hot propellant gas since clearly a high pressure for accelerating the pellet can only be maintained at the pellet as long as the sound velocity of the gas is not much lower than the speed of the pellet. Two stage light gas guns (See Fig. 10) in which the hydrogen propellant gas is heated by adiabatic compression in the first stage to temperatures of $\geq$ 5000 K, accelerated projectiles close to 10 km/s [29]. These experiments have been performed, however, with very high pressures (10^4 bar) and projectiles which were much stronger than hydrogen pellets. Nevertheless numerical calculations at JET showed that with driving pressures at the pellet as low as 100-200 bar (still higher than currently used in pellet injectors) hydrogen pellets should reach similar velocities employing hot propellant gas. Because of the limited strength of the hydrogen pellet it is important to tailor the pressure in the first stage of the gun so that the pressure behind the pellet always maintains the maximum value given by the strength of the pellet ("constant base pressure gun"). For an efficient pellet acceleration it is also advantageous that the pellet starts moving only when the pressure has reached its maximum value (break-away pressure = maximum acceleration pressure). The maximum possible pressure depends on the quality of the hydrogen ice. It is therefore important to find optimal condition for preparing the hydrogen ice. JET has started a development programme for addressing these problems in collaboration with other laboratories.

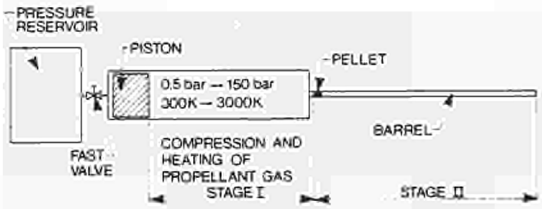

Fig. 10: Schematic diagram of a two stage gun

Heating of propellant gas: JET has started the design of a two stage gun with the propellant gas heated by adiabatic compression. To keep the design as simple as possible but sufficient to prove that velocities of about 5000 m/s can be achieved a dispensable piston will be used. In a second step JET will develop a repetitive two stage gun for pellet acceleration.

As an alternative heating method for the propellant gas the National Laboratory Riso is studying an electric arc heater for JET [30]. With a preliminary set-up pellets (3.2 mm diameter) have been accelerated close to 1800 m/s. Higher velocities should be achieved with optimized arc parameters, i.e. faster current, voltage rise, a higher arc power and a sufficient burning time. Recently the desired pressure-time behaviour has been achieved for the first 200 µs, a higher arc power will be available soon, as a new power-supply and a high pressure arc chamber will be in operation.

"Constant base pressure gun": As an intermediate step for developing a two stage gun

with the propellant gas heated by adiabatic compression JET has placed a contract with the Ernst Mach Institute in Freiburg to study a constant base pressure gun. This gun uses adiabatic compression to tailor the pressure in the second stage so that the pressure at the pellet remains about constant. To limit the technical problems the compression ratio are small enough to keep the gas temperature low (≈ 700°C). Nevertheless theoretical calculations show that velocities close to 3000 m/s can be expected. The system will be used to accelerate plastic pellets with similar density and strength as hydrogen ice. In order to simulate the influence of the break-away pressure of the pellet on the maximum speed either bursting discs or a fast valve unit can be built into the system between the gas compression stage and the pellet. Rather promising results have been achieved during first tests (pellet velocities of 2600 m/s) already.

Pellet preparation: JET has placed a contract with CEN Grenoble to improve the technique of pellet preparation. At CENG instead of using an extrusion-punching technique [31] the pellet is produced by cryo condensation of the pellet directly in the barrel [32]. For this purpose a short zone (freezing cell) of the barrel is cooled down below freezing temperatures of hydrogen. By selecting the temperature of the freezing cell and the pressure of the hydrogen gas according to the vapor pressure curve of hydrogen, good quality pellets of 6 mm diameter and the right length have been produced. For testing the ice quality - by accelerating the pellets with a high gas pressure pulse - CENG developed a fast valve capable of generating an initial pellet acceleration of about 4.10^6 m s^{-2}. Pellets of 6 mm diameter withstood these acceleration forces without fracturing proving that the ice quality is at least as good as that from extruded ice. For pellet velocities of ≈ 5000 m/s still somewhat higher accelerations (> 10^7 m s^{-2}) are required. Whether the ice can withstand these forces can only be tested when propellant gas with higher pressures and probably higher temperatures will be available.

It has been shown that pellet condensed into the barrel feature rather high break away pressures (≈ 40 bars) which is important for an efficient pellet acceleration.

Since pellet production by cryocondensation generates less excess material than extrusion techniques it is better suited for being used in the tritium phase. Excessive tritium would create problems with cryopumps and the tritium regeneration plant.

REFERENCES

[1] REBUT, P.H., DIETZ, K.J., 12th SOFT, Julich (1982).

[2] REBUT, P.H., et al., JET - Report (85) 03.

[3] HUGUET, M., et al., 11th Symp. on Fusion Eng., Austin, Texas (1985).

[4] WINTER, J., 7th Int. Conf. Princeton, N.J., U.S.A. (1986), 8.I.2.

[5] BEHRINGER, K., JET Report (85) 01.

[6] 7th Int. Conf. Princeton, N.J., U.S.A. (1986). See papers 7.8, 8.1, 8.3, 8.5, 8.8, 8.10, 8.15, 8.22.

[7] REBUT, P.H. and HUGON, M., 10th Int. Conf. on Plasma Physics and Controlled Nuclear Fusion Research (1984), London.

[8] DIETZ, K.J., SONNENBERG, K., DEKSNIS, E. Int. School of Fusion Reactor Technology (1985) p.317.

[9] MASSMANN, P., et al. JET-DN-C (86) 29.

[10] TANGA, A., 12TH European Conf. on Controlled Fusion and Plasma Physics, Budapest, (1985), paper 179.

[11] BRINKSCHULTE, H. et al., 13th Eur. Conf. on Controlled Fusion and Plasma Heating, Schliersee (1986).

[12] COAD, J.P., BEHRINGER, K., and DIETZ, K.J., 7th Int. Conf. Princeton, N.J. U.S.A. (1986) 8.23.

[13] MIODUSZEWSKI, P.K., et al. Report on Beryllium Limiter Experiment in ISX-B.

[14] BESSENRODT-WEBERPALS, M., HACKMANN, J. and UHLENBUSCH, J., 7th Int. Conf., Princeton, N.J., U.S.A. (1986), paper 10.4.

[15] WATSON, R.D., and WHITLEY, J.B., J. of Nucl. Eng. and Design, to be publ.

[16] CELENTANO, G., et. al. this conf.

[17] WAELBROECK, F., J. Nucl. Mat. 111 & 112 (1982) 185.

[18] DOYLE, B.L., et al., J. Nucl. Mat. 103 & 104, (1981), 513.

[19] CAUSEY, R.A. and WILSON, K.L., Sandia Report, SAND 85-8675.

[20] MIODUSZEWSKI, P., et al. J. Nucl. Mat. 121 (1984) 285.

[21] REITER, D., Jul. 1947 (1984) ISSN 0366-0885.

[22] HEMMERICH, J. Private communication.

[23] GREENWALD, M. et al. Phys. Rev. Letters 53 (1984), 352.

[24] SENGOKU, S. et al., Nucl. Fusion 25 (1985), 1475.

[25] MILORA, S.L., et al. pres. for publication.

[26] KAUFMANN, M. 13th Eur. Conf. on Controlled Fusion and Plasma Heating, Schliersee (1986).

[27] MILORA, S.L. and FOSTER, C.A., ORNL TM-5776 (1977).

[28] THOMAS, C.E., ORNL TM-7486 (1981).

[29] SEIGEL, A.E., NATO Report AGARD 91.

[30] ANDERSON, S.A., et al., this conference.

[31] COMBS, S.K. et al., Rev. Sci. Instrum. 56 (1985) 1173.

[32] LAFFERRANDERIE, J., et al., this conference.

[33] GOEBEL, D.M., et al., to be published.

PLANS FOR CURRENT PROFILE CONTROL IN JET

C. Gormezano, J. Jacquinot, P.H. Rebut, G. Bosia, R.J. Anderson, H. Brinkschulte, J. Cordey, C. David*, J.A. Dobbing, A.S. Kaye, D. Moreau*, T.J. Wade

JET Joint Undertaking, Abingdon, Oxon, OX14 3EA, England
*Associated Staff from EUR-CEA, CADARACHE, France

ABSTRACT

Studies for controlling the plasma current with the existing JET equipments (Neutral Beam Injection, Ion Cyclotron Resonance Frequency) are summarized together with conceptual studies of new systems: Lower Hybrid Current Drive, Electron Cyclotron Resonance. A more detailed analysis of the LHCD system, which is the most promising, is given outlining the critical technological issues.

1. INTRODUCTION

The profile of the plasma current in a tokamak is a key parameter in determining the confinement of the plasma. The radial location of the rational q surfaces together with the value of the plasma current gradients at these surfaces are essential parameters for the equilibrium and for the stability of the discharge. Generally, the plasma current is created in tokamaks by ohmic induction. The current density is proportional to the induced DC electric field through the Spitzer resistivity which is a direct function of the electron temperature. The plasma current profile is then determined by the profile of T_e. One important consequence of such a tight link between plasma current and electron temperature is that internal relaxations of the temperature and of the density occur when the electron temperature profile is such that the safety factor is below unity within a significative volume of the plasma column. This effect becomes dramatic when a large amount of additional power is coupled to the plasma. In JET, the amplitude of the sawteeth during ICRH and NBI is increased by a large factor. For P_{HF} = 5.5 MW, T_e increases up to 5.6 keV and drops by 1.8 keV during the relaxation [1].

It is also observed in JET [2], as well as in other several large machines, that the radial profile of T_e is a weak function of the additional heating power and of its localisation and that the peaking of Te and the radial location of the q = 1 surface are mainly determined by the safety factor at the plasma edge. This profile consistency can be interpreted as due to the topology of the magnetic field lines when ordered structures such as magnetic islands coexist with ergodic domains [2]. Other theoretical models on profile consistency such as the tearing mode based model of [3] and the minimal energy principles of [4] also involve the tight correlation between electron temperature and current density profile through resistivity.

Good plasma confinement can then be possibly obtained by controlling the current profile so that the location of the q = 1 surface as well as the local shear are modified. This requires current and temperature profiles not to be coupled through the resistivity. This can be obtained by driving the current with non inductive methods. As well, slide-away regimes, where part of the current is carried by decoupled fast electrons, have a broader current profile.

Discharges where a significant part of the plasma current is produced via non inductive current drive are presently obtained via Lower Hybrid Current Drive (LHCD) and Neutral Beam Injection (NBI). The beneficial effects of non inductive current drive are already observed in LHCD experiments where the OH plasma current was completely or partially replaced by HF induced current (see for instance [5]). Internal relaxations are supressed in a large range of plasma parameters ($\bar{n}_e$ up to $1.3\ 10^{20}\ m^{-3}$) both in OH plasmas and in NBI heated plasmas [6]. Large electron heating with profiles broader than the OH profiles have been observed [7]. The decoupling between electron temperature profile and current profile has clearly been demonstrated [6]. Although there are some indications that the confinement time improves, the behaviour of the energy confinement during strong additional electron heating is not well documented so far.

Preliminary observation of the MHD behaviour of discharges where part of the plasma current is driven by NBI in JET have shown that the sawteeth period increases by a large factor (from 0.06 sec up to 0.4 sec). It is to be noted that long duration sawteeth have been obtained in JET when both NBI and ICRH are applied [8]. With 2.7 MW of NBI and 5.4 MW of ICRH, T_e increases from 3.8 keV up to 6.4 keV staying at this high value for more than 1 sec before an internal relaxation occurs, the MHD activity being at a very low level. Interpretation of this behaviour is still going on and in particular the effect of NBI current drive enhanced by fast ion coupling with ICRF and an eventual change in current profile is under consideration. The loss of energy during the subsequent sawtooth represents 28% of the total stored energy.

JET is presently evaluating means of controlling the current profile with the following aims: (i) to avoid the occurrence of internal disruptions in order to achieve a higher central plasma pressure and to obtain, therefore, a higher fusion reactivity. (ii) to yield information on the mechanism of profile consistency and eventually to improve the energy confinement time.

Current profile control can be obtained either by producing non inductive current drive in the plasma centre, via suprathermal electrons or fast ions, or by producing the current in the outer part of the plasma column. The amount of plasma current which has to be non inductively driven is estimated to be of the order of 30% to 50% of the total plasma current. Studies are made for the two density regimes foreseen for JET:

- at moderate densities ($\bar{n}_e < 5\ 10^{19}\ m^{-3}$) where large fusion yield can be foreseen (hot ion mode)
- at large densities ($\bar{n}_e > 5\ 10^{19}\ m^{-3}$) relevant for ignition type experiments.

Limiter operations ($I_p \leq 7$ MA) and X-point mode of operation ($I_p \leq 4$ MA) have to be considered.

In this paper, controlling the current profile with the existing JET equipments (NBI, ICRF) is considered together with the procurement of new systems such as those at Lower Hybrid and Electron Cyclotron Frequencies.

2. MEANS OF NON INDUCTIVE CURRENT DRIVE IN JET

A large variety of methods can conceptually be used for non inductive current drive. The corresponding physical mechanisms are discussed in [9] and a comparison between estimated efficiencies for various methods is given in [10]. A key factor is the ratio, U_o, between the parallel phase velocity of the wave, or the energy of injected particles, and the thermal electron velocity. NBI and ICRH are optimized for low values of U_o, ECR and LHCD for large values of U_o, ie for energetic electrons. It is to be noted that current drive efficiency of all schemes, except ohmic, is inversely proportional to density. For both beam injection and RF schemes, accessibility of region in which current drive is required for controlling the plasma current is an important parameter. The large size of the plasma in JET allows more flexibility for such a purpose.

2.1 Beam driven current

One neutral beam injection system with the capability of producing 160 keV deuterons with an injected power of 10 MW is presently operated in JET up to a beam energy of 80 keV either in co-injection or in counter-injection. In the near future, it will be operated at full energy and a second similar system will be installed.

First experiments have shown that plasma current of up to 0.5 MA have been sustained for 2 sec, after shut-off of the primary current in the transformer, at densities of 1.10^{19} m^{-3}. Estimate of the NBI induced current has to take into account the back electron current, which is sensitive to the impurity content of the plasma, and the trapped electrons which reduce the number of current carriers and increase the friction of the passing electrons. The latest effect depends strongly upon the electron temperature. For the standard conditions of JET (R = 3 m, a = 1.2 m, K = 1.45, 80 keV, D into D and I_p = 3 MA), an analytical expression fitting the output of a neutral beam physics code [11] is found to be:

$$I_{NBI} = 0.05\ (\bar{T}_e/\bar{n}_e)\ P_{NBI}\ (MA, MW, keV, 10^{19}\ m^{-3})$$

Experimental data are in reasonable agreement with the code output. Specific output of the code are given in Table I. The decrease of the induced current with the density as well as

Table I
Beam Induced Current in JET assuming co-injection and τ_E = 0.4 sec

E_{inj} (keV)	number of boxes	$\bar{n}_e$ 10^{19} cm^{-3}	Z_{eff}	$\bar{T}_e$ (keV)	I (MA)
80	1	2	2.5	2.26	0.57
80	2	2	2.5	4.52	1.60
80	2	2	1	3.84	1.65
160	2	2	2.5	3.02	1.07
80	1	4	2.5	1.20	0.15
80	2	4	2.5	2.40	0.65
160	2	4	2.5	1.61	0.32
80	2	10	2.5	1.26	0.10
160	2	10	2.5	0.845	0.11

the non-linear increase of the current with the number of boxes (one NBI box is assumed to deliver 10 MW to the plasma) are due to the large variation of the electron temperature. The energy confinement time is taken to be 0.4 sec for these runs.

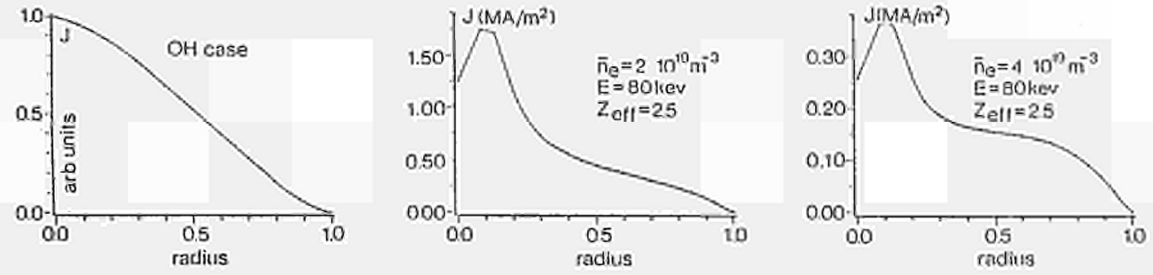

Fig. 1 : Ohmic and Beam Driven Current Profiles

As shown in Fig. 1, NBI induced current profiles are broader than the Ohmic profile. But broadening of the current profile so that the q = 1 surface does not exist any longer can only be expected in medium densities, ie $\bar{n}_e \sim 4\ 10^{19}\ m^{-3}$. At too low densities, the current is still too peaked and at high densities, the induced current is not high enough.

2.2 ICRF Driven Currents

The JET system is presently composed of 3 antennae fed by wide band amplifiers capable of delivering up to 3 MW for 20 sec in each of the antennae in well matched conditions. They can be operated independantly, either as a monopole or as a quadrupole antenna, at any chosen frequency within the band 23 to 55 MHz [12]. In excess of 6 MW of RF power have been injected so far into the torus. One of the main features of the concept which is the ability to deposit the RF power locally has clearly been observed [1].

In the near future, a complete system made of 8 antennae will be installed in JET. A network allowing the antennae to be locked at the same frequency and to be phased according to a prescribed pattern has been designed and is being constructed. ICRF induced current drive can conceptually be obtained with three possible mode of operations: mode conversion current drive, minority current drive, NBI clamping.

2.2.1 Mode Conversion Current Drive: Most of the original fast wave is converted into an ion Bernstein wave which is damped on electrons. Relativistic and electron trapping effects reduce the current drive and a maximum efficiency for JET of I/P = 0.1 (MA/MW) is to be expected for $\bar{n}_e = 5\ 10^{19}\ m^{-3}$ [13], P being the power absorbed by the electrons. Although, the efficiency is rather low, ICRF induced current can be well localized by properly choosing the position of the ion-ion hybrid resonance and by wave focussing.

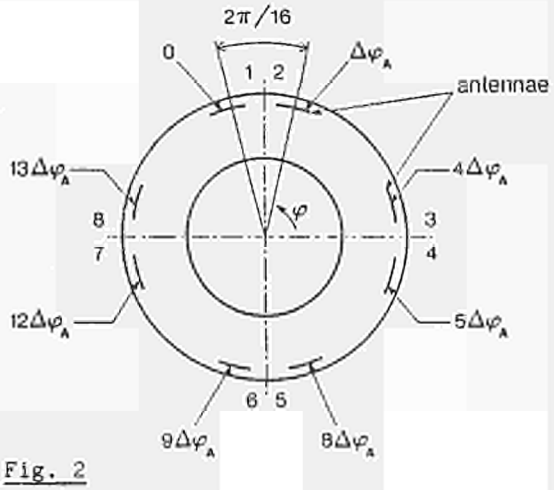

Fig. 2
Arrangement of the ICRF Antennae

The 8 antennae will be distributed in 4 pairs regularly spaced around the torus, the 2 elements of a pair being separated by 2π/16 as sketched in Fig. 2. Resonant fast electron acceleration is given by the phase difference

between antennae which give an integral number of parallel wavelength (m_ϕ). m_ϕ = 3 or 4, ie a phasing of about 90°, will be likely to be chosen for effective current drive.

2.2.2 Minority current drive: Current drive is obtained via cyclotron damping of minority ions at the fundamental resonance. Theoretical estimates have been made for JET [14]for hydrogen minority current drive in a deuterium plasma. The result exhibits a very low efficiency of I/P = 90 A/KW (for T_e = 5 keV, $\bar{n}_e$ = 3 10^{19} m^{-3}) which may be further reduced by electron return current and trapping effects.

2.2.3 ICRH and Neutral Beam Injection: The previous scheme can be significantly increased by heating neutral beam injected minority species instead of minority ion species. In this case, harmonic frequencies can be used. Simultaneous use of ICRH and NBI in JET has already shown that injected ions are accelerated by the RF at energies well above the injected energy. Theoretical estimates [13] have shown higher efficiency for such a scheme as compared to the pure ICRF driven current. It is found that currents of the order of 2 MA could be driven with the planned ICRF and NBI capability. Such a mode of operation does not require a phased antenna array.

2.3 ECRH Current Drive

ECRH experiments have all confirmed that a well localized heat deposition was produced (see for instance [15]) resulting in high electron temperature and eventually to some changes in the MHD behaviour of the plasma due to the subsequent change in the electron temperature profile. In contrast, experiment aimed at ECRH current drive have failed up to now in producing a significant amount of current.

The best efficiency for ECRH current drive is obtained when the resonant frequency is down-shifted by relativistic effects, ie when the wave is absorbed by suprathermal electrons. Such a scheme allows lower frequencies than the resonant frequency for electrons at rest (95 GHz for B = 3.4T) to be used.

Although a good localisation can conceptually be obtained, ECRH current drive should be obtained at the plasma center in order to minimize the trapped electron effects which reduce strongly the current drive efficiency. Off-axis current drive would require injection from the high field side and consequently a higher frequency.

The specific studies made for JET have shown that efficiencies in the range of 60 to 160 kA/MW can be obtained for a central deposition in the vicinity of the q = 1 surface for $\bar{n}_e$ = 5 10^{19} m^{-3} and T_e = 5 - 10 keV, with a deposition length of about 30 cm. It is to be noted that efficiency improves markedly when a suprathermal electron population is present. This is the case at low densities or if an electron tail is already created by Lower Hybrid waves.

The frequency suggested for JET is 70 GHz, although 60 GHz can also be used. Top launch on inside launch have been suggested for which technical developments are required in both cases. Presently, only quasi-DC gyrotrons with an unit HF power of 200 kW can be envisaged.

3. LOWER HYBRID CURRENT DRIVE

3.1 HF Power and Wave Spectrum: the theoretical estimate for current drive efficiency is calculated from a 2D Fokker-Planck code [16] the output of which can be fitted by the following expression:

$$I_{HF} = 20.8 \frac{4}{5 + Z_{eff}} \cdot \frac{P_{HF}}{n_e R} \cdot f(T_e) \cdot \frac{1}{\langle N_{//} \rangle^2} \quad (10^{19}\ m^{-3},\ m,\ MA,\ MW)$$

where P_{HF} is the power coupled to the resonant electrons, $\langle N_{//} \rangle$ the average value of the wave power parallel index and $f(T_e)$ a slowly increasing function which can reach 1.5 for T_e = 10 keV. The corresponding efficiency versus density is plotted in Fig. 3 for the JET conditions assuming that the HF current is peaked at the plasma centre and that 70% of the launched power is coupled to the electrons. The wave parallel index is set so as to meet wave accessibility conditions at the plasma center. It is to be noted that scaling experimental data obtained in the ASDEX and PETULA devices would give for JET efficiencies ranging between 0.1 and 0.15 MA/MW for $\bar{n}_e = 5\ 10^{19}\ m^{-3}$, as compared to the 0.2 MA/MW corresponding to the theoretical formula. The difference is probably related to the uncertainties in the effective HF power spectrum which is coupled to the plasma as compared to the launched spectrum.

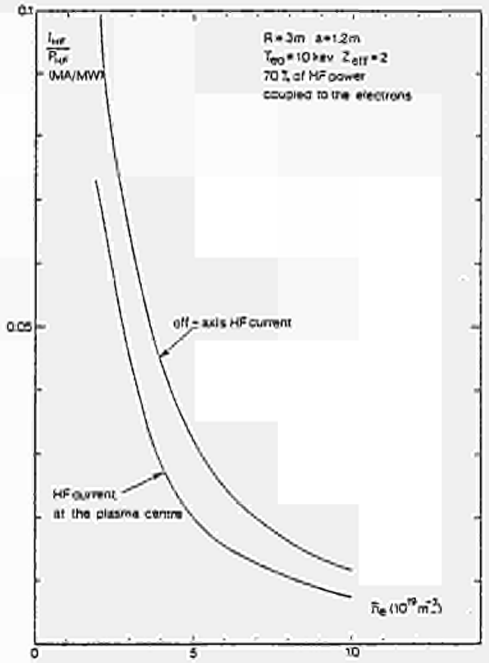

Fig. 3 : LHCD Efficiency Versus Density (from theory)

It has been proposed [17] to make use of the accessibility criteria, which is very dependant upon the density and the magnetic field, to locate the current off-axis, where the density is significantly lower than at the center. As shown in Fig. 3, where wave absorption is assumed to take place at mid-radius, an improved efficiency can be obtained in this way. Although some indications of off-axis current drive have been observed in the Petula experiment, such a scheme has not yet been proven since it requires a narrow wave power spectrum, i.e. a large number of waveguides.

Off-axis current drive is well adapted to allow flat current profiles ($q(o) \geq 1$) to be obtained at higher densities, while central current drive is well fitted for low density operation.

A design project to install a Lower Hybrid system on JET is going on with the following requirements:

- the system has to be as flexible as possible in order to control the current profile by off-axis current drive as well as by other schemes implying current drive in the central part of the plasma.
- a by-product of the use of L.H. Waves being a decrease on the flux consumption and consequently some volt-second saving, the time duration of the pulse has to be long enough.

The main parameters of the L.H. system are then:

- P_{HF} = 10 MW (launched into the torus)
- Δt = 20 sec
- $1.2 \leq N_{//} \leq 2.5$, $\Delta N_{//} \sim 0.3$
- directivity (HF power in the main lobe of the wave power spectrum): 70%

3.2 Choice of the frequency: Frequency has to be a compromise between contradictory arguments, both technical and scientific. In the range of frequencies appropriate for L.H. current drive in JET, klystrons have to be considered, gyro klystrons being more adequate at higher frequencies (≥ 8 GHz). New tubes have been developed for tokamak applications, including modern features such as an anode voltage modulation which allows the HF power to be switched off with a low power and specially designed output cavity so as to sustain high SWR. Table II list the corresponding frequencies together with some relevant figures for a 12 MW output plant allowing the choice of the frequency to be made.

Table II

Critical parameters * (for a 12 MW power plant)

f (GHz)	2.45	3.7	4.6
Number of klystrons *	12-24	24	48
Losses (transmission line) *MW	1.3	1.5	2.3
Losses (conventional grill) *MW	.6	1.1	1.6
Losses (multijunction grill)*MW	.25	.3	.4
p routine (KW/cm^2)	3-4	4	6
Pmax (MW)	7.5-10	10	15
Density limit (10^{19} m^{-3})	5	8-10	15
$N_{\perp}$ (for n = 5 10^{19} cm^{-3})	50	32	26
Resonant ion energy (keV)	375	900	1390
Optimum density at the grill mouth (10^{18} m^{-3})	.9	2	5

One of the main problems is the HF losses in the 40 metre transmission line which has to be foreseen for JET. Losses listed in table II are given for oversized waveguides including losses in some special components: tapers, bends, mode filters, ... and for launchers which have to be copper or silver coated in order to increase the surface conductivity. As compared to conventional grills, the use of multijunction grill [17] where the HF power is split under vacuum is beneficial since the length of the reduced section of the waveguide is significantly reduced.

Multipactoring and plasma edge effects at the grill mouth are thought to limit the power handling capability, p [17]. Routine values are listed in table II together with the corresponding maximum power which can be launched into one of the main JET port assuming that 1/3 of the JET port area is occupied by the HF hardware (waveguide walls, etc..).

Above a certain density ($n_{e\ell}$), the wave is preferentially damped on resonant fast ions and current drive effects disappears. The scaling of this density is: $n_{e\ell} \sim f^{\alpha}$, α ranging between 1.7 and 2.

During the propagation, the wave converts the spectrum into a perpendicular spectrum, with the following scaling: $N_{\perp} \sim n f^{-1/2}$, which can be very harmful because the increase in $N_{\perp}$ results in a change of the $N_{//}$ spectrum due to toroidal effects, so that the wave is eventually unable to reach the plasma center. Moreover the wave can be damped on fast ions, whose corresponding energy is given in Table I and which can be present during combined NBI and ICRH in JET.

Densities corresponding to a minimum in the reflection coefficient are indicated. As shown in Fig. 4, the use of a multijunction grill allows the range of densities at the grill mouth to be markedly extended as compared to a conventional grill.

Higher frequency would be preferable for wave propagation, density limit and power handling capability. Lower frequency would be preferable for lower HF losses and a higher power unit. A good compromise is a frequency of 3.7 GHz together with an oversized transmission line and a multijunction grill.

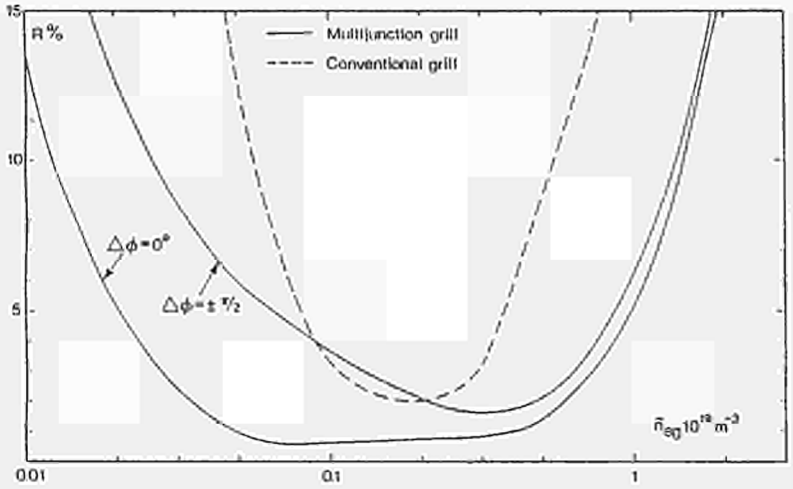

Fig. 4 : Density Dependence of the Reflection Coefficient (f = 3.7 GHz)

3.3 Overview of the Considered HF System: the launcher can possibly be composed of 48 modules of the multijunction type. Current drive and operation of such a multijunction is well documented and good agreement between theory and experimental data is observed [18]. Each module is composed of 2 horizontal rows of 4 waveguides each with a fixed phasing of $\pi/2$ between each waveguide. As shown in Fig. 5, in a JET port, 8 modules can be housed in the horizontal direction and 6 in the vertical direction.

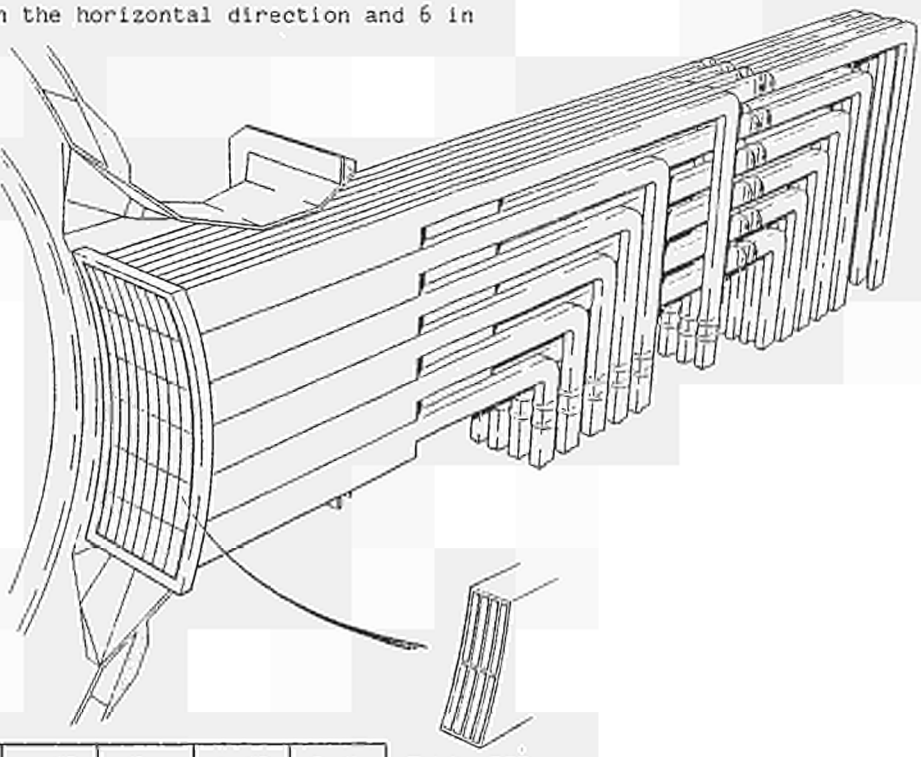

Fig. 5 : Possible Arrangement of a Lower Hybrid Launcher in JET

$\Delta\phi$	$-3\pi/4$	$-\pi/2$	0	$+\pi/2$	$3\pi/4$
N//	1.2	1.4	1.9	2.4	2.6
ΔN//	0.3	0.3	0.3	0.3	0.3
R	4%	1.5%	1%	1.5%	4%
directivity	62%	68%	72%	68%	62%

Table III

Wave spectrum which can be obtained by phasing 8 horizontal modules

The wave spectrum is determined by the waveguide width and the phasing between secondary waveguides. With an inner width of 8.5 mm and a wall width of 2 mm, the same launcher can be operated within the parameters listed in Table III depending upon the phasing $\Delta\phi$ between modules.

A wider spectrum can be obtained with the same launcher with non-equal phasing between modules. Further flexibility can be obtained by using different waveguide widths on some rows.

The reflection coefficient and moreover the directivity depends upon the width of the waveguide walls as shown in Fig. 6. The feasibility of making launchers whose wall width is lower than 2 mm is under consideration.

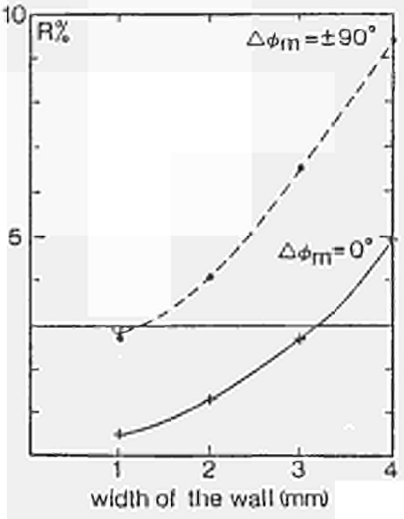

Fig. 6 : R Versus Width of the Walls.

The HF area is about 2500 cm² and the required power loading capability is 4 KW/cm². An eventual extension of unit HF power from 500 KW up to 600 KW will give p = 4.8 KW/cm² which is within the routine operation range. Grill conditioning will be obtained via baking at high temperature and wall coating: carbon coating (PLT technique) or gold coating (ASDEX technique).

The launcher will be housed in a vacuum tank, the whole launcher being movable via a bellow allowing about 30 cm of displacement to be obtained in order to adjust the grill position to various plasma configurations. With the density gradients observed to date in the JET scrape-off layer (decay length of 1.7 cm), it can be seen from Fig. 4 that positioning of the grill should be done within 5 cm for $\Delta\phi = 0$ and within 3 cm for $\Delta\phi = \pi/2$ in order to keep R below 3%. But in X-mode operation where H-mode like plasmas can possibly be obtained, the corresponding large density gradients may require that adjustment of the grill with a precision less than 1 cm has to be made. Positioning of the grill during a plasma shot (~ 1 cm/sec) appears possible.

Vacuum windows can be of the same type of the output windows of the klystron. If no development is made on the vacuum windows, 48 of them will be necessary. Due to the tritium handling, double windows with a pumping system in between are considered. Then, two adjacent modules (in a vertical direction) are fed by a single klystron, the splitting of the HF power being made after the vacuum windows. The overall layout of the launcher and of the transmission line is sketched in Fig. 7. The transmission line is being

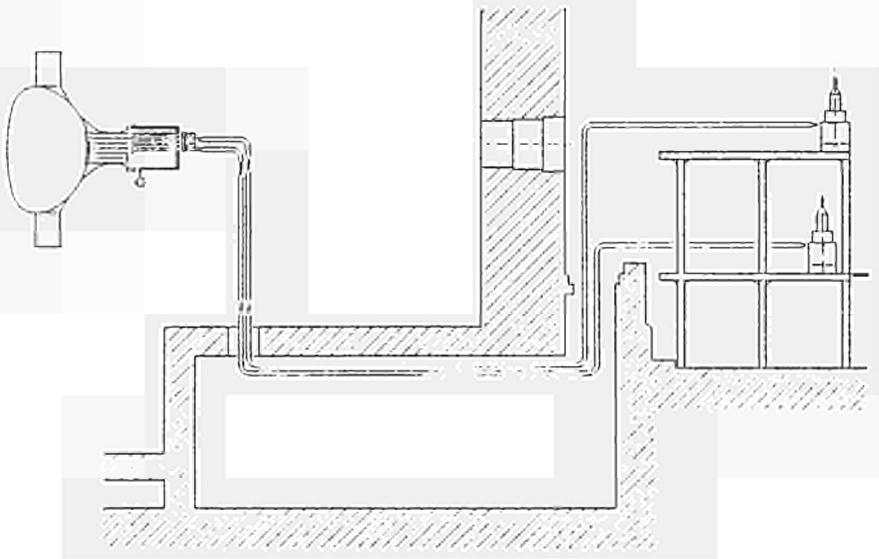

Fig. 7 : Sketch of a Lower Hybrid System for JET

designed so as to minimize HF losses. Preliminary design gives the figures listed in Table III. Part of the transmission line can be evacuated, the rest being SF_6 pressurised. The location of the vacuum windows is not yet fixed.

Table IV : WAVEGUIDE SCHEME LOSS COMPARISONS AT 3.7 GHz

SCHEME / COMPONENT	STANDARD GUIDE WG10/WR284/R32 72.14 mm x 34.04 mm	SINGLE MODE OPTIMIZED DIMENSIONS 80 mm x 40 mm	80 mm x 40 mm SINGLE MODE + AND 77 mm x 175 mm OVERMODE
WG10	0.74 (40 m)	NOT USED	NOT USED
80 x 40 mm	NOT USED	0.588 (40 m)	0.206 (14 m)
OVERMODE	NOT USED	NOT USED	0.159 (26 m)
TRANSITIONS	NOT USED	NOT USED	0.06 ?
SWITCH	0.03	0.03	0.03
FLEXIBLE	NOT USED	NOT USED	0.06
BENDS	0.04	0.04	0.04
2ND HARMONIC FILTER	0.05 ?	0.05 ?	0.05 ?
OVERMODE FILTER	NOT USED	NOT USED	0.05 ?
T O T A L (dB)	1.01	0.858	0.805
	18% loss	15% loss	18% loss

The generator consists of 24 klystrons with a power capability of 500 KW and a pulse length of 20 sec every 10 minutes. The system will be composed of 6 units of 4 klystrons which are fed by one power supply [V = 70 kV, I = 80 A] followed by a crowbar protection. The proposed klystron layout for JET is sketched in Fig. 8. Switch on and off the beam current can be obtained by changing the anode voltage. These units will be housed on two floors, the cooling and ancillaries power systems being located in the basement.

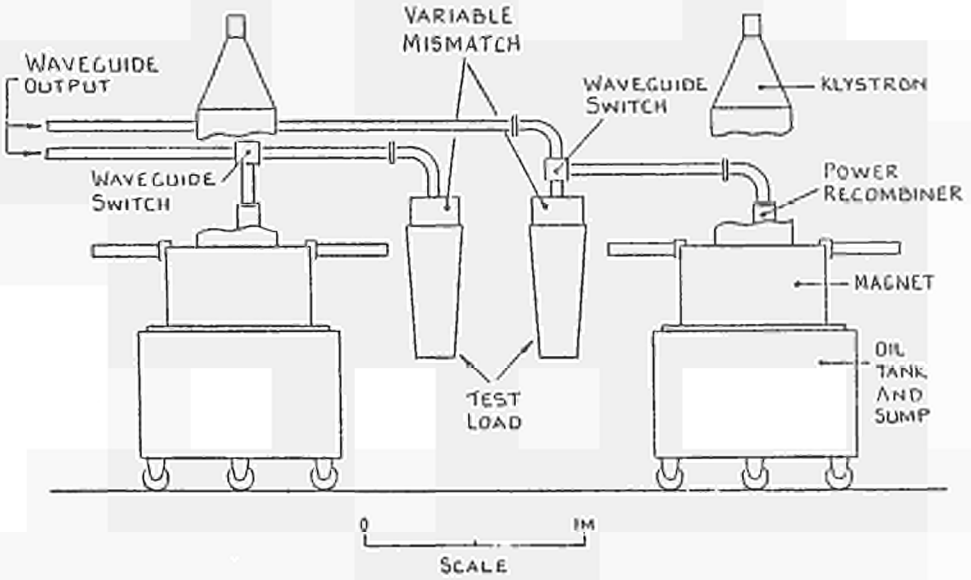

Fig. 8 : Proposed Klystron Layout

Today's 3.7 GHz klystron can sustain SWR of 1.4, ie a reflection coefficient of 3%. Higher values of the SWR can be envisaged, up to 3 (R - 25%) either by lowering the klystron output to about one third of the nominal power or by controlling the phase of the reflected power. It is to be noted that the use of hybrid junctions between 2 modules and the main transmission line can reduce the reflected power taken by the klystron.

A master oscillator gives the frequency and the reference phasing to each klystron. Relative phasing and HF power of each klystron have to be independantly controlled within a large range: 20 dB in power, 2π in phase and with a good accuracy: 5% in power, 10° in phase. Due to the fact that klystrons are amplifiers, such a control can easily be obtained on the low power side by using measurements of the amplitude and of the phase of the HF power at the launcher entrance. Feedback regulation is then obtained via phase shifters and attenuators located just before the klystron input. Special care in the phase measurement is required due to the changes in the length of the transmission line caused by power dissipation. Waveforms of the power and phase pattern will be controlled via the CODAS system.

The present design aims at installing the LH system in JET during the major shutdown at the beginning of 1990. An intermediate step is to have in operation an HF subsystem of 4 klystrons with the corresponding launcher (8 modules, 1.6 MW launched) on a testbed and possibly on JET by the end of 1988.

Summary

Basic features of the various systems which have been considered in JET in order to drive 30 to 50% of the plasma current by non-inductive means so that the current profile can be controlled are summarised in Table V. Moreover, scenarios where non thermal electrons are generated via slide away discharges are studied.

Table V : SUMMARY OF CURRENT PROFILE CONTROL SYSTEMS FOR JET

	NBI	ICRH	NBI + ICRH	ECRH	LHCD
CURRENT DRIVE DATA	OBSERVED (JET, TFTR)	PREDICTED	PREDICTED	NOT YET OBSERVED	ABUNDANT DATABASE
REQUIREMENTS FOR JET	2 BEAM UNITS E = 80 keV	8 PHASED ANTENNAE	2 NBI UNITS + 8 ANTENNAE	15 GYROTRONS AT f = 60-80 GHz TOP LAUNCH OR INNER WALL REFLECTOR	24 KLYSTRONS AT f = 3.7 GHz
POWER COUPLED TO CURRENT CARRYING PARTICLES (MW)	21	5	12	3	7
POWER AT THE GENERATOR (MW)	52	32		4	12
POWER FROM THE MAINS	65	53		10	28
CURRENT DRIVE AT $\bar{n}_e = 2\ 10^{19}\ m^{-3}$ (MA)	1.6			.5	3 to 4.5
CURRENT DRIVE AT $\bar{n}_e = 5\ 10^{19}\ m^{-3}$ (MA)	.4	.4	1 - 2	.3	1 to 1.5
AVAILABILITY OF THE FULL SYSTEM	TO BE OPERATED IN 1987	TO BE OPERATED IN 1987	TO BE OPERATED IN 1987		BEING CONSIDERED 1990

In addition to the systems which are to be installed in JET by the end of 1986: 2 NBI units and 8 ICRH antennae, a 10 MW Lower Hybrid system to be installed in 1990 is presently being considered. A first step will be to build a 1.6 MW prototype which can eventually be operated by the end of 1988.

At low densities, the current profile can be controlled via the Lower Hybrid system, while at high densities all available systems have to be used. It is to be noted that with the potentiality of all the systems: NBI, ICRH, LHCD, there will be a unique opportunity to really shape the plasma current thanks to the fact that these techniques rely on different physical mechanisms and are complementary.

Acknowledgments

Analysis work at JET was supported by Article 14 contracts with several Associations (EUR-CEA, EUR-IPP, EUR-FOM, EUR-UKAE, EUR-ERM/KMS).

References

[1] Lallia, P.P. et al, to be published in Plasma Phys. and Cont. Fusion (1986)
[2] Rebut, R.H., Brusati, M., 12th Eur. Conf. on Cont. Fusion and Plasma Physs. Budapest (1985)
[3] Furth, H.P., P.P.P.L. report 2263 (1985)
[4] Kadomtsev, B.B., paper presented at the Royal Society Meeting, London March 1986
[5] Gormezano, C., to be published in Plasma Phys. and Cont. Fusion (1986)
[6] Soeldner, F., et al, 13th Eur. Conf. on Cont. Fusion and Plasma Phys. Schliersee (1986)
[7] Hosea, J., to be published in Plasma Phys. and Cont. Fusion (1986)
[8] Rebut, P.H. these proceedings
[9] Fisch, N.J. Course and Workshop on Application of RF Waves to Tokamak Plasmas, Varenna, Vol I (1985) 46
[10] Cordey, J., Plasma Phys. and Cont. Fusion 1A (1984) 123
[11] Watkins, M.L. et al, 13th Eur. Conf. on Cont. Fusion and Plasma Phys. Schliersee, (1986)
[12] Jacquinot, J., Tokamak Start up, Erice, 1986 (ed. H. Knoepfel, Plenum Publishing Corporation)
[13] Hammen, H., et al, 13th Eur. Conf. on Cont. Fusion and Plasma Phys. Schliersee (1986)
[14] Cox, M., Start, D.F.H., Nucl. Fusion 24 (1984) 399
[15] Riviere, A.C., Plasma Phys. and Cont. Fusion (1986)
[16] Karney, C.F.F., Fisch, N.J., Phys. Fluids 28 (1985) 116
[17] Briffod, G., et al, 13th Eur. Conf. on Cont. Fusion and Plasma Phys. Schliersee (1986)
[18] Moreau, D., Nguyen, T.K., report EUR-CEA. FC 1246 (1983-84)
[19] Gormezano, C., Course and Workshop on Aplications of RF Waves to Tokamak Plasmas, Varenna I (1985) 422

PREPARATION FOR D-T PHASE OPERATION IN JET

J R Dean, T Raimondi, W Riediker, A Rolfe
JET Project, Abingdon, Oxfordshire, England

ABSTRACT

When tritium is introduced into the JET plasma the tokamak and its surroundings will very quickly become so active that all maintenance must be done by remotely controlled machines. Much of the major robotics equipment, to carry machine components and to place motorised tools in position to carry out fitting tasks, has now been constructed and is being commissioned with its control systems. The development of a variety of special-purpose tools is well advanced: they will be used to install equipment in the torus during the shutdown scheduled to begin in December 1986.

Beryllium will be introduced into the torus in 1987. Because it is harmful when inhaled, equipment has been designed and procured to control the entry of men in air-line suits and the passage of materials.

Because of the high cost of buying and then disposing of tritium, a clean-up and isotope separation plant is being designed and developed to re-process the gases exhausted from the torus and neutral beam injectors.

1. INTRODUCTION

The engineering aspects of the JET tokamak have been comprehensively described eg [1]. The expected future activation will depend on secondary neutrons from the walls produced during disruptions and on the neutrons from neutral beam-plasma interactions. Table 1 (see end of text) from [2] shows how the gamma dose rate inside the torus is expected to increase so that limited human access will be possible until 1991 when tritium will be introduced. Thereafter activation by the neutrons from fusion reactions will prohibit human intervention inside the torus hall and all engineering operations must then be performed by remotely-operated machines.

In addition to these remote-handling machines, equipment and techniques must be developed for preventing the spread of tritium, radioactive dust, beryllium and any other dangerous, dispersible materials and for carrying activated components safely to storage or disposal or, rarely, for repair. Components required to continue operating in tritium and/or neutron radiation, must be made, or shown to be, compatible in respect of material durability and guaranteed leak-tightness.

The tritiated exhaust gases from the torus and some auxiliary systems will be collected and the hydrogen isotopes chemically cleaned, separated and stored for re-use.

The system for this is being developed: it will employ cryogenics for the primary circuit accumulators, transfer pumps and impurity traps, gas chromatography for isotope separation and vacuum vessels as secondary containment.

The experience gained by putting these preparations for the D-T phase into practical effect at JET can serve as a basis for the techniques applied to future fusion machines. Very similar requirements will lead to similar design of details and so also similar solutions to the problems of remote and active handling.

2. REMOTE HANDLING MACHINES

The overall scheme of remote handling equipment is shown in Fig 1, and the bases for the designs have been presented in earlier papers eg [3,4]. There are four principal load-carrying transporters for placing and holding manipulators and other devices called end-effectors, which carry and manipulate components of the tokamak.

Of these, the articulated boom can enter the torus and carry 1 tonne loads over half of the circumference from either of two opposite ports or else 350kg round the whole circumference. Others are the 150 tonne crane, a vertical telescope arm (TARM) mounted on the crane carriage to reach most of the outside of the tokamak, and a low-level floor-mounted transporter to reach under overhangs. A turret truck serves to lift and connect the various parts of the equipment together while they are inside the torus hall, through automatically locking interfaces carrying the many services. A small, tracked, radio-operated vehicle will carry a simple manipulator, lights, television cameras and monitoring instruments on an extensible mast.

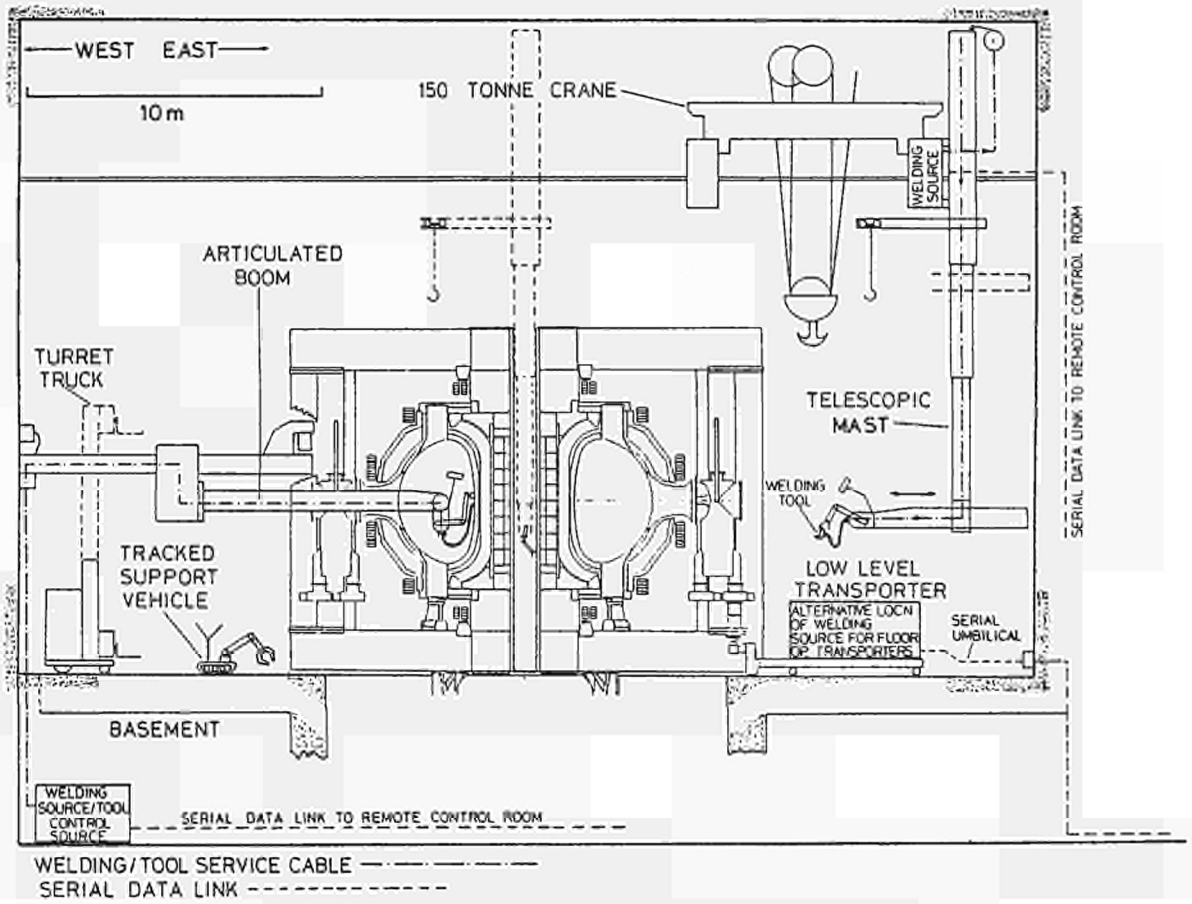

Fig 1 Overall scheme of remote handling equipment

The crane, articulated boom, turret truck and support vehicle have all been put into service, the TARM and low-level transporter are in advanced stages of conceptual design.

One Mascot IV force-feedback servomanipulator has been developed at JET to the compactness necessary to pass through the ports and the kinematic and dynamic performance necessary for its tasks. Two more with up-dated control systems are under construction. It is intended that T Raimondi and JET colleagues will publish a comprehensive paper on the manipulators and their controls, probably during 1987.

3. SPECIAL TOOLS

The manipulators may be required to exercise their dexterity in unpredicted tasks but their principal function, in collaboration with the high-precision transporters, is to place and hold in position automatic tools designed to perform the multitude of detailed and fine operations such as cutting and welding. The design of these tools and matching them in detail with the components they operate on is at the heart of successful remote handling.

3.1. Preparations for 1986-7 shutdown

Some of the new in-vessel components, notably the toroidal (belt) limiters and radio frequency antennae, to be fitted to the tokamak when it is shutdown for several months from the beginning of December 1986, are designed to be fitted by means of automatic tools. This is because of space restrictions and because automatic tools are quicker and cleaner and give better quality and more consistent results than can be achieved by hand. Prototypes of many of the tools have been made and tested and sufficient numbers are being manufactured to meet the work load. They will be placed and operated by hand in the next shutdown, but they are easily adaptable to full remote operation.

These tools are more fully described in the poster presentation HP 42 of this symposium [5]. Examples are described briefly in the following sections.

3.2. Circular ports

Circular ports, with nominal diameters ranging from about 90 - 155mm, do or will contain blanking plugs, windows for diagnostics, or other penetrations such as water pipes for toroidal limiters. About 100 of these need to be changed in the forthcoming shutdown by cutting out an inner sleeve fillet welded to an outer sleeve and welding in a new one.

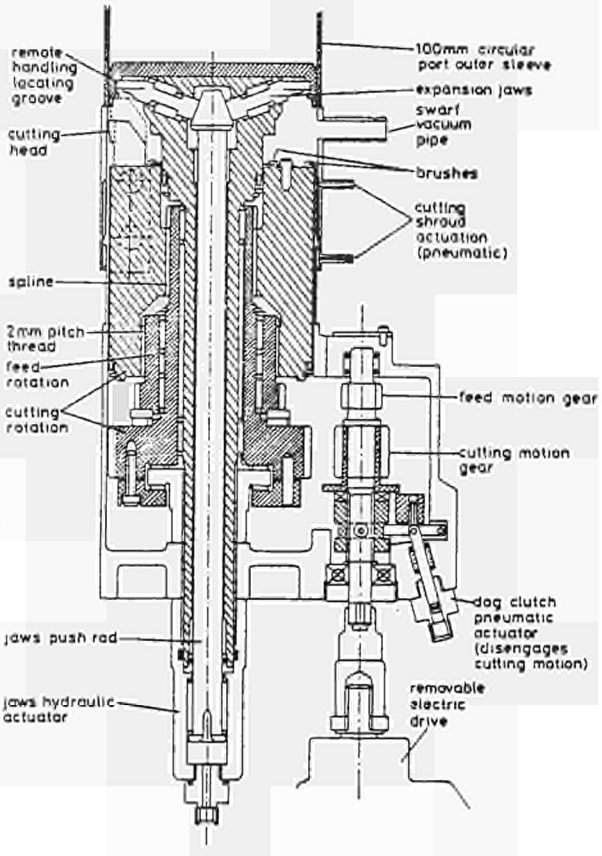

Fig 2 Circular port lip cutter

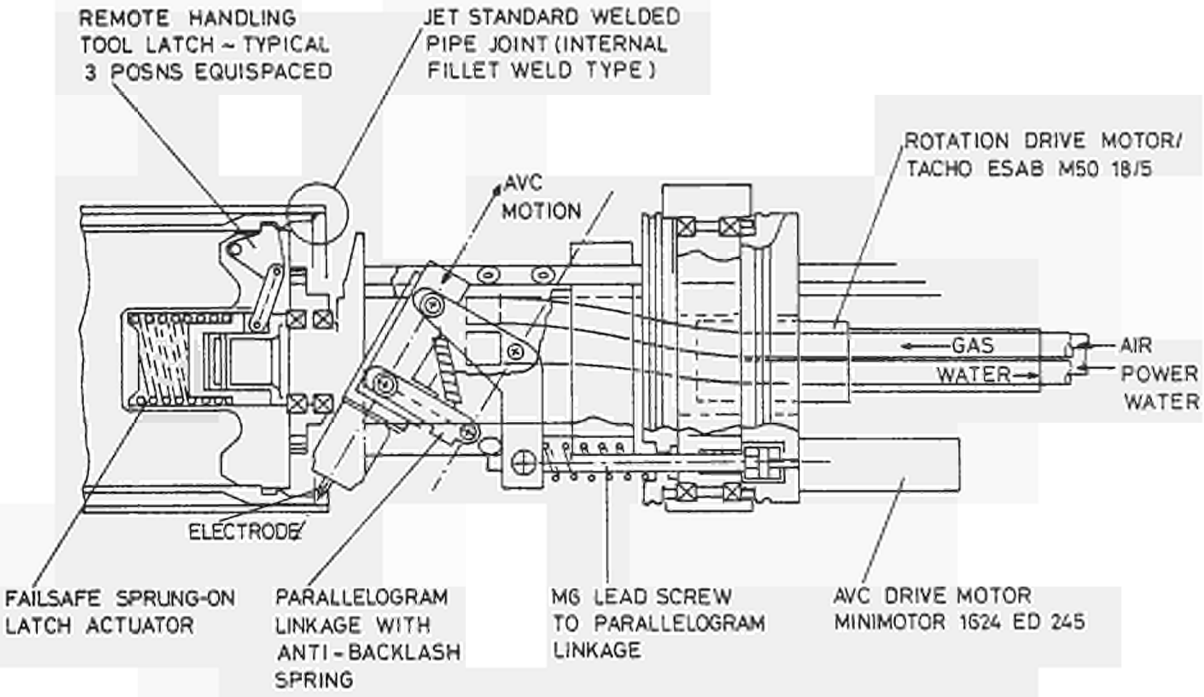

Fig 3 Remote welding tool (one of four weld path diameters) for JET standard pipe joint of internal fillet weld type

Four types of special automatic tools have been developed. One, illustrated in Fig 2 will cut away the welded lip joint, one will pull out the inner sleeve with forces up to 10 tonnes, one will place and expand the new inner sleeve to compensate for clearances and weld distortions and so close the welding gap and finally, as illustrated in Fig 3, the internal weld will be made by an automatic fillet welder supplying filler wire.

These tools demonstrate some important principles. The sizes and shapes of vacuum vessels and similar fabricated components are often outside tolerances, replacement components must be designed to accommodate the variations, and assembly will have been carried out with little regard to dismantling so that large forces or extra cutting are needed to separate components. Also special remote handling features on the components are usually essential, in this case the groove which provides a grip and acts as a reference surface.

3.3. Toroidal (belt) limiters and radio-frequency antennae

One of several operations in fitting or replacing these components is to cut and re-weld the joint in the water pipe just below the bellows as illustrated in Fig 4. Three special tools have been developed. One is a motor-driven slitting saw capable of entering through a gap 40mm deep, gripping a 50mm diameter, 2.5mm wall Inconel pipe with 23mm radial clearance behind it and cutting it square to 0.1mm, so cleanly that the surfaces are ready for re-welding. The second is an orbital welder to make an autogenous butt weld between a new section of rigid pipe and the bellow assembly. A third tool is used throughout these operations to manipulate the bellows assembly, compressing them to remove the rigid section and later realigning the ends to be welded.

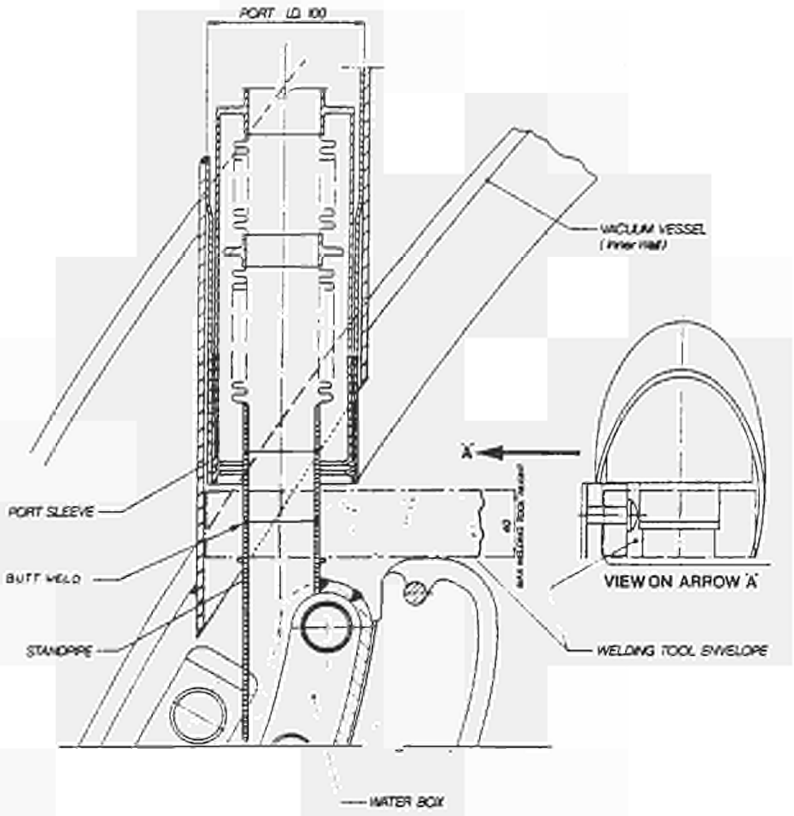

These tools show what can be achieved by collaboration between the tokamak component designers and the remote-handling tool designers and ingenuity in the tool designs in cases where intricate operations in very restricted spaces are unavoidable.

Fig 4 Limited space for cutting and welding toroidal limiter water pipes

3.4. Toroidal limiter tiles

The tile handling tool shown in Fig 5 demonstrates effectiveness with simplicity achieved by practical skills in hands-on development on a mock-up. The tool is held and operated by a servomanipulator gripper. Two prongs are entered between grooves and rotated to free the tiles from their spring-loaded attachments. A safety latch is pneumatically released remotely, but can be operated by the second manipulator arm if the pneumatics fail, following the principle of making any remote-handling device capable of disengagement and retrieval.

3.5. Vacuum flange welding and cutting

Commonly used vacuum joints in JET are welded pairs of 2mm Inconel plate, as used to connect the octants of the torus vessel. A cutter head and a welding torch on self-propelling trolleys to cut off and replace the welds has been described earlier [4]. Because of their universal application and the high quality of the joints they can produce, considerable effort has been devoted to simplifying and improving these tools. They will now follow any plane contour with radii of not less than 70mm and also the edges of concentric cylinders down to 180mm diameter. The cutter leaves extremely even edges suitable for autogenous welding and the welder produces joints of extraordinarily high quality.

Fig 6 shows the simplified and compact trolley, with only two wheels replacing the original four, carrying a cutter head.

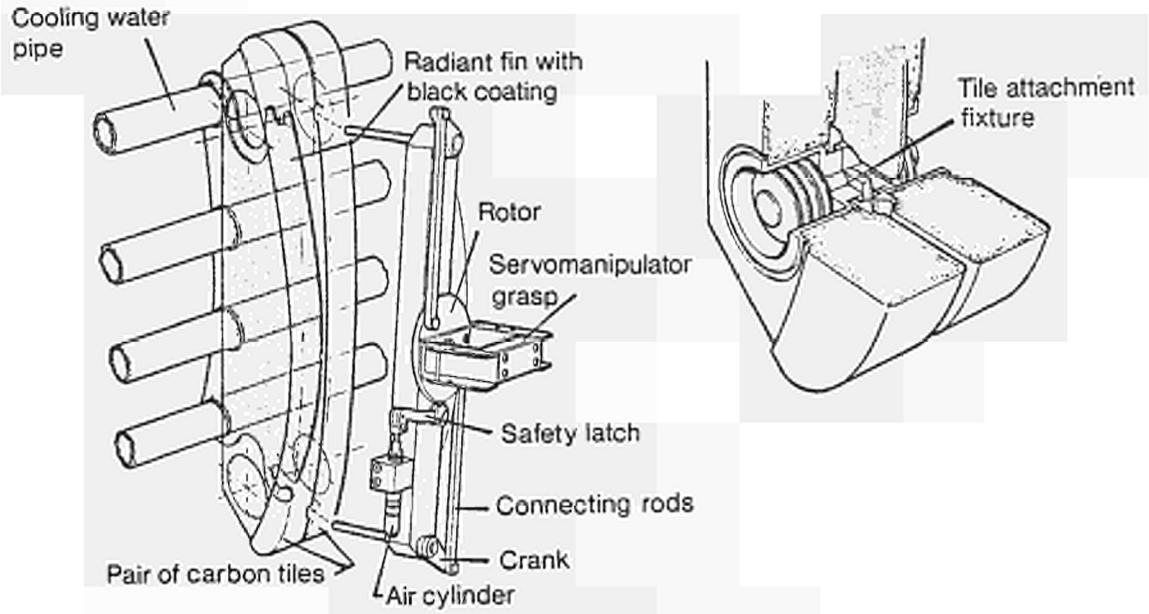

Fig 5 Limiter tile handling tool

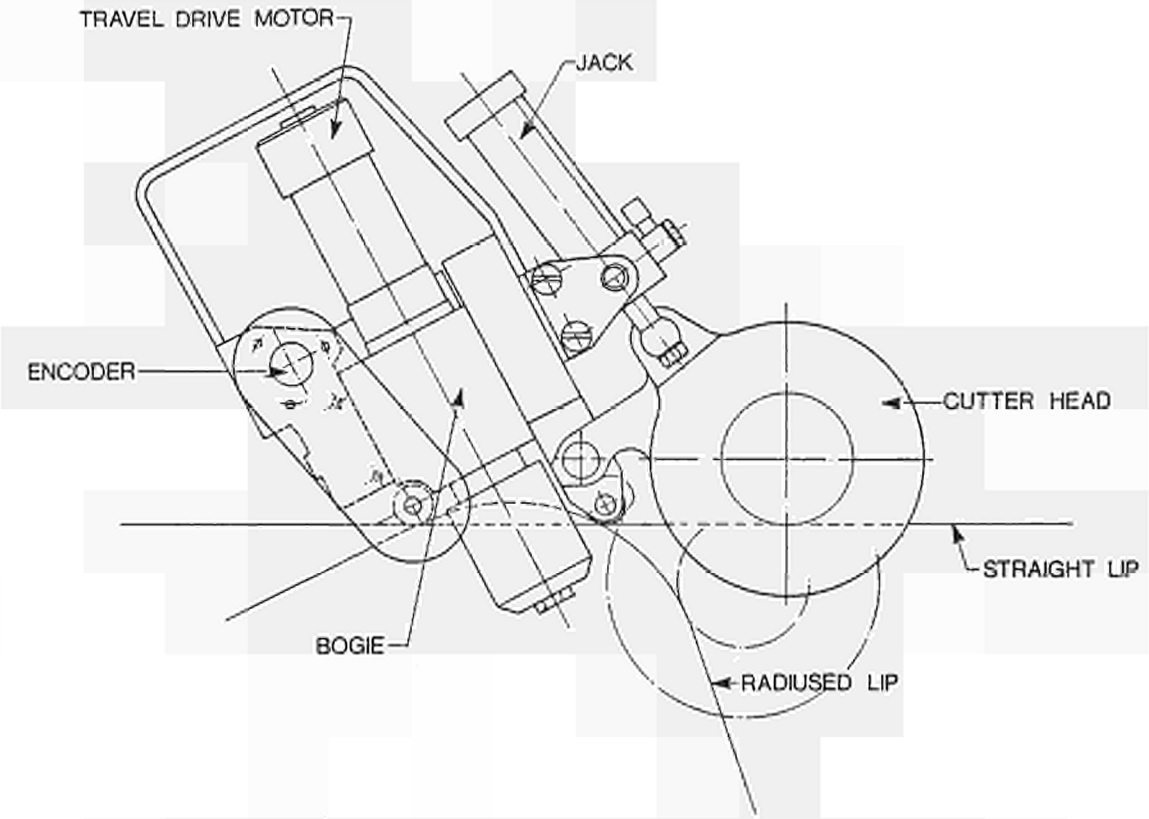

Fig 6 Compact cutting/welding trolley, fitted with cutting head

4. VIEWING SYSTEMS

It is planned to provide 70 fixed locations in the torus hall and other inaccessible parts of the building, any of which can be occupied by one of about 20 TV cameras. Also, up to 30 camera locations will be provided on transporters, end effectors and manipulators.

Two zoom cameras will be mounted on articulated arms attached to each of the transporter booms on a 3-axis "boom extension" located directly behind a manipulator. Their positions can be adjusted to give advantageous viewing of the operations while a third camera mounted on the front of the manipulator body, on a shorter articulated arm, gives a general view in any direction including back along the boom to the tool box.

An in-vessel inspection system (IVIS) comprises four small TV cameras in retractable probes with glass end sections arranged so that they can be inserted into the torus while it is under vacuum. The cameras and their drive mechanisms remain in air. The four cameras between them can scan the whole torus interior by illuminating any camera by flash bulbs in adjacent probes.

This system is fully explained in the poster presentation HP41 of this symposium [6]. It has been used very successfully during the past year and a half, but in its present form the cameras are virtually uncooled and can only be used after the whole torus has been cooled down to 50°C.

In a version now designed, cameras will be kept below 30°C by a water-cooled jacket and glass radiation shields so that they can operate with the torus at 350°C. The zoom facility has been sacrificed because of space restrictions but it has not been used much and the uncooled system, with zoom, can be reinstated if needed. The alternative of using relay lenses to create a scannable image in a cool region was tried experimentally and the loss of optical definition with lenses small enough to fit into the probes was found to be unacceptable.

5. CONTROL OF REMOTE HANDLING EQUIPMENT

The articulated boom and its end-effectors will be controlled by a local control unit (LCU) based on a micro-processor and the crane, the vertical telescopic arm and its end effectors by another, identical LCU so that in-vessel and ex-vessel operations can be performed at the same time. The LCUs will provide the robotic functions of controlling each joint servo, coordinating the joints kinematically, providing teach-repeat and checking the movements for errors and safety.

The force-feedback, master-slave servomanipulators will have their own control systems providing the same robotics functions as the transporter LCUs but with additional operating modes, including weight relief and constraint in a plane. The control systems are being produced in parallel with the mechanical parts of the manipulators.

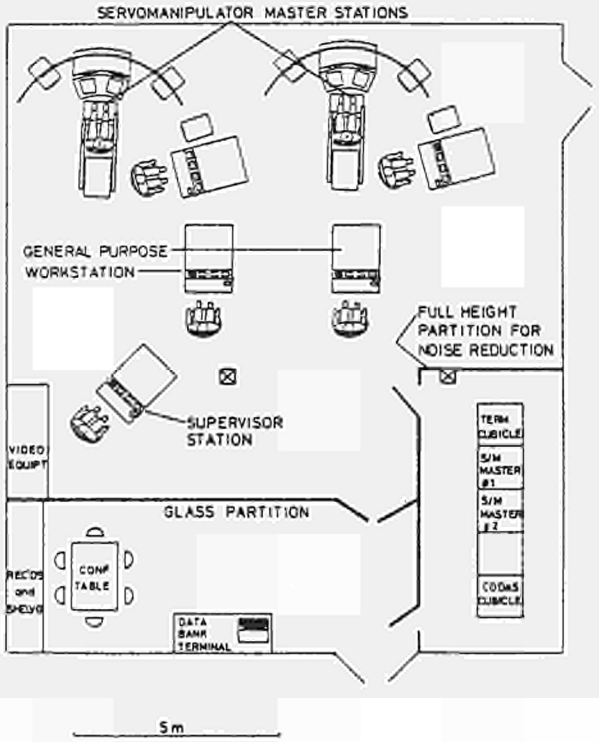

Fig 7 Remote handling control room layout

For in-vessel work one LCU will control the cutting tools and one of the welding tools and an identical pair of LCUs will control the tools for ex-vessel work. They will provide power and control the actuation sequences.

A central control room, Fig 7, will contain five general-purpose consoles. These can be connected to the local control units, as shown in Fig 8, either directly through a multiple switching unit to close the real-time servo loops or through a Nord computer for all other signals. The Nord also controls the multiplexer.

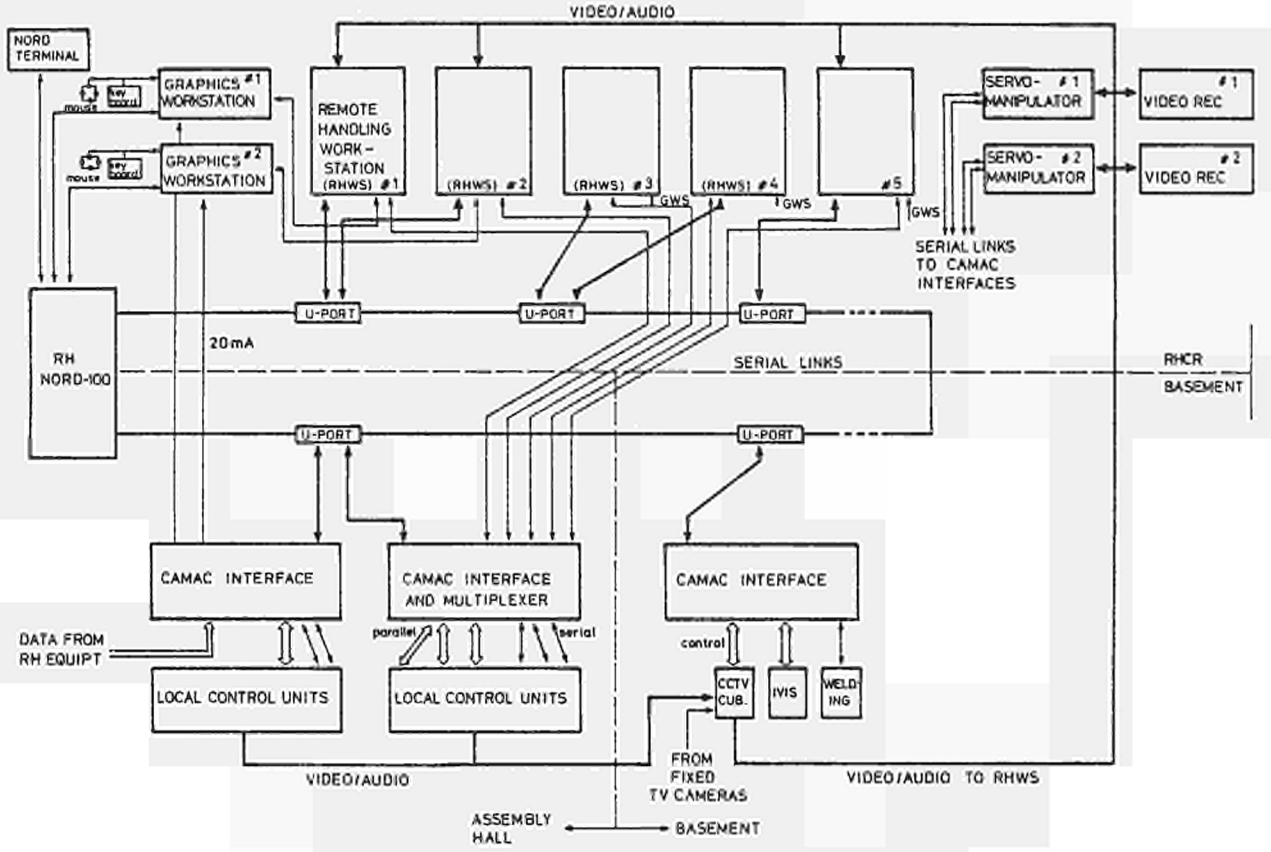

Fig 8 Remote handling control interconnections

Two of the general purpose consoles are incorporated into manipulator work stations which will also have four fixed and two moveable television screens, the latter displaying the views from the two cameras on articulated arms observing the manipulator's work. One operator will control these arms and cameras and the third camera on the front of the manipulator, while another operator controls the manipulator. It is intended to use a prototype manipulator work-station during the shut-down starting in December 1986.

Each manipulator work station will also have a computer graphics display with an expected refresh rate of 5 s^{-1} for the intended portrayal of a solid 3D boom, manipulator and camera arms in 2^6 shades of colour. Accuracy is not expected to be sufficient for fine operations but it will be adequate for avoiding collisions, to help operator orientation by providing overall views and to pre-set TV camera position parameters by choosing viewpoints. It is also intended to use the graphics displays to substitute for large mock-ups in training.

6. CONTAMINATION CONTROL DURING TOKAMAK MAINTENANCE

Until tritium is introduced, probably in 1991, hands-on work will continue both in the torus and outside. However, beryllium is already used in some diagnostics and it is expected that during 1987 beryllium will be purposely evaporated into the plasma and deposited on the torus walls. To protect workers from the dangers of beryllium inhalation and to prevent the spread of beryllium, a torus access cabin (TAC) [7] has been constructed to JET design to support up to six men working in air-line suits and provide a washable stainless steel work-room which can be sealed onto the torus at a main horizontal port. It will also serve to prevent the spread of lightly activated dust which even now is being produced with deuterium plasmas by the secondary neutrons created when runaway electrons bombard protection plates during disruptions.

To prevent the boom and other remote handling equipment carrying contamination outside the torus, it will be fitted with polyurethane gaiters over joints and other intricate parts so that it can be washed down with high pressure water jets while still inside the torus or at the port while being withdrawn. A platform with a structure on which a polyurethane tent can be built to enclose the boom and the equipment it is carrying will be obtained by the end of 1986. The boom will be withdrawn into the tent, checked for contamination and, if necessary, cleaned.

A small beryllium monitoring laboratory, equipped with an atomic absorption spectrometer, will be in operation before the end of the forthcoming shut-down to test swab and air-filter samples. It will take about 30 minutes to collect and test a sample by this method. As a very promising alternative in the near future the laser-induced breakdown spectroscope (LIBS) developed by the US National Laboratory at Los Alamos [8] offers immediate on-line measurement of air-borne beryllium concentrations and of beryllium collected on filters and swabs.

After tritium is introduced the TAC will no longer be used in the torus hall, but it will be used outside as a decontamination or repair facility with workers in air-line suits. Contamination, including tritium, will be washed off remote-handling equipment and tokamak components while still in the torus. Some components can be bagged inside the torus and the bags washed. The gaitering on the remote-handling equipment will be internally pressurised to about 0.1 bar, and this should suffice to prevent significant inward permeation of tritium.

7. JET RECYCLING SYSTEM

7.1. Plant duties

The JET Tritium Recycling System (TRS) is required to process and handle all gases received from the torus and its auxiliary devices such as Neutral Injection (NI), Multiple Pellet Injection (MPI), torus baking loop and auxiliary vacuum systems of diagnostics and RF antennae.

Gases containing mainly elemental hydrogen isotopes will be purified and reprocessed in the isotope separation train to allow re-use of protium, deuterium and tritium, while gases such as argon, air, nitrogen and helium, with only minor levels of (partly) oxidised hydrogen isotopes, will be treated to remove tritium to levels where the effluents can be released safely after tritium oxide has been fixed on disposable dryer beds.

Table 2 (see end of text) shows the separation throughputs needed to deal with the gases from the various sources, including multiple injection of deuterium and tritium pellets. The total amount of gases to be processed for re-use is about 1,050 N&t per day if D_2 pellets are injected. With T_2 pellets the total would be 3,500 N&t per day with 150,000 to 240,000 Ci, based on 25 to 48 JET pulses. Even a reduced test programme with a maximum of 10 pulses per day would still require a daily reprocessing duty of about 320 N&t with D_2 pellets or 1,100 N&t and approx 55,000 Ci with T_2 pellets.

7.2. Design philosophy

In order to minimise accidental, chronic or maintenance-related tritium releases and doses to personnel, the design principle is to use double containment round primary components with major tritium inventories and round equipment that operates at elevated temperatures. Transportable waste and make up containers that have to be connected or disconnected from process lines are also double-contained.

All components, joints and seals must be metallic to allow in-situ decontamination by baking the double containment vessels together with primary components at 200°C under full vacuum before undertaking any maintenance. Furthermore, high reliability components have been evaluated and selected, the primary sensors and cabling of instruments are bakeable and where necessary redundancy is employed to minimise maintenance of process boxes.

Electronics and amplifiers of instruments are located external to double containments.

Advantages of using leaktight and pressure-designed double containments, compared with using glove boxes, are that potential major releases from failed primary components can be kept isolated within the secondary containment, even with overpressure, and also that such releases, or any chronic releases, are not mixed into rather large covergas streams requiring substantial clean up systems.

The long-standing technology of using steel vessels as double containment has been used successfully in cryo technology for reasons of thermal insulation under high vacuum. This containment philosophy lends itself quite naturally to the tritium gas handling, much of which is done under cryogenic conditions, eg hydrogen - helium separation, impurities removal, gas compression.

In order to prevent potential contamination of refrigerator loops or releases to the environment, the system will be equipped with holding tanks that allow safe isolation of cryogenic fluids contained in process and related equipment.

7.3. Plant technology

The front end of the processing plant as shown in Fig 9 consists of 3 parallel cold boxes which receive the neutral injection gas or the torus gas in batches or pulses at a pressure around 1 mbar or less.

Each cold box contains a liquid helium cooled accumulating panel which pumps hydrogen by freezing and separates it from traces of helium that are passed to the helium sorption trap, which adsorbs helium at 5K. Periodically the accumulator panel is warmed up and the frozen hydrogen released to the cryo transfer pump, a small liquid helium cooled condenser which, when warmed up, will compress the gas to 2 - 5 bar, sufficient to push it through the cold adsorber which removes the last traces of impurities at liquid nitrogen temperature.

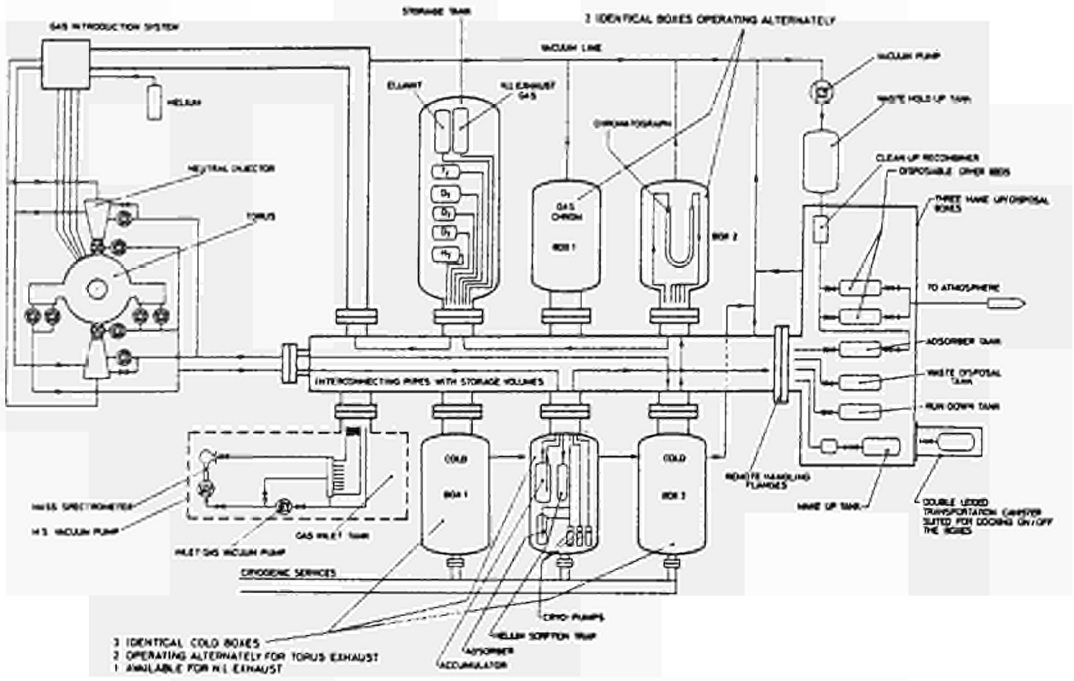

Fig 9 JET tritium plant engineering layout concept

The purified hydrogen isotope mixture is then passed to the separating train whereas impurities and process helium are passed periodically to the make up and disposal boxes where waste containers can be remotely connected and disconnected from process lines. Waste containers are passed out of these vacuum tight and pressure-designed boxes and are transported in double lidded transport flasks to a disposal site. Process helium and other gases, eg nitrogen or air from maintenance, are passed in batches through a recombining clean-up system and released with very low tritium levels.

The hydrogen isotopes are separated in a number of parallel gaschromatographs with palladium packing and using protium as the eluant. As an alternative, cryogenic distillation is being studied in view of the high purity and large throughput requirements of the JET torus and its various auxiliaries.

The separated isotopes are released from the separating train at about atmospheric pressure to the product storage tanks, ready for re-use.

7.4. Development programme

A number of novel key components have had to be designed. They must satisfy the interfacing between a hydrogen isotope separating system, the various high vacuum sources of the process gases and the low maintenance aspect of the design philosophy.

A test rig has been set up at JET for performance testing of these key components using protium and deuterium.

The test rig consists of a cold box with related vacuum pumps, a hydrogen supply system to feed the components with defined gas mixtures, control cubicles with various instrumentation, and automatic controllers to study and establish optimum control

strategies. A gas sampling system with mass spectrometers and catharometers is used to study separating effects and capacities of process units. High frequency generators provide power to heat components with induction coils.

Most of the cryogenic components have been tested to date and the design duties have been confirmed successfully. Double bellow sealed process valves are still being life-tested over many operating cycles and it is expected that the high reliability criteria can be fully met.

7.5. Safety considerations

A number of studies have been carried out to evaluate the expected tritium releases from JET and its auxiliaries during normal operation and as a result of maintenance. The results indicate that the measures taken to contain tritium are adequate and will allow the strict design dose targets to be met.

PERIOD	RF heating	NB heating (a)	Gas	Number of neutrons/pulse	Total neutron production/6 months (b)	Gamma dose rate µSv/hour (mRem/hour)
1987	15MW	10MW(D) 80kV	D,D	6×10^{16}	10^{19}	25 (2,5)
1988	15MW	5MW(D) 80kV				
1989		5MW(D)160kV	D,D	10^{17}	2×10^{19}	50 (5,0)
1990	15MW	10MW(D)160kV	D,D	2×10^{17}	3.5×10^{19}	100 (10)
1991	15MW	10MW(D)160kV	D,T	$10^{19} - 10^{20}$	up to 10^{24} (in 2 years)	> 5000 (> 500)
1992						

Table I Expected additional heating, neutron production and gamma dose rates 1 week after operation has ceased

SOURCE	ISOTOPE SEPARATION REQUIREMENTS	COMPOSITION AT SOURCE, %.
Torus pulsed operation	110 Nlt per day (48 pulses)	> 47D, > 47T, < 5 He or H_2 (1%)*
Glow discharge cleaning	144 Nlt per day (Depleting T_2 inventory of torus)	45 < D < 95, 5 < T < 45 (< 1%)*
Neutral injectors	220 Nlt per day (48 pulses)	> 97.7D, < 1.8T, < 0.5H
Make-up D_2 for NI PINI's	280 Nlt every 2 weeks (8 x 48 pulses)	> 98.9D, < 0.6T, < 0.5H
Multiple D_2 pellet injection	550 Nlt per day (25 pulses)	< 2D, < 0.13T, 97.9H
Multiple T_2 pellet injection	3000 Nlt per day (25 pulses)	< 2D, < 0.13T, 97.9H

* Impurities %, CH_4, N_2, CO, CO_2, DTO

Table II Gases to be processed for re-use of H, T, D

8. REFERENCES

[1] HUGUET, M., Assembly, Commissioning and First Operation of JET, IEEE Symposium on Fusion Engineering, Philadelphia, December 1986. Proceedings pp 834-842.

[2] HUGUET, M. and BERTOLINI, E., Main Features of the JET Facility for D-T Operation, ANS Conference, Reno, USA, June 1986.

[3] ROLFE, A.C., Remote Maintenance of the JET Tokamak, UKAEA Conference, March 1986. Proceedings Paper 8.

[4] DEAN, J.R., Remote Maintenance of the JET Tokamak, EEC Conference, Marseilles, February 1986. Proceedings pp 175-184.

[5] WYKES, M. et al., Remote Handling Tools for JET, Paper HP 42, 14th Symposium on Fusion Technology, Avignon, September 1986.

[6] RAIMONDI, T. et al., The JET In-Vessel Inspection System, Paper HP 41, 14th Symposium on Fusion Technology, Avignon, September 1986.

[7] BOOTH, S.J., Contact Maintenance on JET into the Active Phase, ENC'86, Geneva, June 1986. Proceedings Vol 3 pp 51-56.

[8] CREMERS, D.A. and RADZIEMSKI, L.J., Applied Spectroscopy, 39, pp 57-63.

9. ACKNOWLEDGEMENTS

This paper reports the work of the whole of the three groups comprising the Fusion Technology Division of JET. These are the Remote Handling Development Group, leader T Raimondi, the Remote Handling Applications Group, leader A Rolfe and the Tritium Group, leader W Riediker.

JET Contributed Papers at Fourteenth Symposium on Fusion Technology (SOFT), Avignon, France, September 1986

CONTENTS

CONTENTS PAGE NO.:

OPERATION AND PERFORMANCE OF THE LARGE SCALE JET CRYOPUMP SYSTEM

W Obert, R Haange, A Jones, E Küssel, C Mayaux, R Roberts

JET Joint Undertaking, Abingdon, Oxon, UK.

ABSTRACT

Large scale cryopump systems with a pumping speed of 8 million litres per second each are necessary to provide the pumping requirements of the JET Neutral Injection and the JET Multi-Pellet Injection systems. The first cryopump system has now been operational for more than one year and the performance and operation data are presented. The cryopump system has been operated so far in direct proximity of the extracted particle beam with a total power of up to 32 MW without adverse effect. The compatibility of the system with the Pellet injection requirement of high pulsed gas loads (up to 4×10^3 mbℓs^{-1}) and high inventory (up to 5000 bℓ) has been demonstrated by tests and the related safety aspects have been analysed. The control and instrumentation of the cryopump system performs successfully but the operation of the overall systems showed the need for the decoupling of the system from the main computer and to upgrade the local cryoplant control system.

1. INTRODUCTION

At JET a large scale cryogenic system has been installed for the two cryopump systems for Neutral Injection. By the beginning of 1987 it will also employ an identical cryopump system for the Pellet Injection. Each cryopump system provides 8.5×10^6 ℓs^{-1} pumping speed for H_2 by cryo-condensation on a JET design open structure pump configuration. The design layout and set-up of the system and its cryo-supply system including the cryoplant, the advanced low loss flexible JET cryo-transferline, for the supply of liquid helium and nitrogen, has been reported elsewhere [1] [2] [3].

The complete system (cryopump and cryosupply) for the first Neutral Injection unit has been operated since 1985 and a second cryopump system for the second Neutral Injection system has been commissioned. The cryopump system operates successfully for Neutral Injection in direct proximity to the energetic particle beam with an extracted power of 32 MW so far. The compatibility with the Pellet Injection requirements for large gas pulses and high hydrogen condensate inventory has been tested.

In particular, transitional and dynamic conditions are difficult to quantify theoretically such as cool-down, warm-up and regeneration, and corresponding measured curves under different conditions are now available.

2. CRYOPUMPS

The installation of the cryopump (their design and construction is described in [2] [3] and shown in Fig.1. Table I shows the main data for the cryopump.

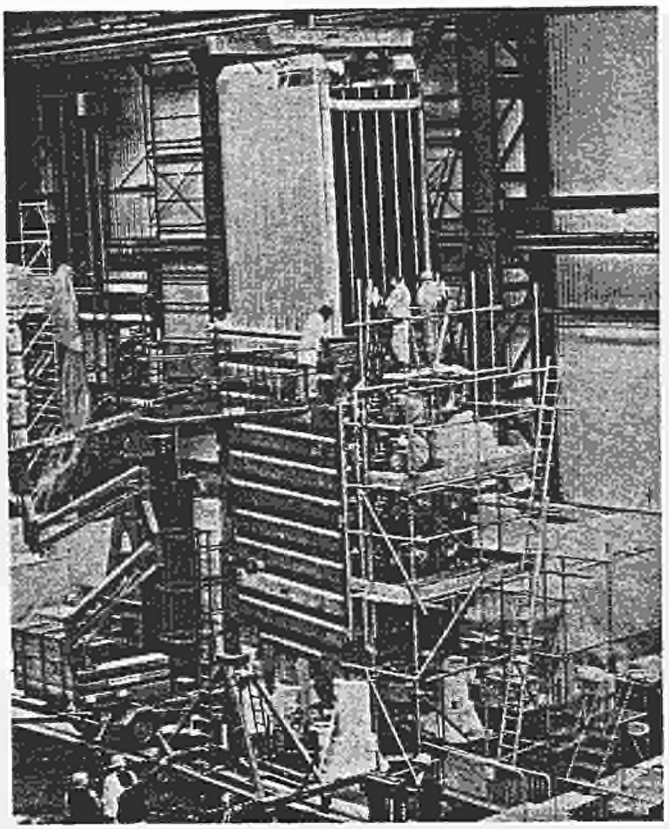

Fig. 1 Installation of the 2nd cryopump into the vacuum box.

Tab. I. JET LARGE SCALE CRYOPUMP SYSTEM DATA PER CRYOPUMP

PUMPING SPEED	8.5×10^6 ℓs^{-1} (H_2)
PUMPING AREA	TWICE 3.5m x 6m = $40m^2$
SYSTEM HEIGHT	6 m
GAS LOAD NI	<300 mb ℓs^{-1}
PI	<2000 mb ℓs^{-1}
CONTENTS	LHe ~ 150 ℓ LN_2 ~ 250 ℓ
WEIGHT TOTAL	~ 5 TONS
LHe STRUCTURE	AL ~560kg StSt ~340kg
LN2 STRUCTURE	AL 2865kg StSt 1385kg
CONFIGURATION	SERIAL OPEN STRUCTURE
SET-UP	20 IDENTICAL MODULES
SYSTEMS DEPTH	0.3 m
MODULE SIZE	EACH 0.3x0.35x6m
COOLING PRINCIPLE	THERMOSIPHON
MATERIAL	
MANIFOLDS	StSt 316L/304L
He PANELS	E.AL MgSi 0,5
N_2 PANELS	AL 99.9 MgSi T7
SURFACES	
He-PANELS	SILVER COATED > 20 μ
N_2 PANELS	BLACK ANODISED
COMPATIBLE WITH -10^{20} NEUTRONS/PULSE -CLOSE VICINITY TO 400A/80keV EXTRACTED PARTICLES	
VACUUM BOX	50 m^3

2.1 Neutral Injection (NI) Cryopumps

For the NI system a base pressure below 4×10^{-5} mb has to be maintained in order to keep the reionisation losses of the neutralised beam below 14%. The gas load from the neutraliser, the ion beam dump and the beam scrapers can be up to 300 mbℓs^{-1}.

The cryopumps had to pump so far most of the time hydrogen but deuterium has also been routinely used for several months. In the long term only deuterium will be used for the neutral injection. For the next subsequent years, however, the use of deuterium for neutral injection may be limited, in order to keep the activation of the JET device due to deuterium beam deuterium plasma collisions below an acceptable level for hands-on operation for maintenance and repair of the JET machine. Therefore hydrogen operation may still be required.

2.2 Multi Pellet Injection (PI) Cryopumps

The cryopump for the Multi Pellet Injection System is identical to the NI cryopumps but the operation conditions are different. The large scale cryopumps are required to cope with the huge gas load from the propulsion of the pellets by means of a pneumatic light gas gun up to several 1000 mbℓs^{-1} (total up to 30 bℓ per pellet and up to 100 bℓ per plasma pulse, mainly H2). Hydrogen is used as a propellant in order to maximise the speed. The pellets themselves will be made of D2 and therefore also D2 due to the pellet ablation has to be pumped.

The total inventory of H2/D2 may be up to 5000 bar litre stp (= 223 mol H2 = 446 g H2 = 5 litre solid H2 at 4 K). This is 10 times the NI cryopump inventory and calls for special safety consideration (see below).

2.3 The effect of hydrogen and deuterium and the base pressure

The heat load to a cryopump consists of several terms:

a) The static heat load due to radiation and heat conductance support structure: this has been measured to be approximately 35 W (or ~ 50 ℓ/h LHe) for the cryopump system.

b) The static heat load due to the thermal conductance of the base pressure of the insulation vacuum: this term can cause a considerable contribution towards the heat load of the overall system. For molecular flow conditions this term can be calculated by Knudsen formula and is shown in Fig.2 based on accommodation coefficients of 1 and ~ 100 m² cold He surface. This shows that operating the cryopump system with hydrogen at atmospheric pressures already increases the heat load close to a factor of two. A further increase of operation temperature/pressure will result in unacceptable high heat loads and runaway of the cryopump. This runaway happened several times during commissioning when the cryo supply plant pressurised the cryopump with He backwards and the cryopump was regenerated within less than 10 minutes. This vapour pressure is so far a very important effect as it contributes continuously to the heat load even outside the actual gas pulse.

In case of H2 operation it also requires to operate the LHe loop below the suction pressure of the cryoplant which is at maximum power output at 1.3 bar and appropriate pumping facilities have to be provided.

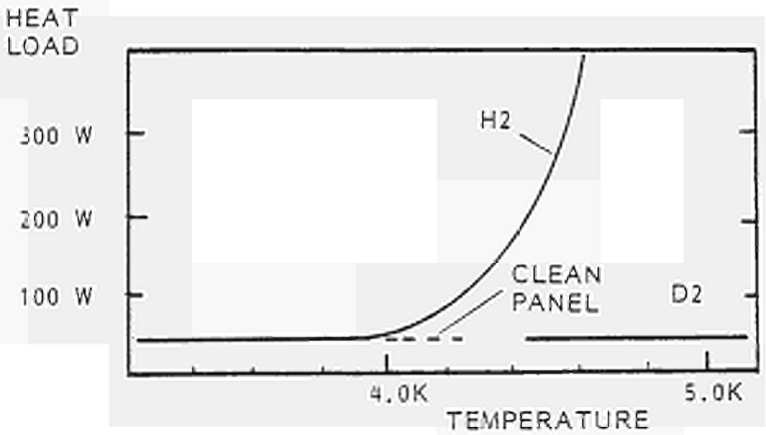

Figure 2
Static heat load on cryopump due to basic heat load (radiation + support) plus the effect of heat conduction due to the vapour pressure of the condensed gas as function of the concondensing surface temperature.

c) The dynamic heat load due to the enthalpy of the gas to be condensed: this enthalpy is the sum of the heat of condensation plus the specific heat of the gas. Heat load measurements as a function of the gas load are shown in Fig.3. The results show a good accommodation of the incoming gas at the LN2 shield to - 100 K.

This dynamic heat load, however, does not affect the cryopump systems at JET due to the very low duty cycle. The 10 sec NI gas pulses cannot be registered with the installed instrumentation (He temperature/He pressure) which can be understood due to to the fact that a 300 mbℓs^{-1}, 10 sec pulse only represents a load of < 500 Joules.

During a pellet pulse the pressure in the vacuum box can rise to values up to several 10^{-4} mb without causing additional heat load due to the thermal conductivity (see b) and the system was tested to maximum loads of up to 4000 mbℓs^{-1} and a corresponding pressure of up to - 5.10^{-4} mb. This is due to the fact that this pressure is rather given by the limit of conductance between the cryopump radiation shields and the cryopumping surface and does not contribute to the static thermal load by conduction (see b) as long as the sticking coefficient for the incoming gas to the surface is close to 1.

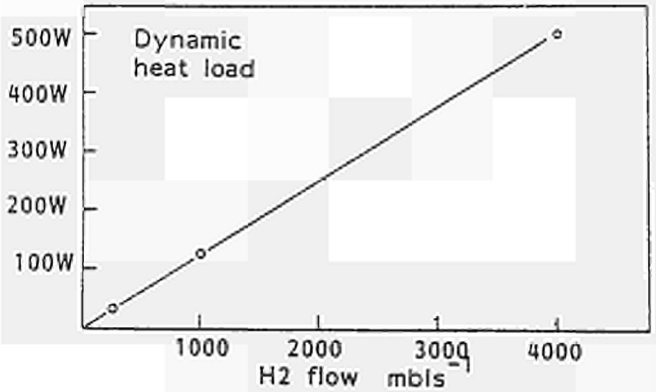

Figure 3
Dynamic heat load on cryopump to condensation of hydrogen as function of the pumped H2 flow rate. Values measured under constant gas flow conditions.

2.4 PUMPING SPEED

The measured pumping speed for H2 of the full scale cryopump system confirmed the measurement of the 1/10 assembly in the Test Bed [2] with

$$S = 8.5 \times 10^6 \ \ell s^{-1}.$$

3. INVENTORY AND SAFETY LIMITS

The inventory, i.e. the maximum gas load of the cryopump is limited by safety consideration due to the use of hydrogen. Usually one restricts the H2 inventory to an amount which gives after defrosting less than 15 mb partial H2 pressure as it is known that below this pressure no flame in a H2/air mixture can be sustained as the thermal loss of a flame due to the thermal conductivity is larger than the produced energy [4].

The safety limit allows for the NI system approximately 1 week of operation before regeneration (Vacuum box 50 m³, inventory maximum 750 bℓ stp corresponding to 250 pulses with 300 mbℓs^{-1} for 10 sec, 50 pulses per day give 5 days of NI operation).

For the advanced Multi Pellet Injection a gas load of up to 5000 bℓ stp (≈446 g H2 ≈ 5 litre solid H2 at 4 K) per day may be required. An ignition in case of an air leak can therefore not be excluded anymore and special safety measures are required such as: Exclusion of all ignition sources such as ion gauges or installation of proper flame stops. Installation of an appropriate relief valve which allows to cope with the pressure rise in case of an uncontrolled ignition. The formation of a detonation shock wave can be excluded for the vacuum box geometry.

4. OPERATION

4.1 Cooldown

The cryopump system is designed for no cooldown restrictions, i.e. no control of the cooldown process itself is necessary as each part of the cryopump system can cope with the thermal contraction due to cooldown separately.

A typical cooldown curve is shown in Fig.4.

The cooldown from ambient temperature is required only after shutdown or after warmup as a consequence of an intervention into the NI or PI system and is therefore an infrequent operation. The cooldown from ambient starts with the supply of LN_2 from the main storage tank (50,000 ℓ) via a subcooler and a flexible transferline of up to 80 m length with a supply pressure of approximately 2-3 bar g. It takes approximately 15 minutes until the H20 residual gas in the vacuum box is cryopumped ($p < 10^{-6}$ mb) and it takes less than 2 hours until the nitrogen part of the cryopump is at LN_2 temperature and full. The cooldown and filling is limited by the LN_2 cryoline impedance and LN_2 supply pressure. A quicker fill up is, however, not desired in order not to stress the cryopump structure unnecessarily.

The liquid helium loop is started only when the LN_2 part of the cryopump is below 150 K in order to have all impurities which could spoil the emmissivity of the He crycondensing surfaces condensed on the LN_2 radiation shields.

The He panels cool down by radiation exchange alone even without active cooling and after approximately 25 h the He panels are close to 150 K.

A way to enhance the cooldown of the He cryopanels is to allow contact gas into the vacuum box (typical pressure 10^{-1} - 1 mbar) which cools the He panels by thermal conductivity of the contact gas down below 100 K within less than 4 h. By this means most of the enthalpy of the StSt and AL structure of the He loop is removed by the LN_2 cooling loop, thus saving time and power for the LHe cooldown.

The cooldown to liquid helium is started at ~ 100 K and is provided by the high pressure supply loop of the He refrigerator. The cooldown is limited by the cooling capacity of the cryoplant and within typically 3 hours the He panels are LHe temperature. In order to enhance the filling rate the liquid helium is then supplied direct from the integrated 5000 ℓ liquid helium dewar.

4.2 Regeneration

For the desorption of the cryodeposited H2 or D2 alternative concepts are possible. The routine method is to shut off the LHe supply valve and to wait for the emptying and defrosting of the panels. This takes, depending on the gas load and whether the condensate is H2 or D2, typically between 20 minutes and 2 hours.

In addition forced regeneration is also possible which means forced emptying of the LHe and quick desorption can be achieved in less than 10 minutes.

After desorption the gas has to be pumped by mechanical pumps which requires about 1 hour in order to achieve a vacuum better than 10^{-4} mb with the given pumping speed and conductances. During this time the complete He-loop warms up to LN2 temperature as the released gas acts as contact gas.

The cooldown to 4 K again and LHe filling is practically the same process as for the cooldown (4.1).

A total regeneration cycle requires approximately 5 hours. Further shortening of this period seems to be possible by provision of enhanced pumping capacity (roots blower or dedicated cryopump) to pump the desorbed gas which would reduce the pump down time but also the warmup of the He panels. The enhancement of the cryoplant refrigeration capacity and/or use of direct LHe supply will also shorten the cycle.

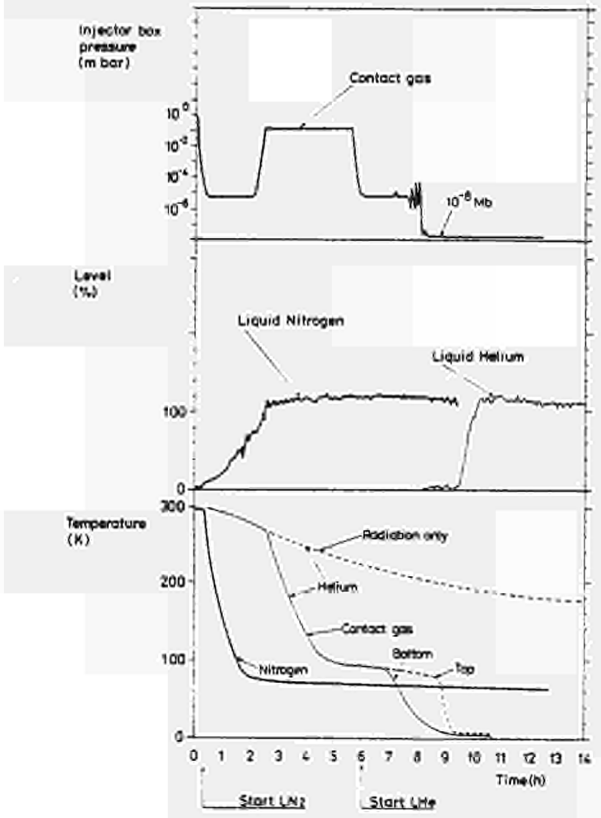

Fig.4 Cooldown curves of the JET cryopump

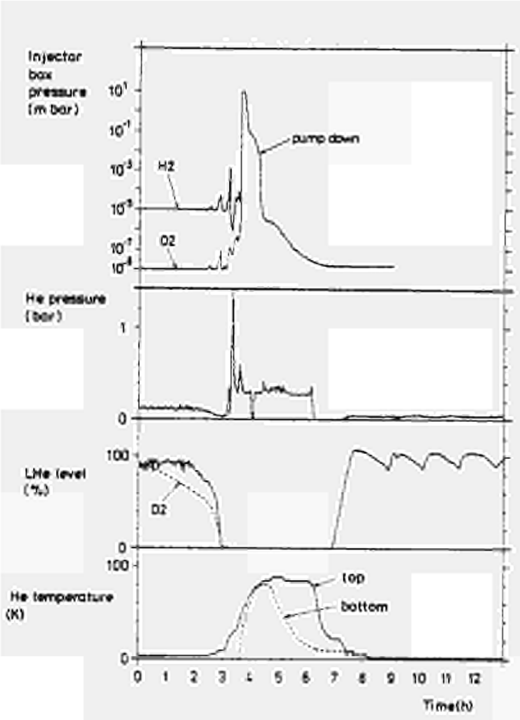

Fig.5 Regeneration curves of the JET cryopump

4.3 Warm up

The warm up of the cryopumps depends, like the cooldown, very much on the pressure in the vacuum box. If the insulation vacuum is better than 10^{-5} mb then it takes several days until the cryopump system reaches ambient temperature.

This is of importance if the NI cryopumps are used as cryotraps for any residual water. Once cooled to LN2 it keeps water pumping for at least 2 days without refilling. If the pressure in the vacuum box is in the range of 10^{-2} mbar or higher, the complete system is close to ambient within less than 10 h and the system can vent to atmosphere.

4.4 Intervention Period

The time required for an intervention in the NI vacuum system due to the cryopumps is

therefore for warmup approximately 10 h and for cooldown approximately 10 h but it seems to be possible to reduce this time (see also 4.2).

5. CRYOSUPPLY

The cryo supply system has been operational for more than 6000 hours without major problem. The operation of the new pellet injection system requires upgrading of the storage and purification facility. It also requires full exploitation of the cryoplant output capacity by installation of increased turbines and replacement of the warm ejector by mechanical vacuum pumps.

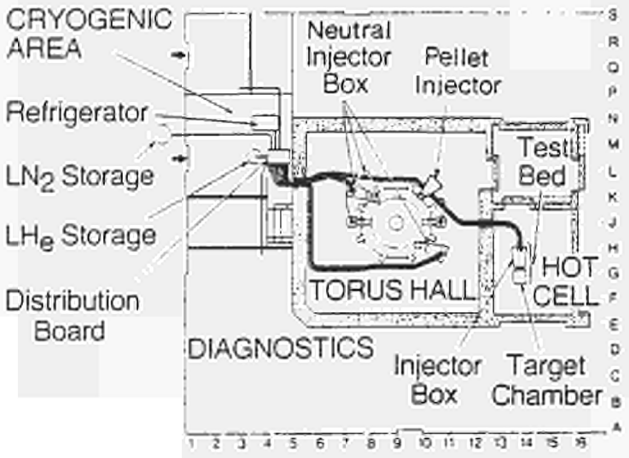

Fig.6 Cryogenic supply system

The cryosupply system has to provide liquid helium and liquid nitrogen to a series of users.

- NI cryopump system Oct 8
- NI cryopump system Oct 4
- NI Testbed with 3 separate cryopumps
- PI cryopump system Oct 2 (1987 onwards)
- PI pellet launcher (1987 onwards)

and future users such as

- Tritium recovery plant
- Supraconducting magnets for ECR heating Klystrons

INSTRUMENTATION AND CONTROL

1. Temperature sensors

type CLTS (linear 400 K to OK, Vichay Micromeasures Malakoff (F)) are on both the LN2 and LHe loop on the top and bottom manifold. They allow to monitor cooldown and warmup.

The exact temperature of the LHe is measured via a pressure transducer on the He loop.

2. Level measurement

fully redundant level measurement is installed for the LN2 and LHe loop.

LN2:	- Pt100 level sensors* low/high	3 sets
	- hydrostatic pressure analog	2 off
LHe:	- supraconducting wire in top manifold (10 cm long) analog	3 off
	- hydrostatic pressure* analog	2 off
	- carbon sensor low/high	1 set

* used for routine control.

The cryo system is controlled by its own PLC (Modicon 584), the control signals (level for LHe and LN2) and other information about the cryopump is received via the main computer (CODAS).

The integration of the main computer into the control loop proved, in several ways, not to be satisfactory.

- the cryopump requires 24 h uninterrupted control independent of the main torus programme,
- control programme development and improving of the cryo system is not compatible with the needs for the operation of the torus,
- the maintenance and shutdown schedule of the cryopumps does not relate to the schedule of the main torus programme and the central computer,
- commissioning of new equipment such as PI interferes with the safe operation requirements of the main torus programme and CODAS.

Therefore after the next main shutdown period the complete cryo system including cryopump will have its independent control loop and use the main computer only for main commands such as cooldown, regeneration and to monitor the status of the cryo system.

Fig.7 shows the basic flow diagramme for the revised instrumentation and control loop.

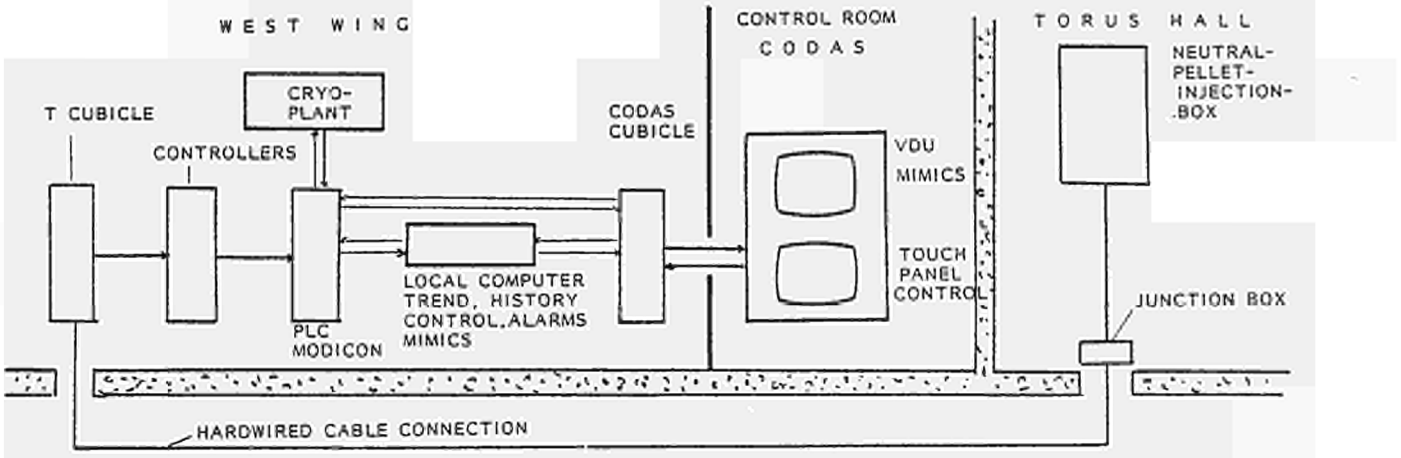

Fig.7 Flow diagramme for the new instrumentation and control loop

REFERENCES

[1] W Obert, et al, 'Cryo Supply and Transfer System for the JET Neutral Injection Cryopumps' 11th Symp on Fusion Techn, Oxford 1980.

[2] W Obert, et al, 'The JET Cryopump System and its Cryolines for Neutral Injection' 13th Symp on Fusion Techn, Varese 1984.

[3] W Obert, P H Rebut, G Duesing 'Cryopump for JET Design of Large Scale System of Open Configuration for High Specific Pumping Speed' 9th Symp on Eng Probl of Fusion Research, Chicago 1981.

[4] M G Zabetakis, 'Safety with Cryogenic Fluids' Plenum Press, New York, 1967.

welding each end of a series of Ø 5 studs (some 580 for each panel on a 40 mm triangular pitch) placed between adjacent titanium sheets.

Rigidity for each panel is achieved by a series of ribs welded between the panel and its support shaft. Panel cooling is provided via concentric feed/return channels within each hollow support shaft. The shaft/panel assemblies are set into a common support frame via a series of journal and thrust/journal bearings placed along the shaft.

Simultaneous rotation of each panel is achieved via two double acting pneumatic actuators, externally mounted at the front end of the injector vacuum box. Penetration of the actuator/panel connecting linkage from atmosphere to the injector box vacuum is achieved via a double bellows assembly. The bellows are required to withstand an axial deformation of some 65 mm with an additional perpendicular pivot displacement of 6 mm.

Panel open/closed positions are sensed by micro switches mounted on each actuator. In addition each actuator has a twin channel linear resistance transducer in order to monitor displacement/time functions for each panel.

Flexible hoses are situated between the water manifold and each panel/shaft assembly in order to accommodate the 65° of rotational movement required during operation of the fast shutter.

In order to inhibit molecular gas flow from torus to neutral injector box when the fast shutter is in the closed position a series of beryllium copper flexible lips are used, providing a low vacuum conductance barrier between the inside face of the injector vacuum box and the support frame, and between the support frame and each titanium shaft/panel assembly.

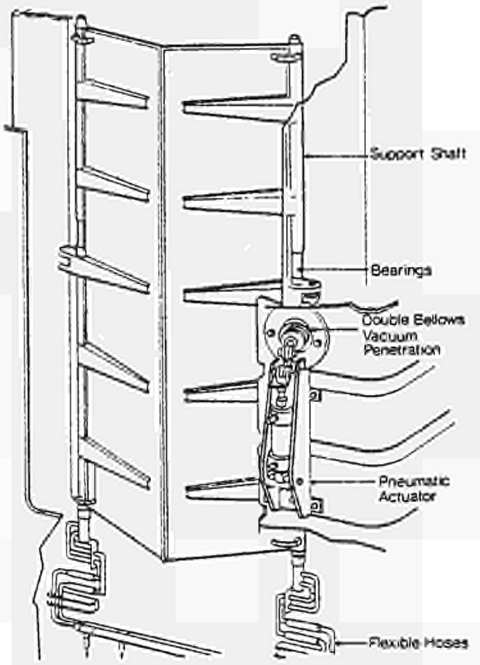

FIG 3
Fast shutter layout

COMPONENT MATERIALS & TESTING

(i) Titanium alloy Grade 5 (6% Al, 4% V) is used for fabrication of each water cooled panel/shaft assembly. Selection of this particular alloy has been made with regard to its following properties:-

- High strength (T.S. > 110 kg/mm²), resistance to corrosion, fatigue and crack propagation.
- Low density, some 60% that of stainless steel.
- Lower affinity (x 5 less) for molecular hydrogen than Grade 2, commercially pure titantium.
- The alloy is weldable via conventional TIG methods. With complex fabrications then post weld stress relieving at 700° C must be carried out.

Titanium is a metal with an unfortunate tribological history, not normally chosen for its sliding properties. Measures have been taken to modify bearing surfaces in order to avoid fretting. Surfaces are subjected to an initial proprietary surface treatment and coated, via high velocity plasma spraying with a Cr_2O_3 compound. The finishing operation involves grinding to a surface finish of 0.4 µm.

A FAST SHUTTER SYSTEM FOR THE JET NEUTRAL INJECTORS

M J Watson, R Haange, D Stork, R Tivey, D Young

JET Joint Undertaking, Abingdon, Oxon OX14 3EA

ABSTRACT

The JET Neutral Injection Beamline [1] is equipped with a pneumatically-actuated Fast Shutter. This shutter is designed to act as a low-conductance path blocking the influx of tritium into the injector boxes of JET following the termination of a JET discharge in the D-T phase. The shutter has been fully operational from January 1986. Mechanical design, control and interlock systems are described together with shutter performance and effect on likely tritium inventory.

INTRODUCTION

A fast shutter is sited at the exit of the JET neutral injection beam lines (Figs. 1,2) [1] serving in the closed position as a low gas conductance device between the torus and the injector vacuum box. Its primary function is to minimise the flow of tritium gas, during D-T operation, from the torus into the injector box, where it would be condensed onto the cryopump.

A secondary function, when in the open position, is to act as a cooled liner for the vertical side walls of the injector box exit ducting.

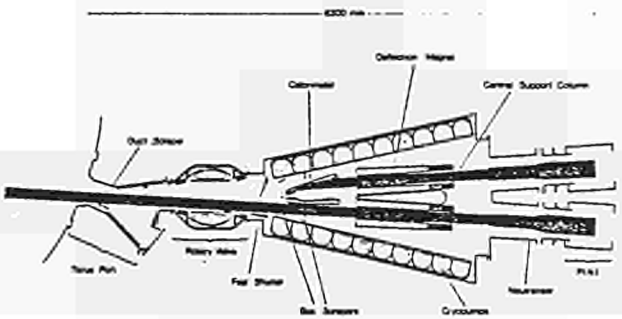

PLAN VIEW OF JET NEUTRAL INJECTOR

FIG 1

Plan layout of JET neutral injection box

DESIGN

The fast shutter has been designed for use with pneumatic operation to 0.4 s and also hydraulic operation to 0.1 s nominal total closing times. Axial forces required to achieve the desired closing times have been minimised by extensive use of a high strength, low density titanium alloy. The cooled panels are designed for a nominal incident flux of 25 W/cm^2 over the complete panel surface area, with a water flow rate of 1 l/s.

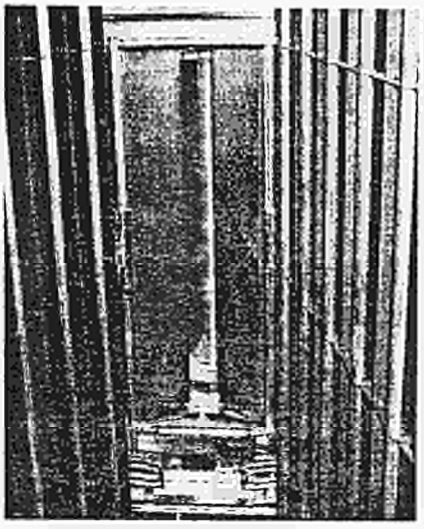

FIG 2

Fast shutter installed at injector vacuum box exit

LAYOUT

Fig (3) displays the fast shutter layout. The assembly consists of two vertical water cooled titanium alloy panels, some 2 m x 0.35 m, each designed to rotate through 65° from the fully open to the fully closed position.

Each panel is constructed from 1.6 mm titanium sheets. A 4.5 mm wide water channel is maintained by

(ii) Compatibility with JET UHV and radiation requirements have led to the choice of a non-galling, self lubricating bearing. Molalloy grade PM-103 is a high load bearing sintered material containing MoS_2, Mo, W and Nb. Tests have been carried out simulating the operational conditions under which the fast shutter bearings will operate, yielding a friction factor of 0.07 after the initial running-in period.

(iii) Inconel 600 flexible hoses used to absorb the $\pm$ 32° of rotational movement between the support shaft and water manifold have been life tested to > 100,000 cycles whilst maintaining a leak rate of $<< 10^{-9}$ mbar l/s.

(iv) The stainless steel double bellows assemblies have also undergone life testing to > 100,000 cycles under simulated operational conditions.

(v) Joining of stainless steel water manifolds to the titanium alloy shaft has been achieved via a pure aluminium insert and two friction welds (Fig 4). The titanium alloy - pure aluminium - stainless steel assembly has been subjected to the following acceptance tests:-

- thermal cycling to 400° C and leak testing.
- thermal shock tests (600 K to 78 K) and leak testing.
- hydraulic burst test (630 bar).
- 'Petal' bend embrittlement tests.

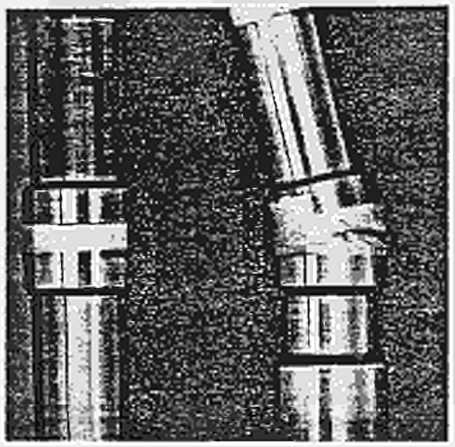

FIG 4

Hydraulic burst test of stainless steel-pure aluminium-titanium friction weld at 630 bar

(vi) Hydraulic pressure testing of the panel results in mecahnical failure of welded studs at 36 bar. Nominal in service operating pressure is 6 bar.

vii) The complete fast shutter assembly (excluding actuators) is subjected to final thermal cycling (x 10) to 300° C plus hot leak testing $<< 10^{-9}$ mbar l/s prior to installation within the injector vacuum box.

ELECTRONIC CONTROL INTERFACE

The Fast Shutter must operate under remote computer control of the JET CODAS [2] system as is standard with all JET 'Local Units'.

The special requirements for the control interface are:

- it must be possible to Open and Close the shutter as part of the timed sequence of the injected neutral beams; the time between opening and closing being minimised to reduce the cryopump tritium load.
- the shutter must close immediately on disruption of the JET plasma.
- the position of the shutter must be interlocked with the beam control in a failsafe manner to switch off the beams once the shutter moves from the fully open position.

The control interface is shown schematically in Figure 5.

The shutter timing control comes from the neutral beam part of the JET Central Timing System (CTS) [3] via fibre optic links for noise immunity. The shutter opening time is set

relative to the 'beam on' periods algorithmically to optimise the time for which the shutter is open [3]. This is indicated in Figure 6.

The timing control only opens the shutter if a signal from the Plasma Fault Protection System (PFPS) is present indicating that the plasma has not disrupted [1], [4]. The signal comes in the form of a maintained pulse train (500 Hz). This has a failsafe action, the disappearance of the pulse train at disruption leads to the activation of the shutter close mechanism in a very short time.

The shutter position is interlocked with the beams via a pulse train from the Plasma Density Interlock system [3]. This is passed via relays which unambiguously are activated by the 'Shutter Open' microswitches and back into the pulse train system which sustains the beam power supplies [1]. When the shutter is fired off its open microswitches the pulse train is interrupted and the beams are switched off within ~ 10 ms. This system is backed up by the sensing of the shutter microswitch positions using the JET Central Interlock and Safety System (CISS) [5]. The reaction time for CISS to switch off the beams is ~ 125 ms - still short enough to protect the shutter from the beam power loading (values in the 1-10 MW/m² range).

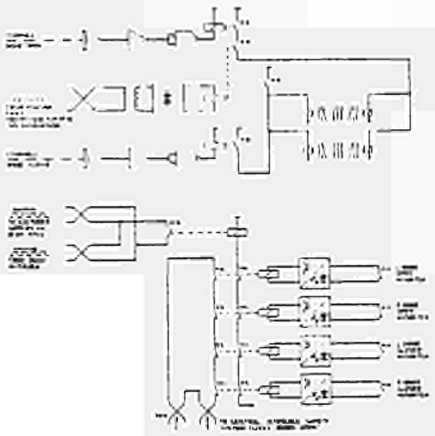

FIG 5
Electronic control interface
(simplified)

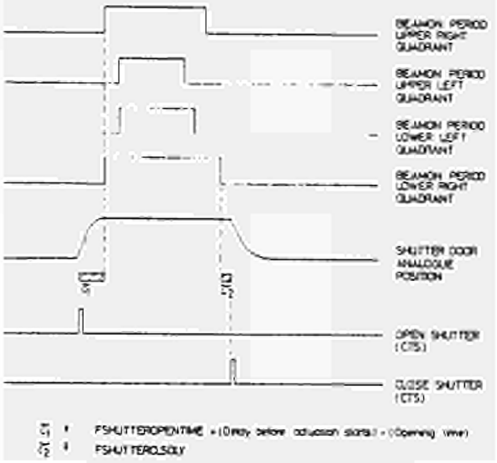

FIG 6
Time setting of shutter

PERFORMANCE OF THE SHUTTER

1. Opening and Closing Times

The opening and closing of the shutter in response to the timing pulses is shown in Figure 7.

Opening time is ~ 330 ms.

Closing time (to the touching of the beryllium copper lips) is ~ 350 ms.

These opening and shutting times can be maintained down to half the normal pneumatic operating pressure (ie. down to 6 bar).

2. Conductance of the Shutter

The time history of the conductance of the shutter whilst opening and closing is shown in Figure 8 (calculated for tritium) and compared with the conductance of the neutral injection duct. It can be seen that the shutter conductance becomes limiting during the last ~ 100 ms of the closing sequence.

The conductance of the closed shutter was measured by filling the Neutral Injector Box (NIB) with H_2 gas with cryopumps off and pumping the NIB through the closed shutter using the torus pumps. The molecular conductance of the closed shutter is hence ~ 50 l/s for tritium. This corresponds to an aperture of ~ 90 μm.

NEUTRAL INJECTOR TRITIUM LOAD CALCULATIONS

From the measured performance of the fast shutter and the behaviour of gas recycling in JET discharges the tritium load on the cryopumps in JET D-T operation can be calculated.

The sources of tritium being condensed on the cryopump will be;

1) The gas feed of 1% tritium-contaminated deuterium through the injector neutralisers (calculated at ~3.5 mg tritium per pulse).
2) Leakage of tritium from the torus through the closed shutter during the interpulse periods.
3) Pumping of the neutral gas and recycling particles at the edge of a JET discharge by the neutral injection duct during the pulse period when the fast shutter is open.
4) For discharges which disrupt the pumping of the released neutral gas by the neutral injection duct whilst the fast shutter is closing.

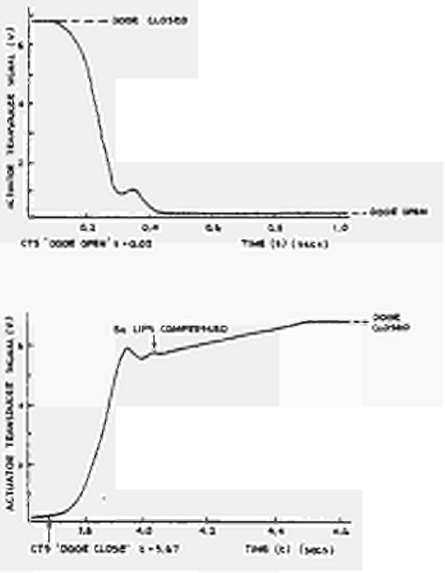

FIG 7
Opening and closing displacement waveforms

Sources (2) to (4) have been those whose minimisation has been addressed by the Fast Shutter design.

With a torus base pressure of < 10^{-7} mbar and the very low conductance of the closed shutter the quantity of tritium pumped into the NIB during the 10 minute interpulse period is a few μ gm and is negligible compared to other sources.

The cold neutral gas pressure at the edge of JET discharges during neutral beams is of the order of 5 10^{-6} mbar during low current (1.0 MA) discharges and should be much less at the high currents to be used in the D-T phase. During a 10 second injector pulse this would lead to an upper limit ~ 0.27 mg of tritium on the cryopump per pulse from this source.

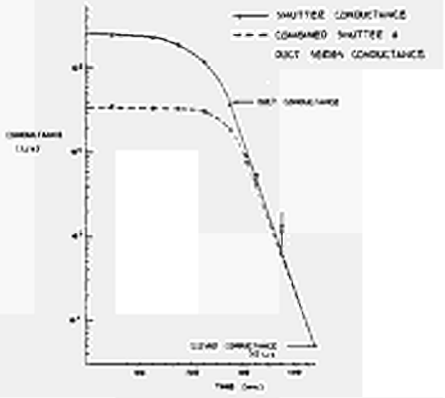

FIG 8
Temporal variation of combined neutral injection duct and shutter conductance

The measured recycling rate during JET beam heated ($P_{NBI} \leq 10$ MW) discharges at medium plasma currents (I_p = 3 MA) is ~ 1.2 10^{22} particles sec^{-1} at average densities (n_e) of ~ 4 10^{19} m^{-3}. The recycling scales roughly linearly with density but drops as the plasma current is raised (which will be the case for D-T plasmas) thus we may take these figures as typical. About 15% of this recycling is from the torus wall in limiter plasmas. Thus taking 200 m^2 of vessel wall area and 0.5 m^2 cross section of the neutral injection duct gives ~ 4.5 10^{18} particles sec^{-1} streaming into the N.I. duct. Roughly 50% of these will be tritium giving (for a 10 second pulse) ~ 0.2 mg on the cryopump from this source.

Disruptions

The pressure rise in the JET vacuum vessel after a disruption with NBI power is shown for 2 JET pulses with NBI in Figure 9. The difference in the way this pressure rise is pumped away when the shutter is open and when it is closed is displayed. (In the first case the NIB cryopump's speed is limited only by the injector duct conductance ~ 4.9 10^4 l/s^{-1} for deuterium).

To estimate the quantity of tritium onto the cryopump from such a disruption we assume:

- torus pressure ~ 3 10^{-3} mbar. 50% tritium.
- closing shutter conductance ~ flat for first ~ 250 ms = 3.5 10^4 l/s^{-1} then exponentially dropping to zero at 450 ms.
- JET vessel volume of 160 m^3.

This gives ~ 0.6 mg of tritium per disruptive pulse.

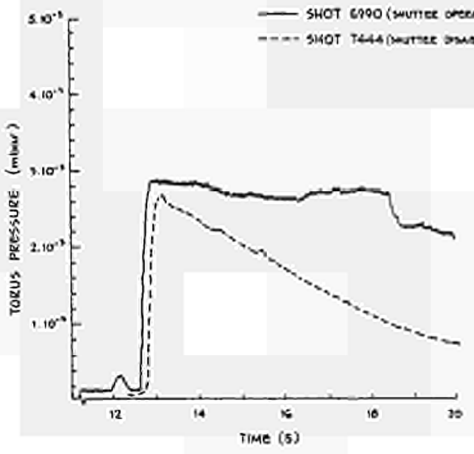

FIG 9

Torus pressure rise after disruption, showing effect of leaving shutter open

TABLE 1 : ESTIMATED SOURCES OF TRITIUM CRYOPUMP LOAD

Source	Quantity per pulse
1. Tritiated deuterium (1%) fed into Beam Neutraliser cell	1% of 300 mbar $l\ s^{-1}$ for 10 secs ~ 3.5 mg
2. Interpulse leakage from Torus through Fast Shutter	~ few ug
3. (a) Cold neutral gas pumped from edge of discharge during shutter open period. (10 secs).	Neutral gas pressure ~ 5 10^{-5} mbar 50% T ~ 0.27 mg Duct conductance (T) ~ 6.10^4 l
(b) Recycling particles streaming into injector duct during shutter open period.	Recycling ~ 4.5 10^{18} sec^{-1} into duct 50% T ~ 0.2 mg
4. Disruptions Unpumped gas pumped during shutter closing period.	Torus pressure ~ 3 10^{-3} mbar 50% T Duct conductance time profile as in figure 9. ~ 0.6 mg

TABLE 1

ESTIMATED FREQUENCY OF CRYOPUMP REGENERATIONS

In the D-T phase there will be 2 injector boxes. Adding up the contributions (1) to (3) for 1 box we have (see Table 1) ~ 4 mg tritium per pulse. In addition an estimate must be made of the frequency of disruptions. For the first 9 months of injector operation these

have been running at ~ 8% of total shots and we take 10% of our estimate. Thus the total tritium per pulse becomes ~ 4.1 mg. For two boxes this corresponds to 8.2 mg.

The acceptable quantity of tritium on the cryopumps is likely to be in the gm range which gives ~ 120 injected pulses between cryopump regenerations. At around 6 pulses per hour this gives 20 hours of operation.

REFERENCES

[1] eg: Duesing, G., JET NEUTRAL BEAM INJECTION SYSTEM : CONSTRUCTION AND COMPONENT TESTS, 13th SOFT, Varese (1984) (also in JET-P(86)01)
Goede, A.P.H.G. et al, PERFORMANCE OF THE FIRST JET NEUTRAL BEAM INJECTOR, these proceedings. (Paper GP13)

[2] Bombi, F., ARCHITECTURE OF THE CONTROL AND DATA ACQUISITION SYSTEM OF THE JET EXPERIMENT, 10th Symposium on Fusion Engineering, Philadelphia, PA (USA), (1983)

[3] Bombi, F., ARCHITECTURE OF THE CONTROL AND DATA ACQUISITION SYSTEM OF THE JET EXPERIMENT, 10th Symposium on Fusion Engineering, Philadelphia, PA (USA), (1983)

[4] How J., et al, JET PULSE TERMINATION NETWORK, these proceedings. (Paper GP06)

[5] Bombi, F., Nijman, J.P., and van Montfoort, J.E., CENTRAL INTERLOCK AND SAFETY SYSTEM OF JET, 13th SOFT, Varese (1984) (also in JET-P(85)02).

OVERVIEW AND OPERATION OF THE CONTROL, SAFETY AND INTERLOCK ON THE JET NEUTRAL BEAM INJECTOR

D Stork, T T C Jones, A Burt, D Cooper, J F Davies, D T Ewers, J G Krom, P McCullen[1], J P Nijman, A Stäbler[2], K D Starley[3], D Young and I D Young.
JET Joint Undertaking, Abingdon, Oxon OX14 3EA.
(1) Assigned to JET under contract from TRASYS (2) Euratom - IPP, Garching, FRG
(3) Assigned to JET under contract from CAP

ABSTRACT The computerised control, safety and interlock system on the first JET Neutral Beam Injector is described.

1. INTRODUCTION

The first JET Neutral Injector [1] is capable of delivering 10 MW of Deuterium beam (full energy 80 kV/atom) or 5.8 MW of Hydrogen beam (full energy 75 kV/atom) to the JET plasma. The injector (shown in figure 1) poses severe problems for safety of operation. These arise from:

- the long-pulse (≤ 10 second) capability of the beams
- the high power densities (10-100 MW/m² range) involved. The beamline components and the JET Tokamak need to be protected against operational errors and plasma or system fault conditions during the pulse.

In addition to the stringent safety requirements, flexibility in the control is needed both asynchronously from the JET Tokamak and synchronously during injection experiments.

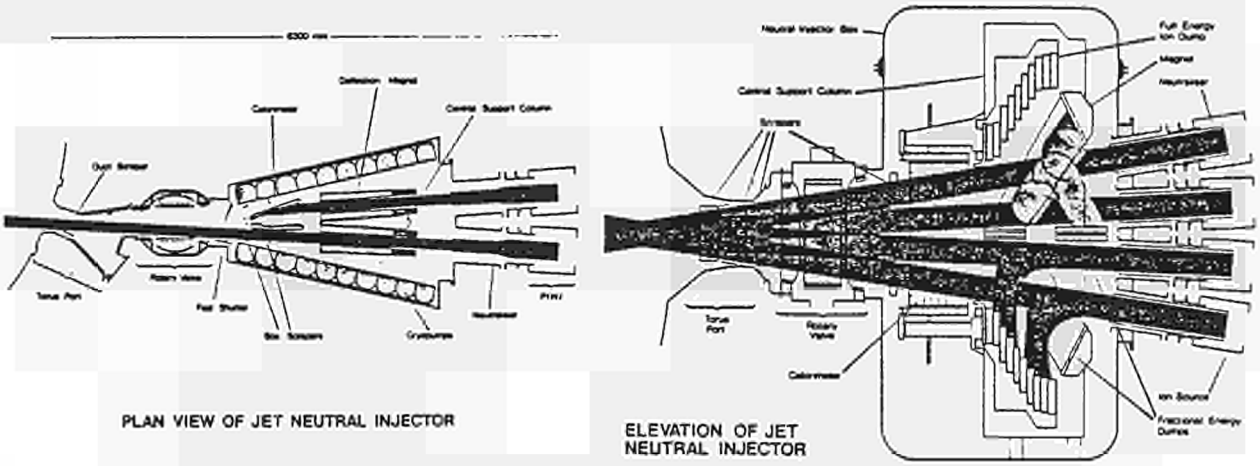

Figure 1 : Plan and elevation of the Neutral Injection Beamline.

2. OVERVIEW OF THE SYSTEM

System control is split amongst 3 JET CODAS [2] subsystem NORD 100 computers. The dedicated 'AH' (Additional Heating) computer, with 2.0 Mbyte RAM plus cache memory and 1 75 Mbyte hard disc, handles the control of the pulsed services to the beamline plus all beamline diagnostics. The pulsed services include the Neutral Beam power supplies (High Voltage and arc); the Deflection Magnet Supplies; Gas Introduction system; Fast Shutter and the Plasma Density Interlock.

Non-pulsed services for the beamline vacuum (turbo pumping, cryopumping etc) and the beamline water cooling are handled by two subsystem computers not dedicated solely to Neutral Beams. The basic interlocks for these systems are integrated by the AH computer however.

A basic feature of the control is the Plant Status Image (PSI); a core-resident map of all the hardware status of the system which includes several pseudo- (or software defined) points.

Basic interlocks for the system are ensured by using a Programmable Logic Controller (PLC)- based system, described below (AH-CISS) and various faster-acting integrated hardware interlocks, eg: the Plasma Density Interlock which is also described below.

3. MODES OF OPERATION AND PULSE TYPES

To achieve high security and flexibility we have defined for the AH beamline system MODES OF OPERATION (OPMODEs) and TYPES OF PULSE (PULSTYPs).

A summary of how control depends on OPMODE and PULSTYP definition is shown in table 1. The Neutral Beam system has 3 distinct OPMODES. One is Asynchronous Mode (ASYNC) with the beamline operated asynchronously from the rest of the JET machine. The Neutral Injector Beamline (NIB) vacuum is isolated from JET and the beam stop calorimeter blocks the beam. Control in this mode comes entirely from the AH computer. The other two modes are synchronous with JET and control is from the Main Control (MC) computer with AH slaved. In these modes a test mode (SYNCTEST) and a fully operational mode (SYNCOP), the NIB vacuum is connected to JET. The SYNCOP mode is the one used for Neutral Beam experiments. SYNCTEST can involve injection into JET without an adequate plasma density and the pulses are kept short (≤ 0.5 seconds beam) by the hardware interlocks. The PULSTYPs available within an OPMODE can be very wide-ranging from simple 'GAS-ONLY' puffing to full 8 beam operation.

Defining →	Leads to definition (by the system) of →	Which defines
OPMODE	· CISS Interlock Logic	· Basic safety of the system (fail safe backup)
	· RED ALARMS presented on AH	· Operator interface to high priority plant faults
PULSTYP	· Setting screens available to operator	· Timing of pulse : Power supply setpoints] via operator Gas system setpoints : PINI selection] input
	· Prepulse checks for prepulse check prog.	· Conditions under which beamline countdown terminated/suspended.
	· YELLOW and TAN ALARMS presented on AH	· Operator interface to other plant faults.
	· CAMAC modules active in Data Acq. Sys.	· Data Acquisition executed during pulse and stored in Subsystem Pulse File.
	· Display Options	· Data display available to AH operator after pulse.

Table 1 : Control via OPMODE and PULSTYP

4. HIGH LEVEL CONTROL

High level control is achieved by a suite of Real Time (RT) programs comprising a TASK-SCHEDULER; a prepulse-check program (NIBLECH); countdown and supervisor programs and dedicated programs to control a particular 'Local Unit' of plant (eg: the Gas Handling System) - the so-called 'Level 2' programs. The relationship between the RT programs controlling phases of operation is shown in figure 2.

4.1 TASK-SCHEDULER

TASK SCHEDULER assures first-line safety by taking the beamline operator systematically through the prepulse-setup and postpulse phases.

The action sequence is defined by the ACTIONS TREE (figure 3), a fixed data structure loaded and read via NORD ISAM File Handling routines. The operator selects permitted options at SELECTION NODES and TASK-SCHEDULER will subsequently activate slave RT programs;

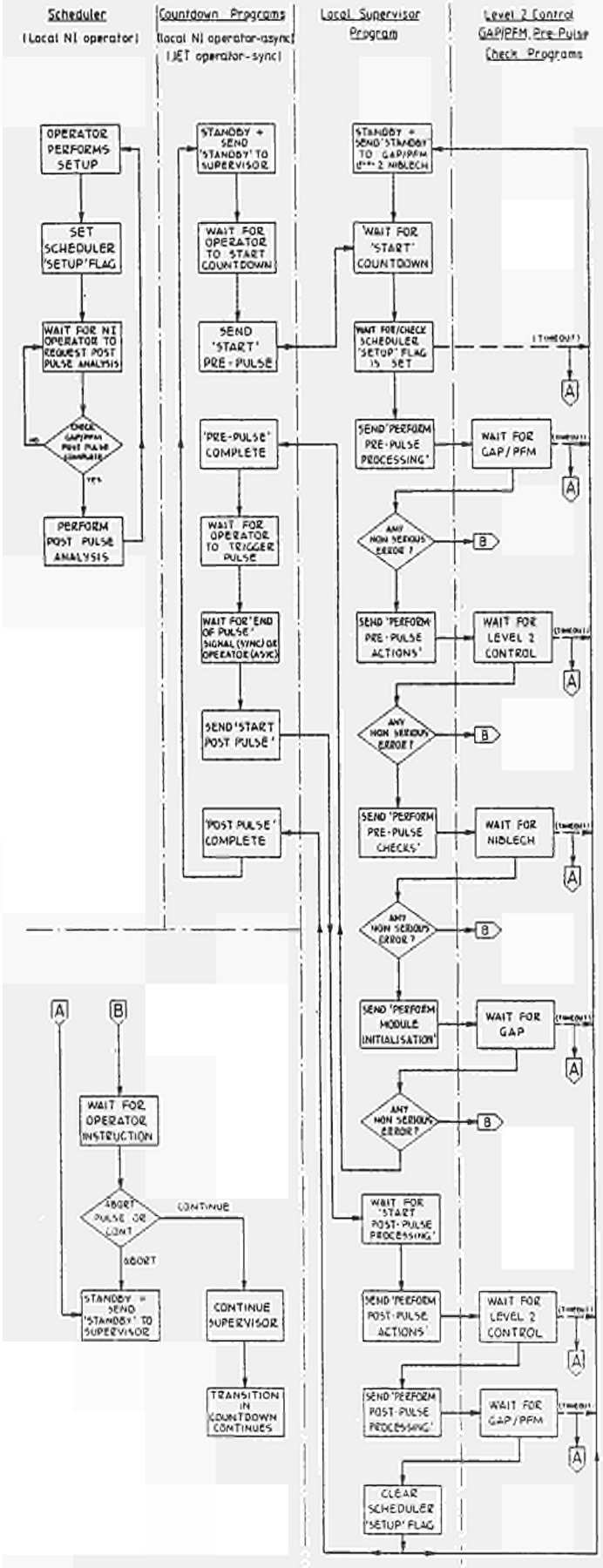

Figure 2 : Controlling RT program relationships.

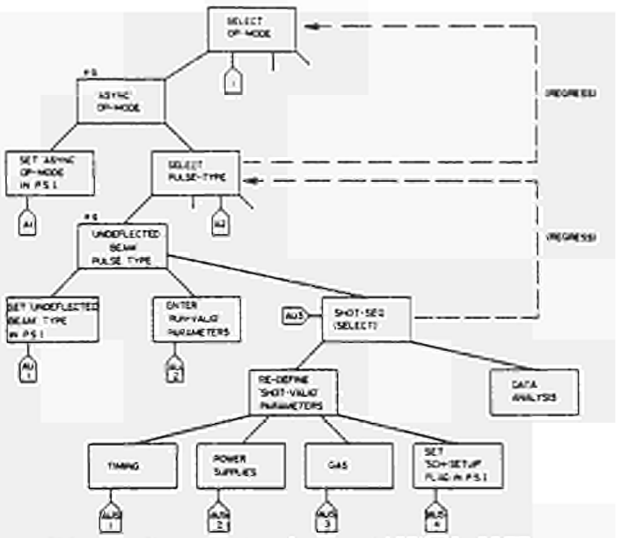

Figure 3 : Part of the ACTIONS TREE.

perform terminal or plant I/O; write to the disc-resident 'tree' representation of the CAMAC (the GAP tree [2]); send messages containing plant data to the Level 2 programs; evaluate pre-specified arithmetic expressions involving database quantities. The GAP tree information is used by the General Acquisition Program to determine which data is collected after the pulse.

4.2 PULSED PARAMETER SETTING

4.2.1 Timing

Pulsed control is achieved using a branch of the JET Central Timing System (CTS) a series of CAMAC timers (figure 4). The basic 'building-block' is a QUADRANT of the NIB (2 vertically adjacent ion sources (PINIs) and neutralisers and the deflection magnet in front of them) and each quadrant is timed independently from the other quadrants with one chain of CAMAC timers for each quadrant. The firing of each chain is inhibited until the defined PULSEON period (see section on CISS).

To avoid error and non-optimum operation, a 'familiar' set of dummy times such as BEAMPULSELENGTH,

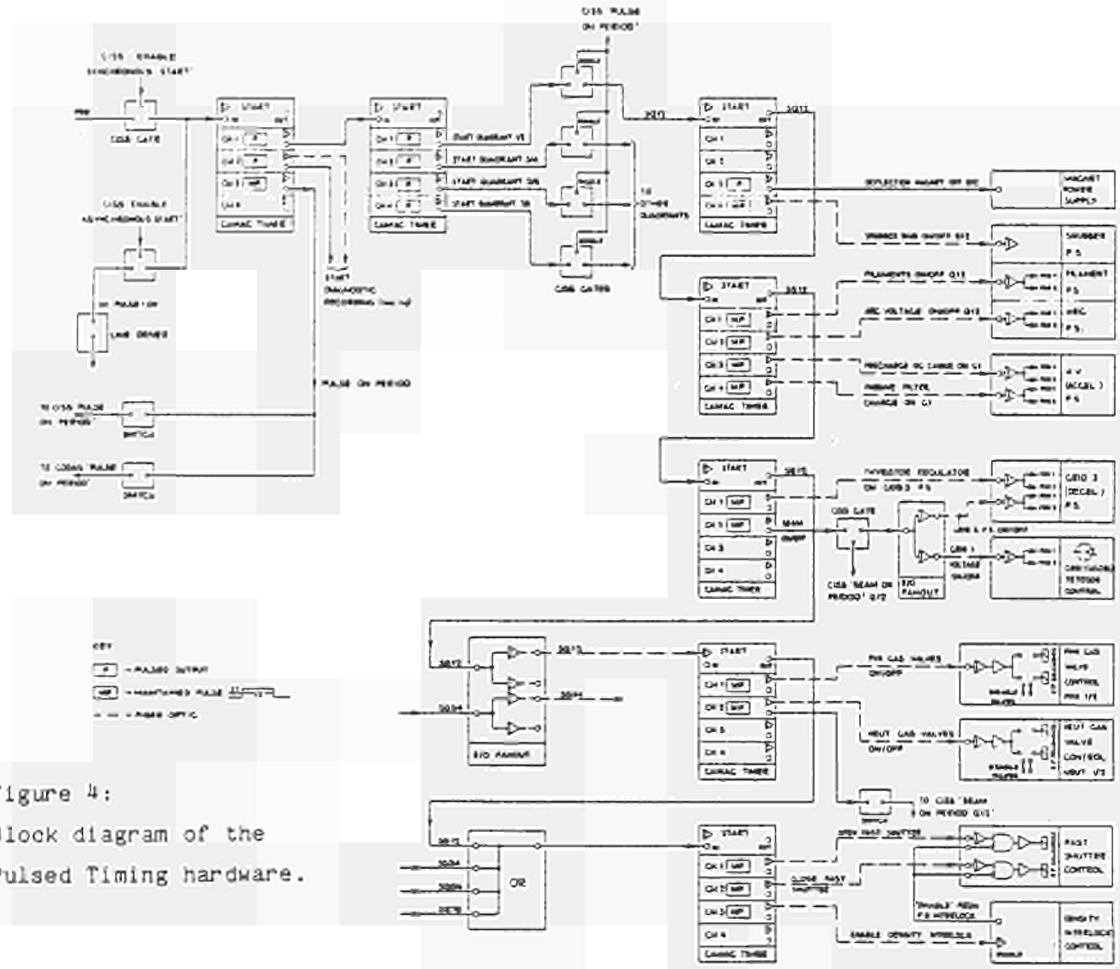

Figure 4:
Block diagram of the
Pulsed Timing hardware.

FILAMENTWARMUPTIME etc are set by the operator and arithmetic expressions are used to rela these to the hardware register times. These expressions form a network, part of which is shown in figure 5. A subset of the 'END-NODE' times determined by a PULSTYP definition are presented to the operator on other parameters from the database, rangechecks important times for error and loads times into the hardware.

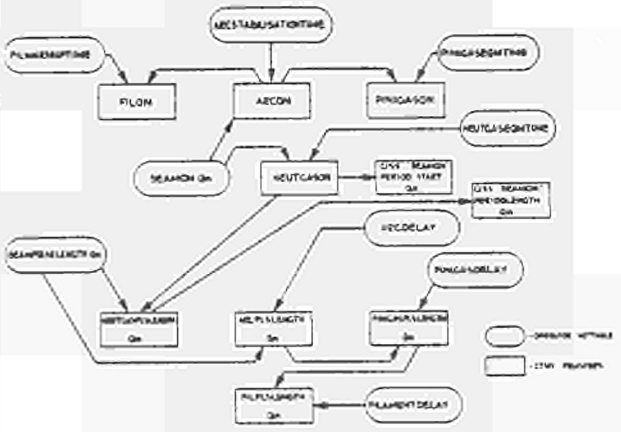

Figure 5 : Timing network of relationships

4.2.2 Voltages and Gas parameters.

The process is essentially similar to that employed for the timing. Mathematical relationships are established between the 'raw' plant set-points and meaningful input parameters. These relationships come from database curves which have been established in ASYNC experiments. An example is the 'ARC model' for an Ion Source (PINI) which relates the beam extracted current (IEXT) to the power supply Arc current setting (IARC) viz

$$IEXT = IARCPARMA + IARCPARMB * IARC$$

where IARCPARMA and IARCPARMB are constants.

The relationships form a network which is shown for one quadrant in figure 6. A large

number of power supply setpoints are fixed by the operator setting only the beam voltage (V_b) and perveance (p) of the PINIs in the quadrant. After evaluation, the raw setpoins are packed into messages and transmsitted to the level 2 software.

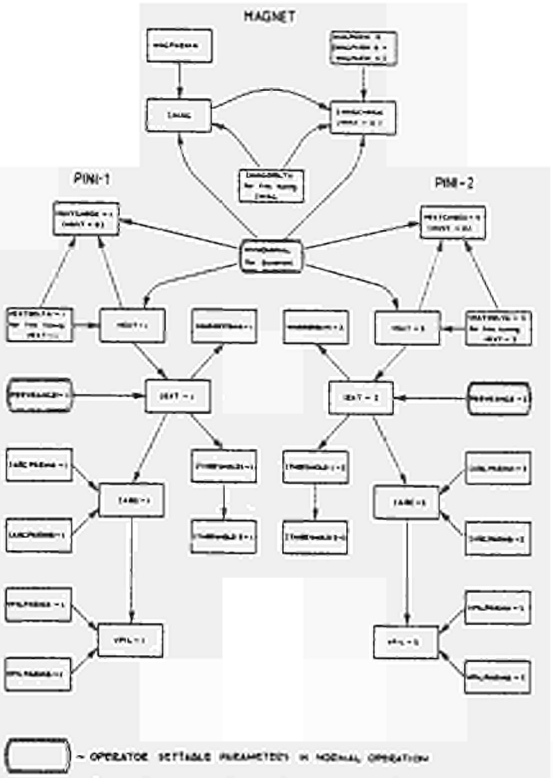

Figure 6 : Power Supply setpoints network

4.3 PREPULSE CHECK PROGRAM ' NIBLECH

NIBLECH confirms the correctness of beamline configuration and critical Power Supply setpoints. The checks which are done by NIBLECH are determined by OPMODE and PULSTYP information in the PSI. If a serious fault is detected NIBLECH aborts the countdown to the pulse and alerts the operator via an Alarm-Handling software. NIBLECH performs several sophisticated plant checks including algorithmic validation of the on load Deflection magnet currents and checks on the Protection Plate Viewing system (see below).

5. BASIC FAIL-SAFE BEAMLINE SAFETY

Integrated hardware interlocks for the beamline are divided into 2 distinct areas (excluding purely Local interlocks).

- CISS INTERLOCKS : which provide for basic safety of the beamline for faults of slow (≥125 ms) timescale. A subsystem of the JET Central Interlock and Safety System (CISS) is used.
- FAST INTEGRATED HARDWARE INTERLOCKS : replace CISS where a fast response is required. An example is the interlock against beam injection into JET with inadequate plasma density (see below).

5.1 CISS

The basic safety is ensured by a subsystem of the JET CISS one of whose Simatic s5-110F PLC's [4], (AH-CISS) is dedicated to the NIB. The important Local Unit status signals are wired to AH-CISS and go/no-go outputs are wired from AH-CISS to important items of Local plant. The PLC is self-checking (dual processors running identical EPROMs) and continually tests all input signals. Outputs are of the maintained (24V) type. Local unit action (eg: supply of HV) is maintained whilst the voltage is present and is terminated on removal of the 24V.

The AH-CISS operational states are defined in a state-transition diagram shown, with explanation, in figure 7. Transitions between states are implemented using a state-machine

AH-CISS States

- NORMAL usual state between pulses. All the enabled sub-units are in safe condition and ready for pulse to be initiated.
- PULSE-ON entered via CTS trigger (which CISS ensures comes from the CORRECT SOURCE). State in which the Ion Source sequence is activated. Timeouts initiated to prevent state being overlong.
- PULSE-INHIBITED State entered from Normal if conditions exist which would not comply with a safe Pulse. All thyristors of Power Supplies are blocked.
- EMERGENCY SHUTDOWN State entered from Pulse On if seriously abnormal condition is detected. Thyristors on Power Supplies blocked thereby removing the beams.
- FULL SHUTDOWN Lowest operational state with all P.S. Circuit Breakers open. Reached by command from JET CISS Supervisor.

Figure 7 : AH-CISS States

resident in the PLC. The PLC executes a complete memory cycle in 125 ms.

The logic templates used by AH-CISS to initiate transitions between states are OPMODE dependent, the OPMODE selection being transmitted by CODAS to CISS. An example of the logic template for INHIBIT PULSE request is shown in figure 8. The status of the CISS inputs is available to the operator via a serial link driven mimic. Plant conditions generating INHIBIT PULSE or EMERGENCY SHUTDOWN requests have parallel signals sent to the PSI where they are used to generate urgent (RED) alarms on the operator's console.

AH-CISS also performs direct interlocks such as ensuring that the Pulse-On transition comes from the correct source by gating the CTS branch; (figure 4) inhibiting the application of High Voltage except in a special CTS-defined 'BEAMON' period (figure 4) and ensuring that the selected neutraliser gas valves are open during the BEAMON period so that properly neutralised beam is extracted.

5.2 PLASMA DENSITY INTERLOCK/FAST BEAM INTERLOCK

The unattenuated 80 kV/ D° neutral beams would put very high power densities(~31 MW/m^2) on the Tokamak inner wall and beams must therefore be switched off quickly (on a few millisecond timescale) if the plasma disappears. Also the position of the Fast Shutter [5] once fired can change significantly on a millisecond timescale. Its position must therefore be interlocked with the beams.

These interlocks are combined in a Plasma density Interlock/Fast Beam Interlock which features signals from the JET Plasma Fault Protection System (PFPS), Fast Shutter Control and the Protection Plate Viewing System (PPVS).

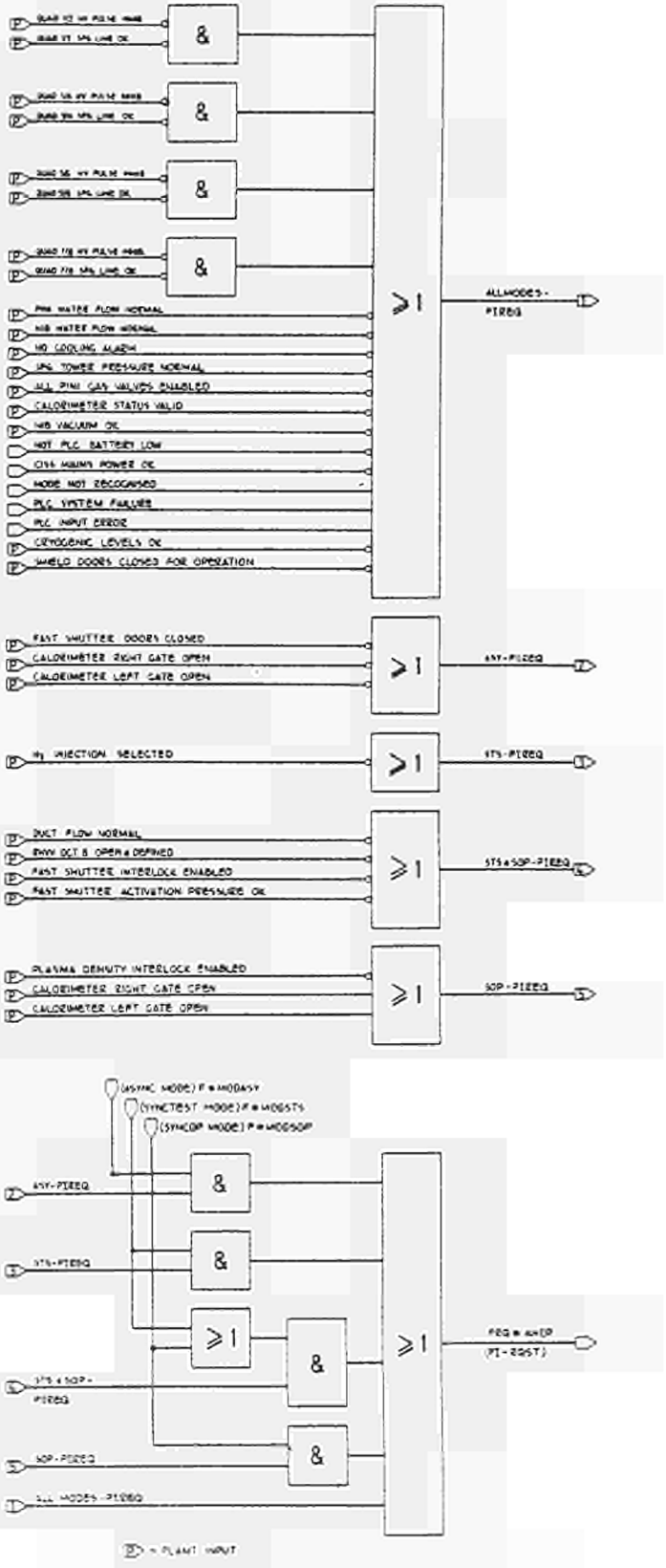

Figure 8 : AH-CISS Pulse Inhibit logic

The total system is shown schematically in figure 9. Fail-safe integrity is maintained by exchange of 500 Hz - 1 kHz pulse train signals. The pulse trains are sent by the

Fast Interlock to the Neutral Beam power supplies. Disappearance of the pulse trains leads to the switch-off of the neutral beam sustaining power supplies (H.V. and Arc). Once off, the beams are permanently disabled until the next shot.

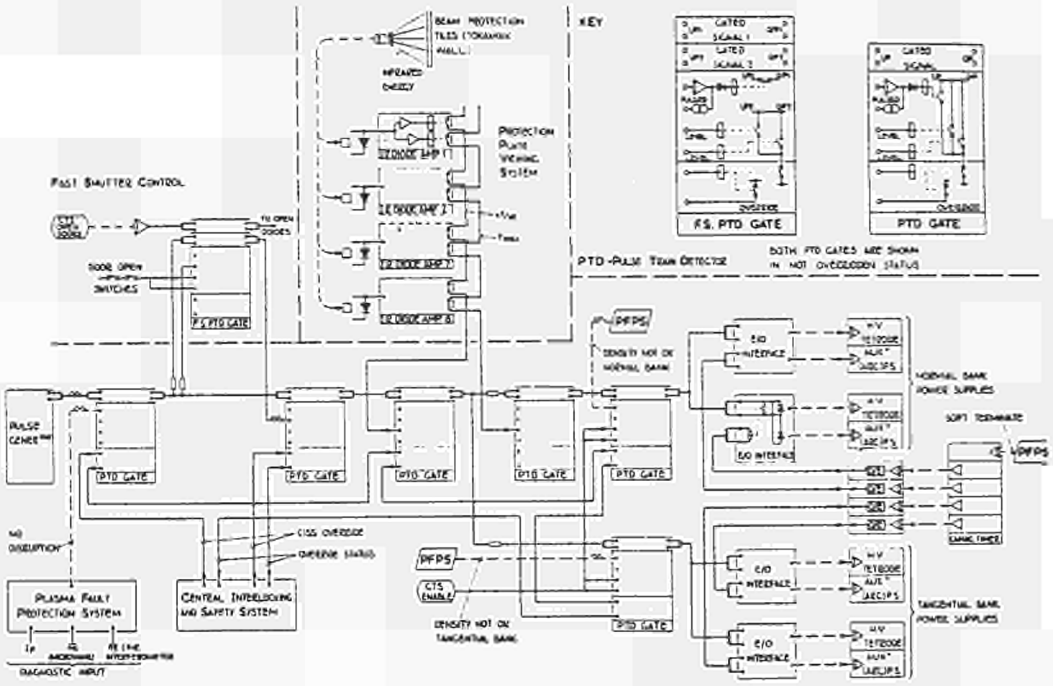

Figure 9 : Schematic of the Plasma Density Interlock/Fast Beam Interlock

The pulse trains can be interrupted by the closure of one of several NORMALLY CLOSED (N.C.) relay contacts across the signal lines. The N.C. relays are kept open by PFPS signals; signals from the Fast Shutter control indicating 'Doors Open' and the PPVS detectorss indicating that the Tokamak protection tiles are not too hot.

5.2.1 PFPS

PFPS is a microprocessor-based system which interrogates signals from plasma diagnostics measuring plasma current (I_p); current derivative ($\dot{I}_p$); plasma density ($\bar{n}_e$) and hard X-ray flux (ϕ_{HXRAY}). It is described in detail in reference[6]. PFPS is preprogrammed before the pulse with the acceptable plasma current and density levels which will keep the beam 'shine through' power on the inner and outer walls below acceptable levels. These levels are based on code runs simulating the beam 'power footprint' at the Torus and on measurements on the neutral Injection Test Bed [7] and during SYNCTEST no-plasma beam pulses on JET [8]. Using real-time evaluation of the diagnostic signals PFPS permits injector operation using the signals shown in table 2.

Signal	Generated by	Output type	Action at NB interloc
PFPS-SOFT (SOFT STOP)	(i) $I_p > I_{p,max}$ (ii) $n_e > n_{e,max}$ (iii) Low validation on density data [6]	Level change (NON FAILSAFE)	Initiates pre-programmed switch off of PINI beams in pairs
PFPS-HDISR	(i) $I_p > I_{p,min}$ AND (ii) $\phi_{HXRAY} < \phi_{HX,MAX}$ AND (iii) $\dot{I}_p < \dot{I}_{p,max}$	Pulse train present whilst conditions satisfied. (FAILSAFE)	Provide immediate switch off of ALL beams (DISRUPTION SIGNAL) Immediately close Fast Shutter [5]
PFPS-DOBT	(i) $I_p > I_{p,TAN,MIN}$ AND (ii) $\bar{n}_e > \bar{n}_{e,TAN,MIN}$	Pulse train present whilst conditions satisfied. (FAILSAFE)	Provide immediate switch off of TANGENTIAL beams. ('DENSITY NOT OK')
PFPS-DOBN	(i) $I_p > I_{p,NORM,MIN}$ AND (ii) $\bar{n}_e > \bar{n}_{e,NORM,MIN}$	Pulse train present whilst conditions satisfied. (FAILSAFE)	Provide immediate switch off of NORMAL beams. ('DENSITY NOT OK')

Table 2 : PFPS signals

Part of the Density Interlock must be overridden in order that injector operation can occur in ASYNC and SYNCTEST modes,

when no plasma is present in JET. This is done in a failsafe manner using AH-CISS which has the OPMODE template in its logic.

5.2.2 PPVS DETECTION SYSTEM

The PPVS detectors are an array of Ge-diodes viewing the Tokamak protection tiles [9] through a sapphire window and long length (~ 50 m) of radiation-resistant low-loss silica fibre-optic. The system is shown schematically in figure 10. The diodes are sensitive to Infra-Red radiation in the 0.8 - 2.0 μm range.

The system has built-in redundancy with two independent diodes viewing one area of tile. The system has self-checking facilities; light sources in the optical head are activated by the NIBLECH prepulse check before each pulse to check fibre and diode; test ramps are also input into the electronics by NIBLECH to check electronic drift.

Signal processing electronics produce both tile temperature (T_t) and temperature derivative (dT_t/dt) signals to provide the trip to remove the Beam Power-Supply pulse trains. To protect the tile supports T_t must be ≤ 1200° C. The diodes' electronics are sensitive to signals ≥ 60 nA corresponding to T_t ≥ 550° C giving a wide safety margin. This high sensitivity is achieved by cooling the diodes and careful electronic circuit design. The PPVS response time is < 10 ms.

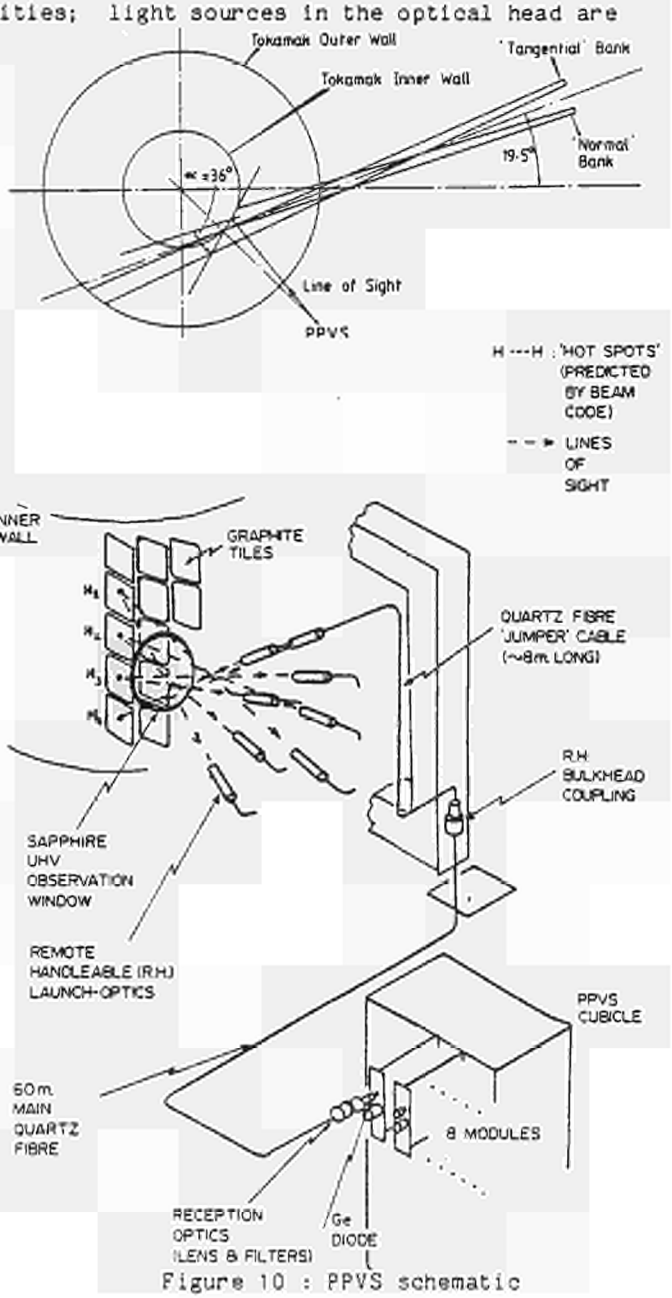

Figure 10 : PPVS schematic

6. SWITCHING BEAMLINE ISOTOPES

Beamline operating conditions are very different for D° beam and H° beam injection with different power densities; different source perveance/arc model relationships; different deflection magnet settings etc.

In order to cope with this two different versions of NIBLECH are used. Each version being flagged with the isotope to which it relates. In

addition the gas type in the supply reservoirs can only be changed over if the reservoirs are evacuated which is ensured by a keyswitch/pressure switch interlock complex. This ensures the contamination of the 'wrong' isotope in the gas feed to the sources is $\leq 0.4\%$.

The selected gas is input to both the PSI and to CISS. Unless the gas flags for NIBLECH, the database and the PSI all agree, NIBLECH aborts the countdown sequence and no pulsing is possible.

7. OPERATIONAL EXPERIENCE

The control system has (by early August 1986) performed more than 4000 ASYNC on-load pulses (with > 1700 with the full NIB system); 20 plus SYNCTEST pulses into the empty JET Tokamak and more than 450 SYNCOP injection pulses into JET plasmas. About 8% of the injection pulses have been terminated by a plasma disruption or soft stop whilst the beams were on. The beam interlock has performed correctly. It is possible for the whole beamline to be controlled routinely by just one operator.

The failsafe backup has coped correctly with a handful of high-danger faults which have occurred. These have included spurious (noise generated) timer firings which have been caught by the BEAMON CISS logic; failure of the Calorimeter pneumatic control; one occasion when the Fast Shutter failed to open and one occasion when register corruption led to a wrong deflection magnet setting.

In the one major accident which has occurred during pulsing, an unscheduled fast time-scale (few seconds) cryopump regeneration led to a pressure excursion and high reionisation power loadings in the duct. Although an AH-CISS Emergency Shutdown was performed (in < 125 ms) melting occurred in the duct liners leading to water leak and extensive down time. As a result the interlocking with the cryogenic supplies has been tightened up.

The cycle time between ASYNC pulses is ~ 5 minutes with minimum interpulse analysis. Pulse data files produced are generally analysed off-line overnight.

ACKNOWLEDGEMENTS

The general software facilities on the system are the responsibility of the JET CODAS division whose help in implementation is gratefully acknowledged.

The help of A Brown in commissioning the system and of T Norman in the preparation of the paper and poster were invaluable.

The authors would also like to acknowledge stimulating and helpful discussions with Drs V Jacobson and E Theil of Lawrence Berkeley Laboratory and Dr M J Mead of JET.

REFERENCES

[1] eg: Duesing, G., JET NEUTRAL BEAM INJECTION SYSTEM : CONSTRUCTION AND COMPONENT TESTS, 13th SOFT, Varese (1984). (also in JET-P(85)01).
Goede, A.P.H., et al, PERFORMANCE OF THE FIRST JET NEUTRAL BEAM INJECTOR, these proceedings. (Paper DP47).

[2] Bombi, F., ARCHITECTURE OF THE CONTROL AND DATA ACQUISITION SYSTEM OF THE JET EXPERIMENT, 10th Symposium on Fusion Engineering, Philadelphia, PA (USA), (1983).

[3] Bombi, F., Nijman, J.P., and van Montfoort, J.E., CENTRAL INTERLOCK AND SAFETY SYSTEM OF JET, 13th SOFT, Varese (1984). (also in JET-P(85)02).

[4] Euringer, M., Reichert, W., SIMATIC S5-110F SAFETY-ORIENTED PROGRAMMABLE CONTROLLER, Siemens Power Engineering Vol 11, No 8, (1980).

[5] Watson, M.J., Haange, R., Stork, D., Tivey, R.B., and Young, D., A FAST SHUTTER SYSTEM FOR THE JET NEUTRAL INJECTORS, these proceedings. (Paper DP48).

[6] How, J., et al, JET PULSE TERMINATION NETWORK, these proceedings. (Paper GP06).

[7] Stäbler, A., Deschamps, G.H., Falter, H.D., Hemsworth, R.S., and Massmann, P., TEST OF GRAPHITE TILES IN THE NEUTRAL BEAM TEST BED, JET-DN-C(85)19 (1985).

[8] Stork, D., and Stäbler, A., OPERATING LIMITS FOR JET PULSES WITH NEUTRAL BEAMS, JET-DN-C(86)32 (1986).

PERFORMANCE OF THE FIRST JET NEUTRAL BEAM INJECTOR

A P H Goede, C Challis, T T C Jones, A Stäbler*, D Stork, E Thompson
JET Joint Undertaking, Abingdon, Oxfordshire, OX14 3EA, England
* attached from IPP Garching, W-Germany

ABSTRACT

The operational performance and beam line physics aspects of the first Neutral Beam Injector installed on JET are reported. Injection of more than 8 MW of 80 keV deuterium beams for several seconds into the Tokamak has been successfully achieved.

1. INTRODUCTION AND SUMMARY

The first JET neutral injector which contains eight individual beam sources was brought into operation for injection experiments at the end of January 1986. This followed limited operational tests in the JET NI Test-Bed [1]. During the first period of operation in excess of 1600 pulses have been obtained, over 450 of which were injected into the torus, virtually all of which have been at power levels > 1 MW and pulse lengths > 1 sec. Accordingly, the availability (≈ 80%; ≈ 17 pulses/day) and reliability of the overall system has proved to be good.

During the first period of operation the following power levels have been injected into the torus,

- over 5 MW of neutral hydrogen beams at 65 keV energy and pulse lengths up to 7 sec,
- over 8 MW of neutral deuterium beams at 80 keV energy and pulse lengths up to 7 sec

both in co- and counter direction. The latter includes combined values of injected power and energy of 8.3 MW and 40 MJ respectively.

As reported elsewhere [2,3], neutral beam injection on JET has been successful in producing large increases in the ion temperature (in excess of 10 keV), significantly extending the density limit (≈ 6 x $10^{19}m^{-3}$) and sustaining beam driven currents (≈ 0.5 MA) for several seconds.

Overall performance is essentially in agreement with the results obtained from single source operation in the JET Test-Bed. The only significant deviation from the design being the effect of the stray magnetic field from the tokamak which had not been simulated in the Test-Bed. This results in a sideways deflection of the beams which is corrected for by deliberately off-setting the beam alignment. It is found that a single setting of the alignment is adequate for the range of 0 to 3 MA plasma current but realignment is necessary for operation at higher currents.

The total mechanical system has proved to be reliable, with only one mechanical failure occurring to date since the start of injection experiments. This fault concerns a leak in one of the protection panels lining the inner wall of the duct (thin-walled quilted nickel structure, water cooled), and developed as a result of excessive power loading from reionised beam particles, following a pressure excursion in the duct. No other components

(including plasma source filaments) have required repair, modification or replacement.

The injector is capable of operation in two distinct modes. The ASYNC mode in which injector operation is entirely independent of the tokamak and the beams are intercepted by the beamline calorimeter, and the SYNC mode in which injector operation is fully synchronised to that of the tokamak and the beams are injected into the plasma. The complete eight beam system requires only a single operator and uses a sophisticated computerised system for the setting of parameters, monitoring and carrying out safety checks in addition to data acquisition and display [4]. During periods of SYNC operation no ASYNC "conditioning" shots are required between injection pulses into the tokamak (which has a pulse repetition rate of 1 per 15 mins at best).

The behaviour of the beam line has been extensively monitored during injection using thermal and optical diagnostics. In this paper we present data on:

- the power loading of the beam line components, and these are compared with the design figures,
- the power injected into the Torus, evaluated with reference to theory and earlier Test-Bed results,
- the effects of the Torus stray magnetic field on the beam trajectory and the reionised beam fractions in the duct.

2. SYSTEM

The JET Neutral Injector is shown schematically in figs. 1 and 2 and has been described earlier in [5] Details of the complex power system are given in [6]. Eight ion sources [PINI's], each rated at 80 kV, 60 A hydrogen and 41 A deuterium at 10 sec pulse length, are grouped in four pairs, the ion fraction of each pair being handled by one bending magnet. The transmitted neutral beams then pass the calorimeter back panels and a set of scrapers at the exit of the Neutral Injector Box. Subsequently, they pass the fast shutter, the rotary gate valve and enter the duct to the torus where further scrapers are positioned together with quilted liners protecting the duct walls against the impact of reionised beam particles. All these components are water cooled, allowing water flow calorimetry to be performed. Temperature rise and water flow rate are monitored continuously by

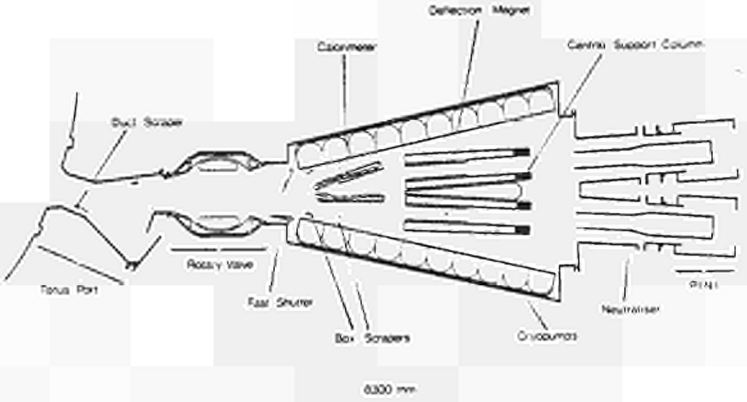

Fig. 1 PLAN VIEW OF JET NEUTRAL INJECTOR

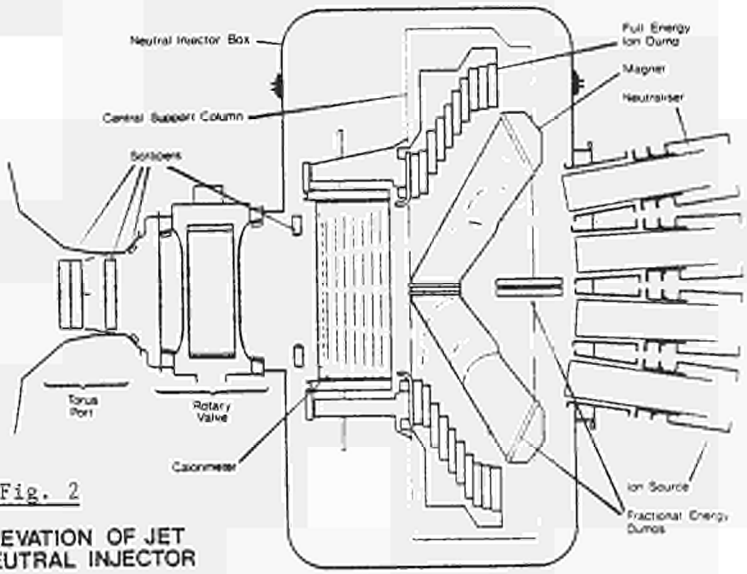

Fig. 2 ELEVATION OF JET NEUTRAL INJECTOR

thermocouples and turbine flow meters respectively; the wave forms are integrated and the power intercepted is displayed after each beam pulse.

3. BEAMLINE PERFORMANCE

Fig. 3 plots the beam power intercepted by the various beamline components downstream of the bending magnet against the toroidal plasma current I_p. Power loadings are expressed as a percentage of the extracted beam power IV where I is the extraction current and V the extraction voltage. The total power intercepted (fig.3b) ranges from 6.5 to 7.5% IV for 65 kV hydrogen to 7 to 8.5% IV in 80 kV deuterium operation and is shown to increase with plasma current. The latter fact is consistent with a progressive misalignment of the beam as the strength of the stray magnetic field increases with I_p. In fig. 3a the power loading to the left-hand duct scraper vertical element (DX-L) is seen to increase with I_p, at the expense of the right-hand scraper (DX-R), consistent with a beam shift to the left during co-injection where the poloidal stray-field points downward. For counter-injection the opposite is observed. Also, it is noted from the horizontal top and bottom duct scraper elements (DX-T & DX-B) that the beam moves slightly upward with increased plasma current, indicating that other than vertical stray-field components also play a part in the beam shift. A similar dependence on I_p is observed on the other beam line components; for instance the power to the calorimeter back panel facing the tangential bank (CB-TB) increases with I_p, at the expense of the calorimeter back panel facing the normal bank (CB-NB), also indicating beam movement to the left.

CB-NB = Calorimeter Backpanel Normal Bank
CB-TB = Calorimeter Backpanel Tangential Bank
BX = Box Scraper
FS = Fast Shutter
RHVV = Rotary High Vacuum Valve
DX-R/L = Duct Scraper Right/Left
DX-T/B = Duct Scraper Top/Bottom
DL-BR = Duct Liner Bottom Right
DL-TL = Duct Liner Top Left

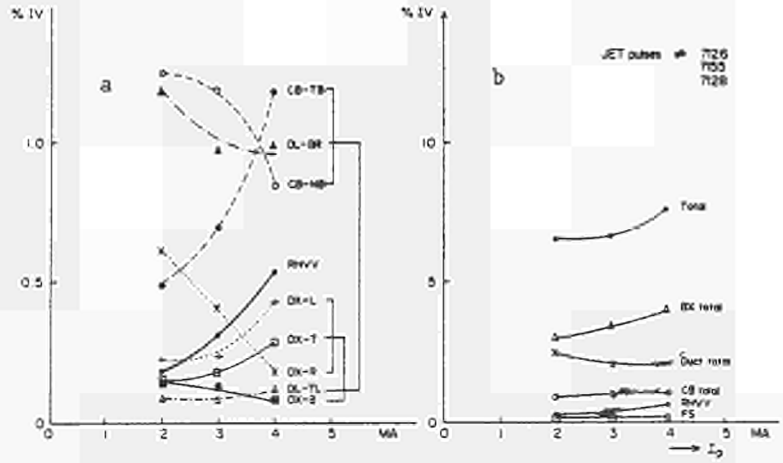

Fig. 3 Power intercepted by beamline components downstream of the bending magnet against toroidal plasma current I_p as a percentage of IV extracted. Co-injection 65 kV hydrogen.

Accurate positioning of the duct- and boxscrapers prevents the duct liners from direct beam interception. The measured power deposition from reionised particles on the duct-liners is predominantly to the bottom/right panel (DL-BR) in co-injection, whilst it is to the top/left panel (DL-TL) in counter-injection. This is expected from the calculated reionised particle trajectories in the vertical field of the Tokamak, which in the duct region points upward in co-injection.

The measured power loadings are compared with theoretical values in Table I. The power intercepted by the scrapers is calculated employing the ZAP-code [7], which models the beam as an array of Gaussian emitters of specified divergence, focus and steering. Beam aberation can be simulated in the code, but has not been included for the present

calculations. Two cases are considered, 65 kV hydrogen and 75 kV deuterium operation, both co-injection. The boxscrapers, which receive most of the intercepted beam power, have a calculated power loading of 1.8% and 2.7% IV respectively. Measured values are about a factor two higher. However, if one takes into account in the calculation a beam misalignment of 0.24°, corresponding to a 2 cm beam shift at the calorimeter, then good agreement with the measurements is achieved (Table I, figures given in brackets). A 2 cm beam shift at the calorimeter is approximately equal to the measured beam shift for an I_p = 4 MA discharge (see section 5). For the vertical duct scraper elements measured and calculated power loadings are also in agreement when assuming a 0.24° beam misalignment.

The power from reionised particles to the duct-liners follows from gas flow calculations and particle trajectory calculations. The calculated pressure in the rotary valve and duct region is approximately 10^{-5} mbar. Particles incident on the duct liner originate from the rotary valve region and display a focussing action of their trajectories near the duct liner leading to local power densities between 50 - 100 W/cm². Total reionised power levels agree well with the calculation both for the thin neutraliser target used in deuterium (figures in brackets in Table I) as well as for the nominal target in hydrogen.

TABLE 1: MEASURED VS CALCULATED POWER LOADING

	ZAP-Code 0.7° div				Measured	
	% Neutral		% IV		% IV	
	Perfect alignment	(0.24° misalign.)	65kV H_2	75kV D_2	65kV H_2	75kV D_2
Box Scraper BX	5.8	(12.9)	1.8 (4)	2.7 (6)	3-4	4.5-6.5
Duct Scraper DX	1.14	(2.3)	0.35 (0.71)	0.53 (1.08)	0.6-0.8	0.55-1.01
	reionised particle calculation				Measured	
Duct Liner	(thin neutraliser target)	nominal neutraliser target				
DL	(3.1)	4	1.3	(1.5)	1.1-1.3	1.1-1.9

4. POWER TO THE TORUS

The power injected into the torus is derived from the neutral power intercepted at the calorimeter in the ASYNC mode and, subsequently, by deducting from this figure the various beamline losses downstream of the calorimeter for each injection pulse in the SYNC mode.

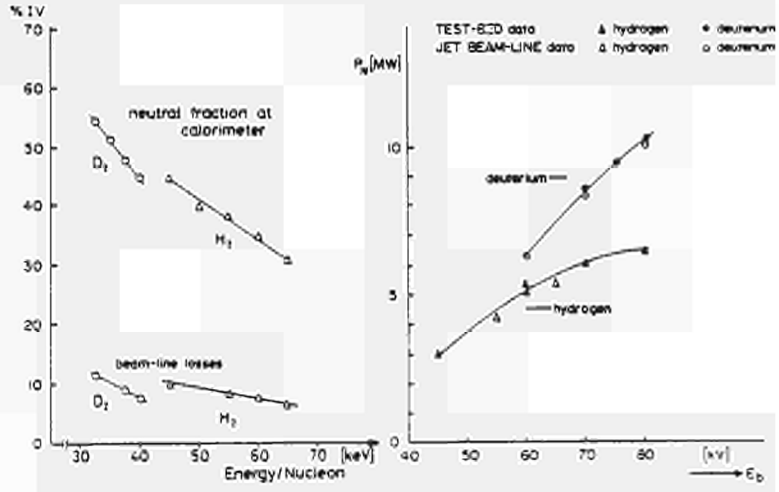

Fig. 4a Neutral fraction at the calorimeter and the beamline losses downstream the bending magnet, as percentage IV, plotted against beam energy per nucleon.

Fig. 4b Power into the torus calculated from fig. 4a, compared with the Test Bed predictions.

In Fig. 4a the neutral fraction measured at the calorimeter, and the beam line losses downstream of the calorimeter are plotted against energy per nucleon for hydrogen and deuterium. The decrease in neutral fraction with energy per nucleon reflects the reduction in

neutralisation efficiency. The graph includes grid and beam line losses upstream of the calorimeter. Data for deuterium refer to a x 0.7 thinner gas target as those for hydrogen, which explains the break in the two curves. The beamline losses decrease with energy, which fact is true also relatively to the incoming neutral beam fraction. Similarly, losses for deuterium beams are relatively smaller than those for hydrogen beams. Both facts illustrate that the beam particles becomes less affected by the stray magnetic field as their momentum increases.

The power into the torus, fig. 4b, is calculated from data of fig. 4a and is compared with the Test Bed predictions. Broad agreement is obtained. The Test Bed prediction is generally a few percent higher which may be attributed to higher beamline losses due to the stray field. This agreement implies confirmation of the thin neutraliser target (leading to reduced neutraliser efficiency) as observed in the Test Bed [8].

An obvious limitation of the above method of determining the power into the Torus is that it relies on 100% power accountability of the beam line which is not achieved. Test Bed results show the power accountability, however, to be in general better than 90% and therefore the error introduced by beam line losses not accounted for will most likely be $\leq$ 10%. The accuracy of the calorimetry itself is estimated to be $\pm$ 5%, which brings the total error bracket of power injected into the torus to (+ 5%, - 10%) IV extracted.

5. BEAM SHIFT

As described in section 3 the neutral beam moves to the left in co-injection depending on the plasma current. A quantitative measurement of the beam shift is obtained from the beam profiles measured at the calorimeter in synchronism with tokamak operation. The beam position and width are derived from a Gaussian fit to thermocouple measurements. As is shown in fig. 5a, for a 3 MA discharge the shift is $\approx$ 1 cm, corresponding to an angular deflection of $\approx$ 0.12°. This constitutes a significant fraction of the duct acceptance angle ($\pm$0.7°). At high stray-fields the beam also broadens. Beam width increases of up to 20% are observed (Fig 5b).

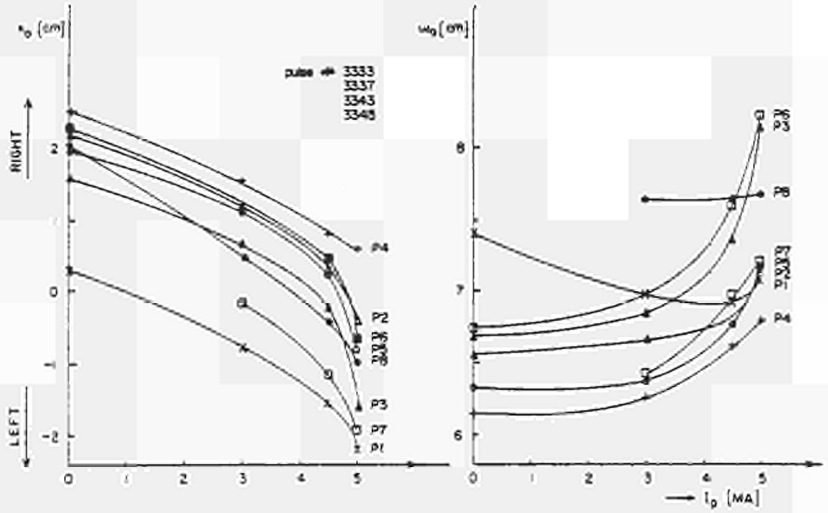

Fig. 5a Horizontal beam shift x_o measured at the calorimeter for each of the 8 PINIs as a function of plasma discharge current I_p.

Fig. 5b Increase in beam half-width ω_o with plasma discharge current I_p.

Hydrogen 65keV co-injection. PINIs are numbered P1 to P8.

The beam shift is related to the current in the poloidal field coil number 1 (plasma current driving coil), which was demonstrated by synchronising the beam pulse with the pre-magnetisation and break-down phase of the plasma (beam sweep by field reversal). During the flat top phase further beam movement is caused by the poloidal field coil number 4 (vertical field), as is shown by the beam shift above 4 MA where the current in the poloidal field

coil 1 actually remains the same. The non-linear increase in beam shift for plasma currents above 4 MA (Fig. 5a) indicates that saturation of the iron circuit takes place.

The magnitude and direction of the beam shift can be explained by the measured stray magnetic field of the poloidal field coils, inside the magnetic shielding of the beam line at the position of the first stage neutraliser, acting on the extracted ion beams before neutralisation. The measured beam deflection angle (averaged over 8 PINI's) is $\alpha = 0.128°$ for a 65 kV hydrogen beam and $\alpha = 0.120°$ for a 70 kV deuterium beam, both at a plasma current $I_p = 3$ MA. The deuterium case refers to a thin neutraliser target. Theoretically the problem has been treated by Conrad [9], solving the ion and neutral kinetic equations for the transverse velocities of the neutrals exiting the neutraliser. Conrad gives the mean angular deflection as

$$\langle\alpha\rangle = \sqrt{m_p/m}\ B\ L\ \langle\omega\rangle\ /\ 79.8\ \sqrt{E} \qquad (1)$$

where B is the magnetic field in Gauss and assumed to be uniform, E the beam energy in keV assumed to be mono-energetic, L the neutraliser length in cm, m_p the proton mass and m the mass of the beam ions. The normalised transverse velocity $\langle\omega\rangle$ is a function of the neutralisation fractions F_o and F_o^∞ and is calculated numerically for a linearly decreasing neutraliser target (Fig. 5, ref 9). Substituting measured values of F_o as derived from the Test Bed neutralisation measurements [8] at an average beam energy of 60 kV in both cases, the magnetic fields consistent with the measured beam deflection are calculated to be 1.4G and 2.2G respectively. This is in good agreement with the measured values of 1.7G to 3.5G.

This measured magnetic field is about a factor 10 larger than the originally computed value during the design of the magnetic shielding by 3D-GFUN [10]. The cause of this discrepancy is probably due to the assumption of 1/16 toroidal symmetry in the calculation and is presently under investigation. Future improvements of the magnetic shielding will most likely include active current compensation, in particular with reference to the envisaged upgrade of the plasma current to 7 MA, as high saturation levels in the iron circuit of the Tokamak and injector shielding already exist under present operation conditions.

6. REFERENCES

[1] H D Falter, R S Hemsworth, G H Deschamps, A P H Goede, T T C Jones, P Massman, M J Mead, 11th Symp on Fusion Engineering, Austin, Texas (1985).

[2] G Duesing et al, Proc Royal Society Meeting, London (1986), to be published. 13th Eur Conf Contr Fus and Plasma Heating, Schliersee (1986), to be published.

[3] E Thompson, Physics Bull., APS-Plasma Physics Div Meeting, Baltimore, Nov 1986, to be published.

[4] D Stork, T T C Jones, A Burt, J F Davies, D Cooper, D Ewers, J Krom, P McCullen, J Nijman, A Stäbler, K Starley, I Young, this Conference, Poster GP13.

[5] G Duesing, 13th SOFT, Varese, Italy (1984), Vol 1, p.59.

[6] R Claesen, U Baur, J Carwardine, G Celentano, C Christodoulopoulos, A Dobbing, P L Mondino, 11th Symp on Fusion Engineering, Austin, Texas (1985).

[7] H Altmann, A P H Goede, R S Hemsworth, B R Nielsen, P Rebut, V Simone, D Stork, E Thompson, 3rd Neutral Beam Workshop, Gatlinburg (1981), CONF-8110118

[8] R S Hemsworth, A Stäbler, H D Falter, P Massmann, G H Deschamps, A P H Goede, 13th Eur Conf Contr Fusion and Plasma Heating, Schliersee, Vol 10C Part II, p297 (1986)

[9] J R Conrad, J Appl Phys 49(7), 3656 (1978) and J Appl Phys 51(6), 2957 (1980).

[10] M J Newman, C W Trowbridge, L R Turner, Proc. 4th Int. Conf. on Magnet Techn., Brookhaven (1972).

CARBON PROTECTION TILES FOR JET

P Massmann, E Deksnis, H D Falter, R S Hemsworth, R Shaw, A Stäbler*
JET Joint Undertaking, Abingdon, Oxon, OX14 3EA
* attached from IPP Garching, West Germany

ABSTRACT

In order to prevent damage and to reduce high Z plasma contamination, approximately 20 m² of the inboard wall of JET is currently covered with graphite protection tiles. Experience and tests have shown that these tiles can provide adequate protection under normal conditions of plasma operation and beam shine- through during Neutral Injection. For extended operation and for the case that the Plasma Fault Protection System fails during Neutral Beam Injection better protection tiles are desirable. Considering high thermal loads together with high mechanical stresses, carbon fibre re- inforced graphite tiles have been tested for the first time with high power particle beams in the Neutral Injection Test Bed. The tests reveal that such tiles are able to protect the inboard wall against an unattenuated 80 kV JET Neutral Deuterium Beam for several seconds without changes in the present support design. Carbon fibre re- inforced graphite tiles will be installed in JET in 1987.

INTRODUCTION

JET was operated initially with Inconel walls and graphite limiters and significant damage was observed on some of the Inconel protection plates located on the inboard wall of the vacuum vessel. In order to reduce plasma contamination by high Z impurities an area of approximately 20 m² of the inboard wall was covered with CL 5890 PT graphite tiles [1, 2] in 1984. Apart from protection during ohmic discharges of various scenarios, one of the most important needs for wall protection originates from the operation with Neutral Beam Injection (NBI). As far as NBI is concerned, tests in the Neutral Injection Test Bed [3] have shown that these tiles fulfil the 'basic requirements', i. e. to withstand shine- through of an 80 kV Hydrogen beam (0.5 kW/cm²) for up to 5 s and and to resist an unattenuated beam (up to 2 kW/cm²) for shorter pulse lengths of about 0.3 s. The investigations have also shown that the tiles are likely to crack if the pulse length is increased beyond a certain limit. Although this limit is not clearly defined because of sample variations one may expect that the tiles subjected to power loadings above 1 kW/cm² for longer than 2.5 s will be damaged. Normally the neutral beams are injected into a plasma and should be switched off by the Plasma Fault Protection System (PFPS) as soon as a plasma fault occurs. Nevertheless it remains desirable to take precautions for the worst case, i.e. the PFPS fails and the inboard wall is exposed to an unattenuated neutral beam for the full pulse length of up to 10 s . The expected peak power density on the wall is then about 1.2 kW/cm² for 80 kV H^0 and about 3.0 kW/cm² for 80 kV D^0 under optimum beam operating conditions. It is well known (aviation, motor racing) that advanced carbon materials (carbon fibre composites) are capable of withstanding both high thermal loads and high mechanical stresses. The purpose of the present test series was to find out whether tiles made from these

materials - preferably without changes in the present support design - can fulfil the requirements of protecting the inboard wall against an unattenuated beam.

EXPERIMENT

The test concentrated on two different makes of carbon fibre re- inforced tiles, one supplied by DUNLOP [4] with the fibres embedded in layers, the other by LE CARBONE LORRAINE [5] exhibiting a random fibre structure. In the following the two samples are called DUNLOP CFC and CL AEROLOR, respectively. The material properties of the samples as far as available are summarised in Table 1. Also included are data obtained during tests with other carbon materials. CL 5890 PT (LE CARBONE LORRAINE) is the material currently installed in JET. UCAR CS (UNION CARBIDE) [6], also non re- inforced but with high thermal conductivity, was tested as a matter of comparison.

The experimental arrangement is shown schematically in Fig. 1. The carbon tiles were attached to an Inconel back plate usually by means of an Inconel rod assembly as it is used in JET (Fig. 2). The plate together with the attached tile was fixed to a probe rod allowing the sample to be positioned in the centre of the impinging beam. The area immediately above the sample was shielded by a piece a of UCAR CS graphite mounted on the probe rod in a stress free position.

The tests were performed with a perveance matched full Hydrogen beam [7] from the JET (160 kV) triode PINI at 60 to 80 kV according to the desired impinging power density. The beam power density and position was determined by means of a retractable calorimeter array (Pendulum Probe) in front of the sample about 7.2 m away from the beam source. Temperatures were monitored with stainless steel sheathed Chromel- Alumel thermocouples. One thermocouple was located approximately at half the depth in the middle of the 20 mm thick tile. A second thermocouple was attached to one of the Inconel mounting bolts.

During the test the tiles were observed with a TV- camera to check the alignment and detect possible damage. For long high- power shots the valves in front of the vacuum windows on the Test Bed were closed during the beam- on time and re- opened immediately after the shot. This was to prevent excessive carbonisation of the windows. For closer inspection or for sample change the tile could be pulled up into the inspection lock without breaking the main vacuum.

MEASUREMENTS

Neglecting alignment shots, a total of 9 shots at 1.5 kW/cm² and 16 shots at 3.1 kW/cm² were fired at the DUNLOP CFC tile. The CL AEROLOR tile was exposed to 15 shots at 1.5 kW/cm² and 10 shots at 3.1 kW/cm². The largest beam- on times realised with both samples are 8.5 s at 1.5 kW/cm² and 4.5 s at 3.1 kW/cm². Fig. 3 and 4 show these tiles after the test series. During the test procedure the beam- on time was increased shot by shot until a maximum was reached caused by an increasing number of beam breakdowns at the end of the pulse. Since no breakdowns occurred with the tile outside the beam it is suspected that these problems are caused by increasing graphite contamination of the source. The temperatures measured for the two composite tiles are plotted in Figures 6, 7. Inspection of the tiles after the test revealed no structural damage despite the considerable temperature gradients caused by the internal holes in the tiles. The

Table 1 SUMMARY OF RECENTLY TESTED TILES

TILE (1)	CL 5890 PT	UCAR CS	DUNLOP CFC	CL AEROLOR
Inconel Rods	yes	no	yes	yes
Dimension (mm)	20 × 140× 150 (2)	25× 160× 150 (3)	20× 95× 150	20× 100× 150
Weight before - after (g)	not measured	not measured	484 - 458	512 - 476
Erosion (mm)	not measured	negligible	2.2	1.4
Density (g/cm³)	1.72	1.73	1.73	1.72
Conductivity (W/mK)	72	220	> 35 parallel > 150 perpend. to beam axis	150 - 300
Tensile strength (MPa)	41	20	> 70	40 - 100
Expansion coefficient ($10^{-6}K^{-1}$)	5.3	1.0	10-13 parallel 1.8- 2.9 perp. to beam axis	10
Young's Modulus (GPa)	10.6	15	not available	17 - 22
Figure of merit for shock resistance (10^6 W/m)	0.7	2.93	not available	0.27- 1.76
Supported power > 3 s (kW/cm²)	< 1	2.8 (4)	3.1 (4)	3.1 (4)

(1) Values at room temperature (2) Rhombus shaped (3) Exposed area (4) No limits tested

gradients were clearly visible appearing, for seconds after the shot, as two bright vertical stripes above each bore on the TV- screen. Note that the cracks in the CL 5890 PT tiles occurred exactly along these bores. Weight loss caused by erosion was about 5 %. The eroded material apeared to be fairly evenly deposited on surfaces inside the vacuum vessel. Carbon coverage of the cryo condensation panels used for vacuum pumping led to a substantial increase in liquid He consumption. The temperature of the Inconel bolt was only monitored during the first test run at 1.5 kW/cm² with the DUNLOP CFC tile, reaching a maximum of about 1000 °C after the last 8.5 s shot. Despite this temperature no deformation or discolouration was found of the Inconel rods or bolts. In all the cases the support assembly could easily be dismantled after the test and could have been

re- used. The Inconel back plates (Fig. 2), however, buckled after dismantling. The plates were actually held flat by the tiles during the test.

DISCUSSION

Although the tile temperatures before the pulse are not identical for the different pulses, Figs 6, 7 indicate the appropriate temperature rise to be expected for a given beam pulse length. Most of the starting temperatures in the test are similar to the temperature of the JET vacuum vessel. Comparison of the two figures shows that within the measured range there is little difference in the thermal behaviour of the two tiles.

A quantitative theoretical verification of Figs. 5, 6 is not straight forward. This is mainly because of the limited accuracy of the temperature measurement and also because of the incomplete knowledge of the temperature dependent material properties. For the same reasons quantitative stress computations are not available. Further tests and analyses are being done. Some physical insight in the thermal behaviour can be obtained if we look at the temperature of the front and rear faces. We assume a slab geometry and apply a 1-dimensional finite element computer code [8] incorporating the temperature dependence of the material quantities as far as available. A temperature- time history of the CL 5890 PT tile, for which the thermal quantities are best documented [2], is shown in Fig. 7. Thermophysical data, although at room temperature, is also available for CL AEROLOR (Table 1). We have scaled the temperature dependence of this data in a manner similar to that of CL 5890 PT. The time history of the CL AEROLOR surface temperatures is plotted in Fig. 8. We have not yet treated the DUNLOP CFC tile because the data is still incomplete. The measurements suggest however that the thermal behaviour is similar to CL AEROLOR.

From Figs 7, 8 it follows that temperature equilibrium at the front surface is reached in the early stages of a pulse and also the maximum temperature gradient is surpassed long before the end of a 4.5 s pulse. The low rear temperature and the measurements of the bulk temperatures indicate that the maximum gradient is located close to the front surface. Note that the CL AEROLOR tile is not only stronger but also exhibits lower gradients because of the higher conductivity. Comparison of the measured bulk temperatures (Fig. 6) with the calculated rear temperatures (Fig. 8) indicates however that the conductivity is not as high as assumed in the calculation. The main heat loss mechanism in the beginning of a pulse is radiation. Sublimation dominates in the later stages. It follows from Figs 7, 8 that sublimation, i.e. the amount of eroded material, is considerably higher for CL 5890 PT also because of the lower conductivity.

Although we have concentrated on localised wall protection against high power fluxes in the order of several seconds, it is of interest for future machines how (inertial) carbon tiles can be used for an integral protection of the inner vessel wall at moderate power levels and for very long pulses. In Fig. 9 we have plotted the calculated thermal behaviour of the two CL tiles for a 1000 s pulse at a surface heat flux of 100 W/cm^2 which is about twice the value expected for NET [9]. In this case we have assumed that the heat is removed only through radiative tranfer to the watercooled wall at the rear of the tiles. Note that the front temperature of CL 5890 PT is substantially hotter for the major part of the pulse.

CONCLUSION

It has been shown that two carbon fibre re- inforced composite materials, DUNLOP CFC and CL AEROLOR, are able to provide local protection against power fluxes of 3 kW/cm² for at least 4.5 s without changes in the design of the present JET tile supports. The thermal behaviour indicates that adequate protection can in principle be obtained even for much longer pulses. The support temperature could be kept at a tolerable level with thicker tiles. The increased level of erosion seems acceptable in the case of an accident caused e.g. by unattenuated beams, re- ionised particles or high power plasma contact with the wall.

REFERENCES

[1] P Deschamps, J Dietz, M Yvars, 13th SOFT 1984, Vol 2, p. 1243

[2] M Yvars, CEN- Saclay, Report No BE 76- 068- 53425 (1976)

[3] A Stäbler, G H Deschamps, H D Falter, R S Hemsworth, P Massmann, JET- DN- C(85)19

[4] DUNLOP AVIATION DIVISION, Holbrook Lane, Foleshill, COVENTRY CV6- 4AA, England

[5] LE CARBONE LORRAINE, Dept Prod. Spec., 41 rue Jean Jaurès, 92231 GENNEVILLIERS, France

[6] UNION CARBIDE U.K., Carbon Prod. Div., Claywheels Lane, SHEFFIELD S6- 1NE, England

[7] H D Falter et al., 11th Symp. Fusion Eng., Austin, USA (1985)

[8] E Deksnis, to be published

[9] NET Status Report 51, EU- FU/XII- 80/86/51

FIGURE 1

Schematic of the test set up in the N.I. Test Bed.

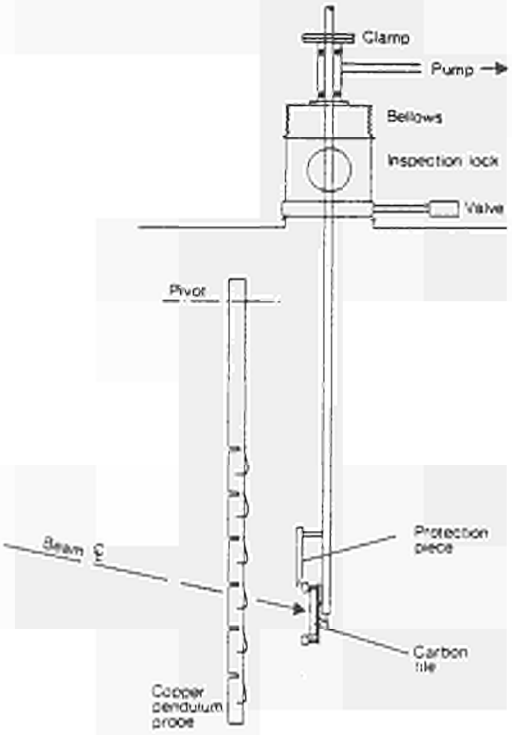

FIGURE 2

Schematic view of the tile mounting assembly. The tiles with the Inconel rods are bolted to an Inconel back plate. The whole is attached to the torus wall by means of a dove tail construction.

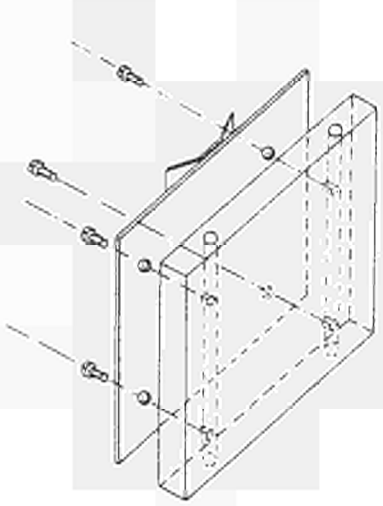

FIGURE 3

Photograph of a DUNLOP CFC graphite tile after being exposed to several shots at 3,1 kW/cm² for up to 4,5 s, There has been no damage, Surface erosion is moderate,

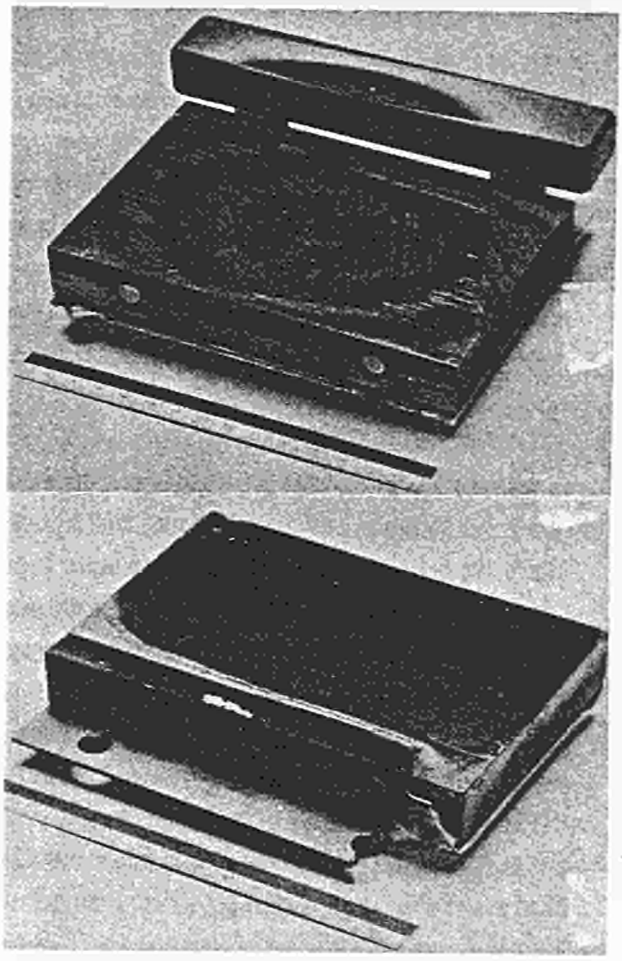

FIGURE 4

Photograph of a CL AEROLOR graphite tile which also withstood 3,1 kW/cm² for 4,5 s, The erosion is comparable to the one of the DUNLOP CFC tile,

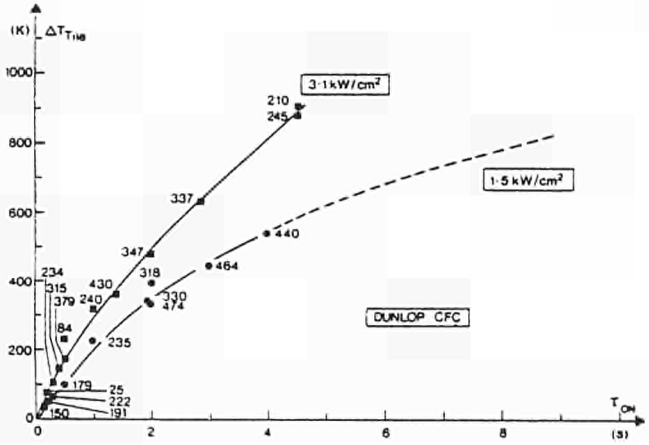

FIGURE 5

Body temperature rise versus actual beam- on time for the DUNLOP CFC tile, The numbers indicate the temperatures at the beginning of each pulse in centigrades,

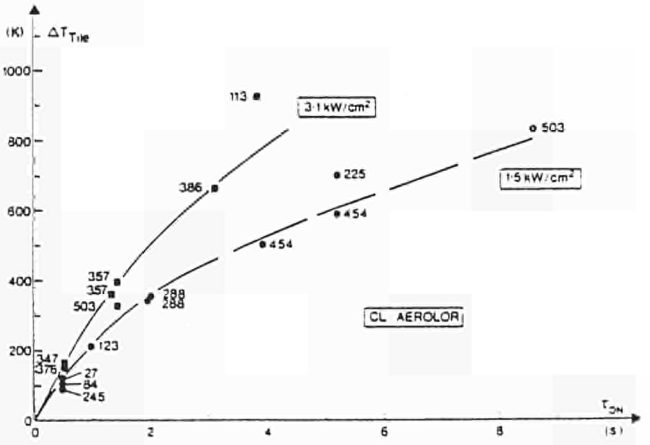

FIGURE 6

Body temperature rise for the CL AEROLOR tile, The figure indicates a thermal behaviour very similar to the DUNLOP CFC tile

FIGURE 7

Variation of temperature and heat transfer parameters with time for the case of a tile of relatively low conductivity.

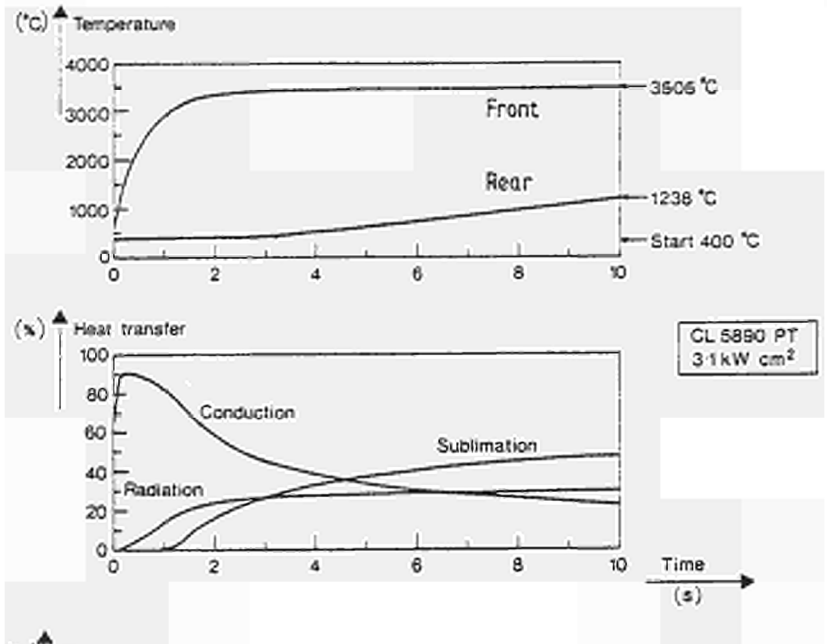

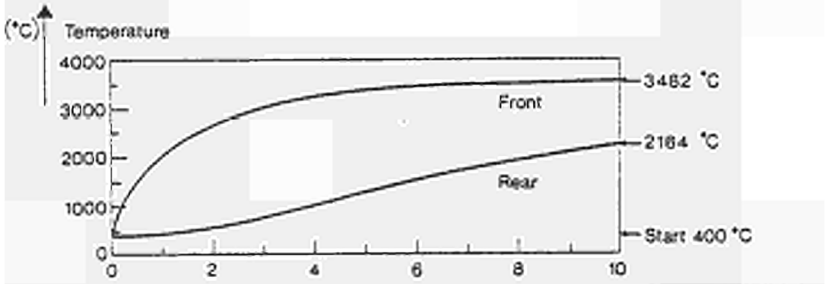

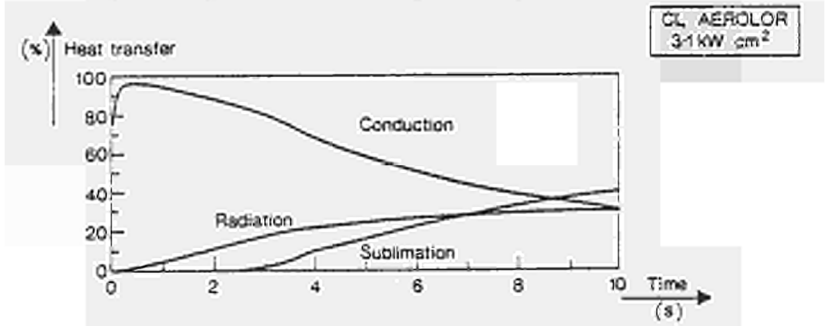

FIGURE 8

Thermal behaviour with time for a material with relatively high conductivity. The temperature dependence of the material quantities is derived from the manufacturer's room temperature data.

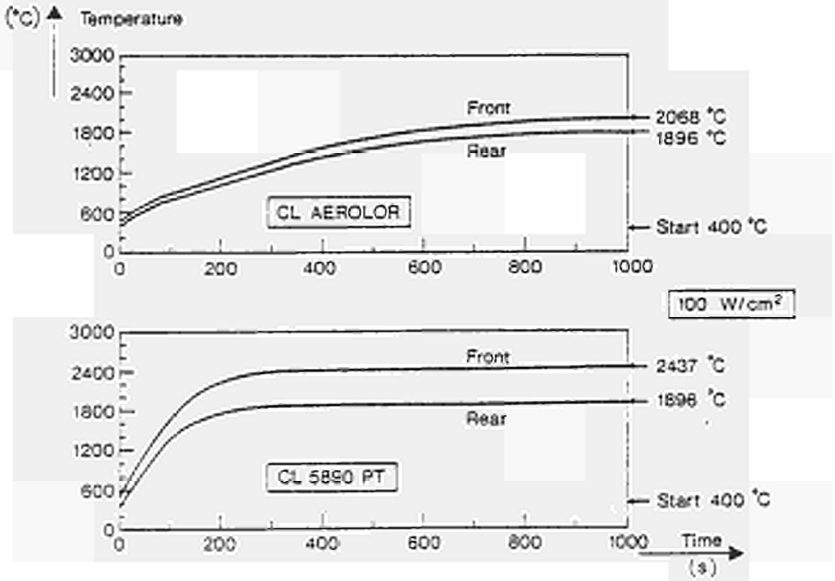

FIGURE 9

Thermal behaviour for very long pulses. Note that for an integral protection the heat removal occurs only at the rear of the tiles.

THE JET BELT LIMITER

G. CELENTANO, E. DEKSNIS, R. SHAW, K. SONNENBERG, J. BOOTH*
JET Joint Undertaking, Abingdon, Oxon OX14 3EA, UK
* Culham Laboratories, Abingdon, Oxon,OX14 3DB, UK

ABSTRACT

A limiter with an effective area in contact with the plasma of about 16 m^2 is presently being manufactured for installation in 1987. This belt limiter consists of two toroidal rings located above and below the equatorial plane of the vacuum vessel. Each of the two rings comprises a structure with water cooling pipes and fins welded to the pipes. The limiter material in contact with the plasma (graphite or beryllium) is inserted between fins in the form of tiles. The belt limiter is designed to handle up to 40 MW of total power at flux densities of 3 - 5 MW/m^2 for 10 s and to permit rapid exchange of different limiter materials. This paper describes the design and manufacture of the belt limiter and the results of thermomechanical analysis for different edge properties, power levels and shot repetition rates.

1. INTRODUCTION

Eight discrete carbon limiters are presently installed in JET with a total area of ~ 3 m^2 in contact with the plasma [1]. The maximum possible heating power into the plasma is about 14 MW for 6 seconds. In early 1987 when the additional heating will be increased, the total power deposited inside the vacuum vessel will reach approximately 40 MW for 10 seconds [2]. This heat load will have to be taken by tiles placed between the fins of the toroidal belt limiter (fig 1 and 2). The tiles are inertially cooled during the pulse and radiation cooled during and between pulses. The heat load is dissipated by radiation to the fins that eventually are cooled down by demineralised water flowing in the pipes. The total tile area facing the plasma is 17 m^2 for graphite and 13 m^2 for beryllium tiles. The radiant fin surface is about 51 m^2 for graphite and 54 m^2 for beryllium and the available overall water flow is 112 ℓs^{-1}.

The belt limiter tiles must be capable of withstanding the full power injected into the vessel (i.e. radiation neglected). The tiles must not melt (beryllium) or sublimate (graphite) under normal operating conditions. A further functional requirement for the design is the possibility of a rapid change from graphite to beryllium tiles and of a fully remote handling replacement of either a segment of the limiter structure or of tiles.

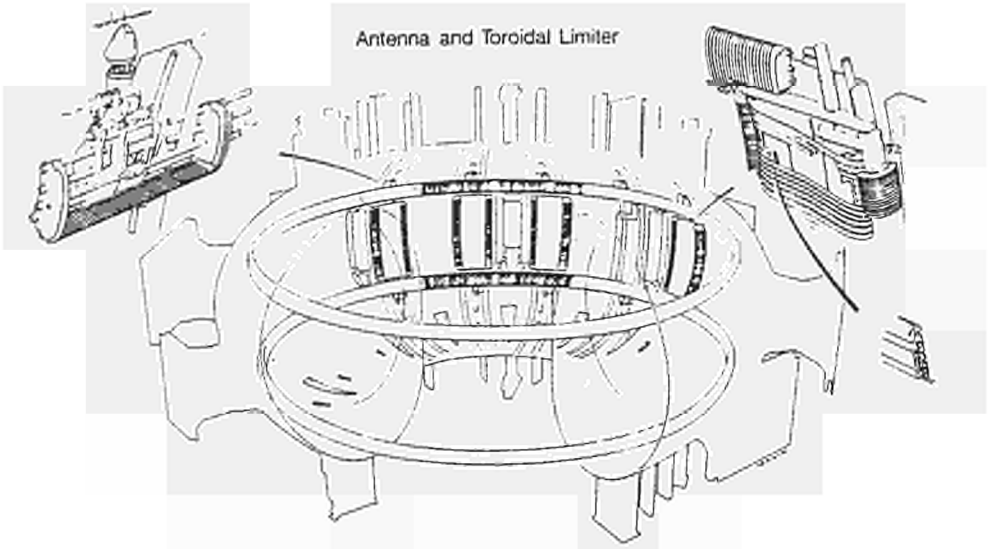

Figure 1. JET belt limiter overall view.

2. MECHANICAL DESIGN

The overall arrangement of the belt limiter is shown in Fig. 1. The ICRF antennas are placed between the upper and lower limiter rings and they share the same cooling system. Each poloidal ring is made up of sixteen equal modules shaped to both poloidal and toroidal radius. They are electrically and mechanically connected to each other but thermally decoupled.

Each module is basically a "radiator structure" made up of two water manifolds at either end joined together by four water cooling tubes on which nickel fins are welded at equal spaces. The tiles are placed between the fins with the edge towards the plasma.

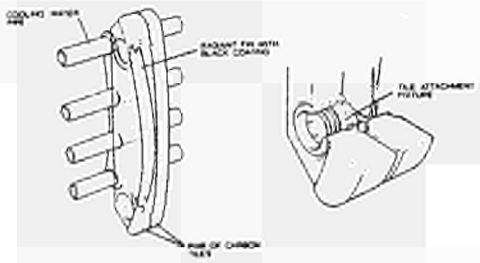

Figure 2. Tile pair showing extent of blackening on fin and attachment.

The belt limiter comprises 1716 tiles (858 for each ring) installed in pairs and supported by alternate fins (fig 2). In order to increase the radiative heat transfer the side faces of the fins and in the case of beryllium, also part of the side of the tiles, are blackened. Sixteen inlet and outlet water pipes enter the mechanical structure and the vacuum vessel through 90 mm diameter vertical ports. Inside the vacuum vessel each belt limiter segment of the lower ring is connected in series with the corresponding segment of the upper ring through the RF antennae or through a bypass pipe (fig. 3).

The different parts of the belt limiter have been thermally decoupled, wherever possible, so as to minimise transient thermal stresses during temperature excursions. The fins adjacent to the rigid water manifold boxes and the supports, have been partially cut in order to reduce bending stresses in the longitudinal water pipes and adjacent weldings. Each segment of the belt limiter structure is rigidly attached to the vacuum vessel wall at only one position, thus allowing for the other supports to slide tangentially (fig.4).

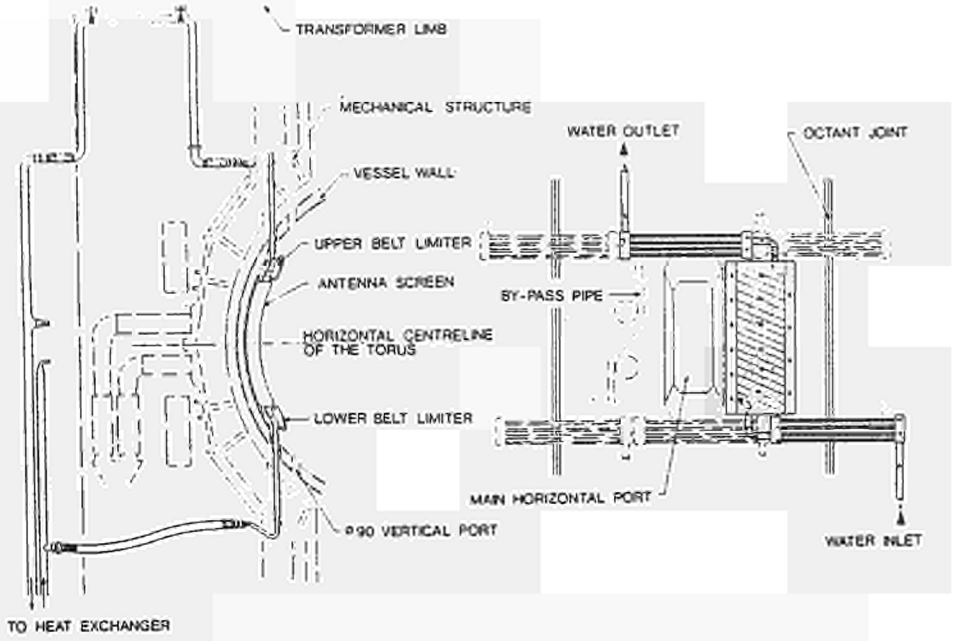

Figure 3. Cooling circuit (schematic) for demineralised water.

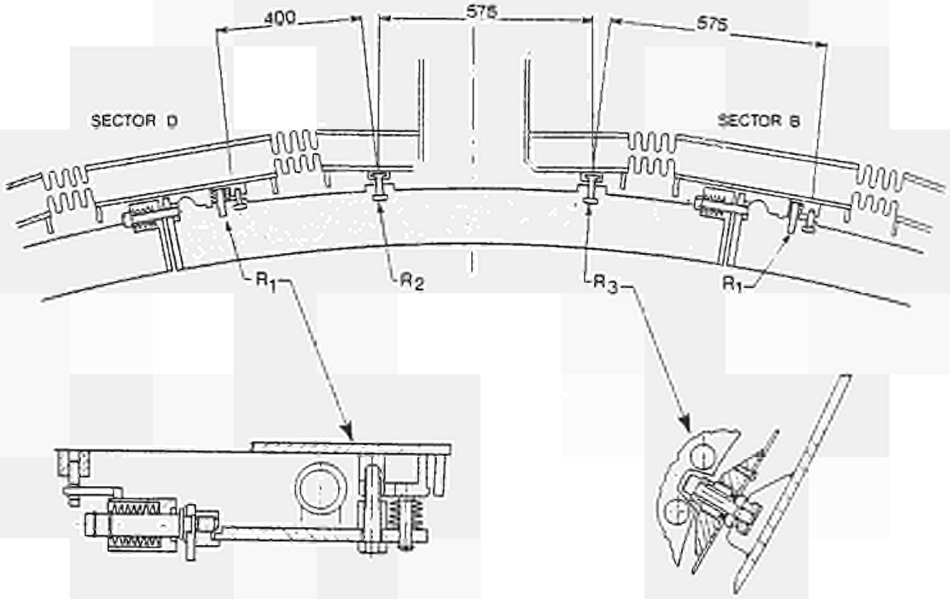

Figure 4. Supports for belt limiter structure. R^1 - main support to align the radial and tangential position of each segment. R^2 and R^3 - idle supports that work only in case of a plasma disruption. R^2 and R^3 are electrically insulated from the vacuum vessel.

The electromagnetic forces acting on the limiter result from eddy currents produced by either the poloidal flux change during plasma disruption or by eddy currents flowing in the loop formed by the vessel wall and the water pipes through the mechanical attachments or by conservation of poloidal flux trapped in the volume of the limiter tiles. Electrical straps and good electrical contacts have been provided to minimise any risk of arcs and of

spot welding of the bolts. Forces due to eddy currents have been conservatively calculated and can easily be resisted by the structure. Eddy currents circulating in the toroidal direction of the belt limiter due to a sudden plasma disappearance produce forces along the toroidal water pipes of about 40 000N/m^{-1}. They are directed towards the centre of the vessel and will be taken by the main bolted supports.

3. BELT LIMITER TILES

Energy scrape-off thicknesses in JET of about 15 mm have been found with the discrete limiters. For the belt limiter arrangement the connection lengths are expected to be similar. However, due to uncertainty in energy scrape-off thickness, the JET belt limiter tiles have been shaped to be capable of handling power for a range of scrape-off thicknesses, i.e. between one-half and double the nominal values. The limiter surface was shaped in such a way that for any scrape-off thickness within a given range the ratio of peak to average flux is the same. The power deposition curves shown in figure 5 for

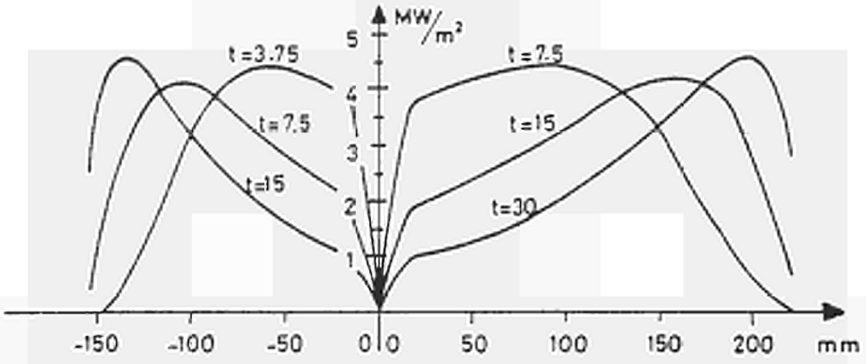

Figure 5. Flux deposition profiles for 40 MW onto 1716 beryllium tiles for different SOL,t. Zero position corresponds to tangency point of the plasma..

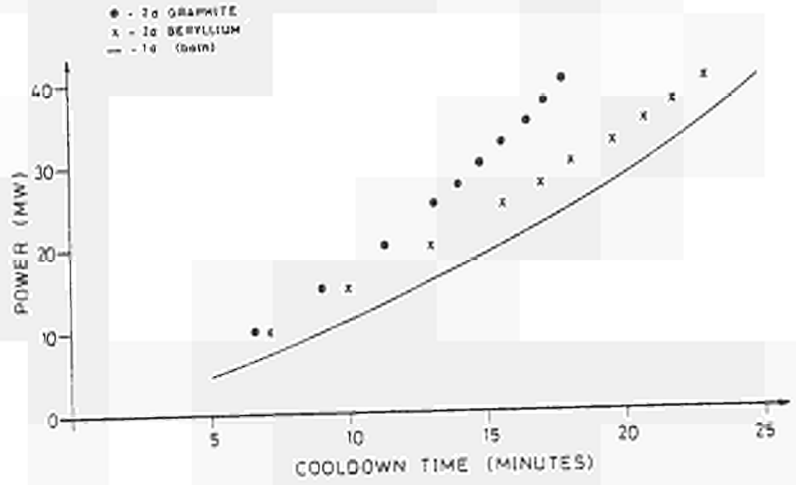

Figure 6. Calculated cooling down times, i.e. surface temperature of tile returns to 300°C. 1-d is a closed form result; 2-d is obtained using a finite difference code for heat transport in the tile.

beryllium are qualitatively the same for graphite (but lower by a factor of 0.765 due to the larger area of the graphite limiter) [3]. The nominal scrape-off thicknesses are 7.5 and 15 mm for the tile segments facing towards and away from the equatorial plane.

It is assumed that the surface of the belt limiter segments can be adjusted with respect to the magnetic axis to give uniform deposition of heat on all of the tiles. The surface of the tiles has been shaped to give an average flux density to the tiles of 2,35 MW/m² for graphite (3,05 MW/m² for beryllium) and a peak flux density of 3,75 MW/m² for graphite (4,85 MW/m² for beryllium). Under these heat loads tiles which are initially at 300°C, will reach an average surface temperature of 800°C (beryllium) at the end of the discharge, and 1250°C (graphite). Immediately after a discharge the temperature of the tiles equilibrates (on a time scale of approximately 100 seconds) to 380°C (beryllium) and 450°C (graphite). They then cool down by radiation within 25 minutes (see fig 6).

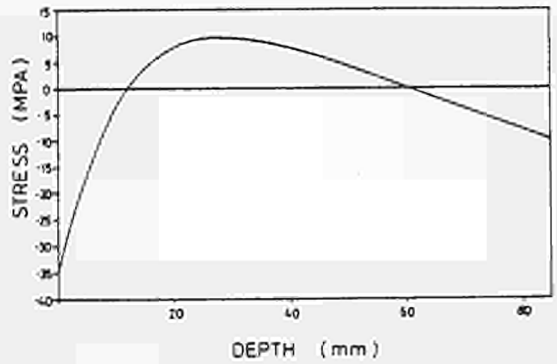

Figure 7. Elastic response of LCL PT 5890 graphite to 10 seconds irradiation at 3.75MW/m².

The peak values of thermal stress are produced by the peak flux densities. Elastic response is predicted for graphite (fig 7) whereas for beryllium plastic zones will develop. Tests have been done by Sandia National Laboratories [4] on samples. At flux densities approaching those for JET damage to the irradiated surface was observed after 2000 cycles. Relatively large numbers of surface cracks developed but did not grow to a depth of more than 3 mm. No gross mechanical failure of the beryllium tiles was observed after 10^4 cycles. Further tests are under way on tiles with dimensions close to those of the JET belt limiter.

The pulse repetition rate is determined by the time required for the tiles to cool to 300°C. A series of analyses was carried out to determine the repetition rate for 10 second

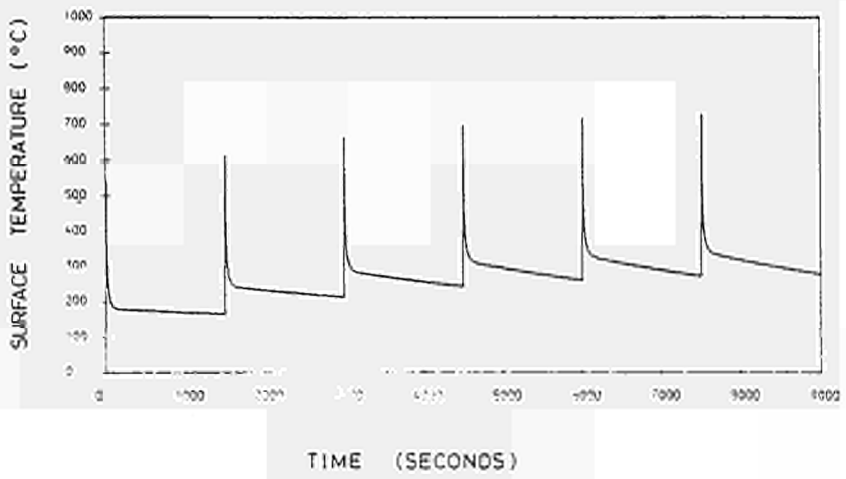

Figure 8. Development of average surface temperature of the beryllium tiles subjectyed to pulses of 40 MW. Pulse repetition rate 25 mins.

discharges at various power levels, (figure 6). The average heat flux density was applied to a 2-dimensional model of the tile and heat losses were due to thermal radiation from the irradiated face to the vessel as well as from the (blackened) side face to the blackened nickel fins. A time history of the average surface temperature of beryllium tiles (figure 8). The peak surface temperature reaches 1000°C, which is well below the melting point (1280°) of beryllium. For graphite the peak temperature is expected to reach 1250°C.

4. MANUFACTURE

The manufacturing contract of the belt limiter was placed in 1984. Materials were procured under tight specification. Nickel has been selected as the fin material because of its high thermal conductivity and its good mechanical properties at elevated temperature. It has been specified in the quarter hard state to ensure mechanical stability of the structure and easy assembly of the tiles. Holes and welding lips around the holes are stamped in the fins for welding to tubes (Inconel 600). During manufacture, each fin is precisely located by a jig and the fin to tube welds are carried out by automatic orbital welding machines. Water manifolds at the extremities of each sector are machined out of forged Inconel bars which are ultrasonically tested. All Inconel pipes which have to be welded without filler material during final assembly inside the vessel to other components (e.g. antennae - water pipes) come from the same production batch in order to avoid metallurgical problems. This will facilitate as well maintenance by remote handling. A clean area workshop enclosing all facilites and fixtures required by the belt limiter production was set up and a prototype module was fabricated. It underwent a comprehensive dimensional control, cold leak test, water flow and pressure test, carried out before and

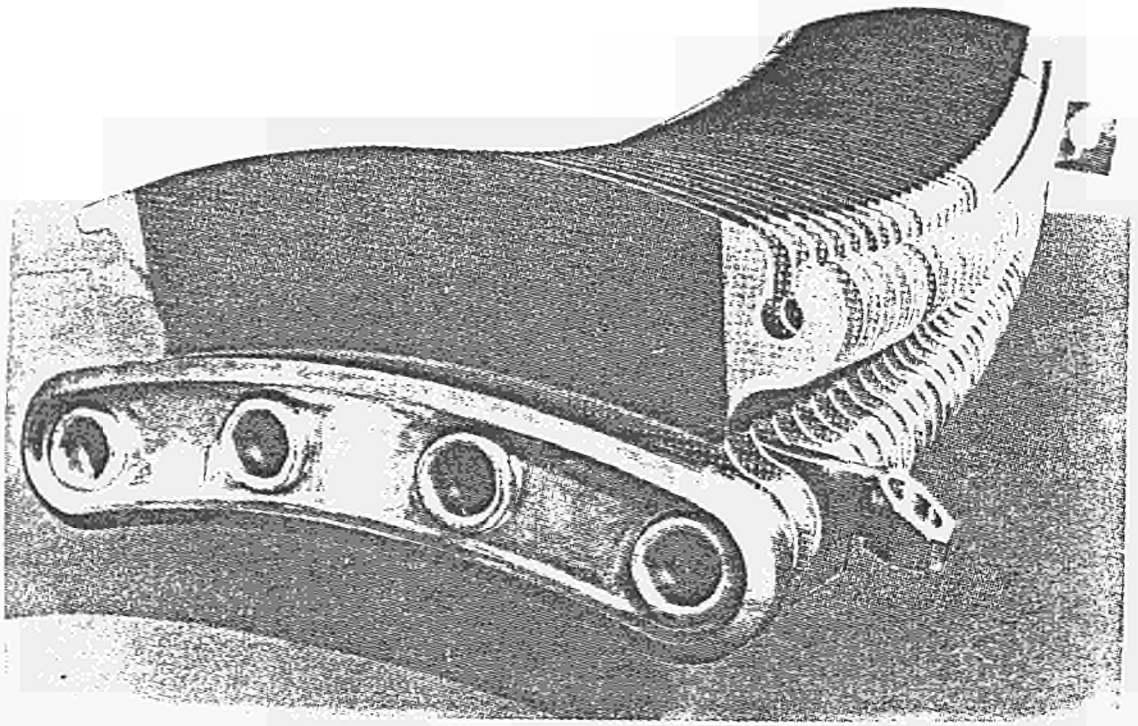

Figure 9. Series limiter module under manufacture. The fins show the plasma coating to improve the emissivity.

after a thermal cycle from room temperature to 550°C. The prototype has been hot leak tested at later stage at JET site using a test vessel manufactured for the purpose. Corrosion tests were carried out on a sample of the actual materials as delivered an on welding samples. Corrosion problems have been looked at in detail also for the thin-walled bellows and as a consequence all bellows welds are performed from the inside. To maintain the required mechanical precision as a prerequisite for interchangebility of the module an extensive set of jigs and fixtures for manufacturing and dimensional checks were required. They were set up and tested for the prototype fabrication. Fig. 9 shows a module under manufacture.

The nickel fins have been blackened to increase the emissivity. A plasma spraying technique under vacuum to coat the nickel fins with a thin (≈ 15 μm) layer of Al_2O_3 + 13% TiO was developed. The emissivity measured for the coating is higher than 0.8. Bending test and thermal fatigue tests showed an excellent bonding strength of the coating.

The production of the belt limiter segments together with water pipes and by-pass pipes is expected to be finished in January 1987, in time to install the components into the JET machine during the shutdown in early 1987.

5. REFERENCES

[1] REBUT,P.H., First Experiments on JET, 10th International Conference on Plasma Physics and Controlled Nuclear Fusion, London (Sept 1984).

[2] HUGUET,M. et al, Limiters and First Wall on JET, 11th Symposium on Fusion Engineering Austin, November 1985.

[3] DEKSNIS,E, in publication.

[4] WATSON,R., Whitley J., Thermal Fatigue Tests of a Prototype Beryllium Limiter for JET, J. of Nuclear Engineering and Design/Fusion (to appear)

[5] WYKES,M. et al, Remote Handling Tools for JET, 14th Symposium of Fusion Technology. September 1986.

COMPUTER-TO-PROCESS INTERFACE IN JET's CONTROL AND DIAGNOSTIC SYSTEMS

K FULLARD, SE DORLING & JE van MONTFOORT
JET Joint Undertaking, Abingdon, Oxfordshire OX14 3EA, England

ABSTRACT

The JET Control and Data Acquisition System, CODAS, uses some 40,000 electrical signals to control and monitor JET's various systems. This paper describes the electronic equipment and the data transmission techniques which are used to route these signals to and from the centrally-located computers. Special emphasis has been placed on the practical aspects of building and maintaining such a large system of approaching 8,000 modules. Quantities and costs of the various classes of modules and cables are given together with an outline of the quality assurance and organisational techniques adopted.

1. INTRODUCTION

CODAS, uses 21 Norsk Data mini-computers to control and monitor JET's systems and to provide semi-automatic preparation, execution and recording of JET pulses, using parameters set by the Operations team in the control room. This system as a whole has been described by F Bombi [1]. However, in this paper we explain how the 40,000 signals which are involved and which arise at various points in the extensive JET site are marshalled and transmitted. Detailed electronic techniques and circuits are not discussed, the emphasis being instead on practical matters such as cost (1986 prices), quantities and sizes. The aim of this approach is to help those planning and building similar sized systems because, as we found ourselves, estimating such quantities can be difficult for a newly assembled team.

The scope of the paper is from the point where the signals leave a local unit to the computer. A local unit is typically a plasma diagnostic assembly provided by an experimental team or else a set of control equipment, usually provided under a single contract with an industrial company. One local unit, or occasionally a few such units, are served by a CODAS interface cubicle which contains Eurocard signal conditioning and CAMAC computer-controlled electronic modules. These marshal and digitize signals onto high-speed CAMAC-standard serial highways which convey the encoded signals to the computers. Each computer has one Serial Highway to which are connected the cubicles of one subsystem of JET, as listed in Table I. Various related systems are excluded from the paper for reasons of space, in particular the 55 bays of console equipment and the Central Interlock and Safety System [2].

2. THE SERIAL HIGHWAYS

These critical elements of CODAS use the CAMAC standard protocol so that it is possible to use standard crate controllers, but the Serial Highway Driver (SHD) and transmission techniques were specially developed for JET. The driver consists of two printed-circuit boards which fit within a Norsk Data subsystem computer. They are complex autonomous devices capable of various block-transfer modes. Interrupt messages are acknowledged automatically and stored and there are built-in diagnostic utilities.

To guarantee reliable transmission of the 5MHz CAMAC messages in JET's electrically noisy environment, and to overcome ground-potential problems, transmission from the SHD to the individual CAMAC crates is by fibre optics. Conversion between electrical and optical standards is made in U-port adaptors. There is such an adaptor at each point where CAMAC is used and a further one close to the SHD. They are inter-connected to form a ring, using two fibres to form each link in the ring. This duplication allows continued, full operation, even if one link is damaged. The combined effect of the SHD and U-port adaptor designs is to allow the rapid transfer of the digital data between the computer's memory and any point on the JET site regardless of distance, ground potential or interference sources.

Several of the fibres reach remote parts of the site in buried ducts but the majority is laid indoors, in steel trunking. This trunking forms part of the CODAS Service Route whose 2km long web reaches the whole JET site. The route is traversed by three parallel trunkings, one for the fibres, one for safety cables and one for other functions. The cross-section varies from 50 x 50mm to 100 x 150mm, though we have found the smaller size too restrictive. Installation of this extensive trunking has proved invaluable for urgent changes to the subsystems.

3. INTERFACE CUBICLES

To exploit the high capacity of the Serial Highways to the full, the local units' signal cables are kept short by placing the CAMAC crate in a cubicle as close as possible to the unit. Because the local units are manufactured by many firms throughout Europe, the interface between CODAS and the local unit had to be defined at the conventional level of terminal blocks. Each cubicle can therefore deal only with some 1,000 signals. The terminal blocks contain knife switches which have proved essential for commissioning work. In practice the cubicles are manufactured in the workshop, installed and then computer-commissioned, with the knife-switches open, before any attempt is made to commission with the local unit. Using this technique, it has proved possible always to have the CODAS connection available before the local unit required it. We have found that, in the majority of cases, a single CAMAC crate has enough capacity to service the needs of all the signals that can be terminated in a cubicle, the average density being 1.33 crates/active cubicle. Some local units require a second termination cubicle.

An important advantage of the fibre-optic computer connection is that the cubicle can be earthed at local unit potential and this freedom is retained by supplying each cubicle with its 240V power through a 2kVA isolation transformer. Occasionally, the local unit has an uninterruptible power supply available, but this is not a general practice in CODAS. Typical power consumption is 1.4kW/cubicle, with a maximum of 1.9kW.

4. CAMAC

All the sophisticated electronic functions in the cubicles are performed by CAMAC modules. The cost of each station in a crate, when account is taken of the crate, its power supply, and crate controller suite, is about £200, which is included in the costs of Table II. This precludes the use of CAMAC for simple non-computer-controlled buffering functions, and makes multichannel modules attractive.

4.1 Analogue-to-Digital Conversion

The main CAMAC role is in analogue to digital conversion and Table II shows the typical costs of a channel, in broad classes of performance. An important point to note is the widespread use of transient recorders which consist of an ADC and digital memory recording the basic waveforms of JET. Although the modest 5 kHz sampling rate suits most purposes, channels can effectively be combined to give up to 40 kHz rate (using 8 channels). Higher sampling rates are used in smaller numbers of applications. Conversion resolution is generally 12-bit which has proved to be useful without being excessively expensive. The use of lesser resolution would have involved the complication of variable gain pre-amplifiers which have generally been avoided.

4.2 Auxiliary Crate Controllers

Local intelligence is provided by these programmable modules for those applications which cannot tolerate the inevitable delays of the busy subsystem computer. Seventy such controllers are installed, running some 21 different programmes. Major roles have been in waveform generation (by controlling a local DAC) and handling serial data-link protocols. The compactness of the TMS99000-based, single-width module has proved most economical, with some CAMAC crates having five controllers, each running its own task.

4.3 Timing Modules

The main role of these modules is to generate, during the JET Pulse, pre-set sequences of pulses to initiate activities and to trigger the sampling of ADCs. Resolution can be as low as one microsecond. The tree structure of timing signals is based on six pre-programmed reference pulses from which further vernier delays are made. The pulse pattern generator modules create complex sequences to cause ADC samples to be taken only where they are of most value. Because timing signals must be most secure and must travel between subsystems, fibre optic cables are used for intercubicle connections.

4.4 Spread of CAMAC Types

There are 80 types of CAMAC module now in use in CODAS, despite every effort to keep this number down. However, 80% of the modules are covered by 23 of the 52 preferred types, 50% by 9 types. The cost of providing proper test procedures, spares back-up and working knowledge in the team for each type means that only the preferred types can have full support. The cost of CAMAC modules in the process interface is £1180 each, a weighted average over 1150 of our 3300 modules.

5. SIGNAL CONDITIONING MODULES

Virtually all CODAS signals pass through a signal conditioning module. This applies even to signals which apparently do not require conditioning, when we use a passive module to enable standard cabling techniques to be retained and to reserve space for active modules to be inserted at a later date. The modules are Eurocards of the 100 x 220mm size which has proved a convenient, low-cost choice.

All the designs are purpose-built for JET by commercial companies to JET's standards. Table II shows the usage of different classes of function. Signals arising from the Torus or other electrically noisy sources (which form a majority) are isolated to general standard of 1 kV ac. This must be maintained through cabling and connectors. This practice is part of a carefully designed and early-defined JET cable routing and earthing policy which minimizes both screen currents and linked magnetic fluxes from the JET machine.

5.1 Line Surveyor/Driver (LSD)

The largest group of signals are the slow digital ones, such as arise from electro-mechanical contacts or which drive relays. In CODAS we have installed modules with a capacity for 40,000 LSD signals, typically 300 signals per cubicle. Each requires isolation, filtering and cabling which would be too bulky for CAMAC. The LSD system was devised to meet this requirement.

The system consists of either one or two Eurocard subracks, each containing up to 16 simple input/output modules. Each module has 16 input or 16 output channels, giving a system capacity of 512 channels. The subracks have fixed wiring, in the form of a printed board backplane which carries a simple 8-bit data bus with strobes. A connector module occupies the 17th position in each subrack. It contains drivers for the 12V bus signals and an address decoder so that each I/O module can receive a single address line. The effectiveness of the system depends on the associated single-width CAMAC module. This contains a Z80, 8-bit microprocessor and a CAMAC-accessible memory. The microprocessor continuously transfers data between the input cards and the memory and from the memory to the output cards. In this way a single block-read and a block-write between the computer and the memory transfers all 512 input and output bits. A scan of the I/O modules occurs every 10ms. For most signals it is sufficient to make the block transfer every second or so but, for those signals requiring a more rapid response, the microprocessor will create a computer interrupt whenever the state of an individual bit changes. This facility may be enabled for each individual bit. There is a 'watchdog' scheme which checks proper functioning of both the CAMAC module and the sub-rack power supplies. The watchdog forces all output bits into a defined state should the LSD power fail, but leaves the outputs as they were on the last scan should the CAMAC module fail. There are 3 input types and 3 output types of I/O module. These offer both relay contact and solid-state options. The use of an opto-isolator which has hysteresis and precise thresholds (HCPL-3700) has important advantages.

The LSD system has proved to be most successful showing good reliability, ease of application and economy. Major contributions to this performance have been made by its use of a single 12V power supply, 12V signals, modest data rate (10us/bit) and heavily filtered, 1kV-isolated plant connections.

5.2 Analogue Signal Conditioning

Again the Eurocard format is used to house a range of isolation amplifiers, integrators, filters and some special-function modules. Bandwidths are usually less than 10kHz. It has proved possible to include 4 channels of amplification or 8 channels of the simpler filter circuits in one 100 x 220mm card. Differential inputs and single-ended outputs are normally used, usually with a ±10V, 20mA range.

6. QUALITY, ASSURANCE & RECORDS

The equipment has been built to a good industrial standard, with a 0°C to 50°C environmental range. All the modules have been produced by commercial companies with a requirement to deliver tested equipment. For each new type, JET has carried out laboratory tests on a sample module to establish 'Type Approval'. Wherever possible a computer test program is devised. Production units are again tested on delivery or after repair using the 'Acceptance Test'. Some testing work has been done successfully for JET by external organisations, but experience has shown that it is essential to have acceptance testing capability on site to prevent an accummulation of suspected modules which inevitable arise from our repair-by-interchange policy. About 40% of suspected modules prove to be sound.

Details of all modules are stored in a 20Mbyte database accessed by 6 on-line terminals. The information stored deals with orders, deliveries, stock-levels, the required inventory of all existing or planned cubicles and the current status and location of some 19,000 serial-numbered items. A history of each item is recorded together with its configuration and modification status. About 60% of our standard equipment types can be set into particular configurations, with an average of 2.9 configurations,for each of these types. Modifications are permanent changes which are fitted to all modules of a type. For the standard CAMAC types, an average of 1.8 modifications have been specified. The database has been extremely valuable in planning an efficient procurement and upgrading programme.

7. CONCLUSIONS

The amount of equipment required to control and monitor JET has proved to be large, but by adopting a very modular design and by exploiting multiplexing to the full, it has been possible to build a system which is maintainable and which does not involve an overwhelming amount of cable. The procurement of modules had three phases: the specification of a basic set of modules tailored to match our high-volume applications, the selection of commercial modules for a host of lesser applications, the specification of a large range of low-design-cost buffer modules to match the intricacies of the plant to our established standards. The selection of CAMAC and Eurocard suited each of the phases well.

Interference could have been a major problem but it has proved not to be so. We feel this is because of the various precautions taken at all points in the system: the use of signal isolators, mains isolation transformers, properly-earthed screened cables for analogue signals and the use of only 12, 15 and 24 V signals at interfaces, have all helped. The use of fibre optics has been particularly successful (see Table III).

We would like to acknowledge the major contributions to this system which have been made by all the past and present members of the Electronics and Instrumentation Group.

Table I CODAS interface subsystems

Code	Subsystem	CAMAC Crates
AH	Neutral Injection (Oct 8)	13
DA	4 Diagnostics	9
DB	3 Diagnostics	5
DC	3 Diagnostics	8
DD	4 Diagnostics	9
DE	2 Diagnostics	7
DF	4 Diagnostics	9
DG	8 Diagnostics	14
GS	General Services	8
PF	Poloidal Field	13
RB	RF test bed	4
RF	Radio Frequency Heating	9
RH	Remote handling(part)	1
SS	Safety & Access	6
TB	NI test bed	10
TF	Toroidal Field	6
VC	Vacuum	10
YC	Neutral injection (Oct 4)	11
Total for 18 subsystems		152

Table II Various costs & Capacities

Equipment Class	Cost £ per channel	Installed Channels
Interface cubicles		112
U-port adaptors	1400	112
ADC&DAC,(CAMAC)		
Relay multiplexed DVM	50	2650
Slow scanning	70	8050
5kHz transient recorder, 1k	98	3360
250kHz transient recorder, 4k	1080	236
1ms DAC	38	868
TIMING, (CAMAC)		
Timing pulse	280	668
Pulse pattern generators	1050	150
Time measurement	285	300
Optical signal buffers	94	408
LSD		
Output modules	14.0	14900
Input modules	14.1	23900
CAMAC LSD Controllers	850	178
ACC		
Auxiliary crate controllers	1880	77
ANALOGUE SIGNAL CONDITIONING		
Isolation amplifiers	98	1030
Other active devices	211	525
Passive devices & filters	6	4856

References

1. BOMBI,F., 10th Symposium on Fusion Engineering, Philadelphia, December 1983.

2. BOMBI,F., NIJMAN,JP., van MONTFOORT JE, 13th Symposium on Fusion Technology, Varese, September 1984.

Table III use of fibre optic cables

Fibre type	200 micrometre core PCS
Wavelength	820nm
Connectors	SMA, Amphenol 905 compatible
Number of fibres	1340
Total length	60km single-fibre cable
Total length	4km quad-fibre cable
Fibres 0 to 50m	60%
Fibres 51 to 300m	40%
Longest fibre	300m
Approx cost/m	£1

THE JET PULSE TERMINATION NETWORK

J A How, M L Browne, S R Cooper, B J Green, P J Lomas, P Noll, F C Schüller, C A Steed,
M Tilley, H van der Beken
JET Joint Undertaking, Abingdon, Oxfordshire, OX14 3EA, UK

ABSTRACT

Should potentially-damaging conditions for JET arise during a pulse, then the pulse must be terminated in such a way as to protect JET equipment. This paper describes the present state of the JET pulse termination network which performs this function.

I INTRODUCTION

The JET Pulse Termination Network (henceforth designated as PTN) is designed to ensure the orderly termination of a JET pulse should an undesirable or dangerous condition arise. All sub-systems within JET are designed to be self-protecting with direct hardware connections between the fault detection device and the plant sub-systems involved for fast (<125ms) actions. For slow actions a network of PLC's implements the Central Interlock and Safety System (CISS) [6]. The PTN is a complementary protection which provides a link between the various sub-systems and the plasma condition, and can thus take global action across key JET sub-systems involved in a JET pulse. A block diagram showing these links is given in fig 1.

Central to the PTN is a hard-wired logic network, which receives fault condition signals from various sources including the plasma and distributes permit and inhibit signals to the JET sub-systems involved in a pulse. The main plasma parameters are monitored and compared with user-set conditions in the Plasma Fault Protection System (PFPS) microprocessor [1] which outputs signals to the logic matrix and directly to certain sub-systems. All events occurring to and from the PTN are recorded by latched timers and data acquisition channels for post-pulse analysis.

Figure 2 shows the logic diagram for the PTN. In section II the outputs of the PTN, shown on the right hand side of fig 2, are described. Section III deals with the fault protocol, ie, how the faults are detected, and what action is taken for each fault condition. Three classes of fault are described;

i) those requiring a modification of pulse parameters,

ii) those requiring a controlled pulse termination,

and iii) plasma disruption.

The set-up and post-pulse display features of the PTN are described in section IV. Finally, future extensions envisaged for the JET PTN are discussed in section V.

II PULSE TERMINATION NETWORK OUTPUTS

II.1 Close All Gas Valves

There are eight gas introduction valves on JET, for prefill, feedback and injection of puffs of various gases. The PTN provides a single signal that overrides all other inputs, and closes all the valves so that no further gas introduction is possible.

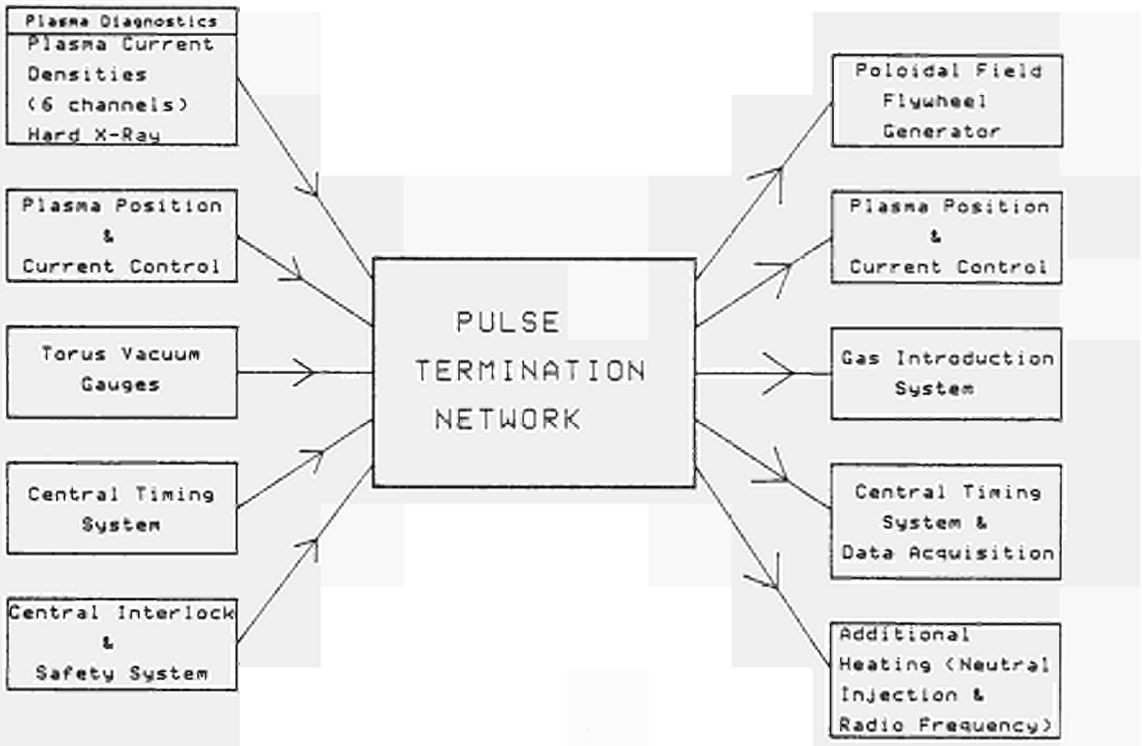

Fig 1. Block diagram of Pulse Termination Network Interface.

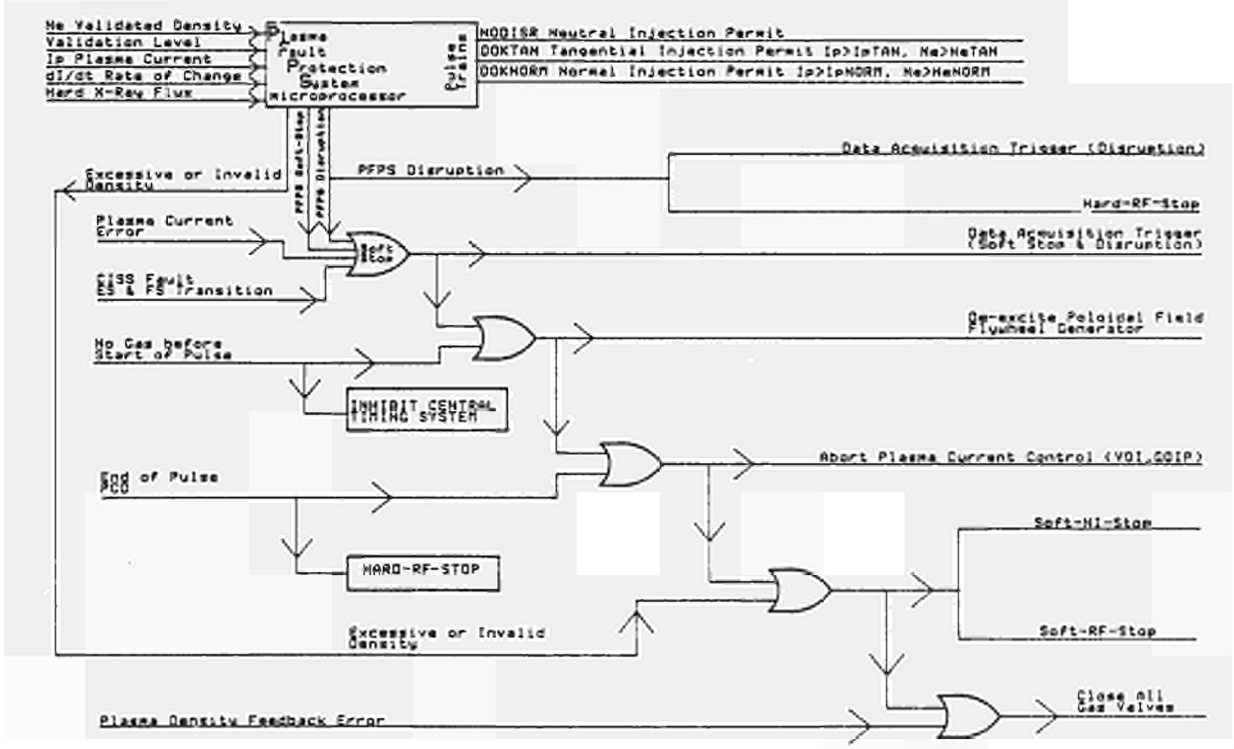

Fig 2. Pulse Termination Network Logic diagram.

off all gas valves. Further, if PFPS sees that the density is above a user-defined limit (NEMAX), or that the density measurements are unreliable ("invalid density") then the additional heating systems are ramped off with a soft-RF-stop and a soft-NI-stop as well as closing the gas valves.

III.2 Conditions Requiring a Soft Pulse Termination

A controlled termination to the plasma pulse is achieved by removing the excitation signal to the ohmic heating flywheel generator (PF/FGC) whilst maintaining control of the position control amplifiers for a further 10 seconds, thus allowing a normal resistive plasma current decay (several seconds). The PTN also sends out soft-RF and- NI-stop signals (see II.2) and closes the gas valves. However, this sometimes results in a disruption because the plasma current is not high enough to support the density so we are also considering moving the plasma to the inner wall at the same time as the soft stop (see V.2).

Several conditions lead to a soft pulse termination (soft-stop):

i) If a difference of more than 500kA develops between the plasma current and the requested current then a soft-stop is initiated [5].

ii) If there is an emergency or full shutdown transition in the CISS [6] then a soft-stop is requested.

iii) If the gas introduction system fails to inject enough gas for plasma breakdown then the central timing system is inhibited and a soft-stop is requested as an additional precaution.

iv) Finally, the PFPS microprocessor [1] compares various plasma signals and requests a soft-stop if an unhealthy plasma develops. The operator can set limits for maximum and minimum plasma current (IMAX and IMIN), maximum rate of change of current (IDOTMX) and hard X-ray flux level (RHXF). A data acquisition trigger is created by the PTN at the soft-stop time for fast data acquisition.

III.3 Plasma Disruption

The sudden loss of plasma current in a tokamak can cause considerable damage. The resistivity rise during a disruption increases the ohmic heating power to the plasma and this, coupled with the existing energy content of the plasma must be dissipated on the walls as direct heat, or as eddy currents. Intense beams of energetic runaway electrons are often created during a disruption, leading to possible local damage. The mechanical forces created by the rapid changes in the plasma and coil currents create severe mechanical stresses. Indeed rapid movement of the JET vacuum vessel during disruptions, of up to 5mm in less than 100ms have been observed. Finally, the transient currents in the transformers, switching gear and in the national grid must be kept below certain limits.

The methods by which we try to avoid disruptions are described in III.1 and III.2 above. Disruptions are usually detected by the dI/dt monitor in PFPS. In some cases they are detected by the sharp rise in the hard X-ray flux level, or by the difference between the actual and requested current. On detection of a disruption, a soft-stop is initiated and in addition the neutral beams are all immediately switched off (see II.5). The plasma control amplifiers are, however, left on for another 10 seconds to control the resistive decay of any plasma that may remain after the disruption.

18:08:46 Soft Termination Timing and Status 30-07-1986

Pulse 9548 Timed at 18:01:46 on 30-07-1986

PRE	STF	SPM	GAS	SCB	PCD
0.00	26.00	36.00	39.50	39.99	58.00

GAS On	39.69	48.27		
GAS Off	40.23	125.48		
SSTOP	48.18	48.19	48.35	58.00
PFPS	48.19			
NOGAS	(no events were recorded)			
CISS	48.35			
PPCC	48.18			

Soft Termination was SET at 48.18 sec from PRE

PPCC was SET at 48.18 sec from PRE

Fig 3. Pulse Termination Network Event Timing Display.

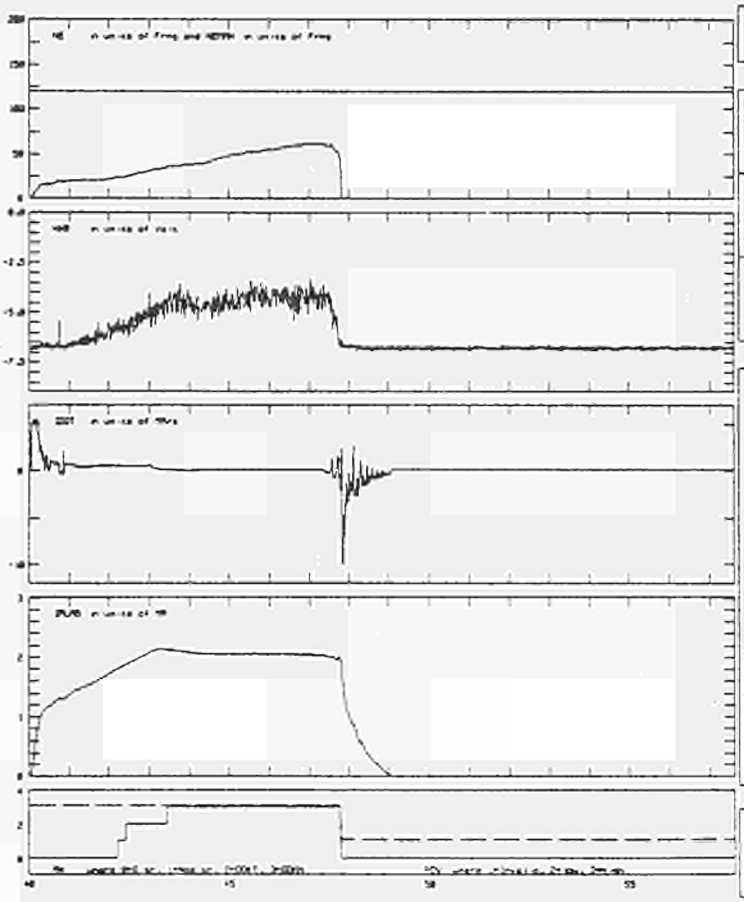

PFPS ALARM PNUM: 9245
7:56: 1 on 17/ 7/1986

AH HARD + RF,GAS OFF
NE INVALID 47.75

SOFT STOP + DISRPTN.
IDOT > IDOTMX 47.80
IDOT =-.10E+02 MA/s

TSCAN =	12	msec
TSTART=	40.60	sec
TSTOP =	58.00	sec
IMIN =	.30	MA
IMAX =	3.00	MA
AUTO =	OFF	
NEMAX =	120	Frng
IDOTMX=	5.00	MA/s
RHFX =	2.00	Volt
IPTAN =	1.80	MA
IPNORM=	1.80	MA
NETAN =	25	Frng
NENORM=	35	Frng

PFPS ENABLED

NODISR=42.20 to 47.74
DOKT =42.40 to 47.74
DOKN =43.43 to 47.74

Fig 4. Plasma Fault Protection System Post Pulse Analysis.

II.2 Soft-NI-Stop and Soft-RF-Stop

The JET additional heating systems (Neutral Injection and Radio Frequency) have elaborate internal self-protection systems [2,3] but the interface with the plasma state is provided by the PTN for both ramp-down (soft) and "immediate" (hard) switch-off. The two PTN outputs "soft-NI-stop" and "soft-RF-stop" trigger a controlled ramp-down of the additional heating power. The RF voltage waveforms are aborted, with a 1 second linear ramp-down, so the power decays quadratically. The eight neutral beam injectors are switched off in pairs, two every half second.

II.3 De-excite PF/FGC and Abort Plasma Current Control

Two methods of aborting the plasma current are used. Firstly the Poloidal Field Flywheel Generator can be de-excited directly simply by shorting the excitation amplifier to earth [4]. Secondly the plasma current control waveforms (VØI feedforward, and GØIP feedback gain) can be set to zero. In both cases the plasma position control amplifiers remain energised for a further 10 seconds in order to allow the plasma to decay smoothly in a controlled manner (the plasma current resistive decay time is several seconds).

II.4 Data Acquisition Triggers

Two data acquisition triggers are provided by the PTN for fast data taking. One results from a disruption or a soft-stop while the other is produced only on a disruption. For most cases the "soft stop or disruption" trigger is used, such that the fault leading to either can be investigated. However, if a disruption occurs subsequent to a soft-stop the relevant data cannot be acquired a second time in this way, so that a "disruption" data acquisition trigger is sometimes useful.

II.5 Hard-NI-Stop and Hard-RF-Stop

These are signals to request an "immediate" switch-off of the additional heating. The hard-RF-stop has not yet been implemented since the reflected power in the RF lines has proved sufficient protection to trip the generators, and further, the present RF poses no immediate threat to the torus. However the hardware is installed and can be quickly implemented if necessary.

The hard-NI-stop is more complicated. For normal neutral injection operation there are three "permit" pulse trains sent directly from the Plasma Fault Protection System microprocessor. The "No Disruption" signal basically says that the plasma exists and no disruptions have been detected. The two other signals are a "tangential beam permit" and a "normal beam permit", which are sent when certain conditions on plasma density and current are satisfied. Loss of these signals causes an immediate "hard-stop" of the relevant beams [2].

III FAULT PROTOCOL

III.1 Faults not Requiring a Pulse Termination

Some faults do not require a full termination of the plasma pulse, but only modification of the pulse parameters. For example, if the plasma density feedback detects an unreasonable error between the requested and the actual density, existing for too long, the PTN switches

IV THE PULSE TERMINATION NETWORK DISPLAYS AND PARAMETER SETTING

IV.1 Parameter Setting

Parameters for the detection of undesirable conditions are set in a number of ways. The pressure trip for the detection of the prefill gas, and the 0.5MA plasma current error detection are hard wired trip amplifiers, but enabled and disabled by computer-controlled timing windows from the central timing system. The plasma parameters are monitored via three microprocessor modules; the Plasma Density Validation system, the Plasma Density Feedback processor, and the Plasma Fault Protection System. Each of these modules has an associated mimic and touch panel in the JET Machine Control Room for parameter setting and confirmation. Similarly alarm points are defined to indicate immediately if any of these systems fail. An example of typical PFPS parameters is shown in fig 4.

IV.2 Post Pulse Display

All of the outputs of the PTN are monitored with latched timers with alarm points defined for each action. Thus alarms are immediately displayed for the JET operation staff should an abnormal pulse termination occur. The only problem then is to determine which of the PTN inputs created the termination. Several displays are available on request to establish the sequence of events during a pulse. Figure 3 shows a display of the main JET timing values, and the various latched fault and event times. The first event causing a pulse soft termination is highlighted, and the reason for this fault clearly indicated.

A further analysis is necessary for the Plasma Fault Protection System, and a display mimic and debug page is available for every pulse. Up to three consecutive faults and actions can be handled presently by PFPS [1]. For example, the density could go above the maximum allowed density for that pulse, and so the gas valves would be closed and a soft-additional-heating-stop sent out. Then a soft-stop could occur from the plasma current greater than IMAX, and finally a disruption could occur, detected by dI/dt or hard X-rays. Figure 4 shows an example of the PFPS analysis page, where invalid density occurred first, and subsequently a disruption. Similar pages are available for the density validation and the plasma current control microprocessors.

V REFERENCES

[1] GONDHALEKAR, A, et al, 13th SOFT, Varese (1984), 1661-1665.
[2] STORK, D, et al, 14th SOFT, Avignon (1986), Paper GP-13.
[3] WADE, T, et al, 13th SOFT, Varese (1984), 727-732.
[4] CORBYN, D, et al, 13th SOFT, Varese (1984), 843-850.
[5] NOLL, P, et al, 13th SOFT, Varese (1984), 503-509.
[6] BOMBI, F, et al, 13th SOFT, Varese (1984), 1133-1139.

THE DEVELOPMENT OF THE JET POLOIDAL FIELD POWER SUPPLIES TO REACH THE NOMINAL FLUX SWING CAPABILITY

P.L.MONDINO, T. BONICELLI, M. HUART, A. SANTAGIUSTINA
JET Joint Undertaking
Abingdon, Oxfordshire, OX14 3EA, England

ABSTRACT

After a review of the results obtained and of the modifications performed, on the poloidal field system, during the first three years of operation, the paper describes the progress development, on the power supplies, to reach the nominal flux swing capability of JET.

1. THE FIRST THREE YEARS OF OPERATION

1.1 The design and the operation till 1985

JET was designed to obtain breakdown with a loop voltage of about 140V and a rise of the plasma current to 4.8MA in 1s [1], followed by several seconds flat top. The nominal flux swing capability was 34Wb. Fig.1 shows the cross section of JET where the various poloidal field coils can be identified. Fig.2 shows the connection of the poloidal field coils to the generator and to the Ohmic Heating Circuit [2] as foreseen in the design [1] and is used in 1983-84. The experimental results up to 1985 show that loop voltages of about 10V are sufficient to obtain breakdown with good reliability at low premagnetisation currents and that the rate of rise of the plasma current has to be limited to 1-2MA/s to avoid high MHD activity and possible disruptions in the early flat top phase. Routine operations were performed at 40kA of premagnetisation current, half the nominal value, losing in this way part of the flux swing available. The commutating resistors were set to the minimum value of 0.15Ω. A loop voltage of about 20V was obtained at breakdown with a plasma current derivative sufficiently low (1MA in the first 0.5s).

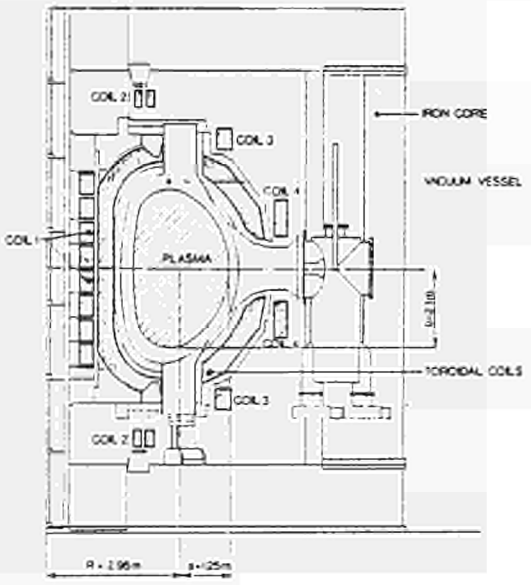

Fig.1. Cross Section of JET.

The operation was also limited by the current capability of the Poloidal Field

Generator (PFGC) at the end of the flat top phase. In fact the PFGC had to provide 80kA of magnetising current for P1, 10-15kA drained by the commutating resistors and a radial equilibrium current of about 4kA per MA of plasma current through the P4 coils. The generator limit (100kA) was already reached in a 3MA pulse [3].

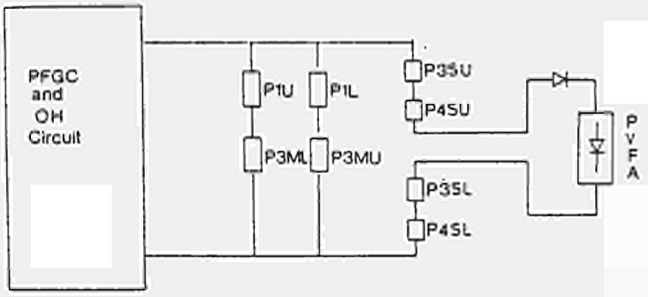

Fig.2. Poloidal field system configuration in 1983-1984.

1.2 The new configuration from 1985

The transformer primary coils (P1) were reconfigured, in early 1985, from parallel to series connection (Fig.3), increasing the transformer ratio to make better use of the available voltage capabilities and to reduce primary current requirement. Active control of the plasma elongation was implemented, by feeding the shaping coils P2S and P3S, independently, from the Poloidal Shaping Field Amplifier (PSFA). The vertical field coils P4 were disconnected from the transformer primary coils P1 and were supplied by the Poloidal Vertical Field Amplifier (PVFA) alone.

In fact the necessary P4 single turn voltage to maintain the radial equilibrium of the plasma column during early fast rise phase, determined by Shafranov equilibrium equation and by circuit equations, is given by:

$$\frac{V_{P4}}{n_{P4}} \simeq K\frac{V_{P1}}{n_{P1}} - hV_{PR} \qquad (1)$$

where h=1 and K=2.2 are geometry factors related also to the plasma size and position and V_{PR} is the plasma resistive voltage drop. The turn number n_{P1}, n_{P4} of P1 and P4 coils were chosen during the design phase to obtain $K\frac{n_{P4}}{n_{P1}} = 0.95$ and $V_{P4} - V_{P1}$; the PVFA had to provide only a small voltage adjustment. With series connection of the P1 coils the P1 number changed from 284 to 568 and the voltage needed by P4 became half of the voltage provided by the OH circuit to P1. For better use of the PVFA low voltage capabilities (2.3kV at 25kA and 2.8kV at no load), P4 was disconnected from the OH Circuit and the P4 number of turns was reduced from 122 to 78.

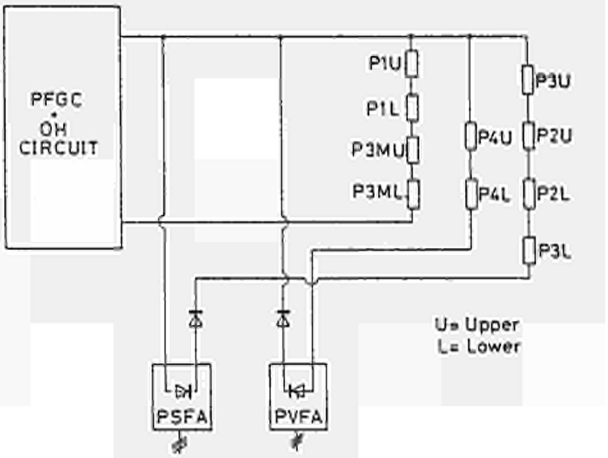

Fig.3. Poloidal field system configuration from March 1985.

Other changes, planned in parallel with the re-configuration of P1, were the increase in P1 coil current (to 40kA per turn) and the setting of the commutating resistors R3 and R4 to a value of 0.34Ω, with the aim of maintaining about the same P1 single-turn voltage previously used (20V), but to use the complete flux swing available (34Wb). The experiments showed that breakdown cannot be sustained with low loop voltages and high P1 coil currents. Strong stray fields produced by P1 were the main reason for this failure [7]. These fields increase proportionally to the square of the P1 coil

current due to the saturation of the JET magnetic circuit. Sustained breakdown in JET requires that $E_{TOR}B_{TOR}/B_{STRAY} > 10^{3}Vm^{-1}$ where E_{TOR} is the electric field on the loop, B_{TOR} the toroidal field (≤3.45T) and B_{STRAY} the vertical component of the stray field.

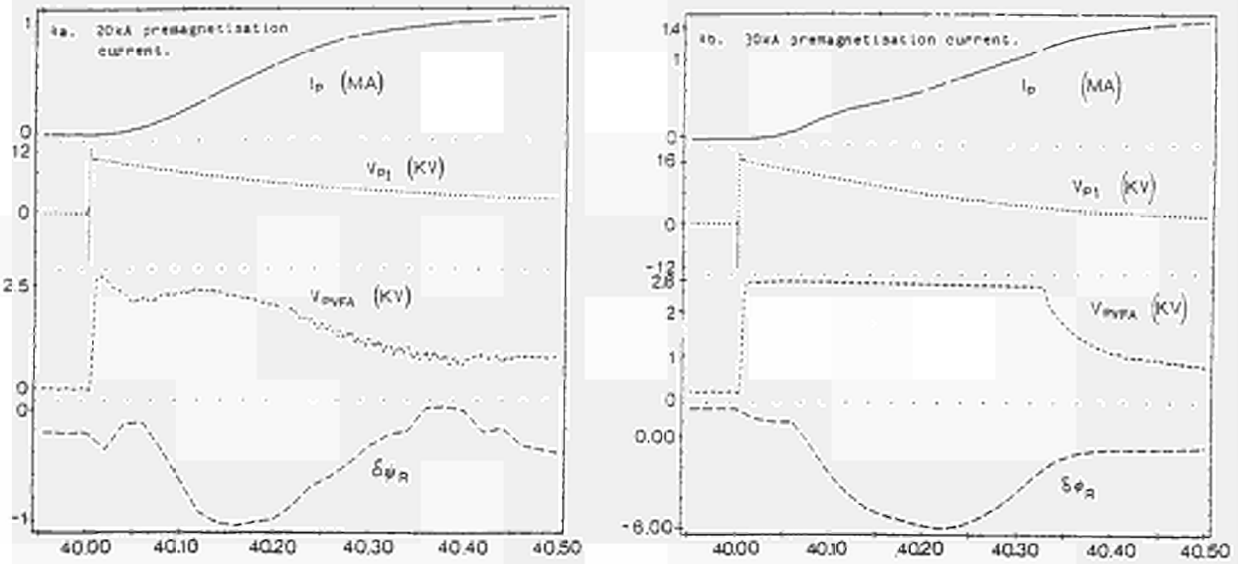

Fig.4. Fast rise phase: plasma current I_p, primary voltage V_{P1}, PVFA voltage V_{PVFA}, radial position error (vertical flux) $\delta\psi_R$.

As a result of the limitation of the ratio $\frac{E_{TOR}}{B_{STRAY}}$ the commutating resistors R3 and R4 have been kept at a high value of 0.6Ω. 20-25kA premagnetisation has been used routinely with a flux variation of 26.5 - 28.5 Wb, respectively. The premagnetisation at 30kA has shown a narrow parameter range for breakdown and could be established only by means of an extremely well calibrated start-up scenario. For the high level of stray fields and the lack of voltage on P4, any attempt at break-down at 40kA has failed.

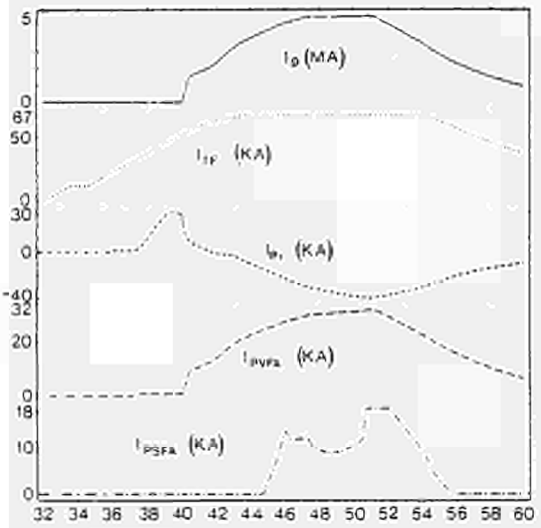

Fig.5. Pulse 8863: 5MA plasma current: plasma current I_p, toroidal field coil current I_{TF}, primary coil current I_{P1}, PVFA current I_{PVFA}, PSFA current I_{PSFA}.

Fig.4 shows the beginning of two typical pulses with different currents flowing in the transformer primary coils at the end of premagnetisation. With 20kA premagnetisation (see Fig.4a), 10.7kV was produced across P1 (-20V loop voltage), PVFA was preprogrammed to produce 2.5kV marginally reduced by feedback during the first 50ms at which time the plasma current was already detectable. During the following 200ms, the plasma current rose quickly (-3.5MA/s), requiring a voltage in the

range 2-2.5kV across P4 to maintain radial equilibrium. The radial position (vertical flux) error signal $\delta\psi_R$ (1V=0.22Wb) [4] reached a maximum, 150ms after current interruption, inside the acceptable range. With 30kA premagnetisation (see Fig.4b), 16kV was produced across P1 (-30V loop voltage). PVFA was preprogrammed to produce full voltage (2.8kV) that was maintained by feedback for more than 300ms. More voltage would be necessary to maintain proper radial equilibrium: in fact the error signal $\delta\psi_R$ reaches a maximum six times higher than before. Nevertheless, the plasma current rises, reaching 1MA at 270ms and 1.4MA at 420ms.

With 30kA premagnetisation, the flux swing produced by P1 was 30Wb. This flux allowed the establishment in JET of the record performance of 5MA plasma current with 4s flat-top (fig.5).

2. OPERATION REQUIREMENTS [8]

An analysis of the various physical processes that take place during plasma current rise is reported in [5], where several operational requirements are identified. These requirements are the guidelines for improvement of the electromagnetic system to optimise plasma formation, for increasing breakdown reliability, for decreasing flux variation losses and for avoiding disruptions.

Stray fields at breakdown. The region with $B_{STRAY}/B_{TOR} < 10^{-3}$ should be a large part of the vessel volume, the null should be inside the vessel as soon as possible after interruption.

Loop voltage. At breakdown, the loop voltage should be large with respect to stray fields ($E_{TOR}\ B_{TOR}/B_{STRAY} > 10^3$ V m^{-1}) and to the filling pressure ($E_{TOR}/P > 5 \times 10^3$ V m^{-1}mbar^{-1}). During plasma build-up, the loop voltage should be large compared to its resistive component: the ohmic input should be sufficient to burn through the radiation barrier. Moreover, the plasma current should rise quickly (2-5MA/s) to avoid high flux loss. When this phase is completed, (I_p=300-500kA), the loop voltage should be reduced to maintain a plasma current derivative in the range 0.5-2.0MA/s. In this way, excessive MHD activity and disruptive behaviour during the early part of flat top can be avoided.

Voltage across the vertical field coils. The voltage induced by P1 should be compensated; moreover, the appropriate current derivative in P4 must be sustained to match the plasma current rise, keeping a good plasma radial equilibrium already from the start of the discharge.

3. PROGRESS DEVELOPMENT

3.1 Stray field compensation

To reduce the stray fields, two P1 subcoils will be added to the eight existing, increasing the number of turns of P1 from 568 to 710 [6]. This first step should allow a reduction of stray fields produced by 40kA premagnetisation to values smaller than with the present 20kA premagnetisation. A further stray field reduction could be obtained by the non-uniform distribution of the current in the various P1 coils. The necessary modifications, under study, are reported in [7].

3.2 Voltage Shaping across P1 and P4

The Additional Switching Network and the Poloidal Vertical Field Boost Amplifier (PVFB) will allow shaping of the voltage across P1 and P4, as shown in Fig.6. The new poloidal

field system configuration is shown in Fig.7: the voltage shaping across P1 will be performed, switching in sequentially the R8 resistors. At interruption, 24kV will be applied to P1 (-34V turn voltage) after 20-100ms, the voltage will be reduced, stepwise, to an intermediate level around 4-6kV (6-9V turn voltage) and after 50-500ms from interruption, the voltage will be reduced even further to about 2-4kV (3-6V turn voltage).

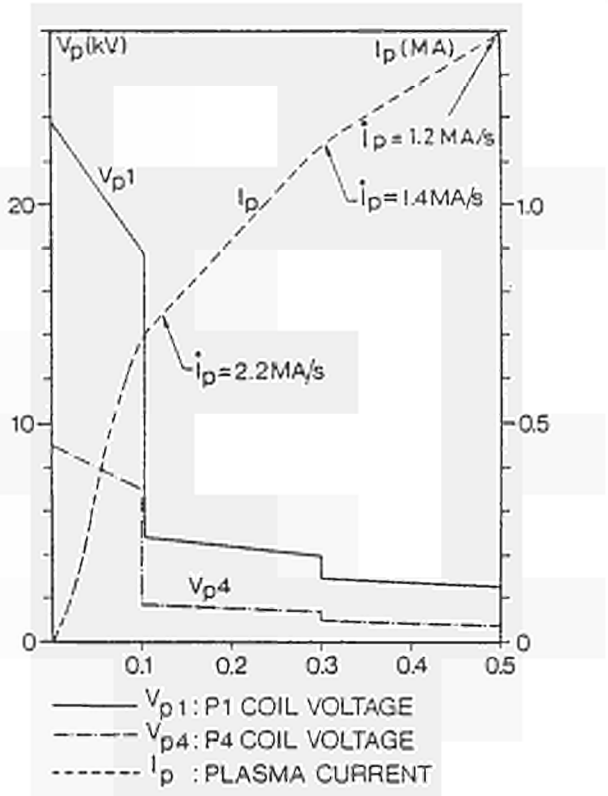

Fig 6 Shaping of P1 voltage V_{P1} and P4 voltage V_{P4}.

4. ADDITIONAL SWITCHING NETWORK

The Additional Switching Network consists of six identical branches connected between the main OH circuit busbars in parallel to P1 (see Fig.7). Each branch is set up with a Thyristor Make Switch, an Additional Commutating Resistor, a Limiting Inductor and a Current Detector, all connected in series. Each branch has a nominal resistance of 0.9Ω and their total parallel resistance is 0.15Ω.

4.1 Thyristor Make Switch

Instead of more traditional electromechanical make switches, thyristors were chosen on the following basis. Suitable electromechanical switches would not have been immediately available and would have any way required some development work on existing equipment, to cope with the expected pre-arcing current. A limiting inductor would have been required even for the electromechanical solution to limit the di/dt before the contact is made. Two electromechanical switches would have had a cost comparable with six static ones, whereas a higher number of branches allows more flexible operation. The technology developed for HVDC systems offers a suitable and well-established design, which is immediately applicable. The thyristor switches are expected to be almost maintenance free and the overall reliability of the static solution is expected to be higher.

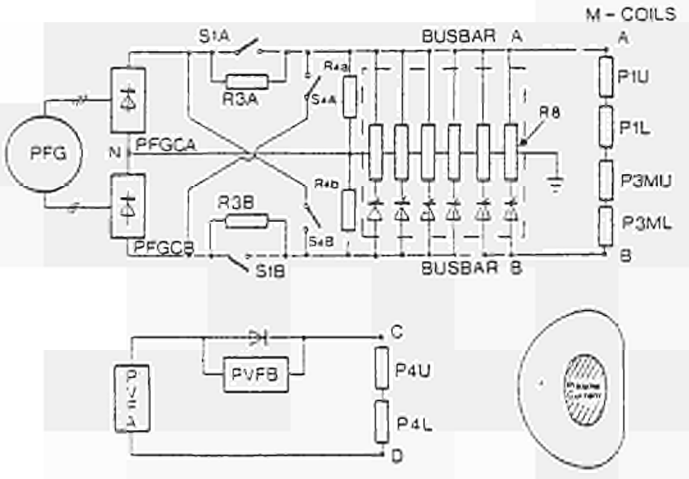

Fig.7. New poloidal field system configuration.

The design finally chosen is based on the following main features: The largest thyristors presently available (wafer with Ø=100mm, V_{DRM}=4200V, I_{TAV}=3000A) are used without parallelling; the thyristors are water cooled on both sides. The voltage safety factor is 1.5, plus one redundant thyristor. Each thyristor make switch is therefore built with 10 thyristors in series. A limiting inductor (1.25mH), air cored, is series connected to limit the di/dt at a conservative 20A/μs. As a first step, at least three branches will be switched in simultaneously to limit the thermal stresses on each thryistor. The reference nominal current waveform is shown in Fig.8a. Each thryistor make switch will be capable of withstanding the stresses due to the current waveform shown in Fig.8b, corresponding to the firing of only one switch (this is regarded as a fault condition).

The energy necessary to fire each thyristor is directly taken from the main busbars through the RC snubber circuit, connected in parallel. The trigger signals, generated at earth potential, are sent, through optical fibres, to the high voltage thyristor stacks. Each thyristor is provided with a firing circuit, which converts the light signal into a current pulse. At the same time, an answer-back signal is generated and sent, through an optical fibre, to earth for monitoring purposes. A self-firing protection is implemented in the firing circuit. If for any reason the voltage across an individual thyristor exceeds 4000V in forward direction, the thyristor itself is immediately fired as a protective action.

4.2 Resistors

Each resistor is internally arranged in twelve elementary banks of 1.2Ω; with four parallel and three series connections, the nominal resistance 0.9Ω is obtained. The energy capability of each resistor is 135MJ every ten minutes (nominal JET duty cycle) but a 50% overload (200MJ) would not cause damage. The active material is stainless steel AISI 310 which has low resistivity variation coefficient with temperature ($\sim 0.5\ 10^{-3}°C^{-1}$ in the temperature range between 20° and 400°C) and allows high working temperature (above 800°C). Actually, in order to limit the resistance variation, the maximum average working temperature will be only 350°C. The resistors are forced air cooled with air to water heat exchangers.

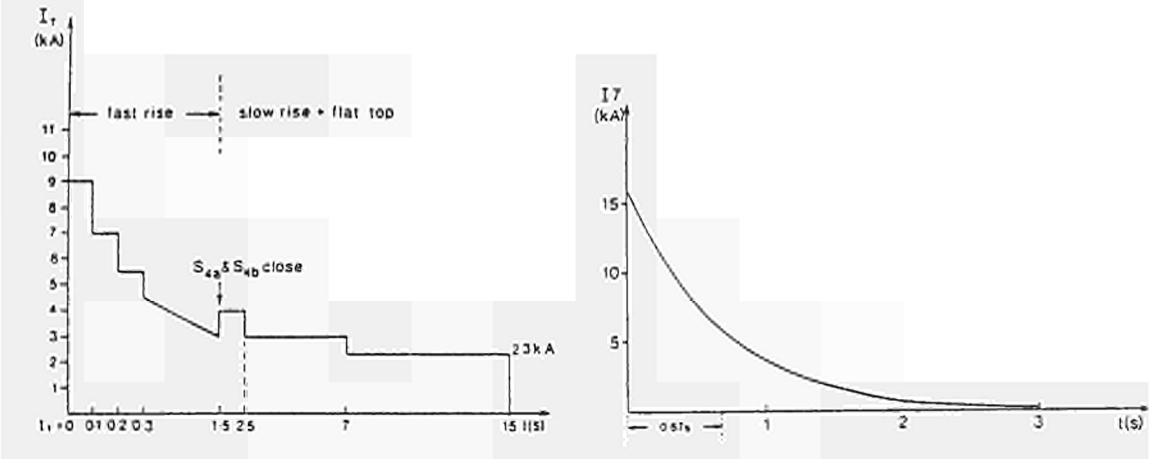

Fig.8. Poloidal vertical field boost amplifier: reference design.

5. Poloidal Vertical Field Boost Amplifier

A voltage capability of 12kV DC will be provided across the coil P4 connecting a boost amplifier PVFB in series with the existing PVFA (PVFA3-4)(Fig.7). The PVFB will be connected by cables in parallel with the existing blocking diode of PVFA, which will act as a freewheel diode. The PVFA and PVFB will be operated in sequential control. The controller will be built in the PVFB control system. The total voltage reference will be given by the Plasma Radial Position Control. For high voltage demand, the PVFA will work at full rectification and the control will be made by the PVFB voltage feedback loop. For low voltage demand, the PVFB will be driven to full inversion to force the current to freewheel in the by-pass diode (BD) and the control will be achieved by the PVFA voltage feedback loop. As the high voltage is only required for a short time, typically 0.5s, at the beginning of the pulse, this mode of control enables a limit to be imposed on the current rating of PVFB and the reactive power consumption, at a reasonable level. The boost amplifier PVFB is specified for an output voltage of 9.2kV DC at 1kA DC and 2kV DC at 6kA DC. The nominal pulse current rating is 6kA DC for 0.5s every 10 minutes. The PVFB will be composed of four identical units, each consisting of dry-type transformer for indoor use with two secondary windings each connected to a single thyristor bridge (Fig.9). The primary of each dry-type transformer will be connected to each secondary winding of the PVFA 33kV/1.05kV transformers. All dry-type transformers will be identical, the phase shifting between series connected units being achieved on the PVFA transformer. The transformer ratio is close to 1:1. The thyristor bridge of PVFB units includes only one naturally air-cooled thyristor per arm. In view of the high impedance of the system (short circuit current required -9kA DC) and the surge rating of the thyristors proposed (22-35kA), the design foresees no fuses. The protection against thyristor failure will be by detection of reverse current and tripping of PVFA 33kV circuit breakers. Various fault conditions have been considered. One of them includes a failure in the control system of PVFB, giving full rectification when the PVFA current of

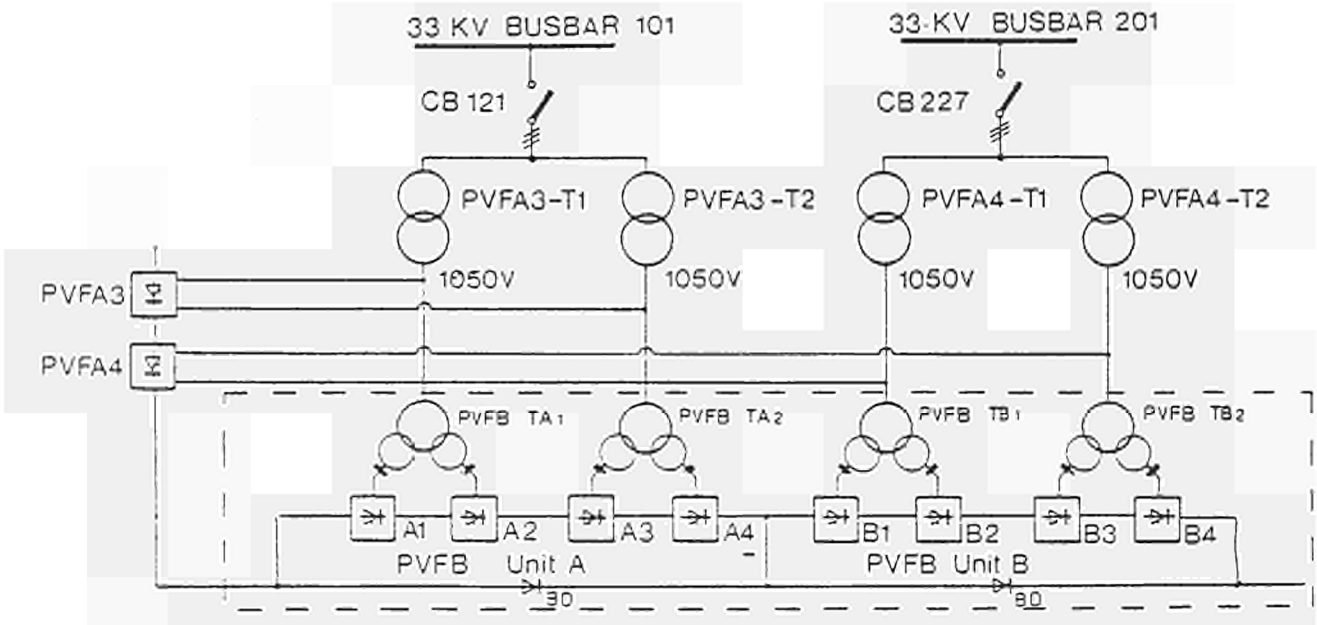

Fig.9. Poloidal vertical field boost amplifier: reference design.

35kA DC freewheels in the by-pass diode BD (during plasma current flat top). The PVFA will in fact be in short circuit and will have to withstand its short circuit current until the PVFA circuit breaker trips (assuming that the protection by inversion of PVFB does not work). As an additional precaution, it has been specified that the PVFB should include a control inhibit, disabling the firing pulses once the PVFA current exceeds a preset level. In the new configuration, the coil P4 will be fed with new independent busbars, galvanically decoupled from the Ohmic Heating Circuit. The vertical field circuit will be grounded by means of a high impedance resistor.

6. CONCLUSIONS

The components of the additional switching network are being manufactured and will be installed during the late 1986 shutdown. Integrated tests with the existing poloidal field system will be performed in Spring 1987. The Boost Amplifier will be ordered during late 1986 and should be operational early in 1988. When this equipment is operational, it should be possible to break-down, at 40kA premagnetisation, using the nominal flux swing available (34Wb). The large flexibility in voltage and timing should allow minimisation of flux losses during breakdown and plasma current rise.

7. ACKNOWLEDGEMENTS

The authors would like to thank E. Bertolini for his technical and managerial supervision; F.C. Schueller for many helpful discussions on operational requirements; D Hrabal (Siemens, Erlangen, FRG) for his contribution to the thyristor make switch, which is now being manufactured by Siemens; and F. Jaselli (Microelettrica, Milano) for his contribution to the additional commutating resistors now being manufactured by Microelettrica.

REFERENCES

[1] The JET Project, DESIGN PROPOSAL FOR THE JOINT EUROPEAN TORUS, EUR5516e, Commission of the European Communities (1976).

[2] Eriksson, T., Mondino P.L., Raymond, C., Stella, A., FABRICATION, INSTALLATION AND TESTING OF THE JET OHMIC HEATING CIRCUIT, Proceedings of the 10th Symposium of Fusion Enginering, pp. 2070-2076, Philadelphia, 1983.

[3] Mondino, P.L., THE JET POWER SUPPLIES: A REVIEW AFTER ONE YEAR OF OPERATION, Proceedings of the 13th Symposium of Fusion Technology, pp. 119-131, Varese, (Sept 1984).

[4] Noll, P., et al, THE JET PLASMA POSITION AND CURRENT CONTROL SYSTEM, Proceedings of the 13th Symposium of Fusion Technology, pp. 503-509, Varese, (Sept 1984).

[5] Schueller, F.C., et al, PLASMA EVOLUTION AND SKIN EFFECTS IN JET", Proceedings of 12th European Conference on Controlled Fusion and Plasma Physics, pp. 287-290, Budapest, Sept.1985).

[6] Last, J., et al, THE JET MAGNETIC OPERATIONAL EXPERIENCE AND PLANS FOR UPGRADE, presented at the 14th Symposium of Fusion Technology, Avignon, (Sept.1986).

[7] Bertolini, E., et al, THE DEVELOPMENT OF THE JET ELECTROMAGNETIC SYSTEM, presented at the 14th Symposium of Fusion Technology, Avignon, (Sept.1986).

THE JET NEUTRAL INJECTION 160kV TRANSMISSION LINES, THE ASSOCIATED SNUBBERS AND THE SF6 TOWER FOR THE TERMINATION OF THE TRANSMISSION LINES HOUSING OF THE SNUBBERS AND VOLTAGE BREAKS

R Claesen, U Baur, E Bertolini, G Celentano, P L Mondino, P H Rebut
JET Joint Undertaking, Abingdon, Oxfordshire, UK

1. ABSTRACT

The JET neutral injection system consists of 16 injectors for operation on the torus plus 2 injectors in the Testbed. The 16 injectors are divided into two groups of 8. One feature of JET is that it is designed for active operation with Tritium. As a consequence, no components requiring regular maintenance can be installed in the active zone. Therefore, the neutral injector power supplies are installed in an adjacent building. A special cable (called transmission line) was constructed to connect the power supplies to the neutral injectors (see Fig 1). Due to the length of these transmission lines, snubbers are necessary to limit the short circuit energy and the maximum current in the injector in case of breakdown. A special vessel (called the SF6 Tower) was constructed to house the snubbers, the high voltage breaks in the cooling water circuits, etc.

2. INTRODUCTION

The design, construction and testing of the power supplies for the neutral injectors have been described in more detail [1], [2], [3], [4]. The early tests of the 160kV power supply system are described in [5]. This paper describes the other components of the system (eg. the transmission line, the snubbers and the SF6 tower). Firstly, the main design constraints will be presented and then the construction and test procedure will be described.

3. DESIGN CONSTRAINTS

JET has been designed to operate in Tritium. Therefore, all components requiring regular maintenance cannot be installed inside the Torus Hall and to a lesser extent inside the Basement. In addition, all components installed in the Torus Hall must be remote handleable to a greater or lesser extent. For the components described in this paper, the connections to the neutral injectors only require remote handling. If a failure occurs inside the SF6 tower, the complete SF6 tower must be removed and placed in the Hot Cell for repair.

The relevant power supply data which are important for the definition and the design of the other components are:

- The accelerating grid (grid 1) and the ion source are at high voltage potential; as a consequence, all auxiliary power supplies and auxiliaries for the ion source, such as cooling pipes, require the same isolation level as grid 1.
- The main grid 1 data are:
  - positive against grid 4 (earth potential)
  - 80kV/60 A in hydrogen, 160kV/30 A in deuterium
  - maximum short-circuit current, 300A
  - maximum short-circuit energy in grid 1, 5 joule.
- arc power supply:
  - 200V, 1350A.
- filament power supply:
  - to reduce the cable size, the filament is supplied with AC at 1kV and a stepdown transformer (1kV/24V) can be installed at the ion source.
  - 1kV, 52A.

Electrically, the torus is connected to earth at one point only in order to avoid earth loops. All equipment connected to the torus must therefore either have a voltage break or must be isolated from earth to 10 kV.

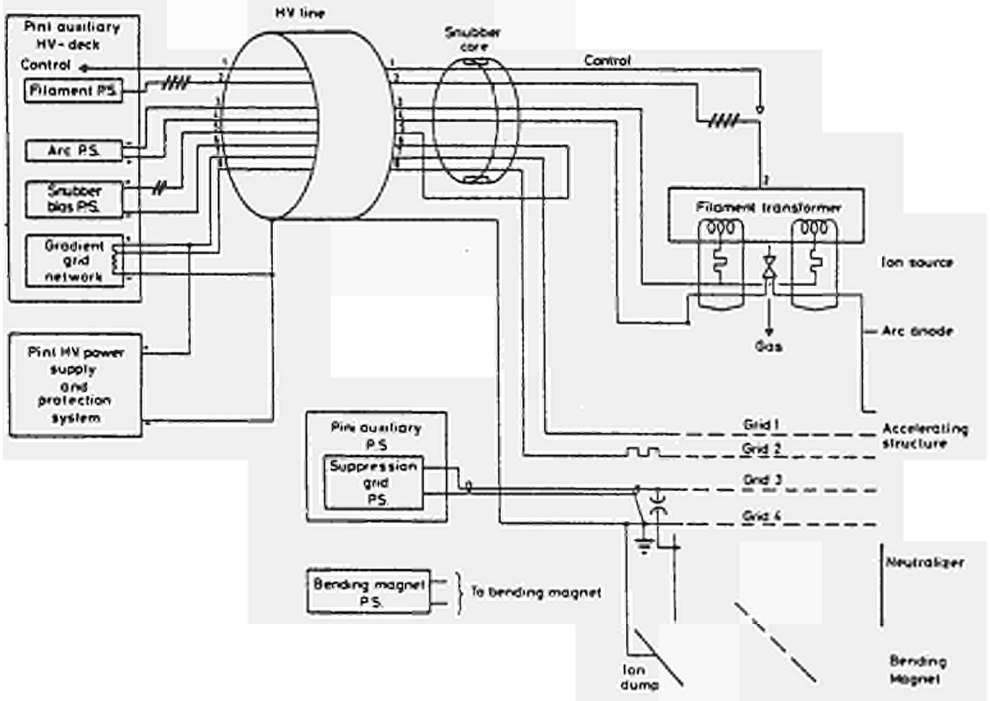

Fig. 1: Overall schematic of the PINI and associated injector power

4. FUNCTIONS AND MAIN DESIGN DATA

4.1 SF6 Tower

The SF6 Tower is installed in the Torus Hall. Because of space restrictions in the Torus Hall, all equipment installed there must have the minimum size possible.

As with all elements installed inside the Torus Hall all components must be able to withstand a minimum level of 10^6 rad.

At the bottom of the SF6 tower, the transmission lines are connected, while at its output, HV bushings are provided for the connection of the different circuits to the neutral injector. The injector side of this bushing requires remote handling as it is supposed that the removing and reinstallation of an ion source will be done on a routine basis during operation.

The components inside the SF6 tower are passive components only. They must be isolated for 160kV operation between each other and against the SF6 tower walls.

4.2 Transmission Line

The transmission line connects the power supply to the SF6 tower. Its maximum operating voltage is: +160kV DC and the rated current in the grid 1 connection is 60A.

To reduce the stored capacitive energy, and as a consequence to keep the size of the snubbers as small as possible the capacitance of the line must be as small as possible.

Due to the complicated installation route the line must be flexible enough (bending radius minimum 3m) but on the other hand must be rigid enough in order to be filled with SF6 under pressure to provide the required isolation.

4.3 Snubbers

The main function of the snubber is to limit the short circuit current to 300A and the short circuit energy to a maximum of 5J if a breakdown occurs inside the neutral injector. The total capacitance of the system is such that a maximum of 100J must be dissipated by each snubber.

5. DESIGN, CONSTRUCTION AND TESTS

5.1 Transmission Line:

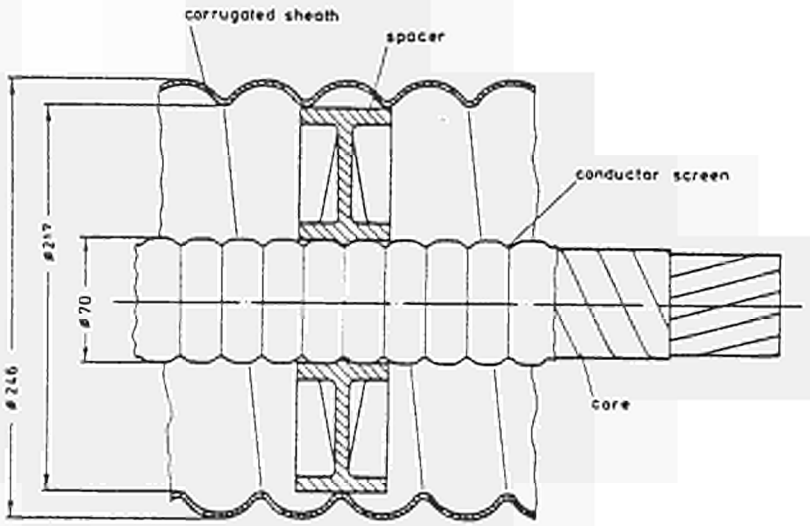

Fig 2: Transmission Line - cross section

As the auxiliary power supplies for the neutral injectors are referenced to the grid 1 voltage level, it is obvious that instead of constructing different cables isolated for 160kV, it is more economical and, in addition, provides the lowest capacitance, if all the cables are bundled together and then isolated against earth. A conventional cable with a PE type of isolation material would have such a high capacitance that the stored energy would be so high that exceptionally large snubbers would be required. A far lower capacitance is reached with a coaxial type of cable with SF6 as the isolation medium.

The inner conductors of the line (for the filament, arc snubber power supply) are conventional cables with 5kV isolation for the conductors, the grid 2 conductor is isolated for 30kV against the others. Around these cables is the corrugated copper conductor for grid 1. This conductor is the inner conductor of the coaxial cable.

The outer conductor is a corrugated AlMn conductor. The corrugation of both the inner and the outer conductor provides the required flexibility of the transmission line.

Spacers installed every 50cm keep the inner conductor in the centre.

The SF6 gas inside the transmission line is at a pressure of 2.3 bar gauge.

Several type tests were performed at a section of 1m length, they are:

- impulse test at 325kV 1.5/50µs.
- at repetitive testing at different voltage levels with pulses of 1 min the first breakdown occurred at 340kV with a pressure of 2 bar gauge.

The site acceptance tests performed were:

- a pressure test at 4 bar gauge
- + 200kV DC for 15 mins
- + 260kV DC for 1 min.

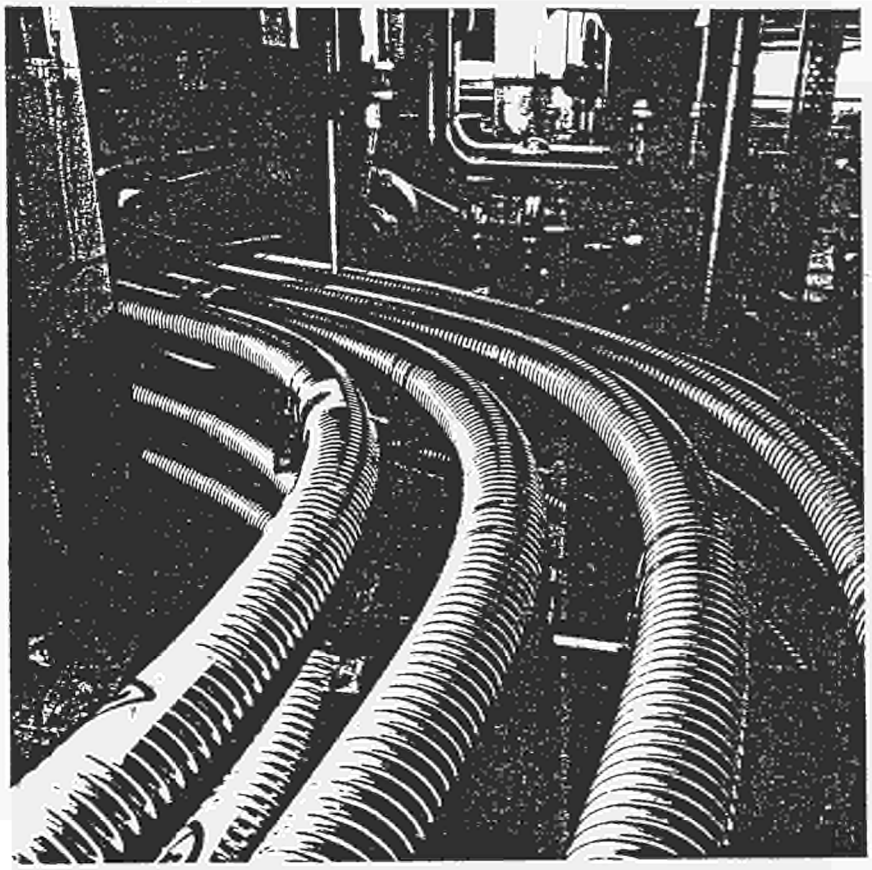

Photo 1: Part of the installation route in the basement

The measured values after the construction are:

- characteristic impedance 67Ω.
- capacitance beween inner and outer conductor < 50pF
- inductance of the arc cables 0.064µH/m
- with 26W/m heating power of the inner conductor its temperature increased by 20°K after 18h
- SF6 gas losses < 0.25%/day.

5.2 Snubber

To minimise size, an active snubber was chosen. The snubber is biased by an independent source of 60V 150A. At the output of the snubber bias power supply, an inductance is inserted in the circuit. It is installed around the magnetic core of the snubber. Its function is to prevent, in case of breakdown in the injector, any short-circuit energy from being dissipated in the small snubber bias power supply.

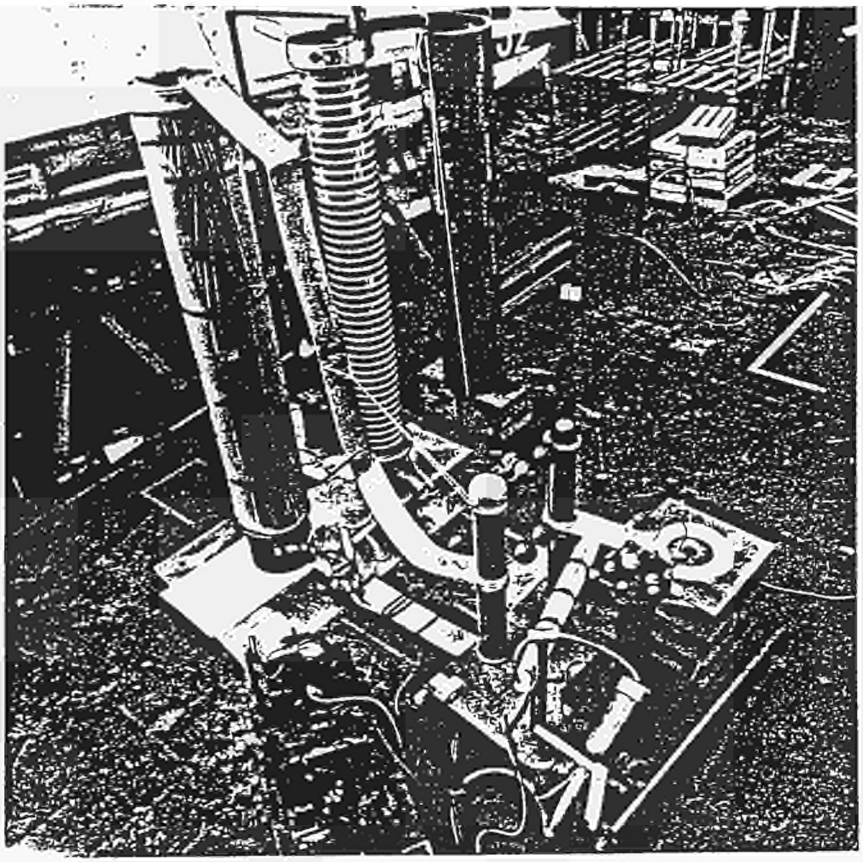

Photo 2: A snubber during its final tests

The snubber is constructed of Si.Fe tape of 2.5cm wide and 50µm thick. This tape is wound like a clockspring with an inner diameter of 100mm and an outer diameter of 340mm. Two of these springs are placed inside a single polyethylene container which provides the required electrical isolation. 48 of these containers are stacked on top of each other and form the snubber. The energy is dissipated in the form of eddy currents.

Each of these wound coils was factory tested with a capacitor of 0.6 µF charged to 2kV. This capacitor was discharged over an inductance of 69 µH and a wire through the centre of the coil. In addition, the coil was biased with a current of 40A. The discharge current was monitored and if the maximum was more than 400A the coil was rejected.

After assembly one snubber was fully tested by discharging a capacitor of 10nF through its centre. The measured maximum current was 270A. In addition the voltage distribution along the stack was measured and found to be linear.

5.3 SF6 Tower

The SF6 tower is electrically connected to the JET machine, and therefore, it must be isolated from local earth. As a consequence it is installed on isolation pads.

The SF6 tower was constructed in three different parts:

- to the bottom part, which is 2.2m high, the transmission lines are terminated. It also serves the purpose of re-routing the inner conductors when the position of the injector box is changed from co- to counter injection.

- The middle part is the main part. It is 7.8m high and has a diameter of 2.15m. In this part the snubbers are installed as well as the high voltage breaks in the cooling water circuits, the hydrogen or deuterium lines for the ion source and the pneumatic actuators for the valves. Each snubber is mounted on a pedestal and connected to the adjacent snubber and to the SF6 tower wall for mechanical support. The hoses hang down from the upper manifold, at the bottom they are guided in vertical rails which allow for movement. At the output of this section the high voltage bushings are mounted. They provide the interface for the connections to the neutral injector.
- the top lid (diam. 2.15m, height 1.6m).

The tests performed were:

- all electrical components were tested to 200kV DC for 15 min and to 260kV DC for 1 min in SF6 pressure of 1.7 bar gauge
- the total vessel was pressure tested at 4 bar gauge for 1.2 hour
- the isolation hoses are factory tested at 50 bar and site tested at 10 bar gauge.

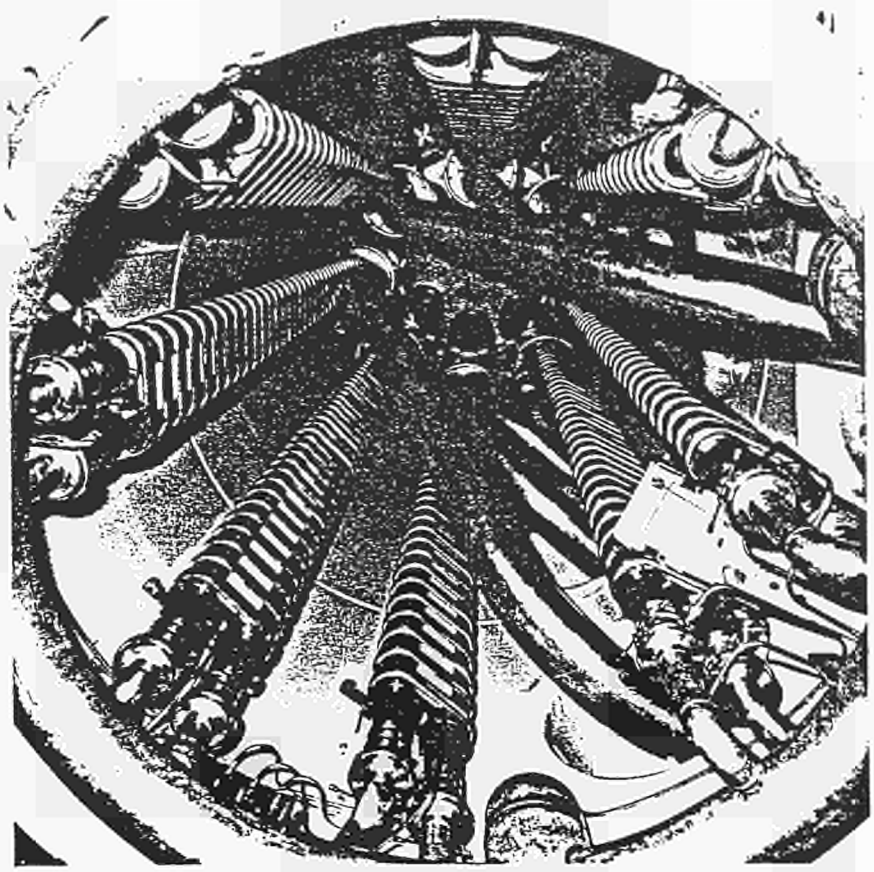

Photo 3: View inside the SF6 Tower: at the bottom, the snubbers; at the left, the connection to the output bushings; and hanging from the top manifold, the DC breaks surrounded by a stack of corona rings to shape the electrical field

6. CONCLUSIONS

The first neutral injection box has been in operation since early 1986, both in hydrogen and deuterium at 80kV. The power supplies will be converted for 160kV operation during 1987. No changes are required to the components described in this paper as the design, construction and all the tests performed during the commissioning were planned for 160kV operation. All tests on the second neutral injection box are completed. Operation is due to start in October 1986.

7. ACKNOWLEDGEMENTS

The authors would like to thank H Fielding for his contibution during the construction and the testing of the equipment, B Shaw for his help in the design of the SF6 Towers and H Altmann for the procurement and testing of the output bushing of the SF6 Towers.

8. REFERENCES

[1] P.L. Mondino and K.I. Selin, "JET ADDITIONAL HEATING POWER SUPPLY AND PROTECTIONS", Proceedings of 7th Symposium on Engineering Problems of Fusion Research, Knoxville, Oct. 1977, pp.1558-1563.

[2] R. Claesen et al., "COMMISSIONING AND EARLY OPERATION OF THE POWER SUPPLY AND PROTECTION SYSTEM FOR THE EXTRACTION GRID OF THE JET NEUTRAL INJECTORS", Proceedings of the 13th Symposium on Fusion Technology, Varese, Sept. 1984, pp.829-834.

[3] G.L. Basile et al, "THE NEUTRAL INJECTION AUXILIARY POWER SUPPLY SYSTEM IN JET: DESIGN, MANUFACTURE AND TESTS", Proceedings of 13th Symposium on Fusion Technology, Varese, Sept. 1984, pp.834-842.

[4] R. Claesen, P.L. Mondino, "NEUTRAL BEAM INJECTION AND RADIO FREQUENCY POWER SUPPLIES", to be published in Fusion Technology Journal, January 1987.

[5] P.L. Mondino et al, "DESIGN, COMMISSIONING AND EARLY OPERATION OF THE POWER SUPPLY AND PROTECTION SYSTEM FOR THE EXTRACTION GRID OF THE JET NEUTRAL INJECTORS AT 160kV", 14th SOFT, Avignon, 1986.

[6] H. Helgesen, "THE PERFORMANCE OF A STRIP WOUND IRON SNUBBER, AN ANALYTICAL APPROACH", JET Internal Report JDN/G/82/160, 1982.

[7] H. Helgesen, "SNUBBERS FOR THE PROTECTION OF THE NEUTRAL INJECTORS DESIGN STUDY", JET Internal Report JDN/G/81/152, 1981.

DESIGN, COMMISSIONING AND EARLY OPERATION OF THE POWER SUPPLY AND PROTECTION SYSTEM FOR THE EXTRACTION GRID OF THE JET NEUTRAL INJECTORS AT 160KV

P.L. Mondino, R. Claesen, J.A. Dobbing, P.A. Baigger*

JET Joint Undertaking, Abingdon, OXON OX14 3EA, UK
*Siemens, Erlangen, FRG

ABSTRACT

The paper describes the design concept, the commissioning and the early operation of the power supply and protection system for the extraction grid of the JET neutral injectors, to produce deuterium beams at 160kV. While the design concept was proposed in 1977, the detailed design was performed in 1982, commissioning took place in 1985 and operation, in a Testbed, started in 1986.

1. INTRODUCTION

Powerful neutral beams, able to penetrate dense plasma ($\sim 10^{20} m^{-3}$), and to deposit the energy in the central region of large machines, require a high voltage applied to the extraction grid of the accelerating structure of the injector. Hydrogen beams are used in Doublet III, JT60 and JET at 80kV. Deuterium beams are used in JET at 80kV, in TFTR at 120kV, and are planned for JET at 160kV during 1988.

Breakdown in the accelerating structure is part of the normal operation of the injectors. Therefore, fast protection systems are necessary, to turn-off the supply quickly (~10μs) and to reapply it shortly afterwards (~10ms), many times (~100) in a pulse. Tetrodes have been extensively used to perform this duty. Direct series connection of up to three tetrodes has been proposed [1]: it implies passive circuits, with resistors, capacitors and non-linear elements, carefully tuned to divide the voltage evenly, especially during the frequent turn-on and turn-off transients. To avoid these problems, a programme was set up in the USA with two leading tube manufacturers, to develop a tetrode [2] for the protection system of TFTR. The main specified parameters were: 200kV hold-off voltage, 65A nominal current, and 2MW anode dissipation. The same tube could not be used in JET because the higher voltage (160kV) foreseen across the accelerating structure of the injector required a power supply able to provide 200kV on load and 240kV at no load.

During the JET design phase, a novel circuit (shown in Fig.1) was proposed [3], in which clipping diodes are connected in parallel to the power supply and the tetrode. These elements constitute a unit, of which several units can be connected in series. The clipping diodes limit the voltage across the tetrodes to the related power supply value,

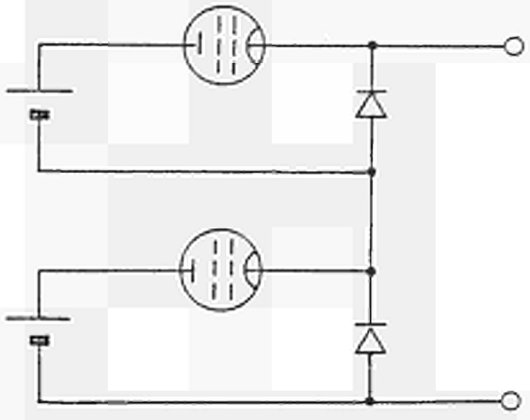

Fig.1. Principle of Series Connection.

in any operating conditions: steady state, turn-on and turn-off transients. The scheme was tested at the CEA Fontenay aux Roses Laboratory, France under a contract with JET. Two units were connected in series, the two tetrodes, made by different manufacturers, were used only as switches. With this limitation, the tests were successful [4] and the scheme was used for the development of the 160kV deuterium neutral beam injector for JET.

2. SIMILAR APPLICATION OF THE SAME DESIGN CONCEPT

A scheme, making use of the same concept (as underlined in Fig.1 for the series connection) was proposed two years ago for Textor [5]. As a series switch, several (~100) GTO are used; because of their low voltage capability the power supplies are divided into many small modules (~1kV). The output voltage can be kept constant (~±1%) varying the number of GTO that are fired. Moreover, if some redundancy is built in, a faulty power supply can be left out of operation, not firing the related GTO. It would be interesting to compare the JET and Textor schemes, for an application with many injectors (~20), working at high voltage (~160kV), taking into account technical aspects, including reliability, and cost implication.

3. DESIGN

In the JET design, two units are used, which are able to operate independently and in series. The tetrodes are used as fast switches and series regulators, to keep constant the output voltage, within a narrow range (±800V), and with large bandwidth (13kHz). The voltage drop across the tetrode (presettable) can be in the range 5-17kV, within the anode dissipation capability (1MW), at nominal current (60A). The nominal output parameters of one module (two units connected in series) are 160kV, 60A, for 20s pulse length every 10 minutes, to supply two injectors connected in parallel (160kV, 30A each). Nine modules are installed at JET: one to supply a Testbed and eight to supply sixteen beams of which eight are operational and eight are being installed.

The design has been carried out taking into account series operation: the insulation level of the two units is carefully graded and tested accordingly. The independent operation has been reported elsewhere: design aspects have been reviewed in [6], commissioning and early operation in [7]. This paper deals with the series operation only. Fig.2 shows the schematic of the series connection of the high voltage power supply and of the protection system. Only the key components are shown, which are essential for the analysis of the series operation. More detailed schematics are given in [6] with the basic design elements of each component.

The protection systems are installed as near as possible to the neutral beam injectors, outside the biological shield [8]. The high voltage power supply, installed outdoors, is connected to the protection system, with three coaxial cables (Z=50Ω) per

module, each ~200m long. The cable shields are connected to the common of unit 1. Therefore, the stray capacitances of unit 2 are: output cable ~20nF, common cable ~20nF, high voltage power supply ~10nf, and protection system ~1nF. These stray capacitances have to be charged and discharged, at turn-on and turn-off.

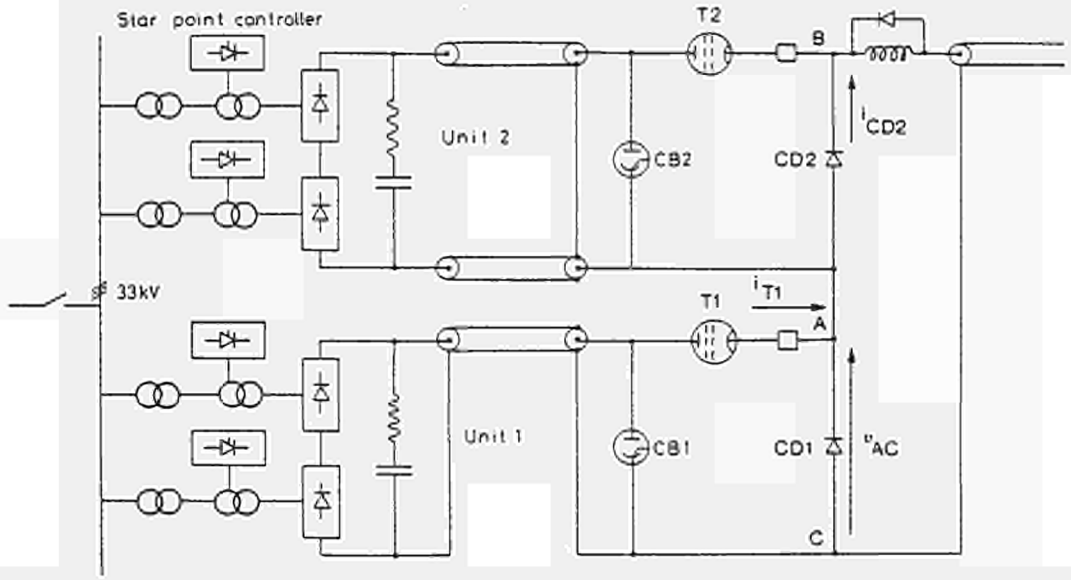

Fig.2. Series Connection of the High Voltage Power Supplies and of the Protection Systems able to produce at the output 160kV 60A.

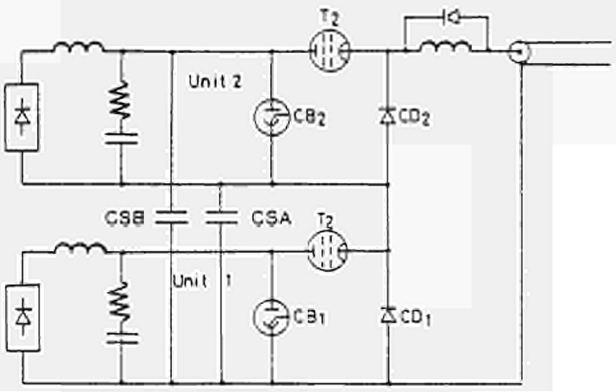

Fig.3. Equivalent Circuit.

At turn-on, the voltage rises, across the load, linearly. Therefore, the unit 1 tetrode must carry a constant current to charge the stray capacitances on the top of the rising load current. Since the nominal current of the tetrode is 80A and the nominal load current is 60A, 20A are available to charge the stray capacitance. The maximum voltage derivative and the minimum rise time (~150μs) are therefore fixed.

At turn-off, the stray capacitances have to be discharged, through the neutral injector. In case of breakdown in the accelerating structure, the peak current is limited, by transferring the unit 1 limiting inductor at unit 2 output. The unit 1 inductor is stacked on the top of unit 2 inductor: due to the effect of mutual coupling, the inductance is ~50mH, which is larger than the sum of each inductance considered separately (~20mH). Fig.3 shows the equivalent scheme of series connection.

4. SERIES OPERATION CONTROL SCHEME

The independent operation control scheme has been reported [7], where the computer architecture has also been described. When operating independently, the protection systems, and their associated high voltage power supply, are controlled by a

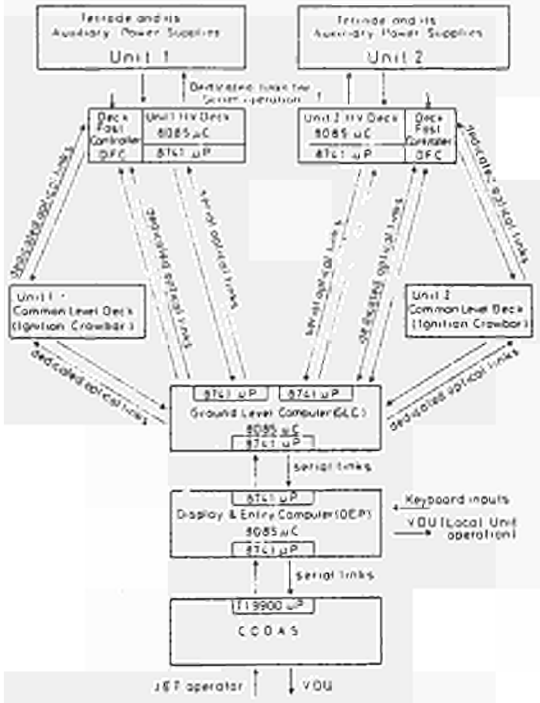

Fig 4. Computer Architecture.

state machine situated on each HV Deck. The state machines have a transition time of 0.5μs, to provide a fast interlock capability. In series operation, the state machines of the two units must act in a coordinated manner. To achieve this addition, fibre optic cables are used to transmit the state of unit 2 to unit 1 (see Fig.4). Unit 1 state machine is reprogrammed to follow the state of unit 2. This coordinates the normal operation of the two units and will turn off both units if unit 2 develops a fault. Conversely to turn off unit 2, if unit 1 develops a fault, two additional fibre optic links are required,. The first detects when unit 1 goes into its Emergency Off state (crowbar fired) and is transmitted directly to unit 2 to block the unit 2 tetrode. The second fibre optic signal blocks the timing signal to unit 2 if an interlock on unit 1 forces it back into the High Voltage Enable, Warm Up or Emergency Off states (see Fig.5).

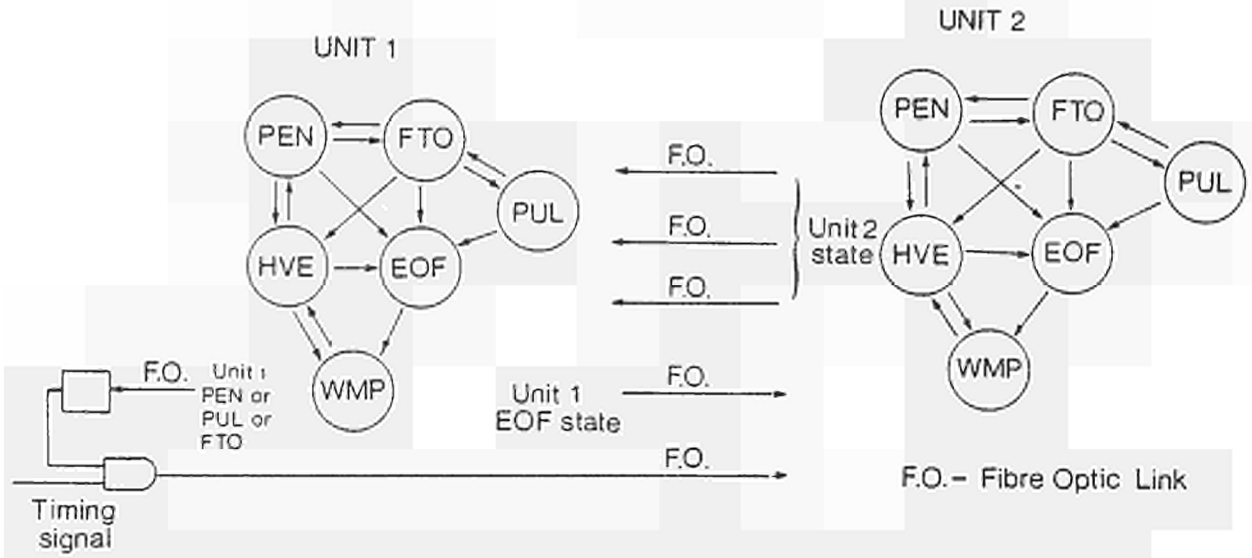

Fig.5. Interconnection of Unit 1 and Unit 2 State Machine for Series Operation.
WMP - Warm up; HVE - High Voltage Enable; PEN - Pulse Enable;
FTO - Fast Turn Off; PUL - Pulse; EOF - Emergency Off.

5. COMMISSIONING AND EARLY OPERATION

A series of commissioning tests were performed to check the operation of each part of the system, culminating in a full power test, with simulated breakdowns on a dummy load.

(a) Test 1. The correct operation of the control system was first checked by connecting the controls for series operation, while leaving the power circuits connected for independent operation to two dummy loads. In this way it was possible to check the synchronous operation of the two units, without the risk that faulty operation would cause damage.

(b) Test 2. The power circuits were next connected in series but with the filament of unit 2 tetrode disconnected, so that it could not produce an output pulse. The clipping diode of unit 2 was also short-circuited, so that unit 2 would float at the unit 1 output potential but remain inactive. The control loop of unit 1 tetrode was then stabilised by modifying the frequency compensation of its error amplifier to take account of stray capacitances in its load. Fig.6 shows the turn on transients. The voltage rise time has been increased to 500μs, because this is the value requested for the operation of the 160kV deuterium injectors. The current Output needed to charge the unit 2 stray capacitance has dropped to 8A from 20A foreseen during design. The first current threshold that detects breakdown in the accelerating structure has been increased to 80A and not inhibited during the turn on transient as foreseen during design.

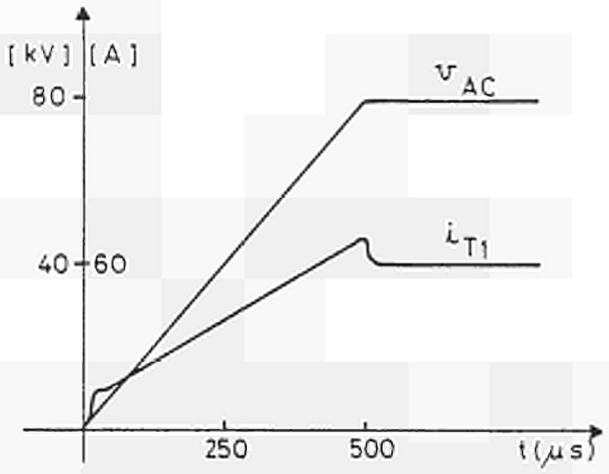

Fig.6. Test 2: Turn on Transient in in Unit 1 (Unit 2 floating): Voltage and Current.

(c) Test 3. With the same conditions as the previous test, the dummy load crowbar was fired, to investigate the discharge of the unit 2 stray capacitance. As foreseen during design, the unit 2 stray capacitance is discharged via the unit 2 clipping diode, limiting inductor and load. The current in the limiting inductor commutates to flow in its freewheeling diode when the stray capacitance voltage is approximately zero. Thus the full stray capacitance of unit 2 is discharged into the neutral injector grid. The current amplitude is limited by the limiting inductor that stores the majority of the energy . Nevertheless fault currents up to 125A for 70μs are produced from this source. A typical pulse termination is shown in Fig.7. It was also found that this discharge current would trigger the second current threshold that detects simultaneous breakdown in the accelerating structure and in the tetrode and fires the protection system crowbar. To overcome this problem, the clipping diodes were reconnected to the output side of the current monitoring shunt.

(d) Test 4. During this test, the firing of the protection system crowbars was investigated. The test conditions were the same as for the previous two tests, except that now the output voltage of unit 2 high voltage power supply was progressively increased, and the unit 2 crowbar, manually triggered, during an output pulse. It was found that, when the crowbar was fired, the positive output cable of unit 2 would pulse charge the common cable of unit 2, so that the output voltage as measured by unit 1

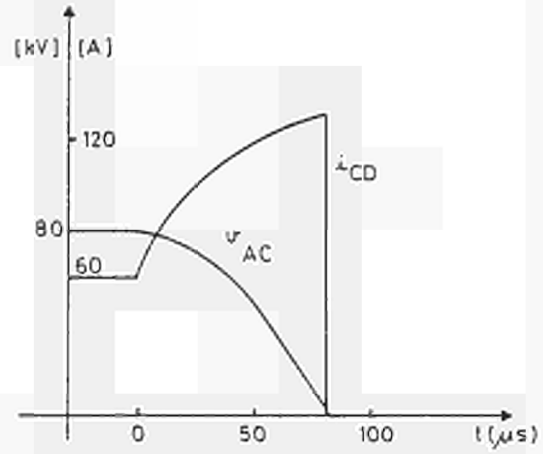

Fig.7. Test 3: Turn off Transients Unit 1 (Unit 2 floating): Output Voltage and Current.

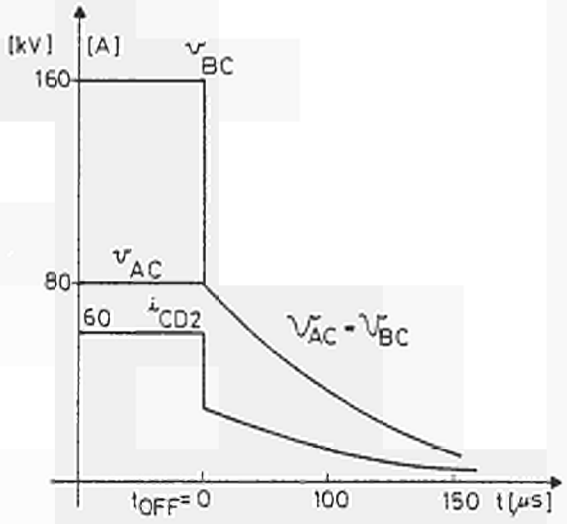

Fig.8. Test 5: Turn off Transients in Units 1 and 2: Output Voltages and Current.

potential divider, was as high as 130kV. According to the design, the two crowbars were fired together so that the 130kV impulse appeared across unit 1 tetrode. To reduce the probability of unit 1 tetrode flashing-over, under these conditions, the firing of the two crowbars was decoupled. This still provides adequate protection for the system, as the relevant crowbar will be fired, if either tetrode flashes-over.

(e) Test 5. With all the modifications identified in the previous tests implemented, the two units were operated in series onto the dummy load. No unexpected results were obtained, except for a small ripple current observed on unit 1 current shunt. This was identified as being due to the capacitance current flowing in unit 2 output cable to ground, then back through unit 1 high voltage power supply and unit 1 protection system to unit 2 common. The turn on transients are as shown in Fig.6. Fig.8 shows the turn off transients: the output voltage drops to 80kV, after tetrode turn off, the load current drops to 30A and consequently the limiting inductor current starts free-wheeling, then unit 2 stray capacitances discharge on the load resistor.

(f) Test 6. Test 5 was repeated while repetitively firing the dummy load crowbar, at 100ms intervals. Some interference problems were initially encountered, that prematurely terminated the pulse and, in some cases, fired one or other of the crowbars. These difficulties were overcome by filtering the inputs to the state machines.

(g) Early Operation. The module that serves the neutral injector Testbed has also been converted to series operation and one neutral injector operated at 160kV, 40A, without the need for further modifications to the protection system or the high voltage power supply.

6. CONCLUSIONS

The commissioning programme was successfully concluded, with full power operation and simulated breakdowns, on the dummy load. The operation, in a Testbed, with a deuterium injector has also been successful. Still the full system foreseen for parallel operation of two deuterium injectors at 160kV in JET [9] has not yet been tested: it

requires the blocking diodes to decouple the two loads, the transmission lines and the snubbers. These integrated tests will be performed after the installation of the 160kV deuterium injectors in the first neutral beam box foreseen for the 1988 shutdown.

Since the concept of series connection, proposed in 1977, has proven successful, its application to three or more units in series can be considered for protection of neutral beam injectors working with voltages even higher to penetrate dense plasmas in future larger machines.

7. ACKNOWLEDGEMENTS

The authors would like to thank E.Bertolini for his technical and managerial supervision; D.Ciscato and B.Tournesac for many useful discussions during design; and H.Arslin (formerly RPC Industries, S.Mateo, USA) for the system analysis performed during design.

8. REFERENCES

[1] Barber, G.C. et al, "THE DEVELOPMENT AND USE OF 60kV, 80kV and 150kV FLOATING DECK MODULATORS FOR HIGH VOLTAGE PROTECTION OF MULTIMEGAWATT ION BEAM ACCELERATORS", Proceedings of the 7th Symposium on Engineering Problems of Fusion Research, pp.1564-1566, Knoxville, (Oct.1977).

[2] Deitz, A. et al, "HV SWITCH TUBE DEVELOPMENT PROGRAMME FOR TFTR", Proceedings of the 7th Symposium on Engineering Problems of Fusion Research, pp.1440-1444, Knoxville, (Oct.1977)

[3] Mondino, P.L., Selin, K.I., "JET ADDITIONAL HEATING POWER SUPPLY AND PROTECTIONS", Proceedings of the 7th Symposium on Engineering Problems of Fusion Research, pp.1558-1563, Knoxville, (Oct.1977).

[4] Desmons, M. et al, "A PROTECTION SYSTEM FOR NEUTRAL INJECTORS WORKING IN THE 120-160kV RANGE", Proceedings of the 8th Symposium on Engineering Problems of Fusion Research, pp.1034-1037, San Francisco, (Nov.1979).

[5] Schwarz, U. et al, "THE HIGH VOLTAGE POWER SUPPLY FOR THE ACCELERATION GRIDS OF THE TEXTOR NEUTRAL INJECTORS", Proceedings of 13th Symposium on Fusion Technology, pp.823-828, Varese, (Sept.1984).

[6] Aslin, H. et al, "THE POWER SUPPLY AND PROTECTION SYSTEM FOR THE EXTRACTION GRID OF THE JET NEUTRAL INJECTORS", Proceedings of the 12th Symposium on Fusion Technology, pp.391-397, Jùlich, (Sept.1982).

[7] Claesen, R. et al, "COMMISSIONING AND EARLY OPERATION OF THE POWER SUPPLY AND PROTECTION SYSTEM FOR THE EXTRACTION GRID OF THE JET NEUTRAL INJECTORS", Proceedings of the 13th Symposium on Fusion Technology, pp.829-834, Varese, (Sept.1984).

[8] Claesen R. et al, "THE JET NEUTRAL INJECTION 160kV TRANSMISSION LINES, THE ASSSOCIATED SNUBBERS AND THE SF6 TOWER FOR THE TERMINATION OF THE TRANSMISSION LINES HOUSING OF THE SNUBBERS AND VOLTAGE BREAKS", Proceedings of the 14th SOFT, Avignon, (Sept.1986).

[9] Claesen, R., Mondino, P.L., NEUTRAL BEAM INJECTION AND RADIO FREQUENCY POWER SUPPLIES", to be published in "Fusion Technology Journal", (January 1987).

THE JET MAGNETS: OPERATIONAL EXPERIENCE AND PLANS FOR UPGRADE.

J.R. Last, D Cacaut, J W Zwart.
JET Joint Undertaking, Abingdon, Oxfordshire, UK.

ABSTRACT

The paper describes the successful operation of the JET toroidal and poloidal magnets and also plans for upgrading the performance of the magnet system for higher plasma current.

1. DESCRIPTION

Fig 1 shows a cross section through the JET machine in which the toroidal and poloidal coil system [1] can be seen.

The toroidal field (TF) comprises 32 D-shaped coils designed to produce a field of 3.45 T at 2.9m radius. The coils are conventional water-cooled, epoxy glass insulated copper coils. The main parameters of the coil system are shown in Table 1. The inward forces of the toroidal coils are supported by poloidal coil 1 and the out of plane forces by a shell type mechanical structure and fluted cylinder at the toroidal/ poloidal coil interface.

Table I: Parameters of the toroidal field coil system

(data are given for maximum performance)

Number of coils:	32
Total number of ampere turns:	51MA
Magnetic field at 2.9m radius:	3.45T
Current:	67kA
Flat top time of pulse:	10s
Effective pulse length:	20s
Resistive power:	280MW
Energy dissipated per pulse:	5.6GJ
Dimensions of one coil (vert/hor):	5.68/3.86m
Weight of one coil:	12 tonnes
Number of turns per coil:	24
Copper cross-section per turn	3900/2700mm²
Centering force per coil:	18MN
Maximum temperature rise of copper:	60°C

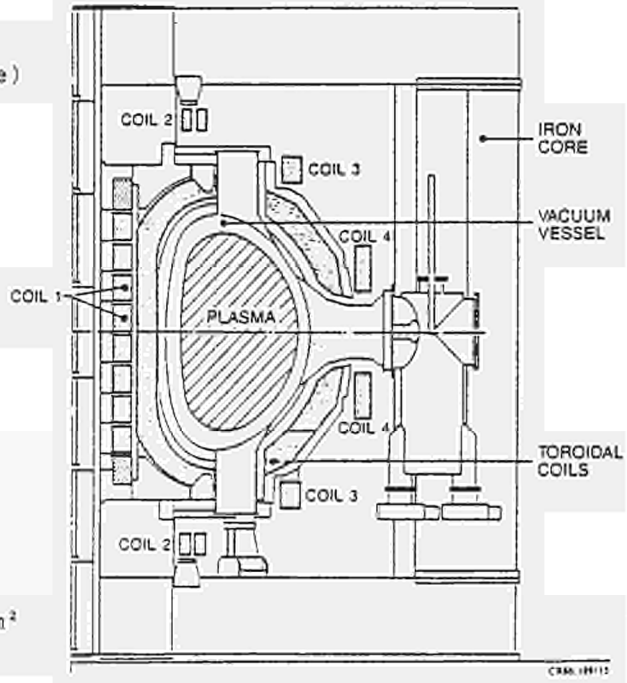

Fig.1 Cross Section through JET machine

The poloidal coils (coil 1, 2, 3 and 4 on fig 1) are also of water cooled, epoxy glass insulated copper. The inner coil (coil 1) carries magnetising currents and the flux of this coil passes mainly through the transformer core. Coils 2 and 3 carry shaping and radial field currents and coil 4 carries vertical field currents. Coil 3 also was a few turns in series with coil 1 to control the magnetising field at breakdown. The main parameters of these coils are given in Table II.

Table II: Main parameters of poloidal field coils

Coil type number	1	2		3			4
Field type	Mag.	Shaping	Radial	Mag.	Shaping	Radial	Vert.
Number of coils	8	2			2		2
Weight (all coils tonnes)	90	28			84		158
Outer diameter (m)	2.17	4.84			8.37		10.91
Conductor size (mm^2)	54x39.5	82x35	35x35	82x35	35x35	35x35	82x35
No. of turns all coils	568	40	32	20	120	40	122
Maximum current (kA)	40	45	20	40	20	20	45

2. OPERATION

2.1 Performance

JET Started operating in June '83 and the coils have operated without faults since then.

The toroidal field coils have operated routinely at full design performance - 3.45 Tesla and 20 seconds effective pulse length (see Table I).

The poloidal magnetising coil (No. 1) has operated at full design current (40kA) in the flat top phase but it has only been possible to use 30kA in the premagnetisation phase due to stray fields making plasma breakdown difficult.

The outer poloidal coils have operated at up to 35kA (i.e. less than design current). This is sufficient to enable the design plasma current to be exceeded. Higher currents will only be needed if the plasma pressure or current are increased.

The poloidal coils have operated at lower voltage than the maximum design voltage (30 volts/turn at breakdown instead of 100v/t) because a low rate of rise of plasma current has been found preferable for stability.

2.2 Measurements

More than 450 channels of magnet system data are measured including mechanical (displacement, strain and crack detection), electrical (voltage, current and magnetic flux) and thermal (cooling water and insulation temperatures) parameters [2]. Signals are fed from the transducers to the data acquisition system (CODAS) via signal conditioning equipment, analogue to digital convertors and an optical link. Data is taken during the JET pulse and permanently stored in the computer. It can be recovered and processed at any time. Alarms and displays are generated by real time software.

Fig 2 shows some typical measurements for a normal and a disrupted pulse. It will be seen that the maximum stress in the mechanical structure is doubled during a disruption. The measured torque on the toroidal coils has a similar behaviour.

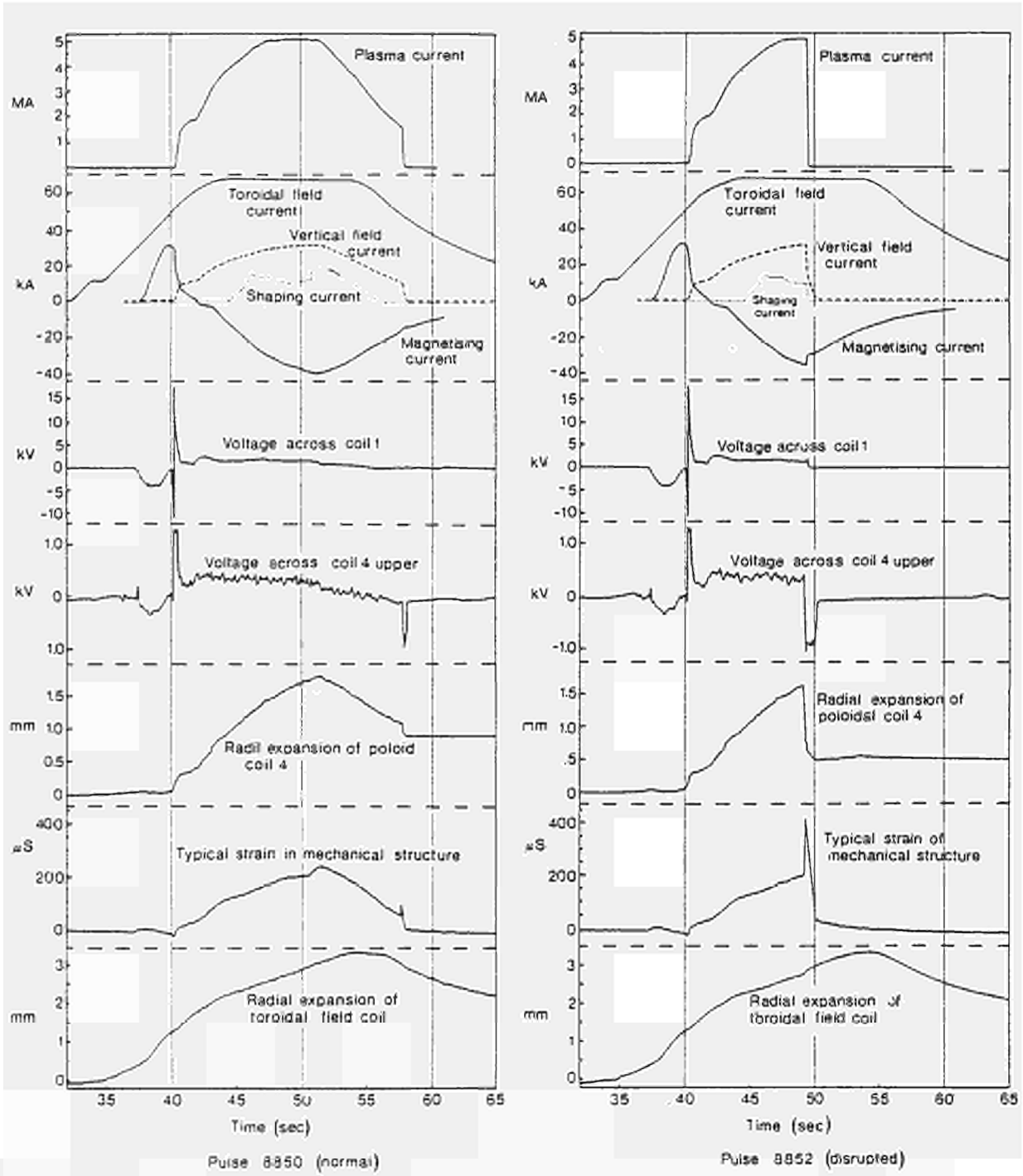

Fig. 2: Typical measurements for normal and disrupted pulses.

3. MODIFICATIONS

3.1 Poloidal circuits

Fig. 3 shows the original connection scheme for the coils. A disadvantage of this circuit was that it was only possible to change the plasma shape by altering the number of turns on coils 2 and 3. This could only be done by closing the machine down. As the elongation of the plasma could not be controlled during a pulse, problems of vertical instability were experienced. Another disadvantage was the parallel connection of coil 1. This was originally designed for high voltages per turn but, as these were not required, merely gave the disadvantage of high currents in the OH power supply.

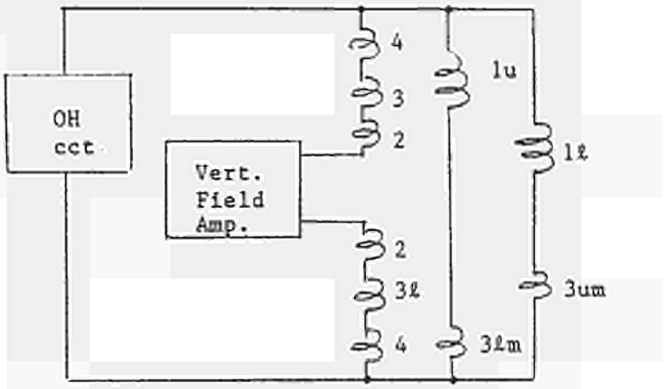

Fig. 3: 1983 p.f. circuit

Fig 4 shows the circuit which was implemented in 1985. This halved the power supply currents for coil 1 and thus increased operating margins to allow other developments and also gave independent control of the plasma position and elongation. To make these circuit changes new busbars had to be ordered and installed.

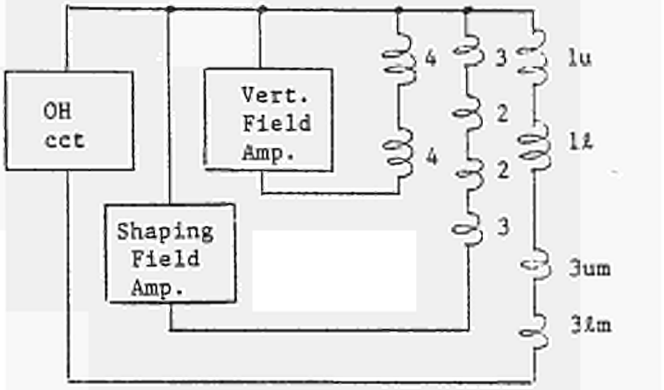

Fig. 4: 1985 p.f. circuit

Fig 5 shows the coil connection arrangement which will be installed in early 1987. The three basic poloidal circuits will be galvanically separated (The radial field circuit is already separated and is not shown). The advantages of this new arrangement will be:

a) less coupling between circuits because lower and symmetric voltages on outer coils will reduce capacitive coupling and ohmic coupling will be eliminated,

b) easier testing and debugging of coils, which will be especially valuable in the remote handling phase.

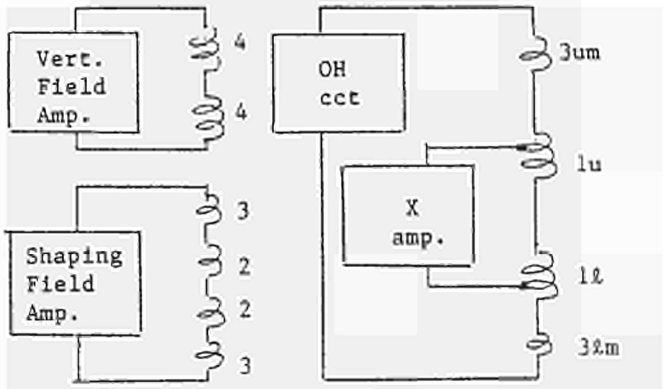

Fig. 5: 1987 p.f. circuit

Also shown in fig 5 are extra tapping points on coil 1. These will enable the end coils of the stack to be fed at a different different current level to the centre set. This will be advantageous in controlling plasma breakdown fields and X-point plasmas.

3.2 Poloidal coil 1

As mentioned in section 2.1 it has not been possible to use full premagnetisation current in coil 1 because stray fields make plasma breakdown difficult. Stray fields will be reduced by replacing 2 dummy coils (pieces of laminated iron in the shape of coils) by

real coils. Thus the coil 1 stack will be 10 coils instead of 8. If the stray fields are not sufficiently reduced by the above it will be possible to change the current distribution in the coil 1 stack using the new tappings shown in fig 5 which should make further improvements. Fig 6 shows the computed effect of these changes.

To make the above changes involves major dismantling and assembly operations on the JET machine. The following major items will have to be removed - cooling water and vacuum rings, 7 central core sections, 8 upper transformer limbs, poloidal coil 2, upper centre piece and coil 1 stack. The stack will be rebuilt and aligned with 10 coils in the JET assembly hall. Meanwhile in the torus hall the base for the rebuilt stack will be aligned. The 10 coil stack will then be transferred to the torus and the machine reassembled. This work will be completed in early 1987.

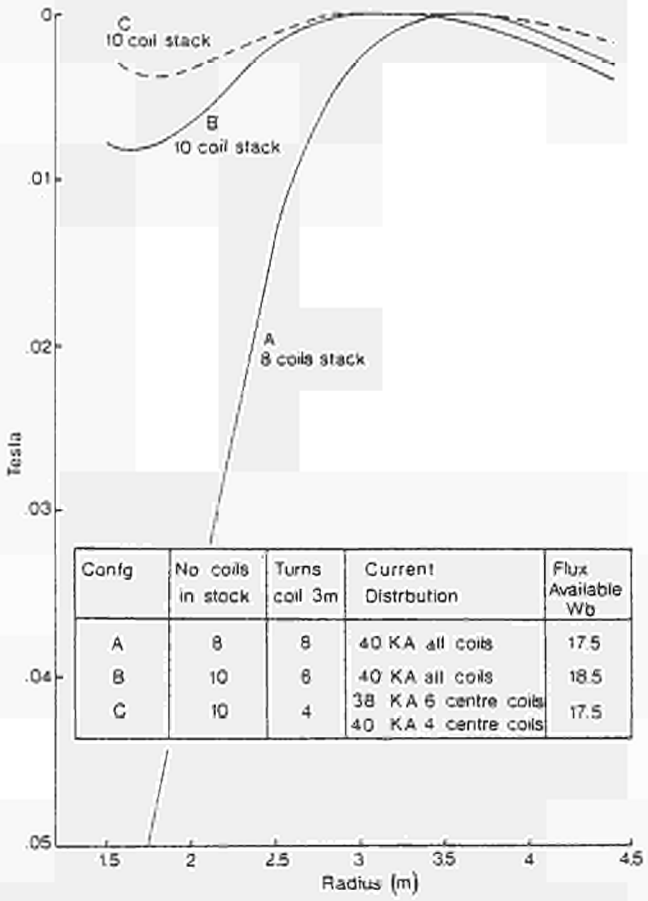

Config	No coils in stack	Turns coil 3m	Current Distrbution	Flux Available Wb
A	8	8	40 KA all coils	17.5
B	10	6	40 KA all coils	18.5
C	10	4	38 KA 6 centre coils 40 KA 4 centre coils	17.5

Fig.6: Stray field at breakdown (Bz vs radius) for 8 and 10 coil magnetising stack

3.3 Other changes

The following changes will also be made in early 1987:

a) Chillers will be installed in the toroidal coil cooling circuit. This will reduce the initial water temperature from 20°C (nominal) to 7°C and enable pulse lengths at maximum current to be extended by about 6.5 sec.

b) The available turns in the poloidal coil 2 shaping circuit will be increased from 40 to 56 by connecting spare pancakes.

c) The supports of poloidal coil 4 will be strengthened to withstand forces during vertical disruptions.

4. UPGRADE

The coil system is being studied to see how the plasma performance can be increased with the following targets:

i) plasma current 7MA in limiter configuration,

ii) plasma current 4MA in 'X-point' configuration

As the toroidal field is believed to be sufficient for a 7MA plasma the main points to be studied are:

i) increased flux swing from poloidal coil 1,

ii) effect of increased poloidal fields on toroidal coils.

iii) required currents and associated forces in outer poloidal coils.

The last point is not expected to be a problem as the coil ampere turns will probably not exceed the design values as the plasma pressure will be less than originally foreseen.

The usable flux swing from poloidal coil 1 is at present 30 Webers. This will be increased to the design value of 34 Webers by the modifications described in 3.2. To further increase the flux swing it will be necessary to increase the coil current above the design value.

This increase may be possible in the 6 centre coils of the stack during the plasma current flat-top because:

i) stray field will not significantly affect the plasma shape and,

ii) the 6 centre coils are pressed inwards by the toroidal coils.

The inward pressure of the toroidal coils at full current is 30MPa. The outward pressure on poloidal coil 1 due to its own field is about 14MPa. Thus if the poloidal field (and current) are increased by about 50% the inward and outward pressures are balanced. This suggests that the coil current can be increased but details such as forces on connections and thermal stresses have to be checked.

The increased plasma current and X-point plasmas with strong shaping fields cause increased poloidal field crossing the toroidal coils and therefore increased out of plane forces. This should not cause problems in the outer shell or inner cylinder regions where the coils are well supported but may cause problems in the collar region where the coils are only intermittently supported by teeth.

To investigate these problems the study program will contain the following elements:

i) development of new finite element models of toroidal coils and poloidal coil 1,

ii) investigation of all electromechanical and thermal stresses using the above models,

iii) analysis of machine data already collected to validate calculations and also for extrapolation to higher performance,

iv) tests to increase information available on properties of material (such as epoxy glass insulation) and components (such as prototype t.f. coil),

v) check on operating conditions of other p.f. coils and of mechanical structure.

5. CONCLUSIONS

The JET magnets have operated at their full design stress level. Full design flux swing plus increased flexibility of the poloidal system should be available in early 1987. The extent to which the coil system is capable of upgraded performance should be identified by mid 1987.

6. REFERENCES

[1] LAST, J.R.: THE TOROIDAL AND POLOIDAL COIL SYSTEMS OF JET, Proc. Inst. Mech. Engrs, Vol.20, No A2, 1986

[2] ZWART, J.W.; KEANE, D.V.; THOMSEN, F.; LAST, J.R.: JET MAGNET COIL INSTRUMENTATION, Symposium on Fusion Technology, Varese, Sept. 1984.

THE HIGH VOLTAGE GRID INTERFACE IN PRESENT AND FUTURE JET OPERATIONAL REQUIREMENTS

K.I.Selin(1), D.Ciscato(2), V.Marchese(1), P.Ashmole(3), B.Jervis(3)

1) JET Joint Undertaking, Abingdon, Oxfordshire, UK.
2) Padova University, Italy
3) Central Electricity Generating Board, London EC1A 7AX, UK

ABSTRACT

A number of limitations surround the JET pulse load and its impact upon the high voltage network in order not to decrease quality and reliability of the electrical supply to other consumers. According to the present agreement with the Central Electricity Generating Board (CEGB) tne active and reactive power swing at the 400kV point of supply should not exceed 575MW and 375MVAr. The voltage drop should be less than 1.5% and the rise and decay of JET load should not exceed 200MW/s. There are also limitations in load power steps the purpose being to protect components of the CEGB power system.

The paper presents two simulated JET scenarios in which the plasma current is Ip=5MA and the additional heating power to the plasma is 25MW. The pulse termination is either normal or abnormal (plasma disruption). In the first case a reactive power compensation of 130MVAr is needed in order to comply with the limits on voltage drop. In case of plasma disruption an active power compensation of 150MW is needed in addition in order that the combined JET load may remain within the present limits of active power step, reactive power swing and voltage drop.

1. INTRODUCTION

Since JET started operation, in June 1983, the level of electric power drawn from tne Central Electricity Generating Board (CEGB) 400kV grid has been growing as increased use has been made of the capacity of the JET power convertors and additional JET loads been put into operation. A point has now been reached at which some measures have to be considered in order to comply with the limits set out in the present agreement with CEGB. This is further emphasised oy the long term plans [1] of JET operation employing even more power supplies thereby increasing the need for the implementation of power compensation .

The paper describes the study of a JET load in 1987 at a plasma current of 5MA, with normal and abnormal termination (plasma disruption), performed via an ad hoc computer model, to determine the degree of power compensation required to stay within present limits. The model has been tested against experimental data from a 1986 JET pulse.

Table I: CEGB Power System and JET load constraints at the 400kV point of connection.

Parameters	Unit	Value
Max. Gen. capacity	GW	52
Kin. energy in system	GJ	150
System X/R ratio	--	10-20
Fault level Scc	GVA	15-35
Maximum voltage drop	%	1.0(step)
" " " Vd	%	1.5(over 1s)
Min. frequency level	Hz	49.75
Maximum active power P	MW	575
Maximum pulse length	s	60
Pulse interval	s	≥600(P>300MW)
" "	s	≥300(P<300MW)
Maximum pulse energy	GJ	15
Reactive power swing Q	MVAr	≤375(at 25GVA)
RSS of volt. harmonics	%	≤ 1.5
Active power		
i) increase to 575MW	s	≥ 6
ii) increase by 200MW	s	≥ 1
iii) decrease	MW/s	≤ 200
Power step	MW	50(≤ 20GVA)
" "	MW	75(≤ 30GVA)
Power ramp	MW	100(in 0.15s)
Occasional power steps	MW	100(140/year)
" " "	MW	150(27/year)
" " "	MW	200(12/year)
Load without pulse restrictions	MW	≤ 120

2. 400kV GRID

JET is supplied at 400kV from the CEGB power system incorporating 79 power stations with a maximum declared capability of 52GW.

Table I shows some parameters of the 400kV supply system and the JET load limitations to avoid undue interference with generation and other consumers.

During a JET pulse the reactive load change should not exceed 375MVAR and should be proportionately less for fault levels (Scc) below 25GVA.

The limitation to load power steps is based on a need to ensure that the JET load will not impose undue electromechanical stresses on the Didcot generating plant less than 5km from the JET site. For a typical CEGB load flow condition, a 50MW JET load step will cause a shock load to a generator, which is less than 2% of its rating.

The maximum active power is limited by the influence which the JET load can have on the system frequency. Studies have shown that a JET load of 575MW is not expected to cause an unacceptable decrease in the level of frequency during normal operating conditions of the supply system.

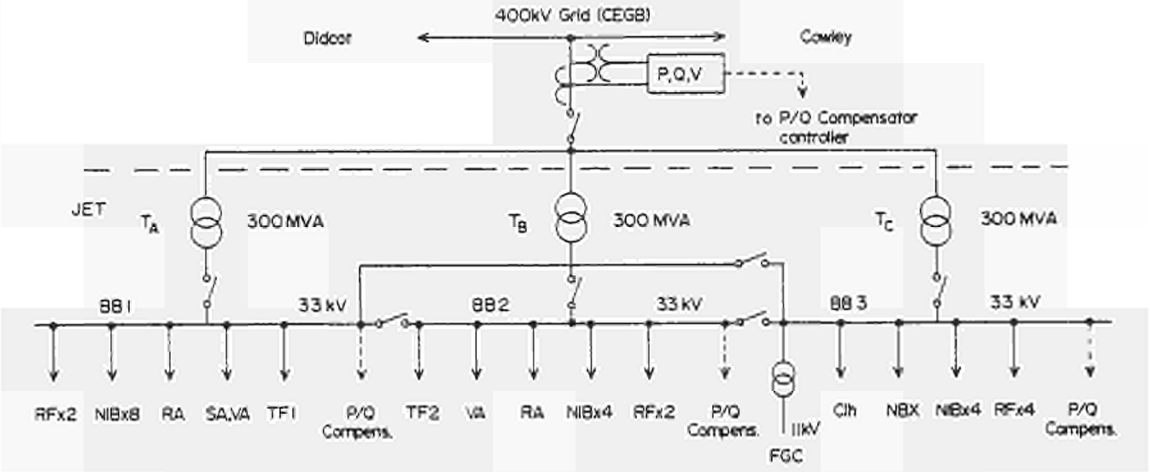

Fig. 1 SINGLE LINE DIAGRAM OF JET PULSED POWER SUPPLIES

3. JET Pulsed Power Supplies Model (PPSM)

Figure 1 shows the AC pulsed power distribution to various JET loads. Most JET loads are AC/DC convertors. Their ratings can be found in [2, 3]. Two thyristor convertor units (TF1 and TF2) in series with one Flywheel Generator Convertor (FGC) constitute the power supply for the toroidal field (TF) coils. A second FGC is used to supply the poloidal field (PF) coils. Radial, shaping and vertical field coils are fed from the radial, shaping and vertical field amplifiers (RA, SA, VA). The Additional Heating (AH) power supplies feed 16 Neutral Beam Injectors (NBI) and 8 Radio Frequency (RF) Generators.

The 400kV supply point is assumed equivalent with a generator of an impedance determined by the system fault level . The voltage drop will be less than computed by the model on account of generator AVR-action. On the other hand is the fault level used in the scenarios 22.5GVA and not the minimum (15GVA).

A P/Q compensator comprising a controllable resistor and capacitor is connected to each 33kV busbar through a 50MVA transformer (X=15% and R=1%). Error signals are derived from the 400kV active power (P), reactive power (Q) and voltage (V) to control the compensators.

The model has been tested against experimental data (JET pulse 5496 of 12.06.1986 at Ip=4MA) [4]. The discrepancy between model and experiment is less than 1% (see fig. 2).

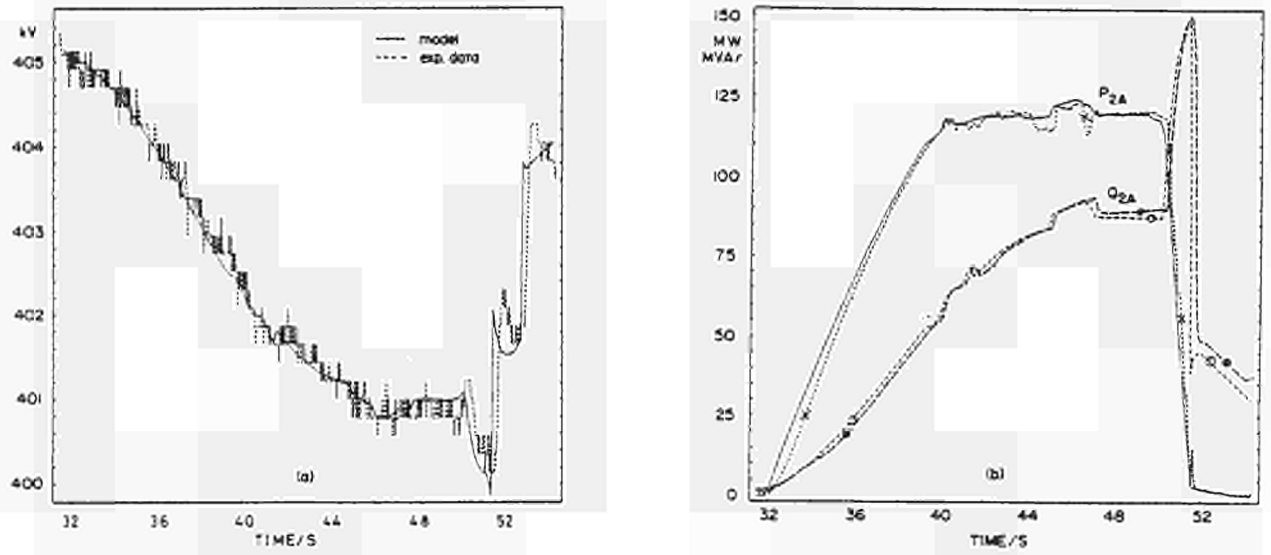

Fig 2. COMPUTER MODEL OUTPUT COMPARED WITH THE EXPERIMENTAL DATA OF JET PULSE 5496.
a. VOLTAGE AT POINT OF CONNECTION
b. ACTIVE AND REACTIVE POWER SUPPLIED BY TRANSFORMER T_A IN FIG. 1.

4. PULSE SCENARIO AND SIMULATION RESULTS

The reference pulse was simulated on the model using the following parameters of the supply system: Scc=22.5GVA, X/R=15. A compensator pulse rated 50MW/MVAr is assumed to be connected to each 33kV busbar and hence the overall installed rating is 150MW/MVAr. Table II lists the JET loads during the flat-top period of the 5MA plasma current pulse, which might

be a typical pulse in 1987.

The plasma current (Ip) is initiated already during the rise of the TF current (It) in order to increase the duration of the plasma flat top time. The shaping current Is is assumed proportional to Ip, for example Is=0.006Ip at plasma elongation e=1.7.

The equilibrium current,

$$Iv(t) = \frac{0.226}{nv} \left[2 + \beta p(t)\right] \cdot Ip(t), \qquad (3)$$

where nv=122 is the number of turns of the vertical field coils and the beta poloidal βp is updated as follows:

$$\beta p(t) = \beta po + \Delta\beta p(t)$$

$$\tau e \cdot \dot{\Delta\beta p}(t) + \Delta\beta p(t) = Kd \cdot Padd(t), \qquad (4)$$

Table II: JET Loads for Ip = 5MA

Load	Description	Value
TFi	TF Static Units(i=1,2)	2x(67kA,1.6kV)
NBI	Neut. Beam Injector PS	16x(60A,92kV)
RF	Radio Frequency PS	8x(400A,22kV)
VA	Vert. Field Amplifiers (prior to AH)	2x(20kA,310V)
RA	Rad. Field Amplifiers	2x(1kA, 15V)
SA	Shaping Amp. (e=1.7)	(30kA,260V)
Clh	Culham Labs. (const)	10MW, 7MVAr
NBX	Neut. Beam Aux.(const)	10MW, 3MVAr
FGC	PF and TF FGCs:	
	Pony Motors (const)	1MW, 14MVAr
	Exciters (pulsed)	1.5MW, 8MVAr

Padd is the additional heating power into the plasma computed from the DC power assuming an efficiency of 11.3% for NBI and 21.3% for RF and Δβp(0) = 0, βpo=0.2, τe=0.5s, Kd=.8/25 (1/MW). Vertical and shaping field voltages (Vv, Vs) are derived from the circuit equations of the relevant coils, taking into account the coupling with the plasma and other poloidal field coils.

Figure 3 shows the results of the simulation with normal plasma termination. It can be deduced from fig.3f that a capacitive reactive power compensation of 0.86·150=130MVAr is required in order not to exceed the contractual voltage drop at the 400kV point of connection. No P-compensation is required in this scenario.

Figure 4 shows the result of the simulation of the reference pulse , when it is terminated through a plasma disruption during 100ms. The AH power supplies are ramped down during the same time. TF1 and TF2 are ramped down in 2s simulating a simultaneous emergency shutdown. During a disruption the VA and SA voltages invert causing the power flow of these amplifiers to reverse and a high negative power step would be generated were a P-compensator not included (assumed rating Pcn).

With Pcn = 150MW the active power step is limited to about 65MW. Following the disruption the resistors of the P-compensator are switched off linearly in 2s (see Fig. 4d) and

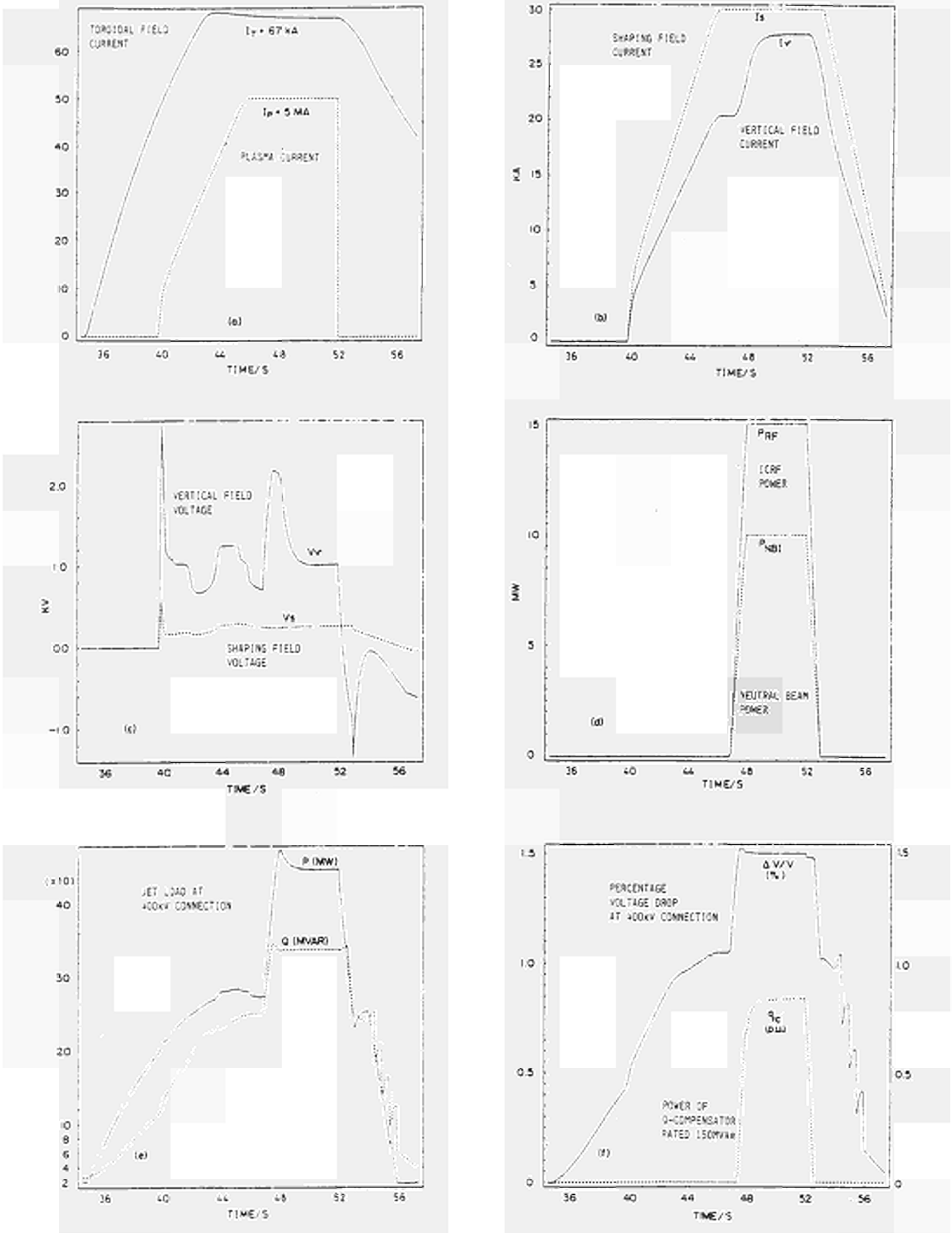

Fig. 3 STUDY OF PLASMA PULSE OF 5MA TERMINATED IN A NORMAL WAY

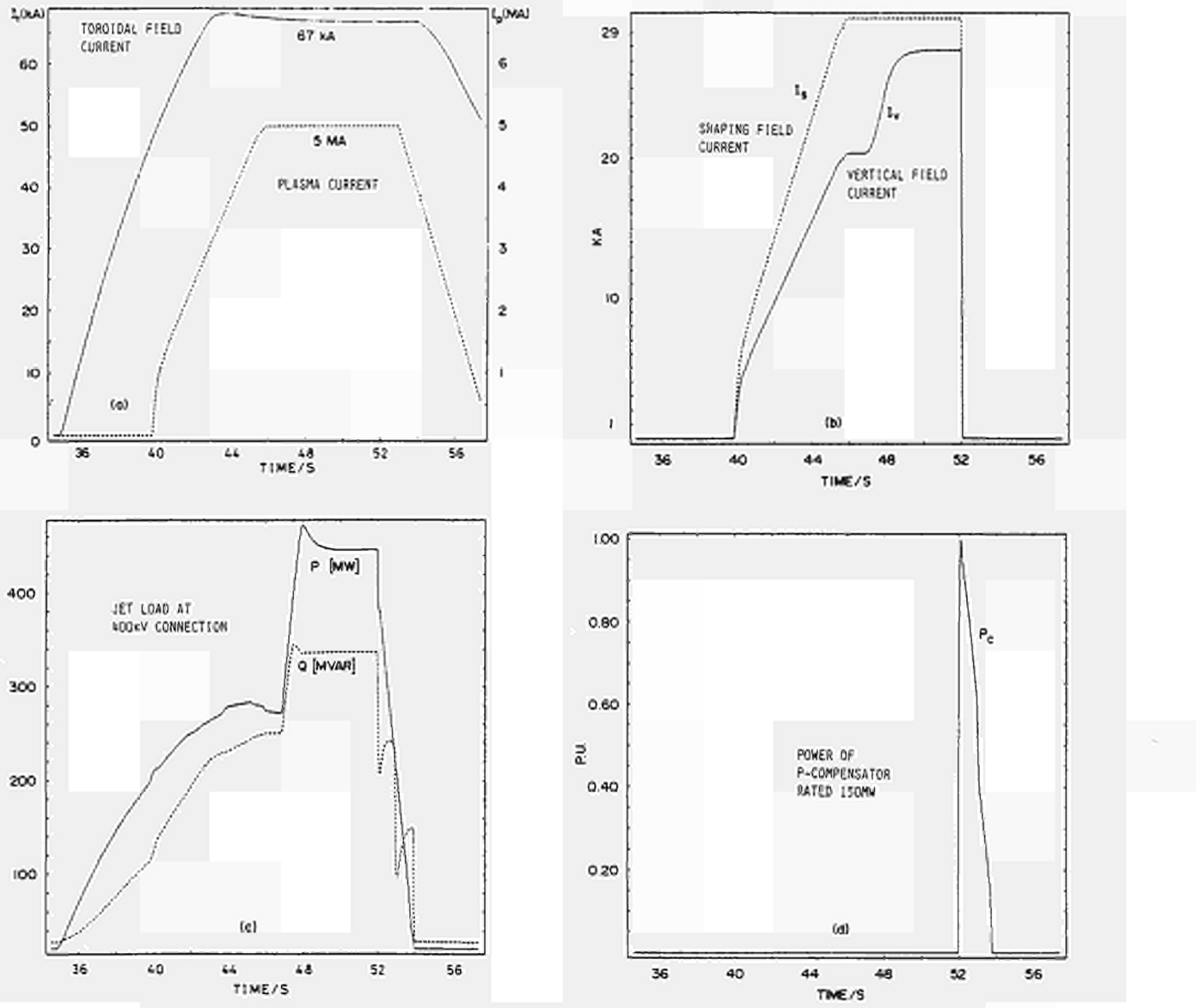

Fig. 4 STUDY OF 5MA PULSE TERMINATED THROUGH PLASMA DISRUPTION

consequently an energy capability of 150MJ would be sufficient for the P-compensator. The compensators will be supplied through a common transformer per busbar, see fig.1. As P- and Q-compensation is not needed at the same time (see fig.3f and 4d) each 33kV transformer may be rated 50MVA for 15-20s every 10 minutes.

5. P/Q COMPENSATION

The design of P/Q compensation is not finalised and several alternatives are considered with the aim to reduce its cost. For example, the tertiary windings of JET main 400/33kV transformers may be used for supplying the P/Q-compensators at 11kV instead of at 33kV.

Figure 5 shows two possible single-line schematics for the Q-compensator. The Thyristor Switched Capacitor (TSC) is expected to give a satisfactory performance if only the voltage drop during a pulse need to be compensated. The Thyristor Controlled Reactor (TCR) with fixed shunt capacitors on the other hand would be preferable in case there is also a lamp

flicker problem present.

The P-compensator of each busbar can be made up of modules of the type shown in Fig.6. and its control can either be made continuous (phase control) or stepwise (switched control). The first one is preferred provided the associated harmonics are acceptable during the short duty period coinciding with other loads being switched off.

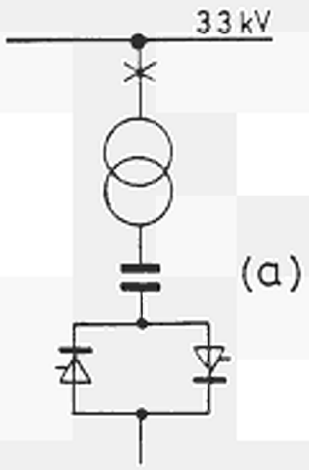

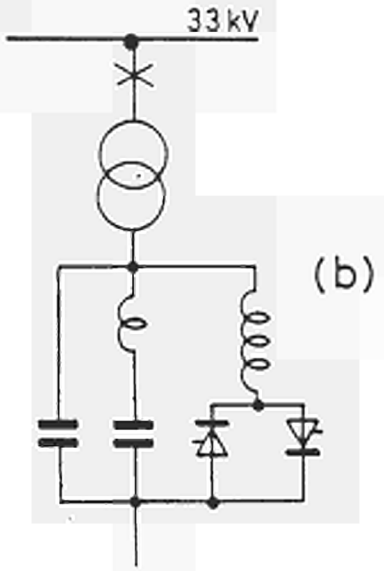

Fig. 5. SINGLE LINE DIAGRAM OF Q-COMPENSATOR
a. THYRISTOR-SWITCHED CAPACITOR
b. THYRISTOR-CONTROLLED REACTOR

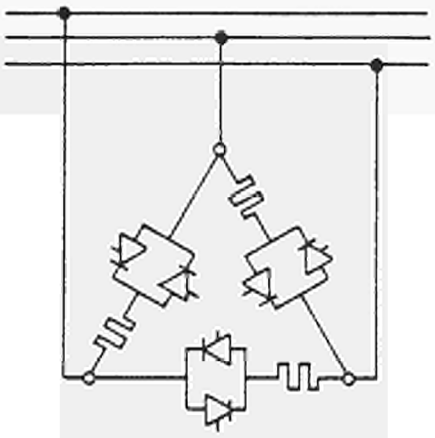

Fig. 6: 3-PHASE P-COMPENSATOR WITH THYRISTOR CONTROLLED RESISTORS

The P-compensator of each busbar can be made up of modules of the type shown in Fig 6 and its control can either be made continuous (phase control) or stepwise (switched control). The first one is preferred provided the associated harmonics are acceptable during the short duty period coinciding with other loads being switched off.

Modifications of the operation of present power supplies are also being considered in order to decrease the amount of compensation needed. NBI might be turned off softly (eg ramp down in 1s) in case of a plasma disruption if an analysis of the heating effect on the carbon tiles in the vacuum vessel proves it feasible. Since the P-compensation is needed only in case of a plasma disruption a signal indicating that a disruption is about to occur could be used to give an early start to the ramping down of some power supplies. Such a precursor signal seems to be available [5] about 0.1s before plasma disruption.

Experiments are also being performed of limiting the negative VA load voltage (to about -360V) or to push the plasma towards the inner wall in order to reduce the VA power drop at a disruption.

P-compensation could be achieved by additional static convertors fed from the grid being connected in series with TF1 and TF2 in the TF coil circuit but by-passed via diodes during

normal operation. To counteract a power drop they would be switched in the circuit for a short time supplying a step of power to the TF coils and increasing the TF current slightly (the TF load has a time constant of about 10s). Costwise this solution is not favoured.

A P-compensation with local resistors installed in the RF and NBI compounds has also been considered but found not practicable.

6. FUTURE EXTENSIONS

The analysis of the 5MA plasma current pulse with AH has shown that P- and Q-compensation is needed if the agreed limits of the JET 400kV load are not to be exceeded.

P/Q compensation is bound to be of importance when additional loads [1] are to be connected. It can be anticipated, even if the ultimate JET scenario is not defined yet, that the effect of a 7MA plasma current pulse on the 400kV system would require a substantial increase of P- and Q-compensation relative to the ratings cited for the 5MA experiment. An implementation in stages of the P/Q-compensation appears reasonable. A relaxation of present 400kV limitations on maximum reactive power and active power step and on voltage drop would be very beneficial in terms of less compensation equipment being necessary.

7. REFERENCES

[1] Mondino, P L; Bertolini, E; "THE JET TECHNICAL AND SCIENTIFIC PERFORMANCE AND FUTURE PLANS", ANS Annual Meeting and 7th Topical Meeting on the Technology of Fusion Energy, Reno, USA, June 1986.

[2] Bertolini, E; "BASIC DESIGN CONCEPT, INSTALLATION, COMMISSIONING AND OPERATION OF THE JET INTEGRATED POWER SUPPLY SYSTEM", in Proceedings of 10th Symposium of Fusion Engineering, Philadelphia, Dec. 1983, pp 1756-1963.

[3] Bertolini, E; Mondino, P L; Noll, P; "MAGNET POWER SUPPLIES AND PLASMA CONTROL", Fusion Technology, to be published, 1987.

[4] Marchese, V; "JET POWER SUPPLIES SIMULATION PROGRAM: COMPARISON BETWEEN MODEL OUTPUTS AND EXPERIMENTAL DATA", JET Report JDN-G-86/001 (1986).

[5] How, J; et al; "THE JET PULSE TERMINATION NETWORK", in these Proceedings.

OVERVIEW OF THE JET ICRF POWER PLANT OPERATION AND DEVELOPMENT

R.J. Anderson, J. Plancoulaine, M. Schmid

JET Joint Undertaking, Abingdon, Oxon, OX14 3EA, England

ABSTRACT

Some salient features of the JET ICRF power plant design are briefly described followed by some important commissioning tests. The working methods adopted during the first two years of operation on JET are covered together with the recent system improvements and enhancements.

1. INTRODUCTION

A full description of the JET ICRF System design was given in the 1984 SOFT conference [1]. Seven 3 MW RF amplifier units have now been installed and tested at JET. Each unit contains two identical amplifier chains consisting of a low power transistor amplifier and three tetrode tube power amplification stages. The final stage is driven by a maximum of 100 kW input power and delivers 1.5 MW via an LC matching network into a coaxial line of 30 ohms characteristic impedance. The amplifiers operate in eight 4 MHz wide frequency bands covering the frequency range 23 to 57 MHz.

Three antennae are currently installed in JET, connected to the RF amplifiers by 84 metres of coaxial line. Motorised switches enable the generators to be tested into 1.5 MW dummy loads. The antennae can present severe impedance mismatches to the coaxial lines. A motorised tuning stub close to the amplifier output together with closed loop control of the input frequency (typically in the range plus or minus 100 kHz) permits minimisation of the mismatch.

Control of the amplifier frequency alone during a JET pulse does not provide a perfect match between amplifier and transmission line, therefore the amplifiers have been designed to operate at full power into loads with a Voltage Standing Wave Ratio (VSWR) of 1.5 to 1 at all phases. Excess endstage anode dissipation is avoided under these conditions by a system which dynamically adjusts the anode voltages provided by the separate high voltage power supplies.

2. COMMISSIONING

2.1 HVDC-RF amplifier combined commissioning

The high voltage (HV) power supplies were installed at JET and commissioned independently of the amplifiers with a separate HV test load. The amplifiers were also tested before shipping at the manufacturer's works with the factory's own general purpose HV power supplies.

Combined commissioning included tests on the fibre optic control link between the HV supplies and the amplifiers and checks on the voltage transients on the 200 m long cables caused if an ignitron crowbar protecting the amplifiers was fired.

The generators were designed to operate in four different pulse modes (Table I). Quasi continuous operation (mode 3) permitted rapid adjustment of the 22 amplifier tuning elements in each of the 8 frequency channels. Full length long pulse tests (mode 1) proved relatively tedious for commissioning owing to the 10 minute interpulse delay.

Mode	Max Pulse Length	Duty Cycle	Total DC Current	Max RF Power	Mode Description
1	20s	1:30	300 A	3 MW	JET pulse
2	100 ms	1:10	100 A	500 kW	antenna conditioning
3	3 ms	1:10	150 A	1.5 MW	amplifier adjustment (1 chain only)
4	infinite	-	60 A	100 kW	continuous wave

Table I : Operation modes provided by the amplifiers.

2.2 Determination of RF output power

Accurate determination of RF output power was not only essential for the satisfactory completion of acceptance tests, but was also required to ensure that the specified endstage anode heat dissipation was not exceeded and for the correct interpretation of the plasma physics. Wideband directional couplers are used both for internal control of the amplifiers and also as a routine means for determination of the power delivered to the antennae.

Initially two independent methods were used to check the power calibration of the amplifiers:

(i) Use of the calibration curves supplied with each coupler and an accurate RF power meter. The calibration accuracy of the couplers and power meter were ± .1 dB and ± .05 dB respectively.

(ii) Calorimetric measurement of the amplifiers feeding soda water test loads. Probably the main sources of inaccuracy here were the finite thermal inertia of the soda load system and the change in inlet temperature of the soda solution during the 20 second pulse.

Differences of up to 0.5 dB found between these two measurement techniques lead to the adoption of the a third measurement method:

(iii) Calorimetric measurement of anode dissipation which is then subtracted from the anode DC input power. Allowance also has to be be made for the driving power in the grounded screen grid configuration of the endstage and for output circuit losses.

In method (iii) the largest source of error was in the measurement of anode dissipation, partly because the instrumentation had not been specified with power calibration as a requirement and partly because of the thermal measurement errors shared by method (ii). The most consistent results from method (iii) were obtained by operating the amplifiers as efficiently as possible and therefore minimising the contribution of anode dissipation errors in the final results. The spread of results between the three measurement techniques suggests the measurement error is now approximately ± 0.25 dB.

2.3 Transmission Line Electrical Performance

2.3.1 General

The JET Transmission Line System (Fig 1) was chosen to permit operation over the full 23 to 57 MHz frequency range while avoiding the need for complex mechanical tuning systems close to the torus. Such a system requires transmission lines with a high voltage breakdown level and low loss, particularly when coping with severe impedance mismatches. Values of VSWR measured on the JET lines have ranged between 3 and 25 depending on the antenna mode and plasma coupling.

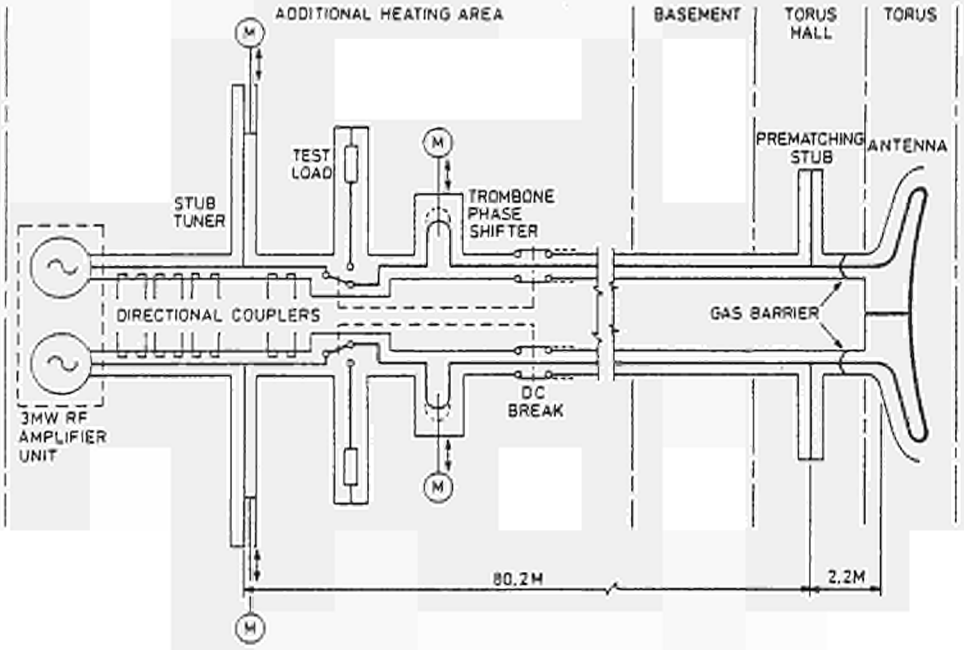

Fig 1 : ICRH Transmission Lines Block Diagram

2.3.2 Voltage standoff tests

After installation, the RF lines began to show a degraded RF breakdown performance. The design of the ceramic supports was suspected at first but the problem was later discovered to be caused by the tin plating on some line components. Single crystals of tin with a diameter of 0.5 µm and lengths of up to 8 mm had formed on the plated parts. As the crystals grew, they progressively reduced the voltage standoff on some of the lines to as little as 16 kV.

More than 600 m of line was dismantled and the plated parts removed. At the same time most of the disk ceramic supports were exchanged with a 3 rod design. The disk ceramic, with an X cross section, was only retained in mechanically critical places such as in the telescopic elements near the torus.

The performance achieved with the lines after these modifications are as follows:

Voltage standoff for 100 ms pulses	+	53 kV
Voltage standoff for 10 s pulses	+	45 kV
Line loss when matched, at 55 MHz		1.57 dB/km
Return loss	++	33 dB

\+ Lines pressurised with dry air at 3 bar gauge

++ Measured on 40 m of line with 3 bends

3. OPERATION

3.1 Multipactor effects

Special attention was paid during the design of both the amplifiers and the HV supplies to possible multipactor discharge phenomena within the ICRF antennae. Modes 2 and 4 in Table 1 were specified for antenna conditioning. In order to pass quickly through the multipactor "power band", a precharged smoothing inductor in the HV supply is synchronised via the fibre optic link, to permit the RF power delivered to the antenna to rise above 1.0 MW within 1 ms [2].

In practice antenna conditioning proved to be very straight forward. The use of mode 2 in Table 1 for one or two hours reduced the top of the multipactor power band to below 20 kW per half antenna. While the HV inductor precharging system has been tested, its use on JET has therefore not proved necessary so far. The ability to drive the antennae at powers as low as 20 kW has brought additional benefits as below this level the amplifiers may be operated into a load with infinite VSWR. This has enabled the use of power waveforms with an initial tuning "porch" and permits the automatic phase control and frequency control systems to lock in before the RF power is increased.

3.2 Antenna matching

Two types of antenna central conductor design have been tried in JET [3,4,5,6]. Both designs exhibit some degree of coupling between the two antenna halves, thus driving the halves with phase differences of more than 1 or 2 degrees away from 0 or π phasing, strongly influences the match seen by the RF amplifiers. The three antennae in JET also exhibit inter-antenna coupling. To the amplifier protection circuits the coupled power is interpreted as load reflections and this complicates the amplifier matching problem.

The variation of power reflected from the antennae back along the transmission lines to the amplifiers can be a sensitive indicator of plasma behaviour. In addition to changes in plasma density or position, the effects of sawteeth and minority gas injection are regularly observed in the fine detail of the reflected power waveforms [6] .

To increase the transmission line efficiency with low antenna plasma coupling, a series of experiments have been performed with prematching stubs connected to the lines close to the antennae (Fig 1). These reduced the voltage stress on all but the last 2.2 metres of transmission line. Non prematched VSWRs of up to 35 are possible in some instances, corresponding to a line efficiency of between 67% to 75% and a peak line voltage of 57 kV. The use of prematching stubs generally limits the operating frequency range to a small portion of one frequency channel and a narrow range of antenna-plasma coupling.

4. RECENT DEVELOPMENTS

4.1 Transmission line insulator improvements

Different designs of ceramic supports with various surface treatments were tested in a half wavelength test resonator at 52 MHz. Test pulse lengths were limited to 100 ms by the power handling capacity of the coupling loop. A maximum of 70 kW was required for the tests. The following points summarise the experiences gained from the tests:

* 50 Hz AC high voltage tests are of limited use for evaluating the high voltage RF performance of transmission line components.

* The increase in voltage standoff with pressure (dry air or nitrogen) is less than suggested in manufacturer's catalogues and text books. An increase from 0 to 2 bar relative pressure improves the voltage standoff at best by a factor of 1.5 compared with the often quoted factor of 2.

* Test results are difficult to reproduce due to the conditioning effect of the voltage breakdowns and the results obtained under laboratory conditions do not carry over well to large installations.

* Long pulses of the order of 10s lead to breakdown at lower voltages than pulses of 100 ms or less. This was experienced consistently on 75 m long lines terminated with a short circuit and pressurised with dry air (dewpoint less than - 40°C) to 3 bars relative.

Test resonator breakdown measurements have been made on a number of ceramic insulator designs. The disc ceramic with an x-cross section withstood approximately 47kV. Better test results were achieved with 3-rod supports which withstood 59 kV and with conical supports which withstood 61 kV. The conical ceramic can take considerable forces (several tonnes) between inner and outer conductor, but only in one direction.

It is planned to replace the remaining x-ceramics in the JET transmission lines with the conical type.

4.2 Variable capacitance antenna prematching stub

In parallel with successful experiments using fixed length prematching stubs described in 3.2, a stub containing a variable capacitance (Fig 2) has been developed. This will confer all the advantages of the fixed length prematching stubs, with increased matching flexibility. The capacitor is driven by a remotely controlled stepper motor. Capacitor voltage, current and temperature are monitored. The unit is compatible with the remote handling requirements of the JET tritium phase. Six units have been manufactured and tested (Table II) in the RF testbed at JET ready for installation in autumn 1986.

Capacitance	20-300 pF
Mechanical adjustment range	50 turns 60 mm stroke
Positioning accuracy	1/12 turn
50 Hz voltage test	90 kV
RF peak working voltage	50 kV
RF peak current	1000 A

Table II : Capacitive Stub Characteristics

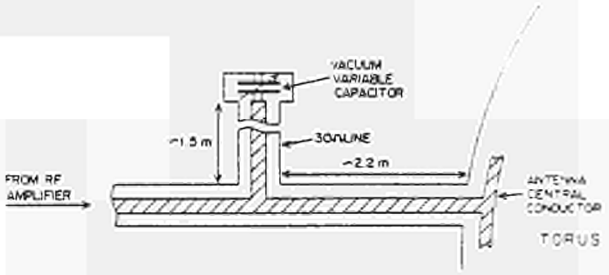

Fig 2 : Capacitively Terminated Stub

4.3 Trombone transmission line phase shifter

The matching system (Fig 1) requires that both antenna halves are powered with a fixed relative phase. So that both antenna halves are matched at the same frequency, the electrical length between stubtuner and antenna must be the same to within 0.4°. Such a precise adjustment is required owing to the low coupling resistance presented by some antenna central conductor designs.

Measurements of phase delay versus frequency on the installed lines have shown that the relative phase delay scatter on a pair of lines is far in excess of this value. The phase delay has been found to vary with a maximum excursion $\Delta\phi$ degrees (eq. 1). This is

expressed as a function of line length (L metres) and frequency (f MHz). The measurements were made on a line containing the disc ceramics.

$$\Delta\phi = 7.8 \times 10^{-4} Lf \qquad (1)$$

In order to enable the matching system to cope with the lower values of antenna to plasma coupling a motor driven trombone phase shifter with an adjustment range of 15° at 25 MHz has been developed. In some experiments at JET all eight antennae will be used in a phase locked mode. Therefore all lines have to have a trombone phase shifter in order to achieve proper matching on all operating frequencies. The first phase shifters were installed in January 1986.

4.4 4 MW Amplifier Upgrade

An installation of ten amplifier units was initially planned for JET, providing a total of 30 MW generated power. The design was based on the Eimac 8973 which produces 1.5 MW per endstage.

Tetrodes with an output power of 2 MW have recently become available from a number of manufacturers and a prototype amplifier is currently being modified to take the Thomson TH525 [7].

Modifications to the generators are limited to the addition of an uprated screen grid power supply, increasing the current carrying capacity of each endstage crowbar damping circuit from 120 A to 172 A, modifications to the endstage tuning network and some minor instrumentation changes. Increasing the capacity of the HV supplies will be achieved by replacing the HV supplies to the driver stage anodes, currently fed from a centre tap of the endstage HV supply rectifier bridge, by a separate driver stage power supply providing 30 A per tube at 12 kV. Uprating of the power handling capacity of the soda water test load from 1.5 to 2 MW will also be necessary.

The upgrade will permit plant costs and space savings to be made over the requirements of the original plan. Eight water cooled antennae will be installed in JET in early 1987 and the upgrade of the last of the eight amplifier units will be completed later in the same year.

4.5 3 MW Power combiner

In anticipation of the 4 MW amplifier upgrade, tests are being performed on the antenna of octant 6B with the combined output power of two generator units. For this purpose two 3 dB hybrid power combiners have been installed with a nominal output power of 3 MW each (Fig 3). The combiners are of the single section quarter wave coupled line type and cover the complete 23 to 57 MHz frequency band without mechanical adjustment.

The original generator testloads are used as balancing loads. The phase between the two outputs of one generator unit is regulated with an electronic phase control system, as is the phase between the outputs of the two combiners. Special arrangements had to be made to limit the output power of all four endstage tubes simultaneously in the event that the automatic protection system of one tube limits its output power.

Fig. 3 : Arrangement of two 3 MW amplifiers to feed one antenna

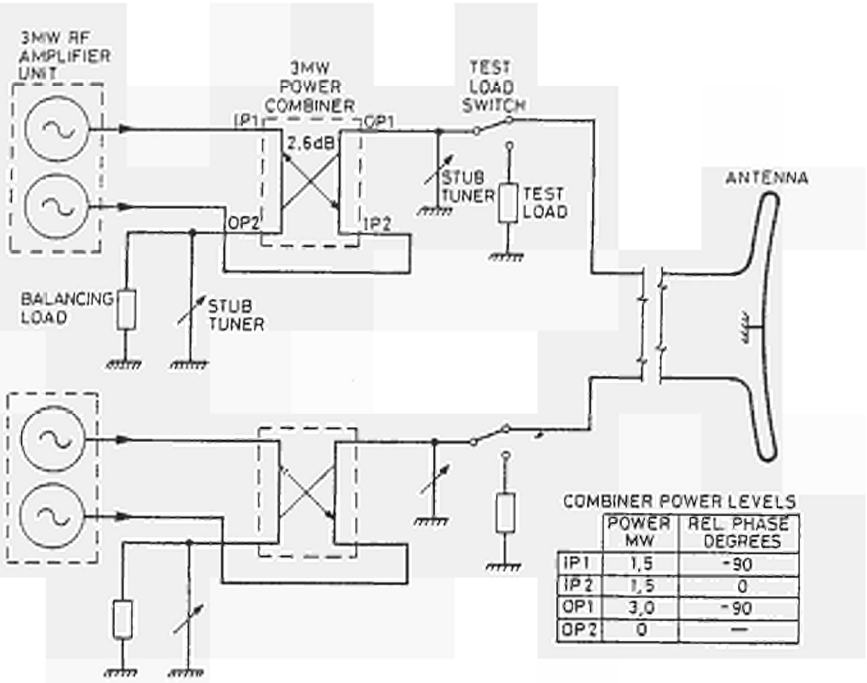

5. CONCLUSIONS

Plant commissioning and operation on JET have proceeded in parallel to enable the ICRF experimental programme to begin approximately 6 months ahead of schedule. With the benefit of experience gained through two years of RF operations with JET, a number of system improvements and enhancements have been identified.

Operations continue until the end of 1986 with up to 12 MW RF Power available from the amplifiers now connected to the JET antennae. In early 1987 eight water cooled antennae will be installed in JET and upgrades of the existing 3 MW amplifiers to 4 MW will begin. In 1988 there will be an installed RF power generation capability of 32 MW corresponding to an additional heating power to the JET plasma of approximately 16 MW.

6. ACKNOWLEDGMENTS

The authors are grateful to the following for their assistance in writing this paper: Dr J. Jacquinot, Mr T.J. Wade, Dr G. Bosia, Dr F. Sand, Mr A.G.H. Sibley, the engineers of Herfurth GmbH (Amplifier system) and Spinner GmbH (Transmission line system).

7. REFERENCES

[1] WADE, T., Thirteenth Symposium on Fusion Technology, Varese, 24-28 September 1984. Proceedings pp 727-732

[2] CLAESEN, R., Eleventh Symposium on Fusion Engineering, Austin, Texas, 18-22 November 1985. Proceedings pp 93-98

[3] KAYE, A., ibidem, pp 1204-1209

[4] ARBEZ J., Fourth International Symposium on Heating in Toroidal Plasmas Rome, 21-28 March 1984. Proceedings pp 1244-1251

[5] SAND, F., ibidem, pp 1121-1127

[6] JACQUINOT, J., Plasma Physics and Controlled Fusion, V28, Nr 1A, 1-15 (1986)

[7] WADE, T.J., Seventh Topical Conference on Technology of Fusion Energy, Reno, Nevada, 15-19 June 1986. Proceedings, to be published.

NON EVAPORABLE GETTER PUMPING FOR JET ICRF ANTENNAE

C.I. Walker, A.S. Kaye, R.A. Horn, F. Mazza[+]

JET Joint Undertaking, Abingdon, Oxon, OX14 3EA, England
[+] SAES Getters SpA, Via Gallarate 215, 20151 Milan, Italy

ABSTRACT

The JET ICRF A_1 Antenna Vacuum Transmission Lines will be pumped with individual non-evaporable getter pumps. The pump is a cartridge type in an all welded body which is heated externally to give activating, operating and regenerating temperatures. The pumped Hydrogen is periodically regenerated back into the torus. This will be particularly advantageous during the tritium phase of operation.

The pump is simple and gives a high reliability. It is tolerant of conditions close to the torus and can be sited within the volume reserved for installation of the RF transmission lines. The all welded system simplifies remote handling.

Tests on prototype pumps are being conducted to establish operational data and confirm contamination, saturation and embrittlement levels. A getter pump has been installed on one of the existing antenna systems on JET, no difficulties have been experienced in operating this antenna.

1. INTRODUCTION

Eight cooled ICRF antennae are to be installed in JET during the next shutdown [1]. Due to the low conductance to the torus, these A_1 Antennae require additional vacuum pumping of the vacuum transmission lines (VTL). Experience with the prototype antenna on JET has shown that the pressure in the VTLs must be less than 10^{-4} mbar throughout the RF pulse to avoid multipactor arcs if the voltage minimum is located inside the vacuum window (ie, above typically 30 MHz).

Fig. 1 shows the equipment and vacuum systems associated with one VTL.

The main parameters of the system are given in Table I.

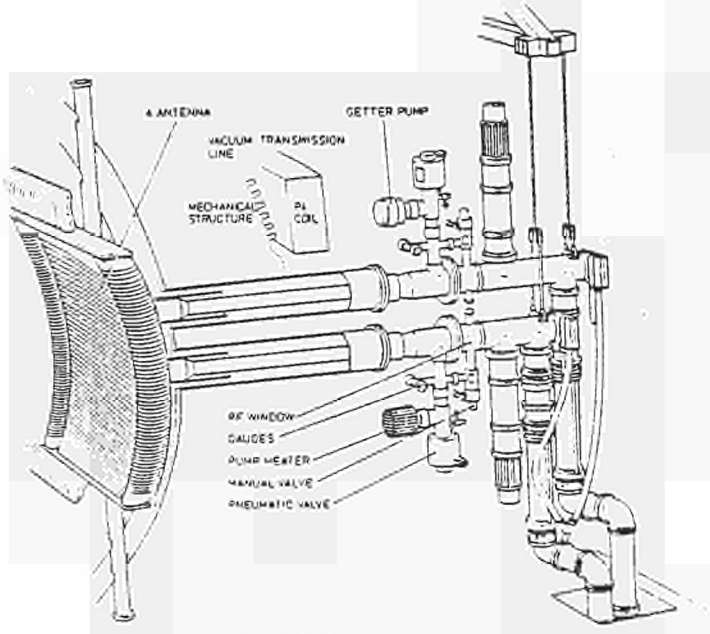

Fig. 1 JET ICRF Antenna Systems with Vacuum System

TABLE I

Main Parameters of A_1 Vacuum System

VTL Volume	=	$3.4\ 10^{-1}$ m³
Surface	=	3.7 m² 1.7 m² RF, 2.0 m² others
Vacuum System Vol	=	$5.2\ 10^{-1}$ m³
Surface	=	1.6 m²
Conductance to Torus	=	34.5 ℓ/s (measured A_0)
	=	35 ℓ/s (measured A_1)
Conductance		
pump to DCF	=	88 ℓ/s
pump to VTL	=	188 ℓ/s
pump to gauge	=	60 ℓ/s

Pumping Speeds (ℓ/s)	After regeneration	Before regeneration
at pump	1,500	500
at VTL port	167	152
at DCF	93	92
at nearest RF surface	110	32
at further RF surface	22	21
to torus	35	35

The Getter Pump was chosen for a number of reasons. The Pump is small enough to be sited close to the torus, in the shadow of the RF Transmission Lines, with no interference with ancillary equipment such as diagnostics and no interaction with the local high magnetic field. No roughing or fore line vacuum system is required as regeneration is performed back into the torus. This is particularly advantageous in the tritium phase. The pump incorporates no moving parts, high voltages, permanent or electro-magnets. Compared with turbo-molecular pumps remote handling and maintenance is reduced and simplified, and services and control systems are minimal. The getter pump thus gives a compact highly reliable system.

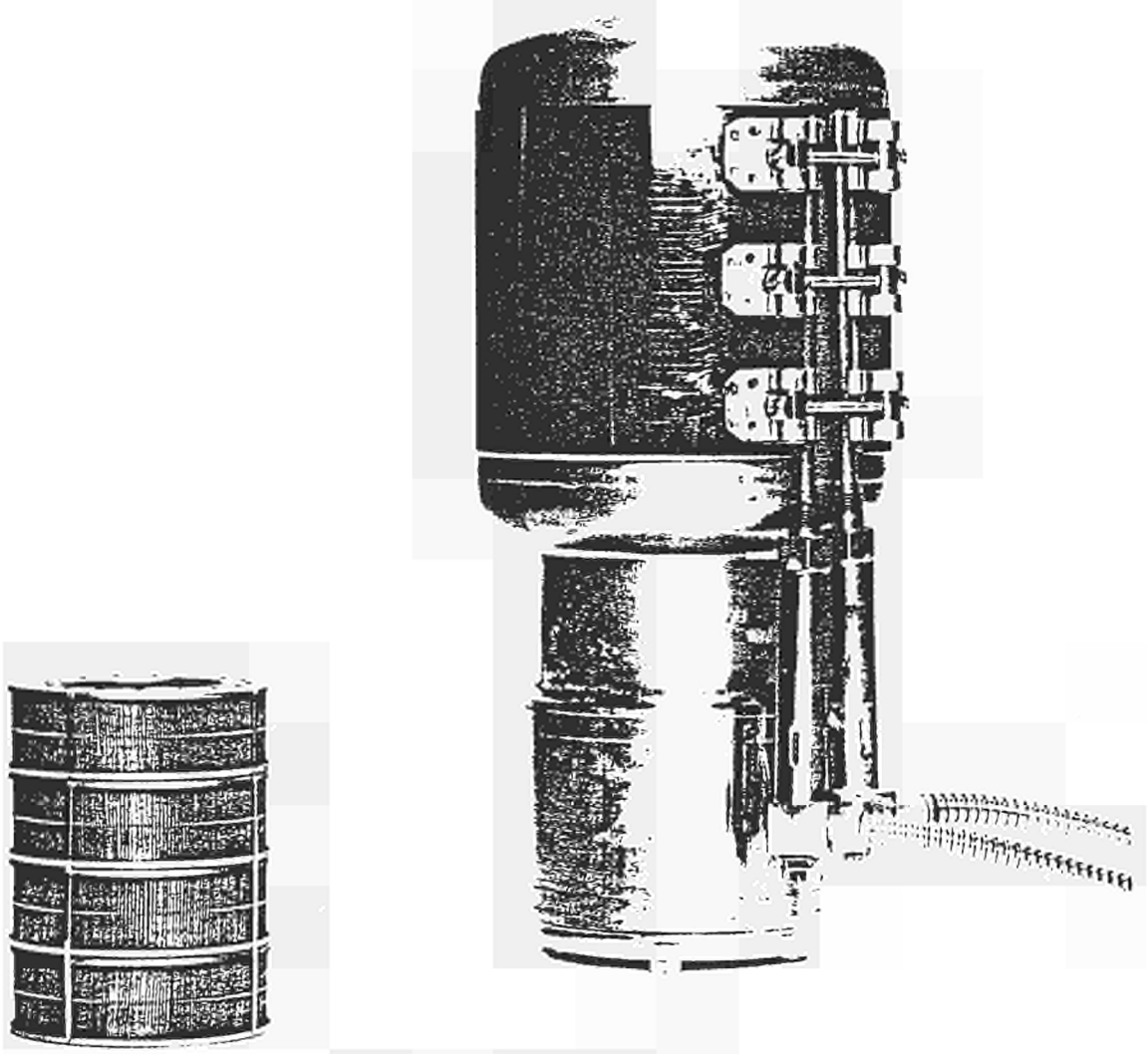

Fig. 2 Getter Cartridge, Pump Body and Heater

2. MECHANICAL DESIGN

The Pump (Fig 2) comprises a

GETTER CARTRIDGE of Pleated Constantan coated with 500 grams of ZrVFe getter alloy [2] (St 707 ® [3]), formed into a cylinder and supported on a central rod with radiation baffles

PUMP BODY of welded stainless steel (304L), with a welded collar of JET standard Remote Handling type.

HEATER of external band type, capable of heating the body above 600°C, insulated.

A pneumatic angle valve has been incorporated to prevent overloading of the getter with hydrogen when at high pressures (10^{-3} mbar) for long periods (> 6 hrs) during discharge cleaning and carbonisation sessions.

3. OPERATION

3.1 Activation

The Getter Cartridge is received passivated with a surface layer of absorbed gases and has to be 'activated' by heating under vacuum to approximately 450°C for up to one hour. When the surface becomes saturated with active gas products, after operation, 're-activation' is performed in a similar way, to restore the original pumping speed. During these processes the active gases are diffused from the saturated surface to the bulk of the gettering material. The low pressure required during activation is provided by the JET torus pumping through the VTL.

3.2 Hydrogen Pumping

During an RF shot, the gas released from a fully conditioned VTL has been measured on the RF testbed to be predominantly hydrogen, see Table II.

The getter material pumps hydrogen isotopes by the formation of solid solutions [4]. The hydrogen pressure above the getter surface is a function of the getter temperature and sorbed hydrogen concentration as shown in Fig 3. The pumping speed of the pump is between 1500 ℓ/s and 800 ℓ/s for operation at 200°C (see Fig. 4).

TABLE II

Measured Partial Pressures of Gases in the VTL and JET

Gases	JET Normal Operation	VTL Conditioning	VTL Conditioned	VTL RF Pulsing
H_2 (D_2)	3×10^{-7}	3×10^{-4}	2×10^{-4}	2×10^{-7}
H_2O (D_2O)	1×10^{-6}	3×10^{-7}	1×10^{-7}	3×10^{-7}
CO	10^{-9}	1×10^{-4}	7×10^{-6}	2×10^{-7}
CO_2	$< 10^{-9}$	3×10^{-7}	-	1×10^{-7}
Hydrocarbons	$1-5\ 10^{-9}$	-	-	-

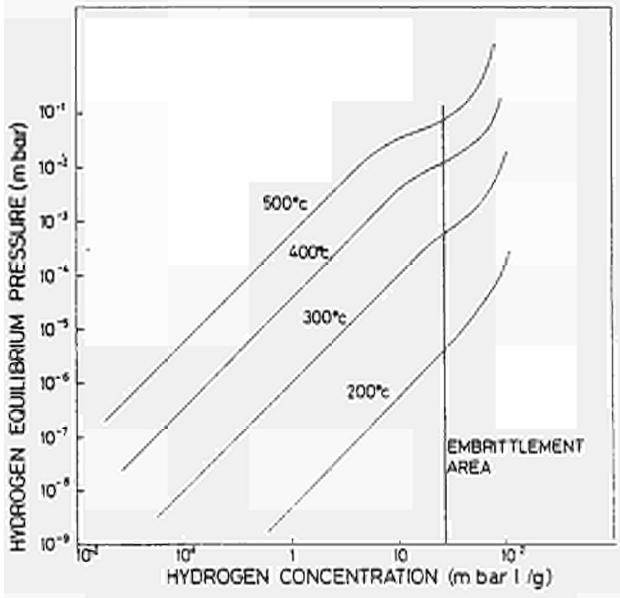

Fig. 3 Hydrogen Equilibrium Pressure on St 707 Getter Alloy

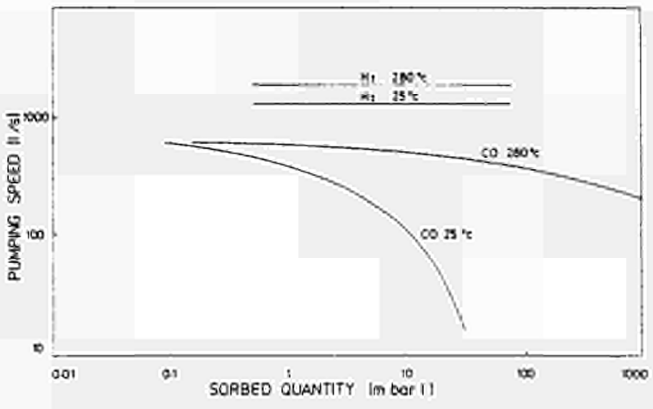

Fig. 4 Getter Pumping Speed Characteristics

The VTL pressure during the RF shot shows two peaks, one at the start and one at the end of the RF pulse as the RF voltage ramps through the multipactor range (typically 0.5 - 2 kV). An additional slow pressure rise is seen, as the VTL heats during long pulses (Fig 5).

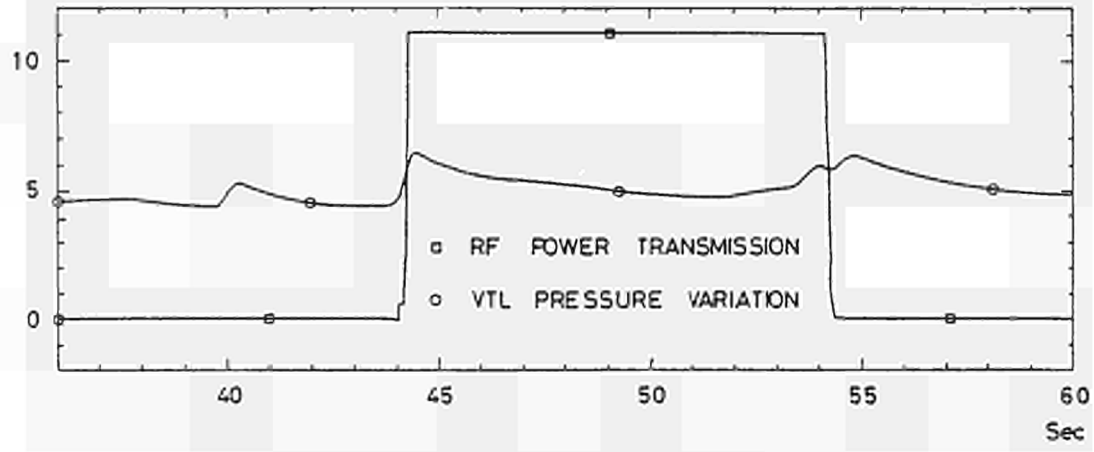

Fig. 5 VTL Pressure Variation with RF Power Transmission

The quantity of gas pumped is 1.2 x 10^{-2}mbar ℓ/hr continuously while the valve is open and the torus pressure is 10^{-7} mbar, with a measured conductance of 35 ℓ/s between VTL and torus. An additional 6 x 10^{-3} mbar ℓ is typically pumped per RF pulse. These results enable the requirement for regeneration to be predicted. The frequency of regeneration will be chosen so that a safe working level of 5 mbar l/g is not exceeded in operation on JET. When the quantity of sorbed hydrogen exceeds 20 mbar ℓ/g the getter material embrittles and tends to spall in flakes.

3.3 Active Gas Pumping

The anticipated volume of active gas generated in the VTL and required to be pumped by the Antenna Vacuum system, during complete conditioning and operation of a VTL is 100 mbar ℓ.

These gases such as CO, CO_2, O_2, N_2, H_2O, chemically sorbed by the getter material with an efficiency that increases with temperature.

Hydrocarbons are pumped very poorly by the the getter (with a pumping speed 1/100 that of CO). Hydrocarbon contamination is carefully avoided during manufacture and installation. The angle valve will be closed during vacuum vessel carbonisation.

The pump provides active gas pumping over 500 ℓ/s with a capacity of 330 mbar ℓ between re-activations; 4500 mbar ℓ in total. Cartridge replacement will be necessary only after five years due to active gas exhaustion.

3.4 Noble Gas Pumping

Noble gases are not pumped at all by the getter system. Such gases, eg Ar from atmospheric leakage or He^3 injected during a pulse for minority heating experiments are pumped only by the torus.

3.5 Operating conditions

The pump operating conditions have been chosen to optimise the active gas pumping during conditioning and the hydrogen pumping when injecting RF power into JET, this corresponds to an operation temperature of 200°C.

3.6 Regeneration

The sorbed hydrogen is regenerated from the getter pump by heating, while pumping to the JET vacuum vessel through the VTL.

The conductance of the system between torus and pump has been measured to be 35 ℓ/s for hydrogen.

A regeneration temperature of 500°C on the getter cartridge has been chosen to enable regeneration to be performed overnight (Fig. 6), with the same heater required for activation. Regeneration would be required at intervals of typically 40 weeks of normal operation. In practice regeneration will be incorporated with re-activation regular planned maintenance periods, typically every 6 weeks, representing four weeks operation.

3.7 Control

The control for the getter pump system has been designed to be minimal, implementing the simplicity and reliability of the pump. A Penning gauge head (plus a spare) is provided on the pump manifold to monitor VTL pressure. The external heaters are supplied only with fixed powers of 56 W and 240 W corresponding to 200°C and 500°C getter temperatures.

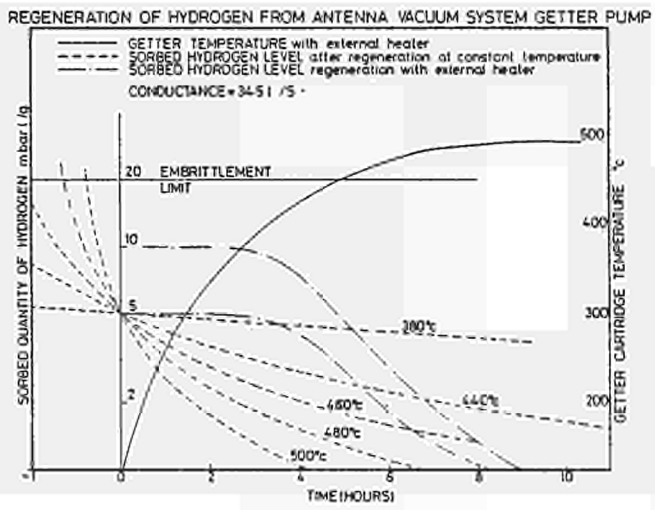

Fig. 6 Regeneration Time for Getter Pump

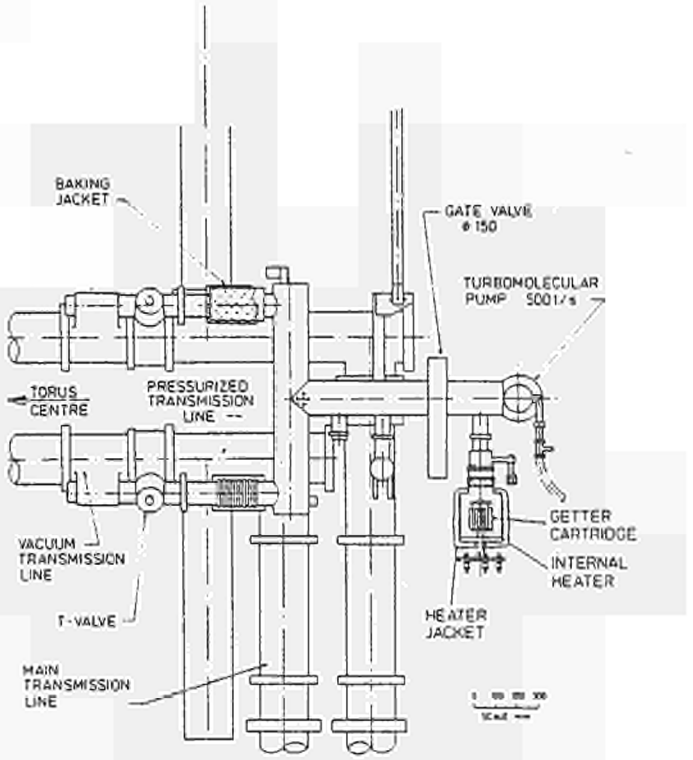

Fig. 7 Surrogate Getter Pump on A_o Vacuum System

4. TESTS

Tests have been carried out on a test rig to measure the pumping speed of the getter cartridge. The data obtained are shown in Fig 4. The pumping speed for hydrogen at 280°C and 25°C is respectively 2000 ℓ/s and 1500 ℓ/s , both higher than the design figures. the pumping speed for CO, chosen as a prototype for active gases, is of 700 ℓ/s at 280°C, again higher than anticipated.

This rig has also been used to assess external heaters for activation, operation and regeneration. It is currently being used to investigate the effect of embrittlement and recovery.

A surrogate getter pump has also been attached to the existing vacuum system on the prototype A_o antenna on octant 2D (Fig 7).

Measurements performed on the 2D VTL have shown a pumping speed for the getter cartridge of about 2000 ℓ/s in agreement with the figures obtained from the laboratory tests. No probleems have been experienced in operating the RF antenna with getter pumping of the VTL.

Direct comparisons have been made between the original turbo-pumped system and the getter pumped system (Fig. 8).

Fig. 8 Relative Performance of Surrogate Getter Pump and Turbomolecular Pump

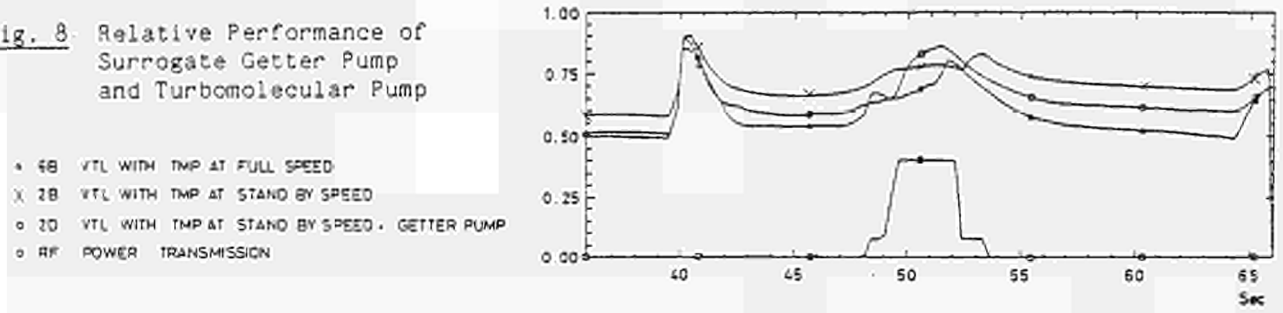

The RF testbed has been used to measure gas generation and conductance to the vacuum vessel (Tab II). Prototype getter pump systems are currently being installed to gain further operational experience.

5. TRITIUM COMPATIBILITY

The development of the pump design continues with respect to the reduction of tritium diffusion through the externally heated pump body. The remaining components of the vacuum system have been designed specifically for tritium operation.

6. CONCLUSION

A non-evaporable, regenerative getter pump has been successfully used to provide the additional pumping required on the vacuum transmission lines of one of the JET ICRF antennae. The characteristics of the pump have been measured. Getter pumping systems are being installed on all of the cooled A_1 ICRF antennae on JET.

7. REFERENCES

[1] Kaye, A.S. et al, Engineering Design and Preliminary Performances of the JET ICRF System, 11th Symposium on Fusion Engineering, Austin, Texas, 1985

[2] Boffito, C., Ferrario, B., della Porta, P., Rosai, L., A Non Evaporable Low Temperature Activable Getter Material, J. Vac. Sci. Technol. 18 (3), April 1981

[3] The St 707 Alloy is Manufactured by SAES Getters, SpA, Milan, Italy

[4] Knize, R.J., Stanton, J.L., Cecchi, J.L., Diffusion of Hydrogen and Deuterium in Zr V Fe. Journal of Nuclear Materials, 122 & 123 (1984) 1553-1557 North Holland, Amsterdam.

DESIGN AND MANUFACTURE OF WATER COOLED ELECTROSTATIC SCREENS FOR JET ICRF ANTENNAE

C.I. Walker, A.S. Kaye, H. Brinkschulte, R.A. Horn, J. Plancoulaine
D. Sigournay, G. Bevilacqua[+], F. Anselmi[*]

JET Joint Undertaking, Abingdon, Oxon, OX14 3EA, UK
[+] De Pretto-Escher Wyss, Schio, Italy,
[*] CSC, Schio, Italy

ABSTRACT

The electrostatic screens for the A_1 JET ICRF antennae are required to be water-cooled in order to extend the pulse length to 20 seconds. Whilst many features found beneficial in the uncooled (A_0) antenna have been retained, the provision of cooling, improvements in shape and interfacing with the toroidal limiter have much increased the complexity. The screens are fabricated in high purity nickel and manufacture has involved the development of machining, forming and welding processes to obtain the required mechanical performance.

Tests of samples, a short proof assembly and a prototype screen have qualified the design and manufacturing processes. Magnetic forces during disruptions are reduced by the use of resistive electrical contacts, and the screen cooling is also used to cool the antenna side protection between pulses.

Keywords: ICRF, Antenna

1. INTRODUCTION

The 8 ICRF antennae, due to be installed in JET from December 1986, are designed to launch a total of 15 MW into the plasma for 20 sec. This pulse length requires the A_1 antennae to be actively cooled. Three uncooled A_0 antennae have been operational on the torus since 1985.

Each A_1 ICRF antenna incorporates an all metal electrostatic screen, as originally developed on TFR [1]. The T-shaped cross-section of the uncooled A_0 screen elements [2], and the tilting of the elements at 15° to align with the tokamak field [3] have been retained. This arrangement has a transparency of up to 90% [4] and successful high power RF transmission [5] [6] [7] has been demonstrated on the A_0 antennae. The screen elements are now curved to follow the magnetic field.

The screens are mounted in series with the belt limiter sectors and are designed for remote installation. Each screen carries graphite or beryllium side protection tiles which are radiatively cooled by, and mounted off fins on the screen manifolds.

The screen is an all welded nickel structure consisting of 79 tubular elements welded into 2 manifolds. To each manifold are also welded 86 fins for the side protection tiles, and the supports for the side electrical contacts. The screen is fixed to the antenna housing with 6 insulated bolts. A section through the screen is shown in Fig. 1 and the complete screen assembly is shown in Fig. 2.

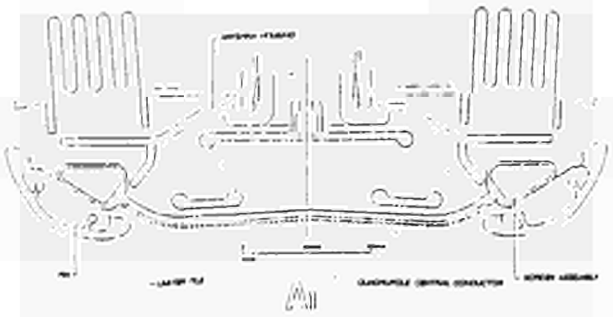

Fig. 1 Section through A_1 Antenna

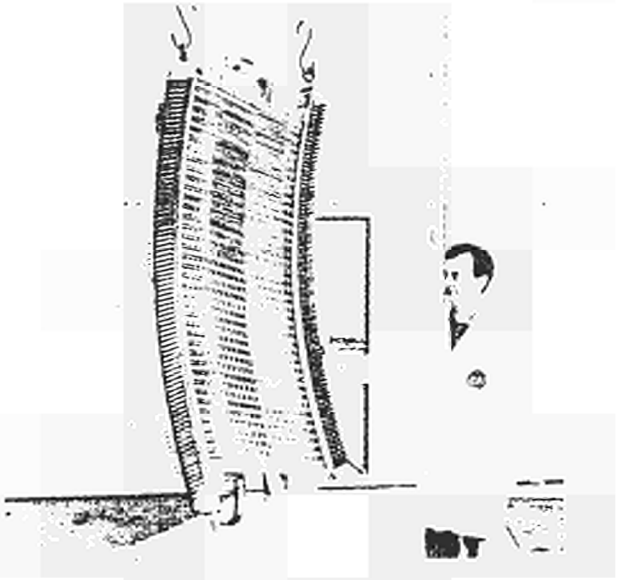

Fig. 2 Antenna Screen

A prototype screen has been tested on the JET RF testbed, and manufacture of the other 8 screens is well advanced. This paper describes the design, manufacture and testing of these screens.

2. DESIGN REQUIREMENTS

2.1 General Requirements

The screen assembly has been designed to withstand the disruption stresses and thermal stresses and handle 50 kV RF voltage without arcing. The screens will experience a 14 MeV neutron flux of 10^{13} n/s for 10s for each of 10^4 shots, integrating to 10^{18} n/cm^2 over the life of the system. The screens are required to have a leak rate of less than 10^{-9} mbar ℓ/s (He) to use the 12 bar cooling water supply of the toroidal limiter, to be bakeable to 500°C, and to be installed remotely.

2.2 Power Dissipation

During the RF pulse the screen is heated (a) by RF losses of up to 300 kW which is non-uniformly distributed giving peak heating of up to 5 x average and (b) by a further 150 kW of uniform plasma radiation. An uncooled element would rise approximately 200°C under this loading. In addition, a mean power of 20-30 kW per antenna has to be removed, due to plasma loading of the side protection tiles and radiation from the hot vessel.

Water cooling at 7 kg/s through the screen gives an overall temperature rise of 15°C and avoids boiling at local hot spots. Variations in temperature between adjacent elements has to be limited to less than 20°C to avoid overstressing and fatigue at the element to manifold joint. Table I summarises the thermal properties of the screen

Table I: Thermal Properties of Screen

Element Material	Nickel	Total Water Flow	7 kg/s
Element Mass	1.19 kg	Water Velocity in Element and Pipe	4.7 m/s
Thermal Capacity	0.54 kJ/°C	Re	4 x 10^4
Hole Diameter	5 mm	Heat Transfer Coefficient	2.3 10^4 W/m²°C
Hole Surface Area	1.1 10^4 mm²		
Screen Assembly Mass	242 kg	Inlet Pressure	6 bar
Thermal Capacity	110 kJ/°C	Pressure Drop	1.6 bar
Internal Volume	9 ℓ	Water Temp Rise during pulse	
		Average	15°C
Tile Thermal Capacity (Total)	165 kJ/°C (Be)	Peak Local	100°C
	48 kJ/°C (C)	Average Element Surface	53°C
Thermal Diffusion Times			
Element Surface to Centre	1.3 sec		
Element ½ Length	90 min		
Hot Spot to Manifold	8 min		
Manifold ½ Length	6 hours		

2.3 Mechanical forces

The forces experienced by the screen in good electrical contact with the housing during a 5 MA plasma disruption in 5 msec are shown in Fig 3. These have been evaluated as 1 kN radially, uniformly distributed on each element and an average of 14 kN on each of the 6 location bolts. It is assumed that the screen will have to withstand 5000 such loadings.

The electrical contact between screen and housing is in practice established by slightly resistive contacts described below. These much reduce the mechanical forces (by a factor 5-10).

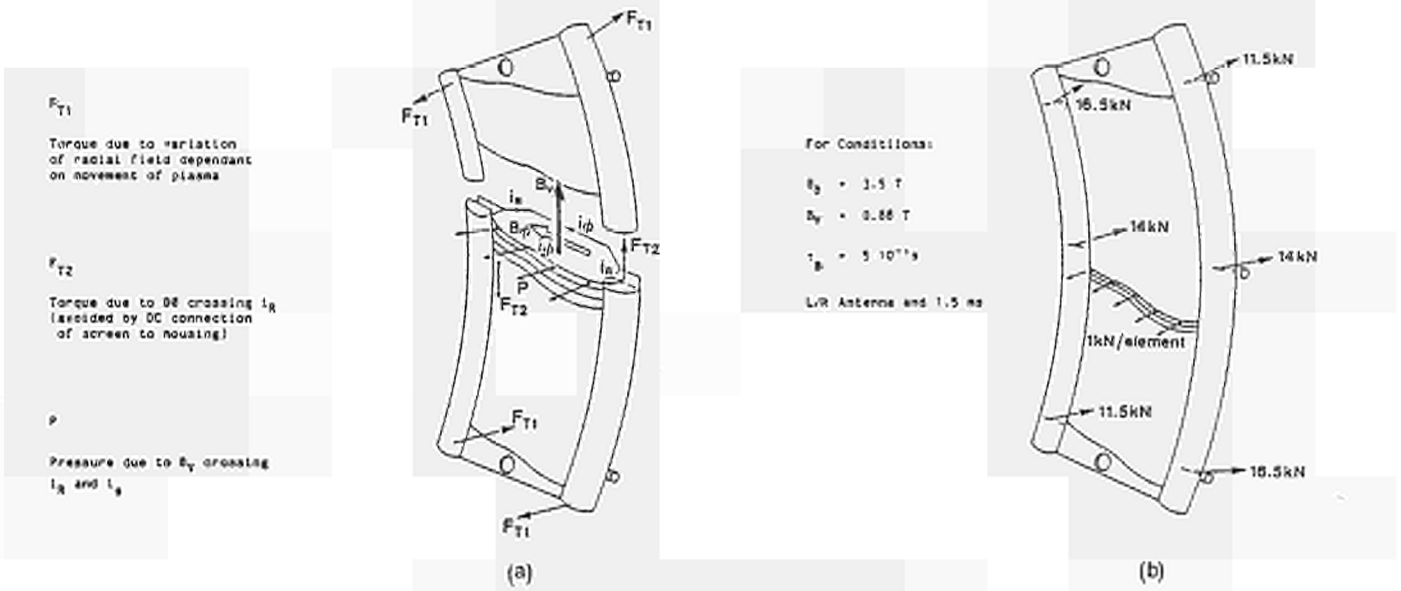

Fig. 3 Forces on Screen During Plasma Disruption

3. SCREEN COMPONENT DETAILS

3.1 Screen elements

A total of 1320 low carbon nickel bars 30 mm diameter, 700 mm long were procured from the same material melt and were processed in one batch after qualification. For subsequent gun drilling, maximum hardness was required. Production from 8 tonne blooms included hot forging, warm rolling, brightreeling, 2 cold drawings and finally centreless grinding. All material was ultrasonic tested for defects. Table II gives the properties of the element material. There is insufficient carbon in this metal to pin grain boundaries. However, testing proved that grain growth only occurred above 500°C.

Due to lack of data, annealed samples were fatigue tested in rotation bending, wet at 60°C. Better fatigue properties were recorded then theoretically predicted with stress to failure at 10^7 cycles at 50% of ultimate strength. Similar fatigue behaviour to the stronger normal carbon nickel 200 was seen, Fig 4. Decrease in strength due to fatigue at ultimate stress levels is seen only above 10^4 to 10^5 cycles.

Table II: Properties of Screen Elements Material

Designation:	Pure Nickel	LC Ni 99.2
Specification:	Cabot Alloy 201	BS 3074 - 3076 Na 11 & 12
		ASME B 160 - 163
		DIN 17740, 17750, 17752

Chemical Composition:

	SPECIFIED	ACTUAL
Nickel	≥ 99.0%	99.77%
Cobalt	≤ 1.0%	< .05%
Carbon	≤ 0.02%	< .01%

Hardness before Annealing: 120 HV min 180 HV Surface
110 HC Centre

Annealing Conditions: 815°C, .75 hr, air cooling

Mechanical Properties after Annealing:

0.2% PS	20°C	≥ 70 MN/m²	134 MN/m² (514 as drawn)
0.2% PS	500°C	≥ 59 MN/m²	78 MN/m²
σ_{ult}	20°C	≥ 350 MN/m²	377 MN/m²
σ_{ult}	500°C	≥ 210 MN/m²	210 MN/m²
Elongation on 50 mm	20°C	≥ 40%	64%
	500°C	≥ 59%	59%
Hardness	20°C	≥ 90 HV	90 HV
Grain Size		3-7	5-6
Max Inclusions		< .25 mm	≤ .02 mm
Electrical Resistivity		≤ 8.4 10^{-8}Ωcm	8.33 10^{-8}Ωcm
Tests Ultrasonic	No indications on 5 passes; ref 1 mm dia to centre		
Eddy Current	No indication on 1 pass ; ref .9 mm dia 3 mm deep		

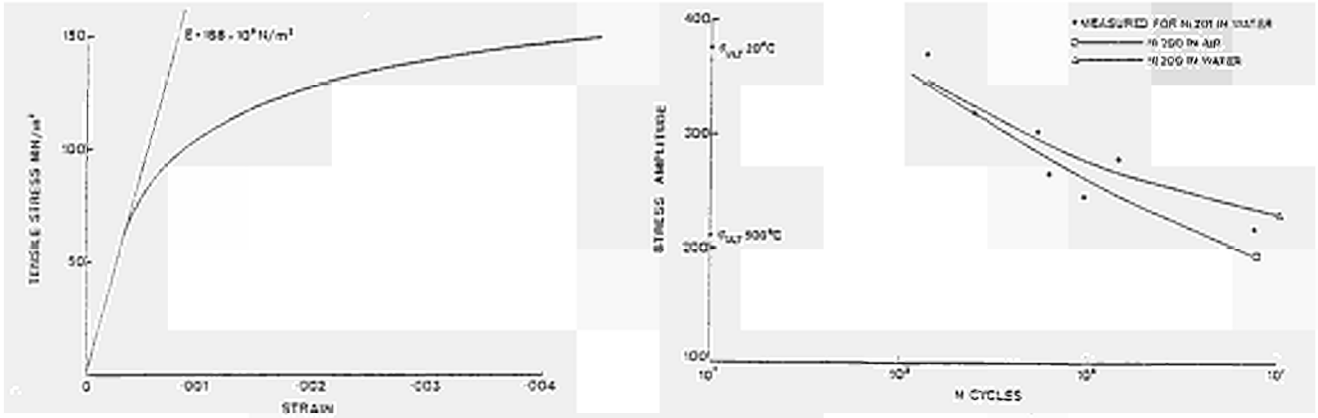

Fig. 4 Tensile and Fatigue Properties of Screen Elements

The 700 mm long bars were gun drilled in 2 passes of 5.02 and 5.00 mm diameter, from one end at an optimized feed rate of 18 mm/min. All drilling was produced within the specified tolerances of 1.0 mm run out over length and straightness of 0.3 mm. Bars were straightened prior to drilling. No drilled bars were rejected.

4. ASSEMBLY

4.1 Element weld

The weld between element and manifold is a critical design area [7]. The weld preparations and procedures have been developed to give in a weld thickness of typically 1.5 mm, and not less than 1 mm on the 1.5 mm wall. Over 100 sample welds of the final geometry have been sectioned and analysed. The resulting weld (Figs 6 and 7) produces a joint withstanding 10 kN axial tension before rupture of the spigot near the weld. In compression the spigot buckles at 20 kN without rupture or failure of weld.

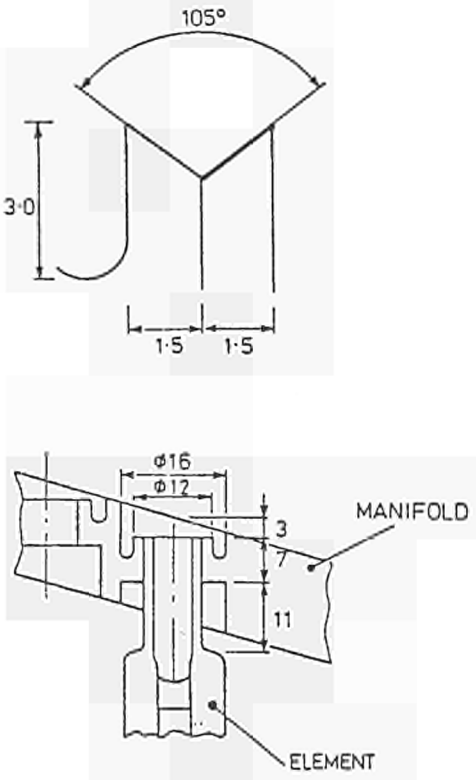

Fig. 6 Element Weld Geometry

Fig. 7 Section of Element Weld

Welding is by hand with DC TIG using Ni 61 filler. Important features of the welding are: the 3 mm castellation of preparation, prior annealing of all material; cleaning immediately prior to welding; deep 'V' preparation.

Some pores are seen but these are not sufficient to affect strength and vacuum integrity is maintained. Pulsed TIG welding with He purge and no filler has been used to produce pore-free welds of typically 0.8 mm thickness. It has been found that the time of the weld run should be maximised, allowing a certain drop off of weld, of up to 0.5 mm, into the tube to produce the largest weld thickness.

Non destructive testing of the weld could only be effectively performed by He leak testing before and after stress relieving and thermal cycling. The manifold shape enables individual leak testing of each weld.

4.2 Proof assembly tests

A short assembly of 5 elements was made to test the design and manufacturing techniques, in particular by cyclic loading to represent the disruptive forces. Initial failure in testing led to the development of improved spigot design, weld preparations and weld procedure.

After drilling, the bars were annealled and machined in a series of operations devised to minimized distortion. Particular attention was paid to the method of clamping. Radiusing the sharp corners at the end of the profiled section was done with electro-discharge machining.

The long profile was formed by cold pressing using tools developed to accommodate spring-back. The elements were finally electropolished.

3.2 Manifolds

The manifolds are also made of nickel to reduce stress in the element weld. They are made of two straight parts, one part machined with weld preparation and the other folded to a V-section. These two parts are then temporarily welded together for rolling to the 2 m radius. The parts are separated for electropolishing and welding of elements.

3.3 Fins

On each side of the screen 87 nickel fins are welded to the manifold. The fins are stamped, grit blasted and coated with a high emissivity Alumina (87%) - Titania (13%) mixture by plasma spraying in low pressure N_2.

3.4 Screen fixing

On each screen are bolted 6 location blocks, electrically isolated from the screen with ceramic cones. The screwed location bolts are made of Nimonic 80A, age hardened and coated with Titanium Nitride by PVD to prevent seizing. If incorrectly assembled these bolts can exert sufficiently large lateral forces on the threads that galling can occur. Tests are continuing with aluminium bronze and titanium alloy bolts.

3.5 RF contacts

The side of the screen is electrically connected to the housing by a series of 55 sprung finger contacts (Fig 5). The contacts have been designed to maximise the DC resistance whilst maintaining good RF contact. The fingers are fabricated in the relatively high resistivity Nimonic 90, which enables the spring to maintain the 10N contact force required at high temperature and to accommodate the differential expansion of housing and screen. Each finger has 5 μm of silver (half skin-depth) electro deposited on the antenna side for the required low RF resistance. It is made in the form of a clip so it can detach itself, during screen removal, if the contact has welded to the housing.

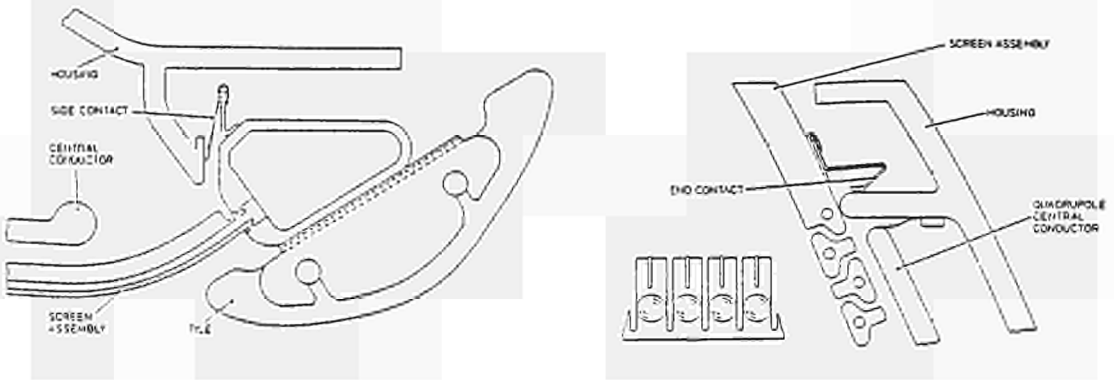

Fig. 5 Detail of Contacts

The end contacts are made to the same specification except high resistance is not required and the fingers are silver plated to 20 μm.

The contacts have been tested at RF currents up to 30A and 60A per contact for the side and end contacts respectively.

The Proof Assembly was centre loaded on each element to 600N with the assembly under 10 bar water pressure. Helium leak testing was performed at 5000 and 10000 cycles. The Proof Assembly successfully withstood this test and also proof pressure testing and 500°C helium leak testing. Deformation of the screen under this loading was measured to be slightly less than predicted by a simple model. This did not allow for non linear plastic behaviour of nickel at low stress levels. The very low notch sensitivity of nickel allows initial yielding to better distribute stresses without crack propagation.

4.3 Assembly procedure

A substantial assembly jig was used to minimise distortion during welding. After welding the elements, and again after welding the manifolds and fins the screen was stress relieved still on this jig at 550°C for 5 hours in 3% H_2/Argon gas. The jig material was stainless steel 310S, the design taking account of the expansion coefficient over the range 10-550°C of 15 10^{-6}/°C compared with 13.3 10^{-6}/°C for nickel.

The jig remained the main dimensional reference throughout assembly. Fins were welded to the manifold referred to the jig, as were the location bolt locations and water feed pipe features.

Pressure proof testing was performed at 20 bar with water. The screen fitted with location bolts was test fitted to a Dummy Housing that represents the features of the real housing. The finished screen was thermally cycled in a vacuum furnace for 10 cycles between 100°C and 500°C. Helium leak testing was performed at 500°C in the final cycle with leak rate of $< 10^{-9}$ mbar li/s. Forced gas cooling of the screen at 50°C per hour was used to accelerate this cycling.

5. RF TESTING

The prototype screen was installed on the prototype antenna in the JET RF Testbed with thermocouples were attached to key points on the screen and antenna.

Initially high voltage testing was performed without cooling. This test was successfully completed with 50 kV pulses of 10 millisec duration. No arcing was seen. The screen temperature profile was monitored using infrared thermography calibration was done using the thermocouples but remains imprecise because of the very high reflectivity of the electropolished nickel. Hot spots are seen on the manifold at a screen gap due to reflections from the hot interior of the antenna. Without cooling, local temperature rises of 80°C are seen. Initial water filling was performed with the screen at 80°C. Cooling of the screen was uniform. This was an important test as water filling on JET will have to be performed frequently.

With water cooling the RF pulse length was increased to 20 secs at 50 kV at the specified duty cycle of 1 shot/10 minutes. The maximum RF power dissipated in the screen was 350 kW at 33 MHz for which screen temperature rises of 90°C were seen at hot spots. The corresponding tile temperature rise was 300°C. A total of about 80 pulses of 20 sec. duration at 42 kV have to date been applied during life tests without failure. These initial test results confirm the design of the screen with regard to both thermal stresses and RF properties.

6. CONCLUSIONS

The water-cooled A_1 Antenna Screens are well into manufacture and will be installed in the major shutdown of JET statring in December 1986 after a rigorous proving of all stages

of design and manufacture. The first screen has been tested, without plasma, and has confirmed design expectations.

7. REFERENCES

[1] J. Jacquinot et al, 11th SOFT Conf. Oxford, UK, (1980)

[2] J. Arbez et al, 4th Int. Symp. on Heating in Toroidal Plasmas, Rome, (1984)

[3] J. Arbez et al, SOFT Conf. Varese, (1984)

[4] F. Sand, 4th Int. Symp. on Heating in Toroidal Plasmas, Rome, (1984)

[5] J. Jacquinot, EPS 12th Eur. Conf. Fusion and Plasma Phys., Budapest, (1985)

[6] J. Jacquinot, Inst. of Phys. 12th Ann. Conf. on Plasma Phys. Glasgow, (1985)

[7] A.S. Kaye, 11th Symposium on Fusion Engineering, Austin, (1985)

8. ACKNOWLEDGMENT

The authors would like to acknowledge the assistance of and many other members of the JET Team in particular P.P. Lallia for the forces analysis and K. Sonnenberg for the fin coating technology. We acknowledge also the contribution of many European manufacturers.

THE JET IN-VESSEL INSPECTION SYSTEM

T Raimondi, R Cusack, L Galbiati
JET Joint Undertaking, Abingdon, Oxfordshire

ABSTRACT

A viewing system was developed for JET so that the interior of the vacuum vessel can be scanned without breaking the vacuum. Four identical TV cameras can be inserted into the vacuum vessel from the top through symmetrically disposed ports of small diameter (~ 60 mm).

To get round the problem of heat from the lamps in a confined space, high energy xenon flash lights are used. The TV raster is recorded immediately after the flash trigger in a high speed digital memory. A new version for inspection at high temperature is being developed.

1. INTRODUCTION

Opening the vacuum vessel to the atmosphere involves a lengthy phase of reconditioning for high vacuum, so a system for inspecting the interior of the vessel without breaking the vacuum seal was required. As penetrations into the Tokamak have to be kept to a minimum, the major constraint on the design was the small size of the ports through which to insert the viewing probes. Four vertical ports of triangular section at the top of the vacuum vessel were allocated. The requirement of preserving the high vacuum meant that all the optical apparatus and mechanisms, as well as the lighting source, had to be contained within a vacuum-tight viewing probe of 54 mm diameter. The large volume of the vacuum vessel which had to be inspected from only four penetrations required high intensity lighting. This posed a severe problem of heat dissipation in the confined space of the viewing probe. The four identical probes of the In-Vessel Inspection System (IVIS) (fig 1), fitted at the beginning of 1984, have since been used successfully.

2. SYSTEM DESCRIPTION (Figs 1 and 2)

Each probe consists of a stainless steel tube terminating in a glass cylinder. The viewing probe is lowered into the vessel by a carriage driven along a guide unit which is suspended from the magnetic limb by means of a gimbal arrangement and centered with the top of the port using a hinge connection. This method of suspension allows the guide unit to comply with thermal deformations of the vessel. The viewing probe itself is centered with the top of the port by flexible phosphor-bronze "fingers" to allow self alignment of the

probe during insertion and reduce shocks due to vibrations of the port. Long vertical bellows, with 6:1 compressions ratio, allow for the vertical stroke of the carriage while forming a vacuum barrier. A separation valve between guide unit and vacuum vessel is opened to insert the viewing probe after checking that the vacuum in the IVIS system matches that of the vacuum vessel.

A high-sensitivity black and white camera is situated at the lower end of the viewing probe. Otherwise relay lenses would be needed to transmit the image along the probe itself resulting in optical losses. Tilt and rotation of a prism in the glass viewing cylinder allows a whole quadrant of the vessel to be explored from any of the viewing positions.

2.1. Suspension method and alignment

Alignment of the guide unit to the port is very important as clearances between viewing tube and port are small, in the region of 1 mm. Therefore before insertion a survey of the relative angle between guide unit and port has to be done, and the position of the hinge point has to be adjusted if necessary, to limit the misalignment to ± 10 minutes. A remote readout of the misalignment has now been implemented in both tangential and radial directions and it has been seen that no readjustment is usually needed.

2.2. Bellows assembly

Bellows 3.2 m in length and edge welded with a compression ratio of approximately 6:1 have been used. Due to the weight of the bellows it was found to be necessary to build in a support system to limit the stretching of the top convolution. The bellows are divided into three sections each being limited to a predetermined length; this is achieved by using stainless steel tapes with a built-in stop. Each tape is attached to a return spring, so that when the bellows are compressed the spring will rewind the tape into a parked position.

In the compressed situation the bellows, shaped in corrugated discs, nest into one another. Calculations led us to choose the following parameters:

Outer diameter	:108.8 mm
Inner diameter	: 64 mm
Thickness	: 0.2 mm
Weight	: 20 kg
Maximum elastic stretching per convolution	: 3.9 mm
Maximum stretching of the top convolution of any of the 3 sections	: 3.7 mm

The bellows were cycled in representative conditions to check that no permanent deformation was occurring.

2.3. Glass cylinders and optics (Fig 3)

The glass chosen was a borosilicate (trade name Kodial) ground and welded to the steel through an intermediate KOVAR collar whose thermal expansion characteristics are compatible with those of the glass.

After an accident to one of the cylinders during a commissioning insertion, a steel cap held in place by pretensioned rods was added to protect them. The rods are thin enough not to impair vision.

The distortion introduced with the viewing cylinder is compensated by a cylindrical lens, rotating with the assembly. A zoom lens, specially designed to fit the small diameter, consists of conventional lenses telescopically operated through thin cylinders by actuators located behind the camera (fig 3). The field of viewing ranges from 20°, to embrace a recognisable portion of the vacuum vessel wall, down to 4° to achieve the required resolution, of approximately 2 mm at 5 mt distance.

In these conditions the aperture is limited to 1:11 and severe problems of heat dissipation are encountered since intense light sources are needed and can only be located in the small volume underneath the telecamera. For these reasons, high energy xenon flash lights (500 joule) were used. The TV raster is recorded immediately after the flash trigger with high speed digital memories, known as "frame grabbers", which are also convenient for image analysis and enhancement. Single frames are recorded every few seconds. Glaring reflections from the wall under certain angles can be avoided by reorienting the reflectors or varying the light energy. Internal reflections in the viewing cylinders are avoided by using one telecamera while flash light is provided from the other cylinders.

Due to the very short duration of the flash light (1 to 2 m/sec) it is not possible to adjust the angular position of the optical axis, zoom, focus, iris and light orientation. Therefore all the co-ordinates of the optical axis and optical parameters, optimised during the tests, are repeated automatically for various angles of viewing. This also allows simplified inspection routines by using a pre-recorded library of positions.

A very small, ϕ 32 mm, black and white camera is used for each viewing probe. The camera is equipped with a Newvicon pick-up tube which is capable of providing a high resolution television picture. A usable picture can be obtained with a face plate illumination as low as 0.1 lux. The Newvicon face plate can withstand high power lighting (10,000 lux) without any damage, and therefore lends itself to using a high energy flash as a light source.

2.4. Control aspects

The following movements are needed for each probe : focus zoom, iris, tilt, reflector, rotation, vertical stroke. Miniature dc motors and incremental encoders for maximum compactness are used within the probe with recirculating ball screws for the linear motions Limit switches provide a reference position.

The movements are controlled by on/off servomechanisms which apply preselected constant voltages to the motors, automatically stepped down at preset thresholds of the position errors as the input reference position signal is approached. Four levels of voltage are used, to obtain a time response and precision comparable to a linear rate control system, which would have entailed use of tachometers. The level of flash energy can also be preset.

2.5. Operation

The co-ordinates of the optical mechanism positions, including the light orientation and level of flash energy, optimised during the tests, are stored in the host computer in the form of "named positions" which identify the various areas of the vessel with significant abbreviations.

For example:

Feature	Octant	Sector	
Lim (limiter)	2	D	→ LIM 2/D

Each movement can also be controlled by a joystick, allocated via a touch panel, or by keyboarding the desired co-ordinate.

After calling a named position, a trial and error adjustment of the focus value is however necessary due to the insufficient repeatability of the reference position. This tiresome procedure can be alleviated by taking all the pictures from the same camera consecutively, since the correction of the focus is the same. Some adjustment of lighting conditions may also be needed from one campaign to the next because of variation of reflectivity of the surface. Initially very bright, the vessel has in fact been carbonised with some shiny and some "matt" areas. These dramatic variations of light intensity and glares are the cause of major difficulties in this type of inspection. With good lighting the quality of the pictures is quite satisfactory (fig 4).

3. ENHANCEMENT PROGRAMME

3.1 The inner part of the vessel is now very dark since it is carbonised and does not receive direct light.

Even increasing the sensitivity by integrating successive flashes, the image remains hazy because direct light impinging on the viewing glass is scattered inside it. Presently a modified version of the glass cylinder is being tested, in which the xenon flash is in a chamber separated from the camera so that it can be used with its own camera to throw its direct light onto the inside wall.

3.2 The present system is designed to operate at 50°C. The cooling and re-heating of the vessel, together with a partial loss of the conditioning entail a down time which one would like to avoid. A version of the IVIS able to inspect at 300°C is being developed. Preliminary calculations and tests indicate that a water cooling jacket is feasible and thermal stresses in the glass cylinder in the region of the 0.4 kg/mm² would be acceptable. Fatigue tests are being carried out.

To make room for the cooling jacket we shall have to eliminate the zoom mechanism. The resolution obtained should be sufficient for routine inspection. When higher resolution is needed, a "cold" campaign with the present system will have to be done.

As an alternative we considered using a number of relay lenses along the viewing probe so that the camera could be located outside. This would have permitted use of a magnifying lens at the eyepiece end and of an image intensifier. However the resolution achievable was so poor, due to the number of relay lenses required, that this made such a solution unworkable.

3.3 Enhancement of the images is achieved using the crystal device, produced by Quantel, that stores in its RAM a complete digitised picture with a resolution of 512 x 512 pixels and 256 grey levels. Several digital filters are available. Particularly important is the "antiflickering" filter which averages out successive lines from two interlaced frames, the second of which is weaker in intensity.

3.4 In DT operation, the glass cylinder would be blackened by a radiation dose of 10^8 rad. Tests done by ENEA-Rome have shown that transparency is restored to 80% when the borosilicate glass is submitted to heating cycles above 250°C. The TV camera is designed to resist 10^4 rad. The objective lenses cannot be heated as they are in the cooling jacket. If we wish to leave the viewing probe permanently on the machine to save time in frequent inspections the lenses will have to be remade in radiation-resistant glass.

4. ACKNOWLEDGEMENTS

Important contributions are acknowledged from:
Prof W Welford of Imperial College London, for the optics design; H Watson and R Govier of Culham Laboratory for the glass techniques; E Gebler (JET) for the electronics and computer interfaces; P Presle (JET) for the alignment procedures.

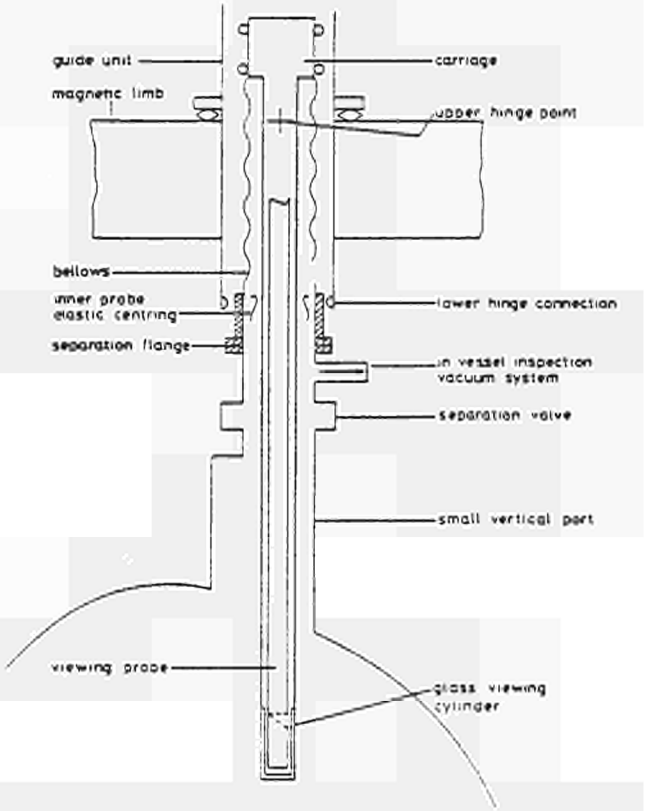

Fig 1 Schematic diagram of inspection system

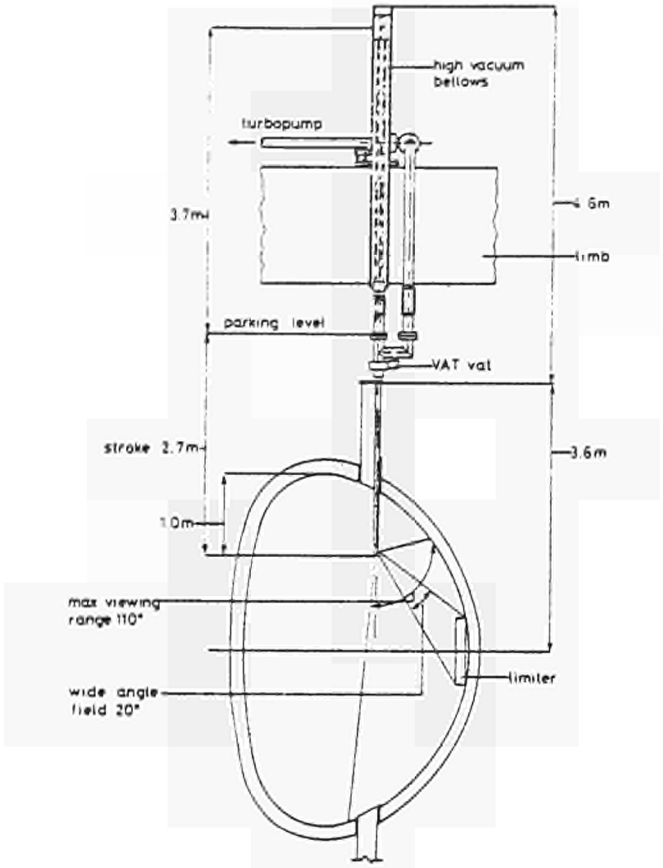

Fig 2 Layout of the system

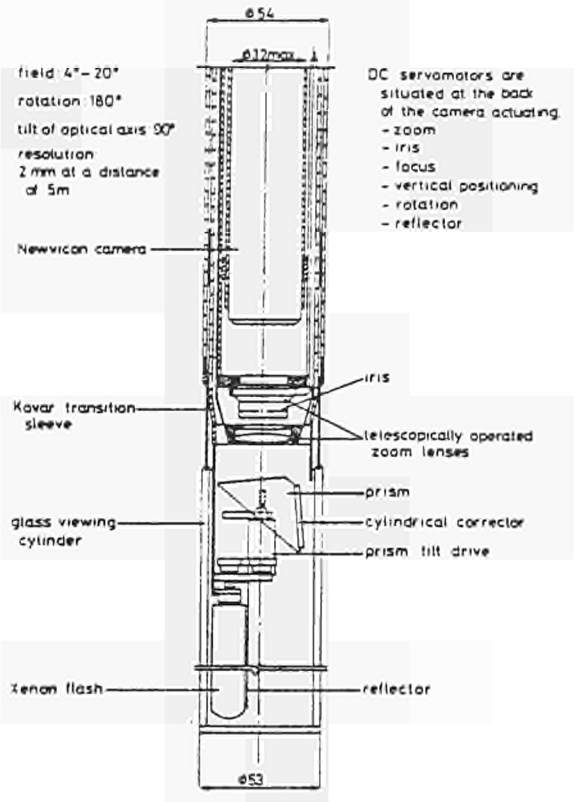

Fig 3 Viewing probe

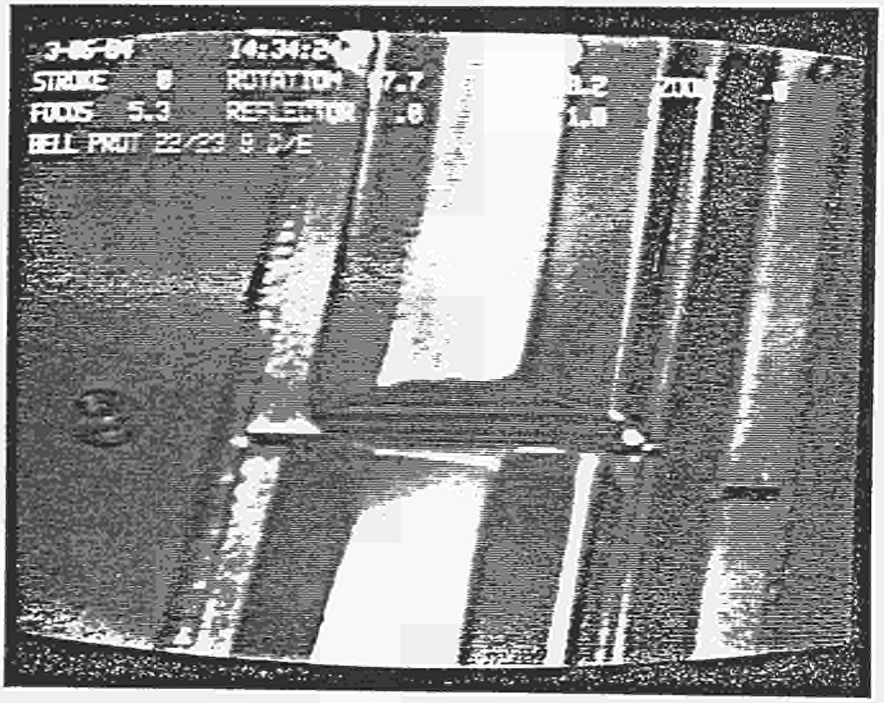

Fig 4 Image of bellows protecting plate with named position and parameters

REMOTE HANDLING TOOLS FOR JET

M Wykes
JET Joint Undertaking, Abingdon, Oxfordshire

ABSTRACT

Hands-on maintenance of the JET machine includes personnel using tools to perform tasks. For remote maintenance, these tasks will be performed by servomanipulators using tools having the same functional requirements as the corresponding hands-on tools, but with simpler handling requirements to reflect the reduced dexterity of servomanipulators as compared to human operators.

Many of the remote handling tools that will be ultimately required for JET have now been designed and procured. They will be extensively used by personnel during the JET 1986/87 shutdown to prove their functional adequacy when operating with actual JET components. This poster describes five typical remote handling tools presently being prepared for shutdown service.

1. ϕ50 EXTERNAL ORBITAL TIG WELDING TOOL

This tool has been specifically designed to perform the connecting welds in the cooling water pipework of the JET toroidal limiters and A1 RF antennae. The pipe material in Inconel 600 with an outside diameter of 50mm and a wall thickness of 2.5mm. The pipe ends are square faced and are TIG welded without additional filler material. Access to the joints is restricted and no proprietory welding tool was available to fit into the 23mm radial clearance and 45mm axial space. There are 96 welds of this style used on JET. The welding tool is shown in Fig. 1.

The water cooled electrode holder is housed in a "Syalon" ceramic arm which articulates on the orbiting ring gear. This articulation accommodates irregularities of pipe diameter and maintains a constant arc length. The ring gear has a side cut-out to allow it to be placed and rotated coaxially with the weld joint. To maintain a continuous drive to the ring gear, two input worm gears are simultaneously driven from a pair of bevel gears, driven in turn by a single motor.

Accurate location of the tool is achieved through a machined trapezoidal section ring which forms part of the weldment.

The tool is hydraulically clamped to this ring which ensures that the tool is supported square to, and the electrode is aligned with, the joint line. The clamping mechanism also ensures that the halves of the joint are aligned coaxially.

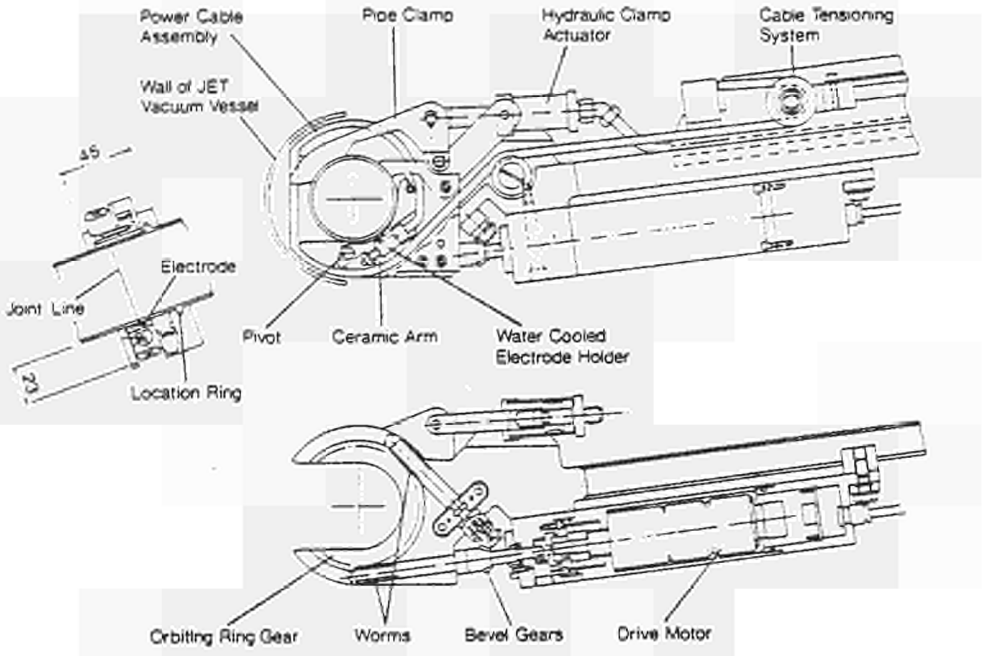

Fig.1 φ50 external orbital TIG welding tool

Welding power and shielding gas are transmitted to the orbiting weld head by means of a water cooled cable assembly. The copper cable is 2mm² in cross section and is fitted inside a silicone rubber hose conveying the cooling water. The cable assembly is maintained under a small tensile load to ensure that it winds onto and off the orbiting head in an orderly manner.

2. CUTTING TOOL FOR INTERNAL FILLET WELDS

JET standard internal fillet welded joints consist of two concentric sleeves, one inside the other. The inner sleeve, which has a remote handling groove, is recessed into the outer sleeve, this recess accommodating an internal fillet weld between the sleeves. This type of remote handling joint is used on JET vacuum windows, port plugs and toroidal limiter bellows sleeve assemblies. A family of remote handling cutting tools has been designed to cut away the internal fillet welds thereby enabling separation of the sleeves.

A sectional view of a typical cutting tool is shown in Fig. 2.

The single point cutting bit orbits at a constant presetable speed. Automatic axial feed is achieved by a lead screw driven by the orbital drive through auxilliary gearing. The feed and orbit motions can be decoupled by a pneumatic clutch to allow fast axial prepositioning of the cutting bit.

The cutting tool is secured to the weldment by three fingers which are pushed into the remote handling groove by a water-hydraulic actuated pushrod.

The cutting speed and axial feed rate have been optimised such that cuts are made in Inconel 600 material without lubricant or coolant. The cutting zone is completely enveloped by a shroud which is evacuated by a vacuum line. The cutting bit has a chip breaker so that all material off-cuts are small enough to be sucked from the shroud and captured. The power unit is a proprietory electric drive motor which has dynamic closed-loop control of orbital speed.

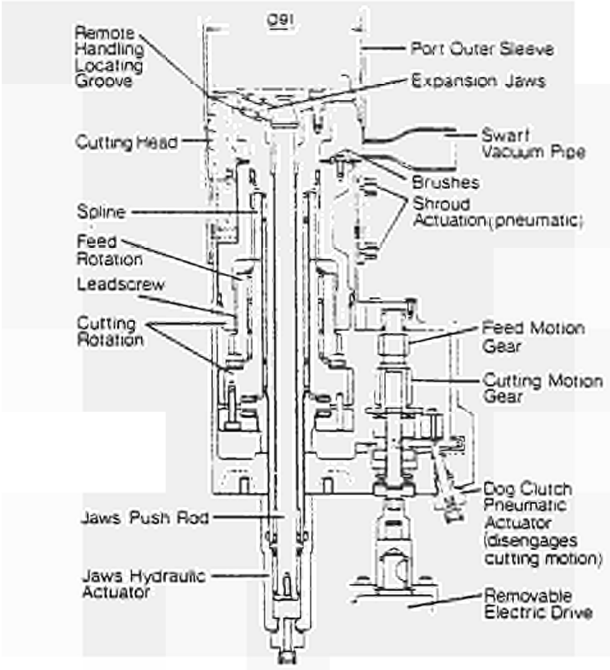

Fig.2 Cutting tool for internal fillet welds

3. WATER HYDRAULIC PIPE EXPANSION TOOLS

For remote handling of the inner and outer sleeved elements of JET standard internal fillet welded joints, there must be sufficient clearance between the elements to compensate for all the effects of tolerances and welding distortion and allow easy insertion. In practice this results in gaps between the assembled sleeve elements which are too large to weld without using excessive filler material and heat input. In order to reduce the gaps prior to welding, a family of remote handling tools is used to locally expand the mouths of the various sizes of inner sleeve elements. Fig.3 shows a sectional view of a typical water hydraulic expansion tool used on all vacuum windows and toroidal limiter bellows sleeve assemblies in the JET vacuum vessel.

The head end of the tool contains pawls which move radially to engage with the inner sleeve remote handling groove when the pawl lever is rotated through 90°. The double-acting piston, which is actuated by distilled water at 200 Bar, displaces the ramp ring axially. This results in a radial motion of the collet segments with considerable force amplification due to the small ramp ring angle. Since the collet segments bear against the tool head, most of the end thrust is reacted within the tool. The amount by which the inner sleeve is recessed into the outer is determined by the stop-collar, the axial position of which can be adjusted using the stop-collar lever.

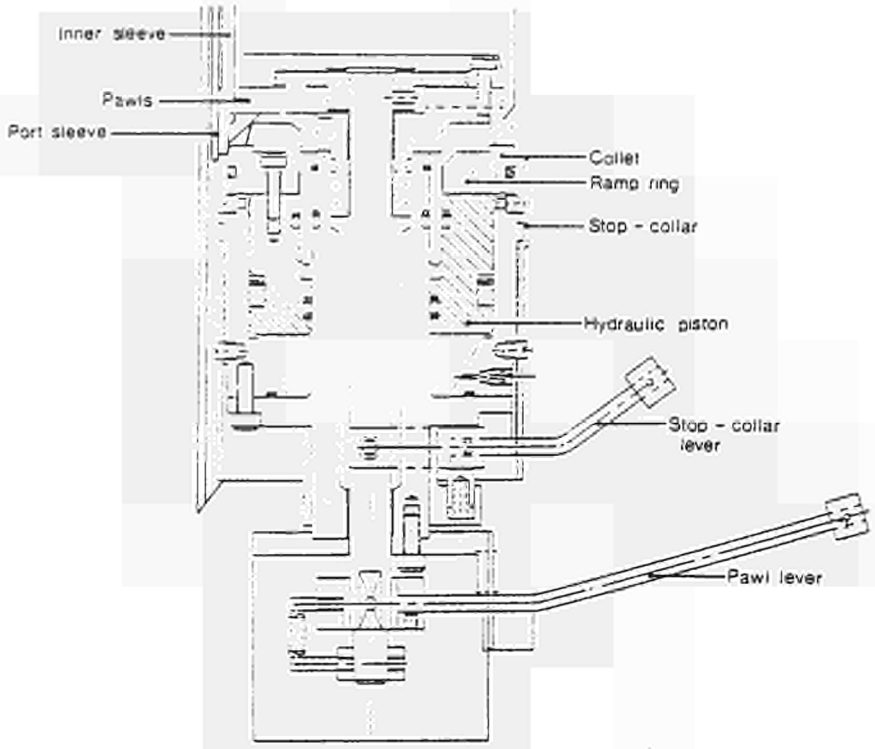

Fig.3 Water hydraulic pipe expansion tool

4. HANDLING TOOL FOR TOROIDAL LIMITER BELLOWS

The toroidal limiter φ50 water supply pipes contain bellows, both to accommodate thermal expansion during operation and to allow displacement of the pipes during remote handling. A tool is required to effect this displacement, which is ±8mm about the free position. The tool is shown in Fig.4.

The leading portion of the tool is in the form of a jaw which fits around the water pipe. The tool is secured to the bellows sleeve assembly by two latches which engage with the remote handling groove. These latches are displaced by a drive plate running in a slideway in the body. Latching is achieved by rotating the latch drive actuator 30°, which disengages a peg from a detent. The two drive springs push the latches into the remote handling groove.

The tool is secured to the water pipe through two trunnions welded to the pipe. Two lead-screwed jaws are engaged with the trunnions by rotating the tool 22° about the pipe axis. The lead-screws run in trapped nuts onto each of which a spur gear wheel is cut. Two spur gear trains connect each geared nut with a common drive wheel. The two pinions which connect with the common gear wheel contain cone clutches so that the tool can accommodate planarity errors between abutting pipes.

The common gear wheel is driven through a bevel gear set and a chain drive. The bellows are displaced by rotating the jaw drive actuator, which contains a clutch to prevent overloading of the mechanism.

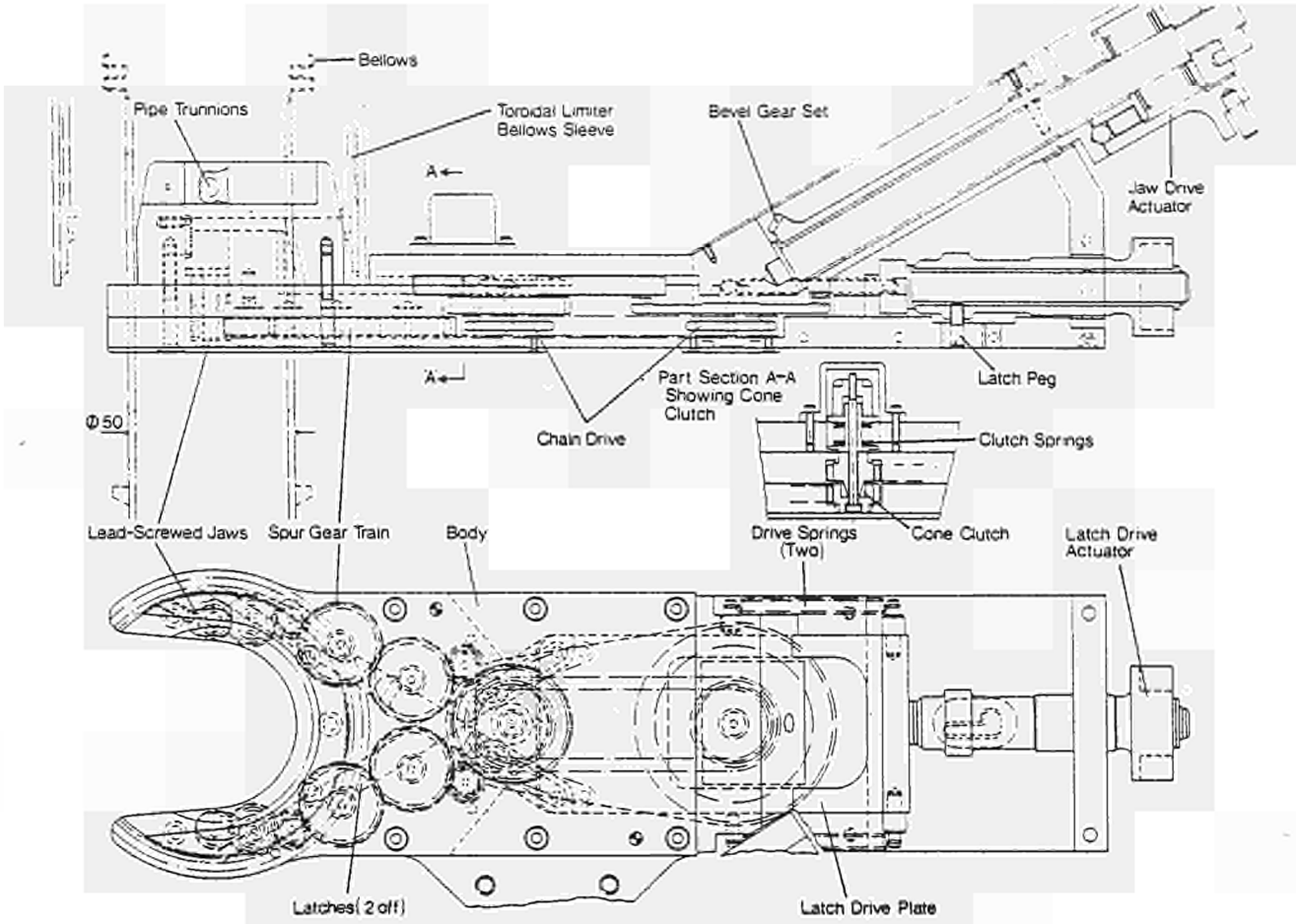

Fig.4 Handling tool for toroidal limiter bellows

5. TOROIDAL LIMITER TILE HANDLING TOOLS

The protective tiles of the toroidal limiters are assembled to their mating fins in pairs. Each tile pair has two locking mechanisms containing disc springs which force the tiles together onto the intervening fin. These disc springs have to be compressed and the tiles separated by a certain amount before the tiles can handled on to or off the fins. Fig. 5 shows the remote handling tool used for this operation.

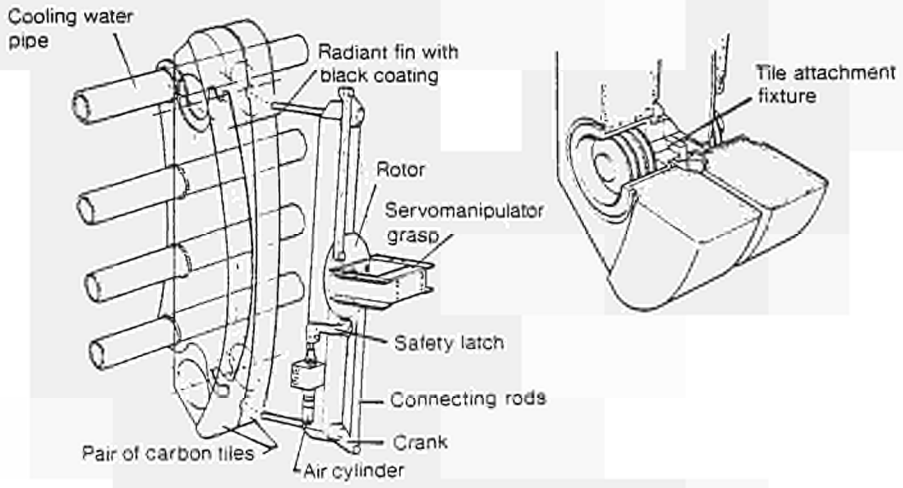

Fig 5 Toroidal limiter tile handling tool

The tool consists of two prongs mounted in and free to rotate within the tool body. The prongs have cranks which are driven by a rotor through two connecting rods. The extent of the rotor, and hence the prong, rotation is governed by the pneumatically actuated safety latch.

During operation the tool is grasped by the tongs of a servomanipulator and the prongs guided between grooves cut into the inner tile faces. By rotating the prongs the tile pack opens sufficiently to allow assembly to the fins. When the lower prong is correctly located in the fin slot, the tile pair is in the appropriate position to be secured onto the fins by the locking mechanism. The upper prong ensures parallel separation of the tile pair.

6. ACKNOWLEDGEMENTS

The author would like to acknowledge S F Mills, J Schreibmaier and A Tesini who have contributed in equal measure to the work reported herein.

OPERATION OF THE MAGNET POWER SUPPLIES.

RELIABILITY AND IMPROVEMENTS

M.Huart, A.Moissonnier, T.Eriksson, C.Raymond

JET Joint Undertaking, Abingdon, Oxfordshire, UK.

ABSTRACT

The JET Magnet Power Supply Scheme includes a combination of flywheel generator-diode rectifiers and mains driven transformer-thyristor rectifiers for the supply of energy to the coils and a switching network with air blast circuit breakers and commutating resistors for inducing the high voltage required for the plasma initiation.

They have now been in operation for three years. During this period, a set of information on the reliability of various power supply equipments under pulsed operation has been obtained.

For each equipment is given a list of faults, indicating potential weaknesses, as well as the remedies and the improvements that have been applied. The Magnet Power Supplies have at present, on average, 6-8 different faults per week with approximately three of them leading to loss of operating time.

1. INTRODUCTION

The JET Magnet Power Supply Scheme consists of two sets of dedicated power supplies to feed energy respectively to the Poloidal Field Coils and to the Toroidal Field Coils. The circuits are shown diagramatically on fig. 1 and fig. 2. The components of these circuits have been described in other papers [1], [2], [3], [4], [5].

The Flywheel-Generators, the Ohmic Heating Switching Network and Stage I of the Transformer-Thyristor Rectifiers started operation on the JET Tokamak in June 1983. The Stage II of these equipments, which corresponds to the duplication of Stage I, started operation in June 1984.

2. ORGANISATION OF THE OPERATION AND MAINTENANCE

The operation of the JET Tokamak is carried out in two shifts since February 1985. The period between major shutdown (~ 12 months) is divided among operation week, maintenance week and commissioning week.

A period of six operation weeks is followed by one week of maintenance and one week of commissioning.

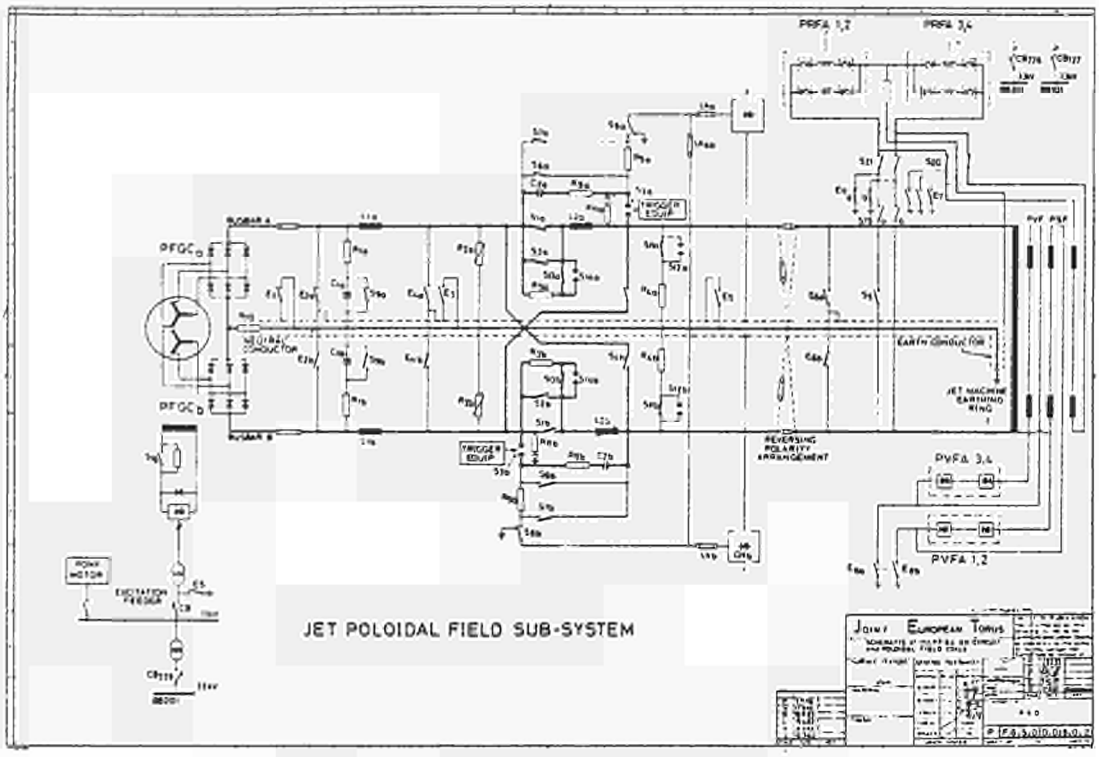

Fig. 1: JET Poloidal Field System

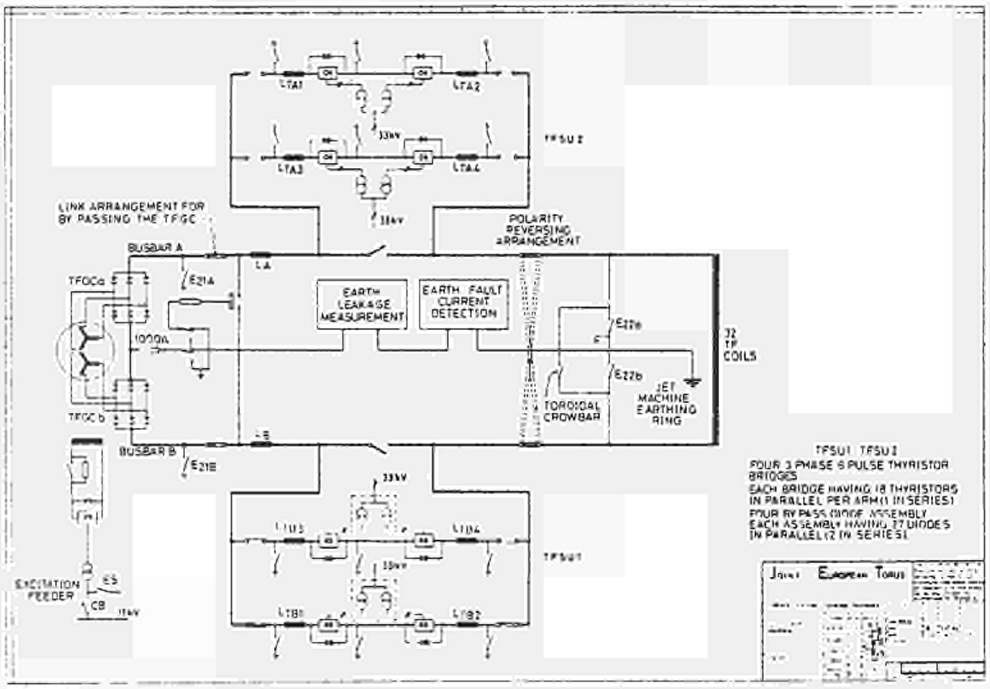

Fig. 2: JET Toroidal Field System

The operation week is divided as follows. The Monday is dedicated to commissioning, the early shift to the machine and the late shift to the diagnostics (with plasma). The Tokamak operation takes place from Tuesday to Friday in two eight hour shifts. The Saturday is a maintenance day. The weekly maintenance is mainly dedicated to routine maintenance and some repair. The maintenance week is used for more extensive routine maintenance as well as trouble shooting, repair of faults and introduce improvements. Annual overhaul of equipments takes place during the major shutdowns of the JET Tokamak.

A centralised and systematic system of recording operation faults in the magnet power supplies has been introduced in February 1985. The records are taken in the Central Control Room by the Power Supply Operation Engineer. These records consist mainly of identification of the system affected and the alarm message received in the control room. They are supplemented by fault reports written by the Site Technician, if an intervention on the equipment has been made.

The records are then transferred to the maintenance team who will investigate the fault in collabration with the various responsible officers and decide upon a replacement, modification of design or alteration in the maintenance procedures.

3. STATISTICS OF FAULTS

The statistics of failures in the magnet power supplies have been grouped in three systems, namely the Ohmic Heating Switching Network, the Flywheel-Generator-Convertors and the Transformer-Thyristor Rectifiers. The later system includes the Toroidal Field Static Units, the Poloidal Vertical Field Amplifiers and the Poloidal Radial Field Amplifiers.

The data have been presented in the following way.

The fault distribution is given in pie-chart for two periods of 15 operation weeks in 1985 and in 1986 to indicate the progress achieved and the most troublesome components (fig. 3, 5 and 7). The failures are then analysed in terms of their cause (component, connection, interference, etc) and in terms of the function affected (monitoring, control, protection, etc). (fig. 4, 6 and 8).

A list of components is then given with their weakness and the remedy applied (tables 1, 2, 3).

3.1 The Ohmic Heating Switching Network

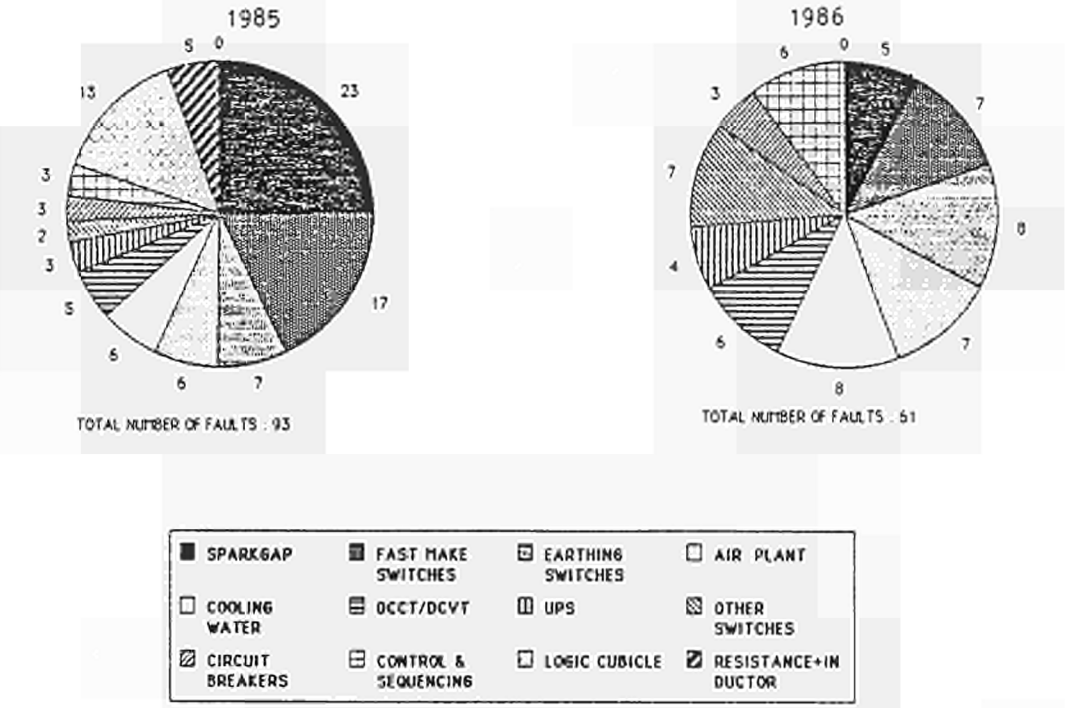

Fig. 3: Distribution of Faults (1985, 1986)

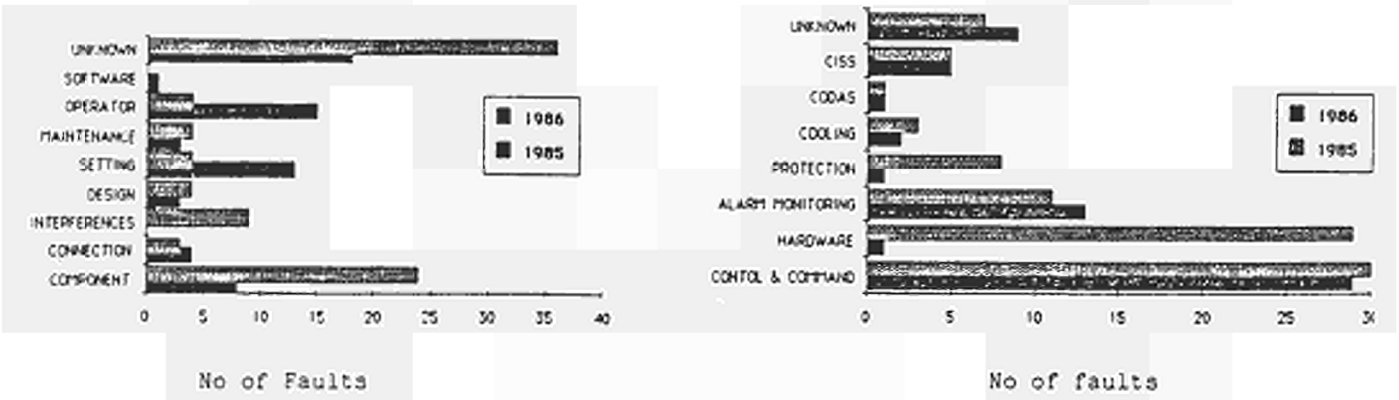

Fig. 4: Fault Analysis

Table 1: Weakness, Remedy

Item	Weakness	Remedy
Sparkgap	mechanical drive	shaft pinned and spring softened
Capacitor bank	control	increase immunity to noise
Fast Make Switch	interlocking ring fracture	changed regularly
Cooling water	sensitivity of flow detector to dirt	change to venturi type
DCCT/DCVT	receiver subject to drift	redesign under progress
UPS	commutation failures	simplify design
Other switches	reliability of control	
Circuit breakers	air leak leading to loss of control	design modification and regular maintenance
Protection logic	spurious intervention	increase immunity to noise
Earthing switches	mechanical drive	shaft pinned, tolerance tightened

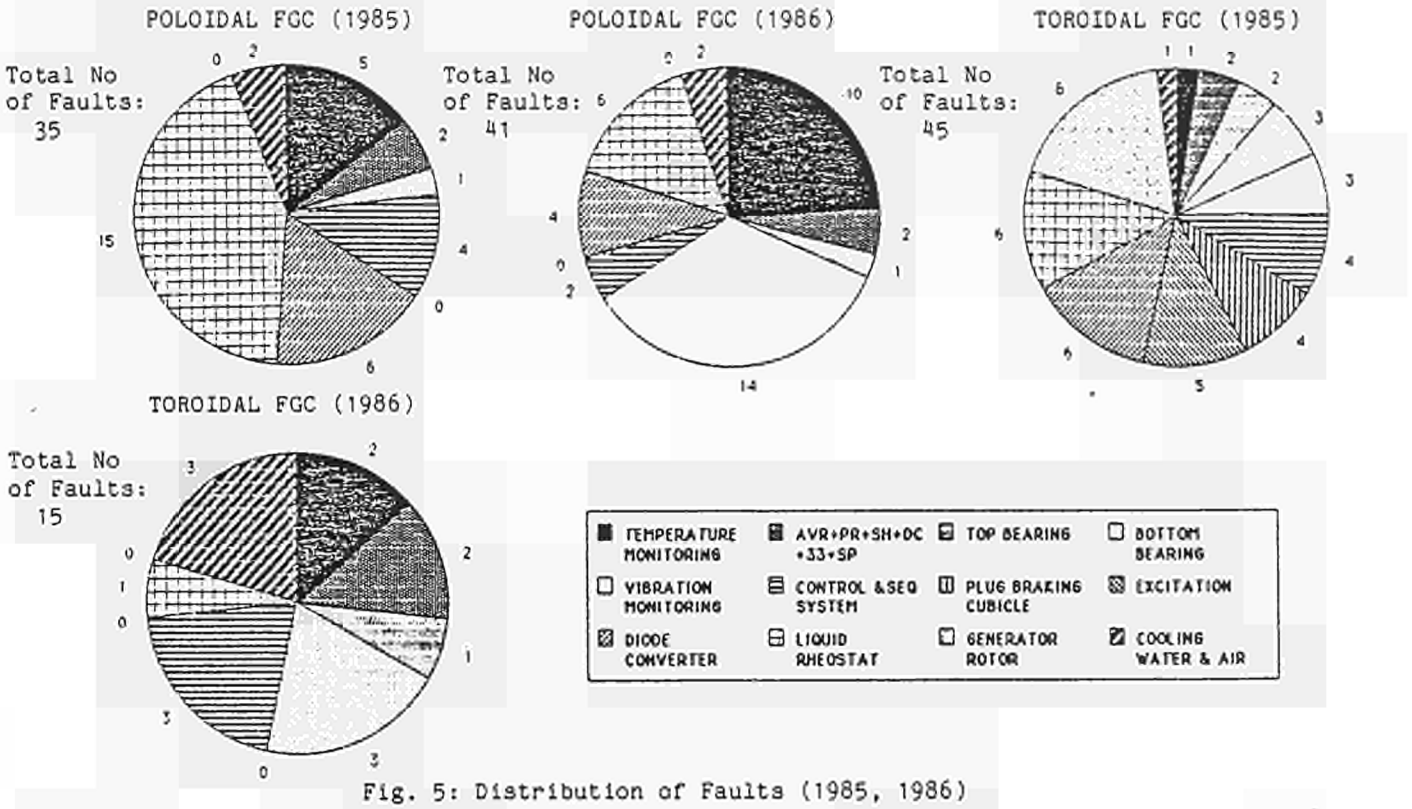

Fig. 5: Distribution of Faults (1985, 1986)

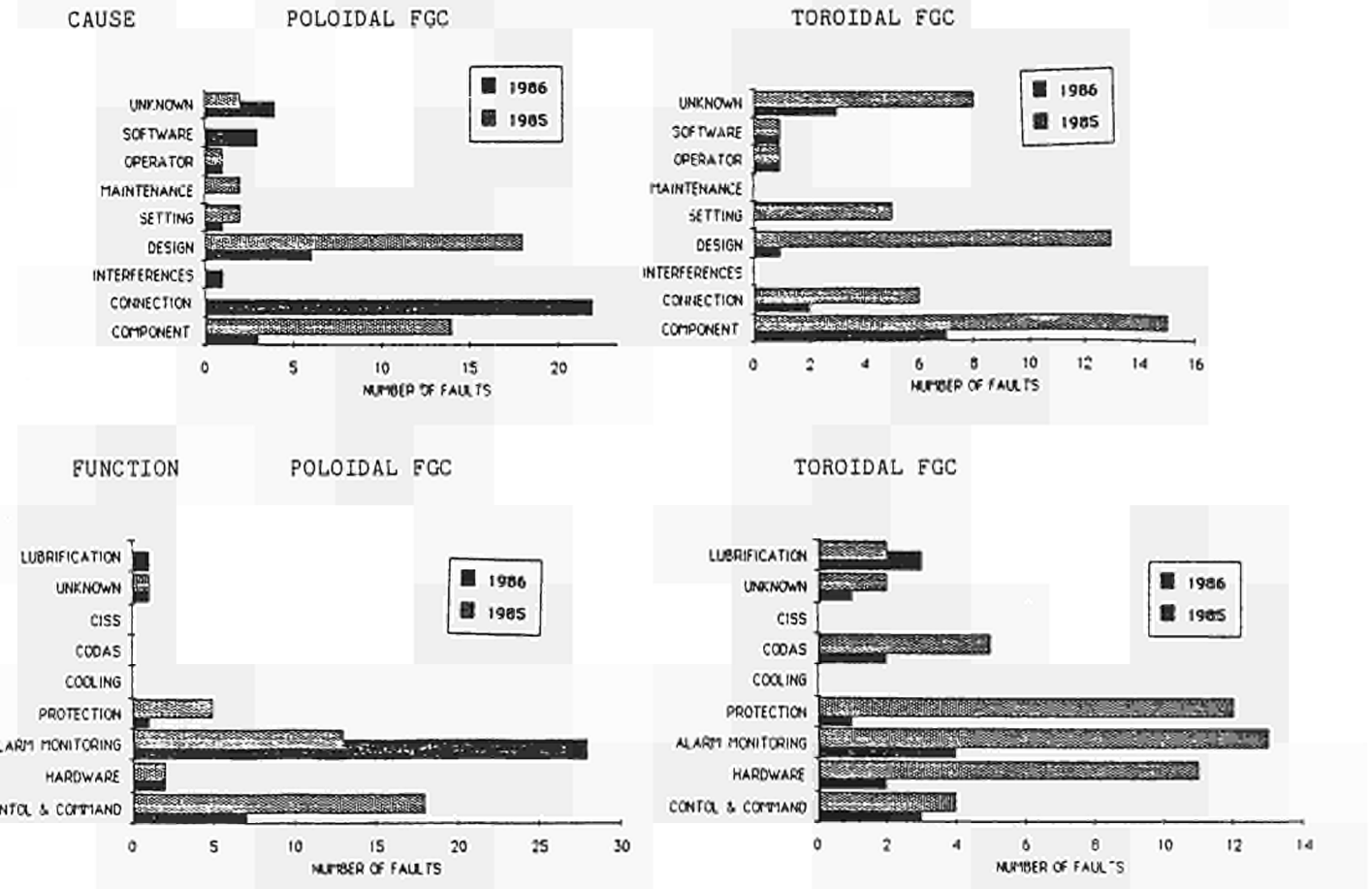

Fig. 6: Fault Analysis

Table 2: Weakness, Remedy		
Item	Weakness	Remedy
Generator rotor	wear of low friction material	Regular balacing run and yearly change
Liquid rheostat	hydraulic drive	change type of servo valves
Diode convertor	spurious alarms	software modification
Excitation	fuse and fuse holder	changed for appropriate type
Plug breaking	mechanical weakness of isolator switches	modify design
Vibration monitoring	poor connection	new termination and wiring
Bottom bearing	oil level measurement L.P. oil pump starter	regular calibration change relay
Temperature monitoring	poor connection	new termination and wiring

3.3 The Transformer Thyristor Rectifiers

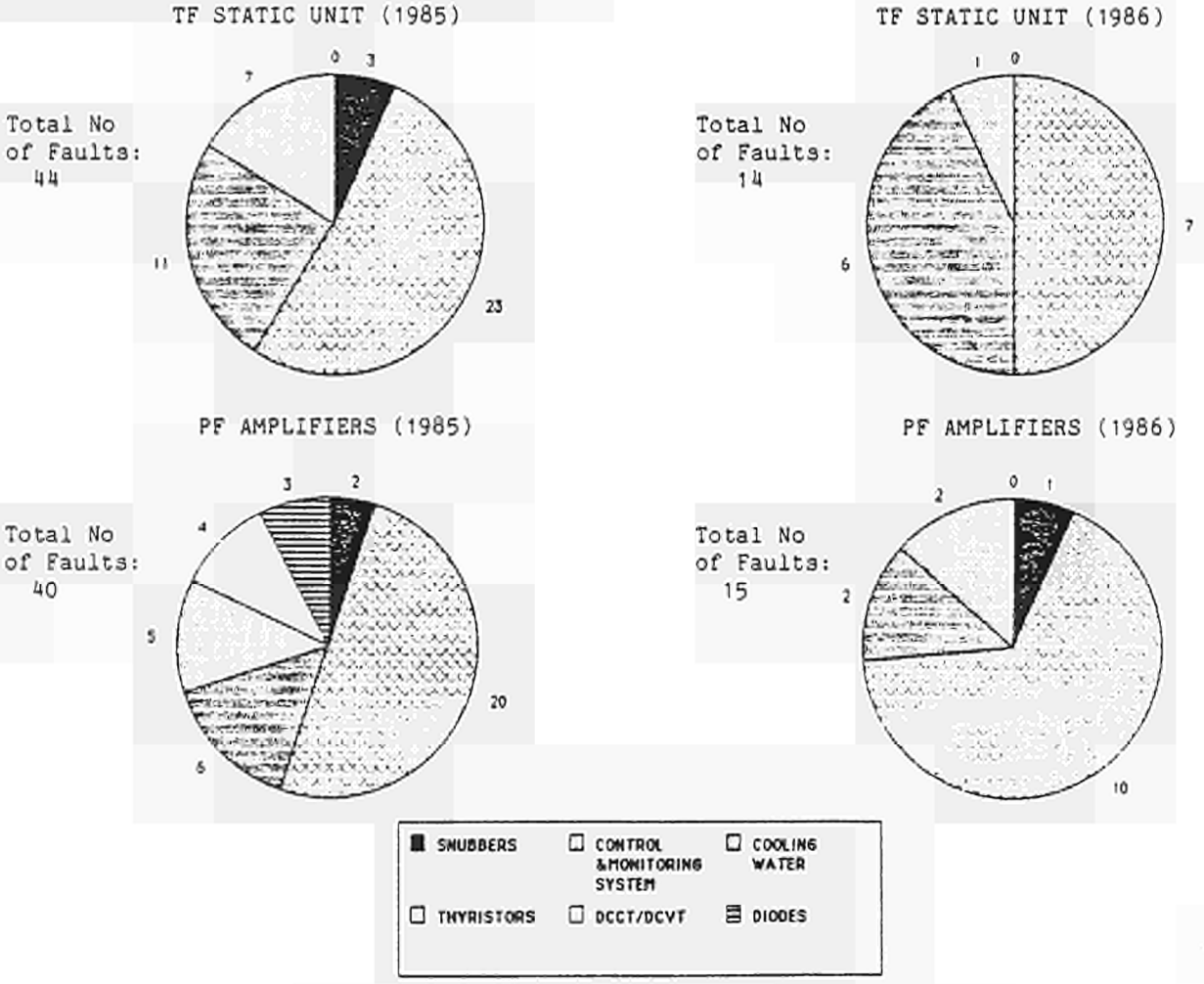

Fig. 7: Distribution of Faults (1985, 1986)

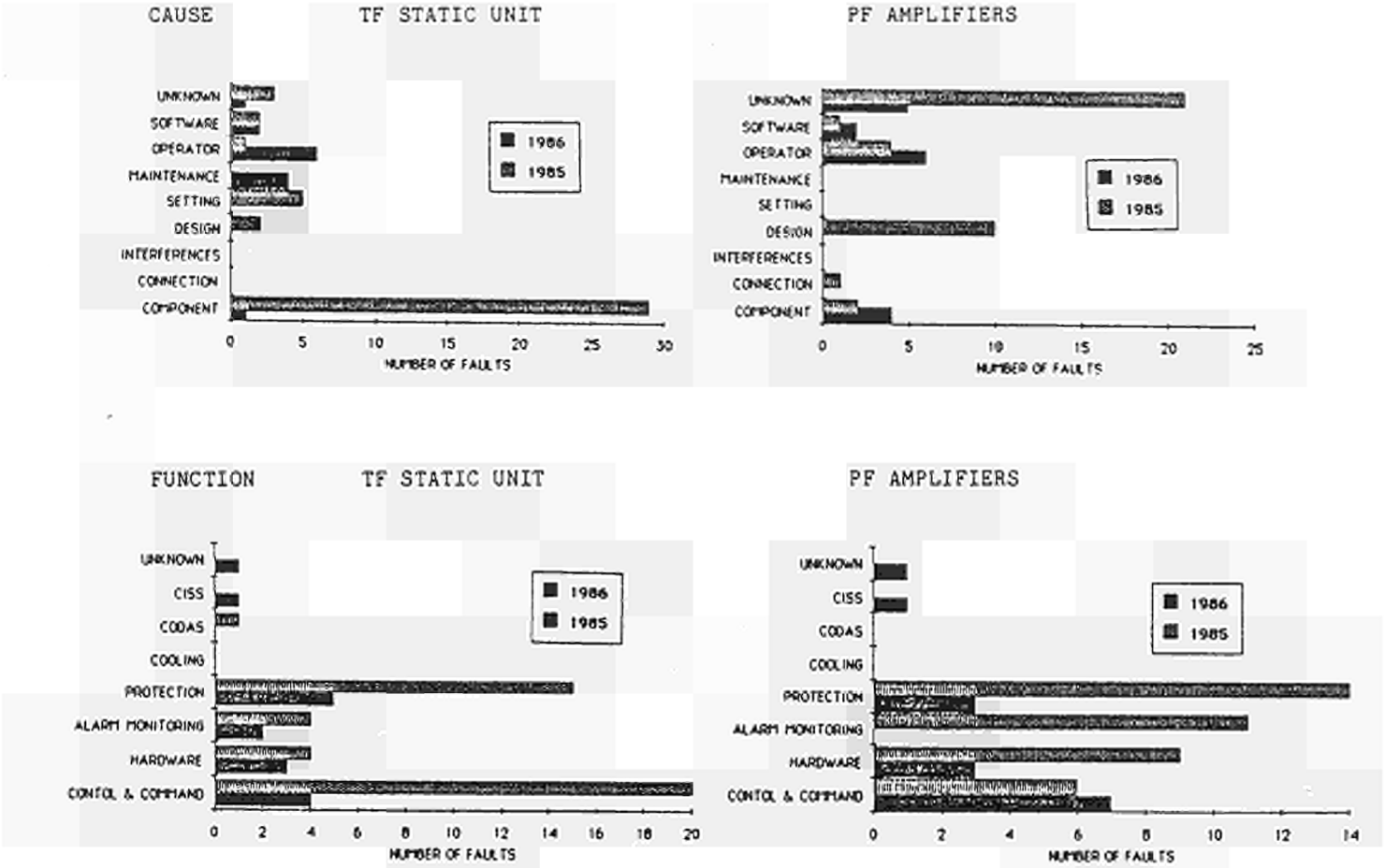

Fig. 8 Fault Analysis

Table 3: Weakness, Remedy

Item	Weakness	Remedy
Snubber circuit	Diode failure	Change to fast recovery type
Control and monitoring systems	Complexity (overall 2000 electronic cards)	Yearly tests
Cooling systems	Sensitivity to foreign material	- flush water circuit regularly - modification of design under review
Blocking diodes	voltage distribution during blocking	regular check

4. CONCLUSION

The introduction of a systematic system of fault recording, analysis and improvements has lead to the improvement of the reliability of the JET Magnet Power Supplies. On average, a reduction of 32% of the number of faults has been achieved in the period 1985-1986 (see fig. 9).

The analysis of the faults shows that the faults on the protection system and high power hardware have been reduced considerably through regular maintenance/testing and design improvements.

The faults on the control and monitoring systems have not benefited to the same extent. For these systems, which are largely relying on electronics, careful selection of components, control of the manufacturing process, (soldering, handling of static sensitive devices), and extensive testing (immunity test for interference, running tests under elevated temperature) need to be carried out at the procurement stage. This is now being implemented for new contracts.

A large number of faults were caused by poor connections. In this instance careful specifications of the type of connections to be used is recommended.

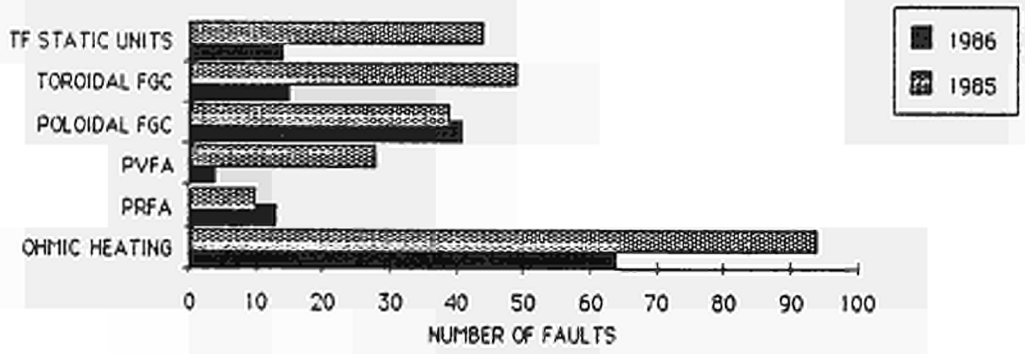

Fig. 9: Global Fault Distribution

5. REFERENCES

[1] M. Huart, E. Beedham, "LARGE FLYWHEEL GENERATOR DIODE CONVERTOR FOR THE JET TOKAMAK", Proceedings of 11th Symposium on Fusion Technology, Oxford, 15-19 September 1980, pp 931-937.

[2] M. Huart, "DESIGN, FABRICATION AND ERECTION OF FLYWHEEL-GENERATOR-CONVERTORS FOR THE JET TOKAMAK", Proceedings of 9th Symposium on Engineering Problems of Fusion Research, Chicago, 26-29 October 1981, pp 382-385.

[3] P.L. Mondino, "INSTALLATION AND TESTING OF THE JET OHMIC HEATING CIRCUIT", Proceedings of 10th Symposium on Engineering Problems of Fusion Research, Philadelphia, December 1983, pp 2070-2076.

[4] T. Eriksson et al, "OPERATION AND CONTROL OF THE JET POLOIDAL FIELD POWER SUPPLY SYSTEM", Proceedings of 13th Symposium on Fusion Technology, Varese, 24-28 September 1984, pp 843-850.

[5] M. Huart, "COMMISSIONING OF THE JET FLYWHEEL-GENERATOR-CONVERTOR SYSTEMS", Proceedings of 13th Symposium on Fusion Technology, Varese, 24-28 September 1984, pp 851-858.

Invited Paper at 7th Topical Meeting on
Technology of Fusion Energy, Reno, USA. June 1986

The JET Technical and Scientific Performance and Future Plans

The JET Team

ABSTRACT

Three years have passed since the Joint European Torus (JET) started operation in June 1983. Phase I of the scientific programme, devoted to ohmic heating studies, has been completed. Phase II, devoted to additional heating studies started in January 1985.

From the technical point of view JET has been entirely successful: indeed the plasma current, an important figure of merit for a tokamak, has reached 5.1 MA for 3s, (exceeding the design value of 4.8 MA). Ion Cyclotron Resonance Heating has added up to 6 MW to the plasma and Neutral Beam Injection has added up to 10 MW.

The energy confinement time in ohmic discharges has reached 0.8s; but degradation has been observed with additional heating. Recently, combined heating (P_{add} up to 14.5 MW) allowed achievement of ion and electron temperatures of ~7.5 keV at densities of ~3 x 10^{19} m^{-3}.

Several proposals for improvements of the JET scientific performance are reported in the paper and summarised in the new development programme.

INTRODUCTION

The JET Project is the key experiment of the European Fusion Programme, which has, as its ultimate aim, the development of a prototype fusion reactor.

In JET, the plasma is confined in a tokamak magnetic configuration, (see Fig 1). A hot plasma of hydrogen isotopes is contained in a large vacuum vessel of toroidal shape and is kept thermally isolated from the wall by a rather complex axisymmetric magnetic field configuration. The main component, the toroidal magnetic field, is produced by 32 toroidal field coils uniformly distributed around the vessel itself. The second component, the poloidal magnetic field, is produced by a current flowing in the plasma itself. This current is induced in the plasma through transformer action pulsing a current of appropriate shape in the primary transformer coils wound along the main axis of the machine. Other coils (equilibrium coils) are used to produce vertical, radial and shaping fields; their interaction with the plasma current controls the horizontal (radial) and vertical position as well as the elongation and the shape of the plasma. The transformer coils and the equilibrium coils constitute the poloidal field coil set.

* (See Reference [20] for definition)

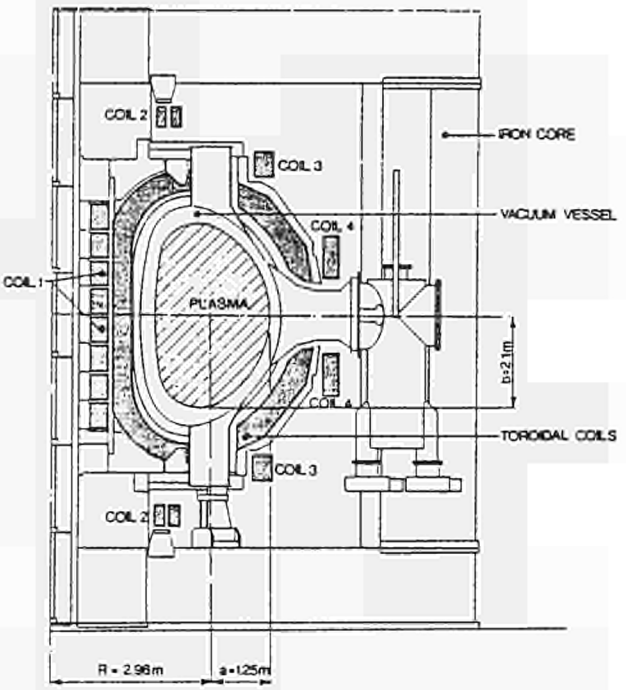

Fig 1: Cross Section of the JET Tokamak.

The plasma current has the purpose both to heat the plasma and to provide a stable equilibrium when below a threshold proportional to the main toroidal field and is a function also of the geometrical parameters. A safety factor, q, is defined as the number of revolutions in the toroidal direction (around the vertical axis) performed by a magnetic line of force to complete one revolution in the poloidal direction (around the magnetic axis).

The objective of JET [1] is to obtain and study plasma in conditions and dimensions which approach those needed for a fusion reactor. The four main aims of the experimental programme are shown in Table I.

Table I: Objectives of JET.

1. The scaling of plasma behaviour as parameters approach the reactor range;
2. The plasma-wall interaction in these conditions;
3. The study of plasma heating;
4. The study of α particle production, confinement and subsequent plasma heating.

Aim 1 is normally qualified by the energy confinement time τ_E, that is the figure of merit of the thermal insulation of the plasma: it is defined as the ratio between the plasma kinetic energy and the necessary power input to sustain it, in steady state conditions.

Aim 2 is normally qualified by the effective ion charge of the plasma, Z_{eff}; that is the figure of merit of the plasma purity. The impurities (all particles in the plasma different from the hydrogenic species and the fusion products) enhance the radiation losses for various reasons and dilute, for a given electron density the ion density that is the important parameter to reach reactor relevant conditions. Aims 3 and 4 are qualified by the comparison of the results obtained with the parameters needed to reach ignition (Lawson criteria). The three key parameters, the ion temperature, T_i, the ion density, n_i, and the energy confinement time have to satisfy the following conditions:

$$n_i \cdot \tau_E \geq 3 \times 10^{20} \text{ s m}^{-3}$$
$$T_i \geq 15 \text{ keV}.$$

Around these values the ignition domain in the Lawson diagram can be approximated with an hyperbola. Therefore only one parameter can be used, sometimes called fusion product $n_i \cdot \tau_E \cdot T_i$ that should reach $50 \cdot 10^{20}$ s m^{-3} keV for a plasma to enter the ignition domain.

The basic design choice of the JET machine defined in 1975 [1], aimed for operation with tritium, to study α-particle production and heating. As a consequence, the machine has the following characteristic features [2], shown in Fig 1 and given in Table II:

- high plasma current;
- large plasma volume and relatively low toroidal field;
- D shape for the toroidal coils, the vacuum vessel and the plasma;
- small aspect ratio (major radius/minor radius)
- poloidal coils all external to the toroidal magnet;
- large access ports;
- modularity of construction (octants);
- life: 10^5 pulses.

From the time of conceptual studies, through the design phase to the construction phase, the experimental evidence gained with other tokamaks and the progress in understanding the physics have created a general consensus in considering the plasma current as a figure of merit for the performance of a tokamak. It is therefore important to stress that JET has, by far, the highest plasma current capability among existing tokamaks.

Aim 4 in Table I had a strong impact on the design concept of JET [3]: all services to the machine including the power supplies for the magnets and additional heating are located outside the Torus Hall. Long busbars or cable connections were therefore necessary.

The two additional heating methods selected were the most advanced at the time when the choice was made (neutral beam injection heating in 1978 and ion cyclotron radio frequency heating in 1981). Beams of neutral particles with very high kinetic energy (80 keV for hydrogen, 160 keV for deuterium) are required to penetrate the target plasma and deposit power in the central region (~ 25% of the volume). The production of powerful beams of neutral particles is rather complex: the basic elements of a Neutral Injection Beam Line are the ion source, the accelerating structure, the neutralizer, the ion dump, etc [4]. The related power supplies are also rather sophisticated because of the fast response time and of the high voltage required [5]. All components of the Neutral Beam Subsystem are designed for long pulse operation (~10s). Two injectors are foreseen in JET each with 8 sources with 4.8 MW of extracted ion beam power per source when operated at full voltage. The total power delivered from the two injectors into the torus is expected to be about 15 MW with 10 MW in the full energy beam component ("high grade power"), both at 80 kV hydrogen and 160 kV deuterium beams.

The Ion Cyclotron Radio Frequency Heating allows RF waves to be coupled to the plasma with large antennae. A wide frequency range was originally chosen (25-55 MHz) in order to heat the JET plasma at full toroidal field with the minority species of hydrogen, deuterium and helium 3. The first group of antennae, called A_0, are designed without active cooling for short pulse operation (1-3s) [6]. The two radiating elements of each antenna are supplied each through long trans- mission lines (83-84m) by 1.5 MW RF amplifier. Eight antennae are foreseen, in total, each driven with two RF amplifiers. The amplifiers will be upgraded to increase the power output up to 2.0 MW for a total of 32 MW, of which 16 MW ("high grade power") are expected to be deposited in the plasma centre (~25% of the plasma volume) and about 25 MW to be delivered into the torus [7].

From the electrical point of view, four different electrical loads can be identified in JET: the toroidal field coils, the transformer primary coils, the equilibrium and shaping field

TABLE II: Main design parameters of JET.

Parameter	Value
Plasma minor radius (horizontal), a	1.25 m
Plasma minor radius (vertical), b	2.10 m
Plasma major radius, R	2.96 m
Plasma aspect ratio, R/a	2.37
Plasma elongation ratio, e = b/a	1.68
Flat top pulse length	10 s
Toroidal magnetic field (plasma centre)	3.45 T
Plasma current, circular plasma	3.2 MA
D-shaped plasma	4.8 MA
Volt-seconds available	34 Vs
Toroidal field peak power	600 MW
Poloidal Field peak power	300 MW
Additional heating power (in plasma)	25 MW
Weight of vacuum vessel	100 tonnes
Weight of toroidal field coils	380 "
Weight of iron core	2700 "

coils and the additional heating equipment. All these pulsed loads require suitable current and voltage waveforms so that the power supply schemes will include AC/DC conversion and power modulation. In JET, as in the majority of the existing tokamaks, the magnets are made with copper coils, water cooled, so that their power and energy requirement are very high. When the additional heating requirements are added, the overall installed power capability is in excess of 1,000 MVA with 11,000 MJ per 20s pulse at a repetition rate of one pulse every 10 minutes. In spite of the large capabilities of the 400 kV supply line, it was necessary to use a combined scheme with two large dedicated flywheel generators that store energy between pulses and provide a large fraction of the peak power required in addition to several AC/DC convertors supplied directly from the mains which are able to provide the majority of the energy [8]. A detailed description of the magnet power supply system of JET is reported in [9], where the various steps in commissioning and operation up to full performance are described.

THE JET PROGRAMME

When JET was approved, five years were allocated to its construction starting in June 1978, and seven and a half years were foreseen to perform the experiments necessary to reach the main aims shown in Table I. The experimental programme of JET is given in Table III showing the four phases originally planned.

TABLE III: JET Development Programme.

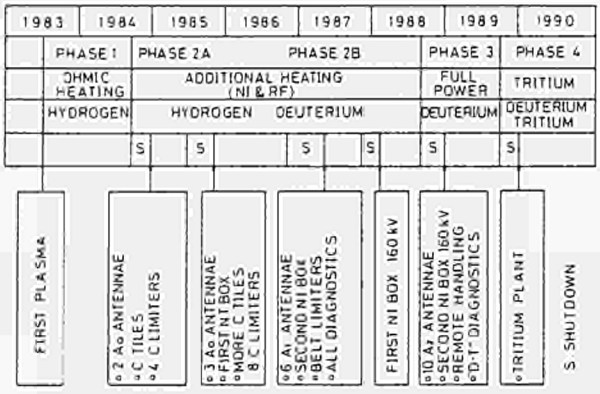

Analysis of the table shows that the experimental programme is performed in parallel with a large manufacturing and development programme dedicated to:

- construction of the additional heating equipment;
- development of the remote handling facility and of the tritium plant, both essential element to start phase IV of the programme [3];
- the progressive upgrade of the various diagnostics;
- implementation of the various modifications that the experimental results progressively require.

The first three items can be planned in advance whereas the last item requires some flexibility and re-adjustment of the programme itself.

Phase I dedicated to ohmic heating studies started in June 1983 according to plan. During 1984, the magnet power supplies were progressively commissioned up to their full performance. In summary, the 1984 experiments extended the plasma current to 3.7 MA with 5s flat top, the plasma elongation to 1.6, with full toroidal field 3.45 T; hydrogen and deuterium plasmas were produced with temperatures up to T_e~3keV, T_i~2.5keV, densities up to $3.5 \times 10^{19} m^{-3}$, maximum energy confinement time of 0.8s and Z_{eff} in the range 2.4 - 10. During Phase I, JET operated with 4 graphite limiters (total area $1.28 m^2$) and inconel walls, "carbonisation" of the vessel walls has been the method used to control metallic impurities [10].

The planned shutdown took place between October and December 1984, during which two A_o antennae were installed inside the vacuum vessel. Moreover, its inboard side was protected with about a thousand carbon tiles for a height of approximately 2m (total protected area $23 m^2$). Finally, to cope with the stresses caused to the vacuum vessel by vertical instabilities (see next section), additional rigid supports were added at the bottom edge of each horizontal port together with shock absorbers on each vertical port (top and bottom).

In 1985, the experimental programme was partly devoted to additional heating studies with ICRF, (Phase II). The power deposited to the plasma was progressively increased up to 4.5 MW. A review of the results obtained during the early phase of operation with ICRF is given in [11].

The development programme was also continued to achieve the full performance of the machine (including IP = 5.0 MA) [10]. Operation with a magnetic separatrix was also established up to 2 MA [12].

The shutdown took place as planned between the mid-June and mid-November 1985. Four additional graphite limiters were installed increasing the total limiter surface to 2.56 m^2 with a heat load capability of 20 MW. Eight graphite belts, in the poloidal direction, have replaced the original Inconel octant joint protections, (12.9 m^2). A small fraction of the outboard wall in Octant 5 in the area of the main horizontal port has been protected with graphite tiles (3.5 m^2) against possible damage made by the "tangential" beams of the neutral beam injector located in Octant 8. A third A_o antenna was also installed.

Since operation started, the main effort of the development programme was put on experiments with the plasma leaning on the limiter, on the inner wall or with the edge determined by a magnetic separatrix (magnetic limiter). Moreover, ICRF Heating used all 3 A_o antennae. Finally, the first injector became operational: deuterium plasmas were injected first, with hydrogen beams (up to 70 keV), and then, with deuterium beams (up to 80 keV and up to 10 MW). A review of the experimental results obtained so far is given in [13].

A review of the status of the machine, of the experience gained in operation and a detailed analysis of the development and enhancement plans, as discussed within the JET Team, during Autumn 1985, are reported in [14]. Preliminary experiments with combined heating were also performed.

The experimental activity will continue with the present machine configuration up to December 1986. A major shutdown will then take place during which the activities foreseen in the JET Programme (Table III) will be implemented. During 1987 and 1988 operation (Phase IIB) the additional heating power will progressively be increased to its maximum capabilities (26 MW of high grade power, 40 MW in total).

TECHNICAL ACHIEVEMENTS

After almost three years of operation, the success of JET from the technical point of view is complete: Table IV shows a comparison between design and operational parameters: indeed the plasma current, already mentioned as an important figure of merit for a tokamak, has exceeded the design value: pulses with I_p = 5.1 MA with 3s flat top have been produced and with I_p = 4 MA for 6s flat top were performed routinely.

TABLE IV: Comparison between design and operational parameters.

Parameter	Design value	Operational values
Plasma minor radius a (horizontal)	1.25 m	0.8-1.2 m
Plasma minor radius b (vertical)	2.10 m	0.8-2.1 m
Plasma major radius R	2.96 m	2.5-3.4 m
Toroidal magnetic field at R = 2.96 m	≤3.45 T	≤3.45 T
Plasma current IP	≤4.8 MA	≤5.1 MA

The plasma current is controlled by feedback; the closed loop is softly brought into operation during slow rise [15],[16]. During flat top, the error is normally ≤3% with response time ~0.5s. The horizontal plasma position is controlled by feedback acting on the voltage applied to a section of the equilibrium coil P4 (see Fig.1) [15], [16]. The system is designed to control the distance from the inboard wall to the last closed magnetic surface that is touching the limiters at its outboard side. During the slow rise and flat top, the error is normally ≤10mm with response time ~30ms. The horizontal position control system can also move the plasma horizontally, decoupling it from the limiters and placing it on the inner wall.

The plasma elongation and shape is controlled by feedback acting on the current flowing in opposite directions on sections of P2 and P3 equilibrium coils [15],[17]. These currents produce a quadrupole poloidal field that helps in elongating the plasma in the range 1.4 - 1.7, at full aperture (maximum horizontal dimensions) and high plasma currents. During flat top, the error in elongation is normally 5% with response time ~20ms.

The plasma vertical position is naturally unstable because of both the quadrupole poloidal field necessary for an elongated plasma and the de-stabilising effects of the ion magnetic circuit, the two contributions are approximately equal, when the elongation is about 1.6. The plasma is stable when the elongation is below a critical value in the range 1.2-1.3. The natural instability (growth rate~50-150s^{-1}) must be stabilised by feedback control of the radial magnetic field produced by current flowing in sections of the equilibrium coils P2 and P3 (opposite direction in the upper and lower coils) [15]. Large vertical forces on the vessel can develop from a failure of this control system. This problem was somewhat under-estimated during JET design and became evident after pulse 1947 during which a vertical force of about 250 tonnes developed on the vacuum vessel. Extensive studies performed afterwards were used to improve the performance of the feedback system, reducing the response time from 4.0 to 2.0ms for small signals. Plasmas with elongations up to 1.9 were experimentally produced (and kept vertically stable)[17]. It was also necessary to strengthen the vessel (action taken in two steps: the first already implemented during the 1984 shutdown, the second will be implemented during the 1986/87 shutdown). With the existing vessel supports, the operating range has been restricted as follows:

$$I_p^2 (b/a - 1.2) < 5.0 \ (MA^2)$$

The final vessel supports will withstand forces up to 1600 tonnes and will allow operation up to I_p = 7 MA at full elongation e = 1.68.

The toroidal subsystem (toroidal field coils and power supplies) has reached the nominal performance of 67 kA that corresponds to 3.45 T on magnetic axis with nominal I^2t=9 $10^{10}A^2s$. The flat top is 12s; (8s are necessary for current rise because only 8 kV are used in order to not stress the interturn coil insulation). Longer flat tops could be obtained, increasing the voltage during current rise and extracting energy during current decay. The limitation on I^2t could also be made less stringent using a lower temperature on the demineralised cooling water (chillers are to be installed on the cooling system).

The poloidal subsystem (poloidal field coils and related power supplies) has been commissioned up to the nominal capabilities of its components: the nominal flux swing of ~34 Vs has been produced.

A dedicated generator is connected to the primary transformer coils (P1) in which, at the end of the premagnetisation phase, the current can reach the nominal 40 kA. This current is then diverted through resistors in order to provide the nominal 40kV across the primary winding. 12kV are normally produced in the experiments with 20kA

premagnetisation. This voltage causes the plasma breakdown and fast rise, the generator is then reconnected to the primary transformer coils to raise slowly the plasma current and finally to maintain it constant (slow rise and flat top phases). At the end of the flat top phase the current in the primary coils normally reaches 40kA in the opposite direction (compared to premagnetisation).

In operation, the total flux swing available to raise and sustain the plasma current cannot be used because the nominal premagnetisation current (40 kA) would create stray fields too high for reliable breakdown. Moreover, even assuming successful breakdown and plasma formation, the current derivative would be too high and the plasma would show an excessive disruptive behaviour (probably due to skin currents).

The RF subsystem has three A_0 antennae operational at 3MW each.

The Neutral Injection subsystem has operated the first injector equipped with 8 sources up to 70 kV in Hydrogen with 50 A extracted current and subsequently has been converted to deuterium and operated at 80 kV with 40 A extracted current. The power ("high grade") delivered to the plasma was 10 MW. A new deuterium source has been tested in the JET Test Bed up to 160 kV with 40 A extracted current: this development is to be considered a great achievement both for the source and the power supply system.

The vacuum subsystem has been operated with the vessel above room temperature (main vessel temperature ~300°C, main port temperature ~150°C) The base pressure before the pulse is about 10^{-7} mbar. During the pulse, the density is progressively increased with feedback control on a dosing valve but the system becomes ineffective when degassing from the walls and/or the limiters is too high. A pumping effect from the walls (especially the inner portion covered with graphite tiles) has been observed but not yet understood.

ANALYSIS OF SIGNIFICANT PULSES.

Pulse 7293 gives the record performance in terms of plasma current using only 30 Vs of the 34 Vs available. The plasma current (see Fig.2) rises in 1s to 2.7 MA (fast rise) and in the following 6s reaches 5.1 MA (slow rise). The length of the flat top (3s) is not enough to reach steady state conditions. The average electron density, $\langle n_e \rangle$, continues to increase during current flat top and reaches the maximum ($4 \times 10^{19} m^{-3}$), 1.5s after the end of current flat top. Then the density drops because the plasma is moved to the inner wall. As usual the electron temperature on axis, T_{eo}, shows a maximum (~4keV) during slow rise when the current density profile is still broad. Afterwards, the current density profile peaks on the centre causing $q<1$ in the region inside the plasma half radius. As a consequence, a relaxation oscillation develops (a phenomenon observed in several tokamaks and known as sawteeth). This characteristic pattern is present also on the electron temperature on axis, T_{eo}, which time average during plasma current flat top is about

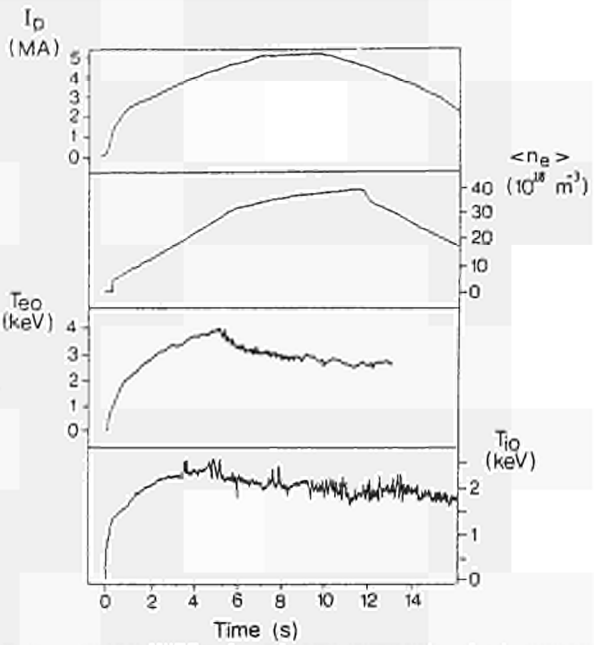

Fig.2: Pulse 7293: I_p plasma current, $\langle n_e \rangle$ average electron density, T_{eo} and T_{io} electron and ion temperature on axis.

2.8 keV. The ion temperature on axis, T_{io}, shows a similar behaviour with 2.2 keV during plasma flat top. The power input (ohmic only) reaches the maximum during flat top (~5 MW), but this number should be treated consciously since the plasma density profile has not yet reached steady state condition. Other significant parameters of this pulse were: toroidal field B_T=3.45 T, elongation e=1.4, energy confinement time τ_E~ 0.6s, impurity content Z_{eff}=2.5.

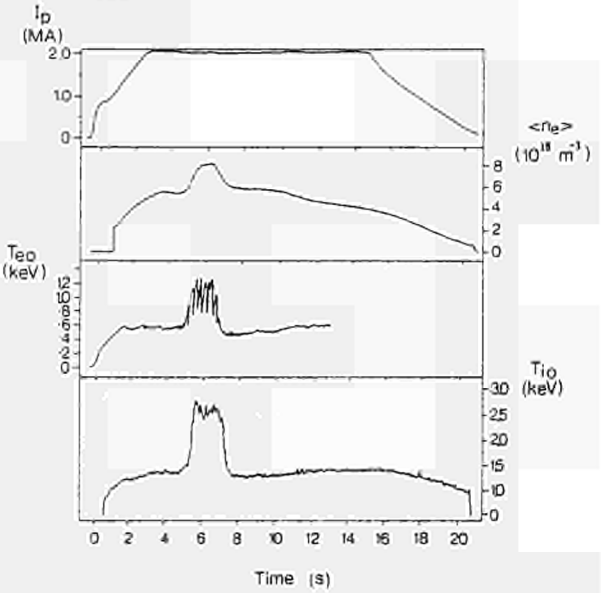

Fig.3: Pulse 7220: I_p plasma current, $\langle n_e \rangle$ average electron density, T_{eo} and T_{io} electron and ion temperature.

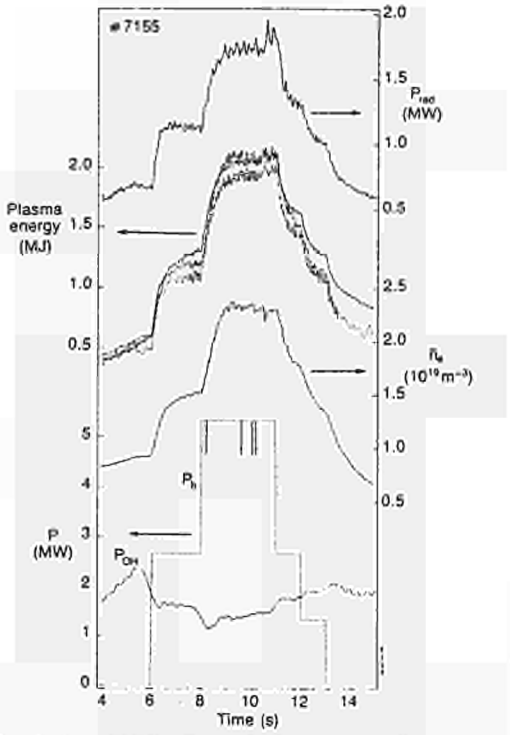

Fig.4: Pulse 7155: P_{OH} ohmic power, P_b neutral beam power, n_e average electron density, plasma energy, P_{rad} radiated power.

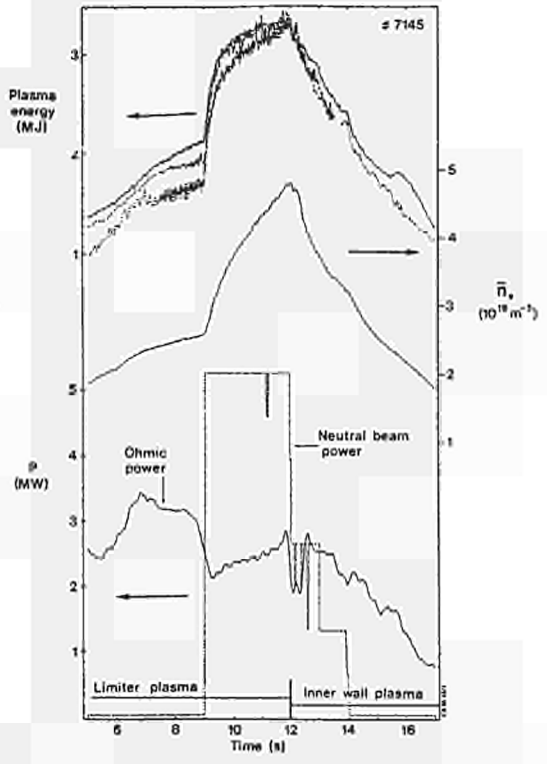

Fig.5: Pulse 7145: ohmic power, neutral beam power, n_e average electron density, plasma energy.

Pulse 7220 shows the consequence of 5.5 MW RF additional heating power (coupled to the hydrogen minority) in a deuterium plasma with 2 MA and 2.3 T. Fig.3 shows the plasma current, the average electron density, the electron and ion temperature on axis. The total power input reaches about 6.0 MW during the 2s RF pulse during which the average electron density increases (about 30%). Giant sawteeth are clearly visible on both electron and ion temperature on axis. The time average temperatures roughly double from the initial ohmic level. The key result is that the plasma stored energy rises from 0.72 to 1.8 MJ only, whereas the total input power rises from 1.5 to 6.1 MW. In other words, the energy confinement time τ_E drops from 0.48s to 0.3s.

Two different plasma regimes can be established with NBI according to the time evolution of the density of the target plasma. The two pulses described in the following are typical of both regimes [18].

Pulse 7155 shows the effect of 5.5 MW NBI additional heating power (hydrogen neutrals at 60 keV) on a low density deuterium plasma with 3 MA and 2.8 T. Fig.4 shows respectively ohmic and neutral beam power, the average electron density, the plasma kinetic energy and the radiated power. The total power reaches a maximum of approximately 7 MW for 3s and is then dropped in steps, the average electron density rises more than 50%. The central electron and ion temperature rise from 4.1 to 4.8 keV and from 2.2 to 6.5 keV. These results are obtained at relatively low density ("hot ion regime"); in order to achieve this, the plasma was moved to the inner wall during current rise. The inner wall pumping effect ensures low initial density when the injector is turned on and mainly minimum density rise during beam pulse.

Pulse 7145 is a typical example of a high density plasma obtained with the same NBI parameters of the previous pulse on a deuterium plasma with 4 MA and 3.4 T which was leaning on the limiters during the beam pulse and was moved to the inner wall during decay. Fig.5 shows the ohmic input power and the beam power respectively. The drop in ohmic power during beam pulse is due to both beam-driven current and a drop in plasma resistivity because of the electron temperature increase and of the impurity content decrease. The average electron density rises sharply during beam pulse from about 2.5 to 4.8 x $10^{19}m^{-3}$ without showing any indication of saturation. The ion temperature shows an increase of 1 keV. The stored plasma energy doubles, reaching 3.3 MJ.

EXPERIMENTAL RESULTS.

Fig.6 shows the fit of the energy confinement time, τ_E, with a widely used scaling law. All JET data obtained in 1984 and 1985 (hydrogen and deuterium) with ohmic heating only are plotted [19]. The strong influence of the plasma geometrical dimension is clearly indicated by the scaling law that confirms the validity of choice made in JET of large plasma volume. An increase in density will be beneficial to increase the energy confinement time. The record performance so far

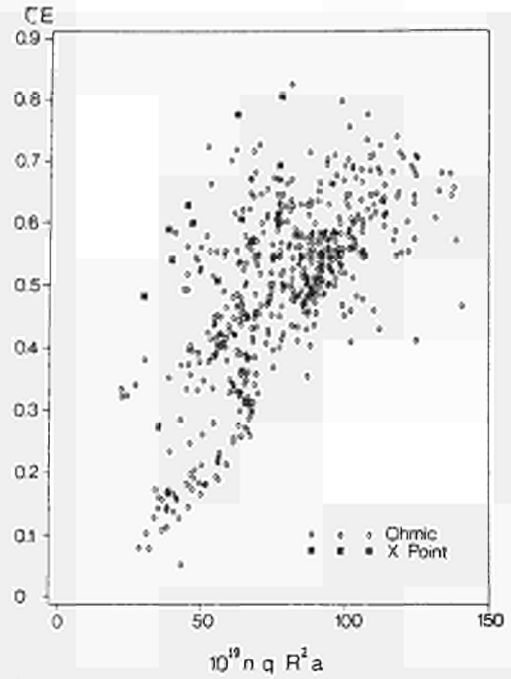

Fig 6: Scaling law of the energy confinement time τ_E

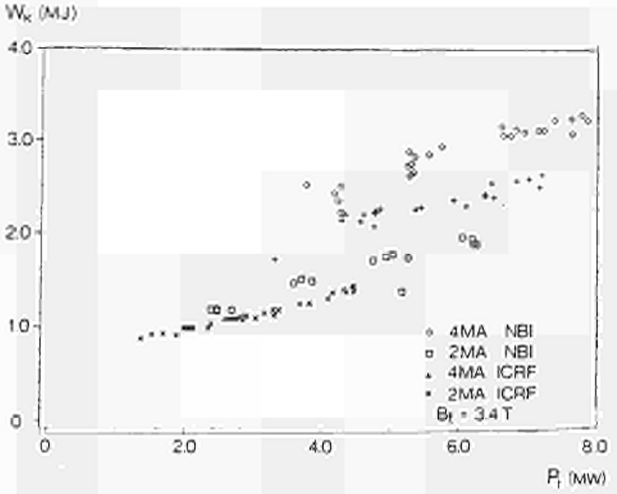

Fig 7: Plasma kinetic energy versus total power input.

obtained in JET (τ_E=0.8s) with ohmic heating only should be noted. The black points show the results with magnetic separatrix: they seem to indicate a better behaviour of the plasma.

The degradation of the energy confinement time with additional heating already observed in other tokamaks is confirmed by the JET results. To analyse better this phenomenon the plasma kinetic energy is plotted (Fig.7) versus the total input power [20]. From present results a linear behaviour can be extrapolated; an increase with plasma current is to be pointed out. The pattern shown in Fig.7 can be represented by the equation:

$$W = \tau_{E_o} P_{\Omega o} + \tau_a (P_{TOT} - P_{\Omega o});$$

in other words the plasma kinetic energy increases with two different rates, τ_a related to the degradiation of confinement is approximately τ_a=0.3 τ_{E_o}.

Fig 8 [19] shows the effective ion charge versus the ratio of density to current density: an increase in density reduces the impurity content, as confirmed by the experiments with neutral injection. On the contrary, experiments with ICRF show an increase in metal impurity content coming from the RF antennae.

Use of low Z materials for the limiters and wall protection has always been in the JET programme. The two alternatives carbon and beryllium have both been studied. Tiles of both materials are being manufactured so that the final choice can be delayed for the time being. By the end of the 1987 shutdown, 48% of the total vessel area will be covered with low Z material. [21].

The experimental results obtained with many different Tokamaks and confirmed by JET show that the electron density is limited. JET results plotted in the form of the Hugill-Murikami diagram are shown in Fig.9 [18]: the electron density is limited for ohmic and RF heating discharges to

$$n_L \sim 10^{20} \frac{B}{Rq}$$

With neutral injection heating n_L has been increased by a ~70% showing that the electron density can be increased if the plasma is fuelled in the centre.

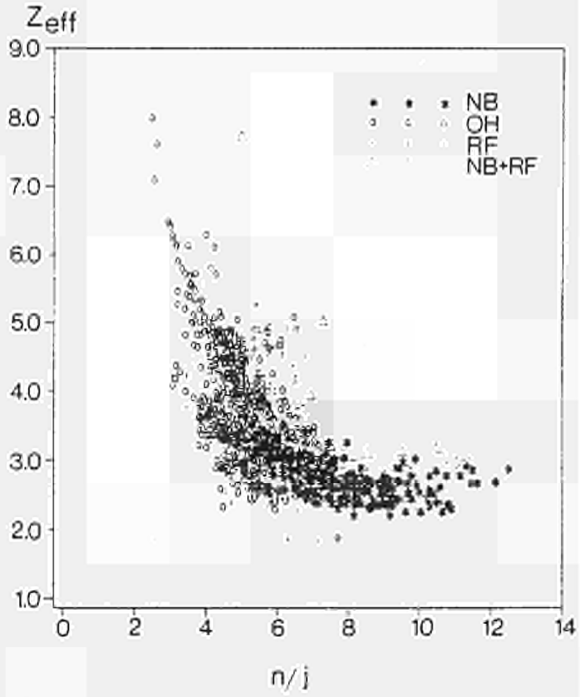

Fig.8: The effective ion charge versus the ratio of average density to average current denaity.

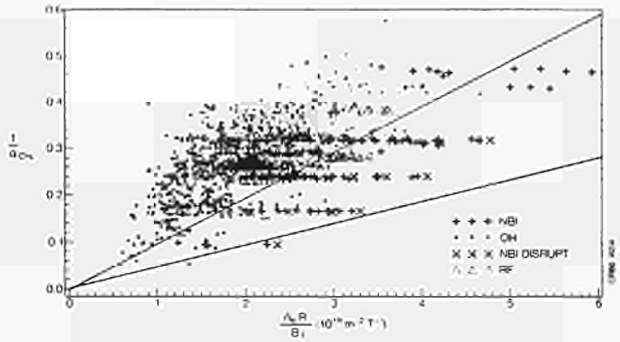

Fig.9: Hugill-Murikami diagram.

Fig 10 [22] shows the JET results plotted in the Lawson diagram. The results obtained with additional heating are only marginally better than the ohmic heating results. The increases in ion temperature and ion density due to additional heating are, at least in part, offset by the degradation in the energy confinement time. The highest value of the fusion product is 6×10^{19} s m^{-3}keV with neutral beam heating only marginally higher than with ohmic heating.

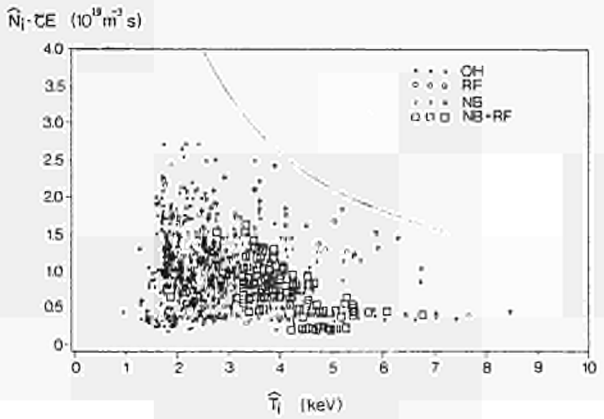

Fig.10: Lawson diagram.

PROPOSALS TO IMPROVE THE JET PROGRAMME

In order to make full use of the total flux swing available (-34 Vs) the primary transformer coils will be increased from 8 to 10, making use of existing spare coils. In this way, the stray fields present inside the vacuum vessel, at full premagnetisation current (40 kA), will be reduced to about the same values that are now produced by 20 kA. Moreover, the voltage across the transformer coils will be reduced in steps to decouple plasma build-up from the current rise. Proper plasma build-up will require high loop voltage (-40 V, 50ms) for fast multiplication of ionised particles (breakdown) followed by intermediate voltage (10-5 V, 300ms) to provide an ohmic power input sufficient to burn through the radiation barrier (I_p-300-500 kA, T_e-T_i>50 eV). The voltage will then be reduced further to meet the requirements on plasma current rise (≤ 1 MA/s). From breakdown onwards, the plasma horizontal position must be kept under control with a vertical field approximately proportional to plasma current, requiring a voltage across the vertical field coils, P4, to be equal to half of the transformer voltage. The new nominal values are 24 kV for P1 and 12 kV for P4.

A non uniform current distribution in the P1 coils (about 40 kA in the central six coils and approximately zero current in the upper and lower two coils) will cause a large stray flux in the top and bottom area of the vessel when the current in P1 (30-40 kA) saturates the iron. This effect combined with appropriate current in the shaping coils (sections of P2 and P3) causes a magnetic configuration with a separatrix inside the vacuum vessel, for plasma current up to 4 MA [23]. Both single null and double null configuration are actively studied: the single null seems more attractive at this stage because plasma currents up to 4.5 MA could be achieved with the X-point 0.2m inside the vessel. A plasma, limited by a magnetic separatrix instead of a material limiter, should show a transition to H-mode behaviour with improved energy confinement time. Preliminary experiments on a magnetic limiter plasma with neutral beam heating have shown improved plasma behaviour.

The following technical implications are carefully analysed:

- localised stresses on TF coils and on the mechanical structure;
- power deposition on inner wall near the X-point (top and bottom of the vessel): additional vessel protection with dump plates will be necessary; water cooled metal plates covered with low Z material are being considered;
- a new power supply configuration to allow different currents in the different sections of P1 is under study.

Preliminary modifications will be performed during the 1986/87 shutdown, whereas the full configuration should become available at the end of the 1988 shutdown.

It is expected that standard plasma discharges in excess of 6 MA, possibly up to 7 MA, are feasible in JET. A task force will be set up in the near future to analyse the various subsystems as built. The aim will be to evaluate how many pulses can be made at increasing performance, taking into account fatigue degradation and built in safety margins. Even in this case, non uniform current distribution in P1 coils will be considered. Current higher than nominal (possibly up to 60 kA) in the central six coils could be accepted since these coils are compressed during the pulse by the toroidal coils working at full field (an aspect not considered in the design of P1 coils).

The performance of the TF subsystem will also be reviewed with the aim of increasing both the amplitude of the toroidal field and its flat top length. These studies should be concluded before Phase III starts (devoted to optimisation studies, see Table III).

It will be necessary to increase the density at the centre of the plasma well above the present

level to reach reactor relevant conditions. Experiments performed with other machines (TFTR, ASDEX, ALCATOR, PDX) indicate that this aim could be reached with multipellet injection.

A staged approach [24] has been chosen, as it fits best the JET development programme. A single pellet injector able to launch pellets of 2.6 to 4.6mm diameter at speeds of 1.2-1.5 km/s is being installed and will be operational during the second half of 1986.

During the 1986/87 shutdown, a multipellet injector will be installed: its main features are:
- sizes: 2.6, 4, 6 mm diameter (same length);
- speed: 1.5 km/s for all deuterium pellets;
- fuel: deuterium, hydrogen;
- number of pellets per pulse: 10, 8, 6 for respective diameters;
- propellant gas: hydrogen up to 120 bar.

Finally a development programme has been undertaken to increase pellet speeds towards 10 km/s. A single shot pellet injector with speed in the range 2-5 km/s is expected for installation during the 1988 shutdown, whereas a multipellet injector with speed in the range 5-10 km/s should be installed during the 1989 shutdown.

An increase of central density should be obtained without increasing the edge density. Therefore, a particle exhaust system is required to control the edge density during pulses with additional heating and pellet injection. Moreover, a controlled pulse termination will be achieved reducing the density to ohmic levels at the end of additional heating, during which the density increases well above the ohmic level.

For this purpose a development programme [25] has started, both of a pump limiter system and of pumping panels. Two steps are foreseen for the pump limiter: firstly a prototype will be installed in the 1988 shutdown: the design implies a limiter blade movable radially by about 20-30mm and able to withstand a power loading of about 10 MW/m^2 for 1-2s.

Assuming a density of $10^{20} m^{-3}$, it will decay with a time constant of ~14s. Second, an actively cooled pump limiter should withstand ~30 MW/m^2 for 10s. Swirl tubes covered with 2.5mm carbon or beryllium will be used. Installation is foreseen during the 1989 shutdown.

Pumping panels have been considered because of the pumping effect of the JET walls, especially of the inboard wall (already mentioned). A systematic study of available data has started, and ad hoc experiments will be performed. According to present estimates, 50 m^2 of pumping panels, radiation cooled, would be required. Installation is foreseen during 1988 shutdown.

Control of current density profile [26] could remove the strong correlation now existing between the current density itself and the electron temperature now caused by Ohm's law ($J \propto T_e^{3/2}$). A flat current profile could keep $q > 1$ everywhere in the plasma, thus avoiding the sawteeth. Higher central electron temperatures could be reached.

Radio frequency waves at lower hybrid resonance (~2-4 GHz) have already been used for this purpose in different experiments. Electron cyclotron resonance (60-100 GHz) should produce current drive (according to theory), but it has not yet been observed. Ion cyclotron resonance could also be used; the JET system is now being prepared to attempt some experiments along these lines: phase locked operation of the 8 A_1 antennae is now planned, and will be attempted after the 1986/87 shutdown. Current drive has also been produced with neutral injection.

Among the various options, JET is proposing to make current drive with lower hybrid; 10 MW would be produced with 24 klystrons (phase locked) at 3.7 GHz. Such a system would be capable of driving 1 MA in the plasma.

Broadening of the current density profile in JET would be achieved using the two injectors available (~0.4 MA capability) in counter injection to reduce the current density in the central region together with the envisaged lower hybrid system able to drive up to 1 MA (positive) in the outer region.

CONCLUSIONS: THE NEW DEVELOPMENT PROGRAMME

The various improvement proposals integrated with the already ambitious JET programme, could clearly not be completed by the end of 1990. So a new development programme has been prepared and the necessary steps have been started to seek approval from the various supervisory bodies as required by the JET Statutes.

Table V shows the new JET development programme [13] that should be considered provisional, for the reasons mentioned above. Although two years longer than the original programme (Table III), the new development plan is very tight. One major shutdown per year is foreseen, during which all necessary modifications needed by the following period of operation, are implemented.

Phase II dedicated to the additional heating studies with progressive increase of performance in terms of power added to the plasma, will be reduced by three months compared to the original programme.

Phase III devoted to optimisation studies with full additional heating is now approximately doubled and is divided in two parts A and B with a major shutdown between, during which all necessary modification for the Tritium Phase should be made.

The last shutdown in the middle of 1991 should only be dedicated to further modifications as required by the tritium operation.

The Tritium Phase (IV) is now envisaged to last for one year. During such a period, about 3000-5000 pulses would be performed to study the alpha-particle production, confinement and heating of the plasma.

A large and solid data base should become available for NET (Next European Torus) [27] that will then be the key experiment of the European Fusion Programme.

TABLE V: **JET PROGRAMME — SCENARIO 1**

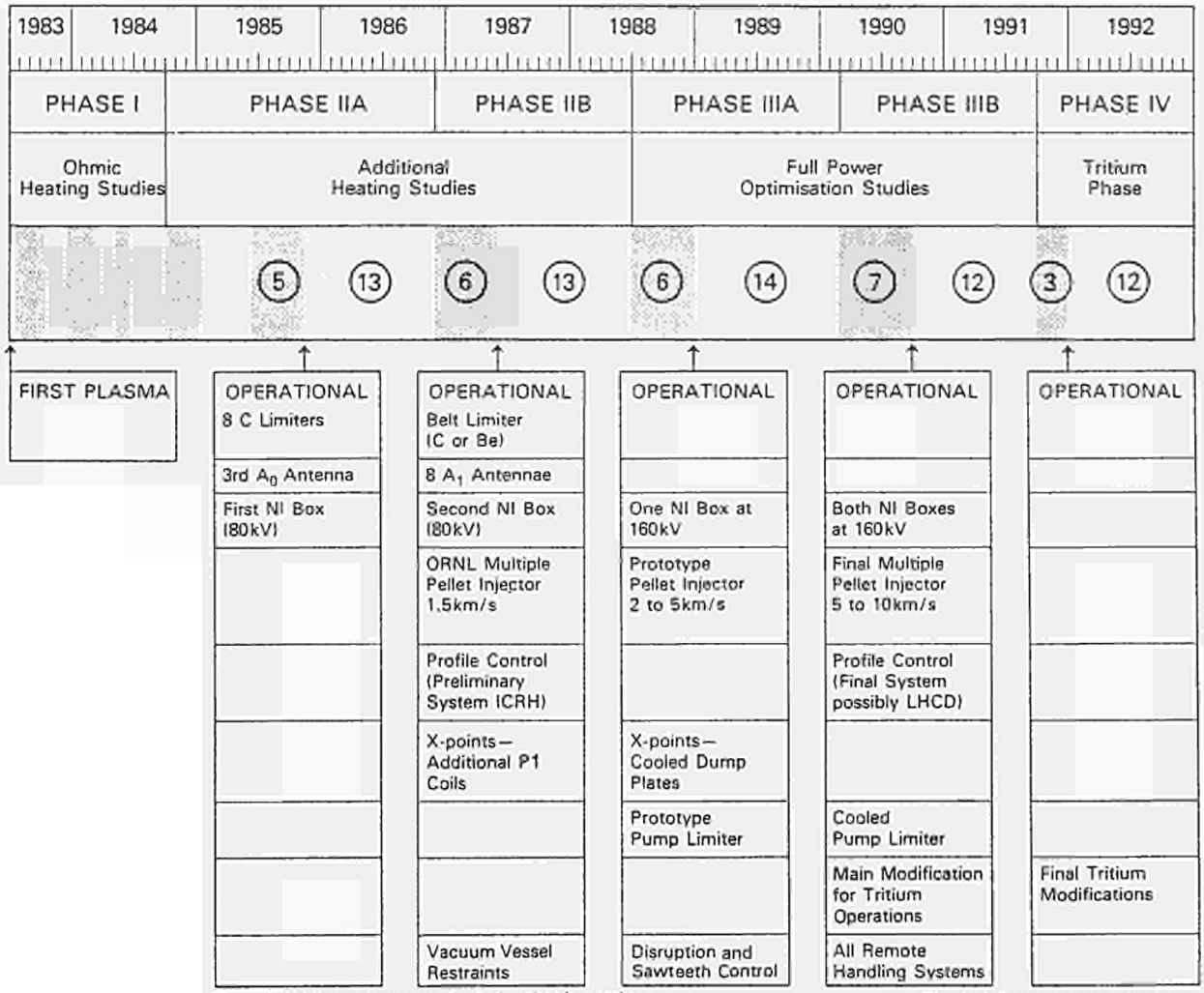

The encircled figures show approximate durations in months.

The shaded areas represent shutdowns.

CR86.2/2 (rev. 28/4/86)

ACKNOWLEDGEMENTS
The authors wish to acknowledge the hard work of the technical staff of JET for their contribution to the operation, maintenance and modifications performed to fulfill the JET experimental programme.

REFERENCES
[1] The JET Project, "Reports of the Commission of the European Communities": EUR 5516e(1976), EUR 5781c(1977), EUR 6831en(1978).
[2] M.Huguet, "Design, Manufacture and Assembly of the JET Machine": Royal Society, London, March 1986.
[3] M.Huguet and E.Bertolini, "Main Features implemented in the JET Facility for D-T Operation": these Proceedings.
[4] G.Duesing, "JET Neutral Beam Injection System, Construction and Components Tests": Proceedings of 13th Symposium on Fusion Technology, pp.59-75, Varese, Sept 1984.
[5] R.Claesen and P.L.Mondino, "Neutral Injection and Radio Frequency Power Supplies", submitted for publication to "Fusion Technology Journal".
[6] A.Kaye, et al, "Engineering Design and Preliminary Performance of the JET ICRF System": Proceedings of the 11th Symposium on Fusion Engineering, pp.1204-1209, Austin, Nov. 1985.
[7] T.Wade, "Technology of the Upgraded JET ICRF System": these Proceedings.
[8] E.Bertolini, "Basic Design Concept, Installation, Commissioning and Operation of the JET Integrated Power Supply System": Proceedings of the 10th Symposium on Fusion Engineering, pp.1756-1763, Philadelphia, Dec. 1983.
[9] P.L.Mondino, "The JET Power Supplies: A review after one year of operation": Proceedings of the 13th Symposium on Fusion Technology, pp.119-131, Varese, Sept.1984.
[10] R.J.Bickerton, et al, "Latest results from JET": Plasma Physics and Controlled Fusion, Vol. 28, No.1A, pp.55-69, 1986.
[11] J.Jacquinot, et al, "ICRF Studies on JET": Plasma Physics and Controlled Fusion, Vol.28, No.1A, pp.1-15, 1986.
[12] A.Tanga, et al. "The Formation of a Magnetic Separatrix in JET": Proceedings of the 12th EPS Conference on Controlled Fusion and Plasma Physics, pp.70-73, Budapest, Sept.1985.
[13] P.H. Rebut and P.P.Lallia, "JET: Evolution, Status and Prospects", Royal Society, London, March 1986.
[14] E.Bertolini, "Operation and Development Plans of JET", Proceedings of the 11th Symposium on Fusion Engineering, pp.8-18, Austin, Nov.1985.
[15] E.Bertolini, P.L.Mondino and P.Noll, "Magnet Power Supplies and Plasma Control", submitted for publication to "Fusion Technology Journal".
[16] P.Noll, et al, "The JET Plasma Position and Current Control System", Proceedings of the 13th Symposium on Fusion Technology, pp.503-509, Varese, Sept. 1984.
[17] P.Noll, et al, "Stabilisation of Vertical Position and Control of Plasma Shape in JET", Proceedings of the 11th Symposium on Fusion Engineering, pp.33-40, Austin, Nov.1985.
[18] G.Duesing, et al, "First Neutral Beam Heating Experiments on JET", Royal Society, London, March 1986.
[19] J.G.Cordey, JET, private communication.
[20] P.Lallia, "Plasma Heating in JET": Proceedings of the 13th EPS Conference on Controlled Fusion and Plasma Physics, Schliersee, April 1986.
[21] M.Huguet, et al, "Limiters and First Wall on JET", Proceedings of the 11th Symposium on Fusion Engineering, pp.1238-1248, Austin, Nov. 1985.
[22] P.Lomas, JET, private communication.
[23] JET document EUR FU 86 / JET-SC 26/6.1 "X-point proposals".
[24] JET document EUR FU 86 / JET-SC 26 6.2 "Pellet injection in JET".
[25] JET document EUR FU 86 / JET-SC 26/6.3 "Plasma exhaust proposals".
[26] JET document EUR FU 86 / JET-SC 26/6.5 "Current profile control"
[27] R.Toschi, "Approach to the definition of NET": Proceedings of the 13th Symposium on Fusion Technology, pp.133-144, Varese, Sept.1984.

Paper at 7th Topical Meeting on
Technology of Fusion Energy, Reno, USA, June 1986

Main Features Implemented in the JET Facility for Deuterium-Tritium Operation

M. Huguet and E. Bertolini

Huguet M, Author No. 1, JET Joint Undertaking
Abingdon, Oxon, OX14 3EA, UK.
Abingdon 0235-28822.

Bertolini E, Author No. 2, JET Joint Undertaking
Abingdon, Oxon, OX14 3EA, UK.
Abingdon 0235-28822.

ABSTRACT

One of the main objectives of the JET experiment is to reach near ignition conditions using deuterium-tritium mixtures so that significant heating of the plasma by alpha particles is achieved. This objective is reflected in the JET development plan which aims at one or two years of active operation and a few thousands deuterium-tritium shots. This approach, where it is believed that a sustained active operation period is necessary for a meaningful study of alpha particle heating, has had considerable design and cost implications on the whole project. The paper first reviews the impact of the active phase on the general design concepts and detailed design of the machine. Buildings, auxilliary systems, power supplies and diagnostics have also been strongly influenced by requirements resulting from the activation of the machine or the use of tritium. The paper reviews also the development programme which is being pursued vigorously in the areas of remote handling and tritium recycling, in readiness for the active phase. An evaluation of the cost of all facilities implemented for the active phase in relation to the overall project cost is also presented.

I INTRODUCTION

The JET experiment, which started operation in June 1983, represents the central pillar of the European fusion research programme, coordinated and supported by the European Atomic Community (EURATOM).[1] The JET machine is shown in figure 1.

The objectives of the JET experimental programme, defined in the EEC Council of Ministers decision establishing the JET Joint Undertaking, are shown in Table I.

The first three objectives are common to other fusion experiments, but JET due to its parameters and size should substantially extend the range of plasma performance beyond the reach of most, if not all, the other tokamaks worldwide. However, the last objective, calling for a deuterium (D) - tritium (T) phase sustained for one to two years, is unique to JET. This is called 'active phase' because thousands of D,T pulses are planned, each producing up to 10^{20} fusion neutrons. The extensive use of the thermonuclear fuel should allow a meaningful study of the confinement properties of the highly energetic alpha particles resulting from the fusion reactions and most important, of their contribution in maintaining the plasma at the required high temperature.

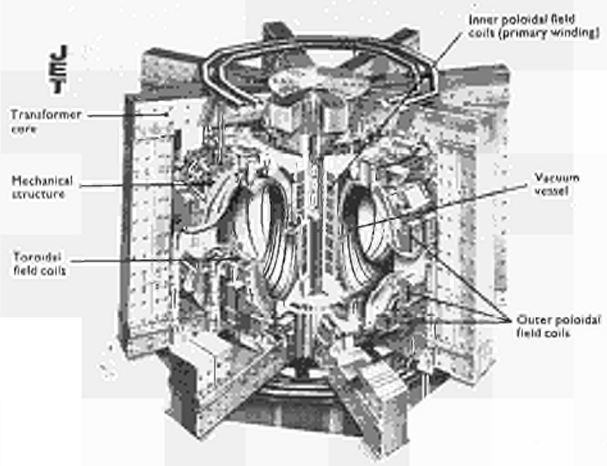

Fig. 1. The JET machine.

TABLE I: OBJECTIVES OF JET

i)	Study of plasma processes and scaling laws in operating regimes of interest for a thermonuclear reactor.
ii)	Study of the interaction of the plasma with the vessel walls, and control of plasma purity.
iii)	Study of plasma heating to temperatures of reactor relevance.
iv)	Study of the behaviour of energetic alpha particles produced by the fusion reactions and consequent plasma heating.

With the above definition of the D.T phase, the fourth objective has been the guiding factor throughout the whole definition process of the JET machine and associated facilities.

The choice of the tokamak parameters (moderate toroidal field, (3.45 T), large plasma current (4.8 MA) and volume (150 m^3)), allows both a safe mechanical design and easy access to the machine with the appropriate remote handling tools, while still maintaining a combination of these parameters suitable for approaching thermonuclear conditions.

Since the early phase of the design, considerable attention has been devcted to the reliability of the technical solutions and their suitability for unmanned interventions. This design philosophy has been applied not only to the Tokamak machine but also to auxilliary facilities and the lay-out and topology of buildings. As a consequence, major design options and the overall design optimization of JET differ from that of other Tokamaks and additional costs on the machine and auxilliary equipment have been substantial, in addition to the cost of remote handling and tritium handling.

In the following sections these aspects will be described and assessed in some detail.

II RADIOLOGICAL ASPECTS OF THE JET ACTIVE PHASE

The JET projet development plan includes a number of operation phases separated by major shut-downs during which important modifications or additions to the machine are implemented. The planned additional heating power on JET, both Radio-Frequency (RF) heating and Neutral Beam (NB) heating is shown on table 2. This table also shows the expected neutron production taking into account the enhancement due to beam-plasma interactions.[2] Activation levels inside the vacuum vessel are also given.[3]

The JET policy is to ensure that personnel access inside the vacuum vessel will be possible up to the 1990 shutdown for major work. Access should also be possible for minor interventions up to 1991 immediately before the active phase. It is also the JET intention that even nominated radiation workers receive as far as possible no more than 5 mSv/year (500 mRem/year). Table 2 shows how operation could be planned to achieve this.

In order to avoid severe manpower and organizational problems, the dose rate inside the vessel will have to be limited to 10 to 20 μSv/hour during the long 1987 shut-down. For the following shut-downs the dose rate will have to be kept below 100 μSv/hour since at this level a worker would receive his annual dose of 5 mSv after 50 hours. This may involve some restriction to the number of high power pulses as is implied in table 2. Another possibility is of course to operate mainly in hydrogen with only a small number of deuterium runs.

D.T operation from 1991 onwards implies a neutron production of at least 10^{19} and perhaps

TABLE 2. ADDITIONAL HEATING POWER AND NEUTRON PRODUCTION ON JET

Period	RF heating	NB heating (a)	Gas	Number of neutrons/pulse	Total neutron production/6 months (b)	Dose rate in μSv/hour (c)
1987	15MW	10MW(D)80kV	D.D	6×10^{16}	10^{19}	25
1988 1989	15MW	5MW(D)80kV 5MW(D)160kV	D.D	10^{17}	2×10^{19}	50
1990	15MW	10MW(D)160kV	D.D	2×10^{17}	3.5×10^{19}	100
1991 1992	15MW	10MW(D)160kV	D.T	10^{19}-10^{20}	up to 10^{24} (in 2 years)	>5000

(a) The power includes only full energy species.
(b) The main long term activation due to D.D neutrons (2.44MeV) comes from Co^{58} (half life = 71 days) and decays by about a factor 5 in 6 months.
With D.T neutrons (14 MeV) the long term activation does not decay significantly over a 6 months period (Mn^{54}=300 days; Co^{60}=5.2 years).
(c) Dose rate inside the vacuum vessel one week after operation. The neutrons are assumed to be produced uniformly over the last 6 to 9 months.

1 Sievert (Sv) = 100 Rem

up to 10^{20} neutrons per pulse. Depending on the neutron production, 100 or 10 such discharges would raise the activation level inside the vessel above 5 mSv/hour and would therefore make access impossible. Therefore full remote handling capability inside the vessel is mandatory from the outset of the D.T phase.

During the full D.T phase, access inside the vessel will be impossible but some strictly controlled access to the torus hall and basement beneath the machine could still be arranged. No general rules can be drawn since the activation level depends critically on the location of the work with respect to the ports of the vessel, or with respect to penetrations through the concrete floor between the torus hall and basement. The dose rate in the torus hall, at a point outside the mechanical structure, but not in the line of sight of a vessel port, is typically 300 times lower than inside the vessel (Table 3). This clearly opens up the possibility of some limited manual interventions by careful radiation monitoring. However extensive work would have to make use of remote handling techniques.

TABLE 3. GAMMA-RAY DOSE RATES IN mSv/HOUR AT SHUT-DOWN.[a]

Zone	1 day cooling	1 month cooling
Inside vacuum vessel	2.5×10^{3}	$1.7\ 10^{3}$
Outer surface of mechanical structure	8.6	6.1
Inner surface of Torus Hall wall at equatorial plane	2.5	1.8
Basement	2×10^{-3}	5×10^{-4}

a) The dose rates are calculated assuming a total of 10^{24} D.T neutrons produced uniformly over 2 years. This is the maximum credible neutron production for JET (10^{4} pulses each producing 10^{20} neutrons).

Tritium contamination must be carefully considered when manual interventions are contemplated in the Torus Hall during the D.T phase. Estimates of tritium permeation through the vessel walls, assuming full internal cladding (see section IV) indicate that the tritium concentration in the Torus Hall could be of the order of 10 $\mu Ci/m^3$ thus giving a dose rate of 10 $\mu Sv/hour$.[4] This takes into account the ventilation rate and assumes one air change per day. Such a concentration of tritium assumed to be in the HTO form would not prevent access to the torus hall although some precautions may have to be taken, depending on the duration of the work.

The other area where significant tritium contamination might be possible is the west wing of the building where the tritium plant is located. Due to the double containment principle used for the plant (see section IX) no access restriction is envisaged in normal conditions. During maintenance periods however special precautions may have to be taken.

Other areas of the JET site, or outside the site should not be affected by tritium release unless a major accident such as a fire, an earthquake or an aircraft crash occurs. Estimates of the maximum tritium release can be derived from the total site inventory of tritium. It will consist of less than 20g in the tritium plant itself and less than 10g firmly embedded on the walls of the vessel and neutral injectors. The latter quantity is assumed inaccessible. The worst possible tritium release is not considered to constitute a serious hazard. These considerations are part of the JET safety analysis still in progress, and are outside the scope of this paper.

III DESIGN PHILOSOPHY IN RELATION WITH THE ACTIVE PHASE

3.1 Design Principles

The design principles of the machine have been deeply influenced by the planned active operation. In particular:

- Established engineering techniques have been used as far as possible in order to limit the technological risk and reduce the probability of failure during the active phase. For these reasons, conventional copper coils are used and the magnetic field is kept at a reasonably low level.
- A modular design was selected for the machine, to ease assembly and maintenance procedures and consequently reduce the down-time when remote maintenance is necessary. The modular concept is apparent in the designs of the vacuum vessel and mechanical structure, which are split into 8 identical octants. Internal components, such as the belt limiter, are also made up of many identical segments.
- The poloidal field coils have been located outside the toroidal field magnet to ease maintenance.
- The vacuum vessel has been provided with large access ports to allow remote handling tools to reach critical welds or components inside the vessel.

3.2 Radiation Resistance

As regards the radiation resistance of insulating materials, the JET policy has been to seek the best materials currently available, rather than develop new products. This policy is consistent with the short time scale of the JET

construction and overall project life time. For this reason, the magnet insulation includes well proven epoxy systems and it is accepted that the life of the magnets may be limited by the deterioration of the insulation after exposure to doses in excess of 10^7 Gray (10^9 rad). It must be said that such a limit, if it were reached, would mean that JET would have been very successful in terms of overall neutron production (section 4.5). Components on the outer surface of the machine are partially shielded by the magnets and the mechanical structure and will not receive doses in excess of 10^6 Gray. Materials for cables, electrical connectors, rubber hoses etc. have been radiation tested to prove their suitability for JET.

3.3 Remote Maintenance

Remote maintenance capability is essential for JET. Although JET has been conceived with remote handling in mind, there are some cases where remote handling requirements were not given an overriding priority, and essential choices were made to optimize the design for better performances, rather than ease of maintenance. To design JET for complete and easy remote repair of any failure which might occur would have led to an unacceptable escalation in cost and construction time and would have represented a major deviation from the essential experimental objectives of the project. A reasonable balance has been struck by assigning priority levels to remote handling tasks.

A high priority level has been allocated to limited interventions on equipment which are known to require frequent maintenance or are vital for operation. For these tasks, remote handling considerations have determined the design, and a large effort is in progress for the development of special tools and procedures. Interventions on components internal to the vacuum vessel fall into this category.

For other tasks with a lower priority level, care has been taken to ensure that the design is remote handling compatible but only a limited effort has been allocated to develop tools and procedures. For example, major interventions such as the replacement of a full octant, fall into this category. It is accepted that a lower level of preparation implies prolonged down-time of the apparatus. The worth of a major intervention in active conditions would have to be assessed against the time required for it.

3.4 Buildings and Systems Layout

The design of the building and the lay-out of the systems around the machine have been determined by considerations related to the active phase. The machine itself is enclosed in a building, with typically 2.5 metres thick walls ceiling and floor, which acts as a biological shield (section VII).

For auxiliary equipment, the design rule has been to retain on the apparatus itself only essential parts. Whenever possible, equipment has been located outside the biological shield to allow hands-on maintenance and avoid radiation damage. This seemingly simple rule has not been easy to implement as will be seen in section VIII, since the long distance between the machine and systems has had far reaching consequences, in terms of design problems and costs. There is, however, no alternative to this design rule and, of course, the same rule will have to be followed for future fusion machines.

IV DESIGN FEATURES OF THE MACHINE WHICH HAVE BEEN IMPOSED BY D.T OPERATION

4.1 The Vacuum Vessel and Remote Handling

The JET vacuum vessel is an all welded, double walled inconel structure made up of alternate rigid sectors and flexible bellows.[5] For ease of assembly and to make an octant replacement possible at all, the vessel is split into 8 identical sectors or octants. The octants are joined by means of special "U joints" featuring a lip weld which can be cut or rewelded several times from the inside of the vessel.

As already mentioned in section III, the vacuum vessel has been provided with large access ports with dimensions to match the "Mascot" servomanipulator, which was selected for remote maintenance early during the design phase. Remotely controlled cutting and welding trolleys, able to run all along the "U joints" between octants, have been developed and were already used for the assembly of the machine in 1983.

For all components internal to the vessel, the capability of remote repair or replacement is mandatory. Tools for the replacement of graphite tiles, limiters and RF antennae are being developed and will be available for use during the 1987 shut-down period. This will enable tools and procedures to be experimentally tested and validated well in advance of active operation. For external connections to the main vacuum, standard welded lip joints or bolted flanges with metal seals have been developed in view of remote maintenance and use of tritium.

Remote leak detection is a daunting task on a machine the size and complexity of JET. At present the JET vacuum vessel has more than 600 vacuum connections in the form of vacuum seals or welds and this number is not expected to decrease although some diagnostics will be removed before the start of the active phase (section 5.3). It is not planned to develop an internal leak detection telescope for JET due to the complexity and cost of such a system. Remote leak detection will be based on conventional helium spraying techniques utilizing a servomanipulator and preinstalled helium spray tubes. Such spray tubes were already part of the original design of

the vacuum vessel, to enable the testing of inaccessible welds. More spray tubes perhaps connected to distribution boards, will be fitted on the machine prior to the active phase.

Since vacuum connections have been standardized, remote repair of leaks will be possible with special tools (section 6.2).

4.2 The Vacuum Vessel and Tritium

One of the major design features of the vessel, i.e. a double walled structure, was selected primarily in view of tritium operation. The double containment constitutes a safeguard against the accidental release of tritium, should a leak develop in the first wall. Moreover, the double wall reduces external contamination due to tritium permeation. Tritium permeating through the bellows of the first wall will be contained within the interspace and diluted in the hot gas which is circulated there to bake the vessel. The tritium concentration in the heat transport gas will be kept low by a clean-up system based on the oxidation of tritium and subsequent absorption of the tritium moisture. This system will be part of the tritium plant (section IX).

Permeation rates are difficult to estimate and depend critically on the oxidation of the metal surfaces. In the case of pressure driven permeation, conservative estimates show that the quantity of tritium released either in the interspace, or directly into the torus hall (the ports are single walled) is well within acceptable limits. Permeation can however be enhanced by atomic or molecular fluxes impinging on the walls during plasma shots or glow discharge cleaning. This "flux driven" permeation could lead to release rates several orders of magnitude greater than that due to pressure driven permeation. For this reason, it has been decided that the vessel walls which are not already protected by graphite tiles would be clad with inconel plates. This internal cladding is planned to be implemented during the 1988 shut-down.

During planned maintenance periods when the vessel is opened, precautions must be taken to minimize tritium emissions in the torus hall. To this end, prior to opening, the vessel will be baked at 300-400°C and glow discharge cleaning runs will be carried out with clean hydrogen or deuterium. This procedure will reduce tritium emissions to a negligible level. The tritiated gas stream from the glow discharge will be treated by the tritium plant.

4.3 The Pumping System and Gas Introduction Valves

The vacuum system is built to ultra high vacuum standard and is therefore tritium compatible since it uses welded joints or metal seals for vacuum connections, and all metal bakeable valves.

Pumping the torus is achieved by four turbo-molecular pumps with a total effective pumping speed at the vessel of 8500 $l.s^{-1}$. This pumping speed requires a large conductance and it was therefore necessary to install these pumps on the machine itself.

It is not expected that the turbo-pumps should be affected by tritium during the planned one or two years of active operation. Tests have shown that the change in viscosity of the bearing oil after an exposure to tritium comparable to that expected on the machine is negligible.

The roughing and backing pumps have been installed outside the torus hall in a service area which will remain accessible when the machine is active.

The backing pumps will consist of a set of tritium compatible pumps, either dry wobble pumps or roots blowers and will compress the gas towards the tritium recycling plant. For roughing operations, the existing roots and rotary pumps are not tritium compatible and will normally not be used. Roughing will be done by means of Normetex pumps which will compress the gas towards the clean-up and disposal system of the tritium plant.[6]

For the gas introduction system, tritium compatible on-off and dosing valves have been specially developed. These valves are all metal and use metal seals and bellow sealed shafts. It is envisaged to use valves of a similar design for the tritium recycling plant.

4.4 The Baking System

The vessel is baked by means of a hot gas circulating in the interspace between the inner and outer walls. The baking plant, including the blower, the heat exchanger and control systems, is located outside the biological shield and only lagged pipes carrying the hot gas penetrate the active area.

So far, air or nitrogen have been used as a heat transport gas. For the active phase, helium is the preferred gas for the following reasons:

(a) Helium is a low Z gas and relatively large interspace to main volume leaks would not affect plasma operation.
(b) Helium is not activated by neutrons, so no activity is transported outside the biological shield.
(c) Tritium contamination is easily removed from helium by oxidation and subsequent trapping of tritium oxide.
(d) Helium has good heat transport properties.

Tritium permeating through the bellows of the vacuum vessel will contaminate the baking loop. For this reason, the loop has been built to ultra high vacuum standard. The blower and its motor will be encapsulated in a metal box so as to

contain the unavoidable leaks through the shaft seal.

4.5 Magnets and Water Cooling Systems

All JET magnets are copper wound and water cooled. Superconductor technology was considered too risky in view of the experimental objectives of JET. As already mentioned in section III, the magnet insulation consists of proprietary epoxy fibre glass systems, which have been developed and extensively tested for particle accelerators. The reduction in the mechanical properties of epoxy resins at radiation doses in excess of 10^7 Gray is accepted since this exposure would be reached at the inner surface of the toroidal field coils after a total production of 10^{24} 14 MeV neutrons. For the poloidal field coils, an insulation system has been developed specially for JET and consists of epoxy resin, fibre glass and interleaved polyimide tapes. Adhesion to copper is also improved by means of a special primer. Up to exposures of 10^7 Gray this system has shown no significant reduction in shear strength.

It must be noted that the toroidal field coils and the mechanical structure act as a very effective radiation shield (Table 3). To improve the shielding effect, the hollow, box like, elements of the mechanical structure have been filled with boronated concrete. This is important to reduce the radiation dose to peripheral equipment and the air activation in the torus hall, and also to ease future decommissioning activities.

Activation of the cooling water of the magnets is significant. The activation is essentially due to $^{16}O(n,p)^{16}N$ reactions. ^{16}N is a γ emittor (6 and 7 MeV) with a half life of 7s. Although short lived, the calculated levels of activation have made it necessary to locate the demineralized water plant within the biological shield. An alternative solution using a holding tank able to store all the water emerging from the magnets during a pulse was technically more complicated. In order to allow hands-on maintenance, the demineralized water loop, including pumps, heat exchangers, valves and filters, is in the basement in an area well shielded from direct radiation. This arrangement also ensures that they will be no activation of the primary water coming from external cooling towers. The resin beds for the water treatment are also within the biological shield but in the access cell for an easy replacement (section VI). These beds will indeed retain all the activated impurities carried by the water. Apart from activation problems, the generation of oxygen in the cooling water by radiolysis and subsequent corrosion, has also been considered. It is planned to monitor carefully the oxygen concentration and if required use deoxygenation techniques.

Contamination of the cooling water by tritium permeating through water pipework or water cooled components inside the vacuum vessel has been found to be negligible.

Therefore the water system requires no significant modification for use during the D.T phase. The only precaution will be to monitor the activity of the primary site water so as to detect any, unlikely, leak in the heat exchangers, between the demineralized and site water loops.

4.6 Design Details

Apart from major design options, there are many design details which have been imposed by remote handling considerations. These design details include features such as welding lips, captive bolts, self locating or self locking mechanisms. Connectors and flanges for vacuum, water or compressed gases have been the subject of a special effort which has resulted in "Standard" JET remote handling designs for general use in the project. Although the monetary value of such design details is not great, they represent a large investment of ingenious design and prototype testing and their incorporation in the machine components requires a considerable design effort. As an example, it has been estimated that the design of the belt limiter including specific remote handling tools, has required 3 to 4 times more design office effort than the same study without remote maintenance requirements.

V OTHER SYSTEMS DIRECTLY CONNECTED TO THE MACHINE

5.1 Neutral Beam Injection Systems

The neutral beam injectors are connected to the main torus vacuum and therefore some tritium is expected to diffuse from the torus to the injector boxes. Tritium back diffusion in each box is minimized by means of a fast shutter which is normally closed and opens briefly during beam injection. This shutter is not a vacuum tight valve but gives, when closed, a low conductance between the torus and the injector box. With this arrangement, tritium contamination is much reduced but nevertheless provisions have been made for full tritium compatibility of the injector boxes. In particular, all components inside the injector boxes have been built to ultra high vacuum standards and use exclusively metal seals or welded joints. The deflection magnets have been lined with stainless steel. Actuactor shafts are bellow sealed. Tritiated gasses from the injector boxes will be exhausted by turbo-molecular pumps and directed to the tritium recycling plant.

The neutral injector systems use large cryo-pumps of a novel design. For the reasons

explained in section 3.4, the cryo plant has been located outside the biological shield, 100 metres away from the cryo-pumps and this made it necessary to develop a new type of advanced cryo transfer lines with a low thermal loss performance.

Activation of the liquid nitrogen used in the cryo-pumps has been considered. It will require either a closed supply loop or a holding system.

5.2 Radio-frequency Heating System

The radio frequency antennae are located inside the vacuum vessel and the power is transmitted through the vessel walls by means of coaxial vacuum transmission lines. Since these lines are connected to the main torus vacuum they have been designed for tritium compatibility using metal seals and bellow sealed valves. The pumping system for these lines presently uses small turbo molecular pumps but it is planned to replace them by getter pumps. These pumps would be fully sealed, with no external connections and could be regenerated through the main torus vacuum. A similar solution is envisaged for some diagnostics (section 5.3).

5.3 Diagnostics

Some of the diagnostics have not been designed to be remote handling compatible as they will be disconnected from the machine before the start of the active phase. Active phase diagnostics however must be capable of at least complete dismantling and in some cases repair by remote handling techniques. Those diagnostics which are connected to the vacuum system must also be designed for tritium operation.[12] This has been achieved by using metal seals or welded joints, all metal valves, and making provision for system baking. The small turbo molecular pumps used for individual diagnostics are all tritium sealed but nevertheless it is envisaged to replace them with getter pumps before the start of the active phase. Such pumps would be fully sealed with no external connections and would be regenerated through the main torus vacuum.

Due to the high radiation level, electronics will not survive inside the torus hall, so all diagnostics designed for the active phase have detectors, electronics and components requiring maintenance, outside the torus hall. This poses problems of efficiency due to signal attenuation and problems of radiation shielding.

The Electron Cyclotron Emission (ECE) diagnostic is an example of a system where the signal can be guided along tortuous paths around shielding labyrinths. The penalty however, is a serious signal attenuation due to the length and many bends of the waveguides, before reaching the detectors which must be located outside the biological shield. (Fig. 2).

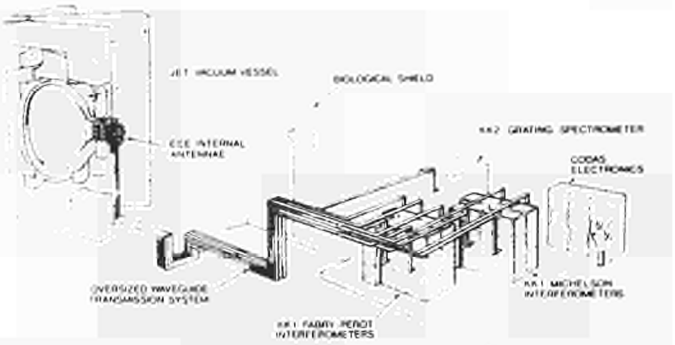

Fig. 2. Layout of waveguides for the E.C.E. diagnostic.

The X-ray crystal spectrometer is an example of a diagnostic requiring a direct line of sight between the plasma and the curved crystal which had to be mounted outside the torus hall. Shielding is necessary outside the penetration window. In this particular case, the problem is made more difficult since a direct line of sight is also required from the curved crystal to the detectors located on the Rowland circle, 15 metres away from the crystal. Additional shielding must contain the scattered radiation all along the beam line. For this diagnostic alone, over 500 tonnes of concrete and blockwork has been erected in the diagnostics hall adjacent to the torus hall.

VI REMOTE HANDLING CONCEPTS AND MAIN FACILITIES

6.1 General Philosophy

As already explained in section III, the JET policy regarding remote handling has been, firstly, to ensure that the design of the components is generally remote handling compatible and, secondly, to provide general purpose remote handling tools able to carry out a great variety of tasks. Special tools designed to carry out specific interventions are also being developed, but only for a limited number of high priority tasks. It has been therefore necessary to classify remote handling tasks, as follows:[8]

Class 1 = Tasks essential to keep the machine in operation, and which are expected to be required during the active phase (e.g. replacement of graphite protection tiles, replacement of a plug-in neutral beam injector).

Class 2 = Tasks essential to keep the machine in operation but which are unlikely to be required during the active phase (e.g. repair within a neutral injection box, replacement of one octant).

Class 3 = Tasks not essential for the operation of the machine. A failure may affect operation only marginally (e.g. replacement of a non essential diagnostic).

Class 4 = No remote handling requirement.

Full remote handling capability, including all special tools and procedures, is being developed for class 1 operations. For class 2 operations, the design is remote handling compatible, but only general purpose tools are available and therefore extensive down time may be required to carry out the work. For class 3 operations, the design has been only marginally influenced by remote handling considerations.

For each component of the JET machine and its auxiliary facilities a TCD (Technical Control Document) has to be submitted for approval to the weekly Design Coordination Meetings. For those components expected to be in an active environment, the design shall specify the remote handling class. The Remote Handling Manual is available to the designers for the definition of remote handling requirements, for following recommended standards and for choosing appropriate "couplings", such as flanges, connectors etc.

6.2 Equipment

An overall view of the remote handling (RH) equipment is shown in Figure 3.: it includes transporters to move components and to position various RH tools, end effectors for special purpose lifting and, among them, servomanipulators to carry out dexterous planned and unplanned operations, special tools for planned operations in confined spaces and finally an in-vessel inspection system to assess the status of the vessel walls without breaking the vacuum.[9]

There are four main transporters. The 150 tonne bridge crane, with a remote control capability of the hook of 2mm horizontally and 0,2mm vertically, has been used throughout the assembly of JET; the telescopic mast, with its articulated arm, and a lifting capability of 3 tonnes, will be used for difficult operations on the outer parts of the machine; the low level transporter will be used to reach components at the bottom part of the machine; finally the articulated boom, for operations inside the vessel, allows the carriage of RF antennae, limiter sections etc. with special tools.

In order to lift equipment onto the transporters, a turret truck will be provided, and support for transporters will be provided by a small tracked vehicle.

While the bridge crane has been extensively used since the early phases of the JET assembly, the articulated boom has been successfully used during the 1985 shutdown for removing and positioning limiters and RF antennae.

End effectors are: the two force reflecting servomanipulators, consisting of two units, master and slave, kinematically similar; the limiter gripper to be fitted at the end of the articulated boom, for lifting and positioning limiters; a similar device for the RF antennae is also provided.

Special Tools are required for specific operation: it is this area where the imagination and the ingenuity of the designers are most required, due to the constraints on weight, accuracy and operational space. A number of automatic cutting and welding devices belong to this category, and they are dedicated to vessel octant joints, 100 mm diameter circular ports, 50 mm toroidal limiter cooling pipes etc.

Finally, a four probe system has been developed for in-vessel inspection, under vacuum with wall temperatures up to 50°C. Each 60 mm probe is terminated with a glass cup and equipped

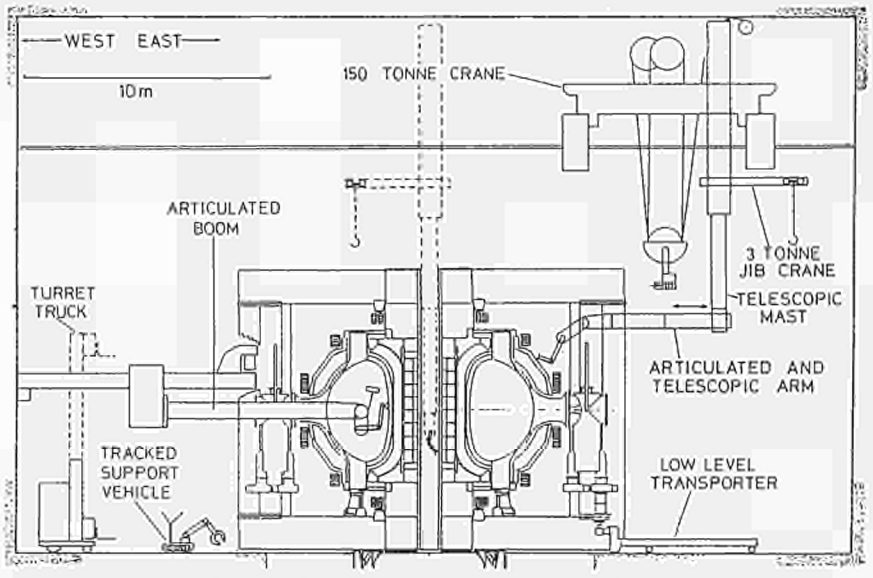

Fig. 3. Remote handling equipment overall pattern

with TV cameras. The system has already been successfully tested to assess the status of the vessel walls.

All remote handling operation will be performed from a dedicated remote handling control room.

6.3 Procedures

Remote Handling Procedures, describing the necessary operations, are required and checked before a particular component is manufactured. These procedures will be used to set up intervention schedules to be checked first by mock up simulations and, for some, on the machine itself before radiological activation.

VII THE JET BUILDING AS A BIOLOGICAL SHIELD

The JET building has been designed to limit the exposure to staff to less than 1 mSv/year, and to reduce the level of radiation at the site boundary to less than the normal fluctuations in background level.[10] The building must provide protection against the following hazards.

a) Direct irradiation by neutrons and X-rays during discharges.
b) Y-ray radiation due to the activation of the apparatus.
c) Release of air activated during discharges.
d) Release of tritium due to chronic or accidental leaks.
e) Release of activated or contaminated water from the apparatus.
f) Activation of ground water under or around the building.

TABLE 4. DOSE RATES DURING D.T OPERATION (Sv/YEAR) (ASSUMING 10^{24} D.T NEUTRONS PRODUCED UNIFORMLY IN 2 YEARS)

Inner surface of Torus Hall wall	3×10^{5}
Outer surface of Torus Hall wall	3×10^{-4}
Control room	1×10^{-4}
Site boundary	2.5×10^{-6}

The biological shield is shown on Figure 4 and its effectiveness is demonstrated in Table 4. In the torus hall, no shielding has been interposed between the apparatus and the walls and there is full accessibility for remote operations. The walls are 2.5 m thick concrete plus an additional 0.3 m lining of boronated (0.7%B) concrete block work. This inner lining attenuates the backscattering of neutrons and thus limits the air activation due essentially to Ar^{41}. The lining also decreases the activation of the main wall, and when removed, would facilitate decommissioning activities. The roof is 2.25 m thick overlapping concrete slabs with an additional 0.04 m thick boronated lining. The roof thickness ensures that radiation levels due to scattering in the air above the building (sky-shine) are low in working areas. The torus hall floor is 0.8 m thick re-inforced concrete with an additional 0.2 m boronated screed. The basement floor adds another 3 m of concrete between the machine and the ground.

There is a radiation shielded cell between the torus hall and the assembly hall. This cell is used presently as a test cell for neutral beam injectors and can be used later as a storage, decontamination or repair cell for active components. Resin beds for the water cooling system are also located in this area (section 4.5). The main function however of this shielded cell is to provide a radiation and air lock allowing the transfer of large pieces of equipment, or the

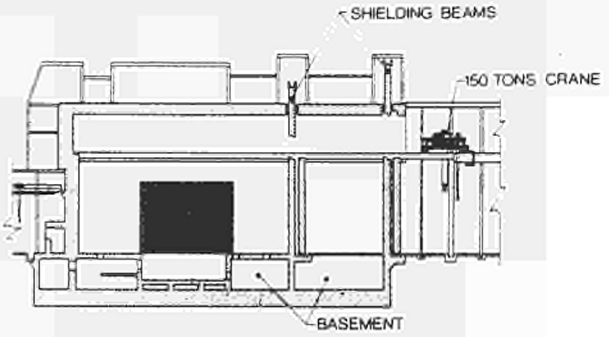

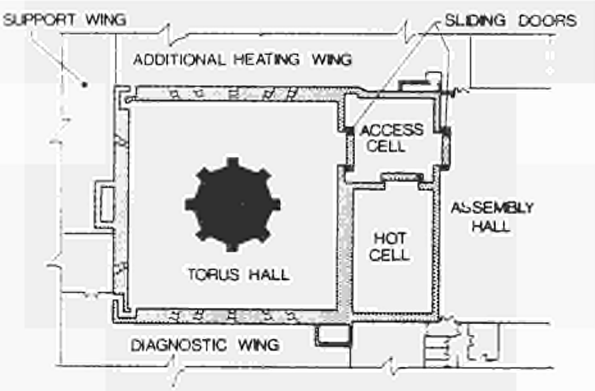

Fig. 4. The JET biological shield.

crane, between the torus and assembly halls. Transit of the crane is possible by raising the 1100 tonnes concrete shielding beams. Crane suspended or floor mounted equipment can pass through massive concrete sliding doors. The two sets of shielding elements must be closed during operation. Outside operation periods and when the machine is activated, the shielding elements can only be operated sequentially. The shielding elements are made airtight by means of inflatable elastomer seals.

A feature of the torus hall is the provision of a pit underneath the machine. This pit contains large manifolds for air, water, primary vacuum and gas, which distribute these services all over the machine. Only a small number of penetrations is therefore required between the pit and the main service basement.

The main service basement provides a radiation shielded route for services, power transmission lines and cables. The basement contains also the water cooling plant and the air ventilation plant which both will circulate activated fluids. Some electronics cubicles are also located in a well shielded peripheral trench.

Release of activated air or tritium must be prevented. To this end, the shielded areas are provided with air seals at all penetrations and access points so that they can be held at a slight under pressure of typically 5 mbar. Furthermore a small differential pressure of 2 mbar is maintained within the shielded areas between the torus hall and the basement and test cell. With this arrangement, the air leak is less than 0.5 m^3/s for the whole shielded area and the air change in the torus hall is less than 1 per day. The supply of air-tight penetrations for all services, cables and power lines has represented a major investment in terms of design, planning of installation, supply and actual installation work. Penetrations are sealed by steel frames carrying tailor made rubber packing elements around pipes and cables.

The building is water tight and includes drain systems which collect into an active sump where radiation levels can be monitored before water disposal.

A comprehensive radiological monitoring system has already been installed within and outside the biological shield to measure the radiation doses equivalent from X and Y radiations and neutrons.[11] As JET progresses towards the D.T phase, tritium monitors and detectors for Ar^{41} and N^{13} (air activation) will also be installed. The large quantity of data from these fixed monitors is computer processed to provide on line displays, integrated or average radiation levels, alarm levels etc.

Personnel monitoring will make use of electronic dosimeters (geiger counters) for short visits in radiation controlled areas. These dosimeters can be plugged in to readers at the access doors, so that the dose increment during the visit and the integrated dose to the individual person is recorded by the computer. Thermoluminescent dosimeters will also be used as a back up system in order to provide the integrated Y ray dose equivalent to individuals, for longer periods up to 1 month. The data base and personnel files for this system are also computerized.

VIII DESIGN FEATURES OF CONTROL AND POWER SYSTEMS FOR D.T OPERATION

In order to minimize remote maintenance requirements, a considerable effort has been made to keep all possible auxiliary components and subsystems away from the torus hall and basement.

8.1 Electronics and Services

The first rule established was not to have electronic cubicles anywhere near the machine, for both avoiding radiation effects on the electronics and remote handling methods for maintenance. All machine and diagnostic cubicles are therefore kept between 50 and 150 m away from the torus, thus requiring long cables through complex penetration paths, to avoid neutron shine through. From the electronics cubicles, the cables run through airtight penetrations into the basement, from the basement to the torus hall through airtight penetrations and finally up the magnetic limbs of the machine to local junction boxes. From there, jumper cables with remote handling connectors, connect to the instruments. Services such as air, water, compressed air etc. are also locally connected by flexible jumper hoses with remote handling couplings. This arrangement allows an easy disconnection prior to maintenance work or dismantling.

The design implication of the above requirement was faced for the first time in fusion research by JET.

8.2 Power Supplies

Most of the site area is occupied by the power supplies and power modulation systems, i.e. ohmic heating circuit, neutral injector protection and RF generators (Fig 5), which in any tokamak are the closest to the machine.

Fig. 5. Aerial view of the JET site.

Since, for JET, they have to be installed beyond the radiological shield, i.e. outside the torus hall and basement, the average length of cables and transmission lines was increased by 100 m. Again this is to avoid radiation damage and remote handling methods for maintenance.

The design of the DC busbars to the tokamak coils is further complicated by the geometry of the penetrations into the basement and from there to the torus hall.

There are two sets of transmission lines which, due to their non conventional features, have required to solve special technical problems: these are the neutral beams (NB) and the radio frequency (RF) power transmission lines.

The key features of the NB transmission lines are the high operating voltage (160 kV DC) and the low capacitance (50 pF/m as compared with conventional cables 200 pF/m), in order to limit the capacitive energy dissipated in the fault, in case of a short-circuit in the neutral beam source. However, due to the length of the NB transmission lines in JET (90 to 120m), the capacitive energy of the transmission line and the other stray capacitances is still too high (~100J) and in order to reduce it and limit the fault current to 300A a set of snubber magnetic circuits to dissipate the extra energy, must be installed near the injectors.[10] Similar consideration, although of different technical nature, apply to the RF power transmission lines and have resulted in a novel design concept.

The scale of this equipment would have been drastically reduced if D.T operation would have not been considered.

IX THE JET TRITIUM RECYCLING PLANT

JET will use a recycling system able to purify the exhaust gases from the machine and separate the hydrogen isotopes for re-use. A "once through" system (where the tritium is supplied and discarded after use) was considered initially but has not been adopted because of the high purchase and disposal cost of tritium. It must be noted that the total quantity of tritium to be used in one to two years is of the order of 1 to 2 kg (250 mg/pulse).

A recycling system appears to be a more economical solution. Moreover, the recycling plant requires a much lower inventory of accessible tritium on site and avoids the problems associated with frequent, almost daily, deliveries of fresh tritium.

The engineering concepts of the JET plant are as follows:

a) Gas chromatography will be used for the separation of hydrogen isotopes.
b) Cryopumps rather than mechanical pumps, are used for gas transfers within the purification and isotopic separation system. It is hoped that such a static system will be essentially maintenance free. The batch operation of the cryopumps is also well suited to the gas chromatography process.
c) Primary circuit components are enclosed in bakeable vacuum vessels which serve as the secondary containment. This should virtually eliminate tritium emissions and the need for complex clean-up systems associated with classical glove box containment.
d) Due to the relatively short utilization time of the plant, and the low throughput, waste handling and disposal facilities will not be provided on site. Wastes will be contained and sent for disposal at existing facilities.

The plant must first purify the exhaust gases. To this end, the gases are first directed to the accumating panel where the gases are frozen and the heavy volatile impurities (H_2O, CO_2..) are retained and accumulated over periods of typically one month. From there, the gases are frozen in a cryopump, which when warmed up, compresses the hydrogen isotopes through the gas chromatographic columns. Two cryopumps and gas chromatographic units, working alternately to process gas batches corresponding to approximately 12 pulses, perform this function. The processed gas fractions are then stored in their respective tanks and are ready for re-use. Gases with a low tritium content coming from the neutral injector boxes, pellet injectors or glow discharge cleaning gas streams, are also processed by the plant.[6]

A clean up system can remove tritium from the gaseous wastes from the plant operation or from gases produced during maintenance. It can also process tritiated air from the torus during pump-down. The removed tritium is fixed as tritium oxide on dessicant beds for disposal.

At present, prototypes of key components designed by JET, such as valves, cryopumps, accumulating panels, are being performance tested in a special rig. The tritium plant is planned to be ready for commissioning in 1990, one year prior to the start of the active phase.

X THE COST OF THE JET ACTIVE PHASE

Additional costs associated with the active operation are difficult to single out since the requirements of the active phase have always been an integral part of the JET design. The additional design and development work in particular is difficult to assess. However it is certain that a considerable engineering effort has been required, not only within the JET division responsible for remote handling and tritium, but throughout the entire project.

Nevertheless there are a large number of clearly identifiable major items, specific to the active phase of JET, for which reliable additional costs can be given. These costs which can be attributed to the active phase are: 10 M$ for the buildings (torus hall walls, hot cell, sliding doors and roof beams, penetrations through the radiological shield, ventilation system); 6 M$ for the tokamak itself (RH compatible flanges, cable junction boxes, vessel large ports and double walls, with helium cooling etc.); 5 M$ for the power supplies (transmission lines for NB and RF, NB snubbers, length of cables and busbars); 11 M$ for diagnostics (14 MeV neutrons, active phase spectroscopy, signal transmissions through the radiation barrier and radiation compatibility of the other plasma diagnostics required); 10 M$ for the development of all the specific RH equipment (see section VI, but excluding the 150 tonne crane); 12 M$ for the tritium processing plant and finally 3 M$ foreseen for handling the tritium waste.

The above figures add up to 57 M $. It is believed that through a detailed analysis of the JET design, a large number of smaller items would have to be considered. In addition, if the considerable engineering costs were also taken into account, the overall costs for the fulfilment of requirements of the extensive D.T operation foreseen for JET, would account for 15-20% of the overall costs of the JET project.

XI CONCLUSIONS

After three years of operation, the JET experimental results are most encouraging. The best, but not simultaneous, plasma parameters achieved are Ti (ion temperature) = 7 keV, n_i (ion density) = $6 \times 10^{19} m^{-3}$, τ_E (global energy confinement time) = 0.8s, while the best simultaneous combination gives a fusion parameter $T_e \times n_i \times \tau_E = 6 \times 10^{19}$ keV.m^{-3}s. Up to 13 MW of additional heating (NB + RF) power has been injected and D.D neutron production rates up to $5 \times 10^{15} s^{-1}$ have been measured. These results are however still far from those required for D.T operation. A meaningful D.T phase with significant alpha particle heating would require a fusion parameter of about 5 to 10 x 10^{20} keV.m^{-3}s. In order to bridge the gap, a programme of enhancements and additions has been initiated. This programme includes pellet injection, magnetic limiter operation, plasma current profile control, disruption control and extension of the maximum current capability from 5 to 7 MA.

From the technical point of view, the work performed so far and the developments underway with a view to make JET and its associated facilities suitable for D.T operation, are considered adequate to attack the ultimate and most important goal of the project that is to study alpha particle heating in a reactor relevant plasma. It must be stressed that the aim to carry out this study during a sustained period of one to two years is unique on the world scene of tokamak research today.

Since the problems associated with a sustained D.T operation had to be faced for the first time in fusion research it is believed that JET has broken new ground in the development of some key technologies. The work undertaken by JET may prove to be most valuable for the design, construction and operation of NET (Next European Torus) now in the conceptual design phase, as part of the European Community Fusion Programme.

ACKNOWLEDGEMENTS:

This paper reports the work of the whole JET team under the leadership of Dr. P.H. Rebut. The authors would like to thank B. Keen, K. Dietz and J. Dean for their suggestions to improve the text.

REFERENCES

1. The JET Project. Reports of the Commission of the European Communities, EUR 5516 e (1976); EUR 5781 c (1977), EUR 6831 en (1980).

2. GIBSON, A. JET Private communication.

3. AVERY, A.F. Dose Rates and Inventories of Active Isotopes at JET, AEE, Winfrith. Work carried out under JET contracts JB0/0079 and JB1/0563.

4. GORDON, C. JET Private communication.

5. DUESING, G. Construction and Commissioning of JET, 9th Int. Vacuum Conf. Madrid (1983).

6. RIEDEKER, W. JET Private communication.

7. MILLWARD, P. et.al. Aspects of Interfacing JET Diagnostics Systems, 11th Symposium on Fusion Engineering, Austin (Texas), (November 1985).

8. RAIMONDI, T., Dean, J. Concept and Status of Remote Handling in JET. 10th Symp. on Fusion Eng. Vol II, Page 1793-1797. Philadelphia (November 1983).

9. ROLFE, A.C. Remote Maintenance of the JET Tokamak, Proceedings of the U.K. prototype and Research Managers conference, (SRD Cultech, UK, March 1986).

10. GIBSON, A. Provisions for the Radioactive Operation of the JET Experiment, American Nuclear Society Meeting, Washington, DC, (November 1982).

11. CALDWELL-NICHOLS, C.J. JET Private communication.

JET Contributions to 11th International Conference on Plasma Physics and Controlled Nuclear Fusion Research

(KYOTO, JAPAN, NOVEMBER 1986)

Dr P. H. Rebut et al

JET LATEST RESULTS AND FUTURE PROSPECTS

The JET Team
(Presented by P. H. Rebut)
JET Joint Undertaking, Abingdon, Oxon, OX14 3EA, U.K.

H. Altmann, R. J. Anderson, J. Arbez, D. V. Bartlett, W. Bailey, B. Beaumont[1], G. Beaumont, K. Behringer, E. Bertolini, P. Bertoldi, C. H. Best, V. Bhatnagar[4], R. J. Bickerton, A. Boileau[15], F. Bombarda[10], T. Bonicelli, S. Booth, A. Boschi, G. Bosia, M. Botman, H. Brelen, H. Brinkschulte, M. L. Browne, M. Brusati, T. Budd, M. Bures, P. Butcher, H. Buttgereit, D. Cacaut, C. Caldwell-Nichols, J. Callen[12], D. J. Campbell, J. Carwardine, G. Celentano, C. D. Challis, A. Cheetham, J. Christiansen, C. Christodoulopoulos, P. Chuilon, R. Claesen, J. P. Coad, S. Cohen[19], M. Cooke, J. G. Cordey, W. Core, S. Corti, A. E. Costley, G. Cottrell, M. Cox[11], C. David, J. Dean, E. Deksnis, G. B. Denne, G. Deschamps, K. J. Dietz, J. Dobbing, S.E. Dorling, D. F. Düchs, G. Duesing, P. Duperrex[6], H. Duquenoy, L. de Kock, A. Edwards, J. Ehrenberg[2], W. Engelhardt, S. K. Erents[11], F. Erhorn, B. T. Eriksson, M. Evrard[4], H. Falter, N. Foden, M. Forrest[11], C. Froger, K. Fullard, G. Fussmann[2], M. Gadeberg[5], A. Galetsas, A. Gallacher, D. Gambier[1], A. Giannelli[10], R. Giannella[10], A. Gibson, R. D. Gill, A. Goede, A. Gondhalekar, C. Gordon, C. Gormezano, N. A. Gottardi, C. Gowers, R. Granetz, B. Green, S. Gregoli, F. S. Griph, R. Haange, J. H. Hamnén[3], C. J. Hancock, P. Harbour, N. Hawkes[11], P. Haynes[11], T. Hellsten, J. L. Hemmerich, R. Hemsworth, F. Hendriks, R. F. Herzog, L. Horton[21], J. How, M. Huart, A. Hubbard[9], J. Hugill[11], M. Hugon, M. Huguet, B. Ingram, H. Jäckel[2], J. Jacquinot, Z. Jankowicz[17], O. N. Jarvis, E. M. Jones, T. T. C. Jones, P. Jones, C. Jupén[20], E. Källne, J. Källne, O. Kaneko[18], A. Kaye, B.E. Keen, M. Keilhacker, G. Kinahan, S. Kissel, A. Konstantellos, M. Kovanen[16], U. Küphnapfel[2], P. Kupschus, P. Lallia, J. R. Last, L. Lauro-Taroni, K.D. Lawson[11], E. Lazzaro, R.C. Lobel, P. Lomas, N. Lopes-Cardozo[7], M. Lorenz-Gottardi, C. Lowry[9], G. Magyar, D. Maisonnier, M. Malacarne, V. Marchese, P. Massmann, G. McCracken[11], P. McCullen, M. J. Mead, P. Meriguet, V. Merlo, V. Mertens[2], S. Mills, P. Millward, A. Moissonnier, P.L. Mondino, D. Moreau[1], P. Morgan, R. Müller[2], D. Murmann[2], G. Murphy, M.F. Nave, L. Nickesson, P. Nielsen, P. Noll, S. Nowak, W. Obert, M. Olsson, J. O'Rourke, M.G. Pacco, J. Paillere, S. Papastergiou, J. Partridge[11], D. Pasini[21], N. Peacock[11], M. Pescatore, J. Plancoulaine, J-P. Poffé, R. Prentice, T. Raimondi, J. Ramette[1], C. Raymond, P. H. Rebut, J. Removille, W. Riediker, R. Roberts, D. Robinson[11], A. Rolfe, R.T. Ross, G. Rupprecht[2], R. Rushton, H.C. Sack, G. Sadler, J. Saffert, N. Salmon[9], F. Sand, A. Santagiustina, R. Saunders, M. Schmid, F.C. Schüller, K. Selin, R. Shaw, A. Sibley, D. Sigournay, R. Sillen[7], F. Simonet[1], R. Simonini, P. Smeulders, J. Snipes[11], L. Sonnerup, K. Sonnenberg, M. Stamp, C.A. Steed, D. Stork, P.E. Stott, T.E. Stringer, D. Summers, H. Summers[13], J. Tagle, G. Tallents[14], A. Tanga, A. Taroni, A. Terrington, A. Tesini, P.R. Thomas, E. Thompson, K. Thomsen[5], F. Tibone, R. Tivey, T. Todd[11], P. Trevalion, M. Tschudin, B. Tubbing[7], P. Twynam, E. Usselmann, H. van der Beken, M. von Hellermann, J.E. van Montfoort, J. von Seggern[8], T. Wade, C. Walker, B.A. Wallander, M. Walravens, K. Walter, M.L. Watkins, M. Watson, D. Webberley, A. Weller[2], J. Wesson, J. Wilks, T. Winkel, C. Woodward, M. Wykes, D. Young, L. Zannelli, J.W. Zwart

PERMANENT ADDRESSES

1 Commissiariat á L'Energie Atomique, F-92260 Fontenay-Aux-Roses, France.
2 Max Planck Instituut für Plasmaphysik, D-8046 Garching bei Munchen, F.R.G.
3 Swedish Energy Research Commission, S-10072 Stockholm, Sweden.
4 EUR-EB Association, LPP-ERM/KMS, B-1040 Brussels, Belgium.
5 Risø/National Laboratory, DK-4000 Roskilde, Denmark.
6 CRPP/EPFL, 21 Avenue des Bains, CH-1007 Lausanne, Switzerland.
7 FOM Instituut voor Plasmafysica, 3430 Be Nieuwegein, The Netherlands.
8 Kernforschungsanlage Jülich GmbH, D-5170 Jülich, F.R.G.
9 Imperial College of Science and Technology, University of London, U.K.
10 ENEA-CENTRO Di Frascati, I-00044 Frascati, Roma, Italy.
11 UKAEA Culham Laboratory, Abingdon, Oxfordshire, U.K.
12 Dept. of Physics, University of Wisconsin, Madison, U.S.A.
13 University of Strathclyde, 107 Rottenrow, Glasgow, G4 0NG, U.K.
14 The Australian National University, Research School of Physics, ACT 2600, Australia.
15 Institute National des Recherches Scientifique, Quebec, Canada.
16 Dept. of Physics, Lapeenranta University, Finland.
17 Cyfronet, Poland.
18 Dept. of Physics, University of Nagoya, Japan.
19 Princeton Plasma Physics Laboratory, New Jersey, U.S.A.
20 University of Lund, Lund, Sweden.
21 Natural Sciences and Engineering Research Council, Ottawa, Canada.

Abstract

During JET's first three years of operation, experiments have been undertaken with up to ~7MW of ICRF, ~10MW of neutral beam and ~18MW of total input power during combined operation. The latest JET results show many advances made during this period. In particular, the especially good confinement (τ_E up to 0.8s), high temperatures (T_e up to 5keV) and fusion product $<\hat{n}_i\tau_E\hat{T}_i> = 10^{20}\mathrm{m}^{-3}$.s.keV achieved with ohmic heating alone have exceeded expectations. Also, very efficient ion heating has been observed ($T_i > 12.5 \pm 1.5$keV) at moderate neutral beam injection power levels ($P_{NB} \leq 8$MW) and at low average densities ($\bar{n}_e \sim 1\text{-}1.5 \times 10^{19}\mathrm{m}^{-3}$). In addition, a fusion product $<\hat{n}_i\hat{T}_i\tau_E> = 2 \times 10^{20}\mathrm{m}^{-3}$.s.keV has been achieved with a separatrix configuration in JET. However, limitations have been encountered in plasma density and electron and ion temperatures due to disruptions and sawtooth oscillations. With additional heating, confinement is degraded, as the electron temperature outside the sawtooth region exhibits only a weak dependence on the input power per particle. As a consequence, additional heating has little impact on the fusion product. The consequent developments to provide significant α-heating in JET are described.

1. Introduction

The Joint European Torus (JET) [1,2] is the largest single project of the coordinated fusion research programme of the European Atomic Energy Community (EURATOM). Its main objective is to obtain and study plasmas in conditions and with dimensions approaching those needed for a fusion reactor (ie $n = 2 \times 10^{20}\mathrm{m}^{-3}$; $T \geq 10$keV, and $\tau_E = 1\text{-}2$s), and is specifically designed to study D-T reactions in the plasma.

This paper concentrates on experiments and advances during the last 2 years (the first additional heating phase) using ion-cyclotron resonance frequency (ICRF) and neutral beam (NB) heating, both individually and in combined situations, and indicates particular developments and additions to JET that are planned to improve performance further towards the reactor regime.

2. Technical Status of the Device

2.1 Machine Conditions

Machine conditions have been progressively improved during the operational phase and all machine systems have now met the stringent design specifications. The achieved parameters are compared with the design values in Table I.

The toroidal magnetic field (B_T) now operates routinely at its maximum design value of 3.45T. The plasma current ($\pm < 3\%$), horizontal plasma position ($\pm \leq 10$mm), plasma elongation $\epsilon(\pm 5\%)$ and shape are all controlled by feedback circuits acting on poloidal field coils. Following considerable work on these systems, stable control has been obtained with elongations in the range 1.2-1.7. However, the plasma vertical position is naturally unstable due to both the quadrupole poloidal field necessary for the elongated plasma and the de-stabilising effect of the iron magnetic circuit. Loss of vertical position feedback control at higher elongations can lead to large vertical forces on the vessel. Some additional vessel support has been introduced, but the plasma current, I_p, had still to be restricted within the operating regime given by $I_p^2(\epsilon\text{-}1.2) < 5.0(\mathrm{MA})^2$.

With a plasma elongation limited to 1.4, the plasma current has been increased to 5.1MA (for a period of 3s within a 20s pulse) exceeding the design value of 4.8MA. In addition, plasma currents have been achieved routinely at 4MA with flat-tops of 6s duration. At present, the full inductive flux (34Vs) is not used as the maximum premagnetisation current creates stray fields, which inhibit reliable plasma breakdown. Strengthening of the

Table I
Principal Parameters of JET: Design and Achieved Values

Parameter	Design Values		Achieved Values
Plasma minor radius (horizontal), a	1.25m		0.8—1.2m
Plasma minor radius (vertical), b	2.10m		0.8—2.1m
Plasma major radius, R_o	2.96m		2.5—3.4m
Plasma elongation ratio, ϵ=b/a	1.68		1.2—1.7
Flat-top pulse length	Up to 20s		Up to 20s
Toroidal magnetic field (plasma centre)	3.45T		3.45T
Plasma current:			
circular plasma	3.2MA		3.0MA
Elongated plasma	4.8MA		5.1MA
Flux Drive Capability	34Vs		28Vs
Additional heating power (in plasma)	1986 Values	Full Values	
RF Power	8MW (3 antenna)	32MW (8 antenna)	<7MW
Neutral beam power	10MW (1 box)	20MW (2 boxes)	<9MW

vacuum vessel, modifying the primary winding and improving the power supply will allow an enhancement of the plasma current to 7MA, at the full elongation of $\epsilon = 1.7$. Stable discharges with $I_p = 3.5$MA, $B_T = 1.7$T, $\epsilon = 1.35$ and $q_\psi = 2.2$ have been studied to simulate 7MA operation.

The vacuum vessel is usually operated with wall temperatures at 250-300°C and with a base pressure of 10^{-7}mbar H and 10^{-9}mbar residual impurities. The vessel is conditioned by glow discharge cleaning (GDC) in hydrogen and/or deuterium. To reduce the level of metallic impurities and oxygen, the torus walls are carbonised by glow discharge cleaning in a mixture of hydrogen or deuterium and hydrogenic methane (CH_4) [3].

In most recent experiments, eight carbon plasma limiters have been located symmetrically on the outer equatorial plane of the vessel. Since disruptions mostly terminate on the inner walls, these have been covered by carbon tiles to a height of ±1m around the mid-plane. Similar tiles also protect the frames of the RF antennae, eight octant joints, and the outer wall from neutral beam shine-through. Additional tiles have been installed at the top and bottom of the vessel to protect the vessel during X-Point (Separatrix) operation. The total surface area covered is 45m^2, corresponding to ~20% of the vacuum vessel area. The inner wall tiles used as limiters and those for X-Point protection have provided powerful pumping (with speeds up to 100mbar.l.s^{-1}). This has allowed operation at low density near the plasma edge and was used to reduce the density after neutral injection to avoid disruptions. Recently, helium discharges prior to normal operation have improved the inner wall tiles pumping capacity.

In early 1987, it is planned to extend the coverage in the machine and the existing limiters will be replaced with two toroidal 'belt' limiters (surface area $\sim 15m^2$), and the existing RF antennae will be replaced with eight water-cooled models. In late 1987, the belt limiter tiles and those from the eight antennae will be replaced by beryllium plates to investigate the expected advantages with this low Z material.

2.2 RF Heating System

Since early 1985, three RF antennae have been installed at the outer equatorial wall. Power is transferred to the plasma at a radiation frequency (25-55MHz) equal to the cyclotron resonance of a minority ion species (H or He^3). Each antenna is fed by a tandem amplifier delivering up to 3MW in matched conditions. The three units have been regularly operated up to 7.2MW for 2s pulses. Experiments with 8s pulse duration have also been performed delivering $\sim$40MJ to the plasma. Recently, a fourth RF generator has been installed so that two generators can be coupled to one antenna [4].

When completed, the JET RF system will have eight generator-antenna units initially delivering 24MW for 20s pulses. Subsequently, each amplifier unit will be upgraded to 4MW, using a more powerful tetrode in the final amplification stage. New water-cooled antennae have been built and tested for insertion inside the toroidal belt limiter.

2.3 Neutral Beam System

A long pulse ($\sim$ 10s) neutral beam (NB) injector with eight beam sources and one integrated beam line system has been operated on JET since early 1986. H beams have been injected into D plasmas with particle energies (in the full energy fraction) of up to 65keV. The neutral power fractions were 69%, 23% and 8% in the full, half and one-third energy components, respectively, giving a total beam power of $\sim$5.5MW injected into the torus. D beams have also been injected into D plasmas, with particle energies up to 75keV (injected power fractions of 76%, 17% and 7%) giving a total power up to 10MW. Up to 40MJ have been delivered to the plasma during a pulse. The second neutral injection box will be available for operation on the machine in mid-1987.

2.4 Diagnostics

About 30 different diagnostics have been installed on JET, allowing cross measurements of the main plasma parameters and detailed analysis of some of the plasma features such as sawteeth oscillations and MHD behaviour [5]. The ECE diagnostic is the main instrument for providing electron temperature profiles and infra-red interferometry is the main technique for density profiles. The ion temperature is measured by three different techniques; charge-exchange neutrals, Doppler broadening of Ni^{26+} and of resonant charge-exchange lines of light impurities. Flux measurements and spectrometry of 2.4MeV neutrons are also used. Z_{eff} is measured by visible bremmstrahlung and is in agreement with estimates from neoclassical resistivity.

3. Experimental Results

3.1 Overall Plasma Parameters

Experiments have been performed in JET in different configurations: limiter discharges on the inner or outer walls and X-Point discharges with single or double null. Various heating scenarios have been used ranging from ohmic heating alone to combinations of ohmic, RF and NB. The variation of the main JET parameters is presented in Table II. Several examples of typical pulses under these various conditions are indicated in Fig.1, which show the density (n), electron temperature (T_e) and safety factor (q) profiles, with ion temperature (T_i) measurements where available.

Each heating method has its own characteristic power deposition profile. For ICRF,

Table II
Range of the Main JET Plasma Parameters

Parameter	Value
Toroidal field (plasma centre) B_t	1.7-3.4T
Plasma current, I_p	1-5MA
Flux safety factor at edge, q_ψ	2.2-16
Volume averaged density, $\bar{n}_e$	$0.5\text{-}5\times10^{19}\text{m}^{-3}$
Central electron temperature, $\hat{T}_e$	2-7.5keV
Central ion temperature, $\hat{T}_i$	1.5-12keV
Energy confinement time, τ_E	0.2-0.9s

it is well localised (half width ~30cm) as shown in Ref. [4], and can be varied across the plasma by changing either the toroidal field or the frequency. The NB deposition profiles are usually less peaked on axis, and are quite flat at high densities.

The following parameters have been obtained under different conditions:

(a) With ohmic heating, peak ion and electron temperatures of 3keV and 4keV, respectively, were achieved with a plasma density $\sim 4.2\times10^{19}\text{m}^{-3}$ and energy confinement times exceeding 0.8s;

(b) With RF heating, the peak electron and ion temperatures have reached 5.5keV with peak ion densities of $3.5\text{x}10^{19}\text{m}^{-3}$. However, the confinement time has dropped to $\tau_E = 0.3$s;

(c) Ion temperatures up to 6.5keV at mean densities of $3 \text{ x } 10^{19}\text{m}^{-3}$ have been produced with neutral beam heating. At lower peak densities ($\sim 1.5\times10^{19}\text{m}^{-3}$), ion temperatures $\geq$ 12.5keV have been observed (Fig.1(e)). Again, there was a degradation in confinement time down to 0.3-0.4s. In addition, with ~7MW of neutral beam injection, current drive of 0.4MA has been observed at a mean density of $2 \text{ x } 10^{19}\text{m}^{-3}$;

(d) Combined RF and neutral beam heating has coupled power up to 15MW to the plasma in a 5MA discharge: the plasma energy content was ~6MJ (Fig.1(d)).

The JET impurity behaviour is similar to that observed in other ungettered tokamaks with graphite limiters [3]. The main impurities in ohmic and neutral beam heated plasmas are carbon and oxygen and principally carbon at high electron density, n_e. During ICRH, moderate metal concentrations (0.1% n_e) are responsible for ~20% of the total radiation power losses. These can be prevented temporarily by carbonisation. Radiation power losses represent 30-60% of the total heating power, P_{tot}, during NBH and 40-70% of P_{tot} for ICRH. Most of the radiated power is emitted from the edge plasma. Z_{eff} varies from 3.5 at low n_e to 2.5 at high n_e. With NB injection, Z_{eff} falls to values of 2-3 and with pellet injection, it can fall to values close to 1 (see Fig.2).

3.2 Density Limits

The Hugill diagram for JET is shown in Fig.3, where the operating domain is limited by disruptive instabilities. In ohmic plasmas, the density limit is n_c (OH)$(\text{m}^{-3}) = 1.2 \text{ x } 10^{20} B_T$ (T)/qR(m). This limit depends on plasma purity. In RF heated discharges, it is only slightly increased, possibly because the effect of the extra power is cancelled by an increase in impurities. In neutral beam heated plasmas, the limit is substantially increased, as shown in Fig.3, to $n_c(\text{NB})(\text{m}^{-3}) = 2.0\times10^{20}\text{B}_T(\text{T})/\text{qR(m)}$. Switching off neutral beams at high den-

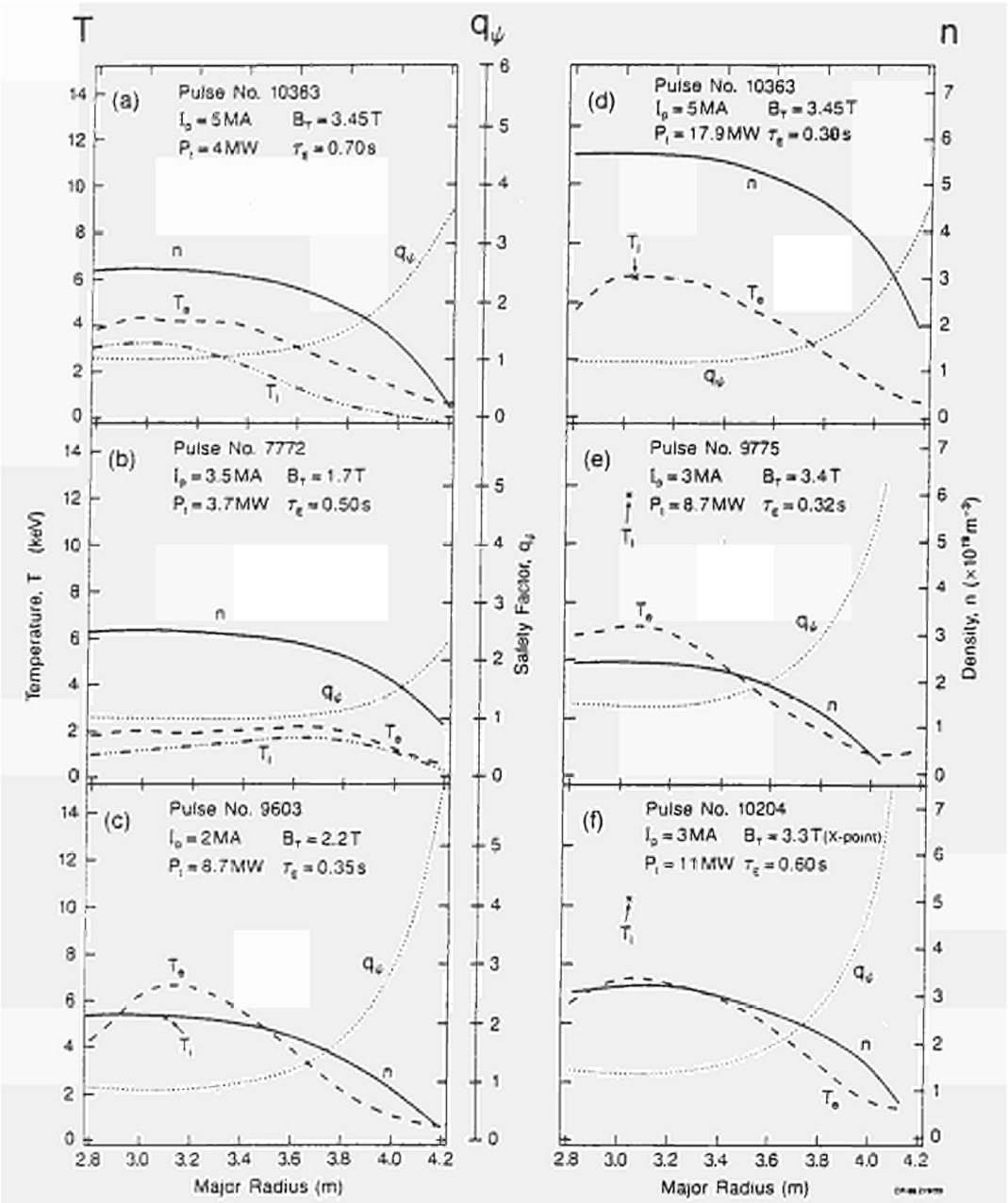

Fig.1: The density (n), electron temperature (T_e) and safety factor (q) as a function of major radius. The ion temperature (T_i) is shown where available. These profiles are indicated for the cases:

(a) 5MA Pulse (No:10363), Ohmic heating only, B_T=3.45T; (b) Low q pulse (No:7772), ohmic heating only, I_p=3.5MA, B_T=1.7T; (c) Monster sawtooth pulse (No:9603), P_{add}=6.1MW; (d) 5MA Pulse (No:10363) with 15.2MW of RF + NB power, B_T=3.45T; (e) High T_i pulse (No:9775) P_{add}=8MW; (f) X-Point configuration pulse (No:10204) I_p=3MA P_{add}=8.2MW;

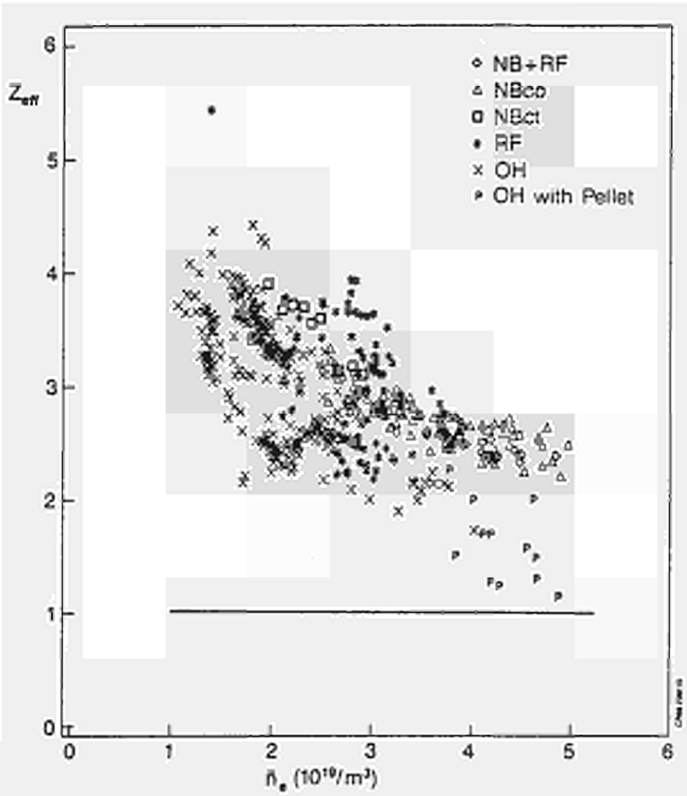

Fig.2: Z_{eff} as a function of average density for various plasma conditions;

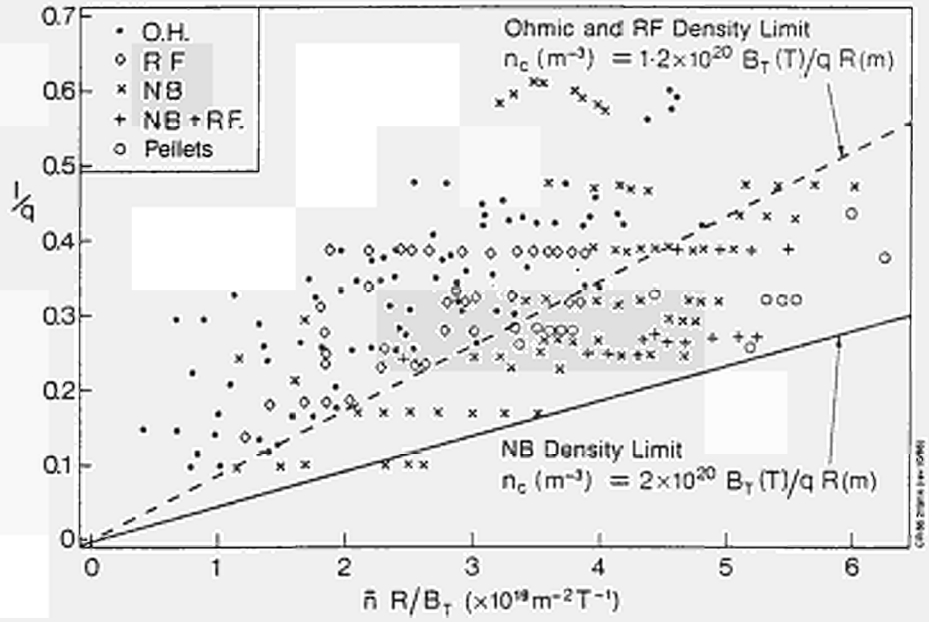

Fig.3: Normalized current [$=(2\pi RI_p/AB_T)=1/q$] versus normalized density [$=\bar{n}R/B_T$];

sity causes the plasma to disrupt, which indicates that the power input plays an important role in the disruption mechanism. Preliminary experiments with a single-shot pellet injector have also exceeded the OH density limit.

Density limit disruptions are always preceeded by an increase in the impurity radiation at the plasma edge [6]. This is seen to cause a contraction of the electron temperature profile, which is followed by the growth of coherent MHD activity (principally $m = 2$, $n = 1$). Alternative theoretical models predict that either the contraction of the temperature profile leads to an unstable current profile [6], or that the increased radiation losses at the $q = 2$ surface lead to a thermal instability [7], but it is possible that both of these effects may be involved. Both models result in the growth of an $m = 2$, $n = 1$ island before the disruption. Observations and theoretical considerations both show that the central plasma density can be increased by deep fuelling.

3.3 Temperature Effects

Sawtooth oscillations occur in almost all JET discharges. As these instabilities, in general, limit the peak ion and electron temperatures, and may affect, in certain cases, the global energy confinement times, they justify a careful analysis. With central deposition of additional power, sawteeth may develop large amplitudes (up to doubling the central electron temperature) and long periods (up to 0.6s) [6]. In some circumstances with combined NB and RF, 'monster' sawteeth have been observed (see Fig.4). They are characterised by long durations of 0.8 - 1.2s and strong reduction of the low m, n numbers MHD activity. The instability mechanism of the sawteeth is described by a model involving ideal MHD [8].

The peak electron temperature $T_e(0)$ can be raised significantly above the value reached in the ohmic phase as shown in Fig.5(a). The dispersion seen in $T_e(0)$ is due to sawteething

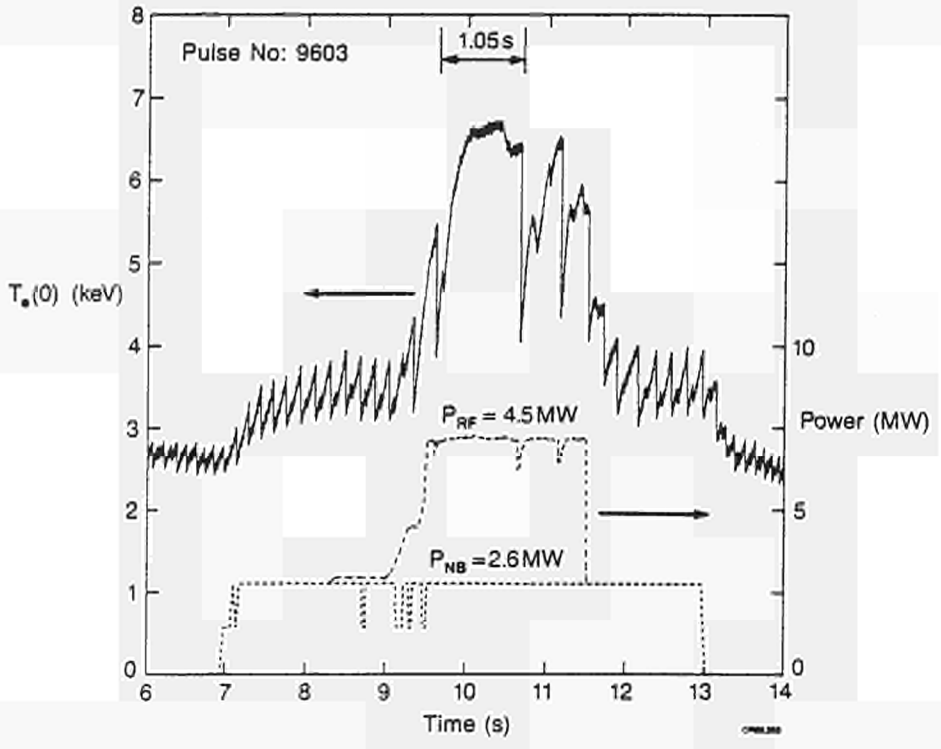

Fig.4: Sawtooth oscillations of the central electron temperature, showing the effects of NB and RF additional heating;

and to variations in profile deposition of the additional power. By contrast, the electron temperature at the inversion radius (q ~ 1 surface) shows only a weak dependence with the power input per particle ($P/\bar{n}$) for a given plasma current and toroidal field (Fig. 5(b), and no explicit density dependence. The radius of inversion is independent of $P/\bar{n}$ in the range shown (Fig. 5(c)).

The ion temperature behaviour appears quite different; the peak ion temperature $T_i(0)$ (deduced from the X-ray crystal spectrometer) is plotted versus $P/\bar{n}$ in Fig. 6(b). Above 4×10^{19}MW/m^{-3}, the ion temperature can greatly exceed the electron temperature and can reach 12.5 keV in JET. A broadening of the ion temperature profile is also observed in cases of off-axis ICRF heating [4].

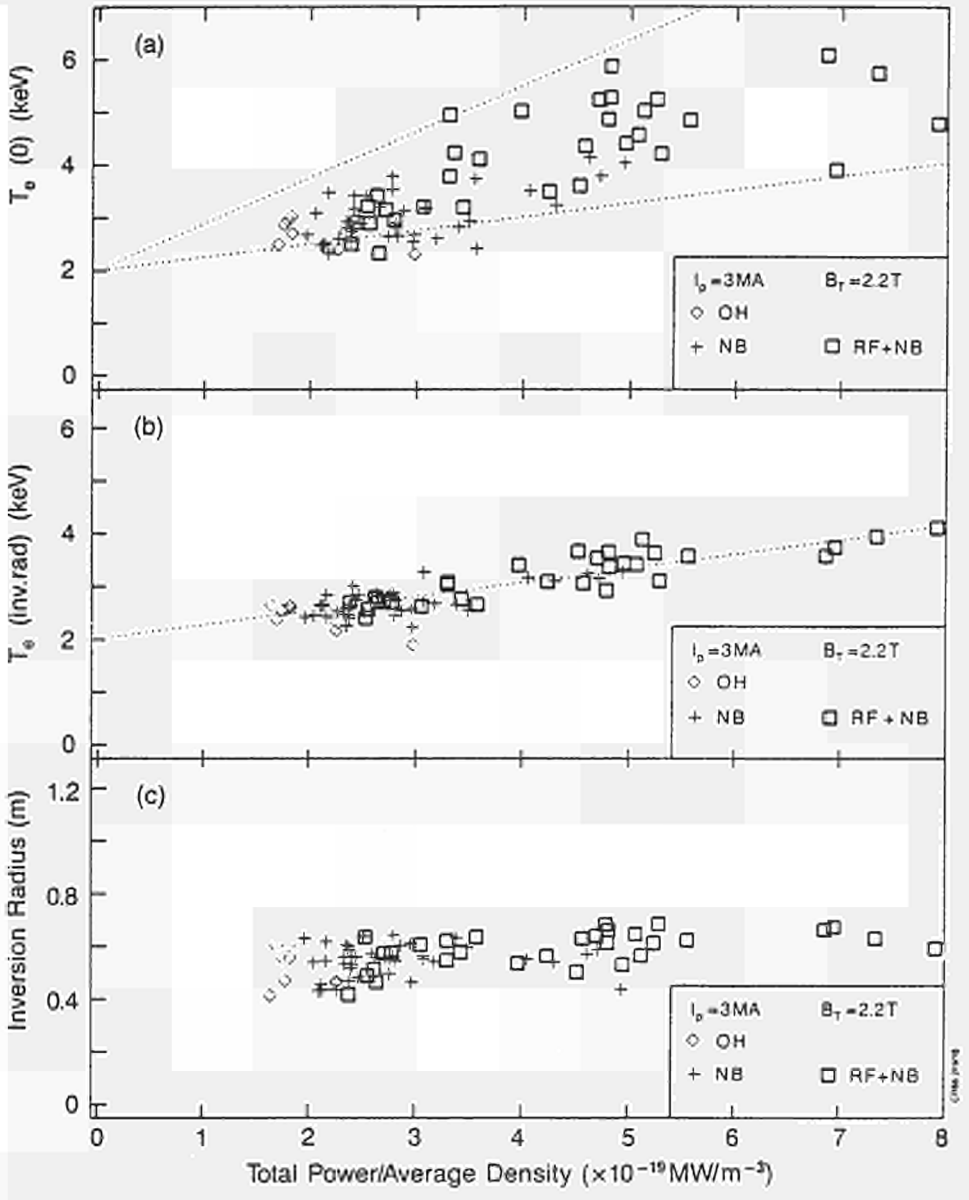

Fig.5:(a) Electron temperature at the centre, (b) electron temperatures at the inversion radius (q = 1) and (c) the inversion radius as a function of the power input per particle, for ohmic, RF, NB and combined heating cases (I_p=3MA; B_T=2.2T);

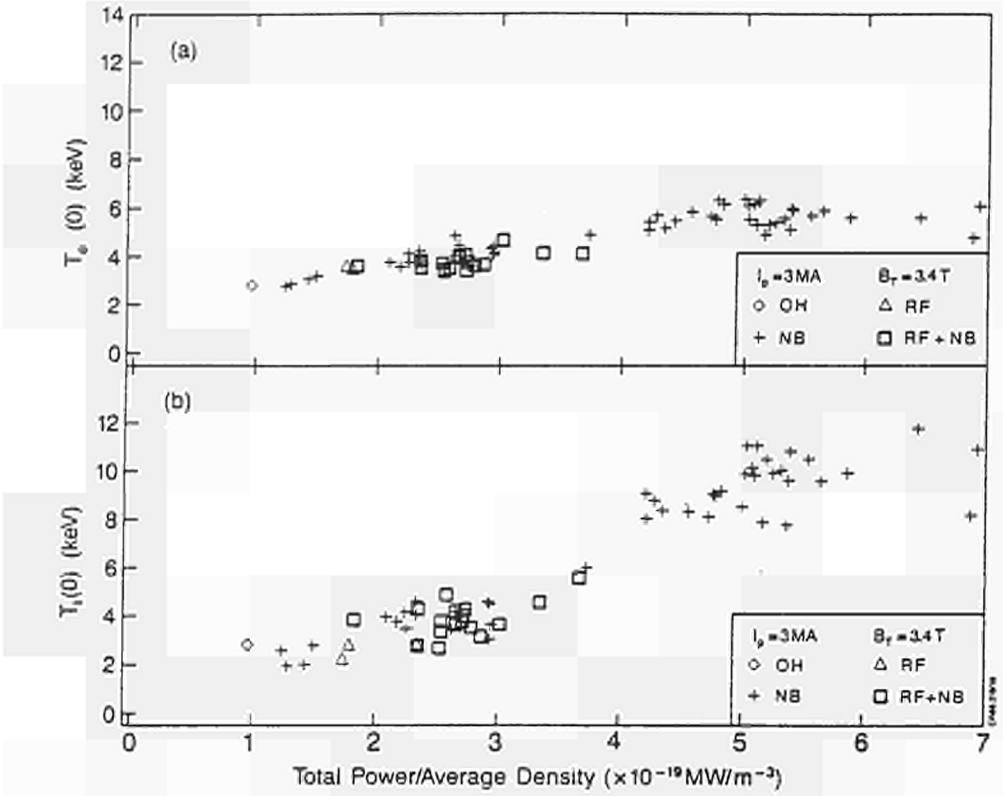

Fig.6:(a) Electron temperature (T_e) at the centre and (b) Ion temperature (T_i) at the centre as a function of power input per particle for various heating scenarios;

3.4 Confinement Degradation

The definition of the total energy confinement time used at JET is $\tau_E = W_k / [P_t - dW_k/dt]$, where W_k is the kinetic energy and P_t is the total input power to the plasma without subtracting radiation losses. Reported values of τ_E are quasi-stationary.

With additional heating, the confinement time, τ_E, degrades with increasing input power (Fig.7(a)), as seen in a number of other experiments. The degradation is independent of type of heating, whether RF, NB or combined. The rate of increase in W_k with $P_t (= \Delta W_k / \Delta P_t)$ appears to reach a limit of 0.1-0.3MJ/MW(=s) at high powers (see Fig.7(b)). This suggests a lower limit to the global confinement time, τ_E, of 0.1-0.3s in JET, independent of type of additional heating. Confinement time depends weakly on plasma density but scales favourably with plasma current.

Since the plasma energy is a function of n_i, T_e and T_i, the degradation in confinement time is consistent with the observation that the electron temperature, at the inversion radius (q=1 surface) increases little with power input and only the central temperature ($T_e(0)$) shows an increase dependent on the central input power (see Fig.7(a) and (b)).

3.5 X-Point Regime

A better confinement regime with additionally heated plasmas has been observed (H-mode) in some Tokamaks with magnetic limiters or divertors. Stable discharges with magnetic separatrix (or X-Point) inside the vessel have been maintained in JET for several seconds, at plasma currents up to 3.0MA with a single null (Fig.8) and up to 2.5MA with a double

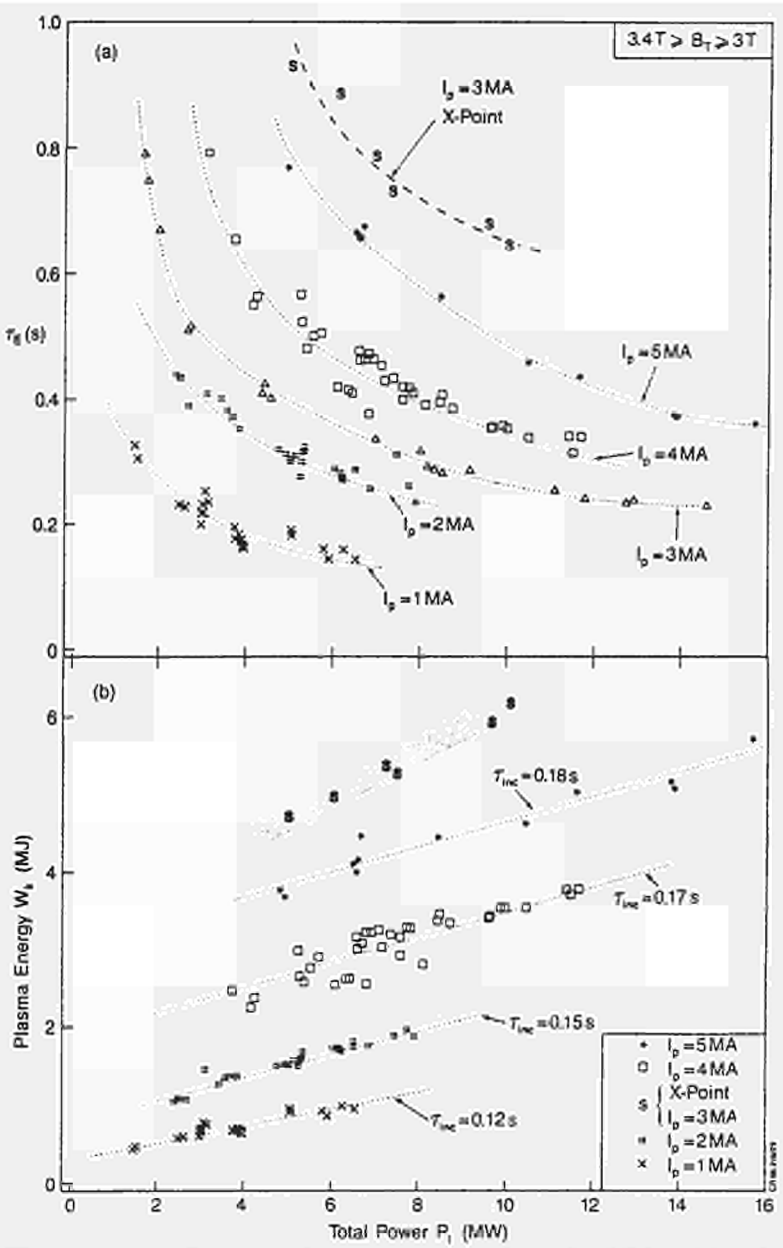

Fig. 7(a): The energy confinement time τ_E as a function of additional heating power (at I_p=1, 2, 3, 4 and 5MA; 3.4T≥B_T≥3.0T; (b) Plasma energy content W_k versus the total input power P_i with NBI and ICRF heating (I_p=1, 2, 4 and 5MA; 3.4T ≥ B_T ≥ 3.0T) X-point values at I_p=3MA are shown for comparison.

null [9]. While interaction of the discharges with the limiters was curtailed, localised power deposition on the top and bottom target plates has limited the total input power to 10MW. The main objectives of these experiments are (i) to study the conditions of creation of a high density highly radiative region at the X-point capable of screening and isolating the main bulk plasma and (ii) to study the global confinement characteristics in comparison with limiter discharges. Evidence exists of the formation of a dense plasma near the X-Point, with average density $1-2\times10^{20}\mathrm{m}^{-3}$, corresponding to an order of magnitude higher

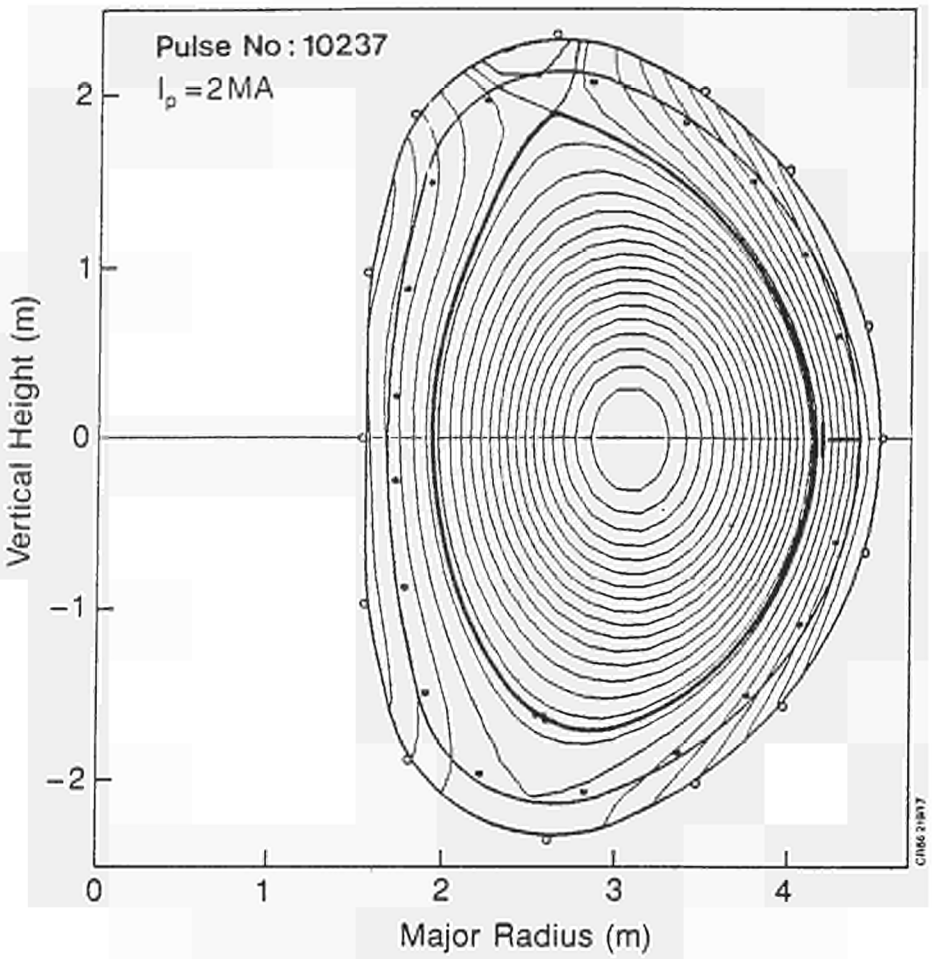

Fig. 8 Single-null X-point configuration at $I_p = 2.0MA$;

than the average value of the main plasma density. There is also evidence that up to 40% of the total input power could be radiated by a ~20cm x 20cm toroidal annulus around the X-Point in the high density discharges with additional power.

As shown in Fig.7, the increase in total energy content (and hence global confinement time) in single-null configurations is observed to be about twice that observed with limiters. In these conditions, both average electron and ion temperatures appear to be higher, and there are indications of changes in edge plasma suggesting an H-mode.

3.6 Slideaway Discharges

A preliminary study of slide-away discharges has also started with a view to decoupling currents and electron temperature. In these conditions, a plasma with 3MA and a mean density just below $10^{19}m^{-3}$ has been obtained with a good confinement time for these conditions (~0.6-0.7s). The voltage per turn was 0.2V. When trying to increase the density by gas puffing, the discharge reverted to normal conditions.

3.7 Progress Towards Breakeven

Neutron yields $>2.8\times10^{13}s^{-1}$ have been obtained with D injection, mainly from beam-

plasma D-D reactions. The best ratio of fusion power to input power obtained was $Q_{DD}=4\times10^{-4}$, which is equivalent to $Q_{DT}\sim0.2$ and would have corresponded to a fusion power production of ~2MW (see Table II).

Fusion products $<\hat{n}_i\,\tau_E\hat{T}_i>\approx 10^{20}m^{-3}$.s.keV have been achieved in JET (compared with the value $5\times10^{21}m^{-3}$s.keV required in a reactor) in a ohmic discharge at 5MA and a value of $2\times10^{20}m^{-3}$s. keV has been obtained in an X-Point discharge at 3MA current. However, additional heating has not yet been optimized into 5MA discharges. Under optimum conditions at lower currents, the values are similar for ohmic heating only, RF, NB, and combined heating cases, the degradation in τ_E with additional heating offsetting gains in other parameters (see Table III).

Table III
Maximum Values of $<n_i(0)\tau_E T_i(0)>$

Experimental Programme	Peak Density	Energy Confinement Time	Ion Temperature	Fusion Parameter	Q_{DT} Equivalent	Plasma Current
	n_i (0) ($\times10^{19}m^{-3}$)	τ_E (s)	T_i (0) (keV)	$<n_i(0)\tau_E T_i(0)>$ ($\times10^{19}m^{-3}$.s.keV)	Q_{DT}	I_p (MA)
Ohmic (4.6MW)	4.2	0.8	3.0	10	0.010	5
ICRF (7MW)	3.7	0.3	5.4	6	0.012	3
NBI (6MW)						
High n_i	4.4	0.4	4.0	7	0.10*	3
Low n_i	1.5	0.4	10	6	0.20*	3
Combined NBI + RF (14MW)	5.0	0.4	3.5	7	0.10*	3
X-point (NB - 10MW)	5	0.65	6	20	0.15*	3

*Beam-Plasma reactions are dominant

4. Progress in Understanding Heat Transport

JET data have been used to assess the status of theoretical understanding of heat transport [10]. Local fluxes have been derived from measurements and compared with presently available theoretical values. No acceptable agreement has been found. However, the scaling of global energy confinement time with the dimensionless plasma physics parameters suggests that the underlying heat transport is a consequence of resistive MHD instabilities [11]. The topology of the magnetic field including chaotic regions and small islands could account for the heat fluxes observed in JET [12]. Such a model is also consistent with the existence of an H-mode.

As α-particles mostly heat the electrons, it is imperative to obtain better control of their temperature, especially inside the $q=1$ surface (ie sawteeth). A possible approach to increase $T_e(0)$ is to control the profile of current and achieve a flat current distribution ($q\gtrsim1$, $q'\approx0$) in the central region, in order to stabilize or at least delay the sawtooth crash significantly.

5. The JET Strategy and Future Programme

The JET strategy is to optimize the fusion product $<\hat{n}_i\hat{T}_i\tau_E>$. Attempts will be made to maintain τ_E with additional heating near to present values, and to increase the central density and temperature.

In order to obtain higher levels of performance, additional equipment is required on JET. Fig.9 shows the plasma profiles which are envisaged. They correspond to an energy content of ~20MJ and would produce ~10MW of α-power. If $\tau_E \sim 0.3$-0.4s, Q_{DT} should reach 1 ~ 2. Such plasma parameters could be obtained in the following ways:

(i) Sawteeth oscillations should be stabilized or have periods of several confinement times. This whould be achieved by flat q profiles ($q \geq 1$, $q' = 0$) over a large plasma cross-

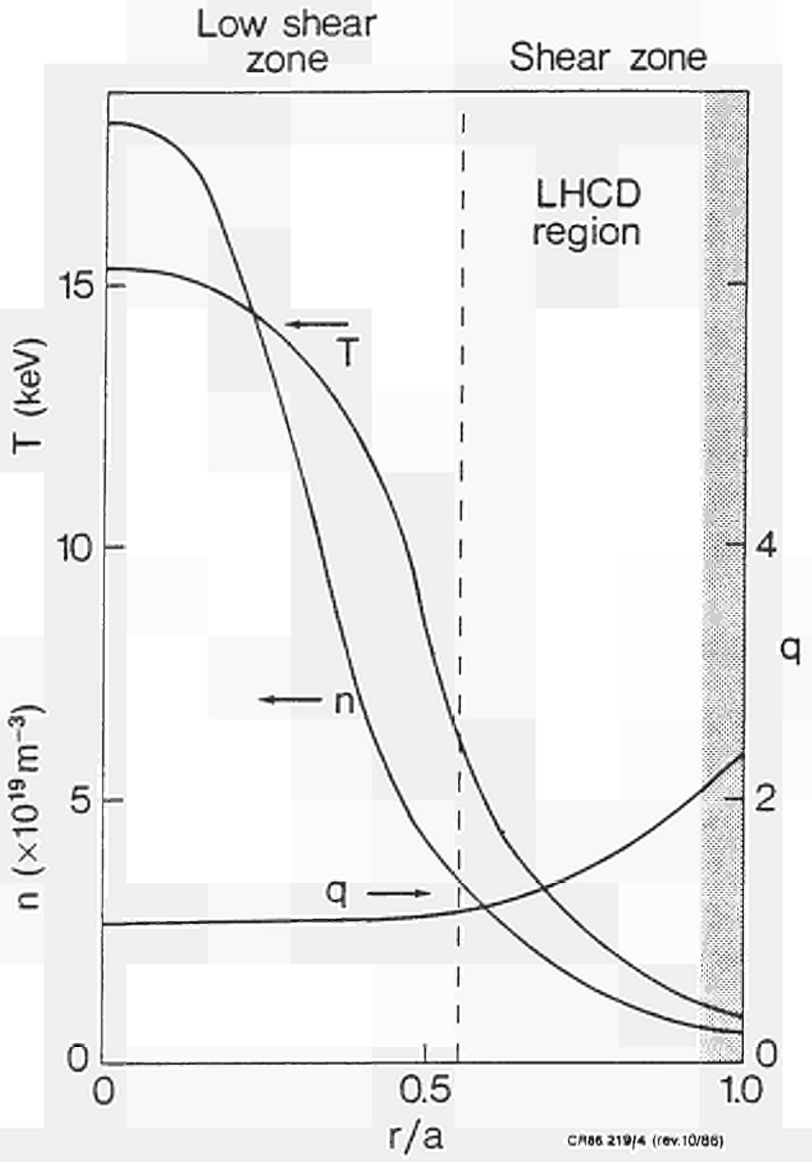

Fig. 9: Density (n), temperature (T) and safety factor (q) profiles aimed for within the latest JET strategy. The shaded area represents the zone q=2.

section, working with a low q boundary and driving part of the current (~2-3MA) in the outer plasma by Lower Hybrid Current Drive (LHCD) (~10MW) and by NB injection. The ICRF antennae with proper phase control could also be used to launch a travelling wave and provide some additional localised current;

(ii) Radiation cooling between the q=2 surface and the plasma boundary would be minimised to allow operation below the major disruption limit and to provide high T_e on the edge. Low Z material (C or Be) would be used to take advantage of its low ionisation potential;

(iii) Since the temperature at the q~1 surface is higher when the density is lowered, edge pumping will be used. Further advantages of low densities in the outer region would be the prevention of disruptions and higher efficiency for LHCD;

(iv) The D-T density on axis would be increased up to 1-2x$10^{20}m^{-3}$ by high velocity pellet injection (>5km/s);

(v) High central temperature (~12-15keV) would be achieved by a combination of 'on axis' ICRF heating, NBI at 160keV and current profile control.

This scheme will be tested in two configurations: (a) with a magnetic separatrix at 4MA and (b) with limiters at current values up to 7MA. Such a low-q discharge has been simulated in JET (see Fig.1(b)).

The main aim of JET operation during the next phase will be to reach maximum performance with full additional heating power in deuterium plasmas, before proceeding to the final phase requiring the introduction of tritium. The starting date for D-T operations is linked to the performance reached in the previous phase and is expected in 1991. α-particle production must be sufficient to analyse its effects on the plasma and to answer the question whether α-particle heating degrades energy confinement as other heating methods. Although degradation is foreseen, this has direct consequences on the ignition margin and on the size of future devices.

6. Implications for a Reactor

Present results suggest that a way for a future reactor is to rely upon tight control of current and density profiles and intense heating inside the q=1 surface to benefit from improved energy confinement and high central temperature (as proposed for JET). Alternatively, a size and current increase could lead to the required ignition temperature, without additional heating. The resulting simplification of the overall system could well compensate for the larger size. Scaling suggests that in a Tokamak with a major radius of ~×2.5 that of JET, plasma volume of ~2000m^3 and magnetic field slightly higher than in JET, a 15keV plasma with a confinement time of 15-25s could be reached with ohmic heating alone at a peak density ~$2\times10^{19}m^{-3}$, satisfying the ignition criterion. Then, the thermonuclear power output of the D-T burner could be increased by injecting fuel pellets: the thermal insulation should degrade as the additional heating provided by the α-particles increases without a strong variation of temperature. Burn control would be performed entirely through density control.

7. Conclusions

The following conclusions can be drawn at this stage:

(a) Both ICRF and neutral beam (NB) injection methods are effective in delivering power into the JET plasma with the expected profile depositions. Large central electron and ion temperature increases have been observed; $\hat{T}_e$ and $\hat{T}_e$ have reached values of 7.5keV at densities of 3x$10^{19}m^{-3}$. At lower density (~$1.5\times10^{19}m^{-3}$), $T_i\approx$ 12.5keV has been measured;

(b) For both heating methods, plasma energy has increased with input power. About 6MJ

energy has been achieved in JET plasmas with ~18MW of total power input. However, the rate of energy increase with power ($\Delta W_k/\Delta P_t$) ~0.1-0.3s is smaller than the corresponding ohmic confinement times (τ_E ~0.6-0.8s). The fusion product $<n_i\tau_E\hat{T}_i>$ has reached values in excess of $10^{20}m^{-3}$.s.keV, both in ohmic at 5MA and with additional heating; the degradation in confinement offsets the gains in density and temperature.

(c) A higher fusion product value of $\sim 2\times10^{20}m^{-3}$.s.keV has been obtained in X-point configuration at lower current (~3MA). Values of $\tau_E \approx 0.6$-0.7s and T_i up 10keV were achieved with neutron production $\sim 2x10^{15}ns^{-1}$ equivalent to a thermal $Q_{DT}=0.1$, the total Q_{DT} being ~0.15;

(d) In the central region (inside the inversion radius) between sawtooth collapses, additional heating is effective in increasing the electron temperature of the plasma (cf monster sawteeth);

(e) Outside this region, electron heating is poor. The electrons seem to be the main energy loss channel, which appears related to confinement properties and not to the heating process;

(f) Good prospects exist on JET for production of several MW of α-particle power at a value $Q_{DT}\approx 1$;

(g) α-particle heating is expected to behave in a similar fashion to other heating methods. Therefore, a reactor must either: (i) work at moderate currents with sophisticated control of the central region; or (ii) work at high currents without the need for complex control and additional heating.

8. References

[1] HUGUET, M. et al, 13th Symposium on Fusion Technology (SOFT), Varese, Italy, 24-28th September 1984. Proceedings Vol.I, pp 91-103

[2] LALLIA, P.P., et al, Plasma Physics and Controlled Fusion, 28, 55 (1986)

[3] BEHRINGER, K. et al, 11th IAEA Conference on Plasma Physics and Controlled Fusion Research (Kyoto, Japan) (1986)

[4] JACQUINOT, J et al, 11th IAEA Conference on Plasma Physics and Controlled Fusion Research (Kyoto, Japan) (1986)

[5] Joint European Torus Progress Report (1985) EUR-JET-PR3 (EUR-10616.EN)

[6] CAMPBELL, D.J. et al, 11th IAEA Conference on Plasma Physics and Controlled Fusion Research (Kyoto, Japan) (1986)

[7] REBUT, P.H., HUGON, M., 10th IAEA Conference on Plasma Physics and Controlled Fusion Research (London, U.K.) (1984) Vol.II, p197

[8] WESSON, J.A. et al, 11th IAEA Conference on Plasma Physics and Controlled Fusion Research (Kyoto, Japan) (1986)

[9] TANGA, A., et al, 11th IAEA Conference on Plasma Physics and Controlled Fusion Research (Kyoto, Japan) (1986)

[10] DÜCHS, D.F. et al, 11th IAEA Conference on Plasma Physics and Controlled Fusion Research (Kyoto, Japan) (1986).

[11] CORDEY, J.G. et al, 11th IAEA Conference on Plasma Physics and Controlled Fusion Research (Kyoto, Japan) (1986)

[12] REBUT, P.H., BRUSATI, M., HUGON, M., LALLIA, P.P., 11th IAEA Conference on Plasma Physics and Controlled Fusion Research (Kyoto, Japan) (1986)

[13] THOMSON, K., et al, Controlled Fusion and Plasma Physics (Proc. of 13th Eur. Conf, Schliersee, F.R.G.), Europhysics Conference Abstracts, Vol 10c. Part 1 p29 (1986)

RF Heating on JET

J. Jacquinot

IAEA-CN-47/F-I-1

ABSTRACT

High power ICRF, $P \leq 7.2$MW has been coupled to the JET plasma in a variety of conditions: outboard limiters, inner wall, combined operation with neutral beams and pellet injection. Long pulse modulation experiments (10s) yield a precise deposition profile which is extremely localised in agreement with expectations. The best heating efficiency is obtained when the minority resonance crosses the magnetic axis. With off-axis heating, the ion temperature broadens more than the electron temperature profile. A new operating regime, called 'monster sawtooth' has been found during combined RF and NBI heating. The MHD quiet regime can last 1.26s and the central electron temperature rises to 7.4keV with a D→D reaction rate of $4 \times 10^{15} s^{-1}$. The temperature profile steepens over the entire profile and $\bar{T}_e$ is enhanced by a factor of 2.5 for combined power of 10MW. RF heating of plasma fuelled with a single mildly penetrating pellet exhibits the normal L-mode behaviour. In combination with NBI, the input power reached 16MW and the plasma stored energy reached 5.8MJ at the highest plasma current of 5MA. Recent experiments in single null X-point configuration with combined heating have shown the transition to an enhanced confinement regime (H-mode).

1. INTRODUCTION

Initial ICRF heating experiments on JET have recently been reported [1,2]. Performed at a maximum power level of 5MW, these experiments revealed a degradation in energy confinement with increased power, following a behaviour previously observed in Tokamaks with a cold plasma edge. It appeared difficult to raise the electron temperature outside the $q = 1$ surface above the ohmic heating value.

The heating sources have now been increased up to 7.2MW using three ICRF antenna-generator units [3] and to 10MW with NBI [4]. Combined ICRF and NBI heating to a maximum power of 16MW has successfully been achieved, and a wider variety of operating regimes have been investigated. These results are summarised below. Experiments performed with ICRF alone are addressed in the first three sections, in which emphasis is placed on power modulation to deduce the deposition profile, on off-axis heating and on the effect of antenna phasing. The last sections described specific aspects of combined ICRF, NBI and Pellet operation. In particular, injected beam ions appear to be accelerated when the RF is applied and, in some conditions, the internal sawteeth are stabilized and a high central electron temperature is achieved ('Monster' mode).

2. MODULATION EXPERIMENT AND POWER DEPOSITION PROFILE

The power deposition profile can be inferred from the change of slope of the temperature evolution during the sharp rise of the applied heating source. A variant is to observe the slope of internal sawteeth [5]. The signal-to-noise ratio is generally mediocre and the method could

only be applied to heating on axis at high power density. Experiments with long and amplitude modulated heating pulses offer the opportunity to use noise rejection techniques, such as the box-car or the fast Fourier transform. The frequency of modulation ν_M can be scanned across the characteristic energy exchange and transport frequencies to reveal the dominant energy channels. In these experiments, ν_M was between 5-62Hz, the heating pulse lasted during 10s and the peak-to-peak modulation was about 1MW. The local perturbation of the electron temperature was measured with a 12 channel polychromator.

When the modulation frequency is high enough, the response of the electron species is adiabatic and it is possible to deduce directly the power density P_e transferred to the electrons, as shown in Fig. 1a,b. In both cases, the peak response is close to the location of the cyclotron resonance and the width of the deposition (FWHM) is ~ 60cm for on-axis heating and ~ 20cm for off-axis heating.

The experimental result is compared with theoretical descriptions using either the ray tracing technique [6] or full wave solutions [7]. Both models take into account the D-shape cross-section and the actual plasma parameters. These both predict that most of the coupled power is first transferred to the minority species, as observed, and is subsequently redistributed by collisions according to Table I. In the ray tracing model, part of the power ($\sim 20\%$) is not absorbed and is assumed lost in the wall or the edge. A very small part ($\simeq 5\%$) goes directly to the electrons and ions. In the full wave model, the pressure anisotropy of the minority is taken into account. A significant fraction of the power is directly coupled to the deuterons (10 to 20%).

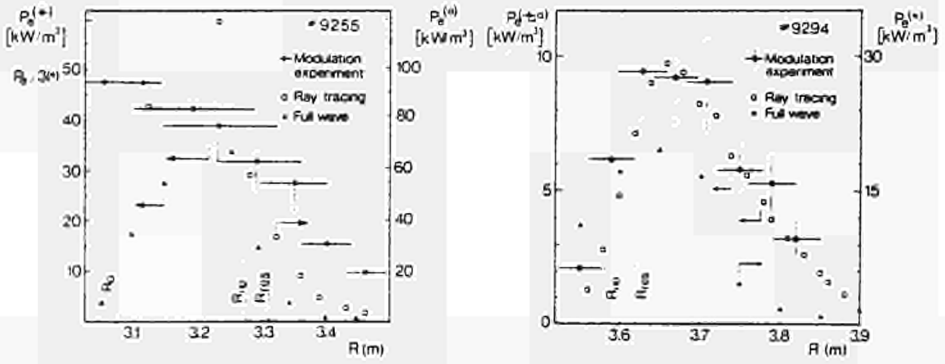

Fig. 1 Net power density P_e *transferred to the electrons deduced from the adiabatic modulation of* T_e *during long pulse ICRF modulation experiments : 1.3 MW peak modulation, 12.5 Hz, H minority. Comparison with theory:*
(a) on-axis heating $B_\phi = 3.4\,T$, $\nu = 47.7\,MHz$;
(b) off-axis heating $B_\phi = 2.9\,T$, $\nu = 37\,MHz$.
Heating via the minority is demonstrated by comparison with theory.

Note that electron heating prevails with heating on-axis, but, as the power density decreases with off-axis heating ion heating increases. At high power, electron heating tends to dominate in all cases. Both models give a good representation of the observed deposition profile (Fig.1a,b). The agreement is excellent for off-axis heating. Central heating is somewhat broader than predicted.

The observed temperature modulation decreases rapidly with $\nu_M (\tilde{T}_e \propto \nu_M^{-2})$. Such a law can only be obtained theoretically if the RF power first transits via the minority before reaching the electron species (direct electron heating would imply $\tilde{T}_e \propto \nu_M^{-1}$). The measurement of $\tilde{T}_e = f(\nu_M)$ has been used to determine the power coupled to the minority. Results are given in Table I.

Table I

Power input (P_c) 1.3MW	Directly to Minority H (P_m/P_c)	To electrons (P_e/P_c)	To deuterons (P_d/P_c)
Ray tracing On-axis	0.75	0.42	0.39
Ray tracing Off-axis	0.71	0.15	0.60
Full wave On-axis	0.80	0.34	0.66
Full wave Off-axis	0.90	0.25	0.75
Observed On-axis	0.6 ± 0.12	≥0.31 ± 0.06	not measured
Observed Off-axis	0.7 ± 0.15	≥0.15 ± 0.03	

3. OFF-AXIS HEATING

The importance of power localisation has been studied in two series of experiments. In the first [2, 8], the minority resonance position is scanned by ramping down the toroidal magnetic field during the RF pulse. In the second, the same effect is obtained by varying the wave frequency in the same plasma conditions. Moreover, the experiment was carried out after a heavy carbonisation to avoid the radiated power increase, when the resonance is far off-axis and with long pulses (≈ 8s) to avoid transient effects. Both series give similar results, for example

- Large amplitude sawteeth on both T_e and T_i were observed only when the ion-ion hybrid resonance was inside the inversion radius [2, 8]. The sawteeth do not disappear with far off-axis heating, but become small and short
- The largest increase of central temperature and stored energy was achieved with central heating (Fig. 2). The increase of $\bar{T}_e$ was only weakly dependent on the resonance location [2].

The deuteron temperature profile (from NPA) appears to broaden with heating off-axis (Fig. 3b). On the contrary, the electron temperature profile is only slightly broadened (Fig.3a) outside the $q=1$ volume.

Transport code simulations of off-axis heating cases indicate that the energy transport coefficient, χ_e, re-adjusts itself to try to conserve a similar T_e profile, by lowering χ_e inside the heating region and by further increasing it outside the heating zone.

4. ANTENNA PHASING AND EDGE EFFECTS

Among the three antennas, two are of the dipole-quadrupole type [1] and internal phasing of the two coupling elements allows the launching of a $k_\parallel$ spectrum which is peaked either for $k_\parallel = 0$ or for $k_\parallel = 7\text{m}^{-1}$. In addition, these two antennas, located on either side of a large horizontal port, can be phased relative to each other. When the dipoles are out of phase, two peaks at $k_\parallel = 2\text{m}^{-1}$ and $7\ \text{m}^{-1}$ are emitted; 90° phase difference produces a small portion of travelling wave (directivity $\approx 5\%$). All these phasing conditions have been compared, using a target plasma which maximizes the impurity effects with ICRF (low density $\approx \langle n_e \rangle = 1.1\times10^{19}\ \text{m}^{-3}$, no carbonisation for several months). The following observations were made:

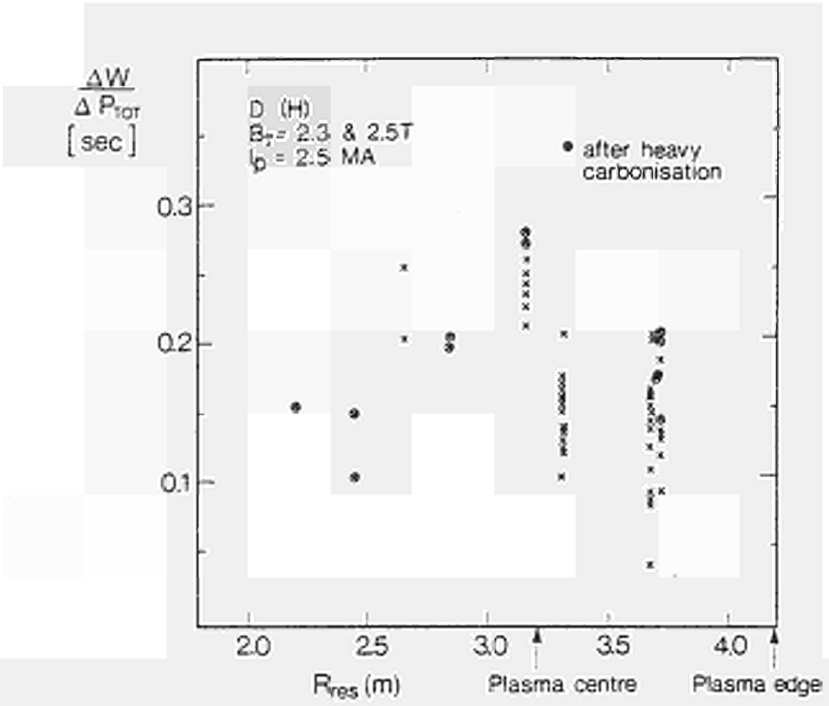

Fig. 2 Incremental confinement time versus position of the H resonance. The frequency was varied between 25 and 48 MHz. Data points following a heavy carbonisation are identified.

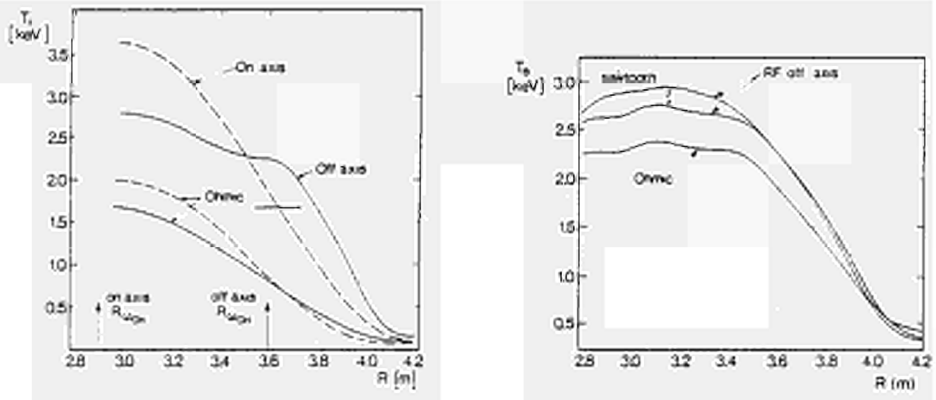

Fig. 3 Electron and D temperature profiles during the ohmic phase (before RF) and during on-axis or off-axis RF heating. The main effect of off-axis heating is a broadening of the T_i profile.
On-axis : $B_\phi = 2.3$, $\nu = 37 MHz$, $P_e = 3 MW$, $I_p = 2.5 MA$, $q(a) = 3.25$
Off-axis: $B_\phi = 2.5$ T, $\nu = 31.8 MHz$, $P_e = 5 MW$, $I_p = 2.5 MA$, $q(a) = 3.55$

- Phasing between the two adjacent antennas, each being in the dipole mode ($k_{\parallel}=0$) did not produce any measurable difference on wave coupling, edge plasma or plasma heating.
- Phasing internally in the quadrupole mode produced not only reduced coupling resistance [1] but also a marked reduction of specific ICRF effect on the edge plasma. In particular, the flattening of scrape-off-layer density and temperature profiles observed with dipoles disappears with the quadrupole, and the increase of metallic ions originating from the activated screen (Cr for one antenna, Ni for the other [9]) is about halved. The density evolution was also different in the two cases: the average density increased more with the quadrupole. Despite this higher density, the radiated power P_{rad} was significantly lower and the carbon released from the wall was typically $\times 2$-3 smaller. The heating efficiency defined by the incremental confinement time $\tau_{inc}=(\Delta W/\Delta P)$ was higher in the quadrupole phasing by typically 25% for similar plasma conditions. Table II summarizes this comparison between the two phasing conditions, in which I_{Ni}, I_{Cr} are the intensities of Ni XXVI and Cr XXII lines and ϕ is total neutral flux.

Table II

Comparison of the dipole and quadrupole phasing for 1 MW coupled power and identical starting plasma conditions

	$\frac{\Delta I_{Ni}}{<n_e>}$ (a.u)	$\frac{\Delta I_{Cr}}{<n_e>}$ (a.u)	ΔP_{rad} (MW)	ΔZ_{eff}	$\Delta \int n_e dl$ (10^{19} m^{-2})	$\Delta\phi$ (10^{21} s^{-1})	τ_{inc} (s)
Dipole	1.8	3.1	0.74	0.34	0.49	0.05	0.17
Quadrupole	1.2	1.5	0.57	0.14	0.79	0.58	0.23

It is clear from these experiments that the edge modification induced with dipole phasing is considerably reduced with the quadrupole. The metallic impurity emitted by the activated screen and the insensitiveness of phasing between adjacent antennas suggest that the RF field pattern immediately in front of each antenna screen plays a key role.

5. HIGH POWER EXPERIMENTS : OPERATING REGIMES

With ICRF alone, it is difficult to couple large amounts of power when the plasma current is low (e.g. at $I_p=1$ MA). The plasma disrupts at only 1 MW, as the density rise during ICRF approaches the density limit. At $I_p \geq 2$MA, no power limit was found. Combined ICRF and NBI operation removed the power limitations at 1 MA.

Experiments with long pulses (5MW, 8s) have shown that quasi-stationary conditions are reached after about 2s. No serious accumulation of high-Z impurity was observed and the plasma central temperatures remained constant after the initial rise.

Neutral beam injection increased the antenna coupling resistance. This increase can be highly beneficial; for instance, when the plasma is in contact with the inner wall and 5cm away from the antenna, the coupling resistance more than doubled. The technical difficulty of coping with large changes of coupling resistance meant that it can be difficult to maintain constant RF power when the beams are switched on during a RF pulse. Injecting RF power during a NBI pulse is normally straightforward. The variation of coupling resistance with the crash of the large sawteeth is often a factor limiting the power during the pulse.

6. COMBINED RF AND PELLET INJECTION

Combining ICRF with pellet injection did not raise any special technical problems. 6MW RF could be applied at the time of injection of a mildly penetrating pellet (3.6 mm, 1km s^{-1}). The power was ramped up over 0.5s. The change of coupling resistance due to the pellet was hardly noticeable. The ratio of radiated power to input power increased only slightly by 10-20% despite a doubling of the average density. The pellet increased the density from $<n_e> = 1.9\times10^{19}$ m^{-3} to 3.7×10^{19} m^{-3}. Without RF, the density decayed typically on a 1s time scale. With RF, the density was sustained at its maximum level and even slightly increased for the duration of the RF pulse (2s). The increase of $T_i(0)$ and $T_e(0)$ with $P_{RF}/<n_e>$ was comparable with the largest increments obtained in the similar discharges without the pellet. The energy confinement during RF was not modified by pellet injection. The incremental confinement time with the pellet becomes $\tau_{inc} = 0.2$s. Large sawteeth appear early in the reheat phase. The pellet penetration was not changed by the presence of ICRF.

7. COMBINED HEATING AND BEAM ACCELERATION

Generally, ICRF plasma heating on the outboard limiters behaves according to the L-mode scaling law [1,2]. Recent combined NBI and ICRF heating up to 16MW has been performed. The energy confinement scaling is reported in [10]. Again L-mode behaviour is found, although inner wall operation and high -q operation perform somewhat better than the 'Goldston L-mode scaling'. Both H and He^3 minority scenarios have been tested, but the stored energy increase is not appreciably different in the two cases.

In combined RF and NBI heating, the H minority scenario has a distinctive feature: power can be coupled to the energetic D beam ions at the harmonic cyclotron resonance. It is calculated [11] that the NBI current drive will be enhanced by ICRF. The beam acceleration also enhances the fusion reactivity.

Figure 4 demonstrates beam acceleration by ICRF. The slope of the energy distribution func-

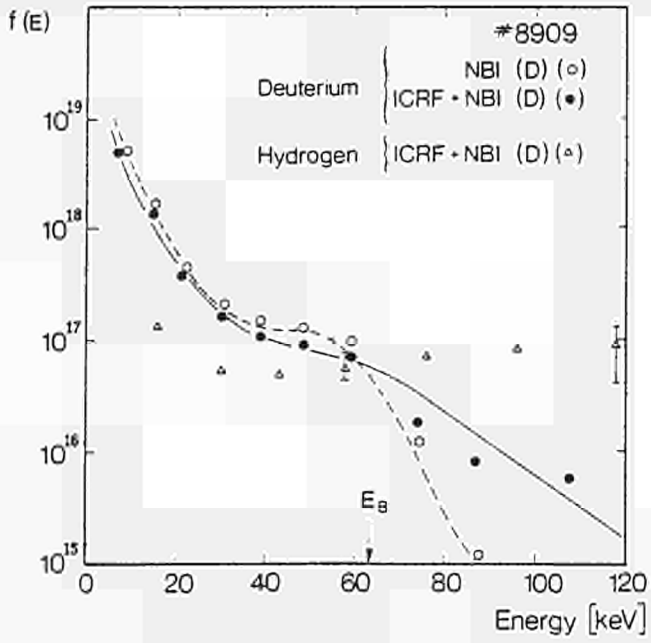

Fig. 4 D and Proton energy spectra before and during a 'Monster' sawtooth ($P_{NBI}=2.5$MW, 65keV; $P_{RF}=7$MW). $I_p=2$MA, $B_\phi=2.13$T, $\nu=31.8$MHz. Acceleration of beam injected ions up to 120 keV is observed.

tion above the injection energy increases from 5keV to 16keV. Simulation by a Fokker Planck calculation [12] requires that a substantial fraction of the incident RF power is coupled to the beam ions. However, note that the high energy tail of the proton still exceeds the D tail (Fig. 4) and most of coupled power is still transferred to the protons. The fraction of power directly transferred to the beam ions is estimated [13] to be about 10%. It is expected to increase non-linearly with RF power.

The fusion reactivity in these D →D injection experiments is dominated by beam-plasma reactions. RF heating increases the reactivity roughly in proportion to the total heating power (cf. Fig. 5) provided the RF power does not exceed the NBI power. Comparison between the He^3 and H minority shows that a higher reactivity is obtained in the H minority experiments ($n_H/n_D \sim 2\times10^{-2}$).

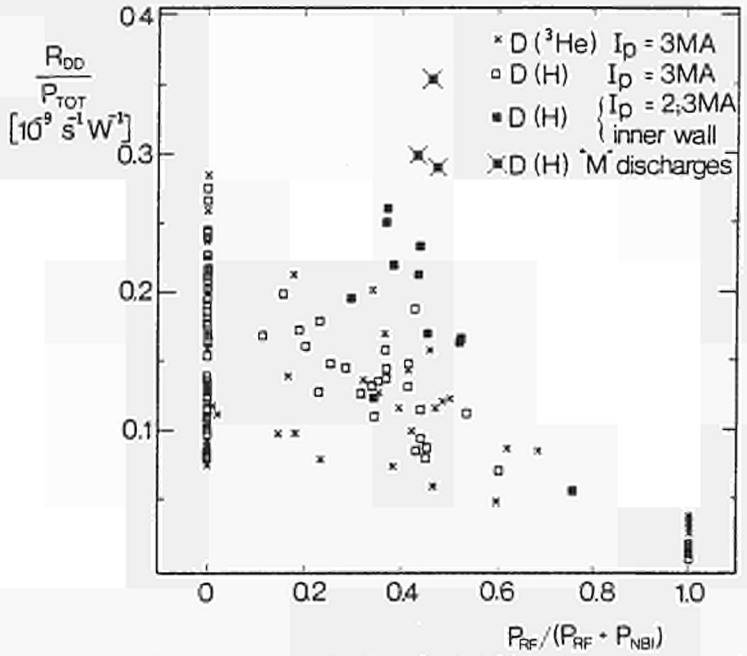

Fig. 5 Fusion D–D reaction rate normalized to the total input power versus the ratio of RF to total additional power. The beam plasma reaction is maintained proportional to the additional power independently of its origin provided $P_{RF}/(P_{NBI}+P_{RF}) \leq 0.5$. Monster sawteeth give a larger fusion yield.

8 MONSTER SAWTOOTH

Unusually long sawteeth and high fusion reactivity have been observed in the so-called 'Monster sawtooth' regime in the following conditions:

— I_p=2 - 2.2MA, B_ϕ=2.1 - 2.2T, Plasmas lying on the inner wall. H minority, RF alone or combined with beams

— I_p=5MA, B_ϕ=3.4T, He^3 minority, combined heating

— $5\text{MW} \leq (P_{RF} + P_{NBI}) \leq 15\text{MW}$

— $2\times10^{19}\text{m}^{-3} < \bar{n}_e < 3.5\times10^{19}\text{m}^{-3}$

Fig. 6 illustrates such a regime when the RF is applied on top of NBI injection. The internal relaxations stop and the plasma is remarkably free from MHD activity for ~ 1s. $T_e(0)$ more than doubles and a peak temperature of 7.4 keV has been obtained with 10MW of additional

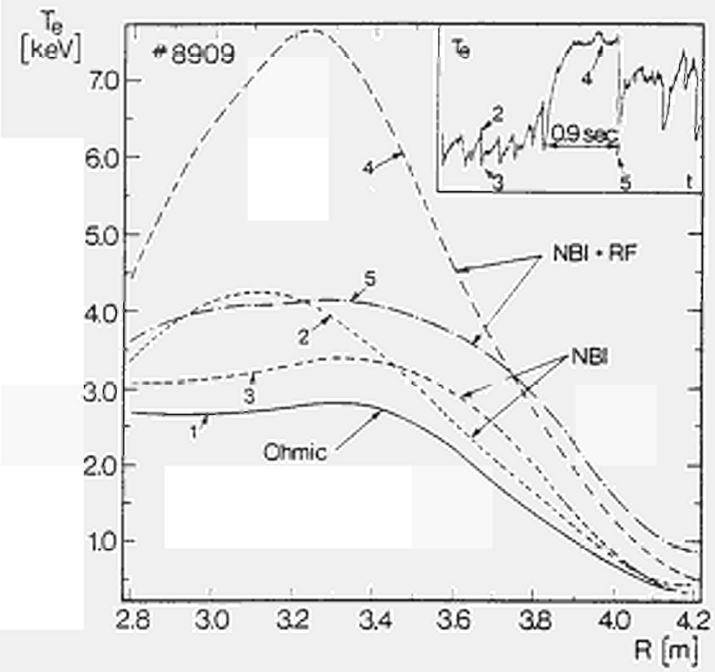

Fig. 6 T_e profile before heating (ohmic) during P_{NBI} (2.5 MW) and during a 'monster' (NBI = 2.5 MW, P_{RF} = 7 MW). In each case, the curves represent the top and bottom of a sawtooth. Note the increase of the inversion radius.

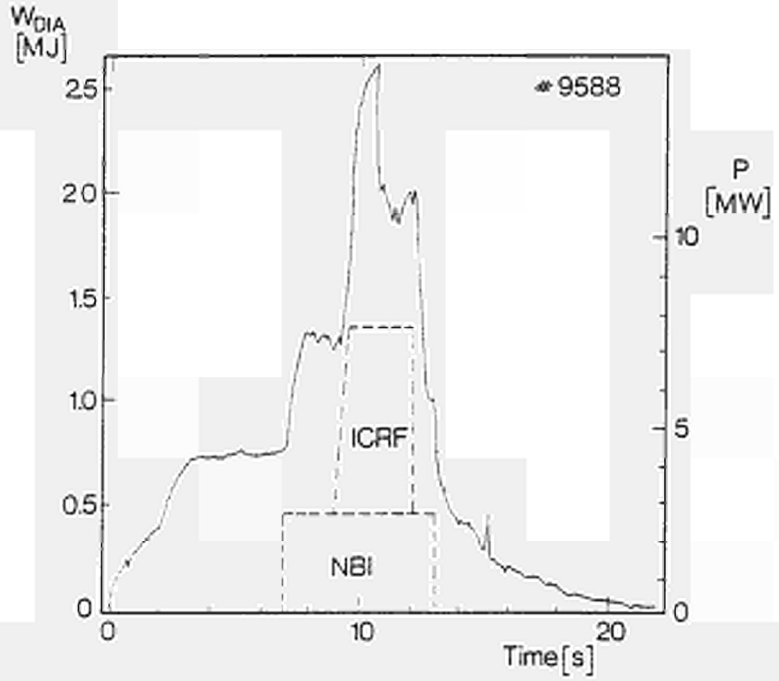

Fig. 7 Evolution of the stored energy during the longest 'Monster' (1.26s.). Although T_e saturates, the density and the stored energy keep increasing. P_{NBI} = 2.6 MW (80 keV). P_{RF} = 5.5 MW, I_p = 2.2 MA, B_ϕ = 2.18 T.

power. The T_e gradient steepens in the entire profile. The inversion radius appears to expand up to mid-radius. In many cases, the stored energy does not saturate before the crash, even after 1.26s (Fig. 7). The incremental confinement time $\tau_{inc} = \Delta W/\Delta P_{RF}$ is somewhat improved over the usual conditions. Typically, $\tau_{inc} = 250$ ms at the end of the 'Monster' instead of 200ms in normally sawteething discharges. The pressure anisotropy is mild: $\beta_{p\perp} = 1.13\ \beta_{p\parallel} = 0.5$. The crash of the monster releases 30% of the stored energy. Thereafter, the MHD activity is high (mostly n=2 modes) and the confinement appears degraded. In these experiments, the poloidal beta reached 0.5 and the ion temperature was between 5 and 7keV.

9. TRANSITION TO AN 'H-MODE'

Preliminary experiments with combined heating in a single null X-point configuration exhibited the change of edge and bulk plasma parameters in the Asdex H-mode behaviour. The transition occurred wiht 7MW of combined heating in the Hydrogen minority regime. After the transition, the density rose, the temperature remaining constant, and the confinement time increased from 0.35s to 0.6s.

10. CONCLUSIONS

After a year of operation on JET, ICRF heating has reached record levels of RF power and electron temperatures in a Tokamak. Eight water cooled antennas will be installed in 1987 and connected to a 32MW power source. Recent results give confidence that JET will demonstrate a fusion output comparable to the heating power input.

REFERENCES

[1] J. JACQUINOT et al., Plasma Phys. and Contr. Fusion **28** 1 (1986)

[2] P.P. LALLIA et al., Plasma Phys, and Contr. Fusion, **28** 1211 (1986)

[3] A.S. KAYE, Proc. of the 11th Symposium on Fusion Engineering, Austin Texas, (1985) Vol II, p1204

[4] G. DUESING et al., Plasma Phys and Contr. Fusion, **28** 1429 (1986)

[5] D. GAMBIER et al., Proc. of the 12th European Conf. on Contr. Fusion and Plasma Phys. Budapest (1985), Europhysics Conf Abstracts, Vol 9F, Part II 152.

[6] V.P. BHATNAGAR, R. KOCH, P. GEILFUS, R. KIRKPATRICK, R.R. WEYNANTS, Nucl. Fusion, **24** No 8 (1984)

[7] T.HELLSTEN and K. APPERT, Proc. of the 13th Eur. Conf. on Contr. Fusion and Plasma Heating, Schliersee F.R.G, (1986) Europhysics Conf. Abstracts, Vol. 10C, Part II, 129

[8] F. SAND et al., Proc. of the 13th Eur. Conf. on Contr. Fusion and Plasma Heating, Schliersee F.R.G, (1986) Europhysics Conf. (1986) Abstracts, Vol. 10C, Part II, 197.

[9] K. BEHRINGER et al., 11th IAEA Conference on Plasma Physics and Contr. Fusion Research (Kyoto, Japan) (1986)

[10] J.G. CORDEY et al., 11th IAEA Conference in Plasma Physics and Contr. Fusion Research (Kyoto, Japan) (1986)

[11] H. HAMNEN et al., Proc. of the 13th Eur. Conf. on Contr. Fusion and Plasma Heating, Schliersee F.R.G, (1986), Europhysics Conf. Abstracts, (1986) Vol. 10C, Part II, 425

[12] W. CORE et al., Proc. of the 13th Eur. Conf. on Contr. Fusion and Plasma Heating, Schliersee, F.R.G, Europhysics Conf. Abstracts, (1986) Vol. 10C, Part II, 73

[13] G. COTTRELL, 1986, Private Communication

ENERGY CONFINEMENT WITH OHMIC AND STRONG AUXILIARY HEATING IN JET

J G Cordey, D V Bartlett, V Bhatnagar++, R J Bickerton, M Bures, J D Callen*, D J Campbell, C Challis, J P Christiansen, S Corti, A E Costley, G A Cottrell, G Duesing, J Fessey, M Gadeberg+, A Gibson, N Gottardi, A Gondhalekar, C W Gowers, M von Hellerman, F Hendricks, L Horton, J Jacquinot, H Jaeckel#, O N Jarvis, T T C Jones, E Kallne, J Kallne, M Keilhacker, S Kissel, L de Kock, P Lallia, E Lazzaro, P J Lomas, N Lopes Cardozoϕ, P D Morgan, P Nielsen, R Prentice, R T Ross, J O'Rourke, G Sadler, F C Schüller, A Stabler#, P Smeulders, M F Stamp, D Stork, P E Stott, D R Summers, A Tanga, P R Thomas, E Thompson, K Thomsen+, G Tonetti**, B J Tubbingϕ, M L Watkins

JET Joint Undertaking, Abingdon, Oxfordshire, OX14 3EA

On attachment from +Riso National Laboratory, Denmark; #IPP Garching, FRG; **CRPP, Lausanne, Switzerland; ++EMS, Brussels; ϕFOM, Instituut voor Plasmafysica, The Netherlands; *Univ of Wisconsin, Madison, USA

ENERGY CONFINEMENT WITH OHMIC AND STRONG AUXILIARY HEATING IN JET

ABSTRACT

The energy confinement properties with strong auxiliary heating are found to be well described by an offset linear law relating the stored energy W to the input power P ($W = \alpha P + \beta$). The scaling of the energy confinement time τ_ε with the non-dimensional plasma physics parameters suggests that the underlying transport mechanism is resistive MHD. Electron heat transport is examined in three different ways and shown to be consistent with a local heat flux model with a constant heat diffusion coefficient χ. The heating profile and impurity radiation are identified as making a substantial contribution to the degradation in the global energy confinement time with auxiliary heating.

1. INTRODUCTION

In this paper the energy confinement properties of the JET plasma with intense auxiliary heating are discussed. In previous papers [1],[2], confinement in ohmically heated plasmas has been reported. The additional heating was provided by neutral beams (60-75keV D and H) at powers up to 9MW and ion cyclotron resonance heating [3] of helium and hydrogen minorities at powers up to 7MW. The two heating methods were also combined to give a total input power of 16MW which was between 4 and 20 times the ohmic input power. The toroidal field B, plasma current I and average density $\langle n \rangle$ were all varied over a wide range ($B = 1.7 - 3.4$ T, $I = 1-5$MA, $\langle n \rangle = 0.5 - 5 \times 10^{19} m^{-3}$) with the geometry kept essentially fixed (major radius $R \sim 3.0$m, horizontal minor radius $a = 1.2$m, elongation $K = 1.45$) so that the dependence of the global energy confinement τ_ε ($= W/P-\hat{W}$) upon I, B, $\langle n \rangle$ and the heating scheme could be assessed.

The plasma edge conditions have, however, been varied by limiting the plasma on the outer mid-plane limiters, the inner-wall or separatrices (X-points) near the top and bottom of the chamber. Generally the confinement time τ_ε degrades with both types of heating from its ohmic value $\sim 0.5 - 0.8$s down to ~ 0.2-0.4s. The smallest degradation occurs for plasmas located on the inner wall or with an X-point.

The remainder of the paper is divided as follows, in section 2.1 a simple empirical scaling law describing the behaviour of the τ_ε with the plasma parameters is derived and then in section 2.2 the scaling of τ_ε with the Connor-Taylor [4] dimensionless constraint parameters is determined. In Section 3

the degradation in confinement is discussed. First the question of whether the heat flux is self-regulating to maintain a fixed electron temperature profile, or whether it is determined by the local temperature gradient, is examined. The latter model is found to be more consistent with the data. Then a procedure is given, for correcting the input power for impurity radiation losses and heating profile effects, and it is shown that these can account for a substantial part of the degradation in confinement.

2.1 Scaling of τ_ε with Plasma Parameters

The plasma confinement properties with additional heating can be most clearly seen by exhibiting the data in a total (diamagnetic) energy W versus total input power P diagram such as that shown in Fig. 1 where examples of power scans with combined heating at four different currents and toroidal fields are shown. The data in Fig. 1 can be represented by an offset linear scaling of W with P in the form:

$$W = W(0) + \tau_{inc} P \qquad (1)$$

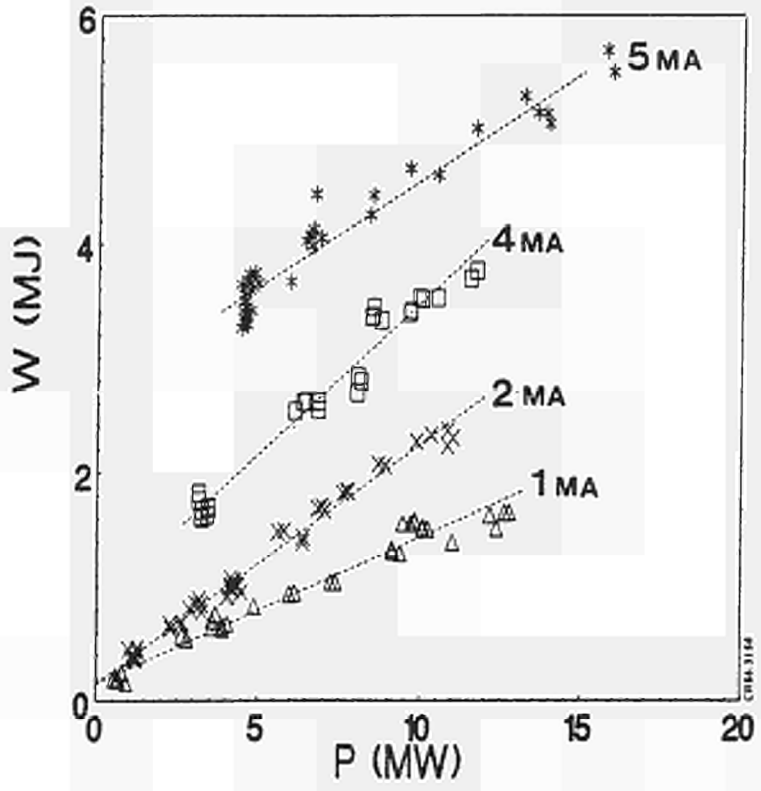

Fig. 1 Total stored energy W(MJ) versus total input power P(MW) for four different power scans: I = 5MA, B = 3.4T; I = 4MA, B = 3.4T; I = 2MA, B = 2T; I = 1MA, B = 2T.

where the incremental confinement time τ_{inc} and W(o) are functions of the I, B, <n>, etc. To make the representation fully general a dependence on power P has to be included in τ_{inc}. The reason for this is that, although the data in Fig. 1 appear linear with P, the density <n> is increasing with P in all the power scans and this could be masking the true power dependence. However, by combining data from scans at different starting densities we have been able to show that the density dependence in τ_{inc} is weak. A good fit to the NBI data set has been found by use of standard regression techniques; it is $W(0) = 0.225\ n^{0.6}\ I^{0.5}\ B^{0.4}$ and $\tau_{inc} = 0.047*I$ (Units, MJ, $m^{-3} \times 10^{-19}$, MA, T). The complete data set (NBI, ICRH and combined heating) is shown against this fit in Fig. 2.

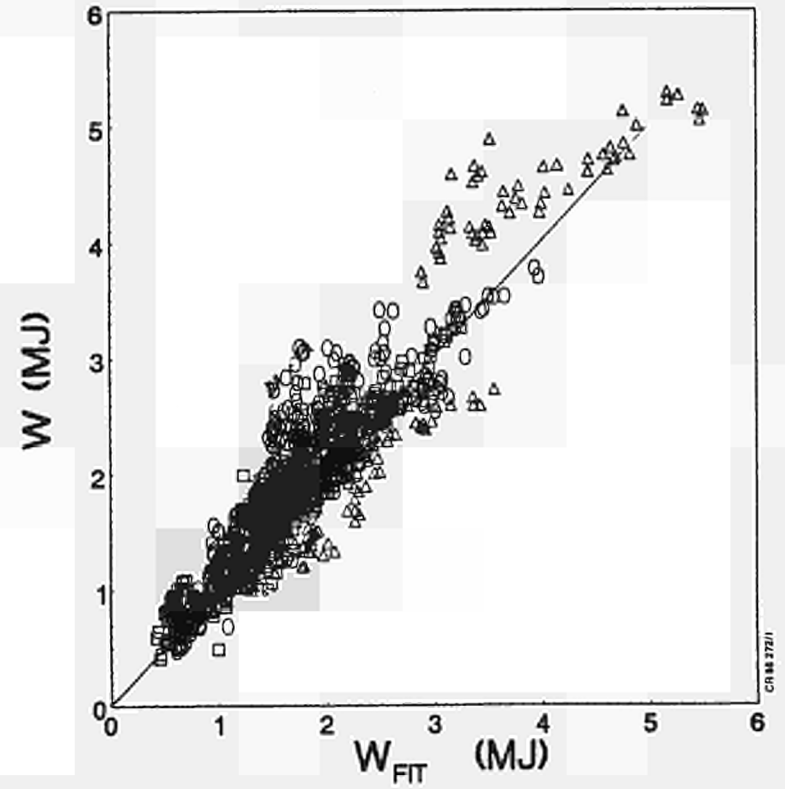

Fig. 2 Total stored energy W versus the fit given in Eq(1). The symbols are neutral beam injection heating alone □, Δ including ICRH with H minority and O including ICRH with He minority.

The scatter in the data in Fig. 2 is thought to be mainly due to the method of heating (NBI or ICRH) and the type of confinement, limiter or inner wall. It is found that the fraction of the input power radiated by the impurities is significantly larger for ICRH and limiter confinement than for inner wall with NBI heating.

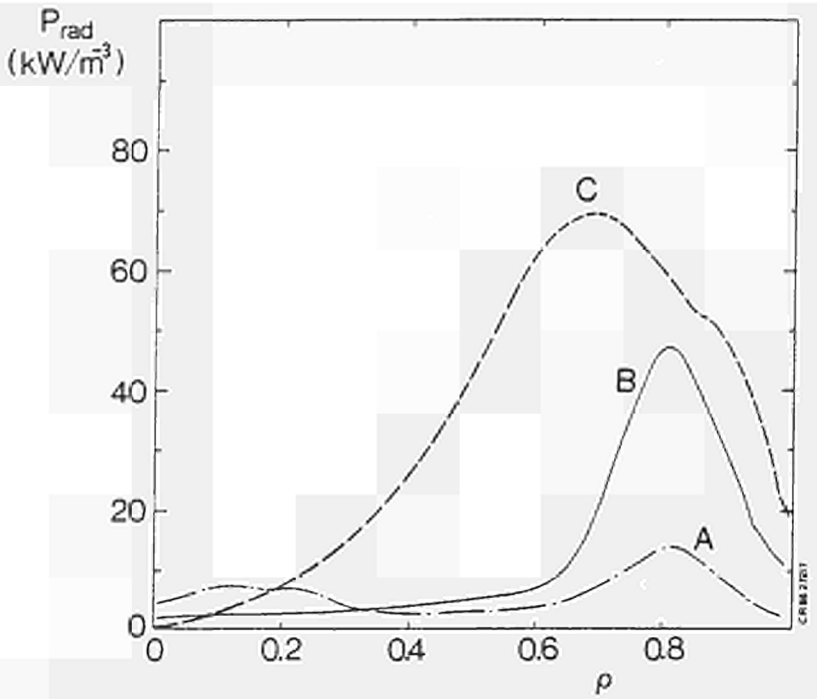

Fig. 3 Radiation profiles for (a) an ohmic discharge located on the inner wall (b) an NBI heated (9MW) discharge located on the inner wall (c) a discharge with combined heating (4MW of ICRH and 5MW of NBI).

In Fig. 3 the radiation profiles are shown for three pulses; (A) a typical ohmic discharge (B) an NBI discharge located on the inner wall (C) a combined heating discharge on the limiter. Typically 30% of the input power is radiated in the central confinement zone ($r/a < 0.7$) in the case (C) and only 8% in case (B), the source and concentration of the impurities is discussed in detail in ref. [5]. The radial heating profiles of the two schemes are also very different: the ICRH profiles are always peaked, ie, similar to the ohmic heating profile, whilst the NBI profile is usually less peaked, and at high densities the NBI profile is quite flat.

The effect on confinement of changing the plasma configuration is shown in Fig. 4 where the global τ_E (diamagnetic) is given as a function of power for the complete 2MA data set; also shown on the same figure is the empirical L mode scaling of Kaye and Goldston [6] derived from data from previous experiments. Although for all configurations and heating schemes the τ_E degrades with power, the inner wall and double null X point data with NBI heating are up to a factor 2 above the Kaye-Goldston law. The single null X point data which had clear H mode characteristics was up to a factor 3 larger than the Kaye-Goldston law.

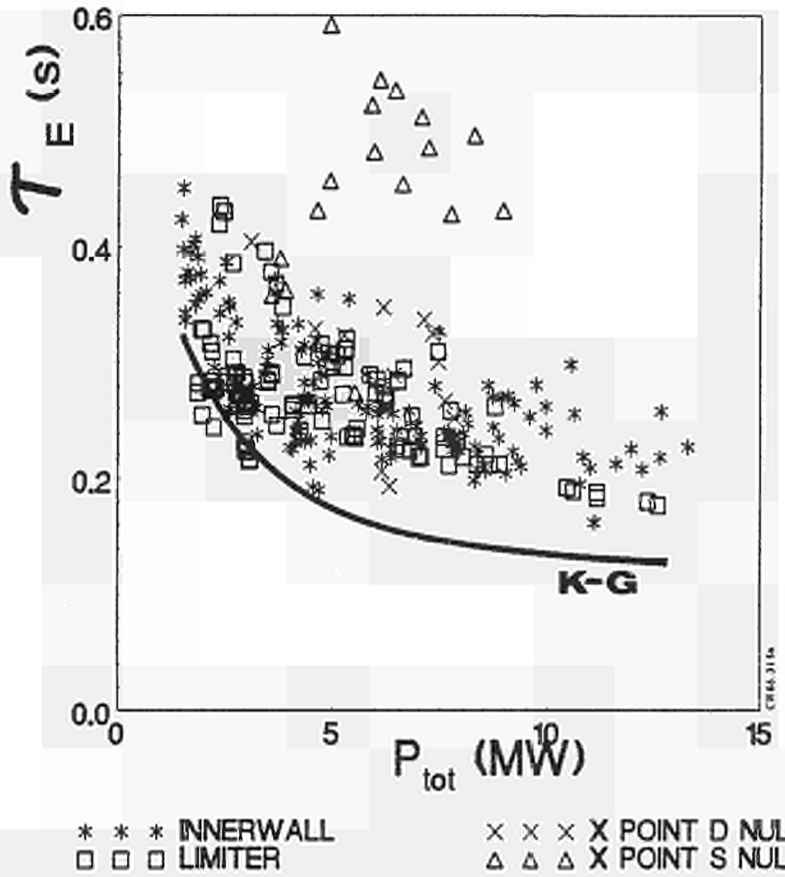

Fig. 4 Energy confinement time τ_ε versus total power P (MW); the symbols are x X-point with double null, S X-point with a single null, * inner wall discharges and outer limiter discharges. The solid line is the Kaye-Goldston fit.

The majority of the NBI experiments have been made with deuterium injection in the co-direction. A few experiments with counter injection using deuterium and also hydrogen injection in the co-direction have also been made. As far as energy confinement was concerned, there was no apparent difference between co and counter injection, and the hydrogen injection results which were reported earlier [2] were similar to the present deuterium injection data.

2.2 Scaling of τ_ε with Dimensionless Parameters

The additional heating data have been compared with the Connor-Taylor models [4]. It is found that the low beta models cannot represent the confinement time scaling, especially when comparison is made with data from smaller devices. The scaling invariants originally given by Connor and Taylor were chosen arbitrarily to represent density, temperature and magnetic field dependences. For the high beta models, it is more appropriate

to use the magnetic Reynold's number ($S = \tau_R/\tau_{Ap}$), the cyclotron frequency times the poloidal Alfven time ($\omega_c\tau_{Ap}$) and the ratio of total to ohmic powers (P_{tot}/P_{ohm}). The latter variable is equivalent to the poloidal beta in power law scaling forms and is used in order to prevent the energy content from appearing in both the dependent and independent variables. This set of scaling variables make the relationship between models more transparent and ensures that geometrical quantities such as safety factor and elongation are included in a natural fashion. The energy confinement time for the collisional high beta model is:

$$\tau_\varepsilon/\tau_{Ap} = F(\omega_c\tau_{Ap},\ S\ ,\ P_{tot}/P_{ohm}) \qquad (2)$$

The collisionless models are obtained by combining the last arguments as $(P_{tot}/P_{ohm})S^{-1}$ and the fluid models by dropping $\omega_c\tau_{Ap}$. It is found that the JET data for $(P_{tot}/P_{ohm})>2$ are best represented by the resistive MHD model as:

$$\tau_\varepsilon = 0.91\ \tau_{Ap}\ (P_{tot}/P_{ohm})^{-0.5}\ S^{0.75} \qquad (3)$$

The fit is shown in Fig. 5. Data from other machines can be reproduced when the aspect ratio ($\varepsilon = a/R$) is included and the resulting scaling law is equivalent to:

$$\tau_\varepsilon = (\tau_R\tau_{Ap})^{0.5}\ (\varepsilon\ \beta_p)^{-1} \qquad (4)$$

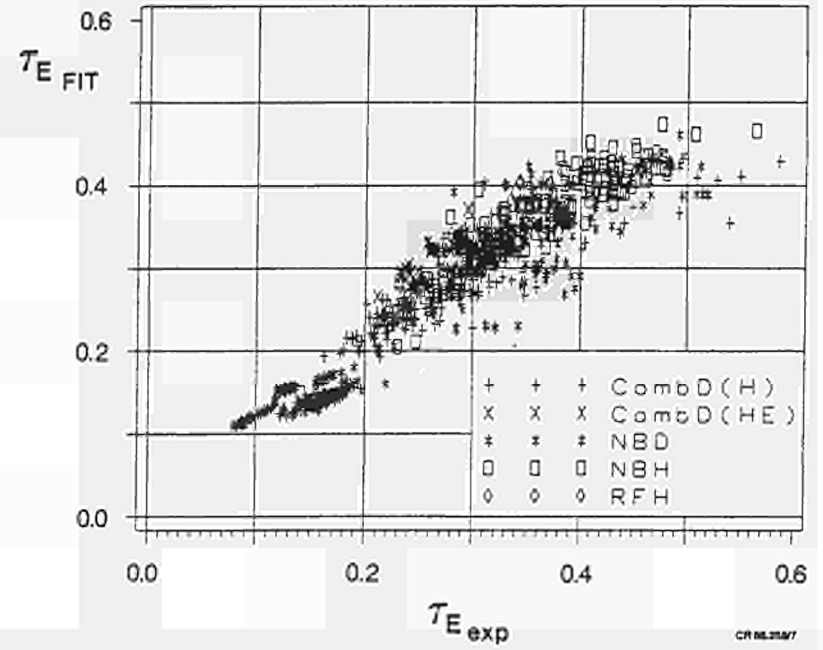

Fig. 5 Energy confinement time τ_ε versus the fit from the resistive MHD model.

In view of the surprising simplicity of this form and the absence of any significant normalising constant, it might be concluded that Eq(4) is indicative of the underlying transport mechanism. However this should be qualified by noting the difficulty in varying S and β_p in such a way as to clearly confirm the separate dependences in a given device. At first sight Eq(3) appears to be inconsistent with the offset linear scaling law Eq(1). In fact the implicit dependence of P_{ohm} and S on power make the two indistinguishable.

3. DISCUSSION OF CONFINEMENT DEGRADATION

There are many possible explanations for the degradation in confinement and some of these are examined briefly in this section. A current popular explanation is that the heat transport is self-adjusting such that the same electron temperature profile is maintained ('profile consistency'). The evidence for profile consistency in JET data was reviewed by Bartlett et al [7], recently. The electron temperature profiles in high current ($I \geq 3MA$) discharges certainly exhibit the conventional profile consistency features, that is $T_e(\rho)/T_e(0)$ is only a function of q and the profile is unchanged by additional heating, at least at the presently available power levels ($P_{tot}/P_{ohm} \sim 4$). In low current ($I = 1MA$) discharges, where $P_{tot}/P_{ohm} \sim 20$, the electron temperature profile appears to respond to the changing heating profile. In Fig 6(a), the temperature profiles are shown for the two cases of low and high current before and during heating and the corresponding heating profiles are shown in Fig 6(b). In the low current case, the initial ohmically heated profile is substantially broadened by the application of NBI heating whilst for the higher current pulse the ohmic and NBI heating profiles are rather similar. Although the change in both temperature profiles is small with additional heating, it is consistent with what is expected for the change in heating profile shown in Fig 6(b). Indeed as Waltz et al [8] have shown, very large changes in the heating profile only produce small changes in the temperature profile shape for discharges in which the central q is limited by internal relaxations (sawteeth).

Thus, in summary, there is no really clear evidence that 'profile consistency' plays a deterministic role in heat transport. There is however evidence that whilst the confinement time degrades with power input the underlying heat transport is independent of the auxiliary heating power. First, the fact that the total energy W increases linearly with power P, as shown in Fig. 1, means that the incremental confinement time $\tau_{inc} = \Delta W/\Delta P$ does not vary significantly with power level. For example, at $I = 3MA$ we have $\chi_{inc} = ab/4\tau_{inc} \sim 2.9 \pm 0.6 m^2/s$. Second, as shown in Fig. 7 the electron heat flux per unit density $P_e(r)/nA = \int d^3x \Sigma Q/n \int dA$ is proportional to the local

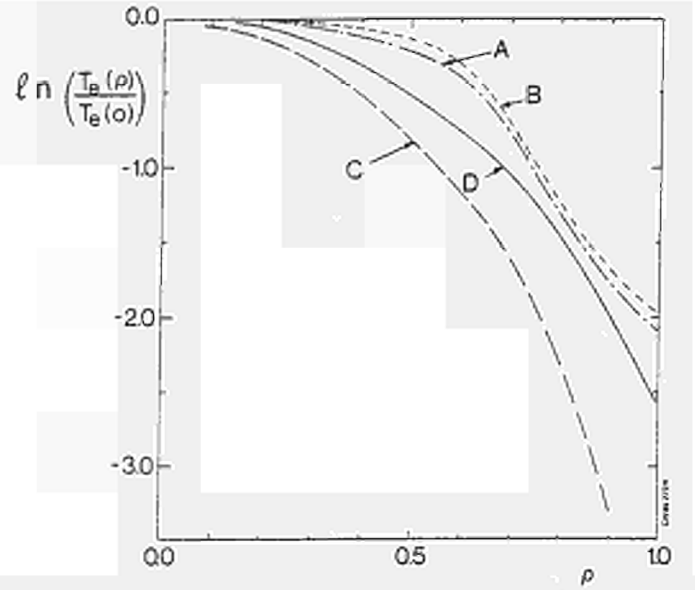

Fig. 6a $\mathrm{Log}_e\ (T_e(\rho)/T_e(0))$ versus ρ for a 3MA discharge before heating (curve A) and after 9MW of NBI heating (curve B) and a 1MA discharge before heating (C) and during 9MW of NBI heating (D).

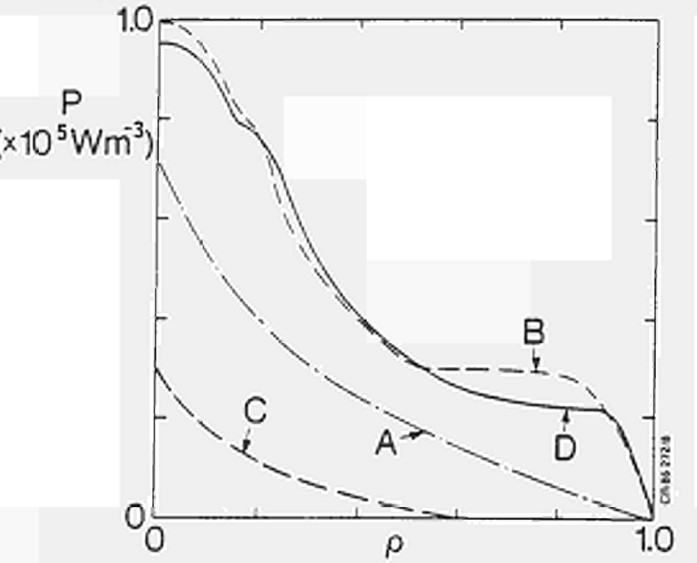

Fig. 6b Power input to the electrons (Wm^{-3}) versus ρ for the four cases of Fig. 6a.

temperature gradient. This implies a $\chi_{flux} = \Delta(P_e(r)/nA)/\Delta(dTe/dr) \sim 1.8 - 3.3 m^2/s$ for the 3MA case. (The reason for the large range in χ_e is due to the uncertainty in estimating the loss through the ion channel.) Finally, and most locally, the χ_{HP} determined using the heat pulse propagation method [9] is found to be approximately constant (for I = 3MA,

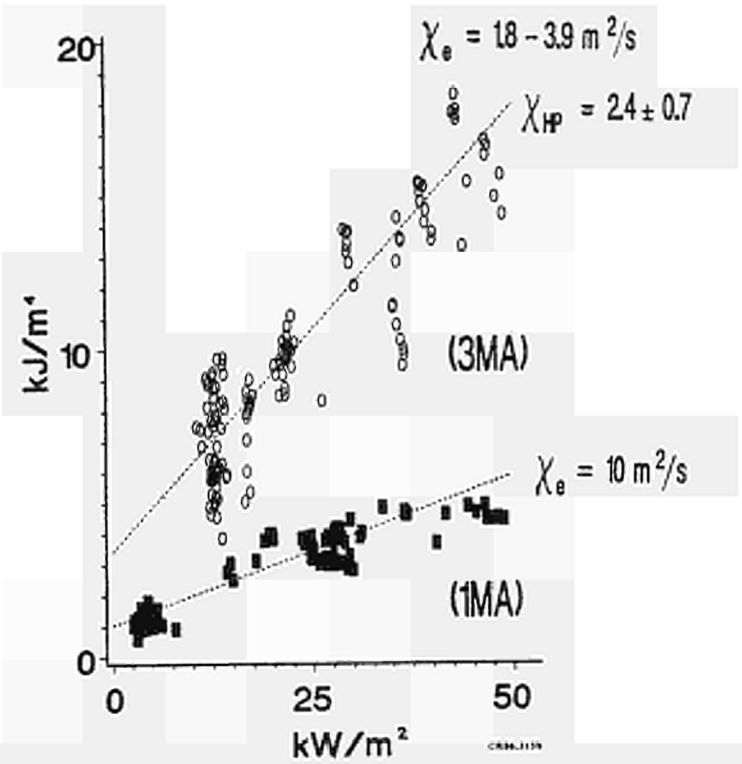

Fig. 7 $n\nabla T_e$(kJ/m²) at ρ = 0.75 versus the heat flux (kW/m²) for a 3MA O and 1MA ■ power scans. The dotted lines are the best straight line fits to the data.

a = 1.2, K = 1.45) at a value of 2.4 ± 0.7m²/s, independent of the heating power [10]. The fact that these three different methods of determining the electron heat diffusivity χ_e yield nearly the same power-independent value ($\chi_{inc} \sim \chi_{flux} \sim \chi_{HP}$) implies that the transition from ohmically to auxiliary heated discharges may be interpretable in terms of a transport model with electron heat conduction characterised by a constant value of χ_e.

An example of such a model will now be developed and used to clarify the heating profile and radiation loss effects. First, assume that the heat flux is given generally by heat conduction plus convection in the form $\underline{q} = -n\chi\underline{\nabla}T + \underline{q}_{conv}$. Utilising this in the equilibrium heat balance, $\underline{\nabla}\cdot\underline{q} = \Sigma Q = Q_{OH} + Q_{aux} - Q_{rad}$ and assuming that χ and q_{conv} are not strongly dependent upon T or ∇T, one can integrate once to determine the temperature gradient and once more to calculate the temperature profile. A further integration over the plasma volume gives the total stored energy W, which in cylindrical geometry has the form,

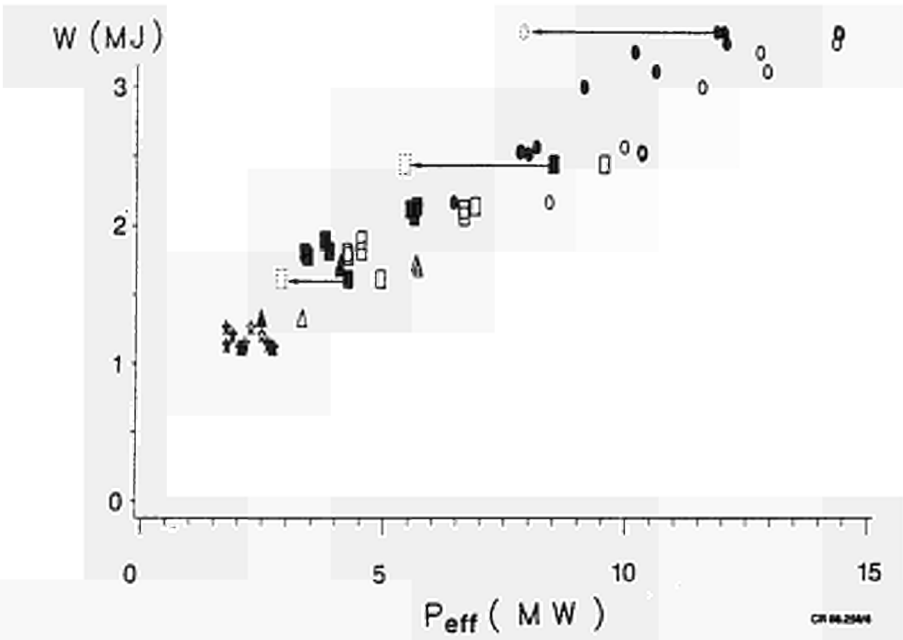

Fig. 8 Total energy density versus effective power, symbols (1) open before correction for radiation losses and heating profile effects (2) solid symbols after correction for radiation (3) dotted symbols after correction for radiation and heating profile effects; ⊽ ohmic □ NBI only Δ ICRH only O combined ICRH and NBI.

$$W = 3\int d^3x\, n(r)\left[\int_r^a \frac{dr'}{rn\chi}\int_o^{r'} rdr''\Sigma Q(r'') - \int_r^a dr'\,\frac{q_{conv}}{n\chi}\right]$$

$$= \tau_{\varepsilon\chi}\,\{[P_{ohm} + P_{aux} - P_{rad}]_{eff} - P_{conv}\} \qquad (5)$$

Here, $\tau_{\varepsilon\chi} = ab/4\bar{\chi}$ and the effective power inputs take account of the effects of heating, radiation, density and χ profiles on the total stored energy W. For constant n and χ, one obtains $P_{eff} = C_o \int_o^a rdr(1-r^2/a^2)Q(r)$ where C_o is a normalising constant.

The main reason for deriving Eq(5) is that it has the same form as the linear offset model Eq(1) used to represent the data, the offset being identified as the convected power. However, it would be negative in this model indicating a heat pinch [11]. An alternative heat transport model without a heat pinch ($q_{conv} = 0$) would require a χ which, while constant over the usual power input (or ∇T) range varies strongly at low values of ∇T [12],[13]. From Fig. 7, either of these models could fit the present data.

An example of the use of Eq(5) is shown in Fig. 8 where the above profile analysis techniques are applied to an I = 3MA, B = 2T power scan with combined heating. The data is shown both

before correction for the power lost by radiation (the open points) and then after correction for the power lost by radiation (solid points). Correcting for radiation losses reduces the scatter in the data and increases the incremental confinement time by 30%. Correcting for the differing heat deposition profile further increases the incremental confinement time (arrowed points) and the degradation in confinement in going from ohmic to strong auxiliary heating is then much smaller. Now the results in Fig. 8 will depend on the assumptions that are made for the radial profile of χ. However this example does demonstrate qualitatively that the degradation in the confinement time τ_E could be due to the broader deposition profile of NBI and/or enhanced radiation; and a change in the basic heat transport mechanism may not be required.

4. CONCLUSIONS

A simple empirical scaling law Eq(1) has been found to adequately describe the energy confinement properties of JET with intense additional heating. The scaling of the energy confinement time with the dimensionless plasma physics parameters suggests that the underlying heat transport is a consequence of resistive MHD instabilities. Electron heat transport with auxiliary heating has been found by three different methods to be describable in terms of a heat flux with a constant coefficient ($\chi_e \sim 2.5 \pm 1.0 m^2/s$ for 3MA discharges). A substantial contribution to the degradation in global confinement with additional heating is shown to be due to the profiles of radiation and heating.

REFERENCES

[1] CORDEY J G et al, EPS Budapest (1985) Vol 1 p26.
[2] THOMSEN K et al, EPS Schliersee (1986) Vol 1 p29.
[3] JACQUINOT J et al, IAEA Conference Kyoto (1986).
[4] CONNOR J W and TAYLOR J B, Nucl Fusion 17, p1047 (1977); Phys Fluids 27, p2676 (1984).
[5] BEHRINGER K et al, IAEA Conference Kyoto (1986).
[6] KAYE S M and GOLDSTON R J, (1985), Nucl Fusion 25, 65.
[7] BARTLETT D V et al, EPS Schliersee (1986) Vol 1, p236.
[8] WALTZ R E et al, GA-A18365 to be published in Nucl Fusion.
[9] CALLEN J D and JAHNS G L, Phys Rev Lett 38 (1977) 971.
[10] TUBBING B et al, "Heat Pulse Propagation Studies in JET" JET Report (to be published). See also 1985 DPP-APS San Diego Meeting paper GP49 and 1985 EPS Budapest paper 142.
[11] FREDRICKSON E D et al, Nucl Fusion 26 (1986) 849.
[12] REBUT P H and BRUSATI M, EPS Budapest (1985).
[13] THOMAS P, EPS Budapest (1985).

IMPURITY PRODUCTION MECHANISMS AND BEHAVIOUR DURING ADDITIONAL HEATING IN JET

K Behringer, A Boileau, F Bombarda°, B Denne, W Engelhardt, M J Forrest*, G Fussmann+, R Giannella°, N Gottardi, M von Hellermann, L Horton, H Jäckel+, C Jupén×, K Lawson, E Källne, G Magyar, G M McCracken*, P D Morgan, R Müller+, N J Peacock*, J Ramette≠, B Saoutic≠, M F Stamp, H P Summers, G Tallents and A Weller+

JET Joint Undertaking, Abingdon, Oxon, OX14 3EA, UK

* EURATOM-UKAEA Association, Culham Laboratory, Abingdon, Oxon, OX14 3DB, UK

\+ EURATOM-IPP Assocation, Garching, FRG

° EURATOM-ENEA Association, Frascati, Italy

≠ EURATOM-CEA Association, Fontenay-aux-Roses, France

× University of Lund, Sweden

IMPURITY PRODUCTION MECHANISMS AND BEHAVIOUR DURING ADDITIONAL HEATING IN JET

ABSTRACT

Impurities in JET are investigated by spectroscopic and plasma edge diagnostics. Impurity influxes are measured by visible spectroscopy allowing identification of impurity sources and conclusions on production mechanisms. Metals and carbon in JET plasmas originate mainly from the limiters; physical sputtering is the release mechanism. Oxygen originates from the walls, presumably by photon or neutral particle desorption. During ICRH, antenna screen material is released by a process not yet understood. Transport studies yield $D \approx 1$ m^2/s for impurities. Ohmic and neutral beam heated plasmas are dominated by light impurities (C, O), in particular by oxygen at high $\bar{n}_e$. Moderate metal levels (0.1% n_e) during ICRH are responsible for radiation losses of $\approx$ 20% P_{tot}. These can be prevented temporarily by carbonisation. Radiative power losses are 30-60% P_{tot} for NBI and 40-70% P_{tot} for ICRH. Z_{eff} ranges between 3.5 at low $\bar{n}_e$ and 2.5 at higher $\bar{n}_e$. During magnetic separatrix operation, a reduction of metals and carbon is observed. The bulk plasma radiation drops compared to limiter discharges, but there is an additional contribution from the X-point regions. To date, no accumulation has been observed during NB counter injection.

1. INTRODUCTION

Impurities in JET plasmas are studied by a variety of spectroscopic diagnostics from the visible to the X-ray range [1], by bolometers and soft X-ray cameras, and by charge-exchange recombination spectroscopy (CXRS). Z_{eff} is derived from visible bremsstrahlung. Hydrogen and impurity influxes, $\phi_{H,D}$ and ϕ_I, are measured at various locations in the torus by visible spectroscopy. For this purpose, line excitation rate coefficients and intensities of specific impurity lines have been computed relating the number of emitted photons to the influx rate [2]. Surface analysis of collector probes, long-term samples and limiter tiles provides information on the status of surfaces in contact with the plasma and on the consequences of cleaning procedures and carbonisation. Langmuir probes are used to measure the plasma edge parameters. The limiter surface temperatures are monitored by infra-red cameras [3].

2. IMPURITY TRANSPORT AND IMPURITY CONFINEMENT

Emission shells of light impurities and low metal ionisation stages in JET are clearly transport dominated requiring a diffusion coefficient $D \approx 1$ m^2/s in order to explain their position and width [4]. Information about transport was also

obtained from accidental injections of iron and nickel. At $\bar{n}_e=2.10^{19}m^{-3}$, simulations using D=1 m^2/s agree best with the observed rise and decay of nickel line intensities as shown in Fig.1 for Ni XXVI. There are indications that D decreases with electron density and increases during additional heating. Investigations of hydrogen particle transport [5] result in similar transport coefficients as found for the impurities.

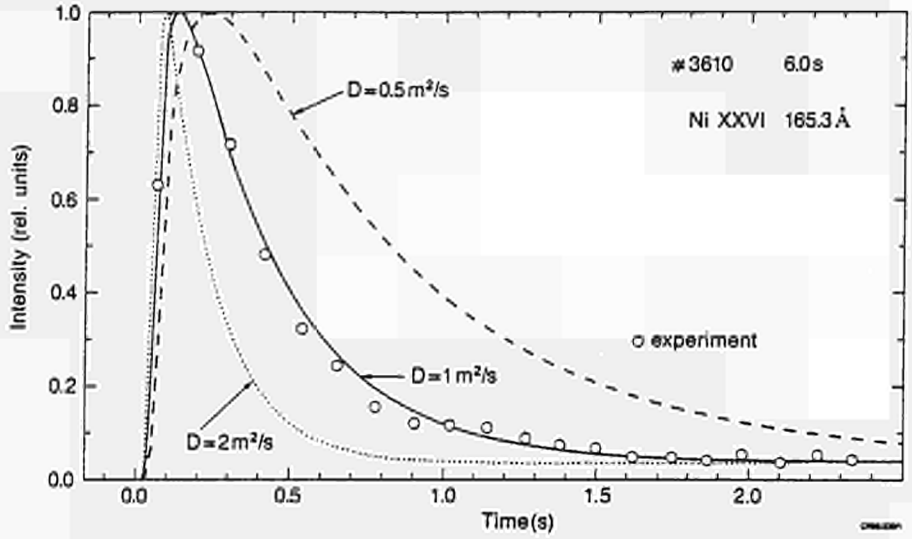

Fig.1: Ni XXVI intensity after accidental nickel injection ($\bar{n}_e=2\cdot10^{19}$ m^{-3}, $I_p=2.8$ MA). Simulations using different D values are shown ($V_D=-2Dr/a^2$). Recycling at the limiters leads to a finite level after the event.

D=1 m^2/s and a drift velocity $V_D=-2Dr/a^2$ are used in standard interpretation of VUV and X-ray spectra and for calculating radiated power losses of individual impurity species by means of an impurity transport code [6]. The resulting, moderately peaked total ion density profiles are confirmed within a factor of two by analysis of a number of metal ionisation stages at different radial positions (eg Ni XVII-Ni XXVII). Sawteeth, observed on lines of higher ionisation stages, can only be partly explained by pertinent variation of electron temperature profiles. It must be assumed that impurities are expelled from within the q=1 surface during the sawtooth crash.

Both the radiated power P_{rad} and $Z_{eff}-1$ are roughly proportional to the square of the nuclear charge Z and the concentration of the impurity species. Therefore, normalized, average radiation losses per unit surface area have been defined

$$P_{norm} = P_{rad}/A\ \bar{n}_e^2(Z_{eff}-1), \qquad (1)$$

(neglecting hydrogen radiation) where A is the plasma surface area. P_{norm} has been calculated by the impurity transport code for a variety of JET plasma conditions and for the important JET

impurities. P_{norm} is found to be about $0.4\text{-}0.9\cdot10^{-38}$ kW m^4 for light impurities and about $0.9\text{-}1.2\cdot10^{-38}$ kW m^4 for metals. The lower end of the range corresponds to peaked n_e profiles and high T_e values, the upper end to flat n_e profiles and low T_e values. The assumption of corona ionisation equilibrium reduces P_{norm} by a factor of 5-10 for light impurities, because the radiation shell is then located in the scrape-off layer at low electron and impurity ion densities. A summary of experimental P_{norm} values as a function of $\bar{n}_e$ is shown in Fig.2 for JET 1986 limiter discharges (500 data points). The vast majority of measured values is found in the predicted range. Fig.2 proves clearly the necessity of including transport in the plasma simulation. Two ASDEX data points [7] demonstrate the validity of the scaling with surface area. The detailed behaviour of P_{norm} with respect to the different heating schemes will be discussed below.

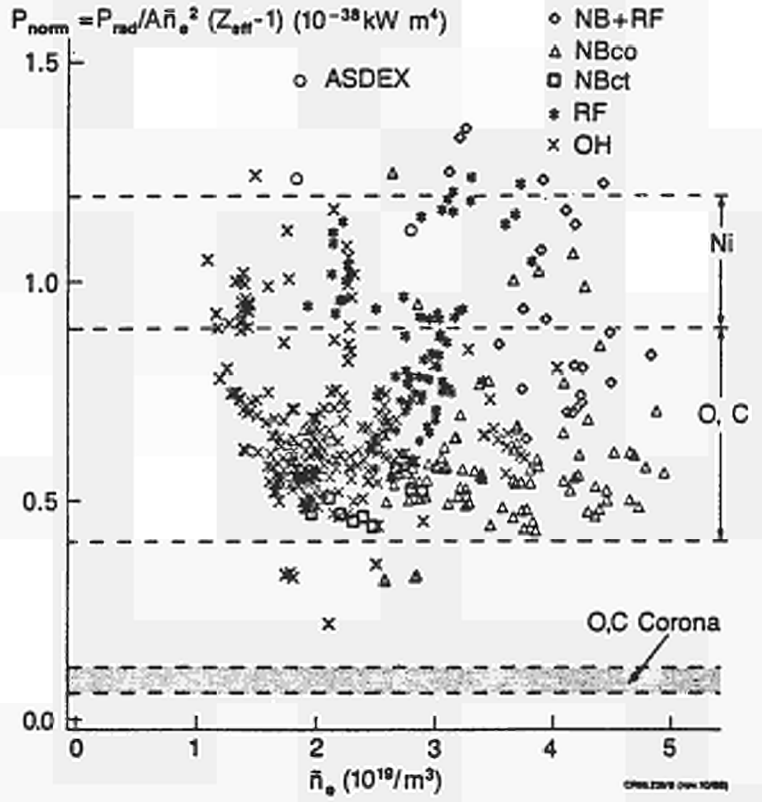

Fig.2: Normalised power per unit surface area for 1986 JET limiter plasmas. The ranges of P_{norm} predicted by the transport code (D=1 m^2/s) for O, C and metals are indicated. Corona assumption leads to much lower P_{norm} values for O and C. One point each is shown for ASDEX limiter and divertor discharges [7].

Impurity particle confinement times, derived from measured influxes and concentrations, agree roughly with calculations on the basis of a simple diffusion model [2] and D=1 m^2/s, if an energy of a few eV is assumed for the neutral particles produced at the limiters. A good correlation of impurity influxes and densities has been observed throughout the JET operation both as a function of plasma parameters and of vessel conditions.

Occasionally, when a steep increase in the Cr influx was observed due to chromium evaporation, the metal concentration in the bulk plasma did not change [2]. These slow particles are ionised in the immediate vicinity of the limiter surfaces and have a high redeposition probability before entering the plasma. This observation demonstrates that the usual impurity influxes of C, O and metals must have a significant kinetic energy to give rise to the measured impurity concentrations.

3. IMPURITY PRODUCTION

The impurity behaviour of JET limiter discharges was dominated by the limiter fluxes (wall contribution ≈ 20% during OH). Metal concentrations were only significant (> 0.1% n_e) if the carbon limiters were metal-coated after accidental melting and evaporation of wall material (Inconel droplets and $\geq 2 \cdot 10^{21} m^{-2}$ uniform coverage [8]). Recently, this has been prevented by covering large areas of the torus by carbon protection plates. A particular metal problem during ICRH will be discussed later.

The release of metals from the limiters can be explained by a combination of sputtering by deuterium and by light impurities taking into account the respective surface coverage of the carbon tiles (ϕ_M/ϕ_D = 0-0.02). The metal fluxes decrease with $\bar{n}_e$ and increase with I_p; they are inversely correlated with the light impurity behaviour. These trends, observed before on many other tokamaks, are due to the temperature dependence of the metal sputtering yields. In JET, gettering of oxygen by chromium has been observed to be a further reason for this anti-correlation.

The carbon concentration in JET has been consistently at a level of a few % n_e throughout operation periods. The carbon production rate behaves similarly to the metal release, but the dependencies are less pronounced [2]. This observation and the fact that the produced C particles must have significant kinetic energy suggest physical sputtering as the prevailing production mechanism. Furthermore, during temperature excursions of the limiter surface from 300°C to over 1000°C no change in carbon production rate was observed, which means that chemical sputtering, expected to manifest itself by an increased yield at about 600°C, is not an important process. There is some evidence for carbon sputtering by oxygen, but only at unusually high oxygen levels [2]. The carbon yields measured (ϕ_C/ϕ_D = 0.05-0.1) can be explained by a combination of deuterium, oxygen and self-sputtering at high $T_e(a)$ values (>100 eV).

The oxygen fluxes and concentrations in JET varied primarily with vessel conditions. The vessel walls constitute the most important oxygen source and, once in the plasma, oxygen recycles at the limiters. This is apparent from the tendency of oxygen limiter fluxes to increase throughout a discharge, even if other parameters are stationary. If the recycling occurs in the form of CO molecules, the O atoms must gain energy in Franck-Condon or charge-exchange processes. Since no dependence of the oxygen yield on plasma parameters is observed, the energy threshold for the respective production mechanism must be very low. During ^{3}He discharges, carbon fluxes remained unchanged ($\phi_C/\phi_{He} \approx 0.13$) while oxygen was substantially reduced. Therefore, chemical processes or CX neutrals must be responsible for the O production.

Due to the above trends, JET plasmas were metal dominated at low electron densities, if there was significant metal deposition on the limiters, otherwise carbon was the most important impurity. At high electron densities metals disappeared, carbon was reduced, and oxygen dominated. Oxygen concentrations increased particularly close to the density limit due to enhanced plasma-wall interaction. Z_{eff} fell steeply with $\bar{n}_e$ when metals were important and was a weak function of $\bar{n}_e$ for metal-free plasmas. During discharges limited by the inner-wall protection tiles, these took over the role of the limiters leading essentially to the same plasma behaviour.

During ICRF heating on JET, screen material (Cr, Ni) has been observed to enter the plasma from the ICRH antennae [2,3]. The measured chromium flux from a Cr coated antenna (10^{16} cm^{-2} s^{-1}/MW) decreased by a factor 5 during five months' operation and was reduced temporarily (some 10 discharges) by two orders of magnitude by means of heavy carbonisation (15% CH_4, 12 hrs). In the course of ICRH operation, screen material was deposited on the limiters and eroded again by the plasma resulting in higher basic metal levels during an ICRH campaign. The metal coverage of the limiter carbon tiles was removed by a few OH or NBI discharges in accord with model predictions [9]. The release mechanism of the screen material is not yet understood.

4. ICRH AND NB CO-INJECTION

Both hydrogen and impurity influxes increased during additional heating, leading to a substantial increase in $\bar{n}_e$, unless the plasma was at the inner wall, which appears to have an efficient pumping capability. Although the wall fluxes gained in importance, the plasmas were still dominated by the limiters. The n_e-profile flattened during ICRH, it was unchanged or peaked during NBI. The hydrogen and impurity particle confinement times decreased in both cases.

Due to the higher electron densities during NBI, oxygen was the most important impurity. The increase in the O/C ratio is well demonstrated by the CXRS results [10], the trends of which are in excellent agreement with the usual VUV spectroscopic

results, while they tend to give somewhat higher carbon concentrations. Z_{eff} dropped during NBI, but not to a lower level than that of OH discharges at the respective higher densities. For constant $\bar{n}_e$, the radiated power fraction P_{rad}/P_{tot} fell with increasing NBI power. However, due to the pertinent $\bar{n}_e$-evolution, radiation losses remained around 45% P_{tot}, on average. These radiation losses were caused by light impurities, in particular, by oxygen (1-2% n_e). Due to the latter fact and a tendency to peaked n_e-profiles during NBI, P_{norm}-values are at the lower end of the range in Fig.2.

The metal release from the antennae screens during ICRH led to significant metal densities in the plasma (≈ 0.1% n_e, contribution to P_{rad} ≈ 20% P_{tot}, see also [11]) except immediately after heavy carbonisation. Z_{eff} remained essentially at the OH value before RF, ie there was no benefit of the higher electron densities. For individual campaigns, the radiated power fraction increased somewhat with P_{RF} and was generally in the range 40-70% P_{tot}. Hydrogen minority heating led to higher metal densities in the plasma than ^{3}He minority heating but the difference in P_{rad} is within the scatter of the data points. Due to some metal contribution and flatter n_e-profiles, the P_{norm} values for ICRH in Fig.2 are at the upper end of the predicted range.

During combined NBI and ICRH, the consequences of the two heating schemes essentially added. The metal densities in the plasma corresponded to the respective RF power. Basic metal levels and limiter coverage built up as during ICRH alone. Z_{eff} and P_{rad}/P_{tot} values for OH plasmas and additional heating are summarised in Fig.3 for 1986 JET limiter discharges. At higher electron densities Z_{eff} was about 2.5 for NBI, ICRH and combined heating, essentially caused by oxygen and carbon.

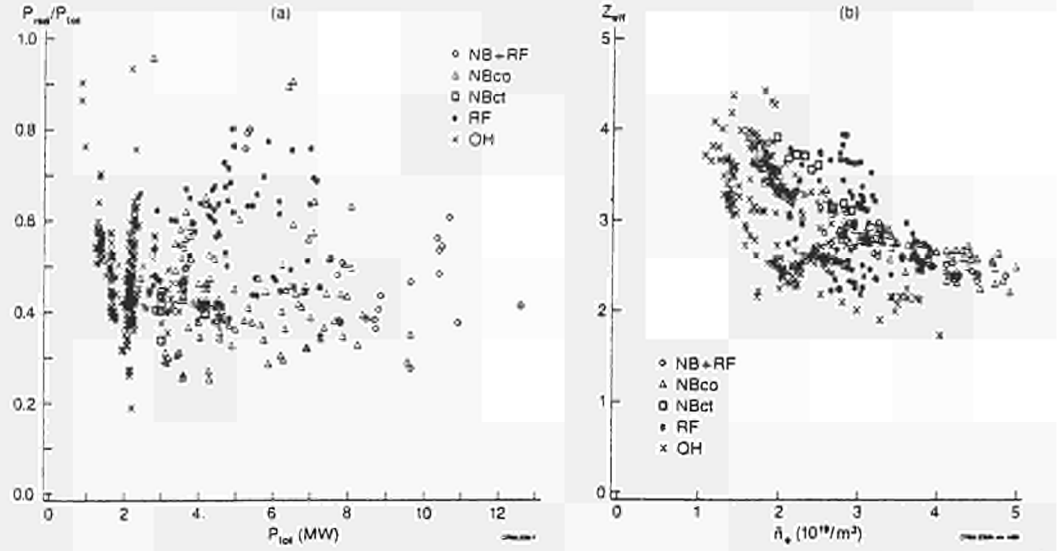

Fig.3: JET 1986 limiter discharges. P_{rad}/P_{tot} as a function of P_{tot} (a) and Z_{eff} versus $\bar{n}_e$ (b) for OH, ICRH (RF), co- and counter-NBI and combined heating (NB+RF).

5. MAGNETIC SEPARATRIX

The magnetic separatrix configuration has been successfully generated in JET (X-point plasmas [12]). In this case, the top and bottom vessel protection tiles act as X-point neutraliser plates. Even when these plates consisted of Inconel (June 1985), no significant metal concentrations were detected in X-point plasmas. With carbon plates, the carbon level was reduced compared to the respective limiter discharges during the OH phase. During NBI, carbon concentrations increased in contrast to the behaviour of limiter discharges as demonstrated again by CXRS [10]. The behaviour of carbon and metals indicates a low plasma temperature in front of the neutraliser plates during OH discharges and therefore a low sputtering yield. After argon puffing into X-point plasmas, no retention of Ar in the X-point regions was observed, ie the same amount was found in the bulk of X-point and corresponding limiter discharges, in contrast to the Doublet III results [13].

The oxygen concentration was not different from limiter plasmas ($\approx 1.5\%\ n_e$). Since metal concentrations were generally low, X-point operation resulted only in a minor reduction of Z_{eff} ($Z_{eff} \approx 3$ at $\bar{n}_e = 1.5 \cdot 10^{19}\ m^{-3}$ and $I_p = 2$ MA). The radiation losses of the bulk plasma were also somewhat lower, but there was an additional contribution of the X-point regions of $\approx 50\%\ P_{bulk}$. The total radiation losses amounted to $\approx 50\%\ P_\Omega$ at low densities ($\bar{n}_e = 1 \cdot 10^{19}\ m^{-3}$) and approached 100% at higher densities. NBI into X-point plasmas led to a low level of wall material in the plasma, probably due to CX particles hitting the walls. The oxygen concentration did not change significantly during NBI.

6. NB COUNTER INJECTION

Counter injection both into limiter and X-point plasmas has been studied for a limited period in JET. The impurity behaviour of these discharges was virtually indistinguishable from the corresponding co-injection cases (see Figs.2 and 3). Some peaking of soft X-ray emission profiles was observed and the line intensities of higher metal ionisation stages appeared to increase more than the lower ones. However, the standard analysis taking into account the respective n_e- and T_e-distributions resulted in the usual impurity ion density profiles within the experimental error bars. For the present NBI power levels (≤ 7 MW) and plasma parameters, no accumulation of impurities has been observed.

7. CONCLUSION

The JET impurity situation is not significantly different from that of other ungettered tokamaks with carbon limiters. Metal concentrations in the plasma were very low during OH and NBI discharges due to coverage of large areas of the wall by carbon tiles. An exception was ICRF heating, where screen

material entered the plasma from the antennae. This will be prevented in the future by a carbon or beryllium coating of the Faraday screens presently under investigation. The carbon concentration was high at moderate electron densities, but, due to the fact that physical sputtering is the production mechanism, it decreased at high densities, which are aimed for anyway. At high $\bar{n}_e$, radiation losses were mainly caused by oxygen. Well below the density limit, P_{rad}/P_{tot} was typically 50% radiated from the plasma edge, while the bulk plasma was transport dominated. A primary aim of future operation must be the reduction of oxygen levels, which could be most easily achieved by gettering. Accumulation of impurities has not been observed in JET.

8. REFERENCES

[1] K Behringer, Rev. Sci. Instrum. 57 (1986) 2000
[2] K Behringer, 7th PSI Princeton, J. Nucl. Mater. 145 & 146 (1987)
[3] W Engelhardt, Plasma Phys. and Contr. Fusion 28 (1986) 1401
[4] K H Behringer et al., Proc. of the Workshop on Basic and Advanced Fusion Plasma Diagn. Techn., Varenna, Italy (1986)
[5] A Cheetham et al, Proc. of the 13th European Conf. on Contr. Fusion and Plasma Heating, Schliersee, FRG (1986) 240
[6] K H Behringer et al., Nucl. Fusion 26 (1986) 751
[7] E R Müller et al., Nucl.Fusion 22 (1982) 1651
[8] R Behrisch et al., as Ref.[2]
[9] G M McCracken et al., as Ref.[2]
[10] M G von Hellermann et al, as Ref.[4]
[11] J Jacquinot et al., No.IAEA-CN-47/F-I-1 these proceedings
[12] A Tanga et al, post-deadline, these proceedings
[13] M Ali Mahdavi et al., Phys. Rev. Lett. 47 (1981) 1602

ANOMALOUS TRANSPORT IN JET PLASMAS

D.F. Düchs, T.E. Stringer, A. Taroni, M. Brusati, N. Gottardi,
T. Hellsten, F. Tibone

JET Joint Undertaking, Abingdon, Oxon., OX14 3EN, UK

ABSTRACT

Local thermal fluxes are determined experimentally for ohmic, RF wave and neutral beam heated JET plasmas through direct power balance calculations and through a modified application of "predictive" equilibrium-transport codes. A realistic way of describing the RF-power deposition profile has been developed. Free boundary plasmas, important for magnetic limiter cases in JET, can now be computed fully self-consistently. The experimental local fluxes have been compared with available analytically derived ones but no acceptable agreement could be found. Many discharges can, however, be modelled empirically by modifying the electron thermal transport equation so that the steady state T_e profile is constrained to fit the observed canonical shape, with both ohmic or additional heat sources.

1. INTRODUCTION

In this paper we attempt to assess the status of theoretical understanding of anomalous transport in JET plasmas. This is done by deriving local fluxes from measurements and comparing them with presently available theoretical ones which are applicable under JET conditions. Sections 2 and 3 present the experimental values which are obtained firstly by the usual method of the integrated power balance, and secondly by applying a full predictive transport code in steady state. The chosen cases include JET discharges where the plasma is heated ohmically, by ion cyclotron waves, and by neutral injection. Those discharges have been selected where a maximum number of diagnostics were available with reliable results so that the uncertainties on the fluxes could be minimised. In Section 4 a number of proposed theoretical formulae are reviewed and checked against JET data. Finally, in Section 5, an empirical approach is outlined by which also the plasma evolution in time is modelled successfully. The highlights are summarised in Section 6.

2. FLUXES FROM INTEGRATED POWER BALANCE

If V_ψ denotes the volume inside a chosen magnetic flux surface S_ψ, we define the average primary electron thermal energy flux density at time point t as

$$f_e(\psi,t) := \frac{1}{S_\psi} \int_{S_\psi} \left(\frac{3}{2} n_e T_e \vec{v}_e + \vec{q}_e\right)_{S_\psi} dS_\psi \qquad (1)$$

consisting of a convective and a conductive term. We prefer this quantity f_e rather than χ_e (or χ_i) because it is closer to the actual measurements and avoids special assumptions and errors connected with local gradients. The flux is calculated as a function of ψ from the power balance

$$f_e(\psi,t) = \frac{1}{S_\psi}\Big\{-\frac{\partial}{\partial t}\int_{V_\psi}\frac{3}{2}\,n_e\,T_e\,dV - \int_{V_\psi} p_{rad}\,dV - \int_{V_\psi} n_e\,\frac{T_e-T_i}{t_{eq}}\,dV + \int_{V_\psi} nj^2\,dV + \int_{V_\psi} p_{RF}\,dV + \int_{V_\psi} p_{NBI}\,dV\Big\}. \qquad (2)$$

An analogous equation holds for $f_i(\psi,t)$. Additional possible terms (e.g. ionisation, adiabatic compression etc.) were estimated as negligible. The geometry, i.e. ψ, S_ψ and V_ψ are taken from solutions of the Grad-Schlüter-Shafranov equation which agree with outside magnetic probe measurements. These solutions also provide the ohmic heating term. The bolometer array signals deliver the radiation loss term after the charge exchange neutral share is computed and subtracted.

The power deposition from ion cyclotron heating is calculated with the global wave code LION [1]. This code calculates wave propagation for the magnetosonic wave in toroidal geometry, assuming the plasma species to be Maxwellian. In the case of on-axis-heating of hydrogen minority at its fundamental cyclotron resonance, the distortion of the velocity distribution of the heated minority ions, as calculated with the Fokker-Planck code BAFIC [2], becomes strong. Finite gyro-radius effects impose a limit on the absorbed power, proportional to the minority density. Since the coupling is usually dominated by the presence of eigenmodes this effect can be included by reducing the power density on axis to this limit and then renormalising the power deposition profile outside this region to account for the total power. At low density, the heating of the minority species away from the magnetic axis is still high enough to produce strong Doppler broadening of the resonance. This further broadens the power deposition. The power transfer to the electrons and ions from that absorbed by the minority ions is calculated with a Fokker-Planck code. Direct electron heating has been neglected. At high temperatures, significant ion heating occurs due to second harmonic absorption by the deuterons. Due to the weaker absorption to ^{3}He minority heating the power deposition extends all along the cyclotron resonance but is still peaked at the mid-plane.

Also the power deposition from neutral beams cannot be measured directly and has been computed by Monte-Carlo or pencil beam codes, with the total power, temperature and density

profiles, and Z_{eff}, as measured input [3]. A major source of uncertainty is the ion temperature profile which we took from the neutral particle analyser diagnostics [4] when available.

These profiles suffice to determine the remaining terms in eq. (2) if the equilibration (t_{eq}) is assumed to be classical.

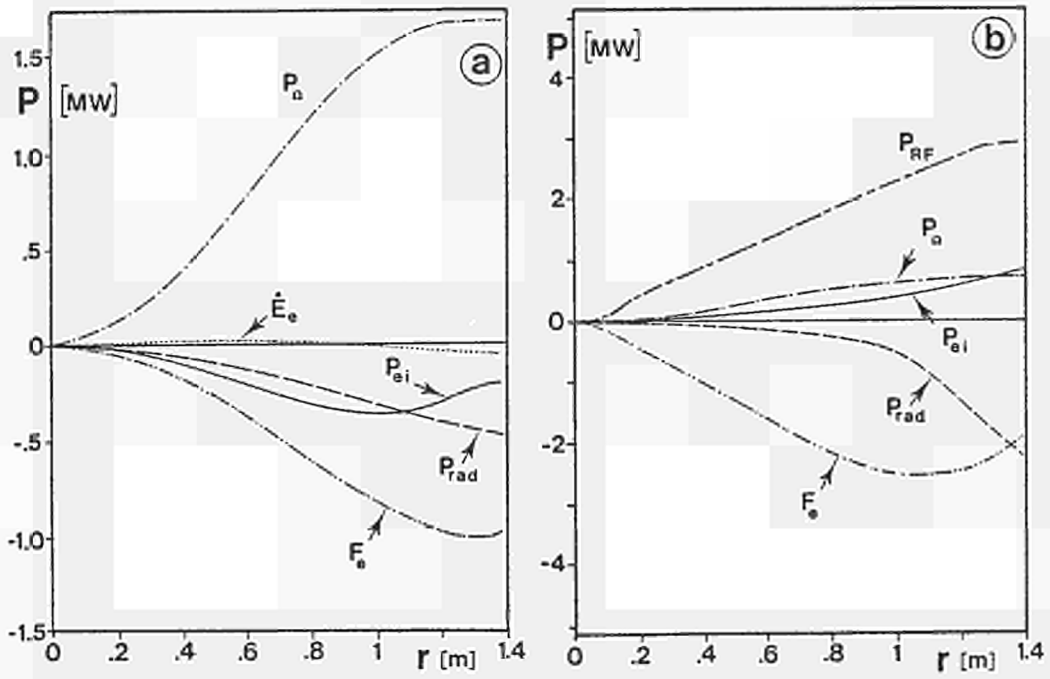

Fig. 1 Local power balance (integrals over magnetic flux surface volume inside r) for a JET pulse during (a) ohmic and (b) RF heating. I_p=2MA, B_t=2.2T, H minority (n_H/n_D ~ 2%) heating in 1b.

Figure 1 shows the single terms of eq. (2) for an ohmically (1a) and an RF heated (1b) JET plasma. The average minor radius r is used here as a flux surface label, i.e. it specifies S_ψ and V_ψ. The integrated ohmic input power is denoted by P_Ω, the RF input by P_{RF}, the power exchanged between electrons and ions by P_{ei}, the radiation loss by P_{rad}, and the temporal change in thermal (electron) energy content by $\dot{E}_e$. The result of the balance is $F_e = f_e \cdot S_\psi$.

These cases have been chosen because F_e is a significant term (i.e. not only a difference of large numbers) over the whole cross section.

In order to set off the difference between ohmic and additionally heated plasmas the figures 1 to 3 refer to two different time slices of the same discharge with a total plasma current I_p = 2 MA and a toroidal field (on axis) of 2.2 T.

Figure 2 presents a typical result obtained through the above procedure for the ohmic case. Figure 2a shows the measured

plasma characteristics, i.e. density, temperature and q-profiles while the local mean thermal fluxes are given in Fig. 2b.

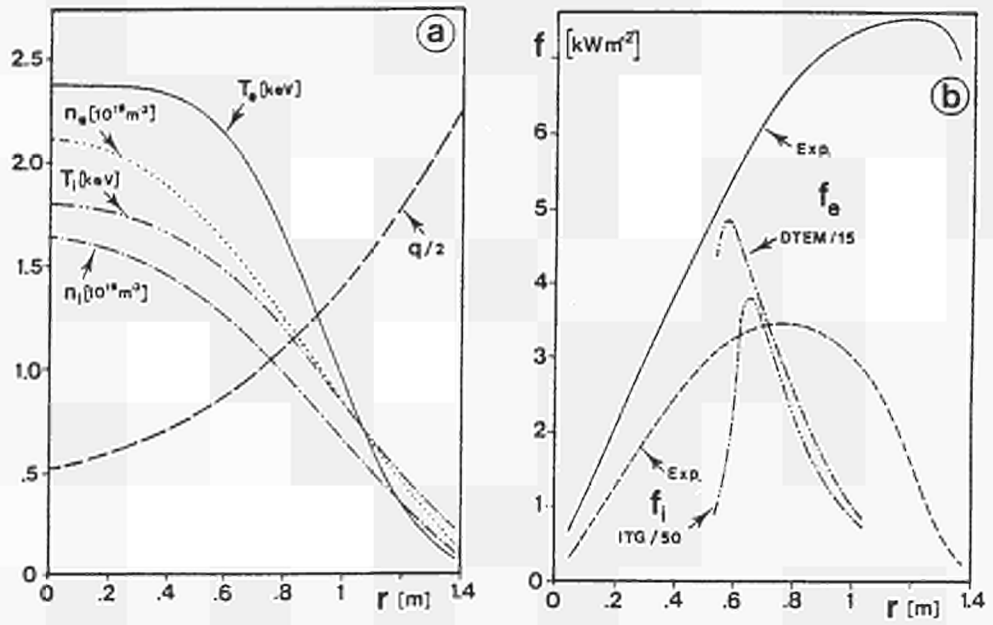

Fig. 2 Measured surface averaged thermal fluxes f for electrons and ions (b) for the ohmically heated JET plasma as Fig. 1(a), plasma parameter profiles (a). Scaled down theoretical prediction (by factor of 15) from dissipative trapped electron mode (DTEM) for electrons and ion temperature gradient instability (ITG) for ions are added in 2b.

The error margin for these fluxes is assessed by varying the terms in eq. (2) within the experimental errors.

3. FLUXES FROM EQUILIBRIUM/TRANSPORT CODES IN STEADY STATE

Our second method to obtain measured fluxes uses a full equilibrium/transport code (in $\psi(R,Z),t$) containing more detailed physics. For example, this code has been restructured to allow fully consistent free boundary equilibrium transport calculations. The mathematical methods have been published recently [5]. The code interacts with the external coils, which is especially important for magnetic limiter cases in JET. In the interpretative application it is, of course, used to reproduce the measured magnetic (probe, loop) signals, thus checking whether the equilibria are consistent with (transport) pressure and current density profiles. In addition, it contains detailed modelling of impurity diffusion and radiation, neutral atom distributions, the sawtooth region, and boundary conditions.

The present method of application is as follows: The measured basic plasma parameters (densities, temperatures, fields) are inserted as initial values. The measured complex quantities such as radiation losses, neutron yields, charge exchange neutrals, are examined immediately through the models

for their consistency with the basic parameters; this leads either to corrections or to an assessment of error bars. In the spirit of "shooting methods" an ansatz for the desired fluxes is guessed and programmed; for example, the result of the previous (cruder) power balance method could be chosen, or any function of the basic parameters and their derivatives. The code is then stepped forward in time, and, in stationary state, must reproduce the input initial value profiles, provided that our ansatz for the fluxes was suitable, otherwise it is to be modified. This method lends itself readily to sensitivity studies by determining those terms which predominantly cause deviation from steady state.

The method can, of course, also be applied to non-stationary conditions, except that then several sets of measurements at consecutive time slices are required.

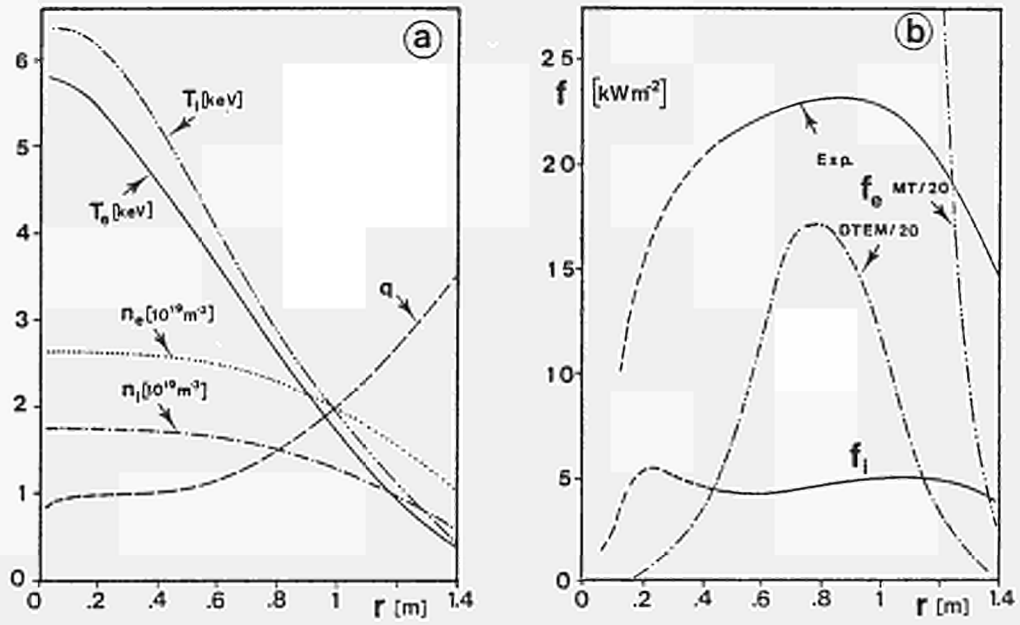

Fig. 3 Surface averaged thermal fluxes f,as derived in Sec. 3, for electrons and ions (b) for an RF heated JET plasma characterised by plasma parameter profiles (a). The uncertainty of f is enhanced within the sawtooth region (dashed in 3b). The electron heat fluxes predicted for the DTEM and microtearing modes MT (scaled down) are shown in (b).

Figure 3 presents the fluxes for an RF-heated JET plasma evaluated by this method.

We have analysed many other cases which are being collected with some attempts at "scaling" for a forthcoming JET report [6].

4. COMPARISON WITH THEORY

Expressions for the anomalous transport, derived analytically for different instabilities, have been evaluated for

JET parameters and compared with the measured fluxes. Space does not permit these expressions to be reproduced here, they may be found in the references quoted. The notation here is the same as in the references.

a) Electron transport

A significant level of agreement has recently been achieved [7,8] between the global energy confinement times measured on several tokamaks and prediction based on the dissipative trapped electron mode (DTEM). However, when the predicted local thermal diffusivity [8], including Z_{eff} in the collision frequency ν_{ei}, is compared with the experimental value in JET, the predicted value is typically an order of magnitude too high within the region where the DTEM should be dominant (see Fig.2b). Because of the strong dependence of the diffusivity on temperature ($\chi_e \sim T_e^{7/2}$ for the DTEM and $\chi_e \sim T_e^{3/2}$ for the collisionless trapped electron mode) and on the characteristic lengths r_n and r_T, the global confinement time is sensitive to the temperature profile, and cannot be adequately expressed in terms of the peak or mean temperature.

It is questionable whether the temperature in JET is low enough, even in the edge region, to satisfy the criteria for the rippling instability [9]. In any case, the predicted diffusivity turns out to be too low by about two orders of magnitude.

The microtearing mode (MT) [10] could develop under JET conditions for mode numbers m such that

$$m < 10^{-11} \frac{r\, r_n n\, B_T\, Z_{eff}}{T_e^{5/2}}$$

in MKS units and eV. The predicted electron thermal diffusivity, $\chi_e \sim T_e^{7/2}/n\, Z\, r_T^2\, B^2$, has a parametric dependence similar to the DTEM, and is larger in magnitude. Close to the plasma edge in JET its value is comparable to the experimental value, but as one moves into the plasma it exceeds the experimental by a rapidly increasing factor, as illustrated in Fig. 3b.

Collisional drift wave transport [13] could occur in the JET edge region; however, the magnitude of the flux comes out too small by 1-2 orders of magnitude.

Stochastic transport due to electrostatic trapping in drift waves has been proposed in Ref [14]. It could occur within the operating range of JET. However, as most of the other models, it reproduces neither the spatial dependence nor the scaling with global parameters obtained in JET.

b) Ion transport

The neoclassical ion heat diffusivity [15] is a factor 1-8 below the experimental value in JET. For example, in Fig. 3b best fit was obtained with once neoclassical.

The observed saturation in τ_E at higher densities has been reproduced in several tokamaks by including in the transport code the diffusivity derived for the ion temperature gradient instability (ITG) [7,8]. However, the predicted thermal diffusivity for this mode in JET is more than an order of magnitude higher than the experimental value (see Fig. 2b).

5. EMPIRICAL FLUX DESCRIPTION

In view of the obvious lack of satisfactory transport theory the development of empirical prescriptions has been pursued further.

A widely applicable prescription is based on the experimental finding that, largely independent of additional heating and radiation losses, two parameters suffice to describe the electron temperature profile $T_e(\rho)$ in all steady states (for $q_b \lesssim 7$) by

$$T_e(\rho) = T_e(\rho_b) \exp\{\alpha[1-(\rho/\rho_b)^2]\}, \qquad (4)$$

or an expression with similar profile characteristics.

The flux surface coordinate ("radius") ρ_b lies towards the inside of the radiation dominated layer, for most JET discharges close to the limiter radius. The parameter α can vary between

$$1.5 < \alpha < 2.2$$

with a strong peak around $\alpha = 1.9$, and no clear dependence on other plasma parameters.

All rigorously derived transport equations are based on such assumptions that the parameters of the system tend towards thermodynamic equilibrium, e.g. flat profiles for vanishing sources. It is possible to restructure the balance equations so that the parameters, here T_e, always approach prescribed equilibrium profiles, e.g. the ones given above in formula (4).

Such apparent neglect of thermodynamic principles might indicate that not all important parameters are computed self-consistently, i.e. that we are dealing with an open thermodynamic system.

A physically consistent model to solve this problem, based on partial ergodisation of the magnetic field, is being developed by P.H. Rebut et al. [12,16].

A restructured balance equation for the electron thermal energy does, of course, allow for temporal deviations from the given equilibrium profiles. In comparison with the experiment it

must satisfy two constraints:

a) The equilibrium profiles for $T_e(\rho)$, obtained from $\frac{\partial}{\partial t}\left(\frac{3}{2} n_e T_e\right) = 0$, i.e. (integrated once over ρ) from

$$0 = \rho\, f_e(\rho) + \int_0^{\rho} (\eta j^2 + P_{RF} + P_{NBI} - P_{rad} - P_{ei})\, \rho\, d\rho \quad (5)$$

must coincide with formula (4), and

b) f_e should reproduce the observed rate of relaxation towards the given equilibrium profile (or the maximum deviation from it for given sources).

It is not clear whether these requirements lead to a unique solution, nor is a sufficiently wide data base available yet for point b.

An application of this procedure to particle transport is given by the popular anomalous inward particle flux term [17,18].

Several practical approaches to solve the above problem for T_e have been reported [19,20], and the connections to widely used empirical formulae have been pointed out. Our method [20] has, in the meantime, been successfully checked against a number of JET discharges with strong additional combined RF and neutral beam heating. The example in Fig. 4 shows practically complete agreement with the measurements.

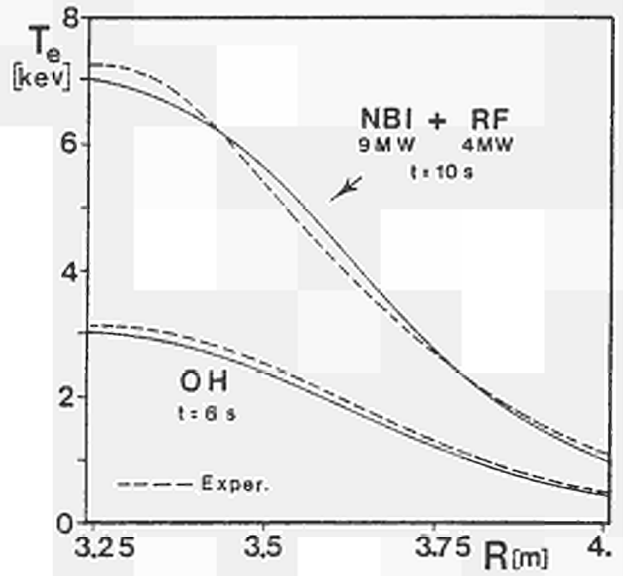

Fig. 4 Comparison between measured and empirically modelled (evolving) T_e profiles for combined ion cyclotron and neutral beam heated JET plasma ($I_p = 2\,MA$; $B_t = 2.2\,T$).

6. CONCLUSIONS

Measured local thermal fluxes in JET plasmas are presented. As a vital ingredient for RF-heated plasmas a new prescription for the RF-power deposition profile has been developed.

The application of predictive transport codes to obtain experimental local fluxes is outlined. The JET code now allows fully consistent free boundary equilibrium/transport calculations.

Available analytically derived anomalous fluxes have been compared with locally measured ones. No acceptable agreement has been found.

Empirically even the temporal evolution of discharges in JET can be reproduced by a prescription which enforces a certain shape of the T_e profile in ohmic and additionally heated steady state plasmas.

ACKNOWLEDGEMENTS

We are indebted to W.G.F. Core, S. Corti, M. von Hellerman, F. Romanelli and E. Springmann for their help and useful discussions.

REFERENCES

[1] APPERT, K. et al., Plasma Physics and Controlled Fusion, 28 (1986) 133.
[2] SUCCI, S. et al., Comp. Phys. Comm., 40 (1986) 137.
[3] WATKINS, M.L. et al., 13th European Conf. on Controlled Fusion, Schliersee, Part I, p 156 (1986).
[4] CORTI, S. et al., Proc. 13th European Conf. on Controlled Fusion and Plasma Heating, Part I, p 109, Schliersee (1986).
[5] CENACCHI, G., TARONI, A., 8th European Conf. on Comp. Phys., Eibsee, May 1986, p 57.
[6] DÜCHS, D.F. et al., JET Report, to be published.
[7] DOMINGUEZ, R.R., WALTZ, R.E., GA Report No. GA-A18184 (1986).
[8] ROMANELLI, F., TANG, W.M., WHITE, B.B., Princeton Report PPPL-2310 (1986).
[9] GARCIA, L., DIAMOND, P.H., CARRERAS, B.A., CALLEN, J.D., Phys. Fluids, 28 (1985) 2147.
[10] DRAKE, J.F., GLADD, N.T., LIU, C.S., CHANG, C.L., Phys. Rev. Lett., 44 (1980) 994.
[11] OHKAWA, T., Phys. Lett., 67A (1978) 35.
[12] REBUT, P.H., BRUSATI, M., Plasma Physics and Controlled Fusion, 28 (1986) 113.
[13] TERRY, P.W., DIAMOND, P.H., Phys. Fluids, 28 (1985) 1419.
[14] HORTON, W., CHOI, D-I., YUSHMANOV, P.N., PARAIL, V.V., to be published.
[15] CHANG, C.S., HINTON, F.L., Phys. Fluids, 25 (1982) 1493.

[16] REBUT, P.H. et al., this conference.
[17] COPPI, B., SHARKY, N., Nucl. Fusion 21 (1981), 1363.
[18] BEHRINGER, K. et al., Proc. IAEA Technical Committee Meeting on Divertors and Impurity Control, IPP Garching, (1981).
[19] TANG, W.M., Report PPPL-2311 (1986).
[20] TARONI, A., TIBONE, F., Proc. 13th European Conf. on Controlled Fusion and Plasma Heating, Part I, p 160, Schliersee (1986).

SAWTOOTH OSCILLATIONS

J.A. WESSON, P. KIRBY*, M.F.F. NAVE

JET Joint Undertaking, Abingdon, Oxfordshire, U.K.

*Euratom-UKAEA Fusion Association, Culham Laboratory, Abingdon, Oxon., U.K.

ABSTRACT

The recent observations of sawtooth oscillations having a very fast collapse phase call for a re-examination of the theoretical description of sawtooth behaviour. One possibility is that the instability involved is an ideal m=1 "quasi-interchange" mode [1]. A calculation of the stability of this mode shows that flattening of the q profile reduces the critical β_p required for instability. Thus, contrary to previous expectations the ideal mode can be unstable even at the low values of β_p observed experimentally. Non-linear simulations show the predicted cellular convection. The distinction between the behaviour of the quasi-interchange and a tearing mode is described and a comparison is made with experimental results from JET. Finally attention is drawn to a fundamental difficulty in explaining the rapid collapse in precursorless sawtooth oscillations.

1. INTRODUCTION

With the advent of larger tokamaks it was found that the sawtooth collapse time did not increase as expected from the Kadomtsev scaling [2] and attention was drawn to this discrepancy by Campbell et al. [3]. An explanation of the observed behaviour was proposed by Wesson [1]. This predicted an mhd timescale for the collapse, in reasonable agreement with the experimental results. The model follows from a simple calculation showing that if the q profile is flat after the sawtooth collapse then it will remain quite flat during the resistive diffusion of the ramp phase. Configurations of this type were shown to be unstable to an ideal m=1 mode.

A further prediction of this model was that the form of the instability would not be a "rigid shift" of the plasma core, as predicted by previous models, but would be a cellular convective motion. This would then lead to the formation of a cold plasma bubble at the centre of the plasma. The magnetic field would not reconnect on this fast timescale but reconnection would occur on a longer, resistive timescale after the collapse.

These predictions were confirmed by subsequent experimental studies on JET. Tomographic analysis of the soft X-ray emission from JET [4] indicated a broad convective motion and the formation of a plasma bubble. The existence of decaying "post-cursor" oscillations after the collapse seems to conform to the prediction of delayed reconnection.

In this paper we report further work on this model in the following areas:

i) Mhd stability and its implications for the plasma motion.
ii) Non-linear simulations of the sawtooth collapse.
iii) Distinction between ideal mode and tearing instability.

Finally, attention is drawn to a fundamental problem in understanding the trigger for the sawtooth collapse.

2. STABILITY OF THE IDEAL m=1 MODE

In reference [1], numerical calculations were presented showing the crucial dependence of the stability of the ideal m=1 mode on the flatness of the q profile within the q=1 surface. These results can also be obtained analytically. In the large aspect ratio expansion the potential energy δW given by Bussac et al. [5] may be written in the form

$$\delta W = a + b\beta_p + c\beta_p^2 \quad \text{where} \quad \beta_p = \frac{2\mu_o R^2}{r_1^2 B_\phi^2}\int_o^{r_1}(-dp/dr)\, r^2 dr, \quad (1)$$

r_1 is the radius of the q=1 surface and the coefficients are determined from the solution of a differential equation which gives the toroidal coupling to the m=2 component. Taking the model illustrated in Fig.1a, for which

$$j = j_c\left(1 - \frac{r^2}{a^2}\right)^\nu, \quad r > r_1; \qquad j = \frac{2B_\phi}{Rq_o}\left(1 - 2(1-q_o)\frac{r^2}{r_1^2}\right), \quad r < r_1$$

where $j_c=(2B_\phi/R)(2-1/q_o)(1-(r_1^2/a^2))^\nu$, the coefficients of eq.(1) were calculated and the criterion for instability was found to be

$$\beta_p > \left(\frac{13}{144}\,\frac{3\Delta q}{\Delta q + 2\Delta q^*}\right)^{1/2}, \quad q_o < 1; \qquad \beta_p > 0, \quad q_o > 1 \quad (2)$$

where $\Delta q = 1-q_o$ and $\Delta q^* (= \nu r_1^2/2a^2)$ is the Δq which would have occurred without flattening.

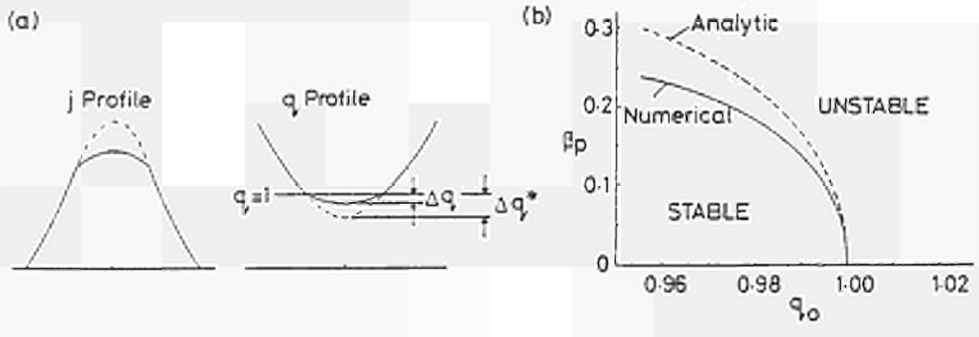

Figure 1 (a) Form of assumed j and q profiles. (b) Stability diagram giving critical β_p against q_o.

It should be noted that in both cases there is a q=1 surface at $r=r_1$. The stability boundary for criterion (2) is shown in Fig.1b for $\nu=1$ and $r_1/a=0.3$ together with the result of a numerical calculation. It is seen that the toroidal stabilising effect is much reduced for a flattened q profile and furthermore that if $q_o > 1$, while retaining the q=1 surface, the m=1 mode is unstable for arbitrarily small β_p.

It was pointed out in reference [1] that for flattened q profiles with $|1-q_o|$ sufficiently small the calculation becomes invalid. The principal, and important consequence of the changed ordering of 1-q is that the plasma flow associated with the instability is completely changed. The "rigid" displacement of the conventional case is replaced by a convective flow in the reduced shear case. The two types of motion are illustrated in Fig.2. The physical basis of this distinction is that, for the more strongly sheared, unflattened q-profile the energy of the instability is inadequate to bend the magnetic field whereas for small shear the magnetic field is carried with the fluid, preserving the flux surfaces but playing a negligible role in the mechanics. This type of behaviour could be called quasi-interchange.

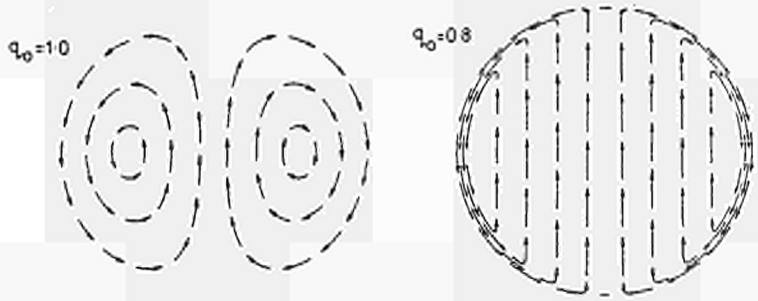

Figure 2 Flow pattern of quasi-interchange (q_o=1.0) and "rigid shift" (q_o=0.8).

3. SIMULATIONS OF SAWTOOTH COLLAPSE

A full simulation of the sawtooth collapse would require a toroidal calculation. However, the essential dynamical features of the present theory should be seen in the simpler case of cylindrical geometry. To this end, calculations have been carried out using a cylindrical, non-linear, incompressible, mhd code with various q profiles. The code has finite resistivity but for the simulations reported here the unstable modes are ideal and the resistivity has no significant effect.

To demonstrate the effect of a flattened q profile, simulations have been made using constant B_z and a model current profile given by

$$j_z = j_{z_o} = \text{const}, \quad r \leq r'; \qquad j_z = j_{z_o} \frac{(c-r^2/a^2)^2}{(c-r'^2/a^2)^2}, \quad r > r'$$

This means that q is constant for $r < r'$, and then rises monotonically for $r > r'$. The runs described here had $S=10^5$, $r'/a=0.3$ and $c=1.26$. In these calculations the higher modes $m/n=2/2$, $3/3$... are unstable with growth rates comparable to that of $m=1$.

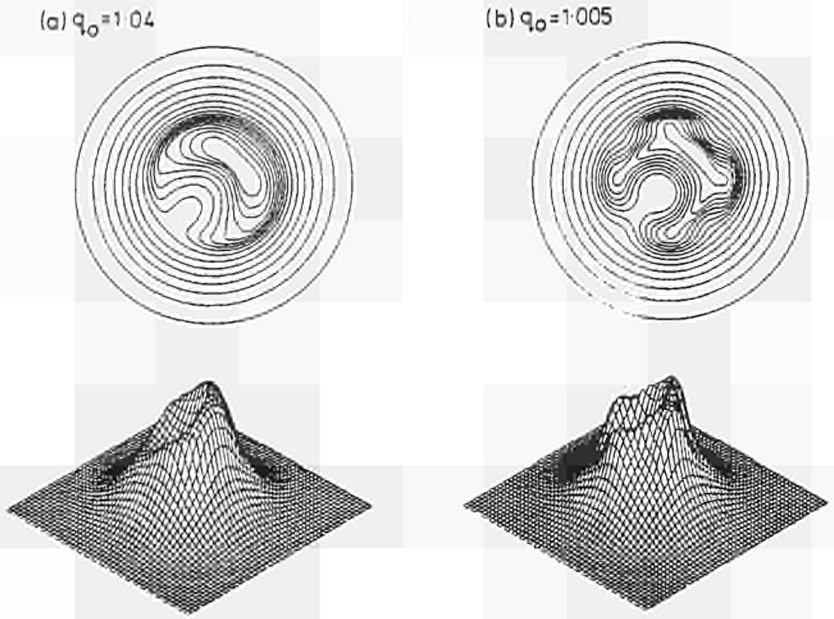

Figure 3 Development of flux surfaces for (a) $q_o=1.04$ and (b) $q_o=1.005$, together with associated soft X-ray emission.

For a relatively large q_o the plasma is displaced a small amount by the $m=1$ instability as shown in Fig.3a for $q_o=1.04$. A small bubble forms but does not penetrate fully because of the magnetic shear. This may represent the behaviour of a partial sawtooth collapse.

As q_o is reduced the instability is more able to sweep the fluid into a full cellular pattern. Figure 3b gives the result for $q_o=1.005$ showing deeper penetration of the bubble.

The corresponding time development of the X-ray emission can be calculated for a given initial profile on the assumption that (given the rapid collapse) the emission is convected with the plasma. The calculated profiles are shown in Fig.3 for the case of an initially Gaussian emission profile. The general form of the development is very similar to that observed in the JET experiment [4]. A further comparison of theory and experiment is made in the following section.

4. DISTINCTION BETWEEN QUASI-INTERCHANGE AND RESISTIVE INSTABILITY

The characteristic form of the radial displacement eigenfunctions for an ideal quasi-interchange mode and a tearing mode are shown in Figs.4a and 4b. The general characteristics of these flows persist into the non-linear regime. The ideal mode leads to a convective flow on the scale of the radius of the q=1 surface. The tearing mode leads to a Kadomtsev type reconnection, the core of the q < 1 region moving almost rigidly to one side and the return flow taking place in a very narrow resistive layer.

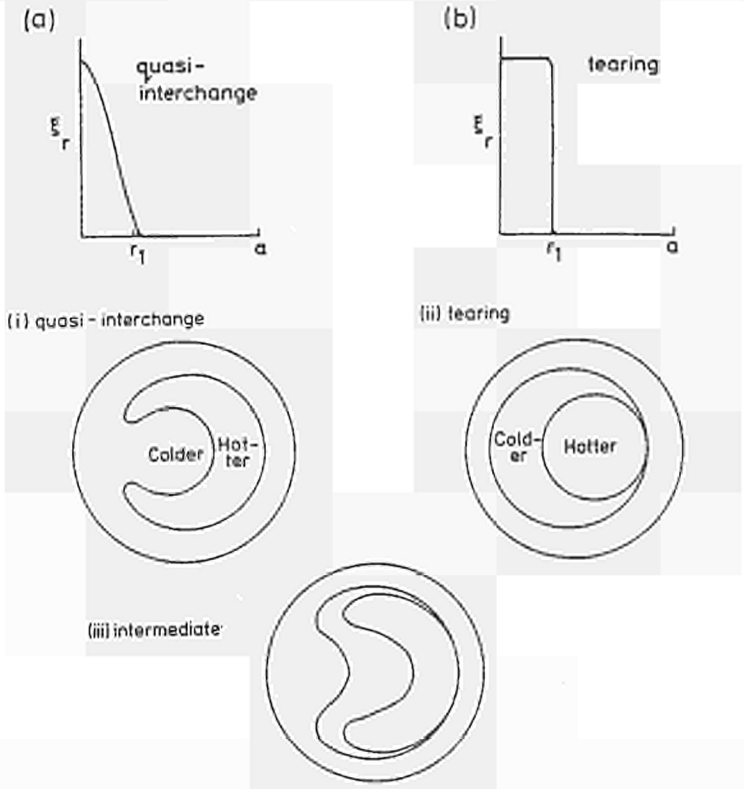

Figure 4 Eigenfunctions $\xi_r(r)$ for (a) quasi-interchange and (b) tearing mode together with diagrams showing the contrasting non-linear topological development for these cases.

The flux surfaces which would develop in the two cases are illustrated in Figs.4(i) and 4(ii). The contours of equal temperature and equal X-ray emission would have a similar topology. The distinction between the two cases is quite clear. It is possible that the type of behaviour will depend upon the plasma parameters and size. If there is a continuous transition from quasi-interchange (4(i)) to tearing (4(ii)) then an intermediate case would take the form shown in 4(iii).

The distinction between the quasi-interchange and the tearing mode is brought out most clearly by considering the

azimuthal displacement eigenfunction $\xi_\theta(r)$. For $R/r_1 >> 1$ this is related to ξ_r by $\xi_\theta = -\frac{d}{dr}(r\xi_r)$. The functions $\xi_\theta(r)$ corresponding to the cases illustrated in Fig.4 are shown in Figs.5a and 5b. Experimental forms for ξ_r and ξ_θ have been derived from the X-ray emission at an early stage of a JET sawtooth collapse. The radial displacement is calculated from the initial emission profile and the profile after 50μsec. The function $\xi_r(r)$ and the derived $\xi_\theta(r)$ are shown in Figs.5c and 5d. Comparison of Fig.5d with Figs.5a and 5b gives clear evidence that the displacement has the form of a quasi-interchange.

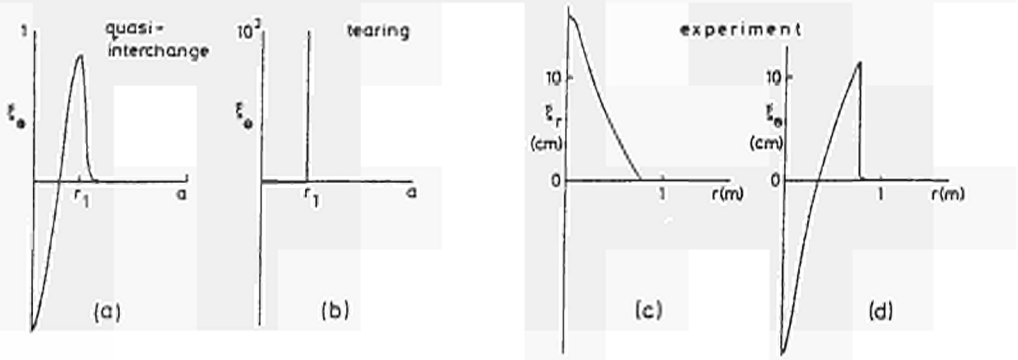

Figure 5 Eigenfunction $\xi_\theta(r)$ for (a) quasi-interchange and (b) tearing mode together with experimental forms for (c) $\xi_r(r)$ and (d) $\xi_\theta(r)$ from the JET experiment.

5. A FUNDAMENTAL DIFFICULTY

In addition to the features described above, the model proposed by Wesson [1] also offered an explanation of the trigger for the rapid sawtooth collapse. Further examination of this problem shows that not only is the proposed explanation inadequate but that there is a fundamental difficulty for all models of "precursorless" sawteeth. This difficulty, which is associated with the rapidity of the onset of the collapse, is described below.

If the collapse time is τ_c, it is necessary for a growth rate $\gamma \sim \tau_c^{-1}$ to develop on a timescale τ_c. Let the change in central q necessary to produce this γ be δq. If this change in q results from resistive diffusion, then

$$\delta q \sim \frac{\tau_c}{\tau_s} \Delta q \qquad (3)$$

where Δq is the change in q during the ramp phase, the duration of which is approximately the sawtooth period τ_s. The magnitude of this Δq can be estimated from the resistive diffusion of the

current [1] and is given by

$$\Delta q \sim \frac{\Delta T}{T}\,\frac{\tau_s}{\tau_R} \qquad (4)$$

where $\Delta T/T$ is the fractional change in the temperature during the sawtooth, and the resistive diffusion time $\tau_R = \mu_o r_1^2/4\eta$. Relations (3) and (4) determine the expected change δq during the collapse time. It is then necessary that the required instability growth rate can be switched on by this δq.

Typical JET values are $\Delta T/T \sim 10^{-1}$ and $\tau_s/\tau_R \sim 10^{-1}$ giving $\Delta q \sim 10^{-2}$. Then since $\tau_s \sim 100$ms and $\tau_c \sim 100\mu$s, relation (3) gives the required sharpness of the switch-on of the instability, $\delta q \sim 10^{-3}.10^{-2} \sim 10^{-5}$.

Even allowing for the uncertainty in the estimation, this δq seems to be improbably small. We can make an estimate of δq required to switch on the quasi-interchange mode as follows. Let the growth rate for zero shear be γ_o, then the destabilising energy density available for the instability is $\sim \tfrac{1}{2}\rho\gamma_o^2\xi^2$. Putting $d\xi/dr \sim \xi/r$ the stabilising energy density [1] is $\sim (1-q)^2(B_\theta^2/2\mu_o)(\xi/r)^2$. Thus the dispersion relation can be characterised by

$$\gamma^2 = \gamma_o^2 - (1-q)^2\,\tau_A^{-2} \qquad \text{where} \qquad \tau_A = r_1/(B_\theta/(\mu_o\rho)^{1/2}). \qquad (5)$$

Although the initial switch-on, $d\gamma/dq$, at $\gamma=0$ is very rapid, it is necessary for γ to grow to give a value (in JET) of $\gamma^{-1} \sim 100\mu$sec. Now for the ideal m=1 mode $\gamma_o \sim \varepsilon\beta_p/\tau_A$, where $\varepsilon = r_1/R \sim 10^{-1}$, $\beta_p \sim 10^{-1}$ and $\tau_A \sim 1\mu$sec. Thus $\gamma_o^{-1} \sim 100\mu$sec and this is of the order of the required growth time. Consequently the change in q necessary to produce the required growth rate is given by equation (5) to be

$$\delta q \sim \gamma_o\,\tau_A.$$

Hence the theoretical switch-on width in q is $\delta q \sim 10^{-2}$, and this is orders of magnitude greater than the required experimental value of 10^{-5}.

The problem is even more severe for tearing modes where the theoretical value for the δq necessary to provide a growth rate γ is [7]

$$\delta q \sim \gamma^{3/2}\,\tau_A\,\tau_R^{1/2}.$$

The typical JET values given above with $\tau_R \sim 1$sec give $\delta q \sim 1$ to be compared with a required switch-on $\delta q \sim 10^{-5}$.

It is clear therefore that a fundamental element is missing in our theoretical understanding of fast precursorless sawteeth. Thus although the experimental evidence on the flow behaviour seems to support the quasi-interchange model, the validity of

this model cannot be accepted while we still lack an explanation of the rapidity of the onset of the collapse.

6. CONCLUSIONS

(i) A flattened q-profile inside the q=1 surface allows instability of the ideal m=1 mode which would otherwise be stable at low β_p.

(ii) Non-linear simulations of the instability illustrate the quasi-interchange behaviour. The broad convective flow takes the outer plasma into the centre to form a colder "bubble".

(iii) The behaviour of the quasi-interchange is quite distinct from that of a tearing mode and is in better agreement with experimental observations of sawteeth in JET.

(iv) The sudden onset of the collapse in precursorless sawteeth presents a fundamental problem for all existing models.

7. ACKNOWLEDGEMENTS

The authors would like to thank J.Hastie for discussions and R.Granetz for help in analysing the soft X-ray results.

8. REFERENCES

[1] WESSON,J.A., Plasma Physics and Controlled Fusion, 28 (1986) 243.
[2] KADOMTSEV, B.B, Sov. J. Plasma Phys. 1 (1975) 389.
[3] CAMPBELL, D.J. et al., Nuclear Fusion Letters, 26 (1986) 1085.
[4] EDWARDS, A.W. et al., Phys. Rev. Letts. 57 (1986) 210.
[5] BUSSAC, M.N. et al., Phys. Rev. Letts. 35 (1975) 1638.
[6] ROSENBLUTH, M.N. et al., Phys. Fluids, 16 (1973) 1894.
[7] COPPI, B. et al., Sov. J. Plasma Phys. 2 (1976) 583.

SAWTEETH AND DISRUPTIONS IN JET

D.J. CAMPBELL, P.A. DUPERREX[1], A.W. EDWARDS, R.D. GILL, C.W. GOWERS, R.S. GRANETZ, M. HUGON, P. LOMAS, N. LOPES CARDOZO[2], M. MALACARNE, M.F.F. NAVE, D.C. ROBINSON[3], F.C. SCHÜLLER, P. SMEULDERS, J.A. SNIPES[3], P.E. STOTT, G. TONETTI[1], B.J.D. TUBBING[2], A. WELLER[4], J.A. WESSON

JET Joint Undertaking, Abingdon, Oxon, OX14 3EA, UK.

[1] CRPP/EPFL, 21 Avenue des Bains, CH-1007 Lausanne, Switzerland.
[2] FOM Insituut voor Plasmafysica, 3430 Be Nieuwegein, The Netherlands
[3] UKAEA Culham Laboratory, Abingdon Oxfordshire, UK.
[4] Max-Planck-Institut für Plasmaphysik, D-8046 Garching bei München, FRG

ABSTRACT

The behaviour of magnetohydrodynamic phenomena associated with sawteeth and major disruptions has been studied for a wide range of discharge conditions with ohmic, neutral beam and ion cyclotron heating. The sawtooth collapse has been investigated in detail and found to be inconsistent with models based on resistive reconnection. Disruptions set limits to JET operation at low q and high density, and the detailed evolution of disruptions at these limits has been studied. A hard operational limit is found at q_ψ=2.0 ±0.1. The highest value of the Murakami parameter achieved in ohmic plasmas is $\bar{n}R/B_T$ = 7.2 $10^{19}m^{-2}T^{-1}$, but neutral beam heating leads to a substantial increase (~50%) in the density limit. Finally, during high power neutral beam heating combined with ion cyclotron heating "monster" sawteeth are observed in which mhd activity of modes with low m and n becomes quiescent for periods ~1s.

INTRODUCTION

Sawteeth and disruptions are well known phenomena in all tokamaks and define the limits on the mhd stability of the discharge. They have been studied extensively in JET and there are some important new features in the results which will be reported here.

Our studies of these phenomena have used all of the JET diagnostics, but in particular we have made detailed measurements of the mode structures using: magnetic pick-up coils and loops outside the plasma boundary; electron cyclotron emission to measure local electron temperatures; and orthogonal arrays of X-ray diodes combined with tomographic analysis to measure the soft X-ray emissivity.

SAWTEETH

Sawteeth are observed in almost all JET discharges. Their general features which have been discussed in earlier papers [1,2] will only be summarised here. In ohmically heated plasmas the modulation of the central electron temperature is up to 20% and the period is between 30 and 250ms. In discharges with ion cyclotron heating (Fig. 1) or co-injected neutral beams the modulation is increased up to 50% and the period extended up to 600ms, whereas with counter injected beams both the modulation and the period are reduced. With combined ion cyclotron and neutral beam heating we have

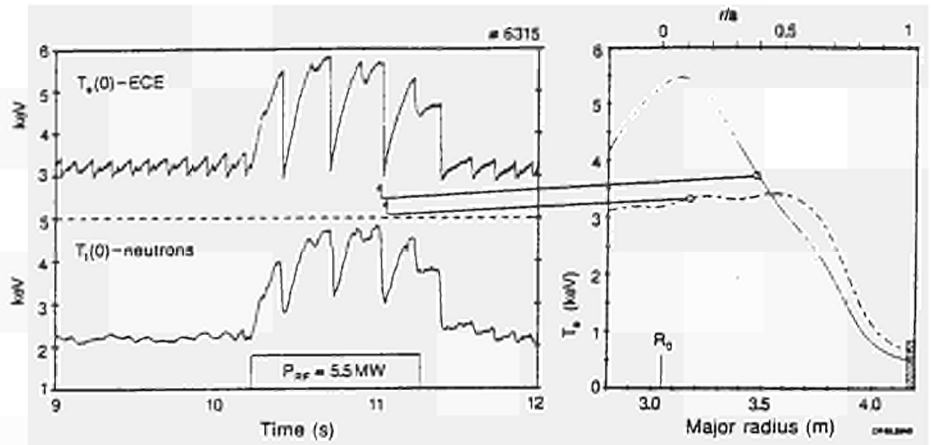

Figure 1 *Central electron and ion temperatures showing the increase in sawtooth modulation and period with 5.5MW of ion cyclotron heating. The electron temperature profiles before and after a sawtooth collapse are shown.*

sometimes seen "monster" sawteeth lasting for more than 1s. We have attempted to determine the scaling of the period with various tokamak parameters, but the only clear trend is that in ohmic discharges the period increases with plasma density. Most JET sawteeth show a compound structure with one or more partial collapses occuring between the main collapses.

As we have reported elsewhere [1] the main collapse of sawteeth in JET occurs on a much shorter time scale (typically - 100μs) than would be consistent with resistive reconnection models. In ohmic discharges the collapse usually occurs spontaneously without any precursor oscillations but often we see successor oscillations. The behaviour is very similar in ion cyclotron heated discharges, but with neutral beam heating we usually see a precursor either as a growing oscillation or sometimes as a saturated mode. When there are precursors, the main collapse appears to be a continuation of the precursor. This suggests that the precursor and main collapse are the same instability, but this has not been proved conclusively.

The collapse mechanism appears to be the same in all JET discharges despite these differences in precursor activity. Detailed studies [3] with the X-ray and ECE diagnostics show that the collapse has an m=n=1 structure and involves the displacement in minor radius of the hot central core of plasma (Fig. 2a). The displaced core spreads poloidally around the magnetic axis into a crescent shaped region (Fig. 3) and at the same time there is a rapid outflow of plasma energy. The successor oscillations are seen to be the rotation of a residual asymmetry in the collapsed state. The soft X-ray

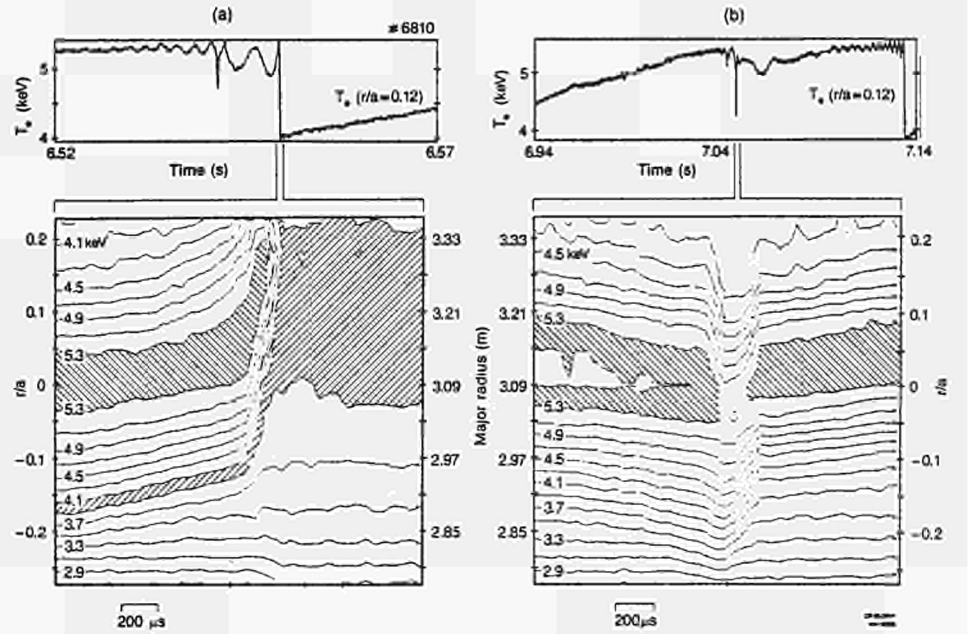

Figure 2 *Temperature contours (each line representing an interval of 0.2keV) during (a) a main collapse (b) a partial collapse. The displacement of the core is seen in both cases, but is smaller for the partial collapse and does not lead to a complete cooling of the core.*

emission profiles after the collapse are sometimes slightly hollow. The time scale of the collapse and the detailed displacement and spreading of the hot core are in agreement with the predictions of the model by Wesson [4] where the sawtooth collapse is an ideal mhd instability. A magnetic signal with n=1 is detected simultaneously with the collapse [5].

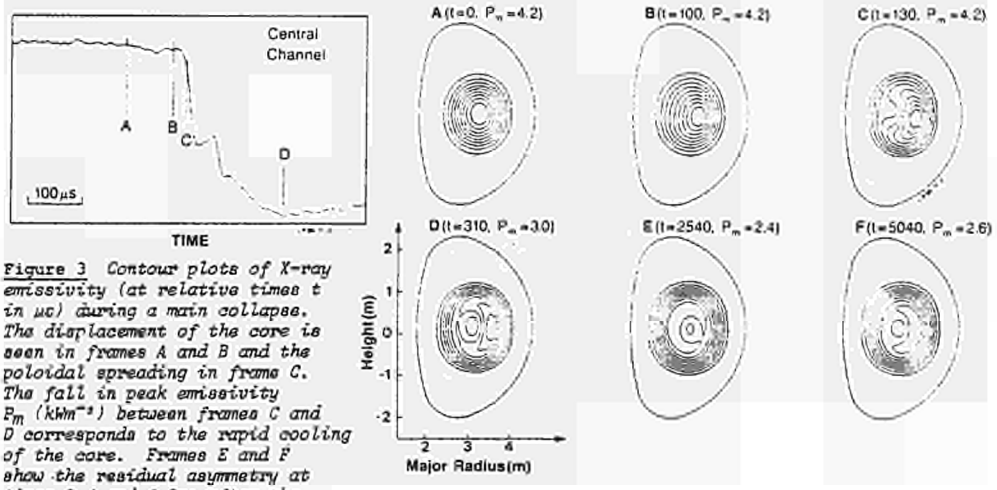

Figure 3 *Contour plots of X-ray emissivity (at relative times t in μs) during a main collapse. The displacement of the core is seen in frames A and B and the poloidal spreading in frame C. The fall in peak emissivity P_m (kWm^{-3}) between frames C and D corresponds to the rapid cooling of the core. Frames E and F show the residual asymmetry at times 2.4 and 4.9ms after the collapse.*

Partial collapses show a wider range of behaviour in precursor and successor oscillations and are more difficult to classify, but there appear to be at least two general types. One is similar to the main collapse, with a sudden (~100μs) but smaller displacement of the hot core (Fig. 2b), and the subsequent propagation of a heat pulse outside the central region. The second type is a much softer relaxation on a longer timescale ~ 10ms with an m = 1 oscillation which shifts inwards but does not lead to a central collapse. Both types of partial collapse have very little overall effect on the central temperature.

MONSTER SAWTEETH

In discharges with combined ion cyclotron and neutral beam

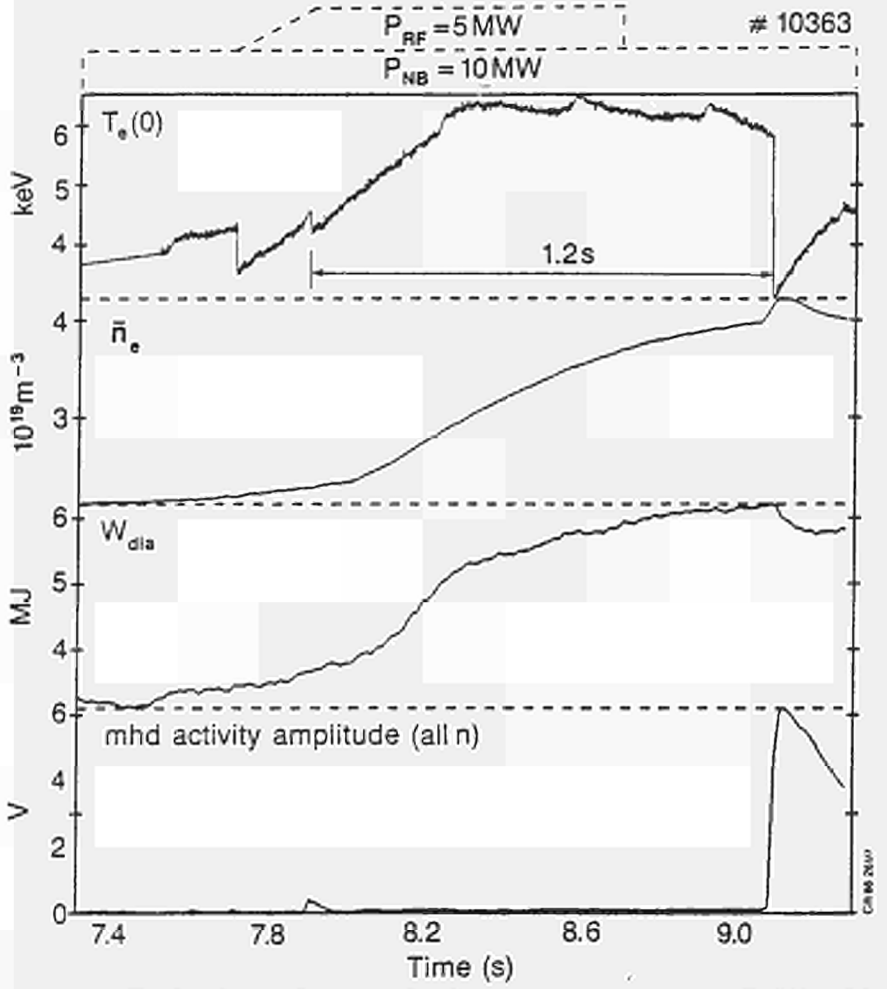

Figure 4 *Evolution of central electron temperature $T_e(0)$, line integral of electron density $\int n_e dl$, total plasma energy from diamagnetic measurements W_{dia}, and the amplitude of total mhd activity during a 5MA discharge with a monster sawtooth lasting 1.2s.*

heating some sawteeth have very long duration (up to 1.26s). These were first seen in relatively low current discharges (I_p ~ 2MA), but similar long duration ("monster") sawteeth have now been seen in discharges with an internal separatrix (I_p = 2MA) and at high currents (I_p = 5MA) as shown in figure 4. These are not simply sawteeth with particularly long periods, as they are characterised by low levels of coherent mhd activity

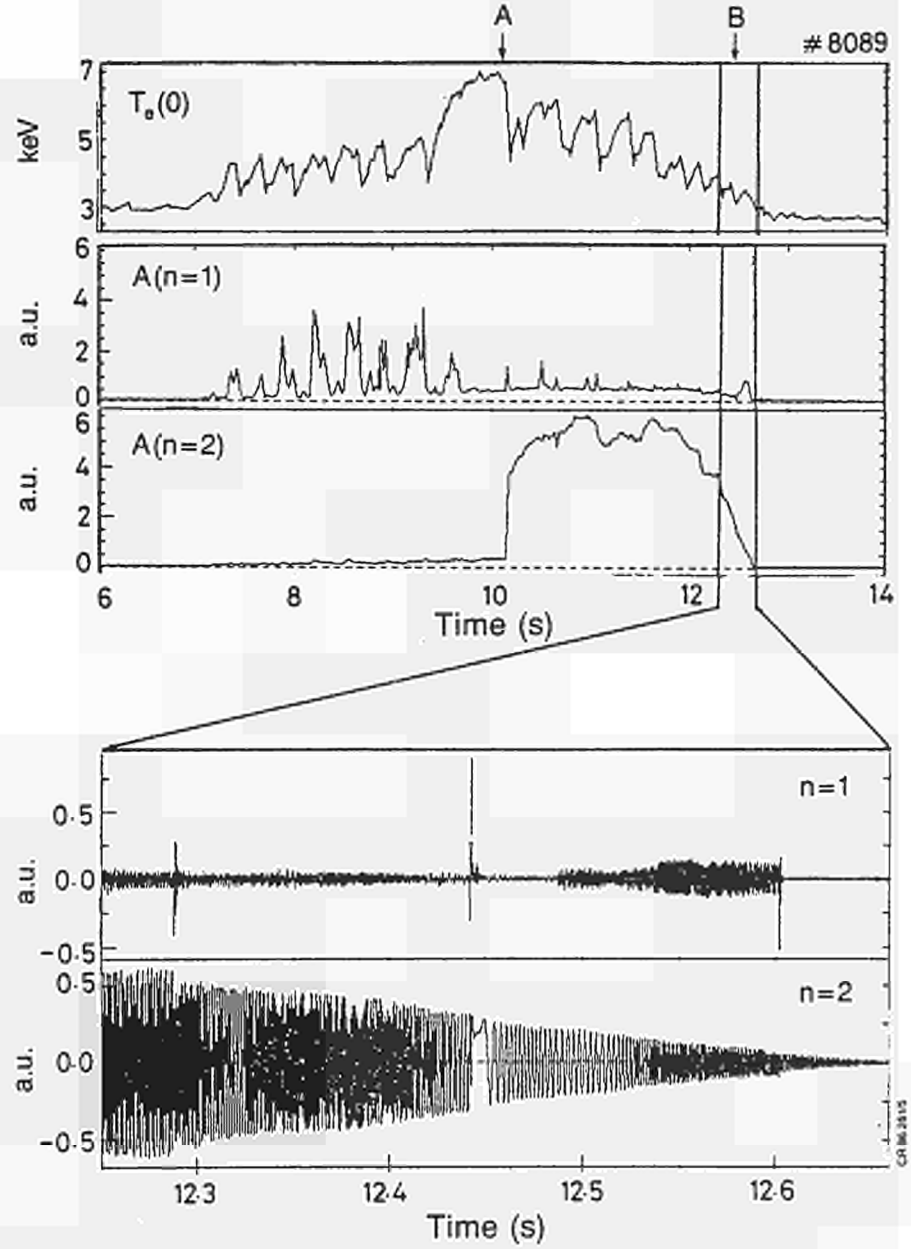

Figure 5 *After the monster sawtooth collapses at time A a large amplitude n=2 mode persists until the end of the neutral beam heating pulse at time B.*

suggesting that the m=1 mode has been stabilised. However after the sawtooth collapse the plasma remains in an unstable state characterised by a large m = 3, n=2 mode which oscillates for several seconds and often persists until the end of the neutral beam pulse (Fig. 5). This seems to prevent the growth of a second monster sawtooth in the same pulse, although there may be several normal sawteeth. The conditions for monster sawteeth have not yet been fully explored, but simultaneous ion cyclotron and neutral beam heating appear to be required. The ratio of ion cyclotron to neutral beam power does not appear to be critical but there does appear to be a threshold of total additional power which increases with plasma current. A possible explanation is that the current profile is modified by the beam driven current which may be enhanced by the ion cyclotron heating.

LOW q DISCHARGES AND DISRUPTIONS

Reproducible, stable ohmic discharges with I_p = 3.5MA, B_T = 1.7T, R = 2.97m, a = 1.2m, b/a = 1.35, q_ψ = 2.2 and $q_c=(5\ 10^6\ abB_T/RI_p)=1.59$ have been studied to simulate the planned operation of JET at I_p = 7MA and B_T = 3.4T. The sawtooth inversion radius is 0.55a. The global energy confinement time of 0.45s is consistent with normal JET scaling. These discharges reach the highest value of the Murakami parameter $\bar{n}\ R/B_T = 7.2\ 10^{19}\ m^{-2}\ T^{-1}$ obtained for JET ohmic plasmas (Fig. 6).

When q_ψ is lowered either by raising I_p, lowering B_T, or by reducing a or b/a, a lower limit to stable operation is always found at $q_\psi = 2.0 \pm 0.1$. These low q disruptions are initiated by a sawtooth collapse and have precursors only on a time scale shorter than the sawtooth period. The total radiated power remains less than the ohmic power input and there is no contraction of the current profile.

DISRUPTIONS AT THE DENSITY LIMIT

Disruptions at the density limit in discharges with $q_\psi \geq 3$ are preceeded by signs of deterioration for up to 1s before the final energy quench. The radiated power rises to equal the total power [6], and although the ohmic power increases due to increased plasma resistance, it fails to keep pace with the radiation. The discharge contracts until just before the quench there is virtually no current flowing outside the q=2 surface. Combining these observations with the assumption that all the energy loss outside q=2 is due to low Z impurity radiation gives an expression for the density limit in JET. An earlier calculation [7] has now been extended to include the effect of additional heating and a more accurate model [8] of

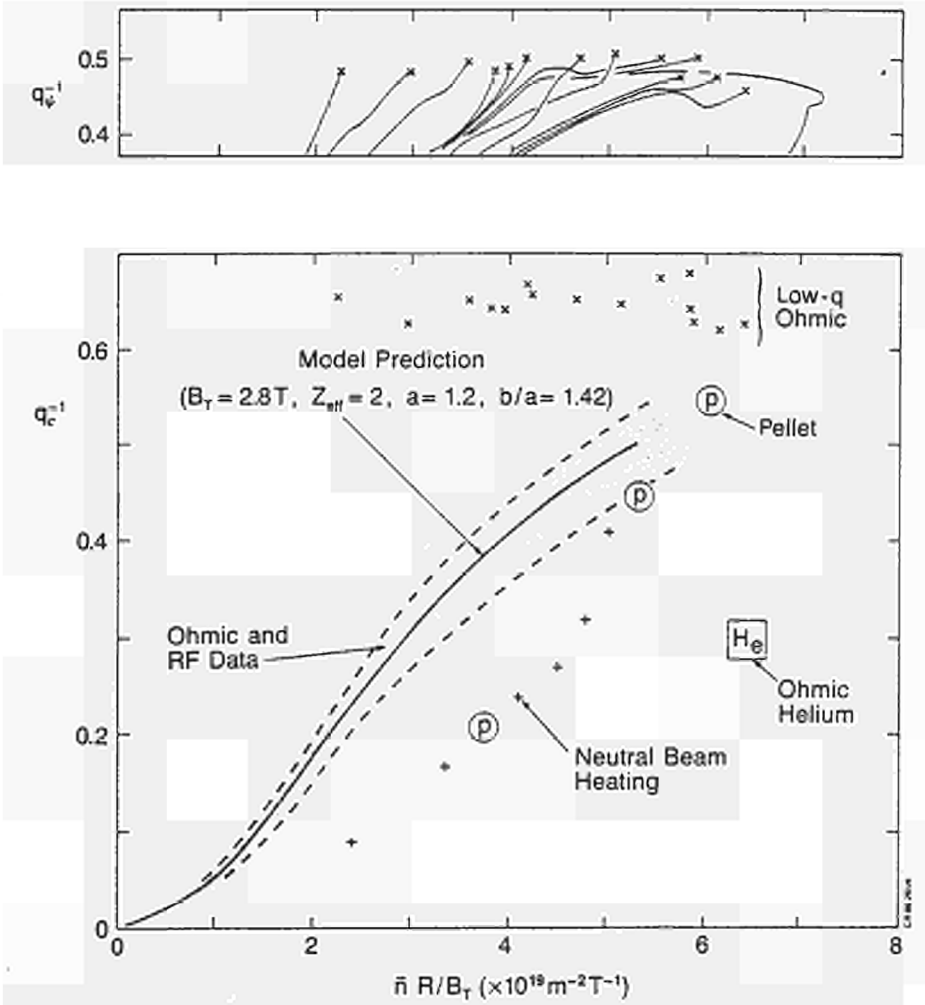

Figure 6 *Hugill diagram summarising the limits of stable operation in JET. The preliminary results of single pellet injection into ohmic discharges which did not disrupt are also shown. The low q limit is more consistently plotted in terms of q_ψ as shown in the upper figure.*

the impurity radiation. The predicted high density limit for low Z dominated discharges with gas refuelling is

$$\bar{n}_{crit} = 3.5\ 10^{16} \left(\frac{P \cdot q_c}{(Z_{eff}-1)\ Rab(q_c - 2a/b)} \right)^{1/2} m^{-3}$$

where P is the total power input (watts). This model clearly breaks down when Z_{eff} is close to 1 and other cooling mechanisms become important. There is good agreement between this expression and observed density limits for disruptions during the current flat top [6], but disruptions during the current rise and decay phases generally occur at lower and

higher densities respectively than the predicted values. The model also indicates that the weakness of the increase in the density limit with ion cyclotron heating is due to the observed increase in Z_{eff} with increasing power, whereas the substantial increase in the density limit with beam heating is slightly assisted by the reduction of Z_{eff} by the beam particles.

DETAILED STUDIES OF DISRUPTIONS

Detailed studies are being made of the sequence of events

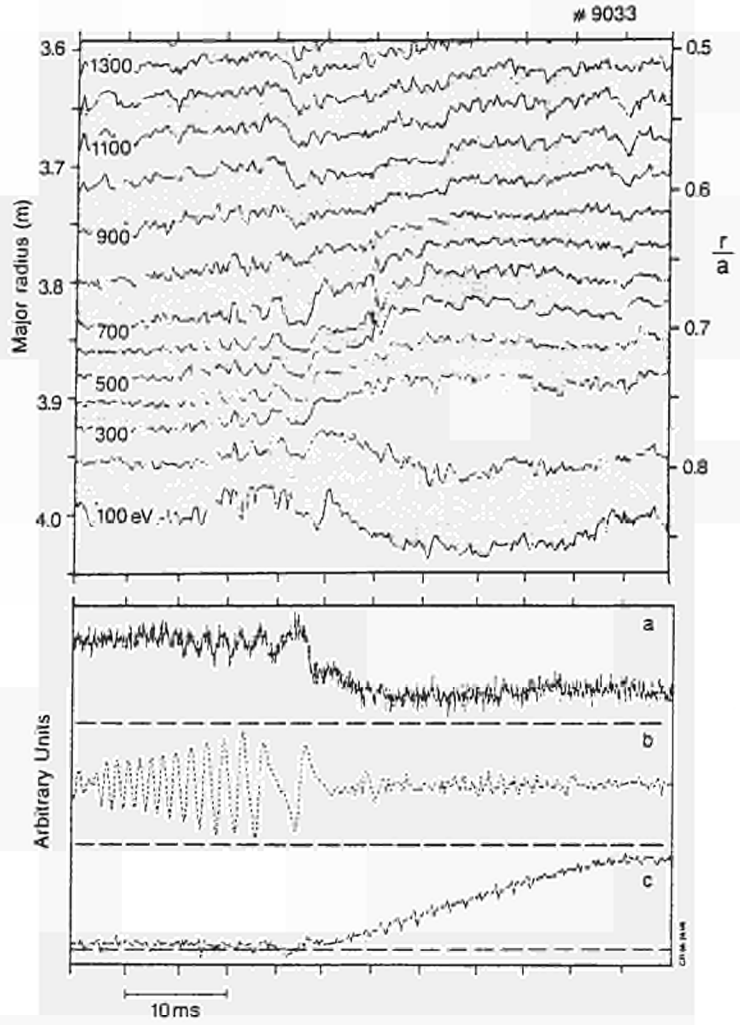

Figure 7 *Contours of electron temperature (at 100eV intervals) versus time during the magnetic activity which preceeds a disruption. The lower traces show (a) the electron temperature at R=3.95m (r/a ∿ 0.8), and the amplitudes (b) of the m=2, n=1 oscillation (c) of the locked mode.*

which preceed a density limit disruption [9]. In a typical case (I_p= 3MA, B_T= 3.4T, q_ψ=5.7) the significant magnetic activity, shown in Figure 7, starts about 700ms before the energy quench with a mode which is predominantly m=2, n=1. This activity grows for about 30ms. The mode then stops rotating and locks in a fixed toroidal position when $\tilde{B}_\theta$ at the wall is 10^{-3}T. During the locked phase the mode continues to grow in amplitude. ECE measurements show that the temperature profile shrinks before the start of the mhd activity. After the mode locks the temperature profile flattens slightly at a minor radius of 0.95 m which is close to the calculated position of the q=2 surface. This is consistent with the growth of a non-rotating magnetic island (the ECE diagnostic views close to the calculated position of the 'O' point) and there may be similar evidence from the soft X-ray emission, but the analysis is at a preliminary stage and there could be other interpretations. The spatial resolution of the ECE diagnostic (at present 40mm in the radial direction) is not quite sufficient to determine whether the 'O' point is colder than the surrounding plasma as predicted by the thermal instability model of disruptions [10].

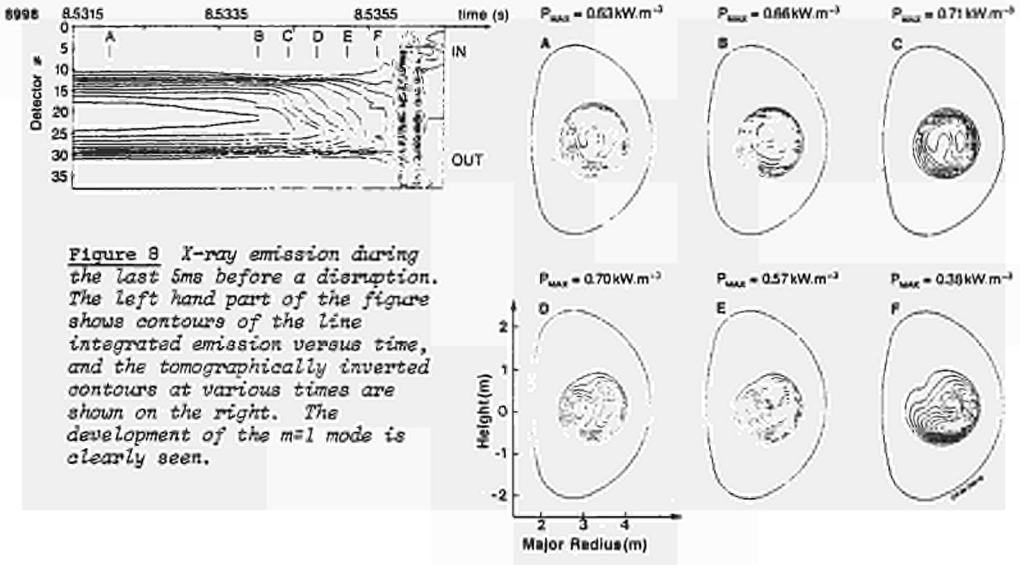

Figure 8 *X-ray emission during the last 5ms before a disruption. The left hand part of the figure shows contours of the line integrated emission versus time, and the tomographically inverted contours at various times are shown on the right. The development of the m=1 mode is clearly seen.*

The locked mode persists for several hundred ms until the final energy quench. This has been studied in detail for the last few ms before the energy quench using the soft X-ray diode arrays. A contour plot (Fig. 8) of the X-ray emission from the vertical camera shows that 2ms before the quench the central core of the discharge is eroded. The emission following the final termination is probably due to contact of the plasma with

the walls and limiter. Tomographic analysis of the X-ray emission shows the growth of a large m=1 asymmetry in the plasma centre. This structure appears to be locked in a specific toroidal phase for most disruptions which suggests that it is n=1 and coupled to the locked m=2 mode observed magnetically.

MAGNETIC FLUCTUATIONS

The magnetic pick-up coils detect incoherent fluctuations as well as coherent mhd activity. These incoherent fluctuations have a broadband spectrum over the whole measured frequency range from 5 to 60kHz.

During typical conditions the frequency dependence of the spectrum is $f^{-1.6 \pm 0.2}$ and the total normalised fluctuation amplitude is $\tilde{B}_\theta / B_\theta \sim 10^{-5}$. The magnetic fluctuations have a short growth and decay time. A strong correlation is observed in the direction parallel to $\underline{B}$. The normalised amplitude is seen to increase with additional heating power which may indicate a possible link with reduced confinement [11].

CONCLUSIONS

Detailed studies of sawteeth, disruptions and magnetic fluctuations are being made in JET with the aim of improving our understanding of these phenomena. The detailed mechanisms involved in the collapse of sawteeth have been investigated and found to be in agreement with an ideal mhd model of the collapse. A new regime which appears to be stable to low m and n modes for more than 1s has been observed with combined ion cyclotron and neutral beam heating. The operational limits to stable operation at low q and high density have been explored and the detailed mechanisms leading to disruptions have been studied. This work is proceeding with the objective of fully understanding the nature of disruptions and attempting to stabilise them by various means.

ACKNOWLEDGEMENTS

It is a pleasure to acknowledge contributions to this work and many helpful discussions with our colleagues in the JET project.

REFERENCES

[1] CAMPBELL, D.J., et al., Nuclear Fusion 26 (1986) 1085.

[2] GILL, R.D., et al., Controlled Fusion and Plasma Heating (Proc. 13th Euro. Conf. Schliersee, 1986) Vol.I 21.

[3] EDWARDS, A.W., et al., Phys. Rev. Lett. 57 (1986) 210.

[4] WESSON, J., Plasma Phys. Contr. Fusion 28 IA (1986) 243.

[5] DUPERREX, P.A., et al., Controlled Fusion and Plasma Physics (Proc. 12th Euro. Conf. Budapest, 1985) Vol.I 126.

[6] WESSON, J., et al., Controlled Fusion and Plasma Physics (Proc. 12th Euro. Conf. Budapest, 1985) Vol.I 147.

[7] SCHÜLLER, F.C., et al., Controlled Fusion and Plasma Physics (Proc. 12th Euro. Conf. Budapest, 1985) Vol.I 151.

[8] BEHRINGER, K., et al., Plasma Physics and Controlled Nuclear Fusion Research (Proc. 11th Int. Conf. Kyoto, Japan 1986) Paper No. A-IV-1.

[9] HENDER, T.C., ROBINSON, D.C., & SNIPES, J.A., Plasma Physics and Controlled Nuclear Fusion Research (Proc. 11th Int. Conf. Kyoto, Japan 1986) (Paper No. A-V-3).

[10] REBUT, P.H., & HUGON, M., Plasma Physics and Controlled Nuclear Fusion Research (Proc. 10th Int. Conf. London 1984) Vol.2, IAEA, Vienna (1985) 197.

[11] MALACARNE, M., and DUPERREX, P.A., JET Preprint-P(86)31.

Magnetic islands and chaos induced by heat flow

P-H. Rebut

ABSTRACT

A theoretical model is presented which addresses the problem of confinement degradation in tokamaks with increasing input power. It will be shown that, when full account is taken of the magnetic field line topology, the adiabatic invariance conditions and the particle motion equations in the guiding centre approximation allow us to relate the heat flow to the level of magnetic perturbation associated with large (M ~ 15) poloidal mode numbers. It will be shown that substantial power can be transported across the plasma by low level magnetic fluctuations and one possible mechanism for the self-sustainment of the magnetic islands is investigated.

1. INTRODUCTION

The degradation of confinement in tokamaks when a substantial amount of heating power is applied is generally ascribed to anomalously high electron losses.

In this paper we show how low level broad band magnetic perturbations ($\tilde{B}/B_p \sim 3.10^{-4}$) associated with large poloidal mode numbers (M ~ 15) are sufficient to account for the losses observed experimentally. To achieve this result it is necessary to take full account of the topological properties of the magnetic field lines.

The calculations are carried out for low collisionality plasmas in steady state regime neglecting curvature and finite Larmor radius effects. The low collisionality assumption is justified by present experimental conditions; for typical JET parameters [1] the electron mean free path ($\lesssim 10^4$m) is much longer than the plasma toroidal length (~ 20m).

2. MAGNETIC TOPOLOGY

The magnetic field in a slab geometry (Fig 1) is described by the components of the vector potential $\underline{A}(x,y,z)$:

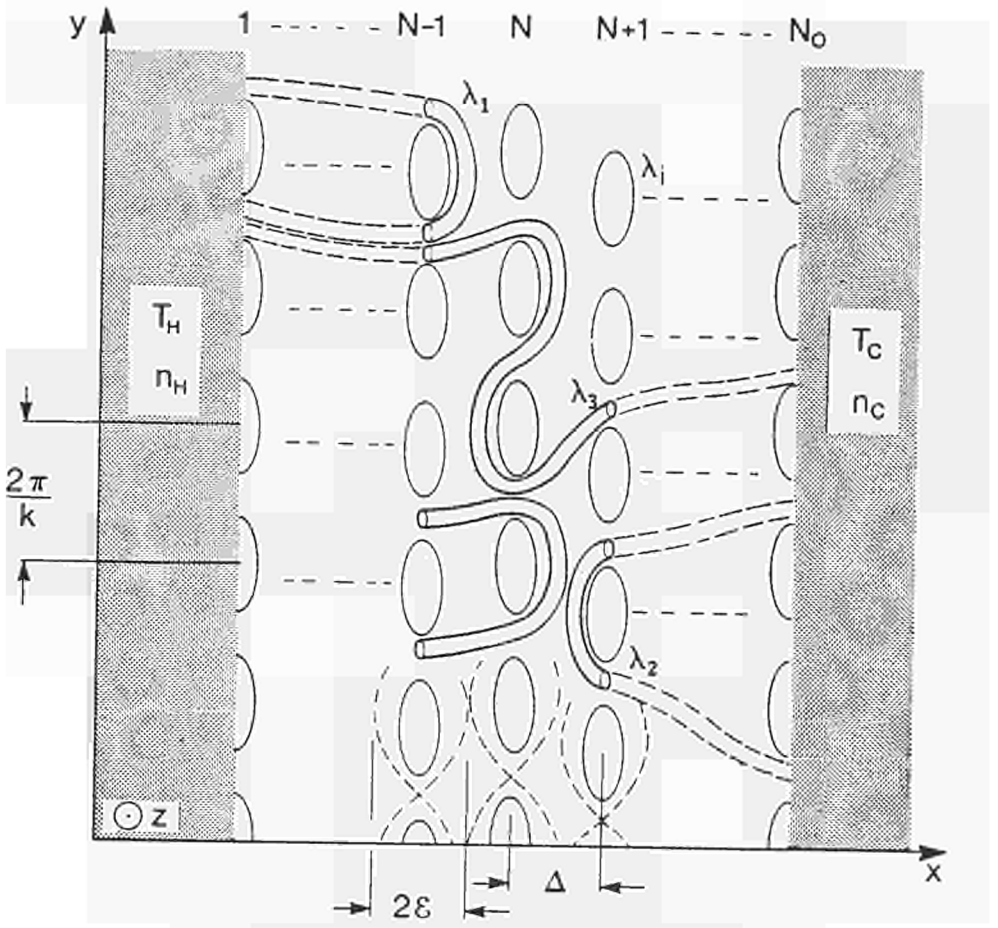

Fig. 1 Schematic diagram of the slab model.

$$A_x = 0$$

$$A_y = B_z\, x$$

$$A_z = \frac{B_o'}{2} x^2 + A \sum_{N=o}^{N_o} \cos k \left(y + \frac{Nz}{kR}\right) \qquad (1)$$

$$\underline{B} = \underline{\nabla} \times \underline{A}$$

$$\varepsilon^2 = -\frac{4A}{B_o'} \; ; \qquad Y = \frac{2\varepsilon}{\Delta}$$

In toroidal geometry:

$$B_o' = \frac{r}{R} B_z \frac{q'}{q^2}$$

where q' is the shear term, ε the virtual island half width and Y the overlapping parameter of the different chains of magnetic

islands; $\frac{2\pi}{k}$ and $2\pi R$ are the periodicities in the y and z directions respectively. Eq (1) corresponds to N_0 chains of magnetic islands [2].

The different chains of islands can be mapped into each other through a translation by Δ (distance between two chains of islands) and a rotation due to the shear. Consequently they are all equivalent and the full slab topology can be deduced from the detailed knowledge of the properties of a single chain of islands. In Fig 2 the (x,y) Poincaré map is shown for five chains of islands with an overlapping parameter $\gamma = 1.0$. The onset of stochasticity affecting neighbouring chains of islands appears at perturbation level above a threshold value $\gamma_c \geq .8$. For $.8 \leq \gamma \leq 1.5$, islands with closed magnetic surfaces are embedded in a chaotic region.

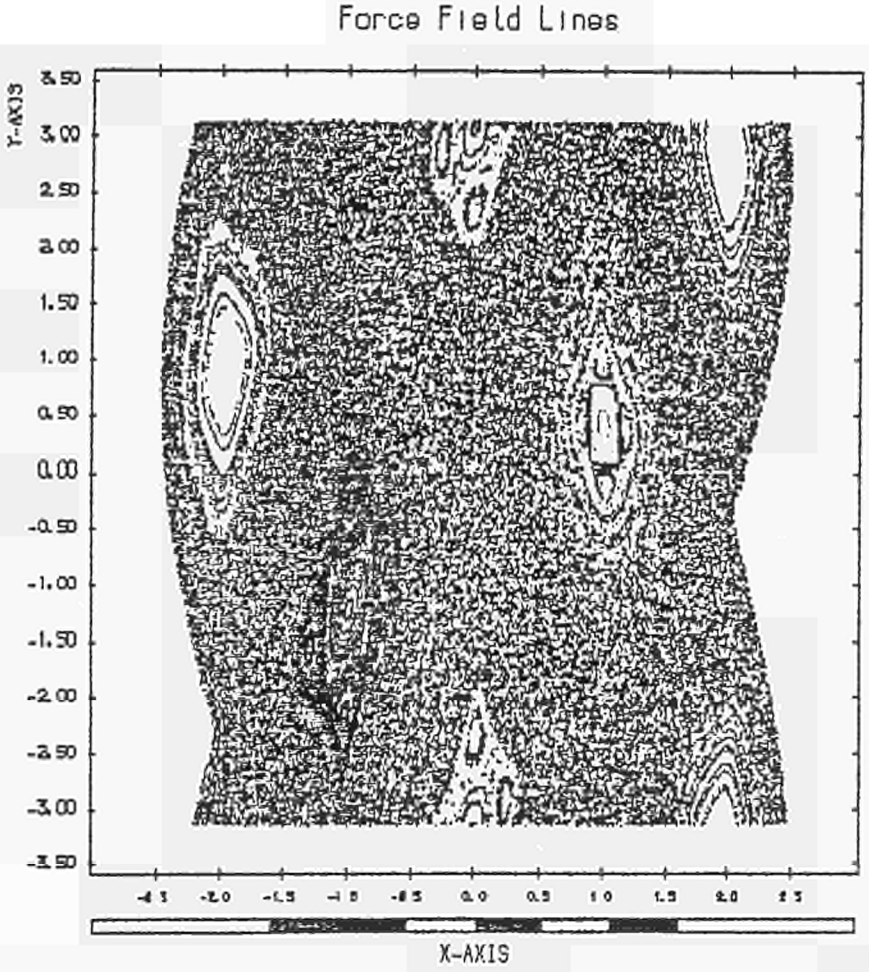

Fig. 2 Poincaré map computed for the field distribution of Eq(1) with $\gamma = 1.0$. Satellites (secondary islands) are visible around the main magnetic island structures.

With reference to Fig 1, the normalised cross-sectional area σ of the tube of flux associated with a chaotic field line and crossing one chain of islands is given by:

$$(2)\quad \sigma(\gamma) = \frac{2}{S}\iint \frac{B_x}{B_z}(\gamma) H(B_x) H_{cross}\, dy\, dz \quad ; \quad S = \iint dy\, dz$$

where $H_{cross} = \begin{cases} 1 & \text{when the field line crosses the island chain} \\ 0 & \text{otherwise} \end{cases}$

Similarly $H(B_x)$ is the Heaviside function for B_x.

Following the same formalism we can define the fraction $\alpha(\gamma)$ of the flux tube which crosses the next chain of islands and the normalised cross-section of the island. Results of numerical computations are shown in Fig 3 for α and the quantity $\frac{\alpha\,\sigma}{1-\alpha}$.

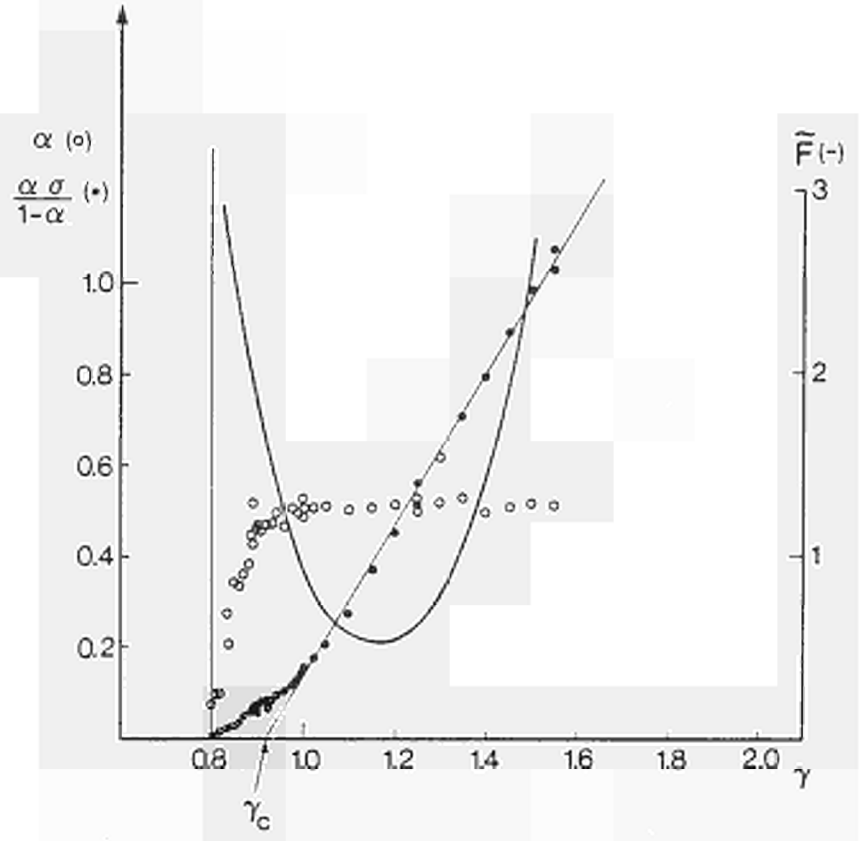

Fig. 3 Plots of α, $\frac{\alpha\,\sigma}{1-\alpha}$ and F as a function of the overlapping paramter γ.

The behaviour of the field lines in the chaotic zone corresponds to a diffusion process through neighbouring chains of islands according to an equation of the type:

$$(3) \quad L_0 \frac{\partial F}{\partial L} = \frac{1}{2} \Delta^2 \frac{\partial^2 F}{\partial x^2} \quad ; \quad L_0 = \frac{S_c(\gamma)}{\sigma(\gamma)} \frac{2\pi R q^2}{M q' \Delta} \qquad (\alpha = \frac{1}{2})$$

where F(L.x) is the probability of finding a field line at x after a path length L and L_0 is the required path length for a field line to cross an island chain; and where $S_c(\gamma)$ is the cross-sectional area of the chaotic region (normalised).

3. PARTICLE MOTION

The following equations are written in a reference frame in which the magnetic islands are at rest and where ϕ is the electric potential which ensures the plasma quasi-neutrality. The electric field satisfies the symmetry invariance of the magnetic field.

Taking into account the constancy of the magnetic field in the chosen frame, the particle adiabatic invariants are:

$$(4) \quad \begin{aligned} U_\perp &= \frac{1}{2} m w_\perp^2 \\ U_{\parallel} &= \frac{1}{2} m w_{\parallel}^2 + q\phi \end{aligned}$$

where subscripts $\perp$, $\parallel$ refer to the field lines. The motion equations in the guiding centre approximation are:

$$(5) \quad \frac{d\underline{r}}{dt} = \frac{\underline{w} \cdot \underline{B}}{|B|^2} \underline{B} + \underline{v}_0$$

They correspond to a motion along the field lines and a perpendicular drift with velocity $\underline{v}_0 = \frac{\underline{E} \times \underline{B}}{|B|^2}$, where $\underline{E} = -\underline{\nabla}\phi$ is the electric field.

From conservation of the number of guiding centres, the total current j_g associated with them satisfies the equation:

$$(6) \quad \underline{\nabla} \cdot \underline{j}_g = \underline{\nabla}.(\underline{j}_{eg} + \underline{j}_{ig}) = \underline{\nabla}.[j_{\parallel g} \underline{e}_{\parallel} + (q_i n_i + q_e n_e)\underline{v}_0] = 0$$

when perpendicular diffusion is neglected.

In conditions of quasi-neutrality and taking into account that the parallel plasma current $j_{\parallel}$ equals $j_{\parallel g}$, we have:

$$(7) \quad \underline{\nabla}.(j_{\parallel} \underline{e}_{\parallel}) = 0$$

Defining a scalar λ by:

$$j_{\parallel} \underline{e}_{\parallel} = \lambda \underline{B}$$

we get:

$$(8) \quad \underline{B}.\underline{\nabla} \lambda = 0$$

Eq(8) shows that the parameter λ is constant on every field line. In particular, λ is constant on a magnetic surface.

When the parallel resistivity $\eta_{\parallel}$ is taken into account, λ is defined by:

$$(9) \qquad \lambda \int_{o}^{L} \eta_{\parallel} \, dl = L \, \frac{1}{B} \, \frac{V}{2\pi R}$$

where L is the field line path and V is the loop voltage. Eq(9) can be solved using Eq(3).

A particular case arises from Eq(8), when all field lines behave similarly; in this case λ is single valued over the whole region [3].

In the chaotic region field lines with different paths have different values of γ, which depend also on the boundary conditions. At a given location, an average value λ_{ch} can be defined statistically over three classes of field lines: field lines connected to each boundary (λ_1, λ_2) and linking both boundaries (λ_3). On the contrary, the field lines in the magnetic islands remain localised and have in general a different λ_i (Fig 1). The guiding centre trajectories can be calculated simply by referring to pseudo field line equations.

In the particular case when $\phi = \phi(x) = -E_o x$ the guiding centre equations become:

$$(10) \qquad \frac{dX}{dt} = w_{\parallel} \frac{B_x}{B_z}$$

$$\frac{dY}{dt} = - w_{\parallel} \frac{B_o'}{B_z} X$$

where $X = x + \frac{E_o}{B_o' w_{\parallel}}$, $Y = y$. For a given $w_{\parallel}$ the guiding centre trajectories have the same behaviour as the field lines and the topological properties summarised in section 2 apply to the particle motion.

The effect of the electric field, is smallest for fast particles; when $E_o/B_o' w_{\parallel} < \Delta$ particles follow closely the field lines, while drift effects dominate when $E_o/B_o' w_{\parallel} > \Delta$ (slow particles).

4. PARTICLE AND ENERGY FLOW

To maintain temperature and density gradients as particles are crossing the various chains of islands, suitable sources and sinks have to be introduced at the boundaries of the slab. These will be schematically represented by hot and cold "seas" of particles with Maxwellian velocity distributions F_H and F_C respectively at temperatures and densities T_H, n_H and T_C, n_C (Fig 1).

Taking into account the symmetry properties of the magnetic islands and the adiabatic invariants (4), it can be shown by recurrence analysis that the electron flow Ψ through N_o chains of islands is given by:

$$(11)\quad \Psi = \frac{\alpha\ \sigma}{N_o(1-\alpha)+1}\left[n_H\sqrt{\frac{2KT_H}{\pi m_e}}\exp\left(-\frac{q_e\phi_o}{KT_H}\right) - n_c\sqrt{\frac{2KT_c}{\pi m_e}}\right] lM\ \frac{q'}{q^2}\ \Delta^2$$

where ϕ_o ($\phi_o = E_oN_o\Delta$) is the potential difference between the hot and the cold sea and l is the slab dimension in the y direction.

In order to maintain quasi-neutrality conditions the electron flow has to equal the ion flow. Assuming similar temperatures for electrons and ions we get:

$$(12)\qquad \exp\left(-\frac{q_e\phi_o}{KT_H}\right) \simeq \frac{n_c}{n_H}\left(\frac{T_c}{T_H}\right)^{1/2} + \left(\frac{m_e}{m_i}\right)^{1/2}$$

In the approximation $(m_e/m_i)^{1/2} \simeq 0$:

$$(13)\qquad E_o = \frac{KT_H}{q_e}\left(\frac{\nabla_x n}{n_H} + \frac{1}{2}\ \frac{\nabla_x T}{T_H}\right)$$

which shows that the velocity v_o of the chosen reference frame follows the diamagnetic velocity of the electrons, a result already obtained for microtearing modes [4].

Similarly, the heat flows are given by:

$$(14a)\quad P_{Heat_{e^-}} = \frac{\alpha\ \sigma}{N_o(1-\alpha)+1}\ n_c\ \sqrt{\frac{8KT_c}{\pi m_e}}\ \left(KT_H - KT_c\right) lM\ \frac{q'}{q^2}\ \Delta^2$$

$$(14b)\quad P_{Heat_{i^+}} = \frac{\alpha\ \sigma}{N_o(1-\alpha)+1}\ n_{iH}\sqrt{\frac{8KT_{iH}}{\pi m_i}}\ KT_{iH}\ lM\ \frac{q'}{q^2}\ \Delta^2$$

The electron distribution function in the chaotic region at the Nth chain of islands is:

$$(15)\quad F_N = F_H(w_{\parallel}) + \frac{N}{N_o}\left(F_c(w_{\parallel}) - F_H(w_{\parallel})\right) H\left[\frac{1}{2}\ m_e w^2 - \left(\frac{N_o-N}{N_o}\right)q_e\phi_o\right]$$

which shows a linear combination of the Maxwellian distribution functions describing the hot and cold "seas".

5. SELF-SUSTAINMENT OF THE PERTURBATION

The necessary condition for self-sustainment is found through the determination of the relative difference $\rho = (\lambda_{ch}-\lambda_i)/\langle\lambda\rangle$ between the values of λ associated to the chaotic zone and to the islands respectively. In presence of

perturbations with a range (ΔM) of poloidal mode numbers around an average value $\bar{M}$ such as $(\Delta M)/\bar{M} = \mu$, the mean separation Δ between chains of islands in toroidal geometry is:

$$(16) \qquad \Delta = \frac{3}{2\mu} \cdot \frac{1}{\bar{M}^2} \cdot \frac{q^2}{q'} \quad ; \quad q = \frac{rB_z}{RB_p}$$

Ampere's equation and the definition of the overlapping parameter γ leads to the relation:

$$(17) \qquad \sqrt{2\mu} \cdot \bar{M} \cdot \rho = \tilde{F}(\gamma) \cdot \frac{B_z}{\mu_0 . jR}$$

where j is the average current parallel to the magnetic field at the minor radius r and where $\tilde{F}(\gamma)$ depends on the shape and cross-section of the islands. As shown in Fig 3, $\tilde{F}(\gamma)$ has a minimum close to 0.5 for $\gamma \sim 1.1 - 1.2$.

Then by using the definition of λ, the safety factor q_0 and current density j_0 on the axis of a Tokamak we get the necessary condition of self-sustainment of the perturbation:

$$(18) \qquad 4\sqrt{2\mu} \cdot \frac{\bar{M}}{q_0} \cdot \frac{\delta j}{j_0} \geq 1 \qquad ; \delta_j = j_{ch} - j_i$$

where δj is the default of current inside the islands with respect to the chaotic region.

Substituting Eq(16) into Eq(14a) the heat flow can be written as:

$$(19) \quad P_{Heat_{e^-}} = \frac{\alpha\ \sigma}{1-\alpha}(2\pi r\ K\nabla T)\left(\frac{3}{2\mu}\right)^3 \frac{1}{\bar{M}^5} \left(\frac{q^2}{q'}\right)^2 n_c v_c \quad ; \quad v_c = \sqrt{\frac{8KT_c}{\pi m_e}}$$

Eq(19) shows that the heat flow is strongly dependent on the average poloidal mode number $\bar{M}$ which defines the number N_0 of chains to be crossed, and on the temperature and density of the cold "sea".

Combining Eq(17) with Eq(19) leads to:

$$(20) \quad \rho = \left(\frac{1}{2\mu}\right)^{2/5} \left(\frac{1}{3}\right)^{3/5} \tilde{F}(\gamma) . \left(\frac{1-\alpha}{\alpha\ \sigma}\right)^{1/5} \cdot \frac{j_0 q_0}{jq} . \left(q\ q'^2 \frac{P_{Heat_{e^-}}}{2\pi r\ n_c\ v_c\ \nabla KT}\right)^{1/5}$$

The minimum value of ρ occurs at $\gamma = 1.2$.

By reference to Section 3, the average electrical resistivity η along a field line depends upon the relative length of its path in the different plasma regions including the two "seas"; and on the local distribution function given by Eq(15). In case of "infinite seas" the current density in the chaotic zone can be written as:

$$(21) \qquad j_{ch} = \frac{N j_C + (N_o - N) j_H}{N_o} = \frac{V}{2\pi R\, \eta_{ch}}$$

As $\eta \propto T^{-3/2}$, j_{ch} is larger than the current density of a plasma with temperature $T_{ch} = \frac{N T_C + (N_o - N) T_H}{N_o}$. The determination of j_i, the current density in the islands, requires to calculate the local distribution function by integrating the particle trajectories including the $\underline{E} \times \underline{B}$ drift.

For small temperature and density differences between the hot and the cold sea, it can be shown that:

$$(22) \qquad \rho = \nu \frac{(T_H - T_C)^2}{T^2_{ch}}$$

where ν is a numerical coefficient, the value of which depends on the details of the collision and on the relative value of the radial electric field. Using Spitzer conductivity and a Krook collisional model ν is found to be in the range 0.1 - 0.3. A rough estimate of $(T_H - T_C)/T_{ch}$ based on the relative plasma volumes at high and low temperatures leads to a self-consistent ρ value of a few percent.

It must be noted that a full treatment should take into account the ion Larmor radius when it is only marginally smaller than the island size. We should also remark that the crash of a sawteeth can also contribute to ρ as the current expelled from the central region of the plasma should flow preferably in the chaotic zone.

6. Preliminary comparison with JET experimental results have been carried out. Inserting JET data into Eq(20) for $q = 1.5$ we get $\rho = \frac{\delta j}{j} > 2.5 \times 10^{-2}$ and a band of M numbers extending from 10 to 20. The corresponding magnetic perturbation $\tilde{B}/B_p$ has an amplitude of 3.10^{-4} and the chains of islands are separated by a distance $\Delta \sim 10^{-2}$m, i.e. only a few times larger than the ion Larmor radius. From Eq(22) with $\nu = 0.3$, $(T_H - T_C)/T_{ch} \sim 0.3$ and the number of chains of islands between the two "seas" would be in the range 15 to 20.

7. CONCLUSION

The topology of magnetic field lines is a dominant feature affecting the properties of magnetically confined plasmas. An equilibrium could exist ($\gamma \sim 1.2$) between undestroyed magnetic islands and chaotic regions.

This topology may be the key feature which explains the "anomalous" confinement in tokamaks, by allowing transport along field lines linking different regions of the plasma. This transport is affected by the plasma density and temperature at the edge. The reverse field pinch configuration could represent an extreme case of this model.

The current perturbation and then the topology may be self-sustained by the difference of resistivity between chaotic zone and islands, resulting from the field line path and the presence of hot electrons in the chaotic zone. The islands have a phase velocity close to the electron diamagnetic velocity.

Other effects, not taken into account so far, like finite ion Larmor radius, perpendicular diffusion and field curvature could play an important role in the self-sustainment of such a topology.

When the model is applied to JET, the observed heat fluxes can be accounted for by perturbation levels in the magnetic field $\tilde{B}/B_p \sim 3.10^{-4}$ and in the current $\delta_j/j \sim 3\%$, corresponding to average poloidal mode number $\bar{M} \sim 15$.

ACKNOWLEDGEMENTS

We acknowledge the contribution of A. Samain, who is working along similar lines at Cadarache (CEA).

REFERENCES

[1] THE JET TEAM, "JET Latest Results and Future Prospects", IAEA Conference, Kyoto, (1986).

J G CORDEY et al, "Energy Confinement with Ohmic and Strong Auxiliary Heating in JET", IAEA Conference, Kyoto, (1986).

[2] P H REBUT and M HUGON, in Plasma Physics and Cont Nuc Fusion Res (Proc 10th Int Conf, London, 1984) 2, IAEA, Vienna (1985) 197.

[3] J B TAYLOR, Phys Rev Lett 33(1974)19.

[4] A SAMAIN, Plasma Phys and Controlled Fusion 26(1984)5.

EXPERIMENTAL STUDIES IN JET WITH MAGNETIC SEPARATRIX

A. TANGA, D. BARTLETT, K. BEHRINGER, R.J. BICKERTON, A. CHEETHAM, J.G. CORDEY, A. GIBSON, N. GOTTARDI, A. GONDHALEKAR, P.J. HARBOUR, H. JAECKEL, M. KEILHACKER, E. LAZZARO, V. MARTENS, P. NOLL, S. NOWAK, F.C. SCHUELLER, A.J. TAGLE, A. TARONI, P.R. THOMAS, F. TIBONE

JET JOINT UNDERTAKING, ABINGDON, OXON, OX14 3EA, U.K.

ABSTRACT

The main objectives of the experiments described are (i) to compare the global confinement characteristics of separatrix and limiter discharges and (ii) to study the conditions for the creation of a high density, highly radiative, cool plasma region near the X-point capable of screening and isolating the bulk plasma. Compared to similar limiter discharges, the thermal energy content of single null X-point discharges (SN) is roughly a factor of two higher. Plasmas with even modest separation between X-point and target plates show typical signatures of H-mode discharges. Multi-channel infrared interferometer measurements provide evidence of the formation of a high density diverted plasma with average density ~$10^{20}m^{-3}$, an order of magnitude higher than the main plasma. Measurements with a bolometer camera array show that, in high density discharges with additional power, up to 40% of the input power is radiated within a ~0.2x0.2m^2 toroidal region around the torus.

1. INTRODUCTION

The main aim of JET is to study plasmas under conditions approaching those needed for a fusion reactor. At present, in limiter discharges, confinement with additional heating is low (L-mode). Better confinement (H-mode) has been observed in tokamaks with magnetic limiters or divertors. In JET, a magnetic configuration with a separatrix inside the vacuum vessel can be created [1]. Two ("double null configuration", DN) or one ("single null configuration", SN) poloidal field nulls are then produced near the top and/or bottom of the vessel as shown in Figs. 1a and 1b.

In these configurations the plasma is detached from both the limiter and the inner wall and recycling occurs in an open divertor region near the X-point. Experiments have been carried out with plasma currents up to 2.5MA in the DN and up to 3.0MA in the SN configuration. A maximum additional power of 9MW has been injected (D° into D^+).

2. FORMATION OF A MAGNETIC SEPARATRIX

A magnetic separatrix can be formed within the vacuum vessel of JET using the multipolar field normally used to control the elongation and triangularity of the plasma cross-section. In the DN configuration, the present poloidal field equipment allows operation at plasma currents up to 2.5MA. The resulting plasma has an elongation of 1.8; the vertical

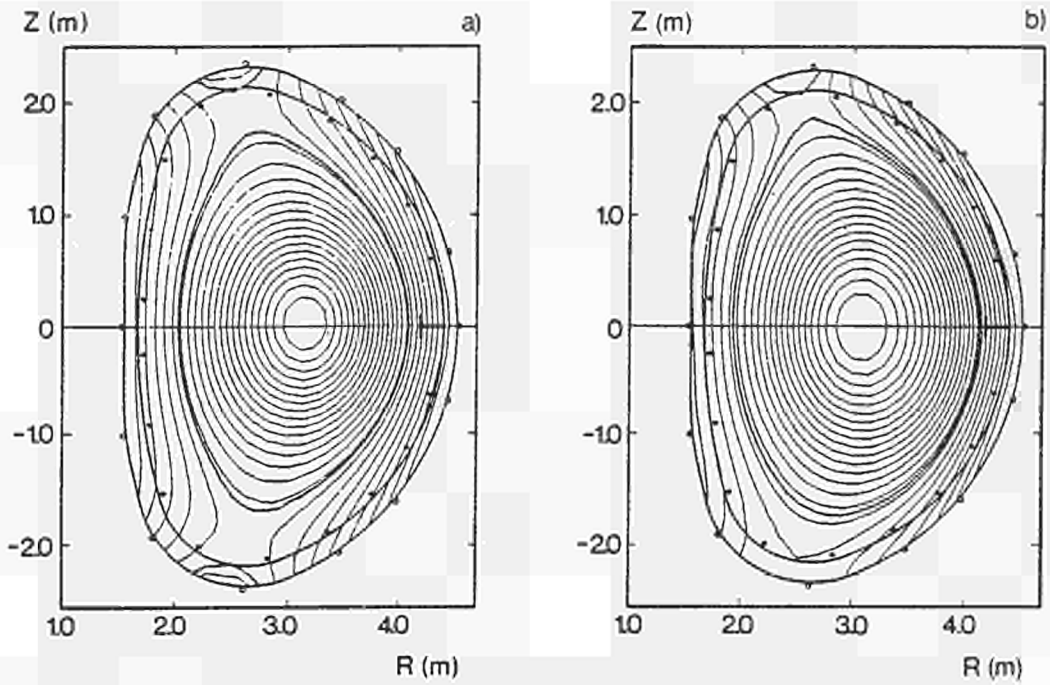

Fig. 1a Flux plot of a double null configuration. Plasma current = 2MA, toroidal field = 2.8T, average electron density = $3.10^{19}m^{-3}$, poloidal beta = 0.44, plasma elongation = 1.8.

1b Flux plot of a single null configuration. Plasma current = 2MA, toroidal field = 2.2T, average electron density = $3.10^{19}m^{-3}$, poloidal beta = 0.6, plasma elongation = 1.65, (#10237 t = 13.5s).

position is unstable with an open loop growth rate of $150s^{-1}$.

The separation between the X-point and the graphite target plates is a linear function of the currents in the shaping coils. For the configuration in Fig.1a the separation is ~0.1m. In the SN configuration, plasma currents up to 3.0MA have been produced with an elongation of 1.65; the growth rate of the vertical instability is substantially smaller than for the DN configuration.

The maximum separation between the X-point and the target plates obtained so far at 2MA with SN is ~0.13m and may be increased by displacing the magnetic axis below the midplane. the radial position of the null point is held constant during the discharge, to within a few centimetres. The distance between the separatrix and the antennae for ICRH is finely controlled by the radial position feedback system and this can allow good coupling of ICRH to the plasma. In both DN and SN configurations, Langmuir probe measurements give the e-folding length for decay of density and temperature as 0.06m and 0.10m, respectively.

The location of the separatrix has been corroborated to within a few centimetres by observations with a bolometer camera array and TV cameras and by the separation between the erosion marks on the graphite target tiles. The magnetic configuration is only slightly sensitive to changes in internal parameters, such as the poloidal beta and internal inductance.

3. HIGH RECYCLING IN THE X-POINT REGION

The formation of a magnetic separatrix within the vacuum vessel produces a significant change in the discharge characteristics. For separations between the plasma and the limiter larger than 0.07m, deuterium recycling (monitored by D_α signals) shifts from the limiters to small regions near the X-points. Both the D_α monitors and TV observations in the near infra-red show the formation of bright regions (~0.2m across) coinciding with the X-points. In high density DN discharges, only one bright region is observed. The application of a radial magnetic field shifts the toroidal plasma column vertically and the bright region moves correspondingly, indicating that the formation of only a single bright region is not connected with slight up-down asymmetries in the poloidal field.

Simultaneous with the shift in recycling characteristics, stronger gas-fuelling is needed to sustain the average plasma density, Z_{eff} is reduced and the bolometer camera array shows a decrease in bulk plasma radiation and a large increase in the radiation from the X-point region. As shown in Fig.2a for a series of ohmic DN discharges, the total radiated power is in most cases between 70 and 100% of the input power and the power radiated in the X-point region increases with plasma density more rapidly than the total radiated power. SN discharges show similar behaviour with the power radiated from the X-point region, following approximately a density-squared dependence. The size of the highly radiative region in the vicinity of the X-point can be estimated to be $\leq 0.2 \times 0.2 m^2$.

The far infra-red multichannel interferometer suggests a similar small region with high electron density near the X-point. When one of the vertical channels of the interferometer passes through the X-point region, the fringe count for that channel shows a substantial increase over the other channels. This can be interpreted as a measurement of the local X-point line density. In Fig.2b, the difference between two adjacent channels of the interferometer has been plotted against the line average electron density. Assuming that the size of this high density plasma region corresponds to that of the highly radiative region the density in the X-point region is estimated to be $\sim 10^{20} m^{-3}$. No data are available for average plasma densities larger than $2 \times 10^{19} m^{-3}$ because the channel of the interferometer intercepting the X-point loses fringes.

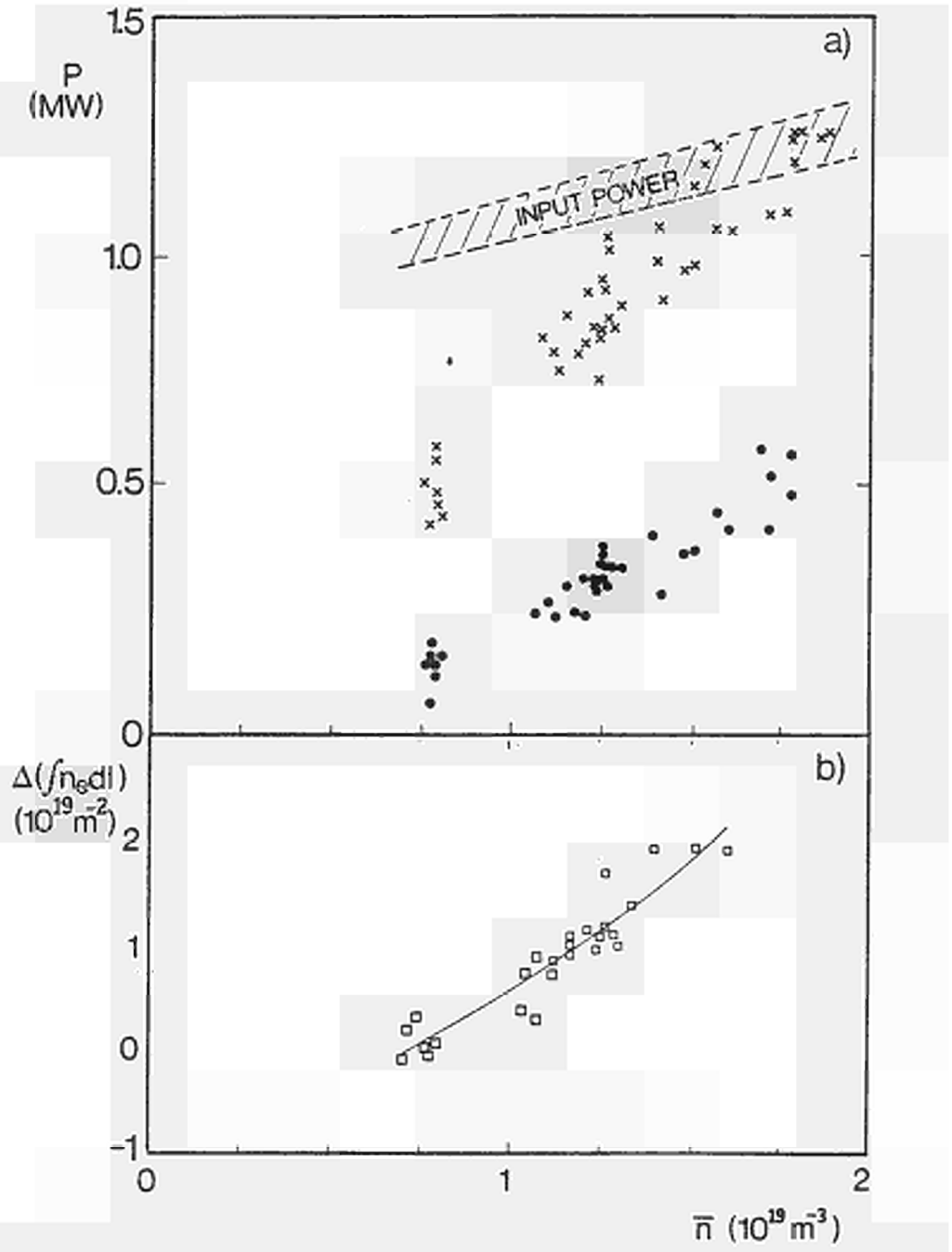

Fig. 2a Radiated power versus line average electron density for ohmic double null configuration. The dots represent the power radiated from the X-point, crosses the total power radiated from the plasma.

2b Difference in line density between two adjacent interferometer channels one of which intercepts the X-point.

Assuming that the thickness of the high recycling region corresponds to the mean free path for neutrals, λ°, the interferometer data provides a measure of [2]

$$n_t \lambda^\circ = \frac{v^\circ}{\langle \sigma v \rangle}$$

where v° is the effective speed of the emitted atoms and $\langle \sigma v \rangle$ is the effective rate coefficient for ionisation. Assuming a single temperature, T_t, for electrons, ions and neutrals, the right hand side of this equation is only a function of T_t. T_t~5-10eV is obtained for $\bar{n}_e > 1 \times 10^{19} m^{-3}$. The density, n_t, may also be estimated from a zero-dimensional model which balances the power flow from the bulk plasma with sonic flow at the high density region in the scrape-off layer. For $\bar{n}_e > 1 \times 10^{19} m^{-3}$, $n_t \sim 4 \times 10^{19} m^{-3}$ is obtained, in reasonable agreement with the estimates made earlier.

This trend towards high recycling is further corroborated by Langmuir probe measurements which suggest that the Mach number of the flow parallel to the magnetic field decreases with increasing plasma density.

4. IMPROVED CONFINEMENT WITH ADDITIONAL HEATING IN THE SINGLE NULL CONFIGURATION

DN X-point discharges show an energy confinement time some 20-30% higher than similar limiter or inner wall discharges. However, no clear H-mode transition was identified as the power levels available. Recent experiments have therefore concentrated on the SN configuration. First results show a substantial improvement of energy confinement in SN X-point discharges compared to similar limiter or inner wall discharges. The experiments have been carried out with neutral beam injection heating with up to 9.0MW power. Ion cyclotron heating has been applied in some of the shots with a power of up to 4MW (but keeping the total input power, $P_{tot} = P_\Omega + P_{NBI} + P_{RF} \leq 20MW$).

In Fig.3 the variation of the total plasma thermal energy content with total input power P_{tot} for two series of SN X-point discharges at plasma currents of 2MA and 3MA is compared with the corresponding data sets for limiter discharges. While the separation of the X-point and the target plates is ~0.13m at 2MA this is reduced to ~0.5m at 3MA and is then rather close to the wall. For either plasma current the energy content of the X-point discharges is up to a factor of 2 larger than that of the corresponding limiter discharge with the same additional power. In general, the trend with increasing heating power is also similar in all cases.

As shown in Fig.4, the electron temperatures (and also the central ion temperatures for such an X-point H-mode plasma are substantially higher than for a limiter plasma with the same parameters of plasma density, plasma current, toroidal field and

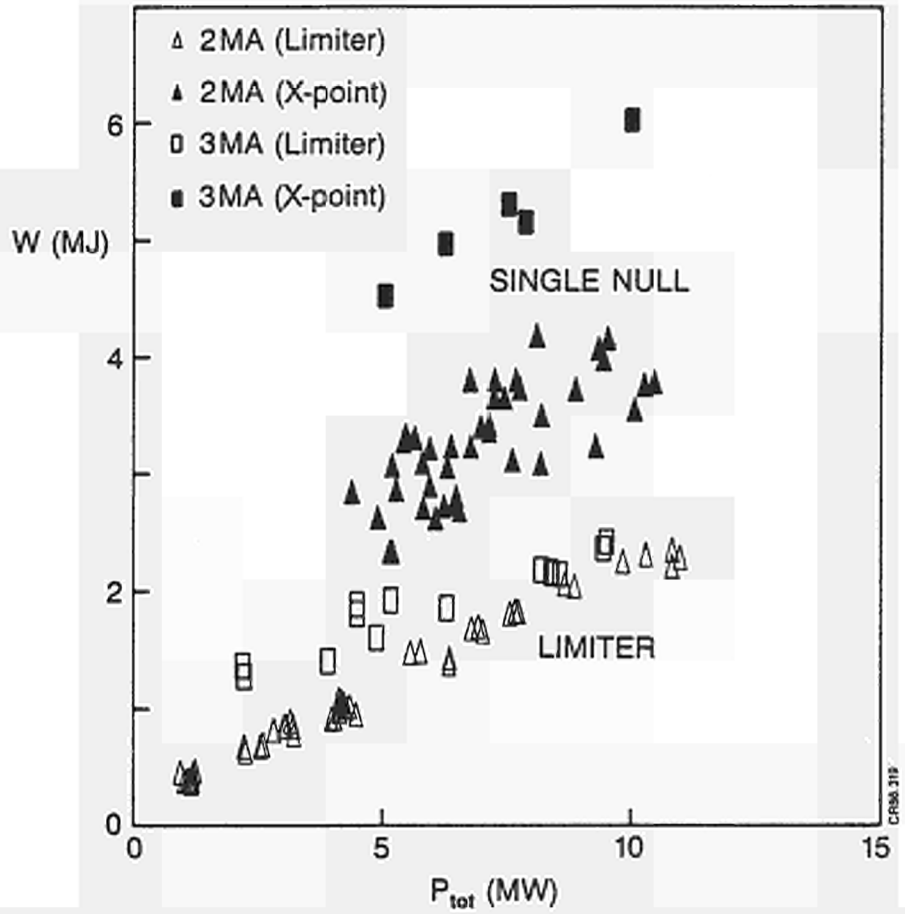

Fig. 3 Total plasma thermal energy content as measured by diamagnetic loop versus total input power for single null and limiter configurations.

P_{tot}. It should be noted that the electron temperature profile is broader, with the edge temperature at R=4.0m being some 2.5 times higher.

As pointed out already the SN discharges at 2MA exhibit clear indications of a transition into an H-mode [3]. As shown in Fig.5 the edge D_α signal (f) drops and the line integrated electron density (d) increases more rapidly. These events occur shortly after the crash of a sawtooth when the edge temperature (e) increases abruptly. The power flow to the target plates (b) is substantially reduced. This phase is subject to an abrupt termination when the average density reaches some limiting value (as evidenced more clearly in other JET Pulses where this event is not obscured by the end of additional heating). The average density, temperature and thermal energy content (c) fall in about 40ms, accompanied by a spike in the X-point radiation. During the H-phase the plasma density profile broadens with steep gradients developing at the edge.

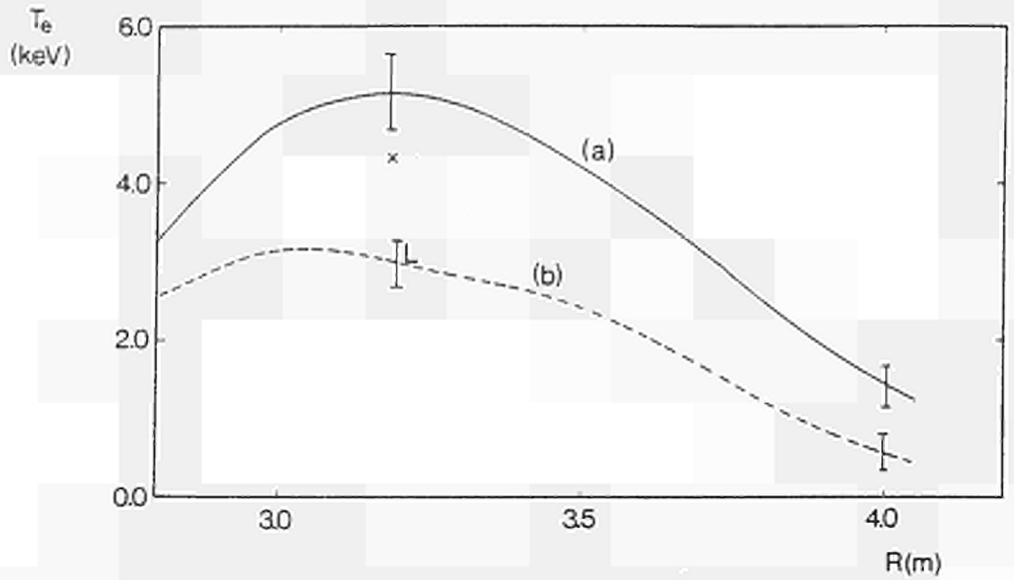

Fig. 4 Electron temperature profiles a) X-point (#10237 t = 13.5s) and b) Limiter discharge (#7709). Central ion temperature for SN (X) and Limiter (L) discharge.

Impurity radiation from the plasma edge (O VI, C IV) falls by about a factor of two at the transition to the H-regime. At this time the ICRH power ceases to be coupled to the plasma (probably due to the changed edge conditions) and the nickel influx from the antenna screen falls to zero. Nevertheless, the total nickel content as observed from the Ni XXV and Ni XXVI line intensities remains constant indicating substantially improved confinement of metals in the interior of the plasma. As indicated by the soft X-ray radiation profiles, however, this does not lead to accumulation of impurities.

A preliminary analysis of transport properties comparing SN X-point with limiter and inner wall discharges has been done with the transport code Jetto [4]. Using the transport models described in [5] good simulations of all the relevant measured quantities (n_e, T_e, radiation profiles, central ion temperature, Z_{eff}) have been obtained in the ohmic phase of these three types of discharges. With additional heating, however, a degradation of the coefficient for the electron energy transport must be introduced for the inner wall and limiter case but not for the X-point discharge. The radial profiles of $n_e \chi_e$ (Fig.6) show that these differences hold over the whole plasma cross-section.

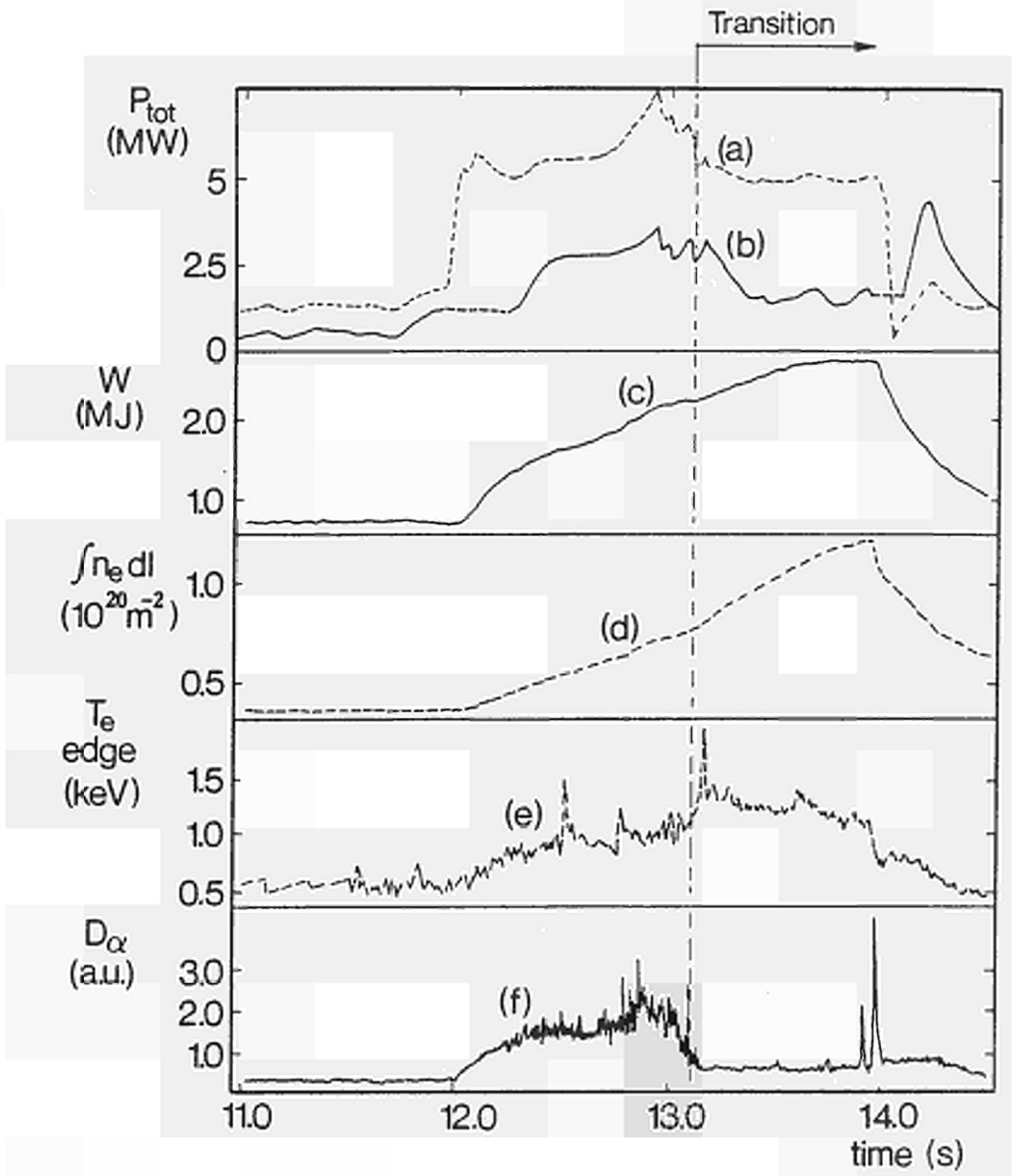

Fig. 5
a) Total input power, P_{tot}, for #10237
b) Power conducted to the target plates from bolometric analysis, $P_{tot} - P_{rad} - W$
c) Total energy content from the diamagnetic loop, W
d) Line electron density, $\int n_e dl$
e) Plasma edge electron temperature, T_e^{edge}
f) D_α signal from the plasma boundary.

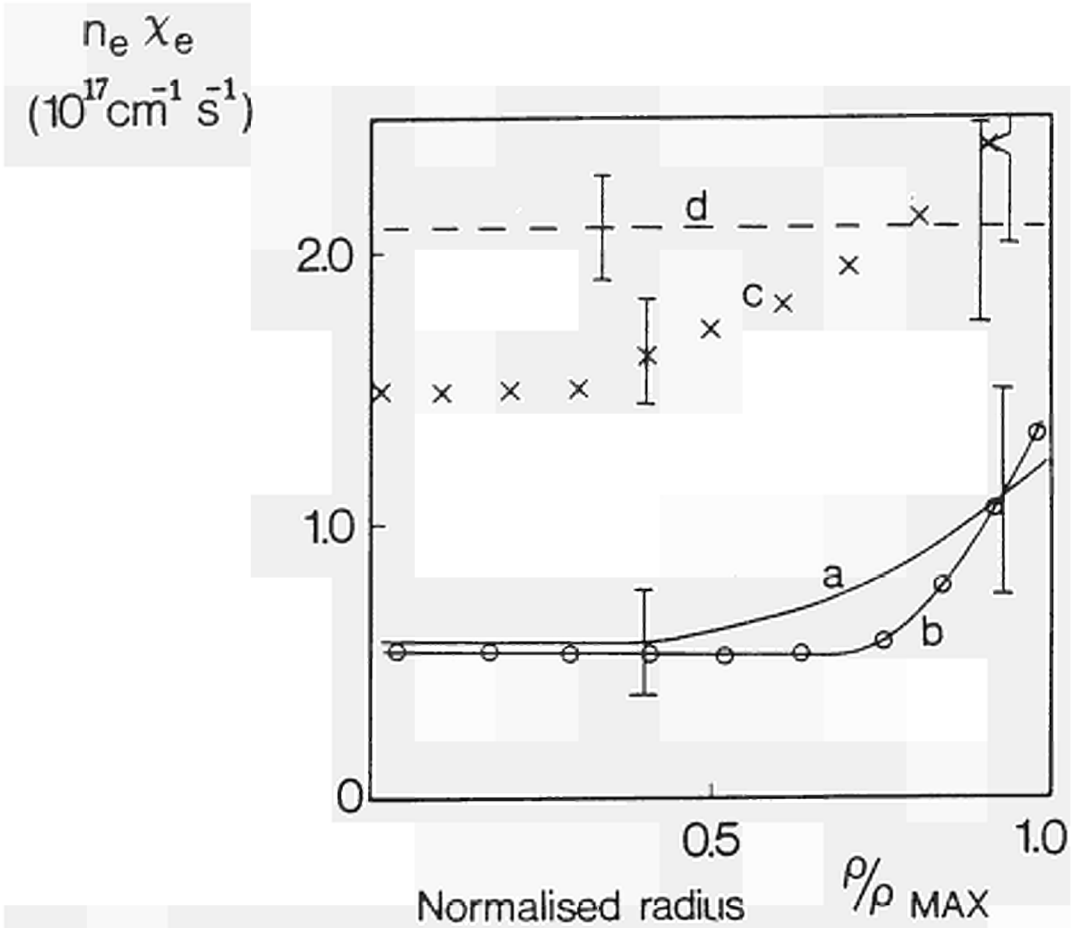

Fig. 6 $n_e\chi_e$ profiles for the SN, limiter and Inner Wall discharges. a) OH phases, b) dots for the discharge of Fig.4 at t = 13.8s, c) for a reference limiter discharge, d) for a reference discharge lying on the inner wall with NBI heating (#8899), with larger input power but lower energy content than b).

5. CONCLUSIONS

Separatrix operation appears to induce substantial changes in the plasma behaviour compared to limiter operation. This is possibly a result of the high shear at the boundary of the plasma. Even with a modest separation of the X-point from the target plates, a high recycling regime has been observed in this region at high plasma densities. With additional heating the stored energy increases substantially above that for corresponding limiter discharges. A further increase in stored energy is observed for both 2MA and 3MA discharges leading to global energy confinement times in excess of 0.6s, about a

factor of two higher than for the corresponding limiter discharges. These discharges also exhibit other signatures (e.g., reduced edge recycling) normally associated with H-modes.

6. ACKNOWLEDGEMENTS

The authors would like to acknowledge the effort of the whole JET team and, in particular,of the RF and NB Divisions.

7. REFERENCES

[1] TANGA, A., Proc. 12th Europ. Conf. on Controlled Fusion and Plasma Physics, Budapest, 1985, Vol.I, p70

[2] NEUHAUSER, J., WUNDERLICH, R., 7th Int. Conf. on Plasma Surface Interactions in Controlled Fusion Devices, Princeton, U.S.A., 1986. To be published in J. Nucl. Mat.

[3] WAGNER, F., et al, Phys. Rev. Lett. 49 (1982) 408, and WAGNER, F., et al, Plasma Physics and Controlled Nuclear Fusion Research, 1982, IAEA, Vienna 1983, Vol.I, p43

[4] DÜCHS, D., et al, Proc. 12th Europ. Conf. on Controlled Fusion and Plasma Physics, Budapest, 1985, Vol.I, p22

PELLET FUELING OF JET PLASMAS DURING OHMIC, ICRF AND NBI HEATING

A Gondhalekar, M Bures, D Campbell, A Cheetham, S A Cohen[1], G Cordey, S Corti, A Edwards, J Ehrenberg[2], R Gill, R Granetz, F Hendriks, W Houlberg[3], H Jäckel[2], T Jones, M Keilhacker, G Magyar, P Mantica[4], V Mertens[2], P D Morgan, P Nielsen, J O'Rourke, G Sadler, F C Schüller, M Stamp, A Tanga, P R Thomas, M L Watkins, A Weller[2]

JET Joint Undertaking, Abingdon, OX14 3EA, UK

ABSTRACT

Pellet fueling experiments have been performed on JET using a single-shot pneumatic injector giving 4.6mm (4.5×10^{21} D atoms) and 3.6mm (2.2×10^{21} D atoms) diameter cylindrical deuterium pellets with velocity $0.8\leq V(km.s^{-1})\leq1.2$. $Z_{eff}<1.5$ with $n_D/n_e\sim1$ on axis has been achieved. In configurations with a magnetic seperatrix, peaked electron density profiles with $n_e(o)/\bar{n}_e\sim2$ are obtained, with $n_e(0)\simeq1.2\times10^{20}m^{-3}$ and $T_e(0)\simeq1keV$. Separately, high value of $n_D(0)\tau_E T_i(0)\simeq1.3\times10^{20}m^{-3}.s.keV$ at $T_i(0)\simeq6.5keV$ has been obtained with pellet fueling followed by NBI heating.

1. INTRODUCTION

The main objectives of pellet injection experiments on JET are (i) to explore if pellet fueling gives access to regimes of higher plasma density, increased plasma purity, improved confinement characteristics, and improved ICRF and NBI heating, (ii) to diagnose plasma behaviour, and to model the measured response in order to develop predictive methods.

The experiments were performed in different configurations, with plasmas limited by (i) the carbon-tile-protected inner wall, (ii) the outer carbon limiters, and (iii) a magnetic separatrix formed during single-null x-point operation. Both ICRF and NBI heating power were applied to the plasma, during and after pellet injection. The plasma parameters were: major radius R~3m, minor radius a~1.2m, elongation k~1.4 and $2.1\leq B_\phi(T)\leq3.4$, $3\leq I_\phi(MA)\leq5$, with target plasma density $0.6\leq\bar{n}_e(10^{19}\ m^{-3})\leq3$ and peak electron temperature $2.3\leq T_e(keV)\leq6$. The total electron content of the target plasmas was $0.6\leq N_e(10^{21})\leq3$. Immediately after pellet injection this increased by $\Delta N_e=3.2(\pm0.3)\times10^{21}$ (4.6mm pellet) and $\Delta N_e=1.8(\pm0.2)\times10^{21}$ (3.6mm pellet), representing 71% and 82% of the pellet mass respectively. Most of the pellet mass was deposited at $0.25\leq r/a\leq0.5$, with some pellets penetrating to within 0.1m of the axis. We present here a survey of the major findings. Fig.1 shows the temporal evolution of a typical pellet fueled limiter discharge with OH alone.

2. PLASMA EDGE BEHAVIOUR AND DENSITY LIMIT

Flux of deuterium at the plasma edge, its recycling and confinement properties have been studied before for gas fueled JET plasmas [1,2]. Outer limiter discharges fueled by a 3.6mm pellet show a large reduction in the influx of deuterium compared to a gas fueled plasma of the same electron density. The global particle confinement time τ_p is thus larger in pellet

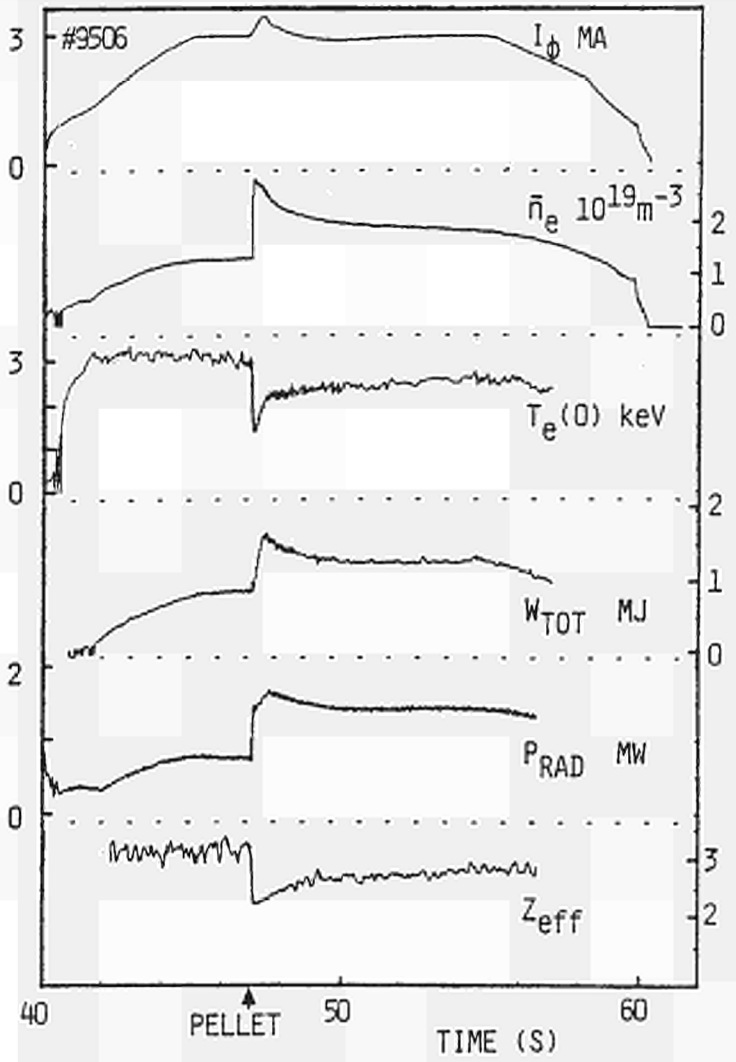

FIG.1 B_ϕ = 2.1T, I_ϕ = 3MA, ohmic heated plasma in deuterium, with 3.6mm pellet injected at 47s. The small increase in I_ϕ at pellet injection is pre-programmed to provide additional power. This feature is not essential.

fueled plasmas, as shown in fig.2. The particle recycling behaviour is also markedly different. Fig.2 also shows (1-R) plotted against $\bar{n}_e$, R is the recycling coefficient measured 1s after pellet injection. Whereas for gas fueled cases $(1-R)\leq 0$, with pellets $(1-R)>0$ for several seconds after injection. This corresponds to a net removal of particles from the system, a pellet induced pumping.

Reduction is also observed in impurity influxes at the plasma edge following pellet injection. However, both the ratio of impurity to deuterium fluxes, and the bolometrically measured total radiated power normalized to the square of the electron density do not show any marked deviation from the behaviour of

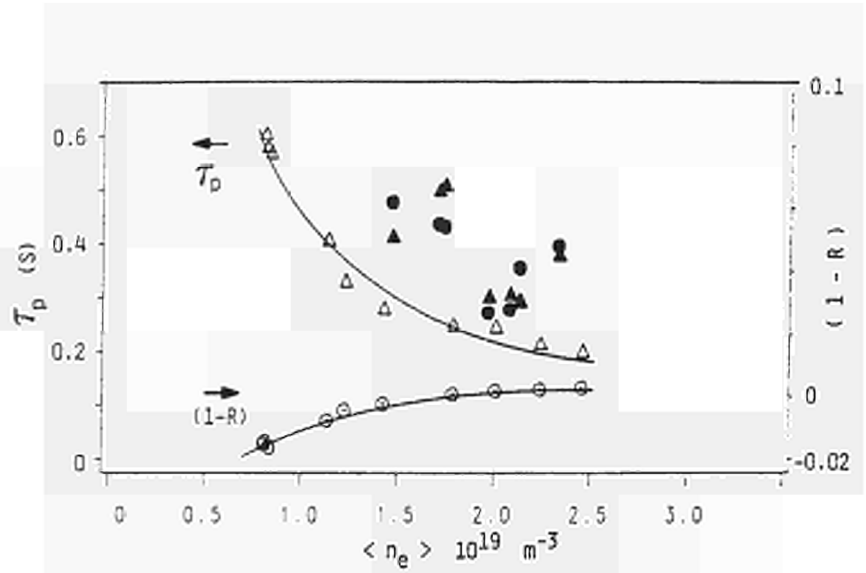

FIG.2 τ_p and (1-R) for limiter plasmas.
O and Δ for gas fueled discharges, ● and ▲ for pellet fueled ones.

gas fueled plasmas. Thus pellet injection effects a reduction of Z_{eff} by reducing the influx of all species, and by diluting the impurities already present. $Z_{eff}<1.5$ have been obtained in limiter plasmas (see fig.2 of [3]). The values are derived from bremsstrahlung measurements taken 0.5s after pellet injection. Eventually, on a time-scale of ≈4s, recycling establishes the higher Z_{eff} concomitant with edge fueling.

The favourable edge behaviour also helps in accessing higher plasma density (see fig.3 of [3]). Both 4.6mm and 3.6mm pellets have been used to probe the limit. The largest increase, by nearly a factor of two above the OH high-density limit in deuterium, was obtained with the 4.6mm pellets at $q_{cyl}≈3.6$. The high-density limit in JET is discussed in [4] in terms of column contraction when the power radiated outside the $q_\psi=2$ surface exceeds the input power. With pellet fueling higher $\bar{n}_e$ can be achieved for a given $n_e(q>2)$.

3. DENSITY DEPLETION AND WALL PUMPING OF THE PELLET FUELED INNER WALL PLASMAS

Gas fueled plasmas placed against the large-area carbon tiles on the inner wall are characterised by a decay of the electron density with a 1s time constant. Increased wall pumping is evident in the post-pellet phase of the plasma. This is an important feature for multiple pellet injection strategies. Pellet fueled inner wall (PFIW) discharges have shown two distinct modes of density behaviour, fig.3. Some show smooth decay in which the volume averaged electron density $<n_e>$ does not return to its pre-pellet value, eg.#9226. This behaviour is similar to that for OH gas fueled inner-wall discharges. In most PFIW plasmas, $<n_e>$ returns to its pre-pellet value in a

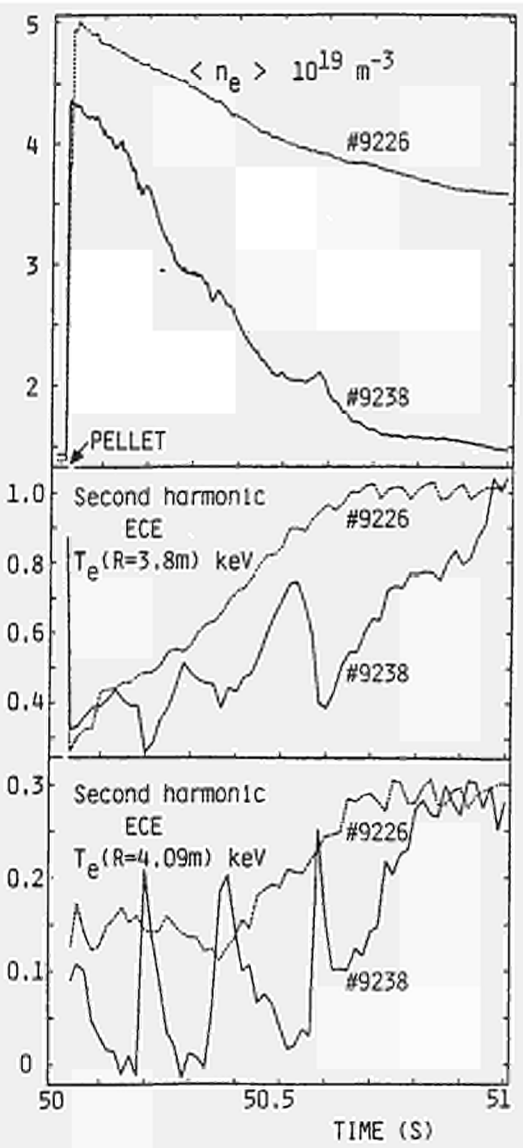

FIG.3 The two modes of density decay for inner-wall plasmas: (a) slow and smooth as in #9226 (b) rapid as in #9238, with mini disruptions at q=2 and corresponding temperature spikes at the edge.

'scallop-like' fashion of ~200ms period, eg.#9238.

The decrease of $\langle n_e \rangle$, whether slow or rapid, depends on transport of plasma ions to material surfaces and then absorption of these ions by the surfaces. The plasma transport process is clearly different in the two modes of behaviour for the PFIW discharges. The scallop-like density decay is synchronous with minor disruptions at the q=2 surface, at R~3.85m, as determined from the magnetics data. A simultaneous decrease in T_e occurs at R~3.8m(q<2), whereas spikes of ΔT_e~100eV occur at R~4.1m(q>2) (eg.#9238 at t=50.2, 50.4 and 50.6sec., for pellet injection at

50s). This same behaviour is shown also in soft x-ray emissions. Interferometry shows a concurrent density increase at large radii. The rise in both $n_e(a)$ and $T_e(a)$ increases the flux of deuterium to the carbon inner wall tiles. Thus minor disruptions give rise to rapid transport of plasma from r=(a-40cm) to r=a. At the edge the particles acquire higher energy due to increased sheath potential, enabling deeper penetration into the wall and thus stronger pumping. During the temperature spikes the D_α emission from the inner wall tiles decreases by a factor of four, showing reduced recycling. Discharges with a smooth decay of $\langle n_e \rangle$ (eg.#9226) do not exhibit such behaviour.

The ability of the $20m^2$ of inner wall carbon tiles to absorb all the deuterium which impinges on it, throughout as many as 20 successive discharges with pellet fueling, is not explicable in terms of the Local Mixing Model [5] of deuterium trapping in graphite. Studies to clarify this are in progress.

4. A PELLET INDUCED OSCILLATION AT THE q=1 SURFACE

Soft x-ray imaging arrays have revealed the presence of a unique phenomenon, the 'snake' oscillation, fig.4. It frequently appears when a pellet is injected, and manifests itself as a small region of enhanced x-ray emissivity with a m=1/n=1 helical symmetry at the q=1 radius. Analysis has shown that this increased emission is due to a density increase in the 'snake', by up to a factor of two, above the background density, as well as a drop of -20% in T_e compared to the surrounding plasma. In contrast to the short-lived m=1/n=1 perturbation rotating in the electron diamagnetic direction observed previously [6], the 'snake' in JET lasts for many hundreds of milliseconds and occasionally up to -1.5s, it rotates at varying frequencies in the ion diamagnetic direction, it sometimes comes to a complete standstill and then resumes rotation. Sawtooth disruptions occur during this activity, without dissipating the 'snake'.

One plausible hypothesis for the 'snake' is that an m=1/n=1 magnetic island is created by the high density ablation cloud from the pellet as it crosses the q=1 surface. This island then traps the excess density, forming the helical 'snake'. If this hypothesis is correct, the radial location of the 'snake' is an accurate indicator of the radius at which q=1. We thus infer that the q=1 region expands by 35% during the sawtooth ramp.

5. ELECTRON DENSITY PROFILES AND RELATED TRANSPORT

Immediately after pellet injection, the electron density profile is hollow ($dn_e/dr>0$). $n_e(r)$ recovers to a centrally peaked shape in ~200ms. The evolution towards a peaked profile is discontinuous when sawteeth occur. An analysis of profile evolution of pellet fueled plasmas using a model of electron particle flux $\Gamma_e = -D\nabla n_e + Vn_e$ indicates that the diffusion

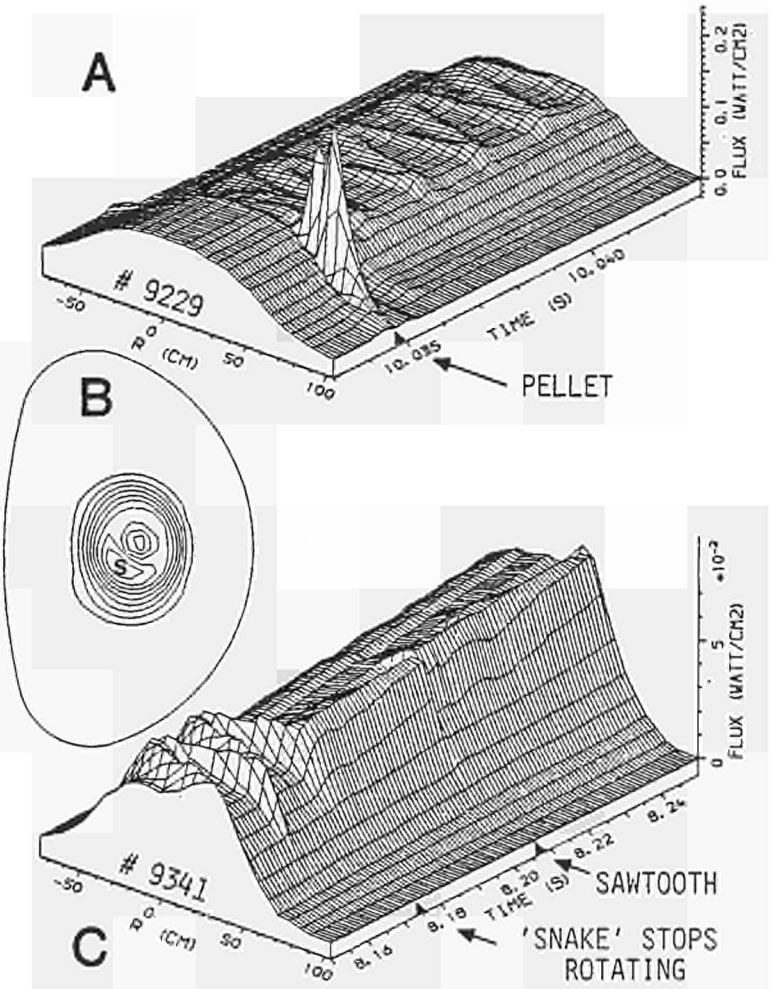

FIG.4 A: Plot of line-integrated soft x-ray fluxes showing the 'snake' oscillation after pellet injection.

B: Tomographic reconstruction showing contours of equal emissivity, and localization of the 'snake'.

C: Plot as in A showing a 'snake' that has stopped rotating, and survives a sawtooth crash.

coefficient D(r) and convection velocity V(r) fall in with those for gas fueled ones [7,2], which showed a large scatter, but no dependence on $\tilde{n}_e$, I_ϕ, B_ϕ or heating mode. Analyses of individual pellet injection cases show that in the outer limiter configuration, V/D increases from $\approx 0.2 m^{-1}$ before pellet injection to $-0.4 m^{-1}$ immediately after, reverting to $\approx 0.2 m^{-1}$ 1.5s later, as evidenced by the more peaked density profile after pellet injection, which subsequently returns to its original form. In the single-null x-point configurations, V/D

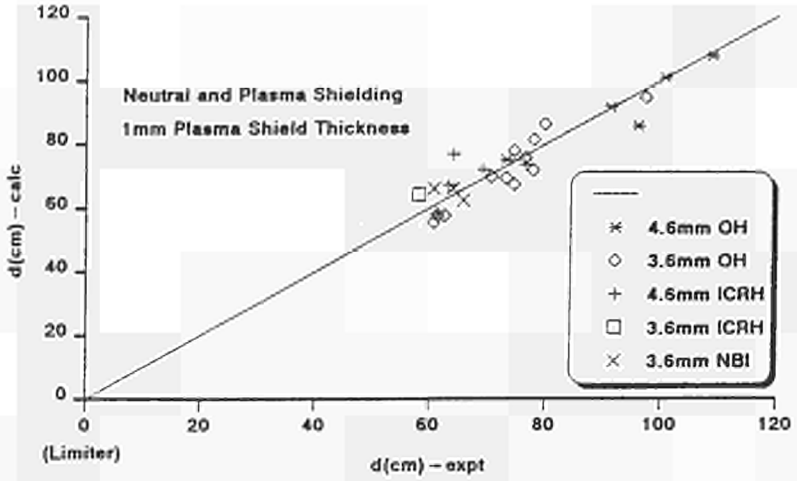

FIG.5 A comparison between the measured penetration, Δ(cm)-exp, and the calculated one, Δ(cm)-calc. The data set includes 4.6mm and 3.6mm pellets, with OH, OH+ICRF heating at $P_{ICRF} \leq 4.6MW$, and OH+NBI heating at $P_{NBI} \leq 4MW$.

increases from $\sim 0.3m^{-1}$ before pellet injection to $\sim 0.6m^{-1}$ after, giving a very peaked density profile that is maintained for a long time. Eventually V/D decreases to $\sim 0.4m^{-1}$.

6. PELLET ABLATION MODELLING

Accurate determinations of penetration of the pellet into the plasma and ablation rate are made using a combination of a soft x-ray camera and D_α detectors viewing the pellet trajectory. As shown in fig.5, the penetration of the pellet into the plasma for all the data considered is successfully modelled with a neutral gas shielding model, modified to include attenuation of the electron heat flux by a cold ionized plasma surrounding the neutral gas [8]. Also included are a multi-group treatment of the incident electrons, plus self-limiting ablation in the collisionless plasma limit. With present heating power levels, the pellets traverse regions with fast ion density $n_{fi} \sim 3 \times 10^{18} m^{-3}$ for NBI heating, and $n_{fi} < 10^{18} m^{-3}$ for ICRF heating. No additional ablation processes associated with such a fast ion population during ICRF or NBI heating have yet been identified.

7. ICRF HEATING OF PELLET FUELED PLASMAS

An important limitation of ICRF heating in JET is the uncontrolled density increase during the RF pulse. Influx of all neutral species from the limiters and wall increases roughly in proportion to the applied power, and Z_{eff} and the ratio P_{rad}/P_{in} remain nearly constant. As a result the density limit during ICRF heating is at most 10% higher than the corresponding value for ohmic heating alone. We have probed this limitation by applying ICRF heating immediately after pellet injection. We

have observed that the initial density increase effected by pellet injection can be maintained with ICRF heating and the high-density limit for OH+ICRF heating can be extended. Both 4.6mm and 3.6mm pellets have been used. The resulting increase in temperature, for both electrons and ions, in the ^{3}He minority heating mode are consistently slightly larger than values obtained with gas fueling under similar plasma conditions and for the same normalized ICRF power. Our future work with multiple pellet injection will further explore and optimize ICRF heating of a densified plasma core.

8. SUMMARY

Deuterium pellets have been injected into plasmas with OH, OH+ICRF and OH+NBI heating. Plasmas with different magnetic configurations were probed. It is shown that pellet fueling gives access to regimes of higher plasma density and increased plasma purity by modification of edge behaviour. Also, pellet injection modifies the electron density transport in the bulk plasma, most markedly in the single-null x-point configuration, giving very peaked density profiles. These effects persist for several seconds. Careful modelling of pellet ablation and penetration measurements has been performed. At present levels of auxiliary heating power, no additional ablation processes associated with application of ICRF or NBI power have been identified. A 'snake' oscillation characterized by an island of dense cooler plasma at the $q=1$ radius is observed. Its small dimensions ($\Delta l_r \approx 15$cm, $\Delta l_\theta \approx 25$cm), and long lifetime ($\tau \approx 0.2 \rightarrow 1.5$s) imply greatly reduced energy and particle diffusion compared to the surrounding plasma.

A critical issue is whether profiles obtained with pellet injection have better confinement properties than those produced by gas fueling [9,10,11,12]. With single pellet injection in JET the behaviour of energy confinement is unclear. In the transient period immediately after injection of a pellet, the confinement time is much larger than the corresponding value with gas fueling, as observed in other experiments employing single pellet injection. However, the duration of the period of apparent improved confinement is shorter than τ_E. The significance of this observation is being investigated. An aim of our future work with multiple pellet injection will be to explore the feasibility of effecting a sustained improvement in confinement properties.

9. ACKNOWLEDGEMENTS

Dedication and enthusiasm of many people has benefited these experiments. The authors are grateful to L Lamb, J-L Bonnerue, J Ryan and K Scheidt for superb technical support, to C Wilson, J Reid, P Roberts and A Tiscornia for excellent engineering support and to C Andelfinger, K Büchl and H-B Schilling of IPP,

Garching, for manufacture of the pellet injector, and for strong support during installation.

10. REFERENCES

[1] MORGAN, P.D., et al., 12th European Conf. on Contr. Fusion and Plasma Physics, Budapest 1985, Europhysics Conference Abstracts, Vol.9F, Part II, p.535.
[2] CHEETHAM, A., et al., 13th European Conf. on Contr. Fusion and Plasma Physics, Schliersee 1986, Europhysics Conference Abstracts, Vol.10C, Part I, p.240.
[3] REBUT, P.H., et al., 11th IAEA Conference on Plasma Physics and Controlled Nuclear Fusion Research, Kyoto, Japan, 1986. Paper IAEA-CN-47/A-I-2.
[4] SCHÜLLER, F.C., et al., 12th European Conf. on Contr. Fusion and Plasma Physics, Budapest 1985, Europhysics Conference Abstracts, Vol.9F, Part I, p.151.
[5] BRICE, D.K., et al., J.Nucl.Materials, 111/112(1982)598.
[6] PARKER, J., et al., MIT Plasma Fusion Center Report, PFC/RR-85-8(1985).
[7] GONHALEKAR, A., et al., Bull.Am.Phys.Society, 30(1985)1525.
[8] WATKINS, M.L., et al., 13th European Conf. on Contr. Fusion and Plasma Physics, Schliersee 1986, Europhysics Conference Abstracts, Vol.10C, Part I, p.156.
[9] GREENWALD, M., et al., Phys.Rev.Lett. 53(1984)352.
[10] SCHMIDT, G.L., et al., 12th European Conf. on Contr. Fusion and Plasma Physics, Budapest 1985, Europhysics Conference Abstracts, Vol.9F, Part II, p.674.
[11] ODAJIMA, K., et al., 11th IAEA Conference on Plasma Physics and Controlled Nuclear Fusion Research, Kyoto, Japan, 1986. Paper IAEA-CN-47/A-III-2.
[12] NIEDERMEYER, H., et al., 13th European Conf. on Contr. Fusion and Plasma Physics, Schliersee 1986, Europhysics Conference Abstracts, Vol.10C, Part I, p.168.

CD-NA-11-113-EN-C